ARISTOTLE UNIVERSITY OF THESSALONIKI
FACULTY OF SCIENCES

SCIENTIFIC ANNALS
OF THE SCHOOL OF GEOLOGY

PROCEEDINGS

XIX CONGRESS OF THE CARPATHIAN-BALKAN GEOLOGICAL ASSOCIATION

September 23-26, 2010
Thessaloniki, Greece

Editors
Christofides G.
Kantiranis N.
Kostopoulos D.S.
Chatzipetros A.A.

Special Volume 100
General Session G11
Special Sessions

Thessaloniki 2010

SET 978-960-9502-00-9
ISBN 978-960-9502-02-3

Printed by Charis Ltd, Thessaloniki, Greece

CBGA Council

President: Georgios Christofides *(Greece)*
Secretary General: Spyros Pavlides *(Greece)*

Councillors (National Representatives)

Albania	Aleksander Cinai
Austria	Volker Hoeck
Bulgaria	Yotzo Yanev
Czechia	Lilian Svabeicka
FYROM	Blazo Boev
Greece	Georgios Christofides
Hungary	Geza Csaszar
Montenegro	Branimir Glavatovic
Poland	Nestor Oszcypko
Romania	Corina Ionescu
Serbia	Milan Sudar
Slovakia	Jozef Vozar
Slovenia	Mirka Trajanova
Ukraine	Volodymir Kolodiy

CBGA Boarder

Georgios Christofides *(Greece)*
Spyros Pavlides *(Greece)*
Aleksandar Grubic *(Serbia)*

Organizing Committee

Georgios Christofides, *President of CBGA*

Vice President

Athanassios Chatzikirkou, *Director of IGME - Central Macedonia Regional Branch*

Secretary General

Spyros Pavlides, *Secretary of CBGA*

Executive Secretary

Alexandros Chatzipetros

Treasurers

Kostas Voudouris
Vasilios Melfos

Members

Kostas Albanakis
Christina Anagnostopoulou
George Christidis
Spyros Dabitzias
Stamatis Dafnis
Nikos Epitropou
Nikos Kantiranis
Theodoros Karacostas
Antonis Koroneos
Dimitris S. Kostopoulos
Ioannis Koukouvelas
Andreas Magganas
Georgios Migiros
Lambrini Papadopoulou
Kostas Papazachos
Michael Stamatakis
Triantafyllos Soldatos
Vasilios Tsikouras
Panayiotis Tsourlos
Georgios Vargemezis

Field trips subcommittee

Kostas Michael
Anne Ewing Rassios
Georgios Syrides
Kostas Vouvalidis

Sponsors

Silver Sponsors

Institute of Geology and Mineral Exploration of Greece

HELLAS GOLD

Thracean Gold Mining

Conference Patrons

Geotechnical Chamber of Greece

Aristotle University of Thessaloniki
Research Committee

Earthquake Planning and Protection Organization of Greece

Municipality of Thessaloniki

Reviewers

Aidona E., Greece
Albanakis K., Greece
Alderton D., UK
Anastasakis G., Greece
Anastasiadis P., Greece
Angelakis N.A., Greece
Antonarakou A., Greece
Argiraki A., Greece
Arvanitidis N., Greece
Astaras Th., Greece
Avdiz M., Bosnia and Herzegovina
Baskoutas I., Greece
Berzina A., Russia
Bilal S., France
Bogdanov K., Bulgaria
Bonev N., Bulgaria
Catchpole H., Switzerland
Chatzitheodoridis E., Greece
Cherneva Z., Bulgaria
Chlögl J., Slovakia
Cholis I., Greece
Christanis K., Greece
Christaras V., Greece
Christidis G. Greece
Christofides G., Greece
Compagnoni R., Italy
Cosztonyi G., Hungary
de Backer H., Belgium
Delfino M., Italy
Dilek Y., USA
Dimitriou E., Greece
Drakatos G., Greece
Dumitru I., Romania
Economou M., Greece
Fassoulas Ch., Greece
Filippidis A., Greece
Fountoulis J., Greece
Fritsch E., France
Fyticas M., Greece
Galan E., Spain
Ganas A., Greece
Georgakopoulos A., Greece
Geraga M., Greece
Godelitsas A., Greece
Golonka J., Poland
Gonthier E., France
Grigorescu D., Romania
Gurk M., Germany
Hajdu A.,Hungary
Halásová E., Slovakia
Hosgoermez H., Turkey
Houssos E., Greece
Hovorka D., Slovakia
Illášová L., Slovakia
Ioannou I., Greece
Ionescu C., Romania
Iordanidis A., Greece
Iosifidis Th., Greece
Kakouros E., USA
Kalampokidis K., Greece
Kalavrouziotis I., Greece
Kantiranis N., Greece
Kapicka A., Poland
Karakitsios B., Greece
Karakostas Th., Greece
Karampelas S., Switzerland
Karymbalis E., Greece
Kassaras I., Greece
Katagas Ch., Greece
Katerinopoulos A., Greece
Kati M. Greece
Kazadtzis S., Greece
Kelepertzis A., Greece
Kilias A., Greece
Kiratzi A., Greece
Klimis N., Greece
Kokinou E., Greece
Kokkalas S., Greece
Komnitsas K., Greece
Kontopoulos N., Greece
Koroneos A., Greece
Koskeridou E., Greece
Kostopoulos D., Greece
Kostopoulos D.S., Greece
Kostopoulou E., Greece
Kostov R., Bulgaria
Koufos G., Greece
Koukis G., Greece
Kouzmanov K., Switzerland
Kyriakopoulos K., Greece
Loiacono F., Italy
Loupasakis K., Greece
Machev P., Bulgaria
Magganas A., Greece
Markopoulos Th., Greece
Mavromatis Th., Greece
Mederer J., Switzerland
Melfos V., Greece

Menzies J., Bulgaria
Méres Š., Slovakia
Michailides K., Greece
Mitropoulos P., Greece
Mladenova V., Bulgaria
Mocanu V., Romania
Morheouse B., USA
Moritz R., Switzerland
Moropoulou A., Greece
Mountrakis D., Greece
Mposkos E., Greece
Nagel T., Germany
Nedyalkov R., Bulgaria
Ntabitzias S., Greece
Ntrinia Ch., Greece
Orlecka-Sikora B., Poland
Oszczypko N., Poland
Ozden S., Turkey
Ozer S., Turkey
Panagiotopoulos D., Greece
Papadopoulos A., Greece
Papadopoulou-Vrinioti K., Greece
Papagianni-Papadopoulou I., Greece
Papanastasiou A., Greece
Papanikolaou D., Greece
Papathanasiou G., Greece
Papazachos C., Greece
Pavlakis P., Greece
Pavlides S., Greece
Pavlopoulos A., Greece
Pe-Piper G., Canada
Perdikatsis V., Greece
Petrakakis K., Austria
Petrescu L., Romania
Plašienka D., Slovakia
Polemio M., Italy
Poli G., Italy
Pomoni F., Greece
Pomonis P., Greece
Pons J.-M., Spain
Potfaj M., Slovakia
Poulos S., Greece
Přikryl R., Czech Republic
Raptakis D., Greece
Rondeau B., France
Samara K., Greece
Saric C., Serbia
Seghedi I., Romania
Selby D., UK
Serafimovski T., FYROM
Sikalidis C., Greece
Skarpelis N., Greece
Sklavounos S., Greece
Sonmez H., Turkey
Soták J., Slovakia
Spassov N., Bulgaria
Stamatakis M., Greece
Stamatis G., Greece
Stamatopoulos L., Greece
Stavropoulou M., Greece
Stolaki S., Greece
Strack E., Germany
Švábenická L., Czech Republic
Syrides G., Greece
Szabo, S., Hungary
Tedesco D., Italy
Theodoridou M., Greece
Theodorou G., Greece
Therrien F., USA
Török Á., Hungary
Tranos M., Greece
Triantafyllou A., Greece
Triantaphyllou M., Greece
Tsapanos Th., Greece
Tsikouras V., Greece
Tsirampides A., Greece
Tsoukala E., Greece
Tsourlos P., Greece
Tzanis A., Greece
Tziavos I., Greece
Udluft P., Germany
Uher P., Slovakia
Valiakos E., Greece
Vargemezis G., Greece
Varsakelis N., Greece
Vaskovic N., Serbia
Vojtko R., Slovakia
Voudouris C., Greece
Voudouris P., Greece
Voulgaris N., Greece
Vozar J., Slovakia
Zaggana E., Greece
Zagorchev I., Bulgaria
Zelelidis A., Greece

Contents

General Session G11
Environmental geosciences

Preface

CBGA 2010 is the XIX Congress of the Carpathian –Balkan Geological Association, one of the longer-lasting series of congresses in Europe. The first CBGA Congress was organized in Poland in 1925 and the penultimate one in Belgrade in 2006.

CBGA 2010, which is a follow-up of previous successful congresses, aims at bringing together academic scientists, institute and industry researchers and scholar students to share their experiences and research results about Earth and Environmental Sciences aspects, discuss the practical challenges encountered, highlight the necessity and the priorities of the geological science, make proposals, and seek for application of policies. It is co-organized by the School of Geology, Aristotle University of Thessaloniki, Greece, the Geological Society of Greece, and the Institute of Geology and Mineral Exploration, Greece.

Earth operates as a constantly changing complex, dynamic system which, however, has not yet been fully understood. The Earth system comprises a lot of interdependent components that interact in complex ways. Planet Earth is changing in all spatial and temporal scales and although investigated in many respects and a huge amount of knowledge, both basic and applied, has been accumulated much more has to be done. The understanding of our Planet system and its reaction to natural and anthropogenic changes must be of predominance concern. Water shortage, environment protection, mineral resources, climate changes, natural hazards, and the Earth's origin and evolution are some of the priorities. Geoscientists have produced enormous amount of knowledge in a great range of topics. However, this knowledge in many cases remains unexploited. We have not found the way to inform or better to convince the politicians and the decision makers for the necessity of using this knowledge. The geo-knowledge we possess must be distributed and used for the benefit of the present and the next generations: for a safer, healthier and wealthier place to live. The XIX CBGA Congress covers a vast spectrum of topics in Earth and Environmental Sciences including Geophysics and Meteorology/Climatology as well as some related disciplines. The quality and quantity of the participants and their works no doubt will contribute towards this direction.

The registration fees have no doubt been the blood donor of the Congress. The sponsors, however, contributed greatly to the success of it and we are grateful to them. Although the worldwide economic crisis has affected the organisation of the congress from the financial point of view, the Organising Committee managed to offer a large number of grants particularly to young scientists giving them the opportunity to attend CBGA 2010 and benefit from it, and facilitated, in some extend, financially the CBGA Council and Board members as well as the invited speakers.

We wish to warmly thank the Conveners of the Special Sessions and all colleagues who offered their valuable time to review the papers included in the Proceeding volumes. We would also like to thank the invited speakers, leading scientists in their field (Gérard Stampfli, Ioan Seghedi and Maria Economou-Eliopoulos), who kindly accepted our invitation to give a plenary talk for the participants.

The Organising Committee is pleased to acknowledge the contribution of all participants in helping to present to the geological community this excellent geological event and to produce the congress proceedings. In total, 130 full papers have been presented in CBGA 2010, of which 81 in oral and 49 in poster mode. Their abstracts, together with 410 stand-alone abstracts that have also been submitted, have been published in the Abstracts volume of CBGA 2010 (Geologica Balcanica). More than 1,400 authors coming from tens of countries all over the world have contributed in making this congress an event of high scientific value.

The President of the Organizing Committee wish to express his gratitude and his sincere thanks to all members of the Organizing Committee, the team of post-graduate and graduate students of the School of Geology of the Aristotle University of Thessaloniki, who worked hard and did their best for the excellent organization of the Congress.

Prof. Georgios Christofides
President of the Organizing Committee
of the XIX CBGA Congress

General Session G11
Environmental geosciences

Scientific Annals, School of Geology, Aristotle University of Thessaloniki Proceedings of the XIX CBGA Congress, Thessaloniki, Greece	Special volume 100	1-5	Thessaloniki 2010

SOCIOECONOMIC INFLUENCE OF NATURAL DISASTERS IN THE WESTERN BALKAN COUNTRIES

Abolmasov B.[1], Mihalić S.[2], Hadži-Niković G.[1], Marjanović M.[3], Krkač M.[2]

[1]*Faculty of Mining and Geology, University of Belgrade, Djušina 7, 11000 Belgrade, Serbia, biljana@rgf.bg.ac.rs, ghinikovic@rgf.bg.ac.rs*
[2]*Faculty of Mining, Geology and Petroleum Engineering, University of Zagreb, Piertottijeva 6, 10000 Zagreb, Croatia, smihalić@rgn.hr, martin.krkac@rgn.hr*
[3] *Faculty of Science, Palacky University, tř. Svobody 26, Olomouc, Czech Republic, milosgeomail@yahoo.com*

Abstract: The Western Balkan region is a region of south-eastern Europe that presents pronounced activities of various types of natural hazards and natural disasters. This paper analyses data sets from two international databases of the main types of natural disasters namely geophysical, hydrological, climatological and meteorological disaster events in the period 1900-2008. The following have been analysed: the number of natural disaster events, natural disaster occurrence by disaster type, the total number of fatalities, the total number of affected people and the corresponding economic damages expressed as a percentage of selected types of natural disasters. The data analysis in this paper aims to confirm the importance of data collection and analysis as a foundation for planning and preparing disaster reduction programs for the Western Balkan countries.

Key words: Western Balkan countries, period 1900-2008, natural disasters, statistical review

1. Introduction

Natural disasters occur all over the world. Climate changes, environmental degradation and development in high-risk zones have all contributed to the increased number of natural disasters worldwide and the increased vulnerability of society, particularly for regions that are prone to natural hazards. An analysis of the total number of natural disasters and the total economic loss reported by natural hazards shows a distinct trend of growth during the last fifty years worldwide. According to data from Munich Reinsurance Company (http://munichre.com) the total economic losses have multiplied in the period 1950-2008. This information can be confirmed if we review the data from (Centre for Research on the Epidemiology of Disasters) CRED (Centre for Research on the Epidemiology of Disasters) (http://www.cred.be) for individual continents or for the entire world. The human and economic losses caused by natural disasters only in 2008 were devastating. More than 235.000 people were killed; 214 million people were affected and the economic cost was over 190 billion US dollars (Rodriquez et al., 2009).

Several definitions of natural disasters emphasize the usage of this term. The Centre for Research on the Epidemiology of Disasters, Catholic University of Louvain, Belgium (Guha-Sapir, 2008) defines natural disaster as "a situation or event which overwhelms local capacity, necessitating a request to national or international level for external assistance; an unforeseen and often sudden event that causes great damage, destruction and human suffering".

It can be said that natural hazards and natural disasters are present all over the world; however, certain types of natural disasters and their total impact differ between geographical locations and the degree of development and vulnerability (social, economic, political or cultural) of the region or country (Abolmasov et al., 2009).

This paper will present the results of an analysis and statistical review of international databases of selected data sets on natural disasters and their impact on the Western Balkan countries.

2. Methodology of collecting data

The collection of information on natural disasters and their impact is complex as it depends on time, funding, the huge variability of definitions, methodologies, sources and data points that have been

collected. There is still no international consensus regarding the best practice for the collection of data on natural disasters (Guha-Sapir, 2008). However, when there are no regional or national databases, internet searches for disaster databases produced an enormous number of references. This paper analyses the data that was obtained by searching two international databases with publicly accessible data: The Emergency Disasters Data Base (EM-DAT) managed by the Centre for Research on the Epidemiology of Disasters (CRED) at the Catholic University of Louvain, Belgium (Accessed September 20, 2009: http://www.emdat.be) and NATHAN disaster database maintained by Munich Reinsurance Company (Accessed September 10, 2009: http://mrnathan.munichre.com).

base, at least one of the following criteria must be fulfilled:

- 10 or more people reported killed,
- 100 or more people reported affected,
- declaration of a state of emergency,
- call for international assistance.

Events are entered on a country-level basis and information collected includes location, date, number of people killed/injured/affected, number of homeless, and estimated damage costs. Sources include governments, UN agencies, research institutions, insurance institutions and press agencies, although priority is given to UN agencies. Amongst disaster databases, both databases provide one of the most comprehensive and transparent explanations of the

Table 1. Definitions of the natural disasters and their main types (Guha-Sapir 2008)

Disaster Main Type	Definition	Disaster Subgroup
Geophysical	Events originating from solid earth	Earthquake, Volcano, Mass Movement (dry)
Meteorological	Events caused by short-lived/small to meso scale atmospheric processes (in the spectrum from minutes to days)	Storm
Hydrological	Events caused by deviations in the normal water cycle and/or overflow of bodies of water caused by wind set-up	Flood, Mass Movement (wet)
Climatological	Events caused by long-lived/meso to macro scale processes (in the spectrum from intra-seasonal to multi-decadal climate variability)	Extreme Temperature, Drought, Wildfire
Biological	Disaster caused by the exposure of living organisms to germs and toxic substances	Epidemic, Insect infestation, Animal Stampedo

The unique classification of natural disasters types in both databases allows for data integration and analysis. Table 1 presents the classification and definitions of certain types of natural disasters, which were established by MünichRe/Geo Risks Research Department and CRED (Guha-Sapir, 2008). The data presented on the biological type of natural disasters was not analysed. Events are entered on a country-level basis and the information collected includes location, date, number of people killed and affected, and the estimated damage costs.

Both databases record data on the number of people killed and affected, in addition to estimated amounts of economic damage expressed in US dollars for the majority of natural disasters. The terms "killed", "affected" and "estimated economic damage" have been identically defined in both databases. For a disaster to be entered into the database, at least one of the following criteria must be fulfilled:

methodology employed. Databases are searchable by country, disaster type or timeframe. As most data was organised on a country-level basis, an additional database was created for this research, containing data organised by disaster-type and by killed-affected-economic damage per disaster type. The Western Balkan countries for which data was collected and analysed in this paper were: Serbia, FYR of Macedonia, Albania, Montenegro, Bosnia and Herzegovina and Croatia (Fig. 1). The data collected covered the period from 1900 to 2008 for the above listed countries.

3. Data analysis and results

The analysis was conducted on selected data sets including all the data for the four main types of disasters and their sub-types, namely: geophysical, hydrological, climatological and meteorological disaster events for the period 1900-2008. Data on the number of disaster events, disaster occurrence

by disaster type, total number of killed and total number of affected people and the corresponding economic damages with percent share by selected types of natural disasters was analysed. Due to the nature of the data provided, i.e. not collected in the same manner in each country and not having an occurrence of a natural disaster event in every year during the period under analysis, only a basic statistical analysis was able to be performed.

Fig. 1. Geographical position of study area.

The basic statistical analysis showed that in the period 1900-2008 in the Western Balkan region, a total of 2.480 people were reported as being killed by all natural disaster types and related subgroups, i.e. 1.299 from geophysical events (8 events), 189 from hydrological events (11 events) and 992 from climatological disasters (13 events). The total number of people killed and the total number of disaster events by disaster types are presented in figure 2.

The analysis of the total number of reported people affected by natural disasters in the same period showed that 6.353.849 persons were affected. Within the total number, 652.220 were affected by ten geophysical events, 885.451 by hydrological events (31 events), 4.290.088 by climatological events (9 events) and 526.090 from meteorological disasters (3 events). The total number of persons affected and the total number of disaster events by disaster types are presented in figure 3.

The analysis of the reported economic damage showed that the total economic cost from natural disasters in the Western Balkan region for the period 1900-2008 amounted to 4.726.886.000 US dollars. The reported economic damages from geophysical disasters was 1.158.600.000 US dollars (5 events), from hydrological disasters was 1.448.973.000 US dollars (8 events) and from climatological disasters was 2.119.313.000 US dollars (9 events) (Fig. 4).

4. Discussion

The review of the natural disasters data from two selected databases for the Western Balkan countries in the period 1900-2008 has shown that in the geographically small study area all types of natural disasters occurred.

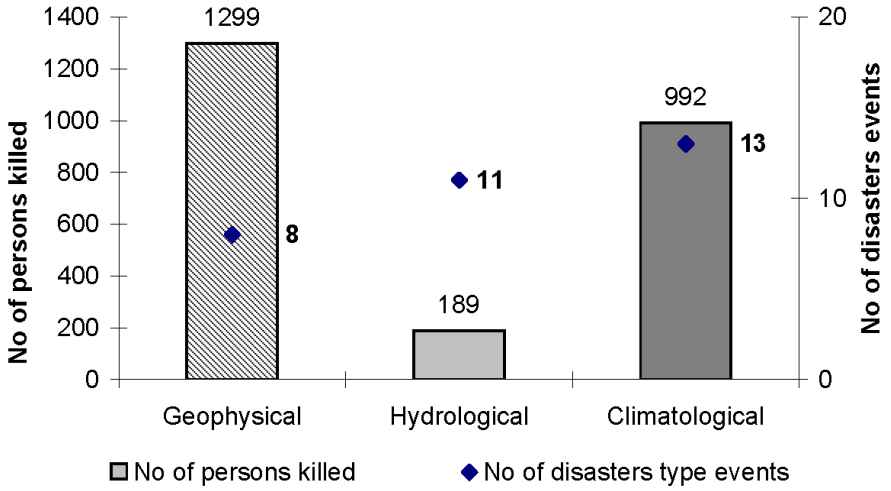

Fig. 2. Total number of persons killed and number of events by disaster type from 1900-2008. Source: EM-DAT and NATHAN.

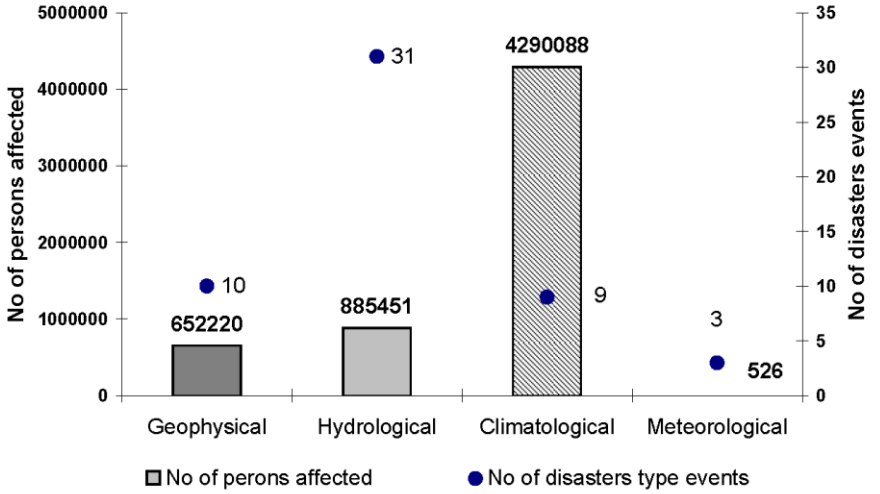

Fig. 3. Total number of persons affected and number of disasters events by disasters type from 1900-2008. Source: EM-DAT and NATHAN.

The analysis of the number of people killed by natural disasters showed that in the Balkan region the greatest number of people killed was by geophysical disasters-earthquakes. A comparison between the percentages of total number of persons killed by the geophysical disaster of earthquakes was 52%, even though the event represents only 25% of the total number of natural disasters events. The earthquake that claimed the most victims was in Skopje on 26th of July 1963 with a death toll of 1.100 people. The disasters type that had the second highest number of people killed was climatological disasters with a total number of deaths of 40% of the total number of people killed by all types of natural disasters (Fig. 2). That number of deaths was in consequence to 13 climatological events, which represent 41% of all events. Only 8% of the persons killed were killed from hydrological disasters, which represent approximately 34% of the total number of disasters events. If we compare the number of persons killed by different types of natural disasters and disaster occurrences, we can conclude that the mortality rate is the highest in the case of earthquakes, where the smallest number of events killed the largest number of people.

The analysis of the total number of persons af-

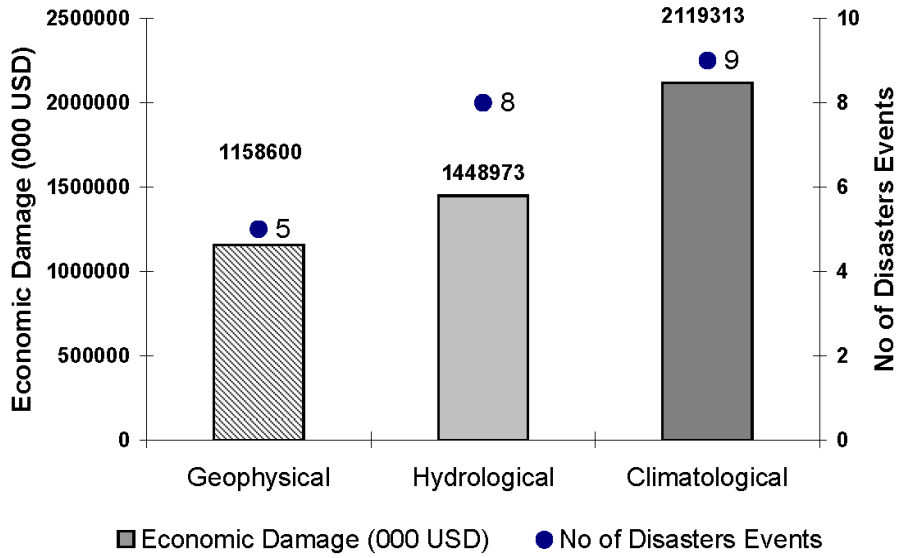

Fig. 4. Total amount of economic damage and number of disasters events by disasters type from 1900-2008. Source: EM-DAT and NATHAN.

fected from natural disasters in the period 1900-2008 shows that the greatest number of people (68%) were affected by climatological disasters and this percentage of people affected came from only 17% of the total number of events, as shown on figure 3. The percentage of the total number of persons reported affected from hydrological disasters was 14% with 10% of persons affected by geophysical events. Only 8% of persons were affected by meteorological disasters. It can be concluded from the results above that of the total number of people affected by natural disasters the greatest number of people was affected by climatological disasters, even though hydrological disasters had the greatest number of events in the same period.

In addition, a review of the economic damages from natural disasters in the Western Balkan countries in 1900-2008 shows that the greatest economic losses were due to climatological disasters (Fig. 4), totalling 44% of the total amount of economic damages, coming from 41% of the total number of natural disaster events. The second highest percentage (31%) of the total amount of economic damages was from hydrological disasters while the reported economic damages from geophysical disasters were only 25% of the total amount of economic damages. The single climatological event that had the greatest amount of economic damages was the drought in the central part of former Yugoslavia during July 1990. The second in order was the hydrological event of flooding during October 1990 in the same region. The earthquake that claimed the most economic damage was in Skopje on 26th of July 1963 which has the third highest reported economic damage, but has the highest number of reported killed.

5. Conclusion

The results of this analysis show that the Western Balkan region, in which more than 22 million people live in approximately 264.000 km^2 (Source: IMF, http://www.imf.org, Accessed October 21, 2009), is affected by all forms of natural hazards and disaster types. Unfortunately, the natural disasters data for all the countries in the region can only be found in the two global databases that were utilised. With differences in the recording criteria and the presentation of data a large amount of local data has not been entered the databases. In addition, many natural disaster types, for example floods or heat waves, are not localized to individual countries, but their effects are often extended to several neighbouring countries, and may not have been registered individually on a country-level basis as they did not fulfil the recording criteria for that individual country. Development and response agencies in the Western Balkan countries have to recognize the importance of disaster data collection and storage in regional databases and local databases in the same way. This is an important issue to the local economy, because the Western Balkan countries are also some of the least economically developed countries within Europe. With the exception of Croatia, whose GNP per capita exceeds 10.000 US dollars for 2009, all the other countries reviewed had a GNP per capita far below that amount. A systematic collection of data related to the frequency and impact of disasters would provide an invaluable tool to local governments and regional institutions charged with the planning of reduction programmes to protect their populations from the effects of natural disasters.

Acknowledgements

The research was supported by the Ministry of Science and Technology of the Republic of Serbia and the Ministry of Science, Education and Sports of the Republic of Croatia, as part of the bilateral Project GeohazardINFO.

References

Abolmasov B., Hadži-Niković G. and Rundić Lj., 2009. The socioeconomic influence of geological hazards. *In*: Aleksić M. (eds.), Proceedings of the XIII International Eco-Conference: Environmental Protection of urban and suburban settlements, Ecological movement of the City of Novi Sad, Novi Sad, 347-355..

CRED (http://www.cred.be/publications)

EM-DAT (http://www.emdat.be; Accessed September 20, 2009)

Guha-Sapir D., 2008. EM-DAT's new disaster classification. In: Disaster data: A Balanced Perspective. CRED CRUNCH News, Issue No 13. Centre for Research on the Epidemiology of Disasters. Brussels, Belgium. http://www.emdat.be/publications/, Accessed September 25, 2009).

IMF (http://www.imf.org; Accessed October 21, 2009)

Munich Re (http://www.munichre.com; Accessed September 10, 2009)

NATHAN (http://mrnathan.munichre.com; Accessed September 10, 2009).

Rodriguez J., Vos F., Below R. & Guha-Sapir D., 2009. Annual Disaster Statistical Review 2008-The numbers and trends. Centre for Research on the Epidemiology of Disasters. Brussels, Belgium. Jaoffset Printers, Melin, Belgium, 25 pp.

Scientific Annals, School of Geology, Aristotle University of Thessaloniki Proceedings of the XIX CBGA Congress, Thessaloniki, Greece	Special volume 100	7-13	Thessaloniki 2010

NATURAL RESERVOIR SYSTEMS IN THE TERTIARY SECTION OF THE EAST RHODOPE DEPRESSION AND PERSPECTIVES FOR STORAGE OF NATURAL GAS AND CARBON DIOXIDE

Balinov V., Doncheva M. and Zaneva-Dobranova E.

University of Mining and Geology, Stoudentski grad, 1700 Sofia, Bulgaria, e-mail: geoenergy@mgu.bg

Abstract: The East Rhodope Depression situated in South Bulgaria is a Paleogene imposed structure. It is mostly filled with Tertiary sedimentary, sedimentary-volcanogenic and volcanic rocks. The tectonic low-order elements distinguished in it are specific volcano-tectonic, block and block-fold structures. The subjects of our study are the aquifer layers (reservoir systems) situated in these structures investigated from the point of view of the possibilities, if other favorable conditions for storage of natural gas and carbon dioxide (CO_2) exist. Special studies carried out by the authors in the limits of the perspective structures are concentrated mostly on the: lithological-physical segmentation of the Tertiary section; defining of permeable and hard-permeable formations and their studying (structure, lithology, reservoir and sealing parameters, spatial behavior); defining of natural reservoirs and studying their spatial relationships; prognosis of possible types of local structures and natural traps. Because of the restricted volume and the absence of specialized information for a number of important geological preconditions and parameters, prognostic assessments are made with the use of indirect data, based on the contemporary ideas about the geological evolution of the examined region. Such are the structural-tectonic, the seismotectonic and the hydrogeological (hydrochemical, hydrodynamic) and the thermo-baric conditions. The prognoses concerning the perspectives for storage of natural gas and CO_2 are connected to the sunken areas within the Dzhebel and Krumovgrad depressions.

Keywords: East Rhodope Depression, natural reservoir systems, CO_2 sequestration; Underground gas storage (UGS)

1. Introduction

The perspectives for storage of natural gas and carbon dioxide (CO_2) in aquifer layers suppose the presence of appropriate natural reservoirs and traps. They should correspond to definite requirements (criteria) that are regulated in the contemporary theory and practice in accordance with the natural conditions of the studied sites.

The territory of South Bulgaria is characterized by a lot of specific features that determine essential differences in the approaches for assessment of the possibilities for storage of natural gas and CO_2 in aquifer layers compared to those, proposed by the authors for a part of the territory of North Bulgaria. These special features are mainly connected to the geological conditions, the degree of studying, from the point of view of the examined problem and the type of the geological exploration works carried out for the present moment.

In North Bulgaria a study subject are the local structures, registered by seismic data and developed by boreholes. In South Bulgaria objects of studying are the reservoir systems, situated in larger-scale graben structures (depressions) in the limits of the imposed Tertiary depressions. The presence of local structures (natural traps of a structural or other type) in them could be registered after carrying out of additional (basically seismic and well-log) exploration works with the purpose of registering these structures.

The subject of more detailed examination in the studied graben structures are the reservoir systems. More general considerations are represented for the other geological preconditions (structural-tectonic, seismotectonic, hydrogeological), because of the absence or the insufficient information with a view to the thoroughness of the prognostic assessments for storage of natural gas and CO_2.

2. Brief information for the geology of the region

The East Rhodope Depression situated in South Bulgaria is a typical Paleogene superimposed structure. It is mostly filled with sedimentary, sedimentary-volcanogenic and volcanic rocks of Paleogene and partially Neogene age (Fig.1). They cover the Pre-Paleogene basement, which has a complicated structure resulting from a multiphase tectonic evolution. It consists of Precambrian metamorphic and Mesozoic metamorphic, mag-

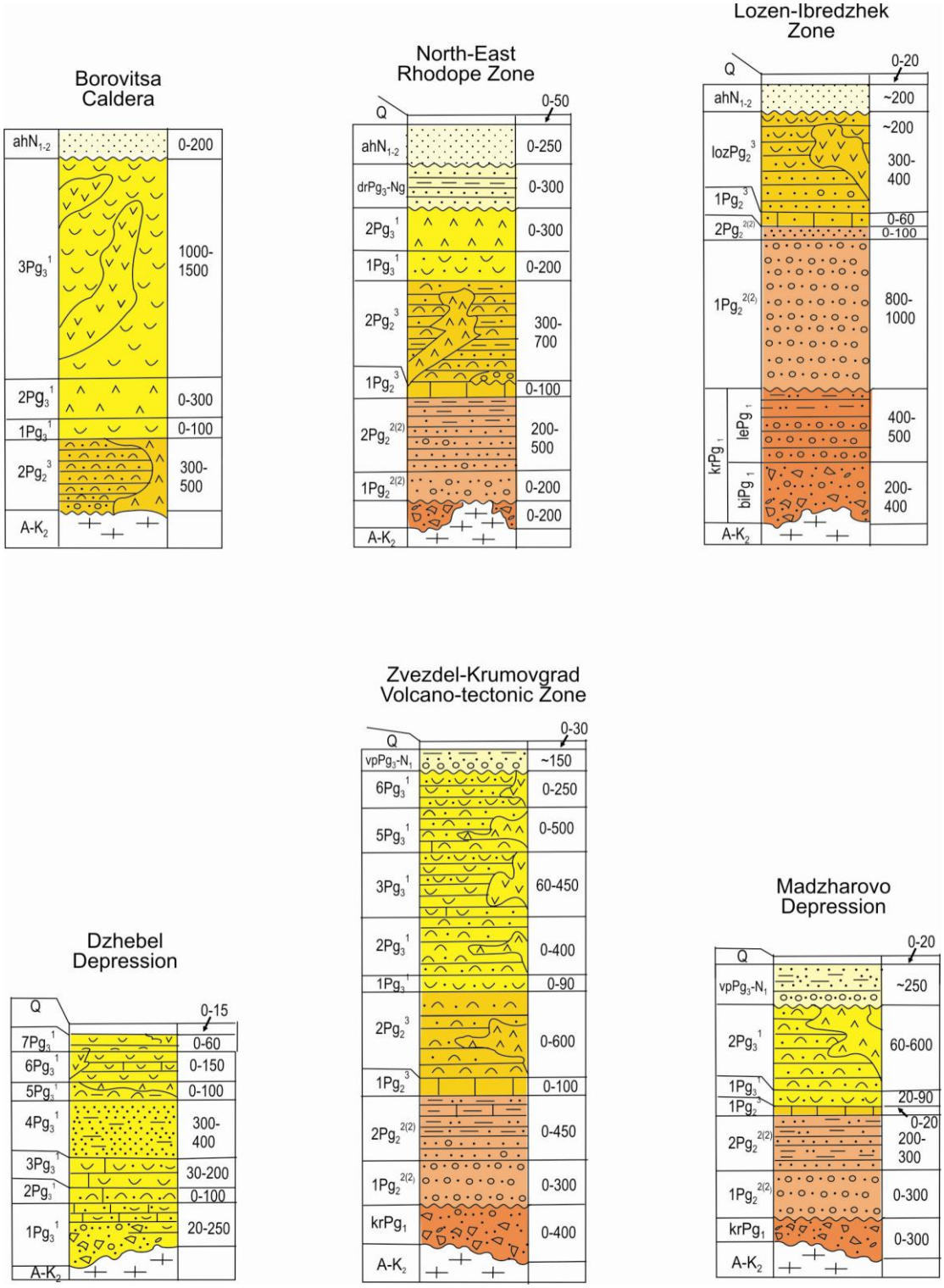

Fig.1. Summarized lithologic-stratigraphic columns in block structures from the East Rhodope Depression (Boyanov and Goranov 1994).

matic and sedimentary rocks. The low-order tectonic elements distinguished in the East Rhodope Depression are specific volcano-tectonic, block and block-fold structures (Borovitsa Caldera, North-East Rhodope Zone, Lozen-Ibredzhek Zone, Dzhebel Depression, Dobromirtsi-Chorbadzhiysko Zone, Zvezdel-Krumovgrad Volcano-tectonic Structure, Madzharovo Depression, Bryagovo Depression) (Boyanov and Goranov, 2001) (Fig.2).

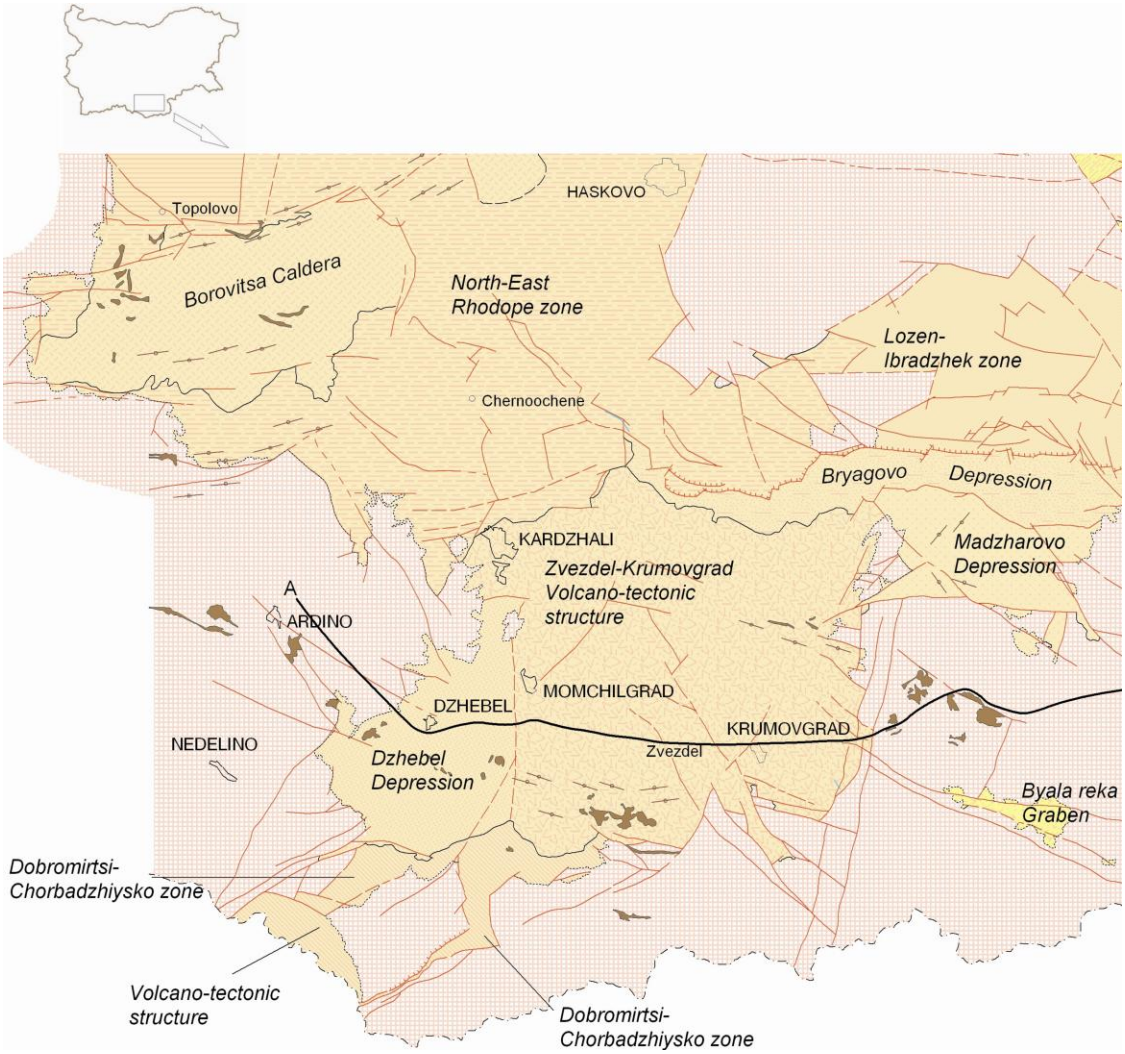

Fig.2. Tectonic map of the East Rhodope Depression (Boyanov and Goranov 2001).

The indicated structures of variable order are too different by their inner structure, dimensions and geological development. Despite of that, they possess some common characteristics. They are depression structures of second and third order. Their structure is complicated and they are built of Tertiary sedimentary, sedimentary-volcanogenic and volcanic rocks. All of them are with graben-like complicated periphery. Reservoir rocks of Paleogene and Eocene age occur in the sections according to data from the outcrops. They consist of coarse clastic and carbonate-terrigenous sediments. It is supposed that they are with unsustained area and vertical distribution and are cracked in some places by dykes. In the Dobromirtsi-Chorbadzhiysko Zone and the Bryagovo Depression the sections are thoroughly built by reservoir rocks. Polymetal deposits of variable scale are registered in the peripheral parts of Borovitsa and Zvezdel-Krumovgrad depressions, as well as in the central parts of Madzharovo and Lozen tectonomagmatic structures.

According to data from the regional seismic section Ivaylovgrad-Ardino in the south-eastern part of the East Rhodope Depression, two depression areas are distinguished. In them the Paleogene sediments are with significant depth (more than 1000 m). They are situated in the region of Dzhebel Depression and the eastern part of the Zvedel-Krumovgrad Zone (Krumovgrad depression). The

Dzhebel Depression is situated in the south-western part of the East Rhodope Depression. Its western slope is slant and its eastern slope is strongly faulted and terraced (Fig.3). The Tertiary section in it consists of Oligocene sediments that in the western and northern part develop on the surface. Two deeper areas are distinguished on the regional seismic section in the central part of the depression. The section's thickness in them reaches up to 1150 m. The Krumovgrad Depression is situated in the southern part of the East Rhodope Depression. It is a complicated depression structure with shallower western part, where the thickness of the Paleogene deposits reaches up to 1400 m (Fig.4). Its eastern part is faulted and the section's thickness reaches up to 2300 m. Probably the regional seismic section doesn't cross the deepest parts of the depression.

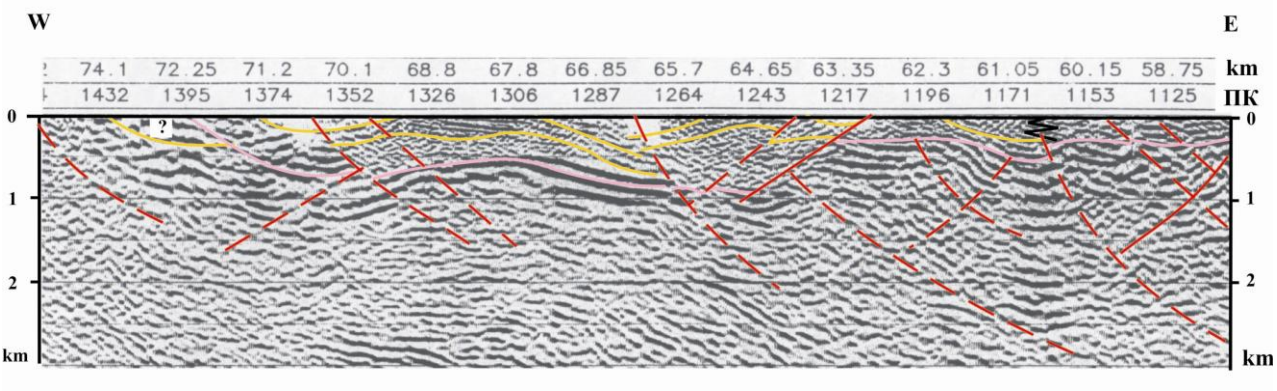

Fig.3. Regional seismic section (Dzhebel Depression) (interpreted by A. Goranov and A. Velev)

Data from the interpretation of the regional seismic studies gives a definite notion about the spatial behavior of the defined reservoir systems and the structural-tectonic environment. In this sense the specialized studies carried out by the authors in the limits of the possible perspective graben structures (depressions) are concentrated mostly on the: lithological- physical segmentation of the Tertiary

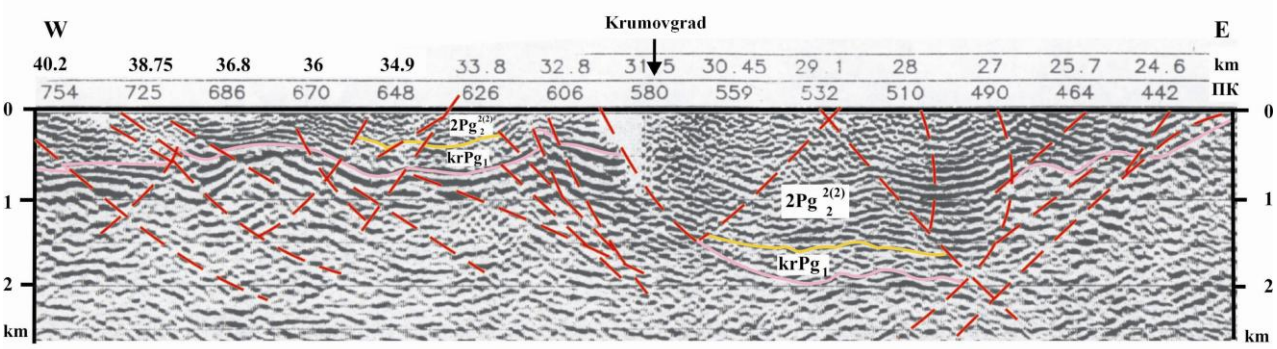

Fig.4. Regional seismic section (Krumovgrad Depression) (interpreted by A. Goranov and A. Velev)

3. Methodical approaches

The methodical approaches worked out by the authors in previous studies for identifying of perspective aquifer structures for storage of natural gas and CO_2 (Balinov et al., 2007, 2008 a,b) are applicable for North Bulgaria. They are based on the main requirements for suitability of the geological sites and are connected to the concrete geological preconditions: lithologic, structural-tectonic, seismotectonic, lithological-physical (petrophysical), hydrogeological and termobaric. They could not be completely applied for South Bulgaria and partially for the Tertiary structures in the East Rhodope Depression. This is due to the specific geological conditions and the poorly studying of this territory. From the point of view of the examined problem the assessment criteria characterize structures of a higher grade – graben depressions.

section; defining of permeable and hard-permeable formations and their studying: structure, lithology, reservoir and sealing parameters, spatial behavior; defining of natural reservoirs and studying their spatial relationships; prognosis of possible types of local structures and natural traps. Because of the restricted volume and the absence of specialized information for a number of important geological

preconditions and parameters, prognostic assessments are made with the use of indirect data, based on the contemporary ideas about the geological evolution of the examined region. Such are the structural-tectonic, the seismotectonic and the hydrogeological (hydrochemical, hydrodynamic) and the thermobaric conditions.

The subjects of our study are only a part of the vary-order graben structures that could be assessed in advance as possible prospective structures according to selected criteria parameters. On the basis of the full complex of parameters, a comparative assessment is made of the perspective graben structures and the reservoir systems containing in them.

4. Natural reservoir systems

The permeable and hard-permeable formations, distinguished in the Tertiary section of the East Rhodope Depression, are with unsustained area and vertical distribution. Late volcanic dykes are often inserted in them. In some cases they are situated in the periphery of the structures, because the central parts are filled with volcanic rocks. In other cases hard-permeable rocks are missing in the section or the formations develop on the surface. Because of this most of the structures are not interesting with a view to storaging of natural gas and CO_2. In this relation, special attention should be paid to the mentioned areas in Dzhebel and Krumovgrad Depression. The interest for them is connected to the presence of reservoir and sealing volcanogenic or sedimentary rocks. On the basis of the carried out litological-physical segmentation of the sedimentary section, two perspective natural reservoirs are distinguished.

4.1. Natural reservoir, connected to the Oligocene Terrigenous – carbonate – pyroclastic reservoir formations in the Dzhebel Depression

The Oligocene Terrigenous-carbonate-pyroclastic Reservoir Formation ($1Pg_3^1$) and the hard-permeable rocks that restrict it from below and above belonging to the Pre-Paleogene basement and the Oligocene Volcanogenic Reservoir Formation ($2Pg_3^1$ и $3Pg_3^1$) take part in building of the natural reservoir (Fig.1).

4.1.1. The Oligocene Terrigenous-carbonate-pyroclastic Reservoir Formation is built by the eponymous formation from the Complex of the first acid volcanism (Lower Oligocene). Its structure is complicated. It consists of clastic and carbonate (reef limestones) rocks, interbedded by acid tuffs and epiclasts. Their spatial behavior could not be followed. In outcrops the thickness of the formation varies from 20 to 250 m. According to data from the regional seismic section the basal conglomerate's thickness is bigger – from 300 to 500 m. The depth of the top of the reservoir formation is variable and reaches up to 800-900 m. The reef and the coarse clastic sediments, situated in the basis of the section are expected to possess the best petrophysical parameters.

4.1.2. The Oligocene Volcanogenic Sealing Formation (cover) consists of rocks from the Complex of the second middle-acid volcanism (Terrigenous-carbonate-epiclastic Formation) and the Complex of the second acid volcanism (Carbonate-pyroclastic-lava Formation and the Terrigenous-carbonate-pyroclastic Formation). The Permeable Sandstone Formation (Dzhebel sandstones) or the hard-permeable deposits of the Complex of third middle-acid volcanism (Lower Oligocene) are situated above the sealing formation. The information for them, according to data from outcrops, doesn't allow conclusions for its spatial behavior to be made. The thickness probably varies in the limits from 200-300 to 800-900 m. The sealing formation is with variable properties. The sediment rocks in it are mainly permeable, but it is supposed that in the sunken areas their presence is insignificant.

4.1.3. Pre-Paleogenic hard-permeable rocks (underlayer) consist of variable metamorphic rocks (Precambrian) and Mesozoic low-crystalline and magmatic rocks.

4.2. Natural reservoir, connected to the Upper Cretaceous –Middle Eocene Terrigenous-Reservoir Formation in the Krumovgrad Depression

The Upper Cretaceous – Middle Eocene Terrigenous Reservoir Formation (krK_2-Pg_1, $1Pg_2^{2(2)}$ and $2Pg_2^{2(2)}$ – lower part) and the hard-permeable rocks that restrict it from below and above belonging to the Pre-Paleogene basement and the Eocene-Oligocene Terrigenous-carbonate-volcanogenic Sealing Formation ($2Pg_2^{2(2)}$.- top, $1Pg_2^3$, $2Pg_2^3$, $1Pg_3^1$, $2Pg_3^1$, $3Pg_3^1$, $5Pg_3^1$, $6Pg_3^1$) take part in building of the natural reservoir (Fig.1).

4.2.1. The Upper Cretaceous – Lower Eocene Terrigenous Reservoir Formation is built of the rocks

of the Krumovgrad Group, the Breccia-conglomerate Formation from the Complex of the varicolored (red) breccia-conglomerate, sandstones and sandy clay and the lower part of the Sandy-coal-bearing Formation (Maastricht – Middle Eocene). The scanty information doesn't allow the spatial behavior of the reservoir formation to be traced. According to data from the outcrops, its thickness varies from 200-300 m (in the western part of the depression) to 400 m (in the eastern part). The thickness near its top is variable and in its eastern part (according to data from the regional seismic section) reaches up to 1900 m and it reduces in western direction to 800-900 m. The quantity data for the reservoir parameters of the permeable rocks are missing. Having in mind their lithologic variation, it is supposed that they posses variable capacity and filtration properties.

4.2.2. The Eocene-Oligocene Terrigenous-carbonate-volcanogenic Sealing Formation (cover) includes the upper part of the Sandy-coal-bearing Formation, the clayey-carbonate (the Marl-limestone Formations) and the volcanogenic (the Complexes from first to third middle-acid and acid volcanism) rocks (middle Eocene-Lower Oligocene). The scanty information doesn't allow their relations to be traced. Obviously, the hard-permeable rocks consecutively situated in the section build the sealing formation with a significant thickness that reaches up to 1900 m. It is covered by the hard-permeable Coal-bearing-terrigenous Formation (Valchepol Molasse). Quantity data for sealing parameters of the formation are missing. Having in mind the lithologic characteristic of rocks, it could be supposed that they posses from high to low sealing properties.

4.2.3. Pre-Paleogenic hard-permeable rocks (underlayer) consist of variable metamorphic rocks of the Rhodope Higher Group (Precambrian) and Mesozoic low-crystalline and magmatic rocks.

5. Structural-tectonic, hydrogeological and seismotectonic conditions

The structural-tectonic characteristics of the Tertiary section suppose the presence mainly of lithologic (stratigraphic) and the combined type of natural traps. An important factor for their forming is the block structure of the basement, determined by the multiple breaks that comprise the Tertiary section as well.

The Tertiary section of the East Rhodope Depression is poorly studied in hydrogeological relation. The direct hydrogeological information from the well data is received only for separate thermo-aquifer and ore zone or fields in the peripheral parts of the graben structures (Antonov and Danchev, 1980). The hydrogeological space in the Paleogene section and in the basement of the depression in the most tectonic units is cut by water-main, fault dislocations and permeable contacts of cutting volcanic bodies. They are open towards the surface. Geostructural and lithofacial preconditions for presence of aquifer bodies and horizons protected from water-exchange with the surface occur only in Ddzhebel and Krumovgrad Depression.

During the regional geothermal separation of South Bulgaria, well-outlined anomalies of the heat flow are distinguished. Their nature is accepted to be endogenous. In the Central Rhodope active geothermal zone the distribution of temperatures to the depth of 5 km is of the rate of 140-180 ^{o}C. The studied region is to the east of this zone and the temperatures are lower than 130 ^{o}C (Dobrev et al., 2004).

The summarized analysis of the seismic activity in South Bulgaria indicates that more intensive seismic shows in the studied region are registered only in the Kardzhali Zone. It is situated in north-northwestern direction, outside the perspective areas.

6. Conclusion

The applied methodical approaches are in accordance with the specific geological conditions and the poorly studied East Rhodope Depression, from the point of view of the examined problem. In this connection the subject of our study are part of the graben structures of variable order with accent put on the studying of the reservoir systems and the conditions for forming of suitable natural traps. In this relation, two natural reservoirs, situated in the Tertiary section of the sunken areas of Dzhebel and Krumovgrad Depressions, are assessed as possible perspective zones. The reservoir formations are mostly built of clastic deposits and their thickness is significant. Sealing rocks are mainly the volcanogenic ones. Natural traps of stratigraphic and combined type are bounded to the perspective reservoir systems. It is supposed that there are favorable hydrodynamic and thermobaric conditions of the aquifer horizons and good hermeticity of the potential storages. The perspective areas are situated in a zone of low seismic activity.

Acknowledgements

The authors are grateful to A. Goranov and A. Velev for the kind permission to use the interpreted seismic sections.

References

Antonov C. and Danchev D., 1980. Underground waters in Bulgaria. Technica, Sofia, 230 p. (in Bulgarian)

Balinov V., Doncheva M. and Zaneva-Dobranova E., 2007. Geological Preconditions for Natural Gas Storage in Aquifer Structures in Paleogene in the Varna Monocline and the Dolna Kamchia Depression (Principles and Methodic Approaches). Annual MGU, p.1, v50, 9-14 (in Bulgarian with English abs)

Balinov V., Doncheva M. and Zaneva-Dobranova E., 2008a. Methodical Approaches for Identifying of Perspective Aquifers for Carbon Dioxide Storage. Scientific technocal conference with international participation "Oil and Gas Prospectivity of the Balkan Black Sea Region. Varna, 172-180 (in Bulgarian with English abstract)

Balinov V., Zaneva-Dobranova E. and Doncheva M., 2008b. Geological Preconditions, Principles and Criteria to the Identification of Prospective Geological Structures of Carbon Dioxide (CO_2) in Bulgaria. Annual MGU, p.1, v. 51, 10-15 (in Bulgarian with English abstract)

Boyanov I. and Goranov A., 1994. Paleocene-Eocene sediments from the Northern periphery of the Borovitsa depression and their correlation with similar sediments in the East Rhodope Paleogene Depression. Rev. BGS, 55, 1, 83-102 (in Bulgarian with English abstract)

Boyanov I. and Goranov A., 2001. Late Alpine (Palaeogene) superimposed depressions in part of South-East Bulgaria. Geol. Balcanica, 31, 3–4, 3–36.

Dobrev T., Dimovski S. and Kostianev S., 2004. Level of study the geothermal field in Bulgaria and methodical approach towards investigating its depth distribution. Annual of the University of Mining and Geology "St. Ivan Rilski", vol. 47, part I: Geology and geophysics, 251-258.

Scientific Annals, School of Geology, Aristotle University of Thessaloniki Proceedings of the XIX CBGA Congress, Thessaloniki, Greece	Special volume 100	15-21	Thessaloniki 2010

GROUNDWATER VULNERABILITY ASSESSMENT TO CONTAMINATION (ERZENI BASIN, ALBANIA)

Beqiraj A.[1] and Cenameri M.[2]

[1] *Department of Earth Sciences, Faculty of Geology and Mining, Polytechnic University of Tirana, Rruga Elbasani, Tirana, Albania, ae_beqiraj@yahoo.com*

[2] *Department of Geoinformatics, Applied Geology and Environment, Faculty of Geology and Mining, Polytechnic University of Tirana, Rruga Elbasani, Tirana, Albania, m_cenameri@yahoo.com.*

Abstract: Groundwater quality has been recently deteriorating in different alluvial aquifers of Albania due to industrialization expansion, waste disposal, and agriculture activity. A preliminary assessment of vulnerability to groundwater contamination in Erzeni watershed area was undertaken because of enormous mining activities of river bed alluviums, the presence of the largest urban solid waste disposal site of Tirana and intensive agricultural and industrial activities at the plane part of the river course. The major geological and hydrogeological factors that affect and control groundwater contamination were incorporated into the DRASTIC model. Moreover, a Geographical Information System (Arc Gis 9.2 INFO) was used to create a groundwater vulnerability map of Erzeni river basin. Aquifer vulnerability assessment aims at predicting areas, which are more likely than others to become contaminated as a result of human activities at the land surface. As a result of the vulnerability assessment, 20% of the Erzeni basin was classified as being very highly vulnerable, 5% highly vulnerable, 15% vulnerable at moderate to low levels and, finally, around 60% of the basin has very low vulnerability.

Keywords: Albania, 2009, GIS-based evaluation, alluvial aquifer, groundwater, vulnerability.

1. Introduction

Groundwater, that represents a major source of water for domestic, industrial and agricultural uses in Albania, is recently suffering a deterioration of its quality especially in the regions with extensive demographic and industrial development, due to excessive groundwater withdrawal and introduction of different contaminants from the surface The concept of groundwater vulnerability is based on the assumption that the physical environment may provide some degree of protection to groundwater against natural impacts, especially with regard to contaminants entering the subsurface environment (Napolitano, 1995). Consequently, some land areas are more vulnerable to groundwater contamination than others. Over the past 30 years, groundwater vulnerability maps have been developed in many countries as a basis for developing land use strategies that take into consideration aspects of protection of groundwater from pollution (Fritch, 2001; Naqa et al., 2006). The final goal of vulnerability maps is the subdivision of the area into several hydrogeological units with different levels of vulnerability. These maps show the distribution of highly vulnerable areas, in which pollution is very common because contaminants can reach the groundwater within a very short time. However, such maps do not replace more detailed studies of the geological and hydrogeological conditions of particular sites for the envisaged use. The aim of this study is to assess the vulnerability of groundwater to contamination for the basin of Erzeni river which flows through Tirana and Durresi regions (Fig. 1). Groundwater vulnerability assessment was done by using a DRASTIC model (Aller *et al.*, 1987) combined with a Geographic Information System (Arc Gis 9.2 INFO). This model has been widely used in many countries because the inputs required for its application are generally available or easy to obtain.

The Erzeni Basin (Fig. 1), which is one of the most important alluvial groundwater basins in Albania (Eftimi et al., 1989; Dhima et al., 2000), consists mainly of Quaternary alluvial gravels that are 2-7.0 m thick (Puca, 2005). The groundwater flow is influenced by the recharge/discharge areas, the topography and the internal characteristics of the aquifer medium. The main recharge occurs from the south-eastern side of the area and groundwater

flows to the north-western part of the basin where the groundwater is under pressure due to the impermeable clay cover layer. The yield for the most of the groundwater wells ranges from 2.0 to 5.0 l/s. The general groundwater mined from this aquifer is around 2000 l/s (Puca, 2005). From the hydrochemical point of view, the groundwater belongs to calcium – magnesium – bicarbonate type having pH, general hardness and general mineralization values of 7.3, 27.9°Gj and 850mg/L, respectively.

2. Materials and Methods

For the assessment of the Erzeni groundwater vulnerability to contamination the DRASTIC (Aller *et al.*, 1987) model and a geographic information system (ArcGIS) (Napolitano, 1995) were used to

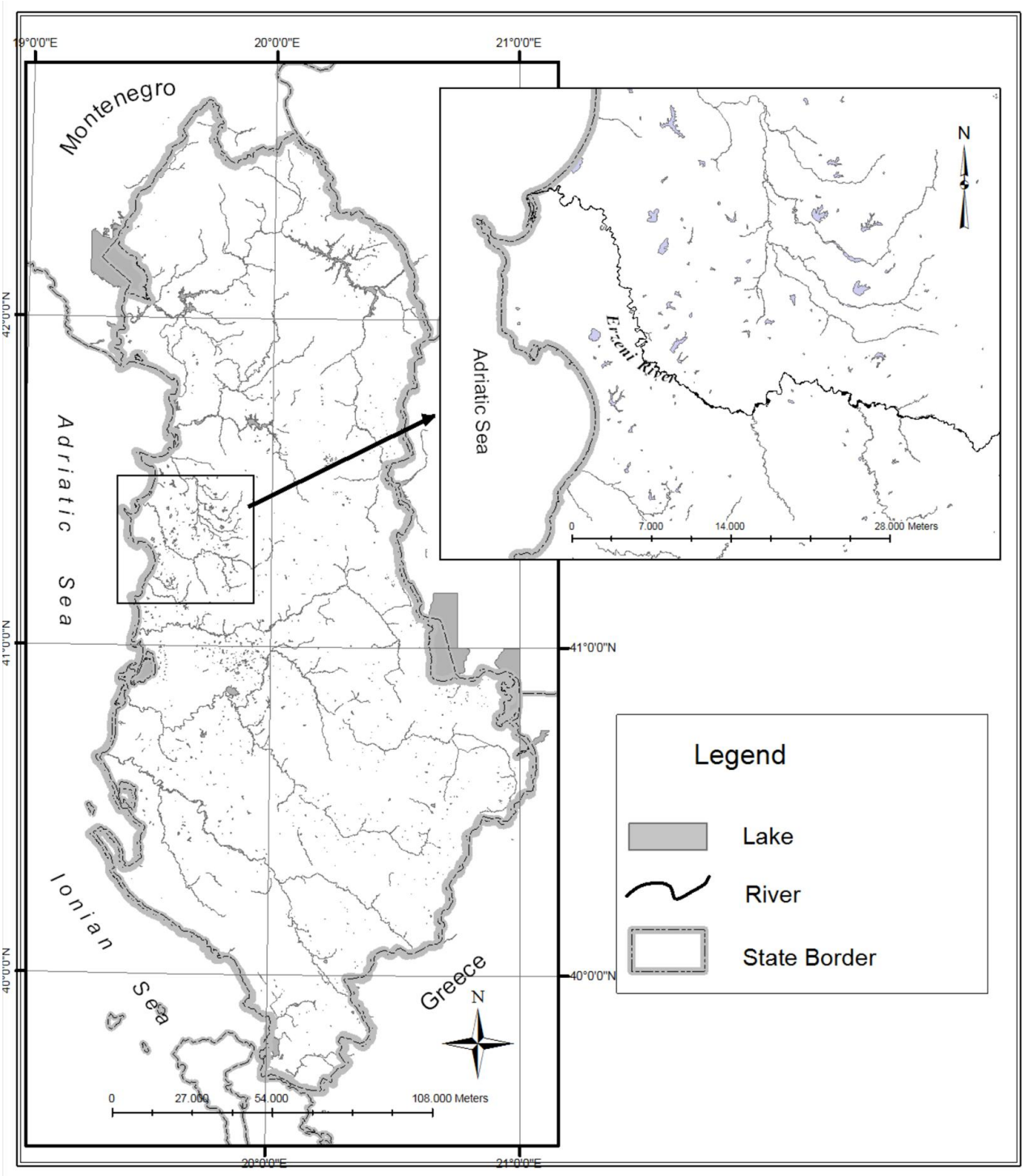

Fig. 1. Hydrographic map of Albania (Erzeni basin is shown on the right).

produce the vulnerability map for groundwater contamination. This involved: (i) data (hydrogeological, geological and pedological) collection, (ii) scanning of toposheets and digitizing (raster to vector) source data, (iii) creating the attribute table, (iv) analyzing the DRASTIC factors for evaluation of Drastic Index, (v) rating these areas as to their vulnerability to contamination and deriving a Graduated Map.

(i) The seven parameters that are involved in arriving at the Drastic Index have been collected from the following sources: Geological Survey of Albania, Institute of Soils and Institute of Topography for the Depth to water, Aquifer media, Hydraulic conductivity and Net recharge, Soil media, Impact of Vadose Zone and Topography, respectively.

(ii)The toposheets were scanned for generating raster images TIF format (Tagged image file) which are then exported to CADD for converting them into a vector format through the digitization process; finally the topographic map was georeferenced.

(iii) the attribute table, that was created in Excel, contains the following data: number and X, Y coordinates of the hydrogeological well, weights and ratings of Drastic parameters, values of Drastic Index. The data of attribute table were imported from Exel to GIS 9.2 through Access.

(iv) Drastic Index formula DR*DW +RR*RW + AR*AW + SR*SW + TR*TW + IR*IW + CR*CW was entered in the calculator (Excel) table where product of ranks and weights of each parameter was summed up and the final output (Drastic Index), as a whole number which assigns the vulnerability, was calculated.

(v) The Graduated Map for each parameter and for the Drastic Index (vulnerability map) was created in Arc Gis 9.2 INFO by using Spatial Analyses.

3. Results and discussion

Vulnerability refers to the sensitivity of groundwater to contamination, and is determined by intrinsic characteristics of the aquifer. It is distinct from pollution risk, which depends not only on vulnerability but also on the existence of significant pollutant loading. In this study, the DRASTIC model and a geographic information system (Arc Gis 9.2 INFO) were used to produce the vulnerability map for groundwater contamination in the Erzeni basin. Different models can be applied to mapping of groundwater vulnerability, but the most commonly used model in assessing groundwater vulnerability in porous aquifers seems to be the DRASTIC model (Aller *et al.* 1985; Aller *et al.*, 1987; Deichert and Hamlet, 1992,).

DRASTIC, that is a methodology for identifying vulnerability to groundwater pollution, was originally developed by the U.S. Environmental Protection Agency. The DRASTIC acronym stands for the seven hydrogeological parameters: Depth to water, net Recharge, Aquifer media, Soil media, Topography (slope), Impact on the vadose zone media, and hydraulic Conductivity of the aquifer. The DRASTIC model has four assumptions (Aller *et al.* 1985; Aller *et al.*, 1987):

1) the contaminant is present on the ground surface;

2) the contaminant is flushed into the groundwater by precipitation;

3) the contaminant has the mobility of water;

4) the area being evaluated by DRASTIC is 0.4 km^2 or larger.

For the determination of the DRASTIC index number (pollution potential) each factor rating was multiplied by its weight and the resulting values were added together:

$$\text{DRASTIC Index} = DrDw + RrRw + ArAw + SrSw + TrTw + IrIw + CrCw \quad (*)$$

where r = rating for area being evaluated (1–10), and w = importance weight for the factor (1–5). Importance weights are found in a generic DRASTIC table (Table 1) that lists weights for factors having greater applicability (Aller *et al.*, 1987) while factor ratings are derived from data on each factor (Table 2-8). Finally, the Drastic Index values are calculated by using the above (*) equation (Table 9). Higher sum values, i.e. higher DRASTIC index, represent a greater potential for pollution or a greater vulnerability of the aquifer to contamination. The DRASTIC index was further divided into five categories: very low, low, moderate, high, and very high. The sites with high and very high categories are more vulnerable to contamination.

Table 1. Assigned weights for DRASTIC parameters.

Feature	Drastic Weights
Depth to Water	5
Net Recharge	4
Aquifer Media	3
Soil Media	2
Topography	1
Impact of Vadose Zone	5

Table 2. Ranges and rating for the depth to water.

Depth to water (m)	
Range	Rating
0-2.0	10
2.0-5.0	9
5.0-10.0	7
10.0-15.0	5
15.0-30.0	3

Table 3. Ranges and rating for the net recharge.

Net recharge (mm/Year)	
Range	Rating
0-5.0	1
6.0-10.0	3
10.1-16.0	6
16.1-25.0	8
>25.0	9

Table 4. Ranges and rating for the aquifer media.

Aquifer Media	
Range	Rating
Coarse-grain gravel	8
Medium-grain gravel	7
Fine-grain gravel	6
Medium-grain sand	5
Fine-grain sand	4

Table 5. Ranges and ratings for soil media.

Soil Media	
Range	Rating
Silty clay	3
Silty sand	4
Loam	5
Sandy loam	6
Sand	9
Gravel	10

Table 6. Range and rating for topography.

Topography (Percentage slope)	
Range	Rating
0-2.0	10
2.0-4.0	9
4.0-6.0	5
6.0-8.0	3
>8.0	1

Table 7. Ranges and ratings for impact of the vadose zone media.

Vadose Zone Media	
Range	Rating
Sandy gravel	8
Silty sand	6
Silt	4
Sandy silt	3
Sandy clay	2
Clay	1

Table 8. Ranges and ratings for hydraulic conductivity.

Hydraulic Conductivity (m/day)	
Range	Rating
0-5.0	1
5.0-10.0	2
15.0-25.0	3
25.0-50.0	6
50.0-100.0	8
>100.0	10

The Arc Gis 9.2 INFO was used to compile the geospatial data and to generate the final vulnerability maps. The DRASTIC index map (Fig.2) was prepared to determine the vulnerability to groundwater contamination (*i.e.*, pollution potential). This map shows that the vulnerability of the Erzeni alluvial aquifer to contamination ranges from very low (DI=65) to very high (DI=200). The most vulnerable areas of the aquifer to groundwater contamination – showed by the highest DRASTIC indexes – are located in the southeast area of the basin where the soil cover and/or vadose zone are absent or very thin and aquifer media consists mainly of gravel and pebbles (Table 10). On the contrary, along the northwestern sectors of the Erzeni basin, where a thick (20-30m) vadose zone with a well developed soil cover are present, the lowest vulnerable areas of the aquifer to groundwater conta-

Table 9. Calculation of Drastic Index values.

D factor	R factor	A factor	S factor	T factor	I factor	C factor	Di number
DrDw	RrRw	ArAw	SrSw	TrTw	IrIw	CrCw	ID
45	36	27	20	3	40	27	199
45	36	27	20	3	40	27	200
45	36	27	20	3	40	27	198
45	36	27	20	3	40	27	198
45	36	27	20	3	40	27	198
45	36	27	20	3	40	27	198
45	36	27	20	3	40	27	198
45	36	27	20	3	40	27	198
10	8	15	6	10	15	12	76
10	8	15	8	10	15	12	78
10	8	15	6	10	15	12	76
50	28	24	10	5	30	24	171
50	28	24	10	5	30	24	171
50	28	24	10	5	30	24	171
50	28	24	10	5	30	24	171
50	28	24	10	5	30	24	171
50	28	24	10	5	30	24	171
50	32	21	18	5	40	24	190
50	28	21	12	5	40	24	180
50	36	21	12	5	40	24	188
50	36	21	12	5	40	27	191
25	28	21	10	5	30	27	146
35	24	24	12	5	30	27	157
25	20	21	12	5	30	27	140
25	20	21	12	5	30	27	140
25	20	21	12	5	30	27	140
15	20	21	12	5	25	27	125
15	20	21	12	5	25	27	125
15	20	21	12	5	25	27	125
15	20	21	12	5	25	27	125
15	20	21	12	5	25	27	125
15	20	21	12	5	25	27	125
15	12	18	12	6	15	15	93
15	12	18	12	6	15	15	93
15	12	18	12	6	15	15	93
15	12	18	12	6	15	15	93
15	12	18	12	7	15	15	94
15	12	18	12	7	15	15	94
10	12	15	6	7	15	15	80
10	12	15	6	7	15	12	77
10	12	15	6	7	15	12	77
10	12	15	6	7	15	12	77
10	12	15	6	7	15	12	77
10	12	15	6	7	15	15	80
10	12	15	6	7	15	15	80
10	12	15	6	7	15	15	80
5	8	15	8	9	10	12	67
5	8	15	8	9	10	12	67
5	8	15	8	9	10	12	67
5	8	15	6	9	10	12	65
5	8	15	6	9	10	12	65
5	8	15	6	9	10	12	65
5	8	15	6	9	10	12	65
5	8	15	6	9	10	12	65
15	8	15	8	10	15	12	83
15	8	15	8	10	15	12	83
15	8	15	6	10	15	12	81

mination are located. Even the very high vulnerable area represents only 20% of the basin, it has a strong impact on aquifer vulnerability because it represents the recharge area of the basin. After entering the aquifer in this area the contaminant can be distributed in other parts downward the aquifer flow.

Table 10. Indicative values of hydraulic conductivity and vadose zone thickness.

Well No.	10	19	14	2-Φεβ	2-Ιαν
Drastic index	198	171	140	94	67
K (m/day)	110	75	15,5	12,3	8,5
Thickness of Vadose zone (m)	1	4	18	20	36

Table11. Representative data of qualitative monitoring.

Well No.	10	19	14	2-Φεβ	2-Ιαν
Drastic index	198	171	140	94	67
NO_3 (mg/l)	2,8	1,8	1,3	1	0
PO_4 (mg/l)	1,8	1,1	0,9	0,9	0,8
NH_4 (mg/l)	0,1	0,05	Trace	0	0

The above configuration of the vulnerability to groundwater contamination fit very well with the data of the qualitative monitoring. This later has detected different levels of ammonium ions, nitrites, nitrates, phosphates, etc, in the groundwater of the southeastern sectors (Table 11) of the aquifer as it could be expected from the vulnerability map.

4. Conclusions

The DRASTIC model and a geographic information system (Arc Gis 9.2 INFO) were used for the assessment of the groundwater vulnerability to contamination in the Erzeni basin. This assessment along with a continuous qualitative monitoring are indispensable for this aquifer because its groundwater represents an important water source for potable, industrial and agricultural needs of the Tirana – Durresi region where Erzeni river flows. According to values of the DRASTIC index, five categories of aquifer vulnerability to contamination are distinguished: very low, low, moderate, high, and very high which fit very well with the data of the qualitative monitoring. The areas with high and very high categories, i.e. the more vulnerable areas to contamination are located in the southeastern part of the basin, whereas the lowest vulnerable areas of the aquifer to groundwater contamination are located along its northwestern sectors.

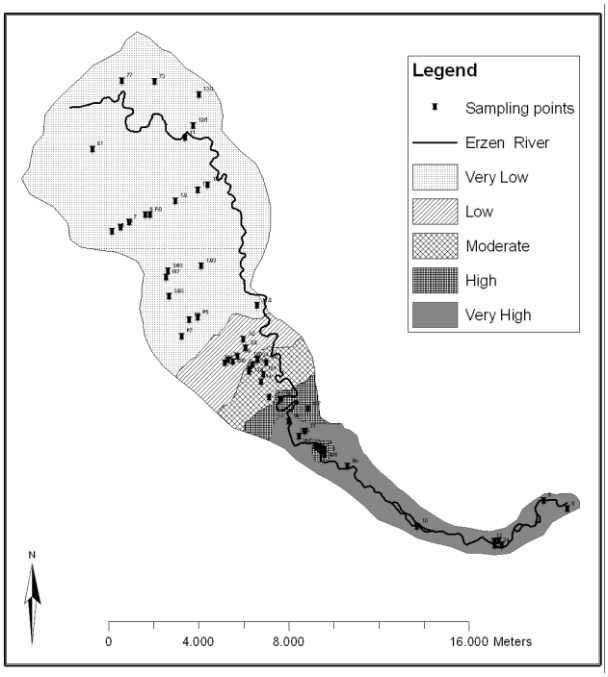

Fig.2. Vulnerability map based on DRASTIC Index.

Acknowledges

We would like to thank the Geological Survey of Albania for providing the hydrogeological and geological data. Also we would like to thank our students (Ernilda Faruku, Flora Progni, Tefta Gogallari, Petro Ranxha, Bledar Voci) who help us during data collection and elaboration.

References

Aller L., Bennett T., Lehr J.H., Petty R.J., 1985. DRASTIC; A standardized system for evaluating groundwater pollution potential using hydrogeologic settings: Ada, OK, United States Environmental Protection Agency, Robert S. Kerr Environmental Research Laboratory, EPA/600/2-85/0108, 163 p.

Aller L., Bennet T., Lehr J. H., Petty R. J. and Hackett G., 1987. DRASTIC; A standardized system for evaluating groundwater pollution potential using hydrogeologic settings: EPA-600/2- 87-035, 622 p.

Deichert L.A., Hamlet J.M., 1992. Non-point groundwater pollution potential in Pennsylvania, *in* American Society of Agricultural Engineers (ASAE) International Winter Meeting, Nashville, Tennessee, 15-18 December, 1992: Paper No. 922531.

Dhima K., Kalaja F., Saraci., 2000. Hydrogeological Resources in Albania: State of their Administration. Italian – Albanian Symposium: Administration of Georesources, 64-71, (in Albanian-Italian).

Eftimi R., Tafilaj I., Bisha G., 1989. Hydrogeological characterization of Albania. Bulletin of the Geological Sciences, 4, 303-316 (in Albanian with English abstract).

Fritch T.G., Mcknight C.L., Yelderman Jr.J.C., Arnold J.G., 2000a. An aquifer vulnerability assessment of

the Paluxy Aquifer, central Texas, USA, using GIS and a modified DRASTIC approach: Environment Management, 25(3), 337–345.

Napolitano P., 1995. GIS for aquifer vulnerability assessment in the Piana Campana, southern Italy, using the DRASTIC and SINTACS methods: Enschede, The Netherlands, International Institute for Geo-Information Science and Earth Observation (ITC), unpublished M.Sc. Thesis, 172 p.

Naqa A. E., Hammouri N. and Kuisi M., 2006. GIS-based evaluation of groundwater vulnerability in the Russeifa area, Jordan. Revista Mexicana de Ciencias Geológicas, 23/3, 277-287.

Puca N., 2005. Scientific report: Monitoring of groundwater in the main aquifers of Albania- Erzeni – Ishmi aquifer. 45p. Archives of Geological Survey of Albania (in Albanian).

Scientific Annals, School of Geology, Aristotle University of Thessaloniki Proceedings of the XIX CBGA Congress, Thessaloniki, Greece	Special volume 100	23-29	Thessaloniki 2010

QANATS BETWEEN MENIKION AND PANGEON MOUNTAINS. A FORGOTTEN AND ENDANGERED RESOURCE FOR LOCAL WATER SUPPLY

Blumenstein O.[1], Weingartner H.[2] and Vavelidis M.[3]

[1] *Department of Geoecology, University of Potsdam, 14476 Potsdam, Germany, oblustei@uni-potsdam.de*
[2] *Department of Geography and Geology, University of Salzburg, 5020 Salzburg, Austria, herbert.weingartner@sbg.ac.at*
[3] *Dept. of Mineralogy, Petrology and Economic Geology Aristotle University of Thessaloniki, GR-54006 Thessaloniki, Greece, vavelidi@geo.auth.gr*

Abstract: Due to the growing water shortage in the summer-dry Eastern Mediterranean, the question of water supply has become an important issue. Since antique times subsurface channels (qanats) have been built, which gather groundwater and take it due to the natural slope to places, where the water is needed. In Greece qanat technology has definitely been used during the Ottoman period. After the liberation and the following Greek-Turkish population exchange the knowledge about the systems has disappeared. There is evidence that many of the subsurface galleries are decayed. On the foothills of the Menikion and Pangeon Mountains active qanate systems have been investigated only recently in order to check their activity, contribution to the local water supply and water quality. The results reveal still working qanate systems, which are endangered by regional land use as well as by system-destructive building measures.

Keywords: Qanat, water supply, water pollution, water shortage, sustainable water use

1. Introduction

In the year 1992 March 22nd was appointed as World Water Day by the United Nations, in order to annually remember one of the most serious problems on our planet – the supply with clean water. The freshwater resources are an indispensible part of all ecosystems and there is no aspect of life without need of water. The enormous population growth on our planet as well the disproportional urbanization gives a new dimension to the aspect of water supply, especially concerning the growing water demand for food production (Scheumann, 2001). To cope with the water demand various technical solutions are applied to defeat water shortage, mostly without implementation of principles of sustainability.

The socio-economic development of societies was ever since dependent from freshwater resources. Especially in the drier regions of the world with little or almost no precipitation it was necessary to develop techniques for water supply as a means of livelihood.

Many ancient remains indicate highly developed technical methods of water utilization in perished civilizations and cultures within dry regions (Garbrecht, 1995). One of the most fascination techniques was and still is the subsurface water use by qanats.

2. Qanats in Mediterranean Europe

Although qanats are even found in central European areas like Luxembourg (Kayser and Waringo, 2003) and Trier (Kremer, 2003), linked to the former influence of the Roman Empire, in Europe qanats are mainly bound to adjacent regions of the Mediterranean Sea, where the regional climate supports the development of a dry summer period or a even longer dryness, especially on the southern borders of the Mediterranean. This climatic situation is linked to the remarkable summer influence of the Azores High in the West Mediterranean and the steady blowing dry Etesian winds (Meltemia) in the East.

An overview about typical climate regimes in the Mediterranean (Fig. 1) reveals dry periods in the southern Mediterranean for almost the whole year (e.g. Mersa Matruh). But in Spain and in the East Mediterranean the dry summer period can reach

similar dimensions. Thus water shortage is a common consequence. Generally qanats are found where precipitation is less than 500 mm / year. Mostly they are inclined to an annual precipitation between 100 and 300 mm (Bazza, 2007).

A short glance at the distribution of qanats in the Mediterranean reveals a concentration to central and southeastern Spain (Weingartner, 2007). The Spanish capital Madrid was supplied by qanat water until the 19th century (Braun 1974). But qanats can be found in the northern Adriatic (island of Pag, Croatia) and in southern Italy (e.g. Palermo) as well. On the island of Pag (Croatia) a water conduit with shafts up to 44 m and a total length over 1.160 m with a gentle slope of 1 ‰ leads to the city of Novalja (Božić, 2001). As the actual knowledge about the qanat distribution – especially in the European Mediterranean - is very fragmentary it is too soon to draw further conclusions.

Within the region of the Mediterranean borderlands Morocco, Algeria, Tunisia, Libya and Egypt qanats are well known. Here they were already responsible for early state formation (Wilson, 2003). At the moment qanats are still in use in these countries although many of them have dried up due to groundwater drawdown, usually connected to water overuse and dam construction (Lightfoot, 2003).

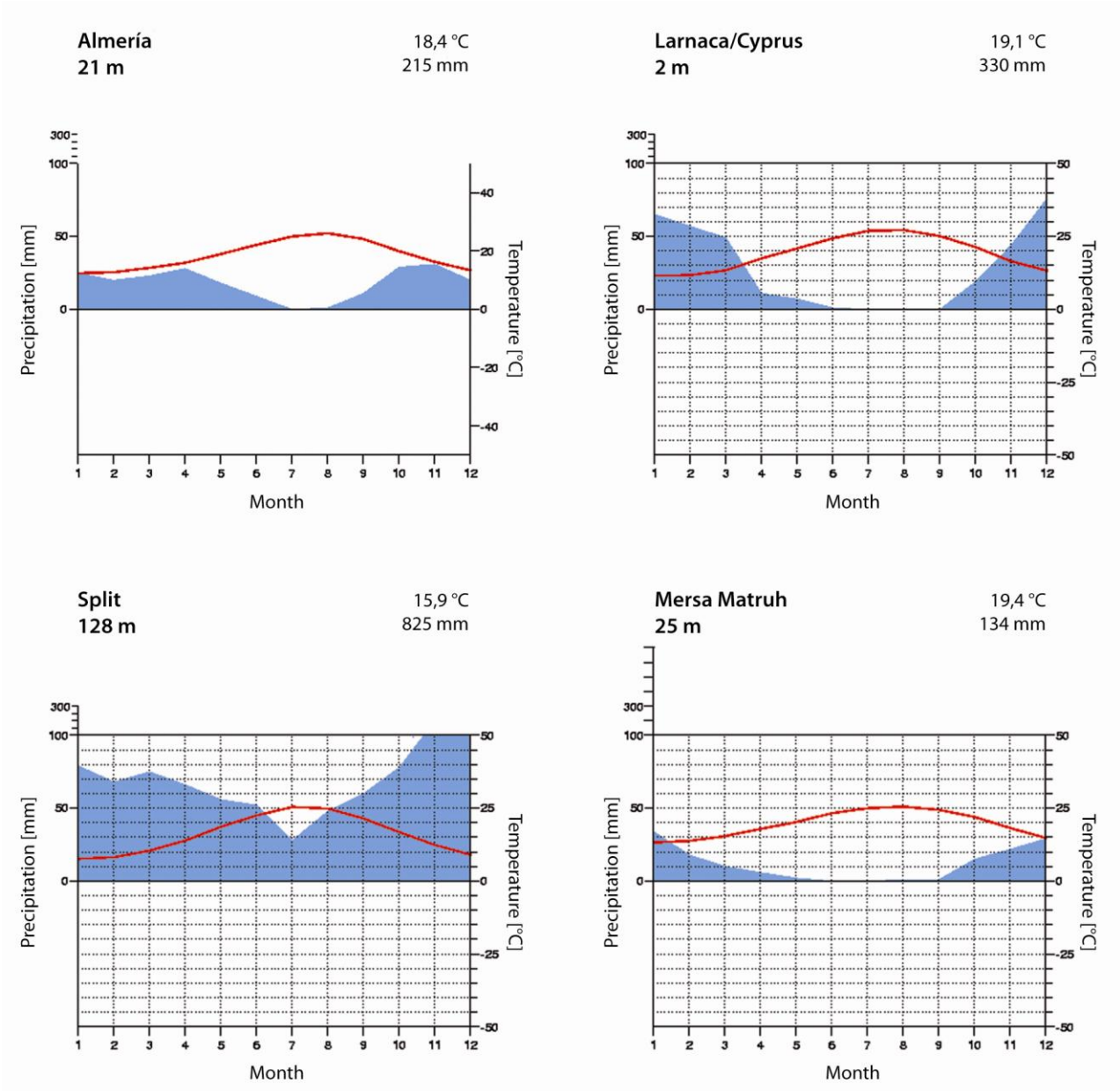

Fig. 1. Mediterranean Climate – typical climographs (Source: www.klimadiagramme.de)

In central Europe – after the fall of the Roman Empire–evidence of qanat construction is missing. However similar water supply conduits reappear together with monasteries. During the Middle Ages the Fulbert-gallery (Maria Laach, Germany) and the Mönchsbergtunnel (Salzburg, Austria) are refereed as the most important tunnels built with qanate technique (Garbrecht, 1995).

3. The qanats of Nea Zichni and Angista

Apart from qanats of ancient and antique times (Crouch, 1993) modern ones have been described as recently as 1993 (Vavliakis). They appear at the margins of the Menikion and Pangeon Mts and are situated at a very typical topographical position, as these mountains have a lasting effect as a big catchment area and are responsible for the recharge of the groundwater flow. Moreover, the mentioned water conduits are qanats in every sense, comparable to the original ones in the homeland of qanats – Iran.

There are indicators for 18 qanats in the region and there is high evidence and proof that the qanats in Phyllis have been built after the occupation of Greece by the Turks, the youngest ones only in 1895 (Vavliakis, 1989). Due to the population exchange between Greece and Turkey knowledge about the communal water supply systems disappeared.

3.1. Water discharge of the qanats of Nea Zichni and Angista

The Nea Zichni qanat is strictly bound to a dry valley, which is incised into Quaternary conglomerates. The Angista qanat traverses ridges and valleys, thus reaching maximum depths of 25-30 meters (Vavliakis, 1989). From a hydrological point of view, the subsurface geological border between Neogene clay and Quaternary conglomerates acts as the key element for the construction and the course of the galleries.

At the bottom of the subsurface waterways the groundwater is collected and forced to move along the gallery. The starting point of the qanat is usually characterized by peripheral tributary galleries, in order to optimize the drainage of the subsurface water source.

Outside, the dry valleys serve to gather and concentrate the surface water inflow. The qanat water in Nea Zichni is discharged through a pipe of 235 mm diameter. Using a flowmeter the runoff in the pipe was measured continuously (liters per hour) during several periods since the year 2006.

The runoff-scheme in Nea Zichni is clearly marked by 2 different discharge periods. During the winter period distinct runoff oscillations are visible. The rest of the year is characterized by rather uniform discharge and only little oscillations occur (Fig. 3). The hourly runoff displays volumes up to 43 m^3. Similar observations were made during the measuring period 2006-2007 (Weingartner 2008). The striking periodic discharge difference and the oscillations in winter may be allocated to the karst environment of the greater catchment area of the qanat - the Menikion Mountains.

The monthly runoff oscillates between 1.908 m^3 (January) and 8.918 m^3 in November. The whole

Fig. 2. Dry valley with subsurface qanat (dried up part), Nea Zichni.

period reveals a water discharge of almost 55.000 m^3.

The Angista qanat reveals a different environment.

a) There is evidence of a subsurface gallery length of 4 km (Vavliakis 1989)
b) The immediate roots of the surface catchment area are in the Pangeon Mountains
c) The geology is dominated by crystalline bedrock

This situation reveals a stronger influence of surface water inflow (compared to Nea Zichni). The flowmeter in the qanat of Angista never registered a drying-up of the system. Obviously the lengths of the system as well as its catchment area have an important influence on the permanent water discharge. Generally the discharge amount of both qanats is reduced due to human impact on the qanat system by system-destructive building measures (concrete shafts which disturb regular water flow).

Several sudden water discharge peaks occur during the measuring period. Usually a clear correlation between precipitation and qanat water discharge can be concluded. The 18th November 2007 precipitation event (Fig. 4), which caused extensive flooding in the region, resulted in a significant rise of qanat water runoff! Within 3 hours only, the amount of qanat water flow increased from 9.66 to 60.12 m^3.

3.2. Contemporary qanat water use and water quality

Currently the water of the known active qanats of the area is used for drinking (Rodolivos) as well as

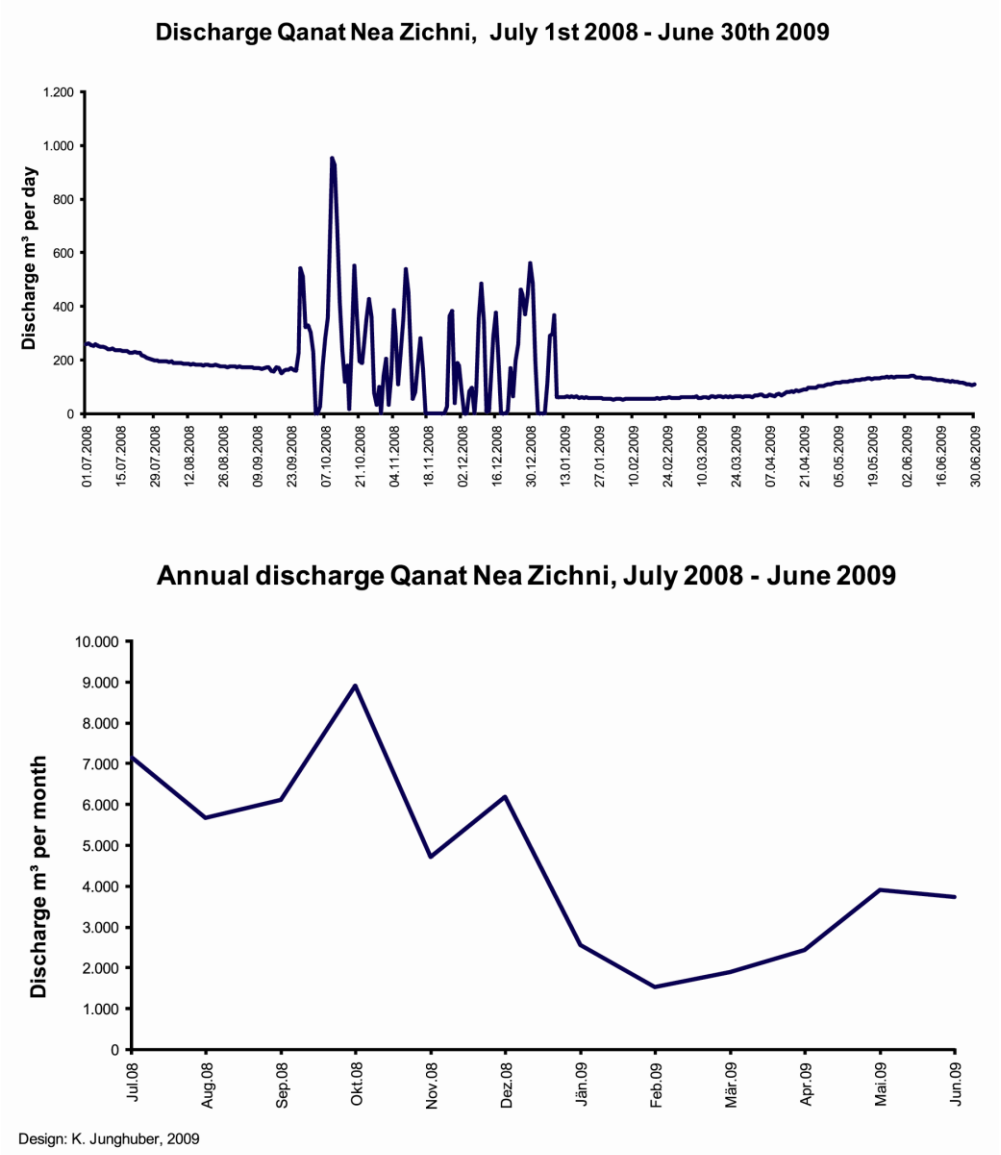

Fig. 3. Discharge and annual course of discharge, Qanat Nea Zichni, July 1st, 2008 – June 30th, 2009.

for irrigation and animal water supply (Nea Zichni and Angista). The contribution of qanat water to the entire water supply of the communities is still a matter of discussion. But the measurements indicate a reliable contribution to the local human and animal water consumption.

The hitherto existing field and laboratory chemical water analyses show the following results: Field as well as laboratory water analyses display conformity with the European Drinking Water Directive (EUDWD). Only two significant deviations occurred: The contents of heavy metals as well as the amount of nitrate (NO_3). The excessive nitrate level can be explained by the rather intensive use of fertilizer within the catchment of the qanat (Angista). An explanation of the heavy metal contents seems to be difficult. Field observations indicate a possible connection to illegal dumping. Further research will be necessary to explain the high heavy metal and nitrate concentrations.

In any case, although qanat water reveals a high potential as a drinking water resource, it displays that even 6 m of soil and sediments (and more) above the qanat channels cannot prevent the groundwater from local human land use impact. Furthermore it has to be taken into account, that qanat water catchments include – from a hydrographic point of view – vast areas of the mountain foothills as well as relief controlled surface water from the adjacent mountains. Thus, mapping of the (still unknown) subsurface qanat water ways is an important future challenge to get more information about the distribution and surface/subsurface relations of the qanat systems.

4. Conclusion and outlook

From a global point of view qanats are of significant meaning for the development of human culture. Considering the global water shortage, especially within dry areas, qanat systems represent an ecological sustainable system with a considerable potential in water supply. Some main advantages of qanats are:

- Saving of energy: No additional input of energy is needed.
- Efficiency: No water loss through evaporation (e.g. in comparison to reservoirs).
- Improvement of quality: Clean water is being produced by the natural process of interaction between water and substrate. The water is largely protected from atmospheric immissions. Water quality enhancement through ventilation (shafts).
- Continuity of the system: Water is available during dry periods.
- Landscape ecological sustainability: Negative secondary effects like salinisation are avoided.
- Contribution to a balanced water household. No burden for the water balance of the area where water is used.

The recent investigation results clearly demonstrate the meaning of qanat water and its contribution to a more sustainable use of water resources. Further research will be necessary to recover the forgotten subsurface water ways in order to get closer insight to their local or even regional water supply potential.

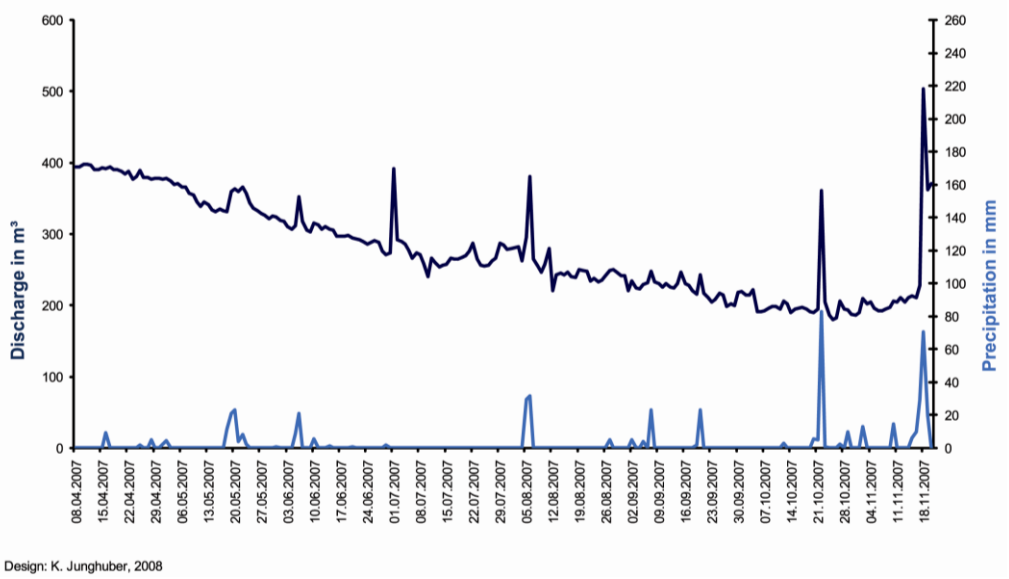

Fig. 4. Discharge and precipitation, Qanat Angista, April – November 2007.

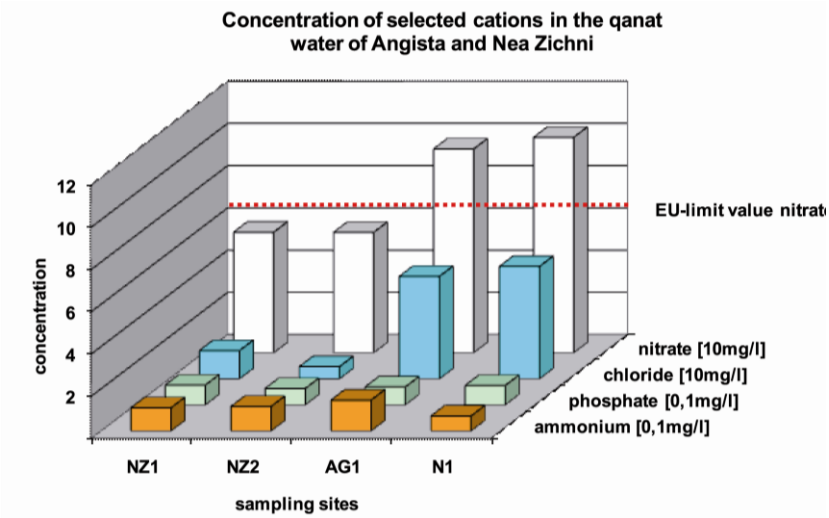

Fig. 5. Concentration of selected cations in the qanat water of Angista and Nea Zichni.

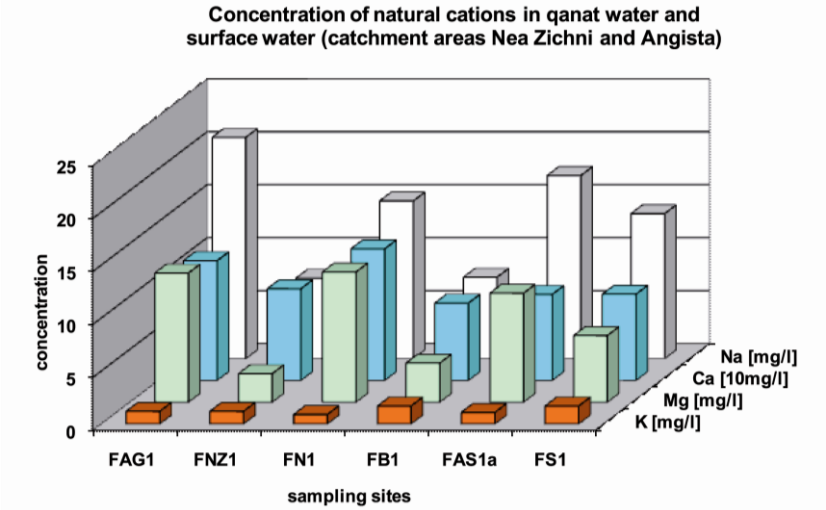

Fig. 6. Concentration of natural cations in qanat water and surface water (catchment areas Nea Zichni and Angista).

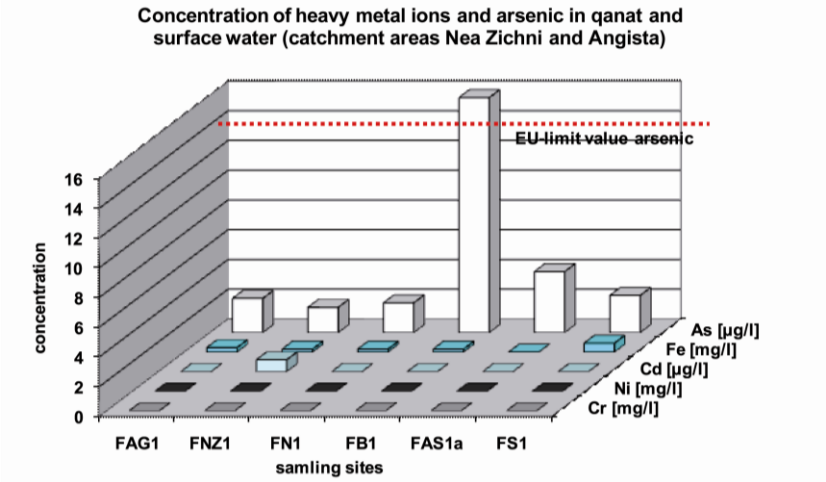

Fig. 7. Concentration of heavy metal ions and arsenic in qanat and surface water (catchment areas Nea Zichni and Angista).

References

Bazza M., 2007. Overview of the History of Water Resources and Irrigation Management in the Near East Region.- Water Sci. and Techn., Water Supply, 7 (1), 201-210.

Božić V. 2001. Schauhöhlen in Kroatien. Ein Führer durch die hergerichteten und zugänglichen Karsthöhlen und –schächte.- Zagreb.

Braun C., 1974. Teheran, Marrakesch und Madrid: ihre Wasserversorgung mit Hilfe von Qanaten; eine stadtgeographische Konvergenz auf kulturhistorischer Grundlage.- Bonn: (Bonner Geographische Abhandlungen, 52).

Crouch D. A., 1993. Water Management in Ancient Greek Cities.- New York, Oxford University Press.

Garbrecht G., 1995. Meisterwerke antiker Hydrotechnik.- München, Teubner.

Kayser P. and Waringo G., 2003. Die unterirdische Wasserleitung der Raschpetzer, ein Monument antiker Ingenieurbaukunst aus Luxemburg.- Internationales Frontinus-Symposium "Wasserversorgung aus Qanaten – Qanate als Vorbilder im Tunnelbau", 2.-5.Okt. 2003, Walferdange, Luxemburg (=Schriftenreihe der Frontinus-Gesellschaft, H. 26), 277-292.

Kremer B., 2003. Neue Forschungen zum Qanat in Pölich/Mosel sowie eine archäologische Neuentdeckung im Trierer Stadtgebiet – Der Qanat bei St. Matthias.- Internationales Frontinus-Symposium 2003, Walferdange (Luxemburg), 2.-5.Okt. 2003, Walferdange, Luxemburg (=Schriftenreihe der Frontinus-Gesellschaft, H. 26), 127-142.

Lightfoot D., 2003. Traditional Wells as Phreatic Barometers: A View from «qanats» and Tube Wells in Developing Arid Lands. Proceedings of the UCOWR Conference on Water Security in the 21stCentury. Washington, DC.

Scheumann W. 2001. Weg vom Staat – Reformen in der Bewässerungslandwirtschaft der Türkei.- Inamo, Nr. 27, Jg. 7, 32-34.

Vavliakis E. and Sotiriadis L., 1993. Die aktiven Qanatsysteme in Griechenland. Untersuchung der aktiven Qanatsysteme in der Provinz Phyllis (Nomos Serres) aus morphologischer und hydrographischer Sicht.- W. Kern, E. Stocker, H. Weingartner (Hrsg), Festschrift Helmut Riedl (= Salzburger Geographische Arbeiten, 25), 193-205.

Vavliakis E., 1989. Die Qanatsysteme in Griechenland. Untersuchung der Qanatsysteme in der Eparchia Phyllis von Serres aus morphologischer, hydrographischer und sozioökonomischer Sicht.- Thessaloniki, Aristoteles Universität, 93 S. (neugr.).

Weingartner H., 2008. Wasserknappheit im Mittelmeerraum. Können Qanate zu einer nachhaltigen Wasserversorgung beitragen? Ein Beispiel aus Ostmazedonien (Griechenland).- Blumenstein, O., W. Krüger & H. Schachtzabel (eds.), Arbeiten der AG Landschaft und Nachhaltige Entwicklung der Universität Salzburg (= Stoffdynamik in Geosystemen, Bd. 14), 49-66.

Weingartner H., 2007. Water supply by Qanats. A Contribution to Water Shortage in Mediterranean Areas?- In: Lekkas T.D. (ed.), Proceedings of the 10th International Conference on Environmental Science and Technology, Kos island, Greece, 5-7 September 2007, p. 1555-1561.

Wilson A., 2003. Foggara irrigation and early state formation in the Libyan Sahara.- Internationales Frontinus-Symposium "Wasserversorgung aus Qanaten – Qanate als Vorbilder im Tunnelbau", 2.-5.Okt. 2003, Walferdange, Luxemburg (= Schriftenreihe der Frontinus-Gesellschaft, H. 26), 223-234.

Scientific Annals, School of Geology, Aristotle University of Thessaloniki Proceedings of the XIX CBGA Congress, Thessaloniki, Greece	Special volume 100	31-38	Thessaloniki 2010

ON THE MINERALOGY, PHYSICAL CHARACTERISTICS AND THE MAIN ELEMENTAL CONTENT OF URBAN ROAD DUST PARTICLES FROM THE HISTORIC CENTRE OF THE CITY OF THESSALONIKI, NORTHERN GREECE

Bourliva A., Papadopoulos A., Giouri A., Papadopoulou L., and Kantiranis N.

Department of Mineralogy-Petrology-Economic Geology, School of Geology, Aristotle University of Thessaloniki, 54124, Thessaloniki, Greece, annab@geo.auth.gr

Abstract: The objective of this study was to characterize urban road dust particles and to study their possible health effects. Road re-suspended dust has been recognized as one of the major contributors to TSP elevating concentrations in Thessaloniki. Eight samples of road dust were collected from the accumulated matter at the edges of major roads in the historic centre of the city of Thessaloniki. The predominant size fraction, according to mass, was 125–500μm, while the mass fraction of the suspendable dust particles (20-63μm and <20μm) was the lowest. Special emphasis was given to the mineralogical characteristics of the urban deposits. Road dusts were mainly composed of quartz, calcite, while plagioclase, dolomite, K-feldspars, amphiboles, micas and chlorite were contained in minor amounts. Amorphous phase was also determined mainly in the finer fractions (20-63μm and <20μm). Scanning electron microscopy shows that dust particles consist of subhedral to anhedral crystalline grains, near-spherical and irregular agglomerates as well as few organic materials. EDS analyses reveal that the composition of dust particles is basically Ca-rich, Fe-rich and silicates.

Keywords: road dust, mineral content, grain size distribution, morphology

1. Introduction

Solid matter, which is composed of soil, anthropogenic metallic constituents, and natural biogenic materials, is called dust. The particles of dust that deposit from the atmosphere and accumulate along roadsides are called road dust particles. Two main sources of road dust are deposition of previously suspended particles (atmospheric aerosols) and displaced soil (Ferreira-Baptista and DeMiguel, 2005). Additionally, the emissions from vehicular traffic, heating systems, building deterioration, construction and renovation, corrosion of galvanized metal structures etc. contribute directly to the road dust load (Howari et al., 2004; Al-Khashman, 2004).

Road dust consisting primarily of mineral matter dominates the total suspended particulate mass (Pakkanen et al., 2001). Apart from the discomfort caused by the dust, respirable mineral particles, e.g. aluminosilicates and crystalline quartz have been implicated in human disease with lung cancer as most severe (Puledda et al., 1999; Powell, 2002). Whether these effects are significant in urban conditions is still unknown. Studies of exposure to mineral and resuspension particles have shown evidence of toxicity and a possibility of adverse health effects (Tiittanen et al., 1999; Salonen et al., 2000).

Furthermore, physical and chemical nature of road dust particles are critical to estimating their potential contributions to environmental and health effects (Brookman and Drehmel, 1981). The physical aspect is basically particle size and shape, while the chemical aspect relates to dust particles composition.

Suspendability of road dust is of paramount importance since this is the principal aspect that relates to human health. The quantity of material suspended depends primarily on particle size (Pye, 1987; Han et al., 2003). Particle size also affects the amount that remains suspended to become part of the TSP (Total Suspended Particles) background and the amount that falls out of the atmosphere

within a short distance from the roadway. Dust particles greater than 500 μm are too large to enter the wind stream and move along the surface during wind erosion by surface creep. Medium size particles, 100-500μm in diameter, may enter the wind stream momentarily, but then settle quickly. Only dust particles less than 100μm (most commonly <63μm) are easily entrained and suspended in the wind stream where they are transported, often for great distances.

The chemical nature of the road dust determines whether or not the material is of a hazardous nature to its surroundings (e.g., toxic to man, harmful to vegetation and water supplies). It also helps establish the origins of the dust and can point the direction towards effective controls.

The city of Thessaloniki is the second largest of Greece and one of the largest urban agglomerations in the Balkans. Historically, Thessaloniki has been encountered serious air-quality problems with air particles, with TSP concentrations exceeding by far the annual limit of 150 mg/m^3. Although a 30% reduction has been obtained during the last decade, the excessive use of cars and ongoing works to build a metro system are keeping TSP levels still high, posing a real risk for the health of Thessaloniki residents. Manoli et al. (2002) found that road dust dominated the coarse particle fraction (3.0-10 μm) in the centre of Thessaloniki, accounting for 57% to its ambient levels, while it was also an important contributor (28%) to the fine size fraction (<3.0 μm) where traffic emissions prevailed. A more recent source apportionment study carried out in Thessaloniki (Samara et al., 2003), estimated the contribution of road dust to ambient PM10 at three sites within the city as ranging between 19 and 22%.

The aim of the present study was to assess the mineralogy, particle size, morphology and the main elemental content of urban road dust particles. Similar studies have not been previously conducted in this region. On the contrary, heavy metals and other toxic elements, polycyclic aromatic hydrocarbons and ionic species found in roadside dusts of Thessaloniki have been investigated (Misaelides et al., 1989; Samara et al., 2003; Ewen et al., 2009).

2. Materials and Methods

2.1. Study area

Thessaloniki (40^o 62′ E, 22^o 95′ N) is one of the most densely populated cities in Greece and in Europe accounting for approximately 16,000 inhabitants km^{-2} (Samara et al., 2003). It is located in the inner part of Thermaikos Gulf, surrounded north, north-eastern by Hortiatis mountain (1200 m height). Numerous residential suburbs circle the city and an extended industrial zone is sited northwesterly. According to Manoli et al. (2002), the climate of Thessaloniki is typically Mediterranean: mild, strongly influenced by the sea breeze. Mean monthly values of relative humidity vary between 47% and 80% (mean annual rainfall is 490 mm), while temperature varies between 5.5^{o}C (in January) and 28^{o}C (in August). Prevailing wind directions are N/NW (25%), S/SW (30%) and calms (20%). This meteorology results to insufficient dispersion of atmospheric pollutants.

2.2. Sample Collection and Preparation

Eight samples of road dust were collected from the accumulated matter at the edges of major roads in the historic centre of the city of Thessaloniki (Fig. 1). Road dust sampling was carried out in November 2009. The dust samples were mainly collected by sweeping an area of about 1 m^2 from road surface using a clean plastic dustpan and brushes for each sampling site. The amount of material from each sampling point varied between 50 and 150 g. The samples were dried in an oven at 35^{o}C for 3 days. The dried samples were passed through a 1000μm stainless steel sieve to remove sand-sized materials and large plant roots. Subsequently, the road dust samples were mechanically sieved into five grain size fractions: <20μm, 20-63μm, 63-125μm, 125-500μm, >500μm. The loss of material during sieving was less than 2%. The three finest fractions were used for further investigations.

2.3 Analytical Methods

Mineralogical characterization of the dust particles as well as semi-quantitative mineral determination was performed by X-Ray powder diffraction (XRPD) using a Philips PW1710 diffractometer. Ni-filtered copper Kα radiation was used energized to 35kV and 25mA. Randomly oriented road dust samples of the <20μm, 20-63μm and 63-125μm fractions were scanned continuously from 3 to 63◦ 2θ angles at a scanning speed of 1.2^o/min. The characterization of the mineral phases was performed semi-quantitatively on the basis of the intensity (counts) of specific reflections, the density, and the mass absorption coefficient (CuKα) of the identified mineral phases.

The percentage of total amorphous material

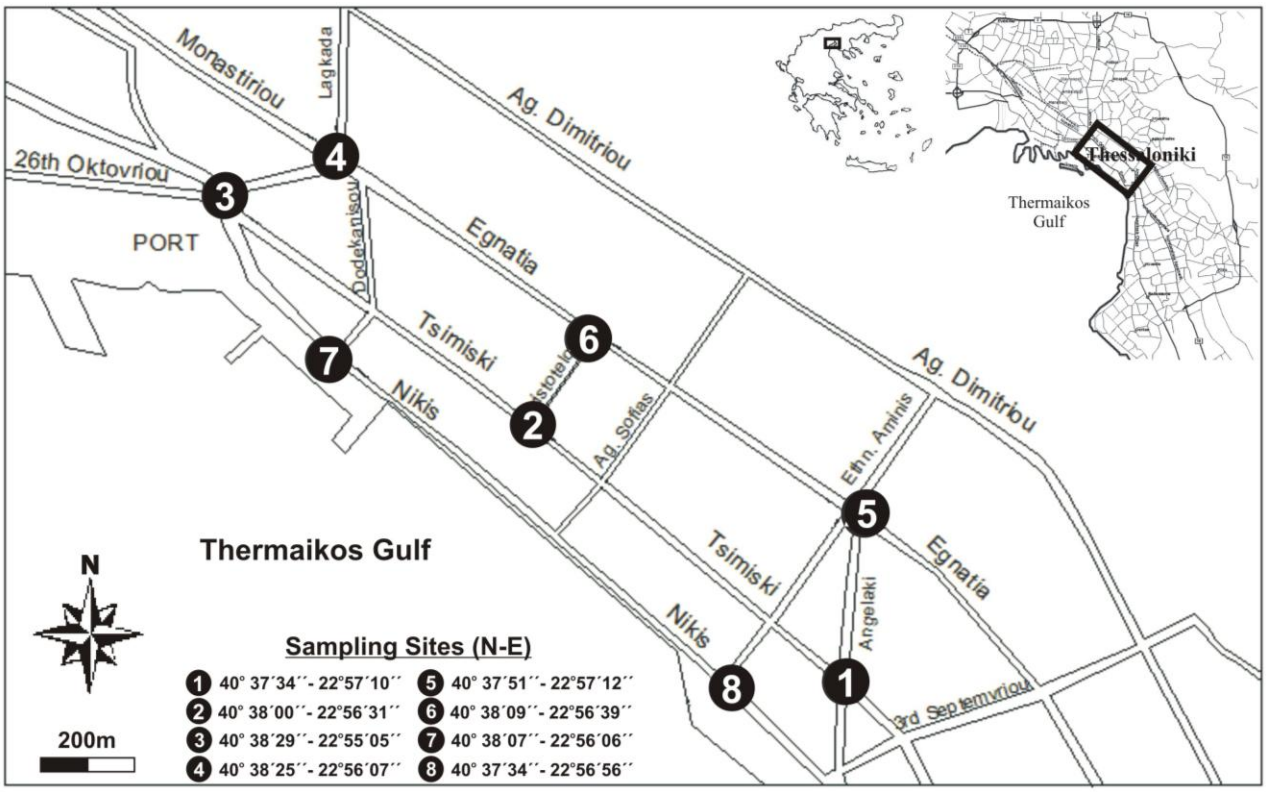

Fig. 1. Location of the sampling sites.

contained in the road dust samples was determined using the methodology described by Kantiranis et al. (2004). The XRPD method is a very good, effective and useful tool for the determination of the percentage of amorphous material contained in a natural or synthetic sample (Kantiranis et al., 2004).

A Scanning Electron Microscope (JEOL JSM-840) connected to an X-ray Energy Dispersion Spectrometer-EDS (LINK-AN 10000) was employed for the morphological and semi-quantitative chemical characterization of the 20-63μm and 63-125μm grain size fractions of the urban road dust samples. This technique allows the definition of the particles with respect to their size and morphology as well as the identification of other properties such as particles association or aggregation (Buseck and Bradley, 1982; Zou and Hooper, 1997).

3. Results and Discussion

3.1. Particle size distribution of road dusts

The grain size distribution of the road dust samples is presented in Figure 2. According to weighted mass, the predominant grain size fraction was 125–500μm varying between 41.9 and 51.8%, while the second most dominant grain size fraction was 63–125μm ranging between 16.6–25.2%. Dust particles which could easily be entrained and suspended in the wind stream were those which had the smallest particle sizes (20-63μm and <20μm). The mass fraction of these suspendable dust particles was the lowest ranging from 7.8-23.2% to 0-0.6%, respectively. This size distribution trend of the road dusts was similar in all sampling sites.

3.2. Mineral Content

The results of the semi-quantitative estimation of the mineralogical composition of the studied road dust samples are summarized in Table 1, while representative XRPD patterns are given in Fig. 3.

The dominant minerals present in the road dust samples were quartz (SiO_2) and calcite ($CaCO_3$). Lower abundances of plagioclase (mostly albite-$NaAlSi_3O_8$) and dolomite ($CaMg(CO_3)_2$) occur in almost all the studied samples. Other minerals identified in small quantities were K-feldspars (mostly orthoclase-$KAlSi_3O_8$), amphiboles (mostly tremolite-$Ca_2Mg_5Si_8O_{22}(OH)_2$), micas (mostly muscovite-$KAl_2(AlSi_3)O_{10}(OH)_2$), and chlorite (mostly clinochlore-$Mg_6Si_4O_{10}(OH)_8$). The prevailing identified minerals were the same in all the studied fractions of the urban road dust samples.

The data available on the mineralogical compositions of urban deposits worldwide, principally based on road dust samples is limited (Kuang et

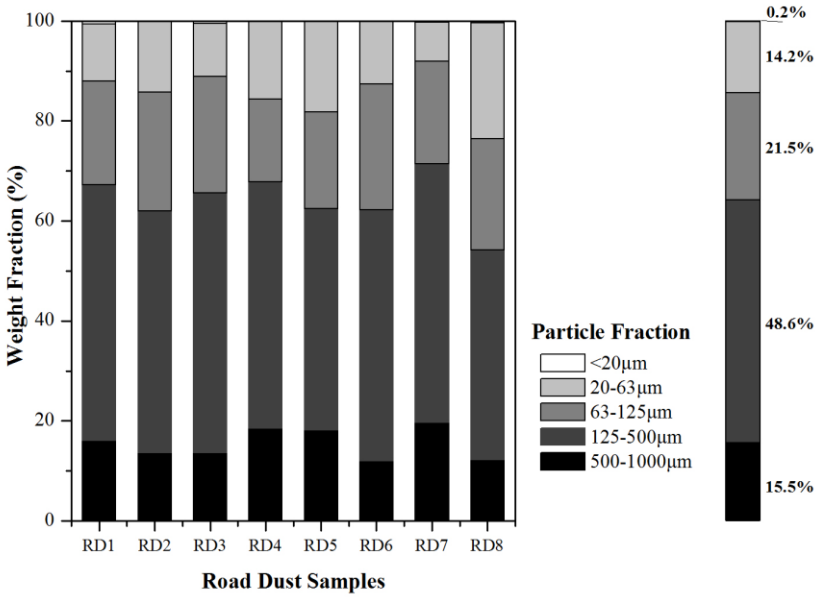

Fig. 2. Grain size distribution (wt%) of the urban road dust samples. The total average value (wt%) of each particle fraction is shown at the right.

al., 2004, Duzgoren-Aydin et al., 2006). Despite a significant variation in the level of contamination and the differences in urban natural and anthropogenic settings, the major mineral components of the road dusts appear to be similar, and are dominated by quartz, calcite and feldspar minerals (including plagioclase and K-feldspars). Quartz, the most resistant mineral to physical and chemical weathering, dominates the overall mineralogy of the urban deposits. Calcite, one of the most abundant minerals in the road dusts, derives probably from the erosion of concrete pavements and other construction materials (Tossavainen and Forssberg, 1999).

The amount of quartz decreases with decreasing particle size (Tab.1). The quartz percentage varies

Table 1. Semi-quantitative mineralogical composition (mass/mass, %) of separated particle size fractions (in μm) of urban road dusts from Thessaloniki city.

Sample	Particle Size	Q	C	Pl	D	Kf	Amp	M	Chl	Amorphous
RD1	63-125μm	78	16	2	2			2		
	20-63μm	47	19	4	3	1		1		25
	<20μm	20	44	1	3	3				29
RD2	63-125μm	83	11	3	1	1		1		
	20-63μm	69	23	5	1		1	tr	tr	
RD3	63-125μm	77	13	1	7	tr	tr	1	tr	
	20-63μm	46	25	2	8				tr	19
	<20μm	18	52	1	6		1			22
RD4	63-125μm	62	19	13	tr		1	1	tr	3
	20-63μm	49	25	4	1	1	1			19
RD5	63-125μm	64	29	4	tr			2	tr	
	20-63μm	27	55	9	tr	tr		tr	tr	8
	<20μm	13	51	1	tr					35
RD6	63-125μm	64	10	2		1	1	tr		21
	20-63μm	80	18	2						
RD7	63-125μm	64	25	5	3		1	1	tr	
	20-63μm	60	29	3	3			1	tr	4
	<20μm	26	43	1	4		tr			25
RD8	63-125μm	77	16	4	2			1		
	20-63μm	64	29	4	2	tr		tr	tr	
	<20μm	29	35	2	2					32

Q: quartz, C: calcite, Pl: plagioclase, D: dolomite, Kf: K-feldspars, Amp: amphibole, M: mica, Chl: chlorite, tr: traces

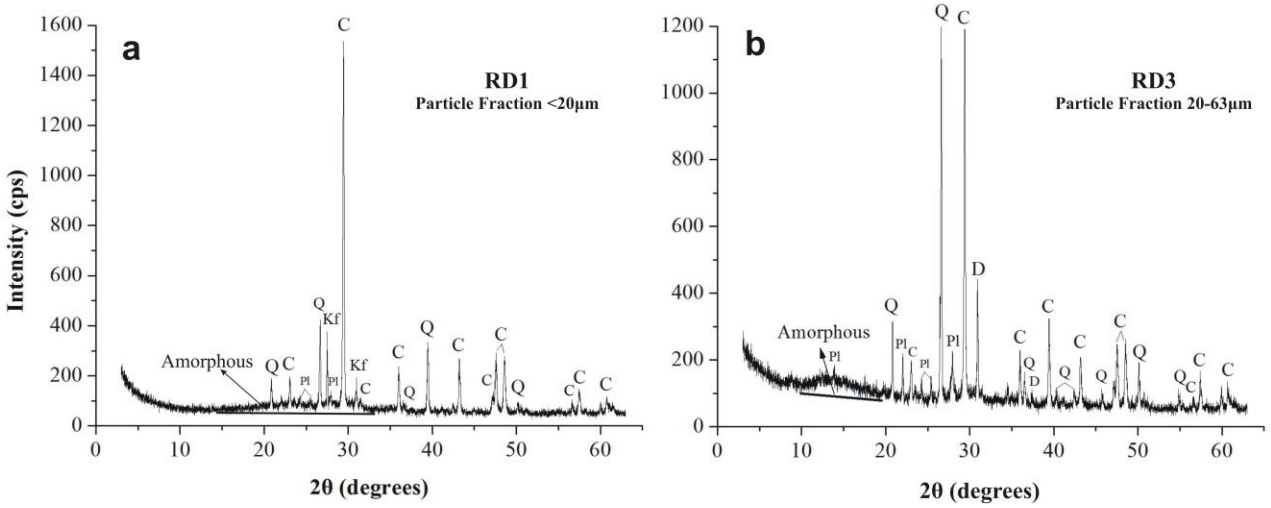

Fig. 3. Representative XRPD patterns of suspendable particle size fractions of road dust samples, a) RD1 and b) RD3. Q: quartz, C: calcite, D: dolomite, Pl: plagioclase, D: dolomite, Kf: K-feldspars.

from 62-84% and 26-80% in the 63-125µm and 20-63µm, respectively. Lower abundances (13-30%) occur in the finer fraction (<20µm). The opposite trend is noticed for calcite. The calcite amount increases with decreasing particle size. In the 63-125µm fraction the calcite percentage varies from 11-29%, while in the finer fraction calcite ranged from 36-56%. This fact is correlated with their erodibility.

The potential health risks associated with crystalline silica are of enhanced interest (Ikeda et al., 1986, Puledda et al., 1999). The latest monograph that the International Agency for Research on Cancer (IARC) devoted to crystalline silica establishes that exposure to this substance can be associated to lung cancer. On this basis, IARC has classified crystalline silica as carcinogenic to man (Category I) (IARC, 1997). By reference to its physical characteristics, there is great concern about the potential health risks resulting from exposure to quartz, the most common mineral phase of crystalline silica. In the present work, relatively high quartz amounts (13-80%) were determined in the suspendable fractions (20-63µm and <20µm) of the road dust samples. However, these results do not permit an assessment of the actual risk for the general population. Health risk depends largely on quartz morphology.

Finally, amorphous phase was also determined. The amorphous phase was mainly in the finer fractions (20-63µm and <20µm). In the <20µm fraction, the amorphous ranged from 19-35%, while in the 20-63µm fraction varied between 4-25%. Only two samples, RD4 and RD6, presented amorphous phase in the 63-125µm fraction. The amorphous phase could probably consist of amorphous silica or Fe-Mn oxyhydroxides which can be found in road dust samples and present poorly crystallized nature.

3.3. Morphology and Chemical Composition

SEM can provide size and morphology information of particles. SEM observation showed that dust particles were present in a wide range of size and shape. Depending on the origin of dusts, the dust particles mostly consist of subhedral to anhedral crystalline grains, plate like and near-spherical particles, and finally irregular agglomerates that contain variable size and amount of particles. The EDS results reveal that the composition of dusts is dominated by Ca-rich or Fe-rich particles and silicates.

Road dusts particles are mainly composed of silicates presenting angular and irregular shapes, which is characteristic of natural sources. Si-rich particles of road dusts are shown in Fig.4. Most of the Si-rich particles contain Si, Al, Fe, and Mg. Si-rich particles are mainly composed of amorphous or crystalline silicate minerals, while Si-rich particles with high iron content are mainly derive from building sites.

Electron micrographs of Ca-rich particles are shown in Figure 5. Ca-dominant particles are mainly composed of $CaCO_3$ (Fig. 5a). The size of Ca-rich particles is typically 10–70µm. Agglomerates of Ca-rich particles are composed of calcium with traces of Si, Al, Mg, K and S (Fig. 5b-c). Additionally, agglomerates of Ca-aluminosilicates are

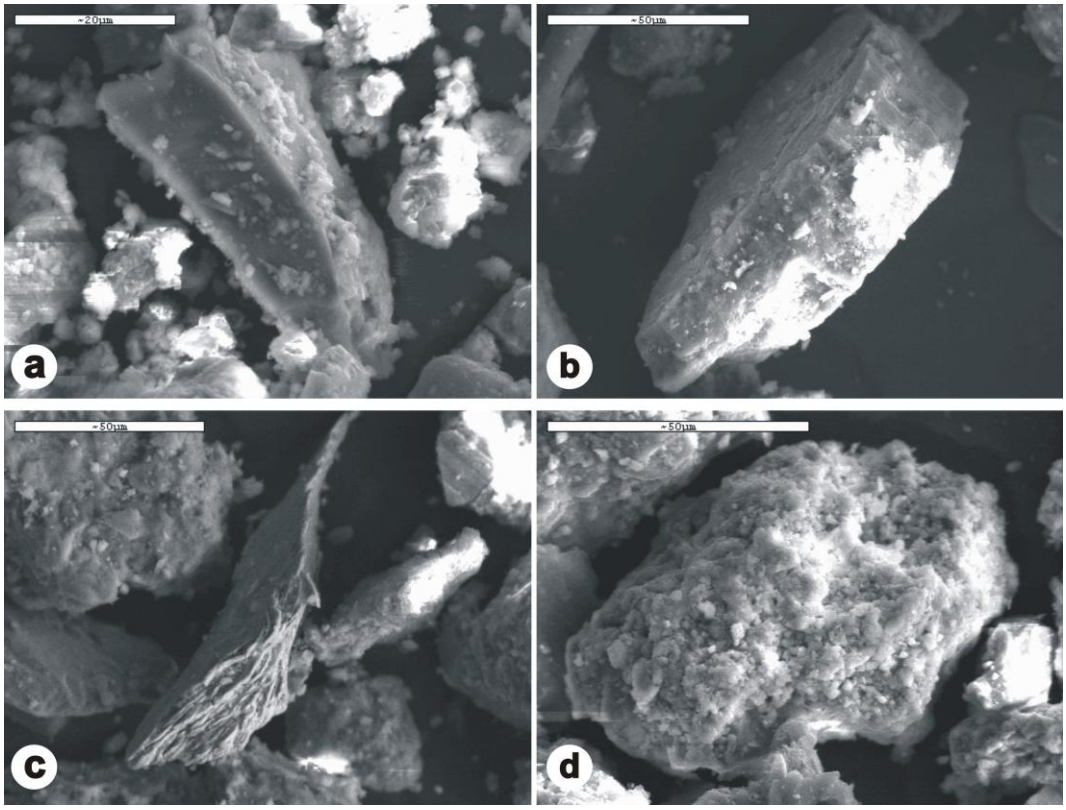

Figure 4: SEM images of Si-rich particles, a) irregular quartz crystal, b) oblate particle of alumino-silicate , c) plate like mica crystal and d) agglomerate of Si-rich particles.

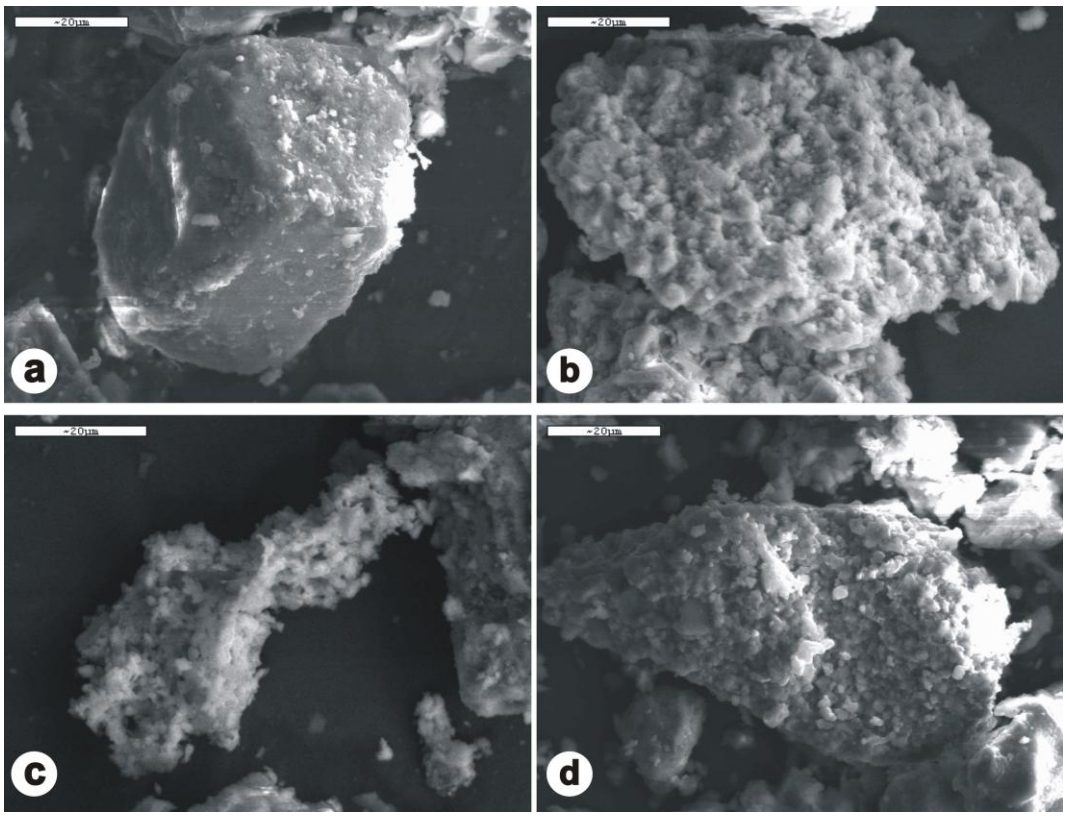

Fig. 5. SEM images of Ca-rich particles. a) calcite crystal, b) agglomerate of Ca-rich particles, c) spongy like agglomerate of Ca-rich particles and d) agglomerate of Ca- and Si-rich particles.

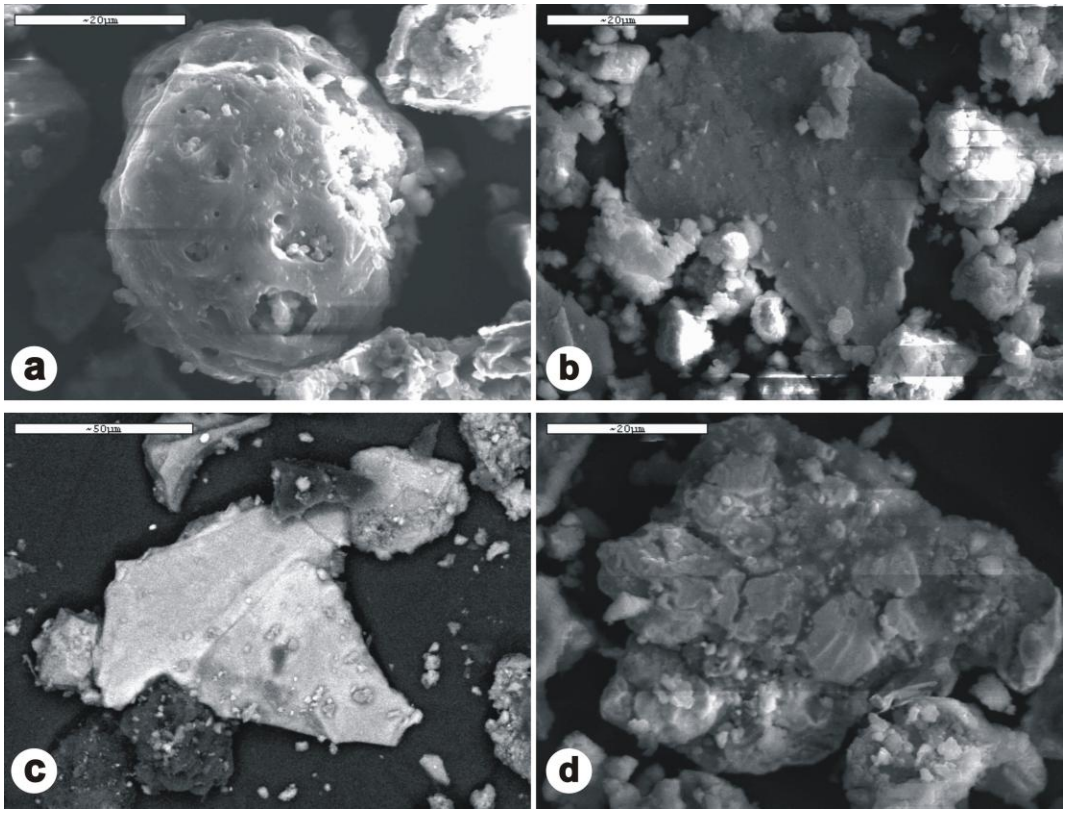

Fig. 6. SEM images of Fe-rich road dust particles, a) near spherical Fe-rich particle, b) plate like and c) irregular plate like Fe-rich particle and d) agglomerate of Fe-rich particles.

determined. The chemical composition of these particles is mainly Si and Ca with minor S, Mg, Fe, Al and K. Ca+Si particles are believed to be a mixture of $CaCO_3$ with silicates (Fig. 5d). Ca-rich particles derive from the erosion of concrete pavements and other construction materials. Sulphur, which produced during fuel combustion is seen as a coating on the surface of Ca-rich dust particles and/or as gypsum from the degradation of the building mortars. As indicated sulfur content in these particles has a range of 0.43–3.13%.

Fe-rich particles are mainly in shapes of near-sphere, plate and agglomerate (Fig. 6). The Fe-rich near-spherical grains exhibit smooth textures (Fig. 6a). The chemical compositions of particles determined by EDS shows that the spherical grains have very high iron content (~70%) with small amounts of Ca and Si. The size of plate Fe-rich particles is typically 10–50μm (Fig. 6b-c). Plate Fe-rich particles contain traces of Si, Al, Ca, Mg, Ti, S and Cr. These non-spherical Fe-rich particles are suggested to be released from vehicles via exhaust emission and the abrasion or corrosion of the vehicle engine and body work (Hoffmann et al., 1999). Agglomerate of Fe-rich particles exhibits cluster texture (Fig.6d).

4. Conclusions

A mineralogical, morphological and chemical characterization of road dust from the historic centre of the city of Thessaloniki was performed. The prevailing identified minerals were quartz and calcite. Numerous studies in literature deal with the potential health risks that could be associated with the occupational exposure to quartz. Additionally, Ca-bearing minerals (e.g. calcite), which are among the most common minerals in the urban environment are strongly linked to certain contaminants (such as Pb and Zn) known to be strongly associated with the operationally defined carbonate fraction. The road dust particles, which are variable in morphology and chemical composition, are mainly composed of near-spherical, plate and irregular agglomerate Fe-rich particles, Ca-rich, and silicate particles. Some of the dusts in the present investigation were rich in potential toxic heavy metal elements (e.g. Cr), which are significant environmental issues. Road dust is often considered only as a nuisance or minor safety hazard. However, environmental consequences in terms of air and water pollution and associated health hazards, primarily those linked to respiratory diseases, render

essential further investigation regarding the problem of urban road dust.

References

Al-Khashman O.A. 2004. Heavy metal distribution in dust, street dust and soils from the work place in Karak Industrial Estate, Jordan. Atmospheric Environment, 38, 6803–6812.

Brookman E.T., and Drehmel D.C. 1981. Future areas of investigation regarding the problem of urban road dust. Environment International, 6, 313-320.

Buseck P. R. and Bradley J. P. 1982. Electron beam studies of individual natural and anthropogenic microparticles: Compositions, structures and surface reactions. In: Heterogeneous Atmospheric Chemistry, American Geophysical Union, Washington DC, USA, 57–76.

Duzgoren-Aydin N.S., Wong C.S., Song Z.G., Aydin A., Li X.D. and You M. 2006. Fate of heavy metal contaminants in road dusts and gully sediments in Guangzou, SE china: a chemical and mineralogical assessment. Human and Ecological Risk Assessment, 12, 374-389.

Ewen C., Anagnostopoulou M.A., and Ward N.I. 2009. Monitoring of heavy metal levels in roadside dusts of Thessaloniki, Greece in relation to motor vehicle traffic density and flow. Environmental Monitoring and Assessment, 157, 483-498.

Ferreira-Baptista L. and DeMiguel E. 2005. Geochemistry and risk assessment of street dust in Luanda, Angola: a tropical urban environment. Atmospheric Environment, 39, 4501–4512.

Han Y.M., Du P.X. and Li Z.M. 2003. Cyclic model, transport and deposition of urban dust in Xi'an city. Geophysical and Geochemical Exploration, 27, 227–229.

Hoffmann V., Knab M. and Appel E. 1999. Magnetic susceptibility mapping of roadside pollution. Journal of Geochemical Exploration, 66, 313–326.

Howari F.M., Abu-Rukah Y. and Goodell P.C. 2004. Heavy metal pollution of soils along North Shuna–Aqaba Highway, Jordan. International Journal of Environment and Pollution, 22, 597–607.

IARC 1997. Silica, Some Silicates, Coal Dust and para-Aramid Fibrils. International Agency for Research on Cancer (IARC) Monographs, 68, 506p.

Ikeda M., Watanabe T., Hayashi H. and Tsunoda A. 1986. Toxicological evaluation of quartz and silica contents in studded tire-generated dust in the city of Sendai. The Tohoku Journal of Environmental Medicine, 148, 207-211.

Kantiranis N., Stergiou A., Filippidis A. and Drakoulis A. 2004. Calculation of the percentage of amorphous material using PXRD patterns. Bulletin of Geological Society of Greece, 36, 446.

Kuang C., Neumann T. and Norra S. 2004. Land use-related chemical composition of street sediments in Beijing. Environmental Science and Pollution Research, 11, 73–83.

Manoli E., Voutsa D., and Samara C. 2002. Chemical characterization and source identification/apportionment of fine and coarse air particles in Thessaloniki, Greece. Atmospheric Environment, 36, 949-961.

Misaelides P., Samara C., Georgopoulos M., Kouimtzis Th. and Synetos S. 1989. Toxic elements in the environment of Thessaloniki, Greece. Part 1: Roadside dust analysis by I.N.A.A. and A.A.S. Toxicological & Environmental Chemistry, 24, 191-198.

Pakkanen T.A., Loukkola K., Korhonen C.H., Aurela M., Mäkelä T., Hillamo R.E., Aarnio P., Koskentalo T., Kousa A. and Maenhaut W.2001. Sources and chemical composition of atmospheric fine and coarse particles in the Helsinki area. Atmospheric Environment, 35, 5381 –5391.

Powell JJ. 2002. Analysis of aluminosilicate particles in biological matrices using histochemistry and X-ray microanalysis. Analyst, 127, 842 –846.

Puledda S, Paoletti L. and Ferdinandi M. 1999. Airborne quartz concentration in an urban site. Environmental Pollution, 104, 441 –448.

Pye, K. 1987. Aeolian dust and dust deposits. Academic Press, San Diego, California.

Salonen R.O., Pennanen A.S., Halinen A.I., Hirvonen M.R., Sillanpaa M., Hillamo R., Karlsson V., Koskentalo T., Aarnio P., Ferguson S. and Koutrakis P. 2000. A chemical and toxicological comparison of urban air PM10 collected during winter and spring in Finland. Inhalation Toxicology, 12, 95 – 103.

Samara, C. and Voutsa, D. 2005. Size distribution of airborne particulate matter and associated heavy metals in the roadside environment. Chemosphere 59,1197–1206.

Samara C., Kouimtzis Th., Tsitouridou R., Kanias G., and Simeonov V. 2003. Chemical mass balance source apportionment of PM10 in an industrialized urban area of Northern Greece. Atmospheric Environment, 37, 41-54.

Tiittanen P., Timonen K.L., Ruuskanen J., Mirme A. and Pekkanen J. 1999. Fine particulate air pollution, resuspended road dust and respiratory health among symptomatic children. European Respiratory Journal, 13, 266 –273.

Tossavainen M. and Forssberg E. 1999. The potential leachability from natural road construction materials. Science of Total Environment, 239, 31–47.

Zou L. Y. and Hooper M. A. 1997. Size resolved airborne particles and their morphology in central Jakarta. Atmospheric Environment, **31**, 1167–1172.

Scientific Annals, School of Geology, Aristotle University of Thessaloniki Proceedings of the XIX CBGA Congress, Thessaloniki, Greece	Special volume 100	39-45	Thessaloniki 2010

ACCUMULATION AND DISTRIBUTION OF ORGANIC MATTER IN SEDIMENTS OF SALT-AFFECTED SHALLOW LAKES AT SZEGED, HUNGARY

Bozsó G., Pál-Molnár E.,Nyilas T., Heténi M.

Department of Mineralogy, Geochemistry and Petrology, Faculty of Science and Informatics, University of Szeged, H-6722 Szeged, Hungary, bozso.gabor@geo.u-szeged.hu

Abstract: The primary aim of the research is to investigate the accumulation and distribution of organic material [OM] in saline shallow lacustrine sediments. This study focuses on the OM parameters of sediments at two areas with different hydrology, land use and vegetation cover. The study area is located at the Fehér Lake, Szeged (Hungary). The studied salt-affected lake system has been under intensive fish breeding from 1970. Sampling was made during the spring of 2007. In case of the profiles a 4 m deep 10 cm diameter sediment core was extracted. The OM data were measured with Rock-Eval pyrolysis, and the proportion of different OM groups was determined by the mathematical deconvolution of Rock-Eval pyrograms. It is showed that there are significant differences in OM distribution and characteristics if the different study sites are compared. In case of both profiles similar changes can be detected in the origin, quantitative and qualitative parameters of OM at depths of 15, 30, and 65-70 cm, which proves that the two sites belonged to the same depositional system, and similar changes affected them during sediment formation. Although both profiles have the same depositional environment, significant difference can be seen between the profiles. The profile 1. used to be located in coastal natural territory till 1970 and the profile 2. represents a constant water-irrigated fields. The fluctuation of F1+F2 and F3 values in Profile 1. suggests that the OM content of the marginal territory (both in its natural and present state) is determined by the alternation of dry and wet periods, sometimes with a high algae production in slack waters. Based on the quality parameters of OM, dry and wet accumulation periods can be separated, and signs of human influence can also be identified.

Key words: organic matter distribution, shallow lake, salt-affected sediment

1. Introduction

The quality and quantity of organic material [OM] preserved in sediments provide trustable information on the circumstances of accumulation, the characteristics of natural and human sources, and post-sedimentation processes influencing OM distribution (Meyers, 2003). While OM in marine sediments has implications on long term phenomenon, the quantity, quality and distribution of OM in the sediments of shallow lakes is primarily determined by short term and local processes. The preservation and transformation of OM is highly influenced by actual hydrologic, climatic and geochemical parameters (Ariztegui et al., 2001; Sebag et al., 2006). Most of the researches focus on the OM of marine and deep water lacustrine environments, the organic geochemistry of shallow, continental lakes is usually out of the scope of these studies. On the other hand due to global climate change, the area of shallow lakes and territories with water-affected soils, usually both influenced by salinization processes, is continuously increasing (Das et al., 2008; Tóth et al., 2006). As a consequence, the investigation of the organic geochemistry of these territories is getting more and more important. The extreme evaporation and hydrological conditions on saline territories can considerably affect geochemical processes (Bozsó et al., 2008), and thus the accumulation and preservation of OM.

An adequate analytical procedure for determining the quantitative and qualitative parameters of OM, influenced by the above processes, is Rock-Eval pyrolysis (Disnar et al., 2003). By the mathematic analysis of the measured pyrograms stable and un-

stable biopolymers (F1, F2), immature and mature refractory geopolymers (F3, F4) can easily be separated (Sebag et al., 2006), and accumulation events can also be delineated and identified in the sediment record (Hetényi et al. 2005).

The primary aims of the present research are to determine the quantity of OM in sediments of shallow lakes affected by salinization, to identify the origin of OM, to investigate the transformation processes of bio and geopolymers, and finally on the basis of the above data, to identify the depositional conditions.

2. Materials and methods

In accordance with the aims of the research the sampling sites were chosen to be at Lake Fehér near Szeged, Hungary (Fig. 1). The lake system and its environment were formed by the fluvial and aeolian accumulation processes of the Carpathian Basin (Keveiné et al., 2000). The studied lake system, with a catchment of 200 km^2 and a net area of 14 km^2, is affected by intensive fish breeding, though some areas are still considered natural and protected by the Kiskunság National Park.

Sampling was made during the spring of 2007 at four different locations with different hydrogeology and land use. Because of the lack of space only two profiles are presented in this paper.

In case of the profiles a 4 m deep 10 cm diameter sediment core was extracted. The cores were dissected into 5 cm units and dried on room temperature for 3 weeks.

2.1. Description of sampled areas

Profile 1

Control site on a saline tussocky meadow. It is the farthest from human activity. It is marshy, and inundated by water for 1-2 months during the spring period. By the 1970s the territory was at the margin of the natural lake system, since then, for almost 40 years it has been a buffer zone for the artificially created lake system too (Keveiné et al., 2000). However, conditions of hydrology and vegetation cover hardly changed.

Stratigraphy of profiles 1

The soil type along the profile is mostly sandy loess (Fig. 1) (Molnár, 1996). The ratio of the sand fraction (> 63 μm) is about 10 % in the whole depth of the profile (Fig. 2). The ratio of the aleu-

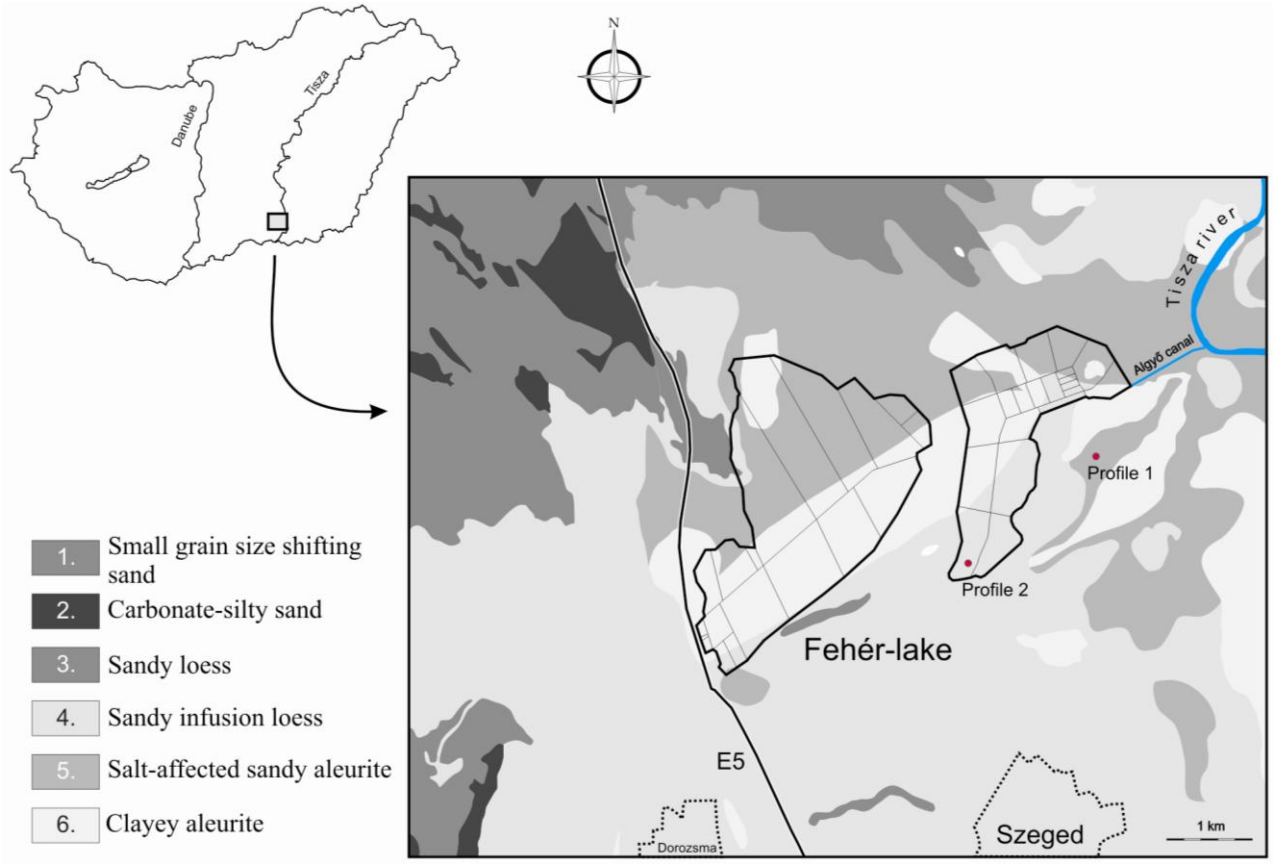

Fig. 1. Geological map of the sampling area and the location of profiles

rite fraction (63-2 μm) is the highest in the profile and with the exception of the upper 10 cm it is increasing with depth. The ratio of the clay fraction (< 2 μm) is the opposite of the aleurite fraction, it is decreasing with depth. The horizon A (from 0 cm to 30 cm) of the profile contains over 3 % of total organic carbon (TOC) that is decreasing to 0% at 100 cm. This level has a loose structure and a light brownish black color. The accumulation of salt can be founded in the depth of 50 cm. It is a level of the horizon B, too. Under this layer the carbonate starts to appear in the profile, it is indicated by the yellowish grey color of the sediment, too.

Profile 2

Directly affected by human activities. It is inundated artificially each year by 1-1.5 m water from April till October. During March-April 10-20 cm high vegetation can develop. By the 1970s this area was located in the central part of the natural lake system. Following the earthworks of the 1970s it has been used for fish breeding (Keveiné et al., 2000).

Stratigraphy of profiles 1

The soil type along the profile is mostly sandy infusion loess (Fig. 1) (Molnár, 1996). The grain size ratios show more difficult distribution than in the case of profile 1 (Fig. 3). The ratio of the sand fraction is higher than in the first case (20-30 %), it is decreasing from the surface to 60 cm and it is apparently increased in the level of 75-95 cm. The distribution of aleurite (~ 50%) and clay (~ 20%) fraction is quite uniform. The horizon A of the profile is relatively thin (10 cm depth from the surface) and contains only about 1 % of TOC. The amount of TOC is 0% below the level of 100 cm. This level has a loose structure and a light yellowish brown color. The boundaries of horizon B and C are not distinguished because this profile looks like disturbed by the water flow.

2.2. Analytical methods

Data of the Rock-Eval pyrolysis were measured with Oil Show Analyzer: preheat for 4 minutes on 108 °C, programmed pyrolysis with a 25 °C/min ramp rate till 600 °C. Subsequently, the samples were oxidized in a constant airflow for 7 minutes on 600 °C. The proportion of different OM groups was determined by the mathematical deconvolution of Rock-Eval pyrograms (Disnar et al., 2003). In order to determine more precisely the origin of OM the C_{org}/N ratio (Meyers, 2003) was also measured in 7 samples.

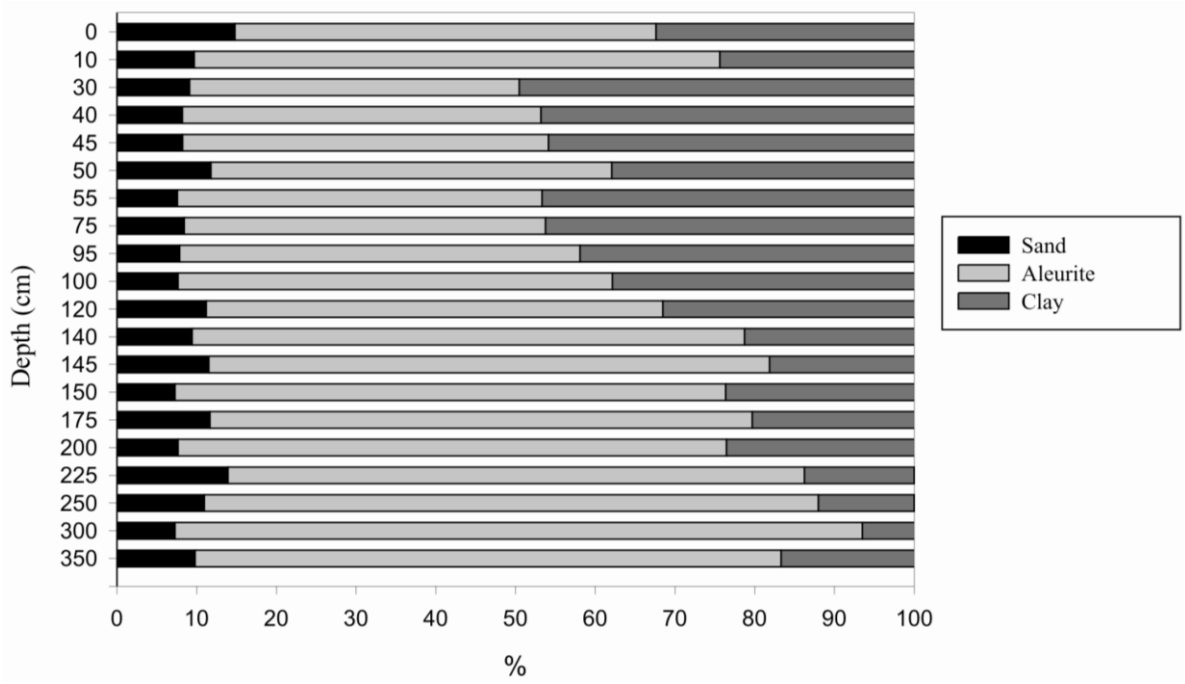

Fig. 2. Grain size distribution of profile 1.

3. Results and discussion

Total organic content (TOC) was measured from 160 samples concerning the two profiles. Based on the results, only the upper 100 cm section of both profiles contained an appreciable amount of OM, going deeper the concentration of OM was below

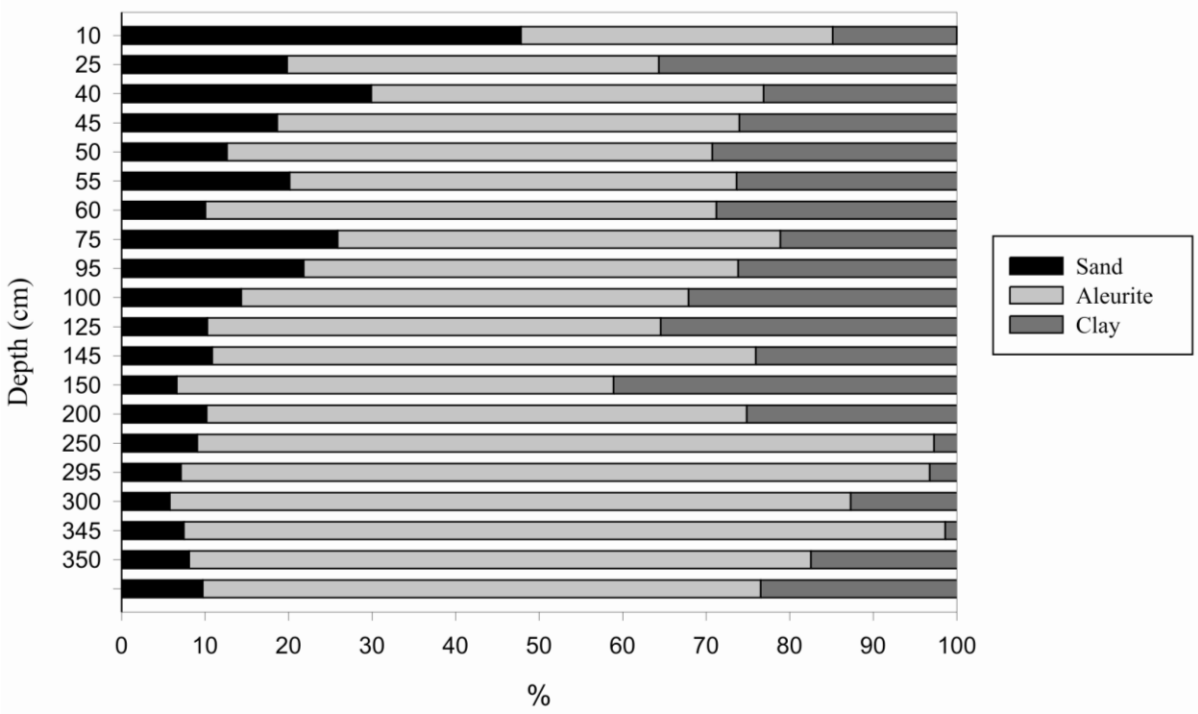

Fig. 3. Grain size distribution of profile 2.

the detection limit. As a consequence, detailed Rock-Eval analyses were only performed on the upper 100 cm layer of the profiles.

Concerning both parameters the differences between the two sites are striking (Table 1). TOC values varied between 0.2 and 2.0 % in the samples. These values are lower than usual OM concentrations measured in lake sediments (Das et al., 2008). In Prof.1 TOC values are higher and show a continuous decrease with depth (Fig. 4).

Nevertheless, the amount and distribution of TOC measured in Prof.2 are very much different (Fig. 4).

Table 1. Average values of organic carbon contents, HI and the relative contribution of major classes in the profile 1 and profile 2.

Depth (cm)	TOC (%)		HI (mgHC/gsoil)		F1 (%)		F2 (%)		F3 (%)		Corg/N	
	Prof1	Prof2	Prof1	Prof2	Prof 1	Prof 2	Prof 1	Prof 2	Prof 1	Prof 2	Prof 1	Prof 2
0	2.00	1.34	135	115	2.71	1.78	40.26	36.38	57.03	61.85		
5	2.10	1.13	135	80	4.05	4.10	35.79	39.73	60.16	56.17		
10	1.82	1.02	117	52	1.32	0.00	41.96	43.28	56.72	56.72	19.30	
15	1.09	0.83	67	49	0.00	1.51	53.63	39.42	46.37	59.07		16.10
20	1.03	0.89	64	58	1.74	3.30	49.13	38.91	49.13	57.79		
25	0.92	0.46	58	73	0.00	1.16	48.36	36.29	51.64	62.55	15.30	10.70
30	0.82	0.58	57	84	2.49	0.82	38.91	37.16	58.60	62.02		
35	0.73	0.79	60	78	3.05	0.87	50.61	36.29	46.34	62.84		
40	0.80	0.84	50	55	0.39	0.00	49.25	35.66	50.36	64.34		
45	0.67	0.43	46	79	3.62	2.70	44.43	35.28	51.95	62.02		
50	0.59	0.58	45	70	2.92	5.88	37.83	35.58	59.26	58.54		16.90
55	0.62	0.63	48	53	2.70	1.43	60.11	36.08	37.19	62.50		
60	0.53	0.58	116	67	22.52	0.89	25.85	40.72	51.62	58.40		
65	0.39	1.19	56	105	3.43	3.07	36.47	31.77	60.10	65.16		
70	0.35	1.37	45	91	1.69	3.12	35.35	30.52	62.96	66.36		13.30
75	0.29	1.13	51	74	1.76	0.00	36.36	33.97	61.88	66.03	8.80	
80	0.32	0.99	43	68	4.03	0.00	37.81	36.00	58.17	64.00		
85	0.24	0.87	79	71	8.04	0.00	47.50	35.21	44.46	64.79		
90	0.21	0.75	69	67	0.00	0.00	5.78	37.85	94.22	62.15		
95	0.20	0.60	64	60	3.97	0.00	28.35	32.43	67.68	67.57		

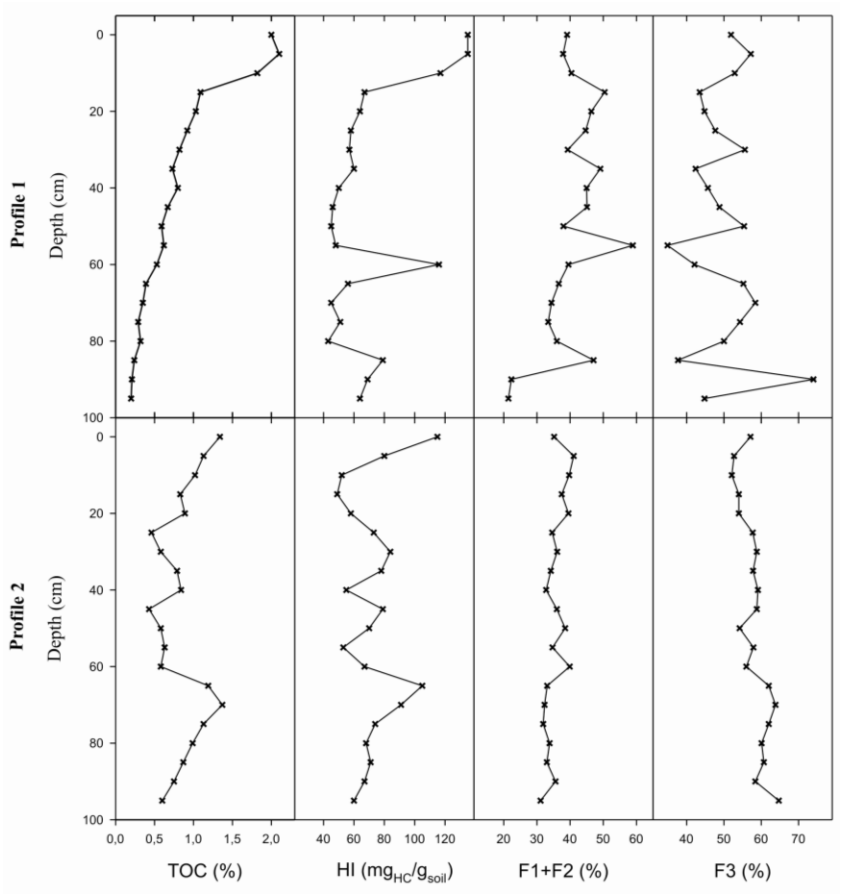

Fig. 4. TOC, HI, F1+F2, F3 values of the profiles.

TOC values are lower, and their downward change is uneven. From the surface till 60 cm with some smaller exceptions a decreasing tendency can be seen, but below 80 cm its value increases above 1 %. In both profiles the upper 15 cm has a higher TOC, which can be explained by the introduction of fish breeding in the 1970s. The distribution of Hydrogen Index (HI) is similar to that of TOC in both profiles, thus it is less even in case of the lake profile. The proportional variation of bio and geopolymers also refers to diverse sedimentation and transformation processes. Basically, the amount of biopolymers (F1, F2) in the sediment is similar to that of immature geopolymers (F3). However, the values measured for inert geopolymers (F4) are negligible compared to the previous three parameters, thus values of polymers are represented on ternary plots (Figs. 5). On the basis of ternary plots representing the proportional distribution of bio and geopolymers, it is obvious that the values in Profile 1 can be classified into several groups (Fig. 5), while in Profile 2 they are almost entirely homogenous. These distributions and the change of F1+F2 and F3 with depth suggest that Profile 1. was periodically inundated and then desiccated in its natural state on the margin of the lake system. Both in its natural and present situation Profile 2 has been the farthest from dryland environments, therefore the accumulation and preservation of OM was more even here. This is also reinforced by C_{org}/N ratios. In Profile 1 values refer to low algae (8.8) and much higher dry land (19.3) origin of OM (Meyers, 2003), which can be another proof of temporary water cover. On the contrary, in Profile 2 C_{org}/N values mostly sign a dry-land origin, i.e. in the middle of the lake system sediments preserved the remainings of dry-land plants, transported there presumably by wind. Although the amount and maturity of OM varied over time on the basis of TOC and HI values, the dry-land supply seems to be inevitable.

4. Conclusions

In our work we mainly aimed at the characterization of OM accumulating in shallow saline lake sediments with special hydrological conditions. We also attempted to answer whether human activity can result in detectable changes in OM characteristics. In general, the OM parameters measured in the two geologically and pedologically similar

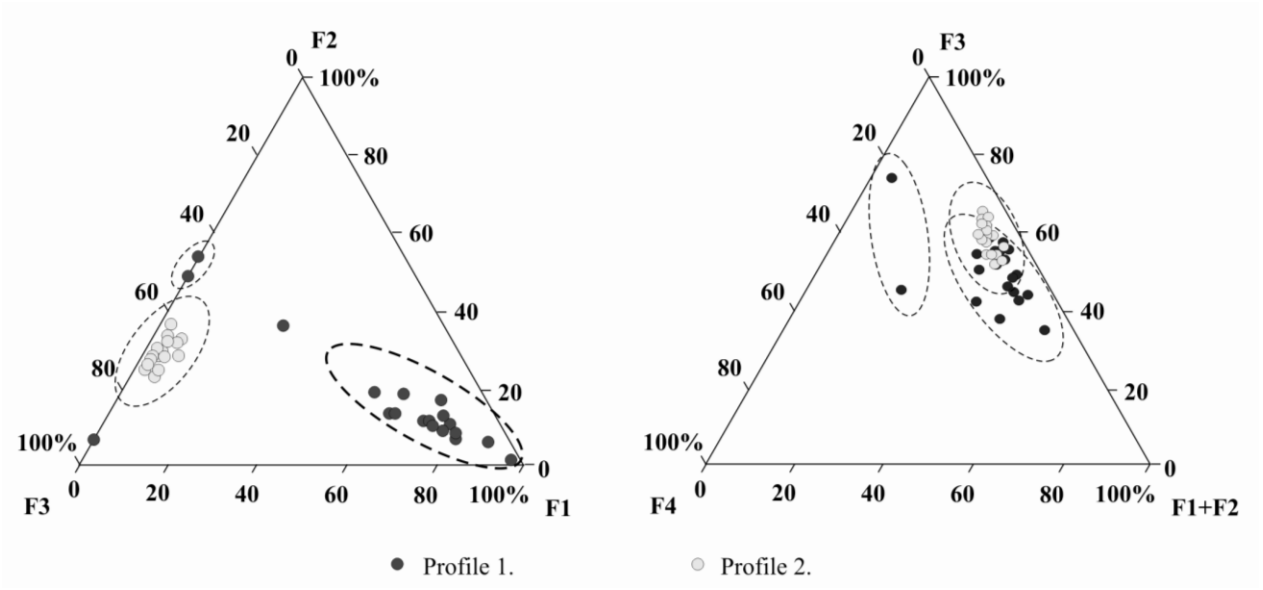

Fig. 5. Rates of F1, F2, F3, F4 fractions in the profiles.

profiles were very different, and values mainly depend on hydrological conditions and the degree of human influence. In both profiles the increased TOC above 15 cm refers to human activity. Although both profiles have the similar depositional environment, significant difference can be seen between the profiles. The profile 1 used to be located in coastal natural territory till 1970 and the profile 2 represents a constant water-irrigated fields. The TOC distribution in profile 1 corresponds well to the OM distribution in meadow soils (Dismar et al., 2003): due to permanent vegetation cover and a continuous OM supply, in the oxidative environment of the porous media the transformation of OM is even. The fluctuation of F1+F2 and F3 values in Profile 1. suggests that the OM content of the marginal territory (both in its natural and present state) is determined by the alternation of dry and wet periods, sometimes with a high algae production in slack waters (It can be seen on the increased HI in fig. 4). The variation of values in case of profile 2 refers to periodical differences in sedimentation conditions. These results are also reinforced by C_{org}/N ratios. In profile 2 F1+F2, F3 values and C_{org}/N ratios suggest that OM has always had a dry-land origin, however in terms of the quantity and maturity of OM well definable sedimentation cycles can be identified here as well. In case of profile 2 the increased amounts of TOC and HI in depth of ~30 cm and ~70 cm indicate the water covered period and the high algae production. In case of both profiles significant changes can be detected in the origin, quantitative and qualitative parameters of OM at depths of 15, 30 and 65-70 cm, which proves that the two sites belonged to the same depositional system, and similar changes affected them during sediment formation. Based on the F1, F2 and F3 values, the OM in the sediment of the study areas is primarily young and unaffected by transformation processes. The downward change of biopolymers (F1+F2) and immature geopolymers (F3) is highly variable in case of the meadow profile, while it is much more even in the lacustrine profile.

Based on the data it can be assess that the lake sediments can preserve the small changes in the OM accumulation. If the present results are compared to pH values and mineral compositions (Bozsó et al., 2008) then it turns clear that salinization processes do not have fundamental influence on the synsedimentary characteristics of OM, and preservation is more directly determined by the actual deposition and hydrological conditions.

Acknowledgements

The financial background of this work was ensured by the Hungarian National Science Found (OTKA), Grant No. T-48325.

References

Ariztegui D., Chondrogianni C., Lami A., Guilizzoni P., Lafargue E., 2001. Lacustrine organic matter and the Holocene paleoenvironmental Record of lake Albano (central Italy). J. of Paleolimnology 26, 283-292.

Bozsó G., Pál-Molnár E., Hetényi M., 2008. Relations of pH and mineral composition in saltaffected lacustrine profiles. Cereal Research Communications 36, 1463-1466.

Das B., Nordin R., Mazumder A., 2008. An alternative approach to recontructing organic matter accumulation with contrasting watershed disturban-ce histories from lake sediments. Environmental Pollution 155, 117-124.

Disnar J.R. Guillet B., Keravis D., Di-Giovanni C., Sebag D., 2003. Soil organic matter (SOM) characterization by Rock-Eval pyrolysis: scope and limitations. Organic Geochemistry 34, 327-343

HeténYi M., Nyilas T., M-Tóth T., 2005. Stepwise Rock-Eval pyrolysis as a tool for typing heterogeneous organic matter in soils. J. of Anal. Appl. Pyrolysis 74, 45-54.

Keveiné B.I., Mucsi L., Tímár B., 2000. The changes of state of the Fehér Lake at Szeged. In: Frisnyák, S. (Ed.), The historical geography of the Hungarian Great Plain. Nyíregyháza, pp. 53–66. (in Hungarian with English abstract).

Molnár B., 1996. The geological and hydrogeological characteristic of Fehér-lake at Szeged, Hungary. Hidrology Bulletin 76/5, 266-271. (in Hungarian with English abstract).

Meyers P.A., 2003. Applications of organic geochemistry to paleolimnological reconstructions: summary of examples from the Laurentian Great Lakes. Organic Geochemistry 34, 261-290.

Sebag D., Disnar J.R., Guillet B., Di Giovanni C., Verrecchia, E.P., Durand, A., 2006. Monitoring organic matter dynamics in soil profiles by Rock-Eval pyrolysis: bulk characterization and quanti-fication of degradation. European Journal of Soil Science doi: 10.1111/j.1365-2389.2005.00745.x

Tóth T., Szendrei G., 2006. Types and distribution of salt affected soils in Hungary, and the characterization of the processes of salt accumulation. Topographia Mineralogica Hungariae IX, 7-20.

Scientific Annals, School of Geology, Aristotle University of Thessaloniki Proceedings of the XIX CBGA Congress, Thessaloniki, Greece	Special volume 100	47-54	Thessaloniki 2010

ENVIRONMENTAL IMPACT OF Pt, Pd, Rh AND Au FROM CATALYTIC CONVERTERS ALONG ROADSIDES: THE CASE OF ATTICA, GREECE

Economou-Eliopoulos M. and Sfendoni T.

Department of Geology and Geoenvironment, University of Athens, Panepistimiopolis, 15784 Athens GR, econom@geol.uoa.gr

Abstract: Platinum (Pt), palladium (Pd), rhodium (Rh) and gold (Au) were investigated along highways of Attica, Greece, with varying traffic, like Katehaki, Messoghion, the intersection between Katehaki, Messoghion and Acharnon avenues, and residential roads, like Pindos and Navarinou roads. Platinum ranges between 110 and 960 ppb in dust samples and from 44 to 820 ppb in soils, Pd ranges between 90 and 1300 ppb in dust samples and from 36 to 1100 ppb in soils. The analysis of dust collected from parts of the roadsides closed to water sewerages reached as high as 2070 ppb Pt and 1980 ppb Pd contents. Gold ranges from 14 to 990 ppb Au (average 230) in dust samples and from 27 to 160 ppb Au (average 95) in soil ones. Any relationship between Au and Pt or Pd is not obvious. The significant fraction of the traffic-related emissions, reaching values over 4 ppm (Pt+Pd), suggest that they may be concentrated into local water systems resulting an environmental risk. Palladium was the most abundant PGE in the grasses ranging from 0.6 to 23 ppb (average 6.8 ppb), Pt ranges between 2.3 and 6.6 ppb (average 4.2 ppb) while Rh is < 0.1 ppb. Average values of the Pd/(Pd+Pt+Rh), Pt/(Pd+Pt+Rh) and Rh/Pd/(Pd+Pt+Rh) ratios decrease from 0.62 to 0.33 and 0.05 respectively, suggesting the Pd>Pt>Rh bioavailability order.

Key words: catalytic converter, recycle, environment, automobile emission, bioavailability, Greece

1. Introduction

The increased use of platinum (Pt), palladium (Pd), and/or rhodium (Rh) in automobile catalyst converters, has led to their release into the environment and biological accumulation on roadsides, since 1974 in USA and 1993 in European countries (Hoffman, 1989; Zereini et al., 1998; Palacios et al., 2000; Ely et al., 2001; Jarvis et al., 2001; Kendal, 2004; Croy et al. 2008). Catalytic converters are used to treat automobile emissions by catalysing the oxidation of carbon monoxide and hydrocarbons, and the reduction of NOx. They are constructed by applying a film of 1-3g Pt- Pd-Rh alloy, in proportion typically 0.08% Pt, 0.04% Pd and 0.005-007% Rh, on a ceramic "monolith" (Hoffman, 1988, 1989). The amount and rate of the Pt, Pd and Rh release from catalytic converters is affected by the speed of the automobile, type of engine, type and age of catalyst, and type of fuel additives (Ely et al., 2001; Whiteley and Murray, 2003).

The investigation of samples from road dust, soil and grass indicated that greater proportion of PGE emissions is from automobile catalysts, in the form of nanometer-sized catalyst particles, which deposit on roadside surfaces. In soil, PGE can be transformed into more mobile species through complexation with organic matter and can be solubilised in low pH rainwater. There are indications that environmentally formed Pd species are more soluble and hence more mobile in the environment than Rh and Pt (Dahlheimer et al., 2007).

Average Pt and Pd concentrations in rural and suburban roadside top soils (2.0 and 1.4 ppb, respectively), and high-way roadside top-soil (140 ppb Pt, and 130 ppb Pd) have been determined in Athens, Greece, recently (Riga-Karandikos et al., 2006). In the present study platinum, palladiun, rhodium and gold along with other traffic related elements were determined (a) in road dust and roadside soils and (b) in grasses and tree-leaves close to highway roads of Attica, Greece, in an attempt to present an assessment of the autocatalyst derived PGE in Greece. They are compiled with published data and the possibility for their bioavailability is discussed.

2. Material and methods

The sampling areas selected for this pilot study include sites with varying traffic and driving style

(stop/start vs. constant speed): (a) parts of the Katehaki high-way road, to the east peripheral of Athens, from the intersection between Katehaki and Messoghion road to the turn to the Panepistimiopolis of Zografou, where there is a change in its geomorphological feature from almost flat to a relatively higher positive slope (b) the urban Messohgion road, from the intersection between Katehaki to Aghia Paraskevi, (c) the Pindos and Navarinou residential roads (d) a few only samples from the National high-way road Athens - Thessaloniki, from about 50 km, (e) the Iera odos and the (f) Acharnon high-way road (Fig.1).

of Geology and Geoenvironment, University of Athens.

All samples were analysed at ACME Laboratories, for Pt, Pd, Rh and Au, using the litharge (PbO) - collection fire-assay fusion for total sample decomposition, digestion of the Ag bead and ICP-MS analysis technique. Detection limits are 0.5 ppb for Pd, 0.1 ppb for Pt and Rh, and 1 ppb for Au. Trace element concentrations (Fe, Mn, Pb, Zn, Cu, Ni, Zr etc) in whole dust samples were determined by ICP/MS analysis at Activation Laboratories, Ltd, Canada, after an alkaline peroxide.

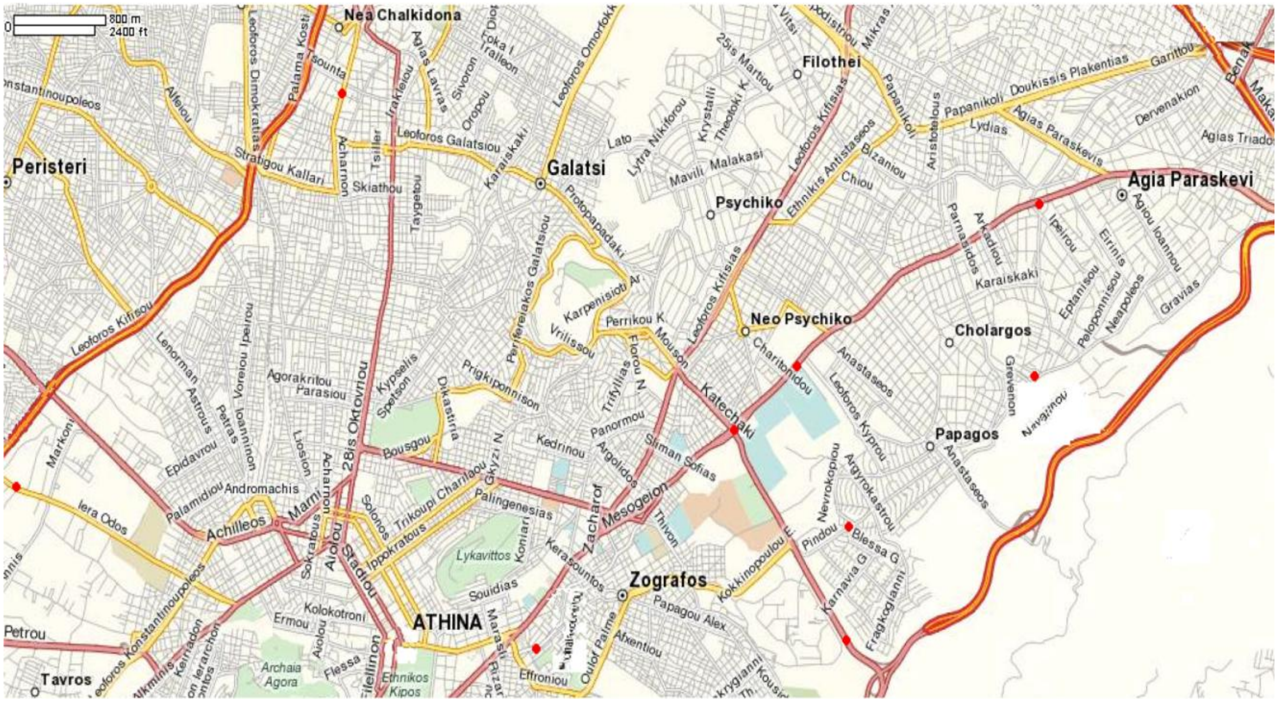

Fig. 1. Location map of Attica, showing the sites (●) of sampling.

Roadside dust samples (n = 29) were collected from the surface along roadways from the above major highways, major intersections and residential roads. Topsoil samples (n = 9) were taken from areas directly exposed to traffic emissions along the highways roadside and also from residential side streets, where traffic flows were low. They were collected from the surface soil (0-4 cm depth) with a plastic spatula in an area approximately 10 cm^2 and stored in plastic sample bags. They were air dried and then sieved using a nylon sieve to produce a 2 mm fraction. Grass samples (n = 22) and leaves from olive and *Laurus nobilis* trees (n = 7) were dried in an oven at 70 ^oC, and then powdered in an agate mortar. Sample preparation was undertaken at the Laboratories of the Department

Polished sections prepared from the most PGE-rich road dust samples (Katehaki road) were examined by reflected light microscopy and scanning electron (SEM). Quantitative analyses were carried out at the University of Athens, Department of Geology, using a JEOL JSM 5600 scanning electron microscope, equipped with automated OXFORD ISIS 300 energy dispersive analysis system. Analytical conditions were 20 kV accelerating voltage, 0.5 nA beam current, b2 μm beam diameter and 50 s count times.

3. Results

The presented analytical platinum-group element data demonstrate significant abundances of Pt, Pd and Au above background in each of the dust and

Table 1. Precious metal content in dust and soils along roadside.

Date (year, month)	**(ppb)**				
Sample location	Pt	Pd	Rh	Au	Pd/Pt
2006-10-KAT1.dust	710	1000	4	14	1,41
2006-10-KAT2.dust	960	1300	5	51	1,35
2007-3-KAT3.dust	440	630	130	60	1,43
2007-04-KAT6.dust	900	670	3	360	0,74
average	*750*	*800*	*35*	*121*	*1,23*
2007-04-KAT.S4.dust	1720	1570	6	71	0,91
2007-04-KAT.S5.dust	2420	2400	4	180	0,99
average	*2070*	*1980*	*5*	*125*	*0,95*
2007-03-KAT2-3.soil	200	196	bdl	93	0,98
2007-04-KAT-MES1.soil	440	510	bdl	160	1,16
2007-04-KAT-MES2.soil	820	1100	3	120	1,34
average	*610*	*800*		*140*	*1,25*
2007-04-Pi.soil	60	70	1,5	56	1,17
2006-10-MES1.dust	290	500	3	220	1,72
2007-03-MES2.dust	210	300	26	460	1,43
2007-04.P.MES3.dust	210	300	3	240	1,43
average	*255*	*365*	*17*	*307*	*1,53*
2006-10-MES1.soil	44	90	8	150	2,04
2006-10-MES2.soil	36	74	10	6	2,06
average	*40*	*82*			*2,05*
2007-03-P.MES.soil	230	360	2	143	1,58
2007-03.NAV.soil	150	230	34	26	1,5
2007-04-MIXAL.dust	400	550	bdl	990	1,38
2006-10-Iera Odos1.dust	500	750	22	90	1,5
2006-10-Iera Odos2.dust	230	350	24	25	1,52
average	*665*	*550*	*23*	*58*	*1,51*
2006-10-N.h.Ath-Th1.dust	190	220	20	27	1,16
2006-10-N.h.Ath-Th2.dust	120	180	16	70	1,5
average	*155*	*200*	*18*	*47*	*1,33*
07-03-N.h.Ath-Th1.soil	92	100	35	27	1,11
2007-05-ACHAR1.dust	380	650	24	120	1,7
2007-05-ACHAR2.dust	240	280	7	530	1,2
2007-05-ACHAR3.dust	140	180	2	120	1,3
2007-05-ACHAR4.dust	200	300	2	660	1,5
2007-05-ACHAR5.dust	320	660	47	1340	2,1
2007-05-ACHAR6.dust	170	260	bdl	160	1,5
2007-05-ACHAR7.dust	350	490	2	1000	1,4
2007-05-ACHAR8.dust	320	460	44	210	1,4
2007-05-ACHAR9.dust	300	450	49	300	1,6
2007-05-ACHAR10.dust	220	320	9	1040	1,4
2007-05-ACHAR11.dust	160	190	bdl	570	1,2
2007-05-ACHAR12.dust	110	90	bdl	210	0,8
2007-05-ACHAR13.dust	160	260	15	900	1,6
2007-05-ACHAR14.dust	170	220	13	550	1,3
2007-05-ACHAR15.dust	170	210	5	260	1,2
average	227	335	15	530	1,4
STANDARD FA-100S	48,1	48,6		49	

Symbols: KAT = Katehaki; MES = Messoghion; P.MES. = Aghia Paraskevi; NAV = Navarinou; MIXAL. = Michalakopoulou; N.h.Ath-Th = National high-way Athens-Thessaloniki; ACHAR = Acharrnon; bdl = below detection limit

soil samples, especially those closest to the road, whilst Rh is decreased to within error of background level (Table 1). Although present data are limited, they suggest an increasing trend between platinum and palladium contents in plants and the associated soils (Fig. 2, Tables 1 & 2) confirming previous aspect that the catalytic converter attrition is responsible for the elevated abundances along highways (Ely et al., 2001; Dahlheimer et al., 2007). Platinum ranges between 110 and 960 ppb (average 550 ppb) in dust samples and from 44 to 440 ppb (average 200 ppb) in soils (Table 1). Palladium ranges between 90 and 1300 ppb (average 680 ppb) in dust samples and from 36 to 820 ppb (300 ppb) in soils. Dust samples showed extremely high concentrations in those collected from small cavities on the road substrate, at the contact with water sewerage (Table 1, samples labelled as KAT.S4 and KAT.S5) exhibit as high as 2070 ppb Pt and 1980 ppb Pd. Gold ranges between 14 and 990 ppb Au (average 230) in dust samples and from 27 to 160 ppb Au (average 95) in soil samples. The lack of any relationship between Au and Pt or Pd is obvious (Table 1).

Representative dust samples from Katehaki, Messoghion, Iera odos roads and the National high-way road Athens - Thessaloniki, were analysed for several trace elements indicated Pb, Cr, Zn, Cu, Ni and Zr contents (Table 3). They range from 130 to 830 ppm Pb, 320 to 530 ppm Zn, 290 to 480 ppm Mn, 100 to 370 ppm Cu, 70 to 135 Cr, 60 to 160 ppm Ni, 11 to 18 ppm Ce, 3.1 to 4.6 ppm Y and 0.5 to 1.3 ppm Zr. Although the roadside dust is derived by various sources, such a composition fell within the typical range of traffic related metals in highways (Ely et al., 2001; Jarvis et al., 2001; Moldovan et al., 2002; Riga-Karandinos et al., 2006). Road dust (polished sections) and atmospheric particle emissions (collected on multiple filters, one day) from the Katehaki high-way peripheral road and were investigated by scanning electron microscope with energy-dispersive X-ray analysis. They showed abundant PM10 (smaller than 10 μm) and PM2.5 (smaller than 2.5 μm) particles which are dominantly crystalline materials such as quartz, calcite, barite, Al, Mg, K, Na-silicates, Fe, Ti, Mn-oxides, metal iron showing a varying degree of oxidation, Cr- , Pb- , and Ce-phases, and zirconium (Fig. 3). Elevated contents and and such Zr, Ce, Cr, Cu, Zn, Mn-phases may be related to brake wear emissions (Schaller, 1991).

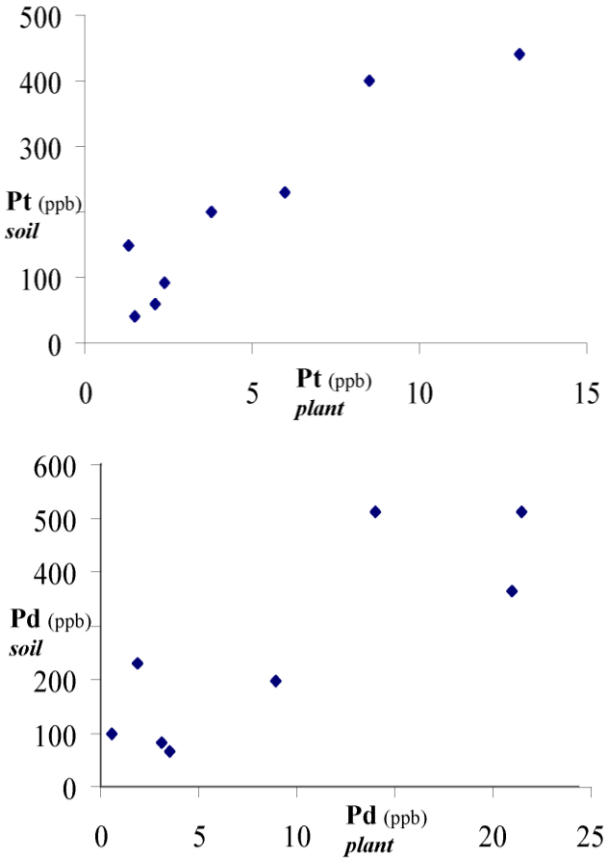

Fig. 2(a,b). There is an increasing trend between platinum and palladium contents in plants and the associated soils, along roadsides of Greece. Data from Tab. 1 & 2.

Palladium was the most abundant PGE in the grasses ranging from 0.6 to 23 ppb (average 6.8 ppb), while Pt ranges between 2.3 and 6.6 ppb (average 4.2 ppb), but compared to the analysed soils, the grasses contained the lowest PGE abundances. There is a good relationship between both Pd and Pt contents in plants with their corresponding contents in soils (Tables 1 & 2; Fig 2a,b). Concentrations below of 0.5 ppb Pd and 0.1 ppb Pt were found in two grass samples in about 100 m distance from the roadside confirming previous studies, e.g. PGE abundances in soils decreased away from road surfaces (Ek et al., 2004; Dahlheimer et al., 2007).

4. Discussion

The presented PGE data from highways of Greece (Table 1) demonstrate that catalytic converter attrition is responsible for the elevated abundances and that concentrations of PGEs increased with traffic density, reaching values up to 2070 ppb Pt and 1980 ppb Pd in dust. Gold, ranging between 14 and 990 ppb (average 310) in dust samples and from 27 and 160 ppb Au (average 95) in soils, is much lower than PGE and does not show any relationship with Pt and Pd, confirming previous study in U.K. (Farago et al., 1996).

Table 2. Precious metal content in grasses and tree-leaves along roadside.

Date (year, month),	(ppb)				
sample location	Pt	Pd	Rh	Au	Pd/Pt
Grassy					
2006-10-KAT.G1	2	3,8	bdl	21	1,9
2007-03-KAT.G2	7	20	bdl	25	2,9
2007-03-KAT.G3	10	23	5	22	2,3
2007-04-KAT.G4	3,2	5,3	0,1	13	2,3
2007-04-KAT.G5	1,2	2,1	bdl	5	1,75
2007-04-KAT.G6	1,5	1,7	bdl	38	1,13
2007-04-KAT.G7.	1,8	4,8	0,2	10	2,67
average	*3,8*	*8,9*			*2,2*
2007-03-MES-KAT.G8	16	20	1,4	22	1,2
2007-03-MES-KAT.G9	10	8	bdl	120	0,8
average	*13*	*14*			*1,07*
2006-10-MES.G10	2	4,4	bdl	250	2,2
2006-10-MES.G11	1	1,8	bdl	16	1,8
average	*1,5*	*3,1*			*2,07*
2007-03-P.MES.G12	6	21	bdl	16	3,5
2006-10-Pi-G13	0,2	4	bdl	7	
2006-10-Pi-G14	1,1	6,5	bdl	2	5,9
2007-03-Pi.G15	2,5	2,4	bdl	1350	1
2007-03-Pi.G.16	4,6	1	bdl	35	0,22
average	*2,7*	*3,3*			*2,37*
2006-10-NAV.G.17	1,3	2	bdl	16	1,5
2006-10-NAV.G.18	0,8	4,7	bdl	170	1,5
2007-03-NAV.G19	1	0,6	bdl	8	0,6
2007-03-NAV.G20	3,6	4,2	bdl	48	1,2
2007-03-NAV.G21	0,8	1,6	bdl	28	2
average	*1,5*	*2,2*			*1,36*
2007-03-N.h.Ath-Th3.G	2,4	0,6	bdl	21	0,25
2007-03-KAT-T1	3,5	4	0,7	110	1,1
2007-03-KAT-T2	5,2	4,4	0,7	30	0,9
2007-04-KAT-T3	4	6,1	bdl	7	1,52
average	*4,2*	*4,6*			*1,17*
2007-03-P.MES.T4.	2,8	2,5	bdl	44	0,9
2007-03-MES.T5	4	6	bdl	55	1,5
2007-03-P.MES.T6	1,2	3,8	bdl	67	3,2
2007-03-P.MES.T7	2,2	2,3	bdl	36	1,05
average	*2,5*	*3,6*			*2,22*
background-G1	<0.1	<0.5	bdl		
background-G2	<0.1	<0.5	bdl		
STANDARD FA-100S	41	40,6	38,2		

Symbols: G = grass; T = tree; KAT = Katehaki; MES = Messoghion; P.MES. = Aghia Paraskevi; NAV = Navarinou; MIXAL. = Michalakopoulou; N.h.Ath-Th = National high-way Athens-Thessaloniki, bdl = below detection limit.

Traffic emissions and their impact on urban air quality, health, and atmospheric processes have been the subject of increasing interest in recent years (Ely et al., 2001; Dahlheimer et al., 2007). The amount and rate of PGE emissions are affected by the speed of the automobile, and the type and age of the catalyst (Artelt et al., 1999). Several studies have focused on the comparison between the gasoline engine type (Pt-Pd-Rh and Pd-Rh) and diesel engine catalysts (Pt), and the three-way catalytic converter: Reduction of nitrogen oxides to nitrogen and oxygen ($2NO_x \rightarrow xO_2 + N_2$), oxidation of (toxic) carbon monoxide to harmless carbon dioxide ($2CO + O_2 \rightarrow 2CO_2$) and oxidation of unburnt carcinogenic hydrocarbons (HC) to carbon dioxide and water ($2C_xH_y + (2x+y/2)O_2 \rightarrow 2xCO_2 + yH_2O$). Platinum and rhodium are used as a reduction catalysts, while platinum and palladium are used as an oxidization catalyst (Fly et al., 2001; Moldovan et al., 2002; Dahleimer et al., 2007).

The PGE level along the highways of Greece (Table 1) that may be washed by rain and concentrated into local water systems, is comparable to that given for many other countries (Hodge and Stallard, 1986; Ely et al., 2001; Dahlheimer et al., 2007). Although some authors have suggested that such Pt-Pd concentrations are high enough to recover PGE from roadside soils and/or dust (Hilliard and Henry, 1998 Hoffman, 1988; Hilliard, 1998, 2001) available data for Greece are very limited for such an assessment. However the recovery of PGE from scrapped catalysts could contribute to the recycled PGE, in particular Pt, depending on the materials composition of the catalyst (Hilliard and Henry, 19989) in every country.

5. Bioavailability of PGE

Platinum concentrations in urban air have increased by more than two orders of magnitude in the last 20 years. It is present mainly in the small particle size fraction (0.5-8 μm), and pose a poten-

Table 3. Trace element contents in dust along roadside

Samples	KAT1	MES1	MES2	Iera Odos	N.h.Ath-The1	STANDARD
	dust	dust	dust	dust	dust	DS7
Date	2006-10	2006-10	2007-03	2006-10	2006-10	
				(wt %)		
Fe	2,0	1,7	1,8	2,6	2,4	2,41
Al	0,4	0,4	0,6	0,3	0,7	1,03
Ti	0,01	0,014	0,01	0,01	0,01	0,12
Mg	0,7	0,81	0,68	1,24	1,01	1,02
Ca	18,1	21,5	17,2	24,9	20,3	0,93
Na	0,01	0,03	0,02	0,06	0,02	0,12
K	0,08	0,07	0,15	0,1	0,2	0,48
P	0,06	0,04	0,06	0,05	0,11	0,08
S	0,01	0,01	0,03	0,01	0,01	0,17
				(ppm)		
Cr	120	103	71	135	113	252
Cu	370	520	200	650	160	103
Pb	830	130	860	306	230	68
Zn	320	320	370	530	490	410
Ni	66	63	57	68	158	55
Co	7	7	8	6	13	10
Mn	290	400	350	480	400	620
As	12	13	15	9	11	52
Sr	79	100	75	114	331	75
Ba	120	114	123	125	120	390
Cd	0,5	0,4	0,9	1	0,8	6
Sb	17	16	12	14	5	5
La	7	5	6	12	7	13
Ce	18	11	13	14	15	39
Sc	1,1	1,4	1,5	1	2,2	2,8
Zr	0,8	0,5	1	0,2	1	6
Y	3,5	3,1	4,4	2,4	4,6	5,5

Symbols: KAT = Katehaki; MES = Messoghion; NAV = Navarinou; Pi = Pindos; N.h.Ath-Th = National high-way Athens-Thessaloniki

tial health risk (Zereini et al., 2001). The results of the speciation studies indicated that various naturally occurring ligands have the potential to increase the mobilities of Pt, Pd and Rh through the formation of soluble complexes that can easily be transported in environmental and biological systems, (Colombo, 2008). The determination of the PGE content of different plants grown on contaminated soil close to highways shows a transfer of the PGE from the contaminated soil to the plants (Table 2). The enrichment of the Pd and Pt contents in grasses and tree-leaves (average 5.6 ppb and 3.8 ppb, respectively) along roadsides (Table 2) confirm the aspect that under appropriate pH and redox potential conditions (humic or fulvic acids) they are more mobile (Lustig et al., 1997; Lustig and Schramel., 2000; Kraemer, 2004; Dahleimer et al., 2007). The good positive relationship between both Pd and Pt contents in plants with their corresponding contents in soils (Fig 1a,b) is consistent with their solubility in soils. It has been demonstrated that the PGEs can be mobilized by natural organic matter and that humic acids and some organic ligands have been shown to enhance the solubility of various forms of Pt and Pd (Wood, 1990, 2005; Wood et al., 1994; Artelt et al., 1999; Rauch and Morrison, 2000). Experimental data on the bioaccumulation of Pt, Pd and Rh by grass grown with nutrient solutions containing these metals showed that most of the metals were accumulated in the roots, and only a small fraction was metabolized and transported to the leaves (Lesniewska et al., 2004). Klueppel et al. (1998) showed that Pt was bound to sulphur in a mechanism involving a phytochelatine (low molecular mass peptide).

In addition, the presented data on the Pt, Pt and Rh contents in grasses indicated the following bioavailability order Pd>Pt>Rh, as is exemplified by the higher Pd than Pt content (Table 2), and the decreasing average values of the ratios Pd/(Pd+Pt+Rh), Pt/(Pd+Pt+Rh) and Rh/Pd/(Pd+Pt+Rh) from 0.62 to 0.33 and 0.05, respectively. This bioavailability order is consistent with the experimental data on synthetic siderophore desferrioxamine- DFO-B enhances the solubility of Pt and Pd due to the formation of Pt- and Pd-DFO-B aqueous complexes at pH 7 (Danhleimer et al., 2007).

6. Conclusions

Although further detailed investigation of Pt, Pd, Rh and Au contents in dust, soil and plant samples along roadsides is required to define their distribution in space and time, present data lead to the following conclusions:

1) Significant abundances of Pt, Pd and Au were recorded in each of the dust and soil samples, whilst Rh content was very low.
2) Palladium in the grasses was more abundant (average 6.8 ppb) than Pt (average 4.2 ppb) and Rh (< 0.1 ppb), suggesting that it is more bioavailable to plants.
3) An increasing trend between platinum and pal-

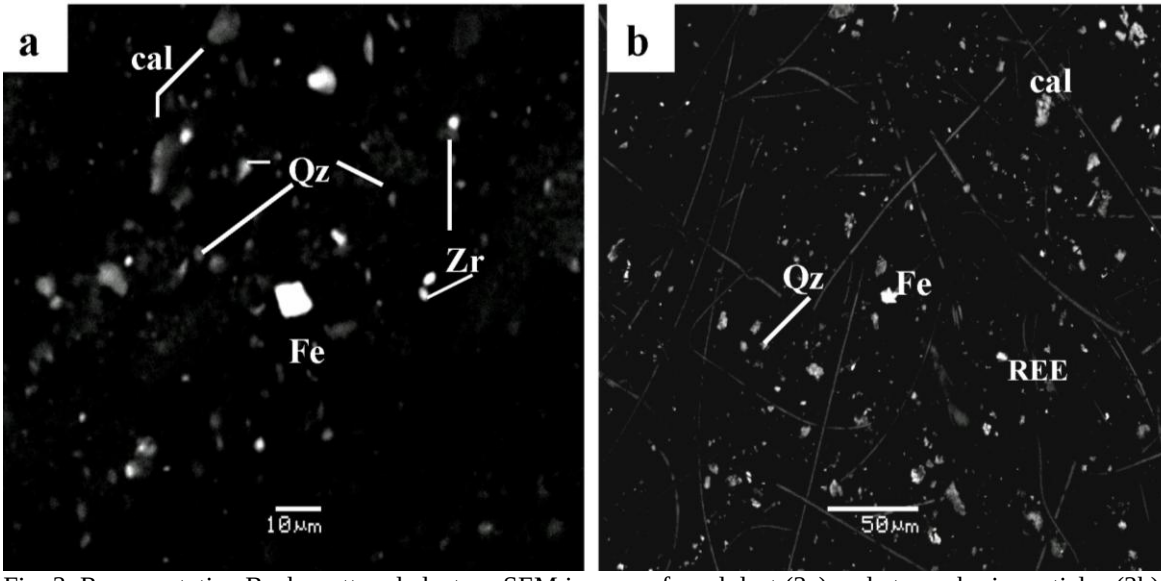

Fig. 3. Representative Back scattered electron SEM images of road dust (3a) and atmospheric particles (3b) collected from the Katehaki high-way peripheral road. There are abundant PM10 and PM2.5 particles, dominated by quartz (Qz), calcite (cal), barite, Al, Mg, K, Na-silicates, metal-Fe (Fe), Fe, Ti, Mn-oxides, Cr-bearing alloy, Ce-minerals (REE) and zirconium (Zr).

ladium contents in plants and the associated soils, along roadsides of Greece is consistent with their solubility in soils and confirm their bioavailability.

4) The highest values up to 2070 ppb Pt and 1980 ppb Pd were determined in dust samples collected from roadsides near water sewerages, although Pd content was higher than Pt in the majority of the analysed dust, soil and plant samples.

Acknowledgements

The University of Athens is greatly acknowledged for the financial support of this work. We thank two anonymous reviewers for their constructive comments and suggestions.

References

Artelt S., Creutzenberg O., Kock H., Levsen K., Nachtigall D., Heinrich U., Rühle T., Schlogl R., 1999. Bioavailability of fine dispersed platinum as emitted from automotive catalytic converters: a model study. Sci Total Environ 228:219–242.

Croy J.A., Mostafa S., Hickman L., Heinrich H., Roldan Cuenya R., 2008. Bimetallic Pt-Metal catalysts for the decomposition of methanol: Effect of secondary metal on the oxidation state, activity, and selectivity of Pt. Applied Catalysis A: General 350, 207–216.

Cowley A., Steel M., 2001. Platinum 2001. Johnson Matthey, UK, 52 pp

Colombo C., 2008. The Speciation and Bioavailability of Platinum, Palladium and Rhodium in the Environment. Ph.D. Thesis, Department of Earth Science and Engineering, Imperial College London, p. 201.

Dahlheimer S.R., Neal C., Fein A., 2007. Potential Mobilization of Platinum-Group Elements by Siderophores in Surface. Environmental Science & Technology 41, 870-875.

Ek K.H., Morrison G.M., Rauch S., 2004. Environmental routes for platinum group elements to biological materialssa review. Environmental Science & Technology 334-35.

Ely J.C., Neal C.R., Kulpa C.F, Schneegurt M.A., Seidler J.A., Jain J.C., 2001. Implications of platinum-group element accumulation along U.S. roads from catalytic-converter attrition. Environmental Science & Technology 35, 3816 –3822.

Farago M.E., Kavanagh P., Blanks R., Kelly J., Kazantzis G., Thornton I., Simpson P.R., Cook J.M., Parry S., Hall G.M., 1996. Platinum metal concentrations in urban road dust and soil in the United Kingdom. Fresenius J Anal Chem 354, 660–663

Hilliard H.E., 1998. Platinum Recycling in the United States. USGS Survey Circular 1196-B. 1998.

Hilliard H.E., 2001. Minerals Yearbook: Platinum-Group Metals. USGS.

Hodge V.F., Stallard M.O., 1986. Environmental Science & Technology 20, 1058-1060.

Hoffman J.F., 1989. Precious and rare metal technologies. In: Thermae AE, Gondolier, I.H. (eds). Process metallurgy, 5. Elsevier, Amsterdam

Hoffman J.F., 1988. Recovering platinum-group metals from autocatalysts. J. Metall 40 (6), 40-44.

Jarvis K.E, Parry S.J., Piper J.M., 2001. Temporal and spatial studies of autocatalyst-derived platinum, rhodium, and palladium and selected vehicle-derived trace elements in the environment. Environmental Science & Technology 35, 1031 –1036.

Kendall T., 2004. Platinum 2004, Johnson Matthey, UK.

Klueppel D., Jakubowski N., Messerschmidt J., Stuewer D., Klockow D., 1998. Speciation of platinum metabolites in plants by size exclusion chromatography and inductively coupled plasma mass spectrometry. Journal of Analytical Atomic Spectrometry, 13(4), 255-262.

Kraemer S. M., 2004. Iron oxide dissolution and solubility in the presence of siderophores. Aquat. Sci. 66, 3-18.

Lesniewska B., Messersserschmidt J., Jakubowskin N., Hulanicki A., 2004. Bioaccumulation of platinum group elements and characterization of their species in Lolium multiflorum by size-exclusion chromatography coupled with ICP-MS. The Science of the Total Environment, 322(1), 95-108.

Lustig S., Zang S. L., Beck W., Schramel P., 1997. Influence of microorganisms on the dissolution of metallic platinum emitted by automobile catalytic converters. Environ. Sci. Pollut. Res., 4, 141-145.

Lustig S., Schramel P., 2000. Platinum bioaccumulation in plants and overview of the situation for palladium and rhodium. In: Zereini F, Alt F, editors. Anthropogenic platinum group element emissions and their impact on man and environment. Berlin: Springer, p. 95 –104.

Moldovan M., Palacios M.A., Gomez M.M., Morrison G., Rauch S., McLeod C., Ma R., Caroli S., Alimonti A., Petrucci F., Bocca B., Schramel P., Zischka M., Pettersson C., Wass U., Luna M., Saenz J. C., Santamaria J., 2002. Environmental risk of particulate and soluble platinum group elements released from gasoline and diesel engine catalytic converters. The Science of the Total Environment 296, 199-208.

Palacios M.A., Moldovan M., Gomez M.M., 2000. The automobile catalyst as an important source of PGE in the environment. In: Zereini F, Alt F, editors. Anthropogenic platinum group element emissions and their impact on man and environment. Berlin: Springer, 3 –14.

Riga-Karandinos A.N., Saitanis C. and Arapis G., 2006. First study of anthropogenic platinum-group elements in Roadside top-soils in Athens, Greece. Water, Air and Soil Pollution 172, 3-20.

Rauch S., Morrison G.M., 2000. Routes for bioaccumulation and transformation of platinum in the urban environment. In: Alt F, Zereini F, editors. Anthropogenic Platinum-Group-Element emissions and their Impact on Man and Environment. Berlin: Springer Verlag.

Schaller K.H., 1991. Zirconium. in: Metals and their compounds in the environment, E. Merian (Ed.), VCH, Weinheim, 1343-1348.

Whiteley J.D., Murray F., 2003. Anthropgenic platinum group element (Pt, Pd and Rh) concentrations in road dusts and roadside soils from Perth, Western Australia. The Science of Total Environment 317, 121-135.

Wood S.A., 1990, The interaction of dissolved platinum with fulvic acid and simple organic acid analogues in aqueous solutions: The Canadian Mineralogist, 28, 665-673.

Wood S.A., 2005. The effect of organic ligands on the mobility of the PGE in soils and natural waters: Implications for exploration and the environment. Geochimica et Cosmochimica Acta 69, A329.

Wood S.A., Tait C.D., Vlassopoulos D., Janecky D.R., 1994. Solubility and spectroscopic studies of the interaction of Pd with simple carboxylic acids and fulvic acid at low temperature: Geochimica et Cosmochimica Acta, 58, 625-637.

Zereini F., Dirksen F., Skerstupp B., Urban H., 1998. Sources of anthropogenic platinum-group elements (PGE): automotive catalysts versus PGE-processing industries. Environ Sci Pollut Res 5, 223 –230.

Zereini F., Wiseman, C., Alt F., Messerschmidt J., 2001. Platinum and rhodium concentrations in airborne particulate matter in Germany from 1988 to 1998. Environmental Science & Technology, 35(10), 1996.

Scientific Annals, School of Geology, Aristotle University of Thessaloniki Proceedings of the XIX CBGA Congress, Thessaloniki, Greece	Special volume 100	55-62	Thessaloniki 2010

PURIFICATION OF MUNICIPAL WASTEWATERS AND PRODUCTION OF ODORLESS AND COHESIVE ZEO-SEWAGE SLUDGE, USING HELLENIC NATURAL ZEOLITE

Filippidis A.

Aristotle University of Thessaloniki, Department of Mineralogy-Petrology-Economic Geology, 54124 Thessaloniki, Hellas, anestis@geo.auth.gr

Abstract: Treatment of municipal wastewaters ($pH_{initial}$ 8.2-8.9), with 7.5 g of Hellenic Natural Zeolite (HENAZE) of a grain-size < 1.5 mm, gave overflowed clear water of pH 7.3-7.8, free of odors and improved quality parameters by 89.9-96.7 % for the color, 89.0-98.5 % for the suspended particles, 93.7-97.2 % for the chemical oxygen demand (COD), 92.9-99.3 % for the P_2O_5 content and 98.3-99.9 % for the NH_4 content. The improvement of the quality parameters for the clear water increases with increasing stirring time of the treatment experiments. The correlation coefficient is 0.9423 for the P_2O_5 content, 0.9323 for the suspended particles, 0.9282 for the chemical oxygen demand (COD) and 0.8854 for the color. The correlation coefficient for the NH_4 content and pH are < 0.60. The HENAZE comes from Ntrista stream of Petrota village of Trigono Municipality of Evros Prefecture, North-eastern Greece. HENAZE contains 89 wt. % HEU-type zeolite and exhibit an ammonia ion exchange capacity (sorption ability) of 226 meq/100g. The mineralogical composition and the unique physico-chemical properties, make the HENAZE suitable material for numerous environmental, industrial, agricultural and aquacultural applications, such as: Animal nutrition, soil amendment for agriculture, pH soil regulation, greenhouse and flowers substrates, durability and health improvement of lawn, purification of industrial and municipal wastewaters, treatment of sewage sludge, odor control, fishery and fish breeding, gas purification and drying systems, oxygen enrichment of aquatic ecosystems, improvement of drinking water quality, constructed wetlands and wastewater treatment units. The treatment gave as precipitate odorless and cohesive zeo-sewage sludge, suitable for safe deposition and also for the reclamation of agricultural soils. The zeo-sewage sludge produced either from the municipal wastewater treatment or from the mixing of HENAZE and sewage sludge, can be used for the reclamation of agricultural soils. The presence of HENAZE in the agricultural soils, increases the crops yield by 17-66 % and improves the quality of agricultural products by 4-46 %, reduces the use of fertilizers by 56-100 %, reduces the usage of irrigation water by 33-67 %, prevents the seepage of dangerous species into the water environment (e.g., NO_3^- by 55-92 %), protecting thus the quality of surface and underground waters. The usage of HENAZE in vivarium units and in the animal nutrition increases the production and improves the quality of the relevant products, reduces the feed cost, the animal diseases and medication, the new-born animal's death-rate and the malodor, converting thus the manure to odorless fertilizer.

Key words: natural zeolite, municipal wastewaters, sewage, sewage-sludge, Evros, Hellas.

1. Introduction

Zeolite comprises a special solid crystalline microporous material, with open structure and void space. Some high quality HEU-type natural zeolites, displays unique physical and chemical features and have a great variety of environmental, industrial, aquacultural and agricultural applications. The large natural zeolite deposits and the low cost of mining, gave access to large-scale utilization (e.g., Pond and Mumpton, 1984; Tsitsishvili et al., 1992; Carr, 1994; Collela and Mumpton, 2000; Filippidis and Kassoli-Fournaraki, 2000; Bish and Ming, 2001; Harben, 2002; Savvas et al., 2002; Inglezakis and Grigoropoulou, 2004; Inglezakis et al., 2004, 2005; Filippidis, 2008; Filippidis et al., 2008g-i).

In the Trigono Municipality (Evros Prefecture) and around the villages of Petrota and Pentalofos, eight different occurrences show varying zeolite con-

tents, on average 39-76 wt. % (e.g., Kirov et al., 1990; Marantos and Perdikatsis, 1994; Filippidis et al., 1995; Arvanitidis, 1998; Stamatakis et al., 1998, 2001; Filippidis and Kassoli-Fournaraki, 2000; Hall et al., 2000; Kassoli-Fournaraki et al., 2000; Yannakopoulos et al., 2000; Zorpas et al., 2000a,b; Barbieri et al., 2001; Moirou et al., 2001; Vlessidis et al., 2001; Koshiaris et al., 2002; Kyriakis et al., 2002; Papaioannou et al., 2002a,b; Savvas et al., 2002; Christidis et al., 2003; Katranas et al., 2003; Krestou et al., 2003; Perraki et al., 2003; Fokas et al., 2004; Inglezakis and Grigoropoulou, 2004; Inglezakis et al., 2004, 2005; Perraki and Orfanoudaki, 2004; Kantiranis et al., 2006; Warchol et al., 2006).

In a specific ground of Petrota village (Ntrista stream) has been located a HEU-type zeolite deposit, the Hellenic Natural Zeolite (HENAZE) of GEO-VET N. Alexandridis & Co O.E. concession (e.g., Filippidis and Kantiranis, 2002, 2005, 2007; Deligiannis et al., 2005; Filippidis, 2005, 2007; Filippidis et al., 2006, 2007a,b, 2008a-f, 2009a,b). The purification of municipal wastewaters, as well as the production of odorless and cohesive zeo-sewage sludge, using 7.5 g HENAZE of grain-size <1.5 mm and stirring time 5-60 min, has been investigated (Filippidis et al., 2007a,b, 2008a-f, 2009a,b). The present study investigates the purification improvement of the municipal wastewaters versus the stirring time. Environmental, agricultural, aquacultural and industrial applications are proposed for the HENAZE.

2. Materials and methods

The Hellenic Natural Zeolite (HENAZE) sample used was selected from a vertical profile of the Ntrista stream within the GEO-VET's concession. Petrographic investigation of HENAZE was performed on thin and polished thin sections. The morphology and chemistry of the HEU-type zeolite were studied by Scanning Electron Microscopy-Energy Dispersive Spectroscopy (SEM-EDS) with Link-AN 10000 EDS system. To minimize volatilization of alkalis, the electron beam spot size was enlarged and the counting time decreased. The mineralogical composition was determined by X-Ray Powder Diffraction (XRPD). Semi-quantitative estimates were performed using external mixture standards of the identified mineral phases. The chemical composition of the HENAZE was determined by Atomic Absorption Spectrometry. The ammonia ion exchange capacity (sorption ability) of the HENAZE was determined according to the Ammonium Acetate Saturation (AMAS) method. The pH variations and the removal ability of metals and anions were performed through butch-type experiments at RT (Filippidis and Kantiranis, 2002, 2007; Filippidis, 2005; Filippidis et al., 2006).

The typical platy crystals of HEU-type zeolite have a grain-size of 5-25 μm (Fig. 1). The chemical formula of the clinoptilolite is $Ca_{1.5}K_{1.4}Mg_{0.6}Na_{0.5}Al_{6.2}Si_{29.8}O_{72}{\cdot}20H_2O$. The minerals content of HENAZE is 89 wt.% HEU-type zeolite, 3 wt.% mica + clays (92 wt.% microporous minerals), 6 wt.% feldspars and 2 wt.% quartz. HENAZE shows a remarkable ammonia ion exchange capacity of 226 meq/100g (Table 1).

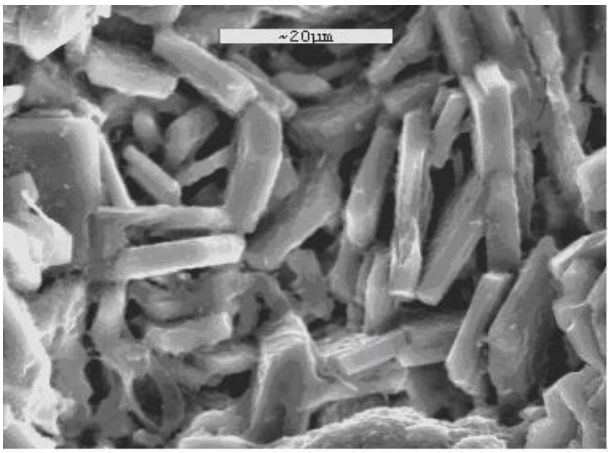

Fig. 1. SEM microphotograph of typical platy crystals of HEU-type zeolite of the HENAZE.

The chemical analysis of HENAZE gave: 68.62 wt.% SiO_2, 11.80 wt.% Al_2O_3, 2.92 wt.% K_2O, 2.14 wt.% CaO, 1.13 wt.% Na_2O and 0.75 wt.% MgO. HENAZE shows a remarkable ability to neutralize the pH of basic water (pH 9.5) from the lake Koronia (Prefecture of Thessaloniki) and of acidic stream mine water (pH 5.5) from NE Chalkidiki Prefecture, exhibiting an amphoteric character. Also found to remove from their aqueous solutions 74 % of Pb, 79% of Ag and 55-57% of NO_3^- (Filippidis and Kantiranis, 2002, 2007; Filippidis, 2005; Filippidis et al., 2006).

Kilkis City municipal wastewaters of different pH were treated at room temperature with HENAZE of < 1.5 mm grain-size (Fig. 2), in butch-type experiments. In 300 ml municipal wastewater 7.5 g of HENAZE was added, the whole was stirred for 5 to 60 minutes (Table 2) and polyaluminium chloride as well as cationic polyelectrolyte was added. The overflowed clear water and the precipitated

zeo-sewage sludge were separated by filtering. The zeo-sewage sludge was dried overnight at room temperature (RT). The starting municipal wastewaters and the overflowed clear waters, were analyzed for (method): pH (electrometric), color (photometric), suspended particles (filtering and centrifugation), COD (method of K_2CrO_6), P_2O_5 and NH_4 (molecular absorption spectrophotometry).

Table 1. Mineralogical composition and cation exchange capacity (CEC) of HENAZE.

Minerals	**Min-Max (wt. %)**	**Average (wt. %)**
HEU-type zeolite	87 – 93	89
Mica + Clays	2 – 4	3
Feldspars	3 – 8	6
Quartz	2 – 3	2
Total	**100**	**100**
Micro-porous minerals	90 – 95	92
CEC, meq/100g	***218 – 234***	***226***

3. Results

The treatment of municipal wastewaters of pH 8.2-8.9 (Table 2) with the HENAZE gave overflowed clear water (Fig. 3) of pH 7.3-7.8, free of odors and improved quality parameters by 89.9-96.7 % for the color, 89.0-98.5 % for the suspended particles, 93.7-97.2 % for the chemical oxygen demand (COD), 92.9-99.3 % for the P_2O_5 content and 98.3-99.9 % for the NH_4 content (Table 2). Simultaneously, the treatment gave as precipitate odorless and cohesive zeo-sewage sludge, dried overnight at room temperature (Fig. 4). The improvement of the quality parameters for the clear water increases with increasing stirring time of the treatment experiments. The correlation coefficient is 0.9423 for the P_2O_5 content (Fig. 5), 0.9323 for the suspended particles (Fig. 6), 0.9282 for the COD (Fig. 7) and 0.8854 for the color (Fig. 8). The correlation coefficient for the NH_4 content and pH are < 0.60.

Fig. 2. The grain-sizes of HENAZE (< 1.5 mm used for the butch-type experiments).


Fig. 3. Left: Starting municipal wastewater, Centre: Odorless and cohesive zoo-sewage sludge, Right: Overflowed clear water.


Fig. 4. Odorless and cohesive zeo-sewage sludge, dried overnight at RT.

4. Discussion and Conclusions

The natural zeolites show a remarkable ability to remove inorganic, organic, organometallic compounds, gas species, metals and radionuclides from their aqueous solutions. The sorption of the different species from their solutions by the micro-meso- and macroporous of natural zeolite can be attributed to absorption (mainly ion exchange), adsorption and surface precipitation processes (e.g., Tsitsishvili et al., 1992; Misailides et al., 1993, 1995; Godelitsas et al., 1999, 2001, 2003; Collela and Mumpton, 2000; Bish and Ming, 2001). The sorption of gas phases results to oxygen enrichment of the air and to the remarkable decrease of the malodor. Also, they show an ability to neutralize the pH of acidic and basic waters, acting either

Table 2. Chemistry of starting municipal wastewaters (SMW), clear water (CW) and relevant improvement (%). HENAZE-treatment: 7.5 g of < 1.5 mm grain-size at RT.

	Stirring time (min)	SMW	CW	± %	Ref.
pH	60	8.9	7.4	-16.9	1
	50	8.4	7.8	-7.1	2, 3
	50	8.4	7.5	-10.7	4, 5
	30	8.4	7.5	-10.7	6, 7
	7	8.6	7.7	-10.5	8
	5	8.2	7.3	-11.0	9
Color, mg/L, Pt scale	60	1470	49	-96.7	1
	50	1390	90	-93.5	2, 3, 4
	50	1390	52	-96.3	5
	30	1230	98	-92.0	7
	30	1214	99	-91.8	6
	7	1280	128	-90.0	8
	5	1180	119	-89.9	9
Suspended Particles, mg/L	60	325	5	-98.5	1
	50	280	10	-96.4	2, 3, 4
	50	280	9	-96.8	5
	30	283	15	-94.7	6
	30	241	15	-93.8	7
	7	272	22	-91.9	8
	5	210	23	-89.0	9
Chemical Oxygen Demand (COD), mg/L O_2	50	670	19	-97.2	4, 5
	30	461	23	-95.0	7
	7	512	29	-94.3	8
	5	410	26	-93.7	9
P_2O_5, mg/L	50	15.86	0.11	-99.3	5
	50	15.86	0.12	-99.2	2, 3, 4
	30	11.15	0.33	-97.0	7
	30	11.22	0.36	-96.8	6
	7	13.26	0.66	-95.0	8
	5	9.24	0.66	-92.9	9
NH_4, mg/L	50	110.76	0.06	-99.9	5
	30	33.80	0.19	-99.4	7
	7	36.92	0.21	-99.4	8
	5	30.52	0.51	-98.3	9

1) Filippidis et al. 2008e, 2) Filippidis et al. 2007a, 3) Filippidis et al. 2008c, 4) Filippidis et al. 2008f, 5) Filippidis et al. 2009a, 6) Filippidis et al. 2008b, 7) Filippidis et al. 2008d, 8) Filippidis et al. 2008a, 9) Filippidis et al. 2009b.

as a proton acceptor or donor, exhibiting thus an amphoteric character (e.g., Filippidis et al., 1996; Charistos et al., 1997).

The Hellenic Natural Zeolite (HENAZE) is of very high quality (> 85 wt. % HEU-type zeolite), removes inorganic, organic, organometallic, gas species, metals, cations and anions from their aqueous solutions. Also, shows an ability to neutralize the pH of acidic and basic waters. HENAZE removes from their aqueous solutions 74 % of Pb, 79 % of Ag and 55-57 % of NO_3^- (Filippidis, 2005; Filippidis et al., 2006). The increase of the pH in the acidic pH-range could mainly be attributed to the binding of the protons to the Lewis basic sites of the zeolite. The decrease of the pH in the basic pH-range could be the result of the removal of protons from surface Brønsted acidic sites or even of the detachment of protons from water molecules surrounding the exchangeable cations, caused by OH^- attack on the zeolite (e.g., Godelitsas et al., 1999, 2001, 2003). The mineralogical composition and the unique physico-chemical properties, make the HENAZE suitable material for numerous environmental, industrial, agricultural and aquacultural applications, such as: Animal nutrition, soil amendment for agriculture, conditioning of acid and basic soils, greenhouse and flowers substrates, durability and health improvement of lawn, purification of industrial and municipal wastewaters, treatment of sewage sludge, odor control, fishery and fish breeding, gas purification and drying systems, oxygen enrichment of aqua ecosystems, improvement of drinking water, constructed wetlands and wastewater treatment units (e.g., Collela and Mumpton, 2000; Harben, 2002; Filippidis, 2007; Filippidis et al., 2007a,b; 2008a-f; 2009a,b).

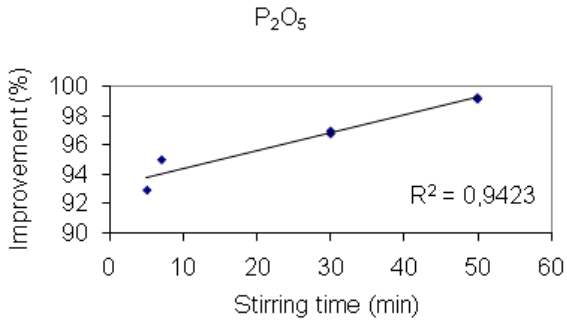

Fig. 5. The P_2O_5 content improvement of clear water vs stirring time of the HENAZE treatment.

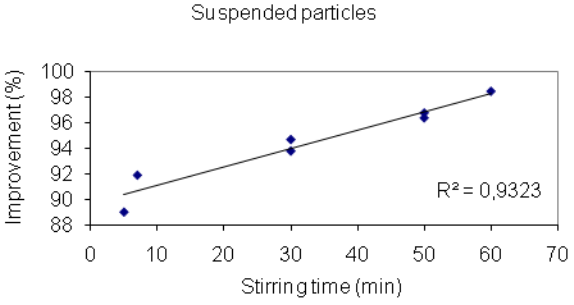

Fig. 6. The suspended particles content improvement of clear water vs stirring time of the HENAZE treatment.

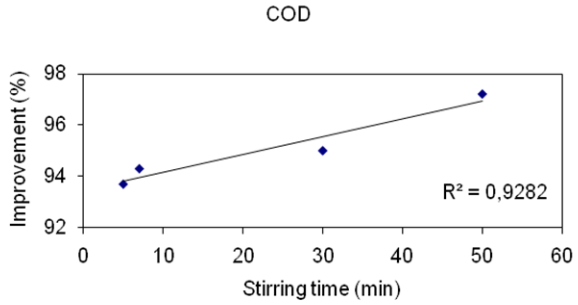

Fig. 7. The Chemical Oxygen Demand (COD) improvement of clear water vs stirring time of the HENAZE treatment.

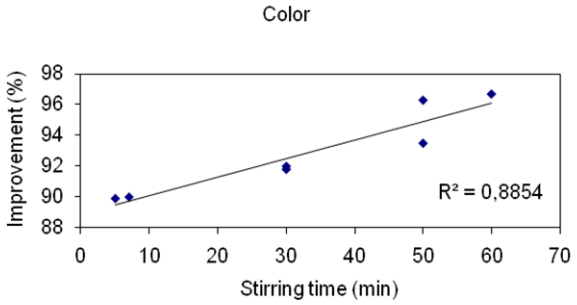

Fig. 8. The color improvement of clear water vs stirring time of the HENAZE treatment.

The HENAZE treatment of municipal wastewaters (pH initial 8.2-8.9) gave overflowed clear water of pH 7.3-7.8, free of odors and improved by 89.9-96.7 % for the color, 89.0-98.5 % for the suspended particles, 93.7-97.2 % for the chemical oxygen demand (COD), 92.9-99.3 % for the P_2O_5 content and 98.3-99.9 % for the NH_4 content. The improvement of the quality parameters for the clear water increases with increasing stirring time of the treatment experiments. Correlation coefficients > 0.88 are observed for the P_2O_5 content, the suspended particles, the COD and for the color, while those for the NH_4 content and pH where < 0.60. These final values of the pH and of the previous mentioned quality parameters, measured in the overflowed clear water, are fulfilling the requirements for disposition as downstream, irrigation, swimming and fish waters.

The HENAZE treatment gave also as precipitate, odorless and cohesive zeo-sewage sludge, suitable for safe deposition but also for the reclamation of

Table 3. The HENAZE in agricultural applications.

Addition of HENAZE in agricultural soils

	Fertilizer		Irrigations		Production (Kg/acre)		
Species	**Kg/acre**	**± %**	**Nr.**	**± %**	**Without HENAZE**	**With HENAZE**	**± %**
Wheat [1]	20				170		+ 29
	0	- 100				220	
	10				70		+ 57
	0	- 100				110	
Rice [1]	90				880		+ 34
	40	- 56				1180	
Maize [1]	120		3		800		
	0	- 100	2	- 33		1200	+ 50
	0	- 100	1	- 67		800	± 0

Production increase (%) by addition of HENAZE in agricultural soils

Species	**%**	**Species**	**%**
Grapes	48 - 66	Carnation (florescence increase) [2]	25
Tomato [1]	48 – 52		
Actinides [2]	45	Cotton [2]	17

Quality improvement of tomato by HENAZE addition in agricultural soils

	Produced		
Quality parameters	**Without HENAZE**	**With HENAZE**	**± %**
Soluble solids (%) [1]	4.20	4.35	+ 4
Vitamin C (mg/100g) [1]	6.81	8.61	+ 26
Firmness (Kg) [1]	0.619	0.906	+ 46

HENAZE as feed additive and farm floor material

17 % increase of milk production in cows [2]	Taste and quality improvement of products (meat, milk,
7 % increase of body weight in broilers [2]	eggs, etc)
Reduction of feed cost	Reduction of new-born animals death-rate
Reduction of animal diseases	Reduction of the malodor
Reduction of animal medication	Conversion of manure to odorless fertilizer

[1]Filippidis et al. 2007b, [2]Filippidis 2007.

agricultural soils. The same stands for the odorless and cohesive zeo-sewage sludge produced by mixing the sewage sludge and the HENAZE. The presence of HENAZE in the agricultural soils, increases the yield by 17-66 % and improves the quality by 4-46 % of agricultural products, reduces the use of fertilizers by 56-100 %, reduces the usage of irrigation water by 33-67 %, prevents the seepage of dangerous species into the water environment (e.g., NO_3^- by 55-92 %), protecting thus the quality of surface and underground waters (Tables 3). The usage of HENAZE in vivarium units and in the animal nutrition increases the production and improves the quality of their products (Table 3), reduces the feed cost, the animal diseases, animal medication, the new-born animals death-rate and the malodor, converting thus the manure to odorless fertilizer (e.g., Filippidis, 2005, 2007; Filippidis et al., 2006, 2007b, 2008e).

Acknowledgments

We express our gratitude to the GEO-VET N. Alexandridis & Co O.E., for the supply and treatment of HENAZE, as well as for their economical support.

References

Arvanitidis N., 1998. Northern Greece's industrial minerals: production and environmental technology developments. *J. of Geochemical Exploration* 62, 217-227.

Barbieri M., Castorina F., Masi U., Garbarino C., Nicoletti, M., Kassoli-Fournaraki, A., Filippidis, A. and Mignardi, S., 2001. Geochemical and isotopic evidence for the origin of rhyolites from Petrota (Northern Thrace, Greece) and geodynamic significance. *Chemie der Erde* 61, 13-29.

Bish D.L. and Ming D.W., 2001. Natural Zeolites: Occurrence, Properties, Applications. Mineralogical Society of America, 654 pp., Washington DC.

Carr D.D., 1994. Industrial Minerals and Rocks. Braun-Brumfield Inc., 1196 pp., Ann Arbor, Michigan.

Charistos D., Godelitsas A., Tsipis C., Sofoniou M., Dwyer J., Manos G., Filippidis A. and Triantafyllidis C., 1997. Interaction of natrolite and thomsonite intergrowths with aqueous solutions of different initial pH values at 25^o C in the presence of KCl: Reaction mechanisms. *Applied Geochemistry* 12, 693-703.

Collela C. and Mumpton F.A., 2000. Natural Zeolites for the Third Millenium. De Frede Editore, 481pp., Napoli.

Christidis G.E., Moraetis D., Keheyan E., Akhalbedashvili L., Kekelidze N., Gevorkyan R., Yeritsyan H. and Sargsyan H., 2003. Chemical and thermal modification of natural HEU-type zeolitic materials from Armenia, Georgia and Greece. *Applied Clay Science* 24, 79-91.

Deligiannis K., Lainas Th., Arsenos G., Papadopoulos E., Fortomaris P., Kufidis D., Stamataris C. and Zygoyiannis D., 2005. The effect of feeding clinoptilolite on food intake and performance of growing lambs infected or not with gastrointestinal nematodes. *Livestock Production Science* 96, 195-203.

Filippidis A., 2005. Mineralogy and physico-chemical characteristics of five natural zeolite samples for N. Alexandridis & Co O.E. Internal report, 10 pp., Thessaloniki, In Greek.

Filippidis A., 2007. Zeolites of Trigono Municipality of Evros Prefecture in industrial, agricultural, cattle-raising and environmental technology. *Proceedings, Scientific Meeting on Development Perspectives of Northern Evros*, Petrota, Greece, 89-107, In Greek.

Filippidis A., 2008. Treatment and recycling of municipal and industrial waste waters using Hellenic Natural Zeolite: A Review. *CD-Proceedings, AQUA 2008, 3rd Intern. Conf. Water Science and Technology*, Athens, 5 pp.

Filippidis A. and Kantiranis N., 2002. Morphology, mineralogy, chemistry, mineralchemistry and ion exchange capacity of five natural zeolite samples for N. Alexandridis & Co O.E., Internal report, 5 pp., Thessaloniki, In Greek.

Filippidis A. and Kantiranis N., 2005. Industrial, agricultural and environmental uses of the natural zeolites of Thrace. *Bull. Geol. Soc. Greece* 37, 90-101, In Greek with English summary.

Filippidis A. and Kantiranis N., 2007. Experimental neutralization of lake and stream waters from N. Greece using domestic HEU-type rich natural zeolitic material. *Desalination* 213, 47-55.

Filippidis A. and Kassoli-Fournaraki A., 2000. Environmental uses of natural zeolites from Evros district, Thrace, Greece, *Proceedings, 5th International Conference on Environmental Pollution*, Thessaloniki, 149-155.

Filippidis A., Kassoli-Fournaraki A. and Tsirambides A., 1995. The zeolites of Petrota and Metaxades (Thrace) and the kaolins of Leucogia (Macedonia), Greece. In: Aleksiev, B.(ed.) *Field Tripe Guide, International Symposium on Natural Zeolites*, Sofia, 49-62.

Filippidis, A., Godelitsas, A., Charistos, D., Misaelides, P. and Kassoli-Fournaraki, A., 1996. The chemical behavior of natural zeolites in aqueous environments: Interactions between low-silica zeolites and 1M NaCl solutions of different initial pH-values. *Applied Clay Science* 11: 199-209.

Filippidis A., Kantiranis N., Drakoulis A. and Vogiatzis D., 2006. Improvement and protection of the lake Koronia using natural zeolite. *Proceedings, 2nd Congress of Aristotle University Environment Council*, Thessaloniki, 273-279, In Greek with English summary.

Filippidis A., Apostolidis N., Filippidis S. and Paragios I., 2007a. Purification of urban wastewaters and production of odorless sewage sludge using porous Hellenic natural zeolite of Petrota (Evros Prefecture). *Proceed-*

ings, 3rd Panhellenic Symposium on Porous Materials, Thessaloniki, 23-25, In Greek.

Filippidis A., Siomos A., Barbayiannis N. and Filippidis S., 2007b. Agriculrural and environmental applications using Hellenic Natural Zeolite of Petrota (Evros), *Proceedings, Jean Monnet Congress*, Veria, Greece, 557-569, In Greek with English summary.

Filippidis A., Apostolidis N., Filippidis S. and Paragios I., 2008a. Purification of urban wastewaters, production of odorless and cohesive zeo-sewage sludge using Hellenic Natural Zeolite. *Proceedings, 8th Internnational Hydrogeological Congress of Greece*, Athens, 2, 789-798, In Greek with English abstract.

Filippidis A., Apostolidis N., Filippidis S. and Paragios I., 2008b. Purification of industrial and urban wastewaters, production of odorless and cohesive zeo-sewage sludge using Hellenic Natural Zeolite. *Proceedings, Second International Conference on Small and Decentralized Water and Wastewater Treatment Plants*, Skiathos, Greece, 403-408.

Filippidis A., Apostolidis N., Paragios I. and Filippidis S., 2008c. Production of odorless sewage sludge, purification of dye-work and urban waste-waters, using Hellenic Natural Zeolite. *CD-Proceedings, 3rd Environmental Conference of Macedonia*, Thessaloniki, 8 pp., In Greek with English abstract.

Filippidis A., Apostolidis N., Paragios I. and Filippidis S., 2008d. Purification of dye-work and urban wastewaters, production of odorless and cohesive zeo-sewage sludge, using Hellenic Natural Zeolite. *CD-Proceedings, 1st International Conference on Hazardous Waste Management*, Chania, Greece, 8 pp.

Filippidis A., Apostolidis N., Paragios I. and Filippidis S., 2008e. Safe management of sewage sludge, produced by treatment of municipal sewage with Hellenic Natural Zeolite. *CD-Proceedings, AQUA 2008, 3rd International Conference on Water Science and Technology*, Athens, 5 pp.

Filippidis, A., Apostolidis, N., Paragios, I. and Filippidis, S., 2008f. Zeolites clean up. *Industrial Minerals*, April, 68-71.

Filippidis A., Kantiranis N., Filippidis S., Vordogiannis I., Apostolidis N. and Paragios I., 2008g. Purification of Textile-work Waste Waters with Natural Zeolite. Patent Number: 1006140, Industrial Property Organisation, Athens, In Greek.

Filippidis A., Kantiranis N., Filippidis S., Vordogiannis I., Apostolidis N. and Paragios I., 2008h. Purification of Sewage with Natural Zeolite. Patent Number: 1006145, Industrial Property Organisation, Athens, In Greek.

Filippidis A., Kantiranis N., Filippidis S., Vordogiannis I., Apostolidis N. and Paragios I., 2008i. Purification of Tanning-work Waste Waters with Natural Zeolite. Patent Number: 1006146, Industrial Property Organisation, Athens, In Greek.

Filippidis A., Apostolidis N., Filippidis S. and Paragios I., 2009a. Purification of sewage effluents and production of odourless-cohesive sewage sludge, using Hellenic Natural Zeolite. *Honorary Volume to Professor Christos Tzimopoulos, Faculty of Engineering, Aristotle University of Thessaloniki, YDROGAIA*, 425-434, In Greek with English abstract.

Filippidis A., Papastergios G., Apostolidis N., Paragios I., Filippidis S. and Sikalidis C., 2009b. Odorless and cohesive zeo-sewage sludge produced by Hellenic Natural Zeolite treatment. *Proceedings, 3rd International Conference, AMIREG 2009*, Athens, 96-100.

Fokas P., Zervas G., Fegeros K. and Zoiopoulos P., 2004. Assessment of Pb retention coefficient and nutrient utilization in growing pigs fed diets with added clinoptilolite. *Animal Feed Science and Technology* 117, 121-129.

Godelitsas A., Charistos D., Dwyer J., Tsipis C., Filippidis A., Hatzidimitriou A. and Pavlidou E., 1999. Copper (II)-loaded HEU-type zeolite crystals: characterization and evidence of surface complexation with N,N-diethyldithiocarbamate anions. *Microporous and Mesoporous Materials* 33, 77-87.

Godelitsas A., Charistos D., Tsipis A., Tsipis C., Filippidis A., Triantafyllidis C., Manos G. and Siapkas D., 2001. Characterisation of zeolitic materials with a HEU-type structure modified by transition metal elements: Definition of acid sites in Nickel-loaded crystals in the light of experimental and quantum-chemical results. *Chemistry European Journal* 7, 3705-3721.

Godelitsas A., Charistos D., Tsipis C., Misaelides P., Filippidis A. and Schindler M., 2003. Heterostructures patterned on aluminosilicate microporous substrates: Crystallisation of cobalt (III) tris(N,N-diethyldithiocarbamato) on the surface of HEU-type zeolite. *Microporous and Mesoporous Materials* 61, 69-77.

Hall A., Stamatakis M. and Walsh J.N., 2000. The Pentalofos zeolitic tuff formation: A giant ion-exchange column. *Annales Geologiques des Pays Helleniques* 38, 175-192.

Harben P.W., 2002. The Industrial Minerals HandyBook. Pensord, 409 pp., Blackwood, UK.

Inglezakis V.J. and Grigoropoulou H., 2004. Effects of operating conditions on the removal of heavy metals by zeolite in fixed bed reactors. *Journal of Hazardous Materials* B112,37-43.

Inglezakis V.J., Loizidou M.M. and Grigoropoulou H.P., 2004. Ion exchange studies on natural and modified zeolites and the concept of exchange site accessibility. *J. of Colloid and Interface Science* 275, 570-576.

Inglezakis V.J., Zorpas A.A., Loizidou M.D. and Grigoropoulou H.P., 2005. The effect of competitive cations and anions on ion exchange of heavy metals. *Separation and Purification Technology* 46, 202-207.

Kantiranis N., Chrissafis C., Filippidis A. and Paraskevopoulos K., 2006. Thermal distinction of HEU-type mineral phases contained in Greek zeolite-rich volcaniclastic tuffs. *European Journal of Mineralogy* 18, 509-516.

Kassoli-Fournaraki A., Stamatakis M., Hall A., Filippidis A., Michailidis K., Tsirambides A. and Koutles Th.,

2000. The Ca-rich clinoptilolite deposit of Pentalofos, Thrace, Greece. In: Colella, C. & Mumpton, F.A. (eds) *Natural Zeolites for the Third Millennium*, De Frede Editore, Napoli, 193-202.

Katranas Th., Vlessidis A., Tsiatouras V., Triantafyllidis K. and Evmiridis N., 2003. Dehydrogenation of propane over natural clinoptilolite zeolites. *Microporous and Mesoporous Materials* 61, 189-198.

Kirov G.N., Filippidis A., Tsirambidis A., Tzvetanov R.G. and Kassoli-Fournaraki A., 1990. Zeolite-bearing rocks in Petrota area (Eastern Rhodope Massif, Greece). *Geologica Rhodopica* 2, 500-511.

Koshiaris G., Marantos I., Tsirambides A., Stamatakis M.G., Kassoli-Fournaraki A. and Filippidis A., 2002. The zeolite deposits of Thrace (North-Eastern Greece). *Field Trip Guide, 6th International Conference on Natural Zeolites*, Thessaloniki, 23 pp.

Krestou A., Xenidis A. and Panias D., 2003. Mechanism of aqueous uranium (VI) uptake by natural zeolitic tuff. *Minerals Engineering* 16, 1363-1370.

Kyriakis S.C., Papaioannou D.S., Alexopoulos C., Polizopoulou Z., Tzika E.D. and Kyriakis C.S., 2002. Experimental studies on safety and efficacy of the dietary use of a clinoptilolite-rich tuff in sows: a review of recent research in Greece. *Microporous and Mesoporous Materials* 51, 65-74.

Marantos I. and Perdikatsis V., 1994. Study of the mineralogical composition, dehydration/adsorption of water and ion exchange capacity of zeolitic tuffs from Petrota-Pentalofos area, N. Evros. Bull. Geol. Soc. Greece 30/3, 311-321, In Greek with English abstract.

Misaelides P., Godelitsas A., Haristos D., Noli F., Filippidis A. and Sikalidis C., 1993. Determination of heavy metal uptake by the sodium form of heulandite using radiochemical techniques. *Geologica Carpathica - Series Clays* 44/2, 115-119.

Misaelides P., Godelitsas A., Filippidis A., Charistos D. and Anousis I., 1995. Thorium and uranium uptake by natural zeolitic materials. *The Science of the Total Environment* 173/174, 237-246.

Moirou A., Xenidis A. and Paspaliaris I., 2001. Stabilization Pb, Zn, and Cd- contaminated soil by means of natural zeolites. *Soil and Sediment Contamination* 10/3, 251-267.

Papaioannou D.S., Kyriakis S.C., Papasteriadis A., Roumbies N., Yannakopoulos A. and Alexopoulos C., 2002a. A field study on the effect of in-feed inclusion of a natural zeolite (clinoptilolite) on health status and performance of sows/gilts and their litters. *Research in Veterinary Science* 72, 51-59.

Papaioannou D., Kyriakis S., Papasteriadis A., Roumbies N., Yannakopoulos A. and Alexopoulos C., 2002b. Effect of in-feed inclusion of a natural zeolite (clinoptilolite) on certain vitamin, macro and trace element concentrations in the blood, liver and kidney tissues of sows. *Research in Veterinary Science* 72, 61-68.

Perraki Th. and Orfanoudaki A., 2004. Mineralogical study of zeolites from Pentalofos area, Thrace, Greece. *Applied Clay Science* 25, 9-16.

Perraki Th., Kakali G. and Kontoleon F., 2003. The effect of natural zeolites on the early hydration of Portland cement. *Microporous and Mesoporous Materials* 61, 205-212.

Pond W.G. and Mumpton F.A., 1984. Zeo-Agriculture, Use of Natural Zeolites in Agriculture and Aquaculture, I.C.N.Z., 305 pp., Brockport, NY.

Savvas D., Samantouros K., Paralemos D., Vlachakos G., Stamatakis M. and Vassilatos C., 2002. Yield and nutrient status in the root environment of tomatoes (*Lycopersicon esculentum*) grown on chemically active and inactive inorganic substrates. *Acta Horticulturae* 644, 377-383.

Stamatakis M., Hall A., Lutat U. and Walsh J.N., 1998. Mineralogy, origin and commercial value of the zeolite-rich tuffs in the Petrota-Pentalofos area, Evros county, Greece. *Estudios Geologicos* 54, 3-15.

Stamatakis M., Koukouzas N., Vassilatos Ch., Kamenou E. and Samantouros K., 2001. The zeolites from Evros region, Northern Greece: A potential use as cultivation substrate in hydroponics. *Acta Horticulturae* 548, 93-103.

Tsitsishvili G.V., Andronikashvili T.G., Kirov G.N. and Filizova L.D., 1992. Natural Zeolites, Ellis Horwood Ltd, 295 pp., Chichester, West Sussex.

Warchol J., Misaelides, P., Petrus, R. and Zamboulis, D., 2006. Preparation and application of organo-modified zeolitic material in the removal of chromates and iodides. *Journal of Hazardous Materials* B137, 1410-1416.

Vlessidis A.G., Triantafillidis C.S. and Evmiridis N.P., 2001. Removal and recovery of p-phenylenediamines developing coumpounds from photofinishing lab washwater using clinoptilolite tuffs from Greece. *Water Research* 35, 1603-1608.

Yannakopoulos A., Tserveni-Gousi A., Kassoli-Fournaraki A., Tsirambides A., Michailidis K., Filippidis A. and Lutat U., 2000. Effects of dietary clinoptilolite-rich tuff on the performance of growing-finishing pigs. In: Colella, C. & Mumpton, F.A.(eds) *Natural Zeolites for the Third Millennium*, De Frede Editore, Napoli, 471-481.

Zorpas A.A., Constantinides T., Vlyssides A.G., Haralambous I. and Loizidou M., 2000a. Heavy metal uptake by natural zeolite and metals partitioning in sewage sludge compost. *Bioresource Technology* 72, 113-119.

Zorpas A.A., Kapetanios E., Zorpas G.A., Karlis P., Vlyssides A., Haralambous I. and Loizidou, M., 2000b. Compost produced from organic fraction of municipal solid waste, primary stabilized sewage sludge and natural zeolite. *Journal of Hazardous Materials* B77, 149-159.

Scientific Annals, School of Geology, Aristotle University of Thessaloniki Proceedings of the XIX CBGA Congress, Thessaloniki, Greece	Special volume 100	63-69	Thessaloniki 2010

ASSESSMENT OF HEAVY METALS CONCENTRATIONS IN SEDIMENTS OF BOGDANAS RIVER AT THE ASSIROS-LAGADAS AREA, NORTHERN GREECE

Giouri A.[1], Christophoridis C.[2], Melfos V.[1] and Vavelidis M.[1]

[1] *Department of Mineralogy-Petrology-Economic Geology, School of Geology, Aristotle University of Thessaloniki, 54124, Thessaloniki, Greece, agiouri@geo.auth.gr*
[2]*Environmental Pollution Control Laboratory, Department of Chemistry, Aristotle University of Thessaloniki, 54124, Thessaloniki, Greece*

Abstract: Bogdanas river flows east of Thessaloniki, in Northern Greece. Its sources are found at the western part of the Vertiskos mountain and flows along the Assiros and Lagada plane towards Koronia lake. In this study, variations of the heavy metal concentrations in Bogdanas river sediments has been evaluated. Sediment samples were collected at 8 representative sampling sites along the river, during two sampling periods. Chemical analysis indicated that the sediment samples show variable concentrations of heavy metals. Sediment quality assessment according to the limits determined by the European Community's legislation indicated that the river sediments were not contaminated, apart from 3 samples and 1 sample concerning Zn and Cu, respectively. On the other hand, sediment quality assessment according to the US EPA Sediment Quality Guidelines (SQG), revealed that there was heavy metal pollution with respect to especially Zn, Cu and Ni. Concerning Zn, only 1 sample is close to the EPA's moderately polluted level, while 10 samples surpass it and 5 samples exceed the EPA's heavily polluted level. Concerning Cu, 7 samples are classified as moderately polluted and 9 samples as heavily polluted. Finally, no pollution is defined for Ni, apart from 2 samples which are classified as moderately polluted. In conclusion, the research showed that the revealed heavy metal pollution is more attributed to the lithology of the area and less to human activity.

Keywords: Bogdanas river, Koronia lake, heavy metals, sediments, Assiros, Lagadas, Northern Greece

1. Introduction

The contamination of the surface water bodies with heavy metals has been attracting considerable public attention over the past few decades. Heavy metals can be added to an aquatic system either by natural or anthropogenic sources.

Heavy metals released to aquatic systems are generally bound to particulate matter, which are eventually incorporated into sediments (Suthar et al., 2009). Thus, sediments are an efficient mean of accumulation and downstream transport of inorganic contaminants, like heavy metals (Espinosa et al., 2009). It is a proven fact that heavy metals induce toxic effects on living organisms, therefore they can pose a high risk when found in high concentrations in sediments (Förster and Salomons, 1991). For this reason limit values for heavy metals have been proposed for the protection of these endangered habitats (Zehl and Einax, 2005).

An example of an aquatic system which is constantly downgrading is that of Koronia lake in central Macedonia, Greece. The water of the lake has been extensively polluted by agricultural and cattle livestock activities as well as by industrial wastes. According to Tzimopoulos et al. (2006) and Gantidis et al. (2006) the quality of the water has worsened–due to the bio-accumulation of the heavy metals and the concentration of toxic algal blooms in the lake.

The pollution of Koronia's water body has increased by the torrents which discharge at the catchment basin of the area and flow into the lake. One of these torrents is Bogdanas river which springs from the western slopes of the Vertiskos Mountain. Bogdanas river flows with a W-SW direction towards Assiros town and then turns to the south. Following that, it passes west of Lagadas

town and finally flows into the northwestern part of the Koronia lake (Fig. 1).

During the field surveys along Bogdanas river various injurious human activities were observed, such as the discharge of untreated urban waste liquids from Assiros and Lagadas towns into the river and the existence of uncontrolled landfills and cultivated fields, which may have played a significant role in the Bogdanas river pollution.

The aim of this study is to determine the concentrations of toxic heavy metals such as Pb, Cd, Zn, As, Cu and Ni in the Bogdanas's sediments, in order to evaluate, firstly, the degree of the river's environmental pollution and secondly to investigate if there is any possible pollution that is caused to the Koronia lake by the river.

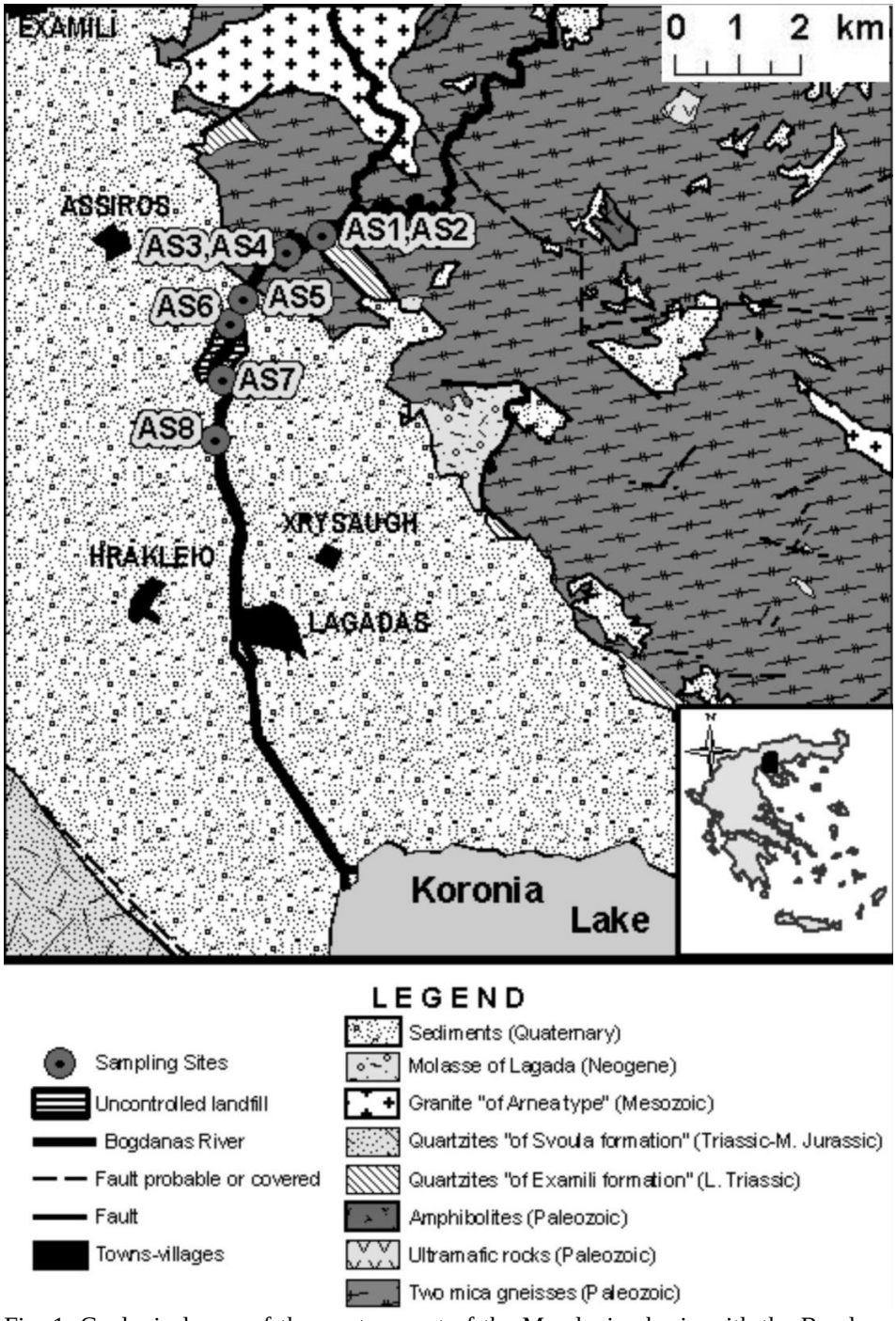

Fig. 1. Geological map of the western part of the Mygdonian basin with the Bogdanas river and the sampling sites (according to Kockel et al., 1978, 1979, with modifications).

2. Geological Setting

The studied area belongs to the boundary between the Serbomacedonian massif and the Circum Rhodope belt, at the western part of the Mygdonian basin, which comprises a tectonic graben (Fig. 1).

The bedrock of the Bogdana's river water catchment basin consists of Alpine and Pre-alpine metamorphic rocks, such as gneisses, amphibolites, quartzites and ultrabasic rocks (Kockel et al., 1978; Kockel et al., 1979). Significant is the presence of a two-mica and biotite granite, of Arnea type, that intrudes these rocks (De Wet, 1989; Kostopoulos et al., 2001). The Mygdonian basin contains Oligocene to Quaternary sedimentary deposits with a thickness of 50 to 450 m. They consist of clays, sands and gravels (Psilovikos, 1977; Tranos et al., 1999). Normal neotectonic faults cut the basement rocks as well as the younger sediments which overlie them (Chatzipetros and Pavlides, 1998).

Numerous restricted ore mineralizations are found in the broader area. According to Vavelidis et al. (1999) and Melfos et al. (2001) mineralized quartz veins are located in Drakontio and Stefania areas, at the northern part of the region. They relate to Cu, Fe, Pb, Zn, As, Bi, Au, Ag, Co, Ni. A small occurrence of a copper mineralization with a old underground excavation is also located east of Assiros town, by the Bogdanas river (Giouri, 2008).

3. Materials and Methods

3.1. Sampling

For the purposes of the present study, 8 sites (AS1 to AS8) were sampled for their sediments downstream Bogdanas river, between Assiros town and Koronia lake (Fig. 1). It should be mentioned that sites AS1 and AS3 are close to AS2 and AS4, respectively, with the first two being at the river banks and the two latter being at the river bed. Sixteen sediment samples were collected at the top of the riverbed and its banks, avoiding the input of ground materials.

Sampling was carried out during July 2006 corresponding to the dry season of the summer. In the meantime, the public authorities of the region tried to apply measures in order to eliminate any human activities in the wider area. Sampling was repeated in February 2009, corresponding after the rainy season, so as to ascertain the measures' adjustment.

3.2. Laboratory treatment of the sediments

All samples were collected with a plastic shovel and were put in plastic bags. At the laboratory, after the removal of organic material, samples were dried in an oven at 60˚C. They were gently ground with rolling pin to disaggregate the samples but not break down the grains themselves, and sieved to collect less than 0.063 mm grain sizes.

The sediment portion with particle size <0.063mm was used to determine the heavy metal concentrations. Contaminants accumulate mainly in the finest particles of sediments (<0.063 mm) due to the larger surface area and the presence of reactive sites. So the environmental available trace elements remain mainly in this fraction (Fernandez-Turiel et al., 2001; Kabata-Pendias and Pendias, 2001). For this reason, fine sediments have been used to investigate river pollution around the world (Salomons, 1995; Murray et al., 1999).

The metals in the sediment samples were extracted using the aqua regia digestion while heated at 120˚C for 12 hours. The samples were centrifugated during 10 min at 2500 rpm. All the extracts were diluted to 50 ml with deionized water in volumetric flasks and stored in polyethylene bottles until analysis.

3.3. Analysis of heavy metals

The sediment samples were analyzed for their concentration in Pb, Cd, Zn, As, Cu and Ni. The concentrations of Pb, Cd and Ni were determined by Graphite Furnace Atomic Absorption Spectrophotometry (GFAAS), with a Perkin Elmer AA400 atomic absorption spectrophotometer, equipped with an HGA 900 furnace programmer. The concentrations of Zn and Cu were determined by Flame Atomic Absorption Spectrophotometry (FAAS) using the same instrument (AA400). Total Arsenic concentration was measured using the hydride generation technique applied with a FIAS apparatus. The heavy metal analyses were carried out by the Environmental Pollution Control Laboratory at the Department of Chemistry in Aristotle University of Thessaloniki.

4. Results and Discussion

The results of the chemical analysis that was carried out in the finest fraction of sediment samples collected in Bogdanas river, are presented in table 1.

Table 1. Heavy metal concentrations at every sampling site of the studied area in mg/g of dry weight.

Sample	Sampling Period	Pb (mg/g)	Cd (mg/g)	Zn (mg/g)	As (mg/g)	Cu (mg/g)	Ni (mg/g)
AS1a	Jul-2006	17.2	bdl	354.1	1.6	104.2	15.4
AS2a		31.0	bdl	133.1	1.6	50.4	13.1
AS3a		22.5	bdl	148.2	1.6	62.4	14.1
AS4a		2.0	0.1	423.1	1.7	117.8	12.1
AS5a		12.2	bdl	178.4	1.5	48.6	0.3
AS6a		3.6	bdl	268.9	1.5	171.1	27.9
AS7a		0.1	bdl	99.6	2.1	72.8	bdl
AS8a		12.3	bdl	316.3	1.5	138.0	0.2
AS1b	Feb-2009	27.5	bdl	112.0	1.4	33.1	bdl
AS2b		33.5	0.1	71.1	1.5	34.1	bdl
AS3b		12.2	0.1	139.3	1.3	44.7	1.6
AS4b		11.7	0.1	102.7	1.4	44.7	21.7
AS5b		0.1	bdl	91.6	1.2	36.4	18.3
AS6b		1.8	0.1	139.6	0.8	69.5	bdl
AS7b		0.2	bdl	156.1	1.0	41.9	bdl
AS8b		0.8	0.2	229.2	1.3	50.4	0.3
Mean		11.8	<0.05	185.2	1.4	70.0	<8

bdl : below detection limit

According to the results, Pb varies from 0.1 to 33.5 mg/g dw with a mean of 11.8 mg/g dw. Cd is generally very low in all sampling sites, reaching 0.1 mg/g dw. Its mean content is <0.05 mg/g dw. Zn concentrations present significant variations in some sites and range from 71.1 mg/g dw to the extremely high value of 423.1 mg/g dw for the sample AS4a. The average content is 185.2 mg/g dw. Arsenic rises up to 2.1 mg/g dw with an average of 1.4 mg/g dw. Cu also shows significant variations at most of the sites, ranging from 33.1 mg/g dw to the elevated value of 171.1 mg/g dw (sample AS6a) with a mean content of 70.0 mg/g dw. Finally, Ni concentrations at some sites are below the detection limit and at the others they reach up to 27.9 mg/g dw for the sample AS6a. The average content for Ni is <8 mg/g dw.

Table 2 shows the maximum allowable concentrations of heavy metals as they are proposed in the directives of the European Community (EC), taken from Kabata-Pendias and Pendias (2001). Additionally, sediments were classified as non-polluted, moderately polluted and heavily polluted, based on the Sediment Quality Guidelines (SQG) of US Environmental Protection Agency (EPA) (Perin et al., 1997).

These limits were compared with the concentrations of the heavy metals measured in the sediments of the Bogdanas river, in order to evaluate the degree of the sediments contamination. The diagrams at figure 2 illustrate the heavy metals concentrations at every sampling site during the two sampling periods, in relation with the sediment quality guidelines.

All the samples contain Pb concentrations which are lower than the limits established by the European Community and EPA. Cd is very low and its concentrations are below the limits of EC and EPA. Zn concentrations show remarkable variations between the two sampling periods and most of them do not fulfill the established sediment quality guidelines. More particularly, samples AS1b, AS2a, AS3a and b, AS4, AS5a and b, AS6b

Table 2. Sediment Quality Guidelines determined by the EC and US EP.

Sediment Quality Guidelines	mg/g dw					
	Pb	Cd	Zn	As	Cu	Ni
EC [1]	300	3	300	20	150	75
EPA [2]						
Non Polluted	< 40	-	< 90	< 3	< 25	< 20
Moderately Polluted	40-60	-	90-200	3-8	25-50	20-50
Heavily Polluted	> 60	> 6	> 200	> 8	> 50	> 50

[1]: Maximum allowable heavy metals concentrations as they are determined by the legislation of the European Community (EC), taken from Kabata-Pendias and Pendias (2001).

[2]: Sediment Quality Guidelines as they are determined by the US Environmental Protection Agency (EPA) (Perin et al., 1997).

and AS7a and b are classified as moderately polluted, while samples AS1a, AS4a, AS6a and AS8a and b are classified as heavily polluted in relation to Zn. Concerning As, its concentrations are lower than the limits determined either by EC or EPA and their values remain relatively in the same level between the two sampling periods. Concerning Cu, most of the samples (AS1a, AS3a, AS4a, ASa and b, AS7a and AS8a and b) are classified as heavily polluted and all the rest as moderately polluted. Based on EC's limits, only one sample (AS6a) exceeds them reaching up to 171.1 mg/g dw. Finally, concentrations of Ni are in general below limits, with an exception of two samples (AS4b and AS6a) which exceed EPA's limit for moderately polluted sediments.

Considering all the data mentioned above, it is assumed that at most sites the concentrations of heavy metals in the sediments of 2006 sampling period are higher than the respective ones of 2009 (Fig. 2). There is no significant pollution detected concerning Pb, Cd and As. In spite of that, concentrations of Pb, Cd and As that were determined in some samples are mostly associated with the lithology of Bogdana's catchment basin than with the anthropogenic activities that were detected in the region. This is due to the fact that the sites in which Pb and Cd concentrations were determined are mainly in the northern part of the basin. In this area, according to Vavelidis et al. (1999) and Melfos et al. (2001) there are ore mineralizations at Drakontio and Stefania areas which contain small quantities of Pb related mainly to galena and of Cd found in the structure of sphalerite. Arsenic concentrations remain at the same level in every sample, indicating that it exists in the sediments along the river and doesn't derive from point pollution sources. Minerals such as cobaltite, gersdorffite and chalcopyrite contain As in the mentioned mineralization (Vavelidis et al., 1999; Melfos et al., 2001). Zn and Cu show almost similar behavior at

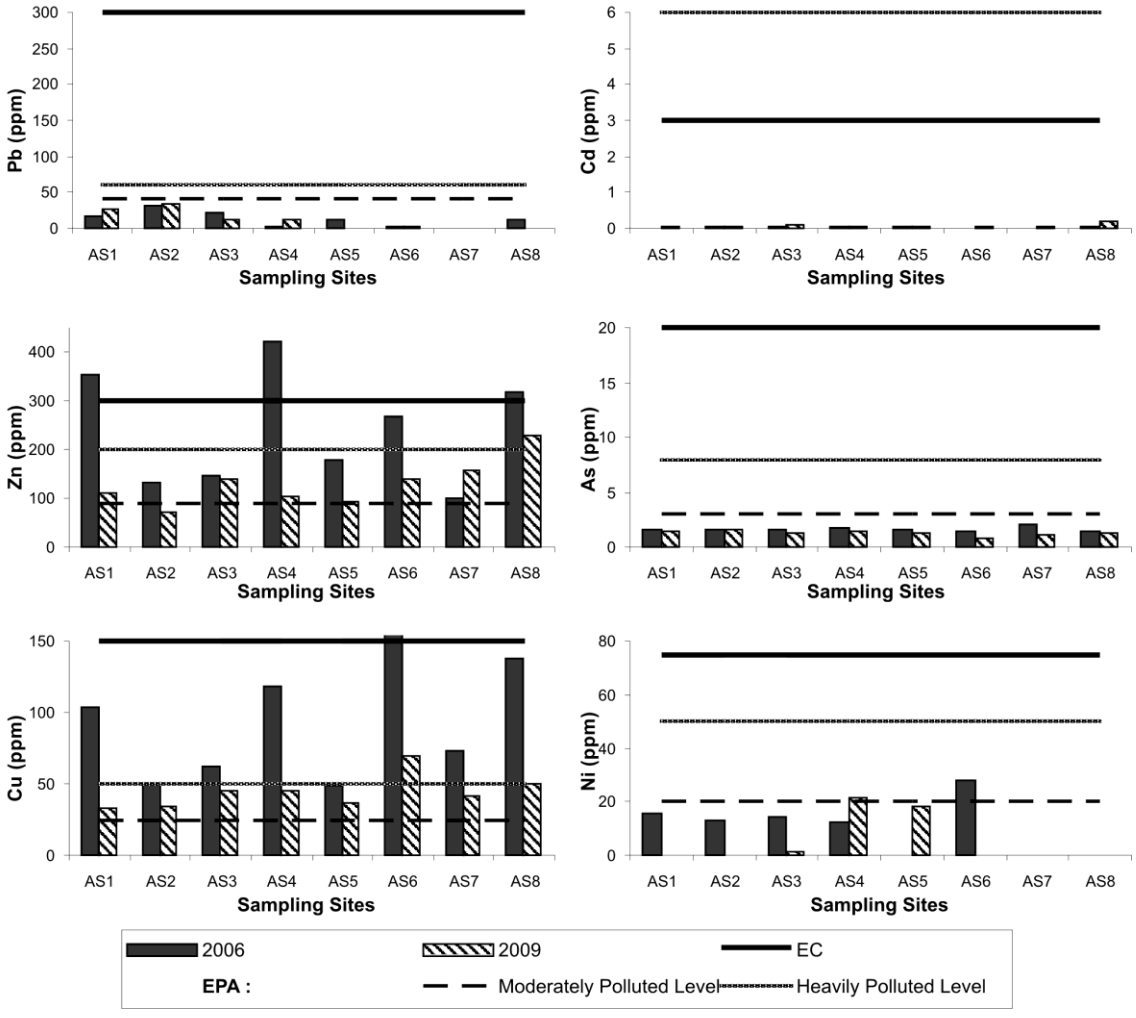

Fig. 2. Concentrations of Pb, Cd, Zn, As, Cu, and Ni in sediments collected from Bogdanas river, in comparison with EC and EPA Sediment Quality Standards.

the Bogdanas sediments and their relatively elevated concentrations are connected probably with the weathering of the ore mineralizations in Drakontio, Stefania and Assiros (Vavelidis et al., 1999; Melfos et al., 2001; Giouri, 2008). This is emphasized by the fact that the higher Zn concentrations coexist at the same sites with the higher Cu concentrations. Similar behavior was observed for Ni, which is probably attributed also to the weathering of the ore mineralizations, which mainly contain gersdorffite and ultramafic rocks that exist in the region contributes to its concentrations. The elevated concentrations of Zn, Cu and Ni at sites AS5, AS6 and AS7, especially in the 2006 sampling period, may have also been affected by the presence of an extensive uncontrolled litter landfill, very close to Assiros town. So the presence of batteries for example, could contribute to the increasing of Ni and Zn concentrations. The fact that the area was evacuated by all the litters meantime, affected the chemical composition of the sediments in the 2008 sampling period, and the Zn, Cu and Ni concentrations were lower.

5. Conclusions

The results of the chemical analyses at the sediments of Bogdanas river showed very limited and insignificant heavy metal contamination. Comparing the concentrations of Pb, Cd, Zn, As, Cu and Ni, with the limits determined by the European Community's legislation it is concluded that sediments are polluted at a percentage of 19% for Zn and 6% for Cu. Comparing these concentrations with the US EPA Sediment Quality Guidelines (SQG) it is concluded that in relation to Zn, 62.5% of the sediments are classified as moderately polluted and 31% as heavily polluted. As for Cu, a percentage of 44% and 56% are classified as moderately and heavily polluted, respectively. In addition, only the 12.5% of the sediments are classified as moderately polluted concerning Ni. The heavy metal concentrations in the Bogdanas sediments are mainly related to the lithology of the broader area and especially to the copper mineralizations in Drakontio, Stefania and Assiros areas, than to human activities. Part of the contamination is possibly attributed to the human activities, and mainly the presence of an extensive uncontrolled litter land fill near Assiros town. This is supported by the differences of some heavy metal contents (Zn, Cu, Ni) between the first sampling period of 2006 and the second sampling period of 2008. The higher heavy metal concentrations in the first period indicate that especially at the sites close to the uncontrolled landfill, metal bearing materials (such as batteries) could contribute to the sediments of the river. The decrease of the heavy metal contents in 2008 show that the public authorities applied the appropriate environmental measures established by legislation.

Acknowledgements

The first author (Giouri A.) would like to thank the State Scholarships Foundation of Greece for the financial support during her post-graduate studies.

References

Chatzipetros, A. and Pavlides, S., 1998. A Quantitative Morphotectonic Approach to the study of active faults, Mygdonia basin. Northern Greece. Bull. Geol. Soc. Of Greece,. XXXII/1, 155-164.

De Wet, A.P., 1989. Geology of part of the Chalkidiki Peninsula, northern Greece. Ph. D. thesis, University of Cambridge, U.K., 117 p.

Espinosa, E., Armienta, M.A., Cruz, O., Aguayo, A. and Ceniceros, N., 2009. Geochemical distribution of arsenic, cadmium, lead and zinc in river sediments affected by tailings in Zimapan, a historical polymetalic mining zone of Mexico. Environ. Geol., 58, 1467-1477.

Fernandez-Turiel, J.L., Acenolaza, P., Medina, M.E., Llorens, J.F. and Sardi, F., 2001. Assessment of a smelter impact area using surface soils and plants. Environ. Geochem. Health, 23, 65-78.

Förster, U. and Salomons, W., 1991. Mobilization of metals from sediment. In: Merian E (ed), Metals and their compounds in the environment. VCH, Weinheim, 379–398.

Gantidis, N., Pervolarakis, M. and Fytianos K., 2006. Assessment of the quality characteristics of two lakes (Koronia and Volvi) of N. Greece. Environ. Monit. Assess., 125, 175–181.

Giouri, A., 2008. Geochemical-minerological environmental study of the Bogdanas river sediments and waters at the Assiros area, Thessaloniki. Master thesis, Aristotle University of Thessaloniki, 115p (in Greek with English abstract).

Kabata-Pendias, A. and Pendias, H., 2001. Trace elements in soils and plants, 3rd ed. CRC Press, Boca Raton, Florida, 413p.

Kockel, F., Mollat, H. and Antoniades, P., 1978. Geological map of Greece, Thermi Sheet, Scale 1:50.000. IGME, Athens.

Kockel, F., Mollat, H., Antoniades, P. and Ioannides, K., 1979. Geological map of Greece, Lachanas Sheet, Scale 1:50.000. IGME, Athens.

Kostopoulos, D., Reischmann, T. and Sklavounos, S., 2001. Paleozoic and Early Mesozoic magmatism and metamorphism in the Serbomacedonian massif,

Central Macedonia, Northern Greece. Jour. Conf. Abstracts of EUG 11, April 8-12 2001, Strasbourg.

Melfos, V., Vavelidis, M. and Arikas, K., 2001. A new occurrence of argentopentlandite and gold from the Au-Ag-rich copper mineralization in the Paliomylos area, Serbomacedonian Massif, Central Macedonia, Greece. Bull. Geol. Soc. Greece, Vol. XXXIV(3), 1065-1072.

Murray, K.S., Cauvet, D., Lybeer, M. and Thomas, J.C., 1999. Particle size and chemical control of heavy metals in bed sediment from the Rouge River, southeast Michigan. Environ. Sci. Technol., 33, 987–992.

Perin, G., Bonardi, M., Fabris, R., Simoncini, B., Manente, S., Tosi, L. and Scotto, S., 1997. Heavy metal pollution in central Venice Lagoon bottom sediments: evaluation of the metal bioavailability by geochemical speciation procedure. Environmental Technology, 18, 593–604.

Psilovikos, A., 1977. Paleogeographic development of the basin and lake of Mygdonia (Langada-Volvi area, Greece), Ph.D. Thesis, Univ. Thessaloniki, in Greek.

Salomons, W., 1995. Environmental impact of metals derived from mining activities: processes, predictions, preventions. J. Geochem. Explor., 52, 5–23.

Suthar, S., Nema, K.A., Chabukdhara, M. and Gupta, K.S., 2009. Assessment of metals in water and sediments of Hindon River, India: Impact of industrial and urban discharges. Journal of Hazardous Materials, 171, 1088–1095.

Tranos, M.D., Kilias, A.A. and Mountrakis D.M. 1999. Geometry and kinematics of the Tertiary post-metamorphic Circum Rhodope Belt Thrust System (CRBTS), Northern Greece. Bulletin of Geological Society of Greece, 33, 5–16.

Tzimopoulos, Ch., Ginidi, P., Yannopoulos, S., Evangelidis, Ch., Chalkides, I. and Giannakopoulou, E., 2006. The problem of the management of Koronia's hydrological basin. Proceedings of the 2nd Conference of the Environmental Council of A.U.Th. "Environmental issues of Thessaloniki and wider area: Opinions of A.U.Th.", June 1-4, Thessaloniki, 265-272.

Vavelidis, M., Melfos, V. and Kilias, A., 1999. The gold-bearing quartz veins in the metamorphic rocks at the Drakontio area, central Macedonia, northern Greece. In: Mineral Deposits: Processes to Processing (ed: C.J. Stanley et al.), 209-212.

Zehl, K., Einax, J.W., 2005. Influence of atmospheric oxygen on heavy metal mobility in sediment and soil. J Soils & Sediments, 5 (3), 164 – 170.

Scientific Annals, School of Geology, Aristotle University of Thessaloniki Proceedings of the XIX CBGA Congress, Thessaloniki, Greece	Special volume 100	71-80	Thessaloniki 2010

ENVIRONMENTAL SYNERGY IN THE ROMANIAN PLAIN (TO THE EAST OF OLT RIVER)

Grecu F.[1], Gherghina A.[2], Ghita C.[1], Comanescu L.[1]

[1] *Dep. of Geomorphology-Pedology, Faculty of Geography, University of Bucarest, Bucharest, Romania, florinagrecu@yahoo.com, chrys_geo_2007@yahoo.com, lauracomanescu@yahoo.com*
[2] *Research Institute for Soil Science and Agrochemistry (ICPA), Bd. Marasti, no. 61, 71331 Bucharest, Romania, alinagherghina@yahoo.com*

Abstract: The objective of the study is the detection of areas and the functioning mechanisms of the oropedo-hydro-geographic and hydrogeologic systems within the Romanian Plain. Geological conditions, especially the hydrogeological ones (groundwater depth and flow) largely influence superficial and underground drainage system. The influence of groundwater dynamics in the padding interfluvial microrelief in direct connection with the thick of loess deposits, is a conditional variable in the occurrence and development of microdepressions towards drainage systems. The analysis of data shows a discrepancy between the supply of the maximum piezometric levels and rainfall, so the groundwater level oscillations are influenced by overlapping rainfall in previous years. To highlight the close link that exists between the microforms of relief and soil covering there have been made correlations between reappearance of padding soils with the distribution of compaction microdepressions. The large arteries assert the direction drainage of the groundwater and the groundwater depth climbs as it bears away from the hydrographic arteries; it results that density relief's fragmentation is directly proportional with the increasing of the groundwater depth.

Key words: Romanian Plain, environment synergy, pading microrelief, geomorphological processes.

1. Introduction

Romanian Plain (Lower Danube) is located in the central-south-east of Europe, the connection with the Black Sea being realized via the Danube River. It corresponds with the accumulation basin within the Carpathian-Balkan mountain arch, being a Quaternary fluvial-lake plane (Fig. 1). Subaerial modeling took place in distinct phases, which imposed various relief, manifested by individualization of several genetic types of plains.

The orogen units situated to the north (Carpathians and Subcarpathians) and the south (Balkans) of that depression influenced the hydrogeological regime of the field by the type of the deposits accumulated in the immediate connection units (gravel of Candesti, gravel of Fratesti), by the position and by the relative high flow of the phreatic water. This is reflected in the high density of drainage network of some sectors of plain (Grecu et al. 2006, 2007). To the south, the Danube, individualized in different stages of time, along with the withdrawal of Pleistocene Lake by E and NE, has contributed to the genetic variety of plain and imposed the general orientation of the hydrographic network (Valsan,1916; Cotet, 1976; Posea, 2002). Also, the Danube river is a major factor in the dynamics of the rivers: the small, young, indigenous to the plain ones (Mostistea, Calmatui), and those allochthonous that cross the plain (Olt, Arges, Ialomita, Buzau).

The neotectonics, manifested in the north-east through movements of different intensities or local

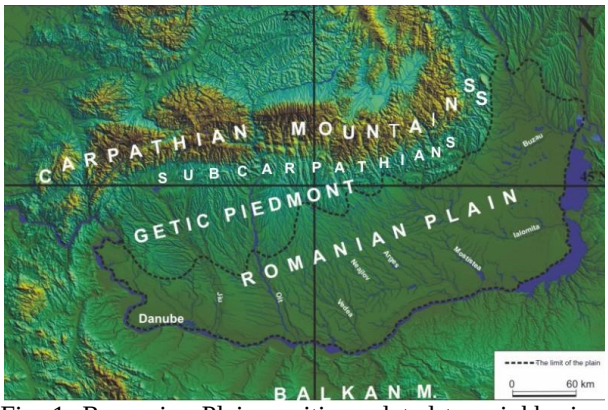

Fig. 1. Romanian Plain position related to neighboring units.

subsidence, is reflected in the morphohydrographic dynamics of the plain as convergence area of the network basins and small depths of the groundwater (0-2 m).

The anthropogenic intervention led to extensive changes in dynamics and drainage regime of the rivers, as well as in the interfluvial hydrophreatic system dynamics (through irrigation), something which is not subject to this study river-interfluve synergism.

Due to these factors, within the Romanian Plain (to the east of Olt River) have been identified the following types of areas according to the interdependent relationships between environmental factors, especially according to:

1. Sectors with high density of river network (between Olt and Arges) imposed by rich aquifers of piedmont deposits.
2. Areas with low density of river network but with common down-sagging processes (Ciornuleasa Field, Burnazul Field);
3. Interfluves with microdepresions of down-sagging and pipping, some of them lacustrine (Baragan Ialomita);
4. Sectors with typical landforms of the Bend glacis.
5. Lower Siret Plain - specific subsidence riverbeds forms.

2. Objectives, materials and methods

The main objective of this study is the detection of areas and the functioning mechanisms of the oro-pedo-hydro-geographic and hydrogeologic systems within the Romanian Plain (to the east of the Olt River). Analytical approach focuses both on the indicator elements (morphometric, morfographic, pedological) and the factor elements (geological data, hydrogeological, climatic, hydrological). Based on field mapping, synthesis reveals specific forms of relief. Conception and systemic approach is supported by the geomorphological one, by the observations and by mapping field.

2.1. Sources and materials

Thematic maps at different scales:
- Hydrogeological map, scale 1:1000000, Liteanu E. 1969;
- Geological map, scale 1:200 000, State Committee of Geology
- Soil Map, scale 1:200 000, L- 35- XXXIV, Calarasi, Institutul Geologic, Comitetul Geologic, Bucuresti
- Topographic maps (scale 1:100000, 1:50000, 1:25000), orthophotomaps (scale 1:5000).
- Data recorded at weather and hydrometric stations;
- Groundwater measurements in wells and field observations (2004-2009).
- ArcGis-ArcMap/Gis, 70 Stereograph projection, Datum S_42 ROMANIA, SRTM (Shuttle Radar Topography Mission) or Corine Land Cover.

3. Results

3.1. Geological and hydrogeological features

Geological conditions, especially the hydrogeological ones (groundwater depth and flow) largely influence superficial and underground drainage system. Deposits characteristic to the central sector of the Romanian Plain (between Olt and Arges) are composed of porous permeable rock, respectively Pleistocene gravel and sand (Fig. 2). Candesti layers, characteristic to the Getic Piedmont, continue on relatively small areas in the field, especially at the contact Piedmont-plain. They are river-lake deposits, composed of stacks of tens of meters of gravel in alternation with marl-clays and sands (Fig. 3). In Piedmont, the groundwater is located at more than 50 m depth, due to gravel. Groundwater drainage to the contact with the plain and within the plain leads to psephitic deposits saturation. Aquifers layers appear as springs that feed rivers in the plains (Liteanu and coord. 1969) (Fig. 2).

Fratesti layers to the south of the alignment Pitesti-Slătioarele, are found in loessic deposits at depths of 20-25 m (Bandrabur 1968). The groundwaters at these depths have free hydrostatic level and flowing from northwest to southeast is consistent with the hydrographic network (within the plain between Olt and Arges).

To the east of Mostistea sands with middle granulation appear, the hydrostatic level ranging between 5 and 20 m being influenced by the presence of sandy clays intercalated in the sands complex (low flow, below 1 l/s) (Fig. 2).

In the Central Bărăgan the Sands of Mostiştea composed of fine sands, pass in clay sands on the east and northeast. They have been encountered in wells in the south of the interfluves Ialomita - Calmatui. Region's counterpane is made of loamy textured deposits with different percentage of sand (loess and loessic deposits), in the southern half of the region and deposits with texture ranging from

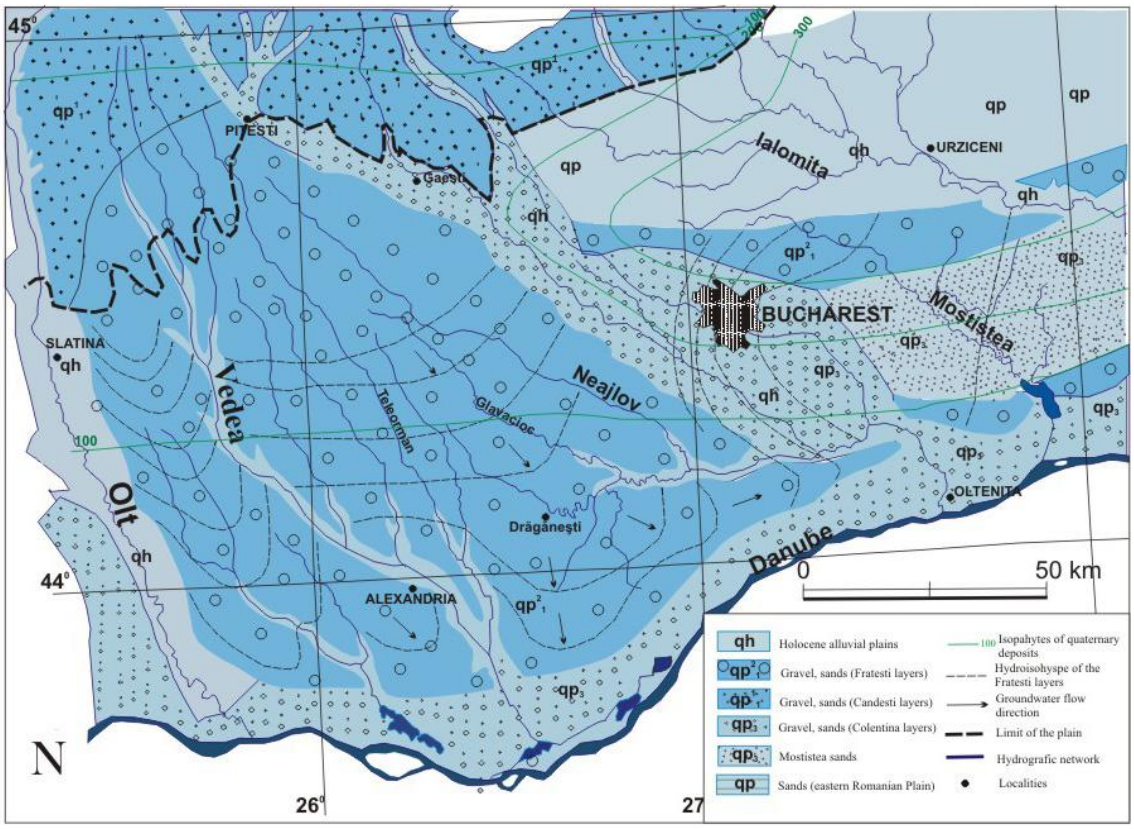

Fig. 2. Romanian Plain to the east of the Olt river. Hydrogeological map (after the *Hydrogeological map*, 1:1000000, E. Liteanu et. all, 1969).

sandy clay to loamy sand and sand (loessic deposits and sand) in the southern part (Tenu et al. 1989) (fig. 4). Under these conditions, the rivers feeding are done in moderate proportions from ground, but considerable for a flat unit. This presents significant variations from west to east (20-25% for Vedea and Neajlov, 15% for Mosti-stea). Rivers in the central plains (Vedea, Neajlov) are characterized by a dense network of drainage (4-6 km/km2). In the eastern sector, however, presents reduced network density (in the Mostistea basin is 0.14 km/km2) (Grecu et al., 2009b).

The hydrographic network is conditioned by geological structure of the Quaternary formations of the plains. The general inclination of the piezometric slope is strongly related to individualization of the hydrographic network: from north to south in the central and east-west (towards the Danube) and even from southwest to northeast in the eastern sector. In periods with excess moisture the levels of groundwater in the northeastern plain grow up near the surface causing flooding in appreciable areas, both in the valley along the corridors and on interfluves (Gastescu et al., 1979; Bogdan, 1979).

Types of groundwater regime in the East Romanian Plain:

¬ fluvial type in river flood-plains, with large amplitudes in normal years and very high in rainy years, returning every year at the same minimum level;

¬ piedmont type in piedmont plains, with large amplitudes (1-3 m) and annual return of the minimum levels around the same level as determined by high permeability of the covering deposits and a good drainage;

¬ divagation plains type, with medium amplitudes (0.5-1 m, rarely 2-2.5 m), with a slight increase of the minimum level in rainy years;

¬ Central Bărăgan type, met in Central Bărăgan, NW of South Bărăgan and in South Bărăgan, west of Ianca Valley, with average annual amplitudes of 0.5-1.5 m and a continued increase of the minimum level in consecutive rainy years, growth that exceed a little the range rainy years;

¬ South Bărăgan type, with a continuous increasing level without annual swings or with very small oscillations, growth that exceeds a lot the rainy consecutive years intervals; this can be meet also in the eastern part of the North Bărăgan.

Fig. 3. Gravels of Candesti in an opening at Milcoiu on the left slope of Topolog (foto 2009).

3.2. The morphology of the drainage network

The inter rivers Olt-Arges is fragmented by a rich local hydrographic network, tributary to Arges, Olt, and Vedea (partially native river, with springs in the Getic Piedmont) (Fig. 5). The rivers have their source in alluvial deposits (alluvial cones of the large rivers, at the exit of the Piedmont or Subcarpathians). For the rivers in the upper sectors of the confluence report presents high values (6.63), leading to a high magnitude in the Horton-Strahler scheme (5,6,7), atypical situation for river plain. For example, in the superior sector, Neajlov, of order 4, is made in terms of number of river segments (I_N = 105%), but under-realized from the length of river segments point of view (I_L = 59%) and also from the average length of river segments point of view (I_l = 56%) (Grecu et al.2009b).

The sub-realization of the lengths sum gives the torrential character of the rivers' segments, most of which are segments of order 1 and 2, respectively glens and gullies, with average lengths between 1 and 4 km, with intermittent flow, whose occurrence is mainly due to geological substrate (sedimentary deposits, friable, poorly consolidated: sand and gravel terrace of Arges - T_2, T_3, loessic deposits, loess) and to modeling processes (rain wash, pouring, down-sagging and pipping).

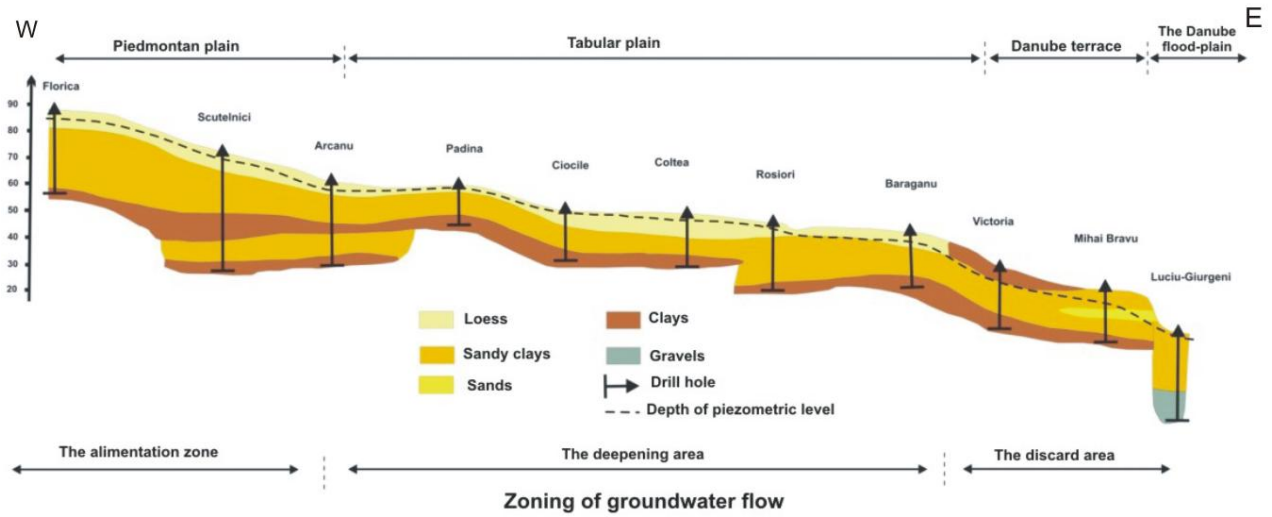

Fig. 4. Hydrogeological transverse profile in the Central Bărăgan Plain on the direction W-E (after Tenu S., Frugina E., 1989).

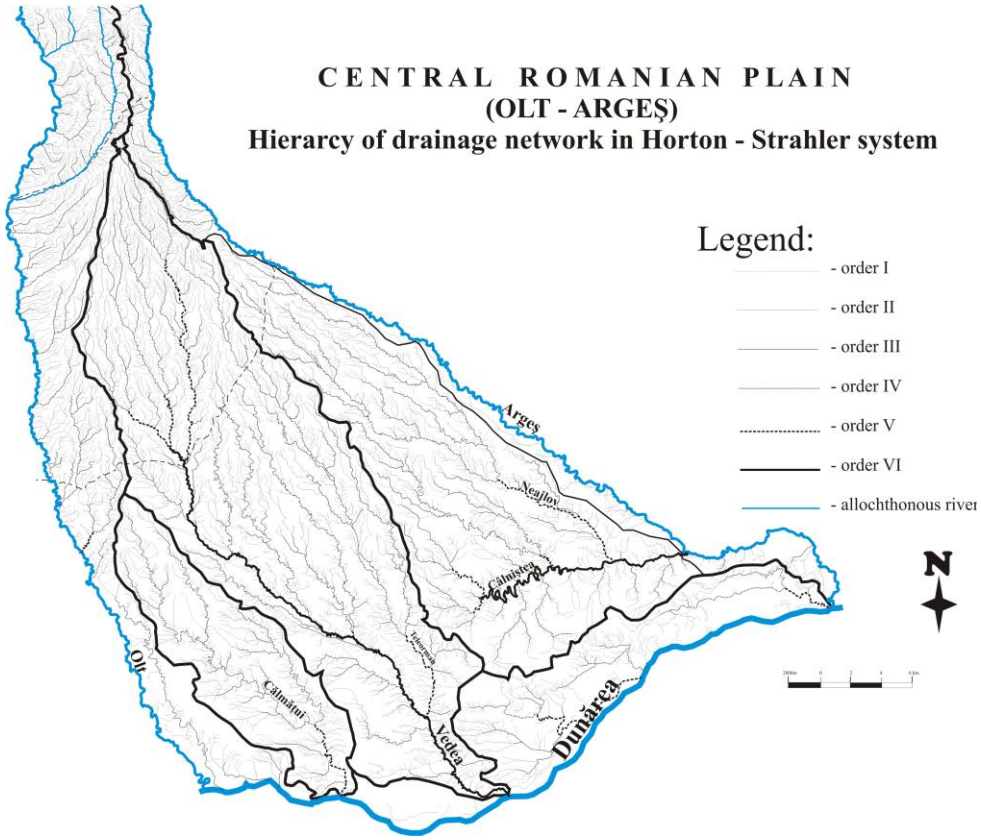

Fig. 5. Olt-Arges sector. The chain of the hydrographic network on Horton-Strahler system it can be observed the high density of the drainage network.

As it regards Cotmeana River a tributary of Vedea in the superior course) with spings in the Piedmont, it should be assessed as a contact river, the medium and the inferior sectors belonging to the plain. On entering the plain, in the basin Cotmeana can be observed a line of springs, making the largest partial confluence report $R_{C_3} = 7.4$.

3.3. The pading microrelief

The influence of groundwater dynamics in the pading microrelief on the fields (inter rivers), in direct connection with the thick of loessic deposits, is a conditional variable in the occurrence and development of microdepressions towards drainage systems.

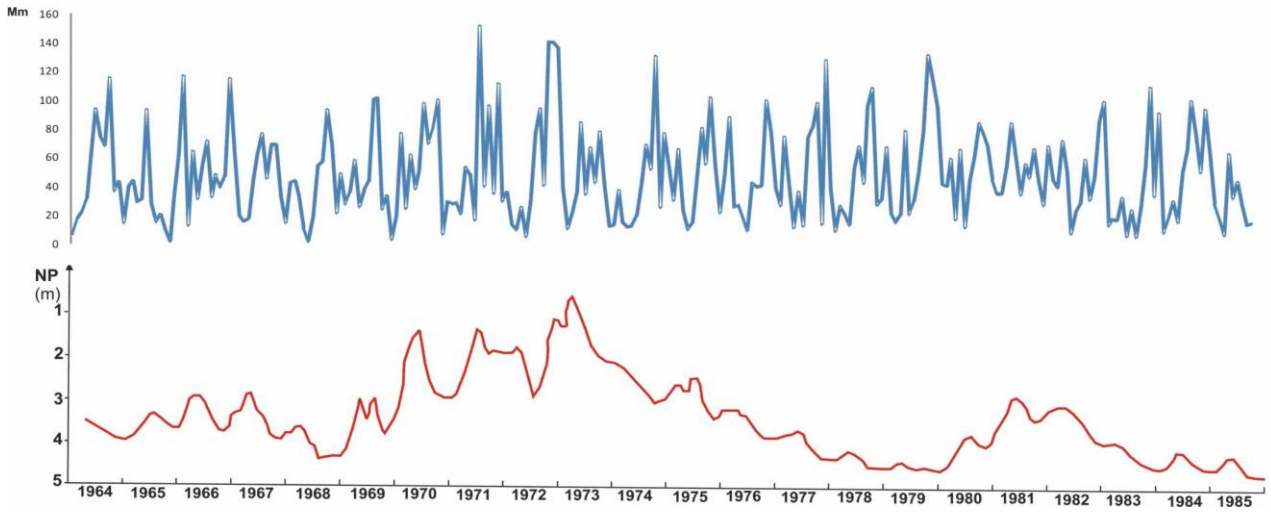

Fig. 6. Relationship between changes in the piezometric level in Grindu area (source's datas Tenu S., Frugina E., 1989) and average monthly rainfall values (station Urziceni) (source data: ANM).

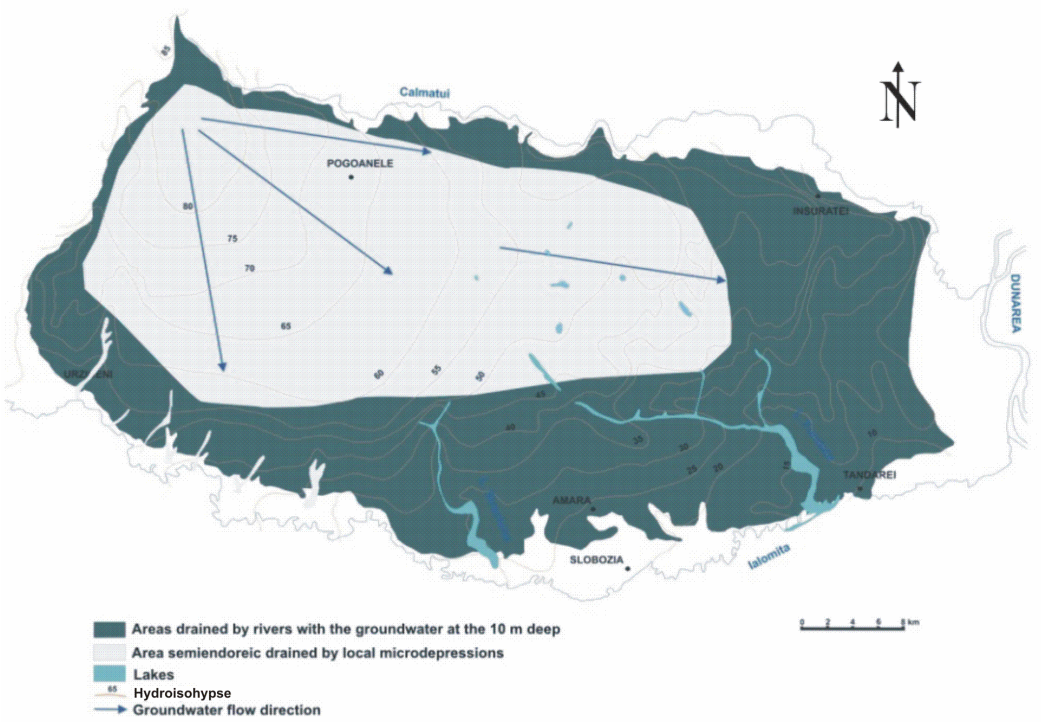

Fig. 7. The general direction of the groundwater flux within Central Baragan (after Florea N., 1976, with modifications and completions based on researches in the field)

In the Central Bărăgan, for example, the main feature of the groundwater system is the very slow horizontal flow, which favours the growth of the salts and raising the hydrostatic level (Florea 1970). The phreatic water is found below the surface of 2-5 m in the central part of the plain, while in the northern, eastern and southern falls to 5-10 m depth, even 15 m, due to the action of draining of Ialomita, Calmatui and Dunarea rivers . The hydroisohypses have general West-East direction, with a slight orientation towards South-East due to strong action of drainage of Ialomița. The cuvettes and the drowned rivers work as natural drains, collecting groundwaters from a small area, water gradually evaporates, increasing the salt concentration of lakes.

The analysis of data shows a discrepancy between production of the maxims piezometric levels and rainfall, so the groundwater level oscillations are influenced by overlapping rainfall in previous years (Fig. 6). The large and sudden level variations of the rivers and the high rainfall determine high variations of the subteran drainage, that draw te sagging of the deposits from above. The general direction of groundwater flow is from NW to the south and east, from intense supply areas in the northwestern and central towards unloading areas. Groundwater flow follows, in general, the direction of decreasing energy relief. In western Central Baragan the underground flow is radial, the download being toward Ialomița, Sărata and Călmățui and in east flow gradually becomes a west-east direction, towards the Danube (Fig. 7).

The high loessic deposit thickness and the great depth of groundwater have led to the apparition of microdepressions with small areas and circular forms, without irregularities (low sinuosity coefficient). The ratio between length and width exceeds the value 2, and the general orientation complies with the general direction of the wind direction and the isopahcytes. Depending on the particular morphohydrogeological features, in the Central Bărăgan (Fig. 8) were identified:

- ***microdepressions with vertical circulation of the water*** (water aquifers at great depth -10-15 m and great thick of loess), circular or elongated, occur in the southern plains, between the valleys Strachina and Fundata. In these depressions the groundwater flow is predominantly downward, the carbonates and the soluble salts are washed from the soil, and the main consequence are the reducing of the total mass of the material and the particles' compacting;

¬ ***interdunes microdepressions*** (at the contact between loess and sand), with excess moisture and accumulation of salts; the low depth situated

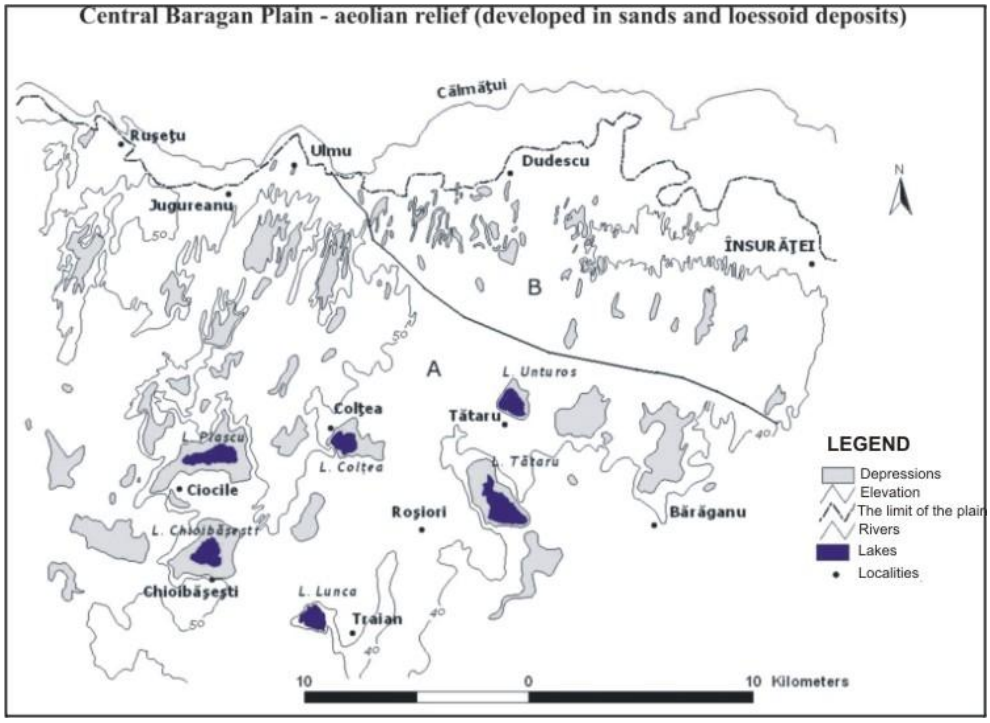

Fig. 8. Central Baragan Plain. Eolian relief (developed on sands and loessic deposits) (after *Topographic map* 1:25 000, *Ortophotoplans* 1: 5 000 and researches in the field).

groundwater intersects the bottom of the depressions, where temporary lakes can even install and water flow is predominantly upward; in dry periods, slightly mineralized groundwater that rises to the surface by capillarity evaporates and contained salts precipitate out, forming crusts of salts;

¬ ***microdepressions with groundwater at 0-3 m, with lakes***. They have large areas and depths of 5 meters and they are situated in the perimeter Tătaru-Ciocile-Traian. Due to large depth in rainy periods the groundwater level rises above the bottom of the depressions, forming lakes (Tataru, Ciocile, Plascu, Chioibăşeşti);

¬ ***low depression areas, with groundwater at 5 m***, that appear in the west of the plain, the area Brădeanu-Glodeanu Sărat-Florica, and in the center, in the area Scutelnici-Cocora-Padina. They have depths of several tens of cm, and during periods of excess moisture can turn into swamps.

¬ ***microdepressions at the contact between terrace and field,*** developed mainly at the contact with the Danube terrace.

¬ ***microdepressions at the contact between terrace and flood-plain***, very numerous, whose development was influenced by human activities (creating holes for exploitation of sand and clay).

¬ ***microdepressions formed at the confluence between the secondary valleys with Ialomita (lake cuvettes)***, formed by sluicing the discharge with materials submitted by Ialomita, behind which formed lakes (drowned rivers). In these valleys there were built human dams for use in agriculture.

3.4. Oropedogeomorphologic report

The correlation between the edaphic and morphologic element may be an important variable in identifying the stage of development, age and current dynamics of the relief interfluves forms. The depressions' microrelief creates conditions for diversifying the edaphic covering where the genetic area type is the chernozem. The great quantity of water that accumulates in depressions, due to internal and external drainage, causes a dampening more pronounced here than on tabular relief and the appearance of eluvium soils (Ghita, 2009).

To highlight the close link that exists between the microforms of relief and edaphic covering there have been made correlations between reappearance of padding soils (cambic and argillic chernozems in paddings and padinies, respectively cambic and phreatic-wet argillic chernozems in paddings and

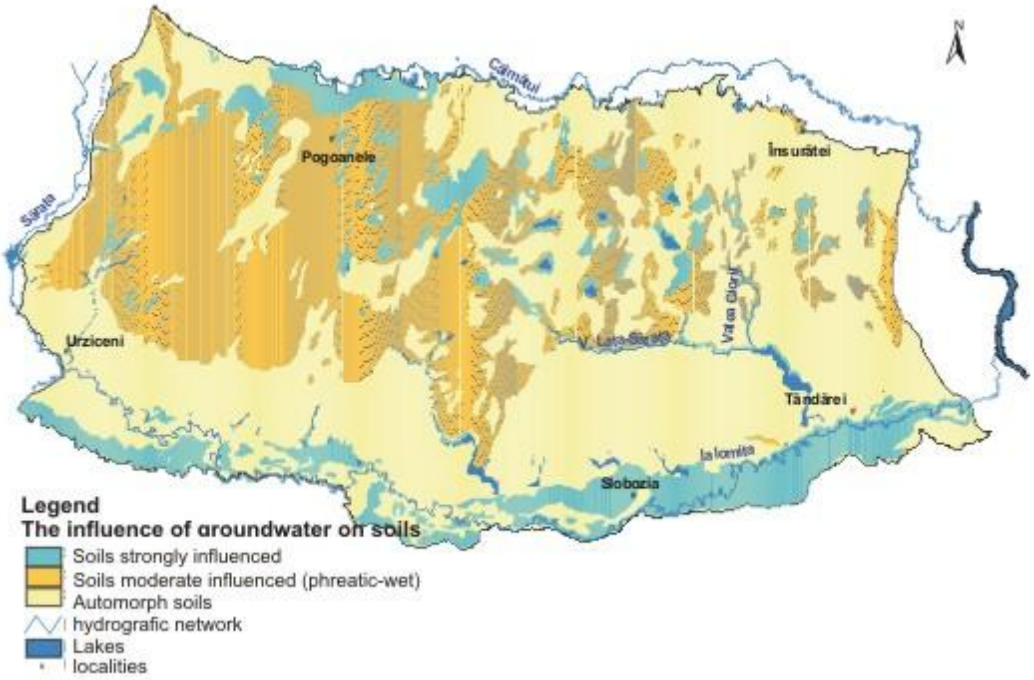

Fig. 9. Central Baragan Plain. Oropedologic relations (after *Topographic map* 1:25 000, *Soil map* 1:200 000, *Calarasi*, and researches in the field).

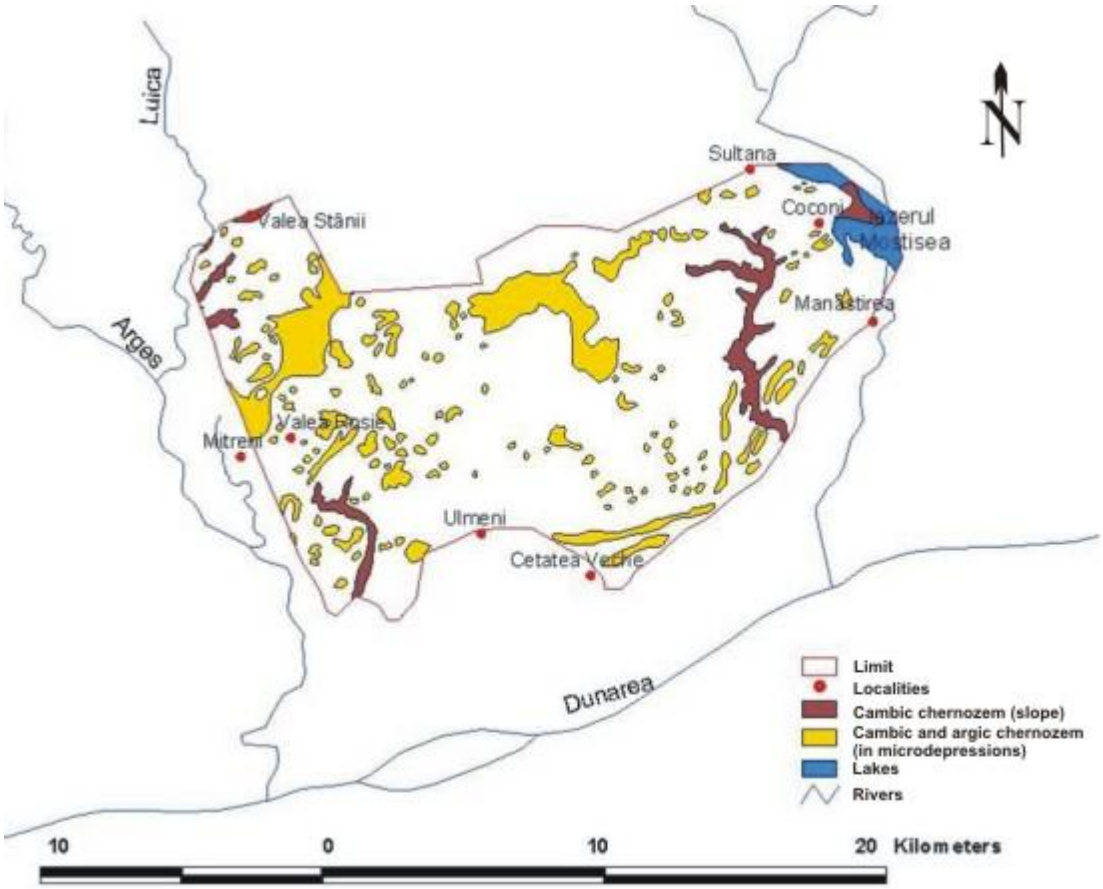

Fig. 10. The Sector Mostiștea-Ulmeni (Arges-Mostistea intefluve). Oropedologic relations (after *Topographic map* 1:25 000, *Soil map* 1:200 000, *Calarasi*, and researches in the field).

padinies and tableland, that chernozems argiloiluviale bill and phreatic-wet, in Crovurilor and tableland) (Fig. 9, 10) with the distribution of compaction microdepressions (Florea et.al. 1959; Florea 1970, Florea, Vespremeanu, 1999).

Thus, the upward movement of water from the profound layers towards the surface, rarely occurs, in short periods of the year, or not at all; therefore, no longer soluble salts are transported to surface by capillary rise of the water. In this way, the carbonates (hardly soluble salts) are at a greater depth as the depression is deeper and provides conditions for accumulation of water here in larger quantities and thus a worsening aerohydric regime, with negative consequences on fertility soil (Chitu, 1975). Parallel to the process of eluviation and podzolization of the soils from padings, there is also a compaction of the mineral material.

4. Conclusions

It can be ascertain the poly-and multi-genetic feature of the padings, the final causal process constituting the compaction in deposits with high porosity.

- In areas with the deep groundwater chemical compaction prevails due calcium carbonate dissolution (eg the central part of Ialomita Baragan, Mostistea Baragan);
-Where groundwater is near the surface, the slope changes of leakage (surface and groundwater) the compaction due hydrodynamic pipping dominates (eg Ialomita Baragan, the northern part);
- The large and sudden variations in level of rivers determine the groeth of the underground drainage and in its turn it determines the pipping of the above deposits. This is the case of the padings and padinies aligned along some glens (eg Mostistea Baragan);
- The large arteries assert the direction drainage of the groundwater and the groundwater depth climbs as it bears away from the hydrographic arteries; it results that density relief's fragmentation is directly proportional with the increasing of the groundwater depth (ex semiendoreic areas of Central Baragan, Mostistea Baragan);
- Groundwater near the surface contributes to the increasing of the intensity of compaction processes (by decreasing the porosity of loessoic deposits), and also to the emergence of numerous springs that influence the high density of river network (the Romanian Plain between Olt and Arges);
- The indicator elements of changes occurred in relief are soils. The soils from the areas with paddings are diversified in small spaces, although it's a plain unit;
- Local peculiarities are due to synergetic relationships between groundwater and the hydrographic network, and between them and the interfluvial dynamics, in addition with the type of rivers feeding: pluvial-nival and underground;
- On a relatively small area there is a great diversity of these relationships that are connected by the general palaeogeographic evolution of the region (Grecu et al. 2009).

Acknowledgements

The research was made within the limits of the PNII, CNCSIS projet " The hydrogeomorphological system in the concepts of geomorphometry and of modern morphological theories.Applications to hazard and risk diagnosis in areas of the Romanian Plain" (Director Prof. Florina GRECU).

References

Bandrabur T., 1968. Cercetări hidrogeologice pe interfluviul Ialomița-Mostiștea – Dunăre, STE, Seria E, Hidrogeologie, Bucureşti, 141-164.

Banu A. C., 1967. Câteva caractere hidrografice ale Bărăganului şi unele concluzii geomorfologice care se deduc pe baza lor, Hidrobiologia, Bucureşti, 205 – 214.

Chitu, C. (1975), Relieful şi solurile României. Raporturi genetice şi de productivitate, Ed. Scrisul Românesc, Craiova.

Conea A., Ghitulescu N., Vasilescu P., 1963. Consideratii asupra depozitelor de suprafata din Campia Romana de Est, Studii tehnice si economice, C, 11, Bucuresti.

Coteț P., 1976. Câmpia Română – studiu de geomorfologie integrată, Ed. Ceres, Bucureşti, 256p.

Cotet P., 1956. Câteva observații asupra formării lacurilor şi rețelei de văi secundare din Câmpia Română, A.U.C.I. Parhon, Şt. Naturii, Bucureşti.

Florea N., Predeal F., Munteanu I., 1959. Cercetări pedologice între Mostiștea şi Argeş, Dari de Seama, Comit. Geol., vol. XLII, Bucureşti.

Florea N., 1970, Câmpia de crovuri, un stadiu de evoluție al câmpiilor loessice, STE, Seria C, Studii Pedologice, Bucureşti, 339-354.

Florea N.,1976, Geochimia ş i valorificarea apelor din Campia Romana de nord-est, Ed.Academiei, Bucuresti, 202 p.

Florea N., Vespremeanu R., 1999. Argumente pedologice pentru precizarea limitelor si evolutiei unitatilor de relief din Campia Romana de la est de Arges, Stiinta solului, XXXIII, nr. 2, 57-70.

Ghita C., 2008. The microrelief as result of morphohydroclimatic conditions in Mostistea river basin., Revista de Geomorfologie, vol. 10, Ed. Universitatii din Bucuresti, 103-111.

Gastescu P., Zavoianu I., Bogdan O., Driga B., Breier A., 1979. Excesul de umiditate din Campia Romana de nordest (1969-1973), Ed. Academiei, Bucuresti, 176 p.

Grecu F. 2010, Geografia campiilor Romaniei, Note de curs, in press

Grecu F., Carciumaru E., Gherghina A., Ghita C., 2006. Semnificația reliefogenă a depozitelor cuaternare din Câmpia Română la est de Olt, Comunicări de Geografie, vol.VI, 21-36.

Grecu F., Comanescu L., Gherghina A., Ghita C., Sacrieru R., Vacaru L., 2007. The geomorphological processes and forms developed by quaternary deposits in the Romanian Plain (Est of Olt river), in Carpatho–Balkan–Dinaric Conference on Geomorphology, 24 -28.

Grecu F., Sacrieru, R., Ghita C., Vacaru L., 2009a. Geomorphological landmarks on the Romanian Plain Holocene Holocene Evolution, Paleoenvironmental dynamics and archaeological sites, Zeitschrift für Heomprphologie, Supplementbände, Volume 53 Supplementary Issue 1, Ed. Pavlopoulos, Kosmos, Stuttgart, 99 – 110.

Grecu F., Ghiță C., Carciumaru E., Vacaru L., 2009b. Diagnostic des aléas detérmines climatiques dans les systèmes hydrogéomorphologiques de la Plaine Roumaine, in vol Extrêmes climatiques: genèse, modélisation et impacts, XXII Colloque de l'Association Internationale de Climatologie, 1-5 Sept. Cluj-Napoca, Geographia Tehnica, Numero special, 229 – 234.

Institutul de Geografie, Academia Romana, 2005. Geografia României, vol. V (Câmpia Română, Dunărea, Podişul Dobrogei, Litoralul românesc al Mării Negre şi Platforma Continentală), Ed. Academiei, Bucureşti.

Institutul Geologic, 1963. Harta solurilor, 1: 200 000, L-35- XXXIV, Calarasi, Comitetul Geologic, Bucuresti

Liteanu E., Ghenea C., Bandrabur T., Mihaila N., Ghenea A., Giurgea P., 1969. Harta hidrogeologica, 1:1 000 000, Institutul Geologic, Comitetul de Stat al Geologiei, Bucuresti.

Posea Gr., 2002. Geomorfologia Romaniei, Ed. Fundatiei Romania de Maine, Bucuresti, 444p.

Tenu S., Frugina E., 1989. Studiul regimului apelor freatice din Subcarpatii de Curbura si zona de influenta (Baraganul Central si de Nord), in Raportul INMH, Bucuresti.

Valsan G., 1916, Campia Romana, B.S.R.G., t. XXXVI, 313-568, Rp. Opere alese, Ed. Ştiinţifică, Bucureşti, 149 – 318.

*** 1967. Harta geologică, 1: 200 000, Foaia Bucureşti, Comitetul de Stat al Geologiei.

*** 1968. Harta hidrogeologică a interfluviului Ialomița-Mostiştea-Dunăre, Comitetul geologic, STE, seria E, nr. 5.

*** 1970. Hărți topografice, 1: 50 000, 1: 25 000.

*** 2005. National Agency for Cadastre and Land Registration, Ortophotoplans 1: 5 000, Bucuresti.

Scientific Annals, School of Geology, Aristotle University of Thessaloniki Proceedings of the XIX CBGA Congress, Thessaloniki, Greece	Special volume 100	81-87	Thessaloniki 2010

CONTINUOUS EXTRA-FRAMEWORK Na^+ RELEASE FROM GREEK ANALCIME-RICH VOLCANICLASTIC ROCKS ON EXCHANGE WITH NH_4^+

Kantiranis N.[1], Sikalidis C.[2], Papastergios G.[1], Squires C.[1] and Filippidis A.[1]

[1]*Department of Mineralogy-Petrology-Economic Geology, Aristotle University, 54124 Thessaloniki, Greece, kantira@geo.auth.gr, gpapaste@geo.auth.gr,anestis@geo.auth.gr*
[2] *Department of Chemical Engineering, Aristotle University, 54124 Thessaloniki, Greece, sikalidi@auth.gr*

Abstract: The continuous extra-framework cations release from Greek analcime-rich rock sample was studied, upon ammonium acetate exchange experiments (agitation time 0.25-720 hours), using atomic absorption spectrometry. The analcime-rich material was examined by X-ray powder diffraction, scanning electron microscopy equipped with energy dispersive micro-analytical system and atomic absorption spectrometry. Its sorption ability was measured using the Ammonium Acetate Saturation method. The monovalent cations K^+ and Na^+ after 720 hours, show only 7 and 10% of exchange, respectively. No steady state achieved for Na^+. The bivalent cations Ca^{2+} and Mg^{2+} show better exchange, 97% for Ca^{2+} and 62% for Mg^{2+}. The calculated rate of ion-exchange was 0.01 ppm/h for K^+ and Mg^{2+}, while 0.13 ppm/h for Na^+ and Ca^{2+}. The recorded behaviour on the multi-component ion-exchange system and the linear release of Na^+ over NH_4^+ observed at a slow rate of ion-exchange, can allow us to propose studied analcime-rich rock as a potential material for waste-water purification and pet litter.

Keywords: tuffs, cation exchange capacity, selectivity, potential uses.

1. Introduction

The analcime structure is made up of linked tetrahedral units proscribing three on-connected channels (Szostak, 1992). Analcime has a relatively compact structure compared with other zeolites and has an idealized unit cell of $Na_{16}(Al_{16}Si_{32}O_{96})16H_2O$ (e.g., Meier et al., 1996; Baerlocher et al., 2001). The cubic unit cell is composed of four-, six-, and eight-membered oxygen rings that form three non-intersecting channels with pore openings of 2.6 Å. These channels encompass 24 small cavities, of which 16 are occupied by sodium cations (Saha, 1959). Analcime has maximum cation exchange capacity 4.9 meq g^{-1} (Sherman, 1978). Small pore zeolites, such as analcime, can constitute a basis for possible future technical innovations in selective adsorption and heterogeneous catalysis (Cheng et al., 2000).

High quality natural zeolites have many applications in industry, agriculture and the environment (e.g., Mumpton, 1978; Pond and Mumpton, 1984; Dyer, 1988; Tsitsishvili et al., 1992; Misaelides et al., 1993; Holmes, 1994; Ming and Mumpton, 1995; Misaelides et al., 1995a,b; Filippidis et al., 1996; Godelitsas et al., 1996a,b; Bish and Mind, 2001). The great majority of these applications employs their cation exchange capabilities and involves the replacement of the existing extra-framework cations with other cations from the surrounding environment. Due to the favourable ion-exchange selectivity of natural zeolites for certain cations, these minerals have been studied for potential use in the treatment of nuclear, municipal and industrial wastewaters and acid mine drainage waters. It is of economic importance that natural zeolites are used in their natural state so that expensive purification is avoided.

The aim of this work is to study the outgoing cations (Na^+, K^+, Ca^{2+} and Mg^{2+}) of analcime-rich volcaniclastic rocks during cation exchange with NH_4^+. The NH_4^+ was selected as the cation of choice as the affinity of zeolites for this cation has led to it being exploited for multiple applications such as in waste water treatment, pet litter and aquaculture. It is also used in the recognized AMmonium Acetate Saturation (AMAS) method (Bain and Smith, 1987) for the determination of the sorp-

tion ability of zeolites. Studies to evaluate how a natural zeolite exchanges with a single-cation or a multi-cation solution often use the Na- exchanged form of the zeolite, which has been shown to lead to higher cation exchange capacities (Yang et al., 1997). Results of these studies however are not applicable where the zeolite will be used in its natural form. Also, most published ion-exchange data on natural zeolites involve the exchange of two cations only. Little attention has been paid to the problem of understanding multi-component ion-exchange equilibrium, despite the fact that ion-exchange processes in natural systems, generally involve more than two ions. In this paper, the exchange of the extra-framework cations Na^+, K^+, Ca^{2+} and Mg^{2+} found in the natural zeolite with a solution of ammonium acetate (NH_4AcOH), as the source of NH_4^+ cations, is studied. Greek analcime-rich rock was selected due to its high zeolite content in order to study its different rates of exchange, while the results of this work are directly connected to the potential applications of the particular Greek zeolite bearing-rock.

2. Materials and Methods

Analcime-rich (AR) volcaniclastic rock sample was taken from the Neogene sedimentary Karlovassi basin of Samos island. The basin's volcanic rocks have been extensively zeolitized to give HEU-type, analcime, chabazite, phillipsite and mordenite of which HEU-type and analcime are the most abundant (e.g., Stamatakis, 1989; Hall and Stamatakis, 1992; Pe-Piper and Tsolis-Katagas, 1991; Kantiranis et al., 2004).

The sample was studied in its bulk form, ground (<125 μm) and homogenized. Sample for mineralogical and chemical analyses was ground further in an agate mortar. Chemical analysis of sample was carried out by AAS on a Perkin Elmer 5000 spectrometer equipped with a graphite furnace. Electron probe microanalysis of the studied zeolite phase was performed on polished thin sections of the zeolite-rich rocks by SEM-EDS (Jeol JSM-840: A scanning electron microscope, equipped with a LINK 10000 AN Energy Dispersion Analyser). Corrections were made using the ZAF-4/FLS software provided by LINK. To minimize volatilization of alkalis in the zeolites framework, the electron beam spot size was enlarged and the counting time decreased. Different minerals (micas, carbonates, feldspars) and pure metals were used as probe standards.

The experimental procedure for the cation exchange experiments entailed placing 100 mg zeolite-rich sample (<125 μm) and 10 mL of 1N ammonium acetate (of pH 7.0) solution into screw-top glass tubes. The tubes were sealed and agitated for 0.25, 0.75, 1.25, 2, 4, 6, 8, 12, 18, 24, 36, 48, 72, 96, 120, 144, 168, 192, 216, 240 and 720 h. The mixtures were then centrifuged and the liquor decanted into a 200 mL volumetric flask. The solid was then washed with 10 mL of deionised water three times and the washings were combined with the liquor and the volume adjusted to 200 mL. The concentration of Na^+, K^+, Ca^{2+} and Mg^{2+} cations in this solution was analyzed by AAS on the Perkin Elmer 5000 spectrometer.

The mineralogical composition of the sample was determined by X-ray Powder Diffraction (XRPD) method. The XRPD analysis was performed using a Philips PW1710 diffractometer with Ni-filtered CuK_α radiation on randomly oriented samples. The counting statistics of the XRPD study were: step size: 0.01° 2θ, start angle: 3°, end angle: 63° and scan speed: 0.02^o 2θ/sec. Quantitative estimates of the abundance of the mineral phases were derived from the XRPD data, using the intensity of a certain reflections and external standard mixtures of minerals.

In order to determine the sorption ability of the studied zeolite-rich sample, the sample was treated with 1M ammonium acetate (NH_4OAc) aqueous solution, according to the AMAS method. Approximately 125 mg of the <125 μm sample was added to a centrifuge tube with 10 mL of the 1N NH_4OAc solution. The suspension was well shaken, agitated for 24 hours, and then centrifuged. The clear liquid was discarded and the NH_4OAc-saturation procedure repeated 9 times, adding fresh 10 mL of NH_4OAc solution each time. After the completion of the 10-day NH_4OAc-saturation, the excess NH_4OAc was washed with 10 mL of 99% isopropyl alcohol, well shaken, and centrifuged. The clear supernatant liquid was discarded and the procedure repeated five times. The sample then was dried in room temperature. Following the NH_4OAc saturation, the NH_4^+ ions retained by the zeolite-rich sample, are converted using a strong base to NH_3 and analysed by an ammonia electrode. The NH_3 concentration was determined using an Orion potentiometric ammonia gas electrode combined with a Jenway 3045 pH/mV/ion analyser. Each air-dried NH_4^+-saturated sample was placed in a 100 mL Pyrex beaker containing a

Teflon covered stirring bar. Deionised nitrogen-free water (50 mL) was added and the solution was stirred to suspend the sample. The electrode was immersed into the suspension taking care to prevent entrapment of air under the concave tip. By addition of 0.5 mL of 10M NaOH, the NH_3 measurements were taken at constant level achievement. The electrode calibration was performed daily using ammonium calibrating solutions of 10, 100 and 1000 ppm provided by Jenway and hourly using the 10 ppm ammonium solution.

3. Results and Discussion

The quantitative mineralogical composition of the studied zeolite-rich sample is shown in Table 1. Analcime, micas (muscovite and/or illite) and clay minerals (mainly smectite) constitute the microporous minerals of the zeolite-bearing rock. The non-microporous minerals found in studied sample are quartz and feldspars. This classification is based on their ability to sorb cations on their structure. Amorphous material (volcanic glass) was also determined in the sample (10 wt %). The analcime content was determined 71 wt %., while in minor amounts micas (5 wt %), and clay minerals (2 wt %, mainly smectite) were also found. The total microporous mineral content in sample AR was 78 wt %.

Table 1. Quantitative mineralogical composition (wt %) of the studied sample.

Sample	A	M	Cl	TMM	Q	F	Am
AR	71	5	2	78	4	8	10

AR: analcime-rich, A: Analcime, M: Muscovite and/or illite, Cl: Clay minerals (mainly smectite), TMM: Total microporous minerals (Zeolite+M+Cl), Q: Quartz, F: Feldspars, Am: Amorphous.

The chemical composition of the studied zeolite-rich sample is shown in Table 2. AR sample was containing 56.11 wt % SiO_2, while the Al_2O_3 content was measured 18.80 wt %. Low amounts (<0.20 wt %) of TiO_2 and MnO were also found, while the Fe_2O_{3T} content was measured 2.98 wt %. The total percentage of oxides of the exchangeable cations Na^+, K^+, Ca^{2+} and Mg^{2+} was 12.07 wt %, with Na^+ being the main exchangeable cation. Loss on ignition was measured 9.43 wt %.

In Table 3 the measured sorption ability (meq/100g), the theoretical and the expected C.E.C. (meq/100g) of the studied zeolite-rich sample are given. The measured sorption ability was derived experimentally by the AMAS method. The theoretical C.E.C. of the sample was calculated from the quantitative mineralogical composition using values of 454 meq/100g for analcime, 20 meq/100g for muscovite-illite and 100 meq/100g for smectite (Mumpton, 1977; Deer et al., 1992). The expected C.E.C. was calculated from the total extra-framework cations of the contained zeolite, measured by SEM-EDS (Table 4). For the calculations of the theoretical and expected C.E.C. values the results were modified according to the zeolite content of the rock.

The measured sorption ability of the sample was too close to the expected C.E.C., meaning that the main process involving the sorption procedure of the studied sample was the ion-exchange.

Table 3. Values (meq/100g) of measured sorption ability, theoretical and expected C.E.C. of the studied sample.

Sample	Measured sorption ability	Theoretical C.E.C.[a]	Expected C.E.C.[a,b]
AR	334	325[c]	329

[a] Values modified according to TMM content (zeolite+micas+clay minerals) of the sample, [b] Measured from the zeolite micronalysis (by SEM-EDS), [c] Amorphous ability to sorb ions was ignored.

3.1. The ion-exchange of extra-framework cations for NH_4^+

The cation exchange behaviour of the zeolite-rich sample was investigated in order to determine which of the exchangeable ions is released first, the rate and the total amount of exchangeable cation occurs at the steady state, and the influence of the multionic system on the exchange behaviour. The SEM-EDS analyses gave accurate zeolite's chemical formula in the sample (several readings were taken for each zeolite and the average values tabulated in Table 4) providing clear data on how many and what species of potential exchangeable cations are contained in the zeolite structure and also the number of water molecules associated with the zeolite. The positions of both extraframework-cations and water molecules depend on the nature of the exchangeable cations of

Table 2. Chemical composition (wt %) of the studied sample.

Sample	SiO_2	TiO_2	Al_2O_3	Fe_2O_{3T}	MnO	MgO	CaO	Na_2O	K_2O	LOI	Total
AR	56.11	0.19	18.80	2.98	0.10	0.50	0.94	6.36	4.27	9.43	99.68

AR: Analcime-rich, LOI: Loss of ignition (at 1050ºC for 2 hours).

the zeolites (Armbruster and Gunter, 1991; Gunter et al., 1994). However, the exact structural arrangement in the channels also depends on the specific Si/Al framework distribution and the water content, which is dependent on the water vapour pressure surrounding the sample. Thus, the exchangeable cations and channel water molecules are interdependent. Changes in cation composition cause changes in the amount and structural distribution of water molecules; likewise, changes in channel water content affect the positions of the channel cations (Bish and Boak, 2001).

and Co^{2+} move into analcime.

Despite the slow exchange, the sorption ability value of 334 meq/100g obtained, using the AMAS technique, is very close to the expected value of 329 meq/100g calculated from the total percentage of extra-framework cations within the analcime structure (Tables 3 and 4). The very low degree of exchange observed in our experiment is probably due to the fact that AR zeolitic material being contacted with the same ammoniacal solution for 30 days. The AMAS method significantly improves the rate of cation exchange by replacing the solution every 24 hours for 10 days thus encouraging cation exchange by removing any competing cations from solution.

Table 4. Formulae and total exchangeable cations (ppm) of the studied zeolite.

Sample	Formulae	Total exchangeable cations			
		Na^+	K^+	Ca^{2+}	Mg^{2+}
AR	$(Mg_{0.20}Ca_{0.28}K_{0.58}Na_{14.97})(Fe_{0.15}Al_{15.80}Si_{31.92}O_{96})\cdot 16H_2O$	913	60	30	13

Micas and clay minerals (mainly smectite) found in AR sample also contain alkaline and alkaline earth exchangeable cations. However, due to their small weight percentages in contrast with the zeolite content of the rock, for the purpose of this discussion it is assumed that the cations released originate from the zeolite phase only.

The kinetic curves of AR sample for cation exchange of Na^+, K^+, Ca^{2+} and Mg^{2+} were presented in Figures 1(a)-1(d). Statistical analysis of the data was obtained using Microcal Origin v.6.0 software, while statistical models and correlation coefficients (R^2) were shown in each figure.

The release of Na^+ cations from sample AR (Fig. 1a) was linear with time over the whole 30 days (720h) period studied and a steady state was not reached. However, it is known that analcime, which has a dense structure, non-intersecting channels and small individual cavities, exhibits very limited ion exchange of its Na^+ for other cations. Particularly, at room temperature analcime does not readily exchange, but at elevated temperatures Na can be completely exchanged by other cations such as K^+ and NH_4^+ (Vaughan, 1978). Balgord and Roy (1974) reported that Na-analcime can be completely exchanged by K^+, Ag^+ ,Tl^+, NH_4^+ and Rb^+ cations at elevated temperatures, whereas only small amounts of Sr^{2+}, Mg^{2+}, Ni^{2+}

After 30 days (Fig. 1b) the concentration of K in solution was 4 ppm (Table 5) indicating the exchange of only 7 % of K^+ cations found in the aluminosilicate framework (Table 4). Bivalent cations Ca^{2+} and Mg^{2+} show better exchange. The Ca^{2+} concentration achieve a steady state of 29 ppm (Table 5) after 216 hours of agitation (Fig. 1c) indicating an almost fully exchange (97%) of Ca^{2+} cations found in analcime framework (Table 4). On the other hand, Mg^{2+} did not achieve a steady state (Fig. 1d), but after 30 days (720 h) its concentration was 8 ppm (Table 5), indicating the exchange of 62% of Mg^{2+} cation found in the analcime framework (Table 4). No steady state achieved for Na^+ (Fig. 1a) and only a percentage of 10% was exchanged from the structure of analcime (Tables 4 and 5).

In Table 5 the agitation time (h), the cation concentration (ppm), the degree of cation exchange (%) and the rate of exchange (ppm/h) once a steady state has been achieved, were summarized for sample AR.

Taking into consideration all the above data, the order of cation release from AR sample, is: Ca^{2+}

Table 5. Ion-exchange statistics for analcime-rich sample.

Extra framework ion	Na^+	K^+	Ca^{2+}	Mg^{2+}
Agitation time until steady state (h)	No steady state	290	216	720
Concentration at steady state (ppm)	After 720 h: 94	4	29	8
Degree of exchange (%)	10	7	97	62
Rate of exchange (ppm/h)	0.13	0.01	0.13	0.01

$>K^+>>Mg^{2+}>>>Na^+$, while the order of the degree of total cation release, is: $Ca^{2+}>Mg^{2+}>>Na^+\approx K^+$. Furthermore, the rate of ion-exchange was calculated for K^+ 0.01 ppm/h, for Ca^{2+} 0.13 ppm/h, for Mg^{2+} 0.01 ppm/h, while Na^+ exchanged in a constant rate of 0.13 ppm/h (Table 5). Using this rate of ion-exchange, the order for sample AR, is: $Na^+=Ca^{2+}>>K^+=Mg^{2+}$. Dyer and Yusof (1989) suggest a systematic-continuous replacement of Na^+ by NH_4^+ in analcime structure, which reduces the water content of analcime.

The linear release of Na^+ over NH_4^+ observed at a slow rate of ion-exchange in our experiments, can allow us to propose studied analcime-rock as a potential material for waste-water purification and pet litter. Analcime can act as an ion sieve (Barrer, 1950; Barrer and Hinds, 1953; Ames, 1966; Balgord and Roy, 1971; Moroz et al., 1998; Seryotkin et al., 2000; Likhacheva et al., 2002), while Dyer and Yusof (1987; 1989) carried out extensive studies on cation and water self-diffusion, concluding that analcime has the potential for use in the storage and disposal of titrated water.

4. Conclusions

The exchange of the extra-framework cations Na^+, K^+, Ca^{2+} and Mg^{2+} found in Greek zeolite-rich rock was studied in its natural form in order to determine its ion exchange behaviour. It is of great importance to understand the behaviour of a multi-component ion-exchange system, because processes of ion removal in natural systems, generally involve more than two ions. Zeolite-rich sample has analcime content 71 wt %. Na^+ was the main exchangeable cation. Loss of ignition was measured 9.43 wt %.

The exchange of initial cations occurs very slow. Monovalent cations K^+ and Na^+ show over the whole period of the experiments (720 hours), only 7 and 10% of exchange, respectively. No steady state achieved for Na^+. Bivalent cations Ca^{2+} and

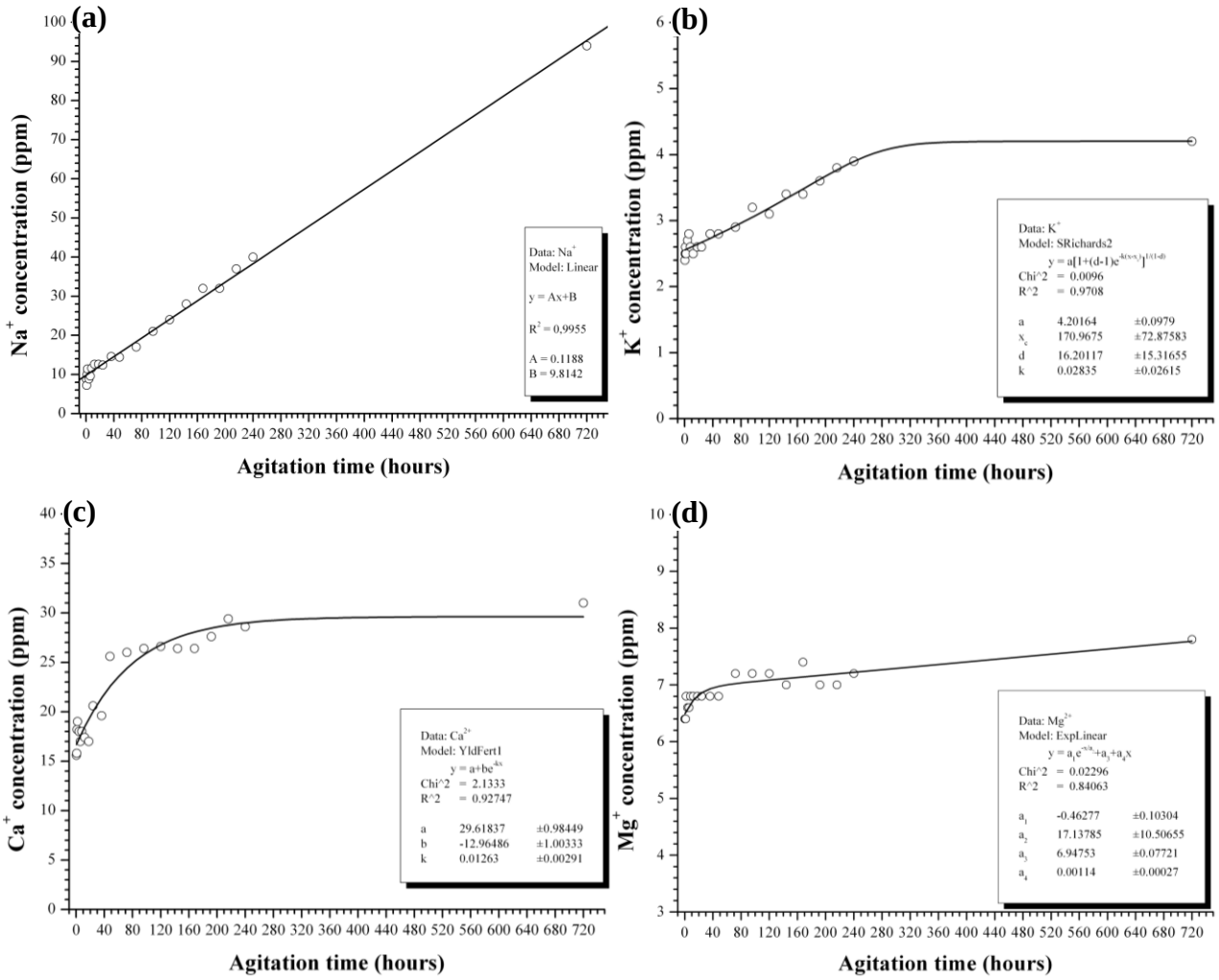

Figure 1(a-d). Kinetic curves of (a) Na^+, (b) K^+, (c) Ca^{2+} and (d) Mg^{2+} for the AR sample.

Mg^{2+} show better exchange. The Ca^{2+} was almost fully exchanged (97%), while Mg^{2+}, despite that did not achieve a steady state after the end of experiments (720 hours), shows an exchange of 62%. The rate of ion-exchange was calculated for K^+ 0.01 ppm/h, for Ca^{2+} 0.13 ppm/h, and for Mg^{2+} 0.01 ppm/h. Na^+ was exchanged in a continuous constant rate of 0.13 ppm/h. Thus, using the rate of ion-exchange, the order for sample AR, is: $Na^+ \approx Ca^{2+} >> K^+ \approx Mg^{2+}$.

The continuous release of Na^+ over NH_4^+ observed at a slow rate of ion-exchange in our experiments, can allow us to propose studied analcime-rich rock as a potential material for waste-water purification and pet litter.

References

Ames L.L., 1966. Cation exchange properties of wairakite and analcime. Am. Mineral., 51, 903-908.

Armbruster T., Gunter M.E., 1991. Stepwise dehydration of heulandite-clinoptilolite from Succor Creek, Oregon, U.S.A.: A single-crystal X-ray study at 100 K. Am. Mineral. 76, 1872-1883.

Baerlocher Ch., Meier W.M., Olson D.H., 2001. Atlas of zeolite framework types, Elsevier, Amsterdam, 308 p.

Bain C., Smith L., 1987. Chemical analysis. In: Wilson, M. (Ed.), A handbook of determinative methods in clay mineralogy. Blackie, Glasgow, pp. 248-274.

Balgord W., Roy R., 1974. Crystal Chemical Relationships in the Analcite Family, I. Synthesis and Cation Exchange Behavior. In Molecular Sieve Zeolites-1, Adv. Chem. Ser., 101, Amer. Chem. Soc., Washington, D.C., 140-148.

Barrer R.M., 1950. Ion-exchange and ion-sieve processes in crystalline zeolites. J. Chem. Soc. Resumed, 2342-2350.

Barrer R.M. and Hinds L., 1953. Ion-exchange in crystals of Analcite and Leucite. J. Chem. Soc., 1879-1888.

Bish D.L., Boak J.M., 2001. Clinoptilolite-Heulandite nomenclature. In: Bish, D.L., Ming, D.W. (Eds.), Natural Zeolites: Occurrences, Properties, Applications, Reviews in Mineralogy & Geochemistry, vol. 45. The Mineralogical Society of America, Washington DC, pp. 207-216.

Bish D.L., Ming D.W., 2001. Natural Zeolites: Occurrences, Properties, Applications. Reviews in Mineralogy & Geochemistry, vol. 45, The Mineralogical Society of America, Washington DC, 654 p.

Cheng X., Zhao P., Stebbins J.F., 2000. Solid state NMR study of oxygen site exchange and Al-O-Al site concentration in analcime. American Mineralogist, 85, 1030–1037.

Deer W.A., Howie R.A., Zussman J. 1992. An Introduction to the Rock-Forming Minerals, 2nd edn. Longman, London, 712 p.

Dyer A., 1988. An Introduction to Zeolite Molecular Sieves. J. Wiley, Chichester, 149 p.

Dyer A., Yusof A.M., 1987. Diffusion in heteroionic analcimes: Part 1. Sodium-potassium-water system. Zeolites 7, 191-196.

Dyer A., Yusof A.M., 1989. Diffusion in heteroionic analcimes: Part II. Diffusion of water in sodium/thallium, sodium/lithium, and sodium/ammonium analcimes. Zeolites 9, 129-135.

Filippidis A., Godelitsas A., Charistos D., Misaelides P., Kassoli-Fournaraki A., 1996. The chemical behaviour of natural zeolites in aqueous environements: Interactions between low-silica zeolites and 1M NaCl solutions of different initial pH-values. Appl. Clay Sci. 11, 199-209.

Godelitsas A., Misaelides P., Charistos D., Filippidis A., Anousis I., 1996a. Interaction of HEU-type zeolite crystals with Thorium aqueous solutions. Chem. Erde 56, 143-156.

Godelitsas A., Misaelides P., Filippidis A., Charistos D., Anousis I., 1996b. Uranium sorption from aqueous solutions on sodium-form of HEU-type zeolite crystals. J. Radioan. Nucl. Ch. Ar. 208, 393-402.

Gunter M.E., Armbruster T., Kohler T., Knowles C.R., 1994. Crystal structure and optical properties of Na- and Pb-exchanged heulandite-group zeolites. Am. Mineral. 79, 675-682.

Hall A., Stamatakis M., 1992. Ammonium in zeolitized tuffs of the Karlovassi basin, Samos, Greece. Can. Mineral. 30, 423-430.

Holmes D., 1994. Zeolites. In: Carr, D. (senior Ed.), Industrial Minerals and Rocks, Braun-Brumfield, Inc., Ann Ardor, Michigan, pp. 1129-1158.

Kantiranis N., Stamatakis M., Filippidis A., Squires C., 2004. The uptake ability of the clinoptilolitic tuffs of Samos island, Greece. Bull. Geol. Soc. Greece 36/1, 89-96.

Likhacheva A.Yu., Paukshtis E.A., Seryotkin Yu.V., Shulgenko S.G., 2002. IR spectroscopic characterization of NH_4-analcime. Phys. Chem. Miner., 29, 617–623.

Meier W.M., Olson D.H., Baerlocher Ch., 1996. Atlas of Zeolite Structure Types, fourth ed. Butterworth-Heinemann, Stoneham, MA, pp. 42–43.

Ming D.W., Mumpton F.A., 1995. Natural zeolites '93: Occurrence, Properties, Uses. International Committee on Natural zeolites, Brockport, New York.

Misaelides P., Godelitsas A., Filippidis A., 1995a. The use of zeolithoforous rocks from Metaxades-Thrace, Greece, for the removal of caesium from aqueous solutions. Fresen. Environ. Bull. 4, 227-231.

Misaelides P., Godelitsas A., Filippidis A., Charistos D., Anousis I., 1995b. Thorium and uranium uptake by natural zeolitic materials. Sci. Total Environ. 173/174, 237-246.

Misaelides P., Godelitsas A., Haristos D., Noli F., Filippidis A., Sikalidis C., 1993. Determination of heavy metal uptake by the sodium form of heulandite using radiochemical techniques. Geol. Carpath.-Ser. Clays 44(2), 115-119.

Moroz N.K., Seryotkin Yu.V., Afanassiev I.S., Belitsky

I.A., 1998. Arrangement of the extraframework cations in NH_4-analcime. J. Struct. Chem. Engl. Tr., 39(2), 281–283.

Mumpton F.A., 1977. Natural Zeolites. In: Mumpton, F.A. (Ed.), Mineralogy and Geology of Natural Zeolites. Mineralogical Society of America Short Course Notes, v. 4, Washington D.C., pp. 1-17.

Mumpton F.A., 1978. Natural zeolites: A new industrial mineral commodity. In: Sand, B.L., Mumpton, F.A. (Eds.), Natural zeolites: Occurrences, Properties, Uses. Pergamon Press, New York, pp. 3-27.

Pe-Piper G., Tsolis-Katagas P., 1991. K-rich mordenite from Late Miocene rhyolitic tuffs, Island of Samos, Greece. Clay. Clay Miner. 39, 239-247.

Pond G.W., Mumpton F.A., 1984. Zeo-Agriculture: Use of Natural Zeolites in Agriculture and Aquaculture. Westview Press, Colorado, 296.

Saha P., 1959. Geochemical and X-ray investigation of natural and synthetic analcites. American Mineralogist, 44, 300-313.

Seryotkin Yu.V., Bakakin V.V., Belitsky I.A., Fursenko B.A., 2000. Ag-exchanged analcime: crystal structure and crystal chemistry. Micropor. Mesopor. Materials, 39, 265-273

Sherman J.D., 1978. Ion exchange separations with molecular sieve zeolites. AIChE Symposium Series 74(179), 98-116.

Szostak R., 1992. Handbook of Molecular Sieves. Van Nostrand Reinhold, New York, 569 p.

Stamatakis M., 1989. Authigenic silicates and silica polymorphs in the Miocene saline-alkaline deposits of the Karlovassi basin, Samos Island, Greece, Econ. Geol. 84, 788-798.

Tsitsishvili G.V., Andronikashvili T.G., Kirov G.N., Filizova L.D., 1992. Natural zeolite. Ellis Horwood, New York, 274 p.

Vaughan D.E.W., 1978. Properties of natural zeolites. In: Sand L.B., Mumpton F.A. (Eds.), Natural zeolites, Occurrence, Properties, Uses. Permangon Press, London, pp. 353-371.

Yang P., Stolz J., Armbruster T., Gunter M.E., 1997. Na, K, Rb, and Cs exchange in heulandite single crystals: Diffusion kinetics. Am. Mineral. 82, 517-525.

Scientific Annals, School of Geology, Aristotle University of Thessaloniki Proceedings of the XIX CBGA Congress, Thessaloniki, Greece	Special volume 100	89-95	Thessaloniki 2010

MAGNETIC PROPERTIES OF SOILS AROUND LOCAL POLLUTION SOURCES (CRETE, GREECE)

Kokinou E.

Department of Natural Resources and Environment, Technological Educational Institute Crete, 3 Romanou Str. Chalepa, Chania, Crete, GR 73133 - Greece, ekokinou@chania.teicrete.gr

Abstract: The main scope of the present study is to investigate the spatial and vertical distribution of the magnetic susceptibility in an area of possible industrial pollution and heavy traffic. For this purpose, a power plant with a dense traffic net around it, located in the SE section of Chania city was selected as the investigated area. In the context of the present work magnetic susceptibility measurements have been contacted in two phases. Surface soil samples have been collected in 2008 from the area under investigation and they were analyzed in order to estimate the spatial distribution of the magnetic susceptibility. Loci of high values of magnetic susceptibility within the study area gave rise to further proceed to coring up to a depth of 120cm at selected sites of the study area. GIS techniques were used for mapping the magnetic measurements on the various topographic and geological features of the area. Maps were created through interpolation algorithms indicating the spatial distribution of the above measurements. Spatial tools and statistical analysis proved the correlation between magnetic properties and the terrain attributes. Both investigations indicate high values of the magnetic susceptibility especially in the eastern part of the investigated area and along the main traffic branch.

Keywords: Magnetic susceptibility, power plant, traffic net, GIS mapping

1. Introduction

Industrial pollution is one of the most important environmental threats, with serious consequences for the future. Thus, its detailed study is of great importance. Apart from expensive and time-consuming chemical methods, several rapid and cheap proxy methods have been developed recently, one of them being based on rock-magnetic parameters.

Routinely used geochemical methods are rather time consuming, laborious in terms of sample preparation, and expensive. Therefore, any other method, although approximative, i.e. not providing absolute threshold values for contamination, but yielding fast information directly in field about relative changes between different sites, can be helpful as indicator for better targeting and selection of sampling sites for subsequent geochemical analysis. Moreover, measurements of temporal changes can serve as simple and rapid monitoring tool. One of such approximative indicators is the concentration of magnetic particles of anthropogenic origin. Magnetometry and especially magnetic susceptibility is a fast and cost-effective method for detection of environmental pollution of soils, sediments and dusts.

Magnetic minerals present in soils may be either inherited from the parent rocks (lithogenic origin), form during pedogenesis or may stem from anthropogenic activities (effluents from power plants, combustion of fossil fuel, metallurgical industries, smelters, road traffic, etc.). In the case of minor contribution of the first two sources to the magnetic properties of soils, susceptibility measurements become very important for monitoring environmental pollution, because, metallurgical dusts, fly ashes and cement dust contain relatively large amount of iron oxides and are therefore highly magnetic (Strzyszcz et al., 1996; Goluchowska, 2001).

Magnetic particles are usually deposited downwind from the industrial units on the surface of soils, streets, buildings and trees. Fly ashes with significant portion of ferromagnetic phase are produced by industrial processes; they are transported through atmospheric pathways and deposited on the ground. In soils, such particles penetrate downwards and accumulate in top layers and their increased concentration can be easily detected us-

ing surface magnetic measurements. Hansen et al. (1981) indicated that chromium manganese, cobalt, nickel, copper, zinc and beryllium are all significantly enriched in the 'magnetic' fraction of coal fly-ash. Beckwith et al. (1984) identified pollution sources in urban drainage systems using magnetic methods. Petrovsky & Elwood (1999) reviewed the application of magnetic susceptibility measurements in various ecosystems. Lately, more researchers investigate the usage of magnetic susceptibility as a tool for contaminated topsoils and sediments (Scholger, 1998; Bitykova et al., 1999; Petrovsky et al., 2001; Boyko et al., 2004; Kapicka et al., 2003, 2008; Sarris et al., 2009).

The aim of this study is to establish links between enhanced concentrations of anthropogenic magnetic particles and known sources of pollution in the catchment area. For this purpose the surface and the vertical distribution of the magnetic susceptibility is examined in an area around a local power plant with heavy traffic. This area was selected because it shows a homogenous geological structure. Therefore it is assumed that magnetic signature of anthropogenic contribution(s) should be well pronounced in the sediments and should be well correlated with heavy metals produced by the respective sources.

This study tries to document that simple and fast in situ magnetic measurements can reflect the anthropogenic influence under certain circumstances.

2. Geological and environmental setting

The study area is located at the SE section of the Chania city in Crete Island, comprising an almost flat area with slopes mainly ranging between 0 and 25%. The softness and horizontality of the geological layers contribute basically in the configuration of the low morphology of the region. A N-S orientated drainage network (Fig. 2) is present near to the local power plant.

The study area is mainly filled by recent alluvial sediments which were sampled in the context of the present study. NW-SE trending faults prevail in the wide area, away from the place that sampling has been conducted. The homogenous geological background justifies the assumption that magnetic enhancement in sedimentary samples can be attributed mostly to sources other than lithogenic.

3. Methodology

3.1. Site description and sampling

In environmental magnetism, the most often used magnetic parameter is the magnetic susceptibility (χ) which is the ratio of induced (temporary) magnetization acquired by a sample in the presence of a weak magnetic field, to the applied field itself. This is because magnetic susceptibility is concentration dependent parameter.

Samples were collected from the study area (Figs. 1a,b, 2) within a depth of 0-15 cm below the surface. GPS coordinates (in EGSA 87 system) were

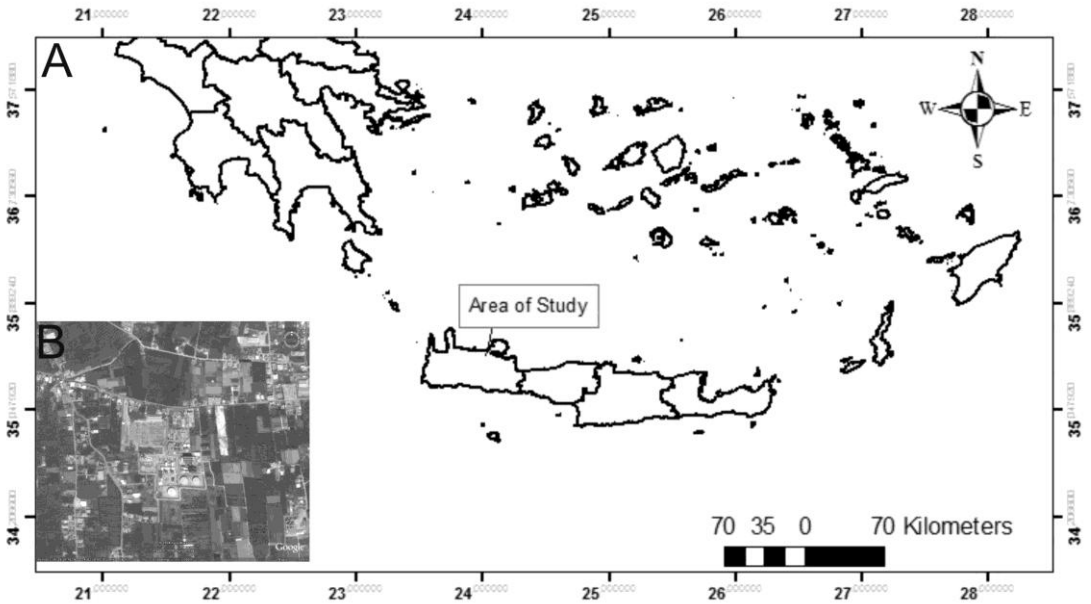

Fig. 1 (A): Location of the study area; (B) the location of the power plant in Chania, Crete. Satellite imagery from Google Earth showing the wider area of interest.

determined at each sampling site in order to be correlated with the available topographic, geological and traffic data. Additionally, coring has been performed at 10 selected sites (Fig. 3) around the local power plant and along the main road, up to a depth of 120 cm, in order to find out the relation of the magnetic susceptibility with the depth.

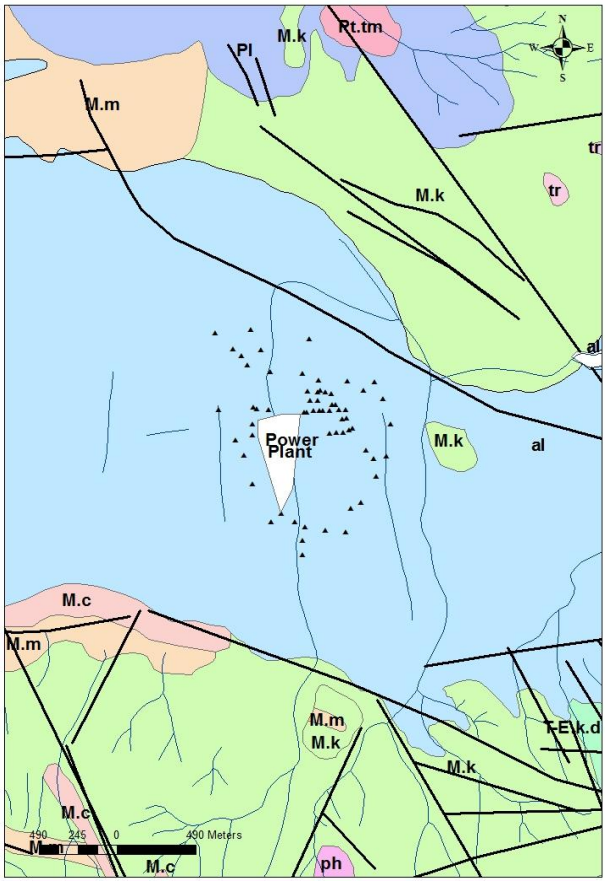

Fig. 2. Geological map of the wider area. Sympols: al-alluvial sed., tr-terra rosa, Pt.tm-marls, sands and conglomerate, Pl-Pliocene sediments, M.m, M.k-Miocene sediments, Black line-fault, blue line-drainage net, Black triangle-sample location.

3.2. Magnetic measurements

Since our samples were of unknown density, mass specific measurements seemed to be more appropriate compared with those based on specific volume. Bartington MS2 susceptibility meter was employed for measuring magnetic susceptibility in two frequencies (f_{low}= 0.43KHz and f_{high}= 4.3KHz). The samples were air-dried and sieved at 2mm in order to remove rock fragments. A sample of 10 cm^3 tightly packed Manganese Carbonate powder (χ= 99.2x10^{-6} emu/gr) was used for calibration of the instrument. The consistency of the instrument calibration was checked by measuring the susceptibility of the calibration sample in the beginning and end of the measuring session. The contribution of the plastic container was measured for 10 pieces and the average value was subtracted from all measurements. 200 samples were generally analyzed.

3.3. GIS techniques

Digitization techniques and GIS were applied for the presentation of the spatial distribution of magnetic susceptibility measurements and the geological features (the geological formations of the region available by 1:50000 scale geological maps of the Institute of Geological and Mineral Exploration, IGME) . Faults, rivers, and the main and secondary roads were also digitized and fused to the Geographical Information System component of the project. Gridding of the data was carried out using the inverse distance weighted method. Similar interpolation methods were used for creating surfaces of the spatial distribution of magnetic measurements.

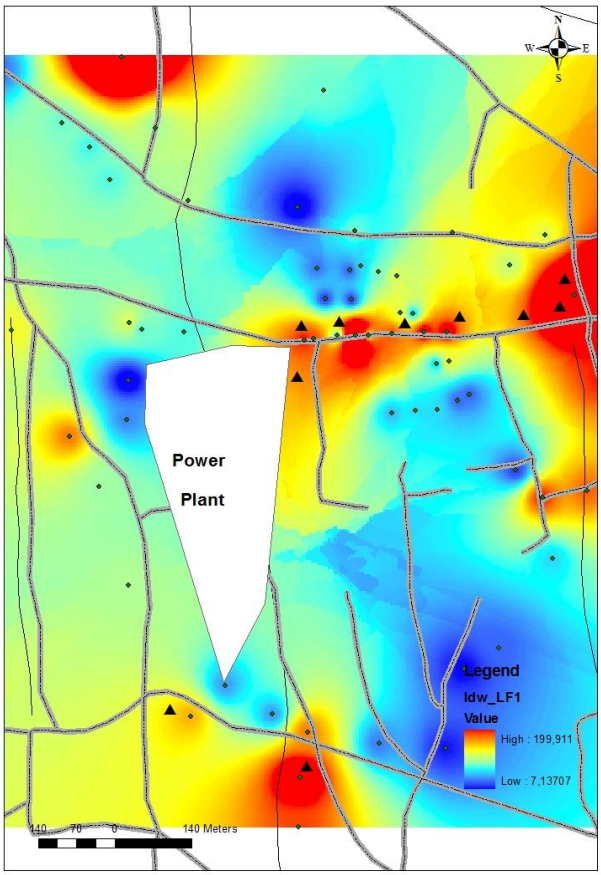

Fig. 3. Mapping of the low field magnetic susceptibility (LFS) in 10^{-6} m^3/Kg. Bullets represent the sample location, black triangle the coring locations, thin solid lines the drainage net and dashed line the traffic net.

4. Results and Discussion

The distribution of the low frequency field magnetic susceptibility susceptibility (LFS) is presented in Figure 3. The susceptibility values corresponding to the topmost samples of cores are not included in this figure. High susceptibility values, indicating possibly polluted sites, are generally detected in the eastern part of the study area, almost parallel to the orientation of the wind currents and along the main road. Additionally some samples, characterized by relative high χ, are indicated across the main branches of the drainage system.

LFS was measured in two phases, i.e. in different days, in order to estimate the influence of the background noise in the laboratory. Figure 4 presents the correlation (R^2=0.8) of the LFS measurements. A 20% influence of the background noise is expected on the measurements. The correlation between LFS and HFS (high frequency field magnetic susceptibility susceptibility) is high as it is expected.

Vertical susceptibility distribution in soil profiles is measured in order to distinguish between lithogenic and anthropogenic contributions to measured topsoil susceptibility values. Figure 5 presents the correlation (R^2=0.91) of the surface susceptibility values around to coring locations with the corresponding values from topmost samples of cores. Figures 6a,b,c show the distribution of the mean low frequency measured magnetic susceptibility, mean high frequency measured magnetic susceptibility and frequency dependent susceptibility in relation to depth, resulting from ten corings up to a depth of 120cm near to the power plant and the main road where high surface susceptibility values were observed. Relative high LFS and HFS values (Fig. 6a,b) are indicated at depths ranging between

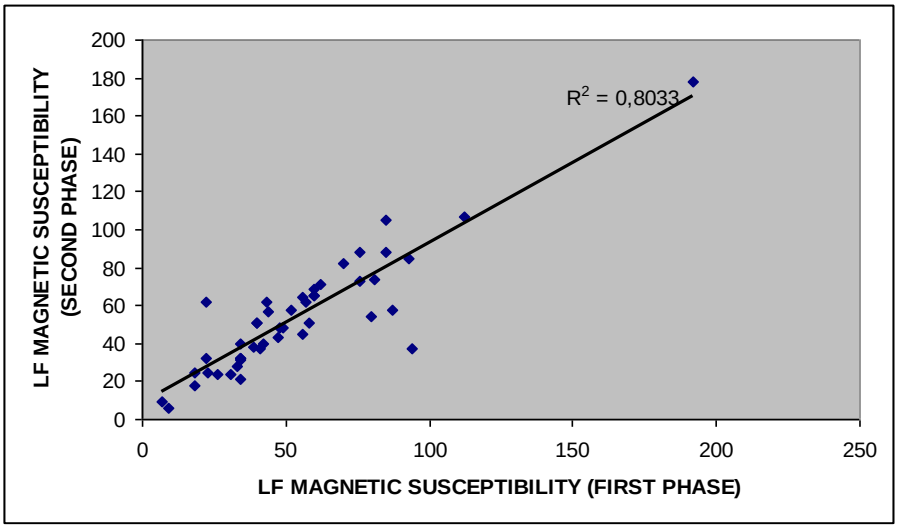

Fig. 4. Correlation of the LFS (10^{-6} m^3/Kg) measured in two phases.

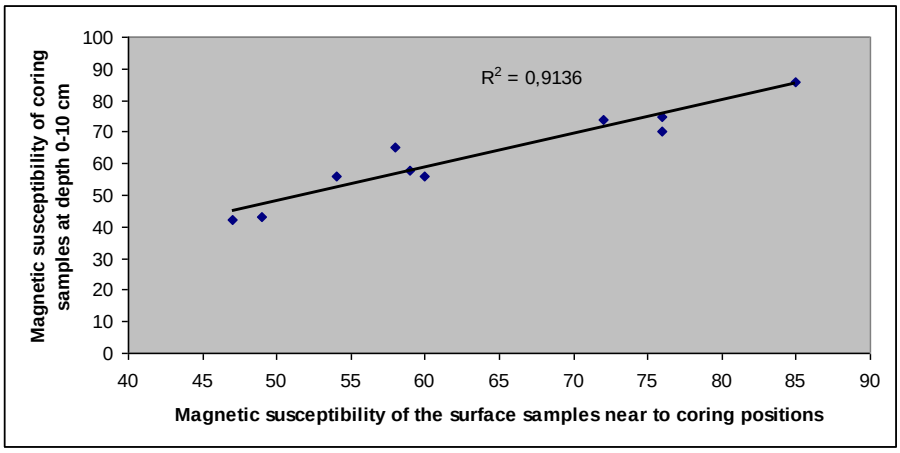

Fig. 5. Correlation of the LFS (10^{-6} m^3/Kg) measured in the two campaigns.

20 and 40cm. The relative deep penetration could be possibly explained by the fact that around the power plant mainly agricultural fields are located, and most of them are cultivated. Therefore polluted dusts can penetrate easier in greater depths. The frequency dependent susceptibility (χ_{fd}) which is given by the following relation: $\chi_{fd} = (\chi_{low}-\chi_{high}/ \chi_{low})$ %, where χ_{low} and χ_{high} refer to mass specific magnetic susceptibility measured at low and high frequency. Frequency-dependent susceptibility (FDS) reflects variations in magnetic grain size from the single domain to superparamagnetic state (Dearing et al., 1996, Kapicka et al., 2003). FDS values in the present case (Fig. 5c) are varying between 4% and 12% (highest values at depths ranging between 60 and 80cm). This suggests that the fined grain sizes have strong contribution to susceptibility due to magnetite formation during pedogenesis.

To eliminate the effect of diagenetic formation of magnetic particles during the sample storage, magnetic susceptibility of raw wet material, measured immediately after sampling, was compared with measurements on the same samples during some days of drying at room temperature. No changes in mass-specific magnetic susceptibility suggest that iron minerals are already stable and no further oxidation or precipitation takes place (Fig. 7).

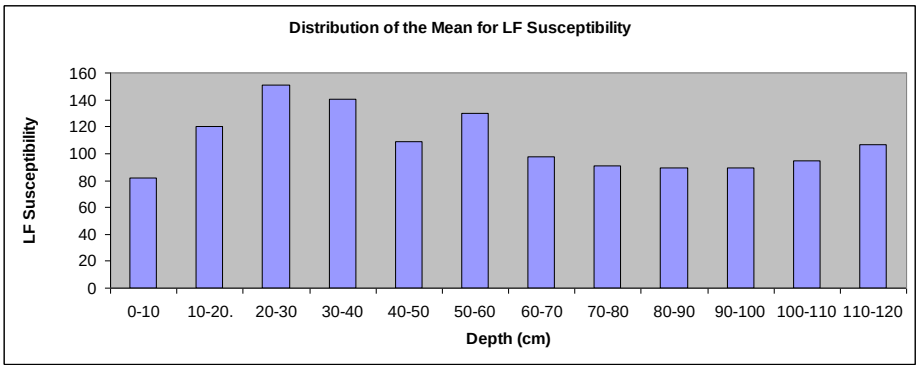

(a)

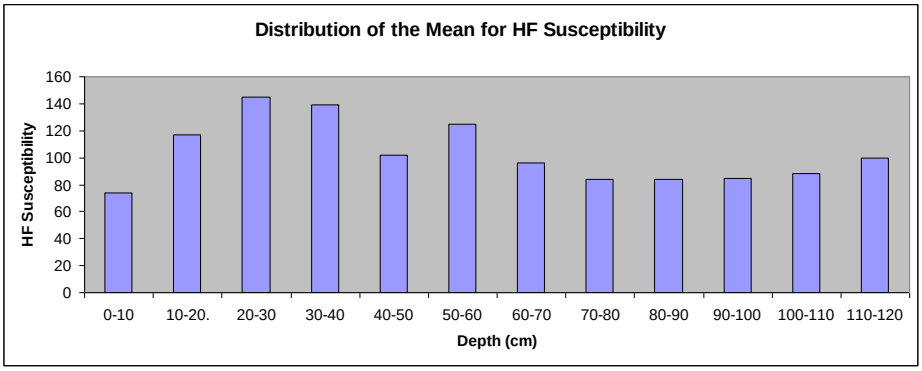

(b)

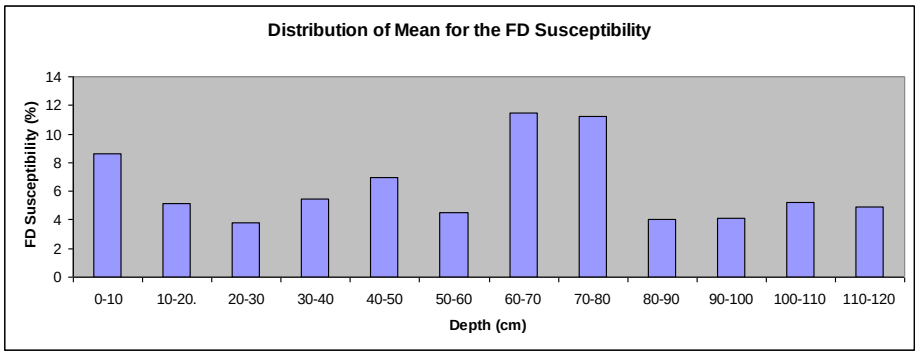

(c)

Fig. 6. Distribution of the Mean for (a) LFS (10^{-6} m^3/Kg), (b) HFS (10^{-6} m^3/Kg) and (c) FDS resulting from 10 corings up to a depth of 120cm.

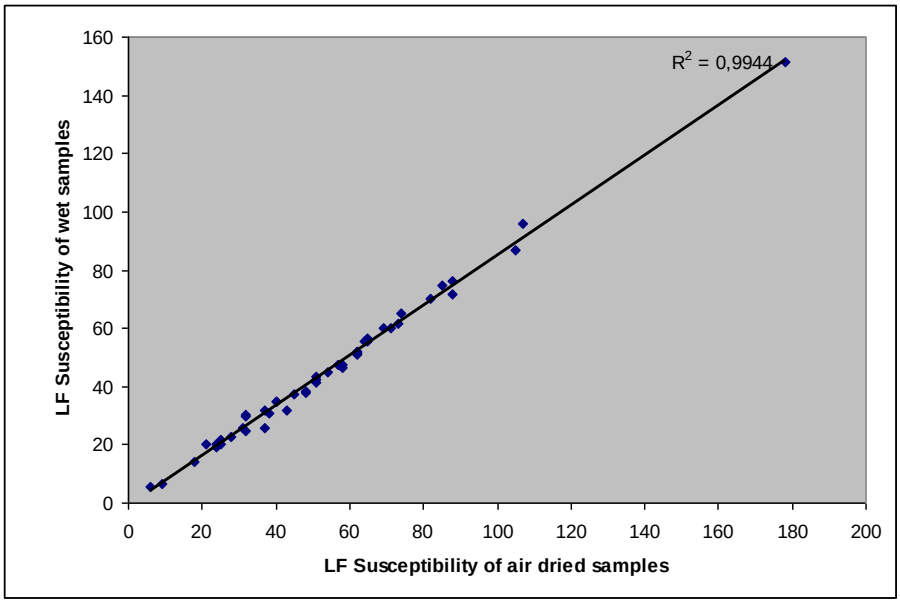

Fig. 7. Correlation of LFS (10^{-6} m^3/Kg) for wet and air-dried samples.

5. Conclusions

In the present work, magnetic susceptibility measurements were conducted around a power plant with a dense traffic net, located in the SE section of Chania city in Crete, in order to examine if the study area is an interesting place for further pollution research.

The main transmission factor seems to be the wind. High values of the magnetic susceptibility χ are orientated east of the power plant and along a major branch of the traffic net. The vertical susceptibility distribution in soil profiles indicates increased values at depths ranging between 10 and 60cm. Frequency dependent susceptibility is moderate and variable, possibly indicating the dominance of SP ferromagnetic minerals and non negligible pedogenesis.

The spatial distribution of magnetic susceptibility in both campaigns verifies the influence of anthropogenic activities and confirms that magnetic susceptibility measurements provide the basis for an environmental study in polluted areas.

In concluding, the study area is of interest and further magnetic analyses (thermomagnetic curves, IRM, ARM, hysteresis loops) as well chemical analyses are proposed in order to examine the possibly polluted sites. In any case, the application of magnetic methods should not be overestimated. Results obtained in one specific region may not be simply transferrable to another region. Instead, detailed analysis should be carried out in order to establish basic correlations (if existent) between various magnetic parameters and concentrations of heavy metals. Only if such relationship is evident, magnetic measurements can be used in tracing and observing future temporal and spatial variations of metal contamination.

Acknowledgements

I am grateful to Koutalakis S., Dagiantas G. and Kleissas N. for being involved in the fieldwork. I wish to thank Dr. Kapicka and an anonymous reviewer for their constructive criticism, which improved a version of this manuscript.

References

Beckwith P.R., Ellis J.B., Revitt D.M. & Oldfield F., 1984. Identification of pollution sources in urban drainage systems using magnetic methods. In: Balmer, P., Malmqvist, P.A., Sjoberg, A., (Eds.), Proceedings of the Third International Conference on Urban Storm Drainage, Chalmers University of Technology, Gotenborg, Sweden, pp. 1313-1322.

Bityukova L., Scholger R. & Birke M., 1999. Magnetic susceptibility as indicator of environmental pollution of soils. In Tallin/ Phys. Chem. Earth, 24 829-835.

Boyko T., Scholger R., Stanjek H. & MAGPROX Team, 2004. Topsoil magnetic susceptibility mapping as a tool for pollution monitoring: repeatability of in situ measurements. J. Applied Geophys., 55, 249-259.

Dearing, J.A., Hay, K., Baban, S., Huddleston, A.S., Wellington, E.M.H. & Loveland, P.J., 1996b. Magnetic susceptibility of topsoils: a test of conflicting theories using a national database. Geophysical Journal International 127, 728-734.

Goluchowska B.J., 2001. Some factors affecting an increase in magnetic susceptibility of cement dusts. J. Appl. Geophys., 48, 103-112.

Hansen L.D., Silberman D. & Fischer G.L., 1981. Crystalline components of stack-collected, size-fractioned coal fly ash. Environ. Sci. Technol. 15, 1057-62.

Kapicka, A., Jordanova N., Petrovsky E. & Podrazsky V., 2003. Magnetic study of weakly contaminated forest soils. Water, Air and Pollution 148, 31-44.

Kapicka A., Petrovsky E., Flavova H., Podrazsky V. & Dvorak 2008. High resolution mapping of anthropogenic pollution in the Giant Mountains national park using soil magnetometry. Stud. Geophys. Geod., 52, 271-284.

Petrovský E. & Ellwood B., 1999. Magnetic Monitoring of Air-, Land- and Water Pollution. In: B. A. Maher and R. Thompson (eds), Quaternary Climates, Environments and Magnetism, Cambridge University Press, Cambridge, U.K., pp. 279–322.

Petrovsky E., Kapička A., Jordanova N. & Borůvka L., 2001. Magnetic properties of alluvial soils contaminated with lead zinc and cadmium. J. Applied Geophys. 48, 127-136.

Sarris A., Kokinou E., Aidona E., Kallithrakas-Kontos N., Koulouridakis P., Kakoulaki G., Droulia K., Damianovits O, 2009. Environmental study for pollution in the area of the Megalopoli power plant (Peloponnesus, Greece). Environmental Geology, 58, 8, 1769-1783, DOI:10.1007/s00254-008-1676-3.

Scholger R., 1998. Heavy metal pollution monitoring by magnetic susceptibility measurements applied to sediments of the river Mur (Styria, Austria). Eur. J. Envirn. Eng. Geophys. 3, 25-37.

Strzyszcz Z., Magiera T. & Heller F., 1996. The influence of industrial emissions on magnetic susceptibility of soils in Upper Silesia. Studia Geophysica and Geodesia, 40, 276 – 286.

Scientific Annals, School of Geology, Aristotle University of Thessaloniki Proceedings of the XIX CBGA Congress, Thessaloniki, Greece	Special volume 100	97-103	Thessaloniki 2010

GEOECOLOGY OF THE BLACK SEA COAST OF GEORGIA

Kvinikadze M., Kuparadze D., Pataridze D., Khundadze N., Kirakosyan V.

Department of Geoecology and Applied Geochemistry, Alexander Tvalchrelidze Caucasian Institute of Mineral Resources; # 85, Paliashvili str., 0162 Tbilisi, Georgia, d.kuparadze@gmail.com, d.pataridze@internet.ge.

Abstract: The combined geoecological works carried out within the bounds of Black Sea coastline (Georgian Section) in 2008 gave the following results: Contamination of sea water surface with oil products does not exceed the regulatory values; Hydrochemical parameters of sea and the rivers discharging into the sea were determined. High concentrations of magnesium and arsenic were observed in the bottom sediments of sea and Rioni River in Poti water area; the composition of copper, lead, zinc, magnesium and arsenic highly exceed the Dutch norms in some samples of toposoils taken along the agricultural terrain and motor road. As a result of radiation measurements carried out in the Black Sea coastline the sites are allotted where radiation is higher than the accepted norms; the concentration of magnesium in the biosamples (tea and eucalyptus) highly exceeds the maximum permissible concentration.

Keywords: Ecology, Geochemistry, Georgia, Black Sea, Radiation, Water Pollution.

A small, but important part of the World Ocean – the Black Sea – borders six countries: Bulgaria, Georgia, Romania, Russia, Turkey and Ukraine, with a total population of 165-167 million. During its history, the Black Sea has sometimes been a lake and sometimes a sea. 250-40 million years ago, it was at the edge of Tetis, which connected the present Atlantic and Pacific Oceans. In the area of the present Black, Caspian and Aral Seas there was formed a landlocked freshwater Sarmat sea-lake. It existed for 2-5 million years, and during this period developed freshwater flora and fauna, remains of which can be tracked up to date.

The shape of the Black Sea is changing: slowly, but firmly taking up its coast. The increase of the Black Sea level compared to its coastal marks has been tracked for as long as there are having been ongoing scientific observations. The ecosystem of the Black Sea has been closed for many thousands of years and slightly opened just seven thousand years ago. This ecosystem is still far from being in equilibrium and is very vulnerable to external factors. That is why changes of the biological structure of the Black Sea still take place.

In order to maintain acceptable water quality of the Black Sea, the main types of possible man-made pollutants need to be examined. One such pollutant is sewage sludge that after being treated is discharged into the sea. This type of liquid waste is usually treated beforehand and possible hazardous components are removed. However, in many cases sewage sludge is discharged into the sea without any treatment. There are cases when the ground that is generated during excavation works (for deepening passage for ships), feces and chemical wastes are discharged in the open sea. Additionally, the solid waste from ships and ballast waters containing petroleum are discharged into the sea. There are other ways for pollutants to enter the sea. The particles of pesticides used from the chimneys, and the exhaust from vehicles and planes enter the sea from the air. From the painted ships, small amounts of toxins are released into the sea. The paint is used in order to avoid ships being overgrown by algae and crustaceans. As a result of forest fires, a large amount of ashes and metal oxides enter the ocean. This particular type of pollution is caused by the accidents of tankers carrying petroleum.

The most significant pollution of the sea is one in which atypical chemicals, such as gaseous and aerosol pollutants, come from the industries and households. The amount of carbonic acid in the air is increasing as well. Further development of this process may result in the unfavorable tendency of increasing the average sea level on the Earth. The pollution of the world ocean with petroleum products is also alarming. Nowadays, 1/5 of the World Ocean's surface is polluted. Such scale of the pollution with the petroleum may result in significant

disturbances in the exchange of gas and water between the hydrosphere and atmosphere. Without a doubt, chemical pollution of soils with pesticides and its increased acidity that result in the collapse of the ecosystems is very significant. Thus, all the above mentioned factors those have polluting characteristics have a significant influence on the processes taking place in the biosphere.

Hydrochemical and climatic characteristics of the Black Sea as well as its socio-economic aspects influence the character of shelf flora.

While making decisions about the realization of certain projects mainly connected with transportation of goods, the transnational corporations mostly focus on profit. Quite often, the governments of states behave the same way and do not always bother themselves with assessing the consequences of the project.

The main problem is the absence of a mechanism for calculating material damage to the state treasury and to the region's population. A population's well being significantly depends on the development of tourism as a result of constructing pipelines and petrol terminals in the coastal zone.

In the beginning of 1980, the world community realized that the environmental crises may become a threat for its existence. During that period, the international mechanisms addressing environmental problems and common usage of natural resources were developed. The special institution – Global Environmental Facility (GEF) – was established to implement the projects related to the global changes in the biosphere. During the conference in Rio de Janeiro in 1992, a number of conventions were adopted that became important instruments for solving existing global problems.

These documents were signed by the countries of Black Sea region as well. These countries also signed the Bucharest Convention on the protection of the Black Sea from pollutants and the Odessa Declaration. In 1996, two documents were adopted in the framework of the Black Sea Environmental Program (BSEP): "Transboundary diagnostic analysis of the Black Sea" and "Strategic Action Plan on Rehabilitation and Protection of the Black Sea". According to these documents, the states of the Black Sea region took on the obligation to develop a joint strategy on the protection and rehabilitation of the Black Sea and on the management of its coastline and marine resources for the coming 20 years.

Fourteen years have already passed, but none of the states has met its obligations. Besides, there are unimplemented provisions of the Bucharest Convention on the creation of the Istanbul Commission and Black Sea Environmental Fund. Measures set in the Bucharest Convention and the Odessa Declaration regarding saving the Black Sea remain unrealized. Mean-while, the situation has drastically worsened. Plans for using resources of Black Sea are mainly worked out in the countries far away from the region. However, the coast for maintenancy of the management and the rehabilitation and protection works of the sea are to be covered by the states of the Black Sea basin.

The radiation pollution caused by humans is related to the accident at the Chernobyl Atomic Power Station. During those days in 1986, radiation was deposited on some area of the Black Sea coastline. According to the radiometric measuring in 1987-1989, strong pollution by radioactive nuclides was determined. On some sections of the coastline the level of radiation was from 30-60 to 90-225 μR/h with the maximum acceptable norm of 10 μR/h. Unfortunately, due to the political and economic cataclysms in Georgia by the end of the century, the monitoring of the radiological and geoecological conditions of the coastline was cut down. Its resumption is very important for the well being of the population and proper functioning of economy of the states of the Black Sea region.

The analysis of the ecological data (Kvinikadze at al. 2006) shows that a large part of the territory of Georgia exposes from geochemical, hydrochemical and biochemical pollution related to the increased man-made waste. This process also concerned the Black Sea coastline. A special concern is raised in relation to the cities and populated sites with the developed industrial activities. In this regard, the port cities of Batumi, Poti and Sukhumi should be mentioned. The negative impact on the environment in these places is caused by the trade and military ships that violate environmental laws. As a result, the Black Sea water was polluted with the petroleum.

Large amount of pollutants are discharged into the Black Sea from the rivers Rioni, Bzib, Enguri, Psou, Choloki, Mzimta, Kodori, Supsa and others. Various mining, metallurgic, chemical or agricultural plants that are located within the basin of these rivers annually discharge into the rivers and as a consequence – into the Black Sea.

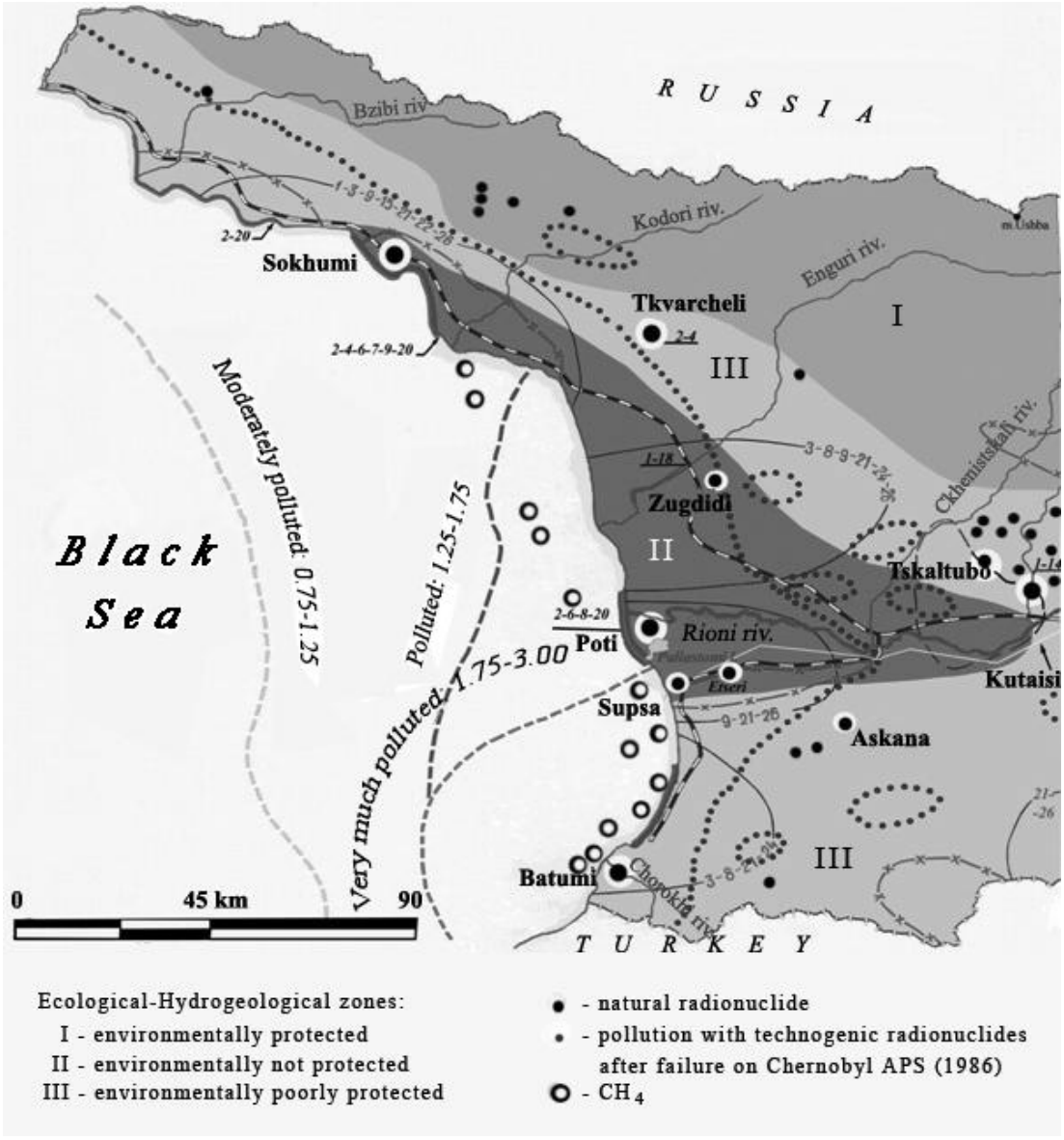

Fig.1. Geoecological map of the Black Sea coast of Georgia. The characters indicates high (in comparison with maximum allowable concentration MAC) contents of chemical elements concentration in underground water: 1-Phenol; 2-Biological need of oxygen; 3-Petroleum; 4-Chloride; 5-Sulfate; 6-Acids; 7-Cyanide; 8-Mn; 9-Fe; 10-Cu; 11-Zn; 12-Pb; 13-Ni; 14-As; 15-Ba; 16-Co; 17-Ag; 18-S; 19-V; 20-Bacterias and feces; 21-Ammonium; 22-Bromine; 23-Flint; 24-Dust;25-Li; 26-NO_2; 27-Synthetic superficially active substances; 28-Cd.

Considering all the above mentioned and based on literary and archive materials the geological map of Black Sea and coastline was developed illustrating actual data of 80-90's of the last century (Fig. 1). Research in the last several years has determined that on the territory of Georgia there are natural radiation anomalies belonging to the group U-Ra-Th-K (Kvinikadze at al. 2007). They are connected to the Paleozoic granites and Mid-Jurassic coal-beds. It was set that unfortunately, 20 years ago, radiation anomalies were located near the settlements.

Today to assess the geoecolgical condition of the Black Sea section of Georgia the following items have to be studied:

- Contamination degree of sea water and coastline by petroleum products;
- Determination of industrial waste qualitative and quantitative contamination parameters of the waters discharging into sea (rivers);
- Contamination of coastline by technogenic origin radiation nuclides – remains of Chernobyl Atomic Power Station accident;

- Contamination of Black Sea and coastline by household waste, toxin-chemicals, fecal waters and etc.

In order to specify these issues in 2008 the integrated geoecological works were carried out in the southern part of Black Sea coastline, the results of which are given in the article. Black Sea water surface, bottom sediments of the surface and the waters discharging into the sea with their hydrochemical parameters has been studied. Also the topsoil used in the agriculture as well as the surface topsoil layers existing along the motor roads have been studied under the present project.

From the Sarpi area, including Rioni River, almost along the total coastline we have conducted radiation measurements. The concentration of the heavy metals in the biological specimens was determined in the plants that are used as food products (corn, nut, mandarin, tea and others).

The radiation measurements have been carried out in Sarpi (Georgian-Turkish Border)–Poti (Sea Port of Georgia) section. As it is known, as a result of Chernobyl accident Black Sea coastline and particularly this section of Georgia was contaminated with radiation nuclides. The measurements made in 2008 (Fig. 2) show that, today in comparison

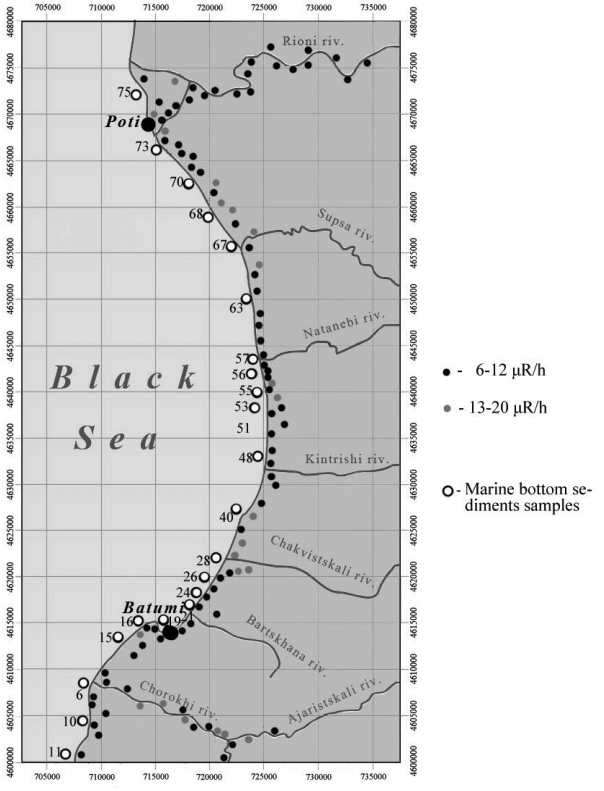

Fig.2 Radiation measurements and marine bottom sediment specimens.

with the established background of radiation in Georgia (8-10 μR/h), high levels of radiation (20 μR/h) were observed only in the plants of Mtsvane Kontskhi (particularly in the tea plantations) and in Batumi and Poti ports adjacent territories (lawns). In some canyon of the rivers (for example Adjaristskali River) and its tributaries the radiation elevations slightly were more than they are permitted (14-17 μR/h). In our opinion the existence of high levels of radiation background are stipulated by peculiarity of topsoil's (where there is high radiation level, the topsoil layers have clay features). As regards to Sea coastline itself (sand of the beach) the radiation background meets all the acceptable values and sometimes is even less.

As the studies show, the distribution of carbohydrate in Black Sea surface water samples does not exceed the acceptable norms. Their existence is observed as a form of trace. Therefore the composition of petroleum products in Black Sea water quite meets the acceptable norms (≤0.04 mg/l). It has to be mentioned that these sea samples were taken in September of 2008, when due to August events (Georgian-Russian conflict) travel by sea was almost stopped.

Besides the petroleum products, the bottom sediments of sea coastline were studied on heavy metals. As it is shown in figure 3, in the area of Poti, where Rioni River joins the Sea, the concentration of manganese (Mn), zinc (Zn) and, in single instances, arsenic (As) is high in the collected marine samples. The analogical type of the samples was taken from all the rivers discharging into the Black Sea.

As figure 4 shows high concentration of heavy metals (copper and zinc) is observed in some samples that were taken from the rivers Kintrishi and Chorokhi. In the bottom sediments of Rioni River analogically in the bottom sediments of the Sea, the composition of manganese and arsenic is high. This fact is very easy to explain as Chiatura manganese and Lukhumi arsenic mines are located at the basin of the above mentioned rivers.

While survey of topsoil two types of topsoil were revealed (Table 1) - topsoil used for pastures located along the roads and topsoil used in the agriculture.

In the second type of the topsoil (used in the agriculture) heavy metals' abnormal data are noted in unit samples. There is high concentration of manganese (11800 mg/kg) and arsenic (25.9 mg/kg) in

Chaladidi (Rioni River right embankment) and Mtsvane Kontskhi (Chakvistskali River) topsoil.

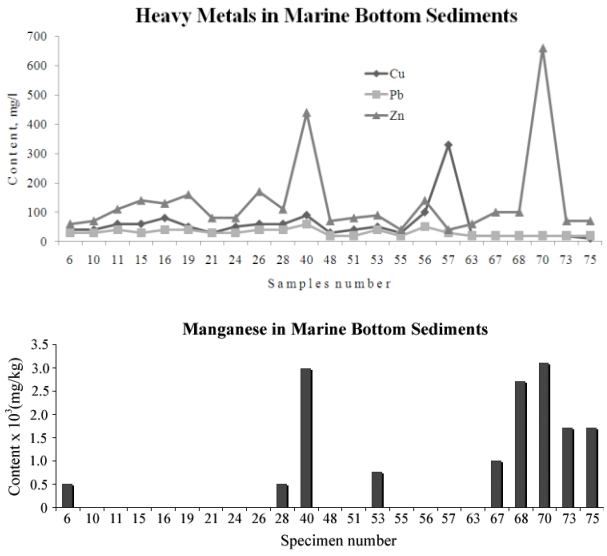

Fig. 3. Heavy metals and manganese contents in the marine bottom sediments (Specimen numbers see on Fig. 1.)

The existence of toxin-chemicals was observed in some samples as a form of large amount of copper. The high concentration of copper is revealed in some samples taken along the motor road. As in the bottom sediments of the sea and rivers, manganese and arsenic concentrations are very high also in the bottom sediments of the topsoil taken in Poti areas.

The plants that are food products are basically used as biosamples. The data in Table 2 show that the manganese in biological samples submitted as a dominant element. In some cases its composition is very high. For example, for the eucalyptus it is 232-255 mg/kg, but for the tea leaves 632 mg/kg. It has to be noted that the species of these both plants are located at the territory of Mtsvane Kontskhi (Chakvistskali river), where the quantitative indications of such elements are very high.

As regards to biological contamination, it basically concerns the waters of Rioni river and Chorokhi river as it is clearly illustrated on the map developed by us (Fig.1). In our opinion this is caused by high coefficient of the settlement in these rivers' basins, so the large amount of household and fecal waters enters these rivers: Chorokhi and Rioni and by means of them the toxic waste joins the Black Sea water.

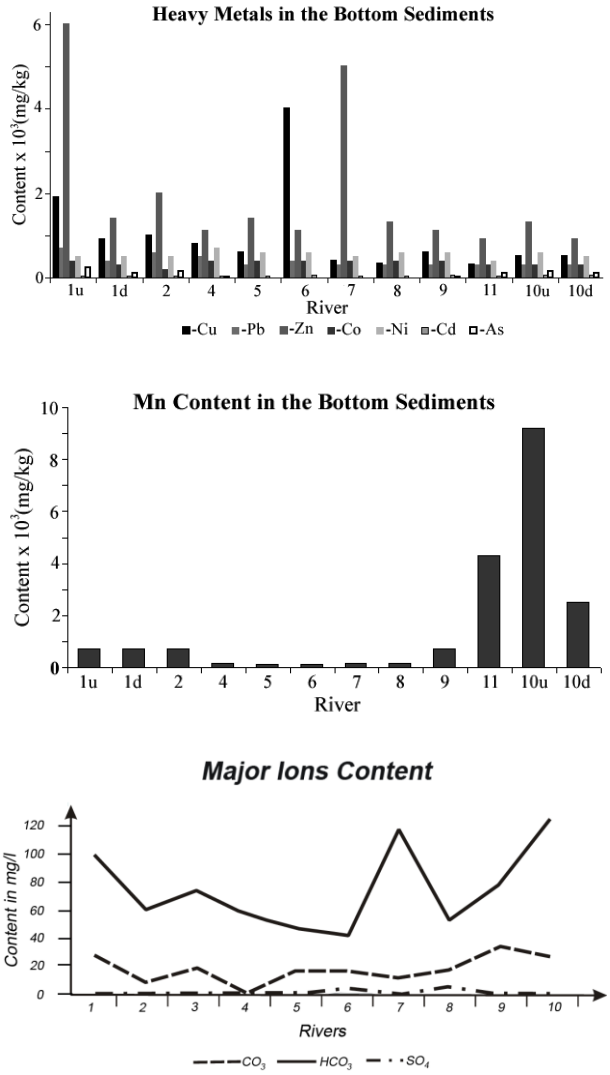

Fig. 4 Heavy metals and manganese contents in the rivers bottom sediments and major ions content in the river water. Rivers: 1-Choroki; 2-Ajaristskali; 3-Bartskana; 4-Korolistskali; 5-Chakvistskali; 6-Kintrishi; 7-Choloki; 8-Natanebi; 9-Supsa; 10-Rioni; 11-Maltakva (u-upstream, d-downstream)

Conclusions

1. The high concentration of manganese and arsenic in the bottom sediments of the sea, river and agricultural topsoils is observed in Poti areas that are due to the precipitation coming from the manganese and arsenic mines located at Rioni River basin.
2. The high concentration of copper, lead and zinc is observed in the topsoils existing along the motor road, what in our opinion is due to the sedimentation processes of vehicles' exhausting gases.

Table 1. Heavy Metals Content in Topsoil along the Roads and Used in Agriculture.

Coordinates		Content (mg/kg)							
N	**EO**	**Cu**	**Pb**	**Zn**	**Co**	**Ni**	**Cd**	**Mn**	**As**
*		36	85	140	20	35	0.8	1500	2.9
Topsoil Along the Roads									
41º 34′ 11.60″	41º 33′ 57.20″	130	70	250	30	40	5.0	-	-
41º 31′ 16.00″	41º 32′ 59.00″	150	70	140	50	120	7.0	-	-
41º 38′ 08.40″	41º 36′ 26.76″	80	50	250	30	40	5.0	-	-
41º 38′ 34.98″	41º 37′ 01.80″	80	40	140	30	30	4.0	-	-
41º 39′ 09.24″	41º 38′ 0.42″	500	60	150	60	50	6.0	-	-
41º 38′ 57.90″	41º 38′ 39.60″	80	60	130	30	60	3.0	-	-
41º 40′ 09.00″	41º 41′ 15.06″	150	80	380	40	60	4.0	-	-
41º 41′ 04.68″	41º 42′ 03.96″	130	70	670	20	50	4.0	-	-
41º 41′ 42.12″	41º 42′ 35.10″	100	60	90	40	50	6.0	990	-
41º 41′ 56.40″	41º 43′ 00.96″	120	70	180	40	60	7.0	940	-
41º 42′ 13.02″	41º 43′ 15.42″	60	40	100	40	40	5.0	2350	
41º 41′ 22.92″	41º 42′ 56.70″	150	40	230	30	30	4.0	-	-
41º 38′ 46.02″	41º 38′ 23.28″	130	110	200	40	50	5.0	1190	-
41º 38′ 13.62″	41º 37′ 05.94″	120	80	1130	30	40	5.0	-	-
41º 43′ 02.76″	41º 43′ 59.82″	60	30	140	40	60	5.0	-	-
41º 44′ 07.80″	41º 44′ 02.34″	100	80	350	500	60	6.0	2270	-
41º 45′ 01.86″	41º 44′ 39.42″	150	60	270	50	60	7.0	-	-
41º 45′ 31.08″	41º 45′ 35.40″	500	70	330	50	150	7.0	-	-
41º 46′ 11.94″	41º 45′ 20.70″	130	60	100	40	40	5.0	1340	-
41º 47′ 15.12″	41º 46′ 00.36″	400	40	1700	30	50	5.0	-	-
41º 49′ 30.72″	41º 46′ 33.48″	500	1400	300	30	60	5.0	-	-
41º 51′ 33.72″	41º 46′ 46.86″	50	40	270	20	60	5.0	-	-
41º 52′ 38.46″	41º 46′ 32.82″	40	30	230	30	110	4.0	-	-
41º 52′ 38.46″	41º 46′ 32.82″	30	20	40	20	50	4.0	-	-
41º 53′ 42.84″	41º 46′ 24.12″	100	50	140	30	40	4.0	-	-
41º 56′ 07.02″	41º 46′ 19.14″	20	20	70	30	60	4.0	-	-
41º 58′ 47.58″	41º 46′ 57.78″	20	30	110	30	60	5.0	-	-
42º 04′ 23.34″	41º 42′ 57.48″	40	130	430	30	60	4.0	1000	6.4
42º 04′ 23.34″	41º 42′ 57.48″	30	30	80	30	50	5.0	1100	8.0
42º 04′ 50.76″	41º 42′ 42.04″	40	30	110	30	400	5.0	900	11.2
42º 06′ 12.90″	41º 42′ 02.46″	20	40	400	30	60	5.0	1200	<1.6
42º 09′ 09.18″	41º 39′ 19.62″	80	40	140	30	60	5.0	1300	8.0
42º 12′ 48.12″	41º 48′ 01.98″	20	20	70	20	40	5.0	-	8.0
42º 10′ 41.04″	41º 41′ 14.70″	60	50	150	30	50	7.0	1700	<1.6
42º 09′ 00.60″	41º 40′ 18.96″	360	150	300	30	50	7.0	4600	8.0
42º 08′ 10.02″	41º 46′ 32.82″	20	30	80	30	40	5.0	1800	14.4
Topsoil Used in the Agriculture									
41º 35′ 43.22″	41º 38′ 31.57″	600	60	330	30	60	5.0	-	-
41º 32′ 50.70″	41º 33′ 51.60″	120	50	120	40	40	5.0	-	-
41º 32′ 50.70″	41º 33′ 51.60″	110	50	150	40	40	5.0	1000	-
41º 38′ 58.74″	41º 39′ 55.10″	50	60	430	30	40	5.0	-	-
41º 41′ 31.44″	41º 42′ 55.74″	150	90	50	30	40	7.0	11800	<1.6
41º 42′ 30.18″	41º 43′ 26.10″	40	60	10	30	40	6.0	-	-
41º 42′ 07.68″	41º 43′ 58.98″	50	40	50	30	80	7.0	-	-
41º 48′ 16.74″	41º 46′ 34.74	700	80	580	40	60	6.0	-	-
41º 50′ 21.00″	41º 46′ 43.20″	400	70	600	30	60	5.0	-	-
41º 50′ 21.00″	41º 46′ 43.20″	50	30	120	30	60	4.0	-	-
41º 56′ 42.60″	41º 46′ 14.58″	40	40	90	40	85	5.0	-	-
41º 57′ 17.70″	41º 46′ 16.50″	60	40	80	30	50	5.0	-	-
42º 12′ 48.12″	41º 48′ 01.98″	50	50	160	30	40	6.0	-	25.6

* Standards, which correspond to natural background (Fomin and Fomin 2001)

Table 2. Heavy Metals Content in Biological Samples.

Biological Sample	Content, mg/kg						
	Cu	**Pb**	**Zn**	**Mn**	**Co**	**Ni**	**Cd**
Eucalyptus (leaf)	0,80	1,10	2,00	7,70	1,00	1,50	0,30
Eucalyptus (stalk)	12,00	6,60	23,00	23,00	4,00	5,00	1,30
Mandarin	3,75	3,90	6,00	6,00	2,30	2,00	0,50
Grass	12,00	8,80	33,00	56,00	6,40	5,50	1,00
Palm	4,00	3,30	14,00	77,00	1,90	2,00	0,50
Broomcorn	4,80	3,50	26,00	23,00	2,00	1,50	0,30
Walnut (foetus)	2,50	2,20	16,00	10,00	1,00	1,00	0,20
Walnut (stalk)	3,80	5,00	36,00	13,50	5,50	6,00	2,00
Walnut (leaf)	6,30	7,00	27,00	60,00	6,50	7,00	2,00
Corn (stalk)	4,50	3,50	39,00	12,00	14,00	1,50	0,25
Corn (husk)	8,50	5,50	28,00	54,00	1,00	1,50	0,70
Corn (ear)	1,50	1,65	29,00	9,50	0,90	1,50	0,30
Corn (leaf)	1,25	1,65	9,00	11,50	0,50	0,50	0,15

3. Rather high radiation data are stipulated by lithological and plant cover peculiarity of the topsoil.
4. The composition of heavy metals in the biosamples has the selective nature and basically is defined by topsoil geochemistry.
5. Biological contamination is connected with the rivers, on which the town type settlements are located. Also it can be caused by bad working of cleaning structures' or their absence on the rivers at all.
6. In October-November of 2009 we are planning to perform the monitoring of the works carried out in 2008, which will enable us to define the received results precisely.

References

Fomin G., Fomin A., 2001. Soil. Inspection of quality and ecological safety according to International Standards. Handbook, Moscow, p.836 (in Russian).

Kvinikadze M., Kuparadze D., Kerestedjian T., Sirbiladze I., 2006. Geoecological assessment of the environment: An example from the territory of Georgia. Bulgarian Academy of Sciences. Geochemistry, Mineralogy and Petrology, Sofia, 44, 131-140 (in English). http://www.geology.bas.bg/ mineralogy/gmp_files/Vol44.html

Kvinikadze M., Kuparadze D., Pataridze D., 2007. About an ecological condition of the Black Sea coast of Georgia. In "Caucasus Environment", Tbilisi, VII, 35-43 (in English and Russian).

Scientific Annals, School of Geology, Aristotle University of Thessaloniki Proceedings of the XIX CBGA Congress, Thessaloniki, Greece	Special volume 100	105-111	Thessaloniki 2010

POLLUTION WITH ARSENIC AND HEAVY METALS OF SOILS AND SOME COMPONENTS OF THE FOOD CHAIN IN THE ENVIRONMENT OF GOLIAM BUKOVETS MINE TAILINGS IMPOUNDMENT, CHIPROVTSI MINING AREA, NW BULGARIA

Mladenova V.[1], Kotsev T.[2], Cholakova Z.[3], Schmitt R.-T.[4], Ivanova I.[1], Dimitrova D.[5]

[1] *Department of Mineralogy, Petrology and Economic Geology, Sofia University St. Kl. Ohridski, 1504 Sofia, Bulgaria*
[2] *Geographical Institute, Bulgarian Academy of Sciences, 1113 Sofia, Bulgaria*
[3] *Department of Landscape Ecology and Environmental Protection, Sofia University St. Kl. Ohridski, 1504 Sofia, Bulgaria*
[4]*Insit. of Mineralogy, Museum of Natural History, Humboldt-University of Berlin, Invalidenstrasse 43, D-10099 Berlin, Germany*
[5]*Geological Institute, Bulgarian Academy of Sciences, 1113 Sofia, Bulgaria,*

Abstract: The Chiprovtsi mining area is contaminated as a consequence of past mining. The 20-year existing of Goliam Bukovets mine tailings impoundment has affected all elements of its surroundings. As a result elevated concentrations of arsenic and heavy metals in upper soil layers and in grass are established. The low distributions of arsenic and heavy metals in depth allow assuming their low mobility which restricts their unfavourable environmental impact. The sheep's milk has elevated Zn and Cu contents and so it transfers them to the humans. The carry-over of Pb, Cd and As from grass to the milk is low. Metal concentrations in livestock's excrements are low and seem not to pose risk for secondary soil contamination if used as organic fertilizer. Although the tailings impoundment is almost recultivated and the dust pollution is finished the contaminated soils of the surroundings contain arsenic and heavy metals and continue to transfer them trough the food chain. Besides, the soil cover of the impoundment is not sufficient to avoid the penetration of grasses root to the mine tailings.

Keywords: arsenic, heavy metals, soil, plants, milk, Chiprovtsi mining area.

1. Introduction

Heavy metals and metalloids released from the mine wastes in mining areas are among the most important sources of environmental pollution.

The Chiprovtsi mining area is located in NW Bulgaria, 30 km W from Montana town (Fig. 1). The area is situated at an altitude from 900 to 400 m. The mean annual precipitation in the region is 756 mm/m^2 per year with maximum in the spring and minimum in the autumn (Koleva and Peneva, 1990). The mean temperature is 10.4^oC, the spring is wet and the winter is mild (Climatic reference book, 1983). The major soil type is strongly eroded grey forest soil (Koinov et al., 1998). The bedrock consists mostly of the rocks of the metamorphic diabase-phillitic complex (DPC) and comprises an alternation of diabase, diabasic tuffs, phillites, marbles, chlorite-sericite- and quartz-chlorite schist and diorite porphyrite. Diabasic tuffs and phillites are the most widespread rocks of this complex (Nikolaev and Tonev, 1961).

The mines in Chiprovtsi region are known to be exploited from Roman times, through Middle Ages, but most intensively from 1950 to 1999, when the last mine ceased its activities. Three types of deposits containing minerals of As, Pb, Zn and Cu have been exploited here: Pb-Zn-Ag Chiprovtsi deposit with main minerals galena, chalcopyrite, tetrahedrite and arsenopyrite (Dragov and Obretenov, 1974;Atanassov and Pavlov ,1982) has produced 4789.1 thousand t of Pb-Zn ore in the period 1951-1995 (Milev et al., 1996); Fe-As-Au Govezhda and Kopilovtsi deposits with main minerals arsenopyrite, galena, sphalerite, tennantite, proustite (Nikolaev and Tonev, 1961; Mladenova et al., 2003) have produced 1105.6 thousand t of ore with average Au content of 3.5 g/t, and 3863 kg pure gold (Milev et al., 1996); Fe-Mo Martinovo deposit with main minerals arsenopyrite, löllingite, chalcopyrite, molybdenite with 79 thousand t of Mo-ore production (Velchev, 1974, Tarasova,

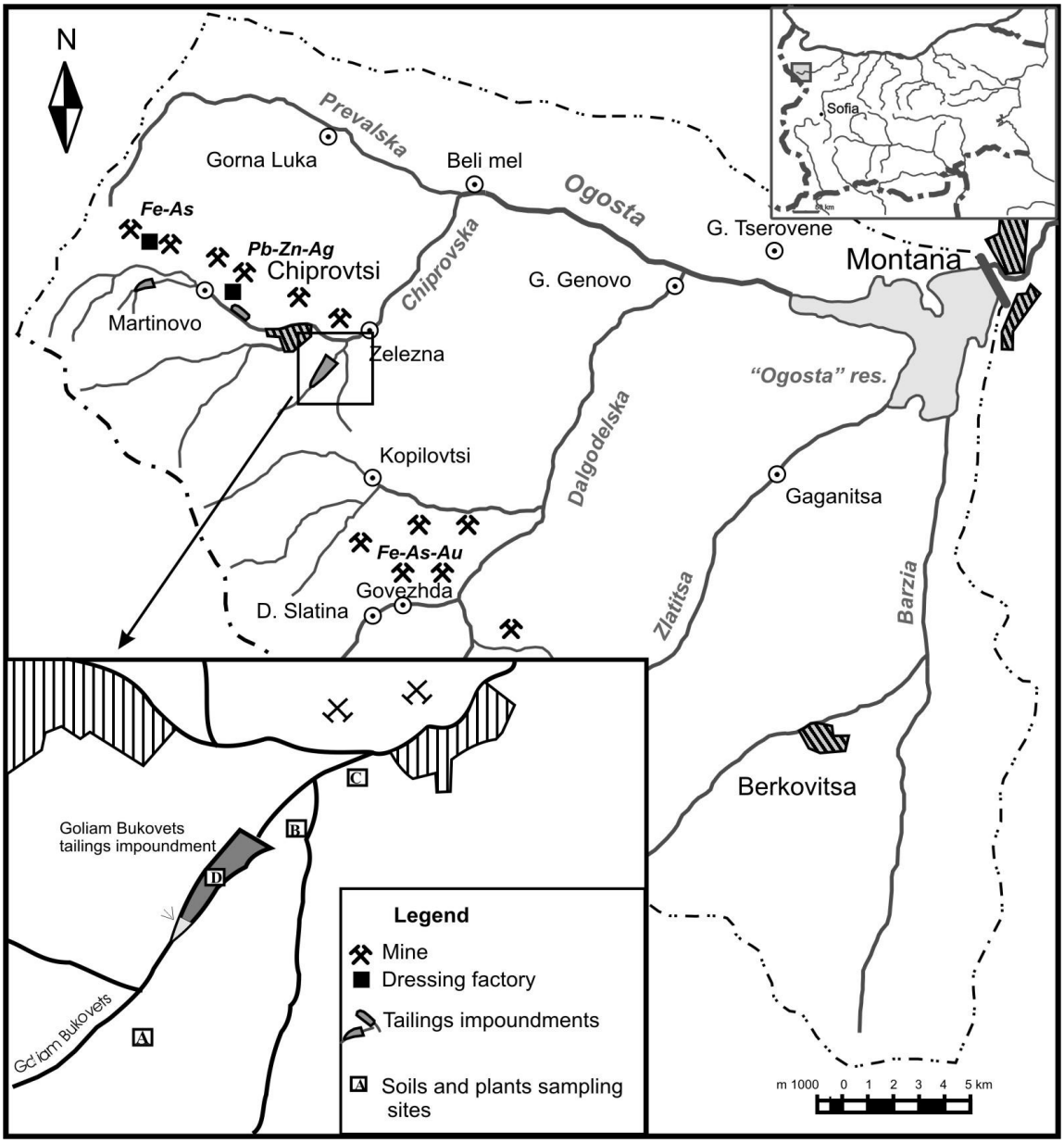

Fig. 1. The Ogosta River catchments and schematic map of the study area with location of sampling sites.

1987; Milev et al., 1996). As a result numerous waste rock dumps and 3.5 million tones mill tailings stored in 3 tailings impoundments are available in the region.

Remediation activities have been carried out in the region since 2000 year, which covered the three tailing impoundments, as well as numerous mine waste dumps. At present almost all mine waste dumps are partially or completely remediated.

The Goliam Bukovets mine tailings impoundment is the biggest one. It occupies a natural negative relief and has surface of approximately 0.16 km^2, volume of about 3.0 million tones and a maximal depth of about 70 m. The impoundment was the main place for the waste storage from the ore processing from the 3 types of deposits. The upper layer is composed only from the wastes of Martinovo deposit because it was the last closed mine in the region. The wall of the tailings impoundment is built up from the oreless massive waste produced by the dry magnitic separation of the iron ore in Martinovo factory (Vesselinov et al., 1996). The main minerals in the impoundment are calcite, siderite, quartz, chlorite, amphibole and magnetite. The sulphide minerals are less 5%, the most abundant are pyrite and arsenopyrite, and galena, sphalerite, chalcopyrite and fahl ore are rare (Mladenova and Zlatev, 2004).

The tailings in the impoundment remained dry and

uncovered until 2001. The emission of dust from Goliam Bukovets tailings with high concentrations of mineral phases with As and heavy metals has impacted waters and river sediments and the agricultural fields and meadows used for farming and livestock breeding. In 2001 Goliam Bukovets tailings impoundment was covered with coating of a slowly soluble, non-reactive synthetic precipitate and about 30 cm of uncontaminated soil and Dutch clover was plant.

The aim of this study is to provide data concerning the contamination with As and heavy metals of soils, plants and some components of the food chain in the surroundings of Goliam Bukovets mine tailings impoundment in Chiprovtsi mining area, NW Bulgaria. The determination of their concentrations is important in assessing of their potential environmental impact.

2. Sampling and analytical methods

Sampling sites were chosen to include sites with background concentrations and sites with expected pollution. Samples were collected in August 2005. Figure 1 shows the location of the sampling points. Samples of primary ores as well as of the tailings were studied to assess the specific pollution sources.

Four soil profiles differing in their position and therefore metal concentration were sampled. The locations of the profiles are given in Figure 1.

The first profile (A) is located in meadow between agricultural fields at about 500 m SW from the impoundment and is considered as unpolluted background reference. It was sampled to a depth of 30 cm from three soil horizons in the following depths: A1- 0-2 cm, A2 - 2-12 cm; A3- 12-27 cm.

The second profile (B) is located at the water shed 100 m NE from the impoundment. It is situated on the main wind directions in the area and was affected by dust pollution during 20 years. The sampling was performed to a depth of 46 cm from four soil horizons in meadow without indication of tilling at least several decades. The following depth intervals have been studied: B1 - 0-3 cm; B2 - 3-13 cm; B3 - 13-23 cm; B4 - 23-34 cm; B5 - 34-46 cm.

The third profile (C) refers to an alluvial terrace on the right bank and 100 m far from Ogosta River and is located in an orchard 800 m NE from the impoundment and is supposed to be polluted through dust emissions as well as through the polluted river waters especially in the period before 1979 when the impoundment has been not yet constructed. The profile is sampled to a depth of 42 cm from three soil horizons. The depth intervals 0-5 cm, 5-12 cm, 12-18 cm, 18-30 cm and 30-38 cm have been analysed.

The forth soil sampling site (D) is from the soil cover of the impoundment and is considered as unpolluted one but its composition is important because it is a growth environment for the plants.

Stems of heterogeneous grasses from all points of soil sampling as well as Dutch clover stems from the surface of the recultivated impoundment were collected. In order to follow the contamination of the food chain livestock milk and excrements from the polluted areas were collected.

The bulk soil samples, grass and excrements were dried naturally. Soils were homogenized and dry sieved at 2 mm then at 63 μm mesh sizes in order to separate two soil fractions – less than 2mm (bulk sample) and less than 63 μm (fine fraction). The samples were then analysed by X-ray fluorescence spectrometry (XRFS) and by ICP- AES, AAS for their major-, minor and trace element contents. The grass and excrements were milled to powder and then analysed by ICP-OES.

The 500-ml raw milk samples were collected and held at 4^0C and arrived at the analytical laboratory within 48 h after their collection. The concentrations of arsenic, cadmium and lead were made by means of absorption spectrophotometer VARIAN AA220Z. Copper and zinc are analysed by IVP-AES. As a references the whole powder milk (RM 8435, National Institute of Standards and Technology, USA) were used.

The mineralogical compositions of selected samples from both soil fractions of the two contaminated soil profiles were determinate by powder X-ray diffraction.

A selected samples of polish samples of primary ores as well of tailings and soil were examined under the optical microscopy in order to characterize the mode of occurrence of As and heavy metals in the ore and in the tailings and the occurrence of secondary minerals concentrating the studied elements.

The pH values of soil samples were measured in the leachates consisting of boiled distilled water and soil in ratio 20 g soil:100 ml H_2O. The composite was shaken 30min and then leached for 1h.

3. Results and discussion

3.1. Soils

3.1.1. Bulk chemical composition

Soil's compositions reflect the composition of the parent rocks and are important of viewpoint for precipitation of secondary phases which potentially might concentrate the heavy metals and metalloids. MnO and P_2O_5 in all of the samples from the 3 profiles are below 1 wt %.

Fe_2O_3 contents in the samples from the two contaminated profiles are almost the same (mean 7.5 wt. % for profile B and 7.9 wt.% for profile C) and these contents are lower than Fe_2O_3 in the background profile (mean 10.13 wt.%).

Significant differences are established in the CaO content also. The two contaminated profiles show lower content (mean 0.9 wt. % for profile B and 1.9 wt. % for profile C) than the background profile (mean 3.6 wt.%).

SO_3 content in the samples from the three profiles is almost the same despite the two contaminated profiles should show higher concentration because of their air pollution with tailings dust.

The loss of ignition (LOI) reflects the content of free and fixed water in minerals and varies in the samples from profile B between 6.6 and 15.0 wt.% (mean 8.8 wt.%), in profil C – between 5.2 and 12.7 wt.% (mean 8.2 wt.%) and in the background profile-between 6.7 and 15.7wt.% (mean 6.8wt.%).

The contents of SiO_2, TiO_2, Al_2O_3, MgO, Na_2O and K_2O vary in narrow range. A close relation with the parent rocks is difficult to obtain because of the complex composition of the metamorphic complex.

3.1.2. As and heavy metals

The soils in the region have high As, Pb and Zn background contents because of the rocks and ore deposits.
The contents of Pb and Zn in the background profile (A) are lower than the maximum accepted concentrations (MAC) for soils with pH 6.2-7.0 by Bulgarian legislation; As vary around the MAC (MAC in mg/kg: As-25; Pb-80; Cu-255; Zn-330) (Instruction Nr.3 2004) (Fig. 2.A).

Arsenic in the two contaminated profiles and in the sample from the impoundment is over the MAC (Fig.2A, 2B). In profile B it varies between 515 and 65 ppm in the bulk sample and between 460 and less than 30 in the fine fraction. In profile C As contents in bulk sample are between 335 and less than 40 ppm and between 295 and 85 in fine fraction.

Cu is below the MAC values for Bulgaria in the both fractions from the two profiles and in the river bank sample and its concentrations vary between 101 to 58 ppm for profile C and between 92 and 69 ppm for both fractions of profile B (Fig. 2B, 2C).

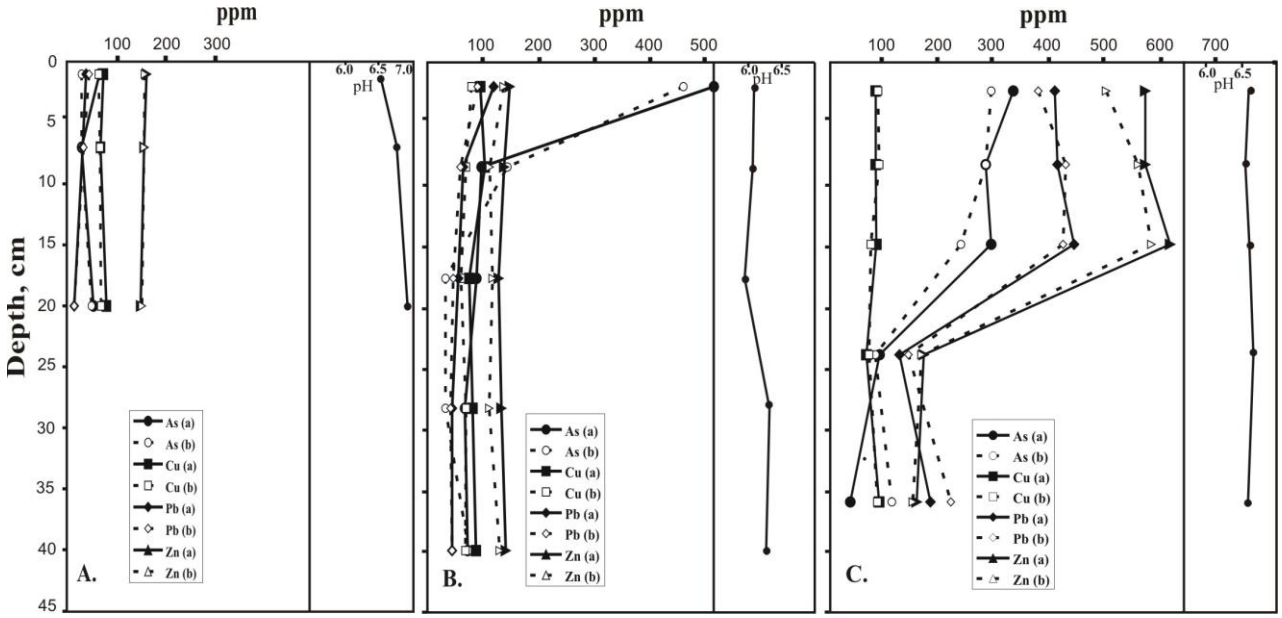

Fig. 2. As and heavy metals distributions and pH changes with depth in bulk (a) and fine (b) soil fractions: A. – *profile A* (background); B.- *profile B* (in meadow at the water shed 100 m NE from the impoundment); C. - *profile C* (in orchard 800 m NE from the impoundment).

Pb in both fractions of profile B is under and close to MAC (from 117 to 42 ppm in bulk sample and 88-39 ppm in fine fraction) (Fig. 2B). The concentrations in profile C are higher and above MAC in the range 445-129 ppm for bulk sample and 430-145 ppm for fine fraction (Fig. 2C).

Zn in the both fractions of profile B is under MAC (in the range 146-126 ppm for bulk sample and 135-109 ppm in the fine fraction (Fig. 2B). In profile C its contents are from 619 to 160 ppm for bulk sample and from 585 to 153 in fine fraction (Fig. 2C).

The two contaminated profiles show enrichment of As and heavy metals in the upper layers. In profile B the highest concentrations are found out in the upper 5 cm, because the contamination was performed by dust and the meadow has not been cultivated. In the alluvial river terrace (profile C) high concentration are established deeper (to 15-20 cm) probably because of the tilling or flooding by the contaminated Ogosta River. In depth 5-40 cm the values of the elements in profile B are almost constant and have concentration close to that in the background profile, while in profile C the values in the depth are higher.

3.1.3. pH and mineral composition

The pH values of soils are nearly neutral with some differences for each of the studied profiles (Fig.2A, 2B, 2C). In background profile (A) the pH values in the 3 sampled depths are as follow: A1-6.6, A2 – 6.7, A3 – 6.9. In the first profile with pollution (B) the pH values in the 5 depths are: B1 -6.0, B2 – 6.0, B3 – 5.9, B4 – 6.3, B5 – 6.3. In the second profile with pollution (C) the pH in the sampled are: C1 – 6.6, C2 – 6.6, C3 – 6.6, C4 – 6.7, C5 – 6.6. The highest pH values have the soil from the cover of the impoundment (between 7.8 and 7.9) which comes not from the surroundings.

The main minerals are quartz, K-feldspar, plagioclase and micas; montmorillonite and chlorite are less abundant. Organic matter occurs in all samples.

In the interval 30-38 cm of soil profile C solid brownish spots were observed. Optically well-shaped oxidised pyrite grains and iron oxides minerals were seen (Fig. 3a, b). No secondary arsenic and heavy metals-bearing minerals have been established. Arsenic in small amount has been determined by microprobe analyses in the iron oxides minerals.

3.2. Grass, milk, excrements

Arsenic and heavy metals can enter the food chain through the plants. Their concentrations in the grass of the background area (profile A) are (mg/kg): As - 0.6, Cd -0.17, Cu -4.64, Zn - 17.33, Pb - 0.6. The concentrations in the heterogeneous pasture grass from the surroundings of the contaminated profiles are (mg/kg): As - 7.0 in profile B, 16.2 in profile C, 3.8 in sample D; Cu - 6.3 in profile B, 14.6 in profile C, 5.2 in sample D; Pb - 1.2 in profile B, less than 0.5 in profile C, 0.5 in sample D; Zn - 27.6 in profile B, 52.5 in profile C, 9.0 in sample D; Cd content is under the detection limit of 0.05 mg/kg in all profiles. The Dutch clover from the recultivated beach of the impoundment contains As-1.7, Cu-6.1, Pb-1.4, Zn-13.6 and Cd - less 0.05. These concentrations are higher compared to their contents in Dutch clover from the polluted with heavy metals Zlatiza-Pirdop region in Srednogorie zone in Bulgaria (As-0.08, Cu-

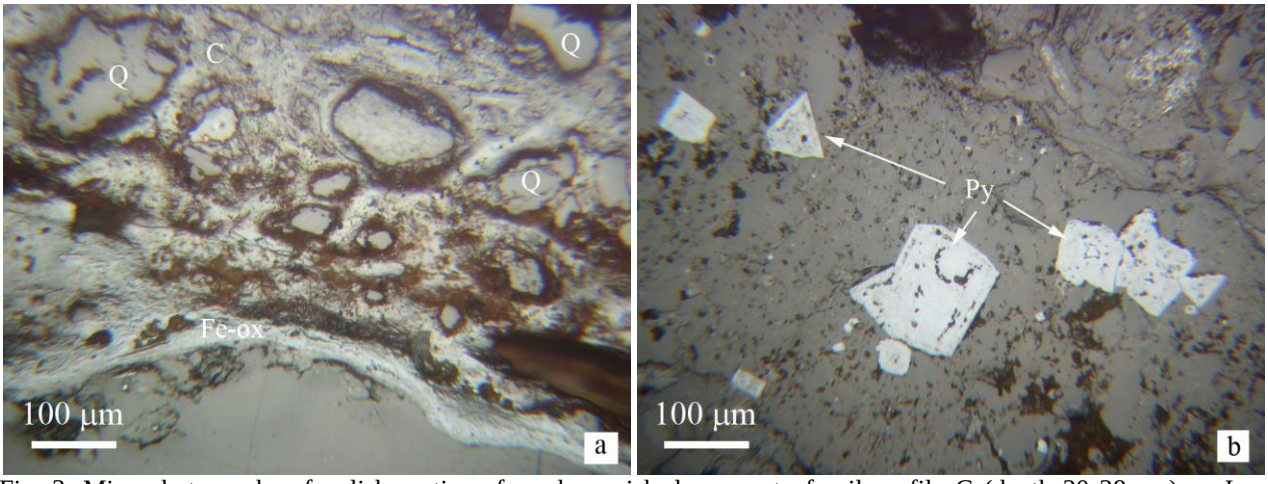

Fig. 3. Microphotographs of polish sections from brownish dense part of soil profile C (depth 30-38 cm). a. Iron oxides minerals (Fe-ox) embracing quartz (Q) and clay (C) particles; b. Well-shaped oxidised pyrite (Py) grains.

2.14, Pb-0.41, Zn-6.96, Cd-0.02) (Stojanov 1999).

As a link between soil and man sheep milk yielded from 200 sheep has been analyzed. The concentrations (in mg/kg) of Zn (6.75±0.11) and Cu (2.75±0.08) are higher than the MAC in foods according Bulgarian legislation (Instruction Nr.31 2004) (Zn-5.0; Cu-0.4). As (0.037±0.005), Pb (0.077±0.008) and Cd (0.005±0.001) are lower than MAC (As-0.05; Pb-0.1; Cd -0.01). These values are higher compared to the sheep's and goat's milk in the area (Kotsev et al. 2009). The low Cd concentration in milk is due to the low concentration of the element in soils as well as to its accumulation in liver and kidney (Prankel et al. 2004) and to the low carry-over to the milk (Blüthgen 2000). Lead concentrations in milk are usually much lower than blood levels and animal tissues with the highest concentrations of Pb are liver, kidney and bone (Biehl and Buck 1987).

The excrements are an integral part of the biocircle. The concentration of the studied elements in the excrements of the same sheep is (in mg/kg): As -13.2±0.8; Zn - 61.7±0.6; Cu – 20.4±1.9; Pb – 4.9±0.3; under the detection limit are Sb (0.5) and Cd (0.05). The concentrations of the elements in the cow's excrements collected on the recultivated beach are: As (8.1±0.5); Zn - (45.9±0.4); Cu – (22.6+2.0); Pb – (4.6+0.3); Sb and Cd are under the detection limit, too. According to EFSA (2005) in mammalian species inorganic arsenic is converted into methylated metabolites, which are rapidly excreted compared to other organic arsenic compounds. The high As contents in sheep's and cow's excrements and the ratios $C_{es}(C_{ec})/C_{soils}(C_{grass}, C_{Dutch\ clover})$ support these statement (Tab. 1). Metal concentrations in both cow's and sheep's excrements are lower than MAC for soils and much lower than the local background and seem not to pose risk for secondary soil contamination if used as organic fertilizer.

The real risk for human health is connected with the plants capability to extract elements from the contaminated soil and to deliver it to milk. The calculated ratios are given in table 1. They show that As is absorbed with low intensity from grass which restricts its transfer to the next element of the food chain.

The grasses and the Dutch clover have extracted most intensively Zn, Cu and Pb and the relations C_{soil}/C_{grass} and $C_{soil}/C_{dutch\ clover}$ give an idea for their bio-absorption capability. The absorption capability of grasses in background part and of Dutch clover on the beach decreases as follows: Zn>Cu>Pb>As and Zn>Cu>As>Pb for the grass of the pasture grounds in the contaminated areas and the beach, relatively.

According to Sirotkin et al. (2000) the ratio $C_{milk}/C_{soil}(C_{grass}, C_{Dutch\ clover})$ indicate the rate of transfer of As and heavy metals from soil and grasses to the milk. The calculated transfer capability in this study decreases in the following order: Zn>Cu>Pb>Cd>As.

Table 1. Ratio between the concentrations of elements in soil, milk, plants and livestock's excrements.

Ratios		*As*	*Cu*	*Pb*	*Zn*	*Cd*
Cgrass/Csoil	bulk	0.02	0.05	0.006	0.05	n.d.
	fine	0.03	0.06	0.006	0.06	n.d.
Cdc/Csoil	bulk	0.01	0.06	0.02	0.08	n.d.
	fine	0.01	0.07	0.02	0.09	n.d.
Ces/Csoil	bulk	0.07	0.19	0.063	0.37	n.d.
	fine	0.09	0.23	0.06	0.43	n.d.
Cec/Csoil	bulk	0.05	0.22	0.06	0.28	n.d.
	fine	0.05	0.26	0.06	0.32	n.d.
Ces/Cgrass		3.47	3.92	9.8	6.86	1
Ces/Cdc		7.76	3.34	3.5	4.54	1
Cec/Cgrass		2.13	4.35	9.2	5.11	1
Cec/Cdc		4.76	3.70	3.29	3.38	1
Cmilk/Csoil	bulk	0.020	2.67	0.1	4.11	n.d.
(x100)	fine	0.024	3.13	0.09	4.72	n.d.
Cmilk/Cgrass (x100)	-	0.97	52.9	15.4	75.1	10
Cmilk/Cdc (x100)	-	2.18	45	5.5	49.7	10

Abbreviations: C- concentrations, dc- Dutch clover, es – sheep's excrements, ec-cow's excrements, n.d. – not detected.

4. Conclusions

The 20 years existing of Goliam Bukovets mine tailings impoundment has affected all elements of its surroundings. As a result elevated concentrations of arsenic and heavy metals in upper soil layers and grass are established.

The low distribution of arsenic and heavy metals in depth of soil profiles indicate their low mobility which restricts their unfavourable environmental impact.

Although the tailings impoundment is almost recultivated and the dust pollution is finished the contaminated soils of the surroundings contain arsenic and heavy metals and continue to transfer them to the food chain. The sheep milk has ele-

vated Zn and Cu contents and so it transfers them to the humans. The carry-over of Pb, Cd and As from grass to the milk is low. Metal concentrations in livestock's excrements are low and seem not to pose risk for secondary soil contamination if used as organic fertilizer.

The soil cover of the impoundment is not sufficient to avoid the penetration of grasses root to the mine tailings and this causes the contamination of the grasses on the surface of the recultivated impoundment. A favourable circumstance is the presence of carbonate minerals in the ore (in the host rocks and as gangue) as well as in the tailings and in soils which increases the pH and avoids acid mine drainage.

Acknowledgments

The authors gratefully acknowledge Ms. Kathrin Koschnik for her help in performing of RFA analyzes. This study was supported financially by the National Science Fund – grant High School-Earth Science–04/05 and by the Cooperation Program between Sofia University "St. K. Ohridski" and Humboldt University in Berlin, Germany.

References

Atanassov V. and Pavlov I., 1982. Notes on the mineralogy and paragenetic zonality of mineral deposits in Chiprovtsi ore district. Ann. Ecole Super. Mines et Geologie, 28, 2-geol., 159-175 (in Bulgarian).

Biehl M.L. and Buck W.J., 1987. Chemical contaminants: their metabolism and their residues. J. Food Protect. 50, 12, 1058–1073.

Blüthgen A.H., 2000. Contamination of milk from feed. Bull. Int. Dairy Feder. 356, 43–47.

Climatic reference book for Bulgaria. 1983. Vol. 3. Air temperatute, soil temperature, frost, Sofia, 440 p (in Bulgarian).

Dragov P. and Obretenov N., 1974. The silver-lead Chiprovtsi deposit. In: Twelve ore deposits of Bulgaria, IV JAGOD Symposium, Varna, 77-98 (in Russian).

EFSA, 2005. Opinion of the scientific panel on contaminants in the food chain on a request from the commission related to arsenic as undesirable substance in animal feed. The EFSA J. 180, 1–35.

Instruction Nr. 2, 2002. Instruction concerning the acceptable concentrations of pollutants in soil. Official Gazette, 39, 1-8.

Instruction Nr. 31, 2004. Instruction of the Health ministry for maximal accepted pollutant in foods, Official Gazette, 88 (in Bulgarian).

Koinov V., Kabakchiev I. and Boneva, K. 1998. Atlas of Soils in Bulgaria. Sofia, Zemizdat, 321 p (in Bulgarian).

Koleva E. and Peneva, R., 1990. Climatic reference book. Precipitations in Bulgaria. Sofia, Publishing house of BAS, 169 p (in Bulgarian).

Kotsev Ts., Mladenova V., Cholakova Z. and Blazhev B., 2009. Heavy metals and arsenic content in sheep's and goat'as milk from the Upper reach of the Ogosta river. Geography, 3, 10-19 (in Bulgarian).

Milev V., Stanev V. and Ivanov V., 1996. Statistical reference book about the proceeded ores in Bulgaria in the period 1878-1995, Sofia, Zemja 93 publ. house, 196 p (in Bulgarian).

Mladenova V., Kerestedjian T. and Dimitrova D., 2003. The Govezhda gold deposit, Western Balkan Mountains, Bulgaria. Geochem. Mineral. Petrol., 40, 109-121.

Mladenova V. and Zlatev, Z., 2004. Geochemical characteristics of Goliam Bukovets mine tailings impoundment, Chiprovtsi mining area, NW Bulgaria. Rev. Bulg. Geol. Soc, 65, 1-3, 141-150.

Nikolaev G. and Tonev, I., 1961. Geological setting of vicinity of Kopilovci village and the mineralization of the gold-quartz-sulfide veins, Ann. Ecole Super. Mines et Geologie, 7, 2-geol., 23-36 (in Bulgarian).

Prankel S.H., Nixon R.M., Phillips C.J.C., 2004. Meta-analysis of feeding trials investigating cadmium accumulation in the livers and kidneys of sheep. Environ. Res. 94, 2, 171–183.

Sirotkin A. N., Rasin I. M., Isamov N. N. and Sokolova, E. A., 2000. Assessment of heavy metals concentrations. Agrochem. J., 2000, 2, 18-19 (in Russian).

Stojanov S., 1999. Heavy metals in the environment and in some foodstuffs, toxic harm of man, clinical treatment and prophylaxis. Ecology and health, 2, Pensoft, 281 p (in Bulgarian).

Tarasova E., 1987. Zoning and mineral composition of the ore bodies in the Martinovo deposit. Ore-Forming Proc. and Miner. Dep., 27, 32-38 (in Bulgarian).

Velchev V., 1974. New data on the parageneses of ore from the skarn-iron Martinovo deposit, Mihaylovgrad district. Ann. Ecole Super. Mines et Geologie, 11, 1-geol., 38-47 (in Bulgarian).

Vesselinov I., Kolarova V., Hadjiev A., Hrischeva E. and Kerestedjian T., 1996. Mineralogical and geochemical characteristics of two tailings ponds of the Martinovo and Chiprovtsi ore-dressing plants. Geochem., Mineral. and Petrol., 31, 89-102 (in Bulgarian).

Scientific Annals, School of Geology, Aristotle University of Thessaloniki Proceedings of the XIX CBGA Congress, Thessaloniki, Greece	Special volume 100	113-120	Thessaloniki 2010

ENVIRONMENTAL ASSESSMENT OF POTENTIALLY TOXIC TRACE ELEMENTS IN SEDIMENTS OF FILIPPOS B PORT, NORTHERN AEGEAN SEA – A COMPARISON WITH OTHER NATIONAL AND INTERNATIONAL COASTAL REGIONS

Papastergios G.[1], Filippidis A.[1], Fernandez-Turiel J.-L.[2], Gimeno D.[3]

[1] *Department of Mineralogy-Petrology-Economic Geology, Aristotle University of Thessaloniki, 54124, Thessaloniki, Greece, gpapaste@geo.auth.gr, anestis@geo.auth.gr*
[2] *Institute of Earth Sciences "Jaume Almera", Consejo Superior de Investigaciones Científicas (CSIC), Lluís Solé i Sabarís, s/n – 08028, Barcelona, Spain, jlfernandez@ija.csic.es*
[3] *Department of Geochemistry, Petrology and Geological Exploration, University of Barcelona, Zona Universitària de Pedralbes, Martí i Franquès, s/n – 08028, Barcelona, Spain, domingo.gimeno@ub.edu*

Abstract: Nine sediment samples from Filippos B port, Kavala, northern Greece were collected, sieved under 200 μm and analyzed for their content in 14 potentially toxic trace elements (Ag, As, Ba, Cd, Co, Cr, Cu, Hg, Mn, Ni, Pb, U, V and Zn). The results indicate that the majority of the elements are found with concentrations similar to other national and international coastal regions. However, Cd seems to be highly enriched in the sediments of the present study. The samples with the highest concentrations of Cd, as well as for the rest of the elements, are found in front of the local, anthropogenic activities. According to their distribution, the elements of the present study can be divided into two groups; group A includes the elements Ag, As, Cd, Hg, Pb and U, group B the elements Ba, Co, Cr, Cu, Mn, Ni, V and Zn. The former are influenced mainly by the activities of a fertiliser plant, while the latter by all the local anthropogenic activities.

Keywords: sea sediment; trace elements; geochemistry; environment; Kavala; Greece.

1. Introduction

Natural and anthropogenic activities are the reasons why many potentially toxic elements, but especially trace elements, are found in aquatic environments. These contaminants may accumulate in bottom sediment and, thus trigger toxic effects on organisms living in the adjacent area (e.g., Michel and Zengel, 1998; Valette-Silver et al., 1999). In fact, the accumulation of potentially toxic and persistent substances in the coastal environment continuously increases due to anthropogenic activities as the estuaries and their nearby coasts are the focus of many economic activities (e.g., Ramessur, 2004; Grigoriadou et al., 2008a,b). Consequently, monitoring the geochemical status of sea sediments is an important and, at the same time, complex task. This was the objective of the present research, as well. En effort was made to assess the environmental status of the sediments of Filippos B port by comparing the concentrations of the elements determined with other coastal regions, national and international.

2. Study area

The study area is located in northern Greece and includes the coastal part of the industrial zone of the city of Kavala (Fig. 1). The climate of the area has general Mediterranean characteristics with mild winters and warm summers. Land uses in the area can be divided into four categories: agricultural, uncultivated, industrial and residential (Fig. 1). The main industrial activities are the Phosphoric Fertilizer Industry (PFI) and the Kavala Oil land facilities. The former industry produces phosphoric fertilizers, pesticides and other similar products and its main by-product is phosphogypsum, while in the latter oil desulphurization takes place. Some contaminants associated with the production of phosphoric fertilizers and similar products (i.e., pesticides), as well as phosphogypsum, are Ba, Cd, Cu, P, Pb, Th, U, and Y (Rutherford et al., 1996; Komnitsas et al., 1999; Chen et al., 2001; Kabata-Pendias and Pendias, 2001; Carbonell-Barrachina et al., 2002; Villa et al., 2009); contaminants associated with the oil industry are Co,

S, Th, and V (Kabata-Pendias and Pendias, 2001). Other activities include some small enterprises that exploit and market local marbles and the Xifias Fishery enterprise which terminated its activities during the undertaking of the present research. Furthermore, near the Kavala Oil land facilities and the Xifias Fishery there are several uncontrolled landfill sites.

The main rock types in the area are (Fig. 2): (a) gneisses, schists and amphibolites, (b) marbles and limestones, (c) granitic and granodioritic rocks and (d) sedimentary deposits (Christofides et al., 1998; 2001; Kilias et al., 1999). Additionally, in the adjacent area, several Pyrite-Blende-Galena (PBG), Mn, and Fe mineralizations exist (Filippidis et al., 1996; Vavelidis et al., 1996;1997). The mineral characteristics of the surface sea sediments in the study area are attributed to the delta of Nestos River and to local sources. The sand fraction mainly consists of quartz, feldspars, micas, amphiboles, biogenic carbonate and pyroxenes, while the respective composition of the clay fraction is illite, kaolinite, smectite and chlorite. The predominant source of clay minerals is Nestos River (Conispoliatis and Lykousis, 1986).

3. Materials and methods

Nine sampling sites in Filippos B port and adjacent areas to the east and west were selected, at variable distances from the coastline (Fig. 1). Surface sediment samples were collected, using a sediment grab sampler, in front of the major industrial activities of the area (S100, S102, S104, S105, S106, S107, S108), but also away from them (S101, S103) (Fig. 1). Samples S100, S106, S107 and S108 were collected in front of the PFI facilities and the phosphogypsum dumps, while samples S102, S104 and S105 were taken in front of the Kavala Oil land facilities and the Xifias Fishery. Sample S103, although it was collected away from the industrial activities of the study area, is located at a point were a water canal connects the aquacul-

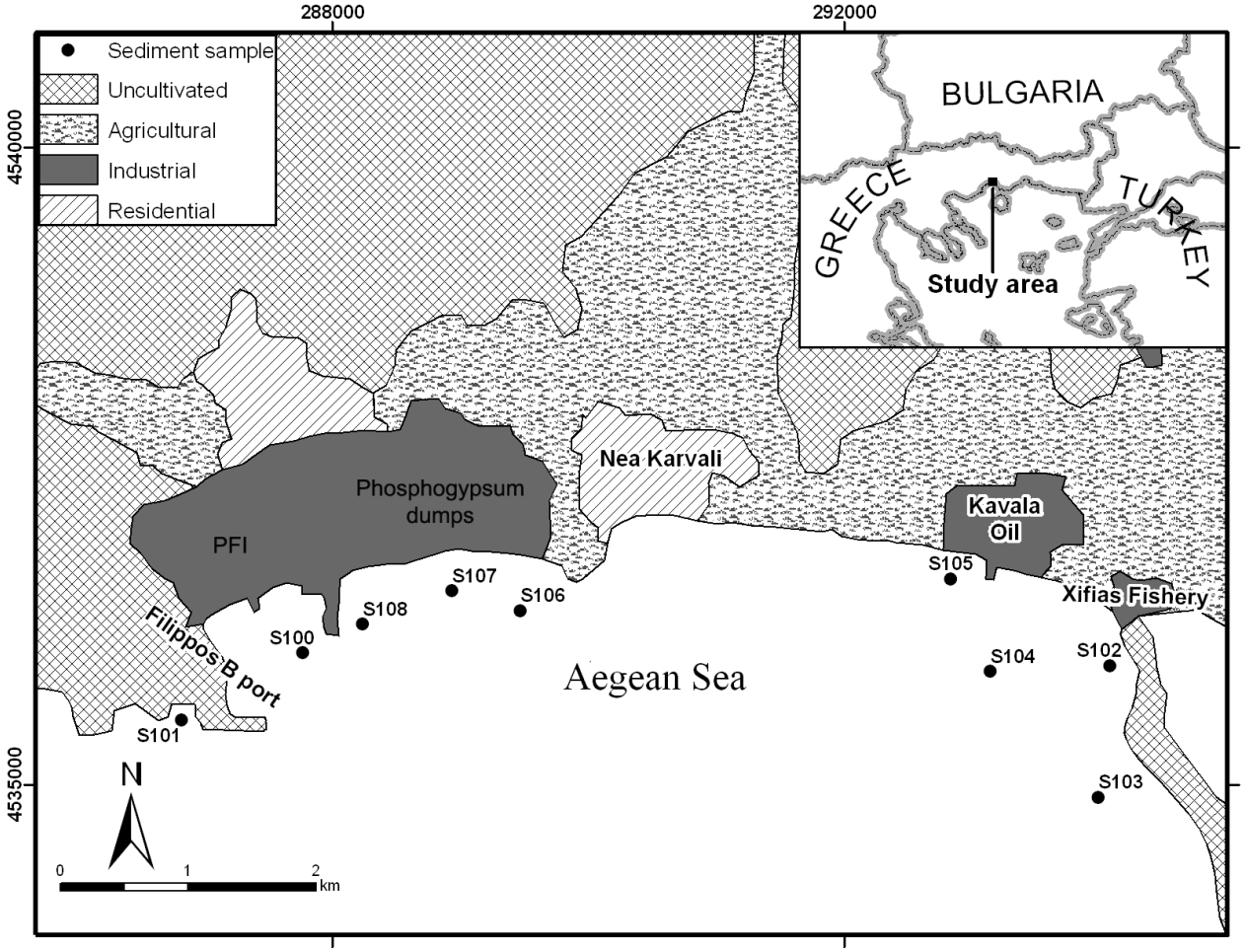

Fig. 1. Map showing the Filippos B port, the sampling locations, the industrial activities and the land use/cover types of the study area (modified after Papastergios 2008).

tures of the Xifias Fishery with the Aegean Sea. Although the present research would benefit from the collection of more samples, unfortunately this was not possible due to various limitations (i.e., accessibility of the area and others). Still, valuable information regarding the status of the sediments in Filippos B port compared to several national and international coastal regions is presented.

All samples were dried in an oven at 40°C, sieved under the 200 μm fraction and the elements determined were extracted using analytical grade, concentrated (65%) HNO_3 (Fernandez-Turiel et al., 2001; Papastergios et al., 2009a; 2010a). The extraction is conducted under extreme analytical conditions, in this way, while at the same time, the compatibility of the leachate with the input solution in Inductively Coupled Plasma – Mass Spectrometry is maintained (direct determination after dilution). Furthermore, the polyatomic interferences produced on analytes by other extraction agents commonly used [e.g., the Cl of aqua regia (3:1, HCl:HNO_3) interferes with elements such as As and V], are avoided.

The concentrations of 14 trace elements (Ag, As, Ba, Cd, Co, Cr, Cu, Hg, Mn, Ni, Pb, U, V and Zn) were determined in all samples by ICP–MS. A Perkin Elmer Sciex Elan 6000 with a Perkin Elmer AS-91 automatic sampler was used. The analyses were performed at the Scientific Technical Services of the University of Barcelona (SCT–UB), Spain. Details on ICP–MS analysis can be found in Fernandez-Turiel et al. (2000). The quality of the results was checked by applying the same procedure to a reference material (CANMET NRCC-MESS-2) as well as to a blank and four replicates of a randomly selected sample. The methodology used, achieved analyses that were very satisfactory, for the work objectives. Many elements exhibited analytical reproducibility values (percent relative deviation-RSD, n=3) lower than 3%. In regard to the extraction procedure's reproducibility, the majority of the elements exhibited RSD values lower than 5% (Papastergios, 2008).

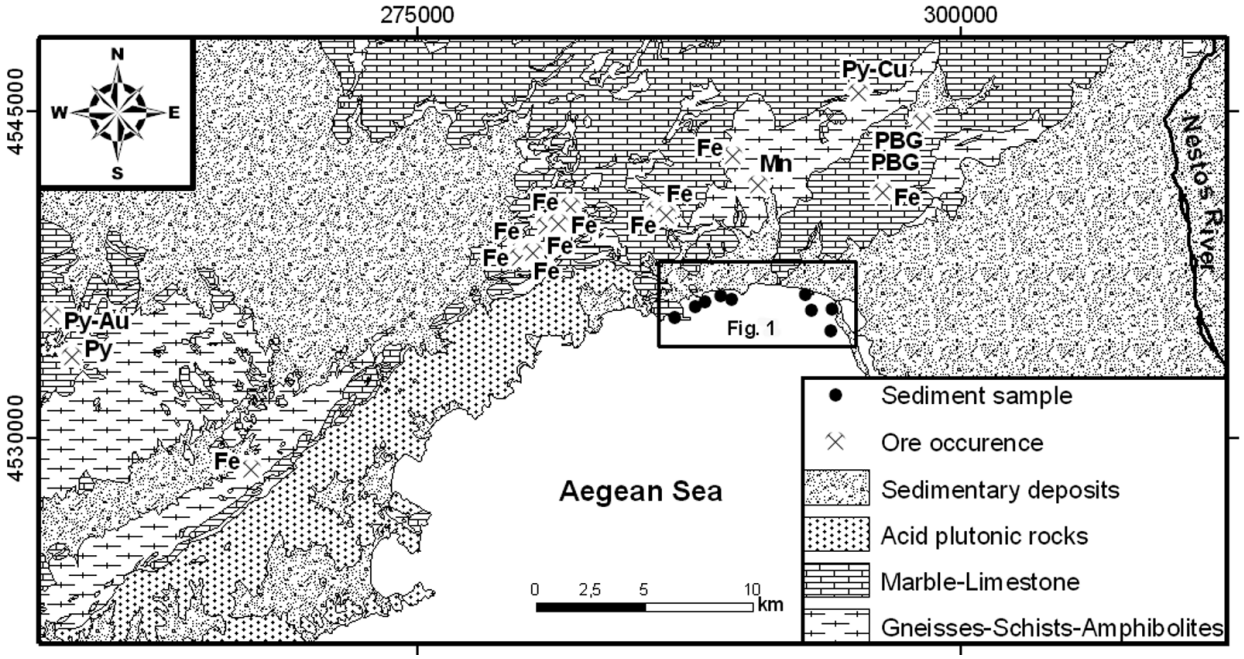

Fig. 2. Simplified geological map of the study area (modified after Papastergios 2008).

4. Results and discussion

Summary statistics regarding the elements determined in the present work are given in Table 1. For the calculation of the descriptive statistics, values that were below the detection limit, for each element, were substituted by half its detection limit. Elements, with average concentrations above 100 mg kg^{-1} are Mn and Zn. Average concentrations between 1 and 100 mg kg^{-1} are noted for Pb, Ba, Cu, Cr, Ni, V, As, Cd, Co and U, while Ag and Hg have average concentrations below 1 mg kg^{-1}.

The concentrations of the elements determined in the present study were compared with the concentrations cited in the literature regarding national and international marine areas (Tab. 2). The average Ag concentration is 0.3 mg kg^{-1}, which is lower than the values cited for Thermaikos gulf and Sydney, and approximately the same with San

Francisco. The two largest values (S100: 0.7 mg kg^{-1} and S108: 0.9 mg kg^{-1}) are noted in front of the PFI facilities. Arsenic's mean concentration is above 15.0 mg kg^{-1}. This value approximates the values given for ports such as Barcelona, Sydney and Thermaikos. The distribution of this element is discussed in detail elsewhere (Papastergios et al. 2010a). The mean concentration of Cd is 7.1 mg kg^{-1}, a value much higher than those reported for both, national and international ports. However, Zabetoglou et al. (2002) have reported similar values (6.2 and 6.3 mg kg^{-1}) of Cd for a specific location (in front of the White Tower) of Thermaikos Bay. The authors attributed the elevated concentrations to anthropogenic sources. The samples with the highest concentrations are found in front of the PFI facilities (S100: 7.8 mg kg^{-1}, S107: 12.3 mg kg^{-1} and S108: 39.2 mg kg^{-1}). Mercury has an average concentration of 0.1 mg kg^{-1}. This value is the same with the one reported for Lesvos' coastal area, lower than the ones reported for San Francisco, Turkey and Italy, and considerably lower than the average values cited for Sydney and Barcelona. However, samples S100 (0.3 mg kg^{-1}), S107 (0.2 mg kg^{-1}) and S108 (0.4 mg kg^{-1}) have similar concentrations with the former, international coastal areas. The average concentration of Pb is above 88.0 mg kg^{-1}. This value is similar or larger to some national or international coastal regions but with Sydney and Barcelona, however, having much larger average concentrations. The largest Pb concentration is noted in front of the phosphogypsum dumps (S107: 274.5 mg kg^{-1}), suggesting that Pb and P are interacting and, possibly forming pyromorphite [$Pb_5(PO_4)_3Cl$], which acts as an important buffer mechanism controlling the migration and fixation of Pb in water, soils, sediments and wastes (Ryan et al., 2001; Manecki et al., 2006). Finally, U has an average concentration of 1.2 mg kg^{-1}. The two largest values (S100: 4.9 mg kg^{-1} and S108: 2.5 mg kg^{-1}) are found in front of the PFI facilities. Unfortunately no values were available for comparison with the other selected coastal sites. All the former elements have been associated with the production of (phosphate) fertilizers, pesticides and other similar products (i.e., Arocena et al., 1995; Martin et al., 1999; Kabata-Pendias and Pendias, 2001; Bolivar et al., 2002; Villa et al. 2009) and because they have their largest concentrations in front of the PFI facilities (samples S100, S107 and S108), it is rather obvious that its activities must play an important role in the distribution that these elements have in Filippos B port.

On the contrary, the rest of the elements have such distributions that they must be influenced by all the industrial activities of the study area, as they have elevated concentrations in front of the PFI and the Kavala Oil facilities and the channel that connects the Xifias Fishery aquacultures with the open sea, as well. The mean concentration of Ba is 45.6 mg kg^{-1}, which is considerably larger than the value reported for Thermaikos gulf. The samples with the largest concentrations are S108 (121.5 mg kg^{-1}), S104 (63.6 mg kg^{-1}) and S103 (46.7 mg kg^{-1}) located in front of the PFI, the Kavala Oil and the Xifial Fishery, respectively. Cobalt's mean concentration approximates 5.0 mg kg^{-1}. This value is much lower than those given for national and international coastal regions. Nonetheless, the samples with the highest concentrations are found in front of the Kavala Oil (S104: 8.6 mg kg^{-1}), the PFI (S108: 8.2 mg kg^{-1}) and the Xifias Fishery (S103: 6.8 mg kg^{-1}). The average concentration of Cr is almost 40 mg kg^{-1}. This value is similar to some

Table 1. Summary statistics for the elemental concentrations of the present study (n=9).

Element (mg kg^{-1})	median	mean	minimum	maximum	std deviation
Ag	0.1	0.3	0.1	0.9	0.3
As	7.4	15.3	2.2	44.8	15.2
Ba	37.9	45.6	11.4	121.5	32.2
Cd	0.4	7.1	0.1	39.2	12.1
Co	4.5	4.8	1.1	8.6	2.7
Cr	33.6	38.0	5.2	76.3	23.9
Cu	18.9	40.9	2.3	119.1	42.1
Hg	0.1	0.1	0.03	0.4	0.1
Mn	130.1	143.9	45.6	264.2	66.1
Ni	22.3	18.7	3.5	40.9	11.6
Pb	49.0	88.3	8.5	274.5	79.0
U	0.5	1.2	0.3	4.9	1.5
V	18.8	17.5	4.0	36.5	10.4
Zn	59.8	133.9	11.8	538.2	157.2

national and international areas. Still, there are ports reported with higher Cr concentrations. Once again, sample S104 (76.3 mg kg^{-1}) in front of the Kavala Oil, samples S100 (61.3 mg kg^{-1}) and S108 (59.9 mg kg^{-1}), in front of the PFI and sample S103 (33.6 mg kg^{-1}) near Xifias Fishery, are the samples with the highest concentrations. Copper has a mean value of nearly 41.0 mg kg^{-1} and has, relatively, similar values with other national ports. Sydney and Barcelona, on the other hand have been reported with much higher concentrations of Cu. Sample S108 (119.1 mg kg^{-1}) has the highest concentration and is followed by samples S100 (103.2 mg kg^{-1}) and S104 (67.9 mg kg^{-1}). The mean concentration of Mn is above 140.0 mg kg^{-1}, but this concentration is lower for almost all other coastal regions used for comparison in the present study, Sydney being the only exception. Samples S104 (264.2 mg kg^{-1}), S103 (229.2 mg kg^{-1}) and S100 (172.8 mg kg^{-1}) have the largest values.

Nickel has an average concentration that is below 20.0 mg kg^{-1}. This value is similar to San Francisco, Sydney and Barcelona but much smaller than those given for Italy or Thermaikos. Again, the highest concentrations are found in front of the local industrial activities (S104, S100 and S103). The mean concentration of V is almost 18.0 mg kg^{-1}. The distribution of this element is very similar to Ni. Finally, Zn has an average concentration above 130 mg kg^{-1}. This concentration is similar to most national coastal areas but notably smaller than the average concentrations of Zn in Barcelona and Sydney. However, the samples with the highest concentrations, especially near the PFI (S108: 538.2 mg kg^{-1}), are found in front of the anthropogenic activities. All the former elements have been associated with the type of activities occurring in the area (Rutherford et al., 1996; Kabata-Pendias and Pendias 2001). Furthermore, the distribution that the elements of the present study have in the sea sediments of Filippos B port is very similar to their distribution in the sea water of the study area (Georgakopoulos et al., 2002).

Research conducted recently in the area of Kavala

Table 2. Average concentrations of the Filippos B port and several national and international coastal areas.

Element (mg kg^{-1})	Filippos B port	Thermaikos gulf (1)	Thermaikos gulf (2)	Evros prodelta (3)	Lesvos coastal area (4)
Ag	0.3	3.1			
As	15.3	19.0			
Ba	45.6	0.4			
Cd	7.1	1.8		0.4	0.1
Co	4.8	33.0			
Cr	38.0	294.0	47.0	76.0	137.8
Cu	40.9	72.0	80.0	39.0	18.3
Hg	0.1				0.1
Mn	143.9	770.0		561.3	294.5
Ni	18.7	98.0		45.3	
Pb	88.3	87.0	77.0	42.7	30.9
V	17.5	160.0			
Zn	133.9	239.0	184.0	104.3	63.8
Element (mg kg^{-1})	San Francisco (5)	Sydney (6)	Barcelona (7)	Turkey (8)	Italy (9)
Ag	0.1	1.8			
As		21.0	21.5		
Ba					
Cd	0.2	2.8	1.5	0.2	0.4
Co					55.3
Cr	21.1	81.0	90.6	216.0	1194.0
Cu		200.0	234.5		
Hg	0.2	1.4	1.8	0.3	0.6
Mn	480.6	120.0			
Ni	39.3	20.0	25.6		1325.0
Pb	21.8	360.0	206.0	58.5	44.5
V					
Zn	65.2	1000.0	515.6		

(1) Violintzis et al 2009, (2) Christoforidis et al. 2009, (3) Kanellopoulos et al. 2006, (4) Aloupi et al. 2007, (5) Lu et al. 2005, (6) McReady et al. 2006, (7) Casado-Martinez et al. 2006, (8) Kucuksezgin et al. 2006, (9) Lafabrie et al. 2007.

has revealed the influence of the local anthropogenic activities, for organic contaminants, on soils, sediments and sea water (Grigoriadou et al., 2008a, b), for heavy metals in street dust and roadside soil along the major national road in Kavala's region (Christoforidis and Stamatis, 2009) and As in sediments of the Filippos B port (Papastergios et al., 2010a). Although there are several ore occurrences (i.e., PBG, Mn, Fe) in the wider study area, which could contribute, as metal sources, to the observed high concentrations, the fact that Nestos River (and, to a lesser extent, local sources) is the predominant source of minerals seems to weaken this alternative, especially since the elemental content of Nestos River sediments and of the surrounding rocks has been found to be within normal ranges (Papastergios et al., 2009a,b; 2010b).

5. Conclusions

All the elements of the present study have their lowest concentrations in either sample S101 or sample S102 and their highest concentrations in either sample S108 or S104. The latter samples are situated in front of the PFI and the Kavala Oil facilities, respectively, indicating that the anthropogenic activities of the study area have modified the geogenic distribution of these elements. However, the contribution of the anthropogenic activities seems to be restricted only in small areas, near their facilities. The concentrations of the elements determined in the present study are similar to many national and international coastal areas but, at the same time, differ as well, reflecting the differences in the local geology and industrial activities. Additionally, some of the differences noted between the present study and those used for comparison purposes could be due to differences in the methodologies applied. Nonetheless, Cd concentrations are significantly larger than compared to any other coastal region used for comparison in the present work, especially for the samples that are found in front of the PFI facilities. A further monitoring of the sediments in the area with additional parameters such as mineralogy of the sediments, pH, redox potential, bioavailability and toxicity of the contaminants etc. is suggested in order to control the evolution of the elemental concentrations in the sediments of this area of Aegean Sea.

Acknowledgments

The authors would like to acknowledge the technical assistance provided by the personnel of the Faculty of Geology of the University of Barcelona, the SCT–UB and ICTJA–CSIC, Barcelona (Spain). Georgios Papastergios during this research was under a scholarship from the Greek State Scholarships Foundation (IKY). This work was partially carried out in the framework of PEGEFA 2009SGR-00972 Research Consolidated Group, funded by AGAUR-DURSI, Generalitat de Catalunya. The PFI provided a small vessel in order to assist to the collection of the samples. The paper benefited from constructive reviews by Drs Mitropoulos P., Samara C. and Skarpelis N.

References

Aloupi M., Angelidis M.O., Gabriel A., Karantanelli M., Koulousaris M., Nikolaou A., Petsas A., Tsirtsis G., Vagi M. and Vlatsiotou F., 2007. Marine monitoring along the eastern coastal area of the island of Lesvos, Greece during 2004 in the framework of MEDPOL III, Global NEST Journal, 9, 83-97.

Arocena J.M., Rutherford P.M. and Dudas M.J., 1995. Heterogeneous distribution of trace elements and fluorine in phosphogypsum by-product. The Science of the Total Environment, 162, 149-160.

Bolıvar J.P., Garcıa-Tenorio R., Masa J.L. and Vaca F., 2002. Radioactive impact in sediments from an estuarine system affected by industrial wastes releases. Environment International, 27, 639-645.

Carbonell-Barrachina A., DeLaune R.D., and Jugsujinda A., 2002. Phosphogypsum chemistry under highly anoxic conditions. Waste Management, 22, 657-665.

Casado-Martinez M.C., Buceta J.L., Belzunce M.J. and DelValls T.A., 2006. Using sediment quality guidelines for dredged material management in commercial ports from Spain. Environment International, 32, 388-396.

Chen M., Ma Q.L., Hoogeweg G. and Harris W.G., 2001. Arsenic background concentrations in Florida, U.S.A. surface soils: determination and interpretation. Environmental Forensics, 2, 117-126.

Christofides G., Soldatos T., Eleftheriadis G. and Koroneos A., 1998. Chemical and isotopic evidence for source contamination and crustal assimilation in the Hellenic Rhodope plutonic rocks. Acta Vulcanologica, 10, 305-318.

Christofides G., Koroneos A., Soldatos T., Eleftheriadis G. and Kilias A., 2001. Eocene magmatism (Sithonia and Elatia plutons) in the Internal Hellenides and implications for Eocene-Miocene geological evolution of the Rhodope Massif (Northern Greece). Acta Vulcanologica, 13, 73-89.

Christoforidis A. and Stamatis N., 2009. Heavy metal contamination in street dust and roadside soil along the major national road in Kavala's region, Greece. Geoderma, 151, 257-263.

Christophoridis C., Dedepsidis D. and Fytianos K. 2009. Occurrence and distribution of selected heavy metals in the surface sediments of Thermaikos Gulf, N. Greece. Assessment using pollution indicators.

Journal of Hazardous Materials, 168, 1082-1091.
Conispoliatis N. and Lykousis V., 1986. Mineralogy of the surficial sediments of Kavala Bay, Northern Aegean Sea. Estuarine Coastal and Shelf Science, 23, 739-749.
Fernandez-Turiel J.L., Llorens J.F., López-Vera F., Gómez-Artola C., Morell I. and Gimeno D., 2000. Strategy for water analysis using ICP-MS. Fresenius Journal of Analytical Chemistry, 368, 601-606.
Fernandez-Turiel J.L., Aceñolaza P., Medina M.E., Llorens J.F. and Sardi F., 2001. Assessment of a smelter impact area using surface soils and plants. Environmental Geochemistry and Health, 23, 65-78.
Filippidis A., Georgakopoulos A., Kassoli-Fournaraki A., Misaelides P., Yiakkoupis P. and Broussoulis J., 1996. Trace element contents in composite samples of three lignite seams from the central part of the Drama lignite deposit, Macedonia, Greece. International Journal of Coal Geology, 29, 219-234.
Georgakopoulos A., Fernandez-Turiel J.L. and Gimeno D., 2002. Influence of oil facilities in seawater quality: trace element distribution near Kavala, north Aegean Sea (Greece). Proceedings of the 6th Geographical Congress of the Greek Geological Society, 343-348.
Grigoriadou A., Schwarzbauer J. and Georgakopoulos A., 2008a. Molecular indicators for pollution source identification in marine and terrestrial water of the industrial area of Kavala city, north Greece. Environmental Pollution, 151, 231-242.
Grigoriadou A., Schwarzbauer J. and Georgakopoulos A., 2008b. Organic geochemical parameters for estimation of petrogenic inputs in the coastal area of Kavala City, Greece. Journal of Soils and Sediments, 8, 253-262.
Kabata-Pendias A. and Pendias, H., 2001. Trace elements in soils and Plants, 3rd ed., CRC Press, New York, 413p.
Kanellopoulos T.D., Angelidis M.O., Karageorgis A.P., Kaberi H., Kapsimalis V. and Anagnostou C., 2006. Geochemical composition of the uppermost prodelta sediments of the Evros River, northeastern Aegean Sea. Journal of Marine Systems, 63, 63-78.
Kilias A.A., Falalakis G. and Mountrakis D.M., 1999. Cretaceous – Tertiary structures and kinematics of the Serbomacedonian metamorphic rocks and their relation to the exhumation of the Hellenic hinterland (Macedonia, Greece). International Journal of Earth Sciences, 88, 513-531.
Komnitsas K., Lazar I, and Petrisor I.,G. 1999. Application of a vegetative cover on phosphogypsum stacks. Minerals Engineering, 12, 175-185.
Kucuksezgin F., Kontas A., Altay O., Uluturhan E. and Darilmaz E., 2006. Assessment of marine pollution in Izmir Bay: Nutrient, heavy metal and total hydrocarbon concentrations. Environment International, 32, 41-51.
Lafabrie C., Pergent G., Kantin R., Pergent-Martini C. and Gonzalez J.L., 2007. Trace metals assessment in water, sediment, mussel and seagrass species – Validation of the use of Posidonia oceanica as a metal biomonitor. Chemosphere, 68, 2033-2039.
Lu X.Q., Werner I. and Young T.M., 2005. Geochemistry and bioavailability of metals in sediments from northern San Francisco Bay. Environment International, 31, 593-602.
Manecki M., Bogucka A., Bajda T. and Borkiewicz O., 2006. Decrease of Pb bioavailability in soils by addition of phosphate ions. Environmental Chemistry Letters, 3, 178-181.
Martin J.E., Garcia-Tenorio R., Respaldiza M.A., Ontalba M.A., Bolivar J.P. and da Silva M.F., 1999. TTPIXE analysis of phosphate rocks and phosphogypsum. Applied Radiation and Isotopes, 50, 445-449.
McReady S., Birch F.G. and Long R.E., 2006. Metallic and organic contaminants in sediments of Sydney Harbour, Australia and vicinity – A chemical dataset for evaluating sediment quality guidelines. Environment International, 32, 455-465.
Michel J. and Zengel S., 1998. Monitoring of oysters and sediments in Acajutla, El Salvador. Marine Polluttion Bulletin, 36, 256-266.
Papastergios G., 2008. Environmental geochemical study of soils and sediments in coastal areas, east of Kavala (Macedonia, Greece) and production of geochemical maps via the use of GIS. Ph.D. Thesis, (in Greek, with English abstract), Aristotle University of Thessaloniki, Greece, 224p.
Papastergios G., Fernandez–Turiel J.L., Georgakopoulos A. and Gimeno D. 2009a. Natural and anthropogenic effects on the sediment geochemistry of Nestos River, northern Greece. Environmental Geology, 58, 1361-1370.
Papastergios G., Georgakopoulos A., Fernandez–Turiel J.L. and Gimeno D., 2009b. A Correlation Study of Major and Trace Elements in Sediments of River Nestos, Northern Greece and Comparison with Other Fluvial Systems, Proceedings of the 9th International Multidisciplinary Scientific GeoConference of Modern Management of Mine Producing, Geology and Environmental Protection (SGEM), Albena Complex, Bulgaria, vol. 2, 431-438.
Papastergios G., Filippidis A., Fernández–Turiel J.L. and Gimeno D., 2010a. Arsenic distribution in Sediments of Filippos B Port, Kavala, Northern Greece. Fressenius Environmental Bulletin, 19, 81-87.
Papastergios G., Filippidis A., Fernandez–Turiel J.L., Gimeno D. and Sikalidis C., 2010b. Natural and Anthropogenic Effects on the Soil Geochemistry of Kavala Area, northern Greece, Proceedings of the 12th International Congress of the Geological Society of Greece, May 19th-22nd 2010, Patra, Greece (in press).
Ramessur R.T., 2004. Statistical comparison and correlation of zinc and lead in estuarine sediments along the western coast of Mauritius. Environment Inter-

national, 30, 1039-1044.
Rutherford P.M., Dudas M.J. and Arocena J.M. 1996. Heterogeneous distribution of radionuclides, barium and strontium in phosphogypsum by-product. The Science of the Total Environment, 180, 201-209.
Ryan J.A., Zhang P., Hesterberg D., Chou J. and Sayers D.E., 2001. Formation of chloropyromorphite in a lead-contaminated soil amended with hydroxyapatite. Environmental Science and Technology, 35, 3798-3803.
Valette-Silver N.J., Riedel G.F., Crecelius E.A., Windom H., Smith R.G. and Dolvin S.S., 1999. Elevated arsenic concentrations in bivalves from the southeast coasts of the USA. Marine Environmental Reseasch, 48, 311-333.
Vavelidis M., Christofides G. and Melfos V., 1996. The Au-Ag bearing mineralization and placer gold of Palea Kavala (Macedonia, N. Greece). In: Terranes of Serbia, The formation of the geologic framework of Serbia and the adjacent regions, Knežević V. and Krstić B., (eds), Belgrade 1996, 311-316p.
Vavelidis M., Melfos V. and Eleftheriadis G., 1997. Mineralogy and microthermometric investigations in the Au-bearing sulphide mineralization of Palea Kavala (Macedonia, Greece). In: Mineral deposits: Research and exploration, where do they meet? Papunen H. (ed), Balkema, Rotterdam, 343-346.
Villa M., Mosqueda F., Hurtado S., Mantero J., Manjón G., Periañez R., Vaca F. and García-Tenorio R., 2009. Contamination and restoration of an estuary affected by phosphogypsum releases. Science of the Total Environment, (in press), doi:10.1016/ j.scitotenv.2009.09.028.
Violintzis C., Arditsoglou A. and Voutsa D., 2009. Elemental composition of suspended particulate matter and sediments in the coastal environment of Thermaikos Bay, Greece: Delineating the impact of inland waters and wastewaters. Journal of Hazardous Materials, 166, 1250-1260.
Zabetoglou K., Voutsa D., Samara C., 2002. Toxicity and heavy metal contamination of surficial sediments from the Bay of Thessaloniki (northwestern Aegean Sea) Greece. Chemospher,e 49, 17-26.

Scientific Annals, School of Geology, Aristotle University of Thessaloniki Proceedings of the XIX CBGA Congress, Thessaloniki, Greece	Special volume 100	121-126	Thessaloniki 2010

THE IMPACT OF A URANIUM MINING SITE ON THE STREAM SEDIMENTS (CRUCEA MINE, ROMANIA)

Petrescu L. [1], Bilal E. [2], Iatan L.E. [1]

[1] *University of Bucharest, Faculty of Geology et Geophysics, Department of Mineralogy, 1 N.Balcescu Ave., 010041 Bucharest, Romania; lucpet@geo.edu.ro*
[2] *Ecole Nationale Supérieure des Mines, Département GENERIC, 158 cours Fauriel, 42023 Saint Etienne, France;bilal@emse.fr*

Abstract: XRF methods were used to evaluate the impact of uranium mine dumps on the stream sediments from Crucea region (Romania). In order to estimate the natural and anthropogenic inputs of radioactive and heavy metals in the sediments, normalization to Al was applied. The pollution degree of the bottom sediments show that U, Th and Pb reach medium and punctual high values, while the rest of the elements appears in concentrations close to the background or lower. The measurements carried out in the surroundings of a local uranium mine show that the impact of Crucea mine on water quality downstream of mining area is insignificant.

Keywords: impact of mine wastes, stream sediments, uranium, thorium

1. Introduction

Uranium and thorium are omnipresent in our human environment. Various anthropogenic activities involving the processing or use of uranium rich-materials in may modify the natural abundance of uranium in stream sediments. These activities include various mining operations and the industrial processing for the manufacturing of nuclear fuel and of other products.

Between 1962 and 2004, the National Company of Uranium (former Romanian Autonomous Administration for Rare Metals), mined over 1,200,000 tones of pitchblende ore in the East Carpathians. Traditional mining methods rely on the relocation of large volumes of mineralized and waste rock. These intensive mining operations have created over 30 solid radioactive mining wastes in Crucea-Botusana area (Bistrita Mountains).

In this paper we present data from four main tributaries of Bistrita River (i.e. Crucea, Troaca Gavanului, Gavan and Cracul Rau creeks) and from two sampling points locating in the upper course of this main stream (one point located downstream and the other located upstream of the confluence with Crucea creek). The aim of this paper is to investigate the impact of mining activities on the stream sediments in the area.

2. The study area

2.1. Geography

The study concerns the uranium mineralization located within Crucea ore deposit, in the East Carpathians, Romania. The uranium ore deposit found in the eastern part of the Bistrita Mountains (40 km southeast of the town of Vatra Dornei) in the headwaters of Crucea, Lesu and Livezi valleys. At present, this is the largest uranium mine in the country. In the past, the mining area covered 18 km^2, but was gradually overtaken by logging activities. The area has a steep mountainous relief cut by narrow valleys. The surface streams are tributaries of Bistrita River.

2.2. Geological background

The host rocks belong to the Crystalline-Mesozoic zone of the northern part of the East Carpathians. The uranium mineralization is confined to a body of brecciated retrometamorphic micaschists, containing carbonates and clay minerals. The richest uranium mineralization is associated with four NW-SE faults with E or W strike. Most mineralized areas occur along fractures, thus denoting a significant structural control over the emplacement of the ore-bodies. Uranium ore bodies form dark-grey lenses or veinlets with thicknesses ranging from decimetres to meters. Primary mineralization consists of pitchblende U_3O_8 included in bitumen.

The intimate association between pitchblende and bitumen is characteristic to this uranium ore deposit. The sulphide content is lower than 10% and consists of pyrite, marcasite, chalcopyrite, and minor galena, sphalerite, arsenopyrite and tetrahedrite in a carbonate gangue. The mineralization is considered to be of hydrothermal origin (Petrescu, 2004).

The geochemical background of uranium in the surrounding area is lower than 3-mg·g^{-1}, whereas in the mining area, it reaches 5.39-mg·g^{-1} in the waste rocks (rocks with sub-economic mineralization) and 7.26-mg·g^{-1} in soils (Petrescu and Bilal, 2007).

The exploration and mining works include thirty-two adits, situated between 780 and 1040 m above sea level. Radioactive waste resulted from mining are disposed next to the mining facilities (Petrescu and Bilal, 2007). The waste rock was disposed in piles of variable sizes that are spread over an area of 364,000 m^2. The average geochemical content of the waste rocks is similar to that of the ore. The average particle size of the waste material is large (>5 cm). Older dumps (18) have been already naturally reclaimed by forest vegetation, which played an important role in stabilizing the waste dump cover and in slowing down the uranium migration processes.

3. Material and methods

The sediment samples were collected at seventeen sampling points (e.g. 1, 3, 6, 11, 16, 19, 23, 25, 27, 29, 32, 33, 35, 41, 43 and 45) (Fig.1) from the bottom of the stream waters. To ensure the representativity of samples, bulk sediments were obtained by mixture of several cores collected. The pool of sediments were collected by manual coring (0–5-cm) from the moist shore and stored in glass jars. They were dried in an oven at 50°C for 48 hr, ground using an agate grinder to pass a 100-µm sieve and analyzed for the following:

3.1. Total elemental concentration

The total metal concentrations of bottom sediments were determined using a SRS3400 Bruker AXS wavelength dispersive X-Ray fluorescence spectrometer (WD-XRF). Thus, 1.3-gram of calcinated powder was added to 1.3-g of oxides (lithium nitrate) and 6.5-g of flux (lithium tetraborate 20%, lithium metaborate 80 %) and then mixed in a crucible that is placed in an automated fusion-fluxing device. The fusion is performed at 1100°C. The cooling is forced to avoid crystallization, and then fused beads with a vitreous, homogeneous structure and flat surface were obtained. The detection limits, in mg·g^{-1}, were: 4 for U, 5 for Th, 5 for Pb and 10 for V.

3.2. Statistical data analysis

The reliability of the chemical analyses was calculated from the four duplicate samples with the analysis of variance. The F-ratio, which is a measure of the ratio of total data variance to error variance (sample inhomogeneity, analytical error) and which has to be > 4 to be significantly high at the 99% level of confidence, was >1000 for Ca, Cr, Cu, Mn, Pb, V, Na and Zn, >100 for U, Th, Sr, Al, Co, Fe, K, P and Mg and 54 and 32 for Si and Ni respectively. Hence, any pattern or absence of pattern of any of these elements in the data set is not due to analytical or sampling error.

Single correlation analysis was performed to assess relationship among heavy elements concentration. Linear correlation coefficients (*r*) were calculated between the different samples parameters. For each correlation, statistical significance (*p-value*) was determined. Traditionally, results that yield *p-value* < 0.05 are considered borderline statistically significant, i.e. the probability of concluding that two variable are different when they are actually the same is ≤5%.

The STATISTICA 7.1 for Windows (StatSoft®) program was used for the statistical analyses mentioned above.

4. Results and discussion

Table 1 shows levels of heavy metals, aluminum oxides and total organic matter (lost on ignition = LOI) found in bottom sediments sampled at the sixteen stations.

In all the areas, similar variations in the concentrations of uranium and thorium in sediment samples were observed. The bottom sediment samples collected from mining area show a wide range of total uranium content from 17.20 to 5023.96-mg·g^{-1} with a mean value of 246.81-mg·g^{-1} (dry wt.) (Fig.2). Total thorium concentration in sediments collected from Crucea site ranged from 18.70 to 6643.92-mg·g^{-1} with an average of 391.17-mg·g^{-1} (dry wt.) (Fig.2). This indicates that the adsorption of the radioactive elements by the sediments is high and variable, influenced by the ore dump – sample relationship. There is a decrease in the con-

centrations of U and Th in the stream sediments downstream from the Crucea uranium ore (Fig.2).

The fate and transport of uranium is governed by its oxidation state, which is either hexavalent (U(VI)) or tetravalent (U(IV)). When mine wastes containing low-grade uranium mineralization are exposed to surface waters containing carbonate ions, the pitchblende is altered, uranium (IV) oxidizing to uranyl carbonates, without producing any megascopically observable changes. This can be illustrated by the following equation:

$$U_3O_8 + 2H_2O + 9\,CO_3^{2-} \rightarrow 3[UO_2(CO_3)_3]^{4-} + 4OH + 2e^-$$

A previous study performed in this area (Petrescu and Bilal, 2006) showed that in the pH range of waters from Crucea area, more than 85% of the uranium was present as the carbonate complexes $UO_2(CO_3)_2^{2-}$, $UO_2CO_3(OH)_3^-$, UO_2CO_3 and $UO_2(CO_3)_3^{4-}$ and 17% as the hydroxide complexes $UO_2(OH)_2$. The anionic carbonate complexes are extremely important because they increase uranium mobility by limiting the extent of uranium adsorption in oxidized waters and by increasing the solubility of uranium minerals (Langmuir, 1997).

Strong correlation of uranium with thorium in the sediments (r = 1; n = 17; p < 0.0001) suggests that unspecific co-precipitation dominates over selective adsorption according to valence and ion sizing.

The lack of correlation between uranium and vanadium in sediments samples (r = 0.16; n = 17; p < 0.0001) is related to ore type. In the Crucea uranium mineralization the vanadium concentration range between 60.7 – 335.9-mg·g^{-1} and we can state that the surrounding rocks are the source of

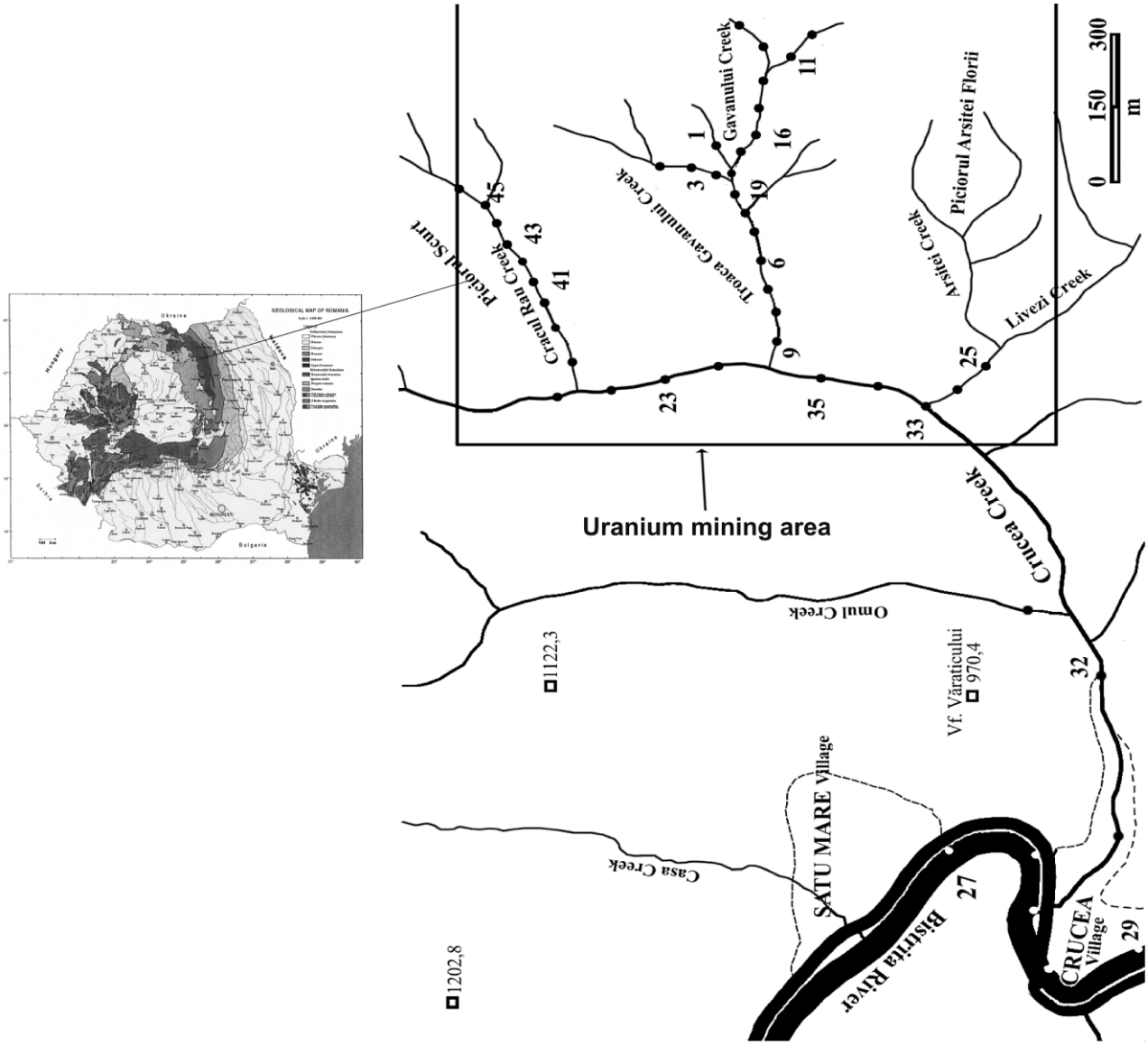

Fig. 1. Topographic map of the investigated area with the distribution of sampling points.

Table 1. Statistics of parameters for bottom sediments samples (n = 17) collected in Crucea region (milligrams per gram $mg \cdot g^{-1}$ except LOI [a] and Al_2O_3 [b]).

Parameter	Minimum value	Maximum value	Median value	Mean value	Standard deviation
LOI (%) [a]	4.59	6.12	5.15	5.19	0.428
Al_2O_3 (%) [b]	14.55	17.77	16.71	18.38	0.948
Co	15.03	21.54	18.34	18.41	1.872
Cr	81.82	110.68	88.88	90.74	6.344
Cu	39.83	70.86	54.64	55.12	9.291
Ni	35.78	125.09	46.03	50.41	19.929
Pb	37.16	371.57	183.54	192.16	97.169
Sr	100.26	120.17	106.57	108.96	7.364
Th	18.70	6643.92	47.78	309.89	391.169
U	17.20	5023.96	63.46	246.81	291.098
V	105.23	123.29	117.39	115.29	5.703
Zn	124.63	161.68	142.00	141.18	10.483

this element. This affirmation confirms the absence of the uranium minerals with vanadium (such as carnotite). Through the weathering of the rocks, vanadium migrates as vanadic acid and in supergene conditions this metal easily concentrates in clay minerals and oxy-hydroxides.

In order to estimate the natural and anthropogenic inputs of actinides and heavy metals into sediments, their total concentrations were correlated with Al concentration. Since Al originated from the natural background it was chosen as the normalizing factor. These data are presented in Table 2. It can be seen that only vanadium shown a linear relationship with the concentration of Al, fact indicates his natural background origin. For the rest of selected elements their origin was anthropogenic. This indicates the impact of mining waste disposal on the environment.

The total concentrations shown in Table 1 have been used for the determination of the degree of pollution with radioactive and heavy metals. At this time, no regulations exist for levels of heavy metals in sediments; however several sets of sediment quality criteria have been reported. Thus, the pollution degree of the sediments was classified using the geo-accumulation index (I_{geo}), which is

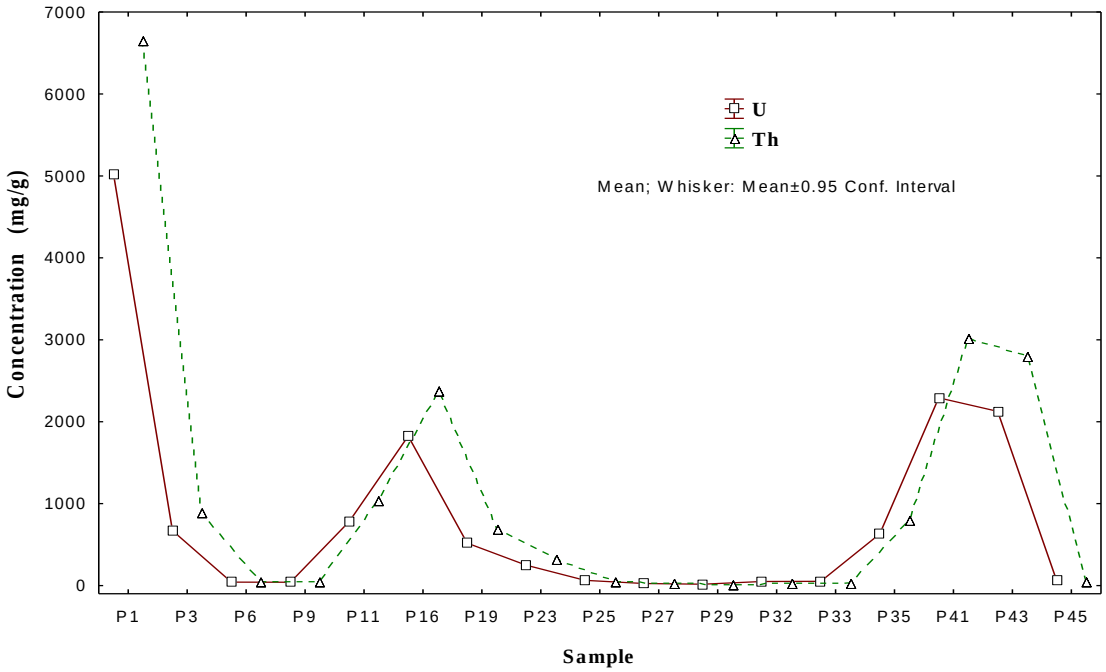

Fig. 2. Variations in actinide concentrations in bottom sediments along Crucea zone. For location of sampling sites see Fig. 1.

Table 2. Relationships between selected elements and aluminum in bottom sediments from Crucea area ($p < 0.001$).

Element	Co	Cr	Cu	Ni	Pb	Sr	Th	U	V	Zn
r (for 4 degrees of freedom)	0.54	0.54	0.50	0.18	(-)0.23	0.17	0.13	(-)0.24	0.97	(-)0.08

Table 3. The background level ($mg \cdot g^{-1}$) for selected elements (Petrescu and Bilal, 2007).

Element	Background level ($mg \cdot g^{-1}$)	Element	Background level ($mg \cdot g^{-1}$)
Cu	13.63	Pb	0.36
Th	10.87	Co	14.36
Sr	107.66	Ni	19.30
U	5.39	Cr	73.58
Zn	66.38	V	97.44

applied for separate element characteristic in the examined sediments and determines the contribution of each element to overall sediment contamination. I_{geo} was calculated as follows:

$$I_{geo} = \log_2 [C_n/(1.5B_n)] \quad \text{(Pinto } et\ al.\text{, 2004)},$$

were: C_n = total element concentration ($mg \cdot g^{-1}$); B_n = background concentration for each element ($mg \cdot g^{-1}$). Therefore, based on the concentration levels of these metals, the stream sediments are categorized into seven classes, with the "0" class corresponding to the values close to the geochemical background. The background concentrations were taken from Petrescu and Bilal (2007) (Table 3).

The pollution degree of the bottom sediments is shown in Table 4. The I_{geo} of U, Th and Pb presents medium and punctual high values that represent sediments belonging to classes of strong to extreme pollution ($I_{geo} > 6$). A proportion of 47.05% of Th and U concentration values are categorized into the highest pollution class (I_{geo} class 6) (Fig.3,a,b), while the rest of the elements presents concentration close to the background values or lowers (Fig.3,d). These high concentrations of U, Th and Pb are distributed preferentially in the proximities of 5, 8, 9 and 1bis mine dumps. Table 4 also shows that I_{geo} of U and Th from the sediments taken from downstream of the mineralized zone (P27 and P29) are lower than those taken from the mineralized areas. This indicates that uranium and thorium are not very mobile in the waters and that these elements are precipitated close to the mining dumps.

5. Conclusions

The knowledge concerning uranium and thorium concentration in stream sediments is essential for predicting natural actinide migration and for drafting strategies concerned with the rehabilitation of contaminated sites.

The pollution degree of the bottom sediments shows that U, Th and Pb are characterized by medium and punctual high values, while the rest of the elements are in concentration close to the background values or lower.

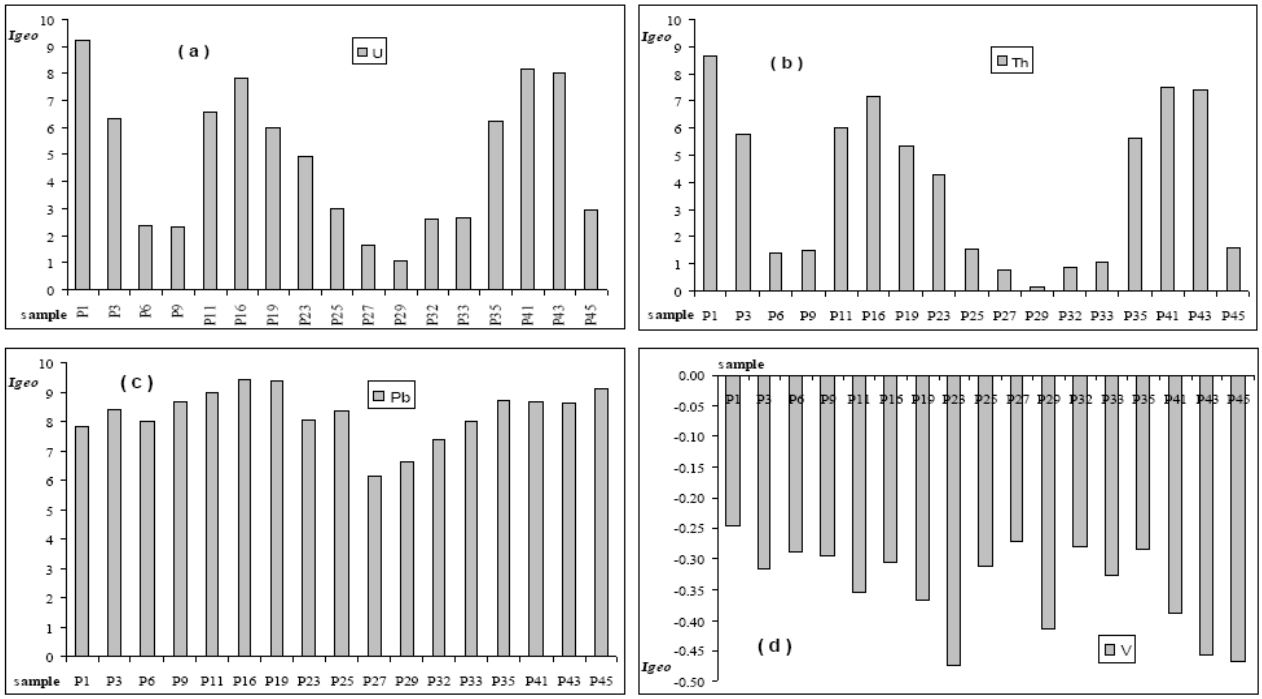

Figure 3. The geo-acumulation index in bottom sediments: (a) U; (b) Th; (c) Pb; (d) V.

Table 4. The geo-acumulation index in bottom sediments for selected elements.

Sample	Cu	Th	Sr	U	Zn	Pb	Co	Ni	Cr	V
S1	1.76	8.67	-0.66	9.28	0.63	7.84	-0.05	0.35	-0.21	-0.25
S3	1.31	5.76	-0.60	6.37	0.39	8.42	-0.10	0.67	-0.34	-0.32
S6	0.96	1.42	-0.50	2.41	0.44	7.99	-0.22	2.11	0.00	-0.29
S9	1.50	1.52	-0.55	2.37	0.56	8.70	-0.13	0.80	-0.31	-0.29
S11	1.00	5.99	-0.67	6.60	0.50	9.00	0.00	0.83	-0.34	-0.36
S16	1.63	7.19	-0.60	7.82	0.70	9.44	-0.29	0.75	-0.23	-0.31
S19	1.42	5.39	-0.68	6.00	0.52	9.42	-0.13	0.93	-0.23	-0.37
S23	0.99	4.30	-0.67	4.95	0.39	8.02	-0.52	0.54	-0.43	-0.47
S25	1.79	1.55	-0.44	2.98	0.51	8.35	-0.20	0.84	-0.22	-0.31
S27	1.37	0.78	-0.49	1.68	0.32	6.12	-0.27	0.58	-0.34	-0.27
S29	1.31	0.20	-0.51	1.09	0.38	6.65	-0.46	0.31	-0.34	-0.41
S32	1.49	0.87	-0.43	2.61	0.39	7.37	0.00	0.60	-0.25	-0.28
S33	1.60	1.11	-0.44	2.69	0.45	8.01	-0.24	0.66	-0.28	-0.33
S35	1.66	5.62	-0.48	6.28	0.52	8.73	-0.26	0.69	-0.32	-0.28
S41	1.50	7.53	-0.67	8.15	0.60	8.70	0.00	0.52	-0.31	-0.39
S43	1.32	7.42	-0.69	8.04	0.56	8.64	0.00	0.57	-0.33	-0.46
S45	1.38	1.61	-0.63	2.97	0.64	9.10	-0.39	0.77	-0.37	-0.47

Although neither U nor Th have an appreciable "exchangeable" fraction, the isolation of specific U- and Th-rich sediment fractions helped to identify connections between bioavailability and genesis of sediments, which control the natural cycling of U and Th. However, if the geochemical conditions it happens to be changes, the surface sediments could act as a future source of actinides and heavy metals to the above water body.

The measurements carried out in the surroundings of a local uranium mine show that the impact of Crucea mine on sediment quality downstream of mining area is insignificant.

Acknowledgements

This work was supported by MIRA Project 050094501 of the Rhone-Alpes Region (France). The inorganic chemical components were determined at Département GENERIC of the Ecole Nationale Supérieure des Mines, Saint Etienne (France). The authors thank Dr. Jacques Moutte and Frederic Gallice for technical assistance. Thanks are due to Dr. G. Ilinca (University of Bucharest) for the reading of the manuscript and for the helpful suggestions. Also, we would like to thank anonymous reviewers for their constructive inputs.

References

Langmuir D., 1997. Aqueous environmental chemistry. Prentice Hall, Upper Saddle River, New Jersey, 600 pp.

Petrescu L., 2004. The impact of the environment of the uranium mine dumps from Crucea and Botusana ore deposit (Bistritei Mountains, Romania): PhD thesis, Department of Mineralogy, University of Bucharest, 196 p. (in Romanian with English abstract).

Petrescu L., Bilal E., 2006. Speciation of natural uranium and thorium in surface waters around a uranium mine (Bistrita Mts., Romania). Geochimica et Cosmochimica Acta, vol. 70, issue 18, supplement 1, pp. A486

Petrescu L., Bilal E., 2007. Environmental impact assesment of a uranium mine, East Carpathians, Romania: Metal distribution and partitioning of U and Th. Carpathian Journal of Earth and Environmental Sciences, vol. 2/1, pp. 39-50.

Pinto M.M.S.C., Silva M.M.V.G., Neiva A.M.R., 2004. Pollution of water and stream sediments associated with the Vale De Abrutiga Uranium Mine, Central Portugal. Mine, Water and the Environment, v. 23, pp. 66-75.

Scientific Annals, School of Geology, Aristotle University of Thessaloniki Proceedings of the XIX CBGA Congress, Thessaloniki, Greece	Special volume 100	127-131	Thessaloniki 2010

EXAMINATION OF THE GROUNDWATER QUALITY IN A SETTLEMENT OF EASTERN HUNGARY

Szabó Gy., Bessenyei É. and Szabó A.

University of Debrecen, Department of Landscape Protection and Environmental Geography, 4010 Debrecen, POB. 9, gyszabo555@gmail.com, alribi@freemail.hu, andial@freemail.hu

Abstract: The water quality from groundwater wells in a small town, called Mikepércs, situated on the SW edge of the Nyírség, eastern part of Hungary, is investigated. By the time of the research, the sewage network had not been yet constructed in Mikepércs, thus the inhabitants collected the sewage in septic tanks. In Mikepércs the tanks usually had not adequate insulation and therefore the majority of the sewage (more than 90% according to our estimations) was emitted into the soil. As there are sandy soils around the settlement the sewage can filter into the soil and reach easily the groundwater level at depth of about 1.5-3 m below ground surface. According to our preliminary expectation we have detected significant pollution in most of the groundwater wells in Mikepércs, especially concerning orthophosphate, nitrate and ammonium pollutants, which concentrations were much over the hygienic limit value. Besides the watering of animals, sometimes people drink groundwater so we can say that consuming of groundwater can cause both human and animal health risk.

Keywords: Eastern Hungary, water quality, groundwater pollution, health risk

1. Introduction

Among the underground water deposits the groundwater is one of the most endangered because the contaminants from the surface can easily reach it (Bolgár and Pál, 2005; Farsang and Fejes, 2009). Some decades ago the groundwater was the most important drinking water resource in Hungary but the situation is markedly changed and nowadays groundwater is rarely used as drinking water. On the other hand, the former dug wells can still be found in the villages and the suburbs, and they are still in use. People use them to water ploughlands and domestic animals but sometimes even to wash cars. Furthermore, the owners of the wells – usually elder people – drink groundwater from the wells saying that they used to drink it from their childhood without any problems and that its taste is much better than that of the tapwater. Knowing the water quality of the wells, this means serious health risk. The percentage of households supplied with sewer system has increased rapidly in Hungary the last years: from 56% in 2002 became 70% in 2008; in this period 700 thousand properties have installed sewer system (MTTE, 2009). Nevertheless, many country settlements where a great deal of the sewage filters into the soil can still be found.

The present quality test was carried out in a settlement where the sewer network had not been constructed by the time of the examination, and the domestic sewage was collected in septic tanks not supplied with adequate insulation, allowing the soil and the groundwater to be exposed to a great demand. Considering the data of the amount of the water consumption and the sniffed sewage we determined that at least 90% of the sewage of the settlement filtered into the soil. In the course of our research the water quality of the dug wells and the temporal changes of these parameters were examined. Moreover, we studied whether the use of groundwater poses any human or animal health risk. Since the sewer network has been constructed after we finished the examinations, this research can serve as a basis to determine the positive effects of the sewerage.

2. Materials and Methods

Examinations were carried out monthly in the 14 dug wells of Mikepércs: from June 2005 to June 2006 and from July 2007 to July 2008 (Fig. 1). Between these two series of measurements a year passed. During the designation of the wells we en-

deavoured to cover the whole area of the settlement.

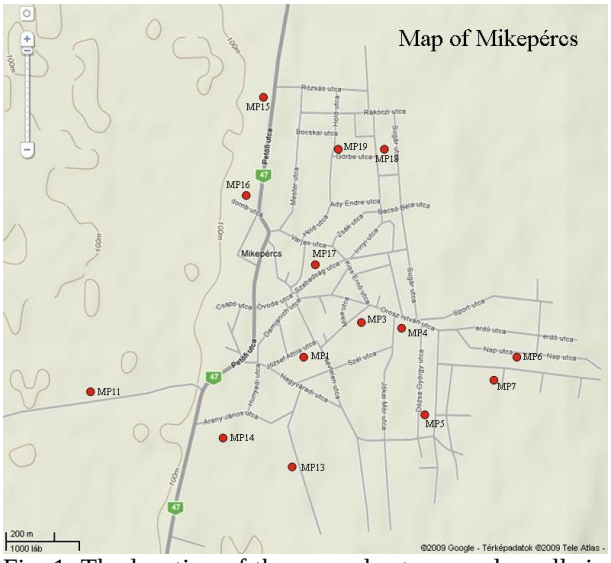

Fig. 1. The location of the groundwater sample wells in Mikepércs

The sampling was carried out with a ball water sampler, and the samples in hermetically closed plastic flacons were transported to the geography laboratory of the University of Debrecen. When the samples were taken, the electric conductivity and the temperature were measured in the field with a Schott electronic conductometer. The depth of the groundwater table was also measured for every sample. The determination of nitrate, orthophosphate, ammonium and organic matter and the measurement of the pH were carried out in the laboratory a day after the sampling (Literáthy, 1973).

The results were saved in an Excel database and the diagrams were also made with this software. In the course of the statistical analyses Kolmogorov-Smirnov normality tests were performed. Since most of the data were not normally distributed, Spearmann correlation coefficient was applied during the correlation analysis. SPSS 8.0 software has been used in the statistical analyses and to make further diagrams.

3. The examined settlement

Mikepércs is situated in the eastern part of Hungary, about 5 Km south from the town of Debrecen. Mikepércs has diverse pedological conditions as the settlement is located at the boundary between the Hajdúság and the Nyírség. The loess area of the Hajdúság extends to the western part of the settlement where chernozem soils were formed. Soils of sandy texture can be found in the greater part of the settlement that belongs to the area of the Nyírség. These soils are much more sensitive than the chernozems because of the coarser granulometric composition, the less content of organic matter and the weaker buffering capacity. The depth of the groundwater in Mikepércs is 1-3 m, but in the higher reliefs more than 5 m deep groundwater table can occur. The groundwater flows from the north-east to the south-west, towards the Kondoros-stream that runs near the west part of the village.

In the Mikepércs settlement of 4000 inhabitants the water supply network is almost complete but the construction of the sewer system has begun only in the second half of 2006. The sensitivity of the confined groundwater bases under the settlement and the significant pollution of the groundwater stress out the urgency of the sewerage program. This program was finished only after the second examination period, by the end of 2008, so the positive effects of the sewerage could not be demonstrable in this examination series.

4. Results and Discussion

During the examined periods the depth of the groundwater was higher than on the average because precipitation was significantly higher that the mean precipitation of many years (600 mm). At the time of the first examination series (from June 2005 to June 2006) precipitation was 904 mm, whereas from July 2007 to July 2008 749 mm precipitation fell (Fig. 2). In most wells the groundwater level fluctuated between 100 and 250 cm during the first examination period but it was at average 80 cm deeper during the second period of the examination (Fig. 3). Beside the less precipitation in the second period, the quite little precipitation (485 mm) during the 12 months between the two studied periods also played a significant role.

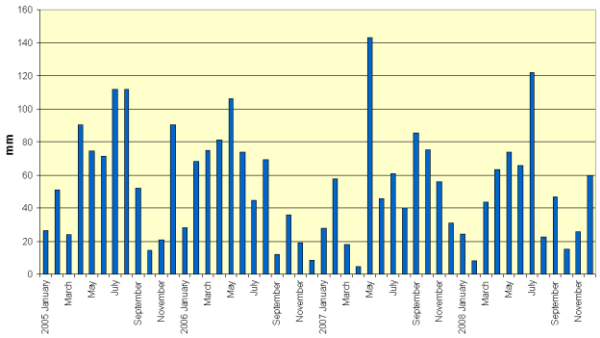

Fig. 2. The monthly precipitation distribution from 2005 to 2008 (Source: VITUKI RT.)

The electric conductivity of the water samples gives the total ion content of the samples (Szabó, 2008; Szalai, 2008). In the first period the conductivity was 1000-2800 µS/cm and in the second period it was a bit less with the values ranging from 900 to 2300 µS/cm, which can be considered as ordinary in a non-sewered settlement (Fig. 4). (Pál and Bálint 2007).

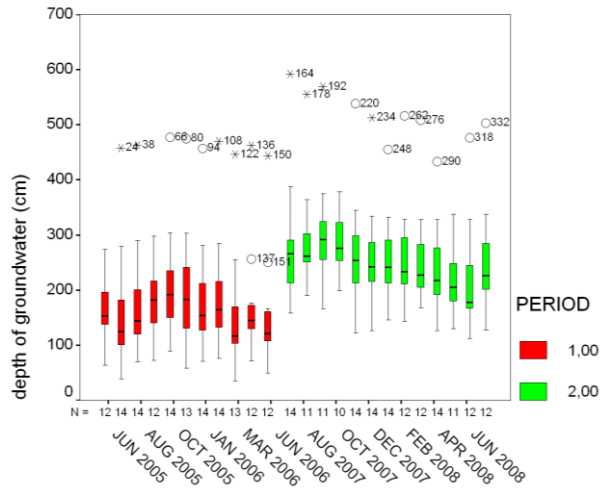

Fig. 3. Changes in the depth of the groundwater in the two examination periods.

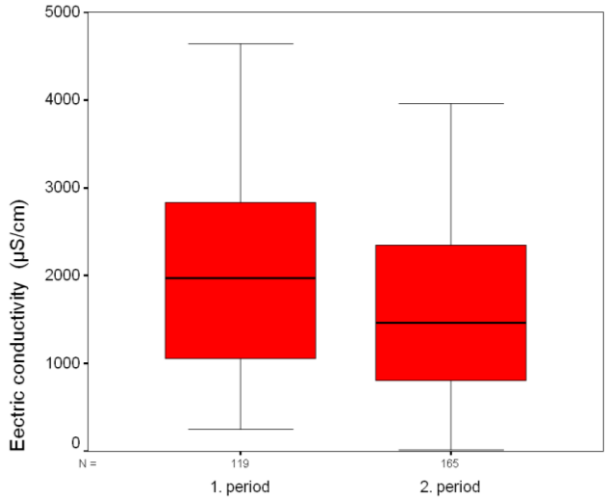

Fig. 4. The electric conductivity in the first and the second examination periods.

Definitely, the less precipitation and the deeper groundwater level gave rise to the weaker values of the second examination period. In the first period the bottom of the non-insulated tanks near several wells got under the groundwater level; that is why the total ion content of the well-water could increase. Although the electric conductivity does not give information about the type of the ion found in large quantities in the sample, certain conclusion can be drawn out with the correlation analysis. Strong positive correlation can be found between the electric conductivity and the nitrate content ($r=0.715$, $p<0.01$). This proves that nitrate accumulated mainly in wells containing other ions – that also play significant role in the change of the conductivity – in high concentration.

The **pH** of the examined water samples were slightly alkaline (Fig. 5). In both examination periods a maximum in the autumn-winter months and a minimum in the spring-summer months can be observed but all the measured values were inside the (B) limit values (pH<6.5 and pH>9.0) determined in the joint decree no. 10/2000 (VI. 2.) KÖM-EÜM-FVM-KHVM.

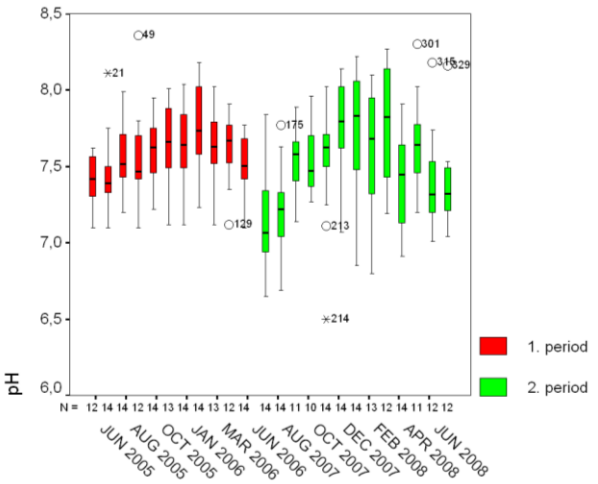

Fig. 5. The pH of the water samples monthly from June 2005 to June 2006 and from July 2007 to July 2008.

The majority of the wells contains **ammonium ion** in really high concentrations; this clearly indicates anthropogenic contamination. In 17% of the samples collected in the first period, the measured concentrations were lower than the contamination (B) level determined in the decree no. 10/2000 (0.5 mg/l) so regarding 83% of the samples the ammonium content exceeded the limit value. Considering the second examination period the situation was better: ammonium concentrations in 38% of the samples were under the contamination level. On the other hand there were extreme contamination values exceeding many times the contamination level; they refer to direct sewage disposal.

In addition to the municipal wastewater the improper management of the manure derived from livestock farming could contribute to the extremely high concentrations. In both periods the highest ammonium concentrations were experienced in the

autumn-winter months. During these months the organic nitrogen is converted into ammonium and the oxidation of the ammonium is retarded due to the cold weather as the activity of the nitrite bacteria slows down below 10 °C and the ammonium ions accumulate into the water (Fig. 6) (Bíró et al., 1998).

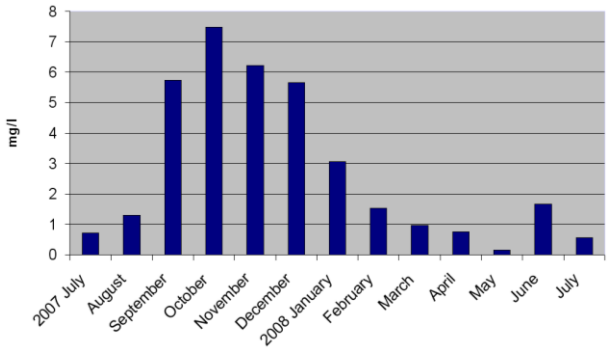

Fig. 6. The ammonium concentrations in the second examination period, means of 13 wells (The data of the well MP19 were excluded because extremely high concentrations were measured in this well).

25 mg/l is the limit value (B) of **nitrate concentration** in underground water bodies, determined in the decree no. 10/2000. Regarding the nitrate content of the wells the results are quite disadvantageous since the nitrate concentration exceeded the limit value in 90% of the collected samples. Moreover, more than fivefold concentration of the limit value was measured in 51% of the samples and values exceeded 500 mg/l also occurred. Knowing the high ammonium concentration, it is no wonder that the water of the wells is strongly polluted as in the presence of oxygen the ammonium is oxidized to nitrite than nitrate (Pál et al., 2009). High nitrate concentration is due to the sewage filtering from the sewage tanks but the nitrogen fertilizers spreading in the vegetable gardens near the wells could also contribute to the high concentrations (Szabó et al. 2007). It can be seen in both examination periods that the highest concentrations were measured in the wells that are situated in areas with the highest groundwater level and where non-insulated sewage tanks were near the wells (Fig. 7).

The **phosphorus** content of the underground water can derive from natural sources, e.g. from the weathering of certain rocks, but the higher concentrations can always be traced back to anthropogenic effects. The most significant anthropogenic source is the sewage but the residues of phosphorus fertilizers used in the agriculture can also cause phosphorus accumulation (Szalai et al., 2004).

The **orthophosphate** pollution of the examined groundwater wells is also significant. Almost 94% of the examined water samples exceeded the 0.5 mg/l (B) contamination limit value determined in the decree no. 10/2000; in 60% the excess of the limit value was more than fivefold (Fig. 8). In Mikepércs the main pollution source is the municipal wastewater, the use of phosphorus fertilizers is not typical in the centre of the settlement. More considerable pollution occurred in the first examination period owing to the higher groundwater level since in most cases of the sewage tanks near the wells the bottom level was situated under the groundwater level and therefore the sewage could directly mixed with the groundwater.

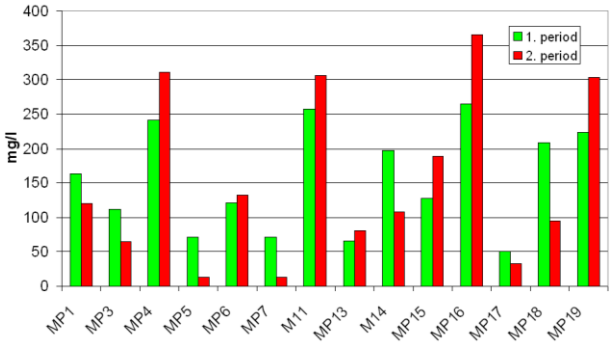

Fig. 7. The mean nitrate concentrations of the examined wells in the first and the second examination periods

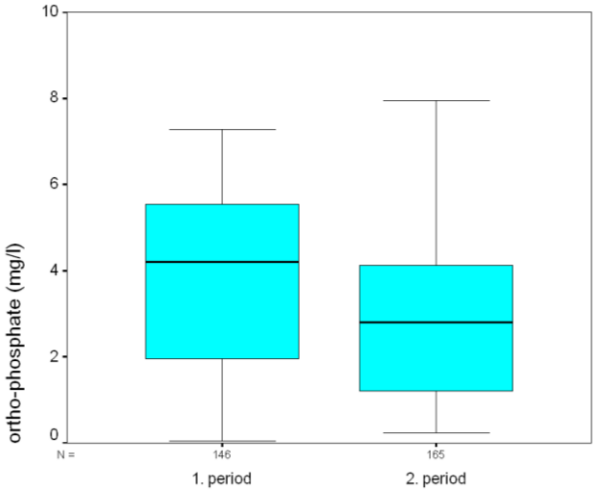

Fig. 8. The orthophosphate concentrations in the two examination periods

5. Conclusions

- The water quality of the examined groundwater wells is extremely inadequate in Mikepércs.
- Regarding the examined water quality parame-

ters the measured concentrations of most collected samples exceeded the limit values. In the cases of the ammonium, nitrate and orthophosphate the situation was extremely adverse.

- The problems occurred because the sewer network of the settlement constructed by the end of 2008 was not put into operation at the time of the examinations so the inhabitants stored the sewage in badly insulated or non-insulated septic tanks. From these tanks 90% of the sewage filtered into the soil, leastways this is backed up by the data of the amount of the water consumption and the sniffed sewage.
- The relatively little depth of the groundwater (1-3 m) and the sandy soils (letting through the pollutants very quickly) found in the most part of the settlement contributed to the pollution of the groundwater.
- The water quality of most examined wells was proved to be worse in the first examination period – because of the higher groundwater levels – since the water levels exceeded the bottom level of several sewage tanks at the times of high water levels and therefore the sewage could directly mixed with the groundwater.
- The decree no. 41/1997 (V. 28.) states that "As far as possible water of drinking-water quality should be used for the watering of animals." Unfortunately, it was not carried out in the cases of the examined households (possessing dug wells) since the inhabitants water the animals everywhere with the water from the dug wells but the quality of this water is not adequate regarding the directions. On the other hand, they had the possibility to use water of drinking-water quality as the water conduit system is entirely constructed in the settlement.
- Knowing the water quality of the wells this practice raises serious questions related not only to the animal but also to the human health since the toxic substances deriving from the polluted water can get into the milk and meat of the animals and the consumption of them can cause several serious problems in the health of human beings.

References

Joint decree no. 10/2000 (VI.2.) KöM-EüM-FVM-KHVM of water management on the limit values necessary to protect the quality of groundwater and the geologic medium www.kvvm.hu (in Hungarian).

Decree no. 41/1997. (V. 28.) FM on Veterinary regulation, www.magyarorszag.hu (in Hungarian).

Bíró T. - Thyll SZ. - Tamás J., 1998. Risk assessment of nitrate pollution in lower watershed of the Berettyó River. In: Filep, Gy. (ed.) Soil water environment relationships. Wageningen – Debrecen, 239-247.

Bolgár B. E. - Pál Z., 2005. Spatial pattern of groundwater pollution on a small Transylvanian village example, Environment, research, protection and management international conference, UBB, Facultatea de Stiinta Mediului, Cluj Napoca, 140-150.

Farsang A. - Fejes I., 2009. Contamination and human health risk of groundwater in Szeged: 11th regional conference on environment and health In: A Papp (ed.) 11th regional conference on environment and health. Szeged, Magyarország, 5p.

Literáthy P., 1973. Unitary water examination methods I. (in Hungarian) Chemistry methods, vol. 1, Vízgazdálkodási Tudományos Kutatóintézet IV. Vízminőségi és Víztechnológiai Főosztálya, 233p (in Hungarian).

Ministry of Transport, Telecommunication and Energy (MTTE), 2009. http://www.khem.gov.hu (in Hungarian).

Pál Z. - Aczél M. - Pál K., 2009. Nitrate contamination of the groundwater in rural settlements – example of Imecsfalva (in Hungarian). Collegium Geographicum 6. sz. Kolozsvár, ISSN. 2065-3859, 43-51 (in Hungarian with english abstract).

Pál Z. - Bálint K., 2007. Settlement groundwater contamination patterns by the examples of forestland villages (in Hungarian). Acta Siculica. Székely Nemzeti Múzeum Évkönyve, ISSN 1843-8385, 49-56 (in Hungarian with english abstract)

Szabó Gy. - Szabó Sz. - Szabó A. - Szemán B., 2007. Spatial and time variations of the groundwater quality of two different landscapes – In: Boltižiar, M. ed. Implementation of Landscape Ecology in New and Changing Conditions, ILE Slovak Academy of Sciences, 421-427.

Szabó Sz., 2008. Methodes of environmental investigations – monitoring – coursebook, Debrecen, 144p. (in Hungarian)

Szalai Z. - Jakab G. - Madarász B., 2004. Estimating the vertical distribution of groundwater Cd and Cu contents in alluvial sediments (River Danube). Saturated and Unsaturated Zone; Integration of process knowledge into effective models (Eds. Per Aagard et al.). La Gordialica Pavese, Rome. ISBN88-7830-387-9, 303-312.

Szalai Z., 2008. Spatial and temporal pattern of soil pH and Eh and their impact on solute iron content in a wetland (Transdanubia, Hungary) AGD Landscape and Environment 2 (1), 34-45.

Water Database – VITUKI Rt., www.vizadat.hu (in Hungarian).

Scientific Annals, School of Geology, Aristotle University of Thessaloniki Proceedings of the XIX CBGA Congress, Thessaloniki, Greece	Special volume 100	133-139	Thessaloniki 2010

MEASURE OF HEAVY METAL LOAD IN THE FLOODPLAIN OF THE RIVER TISZA

Szabó Sz.[1], Gosztonyi Gy.[1], Prokisch J.[2]

[1]*Department of Landscape Protection and Environmental Geography, University of Debrecen, H-4010 Debrecen, Egyetem sq. 1. POB., szszabo@delfin.unideb.hu; gosztonyi.gyongyi@gmail.com*
[2]*Institute of Bio and Environmental Energetics, University of Debrecen, H-4010 Debrecen, Böszörményi str. 138, jprokisch@agr.unideb.hu*

Abstract: The quality of the River Tisza is significantly influenced by the industrial activity of Ukraine and Romania. The main problem is the heavy metal pollution which can be in dissolved form in the water or attached to colloidal particles in the sediments. In this paper an investigation of soil samples taken from the floodplain of the river was carried out. Surface samples were collected and profiles were created. As, Cd, Co, Cu, Ni, Pb and Zn concentrations were determined. The results show significant and continuous heavy metal load. ANOVA test was carried out and the metal concentration in the upper layer of the active floodplain is proved to be considerably higher than in the reclaimed side. Regarding copper and zinc, in addition to the total metal content, their percentage available for plants (Cu and Zn percentages measured in the Lakanen-Erviö solution) is also more in the active floodplain than in the reclaimed side (copper: 27%, zinc: 47%). Discriminance analysis can identify the location of the soil samples (correlate to the levee) with 92% accuracy. Soil profile shows increased heavy metal loads in the top layer of the soil and proved that the accident in 2000 was not the only pollution occurrence. Based on the results we came to the conclusion that the pollution comes constantly with the sediments from the over arm of the River Tisza and its tributaries.

Keywords: Tisza, floodland, heavy metals, accumulation, statistical analysis

1. Introduction

The different anthropogenic productive and social activities load our environment with various contaminations. A great quantity of pollutants can get into the environment especially in the course of industrial production. It often occurs that the wastes and by-products containing toxic materials in large quantities are not properly treated, namely without adequate technical protection the contaminants can get unlimited into the environment. The contaminations can occur in two ways: (1) continuous pollution in various concentrations; or (2) occasional pollution in high concentrations.

In this work the metal contamination of the sediments of the River Tisza was examined so in the followings contaminants getting into the surface water streams will be studied. These contaminants can occur in dissolved form and attached to colloidal particles transported in different quantities depending on the speed of the flow (i. e. the sediment transporting ability).

The River Tisza originates from Romania and, passing Ukraine, enters Hungary near Tiszabecs. Stepping out from the Carpathians, the morphological type of the river changes from upper- and middle-course type to lower-course type. This is an important information in addition to the fact that the River Tisza transports a great deal of floating sediment so contaminants can occur both in dissolved form and attached to the sediment. There are not considerable pollution sources in Hungary that can contaminate the river's water. However, near the bank of the River Tisza and its tributaries several industrial (mining and ore processing) plants can be found in other countries, their technical protection is not always adequate and, based on the accidents happened in the last few years, we can say that we should not keep these plants in mind only as potential pollution sources. In addition to the sudden, unexpected contaminations mentioned by the media, we should also take the minor pollutions into consideration. Metals can get into the water in dissolved form and attached to colloidal particles. During the floods metals at-

tached to colloids are deposited. Thus the metal concentration is significantly influenced by the quantity of the deposited sediment during the flood and the percentage of the colloids. The quantity of the deposited colloids and the rate of the deposition depend on the flow rate. Sluggish stream is favourable for the accumulation and the plant coverage is also important since it increases the roughness and decreases the speed of flow (Szalai, 1998; Braun et al., 2003; Sándor and Kiss, 2009).

The metal pollution examination of the active floodplain of the River Tisza is not new, publications related to this topic can be found from the early years of the 1980s (e. g. Győri and Végvári, 1981; Black and William, 2001; Hum and Matschullat ,2002).

In this research examinations were carried out in a sample area of the Boroszló-kert Holt-Tisza region (near Gulács) – near the River Tisza. Our aim was to demonstrate how the transported sediments contaminated with metals affect the active floodplain compared to the reclaimed side and how effectively the higher concentration of the contaminants can be identified with high-resolution vertical sampling. Moreover, confirming the contaminations water quality data were analyzed to show contamination periods between 2003 and 2009.

2. Materials and methods

Water quality data were taken from Tisza Water Quality Warning System (TWQWS). The network consists of 4 measuring stations in the border sections of the River Hernád, the River Berettyó, the River Szamos and the River Tisza. The data of the monitoring station of Técső (River Tisza) were analysed in terms of the hygienic threshold limits.

In 2006 and 2007 91 surface soil samples were collected from the active floodplain of the River Tisza in Boroszló-kert (Fig. 1). The soil samples were taken from the depth of 0-25 cm and, homogenizing 8-10 subsamples, composite samples were made in order to decrease the errors originated from the microheterogeneity of soil.

High-resolution vertical sampling was also carried out: a 1-meter-deep profile was dug and sampled in every 2 cm (according to Ciszewski, 2003).

The majority of the samples (71) derive from the active floodplain and 20 samples were collected from the reclaimed side (Fig. 1).

The soil samples were dried at 40 °C and then passed through a 2 mm sieve. The granulometric composition (with Köhn-pipette), the humus content (after Tyurin's scheme), the $CaCO_3$-content

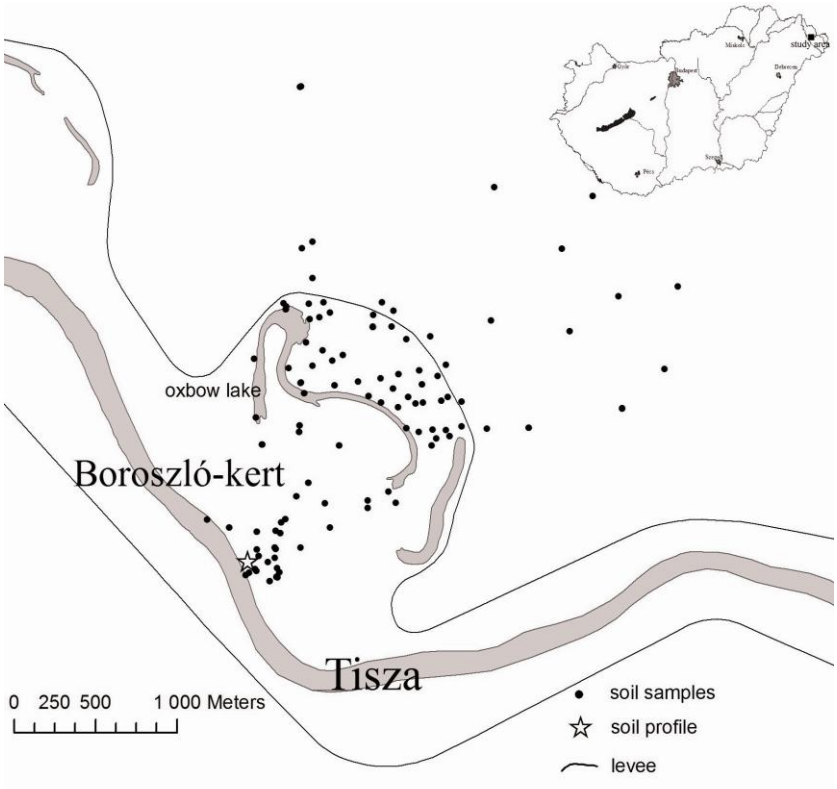

Fig. 1. The locality of the soil samples in the Boroszló-kert Holt-Tisza region.

(with calcimeter, Scheibler method) and the active and potential acidity (pH_{H2O}, pH_{KCl}, y_1, y_2) of the soil samples were determined according to the valid Hungarian standards (MSZ-08-0210:1977, MSZ-08-0205:1978, MSZ-08-0206-2:1978). The humus quality was measured based on Hargitai's method (1981): absorbances of 1% NaF (E_{NaF}) and 0.5% NaOH (E_{NaOH}) extracts were measured at 533 nm (with spectrophotometer).

The metal content of soils was determined according to the MSZ-08-1722-3:1989 Hungarian standard (cc. HNO_3+H_2O_2 acid digestion) with FAAS and ICP-OES. Analyses of the surface samples were carried out with Perkin-Elmer 3000 FAAS appliance (Co, Cu, Ni, Zn) at the Department of Landscape Protection and Environmental Geography (University of Debrecen). The samples from the soil profile were analysed for the same elements as well as As, Cd and Pb at the Central Chemical Laboratory of the Centre of Agricultural Sciences (University of Debrecen). Detection limits are shown in Table 1.

Table 1. Detection limits of the applied methods.

	Detection limits	
Elements	ICP-AES	FAAS
As	12.0 µg/l	300.0 µg/l
Cd	1.5 µg/l	2.0 µg/l
Co	5.0 µg/l	5.0 µg/l
Cu	2.0 µg/l	3.0 µg/l
Ni	5.5 µg/l	10.0 µg/l
Pb	14.0 µg/l	10.0 µg/l
Zn	0.9 µg/l	1.0 µg/l

Total metal content by itself does not give enough information about the dangers caused by metals since they are available for plants to a different extent depending on their form of occurrence. Therefore, in the case of surface samples the available quantity for plants was also determined with Lakanen-Erviö extraction (NH_4-acetate + EDTA, Lakanen and Erviö 1971).

During the data processing the normal distribution of the data was analysed with D'Agustino test. Variance analysis (ANOVA) and discriminance analysis were carried out. Regarding the data of the soil characterizations the distribution is not normal; therefore Mann-Whitney test was applied. TANAGRA software and SPSS for Windows 15.0 were used for the analysis. The data were visualized by C2 (Juggins, 2003) and ArcGIS 9.0 software.

3. Results and discussion

3.1. The heavy metal load of the River Tisza by the industrial activity

Regarding the dissolved metal content the data of the Tisza Water Quality Warning System station in Técső proves the facts described above in the introduction. In this station the dissolved zinc, copper, lead and cadmium content are measured and the data are available from November, 2003 to December, 2009. In this period the measured metal content exceeded at least four times both the warning and the alarming limit values (Table 2): between 21 November 2003 and 14 December 2003; between 9 October 2004 and 15 November 2004; in 3 December 2005; between 2 March 2006 and 17 April 2006. The pH values were under 5.5 (normally they are above 7.2) from 4 May 2008 to 25 June 2008 – heavy metal measurements were not carried out in this period. Since the measurements (because of technical reasons) are not constant, the limit values could often be exceeded.

Table 2. Values of warning and alarm limits in the TWQWS at Técső.

Element	Values of	
	warning (µg/L)	alarm (µg/L)
Zn	600	1800
Cd	10	30
Pb	200	600
Cu	200	600

3.2. Physical and chemical properties of the soil

There is no significant difference in the sand content and the amount of polymerized humic acids (E_{NaF}) between the two sides of the levee. However, significant difference was found in the values of silt and clay content, humus content, the amount of the short carbon chain humic acids, humus quality and pH_{H2O} regarding the two side of the levee (Table 3).

The percentages of the sand and silt fractions are the most considerable ones in the granulometric composition of the sediment. The effect size is average (approximately r=0.3 – see Field 2009) both in the cases of the silt and the clay fraction but extremely significant differences (i.e. the effect of

Table 3. Soil properties and the results of Mann-Whitney test.

Soil properties	Situation	Lower quartile	Median	Upper quartile	Mann-Whitney's U	Effect size (r)
Sand content (%)	floodland	31,2	38,9	47,9	619,5	-0,09
	reclaimed side	32,1	42,3	56,7		
Silt content (%)	floodland	43	48,5	56,8	452,5	-0,26
	reclaimed side	33,8	43,6	50,3		
Clay content (%)	floodland	9,1	10,9	12,9	418,5	-0,29
	reclaimed side	10,3	13,4	17,3		
Humus (%)	floodland	3,2	4,1	5,3	295	-0,33
	reclaimed side	4,9	5,3	5,7		
E(NaF)	floodland	0,25	0,33	0,52	206	-0,12
	reclaimed side	0,16	0,32	0,56		
E(NaOH)	floodland	0,13	0,19	0,28	500	-0,46
	reclaimed side	0,29	0,41	0,61		
Humus quality	floodland	1,41	1,85	2,81	228	-0,46
	reclaimed side	0,37	0,83	1,4		
pH(H_2O)	floodland	6,7	7	7,4	68	-0,64
	reclaimed side	4,9	5,3	5,7		
$CaCO_3$ content (%)	floodland	1,5	2,4	3	-	-
	reclaimed side	0	0	0		

the levee is not noteworthy considering the granulometric composition) are not expected since, before the river regulations, the granulometric composition of the sediment was determined only by the distance from the river (farther from the river bank finer sediments were deposited) and the intensity of the floods. This pattern was also influenced by the shifting of the river channel. However, after the construction of levees and the cut-offs (see the oxbow in Fig. 1) closer to the channel coarser sediments but closer to the levee finer sediments were deposited. The areas outside the levee were always farther from the channel so the sediments are finer there. This also has effects on the chemical linkage of the metals since fine particles as inorganic colloids play an important role in the metal adsorption (Stefanovits et al., 1999). Due to the intensive agricultural activities in the reclaimed side, there is more humus - as organic colloids (Szabó, 2000; Filep, 1999; Farsang et al., 2007) – in the active floodplain than outside the levee. This is proven by the higher concentration of the short carbon chain humic acids. It is important also because the humus quality of the Fluvisols in the active floodplains is generally unfavourable (Stefanovits et al., 1999) but we have got better results in our samples. The pH and quantity of the $CaCO_3$ can be the explanation: the calcareous sediments of the active floodplain result in higher pH (Table 3) and make more advantageous conditions for humification. On the other hand, another factor also affects the pH and the humus quality of the soil: the draining capability of the soil can be improved due to the tillage of the agricultural areas. Thus the leaching is also more intense, which leads to the decrease of the pH and results in the humus of poor quality. The most definite effect size occurs in the case of the pH.

3.3. Heavy metal content of the surface samples

Analyzing the surface soil samples we can get information about the root zone of the plants. The measured metal concentrations are shown in Table 4.

Table 4. The total acid extractable and the Lakanen-Erviö extractable (LE) metal content of the samples from the active floodplain and the reclaimed side (mean ± standard deviation).

Element	Active floodplain	Reclaimed side
Co-LE (mg/kg)	6.7±1.0	4.9±0.8
Co (mg/kg)	18.9±2.7	16.3±2.1
Cu-LE (mg/kg)	15.6±5.8	7.24±1.1
Cu (mg/kg)	32.9±8.3	19.3±4.0
Ni-LE (mg/kg)	10.3±1.3	8.5±1.5
Ni (mg/kg)	46.1±6.9	38.3±7.4
Zn-LE (mg/kg)	15.5±9.8	7.5±6.7
Zn (mg/kg)	118.4±24.2	84.3±30.1

According to the result of the variance analysis zinc, copper and nickel concentrations are higher in the upper 25 cm of the soil in the active floodplain than in the cases of the control samples from the reclaimed side (Fig. 2-3). Regarding copper and zinc, in addition to the total metal content, their percentages available for plants are also more in the active floodplain than in the reclaimed side

(copper: 27%, zinc: 47% more). This can be explained by the fact that the metals are bound to the soil particles in different chemical forms inside and outside the active floodplain. Inside the active floodplain metals are more easily mobilizable and can be accumulated in plants and get into the food chain – in close correlation with the different soil characteristics (pH, humus quality – see above). Regarding the samples from the active floodplain and the reclaimed side discriminance analysis was carried out with zinc, cobalt, copper and nickel as independent variables. After excluding the outstanding values, we can estimate from the results with 92% accuracy ($p<0.01$) whether the sample is from the active floodplain or the reclaimed side (Table 5). The order of the metals based on the structure matrix (Pearson correlation coefficient matrix) values is the following: copper (0.978), zinc (0.703), nickel (0.547) and cobalt (0.444). (As our unpublished results show, the high amount of zinc comes to Hungary by the River Túr where we found 400 mg/kg Zn in the floodplain soil.) Therefore copper and zinc concentrations are very significant in the function and the other two metals are certainly subordinated but their participation in the examination is reasonable since they increase the accuracy of the estimation. Based on the canonical correlation coefficient (0.746) the function explains 55% of the variance of the independent variable.

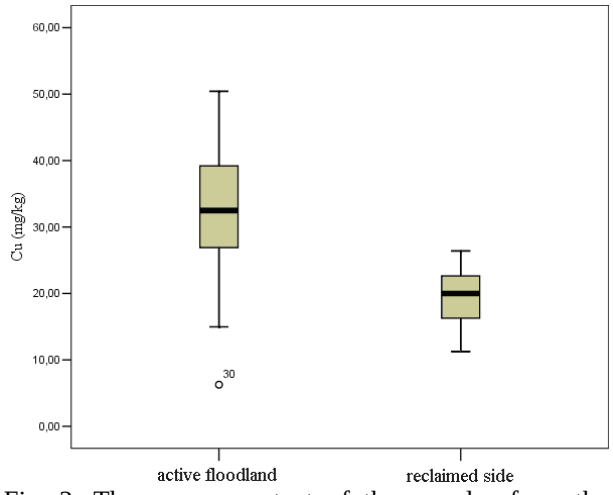

Fig. 2. The copper content of the samples from the floodplain and the reclaimed side ($mg.kg^{-1}$).

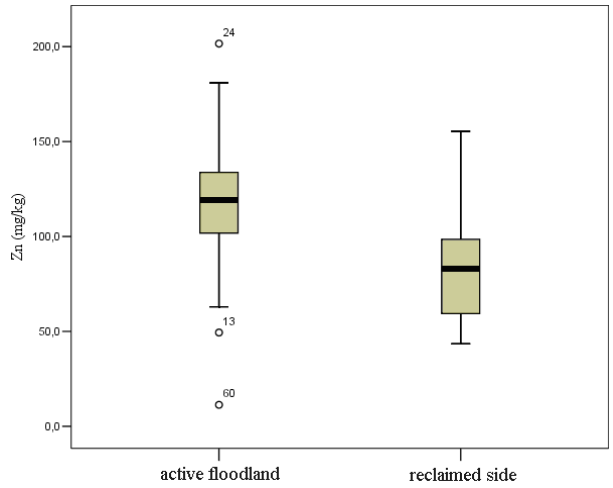

Fig. 3. The zinc content of the samples from the floodplain and the reclaimed side ($mg.kg^{-1}$).

3.4. Heavy metal content in the soil profiles

The analysis of the profiles made the examination of the vertical distribution of the pollutions possible. In Figure 4 the arsenic, cadmium, lead, copper, zinc, nickel and cobalt concentrations of the soil profiles can be seen.

The elemental analysis proves that the accident in 2000 was not the only contamination (Fig. 4). Gamma spectroscopic analyses (Dezső et al., 2009) showed that the ^{137}Cs isotopes, got into the atmosphere by the Chernobyl disaster in 1986 then fallen out, can be found now in the depth of 26 cm in the soil profile (Fig 4/A-line); therefore, the sedimentation rate is approximately 1-1.2 cm/year in this locality of the active floodplain. The highest metal concentrations were measured in this layer – deposited during the last 20 years – and it is exactly the same layer as the plants' root zone. In the cases of As and Cd the limit values (contamination limit value according to the joint decree No. 10/2000; vertical grey line shows the concerned elements in Fig. 4) were exceeded remarkably and the concentrations of the copper, nickel and zinc also approach the limit value. The highest Pb concentration (63 mg/kg) exceeds the background value (25 mg/kg) but does not reach the contamination limit (100 mg/kg). The situation is similar regarding Co: the contamination limit value is 30 mg/kg but all the measured values in the profiles are below 20 mg/kg.

Concerning the essential metals, high metal concentrations in the sediments of active floodplains do not cause problems, we should reckon with deficiency instead (especially in cultivated agricultural areas). However, the concentration of the toxic As and Cd exceeds the limit value, and this is very disadvantageous in terms of the floodplain farming but arsenic is not mobilizable in the soil-plant system (Kádár and Pálvölgyi, 2005). If soil contains humus of good quality, cadmium is bound in insoluble chelates (Livens, 1991; Szabó et al.,

Table 5. The classification table of the discriminance analysis

			Estimated group membership		
			Active floodplain	Reclaimed side	Total
Original	pc	Active floodplain	57	3	60
		Reclaimed side	3	17	20
	%	Active floodplain	95	5	100
		Reclaimed side	15	85	100
Cross-validated	pc	Active floodplain	57	3	60
		Reclaimed side	4	16	20
	%	Active floodplain	95	5	100
		Reclaimed side	20	80	100

92.5% of original grouped cases correctly classified.
91.3% of cross-validated grouped cases correctly classified.

2008a). In the examined floodplain the polymerized long carbon chain humic acids dominate thus either cadmium can not pose any threat. In the course of our examination considerable metal accumulation of plants was not experienced but these examinations are not completed.

4. Summary

At least 4 significant pollution periods can be identified by analyzing the data of the station in Técső so in addition to the well-known contaminations the river is relatively often contaminated by heavy metals. The examination of our samples revealed that the metal concentration is significantly higher in the upper layer of the soil in the active floodplain, and the percentage available for plants is also higher here than in the reclaimed side. Based on the analysis of the soil profiles we proved that sediments contaminated with heavy metals are continuously deposited into the active floodplain. The quantity of the deposited sediment and the metal concentration in the layers depend on the characteristics of the flood: how large area is flooded by the water, what the rate of the flow is in the floodplain and how long the flood lasts. The flow rate is also important in terms of the sediment composition thus the vegetation coverage can also increase indirectly the metal concentration attached to the clay fraction. The effects were shown by the examination of the soil profile.

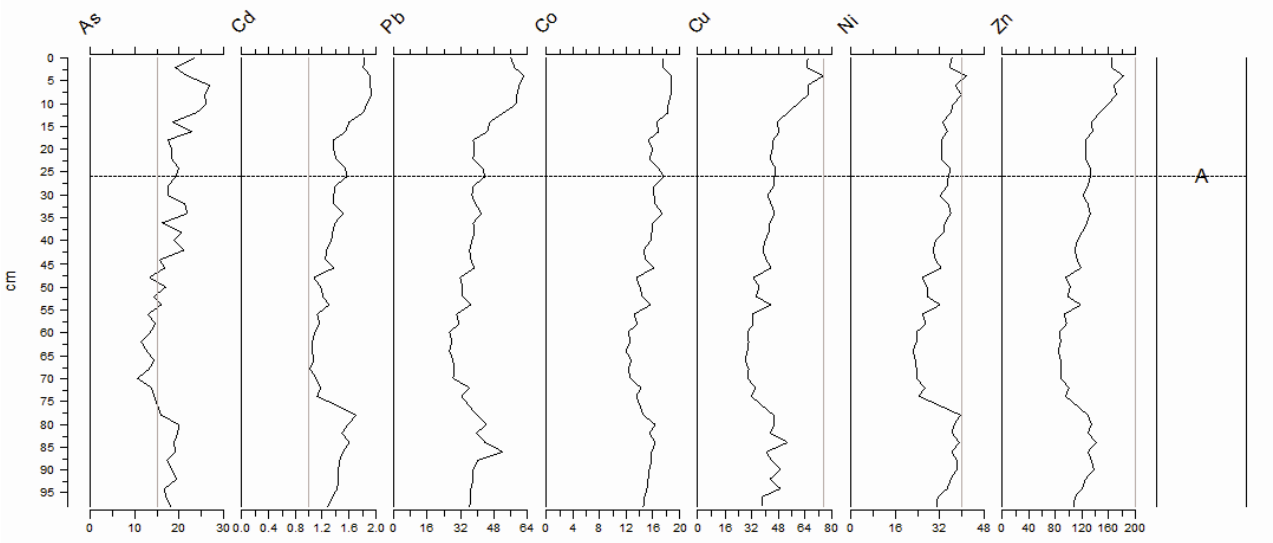

Fig. 4. The metal distribution of the soil profile regarding the arsenic, cadmium, cobalt, copper, lead, nickel and zinc ($mg.kg^{-1}$).

Acknowledgement

The research was supported by the No. 68566 Hungarian Scientific Research Fund.

References

Alapi K. and Győri Z. 2003. Silt examinations in the active floodplain of the River Tisza, loaded by heavy metals. Acta Agraria Debreceniensis 6 p. (in Hungarian with English abstract)

Black M. and William P. 2001. Preliminary assessment of metal toxicity in the Middle Tisza River (Hungary)

flood plain. J. of Soils and Sediments 1(4), 213-216.
Braun M., Szalóki I., Posta J. and Dezső Z. 2003. Estimation of the sediment deposition rate in the active floodplain of the River Tisza. MHT XXI. Vándorgyűlés 2003. július 2-4. CD-Proc. (in Hungarian)
Ciszewski D. 2003. Heavy metals in vertical profiles of the middle Odra River overbank sediments: evidence for pollution changes. Water, Air and Soil Pollution 143 (1-4): 81-98.
Dezső Z., Szabó Sz., Bihari Á. 2009. Investigation of the sedimentation of the active floodplain of Tisza based on gamma-spectrostropic analysis of ^{137}Cs-isotopes. In: Mócsy I. – Szacsvai K. – Urák I. – Zsigmond A R. szerk: Proc. V. Kárpát-medencei Környezettudományi Konferencia, Sapientia-Erdélyi Magyar Tudományegyetem, Kolozsvár pp. 443-438. (in Hungarian with English abstract)
Farsang A., Cser V., Barta K., Mezősi G., Erdei L., Bartha B., Fekete I., Pozsonyi E. 2007. Application of phytoremedation on extremely contaminated soils. 56 (2): 317-332. (in Hungarian with English abstract)
Filep Gy. 1999. Soil Chemistry. Processes and constituens. Akadémiai Kiadó, Budapest, 332 p.
Juggins S. 2003. C2 Software for ecological and palaeoecological data analysis and visualisation. Tutorial Version 1.3 School of Geography, Politics and Sociology, Newcastle University http://www.staff.ncl.ac.uk/stephen.juggins
Győri Zs., Végvári P. 1981. Physical and chemical conditions in the sediments in the sediments of the Tisza and its tributaries. Tiscia 16: 13-43.
Hargitai L. 1981. Determination of the environmental capacity of soils based on the humic substances. Agrokémia és Talajtan 32: 360-364. (in Hungarian with English abstract)
Hum L. 2005. Dirty gold. The floodwaves of 2000 contaminated with cyanide and heavy metals, and the heavy metal content of the sediments. A környezettudomány elmélete és gyakorlata c. konferencia, Szeged, Proceeidings on CD 10 p. (in Hungarian)
Hum L. and Matschullat J. 2002. Heavy metal and arsenic content of the sediments of the River Tisza and its tributaries. Autumn-winter condition of 1999/2000. Hidrológiai Közlöny 82(1): 23-30. (in Hungarian with English abstract)
Hungarian Standard MSZ-08-1722/1989. Soil analysis. Determintaion of soluble toxic element and heavy metal content of the soils (In Hungarian). Magyar Köztársaság Mezőgazdasági és Élelmezésügyi Ágazati Szabvány, 11 p.
Hungarian Standard MSZ-08-0206/2-1978. Analysis of the chemical properties of the soils. Laboratory investgations (pH, alkality, water soluble total salt content, hydrolitic and exchangable acidity) (In Hungarian), Mezőgazdasági és Élelmezésügyi Ágazati Szabvány, 12 p.
Hungarian Standard MSZ-08-0210-1977. Determination of the organic carbon content of the soil (In Hungarian). Mezőgazdasági és Élelmezésügyi Ágazati Szabvány, 6 p.
Kádár I. and Pálvölgyi L. 2005. Effects of microelement loads on sunflower grown on calcareos Chernozem soils. Agrokémia és Talajtan 52 (1-2): 79-92. (in Hungarian with English abstract)
Lakanen E. and Erviö R. 1971. A comparision of eight extractants for the determination of plant available micronutrients in soils. Acta Agr. Fenn. 123: 223-232.
Livens F.R. 1991.Chemical reactions of metals with humic materials. Environ. Pollution 70 (3): 183-208.
Sándor A. and Kiss T. 2009. Land use challenges and their effect on floodplain aggradation along the Middle-Tisza River, Hungary. Acta Geographica Debrecina Landscape & Environment 3 (1): 1-10.
Stefanovits P., Filep Gy,, Füleki Gy. 1999. Soil science. Mezőgazda Kiadó, Budapest (in Hungarian)
Szabó Gy. 2000. Geographycal study of heavy metals in soils and plants in a sample area of the North Hungarian Mountains. Studia Geographica, Debrecen (in Hungarian with English summary)
Szabó Sz., Ágoston Cs., Braun M., Keresztúri P., Szabó Gy. 2008a. Cadmium and zinc uptake of rye-grass as related to soil type and different land use. Cereal Research Communications 36: 427-430.
Szabó Sz., Posta J., Gosztonyi Gy., Mészáros I., Prokisch J. 2008b. Heavy metal content of flood sediments and plants near the River Tisza. Acta Geographica Debrecina Landscape & Environment Series 2 (2): 120-131.
Szalai Z. 1998. Trace metal pollution and microtopography in a floodplain. Geografia Fisica e Dinamica Quaternaria 21: 75-78.
TWQWS - Tisza Water Quality Warning System. The measurement data of the monitoring station in Técső (in Hungarian). www.rivermonitoring.hu. Downloaded: 1. February, 2009.

Special Session S02
Tectonostratigraphic Terranes in the Balkan region

Scientific Annals, School of Geology, Aristotle University of Thessaloniki Proceedings of the XIX CBGA Congress, Thessaloniki, Greece	Special volume 100	141-147	Thessaloniki 2010

THE PALAEOGEOGRAPHIC POSITION OF THE JADAR BLOCK (VARDAR ZONE, NW SERBIA) IN THE EARLY CARBONIFEROUS

Korn D.[1], Sudar M.[2], Novak M.[3] and Jovanović D.[4]

[1] *Museum für Naturkunde, Leibniz Institute at the Humboldt University Berlin, Invalidenstraße 43, 10115 Berlin, Germany; dieter.korn@mfn-berlin.de*
[2] *Department of Palaeontology, Faculty of Mining and Geology, University of Belgrade, Kamenička 6, PO Box 162, 11000 Belgrade, Serbia; sudar@eunet.rs*
[3] *Geological Survey of Slovenia, Dimičeva 14, 1000 Ljubljana, Slovenia; matevz.novak@geo-zs.si*
[4] *Geological Institute of Serbia, Rovinjska 12, 11000 Belgrade, Serbia; djdivna@gmail.com*

Abstract: The Milivojevića Kamenjar section in Družetić (NW Serbia) is the most diverse Carboniferous ammonoid occurrence on the Balkan Peninsula. It contains two faunal complexes, an early Late Viséan and a fauna from the Viséan-Serpukhovian boundary. The early Late Viséan assemblage is similar to time equivalent occurrences of the North Variscides and north-western Africa. It is integrated in a cosmopolitan ammonoid distribution of this time interval. The Viséan-Serpukhovian boundary assemblage is very different to its time equivalents from the North Variscides and as a result indicates provincialism; it belongs to the South Variscan–North Gondwanan faunal realm and is closely related to the occurrences in the Cantabrian Mountains of Spain and the South Urals.

Keywords: Viséan, Serpukhovian, palaeobiogeography, Ammonoidea, NW Serbia

1. Introduction

The distribution of Palaeozoic terranes between the supercontinents Laurussia and Gondwana is poorly understood, in particular, the precise palaeogeographic position of the occurrences of Carboniferous sedimentary rocks on the Balkan Peninsula is still an unsolved problem. Another point of contention is the timing of the closure of the Palaeotethys Ocean; the traditional model postulates a very close approximation of Laurussia and Gondwana in Early Carboniferous times (e.g., Matte, 1991), whereas other authors (e.g., Stampfli and Borel, 2002; Cocks and Torsvik, 2006) postulate a wide ocean between the two supercontinents at this time.

Analyses of time-equivalent ammonoid assemblages, including the occurrences on the Balkan Peninsula, may help to understand the relationships between the various regions with Carboniferous rock successions. We analysed the faunal spectrum of two time intervals, which are widely represented by ammonoid faunas, (1) the early Late Viséan (middle Asbian), and (2) the early Serpukhovian (Pendleian) with respect to similarity and dissimilarity between the regions. Based on the occurrence of ammonoid genera, a cluster analysis was achieved, and the results can be discussed in the context of geological data.

Up to now, only one occurrence of Early Carboniferous ammonoids is known from the Jadar Block, and only one further occurrence, i.e. Prača near Sarajevo (Kittl, 1904), has been described from the Balkan Peninsula. At the Milivojevića Kamenjar site in Družetić (which will be referred to later in the text as Družetić) in north-western Serbia (first described by Stevanović and Kullmann, 1962), two ammonoid-bearing intervals are exposed: (1) an early Late Viséan horizon containing the genera *Entogonites*, *Beyrichoceras*, *Goniatites*, and *Prolecanites*, and (2) a latest Viséan – early Serpukhovian horizon with *Pachylyroceras*, *Dombarites*, *Rhymmoceras*, *Irinoceras*, and *Uralopronorites*. Both intervals can be rather precisely correlated with the time-equivalent ammonoid occurrences in Central and North-western Europe, North Africa, the South Urals, western United States, etc.

2. Geographic and geologic position of the Jadar Block

The Jadar Block is located at the southern margin of the Pannonian Basin: mostly in north-western

Serbia, southern Srem, and partially westward over the Drina River in eastern Bosnia. The name of this tectonostratigraphic unit, which is presently a part of the Vardar Zone, derived from the 'Jadar development of Palaeozoic' (Simić, 1938). The Jadar Block is considered as an isolated, exotic block terrane, in which Dinaridic features predominate. It was incorporated into the Vardar Zone before the Late Cretaceous (Karamata et al., 2000; Karamata, 2006). In this area, deposition of sediments took place during the Variscan and Early Alpine evolution with obvious similarities to time-equivalent successions of the 'Bükkium' (NE Hungary), the Sana-Una terranes (NW Bosnia and Herzegovina), and even the Carnic Alps (Protić et al., 2000; Filipović et al., 2003).

3. Methods

We investigated the ammonoid occurrences of Late Viséan and Serpukhovian age based on the comprehensive database AMMON (Korn and Ilg, 2009) by means of a cluster analysis. In this analysis, we paid special attention to the two stratigraphic ages represented in the Družetić outcrop, for an integration of this occurrence in the global scale. These two time slices are:

3. 1. Early Late Viséan – this time interval is rather easy to characterise because it almost perfectly correlates with the *Entogonites* Genus Zone (Korn et al., 2007). It marks the transition from an interval with rather low ammonoid diversity (Early and Middle Viséan), which is globally represented only by a few considerably rich ammonoid occurrences (North Urals: Kusina, 1980; North England: Riley, 1996; Gourara region of Algeria: Bockwinkel et al., 2010) to the time period in which the Ammonoidea shows a rapid diversification (Late Viséan, Serpukhovian; Ruzhencev and Bogoslovskaya, 1971). For our analysis, we included only those occurrences with at least five ammonoid genera. These seven occurrences are (literature sources in brackets):

- Anti-Atlas (Korn et al., 1999; 2005)
- North England (e.g., Bisat, 1934, 1952; Riley, 1993)
- Rhenish Mountains (e.g., Nicolaus, 1963; Korn, 1988, 1990)
- Antler Foreland Basin (Korn and Titus, unpublished data)
- Alaska (Gordon, 1957)
- South Portugal (Korn, 1997a; Korn and Horn, 1997)
- Družetić (this article)

The revised spectrum of genera recorded in Družetić is composed of the following genera:

Entogonites – *E. tetragonus* (Kullmann, 1962) (very common), *E. grimmeri* (Kittl, 1904), and *E.* cf. *nasutus* (Schmidt, 1941).

Ubites (a genus newly described by Korn (in Korn et al. in press) with the new species *U. filipovici*).

Goniatites – *G. crenistriatoides* (Kullmann, 1962).

Beyrichoceras, *Bollandites*, *Prolecanites*, and an undescribed new genus with undescribed species.

The analysis is based on a very heterogeneous data set. While the north-west Serbian occurrence in Družetić is based on only one single small outcrop, some others (Anti-Atlas, Alaska, South Portugal) are based on a limited area of a few square metres, and some (North England, Rhenish Mountains) contain numerous outcrops and have a long history of investigation. For this reason, a sampling bias may influence the analysis.

Entogonites is present in all the regions except for South Portugal and serves as a good index ammonoid. It is remarkable that the genus diversity within the occurrences ranges between five and nine and that no extraordinarily rich occurrences are known.

3.2. Viséan-Serpukhovian – for our analysis we focused particularly on the latest Viséan/early Serpukhovian transition (i.e., the transition from the Brigantian into the Pendleian). This time interval is somewhat difficult to correlate on a global scale because of significant ammonoid provincialism (Korn 1997b). We included the following occurrences, all with at least seven genera:

- South Urals (Ruzhencev and Bogoslovskaya, 1971)
- Rhenish Mountains (Horn, 1960; Korn, 2006)
- British Isles (Bisat, 1950; Yates, 1962)
- American Midcontinent (e.g., Miller and Furnish, 1940; Gordon, 1965)
- Antler Foreland Basin (Youngquist, 1949; Titus, 2000)
- Béchar Basin, Algeria (Pareyn, 1961)
- Cantabrian Mountains (Kullmann, 1962; Wagner-Gentis, 1963, 1980)
- Družetić (Korn et al. in press and in this article)

The ammonoid fauna from Družetić requires revision, but at the moment it is possible to identify the following genera in the fauna:

Irinoceras – I. stevanovici (Kullmann, 1962).
Dombarites – D. wocklumerioides (Kullmann, 1962) and possibly also *D. serbicus* (Kullmann, 1962).
Rhymmoceras – R. gracilentum Ruzhencev, 1958.
Glaphyrites – G. europaeus (Kullmann, 1962).
Pachylyroceras with an undescribed species.
Dombarocanites – D. chancharensis Ruzhencev, 1949.
Uralopronorites – U. mirus Ruzhencev, 1947.

Some of the determinations have to be confirmed after revision of the fauna. "*Eoasianites europaeus* Kullmann, 1962", for instance was assigned to *Glaphyrites* by Ruzhencev and Bogoslovskaya (1971, p. 37), but the occurrence in Družetić appears to be stratigraphically too old for this genus.

In contrast to the early Late Viséan occurrences, the genus richness differs markedly between the analysed regions, with the South Urals occupying an outstanding position with 27 genera, followed by the Béchar Basin in Algeria with 13 genera.

The cluster analysis was performed using Ward's linkage method, because this is only little sensitive for samples of different size.

4. Results and discussion

4.1. Early Late Viséan

For the early Late Viséan, three major provinces of occurrences of ammonoid genera can be separated (Figs. 1, 2):
(1) An eastern North American province (including Alaska and the Antler Foreland Basin).
(2) A North Variscan province (Central Europe, British Isles, Portugal), and
(3) A South Variscan/ North Gondwanan province with the Anti-Atlas and the Jadar Block.

The analysis is not very stable because of the low number of co-occurring ammonoid genera and their rather cosmopolitan distribution pattern. *Goniatites*, for instance has an almost global distribution and *Entogonites* has been reported from Alaska, Utah, Ireland, England, Germany, Poland, the Czech Republic, Bosnia and Herzegovina, Serbia, and Morocco (Fig. 1). It means that correspondence of these shelf areas must have existed in this time interval. Even more, the presence of the species *Entogonites grimmeri* (Kittl, 1904) at Prača near Sarajevo, Družetić in north-western Serbia, the Rhenish Mountains, and the British Isles suggests that the occurrences on the Balkan Peninsula were rather closely connected with the Rhenohercynian Basin. This pattern indicates that a closed Variscan land barrier had not been established in early Late Viséan times.

Fig. 1. Palaeogeographic map for the North Atlantic region of the early Late Viséan (after Scotese 1997; image (modified) by Ron Blakey, Flagstaff, Arizona, showing the distribution of the genera *Entogonites* and *Goniatites*. [AK – Alaska; YU – Yukon; NV – Nevada; UT – Utah; OK – Oklahoma; AR – Arkansas; MM – Moroccan Meseta; SP – South Portugal; IR – Ireland; BE – Belgium; RM – Rhenish Mountains; GB – England; MS – Moravia and Silesia; HC – Holy Cross Mountains; SU – South Urals; NU – North Urals; CM – Cantabrian Mountains; AA – Anti–Atlas; SV – Saoura Valley; BO – Bosnia and Herzegovina; JB – Jadar Block].

4.2. Early Serpukhovian

The distribution is different in the early Serpukhovian. Two major realms can be separated, both with two provinces (Figs. 3, 4):
(1) A south-eastern realm includes (1a) a Uralian-North Gondwanan province (including the South Urals and the Béchar Basin of Algeria) and (1b) a South Variscan province (Cantabrian Mountains and the Jadar Block).
(2) A north-western realm is composed of (2a) a North Variscan province (Central Europe, British Isles) and (2b) a North American province (American Midcontinent and Antler Foreland Basin).

The analysis is rather robust because of the high number of ammonoid genera (in total 40) and the limited palaeogeographic range of many of them. The strict separation of the two realms, visible in high distance values (Fig. 4) is caused by a partly endemic evolution in the various palaeogeographic regions including limited exchange of faunal elements. The evolution of the important family Go-

niatitidae, for instance, was truncated in the North Variscan province in the mid-Brigantian (with *Lusitanoceras* being the last representative). Occurrences in North America show very few descendents of the Goniatitidae up to horizons near the Viséan-Serpukhovian boundary. In the Urals, the goniatitid descendents are the predominant elements of the faunas on both sides of the Viséan-Serpukhovian boundary; they belong to at least seven genera (*Hypergoniatites*, *Neogoniatites*, *Dombarites*, *Deleshumardites*, *Proshumardites*, *Platygoniatites* and *Delepinoceras*) with numerous species. In the absolute numbers of specimens they outnumber the other co-occurring taxa. Occurrences in the Béchar Basin of Algeria, the Cantabrian Mountains, and in Družetić are similar in this respect. Similarly, the family Neoglyphioceratidae becomes extinct much earlier (mid-Brigantian) in the North Variscan province, but survives with numerous descendents in the Uralian-North Gondwanan province. This pattern is contrasting the evolution of the Girtyoceratids (genera *Girtyoceras*, *Edmooroceras*, *Tumulites*, *Eumorphoceras*), which are well-represented in the North Variscan and North American provinces, but are a lot less common in the other regions.

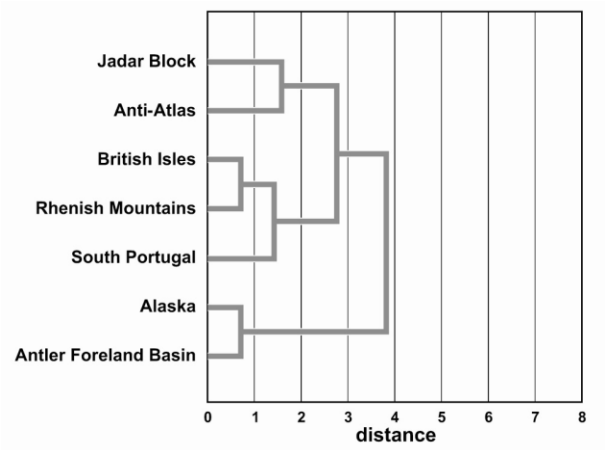

Fig. 2. Dendrogram of a hierarchical cluster analysis using Ward's linkage algorithm for the early Late Viséan ammonoid occurrences.

5. Conclusion

It can be concluded that the single ammonoid occurrence in Družetić indicates, for the early Late Viséan and early Serpukhovian, close relationships to other South Variscan-North Gondwanan occurrences. While for the early Late Viséan correspondence of the ammonoid faunas with the occurrences in Central Europe, the British Isles, as well as North America (Utah, Alaska) can be postulated, clear separation took place until the early Serpukhovian, for which the spectrum of genera suggests a South Variscan position of the Jadar Block.

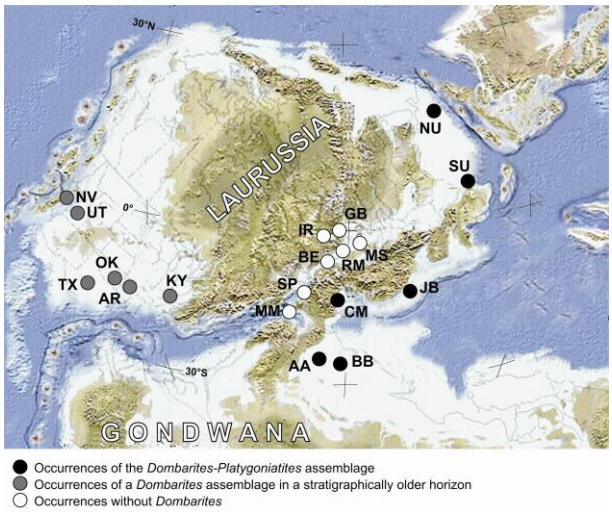

Fig. 3. Palaeogeographic map for the North Atlantic region of the Viséan-Serpukhovian boundary, after Scotese 1997; image (modified) by Ron Blakey, Flagstaff, Arizona. [NV – Nevada; UT – Utah; TX – Texas; OK – Oklahoma; AR – Arkansas; KY – Kentucky; MM – Moroccan Meseta; SP – South Portugal; IR – Ireland; BE – Belgium; RM – Rhenish Mountains; GB – England; MS – Moravia and Silesia; SU – South Urals; NU – North Urals; CM – Cantabrian Mountains; AA – Anti–Atlas; BB – Béchar Basin; JB – Jadar Block].

This interpretation is based on the presence of distinct genera (i.e., *Dombarites*, *Pachylyroceras*, *Rhymmoceras*) in the assemblage from Družetić and the absence of others (i.e., *Edmooroceras*, *Tumulites*), which are to be expected in faunas of this age. Not a single genus from Družetić is known from North Variscan time equivalent strata, but some of them (*Dombarites*, *Ophilyroceras*, *Rhymmoceras*) are characteristic elements in the occurrences of the South Urals and the Cantabrian Mountains.

It means that the generally increasing provincialism of the Early Carboniferous ammonoid faunas can also be observed in the single outcrop in Družetić. Here the stratigraphically older horizon (early Late Viséan) still contains some cosmopolitan elements, but in the younger horizon (with the turn into the Serpukhovian) it becomes separated from the North Variscan province and clearly belongs to the south-eastern biogeographic realm.

According to the ammonoid records, the palaeo-

geographic position of the Jadar Block at the southern flank of the Variscan would be the most likely situation. As Filipović et al. (2003) have pointed out, there exists a close resemblance between the Jadar Block, the Bükk (north-eastern Hungary), and the Carnic Alps (Austria, Italy) in terms of the sedimentological development during the Late Carboniferous and Permian. Unfortunately, there are no Viséan and Serpukhovian ammonoid faunas known from the Bükk and the Carnic Alps, and hence a direct comparison with the Jadar Block is not possible in this respect.

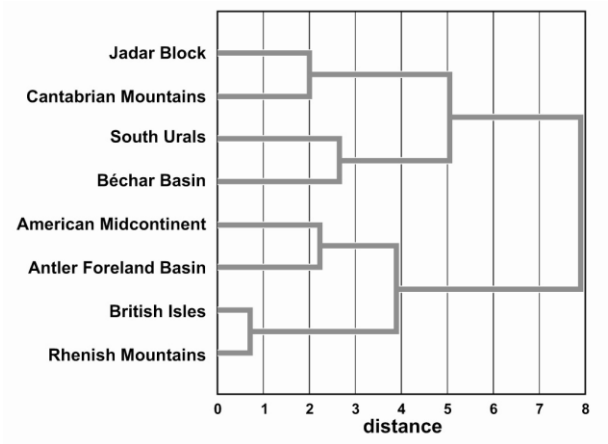

Fig. 4. Dendrogram of a hierarchical cluster analysis using Ward's linkage algorithm for the ammonoid occurrences at the Viséan-Serpukhovian boundary.

The ammonoid results confirm the palaeogeographic reconstruction by Stampfli and Borel (2002) and Stampfli and Kozur (2006), who placed these terranes in a position adjacent to the southern margin of Laurussia. However, these authors postulated a wide (more than 1,000 km) Early Carboniferous (~340 Ma) Palaeotethys Ocean, which was closed until the Bashkirian. Ammonoid relationships between the South Variscan and North Gondwanan shelves, however suggest that such a wide ocean is very unlikely and that at least the western end of the Palaeotethys (north-western Africa) had to be much narrower to allow faunal exchanges between South Variscan and North Gondwanan shelves during the Late Viséan and Serpukhovian.

Ackknowledgements

We thank Sonny Walton (Potsdam) for revising the English text and to the anonymous reviewers for the review of the manuscript.

References

Bisat W.S., 1934. The goniatites of the *Beyrichoceras* zone in the north of England. Proceedings of the Yorkshire Geological Society, 22, 280-309.

Bisat W.S., 1950. The junction faunas of the Viséan and Namurian. Transactions of the Leeds Geologist Association, 6 (3), 10-26.

Bisat W.S., 1952. The goniatite succession at Cowdale Clough, Barnoldswick, Yorkshire. Transactions of the Leeds Geologist Association, 6 (4), 155-181.

Bockwinkel J., Korn D. and Ebbighausen V., 2010. The ammonoids from the Argiles de Timimoun of Timimoun (Early and Middle Viséan; Gourara, Algeria). Fossil Record, 13 (1), 215-278.

Cocks L.R.M. and Torsvik T.H., 2006. European geography in a global context from the Vendian to the end of the Palaeozoic. In: D. Gee, R.A. Stephenson (Eds.), European Lithosphere Dynamics, Geological Society London, Memoirs, 32, 83–96.

Filipović I., Jovanović D., Sudar M., Pelikán P., Kovács S., Less Gy. and Hips K., 2003. Comparison of the Variscan-Early Apline evolution of the Jadar Block (NW Serbia) and "Bükkium" (NE Hungary) terranes; some paleogeographic implications. Slovak Geological Magazine, 9 (1), 23-40.

Gordon M.jr., 1957. Missisippian Cephalopods of Northern and Eastern Alaska. Professional Papers of the United States Geological Survey, 283, 1-61.

Gordon M.jr., 1965. Carboniferous Cephalopods of Arkansas. Professional Papers of the United States Geological Survey, 460, 1-322.

Horn M., 1960. The zone of *Eumorphoceras pseudobilingue* in the Sauerland. Fortschritte in der Geologie von Rheinland und Westfalen, 3,1, 303-342 (in German: Die Zone des *Eumorphoceras pseudobilingue* im Sauerland).

Karamata S., 2006. The geological development of the Balkan Peninsula related to the approach, collision and compression of Gondwanan and Eurasian units. In: Robertson A. H. F. and Mountrakis D. (eds.), Tectonic Development of the Eastern Mediterranean Region, Geological Society of London, Special Publications, 260, 155-178.

Karamata S., Olujić J., Protić Lj., Milovanović D., Vujnović L., Popević A., Memović E. Radovanović Z. and Resimić-Šarić K., 2000. The Western Belt of the Vardar Zone - the remnant of a marginal sea. In: Karamata S. and Janković S. (eds.), Proceedings of the International Symposium "Geology and Metallogeny of the Dinarides and the Vardar Zone", Academy of Sciences and Arts of the Republic of Srpska, Collections and Monographs, 1, 131-135.

Kittl E., 1904. Geology of the vicicity of Sarajevo. Jahrbuch der Kaiserlich-Königlichen Geologischen Reichsanstalt, 53 (for 1903), 515-748 (in German: Geologie der Umgegend von Sarajewo).

Korn D., 1988. The goniatites of the Kulmplattenkalk (Cephalopoda, Ammonoidea; Early Carboniferous;

Rhenish Mountains). Geologie und Paläontologie in Westfalen, 11, 1-293 (in German: Die Goniatiten des Kulmplattenkalkes (Cephalopoda, Ammonoidea; Unterkarbon; Rheinisches Schiefergebirge).

Korn D., 1990. Additional goniatites of the late Viséan from the Sauerland (Cephalopoda, Ammonoidea; Early Carboniferous; Rhenish Mountains). Geologie und Paläontologie in Westfalen, 15, 11-69 (in German: Weitere Goniatiten aus dem Ober-Visé des Sauerlandes (Cephalopoda, Ammonoidea; Unterkarbon; Rheinisches Schiefergebirge).

Korn D., 1997a. The Palaeozoic ammonoids of the South Portuguese Zone. Memórias do Instituto Geológico e Mineiro, 33, 1-131.

Korn D., 1997b. Evolution of the Goniatitaceae and Viséan-Namurian biogeography. Acta Palaeontologica Polonica, 42, 177-199.

Korn, D., 2006. Ammonoids. in: Amler, M.R.W.: Stratigraphie von Deutschland VI. Unterkarbon (Mississippium). Schriftenreihe der Deutschen Gesellschaft für Geowissenschaften, 41, 147-170 (in German).

Korn, D., Bockwinkel J. and Ebbighausen V., 2007. The Tournaisian and Viséan ammonoid stratigraphy in North Africa. Neues Jahrbuch für Geologie und Paläontologie, 243 (2), 127-148.

Korn D. and Horn K., 1997. The Late Viséan (Early Carboniferous) goniatite stratigraphy in the South Portuguese Zone, a comparison with the Rhenish Massif. Newsletters on Stratigraphy, 35, 97-113.

Korn D. and Ilg A., 2009. AMMON, www.wahre-staerke.com/ammon/

Korn D., Jovanović D., Novak N. and Sudar M.N., (in press). The age of the Milivojevića Kamenjar fossil section in Družetić near Valjevo (Late Devonian – Serpukhovian; NW Serbia). Geologica Carpathica.

Korn D., Klug C. and Mapes R.H., 1999. Viséan and Early Namurian Ammonoids from the Tafilalt (Eastern Anti-Atlas, Morocco). Abhandlungen der Geologischen Bundesanstalt, 54, 345-375.

Korn D., Klug C. and Mapes R.H., 2005. The Lazarus ammonoid family Goniatitidae, the tetrangularly coiled Entogonitidae, and Mississippian biogeography. Journal of Paleontology, 79 (2), 356-365.

Kullmann J., 1962. The goniatites of the Namurian Stage (Late Carboniferous) in the Cantabrian Mountains, northern Spain. Abhandlungen der Akademie der Wissenschaften und der Literatur, Mainz, mathematisch-naturwissenschaftliche Klasse, 1962 (6), 259-377 (in German: Die Goniatiten der Namur-Stufe (Oberkarbon) im Kantabrischen Gebirge, Nordspanien).

Kusina L.F., 1980. Saourian ammonoids. Trudy Paleontologicheskogo Instituta Akademiya Nauk SSSR, 181, 1-108 (in Russian).

Matte P., 1991. Accretionary history and crustal evolution of the Variscan belt in Western Europe. Tectonophysics, 196 (3-4), 309-337.

Miller A.K. and Furnish W.M., 1940. Studies on Carboniferous ammonoids: parts 1-4. Journal of Paleontology, 14, 356-377.

Nicolaus H.-J., 1963. The stratigraphy and fauna of the *crenistria* Zone in the Kulm of the Rhenish Mountains. Beihefte zum Geologischen Jahrbuch, 53, 1-246 (in German: Zur Stratigraphie und Fauna der *crenistria*-Zone im Kulm des Rheinischen Schiefergebirges).

Pareyn C., 1961. The Carboniferous Mountains of the South Oran Sahara. Volume II. Stratigraphic palaeontology. Publications du Centre de Recherches Sahariennes, Série Géologie, 1, 1-244. (in French: Les Massifs Carbonifères du Sahara Sud-Oranais. Tome II. Paléontologie stratigraphique)

Protić Lj., Filipović I., Pelikán P., Jovanović D., Kovács S., Sudar M., Hips K., Less Gy. and Cvijić R., 2000. Correlation of the Carboniferous, Permian and Triassic sequences of the Jadar Block, Sana-Una and „Bükkium" terranes. In: Karamata S. and Janković S. (eds.), Proceedings of the International Symposium "Geology and Metallogeny of the Dinarides and the Vardar Zone", Academy of Sciences and Arts of the Republic of Srpska, Collections and Monographs, 1, 61-69.

Riley N.J., 1993. Dinantian (Lower Carboniferous) biostratigraphy and chronostratigraphy in the British Isles. Journal of the Geological Society, London, 150, 427-446.

Riley N.J., 1996. Mid-Dinantian ammonoids from the Craven Basin, northwest England. Special papers in Palaeontology, 53, 1-87.

Ruzhencev V.E., 1947. Evolyution of the family Medlicottiidae Karpinsky. Vestnik Akademiy Nauk SSSR, 8, 37-50 (in Russian).

Ruzhencev V.E., 1949. Systematics and evolyution of the families Pronoritidae Frech and Medlicottiidae Karpinsky. Trudy Paleontologicheskogo Instituta Akademiya Nauk SSSR, 19, 1-206 (in Russian).

Ruzhencev V.E., 1958. Two new genera of goniatites of the early Namurian of the South Urals. Doklady Akademiya Nauk SSSR, 122, 293-296 (in Russian).

Ruzhencev V.E. and Bogoslovskaya M.F., 1971. Namurian time in ammonoid evolution. Early Namurian ammonoids. Trudy Paleontologicheskogo Instituta Akademiya Nauk SSSR, 133, 1-382 (in Russian).

Schmidt H., 1941. A new fauna with *Pericyclus* from Riefensbeek in the Harz Mountains. Jahrbuch der Reichsstelle für Bodenforschung, 60 (for 1939), 148-156 (in German: Eine neue Fauna mit *Pericyclus* von Riefensbeek im Harz).

Simić V., 1938. About the late Palaeozoic facies in western Serbia. Vesnik Geološkog Instituta Kraljevine Jugoslavije, 6, 83-108 (in Serbian, German summary: Über die Jungpaläozoischen fazies in Westserbien).

Stampfli G.M and Borel G.D., 2002. A plate tectonic model for the Paleozoic and Mesozoic constrained by dynamic plate boundaries and restored synthetic

oceanic isochrons. Earth and Planetary Science Letters, 196 (2002), 17–33.

Stampfli G.M. and Kozur H.W., 2006. Europe from the Variscan to the Alpine cycles. In: D. Gee, R.A. Stephenson (Eds.), European Lithosphere Dynamics, Geological Society London, Memoirs, 32, 57–82.

Stevanović P. and Kullmann J., 1962: Namurian at Družetić in western Serbia and its goniatite fauna. Glasnik Prirodnjačkog muzeja, A, 16-17, 45-112 (in Serbian and German: Namurian bei Družetić im Westlichen Serbien und seine Goniatitenfauna).

Titus A.L., 2000. Late Mississippian (Arnsbergian Stage-E2 chronozone) ammonoid paleontology and biostratigraphy of the Antler foreland basin, California. Bulletin of the Utah Geol. Survey, 131, 1-108.

Wagner-Gentis C.H.T., 1963. Lower Namurian goniatites from the Griotte limestone of the Cantabric Mountain Chain. Notas y comunicaciones del Instituto Geológico y Minero de España, 69, 5-42.

Wagner-Gentis C.H.T., 1980. Goniatites from the Viséan-Namurian junction beds in Palencia, NW Spain. Scripta Geologica, 55, 1-43.

Yates P.J., 1962. The Palaeontology of the Namurian rocks of Slieve Anierin, Co. Leitrim, Eire. Palaeontology, 5 (3), 355-443.

Youngquist W., 1949. The cephalopod fauna of the White Pine shale of Nevada. Journal of Paleontology, 23, 276-305.

Special Session S03
Circum Pannonian Terranes – Eastern Alps, Carpathians, Dinarides (tectono-stratigraphy, palaeotectonic evolution and present-day structure-presentation of monography TERRANES)

Scientific Annals, School of Geology, Aristotle University of Thessaloniki Proceedings of the XIX CBGA Congress, Thessaloniki, Greece	Special volume 100	149-156	Thessaloniki 2010

SUBDUCTION RELATED JURASSIC GRAVITY DEPOSITS IN BÜKK-DARNÓ AREA, NORTHEAST HUNGARY

Haas J.[1], Pelikán P.[2], Görög Á.[3], Ozsvárt P.[4], Józsa S.[5], Kövér Sz.[1]

[1] *Geological Research Group of the Hungarian Academy of Sciences, Eötvös Loránd University, Pázmány sétány 1/c, 1117 Budapest, Hungary, haas@ludens.elte.hu, koversz@yahoo.hu*
[2]*Geological Institute of Hungary, Stefánia ut 14, 1143 Budapest, Hungary, pelikan@mafi.hu*
[3]*Paleontological Department, Eötvös Loránd University, Pázmány sétány 1/c, 1117 Budapest, Hungary, gorog@ludens.elte.hu*
[4]*Research Group for Paleontology of the Hungarian Academy of Sciences, Natural History Museum, P.O. Box 137, 1431 Budapest, Hungary, ozsi@nhmus.hu*
[5]*Petrographical and Geochemical Department Eötvös Loránd University, Pázmány sétány 1/c, 1117 Budapest, Hungary, sandor.jozsa@geology.elte.hu*

Abstract: Jurassic sedimentary sequences of pelagic basin facies and slope-related gravity deposits occur in several places in North Hungary (Bükk Mountains, Darnó area, Rudabánya Hills). The aim of the paper is to characterise the Jurassic formations of the study area with special regard to the redeposited sedimentary rocks in order to get information on the provenance of the clasts, and the mode and time of their redeposition. In the Bükk Mts., the Mónosbél Group contains various redeposited sediments showing an upward coarsening trend. They were deposited in Bathonian in subduction-related basins formed in the course of subduction of the Neotethys Ocean. The lower part of the complex is typified by pelagic carbonates, shales and radiolarites with andesitic volcaniclast intercalations. The higher part is characterised by polymict olistostromes. Large olistoliths that are predominantly blocks of Bajocian shallow marine limestones (Bükkzsérc Limestone) appear in the upper part of the sequence. Evolutionary phases of the sedimentry basins were defined from an early extensional stage of the subduction, through island-arc formation, to the compressional stages when onset of nappe stacking gave rise to formation of polymict olistostromes and then redeposition of large blocks derived from out-of-sequence nappes of the previous platform foreland. Remarkable differences between the composition of the redeposited clasts in the olistostromes of the Bükk and Darnó area indicate deposition in different subduction-related subbasins.

Keywords: Bükk Mountains, Jurassic, facies analysis, gravity deposits, subduction-related basins.

1. Introduction

In the Bükk Mountains presence of Jurassic sedimentary and volcanic formations was recognised only at the beginning of the 1980-ies (Bérczi-Makk and Pelikán, 1984). Studies performed in the latest decade led to the conclusions that Jurassic formations akin to those in the Bükk Mts. occur also in the Darnó area, in western foreland of the Bükk Mts. and in the pre-Tertiary basement of the Mátra Mts. (Kovács et al., 2008). The Jurassic formations were interpreted as elements of an accretionary complex formed during closure of the Neotethys Ocean and their close genetic relationships with the ophiolite mélange complex of the Dinarides were suggested (Pamić, 1997, 2003; Haas and Kovács, 2001, Dimitrijević et al., 2003) (Fig. 1). Striking similarity of the Upper Paleozoic and Triassic formations with the corresponding formations of the Dinarides has been known for a long time (Schréter, 1959; Balogh, 1964; Filipović et al., 2003). These considerations inspired the concept that the Bükk together with other terranes in North Hungary derived from the Dinaridic realm and got into its present-day setting via large-scale tectonic displacements in the Tertiary (Csontos and Nagymarosy, 1988).

2. Methods

Interpretation of history of basin evolution and paleo-environmental conditions controlled the accumulation of gravity deposits were based on sedi-

mentological investigations, petrographical analysis of the components of the clastic rocks and biostratigraphic studies of the matrix and the clastic components to get age data.

3. Results

In the area of the Bükk Mts. extensional tectonics led to formation of platforms and basins, that was accompanied by intense andesitic and then basaltic volcanism during the Mid-Triassic. Both platform and basin facies are overlain by red radiolarian chert yielded poorly preserved radiolarians indicating a wide Early Bajocian – Kimmeridgian age range (Bányahegy Radiolarite). Above it, dark grey to black shale occurs, containing sandstone, siltstone and claystone layers deposited via turbidity currents (Lökvölgy Formation). In some places, the Triassic formations are directly overlain by siliciclastic sandstones (Vaskapu Sandstone) in other places similar sandstones occur within or above the Lökvölgy Formation (Pelikán et al., 2005).

In the western part of the Bükk Mts. Jurassic basic magmatic rocks i.e. hyaloclastic lava flows and pillow lavas occur. Relation of the magmatic suits with the sedimentary formations is not perfectly clear. In some places the igneous rocks have thermal contact with the Lökvölgy Formation (Pelikán et al., 2005)

Above the siliciclastic series calcareous and siliceous basin and redeposited slope facies occur, referred as the Mónosbél Group (Pelikán et al., 2005). Within the group several lithofacies can be distinguished. In many cases they show interfingering or transitional features and some of them may appear as redeposited clasts, blocks. Among them the Oldalvölgy Formation is typically made up of alternating dark grey cherty limestone and black shale (silty claystone, sandstone) layers.

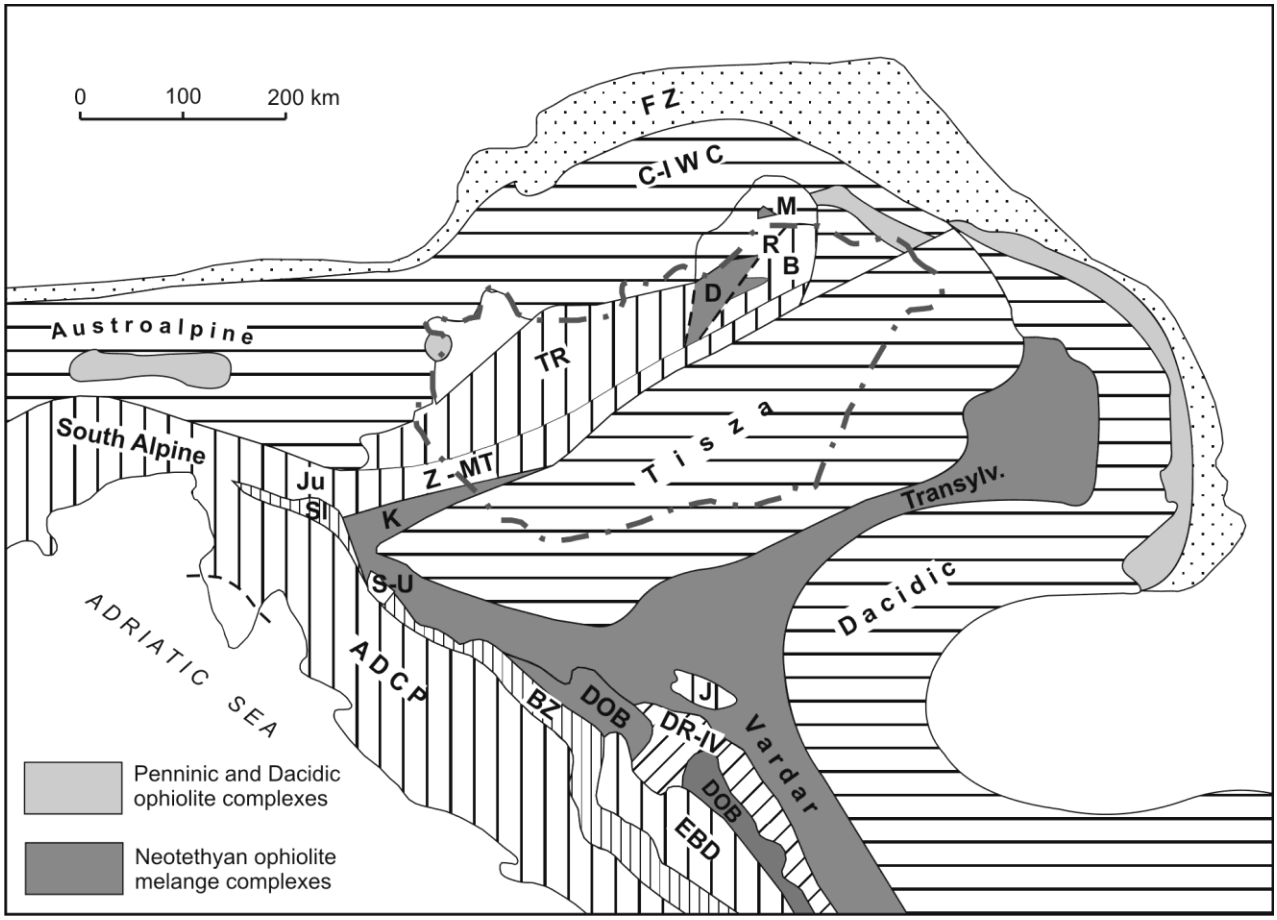

Fig. 1 Geographical and geological setting of the Bükk Unit within the Circum-Pannonian region. Abbreviations: ADCP – Adriatic–Dinaridic Carbonate Platform; B – Bükk Unit; BZ – Bosnian Zone; C-I WC – Central and Inner West Carpathians; D – Darnó Unit; DOB – Dinaridic Ophiolite Belt; DR-IV – Drina–Ivanica Unit; EBD – East Bosnian–Durmitor Unit; FZ – Helvetic and Outer Carpathian Flysch Zone; J – Jadar block; Ju – Julian Alps; K – Kalnik Unit; M – Meliata Unit; R – Rudabánya; Sl – Slovenian Trough; S-U – Sana–Una Unit; TR – Transdanubian Range Unit; Z-MT – Zagorje–Mid-Transdanubian Unit.

Most of the limestone layers have mudstone or peloidal wackestone texture but ooids and shallow marine bioclasts could also be recognised locally. Radiolarian and/or sponge spicule wackestones are also typical textures of the formation. These beds gradually progress into the Csipkéstető Radiolarite. Lateral and vertical transition between the Oldalvölgy Limestone and Csipkéstető Radiolarite are common. Volcaniclastic interbeds were encountered in these formations locally (Fig. 2). Andesite clasts are prevailing in the deepest and thickest bed whereas in the higher beds the basalt clasts are also present.

Polymict olistostrome beds typify the upper part of the series that was assigned to the Mónosbél Formation (Pelikán et al., 2005) (Fig. 2). Along with clasts of siliclastic rocks various volcanites and metamorphic rocks, oolitic carbonates are also common. The volcanic material is extremely variable in these beds including clasts of andesite, dacite, rhyolite and rarely basalt. In the majority of the studied occurrences the carbonate clasts are predominant. Based on their microfacies characteristics and in some cases their microfossil content, the limestone clasts derived from the previously deposited and consolidated Jurassic succession, rarely from carbonate platform and mostly from toe-of-slope (e.g. redeposited oolitic packstone, peloidal grainstone) and basin ("filament" wackestone, sponge spicule wackestone, radiolaria wackestone) facies. The radiolarite clasts are probably derived also from Jurassic basin facies. Limestone clasts containing shallow marine Triassic foraminifera were also encountered. Clasts derived from siliciclastic formations (silty claystone, siltstone, fine to medium grained quartz sandstone) are also common. These clasts probably derived also from the Jurassic succession (Vaskapu Sandstone). Clasts of fillite and micaschist must have been subject to metamorphism prior to the redeposition also occur, rarely.

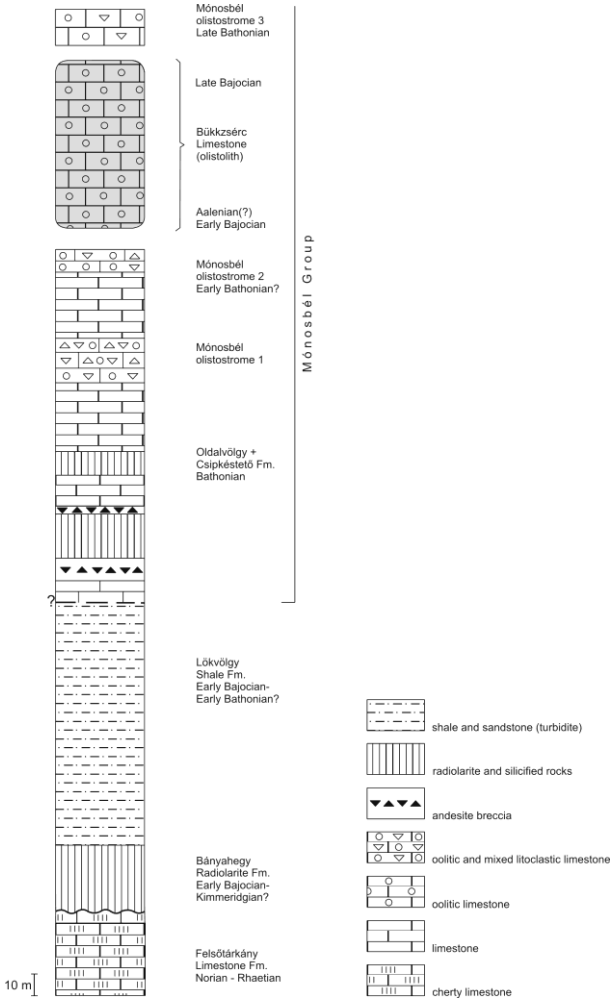

Fig. 2. General lithostratigraphic succession of the study area with indication of age data based on biostratigraphic results of the present study.

The Bükkzsérc Limestone is made up mostly of oolitic grainstone, and peloidal grainstone with intercalations of peloidal-filament wackestone and radiolarian wackestone and packstone representing platform foreslope and toe-of-slope facies (Haas et al., 2006). According to our new biostratigraphic (foraminifera) data this is the oldest unit of the Mónosbél Group. However, this lithofacies occur in the higher part of the Mónosbél Group (above or within the Oldalvölgy–Csipkéstető Formation) usually in smaller or larger redeposited blocks (olistolithes). Although in a lot of cases the geometry of the large blocks could not be unambiguously determined; the anomalous stratigraphic setting of the oolitic limestones suggests their redeposition in the form of olistolithes (Fig. 2).

Interpretation of the lithostratigraphic and biostratigraphic data and construction of a coherent chronostratigraphic scheme is not easy. There are uncertainties in the structural model which influence the assumed relations of the lithostratigraphic units and there are uncertainties in the radiolarian and foraminifera biostratigraphy as well. Evaluation of the new radiolarian data allowed a very wide time-range for the Bányahegy Radiolarite from the Early Bajocian to the Early Kimmeridgian. If the younger age date (younger than Bajocian) is valid, we have to find tectonic solution as it was done by Csontos (2000). However, if the Bányahegy Radiolarite is Early Bajocian, a continuous succession from the Bányahegy Radio-

larite through the Lökvölgy Formation to the Mónosbél Group cannot be excluded either. We have a few foraminifera data from the upper part of the Lökvölgy Formation suggesting Early Bajocian – Early Bathonian age. According to the foraminifera fauna the Oldalvölgy–Csipkéstető Formation can be assigned to the Early Bajocian – Early Bathonian as well. Based on the radiolarian biostratigraphy this interval can be assigned to the Bathonian. Taking into account all of these data, the age of the Oldalvölgy–Csipkéstető Formation is Bathonian, probably Early Bathonian (Fig. 2).

Based on foraminifera Age-range of the Bükkzsérc Limestone encompasses the (Aalenian?) Early Bajocian to Late Bajocian interval. According to the foraminifera fauna the deposition of the lithoclastic beds (Mónosbél Formation) continued at least until the Late Bathonian.

Two, Middle-Late Jurassic sedimentary complex can be found farther to the North, in the Rudabánya Hills. One of them is built up by Bajocian–Callovian black shales, sandstone turbidites and olistostrome beds, and deposited by gravity mass flows. The clasts of the olistostrome are predominantly Middle to Upper Triassic pelagic limestones, rhyolite and basalt (Grill, 1988; Kövér et al., 2009). The other series consists of carbonate turbidite beds containing Jurassic platform derived clasts (ooids, peloids, foraminifera) and olistostrome horizons with Middle–Upper Triassic limestone clasts of red Hallstatt facies. The foraminifera assemblage is similar to that found in the Bükkzsérc Limestone (Kövér et al., 2009).

From Medvednica Mts., Croatia Triassic carbonate olistoliths and matrix-supported polymict conglomerates containing clasts of Triassic radiolarian chert, Jurassic silicified shale and sandstone, basalt and ultramafic rocks were reported. Radiolarians found in the radiolarite matrix proved latest Bajocian–Early Bathonian to Late Bathonian–Early Callovian age of the mélange complex (Halamić et al., 2005). This lithofacies is very similar to those of the Mónosbél Formation in the Bükk as far as both the matrix and the components of the olistostromes are concerned; moreover their ages are also similar.

The Mónosbél Group extends over the limits of the study area in the Bükk Mountains and continues in the Darnó area (Fig. 1). It was also recognised in ore exploratory wells at Recsk, Mátra Mts. (Haas et al., 2006; Kovács et al., 2008). Dark grey shale, siliceous shale, pelagic limestone, radiolarite, carbonate turbidites, debrites containing predominantly siliciclastic sandstone clasts and oligomict olistostomes are the typical lithofacies. Olistoliths of marine Upper Permian and Upper Triassic Hallstatt Limestone were encountered here within Bajocian to Callovian shale and radiolarite. The clasts of olistostromes are mostly radiolaria-bearing silicified rock-types. In a borehole drilled in the central part of Mátra Mts. Bajocian platform derived redeposited carbonates, more proximal than the Bükkzsérc Limestone in the Bükk Mountains, were encountered in a remarkable thickness (Haas et al., 2006).

Magmatites prevail above the Mónosbél Group. These are amygdaloidal basalts with red calcareous inclusions and inter-pillow void fillings, Triassic in age, and greenish usually pillow basalts, probably of Jurassic age. Deep-sea sediments, red radiolarite and dark grey siliceous shale also occur among the magmatic rocks (Kovács et al., 2008). The red radiolarite yielded either Ladinian-Carnian or Bathonian-Callovian radiolarians (Dosztály and Józsa, 1992). The magmatite bodies are probably olistolites in pelagic shale and radiolarite matrix.

The Triassic basalt olistoliths in the Jurassic mélange complex of Kalnik Mts., Croatia show definite genetic relationships with the Triassic volcanite bodies known in the Darnó area (Kiss et al., 2008).

In the Dinarides ophiolite mélange complexes comparable to those in the Bükk area occur in the Dinaridic Ophiolite Belt (Dimitrijević et al., 2003). The ophiolite mélange contains fragments of obducted ophiolites (lherzolite), Triassic and Jurassic limestone olistoplaka, and polymict olistostromes. Carnian to Upper Jurassic radiolarian chert, greywacke, basalt, gabbro, ultramafic rocks, granite and Triassic and Jurassic limestones are typical clastic components of the olistostromes (Robertson et al., 2009).

4. Geodynamic evolution and related sediment deposition

Terranes made up the pre-Tertiary basement of North Hungary approached its present-day setting only during the Tertiary (Late Paleogene to Early Miocene) as a result of multiple large-scale tectonic movements (Csontos and Nagymarosy, 1998). Prior to the large displacements they were located probably somewhere between the South Alpine and Dinaridic domain.

Neotethys rifting in the Late Anisian to Early Ladinian led to segmentation of the former ramp; isolated platforms and grabens were formed. In the Carnian some of these grabens filled up by siliciclasts or platform derived carbonates. In contrast, in the Slovenian Trough the pelagic basin setting preserved during the entire Late Triassic – Jurassic interval (Buser, 1989; Rožič et al., 2009). These tectonic processes led to separation of the Adriatic-Dinaridic Carbonate Platform from the Julian Carbonate Platform. Dismembering of other blocks inclusively the Bükk may have taken place similarly.

In the area of the Bükk Mts., drowning of the carbonate platforms took place by the end of the Triassic. In the Early Jurassic the former platforms transformed to submarine highs. In the Middle Jurassic the deepening continued and a radiolarite veneer formed covering both the previous platform and basin deposits. Than course to fine-grained siliciclastics (Vaskapu Sandstone), and distal siliciclastic turbidites (Lökvölgy Formation) were deposited in a deep-sea basin developed above the attenuated continental crust. The siliciclastic series were intruded by back-arc basalt.

Composition of the Mónosbél Group is complex, reflecting its multi-stage depoisitional history. The oldest biostratigraphically dated element of the Mónosbél Group is the (Aalenian?) Early to Late Bajocian Bükkzsérc Limestone, although these rocks are usually present as smaller or larger redeposited fragments. The large blocks should have slid down from the neighbourhood into the deep depositional basin in the late Middle Jurassic most probably in the Late Bathonian. However, beds containing fine redeposited shallow marine carbonate grains (ooids, cortoids, peloids, bioclasts) are also present in the hemipelagic Oldalvölgy Formation and in some olistostrome beds of the Mónosbél Formation. These facts imply continuing shallow marine input during the Middle Jurassic at least until the Late Bathonian.

The grains of the Bükkzsérc Limestone were formed on a carbonate platform; the redeposited particles were accumulated in the foreland of a platform foreslope. Considering that in the Middle Jurassic the Adriatic-Dinaridic Carbonate Platform (ADCP) remained the only large active platform in the wider region, we suppose that this was the provenance of the Bükkzsérc Limestone. In the Middle Jurassic mostly oolitic sediments were formed in the NE part of the ADCP (Dragičević and Velić, 2002). In several places, coeval slope and toe-of-slope facies of ADCP were also preserved. Textural features and microbiofacies (e.g. foraminifera fauna) of these formations are very similar to that of the Bükkzsérc Limestone (Haas et al., 2006).

Deposition of the Bükkzsérc Limestone and the coeval basin facies represents the passive margin evolutionary stage of the Adriatic (Apulian) margin of the western Neotethys during the Bajocian (Fig. 3). Dismembered and drowned blocks of the former platforms were already deep pelagic basins at that time far from the still existing platform.

Occurrence of the predominantly andesitic coarse clastic beds in the lower part of the Oldalvölgy–Csipkéstető Formation indicates the development of a magmatic island arc formed on continental crust in connection with the subduction of the Neotethys. As a consequence of the island arc development, the distal toe-of-slope and the connected pelagic basin transformed to an arc-related (interarc/backarc) basin. This event can be considered as the second evolutionary stage that may have taken place in the Early(?) Bathonian (Fig. 3).

In the Late Bathonian appearance of the polymict gravity deposits (turbidites and debrites – olistostromes) and later on large slided blocks (olistoliths) suggests the onset of the intense orogenic movements in the third stage of the evolution (Fig. 3). The compressive tectonic movements led to imbrication, nappe stacking and accordingly uplifting and disruption of the previously deposited and already lithified peri-platform carbonate deposits and also the island-arc and back-arc volcanites. In the course of the overthrusting movements, also the older basement rocks may have been exposed and subject to erosion.

The Dinaridic (-Hellenidic) ophiolites are interpreted as mostly supra-subduction zone (SSZ) ophiolites which were crystallized at 171 Ma and emplaced by 169 Ma i.e. during the Bajocian (Smith, 2006). This is roughly coeval with the basic change in the evolution of the area studied, a change from the passive carbonate platform evolution when mostly uncemented carbonate grains accumulated in the foreground of a carbonate platform to the accumulation of volcaniclasts and polymict gravity deposits which clearly indicate the onset of the active subduction period. It was followed by obduction probably in the latest Jurassic to earliest Cretaceous (Balla, 1987; Csontos, 2000) and development of a subduction–collision-related

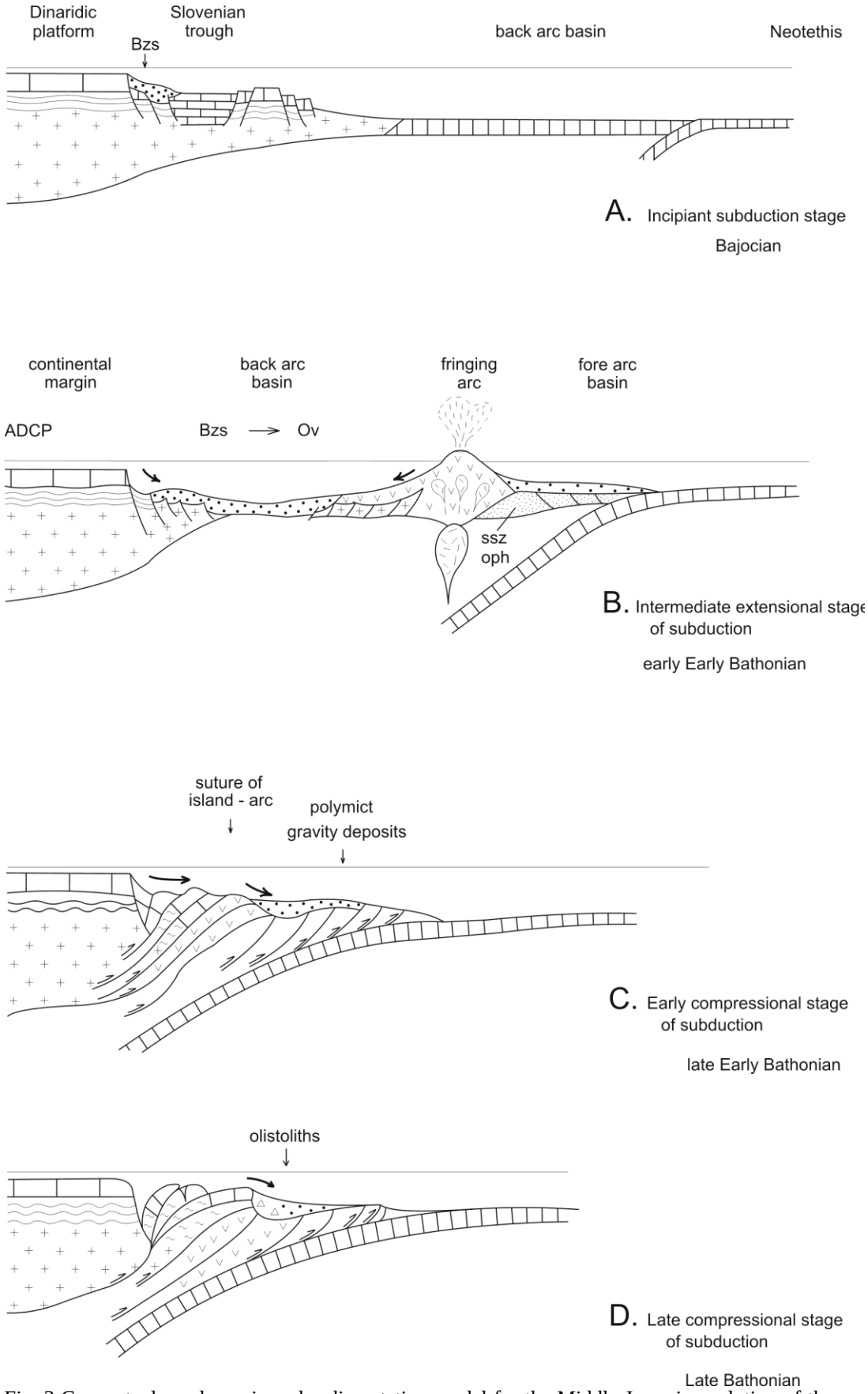

Fig. 3 Conceptual geodynamic and sedimentation model for the Middle Jurassic evolution of the region studied.

mélange complex containing blocks of ophiolites and fragments of the Adriatic continental margin. Further compression resulted in the overthrust of the mélange complex onto the blocks dismembered earlier from the Adriatic margin i.e. the Bükk Parautochthonous, leading to regional metamorphism of the Late Paleozoic to Late Jurassic formations in the late Early Cretaceous (110–120 Ma) and in the Late Cretaceous (90 Ma) (Árkai et al., 1995). The nappe emplacements and the related tectono-metamorphic events took place prior to the Tertiary long-distance displacement of the Bükk Unit.

5. Conclusions

Displaced elements of the Neotethys ophiolite mélange complex occur in the Bükk Mts. and Darnó–Mátra area, in Northeast Hungary. Study of the depositional facies, age determination of the subduction-related sedimentary formations on one hand and detailed petrographic analysis, facies interpretation and age determination of the clastic components of the mélange on the other, provided important data to detect the origin of the clastic material and reconstruction of the complex closure history of the western Neotethys Ocean.

The Bükkzsérc Limestone represents the passive evolutionary stage of a carbonate platform system. It is made up of redeposited platform-derived grains which were deposited in a toe-of-platform foreslope and peri-platform basin setting in the Aalenian(?) Early to Late Bajocian interval.

Based on radiolarians and foraminifera in the matrix of olistostrome interbeds, the Mónosbél Group deposited most probably during the Bathonian. The lower part of the complex is typified by predominance of pelagic carbonates, shales and radiolarites with andesitic volcaniclast intercalations. Intercalations of the andesitic volcaniclasts suggest an island arc provenance and accordingly development of an arc-related basin.

The higher part of the succession is characterised by polymict olistostromes. Large olistoliths that are predominantly blocks of shallow marine "Bükkzsérc-type" limestones appear in the upper part of the sequence.

Appearance of the polymict olistostromes with shallow and deep marine carbonate, siliciclasts, basic to acidic volcaniclasts and metamorphic components implies imbrications, incipient nappe development in a compressional regime probably in the Late Bajocian. This stage is followed by input of large slided blocks mostly of the Bükkzsérc Limestone suggesting disruption and thrusting of the previous passive margin.

Significant difference between the composition of the redeposited clasts in the olistostromes of the Bükk and Darnó area indicate deposition in different subbasins formed along the subducted margin of the Neotethys.

Acknowledgement

The present work was supported by the Hungarian Science Found (OTKA) projects K61872; K68791; F048341 and the Hantken Foundation.

References

Árkai P., Balogh K., Dunkl I. 1995. Timing of low-temperatute metamorphysm and cooling of the Paleozoic and Mesozoic formations of the Bükkium, innermost West Carpathians, Hungary. Geolog. Rundsch. 84, 334-344.

Balla Z. 1987. Tectonics of the Bükkian (North Hungary) Mesosoic and relations to the West Carpathians and Dinarids. Acta Geol. Hung. 30, 25-287

Balogh K 1964. Geology of Bükk Mountains Ann. Inst. Geol. Hung. 48, 245-719 (in German).

Bérczi-Makk A., Pelikán P. 1984. Jurassic formations from the Bükk Mountains. Ann Rep Hung Geol Inst 1982, 137-166 (in Hungarian with English abstract).

Buser S. 1989. Development of the Dinaric and Julian carbonate platforms and the intermediate Slovenian basin (NW-Yugoslavia). In: Carulli GB, Cucchi F, Radrizzani CP (eds) Evolution of the Karstic carbonate platforms. Mem. Soc. Geol. Ital. 40, 313-320.

Csontos L. 2000. Stratigraphic re-evaluation of the Bükk Mts. (Hungary). Földt Közlöny 130, 95-131(in Hungarian with English abstract).

Csontos L. and Nagymarosy A. 1998. The Mid-Hungarian line: a zone of repeated tectonic inversions. Tectonophysics 297, 57–71.

Dimitrijević M.N., Dimitrijević M.D., Karamata S., Sudar M., Gerzina N., Kovács S., Dosztály L., Gulácsi Z., Less Gy., Pelikán P. 2003. Olistrotrome/ mélanges – an overview of the problems and preliminary comparison of such formations in Yugoslavia and NE Hungary. Slovak Geol. Mag. 9, 3-21.

Dosztály L. and Józsa S. 1992. Geochronological evaluation of Mesozoic formations of Darnó Hill at Recsk on the basis of radiolarians and K-Ar age data. Acta Geol. Hung. 35, 371-393

Dragičević I. and Velić I. 2002. The northeastern margin of the Adriatic Carbonate Platform. Geol. Croatica 55, 185-232.

Filipović I., Jovanović D., Sudar M., Pelikán P., Kovács S., Less Gy., Hips K. (2003) Comparison of the Variscan – Early Alpine evolution of the Jadar

Block (NW Serbia) and "Bükkium" (NE Hungary) terranes; some paleogeographic implications. Slovak Geol Mag 9, 3-21.

Grill J. 1988. Jurassic formations of the Rudabánya Mts. *Ann. Rep. Hung. Geol. Inst., 1986*, 69-103 (in Hungarian with English abstract).

Haas J., Görög Á., Kovács S., Ozsvárt P., Matyók I., Pelikán P. 2006. Displaced Jurassic foreslope and basin deposits of Dinaridic origin in Northeast Hungary. Acta Geol. Hung. 49,125-163.

Haas J. and Kovács S. 2001. The Dinaridic–Alpine connection – as seen from Hungary. Acta. Geol. Hung. 44, 345-362.

Halamić J., Marchig V., Goričan Š. 2005. Jurassic radiolarian cherts in north-western Croatia: geochemistry, material provenance and depositional environment. Geol. Carp., 5, 123-136.

Kiss G., Molnár F., Palinkaš L.A. 2008. Volcanic facies and hydrothermal processes in Triassic pillow basalts from Darnó Unit, NE Hungary Geol. Croatica 61, 385–394.

Kovács S., Haas J., Szebényi G., Gulácsi Z., Pelikán P., Bagoly-Árgyelán G., Józsa S., Görög Á., Ozsvárt P., Gecse Zs., Szabó I. 2008. Permo-Mesozoic formations of the Recsk-Darnó Hill area: stratigraphy and structure of the pre-Tertiary basement of the Paleogene Recsk Orefield. In: Földessy J, Hartai É (Eds) Recsk and Lahóca geology of the Paleogene Ore Complex – Geosciences, Miskolc University Press, 33-56.

Kövér Sz., Haas J., Görög Á., Józsa S., Ozsvárt P., Götz A. 2009. Lithofacies characteristics and new age data from the Uppermost Triassic - Jurassic foreslope and basin sediments of Rudabánya Hills, NE Hungary. Geol Carp 60, 351-379

Pamić J. 1997. The northwesternmost outcrops of the Dinaridic ophiolites: a case study of Mt. Kalnik (North Croatia). Acta Geol. Hung. 40, 37-56

Pamić J. 2003. The allochthonous fragments of the Internal Dinaridic units in the western part of the South Pannonian Basin. Acta Geol. Hung. 46, 41-62

Pelikán P. (ed) Less Gy., Kovács S., Pentelényi L., Sásdi L. 2005. Geology of the Bükk Mountains, MÁFI, Budapest, 249p.

Robertson A, Karamata S, Šarić K (2009) Owerview of ophiolithes and related units in the Late Paleozoic–Early Cenozoic magmatic and tectonic development of Tethys in the northern part of the Balkan region. Lithos, 108, 1-36.

Rožič B., Kolar-Jurkovšek T., Šmuc A, 2009. Late Triassic sedimentary evolution of the Slovenian Basin (eastern Southern Alps): description and correlation of the Slatnik Formation. Facies, 55, 137-155.

Schréter Z. 1959. Formations of marine origin of the Bükk Mountains. Földt. Közl. 89, 364-373 (in Hungarian with English abstract).

Schmith A.G. 2006. Tethyan ophiolite emplacement, Africa to Eorope motions, and Atlantic spreading. In: Robertson A.H.F. and Mountrakis D. (eds) Tectonic Development of the Eastern Mediterranean Region. Geol. Soc. London Spec. Publ. 260, 11-34.

Special Session S05
Advances in geology and geodynamic evolution of the Rhodope Massif

Scientific Annals, School of Geology, Aristotle University of Thessaloniki Proceedings of the XIX CBGA Congress, Thessaloniki, Greece	Special volume 100	157-164	Thessaloniki 2010

REGIONAL GEOLOGY AND CORRELATION OF THE EASTERN CIRCUM-RHODOPE BELT, BULGARIA-GREECE

Bonev N.[1], Magganas A.[2] and Klain L.[1]

[1] *Department of Geology-Paleontology-Fossil Fuels, Sofia University "St.Kliment Ohridski", BG-1504, Sofia, Bulgaria, niki@gea.uni-sofia.bg, laslo@gea.uni-sofia.bg*
[2] *Department of Mineralogy and Petrology, Faculty of Geology and Geoenvironment, National and Kapodistrian University of Athens, Panepistimioupolis 15784, Athens, Greece, amagganas@geol.uoa.gr*

Abstract: We review on a regional-scale the distinct units of the eastern Circum-Rhodope Belt (CRB) in Bulgaria and Greece, with the aim to provide an up-to-date synthesis and correlation. The eastern CRB consists of Early-Middle Jurassic supra-subduction zone Evros ophiolite, the MORB related Late Jurassic Samorthaki ophiolite and Middle Triassic-Jurassic clastic, pelitic, carbonaceous and Cretaceous (?) flysch sedimentary successions. Lower Cretaceous shallow-water Aliki limestones seal part of these sedimentary successions already metamorphosed in greenschist-facies. Bulk stratigraphy in ascending order comprises a meta-sedimentary series overlain by a meta-volcanic series. The metamorphic grade increases towards the high-grade basement northwards reaching upper greenschist to epidote-amphibolite facies, and decreases to very low-grade (prehnite-pumpellyite facies) and non-metamorphic stratigraphically up-section. Trace element and REE comparison of the ophiolite basalts and underlying greenschist-facies meta-volcanics of same composition reveals similar geochemistry within the distinct units, implying a regional-scale chemical continuity. The allochthonous eastern CRB units show N-directed internal shear deformation and thrust emplacement, evidently along rarely preserved thrust contacts, and record tectonic overprint by Tertiary collision and extensional tectonics in the region. Collectively, the onshore eastern CRB is a region-wide (180 km long along strike × 80 km wide along meridian) tectonic zone including correlative units with regard to their coherent and comparable stratigraphy, tectonics and geochemistry. These units testify for three paleogeographic domains that include Triassic-Jurassic near Rhodope continental margin shallow-water environment, adjacent to this margin Early-Middle Jurassic intra-oceanic arc system responsible for the generation of the supra-subduction zone Evros ophiolite and related to the ophiolite Middle-Late Jurassic trench-slope environment. Another MORB-related paleogeographic domain is indicated by the Samothraki back-arc ophiolite offshore.

Keywords: regional geology, correlation, eastern Circum-Rhodope Belt, Bulgaria-Greece

1. Introduction

The Circum-Rhodope Belt (CRB) of continuous sedimentary successions was introduced by Kauffmann et al. (1976) as an isopic zone of the Internal Hellenides that surrounds the high-grade crystalline Serbo-Macedonian Massif and the Rhodope Massif in Greece and Bulgaria. This designation followed the works by Jaranov (1960) using the term Peri-Rhodope Zone and Kockel et al. (1971) for the same isopic zone of the Chalkidiki Peninsula. The CRB was discarded as continuous belt representing the sedimentary cover of the high-grade crystalline massifs (Ricou et al., 1998). Nevertheless, the CRB is widely used in the tectonic subdivision of the Hellenides, and the CRB concept is considered still vigorous (Brown and Robertson, 2004; Papanikolaou, 2009). The only attempt for correlation of the units in the eastern CRB was done by Boyanov et al. (1990) for the Mandritsa area in Bulgaria, based on the stratigraphic data presented by Papadopoulos et al. (1989) for the Drimos-Melia and Makri units in Greece. In this contribution, we review distinct units in the eastern segment of the CRB in the light of recent advances in their composition and structure, with the aim to better understand the regional context of this belt in the eastern Rhodope-Thrace region of Bulgaria and Greece.

The eastern CRB consists of greenschist-facies, very low-grade and unmetamorphosed rocks (Papadopoulos, 1982; Boyanov et al., 1990), including

the Jurassic Evros ophiolite (Magganas et al., 1991) and associated Mesozoic sedimentary successions that span Middle Triassic-Lower Cretaceous interval as indicated by published biostratigraphic and radiometric ages in Bulgaria and Greece. We combined available stratigraphic data with own unpublished field observations and tectonic data, and published petrologic and geochemical data on distinct units to provide more comprehensive up-to-date regional synthesis with regard to the materials of eastern CRB.

2. Regional geology

Figure 1 shows the distribution of the Mesozoic low-grade metamorphic rocks of the CRB in the eastern Rhodope-Thrace region of Bulgaria and Greece. The low-grade rocks form the uppermost tectono-metamorphic unit occurring largely as inliers below the Tertiary sedimentary and volcanic cover successions. Partly, these rocks rest tectonically on the high-grade basement units, mostly through extensional detachments where they form part of the hanging wall and locally are limited by thrust contacts (Bonev and Stampfli 2003, 2008, 2009; Bonev 2006a; Bonev and Beccaletto 2007). We use available in the literature names for the distinct units in their description that follows from north to the south. The dispersed areal mode of occurrences of the low-grade successions requires an evaluation of the counterparts of the units, which to be put into a regional-scale frame.

The northernmost unit of the eastern CRB occurs in northern slope of the eastern Rhodope and was originally defined as the Kulidzhik nappe by Boyanov (1969), where Lower Cretaceous radiolarian assemblage (Boyanov and Lipman, 1973) subsequently re-examined as Jurassic in age (Boyanov et al., 1990) was reported in shales. The Kulidzhik nappe tectonically slices the high-grade basement orthogneisses with a greenschist series of arc-related meta-basalts and pyroclastics of IAT to MORB geochemical signature comparable to the similar rocks in the Mandritsa unit (Bonev, 2006b). The greenschist series record upper greenschist to epidote-amphibolite facies conditions, and is conformably overlain by a series consisting of weakly metamorphosed black argillaceous shales intercalated with thin limestone horizon, and phyllites. Both low-grade series are overlain by the Kulidzhik nappe orthogneissic allochthon that cooled in Late Jurassic time ($^{40}Ar/^{39}Ar$ mica ages of 154.23 ± 0.66 Ma and 156.7 ± 0.81 Ma), providing evidence for the Middle-earliest Late Jurassic metamorphism (following Early-Middle Jurassic ophiolite eruptive history) of the greenschist series coeval with a ductile to brittle NNE-directed nappe emplacement (Bonev et al., 2010).

The Mandritsa area is the second large exposure of the CRB rocks in Bulgaria, straddling the Greek-Bulgarian border. This area is usually referred as the Mandritsa unit (e.g. Ricou et al., 1998), whose meta-sedimentary lower section is largely correlated with the Makri unit in Greece (Boyanov et al., 1990). The Mandritsa unit is floored by a horizon of recrystallized limestones that grade into marbles occurring in basal direct contact with the ductile-brittle orthogneiss mylonites of the Byala reka extensional detachment (Bonev, 2006a). The marble horizon contains greywacke knockers and mafic lenses (Bonev, 2005a), and is intruded by boninitic affinity diorite dyke (Bonev and Stampfli, 2008). This horizon is gradually overlain by greenschist unit consisting of meta-sedimentary (common quartz-chlorite-white mica ± garnet) and meta-volcanic (common chlorite-actinolite ± epidote) rocks having arc-related boninitic-tholeiitic affinity. Both lithologies depict an internal NW–NE-directed ductile shear deformation in greenschist-facies conditions (Bonev and Stampfli, 2003). Up-section the greenschist unit is gradually overlain by thin lava flows of arc-related boninitic-tholeiitic affinity basalts to andesites that are geochemically undistinguishable from the greenschists (Bonev and Stampfli, 2008). The lavas are interstratified by chert layers that yielded Lower Jurassic radiolarians (Tikhomirova et al., 1988). Stratigraphically uppermost is mélange-like unit consisting of intercalated conglomerates, gravels, sandstones and black shales. This intercalation contains in olistostromic context reworked blocks and clasts of Late Permian and Middle-Late Triassic shallow-water limestones and siliciclastics (Boyanov and Trifonova, 1978; Boyanov and Bodurov, 1979; Trifonova and Boyanov, 1986; Bonev, 2005b). The subdivided by Boyanov et al. (1990) in the Mandritsa area topmost Late Cretaceous sedimentary-volcanogenic Meden Buk Formation that contains Campanian foraminifera recovered only in drill cores is not considered here because it can not be seen in the field. Instead, we assign the terrigeneous components included in the Meden Buk Formation as belonging to the mélange-like unit. Internal north-directed thrusts locally juxtapose greenschists with very low-grade rocks in the Mandritsa unit.

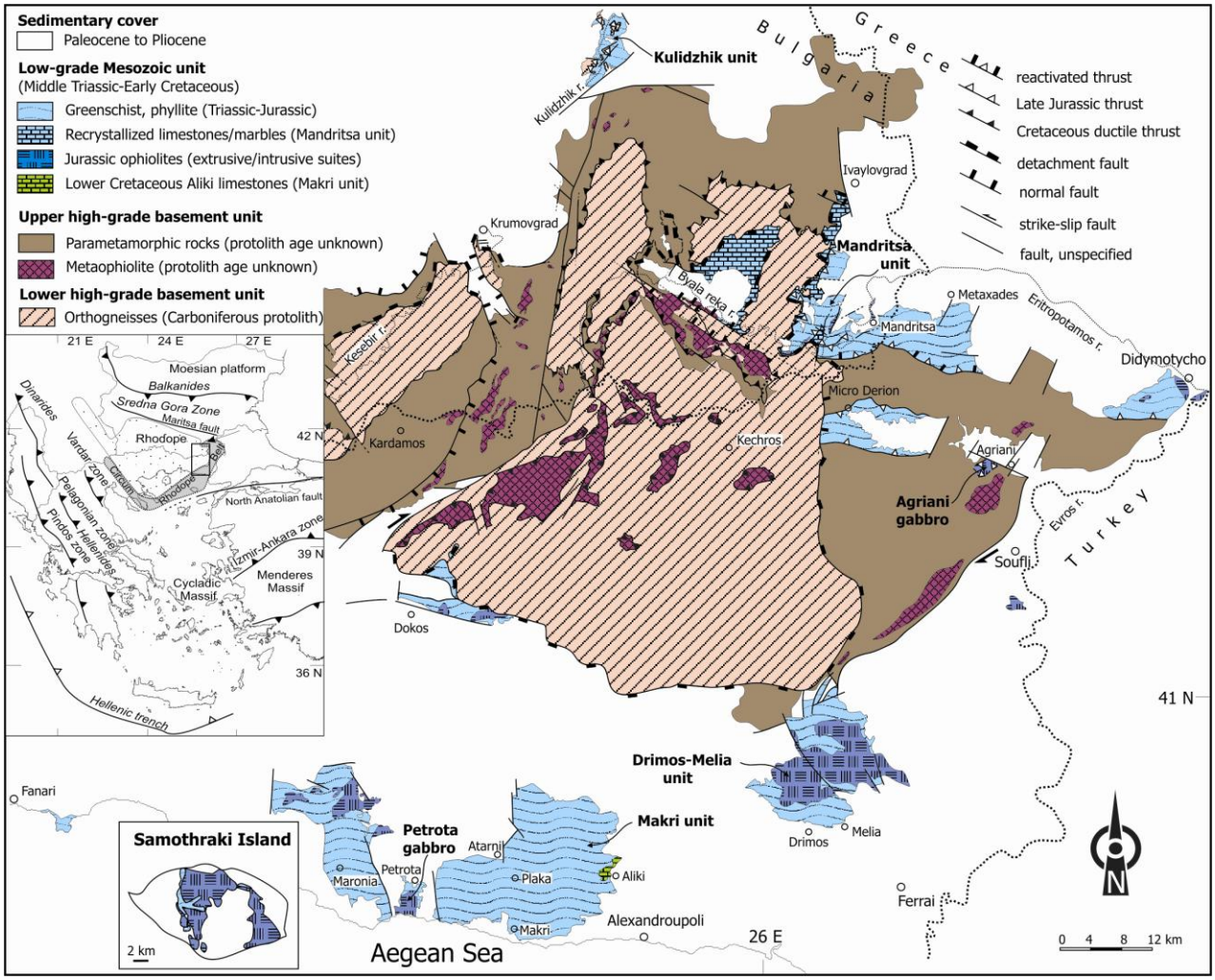

Fig. 1. Geologic sketch map of the eastern Rhodope-Thrace region in Bulgaria-Greece (modified from Bonev and Stampfli, 2008).

The Metaxades-Micro Derion area represents laterally continuous exposure of the greenschist unit from the Mandritsa area. In this area, the meta-lavas and meta-pyroclastics of same lithologic context and metamorphic grade to the Mandritsa greenschist unit belongs to the upper and lower meta-volcanics having an arc-related tholeiitic signature (Magganas, 2002). Field observations in Metaxades-Micro Derion area have shown that the greenschist unit locally exposes a basal N-directed ductile thrust contact with the high-grade basement, which contact is re-activated as normal fault during the Tertiary extensional deformation.

Further east (Fig. 1), a gabbroic body at the village Agriani and the mafic lavas and plagiogranite intrusion at Didymotycho area belongs to the section of the Evros ophiolite (Magganas et al., 1991; Magganas, 2002, 2007; Bonev and Stampfli, 2009). The Agriani isotropic gabbro of tholeiitic affinity is intruded by boninitic basalt dykes and overlain by mafic lava flow. The gabbro lies on the high-grade basement with an inferred thrust contact. The plagiogranite stock at Didymotycho is intruded by microgabbroic and coarse-grained gabbroic dykes, as well as by tholeiitic and boninitic affinity basalt dykes. The massive, rarely pillowed mafic lavas at Didymotycho belong to the upper meta-volcanics of the Evros ophiolite (Magganas, 2002). The basal ductile thrust contact of the ophiolite at Didymotycho, yet locally observed, demonstrates intensely folded thin horizon of the Makri unit-specific meta-sediments with pronounced NE-directed fold asymmetry and tectonic transport direction on top of the high-grade basement.

Southwards, the main exposures of the Mesozoic low-grade rocks encompass the Drimos-Melia and the Makri units (Papadopoulos, 1982). The former unit, which is better exposed between the Drimos and Melia villages, consists therein of massive ba-

salt to andesite lava flows lying usually above the basalt pillow lavas intercalated with rare sheeted-like dykes. This extrusive ophiolite suite is interfingering-with flysch rhythmic shale and sandstone alternation. These relationships imply mutual flysch depositional and ophiolite eruptive history. The flysch supplied find of Callovian-Oxfordian ammonite (Trikkalinos, 1955) and prints of Middle-Upper Triassic bivalve (Dimadis et al., 1996). Detrital zircons in the sandstones cluster at ca. 315-285 Ma, with youngest zircon at ca. 160 Ma providing maximum depositional age of the flysch (Meinhold et al., 2010). Easterly, south of Soufli (Fig. 1), an isolated basaltic andesite lava flow occurs below the Tertiary cover, showing similarity to massive lava flows of the Drimos-Melia unit and at Didymotycho.

The largest development of the Makri unit occurs north of the village Makri and extends into the Maronia area westwards. These two areas are separated by the Tertiary Petrota graben, which exposes in its central part the Petrota gabbroic complex (Biggazzi et al., 1989). According to the latter authors, the Petrota complex consists of cumulitic and isotropic gabbros, gabbro-norites and anorthosites having tholeiitic to calc-alkaline arc-related, supra-subduction zone affinity. Our field observations in the area identified also the presence of tholeiitic basalt dykes. U-Pb zircon SHRIMP age of 169 ± 2 Ma (Koglin et al., 2007) and apatite fission-track ages in the range 161-140 Ma (Biggazzi et al., 1989) were reported for the Petrota gabbro, implying respectively its crystallization or uplift/shallow-crustal emplacement. The contact of the Petrota complex with the surrounding rocks is intrusive (Bigazzi et al., 1989) or tectonic (Frass et al., 1989). In the field, the contact with the Makri unit is uncertain, marked by late faults limiting the graben or traced by gabbro-contact zone altered rocks, but virtually the Petrota complex occurs below the Marki unit. The unit itself includes metasedimentary series consisting of shales, phyllites, quartz-chlorite schists, sandstones and recrystallized limestone horizons overlain by greenschists and greenstone series (commonly chlorite-actinolite) (Kopp, 1969; Papadopoulos et al., 1989), presumably of volcanic and pyroclastic origin. In between greenschists layers of the Makri unit and metasomatic contact zone with them, small serpentinite olistostromic occurrences are found nearby the villages Atarni and Plaka. The greenschists, which form the tholeiitic back-arc-related lower metavolcanics of Magganas (2002), are intruded by gabbroic and minor plagiogranitic rocks. The lower limestone horizon yielded Triassic corals (Maratos and Andronopoulos, 1964), whereas chlorite schists supplied Tithonian-Berriassian ammonite (Dimadis and Nikolov, 1997). The uppermost limestone horizon of the Makri unit, the so-called "Aliki limestones", supplied Lower-Middle Cretaceous foraminifers (Kopp, 1969) which are considered pertaining to Lower Cretaceous (Maratos and Andronopoulos, 1964). The Aliki limestones are debatable because of claimed transgressive superposition onto the Makri unit (Kopp 1969), tripartite intercalation within its higher levels (Maratos and Andronopulos, 1964) or lying with tectonic contact (von Braun, 1993). Our field observations around the hill that only exposes the Aliki limestones revealed no tripartite intercalation with the underlying greenschists that always show very weak shear deformation and the limestones in turn are undeformed. These features indicate that the Aliki limestones unconformably overlie the greenschists. Detrital zircons in the sandstones of the Makri unit cluster at ca.310-290 Ma and at ca. 240 Ma (Meinhold et al., 2010) providing at least Middle Triassic depositional age.

In the Maronia area, both series of the Makri unit are present with same metamorphic grade lithologic assemblage, in turn overlain by forearc tholeiitic basalt to andesite pillow-lavas and flows, boninitic dykes and flysch that exhibit characteristics analogous to the volcanic and clastic sedimentary rocks of the Drimos-Melia unit.

A small area near the village Dokos (Fig. 1) exposing analogous to the Makri unit low-grade successions occur in the hanging wall of an extensional detachment (Bonev and Beccaletto, 2007). All areas exposing the Makri unit provide evidences for an internal N-directed deformation depicted by fold asymmetry, thrust fault propagation in the fold hinges and ductile shearing.

An isolated coastal outcrop east of the village Fanari exposes shale-sandstone rhythmic flysch alternation (Fig. 1). The flysch shows NW-vergent refolded patterns associated with hinge thrusts propagation in the direction of fold overturning. The Fanari flysch strongly resembles the Drimos-Melia unit flysch, despite the later is weakly deformed.

The southernmost occurrence of the eastern CRB units is found in the Samothraki Island. Low-grade

meta-sedimentary rocks consisting mostly of meta-conglomerates and mica-chlorite schists of Late Jurassic age (Heimann et al., 1972) are intercalated by rhyodacitic to andesitic metavolcanics, forming the lower unit in the island. It has been suggested that most rocks from this unit correspond to the Makri unit rocks and constitutes a flyschoid formation deposited in a continental rift (Tsikouras and Hatzipanagiotou, 1998). Ophiolitic rocks of Late Jurassic age (154±7 and 155±7 Ma) tectonically overlay the lower unit. From base to top, the Samothaki ophiolite consists of gabbro, hornblende-diorite with plagiogranite pods and veins, dolerite in massive layers and dykes and basaltic pillow-lavas and flows, almost all showing strong MORB signatures. The diorites intrude locally schists of the lower unit. The ophiolite is unconformably overlain by Eocene sediments, covered by Oligocene to Miocene volcanics and a Miocene granitic body intruded into the ophiolite and the lower unit (Davis, 1963; Eleftheriadis et al., 1989).

3. Correlation and synthesis

Figure 2 summarizes the stratigraphic and tectonic features of the distinct units or studied areas of the eastern CRB, allowing their correlation and establishing corresponding counterparts. Starting from the base of eastern CRB, the meta-sedimentary series of the Makri unit is comparable with the lower meta-sedimentary levels of the Mandritsa unit, both only having relatively thick limestone horizons. The variations in the latter units include the higher abundance of calcareous rocks in the Makri unit, with reminder that the Mandritsa unit lays above an extensional detachment that accounts for stratigraphic omissions. These meta-sedimentary successions stands for the near Rhodope Triassic-Jurassic continental margin shallow-water environment (e.g. Papadopoulos et al., 1989) located adjacent to the Jurassic island arc system that created the supra-subduction zone Evros ophiolite. The very low-grade (prehnite-pumpellyite facies, Magganas, 2005) massive and pillow lavas of the ophiolite extrusive suite, together with its me-

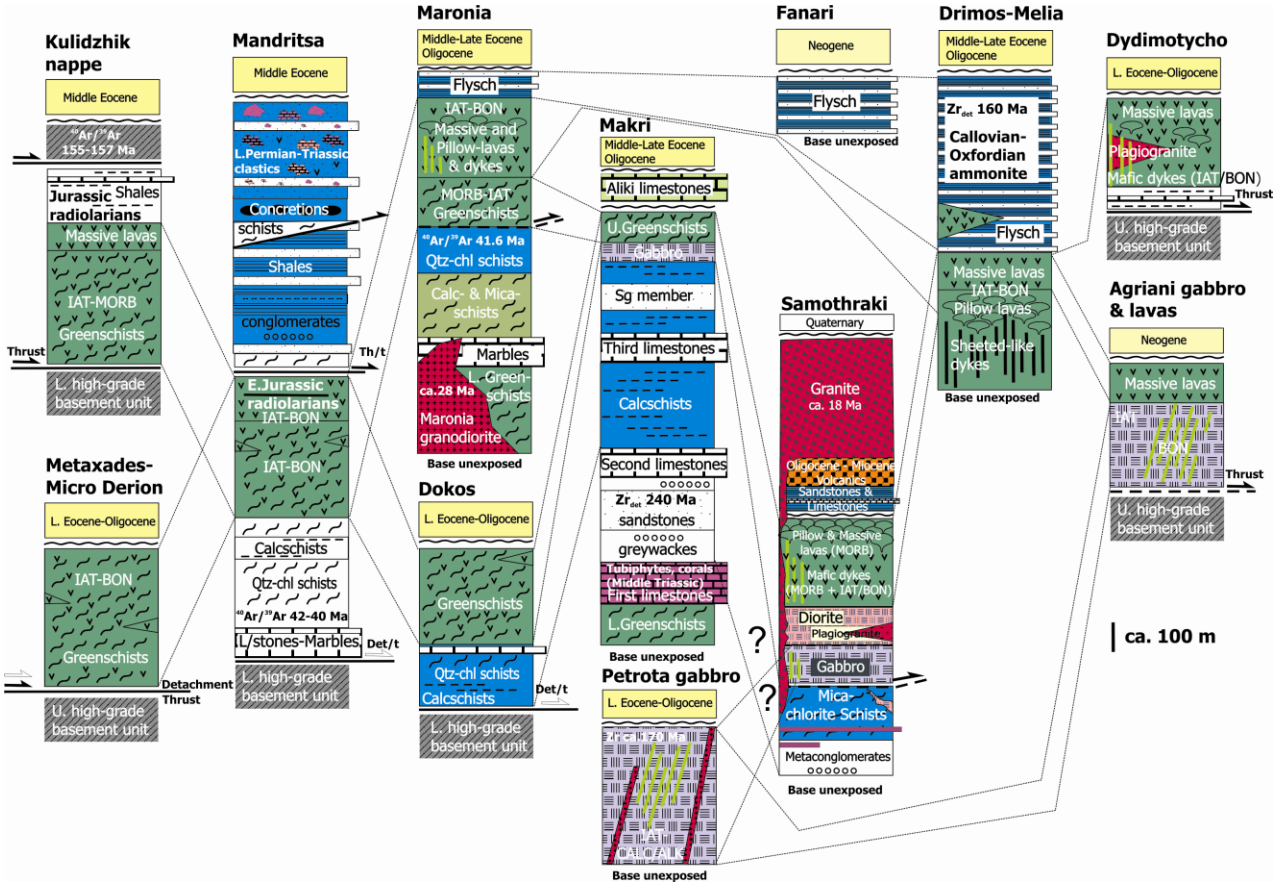

Fig. 2. Tectono-stratigraphic columns for the units or areas of the eastern CRB. The Makri unit stratigraphy after Kopp (1969). $^{40}Ar/^{39}Ar$ ages for the Kulidzhik nappe from Bonev et al., (2010). Unpublished $^{40}Ar/^{39}Ar$ ages for the Mandritsa unit and Maronia area testify respectively for extensional tectonic overprint and burial beneath 5 km thick Middle Eocene sediments (e.g. Ivanov and Kopp, 1969).

tamorphosed members in the greenschist series, both are traced in almost all eastern CRB units. Geochemical comparison of the greenschists and the ophiolite basaltic lavas of same composition show chemical consistency of the trace element and REE patterns in the distinct units, implying common magmatic origin clearly related to a SSZ environment (Fig. 3). Weak MORB and strong IAT and boninitic signatures are revealed, with the latter two compositions depicted mostly in the relatively younger ophiolitic rocks of the Drimos-Melia unit in Greece and the equivalent units in Bulgaria. The deepest crustal section of the ophiolite is represented by Petrota and Agriani gabbroic bodies. Cumulate rocks in the Petrota complex may represent deep magma chamber elements, whereas Makri and Didymotycho gabbroic and plagiogranitic stocks and dykes presumably belong to upper magma chamber layers. The sheeted-like dykes of the Drimos-Melia unit and the basaltic dykes crosscutting plagiogranitic rocks in Didymotycho are forming the likely transition to the extrusive suite in a bulk ophiolite "pseudostratigraphy". Mantle section of the ophiolite is almost absent. However, the serpentinite bodies occurrences at Atarni and Plaka, which are found in close spatial-contact relationship with the greenschists of the Makri unit, showing depleted chemistry and harzburgitic composition can be considered as small slices of the tectonitic part of the ophiolite (Magganas, 2002). The proximal flysch of the Drimos-Melia unit and in Fanari indicates trench-slope environment, which in the Drimos-Melia unit is intimately related to the ophiolite extrusive suite. From a tectonic view point, the Late Jurassic N-directed thrust displacement of the eastern CRB units is recorded elsewhere by internal shear deformation and locally preserved thrust contacts (Bonev et al., 2010; Bonev and Stampfli, 2010), with the strong overprint by the Tertiary final collision and extensional tectonics in the region (Bonev and Stampfli, 2003; Bonev, 2006a; Bonev and Beccaletto, 2007). From a geodynamic view point, the eastern CRB reveals intimately related four paleogeographic environments, namely the Triassic-Jurassic continental margin of the Rhodope, the Early-Middle Jurassic intra-oceanic arc system (including magmatic products specific for the proto/fore-arc and arc regions) responsible for the generation of the Evros ophiolite and the Jurassic trench-slope environment adjacent to the arc-related ophiolite. The last paleogeographic environment is clearly indicated by MORB affinities recognized in most mafic rocks of the Samothraki Island ophiolite. This back-arc extensional setting was active southwards during Late Jurassic (Tsikouras and Hatzipanagiotou, 1998).

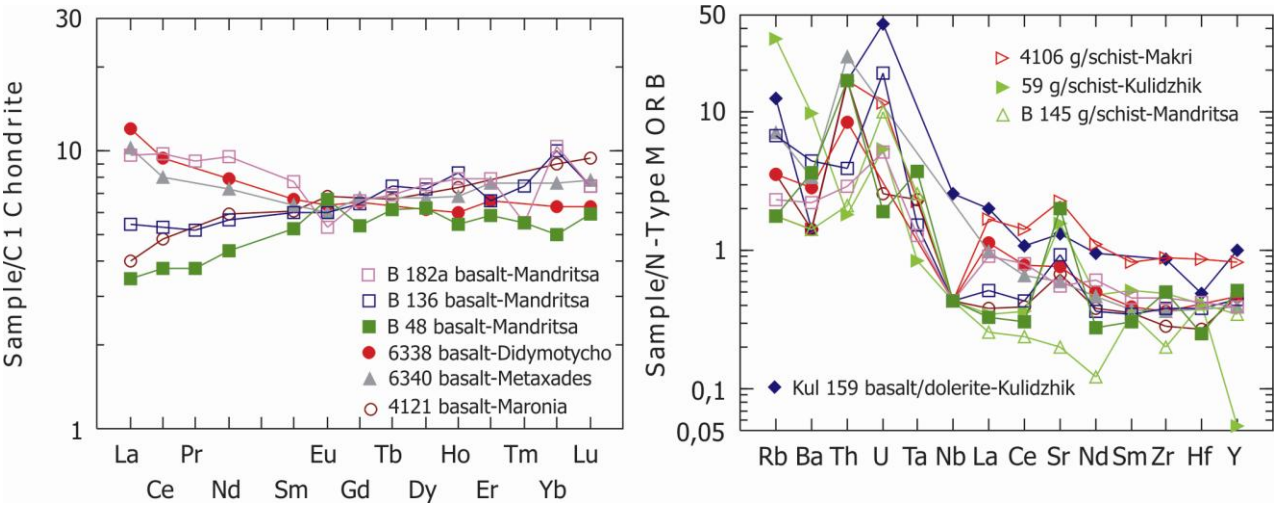

Fig. 3. Comparative geochemistry of the greenschists and ophiolite basalt lavas in the units of the eastern CRB. Data compiled from Magganas (2002), Bonev et al., (2010) and Bonev and Stampfli (2008). Normalization values after Sun and McDonough (1989).

4. Conclusions

- The onshore eastern CRB is a regional-scale tectonic zone including coherent units that can be followed for more than 180 km along the strike from Fanari to Didymotycho and is 80 km wide from the front of the Kulidzhik nappe to the Aegean coast. Offshore element is Samothraki Island ophiolite. The various units contained in this belt show correlative stratigraphy, similar chemical compositions of the ophiolite suites and analogous tectonic features related to their Late Jurassic

thrust emplacement onto the Rhodope margin and the Tertiary Rhodope collisional and extensional overprint. Metamorphic grades are highest northwards close to the high-grade basement in the meta-sedimentary and greenschist series, and generally decrease stratigraphically upwards to ocean-floor metamorphism of the ophiolite and unmetamorphosed flysch.

- The Early-Middle Jurassic supra-subduction zone Evros ophiolite (constrained by radiolarians within the lavas of the Mandritsa unit and the crystallization of the Petrota gabbro) presents mostly an extensive extrusive suite and limited intrusive crustal section, essentially lacking the mantle section. Geochemically, the ophiolite has regionally coherent arc-related dominant IAT signature, with similar affinity greenschist series that systematically underlie the ophiolite in various eastern continental CRB units. In opposite, Jurassic Samothraki ophiolite shows mostly MORB features.

- The weakly or unmetamorphosed sedimentary successions represent deposits related to the supra-subduction zone ophiolite, both depicting three consistent paleogeographic domains of near continental margin shallow-water environment, trench-slope environment and intra-oceanic arc system. A forth setting is indicated by a mid-ocean ridge system developed further south in the marginal basin.

Acknowledgements

The study was supported by Sofia University Scientific Research Fund, grant № 286/09 to N.B and by University of Athens (S.A.R.G.), grant № 70/4/4217 to A.M. D. Papanikolaou and R. Nedyalkov are thanked for constructive and helpful reviews.

References

Biggazzi G., Del Moro A., Innocenti F., Kyriakopoulos K., Manetti P., Papadopoulos P., Norelliti P. and Magganas A., 1989. The magmatic intrusive complex of Petrota, west Thrace: age and geodynamic significance. Geologica Rhodopica 1, 290-297.

Bonev N., 2005a. Siliciclastic knockers in marbles of the eastern Rhodope, Bulgaria: significance for depositional environment and tectonic setting. Annuaire de l'Universite de Sofia, Faculte de Geologie et Geographie, Livre 1- geologie, 98, 28-42.

Bonev N., 2005b. Foraminifers from the exotic Late Permian limestone pebbles in the Mesozoic low-grade sequence of the eastern Rhodope, Bulgaria: paleogeographic and paleotectonic consequences. Neues Jahrbuch für Geologie und Paläontologie Monatschefte, (7), 385-403.

Bonev N., 2006a. Cenozoic tectonic evolution of the eastern Rhodope massif (Bulgaria): basement structure and kinematics of syn- to postcollisional extensional deformation. In: Dilek, Y., and Pavlides, S. (eds.). Postcollisional Tectonics and Magmatism in the Mediterranean Region and Asia. Geological Society America Sp. Paper, Boulder, Colorado, USA, 409, 211-235.

Bonev N., 2006b. Structural and geochemical studies on amphibolite and greenschist-facies rocks in the Kulidjik river valley, eastern Rhodope, Bulgaria: preliminary results. Neues Jahrbuch für Geologie und Paläontologie Abhandlungen, 239, 161-181.

Bonev N., Beccaletto L., 2007. From syn- to post-orogenic Tertiary extension in the north Aegean region: constraints on the kinematics in the eastern Rhodope-Thrace, Bulgaria-Greece and the Biga Peninsula, NW Turkey. In: Taymaz, T., Yilmaz, Y., and Dilek, Y., (Eds.). The Geodynamics of the Aegean and Anatolia. Geological Society London Sp. Publ., Blackwell Scientific Publications, London, 291, 113-142.

Bonev N., Spikings R., Moritz R. and Marchev P., 2010. The effect of early Alpine thrusting in late-stage extensional tectonics: Evidence from the Kulidjik nappe and the Pelevun extensional allochthon in the Rhodope Massif, Bulgaria. Tectonophysics, doi: 10.1016/j.tecto.2010.01.001.

Bonev N.G., Stampfli G.M., 2003. New structural and petrologic data on Mesozoic schists in the Rhodope (Bulgaria): geodynamic implications. Comptes Rendus Geoscience, 335, 691-699.

Bonev N., Stampfli G., 2008. Petrology, geochemistry and geodynamic implications of Jurassic island arc magmatism as revealed by mafic volcanic rocks in the Mesozoic low-grade sequence, eastern Rhodope, Bulgaria. Lithos, 100, 210-233.

Bonev, N., Stampfli, G., 2009. Gabbro, plagiogranite and associated dykes in the supra-subduction zone Evros ophiolites, NE Greece. Geological Magazine, 146, 72-91.

Bonev N., Stampfli G., 2010. Comment on "Geochemistry, petrogenesis and tectonic setting of the Samothraki mafic suite, NE Greece: Trace-element, isotopic and zircon age constraints" N. Koglin, D. Kostopoulos & T. Reischmann [Tectonophysics 473, 53–68 (doi:10.1016/j.tecto.2008.10.028)], 483, 413-419.

Boyanov I., 1969. Notes on the Kulidjik nappe. Bulletin of the Geological Institute of Bulgarian Academy of Sciences, series Geotectonics, 18, 159-165. (in Bulgarian with French abstract).

Boyanov I., Bodurov K., 1979. Triassic conodonts in carbonate breccia within the low-grade metamorphic rocks of the East Rhodopes. Geologica Balcanica, 9, 97-104.

Boyanov I., Lipman P., 1973. On the Lower Cretaceous age of the low-crystalline metamorphic complex in the East Rhodopes. Comptes Rendus de l'Academie Bulgare des Sciences, 26, 1225-1226.

Boyanov I., Trifonova E., 1978. New data on the age of

the phyllitoid complex from the Eastern Rhodopes. Geologica Balcanica, 8, 3-21.

Boyanov I., Russeva M., Toprakcieva V. and Dimitrova E., 1990. Lithostratigraphy of the Mesozoic rocks from the Eastern Rhodopes. Geologica Balcanica, 20, 3-28.

Brown S.A.M, Robertson A.H.F. 2004. Evidence for the Neotethys ocean rooted in the Vardar zone: evidence from the Voras Mountains, NW Greece. Tectonophysics, 381, 143-173.

Davis E.N. 1963. Der geologische Bau der Insel Samothraki. Annales géologique des Pays Hellenique, 14, 133-212.

Dimadis E., Nikolov T., 1997. An ammonite find in the Makri unit (Berriasian, southeast Rhodopes, northeast Greece). Comptes Rendus de l'Academie Bulgare des Sciences, 50, 71-74.

Dimadis L., Papadopoulos P., Goranov A. and Encheva M. 1996. First biostratigraphic evidence for the presence of Triassic at Melia (Western Thrace, Greece). Geologica Balcanica, 26, 37-40.

Eleftheriadis G., Esson J., Christofides G. 1989. Petrology and geochemistry of the Tertiary volcanic of Samothraki (N. Greece). Bulletin of the Geological Society of Greece, 23, 429-442.

Frass A., Hegewald S., Kloos R.M., Tesch C. and Arikas K., 1989. The geology of the graben of Petrota (Thrace, NE Greece). Geologica Rhodopica, 1, 50-61.

Heimann K.O., Lebkuchner H., Kretzler W. 1972. Geological map of Greece, Samothraki sheet, 1:50000. IGME, Athens.

Ivanov R., Kopp K.-O., 1969. Zur tektonik des trakischen Altertiar-Beckens. Geotektonische Forschungen, 31, 1-3, 117-132.

Jaranov D., 1960. Tectonics of Bulgaria. Technica, Sofia, 283 pp. (in Bulgarian with French abstract).

Kauffmann G., Kockel F. and Mollat H. 1976. Notes on the stratigraphic and paleogeographic position of the Svoula Formation in the Innermost Zone of the Hellenides (Northern Greece). Bulletin de la Societe géologique de France (7), 28, 2, 225-230.

Kockel F., Mollat H. and Walther W., 1971. Geologie des Serbomazedonischen Massivs und seines mesozoischen Rahmens. Geologisches Jahrbuch, 83, 575-602.

Koglin N., Reischmann T., Kostopoulos D., Matukov D. and Sergeev S., 2007. Zircon SHRIMP ages and the origin of ophiolitic rocks from the NE Aegean region, Greece. Geophysical Research Abstracts, 9, paper 06848.

Kopp K.-O., 1969. Geologie Thrakiens VI: Der Çoban Dağ (Frenk Bunar) westlich von Alexandroupolis. Geotektonische Forschungen, 31, 97-116.

Magganas, A.C., 2002. Constraints on the petrogenesis of Evros ophiolite extrusives, NE Greece. Lithos, 65, 165-182.

Magganas A., 2005. Subgreenschist to greenschist facies metamorphism of metavolcanics of Circum-Rhodope Belt in Thrace. Bulletin of the Geological Society of Greece, 37, 78-89. (in Greek with English abstract).

Magganas A., 2007. Plagiogranitic rocks of Evros ophiolite, NE Greece. Bulletin of the Geological Society of Greece, 40, 884-898.

Magganas A., Sideris C., and Kokkinakis A., 1991. Marginal basin-island arc origin of metabasic rocks of the Circum-Rhodope belt, Thrace, Greece. Mineralogy and Petrology 44, 235-252.

Maratos G., Andronopoulos B., 1964. Nouvelles données sur l'age des phyllites du Rhodope. Bulletin of the Geological Society of Greece, 6, 113-132.

Meinhold G., Reischmann T., Kostopoulos D., Frei D. and Larionov A.N., 2010. Mineral chemical and geochronoogical constraints on the age and source of the eastern Circum-Rhodope Belt low-grade metasedimentary rocks, NE Greece. Sedimentary Geology. (revised manuscript).

Papadopoulos P. 1982. Geological map of Greece. Scale 1:50 000. Sheet Maronia. IGME, Athens.

Papadopoulos P., Arvantinidis N. and Zanas I. 1989. Some preliminary geologic aspects on the Makri unit (Phyllite series), Peri-Rhodope zone. Geologica Rhodopica, 1, 34-42.

Papanikolaou D. 2009. Timing of tectonic emplacement of the ophiolites and terrane palegeography in the Hellenides. Lithos, 108, 262-280.

Ricou L.-E., Burg J.-P., Godfriaux I. and Ivanov Z. 1998. The Rhodope and Vardar: the metamorphic and the olistostromic paired belts related to the Cretaceous subduction under Europe. Geodinamica Acta, 11, 285-309.

Sun S.S., McDonough W.F. 1989. Chemical and isotopic systematics of ocean basalts: implications for mantle composition and processes. In: Saunders A.D., Norry M.J. (Eds.), Magmatism in Ocean Basins. Geological Society, London, Special Publications, 42, pp. 313-345.

Tikhomirova L.B., Boyanov I. and Zagorchev I., 1988. Early Jurassic radiolarians from the Eastern Rhodopes: a revision of the age of Dolno-Lukovo Formation. Geologica Balcanica, 18, 58.

Trifonova E., Boyanov I., 1986. Late Permian foraminifers from rock fragments in the Mesozoic phyllitoid formation of the East Rhodopes, Bulgaria. Geologica Balcanica, 16, 25-30.

Trikkalinos J.K., 1955. Über das Alter der vortartiären Schichten des Gebietes von Alexandropoulis-Didymotichon, Westthrazien. Annales géologique des Pays Hellenique, 6, 81-82.

Tsikouras B., Hatzipanagiotou K., 1998. Petrogenetic evolution of an ophiolite fragment in an ensialic marginal basin, northern Aegean Sea (Samothraki Island, Greece). European Journal of Mineralogy 10, 551–567.

Von Braun E., 1993. The Rhodope question viewed from eastern Greece. Zeitschrift der deutschen geologischen Gesellschaft, 144, 406-418.

Scientific Annals, School of Geology, Aristotle University of Thessaloniki Proceedings of the XIX CBGA Congress, Thessaloniki, Greece	Special volume 100	165-171	Thessaloniki 2010

METAOPHIOLITE ASSOCIATION IN THE RHODOPE MASSIF AS A STRATIGRAPHICAL AND STRUCTURAL MARKER

Kozhoukharova E.

Geological Institute, Bulgarian Academy of Sciences "Acad. G. Bonchev" Str., Bl. 24; Sofia 1113
evgkozh@geology.bas.bg; ekozhoukharova@abv.bg

Abstract: The paper is a brief survey of the geological setting and metamorphism of the Metaophiolite Association within the metamorphic basement of the Rhodope Massif on Bulgarian territory. It emphasizes the stable stratigraphic level of metaophiolites in the lower layers of the Variegated Formation of the Rhodopian Supergroup. Usually, they crop out in deep tight synclinal folds between anticlinal structures. On the basis of new geological arguments and lithological analysis that take into consideration the syn-metamorphic deformation and metamorphic changes, an attempt is made to reconstruct the primary lithostratigraphy of the metamorphic complex. In addition, some corrections of the current stratigraphic column and geological map of the Rhodope Massif are also made. The view that fold structures dominate instead of thrusts is affirmed. Geological relationships assume that the most likely way for the integration of serpentinites into the Variegated Formation of the Rhodopian Supergroup was obduction of fragments of serpentinized oceanic crust onto an ancient continent consisting of gneisses of the Prarhodopian Supergroup. The ophiolites have undergone various metamorphic changes: hydrothermal ocean and regional metamorphism in the amphibolite facies, culminating in migmatization. It is suggested that eclogitization occurred in local shear zones within the crust, and not along thrust surfaces or within subduction zones to mantle depth. The Metaophiolite Association is an important marker for the stratigraphic correlation of the metamorphic terranes as well as for the structural and metamorphic evolution of the Rhodope massif basement.

Key words: Rhodope Massif, ophiolites, primary lithostratigraphy, eclogitization.

1. Introduction

The Metaophiolite Association in the Rhodope Massif on Bulgarian territory is an important stratigraphic and structural marker for the reconstruction of the internal structure of the metamorphic basement. It is also a suitable indicator for pre-metamorphic geological settings as well as for metamorphic conditions and tectono-metamorphic evolution.

The investigation of metamorphic terranes always faces three interrelated problems: the internal structure, stratigraphy and metamorphic evolution. For their solution, two approaches are applied. The first, preferred by some regional geologists, represents subdivision of metamorphic terranes into tectonic units, often taking into account only absolute age data. This approach, considered as up-to-date, allows more freedom in the interpretation of geological constructions. On the other hand, combining different metamorphic formations into tectonic units is often accompanied by subjective evaluation and sometimes it may lead to significant discrepancy between the concepts and the real geological picture. The second, a traditional lithostratigraphic approach, requires extensive investigations, an extended database for the composition, relationships between the lithostratigraphic units, micro- and meso-scale deformations, and metamorphic petrology. But at the same time it gives a more reliable basis for characterization of the metamorphic terranes.

The Metaophiolite Association with its specific rock composition marks distinct stratigraphic layers and allows the tectonic structure to be decoded. The aim of this paper is to focus attention on some questions concerning mainly the stratigraphic and structural level of the Metaophiolite Association, based on actual geological studies. Clarifying these questions will contribute to a better understanding of both the genesis and metamorphic development of the Metaophiolite Association and the whole Rhodope Massif.

2. Geological settings of the Rhodopian Metaophiolite Association (RMOA)

The primary ophiolite rocks represented by serpentinized harzburgites, gabbros, low potassium-high magnesium tholeiites and tuffs underwent polymetamorphic alteration in different facies and were altered under different metamorphic conditions. As a result, talc-chlorite-actinolite schists, amphibolites, eclogites, pyroxenites, garnet lherzolites and metasomatic gabbroids were produced. The sequence of their formation marks several phases in the metamorphic evolution of the high-grade basement. The ophiolites are not regularly distributed in the Rhodope Massif. They appear widely in the Western and Eastern Rhodopes, where the largest serpentinite bodies and abundant metavolcanics are located, while in the Central Rhodope their appearance is restricted.

3. Stratigraphic position of the RMOA

The well-stratified metamorphic basement of the Rhodope massif is divided into two supergroups: Prarhodopian (PRS) and Rhodopian (RS). The ophiolitic association always has a stable stratigraphic position in the lower levels of the Rhodopian Supergroup. Nowhere does it mark sutures, thrust surfaces or subduction zones as some authors consider (Burg et al., 1990; Sokoutis et al., 1993; Haydoutov et al., 2004). The actual stratigraphic scheme of the metamorphic basement in the Rhodope Massif (Kozhoukharov et al. 1988) represents the sequence of lithostratigraphic units established after metamorphic consolidation of the high-grade basement involving all fold and fault deformations. Nevertheless, the stratigraphic sequence is sufficiently well preserved to allow the original pre-metamorphic sequence to be restored.

A suite of reliable criteria have been used to reconstruct the primary rock composition and relationships of the lithological units, sequences and features of different metamorphic events, periods of hiatus in the evolution, marked by transgression, igneous intrusion or discordance (Kozhoukharova, 2008). The pre-metamorphic reconstruction model distinguishes two lithological complexes (Fig. 1). The lower one is an ancient infracrustal continental complex, the PRS, consisting of highly reworked para- and ortho-metamorphic gneisses, complemented by leptite or porphyroblastic gneisses. The absence of marbles is a specific feature of the PRS. All rocks had already been metamorphosed before the deposition of the upper RS rock complex. Cadomian, Hercynian and Alpine granitoid magmas and several generations of their aplite-pegmatite vein-like derivates penetrated the complex, causing migmatization, granitization, feldspathization and reheating, particularly more intensively in the deeper stratigraphic levels. As a result, the PRS was enriched in components like Si, Al, Na, K, Ba, Rb, Cs, Zr and obtained the geochemical signature of granite-granodiorite. Subsequently, superimposed metasomatic processes considerably altered the composition and structure of the protolith, to the extent that it can be identified only by geochemical methods. The Prarhodopian Supergroup forms the core of anticlines and dome structures (Fig. 1).

The Rhodopian Supergroup (RS) is a new transgressively deposited typical supracrustal variegated complex, consisting of metamorphosed volcanogenic-sedimentary rocks. Its primary rocks were flyschoid pelite-calcareous sediments (Variegated Formation - VF), overlain by limestones (Marble Formation - MF). The ophiolites occupy the lower levels of the VF, where they alternate with or are covered by sediments or are intercalated with them (Fig. 2). A clear lateral variation is observed in the primary composition of the VF.

Two types of VF are distinguished: a) the West Rhodopian (Satovcha) type, and b) the Central Rhodopian (Loukovitsa) type (Fig. 2).

a) The West Rhodopian (Satovcha) type of VF represents a rock assemblage formed in regions with abundant basic volcanism. The volume of basic-ultrabasic orthometamorphic rocks prevails over parametamorphic rocks (Fig. 2). The VF usually commences with ophiolites (serpentinites or amphibolites) lying directly on gneisses of the Prarhodopian Supergroup. Serpentinite lenses and megaboudins of variable size (from several meters to 10-12 km long) are associated with amphibolites. The VF continues upwards as a thick sequence of layered and massive medium- to coarse-grained amphibolites, actinolite-chlorite and biotite schists, interleaved with graphite-bearing garnet quartzites and magnetite-haematite jaspilites. The bulk sedimentation was contaminated by volcanic tuffs, while only very thin and rare calcareous or aluminium-rich metapelite layers appear in the upper levels of the VF. Fine-grained amphibolite dykes, often enriched in ore minerals, cross-cut the layered amphibolites and serpentinites. Rare small gneiss xenoliths with sharp contours, ripped from the sole, occur among the amphibolites. The

chemical composition of the amphibolites corresponds to normal and high magnesium arc tholeiitic and picritic basalts. The Satovcha type of VF is widespread in the Western Rhodope – the valley of Mesta river, and in the Eastern Rhodope – Byala Reka dome, Avren syncline, Chakalarovo syncline and Drangovo horst.

The Kimi Complex, assigned to an "Upper tectonic unit" (Mposkos and Kostopoulos, 2001) in the Eastern Rhodopes on Greek territory, is a direct prolongation of the Vucha Variegated Formation from the Avren syncline (Fig. 1).

volcanism in lower levels of the VF, there are variably thick layers (2-3 to 200-400 m) of porphyroblastic gneisses. The gneiss protoliths are believed to have been coarse-grained or fine clastic sands, rather than porphyroid granite. In the Sakar region the porphyroblastic gneisses are overlain by metaconglomerates. They presumably marked an abrupt change in the palaeoenvironmental setting before the formation of the ophiolite association. The obduction of ophiolite fragments from ocean crust is more likely at present. They ended up in a marginal sea where they were covered by sedi-

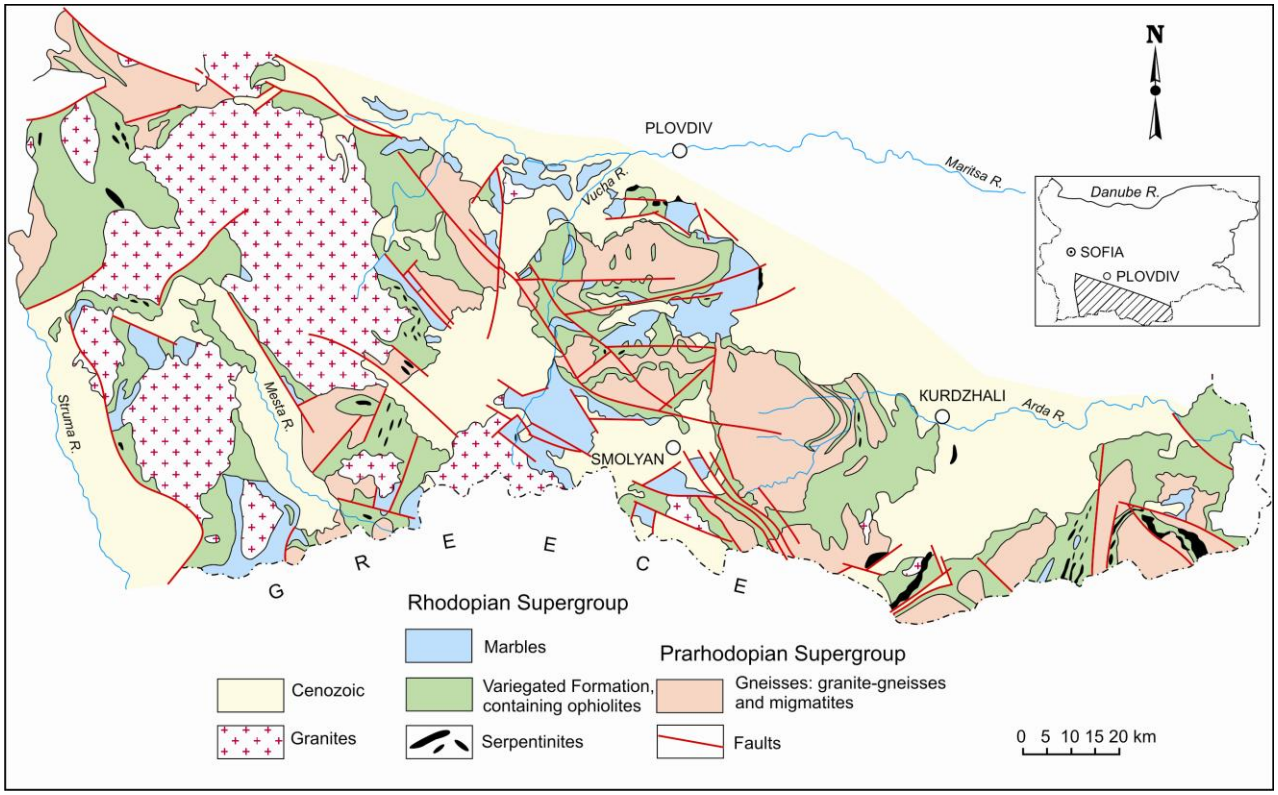

Fig 1. Geological map of the main lithostratigraphy metamorphic units in the Rhodope Massif.

b) The Central Rhodopian (Lukovitsa) type of VF consists mainly of alternating metapelites altered to biotite and two-mica schists (some of them kyanite-bearing), marbles, calc-schists and a few quartzites. Thin layers of amphibolite and lenses of serpentinite occur in the lower stratigraphic levels of the VF (Fig. 2). In some areas of the Central Rhodope (Northern Rhodope anticline), the amphibolites are connected to a sub-volcanic metadiabase body which cross-cuts the leptite gneisses from the base of the VF and includes xenoliths of them. In places beyond the volcanic zones, calcareous and alumina-rich pelites (future marbles and kyanite schists) are more widespread.

Furthermore, in the region of previously active

ments (Kozhoukharova, 2008). The composition of the basic metavolcanic rocks suggests arc tholeiites. Evidence for an autochthonous volcanic origin of the amphibolites includes: relict igneous texture, xenoliths of leptite gneisses derived from the basement, and basic dykes cross-cutting the gneisses of the PRS. These facts suggest possible initial rifting of the ancient continental fragment.

4. Structural position of the RMOA

The Prarhodopian and Rhodopian supergroups were subjected to synmetamorphic folding at least twice. In the general synmetamorphic structural plan, domes and linear positive structures are observed, whose cores consist of gneisses of the PRS.

The spaces between them contain pinched subvertical, inclined or recumbent synclines, filled by rocks of the Variegated Formation containing ophiolites. The largest of the typical inclined and recumbent synclines are: West Rhodopes-Debren syncline, Central Rhodopes-Ardino syncline and East Rhodopes-Zhalti Chal syncline. The last is a complicated doubly folded inclined syncline, such that the serpentinite bodies have been deformed into megaboudins (Fig. 1). The main direction of linear structures in the Central Rhodopes is E-W with a southern vergence, while in the East Rhodopes the direction changes to NNE-SSW (Avren syncline) but later also to NW-SE (Zhalti Chal syncline). The folds observed in the northern part of the West Rhodopes have mainly a NW-SE orientation and are inclined to the SE. They are obliquely cut by the Rila-Rhodopian granite batholith (Fig. 1). In the southern part of the West Rhodopes a later NE-SW direction was imposed (Fig. 1). Usually, the morphology of the folds is variable, and in addition they are complicated by minor isoclines along their limbs. The boudinage structure of the whole Variegated Formation and enclosed ophiolites is clearly expressed. Rod-like structures appear in the axial parts of folds. In places, small fragments of their keels were downfolded into migmatite gneisses, and are now observed as rootless amphibolite or eclogite bodies. In some places the tight synclines become narrow and in their lower parts they pass into shear zones where eclogites and garnet lherzolites occur. An example is the Avren syncline in the Eastern Rhodope, where the ophiolites continue into Northern Greece in the Kimi Complex. A new structural plan was superposed on the earlier synmetamorphic plan during Alpine tectonic reactivation. The folds have a NNE-SSW (10-15^{o}) direction, often associated with retrogression of the metamorphic rocks. Some of the old fold structures were reactivated. Local detachment thrusts formed along the periphery of the Rhodope massif and on the slopes of Palaeogene depressions.

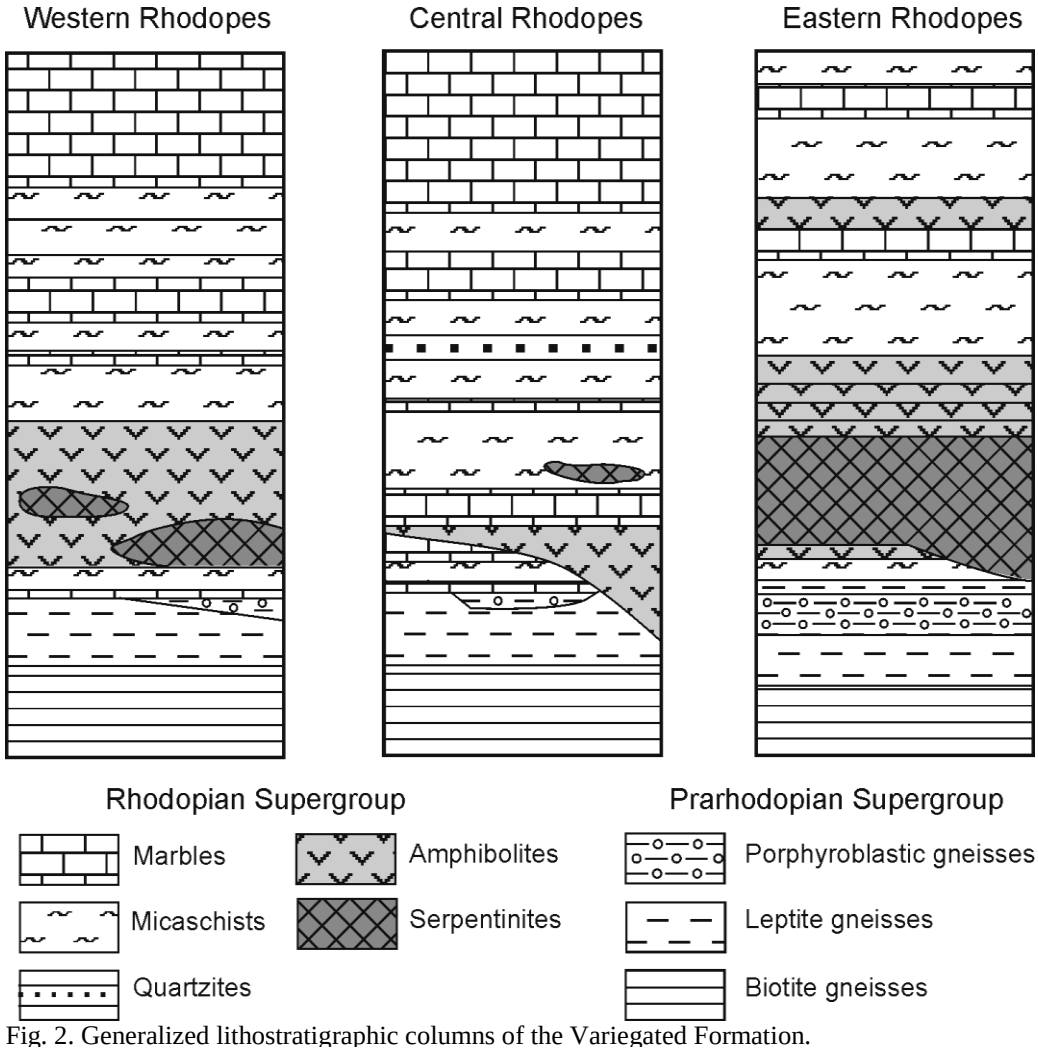

Fig. 2. Generalized lithostratigraphic columns of the Variegated Formation.

5. Brief remarks about the evolution and metamorphism of the Metaophiolitic Association

The primary ophiolite rocks such as serpentinites, gabbros, gabbro-norites, low potassium-high magnesium tholeiites and tuffs underwent polymetamorphic alteration in different facies. Several stages of metamorphism have been identified.

1. Hydrothermal ocean metamorphism – lizardite-chrysotile serpentinitization of peridotites took place in a hydrous environment.

2. Proterozoic tectonic episode – obduction of oceanic crustal fragments (serpentinites) over the marginal parts of an ancient Precambrian continent consisting of Prarhodopian gneisses (metamorphosed during the first Precambrian cycle); igneous activity expressed as basic volcanic and intrusive rocks; sedimentation of politic-calcareous flyschoid sediments that cover the serpentinites. The marbles contain Mesoproterozoic to Neoproterozoic microfossils (Kozhoukharov and Timofeev, 1989; Tchoumatchenko and Sapunov, 1989), indicating a Precambrian age for the ophiolites.

3. Second Precambrian cycle. Regional metamorphism took place generally in the amphibolite facies and synchronous folding of the Rhodopian Supergroup. Two or in some places three metamorphic episodes, marked by two or three consequent mineral assemblages, separated by deformation, were distinguished in the mica schists. Serpentinite bodies have been replaced at their margins by talc-chlorite-actinolite schists. Basic volcanic rocks were transformed into various amphibolites at T = 480-540 ^{o}C and P = 4-6 kbar. Eclogitization took place in local narrow ductile shear zones in the amphibolites, producing omphacite-garnet-rutile assemblages at T = 450-550 ^{o}C and P = 9-12 kbar, while the dominant metamorphism of the country rocks is medium-pressure amphibolite facies (Kozhoukharova, 1980; 1996).

An instructive example for eclogitization "in situ" represents Gr-lherzolite bands within a serpentinite body in the Avren syncline in the Eastern Rhodope (Kozhoukharova, 1996;1999). Thin 1-2 cm stripes, consisting of garnet, enstatite, diopside, olivine and spinel alternate with serpentine bands. The stripes gradually disappear towards the central parts of the body. The P-T conditions of crystallization in the zones is in the range 560-811 ^{o}C/8-15 kbar, while in the country rocks they are 480-540 ^{o}C/4-6 kbar (Fig. 3). The arguments for a metamorphic origin are: lherzolite banded segregations are displayed only at the lithological contact of serpentinite bodies, entirely concordant with the general stratification and metamorphic schistosity of the rock complex; eclogite minerals everywhere replace serpentine, but they themselves are not deformed and altered; Gr-lherzolites are found only in the strongly folded synclines.

The same serpentinite body continues into Northern Greece in the Kimi Complex. Mposkos and Kostopoulos (2001) reported the discovery of microdiamond and coesite inclusions in garnet from eclogites and metapelites. The authors considered that these facts alone are enough to conclude that the rocks had once been transported by subduction to depths exceeding 220 km. However, the ensemble of all the geological and petrographic features of metamorphic complexes in the Rhodope massif does not favour such a traditional decision.

Eclogitization develops locally only in the confined space of shear zones, where a new HP heterofacial mineral assemblage crystallizes synchronously with the dominant amphibolite facies metamorphism of the country rocks (Fig. 3). Preservation of serpentine proves that the temperature of the dominant regional metamorphism does not exceed 580 ^{o}C. Isotopic data indicate a Neoproterozoic age of 610 Ma for the eclogites from the Central Rhodope (Arcadaskiy et al., 2003) and 572±5 Ma for the amphibolites from the Eastern Rhodope (Haydoutov et al., 2004).

The ophiolites located within zones of migmatization and granitization (Cadomian or Hercynian age) are intensively affected by feldspathization and metasomatic processes. Locally, swarms of pegmatite veins cut the serpentinites and form "dykes" of metasomatic gabbroids with xenoliths of partially assimilated serpentinites. Chemical interaction between the serpentinites or amphibolites and aplite-pegmatite veins resulted in various metasomatic gabbroids, outwardly resembling igneous rocks. They are of variable appearance and structure: massive, agglomeratic, streaky, lenticular or schistose. Often lens-shaped segregations of plagioclase with variable anorthite content (from oligoclase to bytownite-anorthite) form a specific spotted ("leopard") structure. Other grey-greenish segregations (which represent reworked ultrabasic inclusions in pegmatite veins), consisting of olivine, pyroxene, amphibole, garnet, talc and chlorite, show reaction textures: coronas, corrosion relationships, different types of pseudomorphs, sym-

plectites and diablastic intergrowths. The formation of metasomatic gabbroids at the expense of basic and ultrabasic ophiolites can be observed at many locations in the Rhodope massif. In the early stages of regional metamorphism, the alteration of ophiolites has a nearly isochemical recrystallization in a compressive regime. During later stages, during decompression, increased mobility of the components occurred and the metamorphism passes into clear metasomatic alteration and assimilation of ophiolites.

6. Discussion

The stable stratigraphic position of the Metaophiolitic Association within the sequence of the Variegated Formation (Rhodope Supergroup) refutes the hypothesis of late post-metamorphic incorporation of the ophiolites into the basement. Nowhere do ophiolites or serpentinites mark sutures, thrust surfaces or deep faults. The ophiolites as an integral part of the volcano-sedimentary Variegated Formation are synchronous with the transgressive Neoproterozoic sedimentation of the Rhodopian Supergroup. It is proposed that only the serpentinites were tectonically obducted onto the margin of an ancient continental fragment (the Prarhodopian Supergroup), where they were covered by peliticcarbonate sediments.

The problem of the origin of eclogites in the Rhodope Massif is similar. The eclogites are not exotic bodies uplifted from mantle depths, and they are always located amongst the ophiolitic amphibolites. Mposkos and Krohe (2006) supposed that the Kimi complex in Northern Greece was subducted to mantle depths (150-200 km), and then rapidly exhumed. But the Kimi complex is not an isolated block, rather it is a direct continuation of the Variegated Formation of the Rhodopian Supergroup cropping out in the Avren syncline and in the whole Rhodope Massif. It is impossible to believe that the whole Rhodope Massif passed through a subduction zone of high deformation, reached mantle depths and was then exhumed, retaining untouched its stratigraphy and fold structures. It is also inexplicable how the serpentine (for which temperature stability reaches only to 580–600^{o}C) was not affected by the extreme P/T conditions. It must be mentioned that reserpentinization in any metamorphic complex in the Earth`s crust is impossible.

On the other hand, the presence of microdiamonds and coesite in the metamorphic rocks is not a sufficient argument for crystallization at mantle depths. A number of experimental data in tribochemistry and tribology provide a new point of view about the realization of high temperatures and pressures in zones of friction, sufficient for the crystallization of diamond and coesite (Kozhoukharova, 2008a).

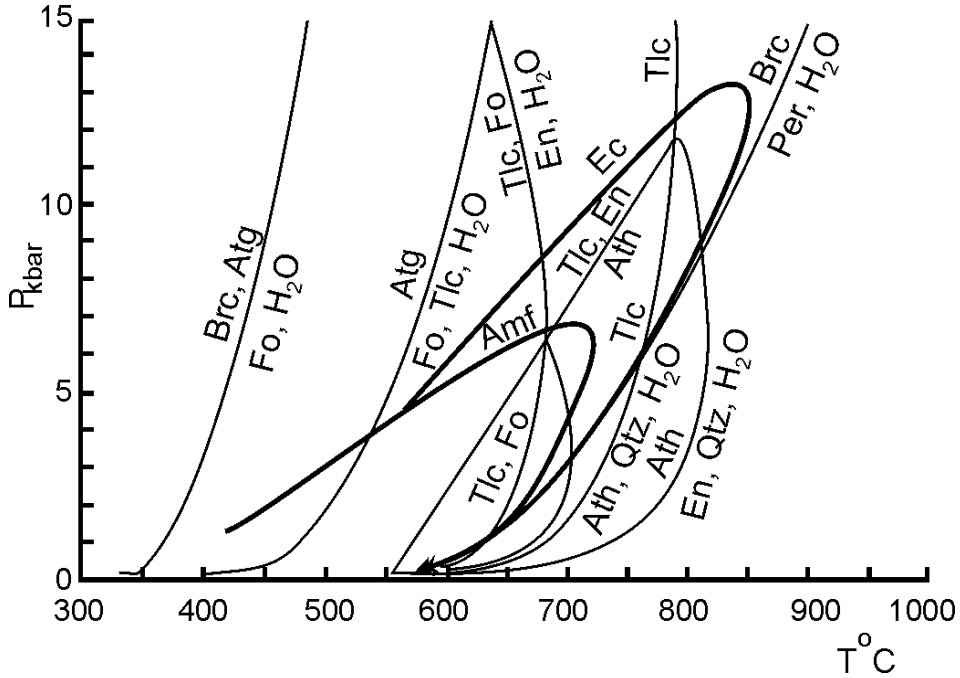

Fig 3. Schematic petrogenetical grid after Spear (1993) with two branches of regional metamorphism: Ec-eclogite facies; Amf-amphibolite facies.

The configuration of the Variegated Formations that contain ophiolites clearly outlines the fold structures in the metamorphic basement (Fig. 1). The idea that the Rhodope Massif represents an Alpine building – a "pile" of several discordant tectonic plates separated by Cretaceous sediments allegedly containing Mesozoic microfossils (Burg et al., 1996), remains unproven. No detailed geological maps, cross sections, descriptions of real tangible overthrusts and their contacts, have been published, except for a few simplified sketches. The alleged Cretaceous sediments have also not been proven, and were later demonstrated to be cataclastic mylonitized marble and calc-schists. The deformation microstructures, shown by the authors cited as evidence for thrusting, are usually observed in all metamorphic rocks that suffered folding. However, it seems that the above-mentioned authors (Burg et al., 1996) probably abandoned the thrust concept, admitting the existence of the Kessebir–Kardamos anticline (Bonev et al., 2006).

7. Conclusions

1) The pre-metamorphic stratigraphy of the Rhodopian Supergroup is represented by two main groups: a lower Variegated Formation and an upper Limestone Formation.

2) The ophiolites occupy a fixed stratigraphic level in the lower part of the Variegated Formation. Nowhere do they mark subduction zones, sutures or thrust surfaces.

3) Eclogites and Gr-lherzolite are crustal metamorphic products after ophiolites; they crystallized locally in narrow ductile shear zones, where HP-metamorphism took place, evidently during syn-metamorphic folding of the complexes. The dominant regional metamorphism is medium-pressure amphibolite facies. Heterofacies mineral assemblages were produced.

4) Feldspathization and granitization caused partial gabbroidization, dioritization and assimilation of the ophiolites at zones of active migmatization.

5) The age of the ophiolite protolith is Mesoproterozoic to Neoproterozoic.

References

Arcadaskiy S. V., Bohm C. Heaman L., Cherneva Z., Stancheva E. and Ovtcharova M. 2003. Remnants of Neoproterozoic oceanic crust in the Central Rhodope metamorphic complex, Bulgaria. Technical Programme, Vancouver 2003.

Bonev N., Burg J.-P. and Ivanov Z., 2006. Mesozoic-Tertiary structural evolution of an extensional gneiss dome-the Kesebir-Kardamos dome, eastern Rhodope (Bulgaria-Greece). Int. J. Earth Sci. 95; 316-340.

Burg J. P., Klain L., Ivanov Z., Ricou L. E. and Dimov D. 1996. Crustal scale thrust Complex in the Rhodope Massif. Evidence from structures and fabric. Terra Nova, 8, 6-15.

Haydoutov I., Kolcheva K., Daieva L. A., Savov I. and Carrigan C. 2004. Island arc origin of theVariegated Formation from the East Rhodope, Bulgaria – Implications for the evolution of the Rhodope Massif. Ofioliti, 92, 2, 145-157.

Kozhoukharov D., Timofeev B. 1989. Microphitofossil data on the Precambrian age of the Rhodope Supergroup in the Central and Western Rhodopes. Geologica Balcanica, 19, 1, 13-31 (in Russian).

Kozhoukharov D., Kozhoukharova E., Papanikolaou D. 1988. Precambrian in the Rhodope massif. In: Zoubek V.(ed.*) Precambrian in Younger Fold Belts.* John Wiley & Sons, Chichester, pp. 723- 820.

Kozhoukharova E. 1980. Eclogites in the Precambrian from the Eastern Rhodope block. Comptes Rendus de l'Academie bulgare des Sciences, 33, 3, 375-378.

Kozhoukharova E. 1996. Eclogitized layered serpentinites in the East Rhodope block. Comptes Rendus de l'Academie bulgare des Sciences, 49, 6, 69-71.

Kozhoukharova E. 1999. Gr-lherzolites into narrow shear zones of serpentinites from Rhodope massif, Bulgaria. Ofioliti, 24, 121-122.

Kozhoukharova E., 2008. Reconstruction of the primary stratigraphy and correlation of the Precambrian metamorphic complexes in the Rhodope massif. Geologica Balcanica, 37, 1/2, 19-31.

Kozhoukharova E. 2008. Application of tribo-principles in Geology. An example for tribochemical genesis of eclogites. 6th International conference on tribology Balkantrib'08, Sozopol, Bulgaria, p. 82.

Mposkos, E., D., Kostopoulos, D., K. 2001. Diamond, former coesite and supersilicic garnet in metasedimentary rocks from the Greek Rhodope: a new ultrahighpresure metamorphic province established. Earth and Planetary Science Letters,192, 497-506.

Mposkos E., Krohe A. 2006. Pressure-temperature-deformation paths of closely associated ultra-high-pressure (diamond-bearing) crustal and mantle rocks of the Kimi complex: implication for the tectonic history of the Rhodope Mountains, northern Greece. Canadian Journal of Earth Sciences, 43, 12, 1755-1776.

Sokoutis D., Brun J. P., Driessche J. Van Den and Pavlides S., 1993. A major Oligo-Miocene detach-ment in Southern Rhodope controlling North Aeg-ean extension. Journal of the Geological Society, London, 150, 243-246.

Tchoumatchenco P. V., Sapunov I.G., 1989. Paleontological evidence of a Precambrian age of the marbles at the Asenova Krepost Castle (Central Rhodopes, Bulgaria). Geologica Balcanica, 19, 1, 33-36.

Scientific Annals, School of Geology, Aristotle University of Thessaloniki Proceedings of the XIX CBGA Congress, Thessaloniki, Greece	Special volume 100	173-181	Thessaloniki 2010

ALPINE POLYPHASE METAMORPHISM IN METAPELITES FROM SIDIRONERO COMPLEX (RHODOPE DOMAIN, NE GREECE)

Mposkos, E.[1], Krohe, A.[2] and Baziotis, I.[1]

[1] *National Technical University of Athens, School of Mining and Metallurgical Engineering, Division of Geological Sciences, 9, Polytechniou Str., Zografou (Athens),Greece, Phone ++3021-07722099*
[2] *Institute for Mineralogy, Laboratory of Geochronology University of Muenster Corrensstr.24, D-48149 Muenster, NRW, Phone: ++49-251-8333405, email: krohe@unimuenster.de*

Abstract: Metamorphic mineral ages from garnet-kyanite gneisses in the area north of Xanthi documented a Jurassic and an Eocene metamorphic event in the Sidironero complex of the Rhodope domain. The two metamorphic events are well imprinted in the mineral assemblages, mineral compositions and textural relationships of metapelites within the Nestos Shear Zone in the Sidironero complex. The Jurassic event at HP-UHP metamorphic conditions is characterized by the mineral assemblage garnet-kyanite-Ti-rich phengite at the peak pressure. The Eocene metamorphic event at moderate HP conditions and minimum pressure > 0.9 GPa is characterized by the mineral assemblages St-Grt-Ms-Ky-Bt with garnet growth at the expense of kyanite or staurolite, and Grt-St-Ky-Bt with peak P-T conditions within the St+Bt+Ky stability field.

Keywords: metapelites, polyphase metamorphism, Rhodope, Sidironero Complex

1. Introduction

The Rhodope Domain occupies a central position in the Alpine belt, between the south west-verging Hellenides and the north-verging Balkanides. It mostly consists of medium-to high-grade pre-Alpine and Alpine metamorphic rocks and granitoids and represents the exhumed metamorphic core of the Alpine orogen of the Hellenides (Mposkos and Krohe, 2000; Ivanov et al., 2000).

Various authors have proposed several schemes for a subdivision of the Rhodope into different tectonic units (see Krohe and Mposkos, 2002 and references therein). Mposkos and Krohe (2000) and Krohe and Mposkos (2002) subdivided the Greek part of the Rhodope Domain into several superimposed tectonic complexes based on differing maximum P-T conditions, P-T paths, geochronological data (known so far), and including structural data constraining the kinematics of emplacement of different tectonic units. These units basically differ in evolution path of Alpine subduction and exhumation. The Vertiscos complex in the west part and the Kimi complex in the east part of the Rhodope Domain underwent mid-Mesozoic high pressure (HP)/ultra-high pressure (UHP) metamorphism and were exhumed to the upper crust in late Cretaceous to early Tertiary time. The underlying complexes Sidironero, Kardamos, Kechros and the lowermost Pangaeon complex including the Albite Gneiss Series underwent Tertiary HP metamorphism (early Eocene in the Sidironero complex, Liati and Gebauer, 1999) and were exhumed to the upper crust in late Eocene (Sidironero Complex) to Miocene time.

Since then, a huge number of new geochronological data have been published that bear witness to the imprint of at least two major Alpine metamorphic cycles, one in the mid-Mesozoic, the other in the mid-Cenozoic with an apparent gap of about 100 Ma in the Sidironero complex (Liati, 2005; Reischmann and Kostopoulos, 2002; Bosse et al., 2009). However, petrological evidences for both metamorphic events within single rocks are still lacking.

In this contribution we present petrological data from selected metapelites from the Sidironero complex, which combined with available geochronological data, indicate that the Sidironero complex underwent two Alpine prograde metamorphic events, a Jurassic HP/UHP metamorphism like that recorded in the overlying Kimi complex and an Eocene moderate HP one.

2. Geological Framework

The Sidironero complex consists of migmatitic quartz-feldspar–and pelitic gneisses, orthogneisses and marbles that host mafic and scarce ultramafic rocks. Partially amphibolitized kyanite eclogites and common eclogites indicate HP metamorphism at peak P-T conditions of >1.9 GPa and 700^{o}C (Liati and Gebauer, 1999). Pelitic gneisses record granulite facies conditions by the mineral assemblage Grt-Ky-Bt-Pl-Kfs-Qtz-Rt (abbreviations after Martin, 1999) (Mposkos and Liati, 1993). Microdiamond inclusions in garnet from pelitic gneisses indicate that lithologies of the Sidironero complex underwent UHP metamorphism (Mposkos and Kostopoulos, 2001; Perraki et al., 2006).

Pre-Alpine ages for magmatic protoliths yielded SHRIMP U-Pb zircon dates (294±8 Ma) in orthogneisses (Liati and Gebauer, 1999). Alpine ages can be classified in two broad groups. The first group at ~185-140 Ma is represented by U-Pb SHRIMP ages in metamorphic rims on zircon, U-Th-Pb LA-ICPMS ages on monazite and Sm-Nd garnet-whole rock age from pelitic garnet-kyanite gneisses near Xanthi town (Liati, 2005; Bosse et al., 2006; Reischmann and Kostopoulos, 2002). This lithology has yielded evidence of diamond inclusions in garnet (Mposkos and Kostopoulos, 2001; Perraki et al., 2006). U-Pb SHRIMP zircon ages of 51 to 42 Ma from amphibolitized eclogites, ~ 36 Ma from cross-cutting pegmatites (Liati and Gebauer, 1999; Liati, 2005) and 55 to 39 Ma Th-Pb monazite ages from deformed pegmatites (Bosse et al., 2009) constrain the second group of the Alpine ages in the Sidironero complex.

A crustal scale shear zone several km in thickness (Nestos shear zone) separates the Sidironero complex and the underlying Pangaeon complex. This shear zone comprises lithologies of the UHP-HT Sidironero complex and the underlying HP Albite-Gneiss Series of Mposkos and Krohe (2000), which is a part of the Pangaeon complex (Mposkos et al., 1998). The Albite Gneiss Series consisting of orthogneisses, paragneisses with pre-mylonitic (pre-Alpine) migmatitic textures in outcrop scale, metapegmatites, minor amphibolites, metapelites and few marbles, record only the Tertiary Alpine metamorphism. In the Drama area, from south to north, the metamorphic grade of the Alpine metamorphism increases from the albite-epidote amphibolite facies to the middle amphibolite facies (Mposkos unpublished data). Pb-Pb evaporation and SHRIMP dating of zircons from orthogneisses yielded Permo-Carboniferous ages (283-297 Ma) for their magmatic protoliths (Liati, 2005; Turpaud and Reischmann, 2010), and 38-40 Ma for the pegmatoid neosomes near the contact with the overlying Sidironero complex (Liati, 2005).

3. Evidence of polyphase metamorphism in metapelites

3.1. Petrography and Mineral Chemistry

Selected samples of metapelites from three localities of the Sidironero complex with textural relationships and mineral assemblages indicating polymetamorphic evolution are studied with optical microscopy, scanning electron microscopy and microprobe analysis. The sample localities are shown in figure 1.

Locality 1: (Fig. 1; coordinates N41^{0}16´59.6´´ E24^{0}24´45.3´´): In locality 1 garnet-kyanite gneisses with migmatitic textures show post-migmatitic mylonitisation. The mineral assemblage of the rock is: Grt+Ky+Bt+Ms+Qtz+Rt±Pl. Garnet porphyroblasts contain single grain inclusions of quartz, biotite, rutile, kyanite, zircon, xenotime, monazite, apatite and inclusions of composite grains consisting of Bt+Qtz+Rt±Xnt±Mnz (Fig. 2a) and Ky+Bt+Qtz±Ms. Rational crystal faces between composite inclusion and garnet host are common. Garnet shows corroded edges and is replaced by biotite and kyanite. The garnet has almost homogeneous composition ($Grs_5Prp_{22}Alm_{70}Sps_3$). Only the outermost rim shows diffusion zoning with decreasing MgO and increasing FeO, CaO and MnO contents (Table 1). Two generations of kyanite occur. Ky-1 occurs as single grain inclusions in garnet. Ky-2 is a major phase in the matrix. It commonly forms aggregates associated with biotite pseudomorphose after former Al-rich phase, probably garnet (Fig. 2b). Biotite inclusions in garnet show higher Mg# values compared to matrix biotite. The Mg# value in single grain biotite inclusions is 0.60, in biotite from polyphase inclusions consisting of Bt+Qtz+Rt± Xnt±Mnz 0.68 and in matrix biotite 0.44 (Table 2), reflecting biotite growth at different metamorphic conditions. Biotite from Bt+Ky+Ms+Qtz polyphase inclusions in garnet shows similar Mg# values to those of the matrix biotite.

Locality 2: (Fig. 1; coordinates N41^{0}20´21.9´´ E24^{0}12´33.1´´): Mylonitic garnet-kyanite gneisses 4 meters in thickness intercalated between underlying mylonitic and retrogressed amphibolites and marbles and overlaying quartz-feldspar gneisses. A

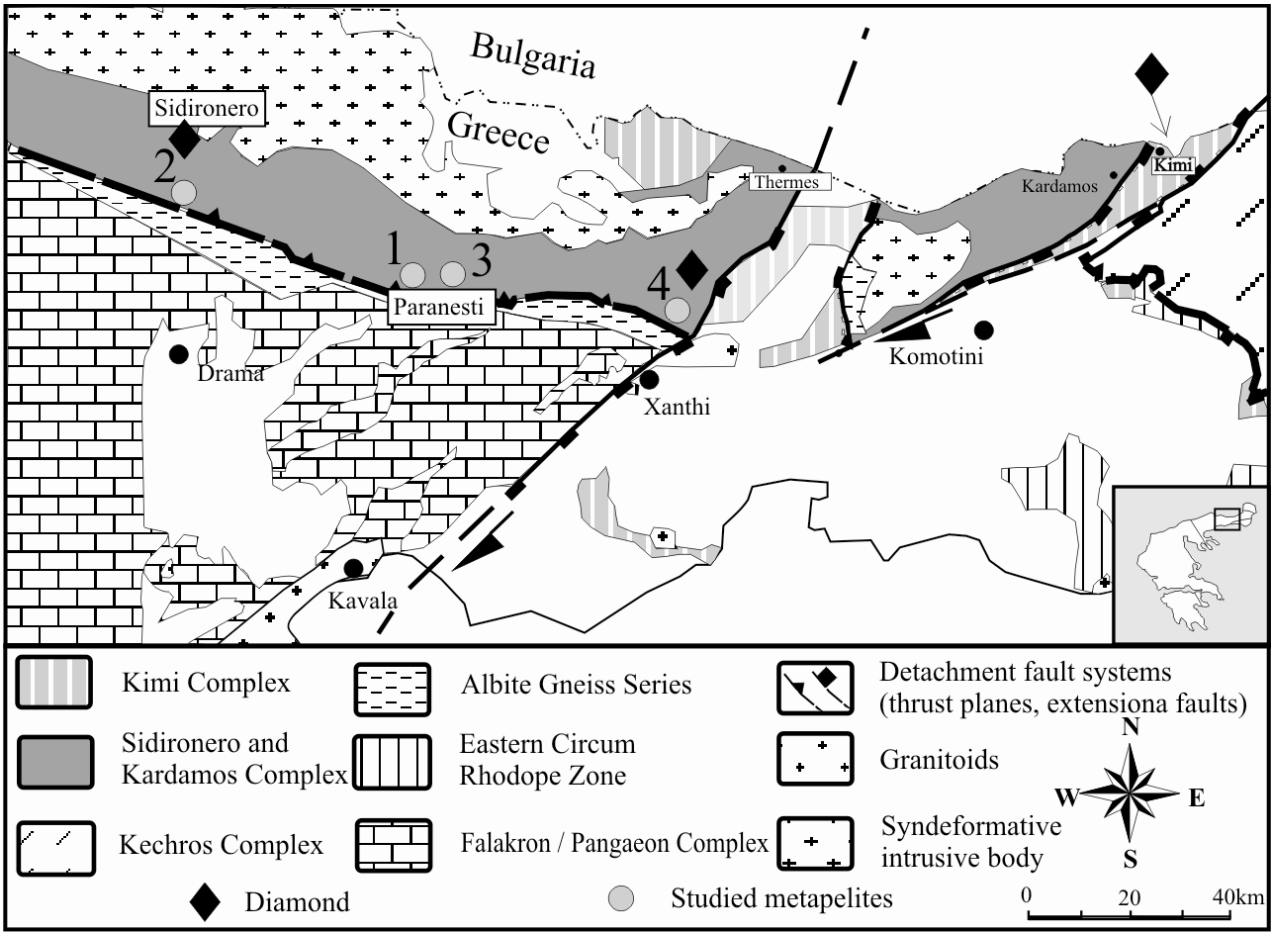

Fig. 1. Simplified geotectonic map of Central Greek Rhodope (after Mposkos and Krohe, 2000). Circles with numbers are localities of metapelites from Sidironero Complex, referred in the present work.

boudin of amphibolitized eclogite ~5m in length overlies the garnet-kyanite gneiss. The mineral assemblage of the garnet-kyanite gneisses is: Grt+ Ky+Bt+Ms±St+Qtz±Pl+Rt±Ilm+Tur+Zr+Ap+Mnz.

Three generations of garnet are distinguished on textural and chemical criteria. Grt-1 (Grs_3 Prp_{18} Alm_{73} Sps_6) occurs as inclusion in kyanite porphyroblasts. Grt-2 (Grs_1 Prp_{26} Alm_{69} Sps_4) forms porphyroblasts up to 20 mm in size. It contains inclusions of rutile, quartz, muscovite, biotite, kyanite, staurolite, graphite, zircon and monazite. Exsolutions of rutile needles oriented in host garnet (triangular pattern, Fig. 2c) are common. Grt-3 (Grs_4 Prp_{18} Alm_{73} Sps_5) overgrows Grt-2 (Fig. 2d) and is commonly associated with matrix muscovite. It forms broad but irregular rims around parts of Grt-2 grains Grt-3 is rich in quartz and rutile inclusions. Inclusions of staurolite, muscovite and biotite are also present (Fig. 2d). Exsolutions of rutile needles are not present in Grt-3.

Two generations of kyanite and two of staurolite occur. Ky-1 forms porphyroblasts up to 15mm in size. Ky-1 contains inclusions of garnet (Grt-1), biotite, muscovite, rutile, quartz and rarely staurolite. Ky-2 (0.05-0.2 mm in size) is associated with matrix biotite, replaces Grt-2 and overgrows Ky-1. St-1 occurs as inclusions in Ky-1 and Grt-2. Matrix staurolite (St-2), if present, overgrows kyanite (Fig. 2e) and is associated with muscovite. It also occurs as inclusion in Grt-3 (Fig. 2d)

At least three generations of muscovite and two of biotite can be distinguished. Ms-1 and Bt-1 occur as inclusions in Ky-1 and Grt-2. Ms-2 is present as porphyroblasts up to 3 mm in size. It contains inclusions of garnet and kyanite, rutile needles interpreted as exsolutions (Fig. 2f), and flakes of biotite. Shape-preferred orientation of medium grained matrix muscovite (Ms-3) and biotite (Bt-2) define the main foliation of the rock. Matrix muscovite contains inclusions of kyanite grains with corroded edges. Rutile is the main Ti-ferous phase. It occurs as inclusions in Ky-1, Grt-1, Grt-2 and Grt-3 and in the rock matrix. Only matrix rutile is replaced by ilmenite.

Table 1. Representative garnet compositions of metapelites from the Sidironero complex.

	Locality-1		Locality-2				Locality-3					
	Grt-c	Grt-r	Grt-1c	Grt-2c	Grt-2r	Grt-3	Grt-1c	Grt-1r	Grt-2c	Grt-2r	Grt-1k	Grt-2k
SiO_2	37.97	37.45	37.65	38.11	37.17	37.52	37.56	37.00	36.90	36.90	37.70	36.79
Al_2O_3	21.43	21.14	21.18	21.54	20.93	21.06	21.15	20.89	20.81	20.80	21.25	20.80
FeO	31.84	32.02	32.91	31.50	33.48	31.70	33.42	35.10	23.98	31.13	32.94	33.95
MnO	1.53	3.49	2.54	1.78	2.79	4.67	2.34	3.70	13.06	5.19	1.64	4.43
MgO	5.56	3.62	4.45	6.64	3.50	3.62	4.87	2.70	1.08	3.24	5.52	2.28
CaO	1.67	2.11	1.07	0.22	1.73	1.33	0.45	0.62	4.12	2.01	0.71	1.40
Total	100.01	99.84	99.80	99.80	99.60	99.99	99.79	100.01	99.95	99.27	99.78	99.68
12 oxygens												
Si	3.000	3.002	3.008	3.002	2.998	3.009	3.000	2.998	2.997	2.992	2.998	2.995
Al	1.996	1.998	1.994	2.000	1.990	1.992	1.991	1.994	1.992	1.988	1.992	1.996
Fe	2.105	2.147	2.199	2.076	2.258	2.127	2.233	2.378	1.629	2.111	2.190	2.311
Mn	0.102	0.237	0.172	0.119	0.190	0.318	0.160	0.254	0.898	0.356	0.111	0.306
Mg	0.655	0.432	0.530	0.779	0.421	0.433	0.580	0.326	0.130	0.391	0.654	0.277
Ca	0.142	0.182	0.092	0.019	0.149	0.115	0.039	0.054	0.359	0.175	0.061	0.122
Mg#	0.237	0.167	0.194	0.273	0.157	0.169	0.206	0.120	0.07	0.156	0.23	0.107

c=core, r=rim, s=inclusion in staurolite, k=inclusion in kyanite, Mg# = Mg/(Mg+Fe)

Locality 3 (Fig. 1; coordinates N41^{0}15′17.7″ E24^{0}28′04.4″): In locality 3 occur garnet-staurolite-kyanite schists with the mineral assemblage Grt+St+Ky+Bt+Ms±Chl±Sil±Pl+Rt+Ilm+Tur+Ap. Garnet is a major phase in the rock matrix. It also occurs as inclusions in staurolite and kyanite porphyroblasts (Fig. 2g). Two generations of garnet are distinguished based on chemical criteria (Table 1). Grt-1 (Grs_2 Prp_{22} Alm_{73} Sps_3 mean composition) shows diffusion zoning with decreasing the pyrope component from the core to the rim. Grt-2 has lower pyrope and higher spessartine component compared to Grt-1 and shows growth zoning with (Grs_{12} Prp_4 Alm_{55} Sps_{30}) core-and (Grs_6 Prp_{13} Alm_{69} Sps_{12}) rim compositions. Grt-2 contains inclusions of rutile, ilmenite and rarely chlorite and biotite. Staurolite and kyanite porphyroblasts (Ky-2) contain inclusions of garnet, biotite, muscovite, rutile and ilmenite (Fig. 2g). Grt-1 and Grt-2 are found as inclusions within a single kyanite porphyroblast (Fig. 2h). Kyanite also occurs as inclusions in staurolite (Ky-1; Fig. 2h). Chlorite is minor phase. Primary chlorite is observed as inclusion in Grt-2 and staurolite. Matrix chlorite is retrograde phase replacing biotite. Ilmenite is formed by replacing rutile. Ilmenite and rutile occur as inclusions in Grt-2, staurolite, kyanite and in the rock matrix. Fibrolitic sillimanite, if present, is always associated with matrix biotite. Replacement of kyanite by sillimanite is not observed.

3.2. Record of polymetamorphic evolution

Locality 1: The stable mineral assemblage Grt+Ky+Bt+Ms+Qtz indicates MP to HP metamorphism at upper amphibolite facies conditions (Fig. 3). The inclusions of kyanite and biotite in garnet porphyroblasts indicate garnet growth at the expense of kyanite+biotite according to the water conserving pressure dependent reaction:

$$2Ky+Bt+Qtz \rightarrow Grt+Ms \qquad (1)$$

Pressures > 1.5 GPa and temperatures >650^{o}C are obtained from reaction 1 (Fig. 3, curve 1). Inclusions of composite grains in garnet consisting of biotite+quartz+rutile±xenotime±monazite (Fig. 2a) suggest much higher P-T conditions. Such inclusions are common in garnets from the garnet-kyanite gneisses of the UHP Kimi complex and are interpreted to be formed from supercritical fluid or melt inclusions in garnet growing at UHP conditions (Mposkos and Krohe, 2006). Matrix biotite (Bt-2) and Ky-2 are formed during decompression according to reaction 1 (running from the right to the left), as indicated by the corroded edges of garnet, the decrease in Mg# at the rims of the garnet, and the lower Mg# values in matrix biotite compared to the Mg# values of single biotite grain inclusions in garnet (Table 2). The composite biotite+kyanite+quartz inclusions in garnet represent decomposition products of former phengite inclusions reacted with the host garnet during decompression.

Locality 2: Textural relationships and mineral compositions in the metapelites of locality 2 record two prograde metamorphic events. The first metamorphic event is recorded by the Ky-1, Grt-2, and Ms-2 porphyroblasts and their inclusions. The overprinting metamorphism is recorded by the matrix staurolite (St-2) overgrown by kyanite and Grt-3 overgrown by Grt-2 (Figs. 2d,e).

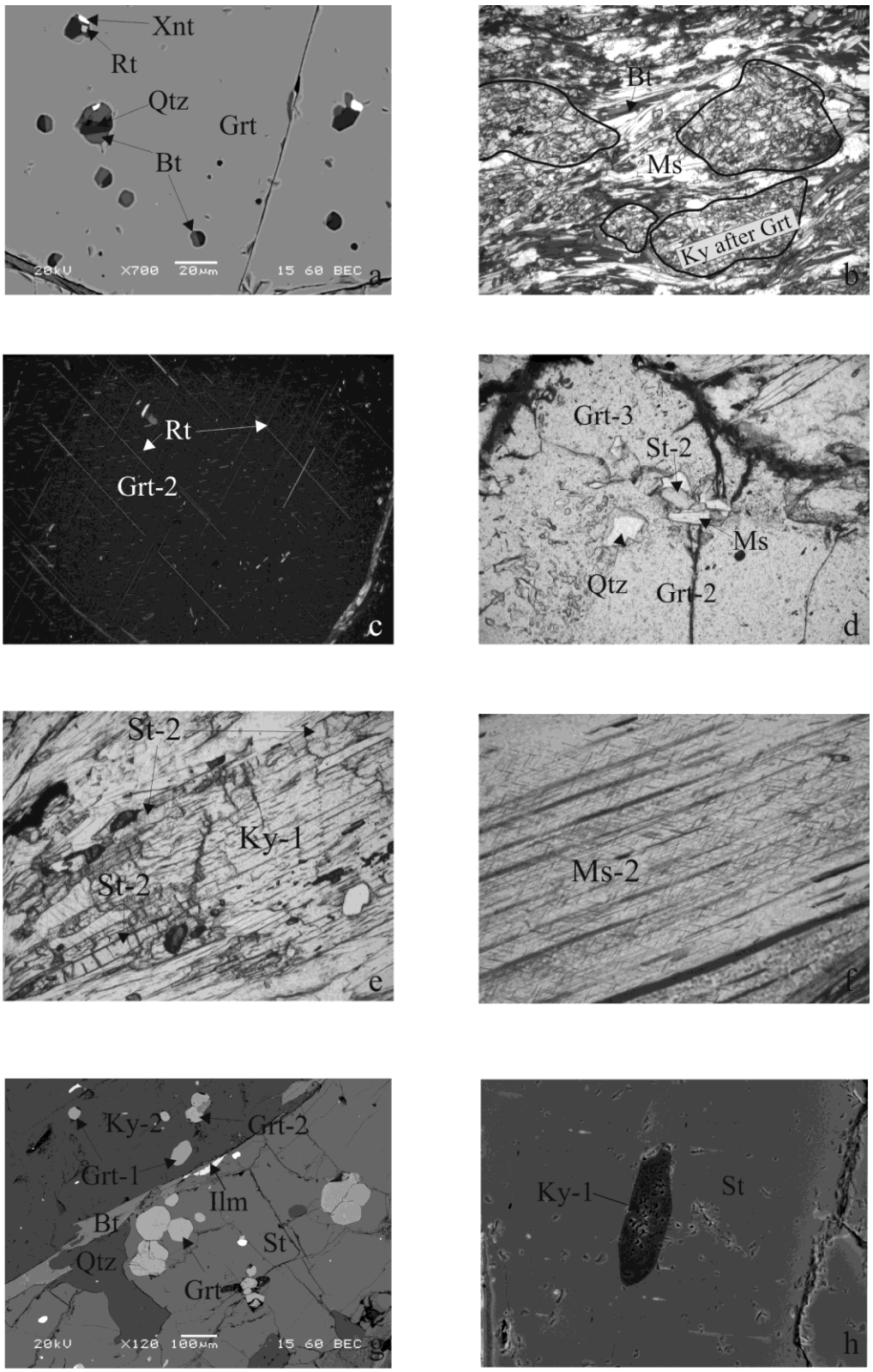

Fig. 2. Locality-1: (a) Composite inclusion consisting of Bt+Qtz+Rt in garnet porphyroblast. (b) Kyanite+biotite aggregates pseudomorphic after garnet. Locality-2: (c) Rutile needles exsolutions (triangular pattern) in garnet porhpyroblast (Grt-2); crossed pollars. (d) Part of garnet porphyroblast (Grt-2) overgrown by new garnet (Grt-3). Grt-3 contains quartz, staurolite (St-2), muscovite (Ms) and biotite (Bt) inclusions. (e) Matrix staurolite (St-2) overgrows kyanite porphyroblast (Ky-1). (f) Muscovite porphyroblast (Ms-2) with rutile needle exsolutions. Locality-3: (g) Staurolite and kyanite (Ky-2) porphyroblasts with inclusions of garnet (Grt-1 and Grt-2). (h) Kyanite (Ky-1) inclusion in staurolite. (a), (g), (h): SEM images and (b),(c), (d), (e), (f): microphotographs.

The inclusions of Grt-1, St-1, Bt and Ms in Ky-1 porphyroblasts indicate formation of kyanite in a prograde path of metamorphism according to the reaction:

$$St\text{-}Ms \rightarrow Grt+Ky+Bt+H_2O \qquad (2)$$

Inclusions of kyanite with corroded edges in Grt-2 porphyroblasts indicate garnet growth at the expense of kyanite (+biotite) according to reaction 1 with pressure increase. Pressures > 1.5 GPa are obtained from reaction 1 (Fig. 3, curve 2). The presence of microdiamond inclusions in garnet porphyroblasts from metapelites of locality 2 (Schmidt et al., 2010), constrains the minimum pressure at 3.5 GPa for assumed temperature of 800°C. We consider that at peak P-T conditions the temperature

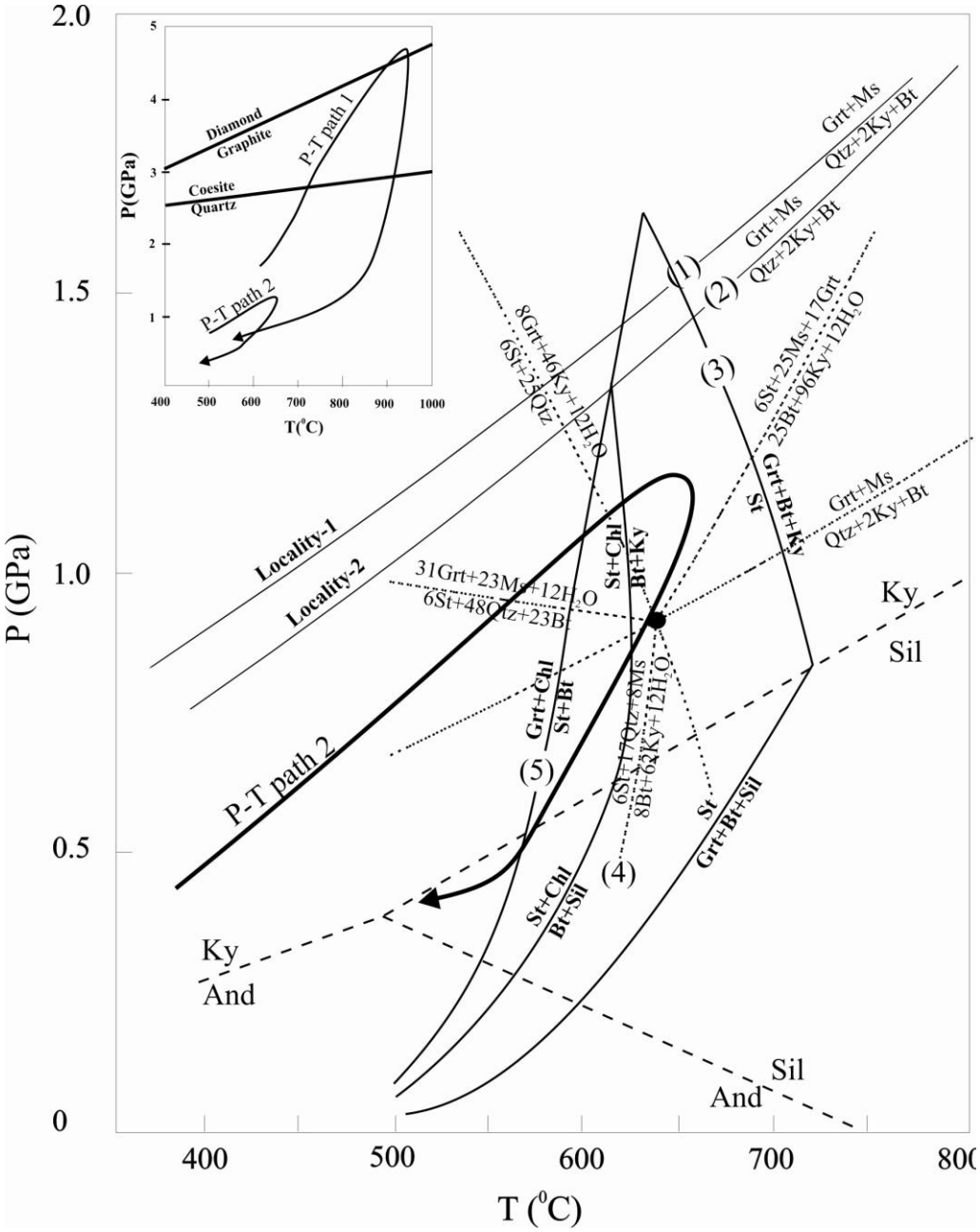

Fig. 3. P-T diagram showing univariant reaction curves in the system KFMASH (taken from Spear 1995). Dotted reaction curves are calculated with the TWEEQU software for the system St+Grt+Ky+Bt+Ms+Qtz+H_2O using mineral compositions representing the second prograde metamorphic event in locality-2. Reaction curves 1 and 2 are calculated using garnet core - biotite inclusion compositions from garnet porphyroblasts of localities 1 and 2. Insert: The Jurassic UHP metamorphism is shown in P-T path 1 and the Eocene intermediate HP metamorphism in P-T path 2.

was very high as shown by the rutile needle exsolutions in garnet and muscovite porphyroblasts (Figs. 2c,f), which suggest that the UHP assemblage contained Ti-rich garnet and Ti-rich phengite. High-Ti phengites are reported from UHP-HT gneisses from Kokchetav massif in Kazakhstan (Hermann et al., 2001) and Ti-rich garnets in eclogites from Sulu UHP terrane and from UHP-HT experiments (Zhang et al., 2003). Matrix biotite (Bt-2) and matrix kyanite (Ky-2) are formed during decompression according to reaction 1 (running from the right to the left), as indicated by the corroded edges of garnet porphyroblasts, the decrease in Mg# at the rims of the garnet, and the lower Mg# values in the matrix biotite compared to the Mg# values of biotite inclusions in garnet (Table 2). Matrix staurolite (St-2) overgrew kyanite (Fig. 2e), indicating that it has been formed by consuming kyanite according to reaction 4 in figure 3. For staurolite formation, the intrusion of water in the rock is needed. Calculated reaction curves for the system St+Grt+Ky+Bt+Ms+Qtz+H_2O using real mineral compositions (Tables 1 and 2) show that staurolite coexists with garnet (Grt-3) at pressures higher than the invariant point (> 0.9 GPa) (Fig. 3). The absence of rutile exsolutions in Grt-3 indicates that Grt-3 grew at much lower temperatures and pressures than Grt-2. Syndeformational ilmenite formed during decompression replaced matrix rutile. Applying the GRAIL geobarometer yields pressures of 0.5 GPa indicating that the dominant foliation in the metapelite formed during the exhumation.

Locality 3: The second prograde metamorphic event is well recorded in the metapelites from locality 3. Grt-1, Rt and Ky-1 are relics of a former metamorphic event at higher P-T conditions as indicated by a) the higher pyrope component in Grt-1 (22%) compared to that of Grt-2 (4-13%), b) the different patterns of chemical zoning (diffusion zoning in Grt-1, growth zoning in Grt-2), c) the kyanite inclusions (Ky-1) in staurolite, d) the rutile inclusions in Grt-1 and e) the replacement of rutile by ilmenite. The presence of ilmenite replacing rutile in the matrix and as inclusion in garnet (Grt-2), staurolite and kyanite indicates that the second prograde metamorphism started within the ilmenite stability field. The first stage of metamorphism was within the garnet+chlorite+biotite stability field as indicated by the chlorite and biotite inclusions in Grt-2. Staurolite+biotite were formed at the expense of garnet and chlorite (Fig. 3, curve 5). With further increase in P-T conditions kyanite+ biotite was formed consuming staurolite and chlorite. Fibrolitic sillimanite associated with biotite was formed during decompression as the P-T path crosses the kyanite-sillimanite boundary.

Table 2. Representative composition of biotite, muscovite and staurolite from metapelites of the Sidironero complex.

	Locality-1			Locality-2						Locality-3		
	Bt-1g	Bt-2g	Bt-3m	Bt-g2	Bt-k	Bt-m	Ms-p	St-g2	St-m	St	Bt-st	Bt-m
SiO_2	38.54	37.95	36.54	37.50	36.02	35.92	47.41	28.26	28.10	28.30	35.77	35.52
TiO_2	2.57	3.11	1.83	1.38	1.39	1.77	1.21	0.83	-	-	1.32	1.85
Al_2O_3	17.45	17.47	18.14	20.53	19.47	19.24	32.51	52.70	53.03	53.85	19.33	19.22
FeO	14.22	11.86	19.51	11.05	15.41	16.72	1.10	10.09	12.67	13.78	19.89	20.31
MnO	-	-	-	-	-	-	-	0.12	0.46	-	-	-
MgO	11.85	14.16	8.59	14.88	12.60	11.20	1.15	2.64	1.62	1.76	9.12	8.42
ZnO	-	-	-	-	-	-	-	3.17	2.45	0.43	-	-
NaO	-	-	-	-	-	-	-	-	-	-	-	-
K_2O	10.39	10.34	9.98	10.38	9.99	9.83	11.48	-	-	-	9.58	9.55
Total	95.01	94.89	94.58	95.72	94.80	94.69	94.86	97.75	98.33	98.12	95.01	94.86
				22 oxygens				47 oxygens			22 oxygens	
Si	5.730	5.600	5.606	5.449	5.407	5.432	6.356	8.002	7.996	7.999	5.463	5.448
Ti	0.287	0.345	0.211	0.151	0.157	0.201	0.122	0.177	-	-	0.152	0.213
Al	3.057	3.039	3.280	3.514	3.445	3.430	5.138	17.63	17.79	17.94	3.479	3.475
Fe	1.768	1.464	2.504	1.343	1.934	2.115	0.123	2.394	3.015	3.257	2.541	2.605
Mn	-	-	-	-	-	-	-	0.029	0.111	-	-	-
Mg	2.625	3.113	1.965	3.222	2.819	2.525	0.229	1.117	0.687	0.743	2.076	1.925
Zn	-	-	-	-	-	-	-	0.664	0.515	0.090	-	-
Na	-	-	-	-	-	-	-	-	-	-	-	-
K	1.971	1.946	1.953	1.924	1.897	1.897	1.963	-	-	-	1.866	1.868
Mg#	0.60	0.68	0.44	0.70	0.59	0.54	0.65	0.32	0.18	0.19	0.45	0.42

g2, k, st = inclusion in Grt-2, Kyanite and staurolite respectively, m=matrix, p=porphyroblast

4. Discussion and Conclusions

The mineral assemblages and textures of the metapelites from locality 2 indicate that the metapelites underwent two distinct metamorphic events; the first at HP or UHP (documented by the microdiamond inclusions in garnet Schmidt et al. 2010) and the second at moderate HP.

North of Xanthi (locality 4 in figure 1), the garnet-kyanite gneisses containing dispersed amphibolitized eclogite boudins, have the mineral assemblage Grt-Ky-Ms-Bt-Pl-Qtz±Kfs±St±Sil+Rt+Ilm. Textures and mineral compositions are similar to those described in locality 2 (Mposkos and Liati 1993). Microdiamond inclusions in garnet porphyroblasts are described by Mposkos and Kostopoulos (2001) and Perraki et al. (2006). Two major Alpine metamorphic events are documented by dating metamorphic minerals from the garnet-kyanite gneisses of the locality 4; a Jurassic and an Eocene (Liati, 2005; Bosse et al., 2009 and references therein). Although mineral ages from the studied metapelites of the three localities are not available, we consider that the HP-UHP event documented in localities 1 and 2 as well as the Grt-1, Ky-1 and Rt relicts from locality 3 are Jurassic in age and the moderate HP overprinting event documented in localities 2 and 3 occurred in Eocene.

Jurassic ages are also reported from the diamond-bearing garnet-kyanite gneisses from the Kimi complex in the Eastern Rhodope (Bauer et al. 2007). The Kimi complex tectonically overlies the Sidironero complex (Mposkos and Krohe, 2000; Krohe and Mposkos, 2002). The metapelites from both complexes seems to have a common Jurassic tectonometamorphic evolution (Mposkos and Liati, 1993; Liati, 2005; Bauer et al., 2007). We hence interpret the Sidironero and Kimi complexes to represent a single, originally connected tectonic block of pre-Alpine continental crust involved in the Jurassic subduction of a branch of the northward subducted Vardar-Axios Ocean under the European continent. The final tectonic juxtaposition of both complexes against each other occurred by Tertiary tectonic processes.

In the Kimi and Sidironero complexes the orthogneisses (most of them are migmatites) yielded U-Pb and Pb-Pb zircon ages in the range of ~165 to 135 Ma, which are interpreted as dating the magmatic protoliths from magmas produced in a magmatic arc setting (Turpaud and Reischmann, 2010; Cornelius, 2008). The wide (20 to 60 Ma) range of U-Pb zircon ages within a single hand specimen, the presence of many pre-Alpine (mostly Variscan) inherited zircon cores in the samples dated by SHRIMP, and that most of the dated gneisses are migmatites (the orthogneiss near the Sidiro village in east Rhodope contains boudins of partially amphibolitized eclogites), suggest that the late Jurassic-early Cretaceous ages of the orthogneisses probably record successive stages of the metamorphic evolution (including high degree of melting) of pre-Alpine magmatic protoliths in a thickened crust after the HP/UHP metamorphic event.

The Nestos shear zone, that contains the studied metapelites, can be traced for about 80 km from Xanthi to the west, to the Bulgarian border. The shear zone includes lithologies from the overlying Sidironero complex, that records two Alpine prograde metamorphic events, one in Jurassic and a second in Eocene (Liati, 2005; Bosse et al., 2009 and references therein), and the underlying Albite-Gneiss-Series that record only one Alpine metamorphic event in the Eocene (Liati, 2005). We consider the migmatitic orthogneiss, which occurs near and below of the metapelites from locality-2 as the upper part of the Albite-Gneiss-Series. At this locality the metamorphic conditions reached those of the granite wet-melting. The U-Pb zircon ages of Liati (2005) only record pre-Alpine and Eocene events, but not any Jurassic event. Both complexes are thrust over the marbles of the Pangaeon complex. Two of the presently known four UHP metamorphic localities in the Greek Rhodope Mountains occur along the Nestos shear zone of the Sidironero complex and two of them within the overlying Kimi complex. The Nestos shear zone represents a major SW directed thrust occurred in Eocene in a compressional regime by underthrusting of the Pangaeon complex (including the Albite-Gneiss Series) under the southern borders of the European continent, part of which was the Kimi complex. With a tectonic erosion mechanism slices of the Kimi complex are brought in the underthrusting plate and suffered the Eocene prograde moderate HP metamorphism, with a P-T path correspond to geothermal gradient < 17^{o}C/km.

Acknowledgments

The reviewers T. Nagel and Z. Cherneva are gratefully acknowledged for their helpful comments and suggestions. We want to express our sincere thanks to N. Bonev for his editorial handling.

References

Bauer, C., Rubatto, D., Krenn, K., Proyer, A. and Hoinkes, G., 2007. A zircon study from the Rhodope Metamorphic Complex, N-Greece. Time recorded of a multistage evolution. Lithos, 29, 207-228.

Bosse, V., Boulvais, P., Gautier, P., Tiepolo, M., Ruffet, G., Devilal, J.L. and Cherneva, Z., 2009. Fluid-induced disturbance of the monazite Th-Pb chronometer: In situ dating and element mapping in pegmatites from the Rhodope (Greece, Bulgaria). Chemical Geology 261, 286-302.

Cornelius, N.-K., 2008. UHP metamorphic rocks of the Eastern Rhodope Massif, NE Greece: new constraints from petrology, geochemistry and zircon ages. Ph.D.Thesis University of Mainz.

Hermann, J., Rubatto, D., Korsakov, A., and Shatsky, V.S., 2001. Multiple zircon growth during fast exhumation of diamondiferous, deeply subducted continental crust (Kokchetav Massif, Kazakhstan). Contributions to Mineralogy and Petrology, 141: 66-82.

Ivanov, Z., Kolkovski, B., Dimov, D., Sarov, S. and Dobrev, S., 2000. Structure, Alpine evolution and metallogeny of the Central Rhodopes area, South Bulgaria. Abstract Volume, ABCD-GEODE, Borovets, 30.

Krohe, A. and Mposkos, E., 2002. Multiple generations of extensional detachments in the Rhodope Mountains (N.Greece): evidence of episodic exhumation of high-P rocks. In: Blundell, D.J., Neubauer, G. and Von Quant, A. (eds.): The timing and location of major ore deposits in an evolving orogen. Geological Society of London, Special Publication, 204, 151-178.

Liati, A., and Gebauer, D., 1999. Constraining the prograde and retrograde P-T-t path of Eocene HP rocks by SHRIMP dating of different zircon domains: inferred rates of heating, burial, cooling and exhumation for central Rhodope, northern Greece. Contributions to Mineralogy and Petrology,, 135, 340-354.

Liati, A., 2005. Identification of repeated Alpine (ultra) high-pressure metamorphic events by U-Pb SHRIMP geochronology and REE geochemistry of zircon: the Rhodope zone of Northern Greece. Contributions to Mineralogy and Petrology, 150, 608-630.

Martin, R.F., 1998. Symbols of the rock-forming minerals. The Nomenclature of minerals: A compilation of IMA reports. International Mineralogical Association 98 Toronto, 148-149.

Mposkos, E., and Liati, A., 1993. Metamorphic evolution of metapelites in the high-pressure terrane of the Rhodope zone, Northern Greece. Canadian Mineralogist, 31: 401-424.

Mposkos, E., Chatzipanagis, I., and Papadopoulos, P., 1998. New data on the boundaring the Pangaeon and Sidironero tectonic units in Western Rhodope. Bulletin of the Geological Society of Greece, 32/1, 13-21. (In Greek with English abstract)

Mposkos, E., and Krohe, A., 2000. Petrological and structural evolution of continental high pressure (HP) metamorphic rocks in the Alpine Rhodope Domain (N.Greece). In: Proceedings of the 3rd International Conference on the Geology of the Eastern Mediterranean, Nicosia, Cyprus, 1999. Edited by I.Panayides, C.Xenophontos, and J. Malpas. Geological Survey, Nocosia, Cyprus, pp. 221-232.

Mposkos, E., and Kostopoulos, D., 2001. Diamond, former coesite and supersilicic garnet in metasedimentary rocks from the Greek Rhodope: a new ultrahigh-pressure metamorphic province established. Earth and Planetary Science Letters, 192, 497-506.

Mposkos, E., and Krohe, A., 2006. Pressure-temperature-deformation paths of closely associated ultra-high pressure (diamond-bearing) crustal and mantle rocks of the Kimi complex: implications for the tectonic history of the Rhodope Mountains, northern Greece. Canadian Journal of Earth Sciences, 43, 1755-1776.

Perraki, N., Proyer, A., Mposkos, E., Kaindl, R., and Honkes, G., 2006. Raman micro-spectroscopy on diamond, graphite and other carbon polymorphs from the ultrahigh-pressure metamorphic Kimi Complex of the Rhodope Metamorphic Province, NE Greece. Earth and Planetary Science Letters, 241, 672-685.

Reischmann, T. and Kostopoulos, D., 2002. Timing of UHPM in metasediments from the Rhodope Massif, N.Greece. Proceedings Goldschmidt Conf., Davos, Switzerland, p. 634.

Schmidt, S., Nagel, T. and Froitzheim, N., 2010. A new occurrence of micro-diamond-bearing metamorphic rock, SW Rhodope, Greece. European Journal of Mineralogy, 22/2, 189-198.

Spear, F., 1995. Metamorphic Phase Equilibria and Pressure-Temperature-Time Paths. Mineralogical Society of America, Monograph, p. 799.

Turpaud, P., and Reischmann, T., 2010. Characterization of igneous terranes by zircon dating: implications for UHP occurrences and suture identification in the Central Rhodope, northern Greece. International Journal of Earth Sciences, 99, 567-591.

Zhang, R.Y., Zhai, S.M., Fei, Y.W. and Liou, Z.G., 2003. Titanium solubility in coexisting garnet and clinopyroxene at very high pressure: The significance of exsolved rutile in garnet. Earth and Planetary Science Letters, 216, 591-601.

Special Session S07
Danube valley geological structure, neotectonic activity and evolution during the Pliocene-Pleistocene time

Scientific Annals, School of Geology, Aristotle University of Thessaloniki Proceedings of the XIX CBGA Congress, Thessaloniki, Greece	Special volume 100	183-190	Thessaloniki 2010

THE LOWER DANUBE VALLEY. GEOLOGICAL STRUCTURE AND EVOLUTION DURING THE PLIOCENE-QUATERNARY

Enciu P.

Institute of Geography-Romanian Academy, Bucharest, Romania, petru_enciu@yahoo.com

Abstract: Stratigraphical and geophysical arguments are put forward, whereby that the beginning of sediments deposition by the Lower Danube and by its tributaries date back to the Upper Pliocene (2.6 Ma) and go up to and into the Lower Pleistocene. During the interval of 2.5-0.9 My, the Danube kept branching out gradually towards the east of the Dacian Basin. Concomitant, a number of intensely flooded low plains developed within the actual Romanian Plain as part of the Lower Danube Basin. Subsequently, during the Middle Pleistocene-Holocene, the Danube River cut the actual profile of the Valley. As a result, the higher relief of the Romanian Plain led to repeated down-cuttings of the 7 (8) stepped terraces. In the eastern half of the Lower Danube Valley, against the background of a mainly subsiding behaviour of the Platform, the upfinning sequences of the 7 terraces were progressively overlayed by the Aeolian Formation (up to 55 m thick). On the Black Sea continental shelf, within the Danube roughly 150 km long deep sea fan, there have been identified 8 seismic sequences, the first two with mass flow deposits, and the other six with alluvial channel fills. They have been ascribed, in accordance with their order of deposition, the indices S1...S8 (Winguth et al., 1997).The S1 sequence may be ascribed to the 800–700 ka interval, and the S2 sequence to the 640–530 ka interval. According to Wong *et al*. (1997), the approximate intervals of deposition of the last six alluvial sequences are: S3 between 480–400 ka, S4 between 400–320 ka, S5 between 320–190 ka, S6 between 190–75 ka, S7 between 75–25 ka and S8 during the last 25 ka.

Keywords: Romania, Danube, Pliocene, Quaternary, stratigraphy, paleogeography.

1. Introduction

In terms of length, the Danube River, ca 2857 km, occupies the second place in Europe after the Volga, ca 3688 km, but, because it connects ten countries and flows through four capitals: Vienna, Bratislava, Budapest and Belgrade, it ranks first from an economic and political point of view. From a geographical perspective, the Danube Basin Network is divided in three; the Upper between its springs (the Black Forest Mountains) and the Passau Passage; the Middle, between above-mentioned point and the watershed of the SW Carpathians (the Iron Gate Passage, Djerdap Gorge), and the Lower Basin which extends from the above-mentioned area to the Black Sea. The main feature of the Lower Danube Basin relief is a W-E decreasing elevation. So, on the eastern slope of the Southwestern Carpathians (Fig.1), the relief has moderate elevation values of elevations (currently around 700 m). Eastwards, the next radial-converging rim is formed of the Prebalkan, the Miroć and the Getic Tablelands, 700 - 300 m altitude. The last one, the Romanian Plain, with altitudes decreasing from west to east, includes three strips: a High Plain (300-160 m altitude), the Danube Valley: having till 7 terraces, 160-35 m high and a large Floodplain, 40 – 5 m a.s.l.

2. Material and Methods

The paper tackles the Stratigraphy and, relying on it, the Geological Evolution of the Lower Danube Basin during the Pliocene-Quaternary. In order to solve the first item, the outcrops existing in the Upper Miocene-Holocene formations on the eastern slope of the SW Carpathians, the Getic Tableland and the western third of the Romanian Plain were studied and sampled out between 1983 and 2000. Beside the two main dating criteria: mollusks biozones and the paleomagnetism of rocks, the fossil micro-mammalia have also been studied (Enciu, 2009). These three categories are major proofs, usually taken into account for dating continental deposits, which were used also to delimit the main four geological formations. Besides the outcrops, the cores of 87 continuous-coring me-

chanical wells, with depths of 250-375 m and 222 samples of rocks and 99 samples of macrofauna were looked into as well (Enciu, 2009).

We have analyzed the lithology, thickness and geometry of rock-bodies on differently-orientated sections through the wells, boundaries of sequences, well log responses a. o. for the four Pliocene-Quaternary formations.

trian, Slovak and Hungarian researchers for the Little Alföld region, i.e. that part of the median Danube catchment area extending between Vienna, Bratislava and Esztergom (Janacek, 1969; Haloužka, 1975; Pecsi et al., 1985, Scharek et al., 2000, Krstić et al., 2004). In the Quaternary series eight distinct terraces have been identified in the higher elevated areas, while in the prevailing sub-

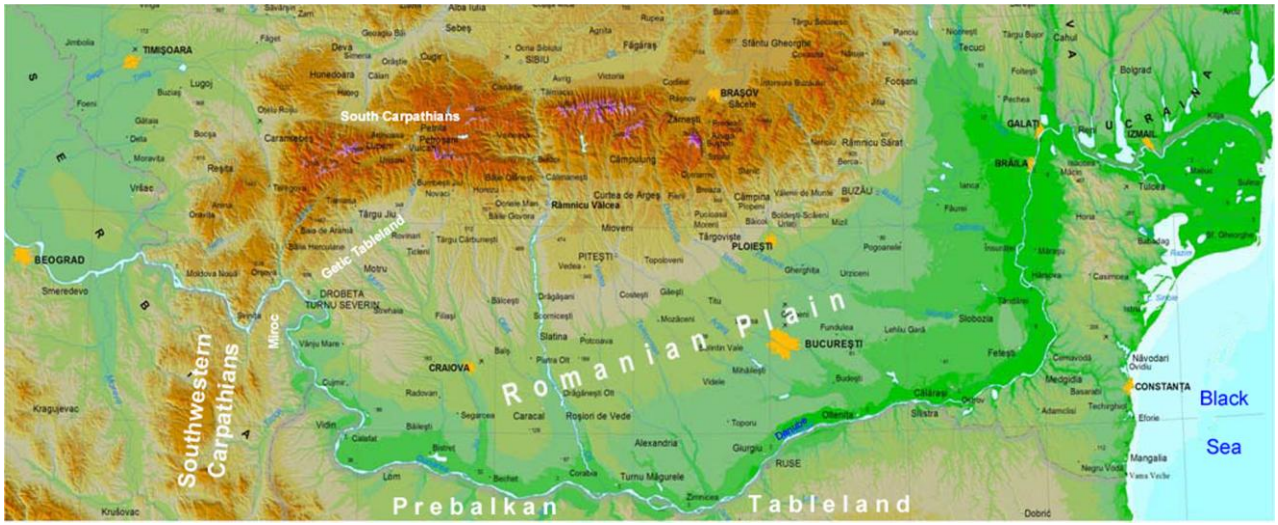

Fig.1 – Physic-Geographical Map of the Lower Danube Basin.

The second topic of this paper seams to harmonize geological hypotheses concerning the Lower Danube Valley modelling (cutting) during the Pliocene and the Quaternary. To this end, the author's own data have corroborated the information provided by the Serbian and Bulgarian researchers' papers about righthandside of the Danube Valley. Information on the mentioned side was published in the sheets of the Geological Map of Serbia on scale of 1:100 000. For the same purpose, the "Bregovo", "Vidin", "Lom" and "Kozlodui" sheets of the Geological Map of Bulgaria on the scale 1:100 000 were also used. The Geological Map of the lefthandside (Romanian area) was integrated with the righthandside ones, Bulgarian and Serbian, on the scale of 1 : 100 000 (Fig. 2).

A short review of previous studies about Pliocene-Quaternary formations in the Middle Danube Valley

1. Since the 20th century, geologists have identified on their national territories (Vienna Basin, Little Alföld, Great Alföld a.o.) the remnants of the Danube Formation. It was firstly, defined in 1938 by Szadeczky-Kardoss in his geological monograph on a large area of the Pannonian Basin. Later on, the Danube Formation concept was used by Aus-

siding areas it was the Danube Series with two complexes that was singled out.

The Danube Series Lower Complex, going down to the depth of 200–300 m, includes deposits belonging to the Danube and to its tributaries (fine and medium-graded gravel). Considering its petrographic content, the Lower Complex was correlated with the first three terraces of the Danube in Austria: Laaerberg (t_8), Wienerberg (t_7) and Arsenal (t_6). It contains fresh water mollusks and has been ascribed to the Final Romanian (?) – Early Pleistocene (Szadeczky-Kardoss, 1938; Halouzka, 1975).

The Danube Series Upper Complex occurs within the last 130-150 m depth, in the middle of the depression. It contains alternating gravel and sands, occasionally with lenses of clay or peat coal. In terms of its petrographic content, this complex correlates with the deposits of the last five terraces of the Danube: Seyring t_5, Simmering t_4, Ganserndorf t_3, Stadt t_2 and Prater t_1.

2. Downstream, as a result of investigations into the margin of the Gerećse – Vishegrad Mountains (located to the SE), revealed only seven terrace levels were identified along the middle course of

the Danube, ascribed to the time intervals of 2.4 – 2.2 Ma, 1.8 – 1.6 Ma, 1.1 – 0.85 Ma, 0.45 – 0.35 Ma, 0.25 – 0.17 Ma, and 0.10– 0.01 Ma (Fig. 1 in: Scharek et al., 2000).According to recent estimations (Ruszkiczay-Rüdiger, 2007, p 52), the onset of the incision of the Danube is ~ 0.90 Ma, consistently younger than the estimated ~ 2400 ka indicated by the previous scientists.

3. In the following, we shall sum up the morphogenetic model of the terraces lying along the Danube in the Southwestern Carpathians. The model was devised by Cvijić in 1908. According to that model, revised by the Rakic, 1977 and Rakić şi Simonović, 1997, one may distinguish in the Danube Gorge the following: the Dacian age of Valley floor at 260–320 m relative altitude (r.a.), the "Šip" terrace t_7 at 200–210 m r.a., the "Brza" terrace t_6 at 150–160 m r.a., the "Ključ" terrace t_5 at 90–115 m r.a., the "Kosovića" terrace t_4 at 60–80 m r.a., the " Turnu" terrace t_3 at 30–50 m r.a., the

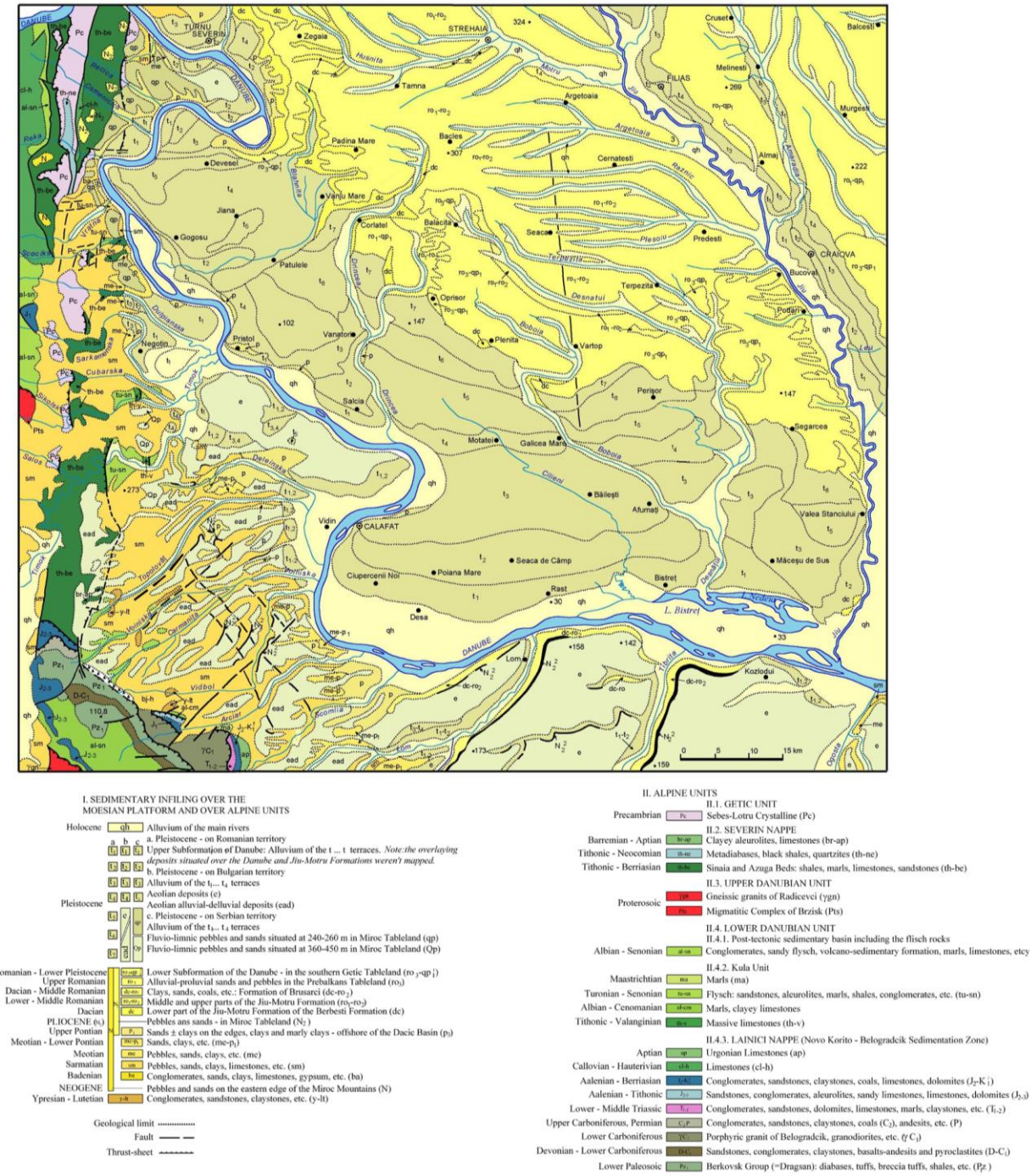

Fig. 2. Geological Map of the western third of the Lower Danube Basin.

″Kladovo" terrace t_2 at 10–20 m r.a., and the lower terrace (t_1) at 6–8 m r.a.

3. The Lower Danube Valley. Results and Discussion

3.1. The pre-Pliocene Structural Settings within the Lower Danube Valley

The Lower Danube Valley ~ 400 km long and ~ 60 km mean width in the W-E and N-S directions, respectively, and the descending average altitude from 170 m in W (Drobeta Turnu Severin) to 20 m in E (Galati City). The Lower Danube Basin is overlying the SW Carpathians (including their Foredeep), the Moesian Platform and in the easternmost part, the North Dobrogea Burried Promontory and the Scythian Platform (Fig.3). The SW Carpathians, just like the whole Carpathian Chain, are allochthonous, coming from SSW, from the Tethysian area. During the Late Cretaceous-Tertiary, these mobile Carpathian units collided with the Moesian Platform's western boundary (Ratschbacher et al., 1993). Owing to the Carpathians' NNE progressive movement and to the corner effect at their contact with the rigid Moesian Platform, the history of the birth of the Lower Danube Valley is governed by the predominantly dextral shearing process along the S-N Poreč-Cerna-Jiu, Timok-Bâlta-Targu Jiu-Calimanesti and other strike-slip crustal faults (Kräuthner şi Krstić, 2002; Tarapoanca 2004). As a result, in the westernmost corner of the Lower Danube Basin, the Foredeep emerged during the Laramie tectonic event (Senonian).

Later on, during the Young Styric tectonic event (Badenian, ca 16 My), the strike-slip processes of the SW Carpathian nappes stack were reactivated. In their median part, over the weak portions, the Zagubica, Kucevo, Rakovo, Krivaco, Liubovca, Donji Milanovač, Bozovici, Orshova and other post-tectonic basins were formed. Usually, for this kind of mutual S-N movement, the magnitude of the SW Carpathians' uplift is in the order of a few hundreds of metres. Laterally, to the east, there is one shallow S-N Foredeep, followed to the east of the Lom Depression (no 2 in Fig.3) by an unequally, progressively, subsiding serie of panels of the Moesian Platform. This cratonic unit (MP) witnessed repeated extensions and warming during the Permian-Triassic, Lutetian, Burdigalian (basanites eruptions), Badenian a.o. (Tarapoanca, 2004).

Starting with the Sarmatian, to east of Intramoesian Fault (fig.3), the main four panels existing in the basement of the Lower Danube Basin were involved in one uneqally SE-NW subsidence, more intense near the Curvature Carpathians Arc as the result of flexural loading (Bertotti et al. 2003). In eastern half of Romanian Plain, some of the paleohydrographic consequences are: the W-E elongation of the Danube Course (Upper Romanian-Lower Pleistocene), the progressive bending of the Danube River from SSE to NNW (between Silistra and Galati) and subsequent flowing in to the Black Sea along the boundary between the North Dobrogea Orogene and the Scythian Platform at the begining of the Middle Pleistocene (Wong et al., 1997).

3.2. The Lower Danube Valley during the last sedimentary cycle

In the western corner of the Lower Danube Valley, the last accretion of mountain slices was therefore most probably Late Badenian, 15-13 Ma to Sarmatian, 13-11 Ma (Sanders, 1999). As a reflex, on the eastern flank of the SW Carpathians, a pile of alluvial fans (few decameters thick), continuing with mini-deltas (sandy) deposits, had been accumulated (Krstić et al., 1997).Then, during the Meotian, the lithofacies was changing from deltas to offshore sandy deposits. The complete infilling of the westernmost part of Dacian Basin is reported to ca 5.5 Ma, with the sands near the edges grades the commonly marly Pontian offshore. The W-E sequential analysis across the margin of Carpathians and its Fore-deep provides constraints both on the last stages of basin filling and on the onset of fluviatile sedimentation related to the development of the paleo-Danube starting with Pontian (Tarapoanca, 2004, fig.3.12).

Starting with the Early Dacian (5,3 Ma.), the communication between the Pannonian and the Dacian basins was reduced to a system of channels and straights along of the post-tectonic Liubcova, Donji Milanovač and Orshova basins. The Dacian Basin became a gulf of the Black Sea. In its westernmost corner, the Lom, the Timok, the Danube and other radial-converging rivers built the sandy, the Berbesti Formation, littoral-lacustrine (Lower Dacian). Then, during the Upper Dacian-Middle Romanian, the Constructive Deltaic Phase was succeded by the Upper Delta Plain and the Floodplain environments (the Jiu Motru Forma-tion):

100-350 m of parasequences with sands, silts, clays, gley paleosoils or 2-9 coal seams.

3.3. Danube Formation in the Lower Danube Valley

Around 2.5 Ma. BP, genetically associated to the general cooling of the northern hemisphere and implicitly to the lowering of the Dacian Basin, starting from the western third, the Danube River and its tributaries extended step by step to the central sector and to the east, towards the Black Sea. Besides, the development of the Danube's fluviatile Network was made possible being stimulated by the last uprising of the Southwestern Carpathians and of the associated Foredeep, genetically connected with the Wallachian compressive event of Upper Romanian age.

a. In the ***Miroć Tableland,*** three sections belonging to a 20 – 60 m-thick formation of gravel and sands with *Mammuthus meridionalis* have been preserved within a ca. 7 km-long strip occurring at +240– +260 m a.a.. On the Geological Map of Serbia, those deposits have been ascribed to the Pliocene and to the ″Sip" terrace of the Danube (200–210 m r.a.). By taking into account the elevation, lithology and age, they can be correlated with the Lower Danube Formation. Using the Serbian Geological Map 1 : 100 000 (Antonijevic 1975; Bogdanovic et al. 1978a, 1978b a.o), we assigned the small mapped surfaces with Pliocene coarse alluvium (N_2) to the Lower Member of the Danube Formation; the Fluviatile-Lacustrine (Qp), the Fluviatile (qp) and the $t_4 \ldots t_1$ terrace deposits to the Upper Member (Fig.2, Legend).

b. On the same right bank, in the Timok-Ogosta interstream of the **Prebalkan Tableland**, an erosive - accumulative formation, mainly built by the Danube righthand tributaries (N_2^2 in Fig. 2) was identified (Filipov et al., 1992; Nikolov and Filipov, 1996). It consists of a 0.5 - 20 m-thick beds of gravels and sands. Still in the Prebalkan Tableland, yet farther east, in the basins of the Vit, Osam and Iantra rivers, relics of a hydrographical network dating from the Pliocene, can be found at a height

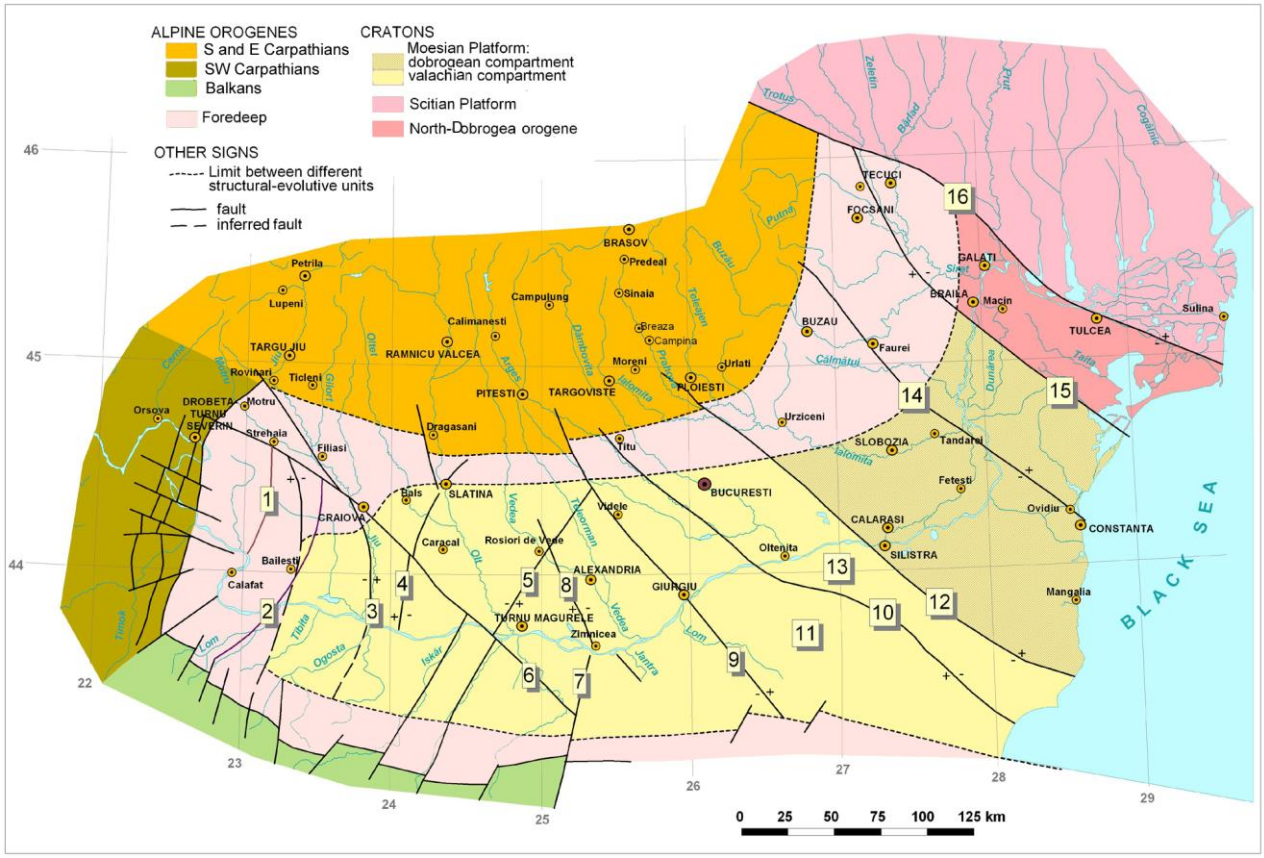

Fig. 3. The main structural elements of the Lower Danube Basin. 1 Strehaia-Vidin uplift; 2 Lom depression; 3 Jiu fault; 4 Campeni fault; 5 Lita fault ;6 Osam fault; 7 „Basalts' fault ; 8. Calmatui fault (Enciu et al., 2001) ; 9 Kubrat-Vetrino fault (Shanov, 2007); 10.Balchik-Dulovo fault (Shanov, 2007); 11. Ludogorie uplift; 12. Intramoesian fault; 13. Tutrakan depression (Shanov, 2007); 14. Capidava-Ovidiu fault; 15. Peceneaga-Camena fault; 16. Trotus-Sfantu Gheorghe fault.

of +190–+200 m. According to Bulgarian researchers, during the Middle Romanian, Danube' righthandside tributaries dissected a roughly 90 m-deep escarpment (Doncev et al.,1985). Subsequently, an ″old abrasive-accumulative horizon" would accumulate on the surface of the escarpment base at roughly 110–100 m r. a. That 7–8 m-thick horizon consists of gravel and sands with *Zygolophodon borsoni, Anancus arvernensis* and *Mammuthus meridionalis* ascribed to the MN_{17} biozone, interval 2.60 – 0.99 Ma, Upper Romanian – Early Pleistocene (Evlogiev *et al*., 1995). In our opinion, this can be reported to the Lower Member of the Danube Formation. Between 0.99 – 0.80 Ma, namely at the end of Early Pleistocene, a formation consisting of mixed clays and gravel accumulated, including relics of cold weather mammalians (*Mammuthus meridionalis, Cervus elaphus* Linne and *Capreolus capreolus* Gray.). The six terraces were shaped during the Middle-Upper Pleistocene (assigned in our opinion to the Upper Member of the Danube Formation).

c. High Plains as part of the Romanian Plain

On the lefthandside of the Danube Valley, the Danube Formation has two members. ***The Lower Member***, Upper Romanian-Lower Pleistocene ($\mathbf{ro_3\text{-}qp_1^1}$), is made up of a flat alluvial fan (Balaciţa High Plain) that continues to the east with braided streams deposits (Salcuţa, Romanati Plains) and with buried, stacked up-fining coarse sequences (Bucharest Plain, a subunit situated in the central part of the Romanian Plain). Using the remnants of the macromammalia found in the elapsed one century within 34 quarries of pebbles and sands (*Anancus arvernensis* Croiset et Jobert, *Mammuthus planifrons* Falconer, *Mammuthus meridionalis* Nesti, *Dicerorhinus etruscus* Falconer) and of the micromammalia (*Mimomys cf. livenzovicus* Alexandrova, *Mimomys pliocaenicus* F.Major, *Mimomys coelodus* Kretzoi , *Kislandia rex* Kormos, *Borsodia langurodontoides* etc), it appears that this prograding process took place during a long interval of time, around one million and a half years, from 2.5 to 1.0 Ma.BP.

The environment of the braided river-type developed against the background of a climate transitional from humid and warm to rather cool. The cumulated surface of the Lower Member of the Danube Formation was around 52 600 km^2. In the outcroppings, on the southernmost edge of the High Plains, an increasing W-E elongated strip (5-20 km wide and over 75 km long) is preserved, representing the lateral north remainder of the Lower Member of the Danube Formation. On the northern rim of this W-E prograding band, approximately on the parallel of Craiova City, debris flow deposits (ca 10-15 m thick of clayey-pebbley sheet) were identified.

d. The Lower Danube Valley

Starting with the second part of the Lower Pleistocene, the Danube began cutting the present profile of its valley. As a result, just the median part of the Lower Member of the Danube Formation was self-evacuated in the Middle-Upper Pleistocene, when the Danube deposited the frontal load in the Black Sea (Wong et al., 1997).Through moulding, the higher relief of the Oltenia Plain ensured repeated down-cutting of the seven stepped terraces. Subsequently, the Danube River deepened in the Dacian-Lower Pleistocene pile, between 160 m deep in the western part of the Lower Danube Valley (Drobeta Turnu Severin City) and 65 m in the central part (Turnu Magurele City). As a result, the higher relief of the Romanian Plain underwent the repeated down-cuttings of the stairway-like seven terraces and the floodplain (Upper Member of the Danube Formation).

The Recent Crustal Displacements Map indicates that structural units in the Romanian Plain basement located eastward of Intramoesian fault valley have been subject mostly to sinking movements. The sinking rates amount to about 0.5 mm/year between the Intramoesian and the Capidava – Ovidiu faults and up to 1–3 mm/year, between Capidava – Ovidiu and Sf. Gheorghe – Galaţi Faults (Enciu, 2009). As a result of the bedrock subsidence, the first 80–100 m depth-interval includes till 6-8 mature alluvial sequences (rounded gravel, sands with gravel, yellow and speckled clays) alternating ephemeral lacustrine sequences (bitumen clays, peat clays, carbonate clays) of Middle-Late Pleistocene age.

On the Black Sea continental shelf, within the Danube roughly 150 km long deep sea fan, there have been identified 8 seismic sequences (the first two with mass flow deposits, and the other six with alluvial channel fills, levee deposits, overbank sediments and mass slide deposits along canyon paths). They have been ascribed, in accordance with their order of deposition, the indices S1...S8. By correspondence with the Dniestr (Nistru) terraces dating scheme (Musinschi, 1999), the S1 sequence may be ascribed to the 800–700 ka interval, and the S2

sequence to the 640–530 ka interval. By using the preliminary relative sea level curve (Winguth et al., 1997), the approximate intervals of deposition of the last six alluvial sequences are: S3 between 480–400 ka, S4 between 400–320 ka, S5 between 320–190 ka, S6 between 190–75 ka, S7 between 75–25 ka and S8 during the last 25 ka (Wong *et al*. (1997). Returning to the Lower Danube Valley's terraces, one should note the very poorly constrained ages of the Lower Danube Terraces. Supposedly, they are ascribed to the Middle and Upper Pleistocene (Enciu, 2009).

4. Conclusions

1.The acceleration of the dextral wrenching of the Carpathian units along the contact with the western edge of the Moesian Platform during the Middle Miocene (Badenian) tectogenetic phase favoured the emergence of Rakovo, Kucevo, Liubovca, Donji Milanovać and Orshova post-tectonic basins within the SW Carpatians and implicitly the connection of the waters of the Pannonian and the Dacian basins through a W-E segmented line of straights and channels, the forerunner of the present Iron Gate Passageway.

2.On the eastern slope of the SW Carpathian ridge, mainly coarse siliciclastic formations were accumulated during the Upper Badenian-Meotian interval and large deltas with dominant prograding seismic facies started developing on the Meotian-Pontian boundary.

3.A sequence analysis of the contact between the SW Carpathian orogene and the Moesian Platform added constraints on the onset of fluviatile sedimentation related to the development of a paleo-Danube. A very dense network of the continuous mechanical corring wells for Lower Pliocene seams of coals (300-400 m deep) made in the westernmost corner of the Lower Danube Valley identified the Gilbert delta of the paleo-Danube Lower Dacian (5.3- 4.6 Ma), containing ca 40 km long and up to 160 m thick monotonous sands.

4. During the Upper Dacian-Middle Romanian, within the western third of the Dacian Basin, the Constructive Deltaic Phase was succeeded by the Upper Delta Plain and Floodplain environments (the Jiu Motru Formation; main mud-filled area of to 300 m parasequences with sands, silts, clays, gley paleosoils or 2-9 coal seams).

5.Climate-controlled changes in the hydrological regime of the Danube Lower Basin induced alternation of erosion and sedimentation cycles.As the result, during the Upper Romanian-Lower Pleistocene, Danube modelled one extensive plain of repeated flooding and have been contributed decisively to the Dacian Basin' infilling (Lower Member of Danube formation). Subsequently, the Danube River deepened in the Dacian-Lower Pleistocene pile, between 160 m deep in the western part of the Lower Danube Valley (Drobeta Turnu Severin City) and 65 m in the central part (Turnu Magurele City). As a result, the higher relief of the Romanian Plain underwent the repeated downcuttings of the stairway-like seven terraces and the floodplain (Upper Member of the Danube Formation). The presented hypothesis about the Lower Danube Valley' evolution is in accordance with the Seismostratigraphy results made on the Black Sea continental shelf along the Danube deep fan.

References

Antonievič I., Kalenič M., Dordevič M., Loncarevič C, Ciculič M., Skuletič T., 1974. Geological Map of Serbia 1:100 000, Bor sheet., Fed. Geol. Surv., Belgrad.

Bertotti G., Matenco L., Cloetingh S., 2003. Vertical movements in and around the SE Carpathians Foredeep. Terra Nova, 15, 5, 299-305. Blackwell Publishing Ltd.

Bogdanović P., Marković V., Dragić D., Dolić D., Rakić M., Babović M., 1978a. Osnovna Geološka Karta SFRJ 1:100 000, foaia Turnu Severin, Fed. Geol. Surv., Belgrad.

Bogdanović P., Marković V., Dragić D., Dolić D., Rakić M., Babović M., 1978b. Osnovna Geološka Karta SFRJ 1:100 000, foaia Donjii Milanovać, Fed. Geol. Surv., Belgrad.

Cvijić J., 1908. Entwicklungsgeschichte des Eisernen Tores, Erganzungshelt, 160 zu Petermanns Geogr. Mitteittlungen, Gotha.

Deceva A., Filipov L, Hajdutev I., Tzankov T., Kojumdjeva Em., Popov N., 1990. Geological Map of Bulgaria 1:100 000, Zaechar-Bor, Inst. Géol. Bulg., Sofia

Dolić D., Rakić M., 1974. Geological Map of Serbia 1:100 000, Negotin, Fed. Geol. Surv., Belgrade.

Enciu P., 2009. Pliocene and Quaternary of the western part of the Dacian Basin. Stratigraphy and Palaeogeographical Evolution, 251 p, in English Language, Romanian Academy, Bucuresti.

Evloghiev J., Sopov V., Popov N., 1995. Correlative geomorphologic and biostratigraphic research on the Quaternary continental deposits in Central North Bulgaria. Rev. Bulg. Geol. Soc., 56, p.47–55, Sofia.

Evstatiev D., Hriscev Hr., Karastanev D., ed-tors, 2000. Nuclear Power Plant – Additional Geological Inves-

tigations. Academic Publishing House "Prof. Marin Drinov", 100p, www.bgob.net/acad_publ_house.asp.

Filipov L., Kojumdjeva Em., Popov N. ,1988, 1989, 1990. Geological Map of Bulgaria 1:100 000, Lom, Kozlodui, Bregovo-Byliesti Sheets. Inst. Geol. Bulg., Sofia

Filipov L., Deceva A., Kojumdjeva Em., Popov N., Țankov T., 1992. Geological Map of Bulgaria 1:100 000, Vidin, Inst. Geol. Bulg., Sofia.

Halouzka R., 1975. Correlation table of the Middle Danube terraces and levels and their parallelization with the main terraces systems in Europe, Antropozoic, 9, Praha.

Janacek J., 1969. Nové stratigrafické poznatky o Pliocenní a Pleistocenní výplni Centrální Části Podunajské Níziny, Geol.Práce, 50, 113-130, Bratislava.

Krautner H. G., Krstic B. ,2002. Alpine and pre-Alpine Structural Units within the Southern Carpathians and the Eastern Balkanides. Proceed. Carpath. Balkan. Geol. Assoc. Congr. CD, Bratislava.

Krstić Nadezda., Mihailović D., Petrović S., Milicević V., 1997. Neogene of Kljuc and Krajina. In: Geology of the Danube Gorge, p 71 – 79, Beograde.

Krstić N., Pantić N., Radosević B. , 2003. Environment of Paludian Beds, p. 94–101, in: Neogen der Zentrale Paratethys, Bd. X, Romanien, Ed.Acad.Rom., Bucureşti.

Mihailova D., Naftali Sn., 1996. Geomorphological Map of Bulgaria 1 : 100 000, Biala Slatina and Kozlodui sheets. Acad.Bulg., Inst. Geogr., Sofia.

Musinschi C., 1999. Correlation of the Quaternary Terraces along the Prut River Valley (in Romanian Language), Abstract PhD thesis, 26p, Inst.Geogr., Rom. Acad., Bucuresti.

Nikolov V., Filipov L., 1996. Geomorphological Map of Bulgaria 1 : 100 000, Vidin, Acad.Bulg de Ştinţe, Inst. Geogr., Sofia.

Pecsi M., Scheuer G., Schweitzer F., Hahn G., Pevzner M.A., 1985. Neogene-Quaternary Geomorphological Surfaces in the Hungarian Mountains. Akad.Kiado, Problems of the Neogene and Quaternary in the Carpathians Basins, p 51-64, Budapest.

Petković V.K., 1948. O fosilnoj „pradelti" Dunava na profilu Kladovo-Turnu Severin-Sip. Glasnik, SGD, 28,1, Beograd.

Rakić M. (1977), The Genesis and Stratigraphy of Quaternary sediments in the drainage basins of Juzna and Zapadna Morava Rivers (with the review of sedimentary conditions in Dacian and Pannonian Basins), Ph.D.Thesis, 88p , Belgrad.

Rakić M., Simonović Slavka., 1997: Quaternary Deposits of Danube Valley between Kostalac and Brza Palanka, p81-87, in: Geology of Danube Gorges, Belgrad.

Ruszkiczay-Rüdiger Z., 2007, Tectonic and Climatic Forcing in Quaternary Landscape Evolution in the Central Pannonian Basin: a Quantitative Geomorphological, Geochronological and Structural Analysis. Vrije Universiteit and Eötvös University, Amsterdam and Budapest, 149p.

Scharek P., Herrmann P., Kaiser M., Pristaš J. (2000), Map of Genetic types and Thickness of Quaternary sediments. Jb.Geol. B.-A., band 142, heft 4, 447–455, Wien.

Shanov S., 2005, Post-Cretaceous to recent stress fields in the SE Moesian Platform (Bulgaria), Tectonophysics 410, 217-233, Elsevier, www.elsevier.com/ locate/ tecto.

Szadeczky-Kardoss E., 1938: Geologie der Rumpfungarländischen Kleinen Tiefebene, Mitt.Berg. u. Hütten., Abt.Kön. Hoech, Sopron., 10,1, 444p.

Tărăpoancă M. (2004), Architecture, 3D Geometry and Tectonic Evolution of the Carpathians Foreland Basin, Vrije Universiteit, 119 p, ISBN 90-9017847.

Winguth C., Wong H.K., Panin N., Dinu C., Georgescu P., Ungureanu G. (1997), Upper Quaternary Sea Level Changes in the northwestern Black Sea: Preliminary Results. Geo-Eco-Marina, 2, 103–114, Bucureşti.

Wong H.K., Winguth C., Panin N., Dinu C., Wollschläger M., Georgescu P., Ungureanu G., Krugliakov V.V., Podsuhveit V. (1997), The Danube and the Dniepr Fans: Morphostructure and Evolution. Geo-Eco-Marina, 2, 77–102, Bucureşti.

Scientific Annals, School of Geology, Aristotle University of Thessaloniki Proceedings of the XIX CBGA Congress, Thessaloniki, Greece	Special volume 100	191-196	Thessaloniki 2010

SEISMOTECTONIC MODEL ON GEOLOGICAL DATA FOR 1892 DULOVO EARTHQUAKE, LOWER DANUBE VALLEY

Shanov S. and Radulov A.

Laboratory of Seismotectonics, Geological Institute, Bulgarian Academy of Sciences, 1113 Sofia, Bulgaria, s_shanov@geology.bas.bg, radulov@geology.bas.bg

Abstract: The potentially active faults in the area of Lower Danube Valley between the arcs of Carpathian and Balkan mountain chains are not properly recognized. The epicentre of the only historically known "strange" earthquake on the territory of Bulgaria with a magnitude evaluated at $M_s = 7$, known as the "1892 Dulovo Earthquake" is situated in this area. The first step for creating a seismotectonic model for this earthquake is the identification of the nearby active fault. The analysis has shown that it is realistic to accept that the earthquake occurred in the frames of the Tutrakan Graben. A fault segment of the Dulovo Fault, the most probably activated during the 1892 Dulovo Earthquake, is recognised. Its length is 42±5 km, and the width is 15±2 km. The offset of the normal faulting from the last seismic events is evaluated at 2 m. Three approaches are used for determination of the maximum magnitude of the earthquake that can be generated. They give M_s in the range between 6.8 and 7.5. The most probable value is 7.0.

Keywords: Lower Danube Valley, active fault, Dulovo Earthquake, seismotectonic model

1. Introduction

The Lower Danube Valley dominates over the territory of the Moesian Platform. The potentially active faults in this area between the arcs of Carpathian and Balkan mountain chains are not properly recognized. The only pretended major active structure passing trough the territory of Bulgaria along the border between Bulgaria and Romania (Cadet and Funiciello, 2004) is the Intramoesian Fault, crossing Danube River from NW to SE. The fault is of a length several times greater than the known active faults generating strong earthquakes of magnitude around 7.0 (Fig. 1). The known strong historical earthquake in the area that could be related (or not) to this structure is 1892 Dulovo Earthquake of magnitude evaluated approximately at 7.0 (Fig.1). The identification of the geological active structure that might generate the 1892 Dulovo Earthquake is the aim of the study. The error of the location of the Dulovo Earthquake by Bulgarian, Romanian and Russian authors is 200 km (Glavcheva and Radu, 1994). Thus, the identification of the active fault structure able to produce such an earthquake is of significant importance for understanding the geodynamics of the area and for the seismic hazard assessment for both countries Bulgaria and Romania.

2. 1892 Dulovo Earthquake

The earthquake occurred the 14th of October 1892. In this time regular seismological observations on the Balkan Peninsula just had been started, and this earthquake has been more than once a matter of study. Handling the entire quantity of reports Glavcheva and Radu (1994) have made new assessments of the isoseismal map according to the MSK-64 scale and relocation of the epicentre. They argued that the contradictory conclusions of previous studies on the 1892 Earthquake are due to the fragmentary use of original descriptions, the incomplete use of reports, the heritage of wrong suggestions and application of different intensity scales. As a result of the analysis of the distribution of the intensity data it was possible to assess the earthquake parameters as presented in table 1.

3. Geology and tectonics of the epicentral area of 1892 Dulovo Earthquake

The epicentral area of 1892 Dulovo Earthquake is situated in the relatively elevated eastern part of the Moesian Platform. This platform**,** dominated by the large plane region of the Low Danube River, was named the Moesian Platform in 1946 (Bonchev, 1971). Its geological and tectonic characteristics, as well as its deep structure**,** have been

studied and discussed by a number of authors (Bonchev, 1946; Muratov, 1949; Popescu et al., 1965; Atanasiu and Chirac, 1965; Dobrev, 1966; Bonchev 1971 and many others). Newly published geophysical and geological data have recently completed the knowledge for the inner structure of the platform and for its geodynamic evolution (Tari et al., 1997; Hausser et al., 2001). For the area of the SE Moesian Platform**,** the difference is that the most important faults inside the platform were recognised only by industrial geophysical works and drilling. Most of them had not been active since the Triassic time (Bokov and Chemberski, 1987). Only a few of the faults, later activated during different tectonic phases and situated near the southern and the eastern periphery of the studied area**,** can be recognised geologically on the surface. Thus, the study of the recent kinematics of the faults is difficult, if possible at all.

Fig. 1. Regional sketch of Lower Danube Valley with the active faults and fault segments, and the probable epicenter of 1892 Dulovo Earthquake.

The present knowledge about the recognized main faults and the principal regional structures was summarized by Tari et al. (1997). The geotectonic evolution of the Moesian Platform is mainly characterized by four main sedimentary cycles: Middle Cambrian-Upper Carboniferous, Permian-Triassic, Jurassic- Cretaceous, and Neozoic, being defined in connection with the tectonic activity. From seismotectonic point of view the Quaternary stage of development of the Moesian Platform is the most important.

The tectonic heritage from the most recent processes for the area of interest is represented by the North Bulgarian Uplift (or Arch) bordered to NE by the Tutrakan Subbasin (or the Tutrakan Depression), to the north – by the Alexandria Subbasin on the territory of Romania, to the south – by the structures of the Fore-Balkan, and to the west – by the Iantra-Iskar Step (Fig. 2). During the Plio-Quaternary stage the North Bulgarian Uplift was submitted to continuous but not very intensive elevation. According to Yaranov (1960) the elevation during the Quaternary was about 80 m for the central part of the Uplift, and of about 50 m towards the periphery.

Table 1. Seismological evaluation for the 1892 Dulovo Earthquake.

Time	1892, October 14, 04 h. 54 min. GMT
Coordinates of the epicenter:	43°45' N, 26°55' E (±10 km)
Hypocentral depth:	35-50 km
Intensity:	Io = 8 [MSK]
Magnitude	Ms = 7 (uncertain)

The differential movements that had superposed North Bulgarian Uplift and the Lom Depression to the west ended at 2,59 Ma BP. The Neotectonic stage is characterized by continuous elevation of the principal tectonic blocks. After the regression of the Dacian Basin (0,82 Ma BP) and till now, the upper level of the alluvium is raised 130,10 m in Yantra-Iaskar Step and at 121,00 m in NE Bulgaria (including the North Bulgarian Uplift).

4. Methodology

The first step for creating of the seismotectonic model is the identification of the active faults. The identification of faults that pose earthquake hazards requires application of a fault-activity criterion to filter out ancient faults that are unlikely to rupture during future earthquakes.

The magnitude of the earthquake can be evaluated using the relationships proposed by Wells and Coppersmith (1994):

$$M_s = 6.04 \pm 0.22 - 0.71(\pm 0.12)\ SRL \qquad [1]$$

where S*LR* is the length of the fault rupture from the earthquake.

Another possibility for normal faults is to use the evaluated geologically offset (average slip on the fault) *D* and the fault area *A.* The fault area *A* is:

$$A = LW \qquad [2]$$

where *L* is the length of the activated fault segment and *W* is its wide in depth. The expected maximum magnitude is:

$$M_s = 6.78(\pm 0.34) - 1.32(\pm 0.26)\ AD \qquad [3]$$

The third approach used for characterizing of an

active fault is based on the relationship between the moment magnitude and the seismic moment. The milestone in this approach is the converting the magnitude M_s onto the moment magnitude scale M_w. The suggestion of Bayliss and Burton (2007) for this part of the Balkan Peninsula was adopted – northern of 43^0 N the most appropriated relationship is:

$$M_w = M_s \qquad [4]$$

The definition of the moment magnitude M_w is:

$$M_w = (2/3) \log_{10} (M_0) - 10.73 \qquad [5]$$

where M_0 is the seismic moment [dyne-cm].

By definition:

$$M_0 = \mu AD \qquad [6]$$

where μ - shear modulus (often *G* in engineering), *A* - fault area, *D* - average slip on the fault. For the conditions of the hypocenters in the Earth's crust it is widely accepted to use the value $\mu = 3.3 \times 10^{11}$ dyne/cm^2.

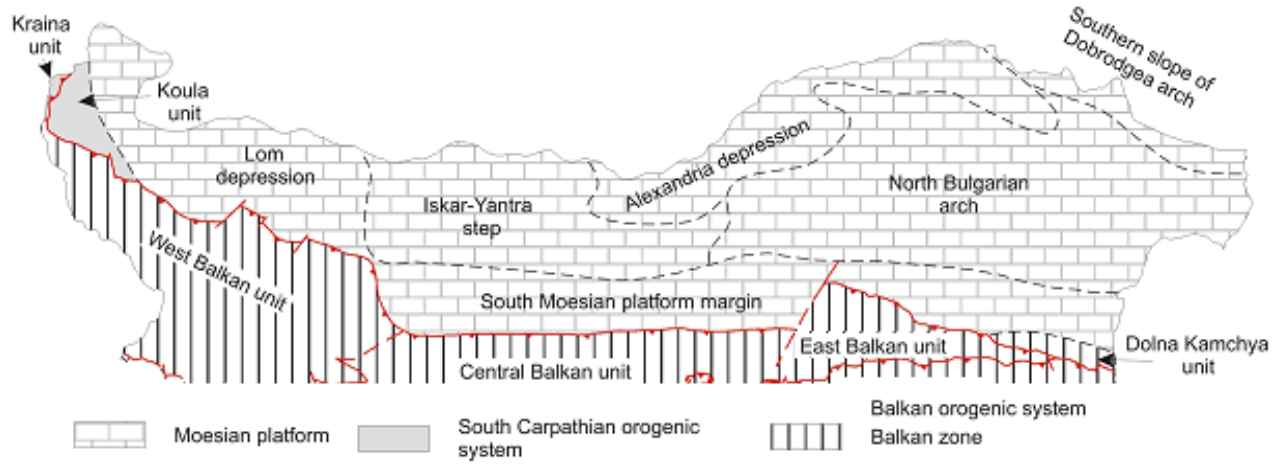

Fig. 2. Tectonic scheme of Northern Bulgaria (according to Dabovski et al. 2002).

The slip rate cannot be determined from the slip and time of only the most recent earthquake, since only an incomplete cycle has taken place. If the magnitude of historical earthquake is known the geometric characteristics of the activated fault segment can be deduced, and vice-versa.

5. Results and Discussion

According to the geophysical data, the inner part of the Moesian Platform has a block structure. Earthquakes with magnitudes of less than 4.5 were recorded (Bonchev, 1979; Visarion et al., 1988**;** Tzvetanov, 1990) in different parts inside the platform. The only historically known "strange" earthquake with a magnitude evaluated at $M_s = 7$ is the 1892 Dulovo Earthquake. The identification of the geologically active structure capable to generate this seismic event is discussed bellow.

5.1. Regional fault structures

A number of sub-parallel faults striking NW-SE have been mapped on the level of the Precambrian - Paleozoic fundament in NE Bulgaria. These faults define the main block structures having the same orientation (Fig. 3). The most important for the geological models are the Intramoesian Fault and Dulovo Fault (named also Balchik – Tervel Fault) framing the Tutrakan Depression (Bokov and Chemberski, 1987). The faults cut also the Mesozoic sedimentary cover (epicontinental sediments of Late Jurassic – Early Cretaceous age).

5.2. Indications for Neotectonic activity

In the frames of Tutrakan Depression, only an important area of Neogene limestones and terrigenous sediments can be found (Fig. 3). On the adjacent and elevated Dobrogea and Vetrino blocks, the Neogene sediments are of insignificant thickness or missing (Geological Map of Bulgaria in a scale 1:100 000, Sheets Dulovo, Tutrakan, Razgrad, Dobritch, Isperih, Russe, Gen.Toshevo, Biala, Popovo, Griaka, Vetovo, Silistra). The spread of the Neogene deposits defines the Tutrakan Depression as an area of sin-sedimentary subsidence. A normal faulting along the bounding Intramoesian and Dulovo faults may be the reason for the recorded sin-sedimentary subsidence.

The enlargement of the Upper Romanian – Lower Pleistocene Basin, north-eastward the Dulovo Fault is a fact demonstrating the continuous tendency of subsidence inside the graben during the

Early Pleistocene. The basin existed till the beginning of Marine Isotopic Stage (MIS) 21 (Evlogiev, 2000).

The differential vertical displacement along the faults during the formation of Danube River terraces after the MIS 21 is confirmed by the lateral distribution of the terraces. All terraces from T6 to T1 are elevated along the Bulgarian Danube riverside between the towns of Tutrakan and Russe. They are not presented eastwards in the Tutrakan Depression (Evlogiev, 2000). The highest river terrace along the Romanian riverside is limited only westward the Arges River outflow (the town of Oltenita). The line Tutrakan – Oltenita separates two blocks with different vertical velocities during the Pleistocene. The western uplifted block contains the all range of terraces, while the eastern block experiences subsidence at the same time. The zone of the differential vertical movements can be identified as a fault segment belonging to the Dulovo Fault (Fig. 3).

The presence of Holocene alluvial fans along the NE block of the Intramoesian Fault and the absence of these sediments in its SW block is an indication for a relative uplifting of the NE block. The different width of the floodplain and terraces from the two sides of the Intramoesian fault also indicates its activity during Pleistocene and Holocene time.

An elevation profile parallel to the Danube River on the surface of the Upper Romanian – Lower Pleistocene Basin shows that the Tutrakan Depression is 26 m lower than Vetrino Block and 19 m lower than Dobrogea Block (Fig. 4). The rate of subsidence of Tutrakan Depression during the Pleistocene reflects the cumulative effect of the displacements along the bordering faults. It is not possible to evaluate the rates of offsets separately for each of the bordering faults.

Another elevation profile along the Danube floodplain shows Holocene deformations, too. The displacement at the Dulovo Fault is evaluated to about 2 m (Fig. 4). Eastward the Intramoesian Fault, the Danube floodplain is also elevated, and even slightly inclined opposite to the flow.

On the base of the elevation profiles and the distribution of the sediments we can conclude that the subsidence in the Tutrakan Depression occurs during the entire Quaternary, even in Holocene time. Hence, the faults bounding the graben should be active at that time.

The first reported data for the Dulovo earthquake (Hepites, 1894) locates the epicentral area near the

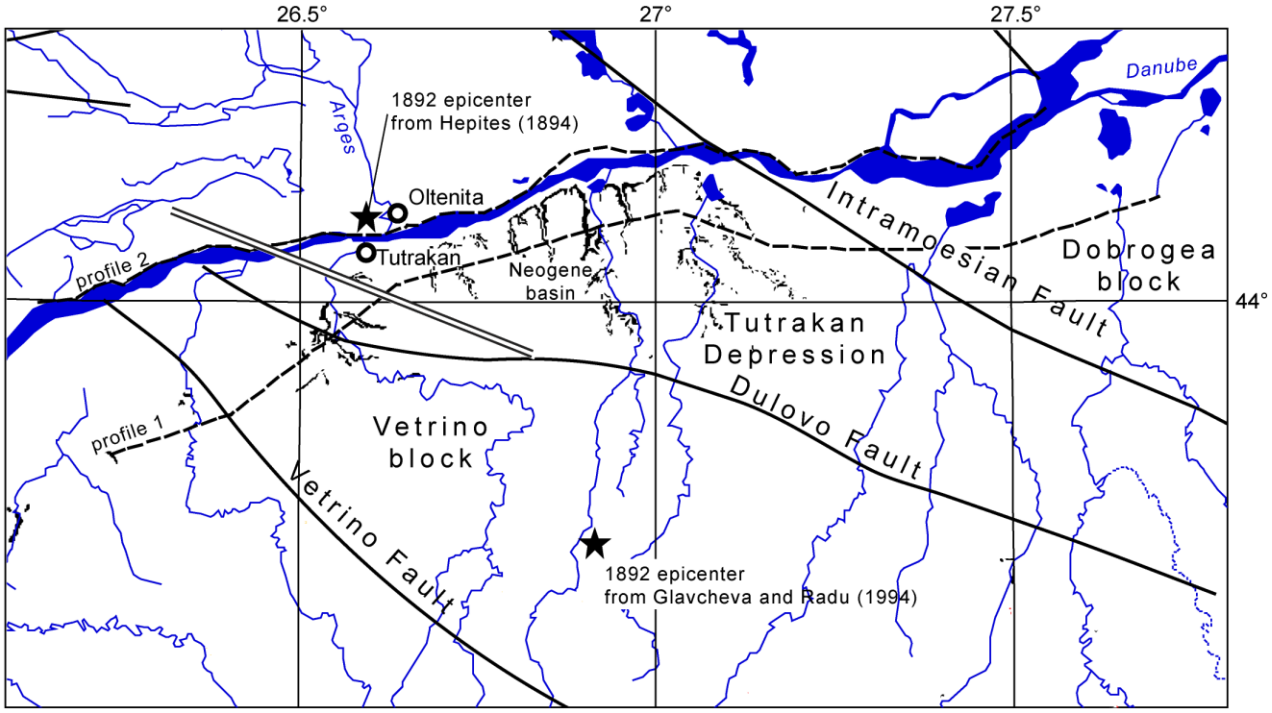

Fig. 3. Structural sketch of the Tutrakan Depression. Main faults in the basement (from Bokov and Chemberski 1987) bound also the Neogene basin (black pattern). Epicenter locations of the 1892 Dulovo earthquake from different authors are shown by stars. Double line shows the segment of the Dulovo Fault controlling relief and Pleistocene-Holocene deposition. Dashed line shows elevation profiles from Fig. 4.

town of Oltenita, situated in the central most subsided part of Tutrakan Depression (Fig. 3). It is realistic to accept that the earthquake occurred in the frames of the graben. The tectonic control on the relief of the segment from the Dulovo Fault crossing the Danube floodplain at the position of the recorded 2 m offset could be traced between the Romanian riverside and an overstep in Bulgaria. This segment may be a seismic source. Its length is 42±5 km. Taking into account the Holocene age of the terrace, the slip rate of Dulovo Fault during the Holocene time is evaluated at 0.28 mm/year.

5.3. Seismotectonic model

The presented above geological consideration give the reason the accept the following characteristics of the activated fault segment during the 1892 Dulovo Earthquake: Fault length (L) - 42±5 km; Width (W) from M_0 – 15±2 km; Depth (H) at dip 60°±10° (normal faults in upper crust) – 13±3 km; Displacement assuming a single event displaced the Danube River floodplain – 2 m.

The maximum possible magnitude of the earthquake that can be generated by the activated segment is evaluated by using the presented relationships [1], [3] and [5]. The results are plotted on table 2. These values are comparable with the Dulovo Earthquake characteristics from table 1 (Glavcheva and Radu, 1994). Following the hypothesis of strict periodicity of the strong seismic events, and using the nomogram of Slemmons and dePolo (1986) the recurrence interval of the strong events is evaluated at 3 000 years, the displacement (vertical offset) is 2 m.

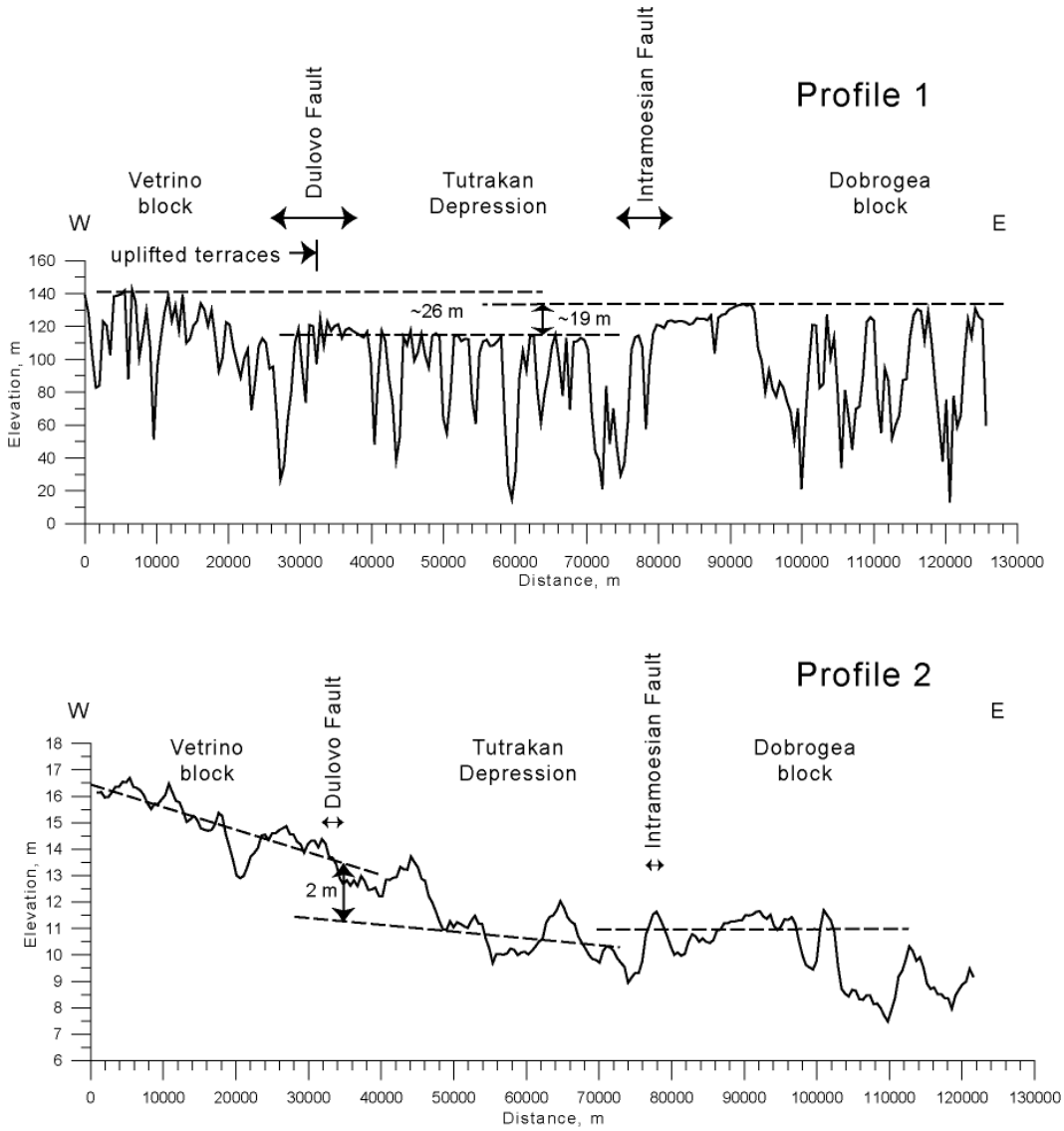

Fig. 4. Elevation profiles across the Tutrakan Depression along the surface of the Upper Romanian – Lower Pleistocene Basin (profile 1) and along the Danube floodplain (profile 2).

Table 2. Dulovo Fault – Seismotectonic model.

Constants and fault characteristics	Magnitude Ms		
	Relationship [1]	Relationship [3]	Relationship [5]
$\mu = 3.3 \times 10^{11}$ dyne/cm^2 Mo = 3.935×10^{26} dyne-cm Vertical offset D = 2 m Fault length = 42±5 km Fault width = 15±2 km	7.2 ± 0.3	7.0 ± 0.1	7,02

6. Conclusions

The study presents a new solution for the epicentre location of 1892 Dulovo Earthquake by recognising the fault structure able to produce an earthquake of magnitude 7. The segment of Dulovo Fault (NE border fault of Tutrakan Graben) is described as the most probable geological structure, activated during the earthquake.

The available data enhanced the creation of an acceptable seismotectonic model. It reflects the latest displacement along the fault. The normal displacement of 2 m created by earthquake of magnitude $M_s = 7$ seems to be reasonable. The model is based also on the assessment that the Holocene slip rate along the Dulovo Fault (vertical component – the most lower possible) is 0.28 mm/y. The recurrence interval of the strong events is evaluated at 3 000 years.

References

Atanasiu L. and Chiriac I., 1965. Considération géologique sur les plates-formes du territoire de la République Populaire Roumanie. 7th Congr. of the Carpatho-Balkan Geol. Assoc., Sofia, Vol. I, 251-255.

Bayliss T.J. and Burton P.W., 2007. A new earthquake catalogue for Bulgaria and the conterminous Balkan high hazard region. Natural Hazards and Earth System Sciences, EGU, 7, 345-359.

Bokov P. and Chemberski, H. (Eds), 1987. Geological conditions for the oil and gas accumulation in North-Eastern Bulgaria. Technika Publ. House, Sofia, 332 p. (in Bulgarian)

Bonchev E., 1946. Bases of the tectonics of Bulgaria. Ann. of the Direction for Geol. and Mining Exploration, part A, v.IV, 336-379. (in Bulgarian)

Bonchev E. 1971. Problems of the Bulgarian geotectonics. Sofia, Tehnika Publ. House, 204 p. (in Bulgarian)

Bonchev E., 1979. The Moesian platform and its role in the Phanerozoic evolution of the Balkan Peninsula. Zavod za Geol. i Geof. Istrazivanja, Beograd, kn. XXXVII, ser. A, 49-58.

Cadet J.P. and R. Funiciello, 2004. Geodynamic map of the Mediterranean. – Commission of the Geological map of the World, 2 sheets.

Dabovski C., Boianov I., Khrischev Kh., Nikolov T., Sapunov I., Yanev Y. snd Zagorchev I., 2002. Structure and Alpine evolution of Bulgaria. Geologica Balcanica, 32, 2-4, 9-15.

Dobrev T., 1966. Structure of the foundation of the Moesian platform in the territory of Bulgaria. Soviet Geology, 11, 44-45. (in Russian)

Evlogiev J., 2000. Quaternary in Northeast Bulgaria. - J. of the Bulg. Geol. Soc., 61, 1-3, 3-25 (in Bulgarian).

Glavcheva R. and Radu C., 1994. On the strong 1892 earthquake in South Dobrudzha. Bulgarian Geophysical Journal, v.XX, No 3, pp. 88-94

Hausser F., Raileanu V., Fielitz W., Bala A., Prodehl C., Polonic G. and Schulze A., 2001. VRANCEA99 – the crustal structure beneath the southeastern Carpathians and the Moesian Platform from a seismic refraction profile in Romania. Tectonophysics, 340, 233-256.

Hepites S., 1894. Le tremblement de terre du 14 octobre 1892. – Analele Inst. Meteor. Rom., 7, 20.

Muratov M.V., 1949. Tectonics and history of the development of the Alpean geosyncline region of the European part of URSS and the adjacent countries. In: - Tectonics of USSR, Moscow, v.II, 204-265 (in Russian)

Popescu M., Patrut, I., Paraschiv, D. and Molnar, M., 1965. Present stage of geolgical knowledge of the Moesic Platform, Romania. Proc. of 7th Congr. of the Carpatho-Balkan Geol. Assoc., Sofia, Vol. I, 333-337.

Slemmons, D.B. and dePolo, C.M., 1986 Evaluation of active faulting and associated hazards. Studies in geophysics — active tectonics: National Academy Press, Washington, DC, 45-62.

Tari G., Dicea O., Faulkerson J., Georgiev G., Popov S., Stefanescu M. and G. Weir. 1997. Cimmerian and Alpine Stratigraphy and Structural Evolution of the Moesian Platform (Romania/Bulgaria). In: - Robinson A. G. (Ed.) Regional and Petrolium geology of the Black Sea and surrounded region: AAPG Memoir 68, 63-90.

Tzvetanov P. (Ed.), 1990. Belene NPP – Investigations and attitudes of the Bulgarian Academy of Sciences, Sofia, BAS Publ. House, 412 p. (in Bulgarian)

Visarion M., Sandulescu M., Stanica D. and Veliciu S., 1988. Contribution à la connaissance de la structure profonde de plate-forme Moesienne en Roumanie. Studii Tehnice si Economice, Seria D, Geofizica, Bucuresti, 15, 211-222.

Wells, D.L. and Coppersmith K.J. 1994. New empirical relationships among magnitude, rupture length, rupture width, rupture area, and surface displacement. Bulletin-Seismological Society of America 84, no. 4: 974-1002.

Yaranov D., 1960. Tectonics of Bulgaria, Tehnika Publ. House, 282 p. (in Bulgarian).

Special Session S09
Geology of the Pieniny Klippen Belt and the role of zones with extensive shortening in the structure of orogenic belts

Scientific Annals, School of Geology, Aristotle University of Thessaloniki Proceedings of the XIX CBGA Congress, Thessaloniki, Greece	Special volume 100	197-207	Thessaloniki 2010

GEOLOGY AND TECTONICS OF THE VRŠATEC KLIPPEN AREA (PIENINY KLIPPEN BELT, WESTERN SLOVAKIA)

Bučová J., Plašienka D. and Mikuš V.

Department of Geology and Palaeontology, Comenius University, Mlynská dolina G, 842 15 Bratislava, Slovak Republic, bucova@fns.uniba.sk, vmikus@fns.uniba.sk, plasienka@fns.uniba.sk

Abstract: The Pieniny Klippen Belt (PKB) is a narrow (merely several km), but lengthy (up to 600 km) zone dominated by Late Oligocene – Miocene wrench tectonics. It separates the Cenozoic accretionary complex of the External Western Carpathians from the Cretaceous nappe system of the Central Western Carpathians. Our investigation was focused on the tectonic structure and evolution of the Vršatec klippen area in the western Púchov sector of the PKB. The studied area includes the Oravic (Czorsztyn, Kysuca, Orava and Transitional Units) and the "non-Oravic" tectonic units (Klape and Drietoma Units). Detailed geological mapping and systematic field structural research of meso-scale deformational structures revealed the record of multistage tectonic evolution during the Senonian – Pliocene times. The oldest recognized stage resulted in formation of the Mesoalpine fold-nappe system of the PKB due to subduction and closure of the Vahic Ocean during the Senonian – Early Eocene times. This compressive stage was accompanied by thrusting of the presently most external Kysuca Unit over the Czorsztyn and transitional units and by formation of macroscopic folds with the NNE-SSW to NE-SW trending fold axes. The main compression was oriented perpendicularly to the strike of the PKB recently trending in the SW-NE direction. The thrusting and folding were followed by several brittle deformation stages. The oldest stages (E-W to NW-SE oriented maximum compression) produced the NE-SW trending dextral positive flower structure along the western boundary of the PKB and resulted in the final morphostructural character of klippen with long axes oriented in the NE-SW direction. The dextral transpression was a result of the continuing shortening and relative counterclockwise rotation of the ALCAPA block in the Late Oligocene – Early Miocene. The younger N-S oriented compression (Early – Middle Miocene) produced mainly sinistral faults roughly parallel to the strike of the belt in the sinistral transpression regime. The apparent shift of the main compression to the N-S direction was an effect of a rigid counterclockwise rotation of the ALCAPA block during the Early Miocene. Mostly strike-slip and normal faults were formed during the next two tectonic events (Middle to Late Miocene) as a product of the transtensive tectonic regime with NNE-SSW to NE-SW trending compression. Active clockwise rotation of the main compressional stress axis from N-S to NE-SW direction, and inversion from the older transpression to the younger sinistral transtension resulted from NE-ward translation of the ALCAPA block. The NE-SW trending normal faults were generated by the NW-SE extension during the final deformational phase under the extensional tectonic regime (Pontian – Pliocene).

Keywords: Western Carpathians, Pieniny Klippen Belt, Vršatec klippen area, Mesozoic successions, tectonic structure, palaeostress analysis.

1. Introduction

The Pieniny Klippen Belt (PKB) represents a tectonic zone connecting the Cenozoic accretionary wedge of the External (Outer) and the Cretaceous nappe system of the Central (Inner) Western Carpathians (Fig. 1). It is an internally complicated narrow structural belt, which stretches in a broad arc for about six hundred kilometres from the Alpine-Carpathian junction area as far as northern Romania. Regardless of its length and intricate internal structure, the PKB preserves its tectonic integrity, indicated especially by the omnipresence of its typical Oravic units that do not occur in other Carpathian zones. In addition, certain parts of the PKB involve also the "non-Oravic" units of the Central Western Carpathian (CWC) provenance which were incorporated into the PKB and attained its tectonic style after their nappe emplacement during mid-Cretaceous times. These are the Klape, Drietoma and Manín Units in western and the Haligovce Unit in eastern Slovakia. Their palaeo-

geographic and tectonic affiliation was interpreted in various ways, most probably all these units represent frontal nappe elements of the Fatric (Krížna) nappe system (see e.g. Plašienka, 1995; Froitzheim et al., 2008 and references therein).

erated in brittle-ductile and brittle deformational conditions at relatively small depths. Its recent shape was a result of mainly Cenozoic destruction of the Mesoalpine fold-nappe system. According to the present views, the main phase of tectonisation

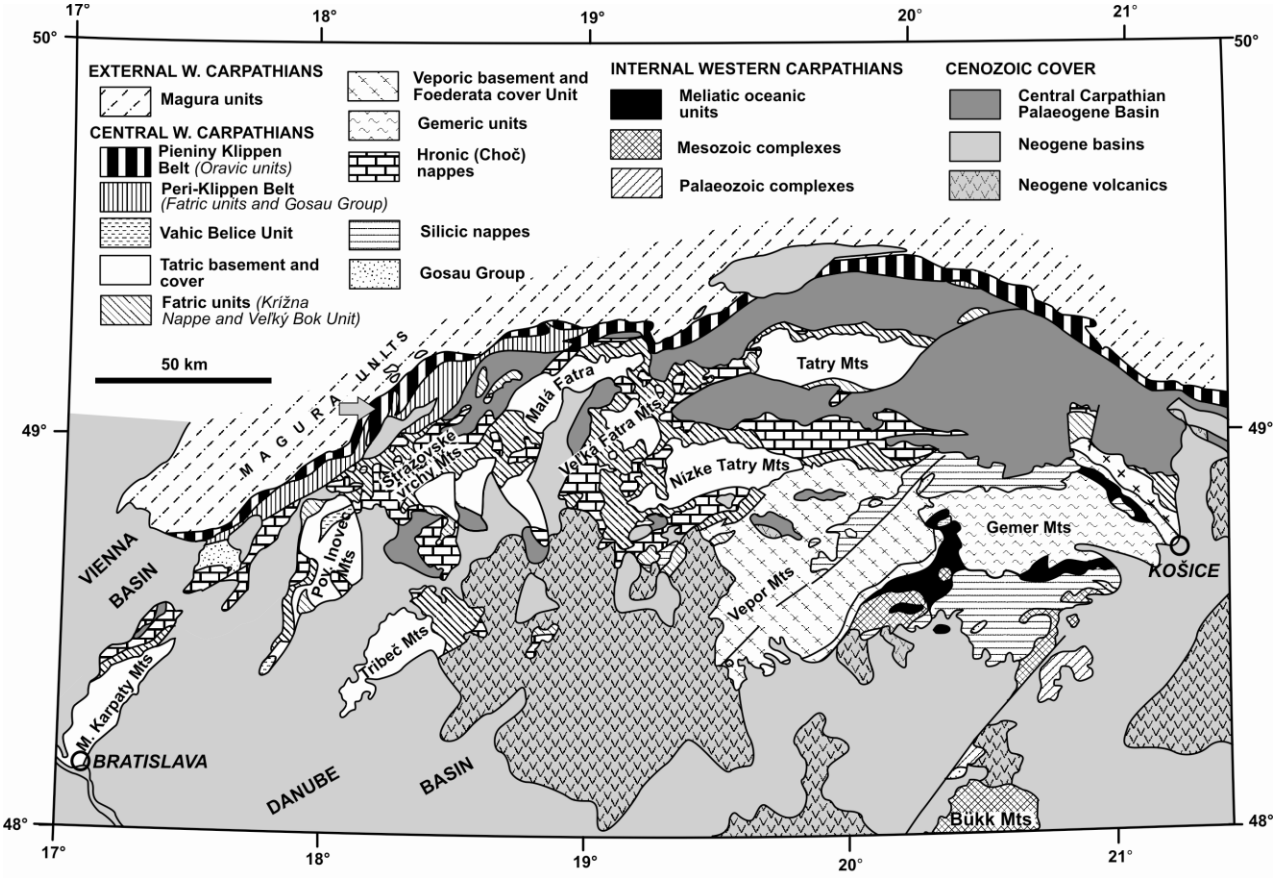

Fig. 1. Simplified tectonic map of the Central Western Carpathians. All boundaries of pre-Cenozoic units are tectonic in origin. Grey arrow in the left part of the figure shows location of the studied area (modified after Plašienka 1998).

The following features are typical for the Oravic units: absence of pre-Mesosoic rocks, scanty representation of Triassic carbonates, variable developments of Jurassic and Cretaceous successions and rarely preserved complete stratigraphic successions. The surface structure of the PKB shows the "klippen tectonic style", where mostly tectonically separated klippen (rigid Jurassic – Lower Cretaceous limestone blocks) are embedded in the "klippen mantle" formed by the Lower Jurassic and Upper Cretaceous to Palaeogene marlstone and flysch formations. Limestone olistolites are present in places as well. The mid-Cretaceous and Senonian marly and flysch formations were originally parts of continuous Oravic successions, but due to higher ductility they were detached and intensely tectonized to form the "klippen mantle".

The complex internal structure of the PKB was caused by several deformational phases, which op-

and separation of the klippen took place after the Eocene – Oligocene and before the Sarmatian (Kováč and Hók 1996; Potfaj 1998). According to Ratschbacher et al. (1993) and Nemčok & Nemčok (1994), the resulting deformation style of the PKB was governed by dextral transpression. The presently observed deformation structures are dominantly brittle. Mesoscopic dislocations prevail and form dense networks in all rock complexes. Well-bedded sequences often exhibit fold structures.

Our study concentrates on the structure and tectonic evolution of one of the most conspicuous parts of the PKB – the so-called Vršatské bradlá group of klippen in the Middle Váh river region of western Slovakia (the Púchov segment of the PKB – see Fig. 1 and 2). Taking as a whole, the Vršatec area represents the largest Czorsztyn-type klippe or a group of klippen in the whole PKB.

2. Geological settings

The Púchov sector of the PKB, located between the Vlára river valley and town of Bytča in NW Slovakia, is a NE-SW trending, approximately 45 km long and up to 20 km wide zone of extremely complex structure. It involves all types of tectonic units known in the PKB, including the Oravic Superunit, as well as the "non-Oravic" units of the CWC affiliation (Fig. 2).

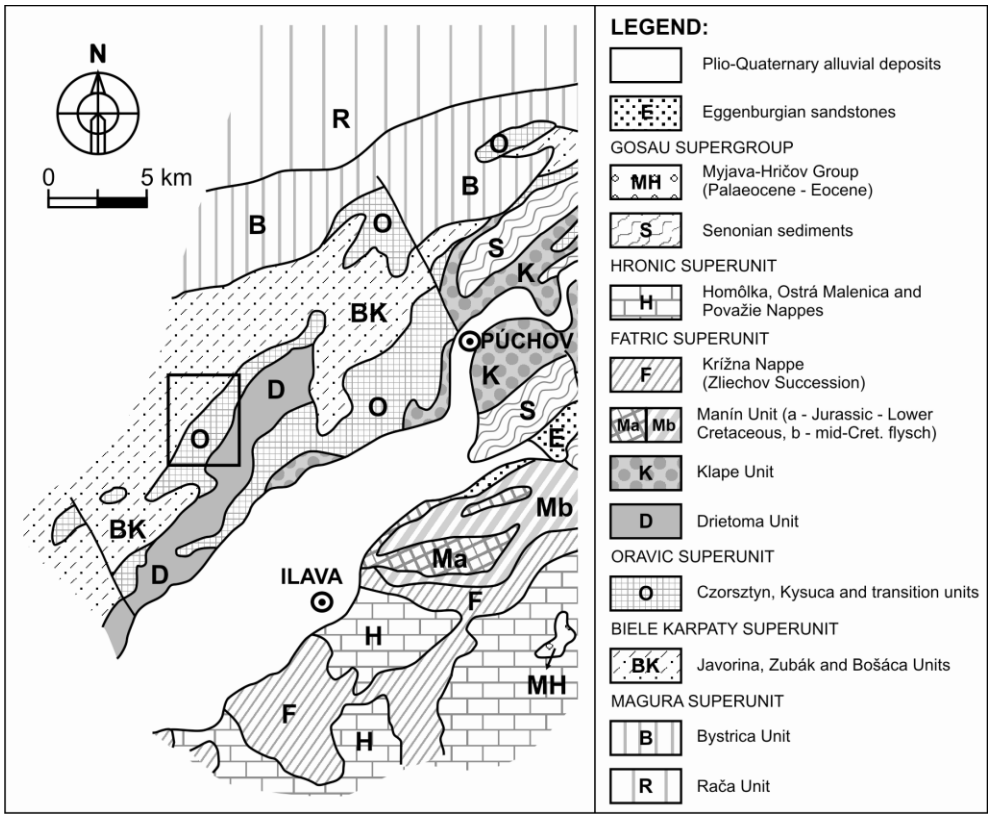

Fig. 2. Distribution of the principal units in the broad vicinity of the Vršatec klippen area. Rectangle in the left part of the figure shows location of the studied area (modified after Schlögl et al. 2008).

The Oravic Superunit includes typical klippen of the ridge-derived Czorsztyn Succession, the basinal Kysuca Succession (corresponding to the Polish Branisko Succession) and several types of "transitional" successions as the Pruské Succession (corresponding to the Niedzica Succession from the Polish part of the PKB – cf. Aubrecht and Ožvoldová 1994), the Orava Succession (Schlögl et al., 2000), the Mariková Succession (Plašienka et al., in press), or the Streženice Succession (Began and Borza, 1963). Klippen of the Oravic Superunit occur along the northwestern margin of the PKB, forming a narrow "Klippen Belt *sensu stricto*". The much broader southeastern part is mostly built by the "non-Oravic" units and their Senonian – Palaeogene overstepping cover (Gosau Supergroup), with occasional tectonic windows of Oravic units. This zone was designated as the "Periklippen Zone" by Maheľ (1980).

The "non-Oravic" Periklippen zone is composed by three large units. The Drietoma Unit, embracing the Upper Triassic – Cenomanian, dominantly basinal succession of likely Fatric (Krížna – Zliechov Succession) provenance, overrides the Oravic units. It forms synclinal tectonic outliers in the Vršatec area, but dominates towards the SW in the Trenčín sector of the PKB. The youngest member of the Drietoma Unit is the mid-Cretaceous (Albian – Cenomanian) synorogenic flysch with "exotic" conglomerates. This provides a link to the huge Klape Unit, which prevails in the Púchov Periklippen Zone. The Klape Unit is composed of some thousand metres thick mid-Cretaceous wildflysch complex (the Klape Flysch) with big olistolites of Triassic and Jurassic carbonates (e.g. the spectacular Klape Klippe; see Marschalko, 1986).

The SE-most component of the Periklippen Belt is the Manín Unit. Its Lower Jurassic – Cenomanian sequence (including the characteristic Urgon-type

platform limestones) closely relates to the Vysoká-type ridge successions of the Fatric Superunit (e.g. the Belá Unit in the adjacent Strážovské vrchy Mts – Maheľ, 1978). However, many authors prefer the Tatric affiliation of the Manín Unit (e.g. Rakús and Hók, 2005). The Manín Unit is dominated by mid-Cretaceous hemipelagic and flysch formations, older solid limestones build several large "klippen" which are in fact brachyanticlines. Senonian sediments within both the Klape and Manín Units were either considered to be their integral continuous sequences (Salaj, 1990), separated by a stratigraphic hiatus in places (Marschalko and Kysela, 1980), or tectonic windows of the underlying Kysuca Unit (Podháj Succession – Rakús and Hók 2005). The mid-Cretaceous flysch of the Manín Unit is from the SE overridden by the frontal Fatric elements with the basinal Zliechov Succession (typical Krížna Nappe).

In places along the NW margin of the Púchov sector of the PKB (Vršatec, Mariková), it can be documented that the Oravic units overthrust various Upper Cretaceous – Eocene flysch formations of the Magura and/or Biele Karpaty Superunits of the External Carpathians. However, this early (probably Eocene) thrust-related structure was strongly overprinted by the Miocene transpression; consequently all units are forming a broad positive flower structure. Oravic units along the NW margin are mostly steeply SE dipping, while the Periklippen Belt is affected by large-scale upright folding. Local axial plane cleavage is developed in the fold hinges. Macrofold axes strike parallel, or slightly oblique to the belt boundaries. They are seldom horizontal, but rather plunging in both directions, thus forming brachyclines. Numerous post-folding faults – slickensides are generally steep to vertical, with gently plunging striae pointing to an oblique- or strike-slip kinematics. In the NE tip of the Púchov sector, near the town of Bytča, the PKB is rapidly narrowing, almost disappearing, due to dextral offset along the W-E trending Bytča fault zone. The next Varín sector of the PKB is W-E trending and located within the southern limb of the structural flower, therefore it is strongly affected by backthrusting (Kováč and Hók, 1996; Marko et al., 2005).

The structural relationships in the Púchov sector of the PKB indicate the emplacement of the Fatric "Periklippen" nappes was the first tectonic event (e.g. Plašienka and Jurewicz, 2006). However, this can hardly be documented by the mesostructural record. This event was followed by the downward (NW-ward) propagated, piggy-back mode of thrusting of Oravic units during the Late Cretaceous – Early Cenozoic succeeded by large-scale upright folding. Shortening passed into dextral wrenching during the Oligocene – Lower Miocene, which incorporated also the Eggenburgian (Burdigalian) sediments in places. The Middle – Late Miocene period is characterized by sinistral transtension along the Mur – Mürz – Leitha – Dobrá Voda – Považie – Žilina wrench corridor, and opening of the small Ilava Basin filled with Pliocene – Quaternary fluviatile sediments (e.g. Kováč, 2000).

The studied terrain of the Vršatec klippen area is formed by two partially independent segments – the Vršatec-Javorník (eastward) and Chmeľová regions (westward) (Fig. 3). The southern, NE-SW trending, Vršatec-Javorník row of picturesque blocky klippen is composed of massive Jurassic – Lower Cretaceous limestones forming a steeply NW-dipping monoclinal slab with overturned stratigraphic sequence belonging to the Czorsztyn Unit. The sequence starts with the Upper Liassic – Aalenian dark hemipelagic marlstones (Krempachy Fm) followed by massive, white bioherm limestones (Vršatec Fm), most probably Lower Bajocian in age (Schlögl et al. 2006). Bioherm limestones are followed by crinoidal limestones (Smolegowa and Krupianka Fms; terminology of lithostratigraphic units mainly according to Birkenmajer 1977), red micritic, locally nodular limestones (Czorsztyn and Bohunice Fms) and whitish to pink biodetrital limestones (Dursztyn Fm). From the SE side, this about 50–150 thick slab of competent limestones is in contact with Upper Cretaceous red pelagic marlstones of the "couches-rouges" type (Púchov Fm). Both Lower Jurassic and Upper Cretaceous marlstones form the so-called "klippen mantle", i.e. a soft matrix in which the stiff klippen are embedded. The lithological contacts, though generally in stratigraphic sequence, are tectonically reactivated in most cases. To the SE, the Púchov marlstones are juxtaposed to various sediments of distinct units participating on the PKB structure (Klape, Orava and Drietoma Units – Schlögl et al., 2000).

In the Chmeľová area, the Oravic Czorsztyn, Kysuca and two transitional successions crop out in a relatively small area, being deformed in a complex fold-fault structure. The Czorsztyn Succession slightly differs from the above-described succes-

sion by lack of the bioherm Vršatec limestones. The Kysuca Unit was discerned in the most external position in this region. It involves deep-water pelagic Jurassic strata (predominantly marlstones and radiolarites), but the Lower Cretaceous sediments are of special type with allodapic biodetrital limestones-the Horná Lysá Fm (Mišík et al., 1994).

The first transitional unit is situated in the eastern margin of the Chmeľová region. The unit contains allodapic crinoidal calciturbidites above the Krempachy and Skrzypny Fms (Aalenian – Lower Bajocian), which are analogous to the Samášky Fm described from the transitional Pruské Succession (Aubrecht and Ožvoldová, 1994). There occur also red crinoidal limestones (Krupianka Fm, Upper Bajocian), which are characteristic rather for the Niedzica than for the Pruské Succession. Younger members are represented by red nodular limestones (Niedzica Fm, Upper Bajocian – Callovian) and radiolarites (Czajakowa Fm, Oxfordian).

The second transitional unit is situated at the southeast margin of the Chmeľová region. Its sedimentary succession contains also volcanic rocks and cannot be assigned to any typical Oravic successions described in the literature so far. Dark grey spotty limestones with intercalations of sandy crinoidal limestones and spongiolites represent the oldest members, which are partly analogous to the Bajocian – Bathonian Samášky Fm described from the transitional Pruské Succession (Aubrecht and Ožvoldová, 1994), or to the Bajocian Flaki Fm known from the Branisko (Kysuca) Succession in Poland (Birkenmajer, 1977). These sediments are overlain by greenish and red platy radiolarites (Sokolica and Czajakowa Fms), followed by red nodular limestones (Czorsztyn Fm). Lower Creta-

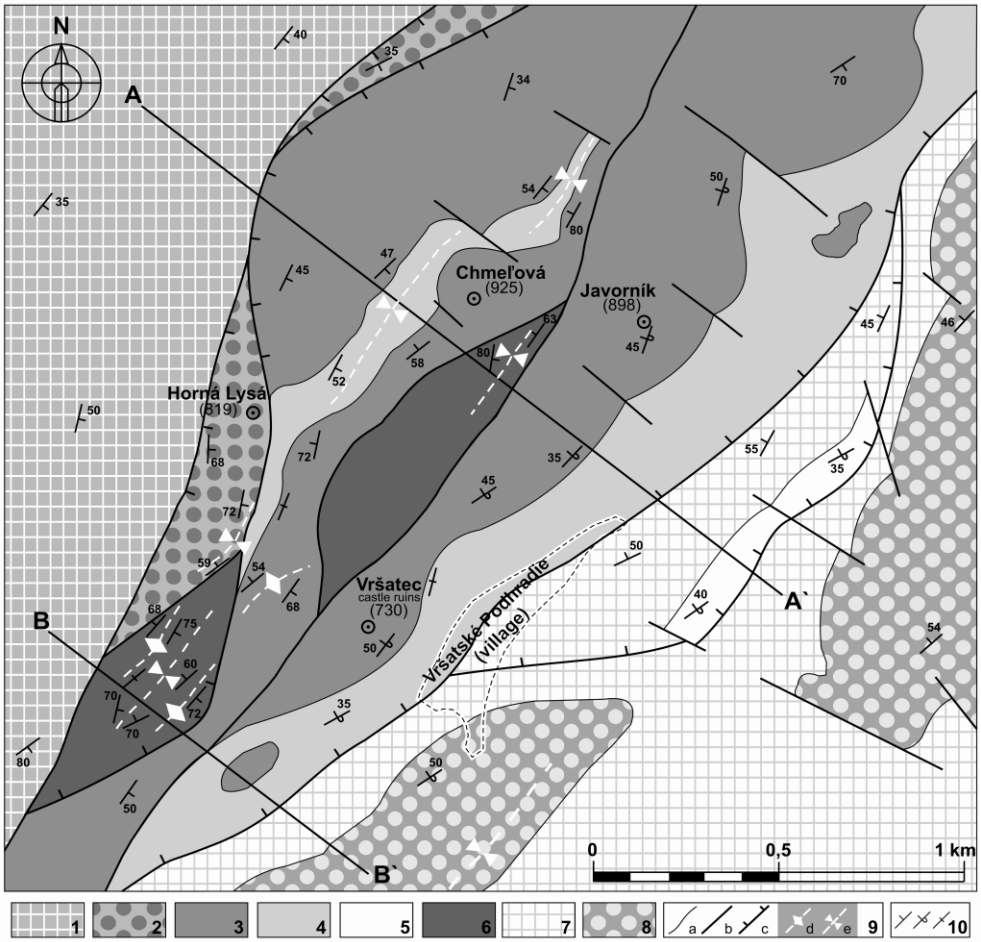

Fig. 3. Simplified tectonic map of the Vršatec klippen area. Carpathian Flysch Belt: 1 – Biele Karpaty Superunit; Pieniny Klippen Belt – Oravic units: 2 – Kysuca Unit; 3 – Czorsztyn Unit: Czorsztyn Sequence (klippes); 4 – Czorsztyn Unit: Púchov-Jarmuta Group ("klippen mantle"); 5 – Orava Unit; 6 – transitional units (undivided); Pieniny Klippen Belt – non-Oravic units: 7 – Klape Unit; 8 – Drietoma Unit; general explanations: 9a – boundaries of tectonic units; 9b – strike-slip faults (undifferentiated); 9c – reverse faults; 9d – anticline axis; 9e – syncline axis; 10 – strike and dip of beds: normal, overturned and upright position.

ceous sediments are represented by pinkish allodapic bioclastic limestones (Horná Lysá Fm – Mišík et al. 1994). Brick-red marlstones, which can be possibly correlated with the Cenomanian Lalinok Fm and the volcanic rocks (alkali basalts of probably Late Cretaceous age – Spišiak et al., 2008) are the youngest components of this succession. The described succession bears features of either a non-typical Kysuca Succession, or the transitional Pruské Succession. Palaeogeographically, both transitional successions most probably occupied a position along a distal slope of the Czorsztyn Ridge at the transition to the Pieniny Basin. To the NW, the Kysuca and the second transitional units are juxtaposed to the flysch sediments of the Biele Karpaty Superunit. Towards the east, these successions are in a tectonic juxtaposition with the typical Czorsztyn Succession of the Vršatec-Javorník region (Fig. 3).

The Maastrichtian – Palaeocene flysch sediments occurring westward of the Oravic units in the Chmeľová area belong to the Biele Karpaty Superunit of the Carpathian Flysch Belt (External Western Carpathians, EWC). The composition and lithostratigraphic succession of this unit is basically different from the other units of the EWC (Potfaj, 1993); the relations to the northern Magura units and to the Klippen Belt are tectonic all along their contacts. Its inner structure has a fold-and-thrust character with NW-vergency, which resulted from formation of the EWC accretionary prism and flysch nappes during subduction of an oceanic crust underlying the EWC flysch basins. The tectonic deformation of the Biele Karpaty nappe group is post-Eocene in age (Potfaj, 1993). The bedding of the flysch sediments neighbouring the Oravic units is generally SE-dipping in normal or reverse position (cf. Mello et al., 2005). This bedding arrangement was primarily a result of the early fold and thrust structure; secondarily it was affected by the Cenozoic transpression. Consequently, the whole Chmeľová area is forming a part of a broad positive flower structure along the strike-slip zone (Fig. 4). The contact with the PKB is most probably followed by a large wrench fault that forms the northern boundary of the PKB.

3. Methods

Our reconstruction of the geological structure and tectonic evolution of the Vršatec klippen area is based on a new detailed geological mapping at the

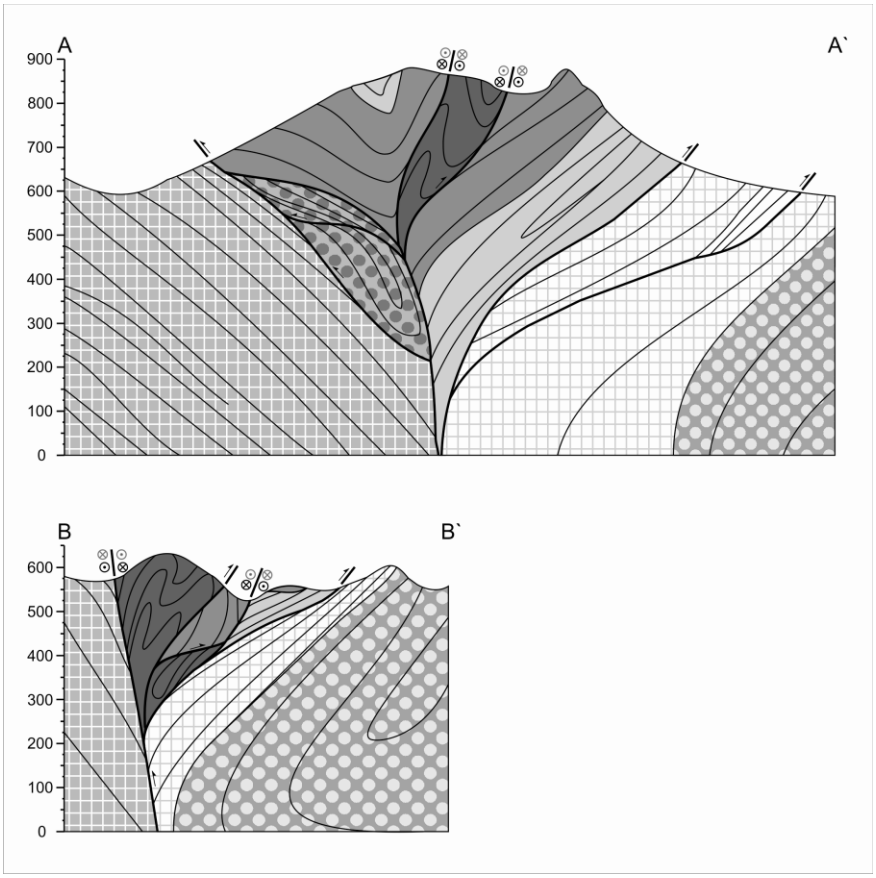

Fig. 4. Cross-section through the Vršatec klippen area. For the location and key see Fig. 3.

scale of 1: 5 000 supplemented by data from the neighbouring areas (Schlögl et al., 2000; Mello et al., 2005). Systematic field structural research of meso-scale deformation elements was focused on fault and fold structures. The analysis of the fault kinematics was based on interpretation of indicators occurring on the slickenside surfaces, along with evaluation of outcrop-scale structures genetically related to faulting. The interactions of the faults observed in the field were used for determination of the relative chronology of the separated homogenous fault groups. The measured slickenside lineations were then processed by analytical palaeostress inversion method (Angelier, 1989; 1994) using the software package Win_Tensor (Delvaux, 1993; Delvaux and Sperner, 2003). The measured bedding and axial plane cleavage attitudes were used for the analysis of fold geometry and orientation. Fold axes are considered to be generally perpendicular to the maximum compression (maximum principal palaeostress axis σ_1). Macroscopic fold axes (β axes) were calculated by the Fabric 7 software (Wallbrecher, 1986).

4. Results

All measured deformational structures were collected from the Oravic units of the Vršatec klippen area. The age range of the investigated rocks is from the Jurassic to the Late Cretaceous. The NW Chmeľová area is internally tectonically complicated, with alternating sectors of normal and reversed stratigraphic sequences. Unlike in the Vršatec-Javorník area to the SE, this region is dominated by macroscopic fold structures (Fig. 3 and 4). Folding was enabled by a much thinner competent limestone layer (ca 10–25 m only) sandwiched between incompetent strata. Folds are mostly upright, slightly asymmetric, with NNE-SSW to NE-SW trending axes and with locally penetrative axial plane cleavage. The cleavage is generally subvertical, but fanwise arranged – steeply northwest dipping in the southwestern sector of the Chmeľová area and mostly steeply southeast dipping in the northwestern sector. The map view and the presence of numerous slickensides postdating the cleavage reveal that folding was followed by brittle deformation that finally shaped the klippen tectonic style of the area.

Meso-scale slickensides were studied in numerous outcrops over the whole studied area. All outcrops exhibit six brittle deformational phases: D1 as the oldest and D6 as the youngest one (Fig. 5; Tab.1). The oldest deformational stage D1 was accompanied by the formation of strike-slip faults (D1a: ENE-WSW trending dextral and NW-SE trending sinistral strike-slip faults) and rarely by NE-SW trending oblique reverse faults with the dextral component (D1b). The horizontal principal compressive stress axis σ_1 was oriented in the E-W direction (in present coordinates). Generally, these faults were activated under the transpressive tectonic regime. NE-SW trending oblique reverse faults indicate the change of the tectonic regime from the pure transpression dominated (E-W oriented σ_1 axis) to the transpressive-compressive regime with the NW-SE horizontal principal compressive stress axis σ_1 (deformational stage D2). Generally NE-SW oriented reverse faults (D2b) were formed; strike-slip faults were still active too (D2a: N-S-trending left-lateral faults and nearly E-W-trending right-lateral faults). Whilst the strike-slip faults are distributed equally throughout the studied area, the reverse faults show different dips in the eastern (only towards the NW), central (both NW and SE-dipping faults) and in the northwesternmost part (mostly SE-dipping) of the area.
The next change of the tectonic regime occurred during the younger N-S oriented compression. Predominantly NNE-SSW trending left-lateral and NW-SE dextral faults (D3a) and rare E-W trending reverse faults (D3b) were formed as the result of the purely transpressive tectonic regime (deformational event D3). On the contrary, mostly strike-slip and normal or oblique normal faults (tensors D4 and D5) were created as the record of the next two strike-slip (transtensive) regimes with NNE-SSW (D4) to NE-SW (D5) oriented σ_1 axis. The last deformation phase D6 is characterized by a number of conjugate normal faults as the result of the extensional tectonic regime with the NW-SE oriented σ_3. Generally, the NE-SW-trending normal faults reactivated the pre-existing weakness zones – either the bedding planes, or older reverse faults. We suppose that normal faulting had already started during the transtensive regimes D4 and D5.

5. Interpretation and Discussion

Summing up, thrusting of the presently most external Kysuca Unit over the Czorsztyn and transitional units was the oldest event recognized in terrain of the Vršatec klippen group. Thrusting was accompanied by formation of macroscopic folds with the NNE-SSW to NE-SW trending fold axes, which are well preserved in the Chmeľová area (Fig. 4). Folding occurred at comparatively greater

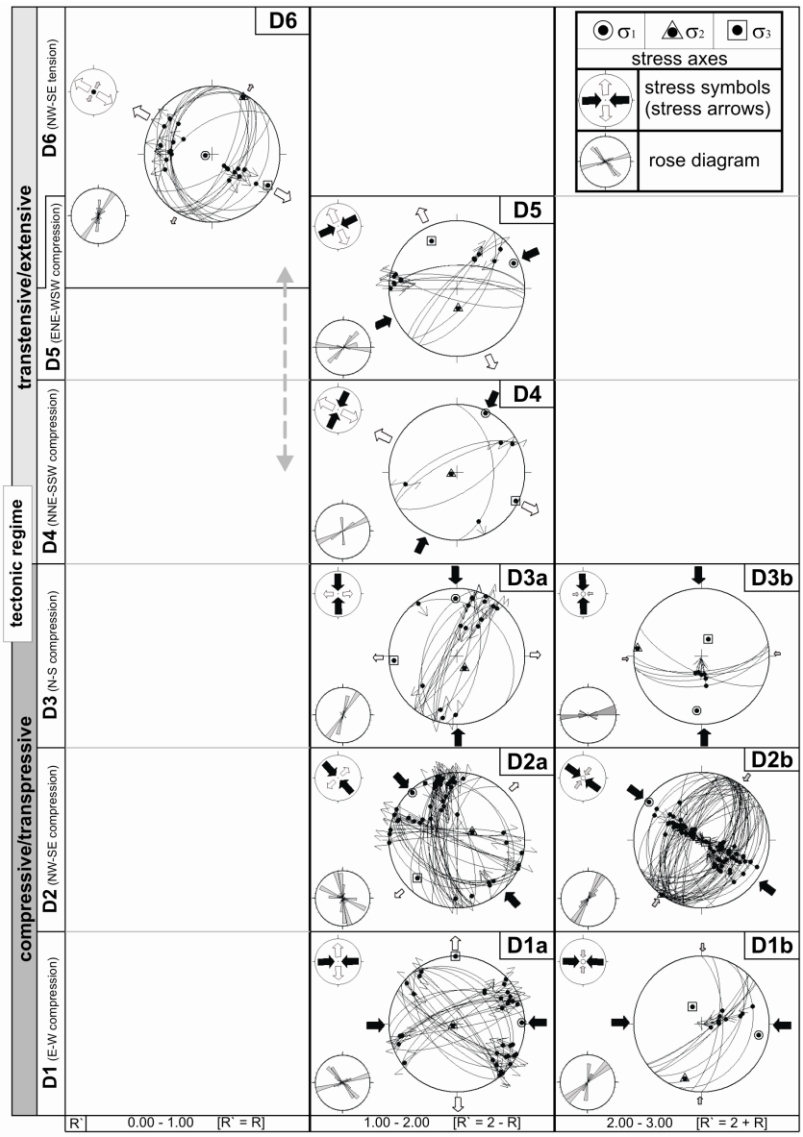

Fig. 5. Synthetic chronological table of all palaeostress tensors from fault slip data (D1a and D1b as the oldest homogenous groups of faults to D6 as the youngest one) and deformational stages (D1 as the oldest to D6 as the youngest one) observed in the Vršatec klippen area. Each homogenous group of faults is represented by stereogram (the fault planes are plotted as great circles with observed slip lines and slip senses using stereographic projection – Schmidt net, lower hemisphere).

depths (but still beyond intracrystalline ductile deformation mechanisms) with development of cleavage formed by pressure solution. The main compression was oriented perpendicularly to the strike of the belt recently oriented in the NW-SE direction. This strong compressive tectonic event resulted in formation of the Mesoalpine fold-nappe system due to subduction and closure of the Vahic Ocean during the Senonian – Early Eocene times (Ratschbacher et al., 1993; Plašienka, 1995). Thrusting and folding were followed by brittle deformation (Fig. 5). The oldest brittle tectonic stages with E-W to NW-SE oriented maximum compression produced mainly reverse, oblique reverse (parallel to the strike of the belt) and strike-slip faults. These meso-scale brittle structures were created under the transpressive to compressive tectonic regime. The distribution of differently dipping NE-SW reverse faults throughout the studied area well documents the NE-SW trending positive flower structure (Fig.4). These tectonic processes were accompanied by the relative counterclockwise rotation of the Central Western Carpathian block with respect to Europe, which generated a

Table 1. Palaeostress tensors from fault slip data. Explanations: Tensor name – name of the homogenous group of faults; n - number of fault-slip data used for stress tensor computation; σ_1, σ_2 and σ_3 - principal stress axes in format azimuth/dip (in degrees); R - stress ratio $(\sigma_2 - \sigma_3)/(\sigma_1 - \sigma_3)$; R` - tensor type (or stress regime) index as defined in Delvaux et al. (1997); α - mean slip deviation (angle between observed and computed slip directions, in degrees); Q (QRw) – World Stress Map project (WSM) quality ranking as defined in Sperner et al. (2003): A (best) to E (worst).

Tensor name	n	σ_1	σ_2	σ_3	R	R`	α	Q (QRw)	Stress regime according to Delvaux et al., 1997
D6	21	258/82	029/05	119/06	0.3	0.3	6.39	B	pure extensive
D5	12	066/09	176/66	332/22	0.4	1.6	9.67	C	pure strike-slip
D4	4	026/04	252/83	116/04	0.52	1.48	13.9	E	pure strike-slip
D3a	16	359/16	147/73	266/08	0.09	1.91	16.46	D	transpressive
D3b	6	185/21	277/06	022/68	0.67	2.67	6.03	D	pure compressive
D2a	50	317/05	062/69	226/21	0.09	1.91	14.63	C	transpressive
D2b	69	306/05	216/01	111/84	0.75	2.75	7.27	A	pure compressive
D1a	34	089/05	246/85	359/01	0.31	1.69	9.88	B	pure strike-slip
D1b	10	101/15	197/17	332/67	0.71	2.71	7.62	C	pure compressive

dextral transpression zone along the western sector of the PKB in the Late Oligocene – Early Miocene (Fodor 1995; Marko et al. 1995, 2005). The activity of a brittle dextral transpression zone resulted in the final morphostructural character of klippen with long axes oriented in the NE-SW direction. Subvertical strike-slips and SE-dipping reverse faults are located along SW-NE contacts of the PKB with the Biele Karpaty Unit. Most of contacts of the Czorsztyn, Kysuca and transitional units are also subvertical strike-slips and NW or SE-dipping reverse faults. Record of younger tectonic events is less clear. Rotation of the σ_1 axis of the regional palaeostress field to the N-S direction is ascribed to a rigid counterclockwise rotation of the entire ALCAPA block during the Early Miocene by some 80° with a stable orientation of the σ_1 axis (Kováč et al. 1994; Kováč and Túnyi 1995; Marko et al. 1995; Kováč and Hók 1996). The N-S compression (Early – Middle Miocene) caused mainly formation of the sinistral strike-slip faults roughly parallel to the strike of the belt and rarely E-W reverse faults under the sinistral transpression. The next two tectonic events (Middle to Late Miocene) are marked by forming mainly strike-slip faults and normal faults as a result of the transtensive tectonic regime with NNE-SSW to NE-SW trending compression. Active clockwise rotation of the main compressional stress from N-S to NE-SW and inversion from the older transpression to the younger sinistral transtension were a result of NE-ward translation of the entire ALCAPA block (Marko et al. 1995; Kováč and Hók 1996). Normal faults oriented in NE-SW direction were created by the NW-SE extension during the last deformational phase under the extensional tectonic regime (Pontian – Pliocene). Finally, the klippen style was affected also by slope movements and some independent blocky klippen are obviously loose blocks transported downslope by landslides.

6. Conclusions

The studied area was formed during multistage ductile-brittle and brittle tectonic evolution that occurred in several deformation stages producing variable fold and fault structures. Probably the oldest stage was thrusting of the presently most external Kysuca Unit over the Czorsztyn and transitional units. Then macroscopic folding due to orthogonal layer-parallel shortening affected especially the Chmeľová region with well-bedded transitional successions, while the thick competent Vršatec-Javorník slab was steepened and partly overturned to the SE. This significant primary compressional stage was followed by transpression and formation of the positive flower structure during the Early to Middle Miocene. Numerous reverse and strike-slip faults truncated the stiff limestones sandwiched between incompetent strata and produced klippen of two distinct morphostructural types: 1) the Vršatec type formed by vertical strata obliquely cut by faults into variously large, lozenge-shaped blocks arranged in one straight zone; 2) the Chmeľová type with a more random arrangement of variously shaped klippen, dependent on which parts of pre-existing macrofolds (cores, limbs) were separated into klippen that slightly moved with respect to each other afterwards. The next brittle deformation regimes – transtension to extension – during the Middle Miocene to Pliocene times are recorded mainly by sinistral strike-slip and normal faults.

Acknowledgement

This work was supported by the Slovak Research and Development Agency under the contracts No.

APVV-LPP-0225-06 and APVV-0465-06, and by Comenius University under the contract No. UK/267/2007 and No. UK/297/2008.

References

Angelier J., 1989. From orientation to magnitudes in palaeostress determinations using fault slip data. Journal of Structural Geology, 11, 1/2, 37–50.

Angelier J., 1994. Fault slip analysis and palaeostress reconstruction. In: Hancock P.L. (ed): Continental deformation. Pergamon Press, University of Bristol (U.K.), London, 53–100.

Aubrecht R. and Ožvoldová L., 1994. Middle Jurassic – Lower Cretaceous development of the Pruské Unit in the Western Part of the Pieniny Klippen Belt. Geologica Carpathica, 45, 4, 211–223.

Began A. and Borza K., 1963. Die neue Streženice-Serie in der inneren Klippenzone der Westkarpaten. Geologický Sborník – Geologica Carpathica, 14, 217–220 (in Slovak with German summary).

Birkenmajer K., 1977. Jurassic and Cretaceous lithostratigraphic units of the Pieniny Klippen Belt, Carpathians. Studia Geologica Polonica, 45, 158p.

Delvaux D.F., 1993. The TENSOR program for palaeostress reconstruction: example from the east African and the Baikal rift zones. Terra Nova, 5, suppl. No 1, Proceedings of EUG VII, Strasburg, 4-8 April, 216.

Delvaux D.F. and Sperner B., 2003. New aspects of tectonic stress inversion with reference to the TENSOR program. In: Nieuwland D.A. (ed): New Insights into Structural Interpretation and Modelling. Geological Society, London, Special Publications, 212, 75–100.

Fodor L., 1995. From transpression to transtension: Oligocene-Miocene structural evolution of the Vienna basin and the East Alpine-Western Carpathian junction. Tectonophysics, 242, 151–182.

Froitzheim N., Plašienka D. and Schuster R., 2008. Alpine tectonics of the Alps and Western Carpathians. In: Mc Cann T. (ed): The Geology of Central Europe, vol. 2: Mesozoic and Cenozoic. Published by the Geological Society, London, 1141–1232.

Kováč M., 2000: Geodynamic, palaeogeographical and structural evolution of the Carpathian-Pannonian region during the Miocene: new view on the Neogene basins of Slovakia. Veda Publ., Bratislava, 202p. (in Slovak)

Kováč P. and Hók J., 1996. Tertiary development of the western part of Klippen Belt. Slovak Geological Magazine, 2, 137–149.

Kováč M. and Túnyi I., 1995. Interpretation of the paleomagnetic data from the western part of the Central Western Carpathians. Mineralia Slovaca, 27, 213–220 (in Slovak with English summary).

Kováč M., Kráľ J., Márton E., Plašienka D. and Uher P., 1994. Alpine uplift history of the Central Western Carpathians: geochronological, paleomagnetic, sedimentary and structural data. Geologica Carpathica, 45, 2, 83–96.

Maheľ M., 1978. Manín tectonic unit: relations of the Klippen Belt and Central West Carpathians. Geol. Zbor. – Geol. Carpath., 29, 197–213.

Maheľ M., 1980. The Periklippen zone: Its nearer characterization and significance. Mineralia Slovaca, 12, 193–207 (in Slovak with English summary).

Marko F., Plašienka D. and Fodor L., 1995. Meso-Cenozoic tectonic stress fields within the Alpine-Carpathian transition zone: a review. Geologica Carpathica, 46, 19–27.

Marko F., Vojtko R., Plašienka D., Sliva Ľ., Jablonský J., Reichwalder P. and Starek D., 2005. A contribution to the tectonics of the Periklippen zone near Zázrivá (Western Carpathians). Slovak Geological Magazine, 11, 37–43.

Marschalko R., 1986. Evolution and geotectonic significance of the Klippen Belt Cretaceous flysch in the Carpathian megastructure. Veda Publ., Bratislava, 139p. (in Slovak with English summary)

Marschalko R. and Kysela J., 1980. Geology and sedimentology of the Klippen Belt and Manín Unit between Žilina and Považská Bystrica towns. Západné Karpaty, séria Geológia, 7–79 (in Slovak with English summary).

Mello J. (ed), Teťák M., Havrila M., Rakús M., Buček S., Filo A., Nagy A., Salaj J., Maglay J., Pristaš K. and Fordinál K., 2005. Geological map of the middle Váh Valley region (in the scale of 1 : 50 000). MŽP – ŠGÚDŠ, Bratislava.

Mišík M., Sýkora M., Ožvoldová L. and Aubrecht R., 1994. Horná Lysá (Vršatec) – a new variety of the Kysuca Succession in the Pieniny Klippen Belt. Mineralia Slovaca, 26, 1, 7–19.

Nemčok M. and Nemčok J., 1994. Late Cretaceous deformation of the Pieniny Klippen Belt, West Carpathians. Tectonophysics, 239, 81–109.

Plašienka D., 1995. Mesozoic evolution of Tatric units in the Malé Karpaty and Považský Inovec Mts.: Implications for the position of the Klape and related units in western Slovakia. Geologica Carpathica, 46, 101–112.

Plašienka D., 1998. Palaeotectonic evolution of the Central Western Carpathians during the Jurassic and Cretaceous. In: Rakús M. (ed), Geodynamic development of the Western Carpathians. Geological Survey of Slovak Republic, Bratislava, 107–130.

Plašienka D. and Jurewicz E., 2006. Tectonic evolution of the Pieniny Klippen Belt and its structural relationships to the External and Central Western Carpathians. Geolines, 20, 106–108.

Plašienka D., Sýkora M., Aubrecht R., Krobicki M. and Józsa Š., in press. New interpretation of the lithostratigraphy and tectonic position of the Michalova hora klippen near Dolná Mariková village (Middle Váh Valley, western Slovakia). Acta Geologica Slovaca.

Potfaj M., 1993. Position and role of the Biele Karpaty Unit in the Flysch Zone of the West Carpathians. Geologické Práce, Správy, 98, 55–78 (in Slovak with English summary).

Potfaj M., 1998. Geodynamics of the Klippen Belt and Flysch Belt of the Western Carpathians. In: Rakús M. (ed), Geodynamic development of the Western Carpathians. Geological Survey of Slovak Republic, Bratislava, 143–154.

Rakús M. and Hók., 2005. The Manín and Klape units: Lithostratigraphy, tectonic classification, paleogeographic position and relationships to Vahicum. Mineralia Slovaca, 37, 9–26 (in Slovak with English summary).

Ratschbacher L., Frisch W., Linzer H., Sperner B., Meschede M., Decker K., Nemčok M., Nemčok J. and Grygar R., 1993. The Pieniny Klippen Belt in the Western Carpathians of northeastern Slovakia: structural evidence for transpression. Tectonophysics, 226, 471–483.

Salaj J., 1990. Geological structure of the Klippen and Periklippen zones in the Middle Váh river valley and lithological classification of Cretaceous sediments from the newly defined sequences. Mineralia Slovaca, 22, 155–174 (in Slovak with English summary).

Schlögl J., Aubrecht R. and Tomašových A., 2000: The first find of the Orava Unit in the Púchov section of the Pieniny Klippen Belt (Western Slovakia). Mineralia Slovaca, 32, 1, 45–54.

Schlögl J., Tomašových A. and Aubrecht R., 2006. Stop B3.5 – Vršatec Klippen – Czorsztyn Succession (Bajocian – Berriasian); Middle Jurassic biohermal limestones; palaeomagnetic interpretations. In: Wierzbowski A. et al. (eds), Jurassic of Poland and adjacent Slovakian Carpathians, Field trip guidebook of 7th International Congress on the Jurassic System, 6-18 September 2006 Krakow, 89–92.

Schlögl J., Plašienka D., Aubrecht R., Michalík J. and Potfaj M., 2008. Composition, structure and evolution of the Pieniny Klippen Belt and adjacent zones in western Slovakia. In: Németh Z. and Plašienka D. (eds), SlovTec 2008 – Proceedings and Excursion Guide, ŠGÚDŠ, Bratislava, 204.

Spišiak J., Bučová J., Plašienka D. and Mikuš T., 2008. Cretaceous alkali volcanites in the Chmeľová region (Vršatec klippen area, Pieniny Klippen Belt, Western Carpathians). In: Németh Z. and Plašienka D. (eds), SlovTec 2008 – Proceedings and Excursion Guide, ŠGÚDŠ, Bratislava, 124–125.

Wallbrecher E., 1986. Tektonische und gefügeanalytische Arbeitsweisen. Enke Verlag, Stuttgart, 244p.

Scientific Annals, School of Geology, Aristotle University of Thessaloniki Proceedings of the XIX CBGA Congress, Thessaloniki, Greece	Special volume 100	209-219	Thessaloniki 2010

LATEST JURASSIC – EARLIEST CRETACEOUS MASS MOVEMENTS IN THE POLISH PART OF THE PIENINY KLIPPEN BELT AND SILESIAN UNIT (OUTER FLYSCH CARPATHIANS)

Krobicki M., Golonka J. and Słomka T.

Faculty of Geology, Geophysics and Environmental Protection, AGH University of Science and Technology, Al. Mickiewicza 30, 30-059, Kraków, Poland, krobicki@geol.agh.edu.pl, jan_golonka@yahoo.com

Abstract: Distribution of sedimentary breccias, mass flows; redeposited clasts, which indicate time and mechanisms of origin of tectonic movements within sedimentary basins, are the main objects of the presented paper. These types of tectonic activity in Polish part of the Carpathians is well documented both in the Outer (Flysch) Carpathians and in the Pieniny Klippen Belt. Neo-Cimmerian tectonic events took place both in the Alpine Tethys and Proto-Silesian Basin. A big geotectonic reorganization, known as the Walentowa Phase, took place in AT during the latest Jurassic-earliest Cretaceous (Neo-Cimmerian) movements resulting in extensive gravitational faulting. Several tectonic horsts and grabens, documented by facies diversification, were formed. These rejuvenated some older structures and Middle/Late Jurassic (Meso-Cimmerian) faults which caused uplift of the shallow intrabasinal Czorsztyn pelagic swell. The over-regional significance of this geodynamic episode in the northernmost margin of the Tethyan Ocean is documented also by foundation of the Proto-Silesian Basin. Chaotic type of sedimentation dominated during Late Jurassic times indicating early stages of the Proto-Silesian Basin opening with increased tectonic activity. The detritic material was supplied from two sources: from the Baška-Inwałd uplift separating the Proto-Silesian Basin and the Bachowice Basin located within the North European Platform, and from the island arcs within the Silesian Ridge separating the Proto-Silesian Basin and the Alpine Tethys. The biogenic material originated within shallow-water reefal and carbonate platform zones was transported by turbiditic currents from the uplifted structures on the Proto-Silesian Basin margins into the deeper zones of this basin. Both the calciturbidites and calcifluxoturbidites formed, constituting the main lithosome within the younger lithostratigraphic unit – the Cieszyn Limestone Formation. These deposits represent the oldest turbiditic currents sedimentation known from the Polish Outer Carpathian Basin.

Keywords: Carpathians, Mesozoic, Cenozoic, palaeogeography, plate tectonics

1. Introduction

Synsedimentary mass movement deposits are a key to understanding tectonic activity of the basins during their geotectonic history. Distribution of sedimentary breccias, mass flows; redeposited clasts are the main objects, which indicate time and mechanisms of origin of tectonic movements within sedimentary basins. Pulses of such activity are connected with wide-oceanic remobilization and are well known in several parts of the whole Alpine Europe. A lot of places of this region are full of very well recorded evidence of synsedimentary movements which originated during Jurassic – Early Cretaceous times. Other sedimentary features like neptunian dykes, omission surfaces, condensation beds, redeposited shelly fauna, clastic sediments input to pelagic deposits as submarine wedges, olistostromes/oli-stoliths etc. also support such events. Such effects are strictly connected with activation and mobility of basin bottoms, especially during strong Alpine phases of tectonic revolutions, mainly of Middle – Late Jurassic/earliest Cretaceous (Meso- and Neo-Cimmerian) movements. Our knowledge on these types of tectonic activity in Polish part of the Carpathians is well documented both in the Outer (Flysch) Carpathians and in the Pieniny Klippen Belt (PKB). The main aim of this paper is presenting of Neo-Cimmerian tectonic movements during the latest Jurassic – earliest Cretaceous episode of evolution of neighboured Carpathian basins.

2. Polish Carpathians *versus* Jurassic Alpine Tethys

The Alpine Tethys (AT), which constitutes important palaeogeographic elements of the future PKB and Outer Carpathians (Figs. 1-3), developed as an oceanic basin, a continuation of the Central Atlantic, during Jurassic as a result of Pangea break-up (Fig. 4). The Mesozoic rifting events caused the origin of oceanic type basins along the northern margin of the Tethys. The Inner Carpathian plate was detached from the Eurasian margin by this AT as part of the separation of Eurasia from Gondwana. It was also dissected by the rift system. The deeper water sediments, like radiolarites, were deposit in these rifts, while shallower water carbonate sedimentation prevailed in the uplifted areas. The central Atlantic and AT went into a drifting stage during the Middle Jurassic times. The oldest oceanic crust in the Ligurian–Piedmont Ocean was dated as late as the Middle Jurassic in the southern Apennines and in the Western Alps. Bill et al. (2001) dated the onset of oceanic spreading of the AT by isotopic methods as Bajocian. The spreading phase follows the rifting during Early Jurassic times. The Jurassic rifting and spreading placed Triassic platform carbonate facies on the basin passive margins. Two major Late Jurassic basin, AT and Proto-Silesian Basin, were later included into the Carpathian thrust- and fold-belt. These basins were separated by Silesian Ridge. The NE part of AT was divided by the Czorsztyn Ridge into Pieniny Basin and Magura Basin, part of the Outer Carpathian Basins (Figs. 5, 6). Major plate reorganization then happened during the Tithonian time. The Central Atlantic began to expand into the area between Iberia and the New Foundland shelf. The Ligurian-Penninic Ocean reached its maximum width and the oceanic spreading stopped (Fig. 5). The Tethyan plate reorganization followed the global pattern. This reorganization was expressed by latest Jurassic/earliest Cretaceous tectonic movements, which affected both AT and Proto-Silesian Basin (Golonka et al., 2003).

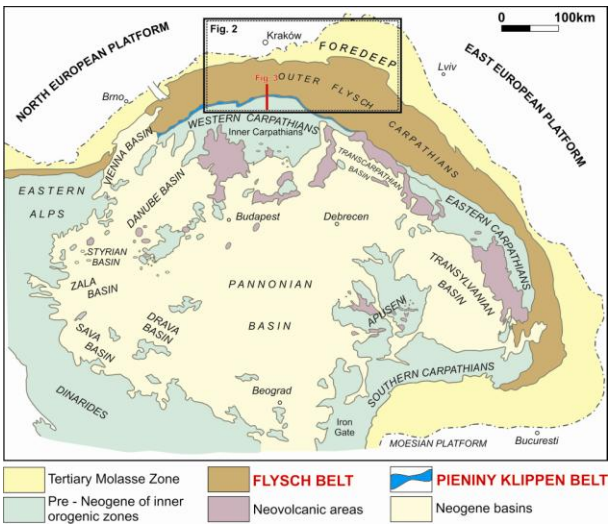

Fig. 1. Tectonic sketch map of the Alpine-Carpathian-Pannonian-Dinaride basin system (modified after Kováč 1998).

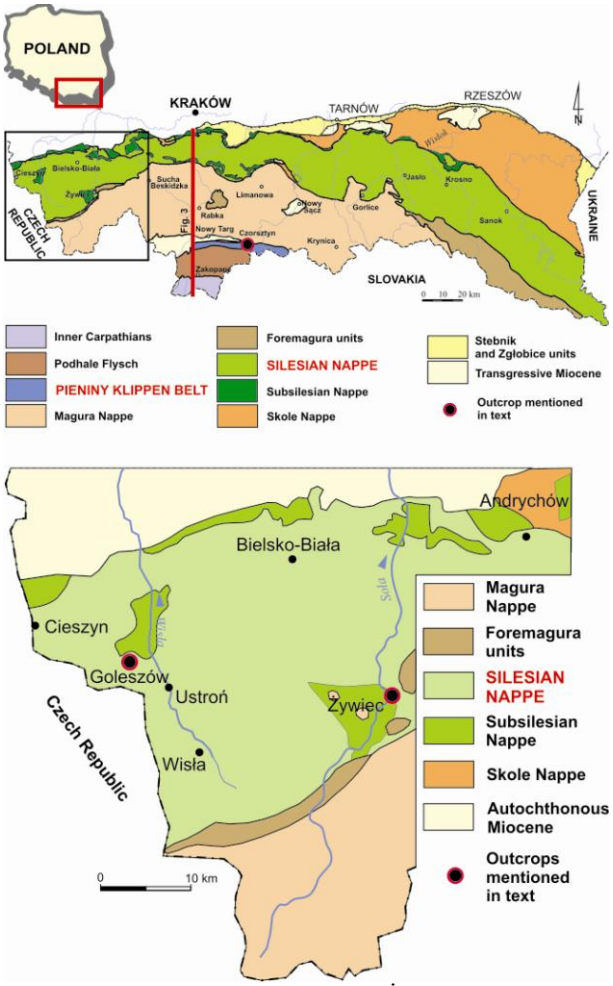

Fig. 2. Geological sketch between Żywiec and Cieszyn towns with location of described outcrops according to geological map of the Outer Flysch Carpathians (after Żytko et al., 1989; simplified).

3. Geological setting and general palaeogeographic sketch

3.1. Pieniny Klippen Belt

The term Pieniny Klippen Belt was first used by Neumayr (1971). The geographic part of this name indicates the mountain range in Poland and Slovakia where numerous klippes build scenic rocks around Dunajec River Gorge, prime geotouristic attraction since 19th century (Krobicki and Golon-

ka, 2008). The "Klippen" are relatively erosion-resistant blocks surrounded by and rising above the less competent rocks, mainly flysch, shales and marls.

and shear zones (Fig. 3), along which a strong reduction of space of the original sedimentary basins took place (Birkenmajer, 1986; Golonka and Krobicki, 2006; Krobicki and Golonka, 2006; 2008).

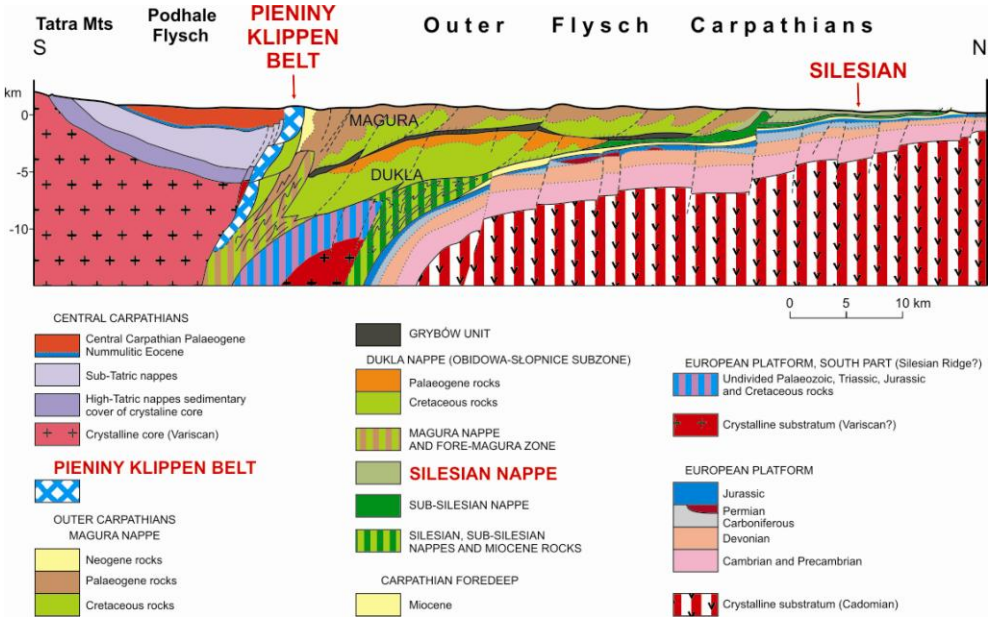

Fig. 3. Generalized cross-section across Polish Carpathians (after Golonka et al., 2006).

The PKB forms a strongly tectonized feature some 600 km long, 1-20 km wide, stretching from Wienerwald in Austria to northern Romania and marking the boundary between the Outer Flysch Carpathians and Inner (Central) Carpathians (Figs. 1, 2). In the modern literature (e.g. Krobicki and Golonka 2008 and references therein) the present day confines of the PKB are regarded as strictly tectonic and characterized as sub-vertical faults

The PKB tectonic components of different age, strike-slip, thrust as well as toe-thrusts and olistostromes were mixed together, giving the present-day mélange character of the PKB, where individual tectonic units are hard to distinguish. Together with the Outer Carpathians the PKB form the northernmost part of the Polish Carpathians.

In palinspastic reconstructions, the Czorsztyn Ridge has the SW-NE orientation which is inter-

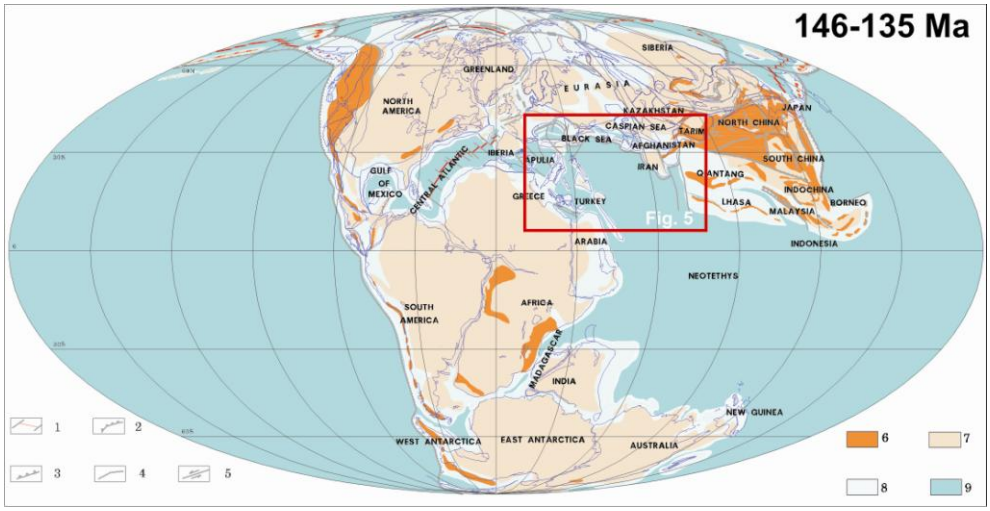

Fig. 4. Global plate tectonic map of latest Jurassic – earliest Cretaceous. Explanations: 1 – oceanic spreading center and transform faults; 2 – subduction zone; 3 – thrust fault; 4 – normal fault; 5 – transform fault; 6 – mountains; 7 – landmass; 8 – shallow sea and slope; 9 – deep ocean basin (from Golonka 2000; modified).

preted by means of palaeomagnetic data, relationship of sedimentary sequences and paleoclimate (see discussion in Golonka and Krobicki, 2001; Lewandowski et al., 2005; Grabowski et al., 2008). The AT basins divided by the Czorsztyn Ridge were dominated by a pelagic type of sedimentation. The deepest parts of AT are well documented by deep water Jurassic – Early Cretaceous radiolarites and *Maiolica*-type cherty limestones (Golonka and Sikora, 1981; Birkenmajer, 1986; Golonka and Krobicki, 2004; Jurewicz, 2005). The shallowest zone is represented by the so-called Czorsztyn Succession which primarily occupied the SE slope of the Czorsztyn Ridge (Birkenmajer, 1986; Golonka and Krobicki, 2004; Krobicki and Golonka, 2006) (Figs. 6-8).

The oldest Jurassic rocks known in the Polish part of the PKB are Pliensbachian to lowermost Bajocian dark marls and spotty limestones, or *Bositra* ("*Posidonia*")-bearing black shales with spherosiderites of widespread Tethyan oxygen-poor *Fleckenmergel* facies (Birkenmajer 1986). Rapid change of sedimentatary conditions took place during the late Early Bajocian, when the Czorsztyn Ridge uplifted, and therefore its SE slope was a good place for sedimentation of well-oxygenated crinoidal limestones. The origin of the mid-oceanic Czorsztyn Ridge was connected with this Bajocian postrift geotectonic reorganization (Golonka et al., 2003; Krobicki, 2006) an

d is coeval with the spreading phase of AT (see also Lewandowski et al., 2005). According to Krobicki and Wierzbowski (2004, 2009), there is no indication of continuous sedimentation between black shales and crinoidal limestones. The hiatus and rapid change of sediments character indicate rapid vertical tectonic movement related to the ridge origin due to Bajocian movements. Plašienka (2002) postulated the thermal uplift above the distal, subcrustal part of detachment fault. During Jurassic – Early Cretaceous times, the Czorsztyn Ridge was submerged and did not supply clastic material into AT basins more. Sedimentation of younger (latest Bajocian – Tithonian) red nodular *Ammonitico Rosso*-type limestones with abundant *Globuligerina* and *Saccocoma* continued on the Czorsztyn Ridge was an effect of vertical movements which subsided the ridge and produced tectonically differentiated blocks, neptunian dykes and scarp-breccias (see Golonka et al., 2003; Krobicki and Golonka 2006 and references therein). Boom of planktonic *Globuligerina* foraminifers in the ridge facies (Oxfordian) was simultaneous with the maximum development of radiolarians within the basinal zones (Birkenmajer 1977, 1986; Mišík 1999; Wierzbowski et al. 1999). This episode marked the beginning of a great facial differentiation between the deepest and shallowest succes-

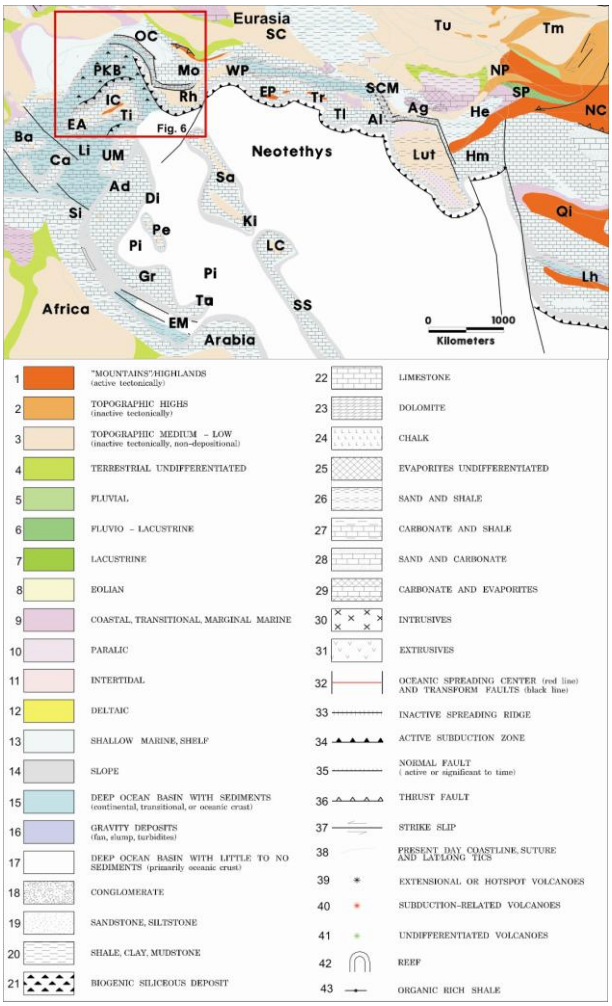

Fig. 5. Plate tectonic, paleoenvironment and lithofacies map of the western Tethys, Central Atlantic and adjacent areas during the latest Jurassic – earliest Cretaceous time (after Golonka 2004; slightly modified). Abbreviations of oceans and plates names: Ad – Adria (Apulia); Ag – Aghdarband (southern Kopet Dagh); Al – Alborz; Ba – Balearic; Ca – Calabria-Campania; Di – Dinarides; EA –Eastern Alps; EM – Eastern Mediterranean; EP – Eastern Pontides; Gr – Greece; He – Heart; Hm – Helmand; IC – Inner Carpathians; Ki – Kirsehir; LC – Lesser Caucasus; Lh – Lhasa; Li – Ligurian (Piemont) Ocean; Mo – Moesia; NC – North China; NP – North Pamir; **OC – Outer Carpathians**; **PKB – Pieniny Klippen Basin**; Pe – Pelagonian plate; Pi – Pindos Ocean; Qi – Qiangtang; Rh – Rhodopes; Sa – Sakarya; SC – Scythian; SCM – South Caspian microcontinent; Sl – Sicily; SP – South Pamir; SS – Sanandaj-Sirjan; Ta – Taurus terrane; Ti – Tisa; Tl – Talysh; Tm – Tarim; Tr – Transcaucasus; Tu – Turan; UM – Umbria-Marche; WP – Western Pontides.

sions. Similar compositions of facies are well known in several European Alpine regions (e.g. Betic Cordillera, Southern Alps, Apennine, Karavanke and Ionian Zone). During latest Jurassic – earliest Cretaceous times (Tithonian – Berriasian) cherty limestones of *Maiolica*-type (=*Biancone*) facies were deposited within deeper environments (Wieczorek 1988). The Late Cretaceous history of AT basin is characterized by deposition of multicoloured green/variegated/red marls marking unification of sedimentary regimes within ridge and slope successions and by formation of syn-orogenic flysch deposits in the basinal parts. Then, the Czorsztyn Ridge collided with the Inner Carpathian terranes around the Cretaceous/Palaeogene boundary (Birkenmajer, 1986).

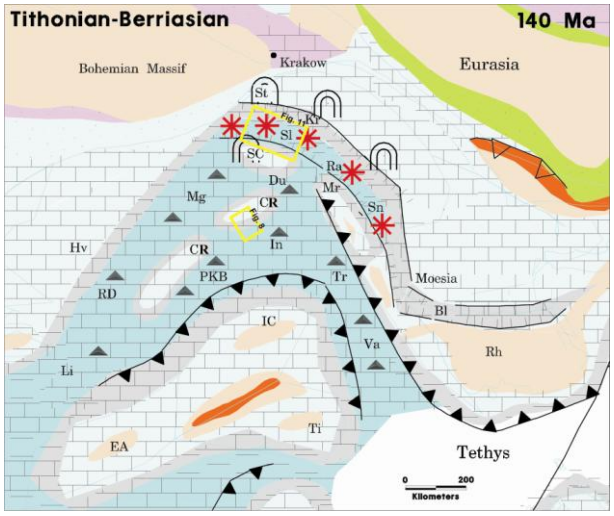

Fig. 6. Paleoenvironment and lithofacies of the circum-Carpathian area during the latest Jurassic – earliest Cretaceous; plates position at 140 Ma (modified from Golonka et al. 2006) with occurrence of rift-related magmatism (red stars). Abbreviations, Bl – Balkan rift; **CR – Czorsztyn Ridge**; Du – Dukla Basin; EA – Eastern Alps; Hv – Helvetic shelf; IC – Inner Carpathians; In – Inačovce-Kričevo zone; Kr – Kruhel Klippe; Li – Ligurian Ocean; Mg – Magura Basin; Mr – Marmarosh Massif; **PKB – Pieniny Klippen Basin**; Ra – Rakhiv Basin; RD – Rheno Danubian Basin; Rh – Rhodopes; SC – Silesian Ridge (Cordillera); **Sl – Silesian Basin**; Sn – Sinaia Basin; St – Štramberk Klippe; Ti – Tisa plate; Tr – Transylvanian Ocean; Va – Vardar Ocean. Explanations of colours and symbols – see Fig. 5a.

3.2. Silesian Unit (Outer Flysch Carpathians)

The Outer (Flysch) Carpathians are composed of Jurassic to Early Miocene flysch sequences. During the Alpine orogenic processes in Miocene times, the north-verging nappes were detached from their original basement (Ślączka et al., 2006).

The Proto-Silesian (Severin-Moldavidic) Basin originated during Late Jurassic times together with syn- and post-rift deposits (Figs. 6, 11). Part of this basin was included into the Silesian Unit, one of the Outer Carpathian nappes. The Silesian Ridge (Fig. 6 – SC) was an uplifted area, originally as a part of the North European platform separating during Jurassic – Early Cretaceous times AT and the Proto-Silesian Basin (Fig. 6). Now it is known only from exotics and olistoliths occurring within the various allochthonous units of the Outer Carpathians. The shallow-water marine sedimentation prevailed on the Silesian Ridge during the Late Jurassic and earliest Cretaceous. The carbonate material was transported from the ridge toward the Proto-Silesian Basin. This basin developed within the North European Platform as a rift and/or back-arc basin. Its basement is represented by the attenuated crust of the North European plate with perhaps incipient oceanic fragments. The sedimentary cover is represented by several sequences of the Late Jurassic – Early Miocene age belonging recently to various tectonic units in Poland and Czech Republic. The Baška-Inwałd Ridge has been located on the opposite side of the Proto-Silesian Basin and its slope contains mainly carbonate deposits and originated as shoulder uplift separating the Bachowice Basin from the Proto-Silesian Basin. The Vendryně Formation (Kimmeridgian – Tithonian/Early Berriasian) represents the oldest deposits of the Silesian Unit (Nappe) (Figs. 2, 9, 10) (lithostratigraphy after Golonka et al., 2008). This formation is built of dark-grey marly shales with rare intercalations of redeposited detrital limestones (Fig. 10) containing fossils of shallow-marine fauna, mainly echinoderms and molluscs. Deposits forming huge sliding slices with numerous deformation structures indicating chaotic type of sedimentation occur within the profile. The rocks of the Vendryně Formation are exposed both in the classic type locality in Vendryně on the Czech side of the Silesian Unit and on the Polish territory (for example – in the abandoned quarry in Goleszów) (Figs. 2, 10). They are covered by the Cieszyn (Těšín) Limestone Formation (Late Tithonian – Middle Valanginian) which are represented by (organo)detrital and pelitic limestones intercalated by grey/black shales. Limestones are usually thin-bedded with typical features of turbiditic deposits: sharp erosive base of beds, gradational fractionation, ripplemark-convolute cross-lamination in the top parts of beds, sometimes with numerous trace fossils on the soles of beds, flutcasts, delicate

ripplemarks in fine-grained type of limestones, resedimented shales and carbonate clasts (often with fractionation) etc., and additionally with rare cherts (comp. Waśkowska-Oliwa et al., 2008). The younger, Middle Valanginian–Barremian Hradište Formation is represented mainly by grey/black shales with intercalations of very thin- to medium-bedded calcareous sandstones (lower part–Cisownica Shale Member; formerly Upper Cieszyn Beds) and thick-bedded sandstones and conglomerates (upper part of formation – Piechówka Sandstone Member; formerly Grodziszcze Sandstones). Also some rocks, formerly known as Wierzowskie Beds are now included into the Hradište Formation. The Hradište Formation is covered by the Veřovice Formation (Aptian) represented by dark and black shales and mudstones rich in organic matter. Younger is the Lhoty Formation (Albian) representing synorogenic flysch-type deposits.

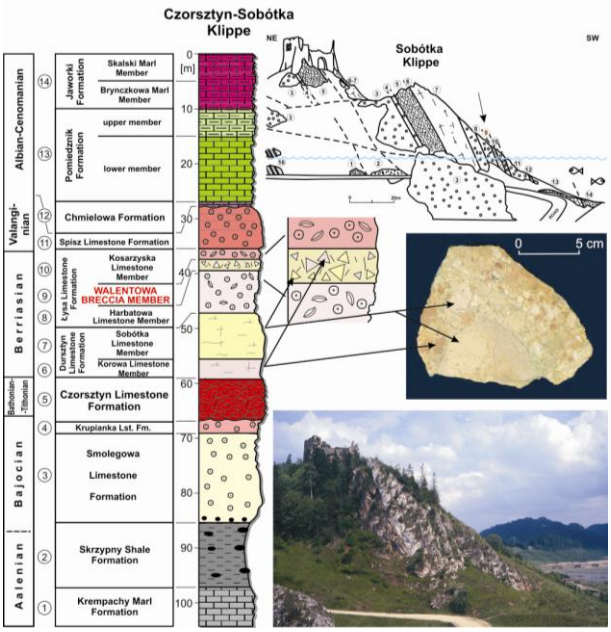

Fig. 7. Stratigraphical section of the Czorsztyn-Sobótka Klippe (PKB) with indication of position of the Walentowa Breccia Member of the Łysa Limestone Formation of the Czorsztyn Succession (lithostratigraphy after Birkenmajer, 1977, slightly modiefied) (photo – state in 1992). Explanations of lithology: 1 – dark-grey/black marls/marly limestones; 2 – black spherosideritic shales; 3 – white cridoidal limestones (with phosphatic concretions in base – black dots); 4 – red/pink crinoidal limestones; 5 – red nodular limestones; 6 – pink micritic *Calpionella*-bearing limestones; 7 – creamy micritic *Calpionella*-bearing limestones; 8 – creamy brachiopodic-crinoidal limestones; 9 – limestone sedimentary breccia; 10 – pink-creamy brachiopodic-crinoidal limestones; 11 – cherry crinoidal limestones; 12 – violet-red marls; 13 – green marls, sometimes with cherts; 14 – green and variegated *Globotruncana*-bearing marls.

4. Synsedimentary breccia and debris flow deposits

4.1. Pieniny Klippen Belt

In the PKB the best example of synsedimentary breccia occurs within widely distributed, exclusively carbonate sedimentation of the Berriasian Łysa Limestone Formation which is tripartite and consists of the Harbatowa Limestone Member, Walentowa Breccia Member and Kosarzyska Limestone Member (Birkenmajer, 1977). The first and third members are represented by crinoid-brachiopod sparitic and micritic limestones. However, the most typical product of synsedimentary tectonic activity is the middle member (*Calpionellopsis* Zone of the Berriasian – Wierzbowski and Remane 1992) composed of pelagic limestones containing pinkish and creamy fragments of underlying beds (so-called *Calpionella* limestones – both Korowa and Sobótka Limestone members of the Dursztyn Limestone Formation), interpreted as synsedimentary scarp breccia (Birkenmajer, 1958; 1975; 1986). Sedimentation of this breccia coincides very well with the moment, when the shallowing effect was strongest, as a change of brachiopod assemblages indicates (Krobicki 1994, 1996; Golonka and Krobicki, 2001). After the Neo-Cimmerian uplift of the Czorsztyn Ridge, the sedimentation depth of the Czorsztyn Succession zone can be estimated between 400-500 m (Cecca 1992), on the basis of palaeoecological considerations of the Lower Berriasian Rogoźnik coquina (partly facies equivalent of the Sobótka Limestone Member). Consequently, the shallowing-upward effect of this vertical movement reached about 100-200 meters. In the Inner Carpathians, both sedimentological and age equivalent of the Walentowa Breccia Member occur – the so-called Nozdrovice Breccia, which is, contrary to our opinion, considered by Slovakian geologists (Reháková and Michalík, 1992; Michalík et al., 1995; 1996; see also Staniszewska and Ciborowski, 2000) as an eustatic-controlled resedimentation event that produced synsedimentary breccias along submarine scarps (Michalík and Reháková, 1995). On the other hand, Plašienka (1999, 2002, 2003) interpreted these resedimentation events as an important rifting phase – the Walentowa Phase – which affected tectonic evolution of the Western Carpathians during the earliest Cretaceous.

4.2. Silesian Unit

The western part of the Polish Carpathians region, between towns of Cieszyn and Żywiec, is the best

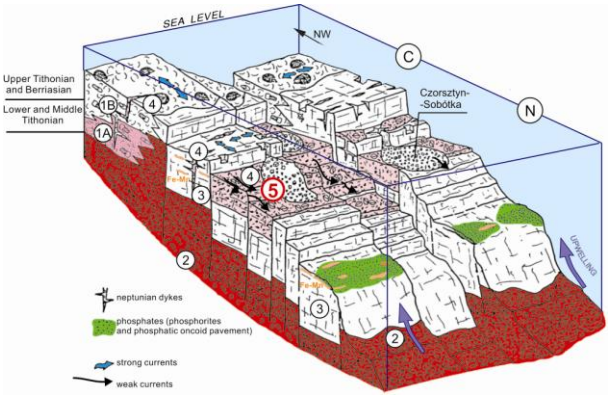

Fig. 8. Model of sedimentation on the intraoceanic Czorsztyn pelagic swell in Berriasian times with effects of pronounced Neo-Cimmerian tectonic movements (after Krobicki 1996; modified). Abbreviations: 1 – Rogoźnik Coquina Member (A – sparitic coquina; B – micritic coquina); 2 – Czorsztyn Limestone Formation (Ammonitico Rosso facies); 3 – Sobótka Limestone Member (Dursztyn Limestone Formation); 4 – Harbatowa Limestone Member (Łysa Limestone Formation); **5 – Walentowa Breccia Member** (Łysa Limestone Formation); successions: C – Czorsztyn; N – Niedzica.

for study of the uppermost Jurassic and lowermost Cretaceous debris flow deposits of the Silesian Unit (Fig. 2). According to the newest lithostratigraphical scheme of the western part of the Outer Carpathians (Golonka et al. 2008) they belong to Vendryně Formation, Cieszyn Limestone Formation and Hradište Formation (Cisownica Shale Member) (Figs. 9, 10) (see above) and cropping out in the Goleszów abandoned quarry (Fig. 10 lower part of photo) and in the Żywiec profile along the bank of the Soła River (Fig. 10 upper part). The thickness of debris flow deposits ranges from 2.5 to 30 meters. The share of the clastic framework does not exceed 30%. These sediments can be correlated with the facies A1.3 of Pickering et al. (1986) and facies GyM of Ghibaudo (1992). They include numerous fragments and pebbles of detrital and pelitic limestones of the Cieszyn Limestone Formation, organodetrital limestones, marly shales, Carboniferous and metamorphic rocks – granitic gneisses, gneisses and crystalline schists. Pebbles are randomly arranged in a mass of structureless, hard, marly silt. Generally, both the clays and embedded lumps of limestone have bends and folds closing towards the north suggesting that the sliding mass moved from the south.

Goleszów (Figs. 2, 10)

In this abandoned quarry, the oldest Outer Carpathian pre-flysch type deposits crop out, which are well visible in the eastern wall of the quarry. These rocks, discovered by Peszat (1968, 1971), belong to the Vendryně Formation, and are represented by dark grey and black marly shales and massive marls with thin, single beds of pelitic, sandy and detritic limestones. All these type of rocks composed huge slumping structures (Słomka 1986a) with well visible deformation structures originated during submarine mass movements (olistostromes, debris flows, gravelstones etc), which dynamically developed on a steep slope presumable during seismic activity in the Proto-Silesian Basin (Słomka, 1986b). Three levels of synsedimentary deformation occur in this quarry. The lowest is 2-4 m in thickness and consists of strongly folded dark marls. The second one has variable thickness (from several to dozen meters) and is characterized by occurrence of dark marls with blocks of detritic limestones and isolated fragments of massive marls, marly shales and thin-bedded flyschoidal rocks. The biggest blocks reach up to 6 m in dimension. *The topmost level (3-5 meters in thick*ness) is represented by dark grey and black shales with irregular blocks of detritic limestones (Fig. 10). Foraminiferal assemblages from the matrix indicate uppermost Jurassic age, but foraminifers and calcareous dinocysts in thin sections suggest Early Tithonian age (Olszewska 2005). However, the oldest part of these units has been earlier determined even as Late Kimmeridgian (Malik, 1994). All sedimentological features indicate a very rapid sedimentation of different kinds of submarine mass movements during large-scale catastrophic (*sensu* Malik 1994) resedimentation events, as it was earlier suggested by several authors (comp. Nowak, 1964; 1973; Peszat, 1968; 1971; Słomka, 1986b).

Żywiec – Soła River valley (Figs. 2, 10)

Geological position of investigated outcrops along

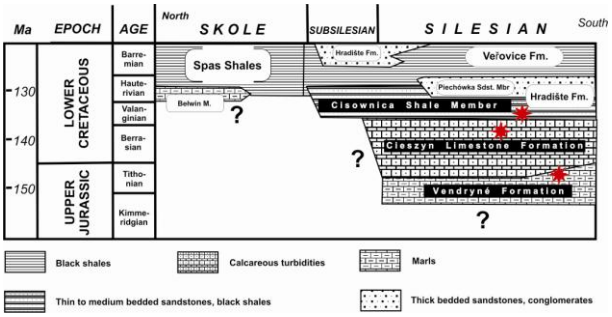

Fig. 9. Stratigraphical position of the Jurassic/Cretaceous boundary units of the Polish Outer Flysch Carpathians (after Słomka 1986, modified; lithostratigraphy – see Golonka et al. 2008) with position of debris flows (red stars).

the Soła River in Żywiec is very complicated by tectonic folding structures and was studied by several authors (Malik, 1994; Słomka, 2001; Golonka et al., 2006 with literature cited therein). More southern part of the long outcrop is built by mass movement deposits (up to 30 m thick) represented by dark grey/black marly shale matrix with abundant exotic rocks, both magmatic/metamorphic and sedimentary ones (Carboniferous coals including); typical exotic-bearing gravelstone of the Cisownica Shale Member of the Hradište Formation (Valanginian in age). Some characteristic exotics are of uppermost Jurassic/lowermost Cretaceous deposits originated a little bit earlier in the Proto-Silesian Basin or surrounding regions. Sedimentological analysis suggests rapid sedimentation of these mass movement deposits with full transitional spectra from olistostromes to debris flows (Tokarski, 1947; Słomka, 1986b; Golonka et

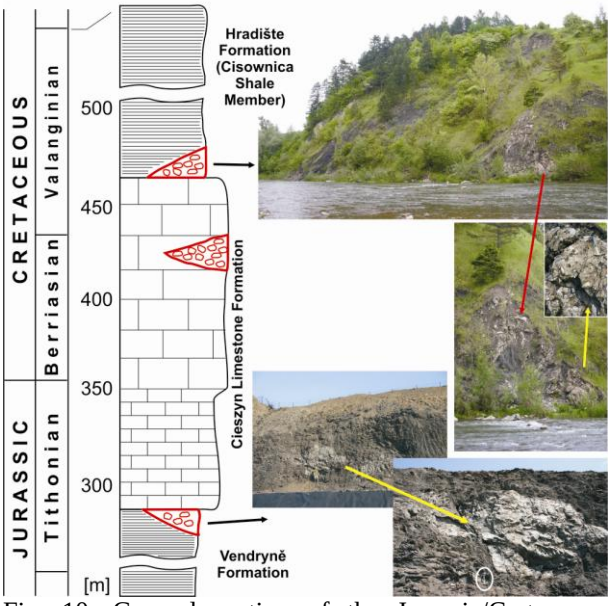

Fig. 10. General section of the Jurassic/Cretaceous boundary units of the Outer Carpathians in vicinity of Żywiec (after Słomka 1986a; changed and modified) with position of debris flows and location of outcrops described in the text – Goleszów (lower photo), Soła River (upper photo); lithostratigraphy after Golonka et al. 2008.

al., 2006) (megaturbidites – *sensu* Malik, 1994).

Such type of redeposited material in olistostromes/debris flows indicates the building of the Silesian Ridge during the initial stage of the active cordillera development, at least since Tithonian – Berriasian times. The tectonic activity caused uplift of the Silesian Ridge, its slope and continental rise of the Proto-Silesian Basin. The deposits of the Cieszyn Limestone Formation were eroded again and redeposited as debris flows. Much greater participation of the coarse-grained facies of the upper part of the Cieszyn Limestone Formation and the appearance of mass-movement debris-flow deposits containing fragments of older rocks and exotics (both metamorphic and Palaeozoic sedimentary rocks) suggest a higher rate of uplift during the latest Jurassic – earliest Cretaceous (Neo-Cimmerian) activity and "cannibalism" of the Proto-Silesian Basin (comp. Matyszkiewicz and Słomka 1994; Waśkowska-Oliwa et al., 2008). Tectonic movements of the Silesian Ridge (and probable also the opposite – Baška-Inwałd Ridge) were presumably connected with development of initial rifting in the Proto-Silesian Basin, as documented by the presence of teschenitic magmatism (Grabowski et al.,

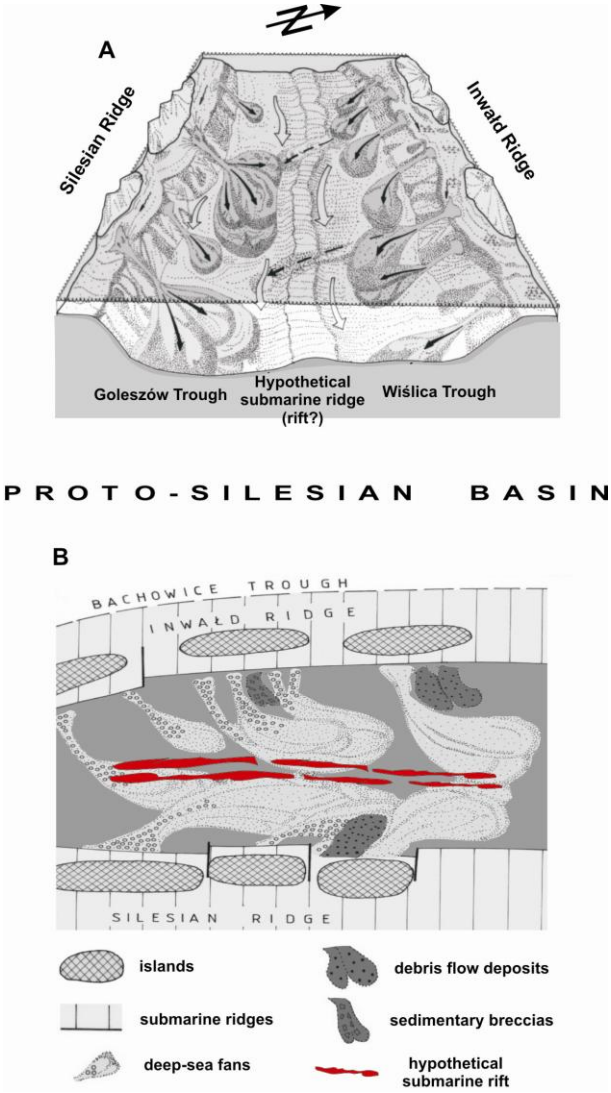

Fig. 11. Palaeogeographical blockdiagram of sedimentation of the oldest flysch deposits in the Proto-Silesian Basin (Jurassic/Cretaceous transition – Tithonian/Berriasian) (A) and its hypothetical palaeogeographical sketch (B) (after Słomka 1986a; slightly modified).

2003; Waśkowska-Oliwa et al., 2008 with references therein) (Fig. 11). Such submarine magmatic processes took place mainly during Early Cretaceous times, but first episodes of magmatic activity could began even during Early Tithonian (148.6 ±1.8 Ma) (op. cit.) during the first step of opening of the Proto-Silesian Basin (Ślączka and Słomka 2001; Golonka et al., 2006).

In the more northern part of this outcrop, typical deposits of the Vendryně Formation occur, with numerous synsedimentarily deformed hard clasts of marls, which were interpreted as resedimentation effect, quite similar to the same-age deposits from the Goleszów quarry (Malik, 1994).

5. Conclusions

Latest Jurassic – earliest Cretaceous tectonic events took place both in the Pieniny Klippen Basin (AT) and Proto-Silesian Basin documenting over-regional significance of this geodynamic episode in the northernmost margin of the Tethyan Ocean. An important geotectonic reorganization, known as the Walentowa Phase, took place in these two regions during the Neo-Cimmerian times, resulting in extensive gravitational faulting. Several tectonic horsts and grabens were formed, rejuvenating some older faults which raised shallow intrabasinal Czorsztyn pelagic swell again and are documented by facies diversification. Additionally, these movements divided the basin into different zones with their own water circulation patterns, probably of an upwelling type. Volcanic activity (both intra-plate alkaline volcanism in the Ukrainian part of the Pieniny Klippen Belt – Krobicki et al. 2005, 2008, and the Proto-Silesian rift-related magmatism) (Fig. 11) and change of oceanographical regimes (upwelling currents) also most probably reflect this geotectonic phenomenon.

Chaotic type of sedimentation dominated during Late Jurassic times indicating early stages of the Proto-Silesian Basin opening with increased tectonic activity. The detrital material was supplied from two sources: from the Baška-Inwałd uplift separating Proto-Silesian Basin and the Bachowice Basin located within the North European Platform, and from the island arcs within the Silesian Ridge separating Proto-Silesian Basin and AT. The biogenic material originated within shallow-water reefal and carbonate platform zones and was transported by turbiditic currents from the uplifted structures on the Proto-Silesian Basin margins into deeper zones of this basin. Both the calciturbidites and calcifluxoturbidites formed, constituting the main lithosome within the younger lithostratigraphic unit – the Cieszyn Limestone Formation. These deposits represent the oldest turbiditic sedimentation known from the Polish Outer Carpathian Basin.

Acknowledgements

We are grateful to Dušan Plašienka (Bratislava) and Vassilis Karakitsios (Athens) for valuable comments and corrections improving the final version of this paper. This research has been financially supported by AGH University of Science and Technology in Krakow, Poland (grant no. 11.11.140.447).

References

Bill M., O'Dogherty L., Guex J., Baumgartner P.O. and Masson, H., 2001. Radiolarite ages in Alpine-Mediterranean ophiolites, Constraints on the oceanic spreading and the Tethys-Atlantic connection. Geologicla Society of America Bulletin, 113, 129-143.

Birkenmajer K., 1958. Submarine erosional breaks and Late Jurassic synorogenic movements in the Pieniny Klippen Belt geosyncline. Bulletin de Academie Polonaise de Science, Sér., sci. chim., géol. and géogr., 8, 551-558.

Birkenmajer K., 1975. Tectonic control of sedimentation at the Jurassica-Cretaceous boundary in the Pieniny Klippen Belt, Carpathians. Colloque sur la limite Jurass.-Crét., Lyon-Neuchâtel (1973). Mémoire BRGM, 294-299.

Birkenmajer K., 1977. Jurassic and Cretaceous lithostratigraphic units of the Pieniny Klippen Belt, Carpathians, Poland. Studia Geologica Polonica, 45, 1-158.

Birkenmajer K., 1986. Stages of structural evolution of the Pieniny Klippen Belt, Carpathians. Studia Geologica Polonica, 88, 7-32.

Cecca F., 1992. Ammonite habitats in the Early Tithonian of Western Tethys. Lethaia, 25, 257-267.

Ghibaudo G., 1992. Subaqueous sediment gravity flow deposits, practical criteria for their field description and classification. Sedimentology, 39, 423-454.

Golonka J., 2000. Cambrian-Neogene Plate Tectonic Maps. Wydawnictwa Uniwersytetu Jagiellońskiego, Kraków, 125 pp.

Golonka J., 2004. Plate tectonic evolution of the southern margin of Eurasia in the Mesozoic and Cenozoic. Tectonophysics, 381, 235-273.

Golonka J. and Krobicki M., 2001. Upwelling regime in the Carpathian Tethys, a Jurassic-Cretaceous palaeogeographic and palaeoclimatic perspective. Geological Quarterly, 45, 15-32.

Golonka J. and Krobicki M., 2004. Jurassic paleogeography of the Pieniny and Outer Carpathian basins. Rivista Italiana di Paleontologica Stratigrafica, 110, 5-14.

Golonka J. and Krobicki M., 2006. Field trip A – From Tethyan to Platform Facies. Outer Carpathians. In, Wierzbowski A. et al. (eds.). Jurassic of Poland and adjacent Slovakian Carpathians. Field trip guidebook. 7th International Congress on the Jurassic System, 6-18 September 2006, Kraków, Poland. pp. 11-15.

Golonka J. and Sikora W., 1981. Microfacies of the Jurassic and Lower Cretaceous sedimentarily thinned deposits of the Pieniny Klippen Belt in Poland. Biuletyn Instytutu Geologicznego, 31, 7-37. (In Polish, English summary)

Golonka J., Krobicki M., Oszczypko N., Ślączka A. and Słomka T., 2003. Geodynamic evolution and paleogeography of the Polish Carpathians and adjacent areas during Neo-Cimmerian and preceding events (latest Triassic-earliest Cretaceous). In: McCann T. and Saintot A. (Eds) Tracing Tectonic Deformation Using the Sedimentary Record. Geological Society, Special Publication, London, 208, 138-158.

Golonka J., Gahagan L., Krobicki M., Marko F., Oszczypko N. and Ślączka A., 2006. Plate-tectonic evolution and paleogeography of the Circum-Carpathian region. In Golonka J. and Picha F.J. (eds), The Carpathians and their foreland, Geology and hydrocarbon resources. American Association of Petroleum Geologists, Memoire, 84, 11-46.

Golonka J., Vašíček Z., Skupien P., Waśkowska-Oliwa A., Krobicki M., Cieszkowski M., Ślączka A. and Słomka T., 2008. Litostratygrafia osadów górnej jury i dolnej kredy zachodniej części Karpat zewnętrznych (propozycja do dyskusji). W, Krobicki M. (Ed.), Utwory przełomu jury i kredy w zachodnich Karpatach fliszowych polsko-czeskiego pogranicza, Jurassica VII, 27-29.09.2008 – Żywiec/Štramberk. Geologia (kwartalnik AGH), 34, 3/1, 9-31. (In Polish, English summary)

Grabowski J., Krzemiński L., Nescieruk P., Szydło A., Paszkowski A., Pécskay Z. and Wójtowicz A., 2003. Geochronology of teschenitic intrusions in the Outer Western Carpathians of Poland – constraints form $^{40}K/^{40}Ar$ ages and biostratigraphy. Geologica Carpathica, 54, 6, 385-393.

Grabowski J., Krobicki M. and Sobień K., 2008. New palaeomagnetic results from the Polish part of the Pieniny Klippen Belt, Carpathians – evidence for the palaeogeographic position of the Czorsztyn Ridge in the Mesozoic. Geological Quarterly, 52 (1), 31-44.

Jurewicz E., 2005. Geodynamic evolution of the Tatra Mts. and the Pieniny Klippen Belt (Western Carpathians), problems and comments. Acta Geologica Polonica, 3, 295-338.

Kováč M., Nagymarosy A., Oszczypko N., Ślączka A., Csontos L., Marunteanu M., Matenco L. and Márton M., 1998. Palinspastic reconstruction of the Carpathian-Pannonian region during the Miocene, In, Rakús M. (Ed.), Geodynamic development of the Western Carpathians. Geological Survey of Slovac Republic, Bratislava, 189–217.

Krobicki M., 1994. Stratigraphic significance and palaeoecology of the Tithonian-Berriasian brachiopods in the Pieniny Klippen Belt, Carpathians, Poland. Studia Geologica Polonica, 106, 89-156.

Krobicki, M., 1996. Neo-Cimmerian uplift of intraoceanic Czorsztyn pelagic swell (Pieniny Klippen Belt, Polish Carpathians) indicated by the change of brachiopod assemblages. In, Riccardi A.C. (Ed.), Advances in Jurassic Research. GeoResearch Forum, 1-2, 255-264, Zurich.

Krobicki, M., 2006. Field trip A – From Tethyan to Platform Facies. Outer Carpathians. Stop A5 – Falsztyn – Czorsztyn Succession (Aalenian-Bajocian). In, Wierzbowski, A., Aubrecht., R., Golonka, J., Gutowski, J., Krobicki, M., Matyja, B.A, Pieńkowski, G. and Uchman, A. (eds.). Jurassic of Poland and adjacent Slovakian Carpathians. Field trip guidebook. 7th International Congress on the Jurassic System, 6-18 September 2006, Kraków, Poland. pp. 39-41.

Krobicki M. and Golonka J., 2006. Pieniny Klippen Belt. In, Wierzbowski A. et al. (Eds.). Jurassic of Poland and adjacent Slovakian Carpathians. Field trip guidebook. 7th International Congress on the Jurassic System, 6-18 September 2006, Kraków, Poland. pp. 15-22.

Krobicki M. and Golonka J., 2008. Geological history of the Pieniny Klippen Belt and Middle Jurassic black shales as one of the oldest deposits of this region – stratigraphical position and palaeoenvironmental significance. Geoturystyka, 2 (13), 3-18.

Krobicki M. and Wierzbowski A., 2004. Stratigraphic position of the Bajocian crinoidal limestones and their palaeogeographic significance in evolution of the Pieniny Klippen Basin. Tomy Jurajskie, 2, 69-82. (In Polish, English summary)

Krobicki M. and Wierzbowski A., 2009. Środkowojurajskie wapienie bulaste sukcesji czertezickiej pienińskiego basenu skałkowego Polski – fakty i kontrowersje. Przegląd Geologiczny, 57, 7, 600-606. (In Polish, English summary)

Krobicki M., Budzyń B., Golonka J., Kruglov S., Malata E., Michalik M., Oszczypko N., Skiba M., Słaby E., Słomka T. and Zych B., 2005. Petrography and mineralogy of the Late Jurassic – Early Cretaceous volcanic rocks in the Ukrainian part of the Carpathians. Polskie Towarzystwo Mineralogiczne – Prace Specjalne, 25, 323-328.

Krobicki M., Oszczypko N., Salata D. and Golonka J., 2008. Intra-plate alkaline volcanism in the Pieniny Klippen Belt (Eastern Carpathians, Ukraine). In: Németh, Z. and Plašienka, D. (eds) SlovTec 08, 6th Meeting of the Central European Tectonic Studies Group (CETeG) and 13th Meeting of the Czech Tectonic Studies Group (ČTS), 23-26 April 2008, Upohlav, Pieniny Klippen Belt, Slovakia. Proceedings and Excursion Guide, 73-74.

Lewandowski M., Krobicki M., Matyja B.A. and Wierzbowski A., 2005. Palaeogeographic evolution of the Pieniny Klippen Basin using stratigraphic and palaeomagnetic data from the Veliky Kamenets section (Carpathians, Ukraine). Palaeogeography, Palaeoclimatology, Palaeoecology, 216, 53-72.

Malik K., 1994. Sedymentacja normalna, katastroficzna i wyjątkowa w mezozoicznym fliszu Karpat Śląskich. III Krajowe Spotkanie Sedymentologów, Przewodnik Konferencji, Sosnowiec, 35-68. (In Polish only)

Matyszkiewicz J. & Słomka T., 1994. Organodetrital conglomerates with ooids in the Cieszyn Limestone (Tithonian-Berriasian) of the Polish Flysch Carpathians and their palaeogeographic significance. Annales Societatis Geologorum Poloniae, 63, 211-248.

Mišík M., 1999. Contribution to the lithology and paleogeography of radiolarites in the Western Carpathians. Mineralia Slovaca, 31, 491-506.

Michalík J. and Reháková D., 1995. Sedimentary records of Early Cretaceous tectonic activity in the Alpine-Carpathian region. Slovak Geological Magazine, 2, 159-164.

Michalík, J., Reháková D. and Vašíček Z., 1995. Early Cretaceous sedimentary changes in West-Carpathian area. Geologica Carpathica, 46, 285-296.

Michalík J., Reháková D. and Jablonský J., 1996. Geodynamic setting of fluxoturbidites in West Carpathian Upper Jurassic and Lower Cretaceous sedimentary basins. Slovak Geological Magazine, 3-4, 325-329.

Neumayr M., 1871. Jurastudien. Der penninische Klippenzug. Jahrbuch der kaiserlich-königlichen geologischen Reichanstalt, 21, 451–536.

Nowak W., 1964. Egzotyki z dolnych łupków cieszyńskich z Jasienicy. Kwartalnik Geologiczny, 8, 973-974. (In Polish, English summary)

Nowak W., 1973. Jura Karpat Zewnętrznych. W, Sokołowski S. (ed.), Budowa Geologiczna Polski. Tom I. Stratygrafia, część 2. Mezozoik, 389-401, 464-4672. (In Polish only)

Olszewska B., 2005. Microfossils of the Cieszyn Beds (Silesian Unit, Polish Outer Carpathians) – a thin sections study. Polish Geological Institute Special Papers, 19, 1-58.

Peszat C., 1968. O wykształceniu dolnych łupków cieszyńskich z Goleszowa. Sprawozdania z Posiedzeń Komisji Geologicznej Polskiej Akademii Nauk, oddział w Krakowie, 11, 370-373. (In Polish, English summary)

Peszat C., 1971. Dolne łupki cieszyńskie w kamieniołomie w Goleszowie. Przewodnik XLIII Zjazdu Polskiego Towarzystwa Geologicznego, Kraków, 12-14.09.1971, 186-191. (In Polish, English summary)

Pickering K.T., Stow D., Watson M. and Hiscott, R., 1986. Deep-water facies, processes and models, a review and classification scheme for modern and ancient sediments. Earth Science Review, 23, 75-174.

Plašienka D. 1999. Tektonochronológia a paleotektonický model jursko-kriedového vývoja centralnych Západných Karpát. Veda, Bratislava, 127 p (In Slovak with English summary).

Plašienka D., 2002, Origin and growth of the West Carpathian orogenic wedge during the Mesozoic. Geologica Carpathica, 53, 132-135.

Plašienka D., 2003. Dynamics of Mesozoic pre-orogenic rifting in the Western Carpathians. Mitteilungen der Österreichischen Geologischen Gesellschaft, 94, 79-98.

Reháková D. and Michalík J., 1992. Correlation of Jurassic/Cretaceous boundary beds in West Carpathian profiles. Földtani Közlöni, 122, 1, 51-66.

Słomka T., 1986a. Statistical approach to study of flysch sedimentation – Kimmeridgian-Hauterivian Cieszyn Beds, Polish Outer Carpathians. Annales Societatis Geologorum Poloniae, 56, 227-336. (In Polish, English summary)

Słomka T., 1986b. Utwory podmorskich ruchów masowych w łupkach cieszyńskich dolnych. Geologia (kwartalnik AGH), 12, 25-35. (In Polish, English summary)

Słomka T., 2001.Osady wczesnokredowych spływów rumoszowych w warstwach cieszyńskich rejonu Żywca. Geologia (kwartalnik AGH), 27, 89-110. (In Polish, English summary)

Staniszewska A. and Ciborowski T., 2000. Dolnokredowa brekcja wapienna w autochtonicznej serii wierchowej w Tatrach Zachodnich. Przegląd Geologiczny, 48, 246-250. (In Polish, English summary)

Ślączka A. and Słomka T., 2001. Stop C1 – Żywiec.W, 12th Meeting of the Association of European Geological Societies and LXXII Zjazd Polskiego Towarzystwa Geologicznego. Państwowy Instytut Geologiczny, 113-115.

Ślączka A., Kruglow S., Golonka J., Oszczypko N. and Popadyuk I., 2006. The General Geology of the Outer Carpathians, Poland, Slovakia, and Ukraine. In, The Carpathians and their foreland, Geology and hydrocarbon resources, Golonka J. and Picha F. (eds.), American Association of Petroleum Geologists Memoir, 84, 221-258.

Tokarski A., 1947. Grojec i żywieckie okna tektoniczne. Biuletyn Państwowego Instytutu Geologicznego, 28, 1-53. (In Polish, English summary)

Waśkowska-Oliwa A., Krobicki M., Golonka J., Słomka T., Ślączka A. and Doktor M., 2008. Stanowiska najstarszych skał osadowych w polskich Karpatach fliszowych jako obiekty geoturystyczne. W: Krobicki M. (Ed.), Utwory przełomu juri i kredy w zachodnich Karpatach fliszowych polsko-czeskiego pogranicza, Jurassica VII, 27-29.09.2008 – Żywiec/Štramberk. Geologia (kwartalnik AGH), 34, 3/1, 83-121. (In Polish, English summary)

Wieczorek J., 1988. Maiolica – A unique facies of the Western Tethys. Annales Societatis Geologorum Poloniae, 58, 255-276.

Wierzbowski A. and Remane J., 1992. The ammonite and calpionelld stratigraphy of the Berriasian and lowermost Valanginian in the Pieniny Klippen Blet (Carpathians, Poland). Eclogae geologicae Helvetiae, 85, 3, 871-891.

Wierzbowski A., Jaworska M. and Krobicki M., 1999. Jurassic (Upper Bajocian-lowest Oxfordian) ammonitico rosso facies in the Pieniny Klippen Belt, Carpathians, Poland, its fauna, age, microfacies and sedimentary environment. Studia Geologica Polonica, 115, 7-74.

Żytko K., Zając R., Gucik S., Ryłko W., Oszczypko N., Garlicka I., Nemčok J., Eliáš M., Menčik E. and Stránik Z., 1989. Map of the tectonic elements of the Western Outer Carpathians and their foreland. In: Geological Atlas of the Western Outer Carpathians and their Foreland (eds. Poprawa D. & Nemčok J.). Państwowy Instytut Geologiczny, Warszawa/GUDŠ Bratislava/Uug Praha.

Scientific Annals, School of Geology, Aristotle University of Thessaloniki Proceedings of the XIX CBGA Congress, Thessaloniki, Greece	Special volume 100	221-229	Thessaloniki 2010

TECTONICS OF THE KLIPPEN BELT AND MAGURA NAPPE IN THE EASTERN PART OF THE PIENINY MTS. (WESTERN CARPATHIANS, POLAND AND SLOVAKIA) – NEW APPROACHES AND RESULTS

Oszczypko N.[1], Jurewicz E. [2] and Plašienka D.[3]

[1]*Institute of Geological Sciences, Jagiellonian University, Oleandry 2a, PL-30-063, Kraków, Poland, nestor.oszczypko@uj.edu.pl*
[2]*Faculty of Geology, University of Warsaw, Żwirki i Wigury 93, PL-02-089 Warszawa, Poland, edyta.jurewicz@uw.edu.pl*
[3]*Department of Geology and Palaeontology, Faculty of Natural Sciences, Comenius University, Mlynská dolina, SK-842 15 Bratislava, Slovakia, plasienka@fns.uniba.sk*

Abstract: The Pieniny Klippen Belt (PKB) is a suture zone, which separates the Central Carpathians from the Outer Carpathians. The PKB successions are built up of the Lower/Middle Jurassic to Upper Cretaceous, dominantly pelagic and flysch deposits. The traditional multi-stage tectonic model of the PKB assumes that during the Palaeocene, retro-thrusting followed by subsidence and deposition of the "Magura Autochthonous Palaeogene" took place. Recently, we have studied the structural relationship of these deposits in the PKB, and we came to the conclusion that they belong to two formations with different tectonic positions. The Kremná Formation (?Oligocene – Lower Burdigalian) belongs to the Magura succession and appears in a tectonic window, beneath the Grajcarek thrust-sheet and the Czorsztyn (Sub-Pieniny) Nappe, while position of the Złatne Beds, which occur inside the Pieniny Nappe, is not clear. In the Slovak part the calcareous flysch sediments of the Jarmuta-Proč Formation described earlier as a "klippen mantle" form the youngest sedimentary member of the lowermost tectonic unit of the PKB, named here as the Fakľovka Unit. These youngest deposits are involved in tectonics of the PKB and document that final folding and thrusting of the PKB took place in the late Early Miocene (after Eggenburgian), corresponding to folding and thrusting of the Magura Nappe.

Key words: tectonic evolution, Pieniny Klippen Belt, Magura Nappe, Western Carpathians, Poland and Slovakia

1. Introduction

The Pieniny Klippen Belt (PKB) is up to 600 km long, but only a few km wide zone that follows the boundary between the External (Outer) Western Carpathian Flysch Belt (Tertiary accretionary wedge) and the Central (Inner) Western Carpathians composed of Cretaceous basement/cover nappe units (Austroalpine system) and its overstepping Cenozoic sedimentary and volcanic cover (Fig. 1A; for the general overview see e.g. Froitzheim et al., 2008). The PKB is a zone with intricate tectonic structure, known as the "klippen style" – block-in-matrix arrangement of stiff Jurassic to Lower Cretaceous limestones, traditionally called "klippen", embedded in soft Upper Cretaceous and Palaeogene marlstones, shales and sandstones, known as the "klippen mantle". Mixture of units with originally distant palaeogeographic provenances (partly "exotic") reveals an extraordinary internal shortening within this narrow zone. Predominantly brittle deformation of PKB rocks occurred in several phases from the latest Cretaceous up to Middle Miocene times. The PKB is therefore often considered as a suture, in spite of the lack of ophiolites in the surface structure of the PKB and adjacent zones.

Lithology and stratigraphy of the klippen successions, i.e. Jurassic and Early Cretaceous sediments, is generally well known (e.g. Birkenmajer, 1977 and references therein) and will not be concerned in this paper. On contrary, the soft rocks of the "klippen mantle", i.e. Late Cretaceous to Palaeogene pelagic and flysch deposits are comparatively less known due to poor outcropping and intense deformation, which obliterated to a high degree their original mutual relations. The same applies for the interrelationships of the PKB to the Magura Nappe (Carpathian Flysch Belt) adjoining from the north and to the Central Carpathian (Podhale)

Palaeogene Basin (CCPB) bounding the southern PKB margin. Thus although having been studied in a great detail over 150 years, many important aspects of the PKB structure and its relationships to neighbouring units remain poorly constrained. This paper is focussed on the so-called Pieniny sector of the PKB and adjacent innermost part of the Magura Nappe, in the eastern part of the Pieniny Mts nearby the Polish-Slovakian state boundary. Based on some new results of detailed sedimentological, biostratigraphical and structural studies, the presented paper aims mainly at the description of local tectonic structure and correlation of some problematic rock units between Poland and Slovakia.

ążkiewicz, 1977 and references therein), the general structure and evolution of the PKB and adjacent zones was established. The generalized view recognizes two main nappe units differing in their Jurassic–Cretaceous lithostratigraphic successions: the ridge-type Czorsztyn and the basinal Pieniny ones, which are interrelated by several "transitional" successions (e.g. Czertezik, Niedzica-Pruské, Kysuca-Branisko). Views on time of the nappe formation were changing during time, but the most widely accepted opinion considers the Late Cretaceous age of the PKB nappe structure (e.g. Birkenmajer, 1986).

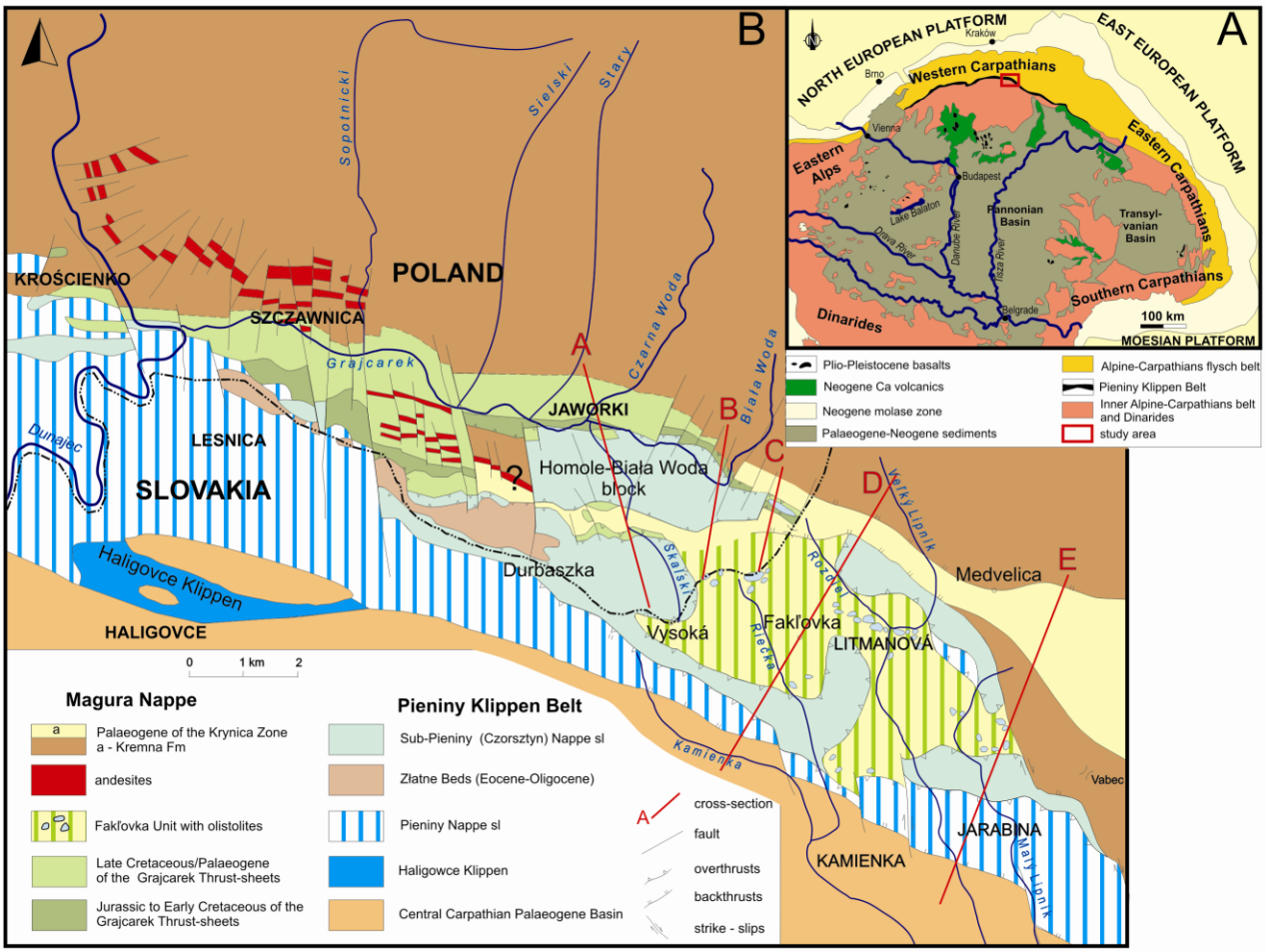

Fig. 1. A – Position of the studied area in the Alpine-Carpathian and Pannonian realm; B – Geological sketch-map of the eastern part of the Pieniny Mts. The Polish Małe Pieniny Mts based on Birkenmajer 1979 (simplified and changed).

2. Previous research

The Polish and adjacent Slovak part of the Pieniny Mts represent the classical area of the PKB geology and tectonics. After the milestone works by Neumayr, Uhlig, Limanowski, Horwitz, Andrusov, Książkiewicz, Birkenmajer and Matějka (see Ksi-

In the Małe Pieniny Mts, the Magura Nappe and PKB are separated by the narrow, strongly deformed Peri-PKB Zone *(s.l)*, known in Poland as the Grajcarek Unit (Birkenmajer, 1977; 1979; 1986) or Hulina Zone (Sikora, 1974). This unit is composed of the Jurassic, Cretaceous and Palaeo-

cene, pelagic and flysch deposits belonging to the Magura succession. According to this concept, the Laramian Grajcarek Unit was thrust back over the PKB, and finally overstepped by the Late Palaeocene to Early Eocene "Autochtonous Magura Palaeogene" (AMP) deposits as a lateral extension of the Magura Basin (see also Birkenmajer and Oszczypko, 1989).

The idea of retro-arc thrusting of the Grajcarek Unit over PKB was questioned by Golonka and Rączkowski (1981) and Jurewicz (1997). According to these authors, the Grajcarek Unit appears in tectonic windows within the PKB. According to Jurewicz (1997, 2005), the terminal phase of nappe thrust-folding was followed by gravitational sliding of the Czorsztyn (Subpieniny) Nappe. This nappe was detached from the basement, defragmented into slices and thrust onto on the southern slope of the Magura Basin, forming numerous olistoliths and olistrostomes (e.g. the Homole-Biała Woda block).

This concept has been recently supported by Cieszkowski et al. (2009).

It was Ján Nemčok late in the last century (e.g. Nemčok et al., 1990), who performed new detailed geological mapping and investigations in the Slovak part of the area and brought many new ideas that partially contradicted the views of older authors. In particular, he characterized the Jarmuta-Proč Formation (Maastrichtian – Early Eocene) as a dominating complex of the "klippen mantle", uniting the various "series", "facies" and "developments" of the Peri-klippen Palaeogene, which were distinguished by older authors (e.g. the Kremná, Ujak, Kyjov, Lackovce, Inovce series etc.). He also stressed the role of "Illyrian" folding before the Late Eocene, which was responsible for creating of the main structures of the PKB. The post-Illyrian sediments (Ombron Group – Nemčok et al., 1990, see also Leško and Samuel, 1968 an references therein) partly seal the deformed substratum and reveal unified sedimentary conditions within the CCPB, PKB and Magura Basin, in spite they were deformed again during the Miocene. Certain aspects of these Nemčok's concepts are accepted also in the present work. On the other hand, we do not follow some other Nemčok's opinions, especially his hypothesis about the megaolistostromatic nature of the whole PKB (Nemčok, 1980). He did not differentiate between various PKB klippen successions and partial nappe units, considered all klippen and even parts of the "klippen mantle" (Late Cretaceous marlstones) as olistoliths and, consequently, questioned the existence of partial PKB nappes differing in lithostratigraphy and position. However, we fully agree that a large part of the klippen (but not all!) are sedimentary slide blocks in the Jarmuta-Proč Formation and not tectonic lenses or boudins, as considered by all other authors.

The last important work dealing with the Palaeogene sediments of the "klippen mantle" in relation to the neighbouring sediments of the Magura Unit was recently published by Oszczypko et al. (2005). These authors established the lowermost Miocene age of the newly-defined Kremná Formation and assign it to the Magura Nappe (Krynica Zone), together with the underlying Eocene – Oligocene Magura Formation. The Kremná-type sediments (Kremná facies or development) were previously considered to be Eocene in age and regarded as constituents of the "Klippen Palaeogene", i.e. part of the transgressive klippen mantle (e.g. Matějka et al., 1963).

3. Methods

During the last few years, new geological mapping of the contact zone between the Magura Nappe and PKB in the Szczawnica and Jaworki area (Małe Pieniny Mts) has been performed by the first author. More or less simultaneously, the authors equally studied relationships between the Magura Nappe, Grajcarek thrust-sheet and the Mesozoic nappes of the PKB (see Oszczypko and Jurewicz 2009). At the same time, we sampled "Autochtonous Magura Palaeogene" flysch (AMP) inside PKB for the petrographic and biostratigraphic purposes (see Oszczypko and Oszczypko-Clowes submitted).

At the same time, new geological mapping in the scale 1:10,000, along with the structural research, has been performed in the eastern Slovakian part of the Pieniny Klippen Belt by the third author. Geographically, the research treated here covers the eastern part of the Pieniny Mts, which are built by units of the PKB and adjacent parts of the Magura Nappe and CCPB. Along with mapping, field-based structural investigations were focused on relationships of minor and major structures, structural relations of klippen to klippen mantle, and spatial/temporal distribution of deformation phenomena. Studied minor structures include bedding-parallel foliation, occasional cleavage and minute folds, and especially shear zones – ductile-brittle in

incompetent shales and marls and brittle (faults, slickensides) in competent limestones and sandstones. Results of the structural investigation will not be treated in detail here, since they are prepared to be published in a special paper.

4. Results

The geological structure of the Małe Pieniny Mts significantly differs from the Pieniny Mts to the west. This is manifested by dissimilarities between the two areas shown in the geological map (Fig. 1B). To the east of the Dunajec River the PKB clearly narrows, while the Peri-Klippen Zone expands. At the same time, the structure of the PKB is changed from the fold-and-thrust belt into block structure. Next to the east, the big blocks of the Mesozoic rocks disappear and their place is occupied by single small klippen (e.g. the Fakľovka Unit between Litmanová and Jarabina villages). Concurrently, the area of AMP significantly extends east of Szczawnica town.

4.1. Lithology, age and tectonic position of "AMP" in the Małe Pieniny Mts

In the Małe Pieniny Mts, the AMP occurs in three, more or less separated belts (Fig. 1B). The first one, 4 km long and up to 1 km wide appears cartographically inside the Czorsztyn (Subpieniny) Nappe, and runs from Slovak-Polish boundary, narrowing towards the west (Fig. 1B), and disappears south of the Homole Block. This area is occupied by thick-bedded, fine to coarse grained sandstones, with sporadic intercalations of fine conglomerates. The sandstones are similar to the Magura type, muscovitic sandstones, while infrequent fine conglomerates, rich in carbonate clasts, show similarity to the Jarmuta type sandstones. The shale intercalations are very rare. Recently these deposits were sampled, south of the Homole block, as well as in the upper flow of the Sztolnia Stream. These samples contain calcareous nannoplankton belonging to Early Miocene NN2 Zone (Oszczypko and Oszczypko-Clowes, submitted). For these very recent age determinations, the Kremná sediments have not yet been cartographically distinguished from the Palaeogene sediments of the Fakľovka Unit – the latter most probably overly them tectonically. This is the reason why the map in figure 1 and sections A – C in figure 2 do not show a contact between these two units.

The second belt of the AMP is located west of the Homole-Biała Woda block, surrounded by the Grajcarek thrust sheet. This area is dominated by thick-to very thick-bedded sandstones of the Magura type without any intercalations of shales, which prevented micropaleontological tests. Taking into account the lithological development of these beds, we can regard them as an equivalent of the Piwniczna or Poprad Members of the Magura Formation, but Kremná Formation also cannot be excluded (Fig. 1B).

The third belt of AMP is located along the Polish-Slovakian state boundary, west of the Durbaszka Mt. From the north this area is bounded by a narrow belt (100–200 m) of Mesozoic limestones and marls similar to the Branisko (Kysuce) succession of the Pieniny Nappe. On the Slovak side this type of AMF passes into the calcareous sandstones of the Jarmuta-Proč Formation (Palaeocene – Middle Eocene; see Nemčok 1992). For unclear reasons, in the map of Janočko ed. (2000) these rocks are shown as the Upper Cretaceous flysch sediments of the Klape Unit. The small exposures of medium to thick-bedded calcareous sandstones, with infrequent claystone intercalations are visible in the upper flows of the Krupianka and Sztolnia streams (Fig. 1B). Taking into account lithology and tectonic position of the AMP in this area, we decided to establish these strata as the Złatne Beds (Golonka and Rączkowski, 1981).

The possible relationship between the AMP (Kremná Formation) and PKB nappes, Grajcarek thrust-sheet and the Magura Nappe is presented in the cross-sections (Fig. 2). The cross-sections A, B and C suggest that major part of the AMP, belonging to the Lower Miocene Kremná Formation, appears in tectonic windows beneath the Grajcarek thrust sheets and PKB nappes.

In the eastern part of the Małe Pieniny Mts, the Kremná Formation has been recognized both at the front of the PKB, as well as in tectonic window inside the PKB. The Kremná Formation is overlapped by two tectonic outliers of the Czorsztyn (Sub-Pieniny) Nappe and Grajcarek thrust-sheet. Towards the south the Kremná Fm. is overthrust by the Mesozoic rocks of Czertezik succession of the Czorsztyn (Sub-Pieniny) Nappe. Towards the west (Fig. 2B, C) position of the Brysztan outlier is occupied by the Homole-Biała Woda Block, composed of both the Czorsztyn and Niedzica successions of the Czorsztyn (Subpieniny) Nappe. This nappe is underlain by the south Grajcarek thrust-sheet up to 100 m thick, composed of the Szlachtowa and Malinowa formations. Both tec-

tonic units of the Homole-Biała Woda Block are thrust over the northern Grajcarek thrust sheet.

The tectonic position of the Złatne Beds (Fig. 1B) of the Durbaszka Mt. and along the Polish/ Slovakian boundary is not clear. On the Slovakian side of PKB, an equivalent of the Złatne Beds is represented by the Jarmuta-Proč Formation.

4.2. Structure of the Slovak part of the Pieniny Mts

Based on the recent geological mapping and structural investigation, the following major tectonic units have been distinguished (in a zonal arrangement from bottom and north to top and south): 1. the Magura Unit (Krynica subunit) of the Outer Carpathian Flysch Belt; 2. Oravic units of the

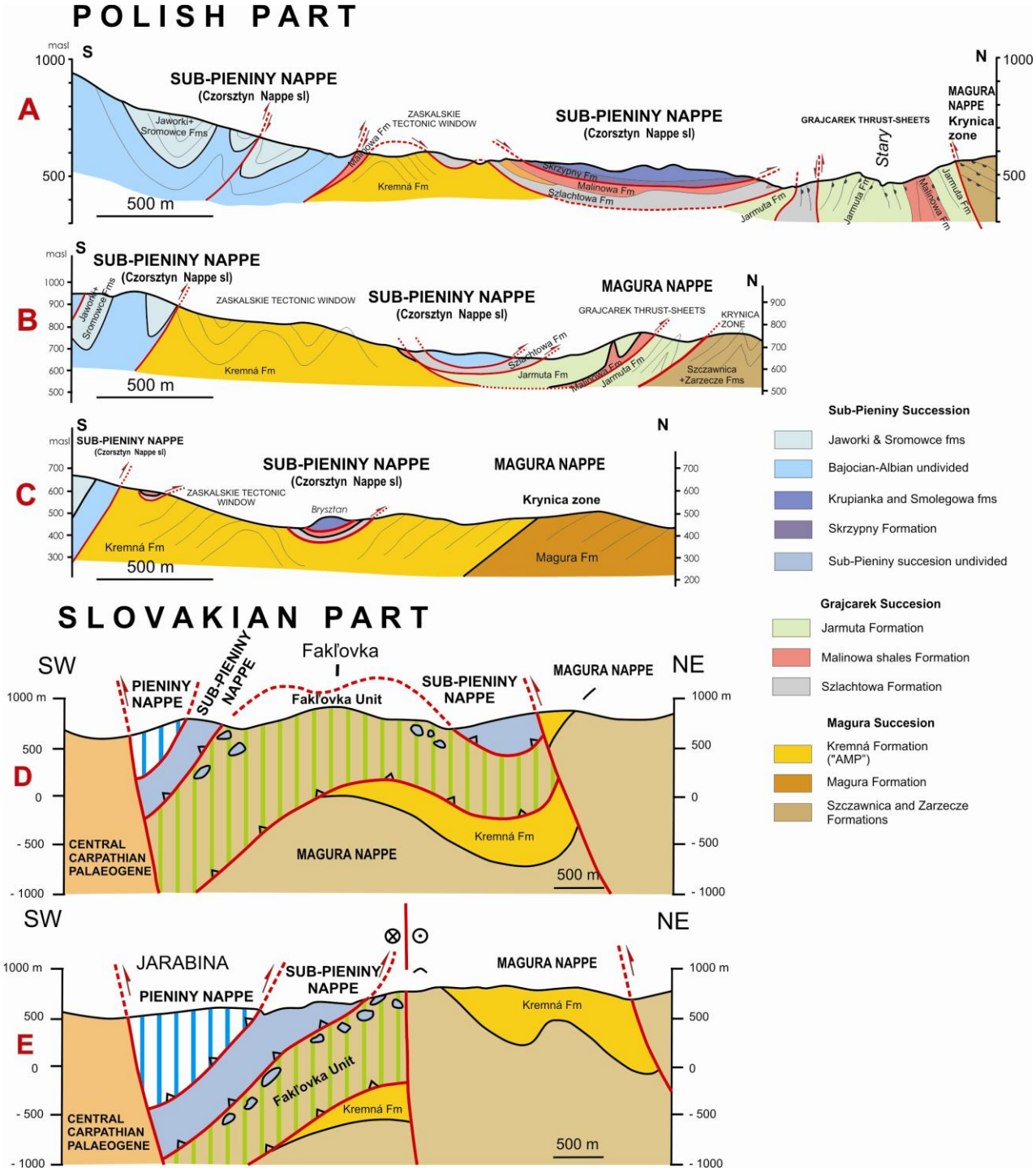

Fig. 2. Geological cross-sections of the area. For their position and key of sections D and E see Fig. 1.

PKB; 3. CCPB (Podhale-Podtatra Group). Further east, out of the area described here, the Magura vs. PKB tectonic contact is partly sealed by the Upper Eocene – Oligocene sediments of the Údol Succession (Ujak facies of older authors, Ombron Group of Nemčok et al., 1990), which is composed of variegated shales, Globigerina marls, menilite shales and calcareous flysch of the Malcov Formation (see Oszczypko et al., 2005 for details). These formations exhibit close facies relationships to the southward adjacent, coeval sediments of the Podhale-Podtatra Group.

The Magura Unit, adjacent to the PKB (Krynica Zone or subunit, Čergov Unit of older Slovak authors), is dominated by the Magura-type sandstones. These are usually thick-bedded, medium- to coarse-grained, siliciclastic, which seemingly do not contain material typical for the PKB formations. From bottom to top, the Magura Formation is subdivided into three members (Oszczypko et al., 2005): Piwniczna Sandstone (Lower – Middle Eocene), Mniszek Shale (Middle Eocene) and Poprad Sandstone (Upper Eocene – Oligocene), which is conformably overlain by the Early Miocene Kremná Formation (NN1-NN2) in a synform close to the northern boundary of the PKB (Fig. 1B). The Poprad sandstones contain conglomerate bodies bearing exotic material dominated by crystalline basement rocks, which considerably differ from exotics found in the Upper Cretaceous – Palaeogene conglomerates of the PKB (Mišík et al., 1991; Oszczypko et al., 2006). Therefore different sources have been reconstructed for the coeval clastic sediments of the Magura and Klippen Belt basins. On the other hand, some authors indicated a gradual transition from carbonate-bearing Palaeogene sandstones of the PKB to siliciclastic deposits of the Magura Unit across their boundary (e.g. Stráník, 1965).

The contact of the Magura Unit with the PKB is always tectonic, formed by steeply NE dipping reverse fault (backthrust) segmented by N-S trending strike-slips with dextral offset (Figs 1B, 2D, E)). Bedding of the Magura sediments is steeply to moderately N-dipping at this contact. This situation indicates oblique dextral backthrusting of the Magura Unit, which occurred late in the tectonic evolution of the area, most probably during the Early – Middle Miocene. This event affected also the PKB units and their overstepping cover (Údol Succession), as well as the southern boundary fault of the PKB and adjacent sediments of the CCPB (Šambron-Kamenica antiform; Plašienka et al., 1998).

The lowermost structural unit of the PKB mostly occurs along the northern boundary of the PKB, in places also more southerly in windows or half-windows. This unit includes Upper Jurassic radiolarites and Lower Cretaceous spotted cherty limestones, variegated, but mostly grey to black, often calcite-free shales and silicites overlain by "black flysch" (mid-Cretaceous?), Upper Cretaceous variegated, mostly red shales and marls with thin turbiditic beds of fine-grained, siliciclastic sandstones, and then hundreds of metres thick calcareous sandstones and conglomerates/breccias (Jarmuta-Proč Formation). Huge slide blocks and mass flows (olistostromes) occur as stratiform bodies or incised channel fillings in the uppermost parts of this succession (e.g. Litmanová, Miľpoš – part of the Gregorianka Breccia in the sense of Nemčok et al., 1989). Sandstones and conglomerates obviously contain material derived mainly from the Czorsztyn and/or Niedzica and Czertezik successions (Pieniny-Kysuca/Branisko might be also present). Their inferred age is Palaeocene – Early Eocene. The lithostratigraphic content of this unit roughly corresponds to the Birkenmajer's Grajcarek Unit (see above), our view on its tectonic position is considerably different, however. Paleogeographically, the unit under question should be placed at the southern margin of the Magura Basin, but structurally it forms the lowermost, not the uppermost thrust unit of the PKB, as reconstructed by Birkenmajer (e.g. 1986). Therefore the term Grajcarek Unit is not used in Slovakia. Instead, a provisional term Fakľovka Unit is proposed here. Moreover, according to the newest results presented here from the Polish Małe Pieniny Mts (see above), the Grajcarek Unit appears to override the Kremná Formation of the Magura Nappe and, vice-versa, is overridden by the typical PKB Czorsztyn and/or Niedzica nappes (see also Jurewicz, 1997).

In addition to clastic material in sandstones and olistostromes, huge olistoliths of typical PKB rocks occur within the Jarmuta-Proč Formation (Figs 1B, 2D, E). These were considered as klippen, i.e. tectonic lenses until now. The overriding Czorsztyn-type units form imbricated thrust sheets, their fronts passing gradually into mass-flows inserted within and above the Jarmuta-Proč flysch, hence indicating close sedimentary and tectonic relationships of the Fakľovka Unit and the overlying

Subpieniny nappe.

For the higher nappe unit of the PKB, we return to the old Uhlig's term Subpieniny Unit (Uhlig 1907). This view corresponds also to the division of Książkiewicz (1977), i.e. the Subpieniny Nappe includes the dominating Czorsztyn Succession, as well as Niedzica, Czertezik and similar "transitional" successions derived from the Czorsztyn ridge and its slopes. Lithology and stratigraphy of these successions were described in numerous papers, readers are recommended e.g. to Birkenmajer (1977, 1986 and others). However, in no case these successions represent independent large-scale units in the tectonic sense as some other authors proposed. The Subpieniny Nappe is a more-or-less continuous overthrust sheet with stable structural position, but strongly imbricated or even disintegrated internally, which at least partly resulted also from the morphological dissection of the original sedimentary area and consequent wavy or upstepping nature of the detachment plane. Especially the frontal parts are very complicated with numerous slices or lenses (klippen) embedded in Upper Cretaceous marlstones ("diapirs" of Birkenmajer, 1979). Nappe fronts were even probably gravitationally detached and form disintegrated bodies above the Jarmuta-Proč flysch (Figs 1B, 2D, E). These slide bodies are closely related to olistoliths and olistostromes within the underlying Jarmuta-Proč Formation of the Fakľovka Unit (sometimes not distinguishable), which originated from gravitationally liberated frontal parts of the Subpieniny Nappe. Only the most internal (but structurally lower) parts of the Subpieniny Nappe, formed by the Czorsztyn Succession with thick rigid crinoidal limestones, are more coherent, but still imbricated. The youngest sediments of the Czorsztyn Succession are Upper Senonian Jarmuta-type calcareous sandstones overlain by olistostrome breccias (Gregorianka Breccia at the type locality near Jarabina–Nemčok et al., 1989). These breccias only contain material from the overriding Pieniny Nappe (Upper Jurassic radiolarites, Lower Cretaceous biancone-type limestones).

The highermost tectonic unit of the PKB – the Pieniny Nappe is clearly independent from the Subpieniny Nappe, but includes several lithostratigraphic successions as well (Pieniny s.s., Kysuca-Branisko, see e.g. Birkenmajer, 1977). The Pieniny Unit is strongly folded and imbricated again, but generally continuous and coherent. It overlies the Subpieniny Unit, but in places directly the Fakľovka Unit (Figs 1B, 2D, E). Except a few places, it forms the southernmost zone of the PKB.

5. Discussion and conclusions

New data on the age and position of the "AMP" allows for the development of a new scenario of tectonic evolution of the PKB (Fig. 3).

1) Late Cretaceous/Palaeocene: detachment of the Pieniny Unit and its thrusting over the Czorsztyn slope and ridge (Gregorianka Breccia).

2) Palaeocene – Early Eocene: detachment of the Subpieniny Unit, its internal imbrication (partially also with the overlying Pieniny Unit) and thrusting over the foreland Jarmuta-Proč Basin facing the Magura Ocean, its frontal parts were disintegrated into slide sheets, olistoliths (the largest one could be just observed in the Małe Pieniny, famed as Homole-Biała Woda block) and debris flows (Milpoš-type breccias of the Proč Formation). This gravitational sliding influenced also the background sediments and caused their folding and forming the Grajcarek thrust-sheets.

3) Eocene: detachment of the Fakľovka Unit, out-of-sequence thrusting in the Subpieniny and Pieniny Nappes, possibly also thrusting of the Fakľovka Unit along with the overlying Subpieniny and Pieniny Units over the innermost Magura elements. Probably during the same time the Grajcarek thrust-sheets could be activated ones more. These gravitational movements at the boundary of PKB and Magura Basin prolonged to the Eocene/?Oligocene (Fig. 4 B,C). Further shortening and first manifestations of dextral transpression took a place (steep shear zones affecting all PKB units).

4) Eocene – Oligocene: Collapse of the thrust stack, flat extensional shear zones in PKB units, subsidence and subsequent deposition of the Údol Succession.

5) Early Miocene (Burdigalian): The youngest thrust of the PKB units onto the Magura Nappe (after deposition of the Kremná Formation) connected with folding and thrusting within the Outer Carpathians (Intra-Burdigalian or Early Styrian movements). Renewed thrusting along the PKB/Magura boundary in the rear part of the developing accretionary wedge of the Carpathian Flysch Belt, affecting also the Lower Miocene Kremná Formation according to present study.

6) Late Burdigalian/ Middle Miocene: dextral tran-

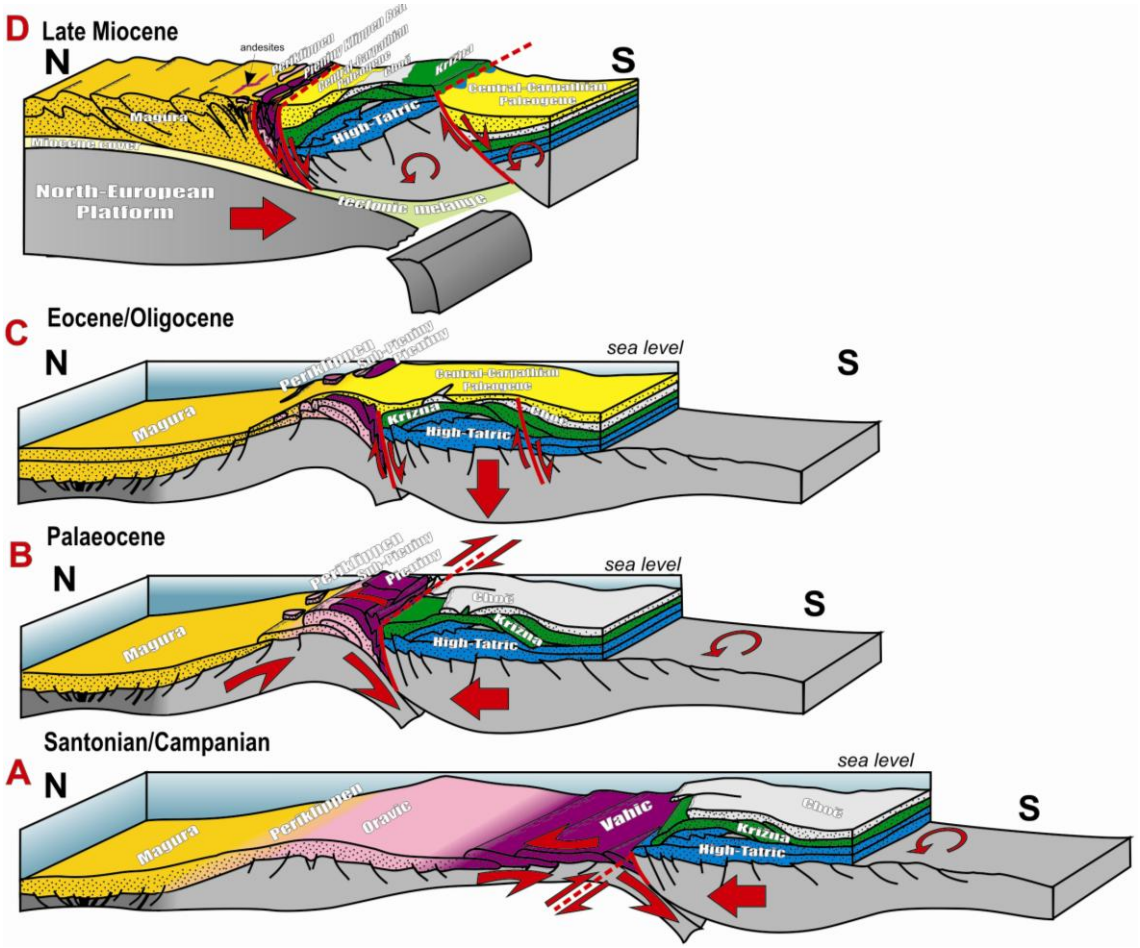

Fig. 3. Late Cretaceous – Late Miocene evolution of the Pieniny Klippen Belt and adjacent areas (based on Jurewicz 2005, supplemented).

spression and shaping of the final "flower" structure of the PKB. The eastwards escape and counterclockwise rotation of the ALCAPA caused involvement of the PKB into strike-slip movements and development of a flower structure, consequently some parts of klippen units were retro-thrust onto the CCPB (Fig. 4D; compare to Fig 3D). This event was apparently accompanied by narrowing and development of the orogen-scale curvature of the PKB.

Acknowledgements

The research was supported by the Polish Ministry of Sciences and Higher Education grant N307 025 31/1997 (to N.O.). Research in the Slovak Republic was performed in frame of the project APVV-0465-06 "Tectogen". D.P. wishes to thank the Slovak Research and Development Agency for the financial support. Authors thank cordially to Prof. Jan Golonka and Dr. Michal Potfaj for reviewing this paper.

References

Birkenmajer K., 1977. Jurassic and Cretaceous lithostratigraphic units of the Pieniny Klippen Belt, Carpathians. Studia Geologica Polonica, 45, 158p.

Birkenmajer K., 1979. Pieniny Klippen Belt of Poland – geological guide. Wydawnictwa Geologiczne, Warszawa, 237p (in Polish).

Birkenmajer K., 1986. Stages of structural evolution of the Pieniny Klippen Belt, Carpathians. Studia Geologica Polonica, 88, 7-32.

Birkenmajer K. and Oszczypko N., 1989. Cretaceous and Palaeogene lithostratigraphic units of the Magura Nappe, Krynica Subunit, Carpathians. Annales Societatis Geologorum Poloniae, 59, 145-181.

Cieszkowski M., Golonka J., Krobicki M., Ślączka A., Oszczypko N., Waśkowska A. and Wendorff M., 2009. The Northern Carpathians plate tectonic evolutionary stages and origin of olistoliths and olistostromes. Geodinamica Acta, 22/1-3, 101-126.

Froitzheim N., Plašienka D. and Schuster R., 2008. Alpine tectonics of the Alps and Western Carpathians. In: The Geology of Central Europe, vol. 2: Mesozoic and Cenozoic (T. Mc Cann, ed.), Published by the Geological Society, London, 1141-1232.

Golonka J. and Rączkowski W., 1981. Detail Geological Map of Poland, Piwniczna sheet. Wydawnictwa Geologiczne, Warszawa (in Polish).

Janočko J. (ed.), 2000. Geological map of the Spišská Magura Mts 1 : 50 000. Geol. Služba SR, Vyd. D. Štúra, Bratislava, 174 p.

Jurewicz E., 1997. The contact between the Pieniny Klippen Belt and Magura Unit (the Małe Pieniny Mts). Geological Quarterly, 41, 315-326.

Jurewicz E., 2005. Geodynamic evolution of the Tatra Mts. and the Pieniny Klippen Belt (Western Carpathians): problems and comments. Acta Geologica Polonica, 55, 295-338.

Książkiewicz M., 1977. The tectonics of the Carpathians. In: Geology of Poland Volume 4. Tectonics (Pożaryski W., ed.), Wydawnictwa Geologiczne, Warszawa, 476-699.

Leško B. and Samuel O., 1968. The geology of the East Slovakian Flysch. Vydav. Slov. Akad. Vied, Bratislava, 245 p. (in Slovak with English summary).

Matějka A. (ed.), 1963: Explanations to the general geological map of ČSSR 1 : 200 000, sheet M-34-XXI Spišská Stará Ves. Geofond, Bratislava, 60-132. (in Slovak)

Mišík M., Sýkora M. & Jablonský J., 1991: Strihovce conglomerates and the south Magura cordillera. Západné Karpaty, Geológia, 14, 7–72.

Nemčok J., 1980. Non-traditional view of east-Slovakian Klippen Belt. Geologický Zborník – Geologica Carpathica, 31, 563–568.

Nemčok J., 1990. Geological map of the Pieniny, Ľubovnianska vrchovina Highland and Čergov Mts in the scale 1:50,000. Geologický Ústav D. Štúra, Bratislava.

Nemčok J., Kullmanová A. and Ďurkovič T., 1989. Development and stratigraphic position of the Gregorianka breccias of the Klippen Belt in eastern Slovakia. Geologické Práce, Správy, 89, 11–37 (in Slovak with English summary).

Nemčok J., Zakovič M., Gašpariková V., Ďurkovič T., Snopková P., Vrana K. and Hanzel V., 1990. Explanation to the geological map of the Pieniny, Čergov, Ľubovnianska and Ondavská vrchovina Mts. Geologický Ústav Dionýza Štúra, Bratislava, 132p (in Slovak with English summary).

Oszczypko N. and Jurewicz E., 2009. The position of the so called autochtonous Magura Paleogene in the Małe Pieniny Mts. (Magura Nappe and Pieniny Klippen Belt, Poland). In: Conference of Environmental, Structural and Stratigraphical Evolution of the Western Carpathians, 2-5.12.2008 (Reháková D. and Józsa Š., eds). Mineralia Slovaca, 40, 3-4, Geovestník, 245-246.

Oszczypko N. and Oszczypko-Clowes M., 2009. Stages in the Magura Basin evolution: a case study of the Polish Sector (Western Carpathians). Geodinamica Acta, 22, 83-100.

Oszczypko N. and Oszczypko-Clowes M., submitted. New Data on the stratigraphy of the Paleogene and Early Miocene of the Beskid Sądecki Range and Ľubovnianska Vrchovina (Magura Nappe, Outer Carpathians, Poland and Slovakia**).** Acta Geologica Polonica.

Oszczypko N., Oszczypko-Clowes M., Golonka J. and Marko F., 2005. Oligocene – Lower Miocene sequences of the Pieniny Klippen Belt and adjacent Magura Nappe between Jarabina and the Poprad River (East Slovakia and South Poland) – their tectonic position and paleogeographic implications. Geological Quarterly, 49, 379-402.

Oszczypko N., Oszczypko-Clowes M. and Salata D., 2006. Exotic rocks of the Krynica Zone (Magura nappe) and their palaeogeographic significance. Geologia, 32, 21-45.

Plašienka D., Soták J. and Prokešová R., 1998. Structural profiles across the Šambron-Kamenica Periklippen Zone of the Central Carpathian Paleogene Basin in NE Slovakia. Mineralia Slovaca, 29, 173–184.

Sikora W., 1974. Outline of the tectogenesis of the Pieniny Klippen zone in Poland in the light of the new geological data. Annales Societatis Geologorum Poloniae, 41, 1, 223-239. (In Russian with English abstract).

Stráník Z., 1965: Geology of the Magura Flysch in the Čerchov Mts and western part of the Ondavská vrchovina Mts. Sborník Geologických Vied, Západné Karpaty, 3, 125–178 (in Czech, German summary).

Uhlig V., 1907: About tectonics of the Carpathians. Sitzungsberichte der kaiserischen Akademie der Wissenschaften, matematisch-naturwissenschaftliche Klasse, 116, Abt. 1, Wien, 871-982 (in German).

Scientific Annals, School of Geology, Aristotle University of Thessaloniki Proceedings of the XIX CBGA Congress, Thessaloniki, Greece	Special volume 100	231-240	Thessaloniki 2010

CALCAREOUS NANNOPLANKTON BIOSTRATIGRAPHY OF THE TERMINAL SEDIMENTS OF THE MAGURA BASIN – A CASE STUDY OF THE POLISH SECTOR (OUTER WESTERN CARPATHIANS)

Oszczypko-Clowes M.

Institute of Geological Sciences, Jagiellonian University, Oleandry 2a, 30-063 Krakow, Poland
m.oszczypko-clowes@uj.edu.pl

Abstract: The Oligocene to Early Miocene closing of the northern sector of the Outer Carpathian sedimentary area is manifested by deposition of the Krosno synorogenic lithofacies in the Grybów-Dukla-Silesian/Sub-Silesian/Skole and Boryslav-Pokuttya basin system. The analogous Malcov synorogenic lithofacies is typical for the Pieniny Klippen Belt and Magura Basin. These lithofacies comprise the fining and thinning upwards sequences. Towards the top, the sedimentary sequences are dominated by marly pelites. In the Pieniny Klippen Belt, as well as in the Krynica and Rača zones of the Magura Basin, the deposition of the Malcov lithofacies was initiated during the NP24 and persisted to NP25 Zone. In the northern part of the Magura Basin (Siary Zone) the youngest deposits (so called Supra-Magura beds) belong to the NP24 Zone. The most important species to determine the NP24 zone in the region is *Cyclicargolithus abisectus*, and for NP25 – *Sphenolithus conicus*. During the Late Oligocene (NP25/NN1) the frontal part of Magura Nappe were thrust northwards onto the terminal Krosno flysch basin. The clastic material derived from eroded front of the Magura Nappe has been found in the Krosno shally facies of the Silesian Basin. The northwards thrusting of the Magura Nappe was also accompanied by formation of the piggy-back basin on the Magura Nappe, filled with synrogenic turbidites of the Zawada and Kremná formations – NN1 and NN2 zones. These nannofossil associations are characterised by the presence of *Sphenolithus delphix* (NN1) and *Sphenolithus disbelemnos* (NN2) while the species of *Dictyococcites bisectus* is absent. At the same time the level of reworked species is high.

Keywords: litho-and biostratigraphy, calcareous nannofossils, Late Oligocene, Early Miocene, Magura Nappe, Outer Western Carpathians

1. Introduction

History of the stratigraphic studies of the Magura Nappe has more than 100 years (Fig. 1A). The first information (beginning of XXth Century) about the Eocene age of the youngest deposits of the Magura Nappe was based on a few determinations of large foraminifera. This point of view has persisted until the mid-50ties of the last century, when the first analyses of small foraminifers were made. These investigations conducted in the northern, marginal part of the Magura Nappe in the Gorlice area (Fig. 1B) revealed the presence of assemblages of small globigerinas, characteristic for the Submenilite Globigerina Marls (SMGM). This datum level marks the Eocene-Oligocene boundary in the more external units (Krosno Zone or Moldavides) of the Outer Carpathians. Few years later, the Malcov Beds (Oligocene) were discovered in the Nowy Sącz area (for references see Osczypko-Clowes, 2001) over the Magura sandstones, regarded as the youngest deposits of the Magura Nappe at that time. For a long time, the SE part of the Magura Nappe, dominated by thick-bedded, turbiditic sandstones, devoid of fauna and microfauna, had a weaker stratigraphic recognition.

A significant qualitative change in biostratigraphic studies took place after application of calcareous nannoplankton. This resulted in the introduction of formal stratigraphic schemes in the Krynica and Bystrica zones (for references see Osczypko-Clowes, 2001). Contemporary research of calcareous nannoplankton from the Krynica and Bystrica zones suggested mainly early-middle Eocene age of formations, while the younger data were found in the outer zones, mainly in the Siary Zone. Such biostratigraphical framework strongly affected the palaeogeographic and palaeotectonic reconstruc-

tion not only for the Magura Nappe, but also for the entire outer Carpathians.

The aim of this paper is to summarize biostratigraphical data on the final Oligocene to Early Miocene stages of sedimentation in the Magura Basin. This is based on the author's latest research and recently published papers by Oszczypko-Clowes (2001), Oszczypko and Oszczypko-Clowes (2002; 2009, submitted) and Oszczypko et al. (1999, 2005).

cies differentiations with regards to the Palaeogene deposits, the Magura Nappe has been subdivided into four facies-tectonic zones, namely the Krynica (Orava), Bystrica (Nowy Sącz), Rača and Siary (Figs. 1B, 2, see also Koszarski et al. 1974). From the South, the Magura Nappe is in contact with the PKB along a sub-vertical Miocene strike-slip fault, and at the same time it is flatly overthrust northward over the For-Magura Group of Nappes and the Silesian Nappe by at least 50 km. During the

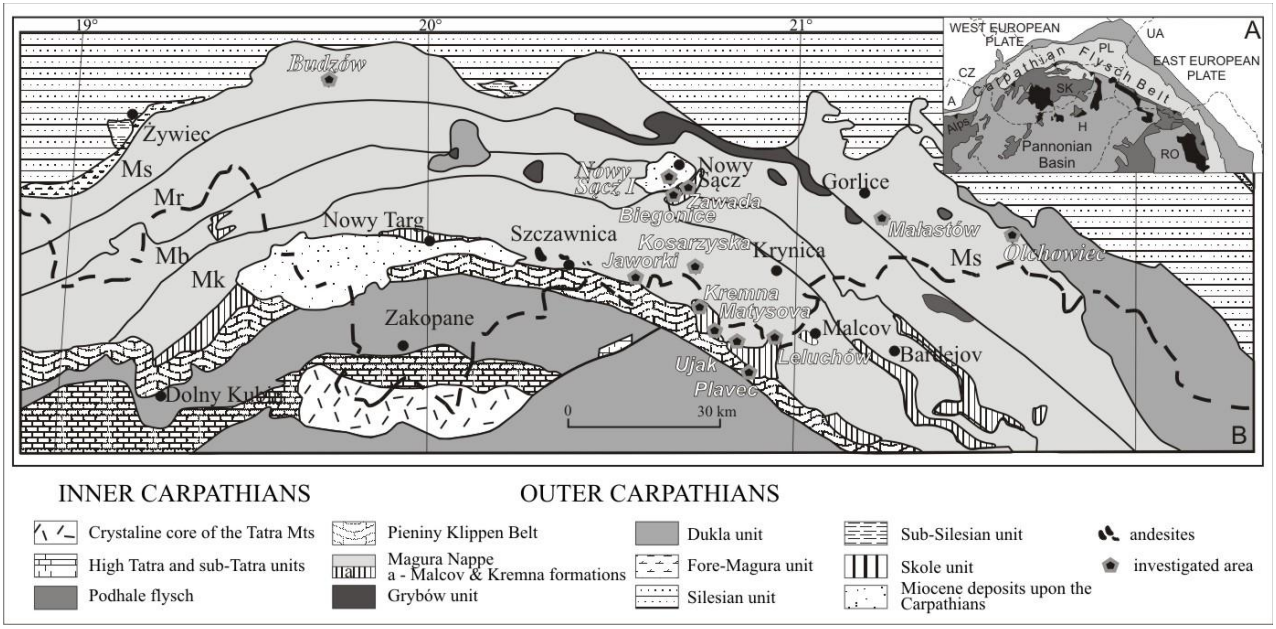

Fig. 1. (A) The geological map of the East Alpine-Carpathian-Pannonian basin system (after Picha et al. 2006), (B) Sketch-map of the Polish Carpathians and their fore-deep (based on Żytko et al. 1989, supplemented). Abbreviations: Su- Siary, Ru- Rača, Bu- Bystrica, and Ku- Krynica facies zones of the Magura Nappe.

2. Geological Setting

The Magura Nappe (Fig.1B) is the largest unit of the Outer Western Carpathians, linked up with the Rheno-Danubian flysch of the Eastern Alps in the west and the Marmarosh Flysch in the east (for references see Oszczypko and Oszczypko-Clowes 2009). The Magura Nappe is mainly composed of Late Cretaceous to the Eocene sediments. The oldest Jurassic – Early Cretaceous rocks are known as Grajcarek Unit from the Peri-Pieniny Klippen Belt (PKB) in Poland and a few localities in Southern Moravia (op.cit.). The youngest (Oligocene to Early Miocene) deposits of the Magura Nappe have been discovered in the Nowy Sącz area (Oszczypko et al., 1999, Oszczypko and Oszczypko-Clowes, 2002), Peri-PKB area (Cieszkowski 1992), and recently in the several other places (Oszczypko et al., 2005; Oszczypko and Oszczypko-Clowes submitted). On the basis of fa-

Late Oligocene – Middle Miocene thrust movements, the Magura nappe has been completely uprooted from its substratum, mainly along ductile Upper Cretaceous rocks (for references see Oszczypko and Oszczypko-Clowes 2009). The Lower Cretaceous (Hauterrivian – Cenomanian) deposits are known only at a few locations in Southern Moravia, whereas the more or less complete sections of the Upper Jurassic – Lower Cretaceous deposits are known only from the Grajcarek thrust sheets from the Peri-PKB area in Poland (for references see Oszczypko and Oszczypko-Clowes 2009).

2.1. Studied sections

For the purpose of this paper the selected profiles from all facies zones of the Magura Nappe and Pieniny Klippen Belt have been used (Fig. 2). This figure shows the synthetic lithostratigraphic profiles of the Palaeogene to Early Miocene deposits,

across the Magura Nappe. These profiles are representative of the eastern sector of the Magura Nappe in Poland (Fig. 1B). As the level of correlation we adopted SMGM, or vicariously the top of the variegated shales with the *Reticulophragmium amplectens* (Middle – Late Eocene).

Palaeogene Basin) and PKB suture zone (Údol section, fig. 2). In the southern part of the Krynica Zone, the youngest deposits belong to the Malcov and Kremná formations (Figs. 2, 3). So far, the only site of Malcov Formation on the Polish side was found in the Leluchów section (for reference

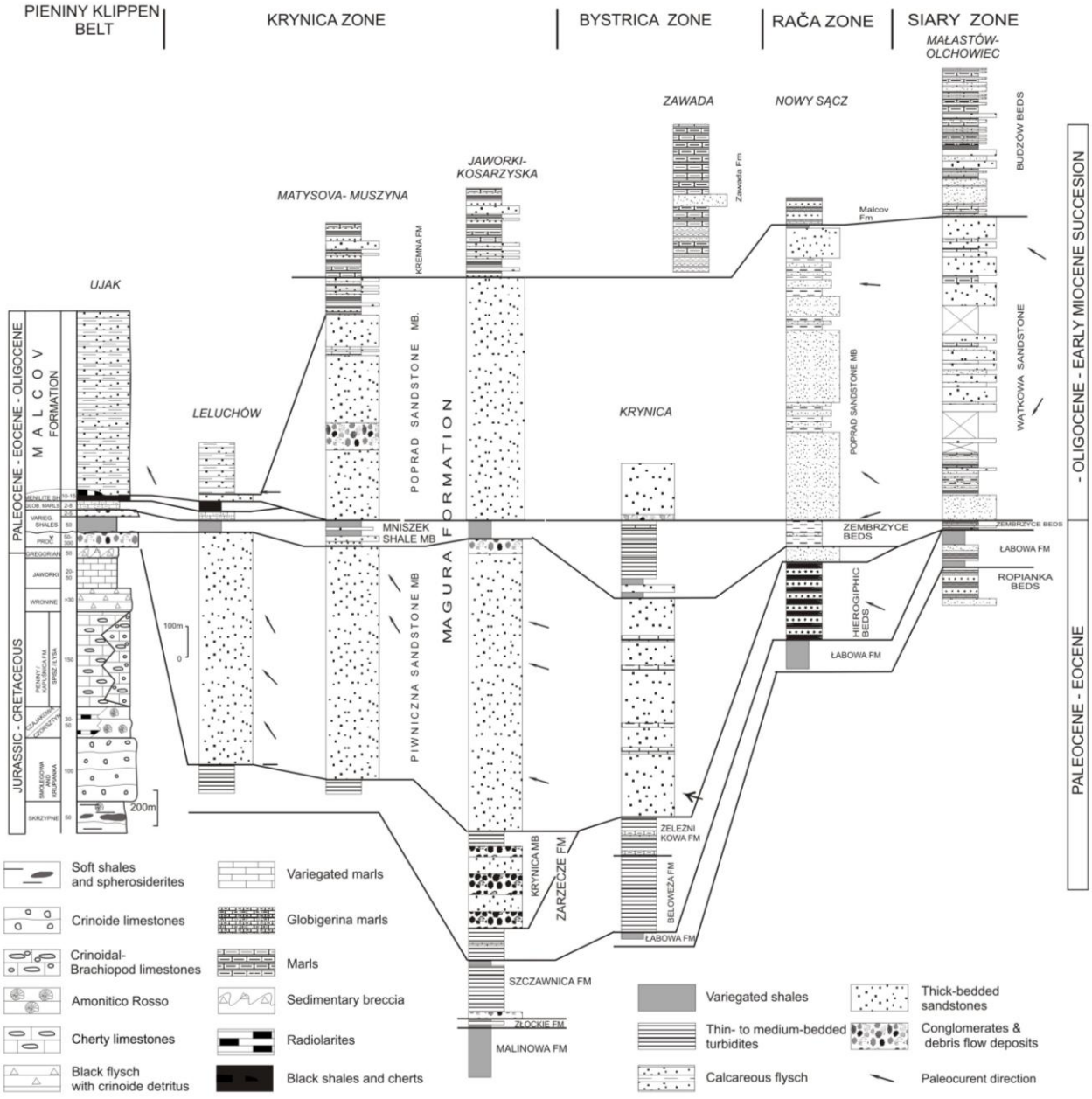

Fig 2. The lithostratigraphic logs of the Magura Nappe (after Oszczypko-Clowes 2001; Oszczypko and Oszczypko-Clowes 2009).

2.2. Krynica Zone

The Krynica facies zone provides an important insight for our understating of terminal history of the Magura Basin. This zone records facies links with post-nappe – Late Eocene to Oligocene basins of the Central Carpathians (Central Carpathian

see Oszczypko-Clowes, 2001). This section is situated close to the Polish-Slovak border, and is directly linked with the Ujak section of the PKB (Oszczypko et al., 2005). In the Leluchów profile, the Malcov Formation is composed of the following, Late Eocene to Oligocene lithostratigraphic

units: the Leluchów Marls Member, Smereczek Shale Member and Malcov Formation s.s. The Leluchów Marl Member (see SMGM) consists of green and grey marly shales with numerous calcite veins covered by a 4 m thick unit of red, greyish-green, greenish and olive marls. The Smereczek Shale Member is represented by dark, silicified, Menilite-like shales (for references see Oszczypko-Clowes 2001). The lowermost portion of this member reveals a marly development with a few tuffite intercalations, and a thin (2-5 cm) intercalation of hornstones at the top. The upper portion of the Menilite Shales consists of black non-calcareous, bituminous shales with a few layers of coarse-grained, thick-bedded sandstone. In the uppermost part of the Leluchów section occur thin-bedded turbidites – dark-grey marly shales with intercalations of thin bedded (10-12 cm), cross-laminated calcareous sandstones. These flat-lying, south dipping strata belong to the Malcov Formation ss.

The similar type of the Malcov Formation is known from exposures in the Údol village near Stará Ľubovňa and Plaveč (Figs. 1B, 2). The upper part of the Malcov Formation is represented by dark grey marly shales with intercalations of thin to medium-bedded muscovite sandstones.

The Kremná Formation has been established by Oszczypko *et* al. (2005). The thickness of the for-

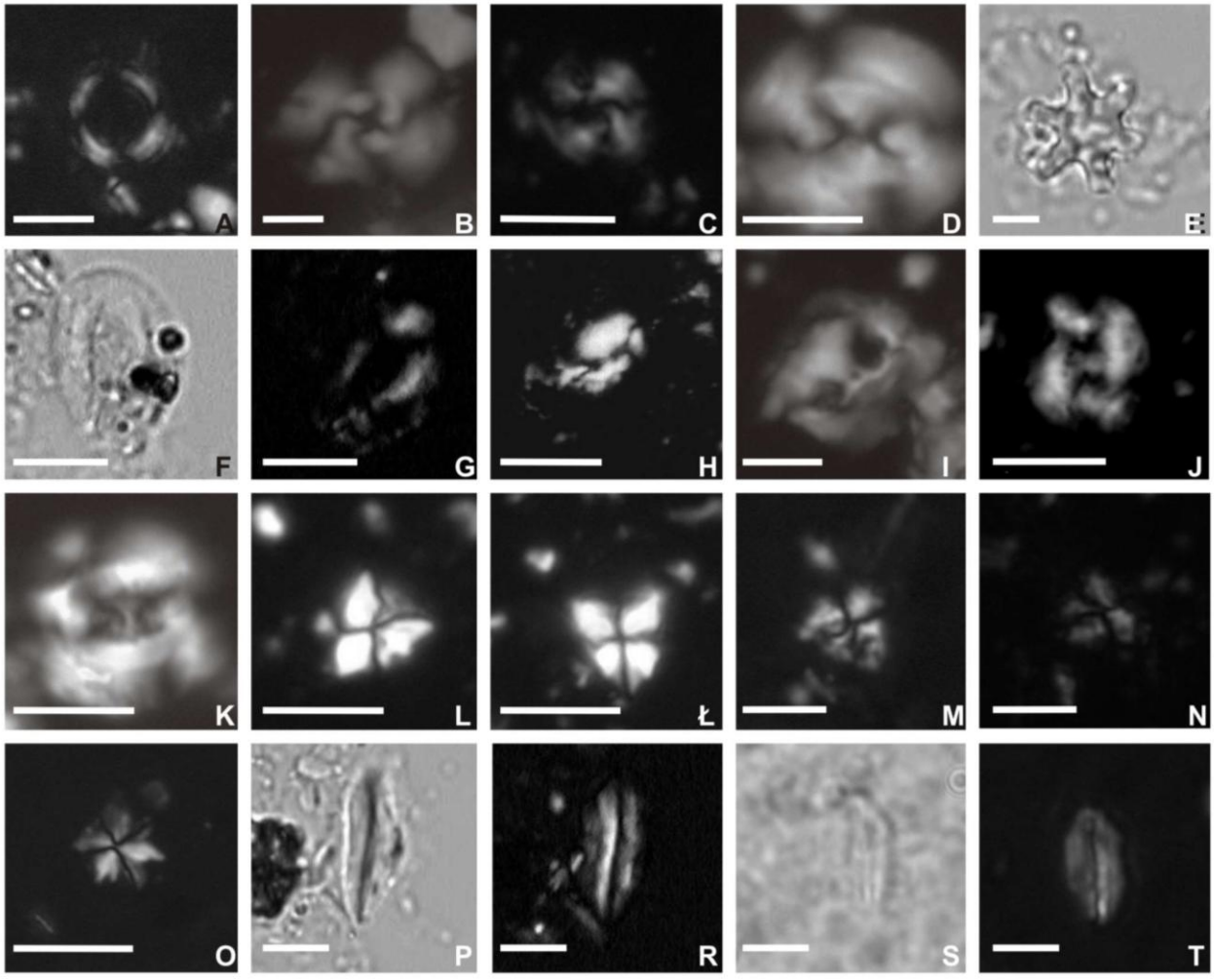

Fig. 3. Light microscope photographs of index nannofossil form Magura Kremná and Zawada formations (for the sample localities see Oszczypko and Oszczypko-Clowes 2002 and Oszczypko et al. 1999, 2005). The length of the scale bar is 5µm. A - *Coronocyclus nitescens*, Kremná Formation, B - *Cyclicargolithus abisectus*, Magura Formation, C - *Cyclicargolithus floridanus*, Magura Formation, D - *Dictyococcites bisectus*, Magura Formation, E - *Discoaster* cf. D. *druggii*, Zawada Formation, F, G - *Helicosphaera ampliaperta*, Zawada Formation, H - *Helicosphaera carterii*, Kremná Formation, I - *Helicosphaera recta*, Magura Formation, J, K -*Reticulofenestra lockeri*, Magura Formation, L, Ł- *Sphenolithus conicus*, Magura Formation, M, N - *Sphenolithus disbelemnos*, Kremná Formation, O - *Sphenolithus dissimilis*, Magura Formation, P, R -*Triquetrorhabdulus milowii*, Zawada Formation, S, T - *Triquetrorhabdulus rugosus*, Kremná Formation.

mation varies from 200-300 m in the Matysová and Dubne section up to 500–600 m in the Kremná and Jaworki-Kosarzyska section (Figs. 1B, 2). The Kremná Formation is composed of thin-to medium-bedded turbidites (T_{bc}) with intercalations of thick-bedded (1.0-2.0 m) massive sandstones. The upper part is dominated by thin-bedded turbidites. The calcareous sandstones are intercalated by gray marly shales.

2.3. Bystrica Zone

The youngest deposits of this zone belong to the Zawada Formation (Figs. 2, 4) which has been documented on the southern periphery of the Nowy Sącz Basin (Fig. 1B). This formation was found in the Nowy Sącz 4 borehole, as well as in the Zawada, Biegonice (Oszczypko et al., 1999; Oszczypko-Clowes, 2001) and Poręba Mała sections (Oszczypko and Oszczypko-Clowes, 2002). The Zawada Formation is represented by medium- to thick-bedded, sometimes glauconitic, sandstones with intercalations of thick-bedded marls and marly claystones. The thickness of the formation is at least 550 m (Fig. 2).

According to Oszczypko et al. (1999), this formation occurs in the southern part of the Rača Subunit, and at the front of the Bystrica Subunit of the Magura Nappe. Due to lack of exposures, the relationship between the Malcov Formation of the Rača Subunit and the Zawada Formation is not clear yet.

2.4. Rača Zone

In the Rača Zone, above the Poprad Sandstone Member of the Magura Formation, marls and shally lithofacies of Krosno-like facies were found in borehole Nowy Sącz I (Figs. 1B, 2, 4). These sediments are at least 100 m thick and were included into the Malcov Formation (see Oszczypko-Clowes et al. 2009).

In the Nowy Sącz 1 borehole, the Malcov Formation was pierced beneath the Late Badenian freshwater deposits (Oszczypko-Clowes et al., 2009) to a depth up to 540 m. Below this depth, folded deposits of the Magura Nappe were reached. The depth interval 540-602 m is dominated by dark-greyish, mainly non-calcareous claystones with sporadic intercalations of mudstones and very fine muscovite sandstones. At a depth of 569-571 m, light marly claystones with sideritic concretions were found. Further down (602.0-606.5 m), fragments of light-yellowish marls occurred. Beneath

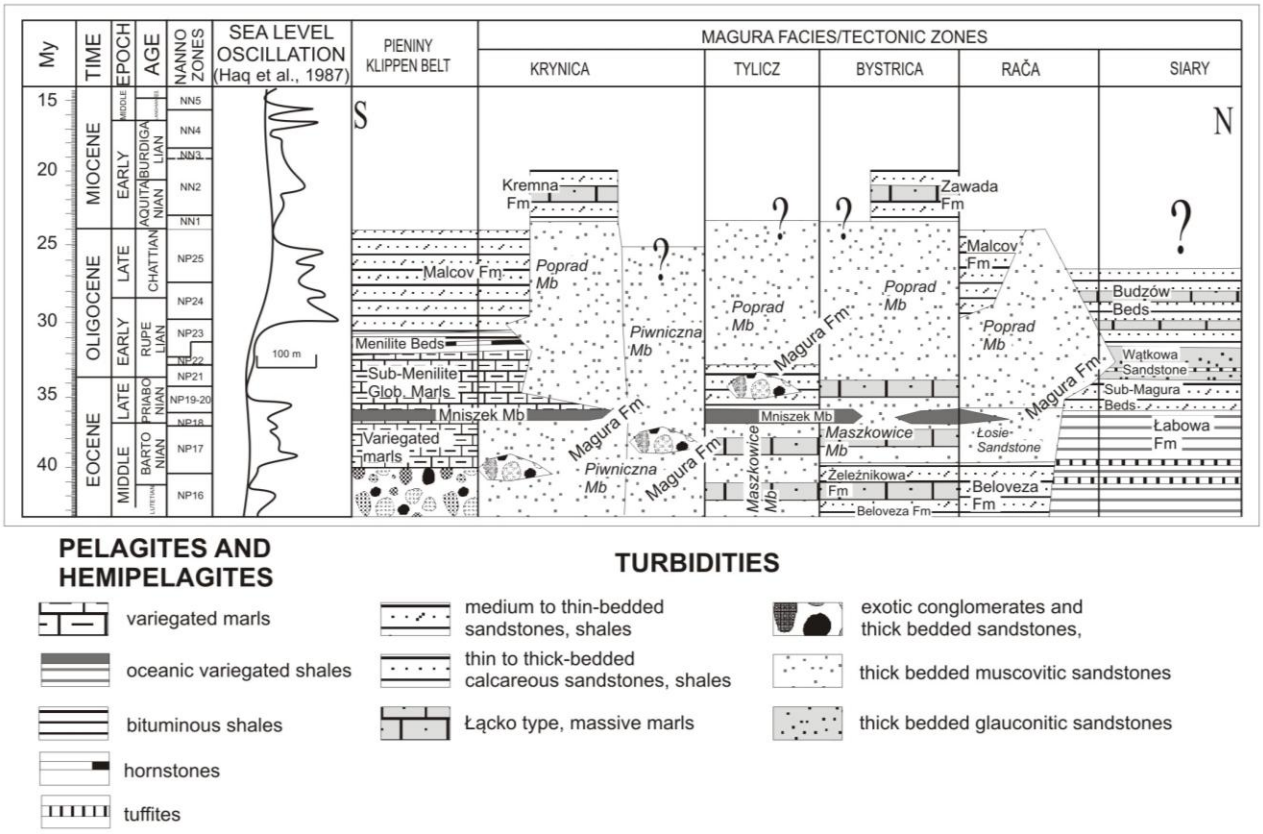

Fig. 4. The lithostratigraphic table of the Palaeogene – Early Miocene deposits of the Magura Nappe and Pieniny Klippen Belt (after Oszczypko and Oszczypko-Clowes, 2009).

the marls, down to a depth of 618.7 m, dark-greyish calcareous claystones and mudstones containing a few thick-bedded intercalations of medium-grained muscovite sandstones were pierced. At depth 618.7-620.8 m a 2 m thick layer of brown-chocolate claystones occurs, followed by dark-greyish claystones. Deeper still, to a terminal depth 704 m, poorly-cemented thick-bedded, muscovite sandstones of the Poprad Sandstone Member of the Magura Formation occur.

2.5. Siary Zone

In the Siary Zone, the Budzów Beds are an equivalent of the Malcov Formationof the Rača and Krynica/PKB zones. In the Małastów and Olchowiec sections (Figs. 1B, 2, 3), these beds occur above the Wątkowa sandstones. Their thickness varies from at least 290 m in Olchowiec, up to 470 m in the Malastów sections. The Budzów Beds are represented by marly claystones, with intercalations of medium to thick-bedded glauconitic sandstones. Subsequently silicified marls and spherosiderites are visible.

3. Material and Methods

A great number of samples (over 100) used for the nannofossil analyses were gathered during the author's field work. The samples were collected from the Malcov Formation in the Leluchów section and Nowy Sącz I borehole (Oszczypko-Clowes, 2001), Zawada Formation (Oszczypko et al., 1999; Oszczypko & Oszczypko-Clowes, 2002) and Kremná Formation (Oszczypko et al., 2005) of the Magura Nappe. Recently, new samples of the Kremná Formation, and Malcov Formation (Údol and Plaveč) have been obtained (Oszczypko and Oszczypko-Clowes, submitted).

All samples were prepared using the standard smear slide technique for light microscope (LM) observations. The investigation was carried out under LM at a magnification of 1000x using phase contrast and crossed nicols. Several of the specimens photographed in LM are illustrated in fig. 3.

The examined samples from the Zawada Formation contain well preserved and diverse calcareous nannoplankton assemblages, highly dominated by the reworked species, especially those of Middle/Late Eocene such as *Chiasmolithus gigas*, *Chiasmolithus grandis, Chiasmolithus oamaruensis, Discoaster barbadiensis, Discoaster bifax, Sphenolithus radians*, as well as some Oligocene species. The level of reworking varies from more than 60%, down to approximately 20-30%.

The abundance pattern for the Kremná Formation is different for certain samples, and varies from more than 15 species (per observation field) down to less than 5. Majority of specimens are easily identifiable. The level of reworking is generally not higher than 30%.

4. Biostratigraphy based on the calcareous nannofosils

For the purpose of this work the standard zonation of Martini (1970) and Martini and Worsley (1970) was used. In the case where the index species have not been observed, it was necessary to use the secondary index species.

Sphenolithus distentus Zone (NP24)
Age: Late Oligocene
Remarks: This zone was identified (Figs.1B, 2, 4) in the Budzów Beds from the Małastów and Olchowiec sections (Fig.1B, 2) and the Malcov Formation s.s. from the Leluchów section. The zone assignment is based on the first occurrence (FO) of *Cyclicargolithus abisectus*. The FO of *Cyclicargolithus abisectus* is usually found close to the FO of *Sphenolithus ciperoensis* (zonal marker for the lower boundary of zone NP24) and thus can be used to approximate the boundary of NP23 and NP24 (Martini and Műller 1986). In addition, *Sphenolithus dissimilis* was also observed. The FO of these species is characteristic for zone NP24 (see Perch-Nielsen 1985).

Sphenolithus ciperoensis Zone (NP25)
Age: Late Oligocene
Remarks: This zone was identified in the Malcov Formation from Údol and Plaveč localities, as well as from the borehole Nowy Sącz I (Figs. 1, 2, 4).
The zone assignment is based on the first occurrence of *Sphenolithus capricornutus* and *Sphenolithus conicus* and *Ponthosphaera rothi*. Slightly less abundant are *Cyclicargolithus abisectus*, *Reticulofenestra lockeri*, *Sphenolitus dissimilis* and *Reticulofenestra dictoda*. The species of *Dictyococcites bisectus* is occurring very rare, but it is still present. The (FO) of *Sphenolithus conicus* has been traditionally used as the base of the NN1 zone. However, Bizon and Műller (1979), Biolzi et al. (1981) and Melinte (1995) have observed the FO of these species as low as in the upper part of the zone NP25.

Discoaster druggii Zone (NN2)
Age: Early Miocene
Remarks: This zone was identified in the Kremná and Zawada formations (Figs. 2, 4).

The zone assignment of the described section is based on a co-occurrence of the following species: *Sphenolithus conicus, Sphenolithus disbelemnos*, *Reticulofenestra pseudoumbilica* and *Triquetrorhabdulus carinatus*. At the same time *Dictyococcites bisectus*, *Cyclicargolithus abisectus* and *Zygrhablithus bijugatus* are absent from the association. According to the standard zonation of Martini (1970) and Martini and Worsley (1970), the first occurrence of *Reticulofenestra pseudoumbilica* takes place in the NN5 zone. However, in the Intra- and Outer Carpathian areas of Romania the FO of *Reticulofenestra pseudoumbilica* coincides with the FO *Discoaster druggii* (Marunteanu 1992), which corresponds to the lower limit of NN2. According to Young (1998), the FO of *Sphenolithus disbelemnos* and/or *Umbilicosphaera rotula* is a reliable biostratigraphical event characteristic for the lower limit of NN2 Zone.

Additionally, the nannofossil association from the Zawada Formation contains *Discoaster druggii* and *Helicosphaera ampliaperta.* The presence of *Discoaster druggii* was documented from more than 50% of investigated samples, whereas the occurrence of *Helicosphaera ampliaperta* is extremely rare. The presence of *Helicosphaera ampliaperta* can suggest the upper part of Zone NN2 (see Holcová, 2002; 2005).

5. Palaeoecology

During the Oligocene, drastic changes in palaeography and palaeoecology took place in Southern Europe. This was connected with transformation of the Western Tethys into the Eastern Paratethys. The transformation was initiated in the nannoplankton zones NP21/22 and resulted in the long lasting anoxic bottom conditions and deposition of the black shales (see Schulz et al., 2005). In the Carpathian sedimentary area, this was recorded by replacement of the pelagic Globigerina Marls by the menilite bituminous shales. These palaeoenviromental changes took place mainly in the northern external part of the Carpathian Flysch Basin (Skole, Sub-Silesian/Silesian and Dukla subbasins), in the lower extend in the Transylvanian and Central Carpathian Palaeogene basins, and to a very small extent also in the Magura Basin.

In the Fore-Magura, Ždánice-Subsilesian and Pouzdřany units of the Czech sector of the Outer Carpathians, the microfossils response on the paleoenvironmental changes has been described by Krhovský and Djurasinovič (1993) and Švábenická et al. (2007). These changes display the nannofossil blooms in the upper portion of the Menilite Formation and reflects the freshwater runoff (floods), decreased salinity, high nutrient input, and sea-level fluctuations connected with gradual isolation of the basin during the Oligocene. Simultaneously, the number of autochtonous species decreased and domination of reworked fossils is observed. This study also of confirmed the diachronous onset of the Krosno lithofacies (Švábenická et al., 2007).

In the Magura Basin, the Oligocene palaeoecological changes are manifested mainly in the Malcov Formation, which was paleogeographically connected with the Central Carpathian Palaeogene Basin. These changes are characterized by the distinct decrease of species diversity, drop of salinity and bloom of *Reticulofenestra ornata, Transversopontis fibula* and *Transversopontis latus* (Oszczypko-Clowes, 2001). In the Lower Burdigalian Zawada and Kremná formations, the palaeoecological changes are not so well manifested. This is probably due to domination of reworked nannofossils derived from the intensively eroded accretionary prism.

6. Palaeogeography

At the turn of the Eocene, the fundamental reorganization of the Magura Basin took place. It was probably related to the first manifestations of an eastwards escape of the ALCAPA (Alpine-Carpathian-Pannonian) Mega Unit to its Early Miocene, pre-orogenic position (Figs. 2, 3, 5, see also Ustaszewski et al., 2008; Oszczypko and Oszczypko-Clowes, 2009). As a result, the Oligocene Magura Basin was occupied by three distinct, interfingering turbiditic lithofacies: glauconitic sandstones in the north (Siary Zone), the Magura type muskovitic sandsones in the middle and southern part of the basin (Rača, Bystrica and Krynica zones), and the black shales and calcareous sandstones (Malcov Formation) in the southernmost part of the basin. These facies were supplied from the different source areas. The Malcov lithofacies records a connection with the PKB and Central Carpathians Paleogene Basin (CCPB), post-nappe basins, and locally overlapped with an angular discordance the Magura type sandstones.

The Oligocene – Early Miocene closing of the northern sector of the Outer Carpathian sedimentary area is manifested by deposition of the Krosno synorogenic lithofacies, which occupied the Gry-

bów-Dukla-Silesian/Sub-Silesian/Skole and Boryslav-Pokuttya basin system (Fig. 5). These lithofacies represent the fining and thinning upwards sequences. Towards the top, the sedimentary sequences are dominated by marly pelites. The beginning and termination of these deposits was diachronic and migrated across the basins towards the north.

The Malcov lithofacies, an equivalent of the Krosno one, is typical for the Pieniny Klippen Belt/Magura Basin. In the PKB and Krynica Zone of the Magura Basin, the deposition of the Malcov lithofacies was initiated during the NP 24 and persisted to NP25 zone, whereas in the Rača zone in NP24 and NP25 respectively. In the northern part of the Magura Basin (Siary zone) the youngest deposits (so called Supra-Magura beds) belongs to NP24 zone (Oszczypko-Clowes, 2001). In the Grybów-Dukla units, the Krosno shaly facies belongs to NP25.

During the Late Oligocene (NP25/NN1), the frontal part of Magura Nappe thrust northwards onto the terminal Krosno flysch basin. The northwards thrusting of the Magura Nappe was accompanied by the formation of the piggy-back basin on the Magura Nappe, filled with the synrogenic turbidites of the Zawada and Kremná formations (NN1 and NN2 zones).

7. Conclusions

1. In the Magura Basin the youngest (terminal) flysch deposits belong to the Supra-Magura Beds, Malcov and Zawada/Kremná formations.

2. The deposition of the Supra-Magura Beds – glauconitic sandstones and massive marly mudstones took place in the deepest, northernmost part of the Magura Basin (Siary facies Zone). During the Late Oligocene (NP24/NP25 zones) this part of the basin was uplifted and transformed in the fron-

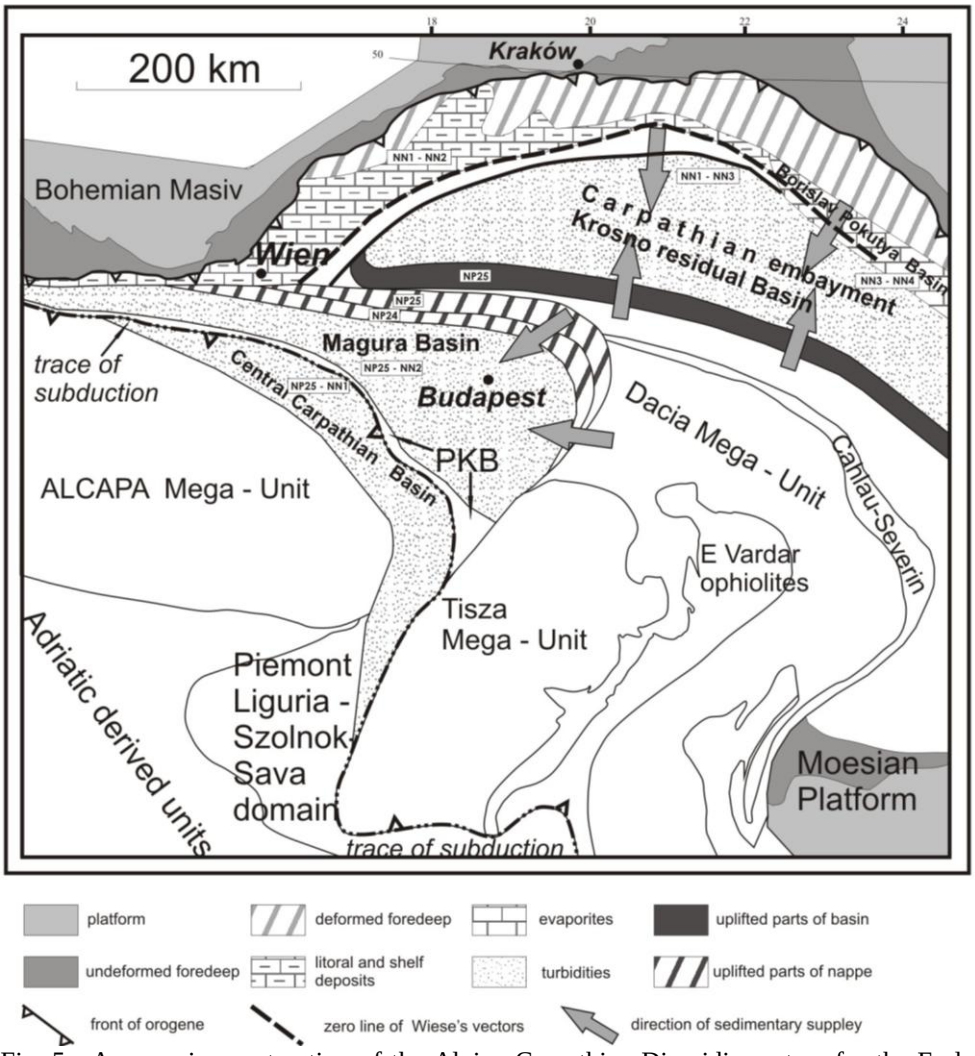

Fig. 5. A map-view restoration of the Alpine-Carpathian-Dinaridic system for the Early Miocene after Ustaszewski et al. (2008).

tal part of the Magura Nappe, overthrust upon the Fore-Magura Basin.

3. The Malcov lithofacies (Rača, ? Bystrica and Krynica facies zones) correspond to the Krosno synorogenic facies and display the same sedimentary development. The termination of the Malcov Formation took place in the Late Oligocene, NP24 and NP25.

4. The youngest deposits of the Magura Basin belong to the Zawada/Kremná formations are of Early Miocene age (NN1, NN2). This synorogenic turbiditic facies, characterized by the high content of carbonate clasts and reworking nanofossils, form the sedimentary infill of a piggy-back basin on the Magura Nappe.

Acknowledgments

The author is gratefully indebted to Dr. Eva Halásová, Dr. Lilian Švábenická and Prof. Dušan Plašienka for their constructive comments which greatly improved this paper.

References

Biolzi M., Műller C. and Palmieri G., 1981. Calcareous nannoplankton. In: In search of the Paleogene – Neogene boundary stratotype, part II, Gelati, R. and Steininger, F. (eds.). Revista Italiana Di Paleontologia i Stratigrafia, 89 (4), 460-471.

Bizon G. and Műller C., 1979. Remarks on the Oligocene/Miocene boundary based on the results obtained from the Pacific and the Indian Ocean. Ann. Geol. Pays Hellen., 1, 101-111.

Cieszkowski M., 1992**.** Marine Miocene deposits near Nowy Targ, Magura Nappe, Flysch Carpathians (South Poland). Geologica Carpathica, 43 (6), 339-346.

Fornaciari E. and Rio D., 1996. Latest Oligocene to Early Middle Miocene quantitative calcareous nannofossil biostratigraphy in the Mediterranean region. Micropaleontology, 42, 1-37.

Garecka M., 2008. The Oligocene/Miocene boundary based on calcareous nannoplankton, in Polish Outer Carpathians. Biuletyn PIG, 432 (in Polish)

Holcová K., 2002. Calcareous nannoplankton from the Eggenburgian stratotype and faciostratotypes (Lower Miocene, Central Paratethys). Geologica Carpathica, 53 (6), 381-390.

Holcová K., 2005. Quantitative calcareous nannoplan-kton biostratigraphy of the Oligocene/Miocene boundary interval in the northern part of the Buda Basin (Central Paratethys). Geological Quarterly, 49 (3), 263–274.

Koszarski L., Sikora W. and Wdowiarz S., 1974. The Flysch Carpathians. In: Maheľ M. (ed.), Tectonics of the Carpathian - Balkan regions. Geol. ústav D. Štúra, Bratislava, 180-197.

Krhovský J. and Djurasinovic, M., 1993. The nannofossil chalk layers in the Early Oligocene Stibořice Member in Velké Němčice (the Menilitic Formation, Zdanice Unit, South Moravia): orbitally forced changes in paleoproductivity. Knihovnička Zemního Plynu a Nafty, 15, 33–53 (Hodonín).

Martini E., 1970. Standard Tertiary and Quaternary calcareous nannoplankton zonation. In: Proceedings 11 Planktonic Conference, Farinacci, A. (ed), Roma, 2, 739–785.

Martini E. and Worsley T., 1970. Standard Neogene calcareous nannoplankton zonation. Nature, 225, 289-290.

Martini E. and Műller C., 1986. Current Tertiary and Quaternary calcareous nannoplankton stratigraphy and correlations. Newsletter on Stratigraphy, 16 (2), 99-112.

Marunteanu M., 1992. Distribiution of the Miocene calcareous nannofossils in the Intra- and Extra- Carpathian areas of Rumania. In: Nannoplankton research.- Proec. Fourth INA Conf., Hamršmíd B. and Young J.,(eds), Prague, 1991, 247-262.

Melinte M., 1995. Changes in nannofossil assemblages during the Oligocene – Lower Miocene interval in the Eastern Carpathians and Transylvania. Abstracts 10th RCMNS, Bucharest 1995, Romanian Journal of Stratigraphy, 76, suppl., 7, 171-172.

Oszczypko N. and Oszczypko-Clowes M., 2002. Newly discovered Early Miocene deposits in the Nowy Sącz area (Magura Nappe, Polish Outer Carpathians). Geological Quarterly, 46 (2), 117-133.

Oszczypko N. and Oszczypko-Clowes M., 2009. Stages in the Magura Basin evolution – a case study of the Polish Sector (Western Carpathians). Geodinamica Acta, 22/1-3, 83-100.

Oszczypko N., Andreyeva-Grigorovich A., Malata E. and Oszczypko-Clowes M., 1999. The Lower Miocene deposits of the Rača Sub-Unit near Nowy Sącz (Magura Nappe, Polish Outer Carpathians). Geologica Carpathica, 50, 419-433.

Oszczypko N., Oszczypko-Clowes M., Golonka J. and Marko F., 2005. Oligocene–Lower Miocene sequences of the Magura Nappe and Pieniny Klippen Belt and adjacent Magura Nappe between Jarabina and the Poprad River (East Slovakia and South Poland) – their tectonic position and paleogeographic implications. Geological Quarterly, 49, 379-402.

Oszczypko-Clowes M., 2001. The nannofossils biostratigraphy of the youngest deposits of the Magura Nappe (East of the Skawa River, Polish flysch Carpathians) and their palaeoenviromental conditions. Annales Societatis Geologorum Poloniae, 71, 139-188.

Oszczypko-Clowes M., Oszczypko N. and Wójcik A., 2009. New data on the late Badenian–Sarmatian deposits of the Nowy Sacz Basin (Magura Nappe, Polish Outer Carpathians) and their palaeogeographical implications. Geological Quarterly, 53 (3), 273–292.

Perch-Nielsen K., 1985. Cenozoic calcareous nannofossils. In: Plankton Stratigraphy, Bolli, H., Saunders, J.S. and Perch-Nielsen, K. (eds), Cambridge University Press, 11, 427-554.

Picha F.J., Stráník Z. and Krejčí O., 2006: Geology and hydrocarbon resources of the Outer West Carpathians and their foreland, Czech Republic. In: The Carpathians and their foreland: Geology and hydrocarbon resources. Golonka J. and Picha F.J., (eds.), Mem. Amer. Assoc. Petroleum Geol., Tulsa 49—176.

Schulz H.M., Bechtel A. and Sachsendorfer R.F., 2005. The birth of the Paratethys during the Early Oligocene: From Tethys to an ancient Black Sea analogue? Global Planet Change 49, 163-176. doi:10.1016/j.gloplacha. 2005.07.001.

Švábenická L, Bubík M. and Stráník Z., 2007. Biostratigraphy and paleoenvironmental changes on the transition from the Menilite to Krosno lithofacies (Western Carpathians, Czech Republic). Geologica Carpathica,, 58, 3, 237-262

Ustaszewski K., Schmid S., Fügenschuh B., Tischler M., Kissling E. and Spakman W., 2008. A map-view restoration of the Alpine-Carpathian-Dinaridic system for the Early Miocene. Swiss Journal of Geosciences, 101/supplementary issue, 273-294.

Young J. 1998. Miocene. In: Calcareous nannofossil Biostratigraphy, Bown P. (ed.), Kluwer Academic Publishers, Dordrecht, 225-265.

Żytko K., Gucik S., Ryłko W., Oszczypko N., Zając R., Garlicka I., Nemčok J., Elias M., Menčík E., Dvořák J., Stráník Z., Rakús M. and Matějovská O., 1989. Geological map of the Western Outer Carpathians and their Foreland without Quaternary formation. In Poprawa D. and Nemčok J. (eds.), Geological Atlas of the Western Outer Carpathians. Państwowy Instytut Geologiczny, Warszawa.

Scientific Annals, School of Geology, Aristotle University of Thessaloniki Proceedings of the XIX CBGA Congress, Thessaloniki, Greece	Special volume 100	241-248	Thessaloniki 2010

PRELIMINARY RESULTS OF PROVENANCE ANALYSES OF EXOTIC MAGMATIC AND METAMORPHIC ROCK PEBBLES FROM THE EOCENE FLYSCH DEPOSITS OF THE MAGURA NAPPE (KRYNICA FACIES ZONE, POLISH OUTER CARPATHIANS)

Salata D. and Oszczypko N.

Jagiellonian University, Institute of Geological Sciences, Oleandry 2a, 30-063 Kraków, Poland
dorota.salata@uj.edu.pl; nestor.oszczypko@uj.edu.pl

Abstract: During the Late Cretaceous to Palaeogene, the Magura Basin was supplied by clastic material from source areas situated at the northern and southern margins of the basin, which are presently not outcropped at the surface. The northern source area is traditionally connected with the Silesian Ridge, whereas position of the southern one is still under discussion. The south-Magura source area supplied the Eocene pebbly paraconglomerates containing partly exotic material. The studied clastic material contains fragments of igneous and metamorphic rocks, derived from a continental type of crust, and frequent clasts of Mesozoic to Palaeogene deep and shallow-water limestones. Volcanites, rarely granitoids as well as schists, gneisses, quartzites and cataclasites were found in the group of crystalline exotic pebbles. Monazite ages of "exotic" pebbles from the Tylicz and Piwniczna-Mniszek sections document the Variscan age of metamorphic rocks. The provenance of these exotic rocks could be connected with the Eocene exhumation of the SE sector the Magura Basin basement or by supply of crystalline material from remote SE source area (Dacia and Tisza mega units).

Key words: exotic rocks, source areas, Magura Basin, stratigraphy and palaeogeography

1. Introduction

The Outer Carpathian flysch basins were supplied with clastics that were derived from external as well as internal source areas, sometimes referred to as "cordilleras" (Książkiewicz, 1962). Our palaeogeographic reconstructions of source areas are based on the investigations of sedimentary blocks and "exotic" pebbles that were transported into basinal areas by submarine gravity flows (see Książkiewicz, 1962). The Eocene deposits of the Krynica facies zone of the Magura Basin contain fragments of magmatic and metamorphic rocks, derived from a continental type of crust, and infrequent clasts of Mesozoic limestones. This clastic material is referred to as "exotic", since the original source areas are not cropping out in the neighbourhood of the Magura Basin at present surface. Mišík et al. (1991) suggested that carbonate material was derived from "the basement of the Magura Basin", that was exhumed during the Early/ Middle Eocene, but differs in composition from that of the adjacent Czorsztyn-Oravicum Ridge. Alternatively, the clastic material may have been derived from an Inner Carpathian type source area, located on the SE margin of the basin (e.g. tip of the ALCAPA Block, see Plašienka, 2000). The aim of this paper is to present preliminary results of the composition study of the Eocene igneous and metamorphic pebbles from conglomerates of the Krynica facies zones.

In the Krynica zone of the Magura Nappe (Fig. 1), the "exotic" conglomerates have been studied for many years (Jaksa-Bykowski, 1925; Mochnacka and Węcławik, 1967; Wieser, 1970; Oszczypko, 1975; Oszczypko et al., 2006, Olszewska and Oszczypko, 2010). The first detailed description of exotic pebbles from the Eocene deposits of the Beskid Sądecki Range (Krynica zone) were given by Oszczypko (1975). This author described granitoids, gneisses, phyllites and quartzites, with a relatively small amount of basic volcanic rocks and Mesozoic carbonates. The exotic carbonate material of the Strihovce Sandstone, an equivalent of

the Piwniczna Sandstone Member of the Magura Formation in Poland, have been studied by Mišík et al. (1991). These carbonates are repre-sentted by deep-water Jurassic-Lower Cretaceous sediments as well as fragments of shallow-water limestones of the Triassic, Upper Jurassic, Lower and Upper Cretaceous, Palaeocene and Lutetian age (Mišík et al., 1991).

2. Geological setting

The studied area is located in the south-eastern part of the Magura Nappe south of the boundary between the Bystrica and Krynica subunits (Fig.1). The Krynica facies-tectonic zone is composed of the Upper Cretaceous to Oligocene deposits (Birkenmajer and Oszczypko, 1989; Oszczypko and Oszczypko-Clowes, submitted). The oldest deposits are known from the Muszyna-Złockie area, 5 km west of Krynica. They consist of the Turonian-Maastrichtian, deep-water variegated shales (Malinowa Fm.) with sporadic intercalations of thin-bedded sandstones (Oszczypko et al., 1990). That formation passes upwards into strongly tectonized, medium to thin-bedded turbidites of the Maastrichtian/Paleocene to Lower Eocene (Szczawnica Fm.), which are rich in calcite veins. Higher up in the succession, thin-bedded turbidites occur (Zarzecze Fm.), with intercalations of thick-bedded Krynica sandstones and conglomerates of the Lower-Middle Eocene. In the Krynica area the youngest deposits of the Krynica facies zone belong to the thick-bedded sandstones of the Magura Fm. (Middle Eocene to Oligocene). The stratigraphic thickness of the Magura Nappe reaches at least 2.6 km. During overthrust movements and tectonic repetitions, the total thickness of the flysch deposits in the Krynica subunit increased up to 5.5-7.5 km, as shown by magnetotelluric investigations (Oszczypko and Zuber, 2002). The Bystrica and Krynica subunits contact along the sub-vertical thrust fault, which dips to the NE. Three NE-SW trending transversal faults cut both the Bystrica and Krynica subunit into several blocks.

The Late Cretaceous to Oligocene flysch formations of the Krynica succession were deposited in a deep-water basin (Oszczypko, 1992). Starting from the Early Eocene, the sedimentary processes in the southern part of the Magura basin were accompanied by growth of the accretionary wedge (Oszczypko and Oszczypko-Clowes, 2009). Gradual shallowing of the basin started during the Late Eocene. This was followed by folding and uplifting of the basin after the Late Oligocene/Early Miocene, and prior to the Late Miocene.

The current study shows that bodies of exotic conglomerates in the Krynica zone are rare. These

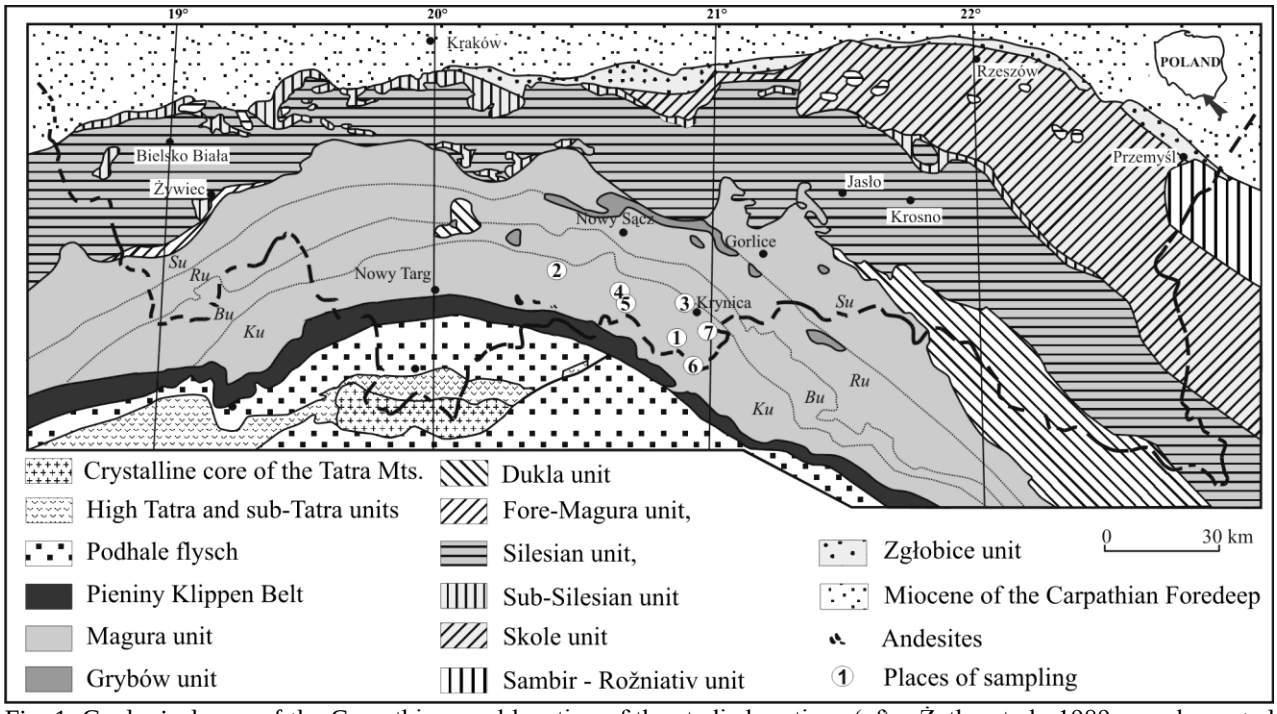

Fig. 1. Geological map of the Carpathians and location of the studied sections (after Żytko et al., 1989; supplemented and modified): Su - Siary, Ru - Rača, Bu - Bystrica, and Ku - Krynica subunits; sample locations: 1-Muszyna, 2-Zarzecze, 3-Łosie, 4-Rytro, 5-Mniszek-Piwniczna, 6-Leluchów, 7-Tylicz.

conglomerates are related to thick-bedded turbidites of the Szczawnica, Zarzecze and Magura formations. The exotic conglomerates of the Jarmuta-Proč Formation of the Grajcarek thrust-sheets, occurring along the contact zone between the Magura Nappe and Pieniny Klippen Belt, occupy a separate position (Birkenmajer, 1977; Birkenmajer and Wieser, 1990).

3. Materials and methods

In this paper, we have concentrated on investigation of the Krynica Sandstone Mb. of the Zarzecze Fm., Piwniczna Sandstone Mb. and Mniszek Shale Mb. of the Magura Formation. It must be mentioned that many of exposures described in literature in 70-ties and 80-ties do not exist today. Several dozens of pebbles were taken from each exposure. The Krynica Sandstone Mb. has been sampled in the Łosie, Muszyna and Zarzecze sections, while the Piwniczna Sandstone Mb. and Mniszek Shale Fm. have been studied in the Rytro, Piwniczna-Mniszek, Leluchów and Tylicz respectively (Fig. 1). Sandstones and conglomerates of the Krynica Mb occur within the thin-bedded flysch of the Zarzecze Fm. as one or more packages of 10 to 300 meters thick sediments.

Exotic rocks of the lower part of the Piwniczna Mb. are known from the Rytro area, whereas exotic conglomerates from the upper part of this member have been found in Piwniczna-Mniszek and Leluchów sections. They occur in a submarine slump body represented by pebbly mudstones. The Krynica and Piwniczna members display paleotransport direction from the south and south-east. The Tylicz conglomerates are underlain and overlain by the thin-bedded shally turbidites of the Mniszek Shale Mb. of the Magura Fm. (Oszczypko and Oszczypko-Clowes, submitted). The conglomerates and thick-bedded sandstones form two bodies 150 m and 50 m thick, which are separated by 50 m packet of thin-bedded flysch. These conglomerates represent a channel infill incised in thin-bedded turbidites (Olszewska and Oszczypko, 2010).

Among the whole spectrum of pebbles only those representing magmatic and metamorphic rocks were taken for analyses. EDS analyses were made using electron microscope (SEM) JEOL 5410 equipped with spectrometer Voyager 3100 (Noran) with accelerating voltage of 20 keV, spot size 7-9 µm and time of counting 100s were used during analyses and Cameca SX-100 with accelerating voltage of 15 keV, spot size 2-7µm. Measurements were performed at the State Geological Institute of D. Štúr in Bratislava, Slovakia. Quality analyses of micas, chlorite, apatite, epidote group and quantity analyses of feldspars, garnets, Fe-sulfides and oxides were made. Calculations of monazite ages were done according to Montel et al. (1996) using author's software DAMON. Geochemical analyses of main elements were made using ICP-ES and trace elements using ICP/MS methods. Immobile elements such as Y, Th, Zr, Ti, Nb were mostly used for classification of rocks and discrimination diagrams, especially for those rocks displaying alterations of minerals. It is to be mentioned that in many cases, the analysed pebbles were too small for geochemical analyses and very often they were altered which prohibited their proper microscopic identification and classification.

4. Results

4.1. Zarzecze Formation

Pebbles of magmatic and metamorphic rocks occurring in Zarzecze are small and usually do not exceed 3cm in diameter, while sedimentary rocks such as sandstones and limestones can reach 11cm. Pebbles from the Muszyna area are much smaller and do not exceed 6cm concerning sandstones and 2cm in case of magmatic and metamorphic rocks. Magmatic and metamorphic rocks comprise 18% and 21% of all pebbles in Muszyna and Zarzecze, respectively (Fig. 2). Among the plutonic rock pebbles from the Krynica Sandstone Mb from the Wilcze stream exposures near Muszyna and Zarzecze section, granitic rocks and aplites were identified. Between volcanic exotics, the following rocks were distinguished: 1) rhyolitic to dacitic rocks formed by feldspar phenocrysts settled in

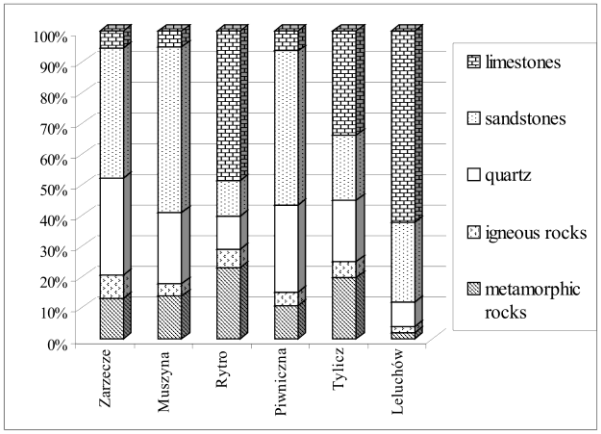

Fig. 2. Petrographic composition of the investigated exotic pebbles (in vol. %).

microcrystalline matrix composed of quartz, feldspars and single flakes of micas (Fig. 3A). Rutile, zircon, monazite, xenotime, apatite and pyrite occur in form of scattered crystals; pyrite also in small veinlets. Products of albitization, calcification and sericitisation are visible in the feldspar phenocrysts as well as in the matrix; 2) trachytic to andesitic rocks with phenocrysts of totally albitised feldspars and primary prismatic minerals (probably amphiboles) replaced by chlorite, epidote and quartz (Fig. 3B). The matrix is built of feldspars, quartz and anhedral minerals (primary biotite?) totally replaced by chlorite and scattered Fe-sulfides. A pebble composed of quartz and tourmaline with schörl-dravite composition, which could be a piece of granitic rock, was found as well.

Among metamorphic rock pebbles the following types were distinguished: 1) fine-blastic quartz-mica (muscovite) schists with sporadically occurring feldspars; 2) quartz-mica schists with biotite, albite, oligoclase ($Ab_{72-99}An_{0-20}Or_{0-9}$) and garnets ($Alm_{56-62}Grs_{19-28}$ $Adr_{9-13}Sps_{3-9}Prp_{0-3}$ in Muszyna and $Alm_{60-83}Adr_{2-18}$ $Sps_{1-15}Grs_{1-16}$ Prp_{1-9} in Zarzecze). In addition, minerals of epidote group, apatite, rutile, zircon and monazite were found there. Composition of garnets suggests that they formed under kyanite, sillimanite (for Zarzecze garnets) and garnet zone (Zarzecze and Muszyna) conditions; 3) gneisses built of quartz, K-feldspars, albite, oligoclase, biotite and garnet porphyroblasts ($Alm_{42-49}Grs_{24-36}Adr_{10-17}Sps_{8-12}Prp_{1}$), in some pebbles totally replaced by chlorite, micas and Fe-

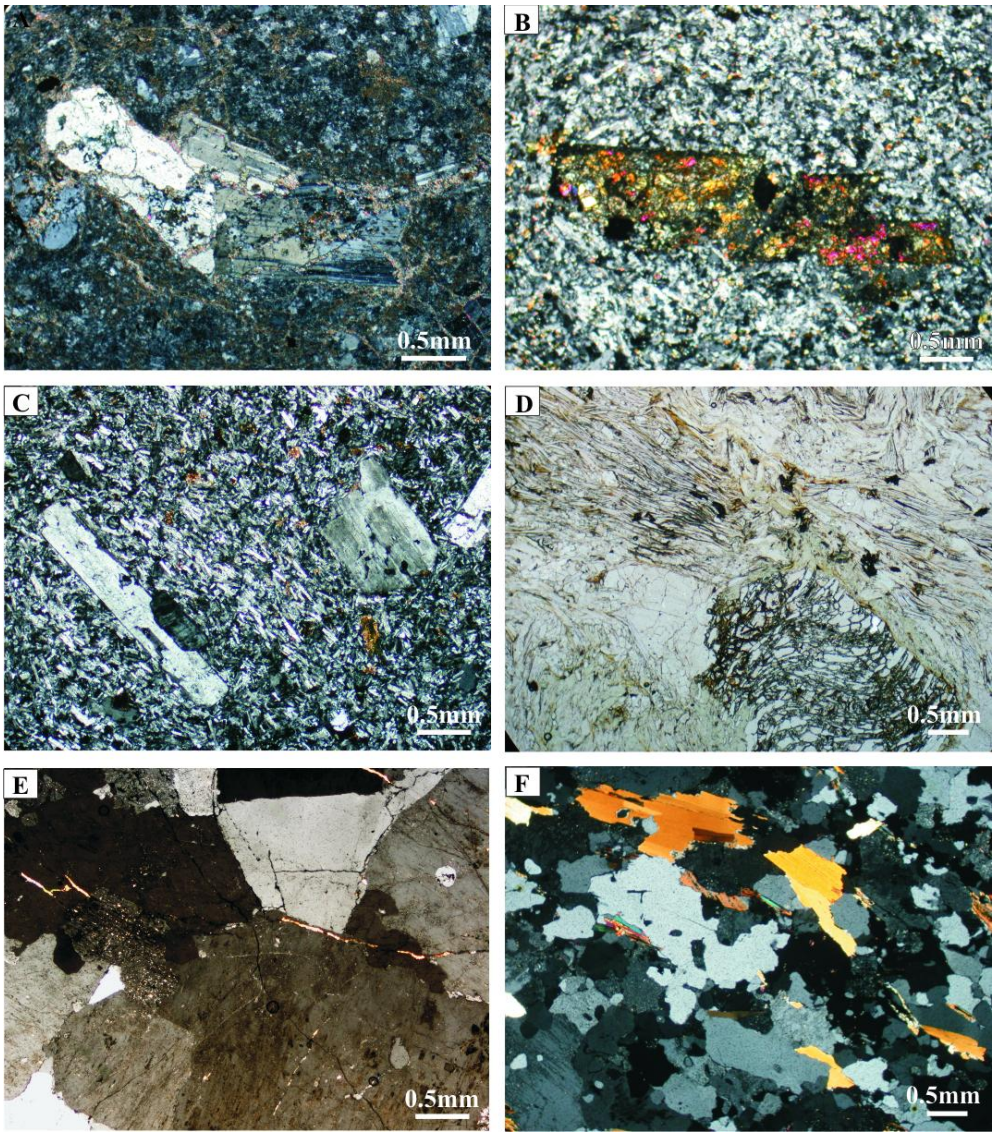

Fig. 3. Microphotographs of the main types of studied magmatic and metamorphic pebbles: A - rhyolitic to dacitic rock, Muszyna (*XPL*); B - trachytic to andesitic rock, Zarzecze (*XPL*); C - trachytic rock, Piwniczna (*XPL*); D - quartz-mica schist with garnets, Leluchów (*PPL*); E – granitic rock, Tylicz (*XPL*); F - fine-blastic gneiss, Tylicz (*XPL*).

oxides. Zircon, rutile and epidote were also found. Composition of garnets represent garnet zone.

The investigated conglomerate sampled in Łosie locality consists mainly of quartz pieces, metasediments and small fragments of schists. Their size does not exceed 0.5cm, sporadically reaching about 1cm.

4.2. Magura Formation - Piwniczna Member

Pebbles in the Piwniczna-Mniszek conglomerates usually reach 7 cm in size and in Leluchów 14 cm in size, from among which sedimentary pebbles (sandstones and limestones) are bigger than those of igneous and metamorphic origin. Among exotic rocks occurring in the Piwniczna-Mniszek and Leluchów localities, only few pebbles of volcanites and metamorphic rocks were found. They comprised 15 % in Mniszek and only 4% in Leluchów (Fig. 2). Among these volcanites we distinguished: 1) rhyolitic rocks with partly altered phenocrysts of $Or_{93-98}Ab_{2-5}An_{1-2}$ feldspars or rarely quartz. Microcrystalline matrix is composed of feldspars and quartz and sporadically micas, zircon, epidote, pyrite and secondary Fe-oxides; 2) trachytic rocks with phenocrysts of feldspars (Fig. 3C). The trachyte-like background is built of feldspars and rarely quartz. Secondary calcite is present as well.

Pebbles of metamorphic rocks are represented by: 1) fine-blastic quartz-mica schist composed of feldspars and biotite. Tourmaline, rutile, minerals

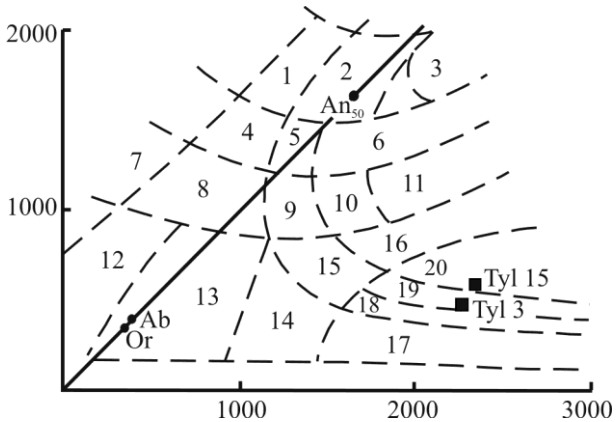

Fig. 4. Points reflecting composition of granitic rocks from Tylicz in the R1 *vs*. R2 diagram. R1=4Si-11(Na+K)-2(Fe+Ti), R2=6Ca+2Mg+Al (in milications) (de la Roche et al. 1980); numeration of fields: 1-Alkali gabro, 2-Olivine gabbro, 3-Gabbronorite, 4-Syenogabbro, 5-Monzogabbro, 6-Gabbro, 7-Essexite, 8-Syenodiorite, 9-Monzonite, 10-Monzodiorite, 11-Diorite, 12-Nepheline syenite, 13-Syenite, 14-Quartz syenite, 15-Quartz monzonite, 16-Tonalite,17- Alkali granite, 18-Syenogranite, 19-Monzogranite, 20-Grano-diorite.

of the epidote group, zircon, apatite and monazite are present as well. Monazites in schists from Piwniczna-Mniszek reach sizes in the range of 20-100 μm. They occur in spaces between main minerals as isolated subhedral grains. They are homogenous in terms of internal features, as well as chemical composition. The average calculated age is about 314±18 Ma (MSWD=1.11) (Fig. 6A). Further pebbles include 2) quartz-mica schists with garnets (Alm_{52-71} $Grs_{12-22}Sps_{0-16}Adr_{4-15}Prp_{3-8}$ in Leluchów and $Alm_{64-69}Sps_{12-17}Prp_{8-12}Adr_{5-10}$ in Mniszek), albite, oligoclase ($Ab_{87-98}An_{2-13}$) and K-feldspars ($Or_{96-97}Ab_{1-2}An_2$)(Fig. 3D). Composition of garnets suggest they crystallisation in conditions of kyanite and garnet zones. Garnets found in Leluchów display features of syntectonic rotation; 3) gneisses composed of quartz, $Ab_{93-98}An_{1-2}Or_{0-6}$ and $Or_{96-97}Ab_{1-3}An_{0-2}$ feldspars, micas, chlorite and accessory zircon and minerals of epidote group; 4) cataclasites; 5) metasandstones.

4.3. Magura Formation - Mniszek Shale Member

Pebbles of sedimentary rocks in the Tylicz conglomerates reach 16cm in size, while crystalline pebbles do not exceed 5cm. In this respect, the pebble population in Tylicz is similar to that found in the Leluchów section. magmatic and metamorphic rocks in Tylicz section compri-sed up to 25% of taken pebbles (Fig. 2). The most frequent pebbles are represented by metamorphic rocks such as schists and gneisses. Plutonic rocks of granite type are rare, while volcanic rocks were not found in this exposure. Two pebbles of plutonic rocks are composed of quartz, perthitic or microcline K-feldspar with $Or_{1-90}Ab_{10-95}An_{1-13}$ composition, subordinate muscovite-like mica and accessory zircon. Values of main elements (Tab. 1) indicate that they represent granitic rocks (Fig. 3E). The values of main cations allow to classify the rocks as monzogranites and granodiorites (Fig. 4). The calculated molar [Al/(Na+K+Ca/2)] para-meter exceeding 1.05 value for the studied grani-tes indicates an S-type of them (Pitcher 1982). The Y versus Nb proportions indicate that these granites represent volcanic-arc and syn-collisional granites, while relation (Y+Nb)/Rb fall allow to precise them as volcanic-arc granites (Fig. 5).

Among the metamorphic rocks in Tylicz, we have recognised: 1) fine-blastic gneisses (Fig. 3F) composed of feldspar, muscovite and biotite, quartz, garnet ($Alm_{68-70}Sps_{17-18}Adr_{8-10}Prp_{3-5}$, $Alm_{64-68}Sps_{16-19}$ $Prp_{8-10}Adr_{3-9}$ and $Alm_{43-71}Sps_{3-31}Grs_{3-20}$ Adr_{4-17}

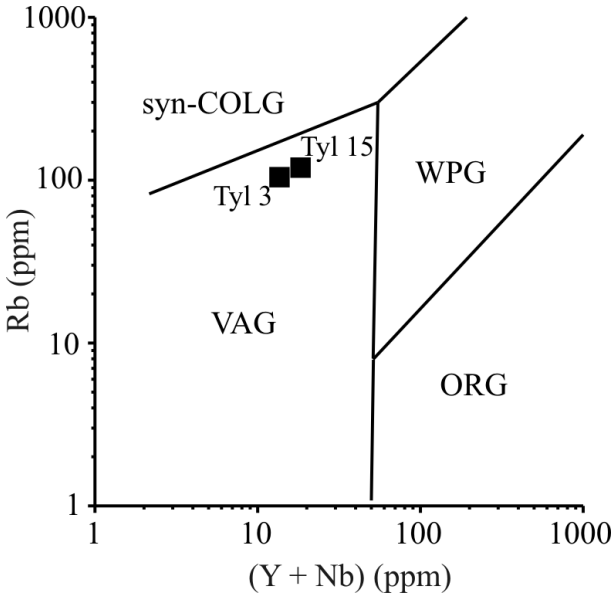

Fig. 5. Points reflecting composition of granites from Tylicz in the Rb *vs.* (Y+Nb) diagram (Pearce et al. 1984). VAG-volcanic-arc granites; syn-COLG-syn-collisional granites; WPG - within-plate granites; ORG-ocean-ridge granites.

Prp_{1-8}), zircon, monazite and apatite. Besides these, sillimanite fibrolites were found in one gneiss pebble. Composition of garnets indicates that they represent medium grade metamorphic conditions of kyanite and sillimanite zone. Monazite crystals are of 20-80 μm size and are present as subhedral isolated grains in spaces between the main minerals. Darker and lighter zones were visible in some grains, but they were homogenous considering U, Th and Pb values. Calculated ages for the monazites oscillate around 300 Ma isochrone. The average age of monazite grains is 303±2 Ma (MSWD 0.96); 2) fine-blastic quartz-mica schists consisting of quartz, $Or_{1-92}Ab_{8-94}An_{1-20}$ feldspars, micas of phlogopite and phengite composition and chlorites. Additionally apatite, zircon (sometimes as inclusions in biotite), rutile, monazite and garnets of $Alm_{42-65}Sps_{16-25}Adr_{6-8}Prp_{5-6}$ and $Alm_{65-67}Sps_{20-22}Adr_{6-9}Prp_{5-6}$ composition suggesting similar conditions as mentioned above. Monazite grains are smaller than those found in gneisses and are 15-30μm in size, but other features are similar. Monazites are compositionally homogenous and the calculated ages generally oscillate around 300 Ma, with average value of 314±2 Ma (MSWD 1.11)(Fig. 6B).

5. Discussion and conclusions

1. In the Palaeogene deposits of the southern part of the Magura Nappe (Krynica Zone), the exotic pebbles have been recognized in two stratigraphical positions:

   a) in the thick-bedded sandstones of the Krynica Sandstone Mb (Zarzecze Fm., Lower/Middle Eocene) and the Piwniczna Sandstone Mb. (Lower/Middle Eocene) of the Magura Fm. and its equivalent - the lower part of Strihovce Sandstone (see Nemčok 1990 a, b; Mišík et al. 1991). These conglomerates are rich in granitoids, medium grade metamorphic gneisses and schists, phyllites and quartzites, with a relatively small amount of felsic and intermediate volcanic rocks and Mesozoic carbonates (Oszczypko, 1975; Mišík et al., 1991; Oszczypko et al., 2006; this paper).

   b) in the thick-bedded sandstones and conglomerates of the Mniszek Shale Mb. (Upper Eocene - ?Oligocene) of the Magura Fm. (see the Tylicz Conglomerate in Olszewska and Oszczypko, 2010) and the upper part of the Strihovce Sandstone (Mišík et al. 1991). Population of pebbles in Tylicz is rich in medium grade metamorphic rocks such as

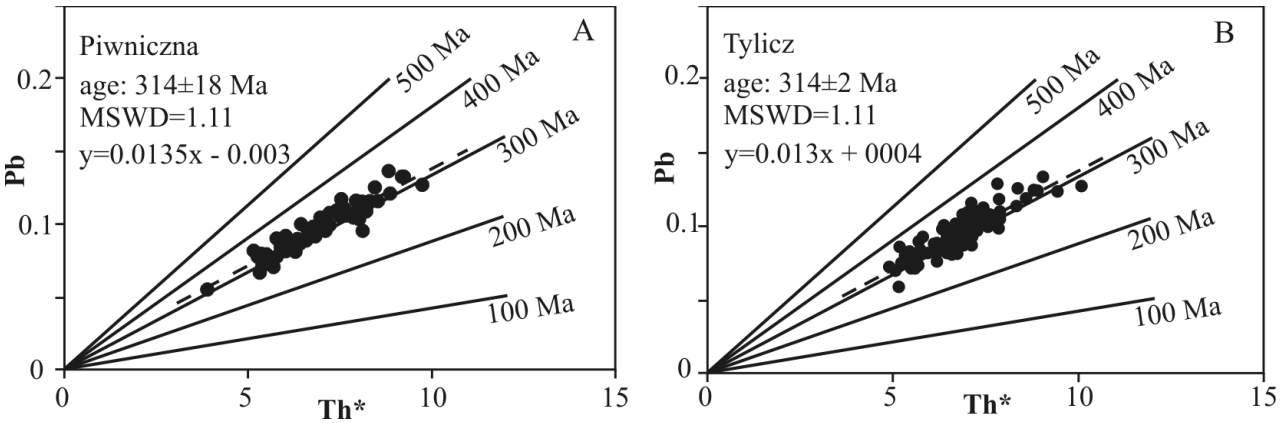

Fig. 6. Isochrones of the analysed monazite ages: A – Piwniczna (Piwniczna Member); B –Tylicz (Mniszek Shale Member).

gneisses and schists and poor in igneous rocks. Contrary to older conglomerates (see point a), no volcanic pebbles are present in the collected population of pebbles in Tylicz. The composition of carbonate material and microfossils assemblages of the Tylicz Conglomerate (Late Eocene – Oligocene) indicates similarity to both to the Jarmuta/Proč and Strihovce exotic pebbles (Olszewska and Oszczypko, 2010).

2. Metamorphic rocks found in all sampled conglomerates are similar and correspond to medium grade metamorphic conditions of epidote-amphibolite or amphibolite facies. Similar results were obtained on the basis of numerous analyses of detrital garnets found in the Jarmuta (Maastrichtian-Palaeocene) and Szczawnica (Palaeocene-Lower Eocene) Formations (Salata, 2004; Oszczypko and Salata, 2005). Monazite dates document the Variscan age of metamorphic rocks, what corresponds to earlier radiometric ages (Poprawa et al., 2004).

3. Plutonic rocks in Tylicz represent volcanic-arc granites and syn-collisional granites of S-type, which are well known from the Western Carpathians (e.g. Petrík et al., 1994; Broska and Uher, 2001). Such granites were also described as protoliths for Carpathian orthogneisses found as pebbles in Palaeocene flysch in the Dukla Nappe (Bąk and Wolska, 2005). According to Pitcher (1982) and Broska and Uher (2001) S-type granites are orogenic granites connected with continental collision. Low-pressure regional metamorphic rocks can accompany them (Pitcher, 1982).

4. The position of the source area for the investigated exotic pebbles is speculative. The obtained data suggest erosion and recycling, during the Late Eocene to Oligocene, material of an older accretionary wedge and deposition of detritus in the southern part of the Magura Basin. The supply of siliciclastic material from SE source area (Dacia and Tisza mega units) and carbonate material from S source area (ALCAPA Mega Unit: Central Carpathian Block and Pieniny Klippen Belt) is also possible. The latter solution can be deduced from the Oligocene?/Early Miocene pre-orogenic palaeogeographic restoration of the Alpine-Carpathian-Panonian realms (Ustaszewski et al. 2008).

Acknowledgement

Authors thank to Prof. Dušan Plašienka and Dr. Pavel Uher for detailed reviews and all critical suggestions. Thanks are also extended to Patrik Konečný from ŠGÚDŠ for calculations of monazite ages and technical support and to Dr. Anna Wolska for content-related discussion. This paper was financed by the Polish Ministry of Sciences and High Education (grant nr 2 P04D 002 28).

References

Bąk K. and Wolska A., 2005. Exotic orthogneiss pebbles from Palaeocene flysch of the Dukla Nappe (Outer Eastern Carpathians, Poland). Geologica Carpathica, 56, 3, 205-221.

Birkenmajer K., 1977. Jurassic and Cretaceous lithostratigraphic units of the Pieniny Klippen Belt, Carpathians. Studia Geologica. Polonica, 45, 1-159.

Birkenmajer K. and Oszczypko N., 1989. Cretaceous and Palaeogene lithostratigraphic units of the Magura Nappe, Krynica Subunit, Carpathians. Annales Societatis Geologorum Poloniae, 59, 145-181.

Birkenmajer K. and Wieser T., 1990. Exotic rock fragments from Upper Cretaceous deposits near Jaworki, Pieniny Klippen Belt, Carpathians, Poland Studia Geologica. Polonica, 97, 7-67 (in Polish with English summary).

Broska I. and Uher P., 2001. Whole-rock chemistry and genetic typology of the West-Carpathian Variscan granites. Geologica Carpathica, 52, 2, 79-90.

De La Roche H., Leterrier J., Grande Calude P. and Marchal M., 1980. A classification of volcanic and plutonic rocks using R1-R2 diagrams and major element analyses-its relationships and current nomenclature. Chemical Geology, 29, 183-210.

Jaksa–Bykowski Cz., 1925. Contribution to petrographic characteristic of the Magura flysch in the area of Krościenko on the Dunajec river. Archivum of the Mineralogical Lab of the Scientific Warsaw Society, 1, 123-130 (in Polish).

Książkiewicz M. (ed.), 1962. Geological Atlas of Poland. Stratigraphical-facies issues. Cretaceous and Lower Tertiary in Polish Outer Carpathians. Geological Institute, Warsaw. (In Polish with English abstract).

Mišík M., Sýkora M. and Jablonský J., 1991. The Strihovce Conglomerate and South-Magura Cordillera. Zapadné Karpaty, ser. geol., 14, 7-72. (In Slovak with English abstract).

Mochnacka K. and Węcławik S., 1967. Paleogene exotic rocks in the Paleogene of the Magura Nappe near Tylicz. Sprawozdania z Posiedzeń. Komisji PAN Kraków XI/ 2, 805-808 (In Polish with English abstract).

Montel M.J., Foret S., Voschambre M., Nicollet C. and Provost A., 1996. Electron microprobe dating of

monazite. Chemical Geology, 131, 37-53.
Nemčok J., 1990a. Geological Map of Pieniny, Ľubovnianska Vrchovina Highland and Čergov Mts. Geologický Ústav D. Štúra. Bratislava.
Nemčok J., 1990b. Explanations to the Geological Map of Pieniny, Ľubovnianska Vrchovina Highland and Čergov Mts. Geologický Ústav D. Štúra. Bratislava, 131 pp.
Olszewska B. and Oszczypko N., 2010. Geological position, sedimentary record and composition of the Tylicz Conglomerate (Late Eocene-Oligocene) - stratigraphical and paleogeographical implications (Magura Nappe, Polish Outer Carpathians). Geologica Carpathica**,** 61, 1, 39-54.
Oszczypko N., 1975. Exotic rocks in the Palaeogene of the Magura nappe between Dunajec and Poprad rivers, Carpathians, Poland. Annales Societatis Geologorum Poloniae, 45, 3-4, 403-431 (In Polish with English abstract).
Oszczypko N., 1992. Late Cretaceous through Paleogene evolution of Magura Basin. Geologica Carpathica, 43, 6, 333-338.
Oszczypko N., Dudziak J. and Malata E., 1990. Stratigraphy of the Cretaceous through Palaeogene deposits of the Magura Nappe in the Beskid Sądecki Range, Polish Outer Carpathians. Studia Geologica Polonica, 47, 109-181. (In Polish with English abstract).
Oszczypko N. and Zuber A., 2002. Geological and isotopic evidence of diagenetic waters in the Polish Flysch Carpathians. Geologica. Carpathica, 53, 4, 257-268.
Oszczypko N. and Salata D., 2005. Provenance analyses of the Late Cretaceous-Palaeocene deposits of the Magura Basin (Polish Western Carpathians)-evidence from a study of the heavy minerals. Acta Geologica Polonica, 55, 237-267.
Oszczypko N. and Oszczypko-Clowes M., 2009. Stages in Magura Basin: a case study of the Polish sector (Western Carpathians). Geodynamika Acta, 22/1-3, 83-100.
Oszczypko N. and Oszczypko-Clowes M., submitted. Lithostratigraphy and biostratigraphy of the Palaeogene to Lower Miocene deposits of the Beskid Sadecki Range (Magura Nappe, Western Flysch Carpathians, Poland). Acta Geologica Polonica.
Oszczypko N., Oszczypko-Clowes M. and Salata D., 2006. Exotic rocks of the Krynica Zone (Magura Nappe) an their paleogeographic significance. Geologia, 32, 1 21-45. (In Polish with English abstract).
Pearce J.A., Harris N.B.W., Tindle A.G., 1984. Trace element discrimination diagrams for the tectonic interpretation of granitic rocks. Journal of Petrology, 25, 956-983.
Petrík I., Broska I. and Uher P., 1994. Evolution of the West Carpathian granite magmatism: source rock, geotectonic setting and relation to the Variscan structure. Geologica Carpathica, 45, 283-291.
Pitcher W. S., 1982. Granite type and tectonic environment. In: Mountain building processes, Hsu K.J. (Ed.), Academic Press, London, 19-40.
Plašienka D., 2000. Paleotectonic controls and tentative palinspastic restoration of the Carpathian realm during the Mesozoic. Slovak Geological Magazine, 6, 2-3, 200-204.
Poprawa P., Malata T., Pécskay Z., Banaś M., Skulich J., Paszowski M. and Kusiak M., 2004. Geochronology of crystalline basement of the Western Outer Carpathians sediment source areas - preliminary data. Mineralogical Society of Poland - Special Papers, 24, 329-332.
Salata D., 2004. Detrital garnets from the Upper Cretaceous-Palaeocene sandstones of the Polish part of the Magura nappe and the Pieniny Klippen Belt: chemical constraints. Annales Societatis Geologorum Poloniae, 74, 351-264.
Ustaszewski K., Schmid S., Fügenshuh B., Tischler M., Kissling E. and Spakman W., 2008. A map-view restoration of the Alpine-Carpathian-Dinaridic system for the Early Miocene. Swiss Journal of Geosciences, 101, Supplementary Issue, 273-294.
Wieser T., 1970. Exotic rocks from the deposits of the Magura nappe. Bulletin of the Geological Institute, 235, 123-161.
Żytko K., Gucik S., Ryłko W., Oszczypko N., Zając R., Garlicka I., Nemčok J., Eliás M., Menčík E. and Stráník Z., 1989. Map of the Tectonic Elements of the Western Outer Carpathians and their Foreland. In: Poprawa D. and Nemčok J. (eds). Geological Atlas of the Western Outer Carpathians and their Foreland. PIG Warszawa, GUD Bratislava, UUG Praha.

Scientific Annals, School of Geology, Aristotle University of Thessaloniki Proceedings of the XIX CBGA Congress, Thessaloniki, Greece	Special volume 100	249-258	Thessaloniki 2010

RELATIONSHIP BETWEEN THE ?CRETACEOUS "BLACK SHALES" AND CRETACEOUS OCEANIC RED BEDS OF THE GRAJCAREK SUCCESSION-A GEOCHEMICAL APPROACH (PIENINY KLIPPEN BELT, WEST CARPATHIANS, POLAND)

Wójcik-Tabol P. and Oszczypko N.

Institute of Geological Sciences, Jagiellonian University, Oleandry 2a, PL-30-063, Kraków, Poland, p.wojcik-tabol@uj.edu.pl, nestor.oszczypko@uj.edu.pl

Abstract: In the Polish Outer Carpathians, the contact zone of the Magura Nappe and the Pieniny Klippen Belt is known as the Grajcarek Succession (Unit). This succession contains the "black flysch" deposits, with controversial age, overlain by the Cenomanian radiolarian shales (CRS), followed by the Turonian through Campanian variegated shales (CORB). All these deposits have been sampled. The major and trace elements were analyzed, as well as relation of trace metals with organic matter content (TOC) was recognized. The studies performed by authors reveal that deposition of the CRS took place under oxygen deficiency condition. The trace-element distribution characterizes the hemipelagic regime of sedimentation of both the upper portion of the "black flysch" (spotty shales) as well as the CRS, which were deposited during increasing sea-level. Enrichment in redox-sensitive elements match was probably due to scavenging by H_2S-rich pore fluids. It suggests that spotty shales and the CRS were deposited under very similar sedimentary conditions. During the Late Cretaceous, crucial change in oceanic sedimentation occurred in the Tethys. The Mid-Cretaceous "black shale" facies were passed into Upper Cretaceous oceanic red beds (CORBs).

Key words: "black flysch", CORB, Cretaceous, geochemistry, anoxic event, Magura Basin, Western Carpathians

1. Introduction

The organic matter-rich black shales in the Cretaceous intervals on a global scale resulted in the concept of „Oceanic Anoxic Events" (OAEs, Schlanger and Jenkyns, 1976.). Three OAEs were introduced for the Cretaceous: the Aptian/Albian OAE 1, the Cenomanian/Turonian OAE 2 and the Coniacian/Santonian. The OAE 1 was further divided into four distinct sub-events of oxygen deficiency separated by oxic conditions: Early Aptian OAE 1a, Early Albian OAE 1b, Late Albian OAE 1c and 1d (Arthur at al., 1990).

Records of the Mid-Cretaceous anoxic events have been found in many localities. In the Mediterranean part of the Tethys, they are related to epicontinental seas, and carbonate platforms (Kuhnt et al., 1990). In the Pieniny Klippen Belt (PKB) basin that is interpreted as the northern branch of the Tethys, OAEs records were described by many authors (Wójcik-Tabol 2006 with references therein).

The Mid-Cretaceous anoxic events developing in deep-water conditions of the trench basins are known from numerous localities, also from the Polish Outer Carpathians (Bąk, 2007; Wójcik-Tabol and Ślączka, 2009). A major change in oceanic sedimentation from mid-Cretaceous organic carbon-enriched deep-sea deposits to predominantly Upper Cretaceous oceanic red beds (CORBs) occurred during the Late Cretaceous in the Tethys. This palaeoenviron-mental reconstruction has been based on sedimentological, micropalaeontological and geochemical data (Hu et al., 2005).

The Grajcarek Succession of the PKB (Birkenmajer, 1977) contains the "black flysch" deposits (the Szlachtowa and Opaleniec forma-tions), overlain by the Cenomanian radiolarian shales (CRS) and CORB. A group of major and trace elements has been analyzed in this succession. The relation of trace metals with organic matter content (TOC)

was searched. The behaviour of the redox-sensitive elements in recent sediments has potential as the proxy indicator of physicochemical conditions of deposition environment. The new data derived from inorganic geochemistry might supply additional information useful in characterizing the basin in which the studied succession was formed.

The aim of our studies is to establish geochemical relationship between these deposits, and compare studied profiles with standard profiles in the Alpine-Carpathian region, which documented transition between the Lower and Upper Cretaceous deposits (e.g. Brumsack, 1986; Bąk, 2007; Wójcik-Tabol, 2006).

2. Geological Setting

The Małe Pieniny Mts. are located in the southern part of the Polish Western Carpathians, between the Dunajec River Valley on the west and Polish/Slovak state boundary on the east and south (Fig. 1). The studied area occupies the contact position between the Magura Nappe and the PKB. The boundary between the Magura Nappe and the PKB runs along the Grajcarek Stream (Fig. 1C). The Magura Nappe, situated north of stream is composed of the Palaeogene flysch deposits belonging to the Krynica facies-tectonic zone (Birkenmajer and Oszczypko, 1989). These deposits are composed mainly of thick- to medium-bedded turbidites of the canal-lobe provenance. Along the Grajcarek Valley, the Magura Nappe is in a contact with narrow, strongly deformed the Peri-PKB Zone, known as the Grajcarek Unit (Birkenmajer, 1979).

The Grajcarek Succession comprises Jurassic, Cretaceous and Palaeocene, pelagic and flysch depos-

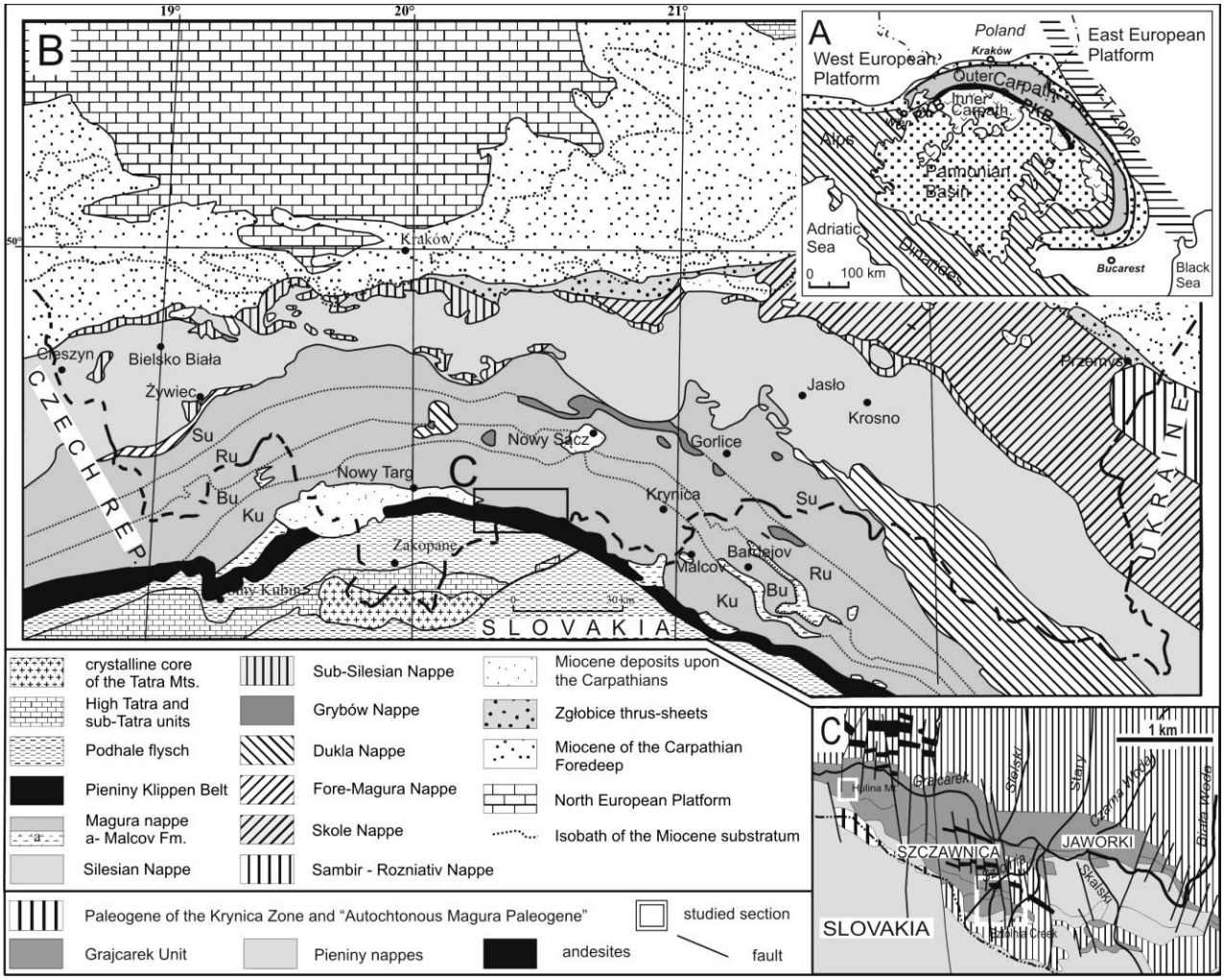

Fig. 1. Location of the studied area at the background of main geological units: A. Simplified tectonic scheme of the Alpine orogens; PKB – Pieniny Klippen Belt (after Kováč et al. 1998, modified); B. Central part of Polish Carpathians (after Oszczypko and Oszczypko-Clowes. 2009); C. Detailed division of the Małe Pieniny region (after Birkenmajer 1979, simplified).

its of the Magura Basin succession, incorporated in the structure of the PKB. The Szlachtowa and Opaleniec formations (black flysch) are up to 220 m thick. Their age, either Jurassic or Early Cretaceous, is a subject to a long-term controversy. Recently Oszczypko et al. (2004) presented new arguments to suggest the Albian-Cenomian age of these sediments, whereas Birkenmajer et al. (2008) support the idea of their Jurassic age.

This black flysch facies is followed by the 2-10 m thick Cenomanian radiolarian shales (CRS, Hulina Fm), variegated shales of the Turonian – Campanian Malinowa Fm. (20-100 m) and the coarse clastic deposits of the Jarmuta Fm (Maastrichtian – Paleocene) reaching 100-400 m (Birkenmajer, 1977). The thickness of the other pelagic formation is highly condensed and does not exceed 15m.

3. Studied Section

The studied exposures are located in the upper course of the Sztolnia Stream along a 250 m long cross-section (Oszczypko et al., 2004; Birkenmajer et al., 2008 and references therein), which comprise three sections (A, B and C; see Fig. 2). In the section Sztolnia A, the Szlachtowa Formation is represented mainly by dark-grey and black marly shales, claystones and siltstones (samples: 12/06, 13/06, 16/06, 17/06, SZT WOD-1, SZT WOD-2, 5/08, 14/08) and fine-grained, calcareous sandstones containing a lot of mica shining flakes (samples: KR 33, KR 34). This formation is overlain by the Opaleniec Fm composed of the light grey marly claystones with intercalations of spotty limestones and sideritic dolomites (samples: 1-2/06). In the Sztolnia section B, this formation is developed as a 20 m thick sequence of dark-grey, green-grey, blue-grey, sometimes fucoid spotty shales with pyrite concretions and intercalations of lenses and beds of grey spotty limestones and sideritic dolomites of a thickness not exceeding a few dozen centimeters (samples: 9-11/06, 6/08, 8/08, 9/08, 15/08, 17/08). The Opaleniec Formation is overlain by the CRS composed of manganese shales, radiolarian shales and radiolarites with pyrite framboids (samples: 3/06, 4/06, 8/06, 15/06;

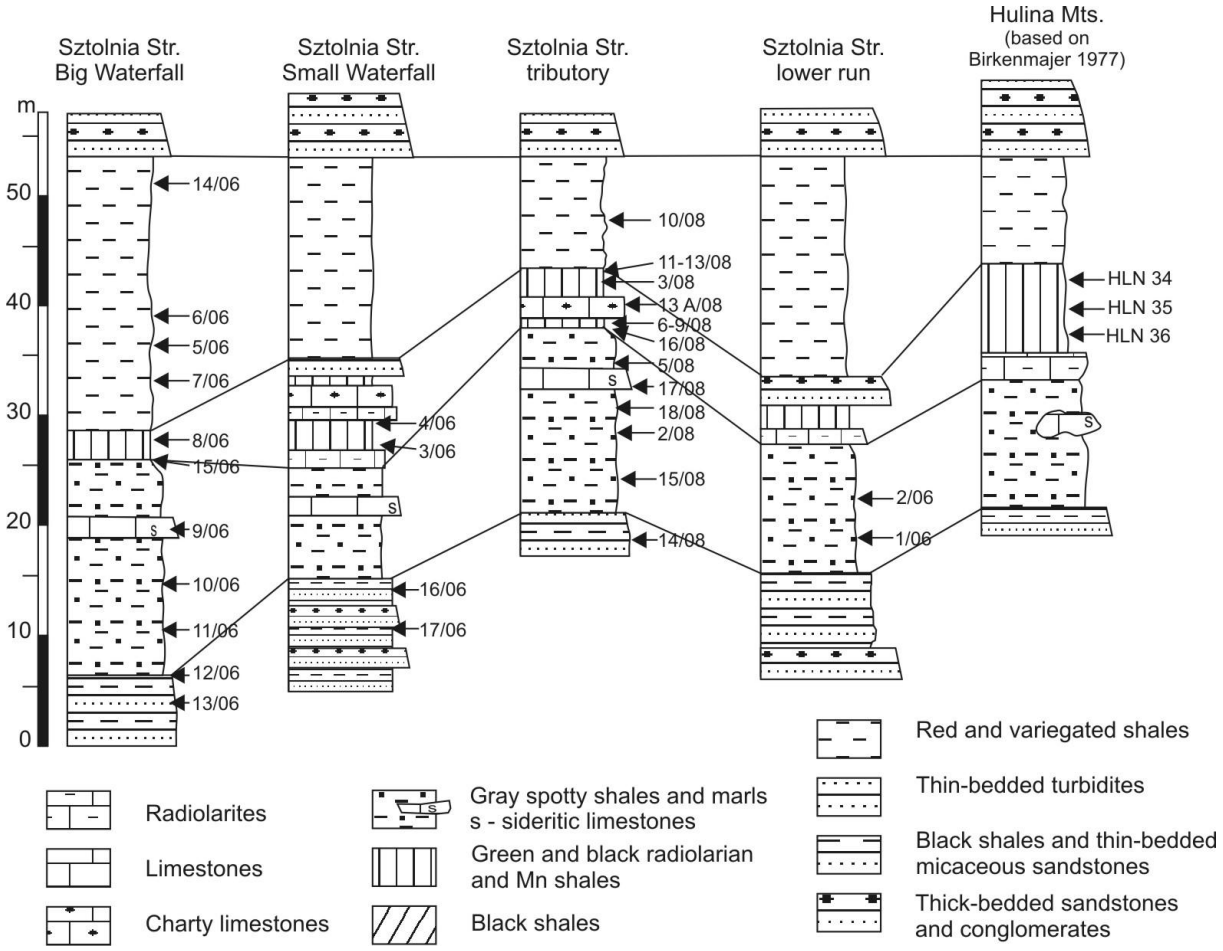

Fig. 2. Lithological log of the Sztolnia sections after Oszczypko et al. (in preparation), Hulina section after Birkenmajer and Gedl (2007), reinterpreted by Oszczypko et al. (in preparation).

3/08, 7/08, 11/08, 12/08, 13/08). These strata have been described by Birkenmajer (1977) as the Hulina Formation (Albian – Cenomanian).

In the Sztolnia Creek section A, C (see Fig. 2), the Cenomanian green shales are followed by non-calcareous, cherry-red and green argillaceous shales (14/06, 5-7/06) of the Malinowa Shale Formation (Birkenmajer, 1977; Birkenmajer and Oszczypko, 1989), whereas in the section B, the lower part of this formation is composed of massive cherry marls (sample 10/08). In the lowermost part of the Malinowa Fm. (section A), on the northern limb of a small anticline, we found a 1 m thick bed of light fine-grained sandstone conformably overlain by 10 cm of green radiolarite, whereas on the southern limb of the anticline, the red radiolarite (5 cm) occurs at top of cherty limestone (sample 22, see Oszczypko et al., 2004).

Additionally, the exposures on the S slope of the Hulina Hill (Fig. 2) have been sampled. The samples (HLN 34B, HLN 34G, HLN 35G, HLN 35A, HLN 35B, HLN 35 Mn, HLN 36G) represent the Hulina Formation.

4. Analytical methods

Microstructures, mineralogy and organic petrological features were investigated in thin-sections using optical microscopy - Nicon ECLIPSE, E 600 POL under transmitted and reflected light. The samples were studied by X- ray diffraction (XRD) both as bulk rocks and in clay fractions (<0.2 μm) separated from these rocks. The clay minerals were separated using the complete Jackson procedure, applied in order to dissolve carbonates and remove organic matter and iron oxides. They were studied as oriented preparations, sedimented on glass slides, both in air- dry and ethylene glycol saturated form. A Philips diffractometer, equipped with a Cu lamp, and a monochromator were used. The identification of clay minerals followed the method outlined by Moore and Reynolds (1989).

The amounts of major oxides were determined in 50 samples using inductively coupled plasma – optical emission spectrometry (ICP-OES). Trace-elements were determined by the inductively coupled plasma – mass spectroscopy (ICP-MS) using a Perkin Elmer Elan 6000 ICP at the ACME Analytical Laboratories, LTD, in Vancouver, Canada.

The amounts of major, minor and trace elements were normalized using Al as a detritus index.

5. Results

5.1. Microfacies and mineral composition

The samples of the Szlachtowa Fm. are represented by dark grey-black mudstones and paper shales. They are parallel laminated, barren of fossils. Rare grains of quartz and light mica occur within clayey or marly matrix. X-ray diffraction analysis defines the clay minerals as kaolinite, illite, smectite and lesser admixture of chlorite. Organic matter is represented by vitrinite.

The spotty marls of the Opaleniec Fm. contain mineral detritus (silty-sized quartz, feldspar, mica) dispersed within marly matrix. Based on XRD, composition of clay minerals appears similar to clay minerals of the Szlachtowa Fm. Calcareous tests (mainly echinoderm spines) are common. The dark spots are cross-section of ichnofossils. There is abundant amorphous organic matter associated with framboidal or massive pyrite.

The CRS from the Sztolnia A, B sections are full of radiolarian tests dispersed within a siliceous-clayey matrix. Clay minerals are represented by kaolinite, illite and traces of chlorite as well. The sulphides concretions are developed at the top of the layer. They have few mm in size. Internal core consists of radial crystals of iron sulphides encircled by euhedra of pyrite.

All of samples of the Hulina Fm., collected from the Sztolnia C section, reveal an abundance of radiolarian tests that are recrystalised by silica. Silica and clay minerals are major components of the matrix. Basing on XRD, clay minerals was identified as illite/smectite admixed with chlorite; presence of small amounts of kaolinite cannot be excluded. Scarce detritus is represented by silt-sized grains of quartz, feldspar and mica. The green shales (HLN 35G, HLN 36) contain higher amount of clay minerals and feldspar relative to black shales. Within ferrous shales (HLN 35A) a negligible amount of illite occurs, as one of clay mineral. Feldspar is absent. Black shales are enriched in organic matter that is developed as black and brownish amorphous matter.

The samples of the Malinowa Fm. are composed of calcite admixed with quartz and clay minerals, i.e. illite and chlorite.

Summing up, the clay mineral composition, lower part of the section (Szlachtowa and Opaleniec Fms) is enriched in kaolinite, the content of which diminishes upwards the section, contrary to in-

creasing amounts of illite and chlorite. Detrital minerals are present through the whole studied interval. Their minimal amounts were recognised in the siliceous shales and radiolarites of the Hulina Fm., but within the overlying Malinowa Fm. amounts of terrigenous material increase again.

5.2. Bulk sediment geochemistry

The chemistry of the studied samples is presented in the table 1. Chemical composition of the studied samples was compared to the standard siliciclastic deposits–Post-Archean Australian Shale (PAAS, Taylor and McLennan, 1985). Determined amounts of the redox-sensitive trace elements were additionally correlated with recent organic matter-rich deposits from the Black Sea and Gulf of California (Brumsack, 1989).

The major chemistry of sediments from the Gulf of California in principle reflects a mixture of terrigenous detritus with a PAAS- like composition and organic-derived silica material (plankton remains). The slight biogenic carbonate component is apparent as well (cf. Brumsack, 1989). The similarity of the Gulf of California deposits to the studied Hulina Fm. is supposed.

The Black Sea marls represent the mixture of detrital clays and biogenic carbonate (coccoliths) with varying amounts of organic matter (Brumsack, 1989). In present paper, they will be compared to the sediments of the Szlachtowa and Opaleniec Fms.

5.3. Detritus index vs. primary productivity

Comparing to PAAS, the tmajority of studied samples are enriched in CaO at the expense of SiO_2. The contents of Al_2O_3 are similar to PAAS. Only the Hulina Formation samples are relatively enriched in SiO_2. They seem to be analogous to upwelling sediments from the Gulf of California (Brumsack, 1989).

The major element composition of the studied material is shown in the triangular plot (SiO_2 – Al_2O_3 x 5 – CaO x 2, Fig. 3). This presentation is based on the assumption that marine sediments may be regarded as mixtures of three components: 1. aluminosilicates (represented by the Al_2O_3 and SiO_2 contents), 2. biogenic silica (partly represented by the SiO_2 contents), 3. biogenic carbonate (largely represented by the CaO contents). It seems to be evident from the diagram that the studied samples represent a mixture of terrigenous detrital material and biogenic silica with various amounts of carbonate, and resemble the Black Sea sediments. Majority of samples plots in the field near the PAAS. The CRS are shifted toward the SiO_2 corner like sediments of the Gulf of California. It suggests that siliceous shales contain the biogenic silica, however presence of diagenetic minerals (carbonate and chalcedony) is supposed. Biogenic derivation of silica finds confirmation in negative correlation between SiO_2 and Al_2O_3 (Fig. 4).

In the SiO_2 vs. Al_2O_3 diagram the correlation is positive for rest of samples. Data describing the Szlachtowa and Malinowa Fms are situated along one, short line. The samples from the Opaleniec Fm. resemble the rest of samples.

The TiO_2/Al_2O_3 diagram illustrates the positive correlation between oxides for all samples (Fig. 4). The samples of the Szlachtowa and Malinowa Fms co-draw line that is shifted towards higher values of TiO_2. The Opaleniec Fm. samples are located irregularly close to other samples.

Contents of TiO_2 in the studied samples are lower than that in the PAAS. The lowest concentration were determined in the Hulina Fm. (e.g. HLN 35 B and HLN 36 Mn or 8/06, 13A/08). TiO_2 distribution trough the Hulina Fm. is parallel to Zr pattern. The TiO_2 distribution through the Szlachtowa and Opaleniec Fms differs in some extent and correlation with Zr is irregular. The brownish-green, marly shale samples (2/08 and KR 33) are enriched of TiO_2, contrary to the clayey shales (calcareous 9-11/06 and non-calcareous 16/06), that are poor. TiO_2 enrichment can be related to presence of both: layered aluminosilicates and "heavy" minerals, whereas Zr occurs in zircon – typical "heavy" mineral. Relatively high and constant amounts of TiO_2 and Zr occur within the Malinowa Fm.

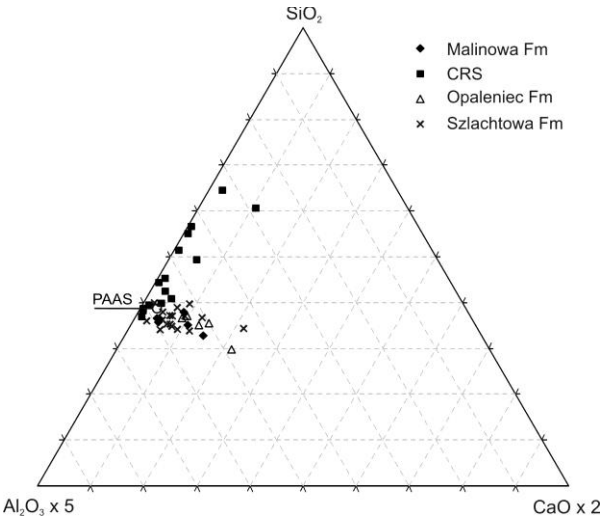

Fig. 3. Triangular plot SiO_2 – Al_2O_3 x 5 – CaO x 2.

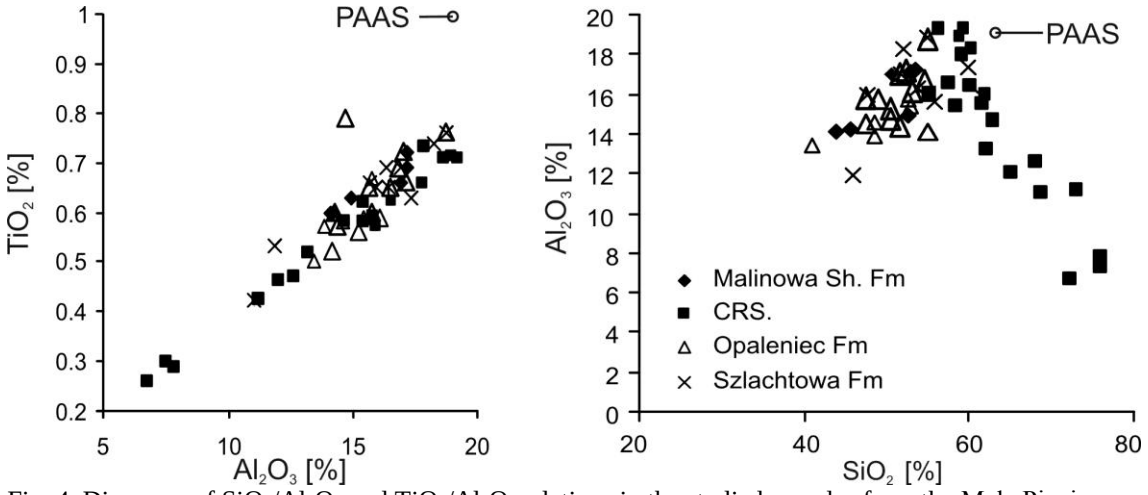

Fig. 4. Diagrams of SiO_2/Al_2O_3 and TiO_2/Al_2O_3 relations in the studied samples from the Małe Pieniny area.

Good correlations between SiO_2, Al_2O_3, K_2O and TiO_2, and correlation with the minor elements Zr, Rb and Nb in the sections depends on the detrital provenance of these elements. The bulk samples are characterised as mixtures of terrigenous-detrital matter comparable to PAAS with varying amount of calcium carbonate.

Variations in the element/Al ratios within the sections are indicative of varying inputs of quartz, heavy minerals and clay minerals. Lower part of the succession consists of abundant clay minerals associations dominated by kaolinite. The fine-grained samples of both: the Szlachtowa and Opaleniec Fms contain higher amounts of detrital quartz, mica and dense minerals. It is probable that the Opaleniec Fm. samples contain Ti-bearing layered aluminosilicates, because no correlation to other "immobile" elements is apparent. The CRS are poor of detrital components.

The studied samples display values of normalized K_2O about 0.2, like in PAAS. The K_2O contents strongly and positive correlate with Rb (r^2 equals 0.9) and K_2O/Rb ratio is constant (Fig. 5).

The investigated samples have the K_2O/Rb ratio similar to detritus derived from the upper continental crust (Plank and Langmuir, 1990).

All studied samples contain small amounts of P_2O_5. Values are rather constant (exception of micaceous sample, KR 33), slightly below that in standard PAAS and organic matter-rich sediments from Gulf of California and Black Sea.

A correlation between P_2O_5, SiO_2 and organic matter is visible in the Hulina Fm.. C, Si and P represent the major nutrient elements and their concentrations suggest an enhanced bioproductivity. Enrichment of Ba and high values of Ba/Sc ratio give evidence of productivity.

The contents of Ba in all studied samples are lower than those in the standard organic matter-rich sediments. Values of Ba are high in the siliceous samples of the Hulina Fm. (max. in HLN 34 B and HLN 35 B, 35 Mn) relative to the other samples. The Opaleniec and Szlachtowa Fms have the lowest contents of Ba. This pattern is followed by Ba/Sc. The highest values of Ba and Ba/Sc ratio were determined for the Hulina Fm. samples. They contain high amounts of Ba and low amounts of Sc. Downward the section (from the Malinowa Marl Fm. to the Szlachtowa Fm.), the Ba and Ba/Sc ratios decrease.

5.4. Redox conditions

The content of MnO and concentration of redox-sensitive elements (Mo, Cu, Ni etc.) are important

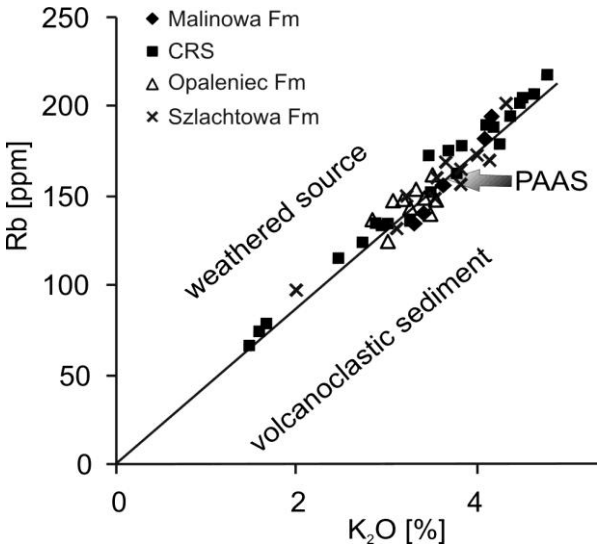

Fig. 5. K_2O vs. Rb diagram. The values of K_2O/Rb ratio in the studied samples are similar to that of the PAAS (McLennan et al., 1990).

Table 1. Major and trace element chemistry of the studied samples. <0.1 or <0.5 – below the detection limit.

			SiO_2	Al_2O_3	CaO	K_2O	TiO_2	P_2O_5	MnO	Ba	Ga	Nb	Rb	U	V	Zr	Y	La	Ce	TOT/S	Mo	Cu	Pb	Zn	Ni	As	Se	V/V+Ni	Ba/Sc	U/Th	TOC
			%	%	%	%	%	%	%	ppm	ppm	ppm	ppm	ppm	ppm	ppm	ppm	ppm	ppm	%	ppm	ppm	ppm	ppm	ppm	ppm	ppm				%
MALINOWA FM	red marls	SZT 10/08	50.49	15.29	6.98	3.69	0.56	0.1	0.2	257	19.9	11.9	168.5	1.9	124	99.5	33.3	34,0	67.5	0.02	0.2	21.6	13.5	80	89.4	1.6	0.5	0.58	18.35	0.15	nd
	red marly shales	SZT 14/06	52.89	17.14	3.34	4.15	0.72	0.125	0.1	304	21.1	14.6	194.4	2.7	153	136.7	28.8	36	74.4	<0.02	0.2	40.4	25.8	67	69.1	1.5	<0.5	0.69	19	0.19	nd
	red marly shales	SZT 5/06	45.57	14.23	7.19	3.41	0.6	0.123	0.14	297	18.4	13.3	147.9	3.1	107	120.8	23.8	28.5	55	<0.02	0.2	17.5	10	58	51.9	1.9	<0.5	0.67	24.75	0.29	nd
	pale calcareous sandstone	SZT 6/06	44.01	14.12	10.2	3.25	0.6	0.122	0.11	273	18.4	12.5	136.3	3.4	107	118.8	24.4	28.1	55.9	0.03	0.2	23.4	12.2	53	40	2.1	<0.5	0.73	19.5	0.29	nd
	red marly shales	SZT 7/06	53.46	17.19	2.89	4.09	0.69	0.14	0.11	302	22.8	14.5	181.3	3	124	128.6	27.4	32.9	65.9	<0.02	0.3	19.1	18.9	66	62.7	3.8	<0.5	0.66	20.13	0.23	nd
HULINA FM	olive-green radiolarian shales	HLN 34G	61.94	13.23	3.43	2.89	0.52	0.06	0.07	251	16.4	14.5	134.8	1.9	130	94.2	18.2	28.6	63.5	0.04	0.4	120.8	24.8	81	49.7	6.3	0.6	0.72	19.3	0.2	nd
	black radiolarite	HLN 34B	75.83	7.44	3.27	1.58	0.3	0.059	0.3	404	9.8	9.7	73.8	1.2	75	58.7	16.7	20.3	46.8	0.1	0.3	88.5	14.1	52	46.7	4.7	<0.5	0.61	50.5	0.21	nd
	green paper shales	HLN 35G	60.33	16.46	0.9	3.83	0.65	0.076	0.09	286	21.6	17.6	178.3	2.2	157	115	24	34	73.6	0.02	0.2	143	26.3	125	62.5	6.2	0.7	0.71	15.9	0.21	nd
	ferric paper shales	HLN 35A	68.7	11.02	0.65	2.46	0.42	0.066	0.38	291	14.6	11.5	115	1.8	106	80.8	16	23.8	74.6	0.04	0.3	139.9	21.7	111	181	10.5	0.7	0.37	24.25	0.25	nd
	black radiolarite	HLN 35B	72.07	6.7	6.7	1.47	0.26	0.06	0.37	222	9.3	7.4	65.8	1	71	50.3	16.7	17.3	40.9	0.18	0.3	107.5	16.4	44	39.3	4.4	0.6	0.64	31.7	0.22	nd
	manganiferrous radiolarite	HLN 35 Mn	76.05	7.77	1.74	1.66	0.29	0.099	1.2	317	11	7.2	78.2	1.4	67	51.3	25.8	27	68.6	0.13	0.5	104	16.8	56	104.7	6.5	<0.5	0.39	39.6	0.25	nd
	beige paper shales	HLN 36G	68	12.59	0.63	2.87	0.47	0.125	0.19	317	16.7	12	135.2	3	130	84.5	25.7	27.1	65.8	0.05	0.5	181.9	22.9	126	106.4	8.7	0.7	0.55	24.4	0.33	nd
	black siliceous mudstones	SZT 3B/08	55.44	15.91	0.07	3.72	0.59	0.09	0.02	282	22.1	11.8	174.7	6.1	202	104.6	21,0	27.2	53.5	2.04	9,0	95.4	48.8	66	89.2	210	5.3	0.69	18.8	0.59	3.26
	green siliceous shales	SZT 3/08-G	59.74	19.29	0.34	4.69	0.71	0.12	0.02	341	26.8	14.3	206.3	3.2	176	121.1	26.4	31.6	71	0.07	0.1	58.1	14.8	115	67.5	10.5	0.6	0.72	17.9	0.24	nd
	black siliceous shales	SZT 3/08-B	59.42	18.82	0.35	4.56	0.71	0.12	0.02	314	26.5	15.6	204.2	4.2	247	118.9	27.1	35.9	82.1	0.13	0.4	166,0	52.2	205	70.3	24.2	6,0	0.78	17.4	0.39	0.73
	black paper shales	SZT 7/08	56.74	19.16	0.78	4.3	0.71	0.14	0.04	338	25.1	14.5	178.4	5.9	253	119.7	25.9	28.7	62.3	0.58	1	97.7	174.1	92	82.4	36.1	8.1	0.75	18.8	0.47	0.59
	black paper shales	SZT 11/08-B	60.08	18.02	0.79	4.53	0.73	0.11	0.04	293	24,0	15.4	201.2	3	167	130.4	31,0	42.8	101.8	0.03	0.1	101.5	40.9	83	139,0	4.5	0.5	0.54	15.4	0.22	0.92
	green paper shales	SZT 11/08-G	59.75	17.97	1.1	4.84	0.66	0.08	0.04	287	25.8	13.7	217,0	2.5	158	115.9	27.8	36,0	83.8	0.02	0.2	125.3	38.1	64	96.6	3.5	0.5	0.62	15.1	0.21	nd
	green spotty cherts	SZT 12/08	62.25	15.93	1.86	4.42	0.57	0.07	0.06	225	21,0	12.7	194,0	2.2	139	106.6	22.2	30,0	68.8	0.04	0.1	117,0	40.1	31	35.4	2.1	0.5	0.79	15	0.19	0.09
	black micaous mudstones	SZT 13/08	63.4	14.73	1.15	3.55	0.58	0.05	0.06	284	19.1	13.2	159.4	3.7	172	103.9	20.1	31.7	71.3	0.54	1.4	190.9	79.7	367	72.5	34	0.5	0.7	18.9	0.39	1.24
	green radiolarite	SZT 13A/08	73.7	11.2	0.55	2.75	0.42	0.03	0.01	176	14.3	10.1	123.6	1.8	128	83.9	14.4	22.2	46.8	1.06	1.3	122.7	49.3	109	66.9	36	2.1	0.65	17.6	0.24	nd
	dark green spotty chert	SZT 8/06	65	12.02	3.61	2.93	0.46	0.058	0.1	246	14.2	11.5	132.8	1.9	100	80	16.6	23.1	49.4	1.18	1	170.8	24.1	84	92.3	111.9	0.6	0.52	20.5	0.25	nd
	green spotty shales with pyrite	SZT 3/06	57.68	16.56	2.59	4.19	0.62	0.069	0.1	225	19.6	15.2	188	2.4	126	102.5	23.4	35.3	84.1	0.39	0.4	74.8	10	62	40.8	1.4	<0.5	0.75	14	0.21	nd
	dark green spotty chert with pyrite concretions	SZT 4/06	61.72	15.45	0.57	4.1	0.62	0.072	0.03	216	19.8	16.4	189.2	2.5	150	105.7	22	33.9	71.8	1.88	5	138.5	56.5	277	79.1	16.9	2.2	0.65	14.4	0.26	nd
	dark green spotty chert	SZT 15/06	58.31	15.41	3.51	3.47	0.58	0.145	0.07	376	18.4	12.5	171.6	2.2	125	104.5	37.8	39.1	94.2	0.05	0.2	215	14	81	77.5	0.5	<0.5	0.62	22.1	0.19	nd
OPALENIEC FM	green marly shales	SZT 6/08	52.57	17.22	3.83	4.04	0.66	0.12	0.16	262	23.2	13.6	172.2	2.8	123	133.6	26.5	32.6	70.1	0.02	0.1	31.5	3.1	100	72.7	0.9	0.5	0.63	17.5	0.24	nd
	grey calcareous mudstone	SZT 8/08	53.09	16.17	4.33	3.53	0.59	0.11	0.14	298	21,0	12.4	147,0	9.2	295	104.6	25.9	31.1	68.6	0.77	0.5	61,0	163.1	85	90.1	43.8	4.7	0.76	18.6	0.83	nd
	green spotty. sideritic shales	SZT 9/08	54.55	16.62	3.65	3.87	0.65	0.09	0.14	271	21.9	13.7	164.6	2.8	135	117.9	24.9	28.2	59.2	0.02	0.2	35.6	7.5	84	71.3	1.3	0.5	0.65	16.9	0.24	nd
	brown marls	SZT 17/08	47.54	14.46	5.94	3.56	0.57	0.11	0.16	261	19.2	12.9	151.9	2.9	126	120.4	24.3	27.5	57.7	0.02	0.2	18.9	11.9	68	63.3	2.9	0.5	0.66	20	0.25	nd
	black shales	SZT 19/08	47.58	15.79	5.62	3.53	0.6	0.1	0.09	315	19.8	12.9	148.8	11.4	298	122.6	23.4	33.5	70.5	0.68	0.6	56.8	104.9	77	89.3	70.1	7.3	0.77	21	0.96	1.73
	grey-green. spotty marly shales	SZT 1/06	48.51	13.84	9.87	2.87	0.57	0.17	0.14	262	17.4	13.2	136.6	2.6	121	92.7	25.2	30.9	52	0.64	0.6	54.6	19.1	79	41	11.2	1.1	0.75	20.15	0.28	nd
	green spotty sideritic shales	SZT 2/06	52.68	15.73	6.37	3.18	0.67	0.105	0.1	222	20.5	14.9	147.4	2.8	125	101.9	18.5	28.5	50.5	0.26	0.6	56.5	19.9	69	30	6.6	0.9	0.8	14.8	0.28	nd
	grey-green. spotty marls	SZT 9/06	41.04	13.42	15.19	2.89	0.5	0.097	0.29	161	16.5	12.4	134.2	2.4	112	97.8	25.6	32	55.8	0.91	1.2	62.5	25.1	60	42.1	16.5	<0.5	0.72	13.4	0.22	nd
	blue-grey marly shales	SZT 10/06	48.61	14.57	8.77	3.02	0.58	0.08	0.13	178	18.3	14.1	134.2	4.6	127	110.6	25.5	31.3	56.6	3.6	7.5	55.3	36.2	95	61	27	1.9	0.67	13.7	0.44	0.17
	grey-green. spotty marls	SZT 11/06	52.88	15.4	6.76	3.32	0.59	0.072	0.19	184	18.3	15.4	153.6	2.5	113	112.6	22.2	33.6	64.1	0.4	0.1	37.5	12.7	66	37.6	3.4	<0.5	0.75	13.1	0.22	nd
SZLACHTOWA FM	black paper shales	SZT 12/06	53.74	16.35	5.06	3.49	0.69	0.104	0.09	273	18.9	15.4	150.9	3.2	141	134.9	22.8	33.2	60.5	0.87	7.5	56.2	34	62	47.5	21.9	1.2	0.75	17	0.29	0.66
	green marly shales	SZT 13/06	47.64	15.94	6.52	3.5	0.65	0.134	0.11	267	20.5	13.8	138.6	2.8	109	126.1	23.4	28.8	57.5	0.05	0.1	25.7	10.3	66	43.7	1.3	<0.5	0.71	19.1	0.26	nd
	green paper shales	SZT 16/06	59.8	17.37	1.41	4.33	0.63	0.104	0.06	253	22.4	13.7	201	2.2	135	107.5	25.9	35.3	81.2	0.03	0.1	105.6	41.8	55	55.1	0.6	<0.5	0.71	15.8	0.19	0.04
	black paper shales	SZT 17/06	52.1	18.24	4.61	3.77	0.74	0.109	0.08	226	22.3	15.9	161.9	2.6	155	114.6	20.4	33.2	62.5	1.08	1.7	61.5	20.5	101	57.5	39.6	0.8	0.73	13.3	0.23	nd
	brownish calcareous siltstone	KR 33	45.91	11.86	14.3	1.99	0.53	0.45	0.14	147	14.1	13.3	96.1	2.7	107	116.9	33.3	33.3	70	0.37	0.3	18.4	15.1	60	23.3	7.8	0.6	0.82	13.3	0.32	nd
	brownish calcareous mudstone with mica	KR 34	55.8	15.65	4.88	3.06	0.66	0.09	0.09	224	19.9	15.1	145.9	2.8	134	108.6	19.3	28.9	51.3	0.54	1	126.7	20.2	83	52.6	6.3	0.6	0.72	14.9	0.28	nd
	black paper shales	SZT WOD-1	55,00	18.79	2.23	4.18	0.76	0.1	0.05	238	23,0	17.5	169.4	3	163	131.6	23.2	38.3	77.2	0.73	0.5	67.3	22.9	88	57.6	30.1	0.6	0.74	14	0.23	0.71
	black paper shales	SZT WOD-2	51.63	16.94	5.6	3.44	0.69	0.19	0.06	211	20.2	16.2	139.8	2.9	137	123.1	27.2	32.9	63.9	1.18	1.1	61.8	23.8	91	75.3	47.7	1.1	0.64	13.2	0.27	nd
	grey marly shales with mica	SZT 2/08	50.7	14.71	6.33	3.21	0.79	0.1	0.07	288	18.8	14.8	137.1	2.8	122	208.9	27.4	31.7	64.1	0.02	0.4	30.5	13.1	69	58.2	1.7	0.5	0.68	19.2	0.25	nd
	black calcareous mudstones with mica	SZT 5/08	49.04	15.7	8.34	3.13	0.65	0.19	0.11	250	20.4	14.8	131.5	2.5	133	102.9	24.1	30.9	59.4	0.61	1.1	65.8	24.1	107	84.9	41.6	1.4	0.61	16.7	0.29	0.87
	black marly shales	SZT 14/08	51.76	14.31	9.19	3.03	0.6	0.12	0.14	189	17.5	13.9	123.5	2.4	115	103.6	19.6	27.9	50	0.73	1.3	55,0	21.7	95	56.9	29.8	1.1	0.67	14.5	0.26	0.66
	grey-green marly shales with mica	SZT 15/08	55.23	14.21	5.99	3.25	0.52	0.04	0.18	169	19.1	13.3	149.4	2	103	96.7	20.3	30.6	68.1	0.06	0.2	61.8	20.3	100	115.1	42.8	0.5	0.47	13	0.2	nd
	black paper shales	SZT 15/16-B	52.28	17.12	4.78	3.86	0.72	0.12	0.12	212	20.2	18.2	155.4	3.4	146	120.2	24.8	34.7	71.1	0.67	0.5	73.5	24.5	201	51.5	25.6	1	0.74	13.2	0.31	nd

indicators of redox condition during deposition. Trace metals could be incorporated into the sediment by reduction with H_2S and sulphides precipitation, or by absorption to organic particles under anoxic conditions, whereas Mn concentration requires the oxic conditions. Therefore, anoxic sediments are characterized by trace metal enrichment and Mn depletion.

The MnO contents vary in the studied sequence in a broad range. The strongest variation is visible between samples of the Hulina Fm. The MnO-poor, green shales co-occur with the manganiferrous shales. Generally, the Hulina Fm. samples are the most enriched of MnO relative to other samples. The Szlachtowa Fm. is the poorest in MnO. If the correlation between MnO and CaO occurs, presence of diagenetic Mn carbonates is supposed. In many samples contents of MnO correlates negatively with V/V+Ni ratio. Most of samples are characterised by values of V/V+Ni ratios above 0.6. The increased V/V+Ni ratio has been applied as an anoxic indicator (Lewan and Maynard 1982).

In the studied section, slight variation is evident in the U/Th profile. Values of the U/Th ratio are below one (mean values are about 0.25) and increase occasionally in the siliceous shales of the CRS and Opaleniec Fm. The U/Th ratio is positively correlated with V/V+Ni ratio and with organic matter accumulation, suggesting development of anoxic conditions during deposition of 3B/08, 13/08, 19/08 and others (Jones and Manning 1994). The samples 3/08-G, 3/08-B show high V/V+Ni ratio

and low U/Th. They are also enriched of Zr, Rb, TiO_2 that suggests an increased siliciclastic input. The black shales intercalations within the Opaleniec Fm (10/06) have lower values of V/V+Ni ratio, but high U/Th associated with high S content. It might be explained by precipitation of sulphides under disoxic conditions.

Absolute contents of the redox-sensitive trace elements in the studied material are similar to PAAS. Relative to the recent, organic matter-rich sediments from the upwelling area of the Gulf of California (see Brumsack 1989), the studied samples are enriched in most of trace elements, but poor in Mo, U, Ba. Concentration of trace elements in the Black Sea sediments is very high (see Brumsack 1989). Amounts of Cu, As, Pb in some samples (mainly CRS) are extremely high, even higher than that in the Black Sea sediments.

The Szlachtowa and Opaleniec Fms are characterized by slightly enhanced amounts of S correlating with accumulation of Mo, Se, As, V. Interestingly, distribution of Cu does not depend on S. The highest concentration of Cu is often associated with accumulation of Pb.

The CRS samples are the most enriched in trace elements . Some samples are enriched in S and trace elements (Mo, Cu, Pb, Zn, Ni and Co, As), while others, in spite of a low content of S, contain high amounts of Cu and Ni. Distributions of Ni and As are parallel, partly affected by concentration of S and/or organic matter (OM) (HLN 34B, HLN 35B).

The Malinowa Fm. is depleted in trace elements and S. Only 14/06 sample displays slightly increased amounts of Cu and Pb.

Irregular distribution of the trace metals is difficult to interpret in terms of redox conditions during deposition. The chemical composition of the studied samples might be altered by diagenetic processes, i.e. pyritization .

6. Discussion

The Outer Carpathian and PKB basins were situated in the northern part of the Western (Alpine) Tethys, therefore the studied sections resemble lithologicaly other Cretaceous successions of the western Tethys. In the Outer Carpathians black shales and mudstones of the Věřovice Beds were formed during the Barremian – Early Aptian. They were followed by the turbiditic sedimentation that directly preceded the Cenomanian radiolarian shales (Barnasiówka Radiolarian Shale Formation), overlain by the Turonian Variegated Shales (CORB). In the Grajcarek Succession, the CRS belonging to the Hulina Fm. are followed by red shales of the Malinowa Fm. (CORB), while black shales of the Opaleniec and Szlachtowa Fms might be correlated with the Early Creataceous black shale facies.

The chemical character of the Szlachtowa and Opaleniec Fms is similar Relative to the CRS, they are enriched in CaO associated with P_2O_5 and MnO. The Szlachtowa and Opaleniec Fms contain also high amounts of such elements as Ga, Nb, Zr, Rb and TiO_2 indicating a rise of the terrigenous supply.In terms of content of major oxides, they are similar to the Black Sea sediments. However, the contents of TOC and trace elements are not high enough. The Black Sea exemplifies the type locality for a stagnant, anoxic basin. Geochemical indicators do not allow interpreting the environment of the Szlachtowa and Opaleniec Fms by a direct interpolation to the model of anoxic basins. The Szlachtowa and Opaleniec Fms can be related to the Early Cretaceous OAE 1. Taking into account the mineral composition and geochemical indices, they can be compared to the upper part of the Kapuśnica Fm of the Niedzica Succession of the PKB (see Wójcik-Tabol, 2006).

The clay minerals assemblage within the Szlachtowa and Opaleniec Fms resemble those of the Albian Lhoty Fm. of the Silesian Nappe of the Outer Carpathian (Wójcik-Tabol and Ślączka, 2009).

The records of the Cenomanian/ Turonian Boundary (CTB) in the Polish Outer Carpathians have been recently investigated by Bąk (2007) and Wójcik-Tabol and Ślączka (2009). This CTB interval including OAE-2 is recognized as the Barnasiówka Radiolarian Shale Formation. In the Pieniny Succession of the PKB, the Cenomanian-Turonian OAE 2 is recorded as the Magierowa Member of the Jaworki Fm (Wójcik-Tabol, 2006). The studied CRS are comparable to the Barnasiówka Fm. and Magierowa Mb. The contents of major elements in the CRS are similar to those in the Gulf of California sediments. Extraordinary enrichment of sulphide forming metals may be explained by diagenetic pyritization.

The mid-Cretaceous black shales facies are replaced by the Upper Cretaceous oceanic red beds (CORB). They are distributed in a broad belt extending from the Caribbean across the Central At-

lantic, Europe to eastern Asia and record changing deposition conditions from anoxic/disoxic to oxic. The studied Malinowa Fm. samples are lithologically, geochemically and mineralogically similar to other CORBs (see Hu et al., 2005 and references therein).

7. Conclusions

Considering the lithological, mineralogical and geochemical characteristics, the Szlachtowa and Opaleniec Fms resemble the Věřovice Beds/Lhoty Fm. of the Outer Carpathians and upper part of the Kapuśnica Fm. of the PKB. Thus, they can be related to the Early Cretaceous OAE 1. It is supposed that studied sediments were formed under disoxic/anoxic environment of the stagnant basin. Trace metals were trapped into reactive organic matter and sulphides during sedimentation, and/or later due to diagenetic pyritization.

The studied Cenomanian radiolarian shales (CRS), like Barnasiówka Fm. and Magierowa Mb., record the OAE-2. The studied CRS resample recent sediments of the upwelling area (Gulf of California). The CRS are interpreted as settled through the mid-water oxygen minimum zone. The periods of anoxia were interrupted by intervals of disoxic conditions at the sea bottom, related to changes in surface productivity and fluctuations in bottom water circulation. The enrichment of trace elements may be explained by diagenetic pyritization.

Analysis of the detrital flux revealed that the material supply to hemipelagic sediments was mainly derived from a continental crust. Upward the section, detrital input decreases, reaching its minimum in the CRS and then it increases in the Malinowa Fm.

Deposition of the Malinowa Fm. might have been influenced by several processes: excess of organic carbon burial, global cooling, and/or intensification of bottom circulation. It is possible, that the Malinowa Fm. was developed under analogous conditions.

Acknowledgments

This work has been supported by the Polish Ministry of Science and Higher Education (grant 2 PO 4D 080 29 to PWT and grant 1997/PO1/2006 to NO).

References

Arthur M.A., Brumsack H.J., Jenkyns H.C. and Schlanger S.O., 1990. Stratigraphy, geochemistry and paleoceanography of organic carbon-rich Cretaceous sequences. In, R.N. Ginsburg and B. Beaugoin (eds.), Cretaceous Resources, Events and Rhythms, Elsevier; Amsterdam, 75-119.

Bąk K., 2007. Environmental changes during the Cenomanian–Turonian Boundary Event in the Outer Carpathian Basins, a synthesis of data from various tectonic- facies units. Annales Societatis Geologorum Poloniae, 77, 171–191.

Birkenmajer K., 1977. Jurassic and Cretaceous lithostratigraphic units of the Pieniny Klippen Belt, Carpathians, Poland. Studia Geologica Polonica, 45, 1-159.

Birkenmajer K., 1979. Geological guide to the Pieniny Klippen Belt (in Polish). Wydawnictwa Geologiczne, Warszawa, 3–236.

Birkenmajer K. and Oszczypko N., 1989. Cretaceous and Palaeogene lithostratigraphic units in the Magura Nappe, Krynica Subunit, Carpathians. Annales Societatis Geologorum Poloniae, 59, 145-181.

Birkenmajer K. and Gedl P., 2007. Age of some deep-water marine Jurassic strata at Mt Hulina, Małe Pieniny Range (Grajcarek Unit, Pieniny Klippen Belt, West Carpathians, Poland) as based on dinocysts. Studia Geologica Polonica, 127, 51-70.

Birkenmajer K., Gedl P., Myczyński R., Tyszka J., 2008. "Cretaceous black flysch" in the Pieniny Klippen Belt, West Carpathians, a case of geological misinterpretation. Cretaceous Research. 29, 3, 535-549.

Brumsack H.J., 1986. The inorganic geochemistry of Cretaceous black shales (DSDP 41) in comparison to modern upwelling sediments from the Gulf of California. Geol. Soc. Spec. Publ., 21, 447-462.

Brumsack H.J., 1989. Geochemistry of recent Corg.-rich sediments from the Gulf of California and the Black Sea. Geol. Rundschau, 83, 851-882.

Hu X., Jansa L., Wang C., Sarti M., Bąk K., Wagreich M., Michalik J., Soták J., 2005. Upper Cretaceous oceanic red beds (CORBs) in the Tethys, occurrences, lithofacies, age, and environments. Cretaceous Research, 26, 3-20.

Jones B. and Manning D., 1994. Comparison of geochemical indices used for the interpretation of palaeoredox conditions in ancient mudstones. Chemical Geology, 93, 111–129.

Kováč M., Nagymarosy A., Oszczypko N., Ślączka A., Csontos L., Marunteanu M., Matenco L. and Márton E., 1998. Palinspastic reconstruction of the Carpathian-Pannonian region During the Miocene, In: Rakús, M. (ed.), Geodynamic development of the Western Carpathias. Slovak Geol. Surv., Bratislava, 189-217.

Kuhnt W., Herbin J. P., Thurow J.W. and Wiedmann J., 1990. Distribution of Cenomanian-Turonian organic facies in the western Mediterranean and along the Adjacent Atlantic Margin, AAPG Stud. in Geol., 30, 133-160

Lewan M. and Maynard J., 1982. Factors controlling enrichment of vanadium and nickel in the bitumen of organic sedimentary rocks. Geochimica et Cosmochimica Acta, 46, 2547-2560.

McLennan S.M., Taylor S.R., McCulloch M.T. and Maynard J.B., 1990. Geochemical and Nd-Sr isotopic composition of deep-sea turbidites, crustal evolution and plate tectonic associations. Geochimica et Cosmochimica Acta, 54, 2015-2050.

Moore D.M. and Reynolds Jr. R.C., 1989. X-Ray Diffraction and the Identification and Analysis of Clay Minerals. Oxford Univ. Press, Oxford. 332 pp.

Oszczypko N., Malata E., Švábenická L., Golonka J., Marko F., 2004. Jurassic-Cretaceous controversies in the Western Carpathian Flysch, the "black flysch" case study. Cretaceous Research. 25, 1, 89-113.

Oszczypko N. and Oszczypko-Clowes M., 2009. Stages in the Magura Basin: a case study of the Polish sector (Western Carpathians). Geodinamica Acta, 22/1-3, 83-100.

Oszczypko N., Malata E. and Olszewska B., in preparation. Lithostratigraphy and biostratigraphy of the Cretaceous flysch deposits in the Beskid Sadecki Range (Krynica and Grajcarek Subunits, Magura Nappe,Western Flysch Carpathians, Poland).

Plank T. and Langmuir C.H., 1998. The chemical composition of subducting sediment and its consequences for the crust and mantle. Chemical Geology, 145, 325-394.

Schlanger S.O. and Jenkyns H.C., 1976. Cretaceous oceanic anoxic events: causes and consequences. Geologie en Mijnbouw, 55, 179-184.

Taylor S.R. and McLennan S.M., 1985. The Continental Crust: its Composition and Evolution. Blackwell Scientific Publications, Oxford.

Wójcik-Tabol P., 2006. Organic carbon accumulation events in the mid-Cretaceous rocks of the Pieniny Klippen Belt (Polish Carpathians) - a petrological and geochemical approach. Geological Quarterly (Warszawa), 50, 4, 419-437.

Wójcik-Tabol P. and Ślączka A., 2009. Provenance and diagenesis of siliciclastic and organic material in the Albian-Turonian Sediments (Silesian Nappe, Lanckorona, Outer Carpathians, Poland): preliminary studies. Annales Societatis Geologorum Poloniae, 79, 53-66.

Special Session S13
Neogene palaeoenvironmental reconstructions and climatic records in South-Eastern Europe

Scientific Annals, School of Geology, Aristotle University of Thessaloniki Proceedings of the XIX CBGA Congress, Thessaloniki, Greece	Special volume 100	259-268	Thessaloniki 2010

PLANKTONIC FORAMINIFERAL BIOSTRATIGRAPHY AND PALAEOENVIRONMENTAL IMPLICATIONS OF A MIDDLE MIOCENE TRANSGRESSIVE SEQUENCE ON THE IONIAN ZONE OF LEVKAS ISLAND, IONIAN SEA, GREECE

Antonarakou, A., Drinia, H., Kontakiotis, G.

Department of Historical Geology and Palaeontology, Faculty of Geology and Geoenvironment, University of Athens, Panepistimiopolis 15784, Athens, Greece, aantonar@geol.uoa.gr, cntrinia@geol.uoa.gr, gkontak@geol.uoa.gr

Abstract: Asprogerakata section, located in the northeast part of Levkas Island, Ionian Sea, consists of well-bedded grey-brown calcareous sandstones and silty to sandy marls and represents part of the Miocene transgressive cover of the Ionian zone. Biostratigraphic data and palaeoenvironmental conditions are inferred based upon the planktonic foraminifera. A rich, highly to moderately diverse and well preserved planktonic foraminiferal association enabled biostratigraphic zonation of the Lower-Middle Miocene deposits. On the basis of the composition of the foraminiferal assemblages, palaeoecological and palaeoclimatic interpretations have been made. Quantitative and qualitative analyses provide a detailed distribution of the identified taxa and defined a number of bioevents for the Middle Miocene. The recognition of the first Acme End (AaE) of *Paragloborotalia siakensis* proved that the neogene deposits in Levkas Island have an age of 15.435 Ma and belong to the MMi4 planktonic foraminiferal zone. The MMi4c-MMi4d boundary has been defined by the presence of *Praeorbulina glomerosa circularis* dated at 14.89 Ma. Planktonic foraminiferal assemblages identify a significant change in variability of climate system at around 15.2 Ma, probably corresponding to the global cooling events superimposed to the Middle Miocene Climatic Optimum. In particular, faunal composition suggests a warmth phase in the lower part of the section followed by a cooling phase.

Key words: planktonic foraminifera, Middle Miocene, Eastern Mediterranean

1. Introduction

Levkas Island belongs to the Ionian Islands, which are located in the west segment of the Hellenic Arc, the most active plate margin of the Mediterranean region. The tectonic setting of the wider area is determined by the continental collision between northwestern Greece in the east and the Apulian platform in the west, as well as by the subduction of the African plate under the Aegean microplate along the active Hellenic Arc in the southwest. The Ionian Islands are situated in a transitional zone between the northwestern end of this active subsidence and the continental collision in the north.

The Ionian Islands form part of the para-autochthonous Apulian foreland of the Hellenide orogen and include rocks of the Pre-Apulian (or Paxos) and Ionian isopic zones (Aubouin, 1965; Underhill, 1989).

The Ionian zone represents one of the major tectonic lineaments within Apulia (Adria), and was situated at the southern margin of Neo-Tethys Ocean during Mesozoic times. Palaeogeographically, the Ionian zone originated as a deep-water basin when a pre-existing carbonate platform collapsed during Early Jurassic crustal extension. Early Jurassic syn-sedimentary faulting gave rise to intrabasinal differentiation, which resulted in basinal successions with continuous sedimentation, and reduced sequences deposited on intrabasinal swells, punctuated by stratigraphic gaps (IGRS-IFP, 1966). Pelagic sediments (mainly carbonates, but also argillaceous and siliceous) with local intercalations of cherts and shales accumulated up to Eocene time in a depositional environment remote from any major siliciclastic input. The transition into flysch-type sedimentation took place during the Early Eocene already and ended in the Aquitanian, when the eastern part of Levkas

emerged. Several local formations unconformably rest over the flysch of the Ionian zone that as a whole correspond to a Miocene transgressive cover, which is interesting both from the stratigraphic-palaeontological and the structural point of view.

However, Miocene sediments in Levkas Island have not yet been studied adequately palaeontologi-cally and furthermore a biostratigraphic framework has not yet been properly established.

The purpose of this study is to provide the first comprehensive account of the micropalaeontology of the Early to Middle Miocene in Levkas Island, by using a reference section (Asprogerakata section). Depending on the lithology, the biotic content changes remarkably and, consequently, its potential resolution. Although no formally established biozones have been generally used because of the rarity of species useful for biozone recognition, a biostratigraphic framework has been developed using plenty of age-diagnostic taxa recovered. Information derived from the planktonic foraminiferal assemblages and analogy with present day phylogenetically related taxa, have been also used for the palaeoenvironmental analysis.

2. Materials and methods

2.1. The studied section

The Asprogerakata section (Fig. 1) gives a representative picture of the Miocene sedimentary record of the Ionian zone, in Levkas Island. The section is located along a roadcut just south of the village Aprogerakata. A conspicuous steep fault separates white non-detrital limestones of Late Eocene age from approximately 65 m of grey marls and intensively burrowed, medium to fine-grained calcareous sands. Coarse intercalations were not observed in the succession.

The grey-brown, medium to fine-grained, calcareous sandstones, which predominate in the lower and middle parts of the section, are well bedded and generally ill-sorted. Primary sedimentary structures are obscured by the intense bioturbation (Fig. 1).

Beds are generally parallel sided, while the burrows (*Skolithos/Ophiomorpha*) are commonly vertical, penetrating downwards from the upper surface, and have hard, brown meniscoid sandy walls, filled with loose, clean white sand.

From bottom to top the sandstone beds are decreasing in number and thickness. Silty and sandy, burrowed marls with some intercalations of thin, calcareous sandstone beds are prevailing in the upper part of the section.

These facies are believed to have been deposited in both inner shoreface and middle to outer shelf settings below the fair-weather wave base by slow and semi-continuous fall-out from storm-generated suspension clouds, enabling infaunal reworking to keep pace with sediment accumulation. The sediment was supplied from the upper shoreface by relatively frequent and strong wave and storm reworking. During calm intervals, various organisms thoroughly reworked the sediments, obliterating the primary sedimentary structures.

2.2. Planktonic foraminifera

Planktonic foraminiferal analyses were carried out on a total of 58 samples collected from Asprogerakata section at a mean interval of 0.50 to 0.60 cm.

All the samples were washed with a 63μm sieve. Quantitative analysis was performed on the whole samples. For the biostratigraphy semi-quantitative and qualitative analyses have been carried out on survey of the >125 μm fraction. Distribution patterns have been reconstructed counting about 300 specimens of all planktonic species from splits of the total sample. The distribution of selected taxa and their estimated abundance, for the two sequences are expressed in percentages of the total planktonic fauna and are reported in Fig. 2.

The palaeoclimatic record was determined using biogeographic indicators as proxies of temperature. Therefore, a palaeoclimatic curve was constructed using the formula (w-c)/(w+c)x100 of Amore et al. (2004), where *w* represents the warm-water indicators and *c* the cold water indicators. *Paragloborotalia siakensis, Globoquadrina dehiscens, Globoturborotalita decorapeta, Dentoglobigerina altispira, Globigerinella obesa, Globigerinoides subquadratus., Globigerinoides quadrilobatus, Praeorbulina* spp. are considered warm water species (Hemleben et al., 1989; Rohling and Gieskes, 1989; Turco et al., 2002). *Globorotalia praescitula, Globigerina praebuloides, Catapsydrax parvulus,Globigerinita. glutinta*, and *Turborotalita quinqueloba* are considered cool water indicators (Hemleben et al., 1989; Pujol and Vergnaud-Grazzini, 1995).

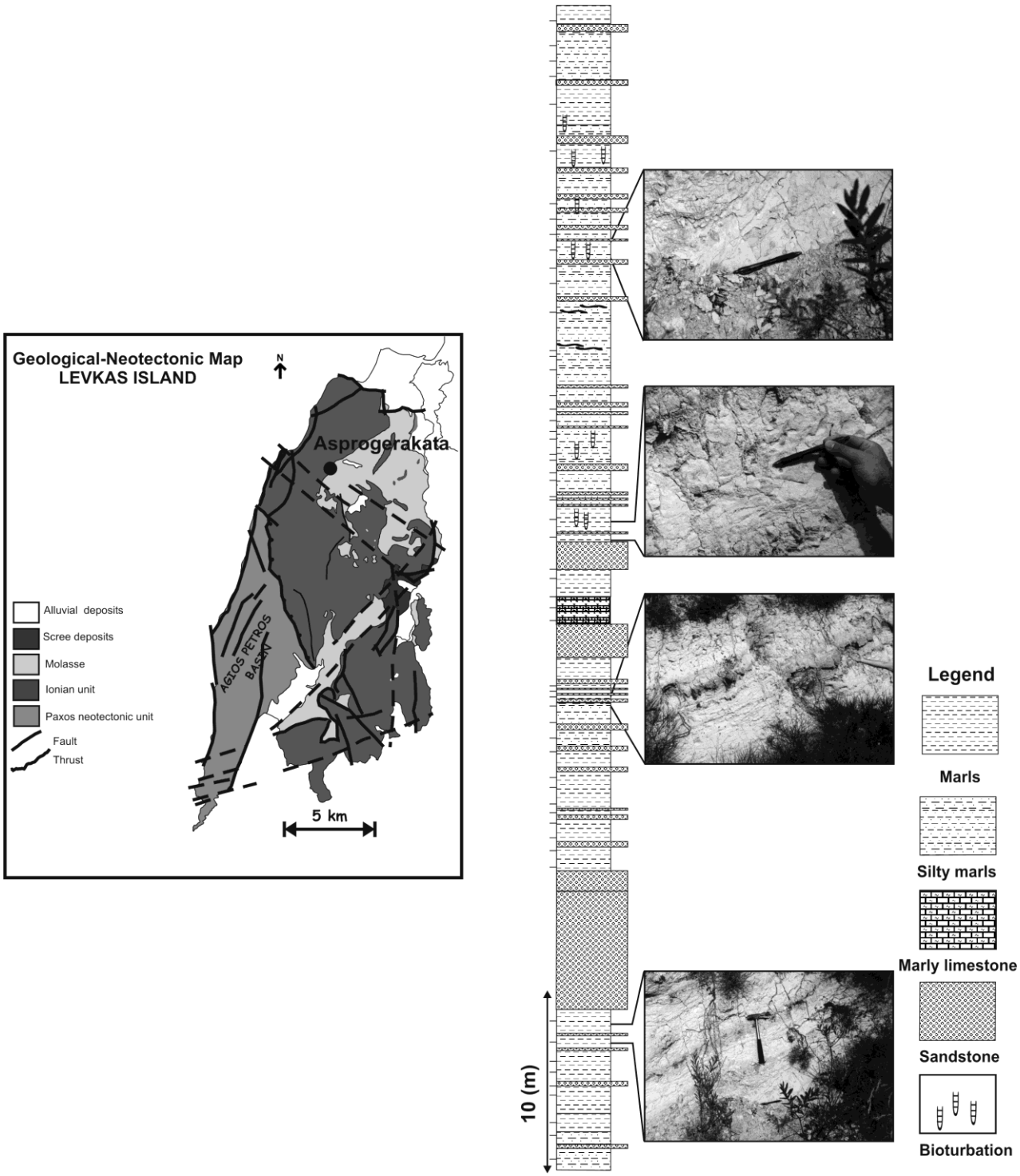

Fig.1. Geological and Neotectonic map of Levkas Island (after Lekkas et al., 2001, modified), depicting the location of the studied area. Lithology and position of samples of Asprogerakata section.

3. Results

3.1. Faunal changes

Planktonic foraminifera are abundant in the studied section, showing generally a moderate preservation. In spite of a minor resolution, planktonic foraminiferal bioevents are recorded as in the time equivalent Mediterranean sequences.

The quantitative distribution pattern of 20 planktonic foraminiferal categories are presented in fig. 2, showing biostratigraphic and/or abundance significance. Some categories represent different taxa linked by morphological or philetic affinities. *Globigerina praebulloides* group contains the species *G. praebulloides*, *G. falconesis* and *G. bollii*. *Glo-*

bigerina bollii has been considering as a synonym of *G. falconensis* (Blow, 1969), a characteristic species for the Medirerranean Middle Miocene (Foresi et al., 2002). In the studied section this species shows a limited distribution so it is included in the *G. praebulloides* group. In the *G. obesa* group specimens *of G. praesiphonifera, G. obesa* and *G. pseudobesa* are also included. *Globigerinoides quadrilobatus* group contains *G. quadrilobatus, G. trilobus* and *G. sacculifer*. *Dentoglobigerina* spp. is referred to the *D. baromoensis* and *D. langhiana* species, which have been considered by many authors as synonyms (Kennett and Srinivasan, 1983). Both species were recognised in the studied section, but because of their limited distribution we incorporated them in the same group. *Globigerinoides obliquus obliquus* specimens sporadically occur in the section and because of its low percentages in the assemblage it is not plotted.

tains the *G. praemenardii, G. miozea* and *G. archeomenardii*.

The taxa *T. quinqueloba, G. druryi. G. Decoraperta, C. parvulus, D. altispira, Dentoglogerina* spp., *G. obesa, G. quadrilobatus* are continuously present and show abundance fluctuations throughout the studied sections. The most abundant species are those of *G. praebulloides* group and *G. glutinata*. Among the species having discontinuous distribution *Glolobigerinoi-des subquadratus* and keeled globorotaliids, occasionally reach significant percentages.

In the following paragraphs we only consider the appearance/disappearance of marker species which are used as biohorizons. The results, as well as an adopted biozonal scheme, are presented in Fig. 3.

Paragloborotalia siakensis (Le Roy): In Asprogerakata section *Paragloborotalia siakensis* is

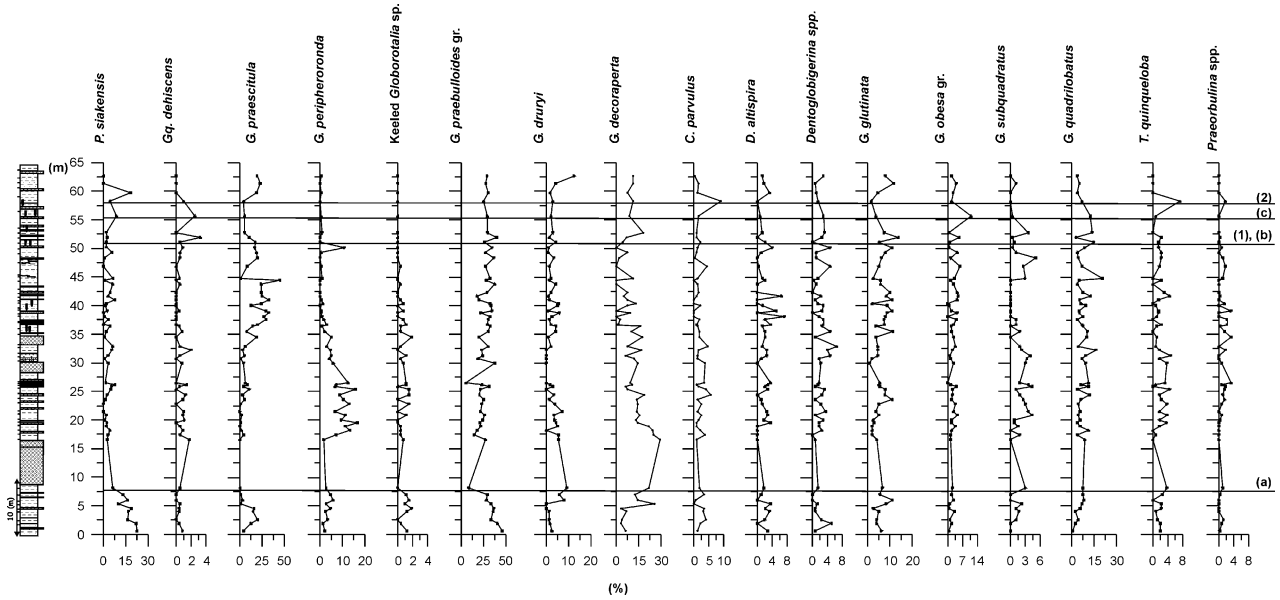

Fig.2. Quantitative distribution pattern of planktonic foraminiferal marker species and the position of the main bioevents: (a) AaE1 *P. siakensis*, (1) FAD *P. glomerosa glomerosa*, (b) high abundance of *G. dehiscens* (c) AbB2 *P. siakensis* (2) FAD *P.glomerosa circularis*.

The qualitative analysis reveals the occurrence of *Paragloborotalia birnageae* in some levels, but because of the small numbers of abundance this species was not plotted. This species was previously reported by Zachariasse, (1992) in N4 zone and in the N7 Zone by Kennett and Srinivasan (1983). Foresi et al. (2002) found this species in Tremiti Island in the *Praeorbulina gl. sicana* zone. *Praeorbulina* spp. consists of *P. transitoria, P. glomerosa sicana, P. glomerosa glomerosa* and *P. glomerosa circularis*. Keeled globororaliids con-

nearly absent from 10 to 55 m of the section, but is abundant in the lower part up to 10 m, where the Acme End (AaE) of this taxa is recorded for the investigated interval (Fig. 2). The percentages of its abundance are ranging between 21 to 45% of the total planktonic foraminiferal assemblage. After an interval of its near absence, *P. siakensis* appears in the top part in significant percentages. The coiling direction of *P. siakensis* is random from 0-10 m, while from 25 m and upwards seems that the sinistral coiling forms prevail. A second distinct

interval of high abundance of *P. siakensis* is observed just below the FO of *P. gl. circularis*, up to the top of the section. The prevailed coiling direction of the taxon in this interval is sinistral. *P. siakensis* is a long ranging species displaying several distributional changes of biostratigraphic significance. The age of the Acme End (AaE) of *Paragloborotalia siakensis* has been magnetostratigraphically dated at 15.435 Ma (Abdul-Aziz et al., 2008).

The interval of the Acme End of *P. siakensis* in Levkas Island seems to be synchronous with the AaE in Site 372 and in Tremiti Island (Abdul-Aziz et al., 2008; Di Stefano et al., 2008) The reabundance of the species, at the top of the section (56 m), is recorded just below the first appearance of *P.gl. circularis* and can be compared with the AbB bioevent recorded in the previous sections (Di Stefano et al., 2008).

Praeorbulina spp. Olsson: Several specimens of *P.gl. sicana* were recognized in the middle part of the record, while the FO of *P. gl. glomerosa* occurs in the upper part (51 m) of the section. The topmost part of the studied record is characterized by the FO of *P. gl. circularis*, exactly at the 58 m of the section.

Globoquadrina dehiscens Chapman, Parr and Collins: Although this taxon occurs in small percentages, rather continuously, its distributional pattern reveals a distinct interval in which the species shows an elevated abundance between the first occurrences of *P. gl. glomerosa* and *P. gl. circularis*. The influx of *G. dehiscens* is associated with peak in abundance of *G. subquadratus* and *C. parvulus* and absence of *G. praescitula*. This event can be considered of secondary significance and has been recognised also at the same stratigraphic level in northern Italy (La Vedona section, Hüsing et al., 2010).

Globorotalia praescitula Blow: Dextral and sinistral specimens reveal two significant intervals of maximum abundance. The first interval is recorded at the base of the investigated section and the second in the middle part of the section, where the dextrally coiled specimens dominate the assemblage.

Globorotalia peripheroronda Blow and Banner: This species shows a discontinuous distribution pattern. It is present at the base and then it occurs in significant numbers at 17-35 m of the section. At 50 m of the investigated interval a remarkable peak in abundance of the sinistral coiled specimens is obvious. The species exists in the Mediterranean from the Aquitanian stage and ends within the lower part of the Serravallian (Foresi et al., 2002; Di Stefano et al., 2008).

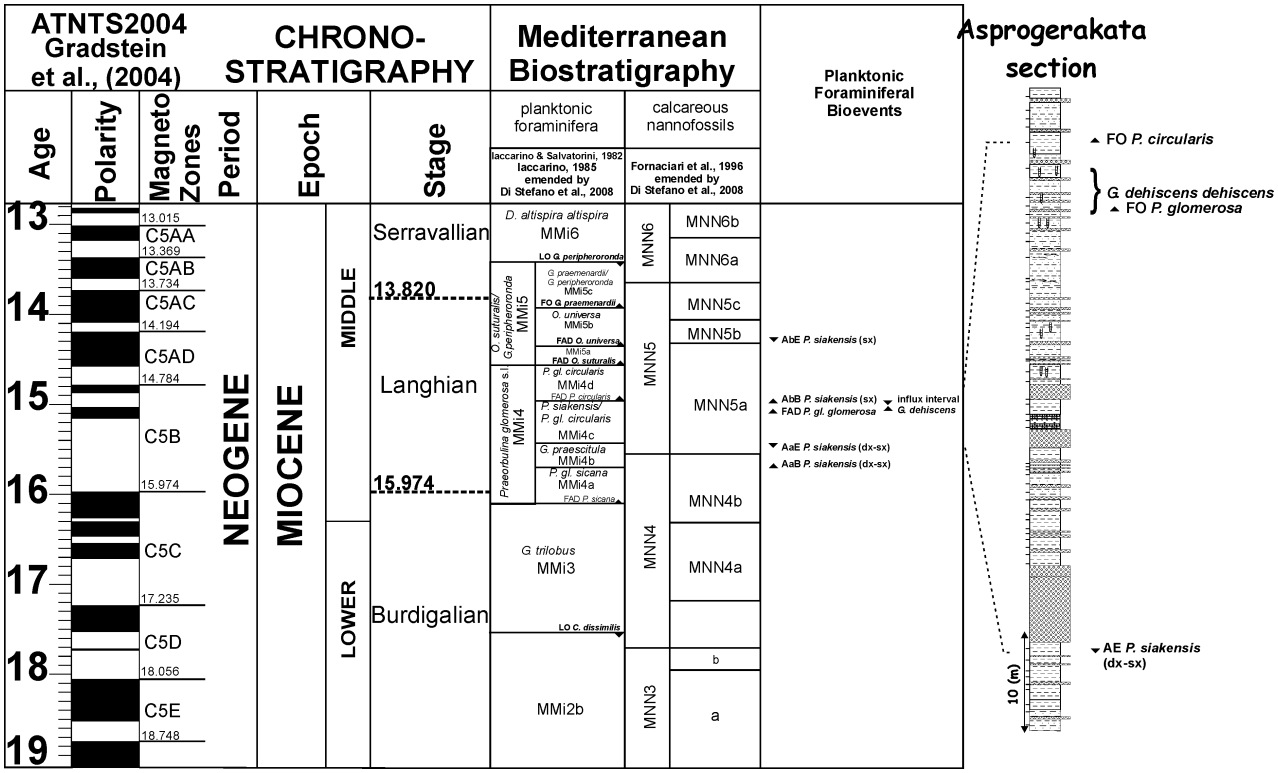

Fig. 3. Planktonic foraminiferal biostratigraphy of the Asprogerakata section.

3.2. Biostratigraphy

Several biostratigraphic schemes, based on planktonic foraminifera (Iaccarino and Salvatorini, 1982; Iaccarino 1985; Foresi et al. 1998; Sprovieri et al., 2002), have been proposed in the last decades for the Mediterranean Middle Miocene. Recently, Di Stefano et al. (2008) emended the biostratigraphic zonal scheme of Iaccarino & Salvatorini, 1982 and Iaccarino, 1985 by the addition of two subzones using the $Acme_a$ interval of *P. siakensis*. Following these pioneer works, as well as the abundance pattern of the taxa, the appearance of marker species and acme interval of selected taxa, which are used as biohorizons according to the integrated biostratigraphic scheme of Di Stefano et al. (2008), we are able to date the section.

The planktonic foraminifera which have been identified in the investigated succession characterize the Langhian interval. The main planktonic foraminifera events recorded in Asprogerakata section in stratigraphic order are: (1) the First Appearance Datum (FAD) of *Praeorbulina gl. glomerosa (*dated at 15.102 Ma, Abdul Aziz et al., 2008) and (2) the FAD of *P.gl. circularis* (14.89Ma, Abdul Aziz et al., 2008). In addition, the quantitative distribution patterns of planktonic foraminifera taxa reveal additional faunal changes of biostratigraphic significance, such as two acme intervals of *Paragloborotalia siakensis* (a, c, Fig. 2) and an interval of high abundance of *Globoquadrina dehiscens* (b, in Fig. 2). The AaE (Fig. 2, a) of *P. siakensis* has been dated at 15.435 Ma and the AbB (c) at 14.93 Ma (Abdul-Aziz et al., 2008; Di Stefano et al., 2008). The chronostratigraphic level of the observed high abundance of *G. dehiscens* is consistent with the one of FAD of *P. gl. glomerosa* and is followed by an Acme interval of sinistrally coiled *P. siakensis.* The influx of *G. dehiscens* is also defined in northern Italy (La Vedona section).and dated 14.915-15.098 Ma, which is in accordance with the studied chronostratigraphic record (Hüsing et al., 2010).

The bioevents listed above allow the identification of *P. siakensis-P.gl.circularis* subzone of MMi4 planktonic foraminiferal Zone for the Langhian of the Mediterranean region of Di Stefano et al. (2008). The first occurrence of *P .gl. circularis* defines the MMi4c/MMi4d boundary.

According to the astronomical ages derived from other astronomical tuning sections in the Mediterranean Sea the investigated section spans from 15.435 to 14.89 Ma, corresponding to Langhian.

3.3. Palaeoenvironmental-palaeoclimatic implications

The palaeoclimatic curve and the different abundance patterns of planktonic foraminifera allowed the recognition of four main intervals in the Middle Miocene sequence of the section (Fig. 4).

0-7.5m: The lower part of the section is characterized by *P. siakensis* random coiled, a warm species (Turco et al., 2002), *G. praebulloides* and *G. praescitula*. The last two species are closely related to the extant species *G. bulloides* and *G. scitula* respectively, which have the same environmental preferences (cool water indicators) (Hemleben et al., 1989).

7.5-20 m: Just after the acme end of *P. siakensis* the interval is characterized by the elevated percentages of *G. druryi, G. decoraperta*, and *G. quadrilobatus.* These taxa are relatively warm water forms, which are inhabited in warm subtropical environments (Pujol and Vergnaud-Grazzini, 1995).

20-32m: The palaeoclimatic fluctuations towards cool conditions are due to the dominance of cool water species such as *G. glutinata* and *G. praebulloides* (Pujol & Vergnaud-Grazzini, 1995), while

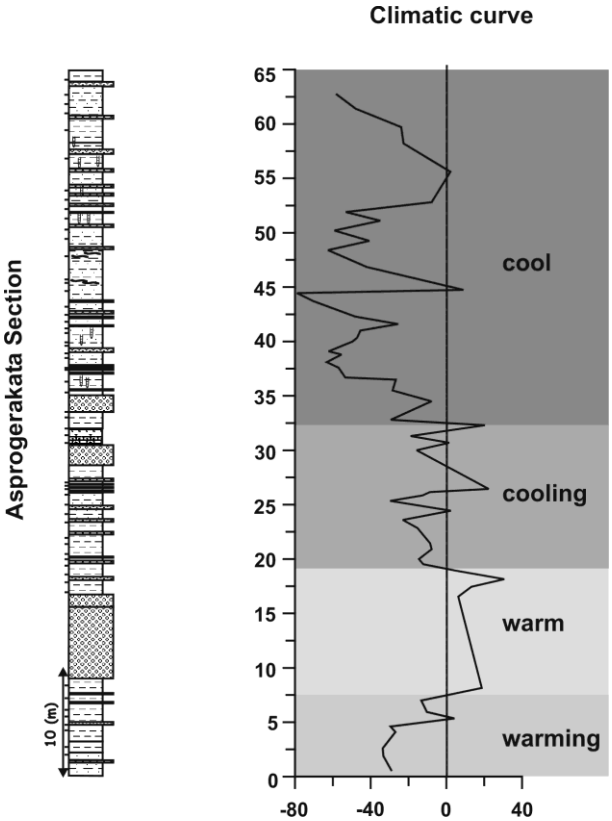

Fig. 4. Palaeoclimatic curve based on warm vs cold water plantkonic foraminiferal species.

warm water species display several peaks in abundance.

32-65 m: The palaeoclimatic curve implies that cool sea surface conditions prevailed in this period, due to the elevated percentages of the cool water indicators and the lack of warm water taxa. A major cooling step is recorded at 45 cm, whereas two warming steps are recorded within the cool interval. The first follows the significant cooling shift and the second is described between the first occurrence of *P. gl. glomerosa* and the first occurrence of *P. gl. circularis*. The latter event is characterised by a shift in abundance of *G. dehiscens* and reflects the warming (deepening) of the thermocline while surface temperatures are also warmed.

Planktonic foraminiferal abundance identify a significant change in variability of climate system prior to 14.89 Ma probably corresponding to the global cooling events superimposed to the Middle Miocene Climatic Optimum (D Event of Shevenell and Kennet, 2004 recorded at 14.8 Ma and/or affected by the Mi3a event of Miller et al., 1991).

In particular, the lower part of the section up to 20m seems to be subjected to more ameliorated conditions implied by the occurrence of *Paragloborotalia siakensis* (Turco et al., 2002). More deteriorated climatic conditions are evident for the middle–upper part of the sequence.

4. Discussion

Asprogerakata section was previously dated to the Lower Miocene (Burdigalian) on the basis of the presence of *G. trilobus, G. obliquus, G. subquadratus, G. praescitula* and the absence of *Orbulina* (de Mulder, 1975). According to Fornaciari et al. (1996) and Rio et al. (1997), the Langhian Epoch is defined by the FO of *Praeorbulina* and the LO of *Sphenolithus heteromorphus*.

The biostratigraphic data referred to this study, based on planktonic foraminifera, allowed us to characterise and date the beginning and the end part of the section.

In particular, at the lower part of the section the distribution pattern of *P. siakensis* led to the recognition of the AaE event, which has been dated at 15.435 Ma (Abdul-Aziz et al., 2008). Going upwards, the FAD of *P. gl. glomesa* recorded at 51 m and the FAD of *P. gl. circularis* at 58 m as well as the acme interval of *G. dehiscens* and the AbB of *P. siakensis* sinistrally coiled made our data comparable to that of Tremiti Island and other Mediterranean sites (Di Stefano et al., 2008; Hüsing et al., 2010), dating the top part at 14.89 Ma.

In the climate evolution of Cenozoic, this interval represents the Middle Miocene climatic transition from relative global warmth of the Late Oligocene-Early Miocene to the Neogene "ice-house" From the early-middle Miocene, global temperatures cooled dramatically through a series of major changes in climate, polar ice volume and ocean circulation (Roth et al., 2000; Mutti, 2000). Following the Miocene Climatic Optimum, between 16-14.5 Ma, the Middle Miocene is characterized by a major period of expansion of Antarctic ice. The major phase of East Antarctic ice sheet growth took place between 15 Ma and 13 or 12 Ma (Zachos et al., 2001; Billups and Schrag, 2002; Winkler et al., 2002). During this period the global climate changed to colder conditions with increased zonality (Flower and Kennett, 1993; Zachos et al., 2001). At this time, the ocean climate evolved into modern state conditions dominated by strong meridionality and vertical thermal gradients and dominance of high-latitude deep water source (Miller et al. 1987, 1991; Woodruff and Savin, 1989, 1991; Flower and Kennett, 1993; Roth et al., 2000). This long term climatic Cenozoic evolution was punctuated by several brief periods of glaciation based on the recognition of prominent isotope events (Mi1-6) (Miller et al., 1991) with potential for global correlations. The Mi-events have been recently correlated and dated in several Mediterranean sections (Turco et al., 2001; Abels et al., 2005) on the basis of magnetostratigraphic data integrated into orbitaly-derived timescales (Lourens et al., 2004).

In Asprogerakata section, palaeoclimatic curve identify a significant cooling phase above the 15.4 Ma at the middle-upper part of the record. This phase follows a warming phase recorded at the lower part of the section, which may correspond to the later phase of the MCO as this has been recorded in site 608 of North Atlantic. Indeed, the Mi3 event recorded in site 608 in North Atlantic reveal two peaks in oxygen isotope record dated at 14.9 and 13.6 Ma (Miller et al., 1991) and labeled Mi3a and Mi3b respectively.

The astronomical dates for the Mi3a and Mi3b events have estimated at 14.2 Ma and 13.8 Ma (Shevenell and Kennett, 2004) while a major isotope enrichment event in Mediterranean dated at 13.82 Ma has been interpreted as related to Mi3b

event (Abels et al., 2005; Holbourn et al., 2005), which is influenced by the 100-kyr of eccentricity cycles and coincides with a period of minimum amplitudes in obliquity. This orbital configuration was also recognized by Holbourn et al., 2007 during the lond-term cooling phase II from 14.7 to 13.9 Ma bounded by oxygen isotope increases.

On this basis, the two major climatic pahses recorded in Asprogerakata section is interpreted to have been affected by the global climatic deterioration recorded from 15 to 14.5 Ma (Zachos et al., 2001; Holbourn et al., 2005; 2007), whereas the cooling phase is affected by the global climatic transition to colder mode conditions (Miller et al., 1991; Shevenell et al., 2004; Wright and Miller, 1992).

From Langhian time onwards the only connection between the Mediterranean and the world's ocean was via Atlantic. Our data further support the inflow of cold North Atlantic water in the Mediterranean. The entry of cold Atlantic water was made possible by deepening of "Gibraltar sill", so an estuarine circulation can be assume for Langhian time (Gebhardt, 1999)

5. Conclusions

This study refers to the early Middle Miocene palaeoclimatic evolution of eastern Mediterranean, based on the planktonic foraminiferal assemblage changes. The biostratigraphic analyses reveal that the investigated section spans from 15.435 -14.89 Ma. The interval from the base (15.435 Ma AaE of *P. siakensis*) to the top part is characterised by an overall warming trend which is mainly represented by warm-temperate water taxa.

The relatively warm period is followed by a gradually cooling resulted at a major cooling event at 45 m of the section.

The undertaken analyses indicate that climatic and oceanographic cooling occurred during 15-14.89 Ma in the Eastern Mediterranean area coincides closely with the end of the Middle Miocene Climatic optimum between 17 and 15 Ma (Zachos et al., 2001).

Acknowledgments

Funding has been provided by Research Projects 70/4/8642 financed by National Kapodistrian University of Athens. The authors would like to thank G. Goumas for help during field work. Special thanks are due to Dr F. Lirer and Dr. L.M. Foresi for their fruitfull recomendations.

References

Abels H.A., Hilgen F.J., Krijgsman W., Kruk R.W., Raffi I., Turco E., Zachariasse W.J., 2005. Long-period orbital control on middle Miocene global cooling: integrated stratigraphy and astronomical tuning of the Blue Clay Formation on Malta. Paleoceanography 20, PA4012, 11 pp.

Abdul-Aziz H., Di Stefano A., Foresi L.M., Hilgen F.J., Iaccarino S.M., Kuiper K.F., Lirer F., Salvatorini G., Turco E., 2008. Intergrated stratigraphy and $_{40}Ar/_{39}Ar$ chronology of early Middle Miocene sediments from DSDP Leg 42°, Site 372 (Western Mediterranean). Palaeogeography, Palaeoclimatology, Palaeoecology, 257, 123-138.

Amore F.O., Caffau M., Massa B., Morabito S., 2004. Late Pleistocene–Holocene palaeoclimate and related palaeoenvironmental changes as recorded by calcareous nannofossils and planktonic foraminifera assemblages in the southern Tyrrhenian Sea (Cape Palinuro, Italy). Marine Micropalaeontology, 52, 255–276.

Aubouin J., 1965. Geosynclines. Developments in Geotectonics; 1. Elsevier, Amsterdam.

Billups K. and Schrag D.P., 2002. Palaeotempeatures and ice volume of past 27 Myr revisited with paried Mg/Ca and 18O/16O measurements on benthic foraminifera. Paleoceanography, 17, 1-11.

Blow W.H., 1969. Late middle Eocene to Recent planktonic foraminiferal biostratigraphy. In: Bronniman P. and Renz H.H. (Eds.), Proc. First Int. Conf. Planktonic Microfossils, Geneva, 1967. Leiden (E.J. Brill), 1, 199-422.

De Mulder E.F.J., 1975. Microfauna and sedimentary-tectonic history of the Oligo-Miocene of the Ionian Islands and Western Epirus (Greece). Utrecht Micropalaeontol. Bulletin. 13, 1–139.

Di Stefano A., Foresi L.M., Lirer F., Iaccarino S.M., Turco E., Amore F.O., Morabito S., Salvatorini G., Mazzei R., Abdul Aziz H., 2008. Calcareous plankton high resolution bio-magnetostratigraphy for the Langhian of the Mediterranean area. Rivista Italiana di Paleontologia e Stratigrafia, 114, 51-76.

Flower B.P. and Kennett J.P., 1993. Middle Miocene ocean-climate transition: high resolution oxygen and carbon isotopic records from DSDP Site 588A southern Pacific. Paleoceanography, 8, 811-843.

Foresi L.M., Bonomo S., Caruso A., Di Stefano A., Di Stefano E., Iaccarino S. M., Lirer F., Salvatorini G. and Sprovieri, R. 2002. High resolution calcareous plankton biostratigraphy of the Serravalian succession of the Tremiti Islands (Adriatic Sea, Italy). In Iaccarino, S.M. (ed.), Intergrated Stratigraphy and Palaeoceanography of the Mediterranean Middle Miocene. Rivista Italiana di Palaeontologia e Stratigrafia, 108: 257-273.

Foresi L.M., Iaccarino S.M., Mazzei R., Salvatorini G., 1998. New data on Middle to Late Miocene calcareous plankton biostratigraphy in the Mediter-

ranean area. Rivista Italiana di Paleontologia e Stratigrafia, 104, 95–114.

Fornaciari E., Iaccarino S., Mazzei R., Rio D., Salvatorini G., Bossio A. and Monteforti B., 1997. Calcareous plankton biostratigraphy on the Langhian historical stratotype. In: Miocene Stratigraphy: An Integrated Approach, 89-96.

Hemleben C., Spindler M. and Anderson O.R., 1989. Modern Planktonic Foraminifera. Springer-Verlag, New York, 1-363.

Holbourn A., Kuhnt W., Schulz M., Erlenkeuser H., 2005. Impacts of orbital forcing and carbon dioxide on Miocene ice-sheet expansion. Nature, 438, 483-487.

Holbourn A., Kuhnt W., Schulz M., Flores J.A. and Andersen N., 2007. Orbitally paced climate evolution during the middle Miocene 'Monterey' carbon-isotope excursion. Earth and Planetary Science Letters, 261, 534-550.

Hüsing S.K., Cascella A., Hilgen F.J., Krijgsman W., Kuiper K.F., Turco E. and Wilson D., 2010. Astrochronology of the Medietrranean Langhian between 15.29 and 14.17 Ma. Earth and Planetary Science Letters, 290, 254-269.

Gebhart H., 1999. Middle to Upper Miocene benthonic foraminiferal palaeoecology of the Tap Marls (Alicante province, SE Spain) and its palaeoceanographic implications. Palaeogeography, Palaeoclimatology, Palaeoecology, 145, 141-156.

Iaccarino S., 1985. Mediterranean Miocene and Pliocene planktic Foraminifera, *in* Bolli H.M., Saunders J.B. & Perch-Nielsen K. (eds.), Plankton Stratigraphy. Cambridge Univ. Press, London, 283-314.

Iaccarino S. and Salvatorini G., 1982. A framework of planktonic foraminiferal biostratigraphy for Early Miocene to Late Pliocene Medoterranean area. Paleontol. Stratigr. Evol., 2, 115-125.

IGRS-IFP, 1966. Etude géologique de l' Epire (Grèce nord occidentale). Editions Technip, Paris, 306pp.

Kennett J.P. and Srinivasan M.S., 1983. Neogene Planktonic Foraminifera: A Phylogenetic Atlas: Stroudsburg, PA (Hutchinson Ross).

Lekkas E., Danamos G., Lozios S., 2001. Neotectonic structure and neotectonic evolution of Lefkada island. Bulletin of the Geological Society of Greece, XXXIV/1, 157-163.

Lourens L.J., Hilgen F.J., Shackleton N.J., Laskar J. and Wilson D., 2004. The Neogene Period. In: Gradstein F. et al. (Eds), A Geologic Time Scale 2004, Cambridge Univ. Press, 21, 409-440.

Miller K.G., Fairbanks R.G. and Mountain G.S., 1987. Tertiary oxygen isotope synthesis, sea level history and continental margin erosion. Paleoceanography, 2, 1-19.

Miller K.G., Wright J.D. and Fairbanks R.G., 1991. Unlocking the ice house: Oligocene-Miocene oxygen isotopes, eustasy and margin erosion. Journal of Geophysical Research, 96B, 6829-6848.

Mutti M., 2000. Bulk δ18O and δ13C records from Site 999, Colombian Basin, and Site 1000, Nicaraguan Rise (latest Oligocene to middle Miocene): diagenesis, link to sediment parameters, and palaeoceanography. Proceedings of the Ocean Drilling Program, Scientific Results, 165, 275-283.

Pujol C. and Vergnaud-Grazzini C., 1995. Distribution patterns of live planktic foraminifers as related to regional hydrography and productive systems of the Mediterranean Sea. Marine Micropaleontology., 25, 187-217.

Rio D., Cita M.B., Iaccarino S., Gelati R., Gnaccolini M., 1997. Langhian, Serravallian and Tortonian historical stratotypes. In: Montanari, A., Odin, G.S., Coccioni, R. (eds.), Miocene Stratigraphy: An Integrated Approach. Developments in Palaeontology and Stratigraphy, vol. 15, pp. 57–87.

Rohling E.J. and Gieskes W.W.C., 1989. Late Quaternary changes in Mediterranean intermediate water density and formation rate. Paleoceanography, 4, 531-545.

Roth J.M., Droxler A.W. and Kameo K, 2000. The Caribeancarbonate crash et middle to late Miocene transition: linkage to the establishment of modern global ocean conveyor. Proceedings of the Ocean Drilling Pr gram, Scientific Results, 165, 249-273.

Shevenell A. E., and Kennett J. P., 2004. Palaeoceanographic change during the middle Miocene climate revolution: An Antarctic stable isotope perspective, in The Cenozoic Southern Ocean: Tectonics, Sedimentation, and Climate Change Between Australia and Antarctica, Geophys. Monogr. Ser., vol. 151, edited by N. Exon, J. P. Kennett, and M. Malone, pp. 235–252, AGU, Washington, D. C.

Shevenell A. E., Kennett J. P. and Lea D. W., 2004. Middle Miocene Southern Ocean cooling and Antarctic cryosphere expansion. Science, 305, 1766–1770.

Sprovieri M., Caruso A., Foresi L. M., Bellanca A., Neri R., Mazzola S. and Sprovieri R., 2002. Astronomical calibration of the upper Langhian/lower Serravallian record of Ras Il-Pellegrin section (Malta Island, central Mediterranean). Rivista Italiana di Palaeontologia e Stratigrafia, 108(2), 183– 193.

Turco E., Bambini A.M., Foresi L.M., Iaccarino S., Lirer F., Mazzei R., Salvatorini G., 2002. Middle Miocene high-resolution calcareous plankton biostratigrphy at Site (Leg 154, equatorial Atlantc Ocean): palaeoecological implications. Geobios, special volume 24, 257-276.

Turco E., Hilgen F.J., Lourens L.J., Shackleton N.J. and Zachariasse W.J., 2001. Punctuated evolution of global climate cooling during the late Middle to early Late Miocene: High-resolution planktonic foraminiferal and oxygen isotope records from the Mediterranean. Paleoceanography, 16, 405-423.

Underhill J.R., 1989. Late Cenozoic deformation of the Hellenic foreland, Western Greece. Bulletin of the Geological Society of America, 101, 613–634.

Winkler A., Wolf-Welling T.C.W., Stattegger K., 2002. Clay mineral sedimentation in high northern latitude deep-sea basins since the Middle Miocene (ODP Leg 151, NAAG). *Journal of Earth Sciences* (Geol. Rundsch), 91, 133-148.

Woodruff F. and Savin S., 1989. Miocene deep water oceanography. Paleoceanography, 4**,** 87-140.

Woodruff F. and Savin S., 1991. Mid-Miocene isotope stratigraphy in the deep sea: High-resolution correl tions, palaeoclimatic cycles, and sediment preservation. Paleoceanography, 6**,** 755-806.

Wright J.D. and Miller K.G., 1992. Miocene stable isotope stratigraphy, Site 747, Kerguelen Plateau. Proceedings of the Ocean Drilling Program, Scientific Results, 120, 855- 866.

Zachariasse W.J., 1992. Neogene planktonic foraminifers from Sites 761 and 762 off northwest Australia. In: von Rad, U, Haq, B.U., et al., 1991, Proceedings of the Ocean Drilling Programn Scientific Results, 122, 665-675.

Zachos J.C., Shackleton N.J., Ravenaugh J.S., Pälike H., Flower B.P., 2001. Climate response to orbital forcing across the Oligocene–Miocene boundary. Science, 292, 274–278.

Scientific Annals, School of Geology, Aristotle University of Thessaloniki Proceedings of the XIX CBGA Congress, Thessaloniki, Greece	Special volume 100	269-278	Thessaloniki 2010

PALAEOCLIMATE RECONSTRUCTIONS FOR THE LATE MIOCENE IN SOUTHEAST BULGARIA USING POLLEN DATA FROM THE TUNDZHA BASIN

Ivanov D.

Institute of Botany, Bulgarian Academy of Sciences, Acad. G. Bonchev Str., Bl. 23, BG-1113 Sofia, Bulgaria; dimiter@bio.bas.bg

Abstract: The results of palaeoclimate reconstructions of Neogene freshwater deposits of the Tundzha Basin (South Bulgaria, SE Europe) are presented. We analysed pollen and spores complexes with the aim of obtaining data about the climate conditions. The palynological analysis was performed on clayey sediments of the Elhovo Formation intercalated between coal layers from core C-432 situated in the central part of the Basin. The climate data reconstructed by the Coexistence Approach indicate a warm temperate climate with mean annual temperatures around 16 ºC and with mean temperature of at least 5 ºC during the coldest month. With annual precipitation rates commonly around 1000 mm climatic conditions were overall humid. Partly seasonally drier conditions suggested for the topmost part of Elhovo Formation by previous studies, were not evident from recent analyses. The Early Pontian climate was about 3-4°C warmer than today, with rainfalls at least 300 mm higher. These data coincide with the warming trend recognised in other regions in Bulgaria during the Early Pontian. Thus the data from current study contribute to the elucidation of the evolution of the local and regional Late Miocene climate patterns and contribute to the palaeoclimate model for the Balkan Peninsula.

Key words: Late Miocene, Bulgaria, Southeast Europe, palynology, climate, coexistence approach.

1. Introduction

Palaeoclimate reconstructions are essential for understanding the recent and future changes in the climate system under the pressure of internal and external forcing factors. In general the records of changing climate that are preserved in sedimentary archives provide data for describing the history of climate. In particular, the long and continuous sedimentary successions contain a unique record of climate changes. The fossil plant record helps to understand past climates, because of strong dependence flora and vegetation composition and structure on climatic conditions. In recent years, a different quantitative techniques have been developed, e.g. CLAMP (Wolfe, 1993); Coexistence Approach (Mosbrugger and Utescher, 1997); Climate Amplitude Method (Fauquette et al., 1998); ELPA (Traiser et al., 2005, 2007) and improved (e.g. Utescher et al., 2009b) making an effort to obtain more precise climate data from plant fossils. As a result a numerous climate reconstructions have been carried out for the Neogene period, aiming at the reconstruction of local and regional climatic patterns (Fauquette et al., 1999; Gebka et al., 1999; Utescher et al., 2000; Bruch and Gabrielyan, 2002; Ivanov et al., 2002; Bruch and Kovar-Eder, 2003; Fauquette and Bertini, 2003; Uhl et al., 2003; Bruch et al., 2004; Jiménez-Moreno et al., 2005; Bruch et al., 2006; Fauquette et al., 2006; Uhl et al., 2006; Akgun et al., 2007; Bruch et al., 2007; Fauquette et al., 2007; Ivanov et al., 2007a,b,c; Jiménez-Moreno et al., 2007a,b; Syabryaj et al., 2007; Uhl et al., 2007; Utescher et al., 2007; Akkiraz et al., 2008; Jiménez-Moreno et al., 2008,b; Kayseri and Akgun, 2008; Ivanov, 2009a; Utescher et al., 2009a).

Terrestrial climate records during the Miocene have been reconstructed recently from the microfloral record of Central and Eastern part of Balkan Peninsula. Quantitative climate data were calculated for Middle and Late Miocene palynological records from marine/brackish sediments of the Forecarpatian and Euxinian Basin (Ivanov et al., 2002, 2007c). The temperature records obtained reveal continental cooling from sub-tropical conditions in the Middle Miocene to warm temperate climate at the Miocene/Pliocene transition. Major global cli-

matic events known from marine data archives (Zachos et al., 2001) such as the Mid-Miocene Climatic Optimum and Late Miocene Cooling trend are mirrored in the terrestrial curves. In general the temperature records coincide with overall climate trend for North Germany and Central Europe (Utescher et al., 2000; Mosbrugger et al., 2005). As regard the precipitation pattern, differences with Central European model were observed for the Late Miocene (Ivanov et al., 2007c; Ivanov, 2009a). In addition, fluctuations occur in all climate parameters and display cycles of humid/dryer and warmer/cooler conditions for the Late Miocene (Maeotian) in Bulgaria (Ivanov et al., 2002), which required more detailed studies of these events. Other recent studies on Late Miocene (Pontian) floras and vegetation revealed additional information for climate change (Ivanov et al., 2007a), incl. cyclic vegetation and climate pattern referred to orbital climate forcing (Utescher et al., 2009a).

The present study of the Upper Miocene sediments from the Tundzha Basin (Fig. 1) aims to elucidate the evolution and the variations of past climate, not sufficiently known in this area up to now.

2. Geological settings

The Tundzha Basin (also known as Elhovo or Elhovo-Yambol Basin) is situated in the South-eastern part of Bulgaria (Fig. 1). It provides important information on both dynamics of the system of fresh-water basins on Balkan Peninsula (Burchfiel et al., 2000; Nakov et al., 2001) and climate change and vegetation evolution in south-eastern part of Europe (Ivanov et al., 2007a). The basin is considered as a graben structure, which was formed as a result of movements in faults and extensions in the beginning of Late Miocene.

The Neogene sediments of the Tundzha Basin are assigned to the Elhovo Formation (Kojumdgieva et al., 1984) with two members (Fig. 1): Izgrev Member and Duganovo Member, and an undivided part. Angelova et al. (1991) have described the infiltration limestone sediments of the Duganovo Member as the Prustnik Limestone Formation, and dated it to the Pleistocene. The Elhovo Formation is unconformably overlain by a few meters of Pleistocene-Holocene sediments.

The sediments of Elhovo Formation are entirely of continental origin, were deposited in alluvial, fluvial and locally lacustrine-marshy environments (Nakov et al., 2001), and consist of an irregular alternation of claystone, sandstone and rare conglomerates. The thickness of the Formation is ca. 150 m to 200 m, but locally it reaches up to 300 m (Kojumdgieva et al., 1984). Within these deposits large lenses of gray and black clays, diatomite clays and lignite coal are grouped as Izgrev Member, which is locally present in the middle part of the basin (Fig. 1). The total thickness of the Izgrev Member reaches up to 40 m, with three main coal seams, each of them with a thickness varying from 3 m up to 8 m. Lignite was formed in an environment, characterized by low subsidence rate. Peat accumulation was terminated by a major flooding event resulting in a short-term establishment of a lake (Zdravkov et al., 2007).

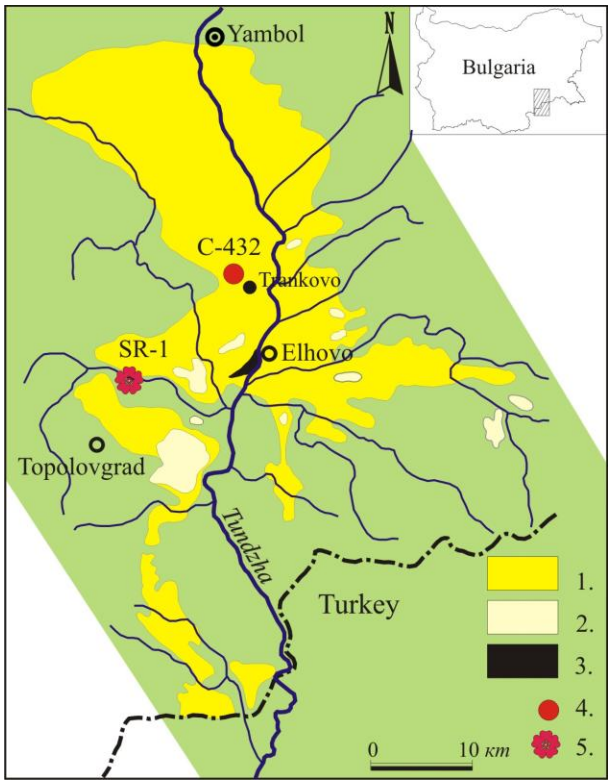

Fig. 1. Geological map of the Toundzha Basin, SE Bulgaria (redrawn from Kojumdgieva et al., 1984). Legend: 1. Elhovo Formation; 2. Douganovo Member of Elhovo Formation; 3. Izgrev Member of Elhovo Formation; 4. Position of core C-432, Trankovo; 5. Outcrop SR-1, Sinapovska River.

Diatom analysis of the clays from Izgrev Member has yielded a Pontian age for Elhovo Formation (Temniskova-Topalova et al., 1996; Temniskova-Topalova and Ognjanova-Rumenova, 1997). Among the vertebrate fauna discovered in the sediments from the upper part of the Elhovo Formation the following species were identified: *Deinotherium giganteum* Kaup, *Tetralophodon longi-*

rostris Kaup, *Anancus arvernensis* Croizet & Jobert, and *Zygolophodon borsoni* Hayes (Bakalov and Nikolov, 1962; Kojumdgieva et al., 1984; Nikolov, 1985). On the basis of these finds Kojumdgieva et al. (1984) assumed that the upper part of the Formation is Pontian-Pliocene, while the Elhovo Formation in was deposited in the Meotian-Early Pliocene time interval.

3. Materials and Methods

The sediments studied originate from core 432 (Fig. 1.) drilled near the village of Trankovo, Elhovo district. The profile comprises of browncoals, (diatomaceous) clays, and sandy clays (Fig. 2). The samples from the studied profile originates from the diatom clays and clays contacting to the lignite coals of the Izgrev Member. They were processed according to the standard technique for disintegrating Cenozoic sediments, which includes successive treatment by hydrochloric acid (HCl), fluoride acid (HF), potassium base (KOH), heavy liquid separation ($ZnCl_2$), and acetolysis.. The studied samples contain sufficient and well-preserved pollen grains, which enable us to apply quantitative techniques for climate reconstructions, and to analyse and interpret the results. On the basis of pollen/spore counts a percentage pollen diagram was plotted (Fig. 3.) showing the palynological record of the complete section. The percentage of each palynomorph taxon identified in the pollen spectra was calculated with respect to the total sum of arboreal (AP) and non-arboreal (NAP) pollen (AP+NAP=100 %). Local elements (L), such as spores, aquatic plants, were calculated on the basis of the sum AP+NAP+L=100 %. Total pollen sum for each sample is given in Append. 1, and graphically presented on the pollen diagram (Fig. 3).

To reconstruct palaeoclimate from the palynological record of theTundzha coal basin, the Coexistence Approach (CA) method was applied (Mosbrugger, 1995; Mosbrugger and Utescher, 1997). This method uses the climate tolerances of all Nearest Living Relatives (NLRs) known for a given fossil flora to determine a coexistence interval for each considered climate variable which allows the majority of NLRs of a fossil flora to coexist. The resulting intervals obtained for the different climate variables were then interpreted as the most probable ranges of palaeoclimate parameters for the fossil flora analysed. The Palaeoflora data base (Utescher and Mosbrugger, 1990-2007) was used for identifying the living relatives and their climatic requirements.

In the present study, four climatic parameters are considered and discussed below, namely:
- MAT: mean annual temperature (°C),
- CMT: mean temperature of the coldest month (°C),
- WMT: mean temperature of the warmest month (°C),
- MAP: mean annual precipitation (mm).

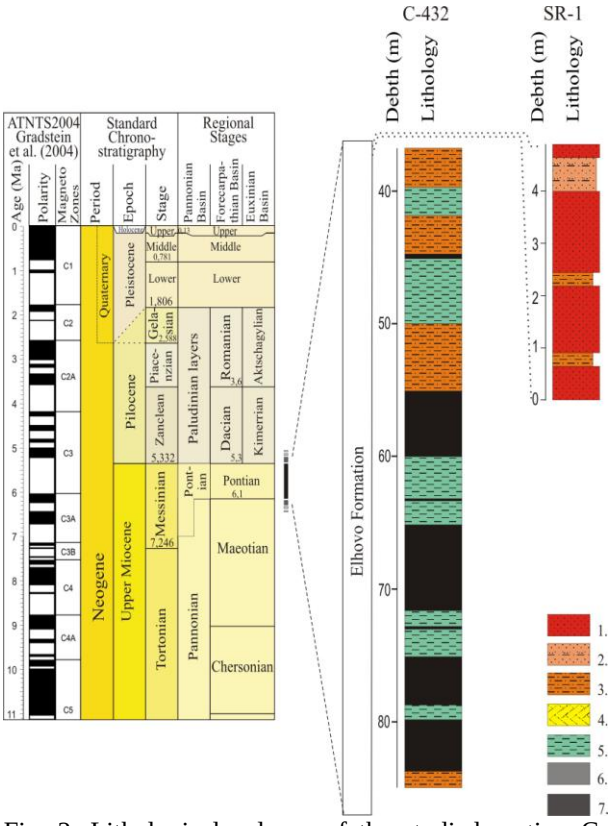

Fig. 2. Lithological column of the studied section C-432, Trankovo. For completeness the litological column of outcrop SR-1, Sinapovska River is given. Legend: 1. Sands and sandstones; 2. Sands with clayey interbedding; 3. Silty clays; 4. Yellow clays. 5. Diatomaceaous clays; 6. Clayey lignites; 7. Lignite coal.

These are the parameters which most reliably represent changes in palaeoclimatic conditions because their effect on plant distribution is most important. They are also best developed in terms of methodology (see (Ivanov et al., 2002; Mosbrugger and Utescher, 1997). As shown by previous palaeoclimate reconstructions for the Bulgarian Neogene, significant changes primarily involve mean annual temperature, temperature of the coldest month and mean annual precipitation, while temperatures of the warmest month are more constant and show smaller fluctuations (Ivanov et al., 2002).

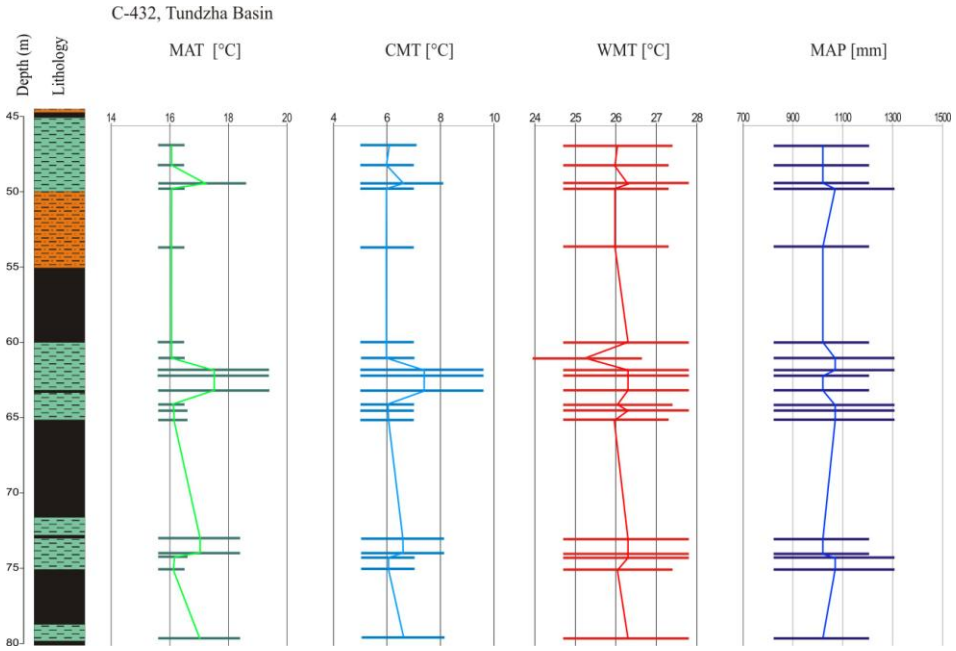

Fig. 3. Simplified percentage pollen diagram of core C-432, Trankovo, Tundzha Basin.

For the analysis, 19 microfloras from core 432 were selected providing required plant diversity for climate analysis. One sample (the top of section) was excluded because its diversity was below the limit of the method to produce reliable results (Mosbrugger and Utescher, 1997). Climate data calculated for the single microfloras, number of taxa contributing climate data, lower and upper limit of climate range obtained for the different variables are presented in Table 1, and illustrated on Fig. 4. In addition, the climate data from outcrop Sinapovska River (Ivanov et al., 2007b) are also used in terms to compare climate data and draw conclusions about climate dynamics.

4. Results and discussion

The fossil flora from Tundzha Basin is not sufficiently studied up to now. Recently studies on fossil macro- and microflora from upper part of Elhovo Formation (Ivanov et al., 2007b; Palamarev and Bozukov, 2004) have been undertaken, including also palaeoclimate interpretations (Ivanov et al., 2007b). Pollen analysis was applied on clayey sediments of Izgrev Member (Elhovo Formation)

Table 1. Climate data calculated for the single microfloras of core C-432. No taxa – number of taxa contributing climate data; min/max – lower/upper limit of climate range.

Depth (m)	No taxa	MAT min	MAT max	TCM min	TCM max	TWM min	TWM max	MAP min	MAP max
46	32	15,6	16,5	5	7,1	24,7	27,4	823	1206
47	34	15,6	16,5	5	7	24,7	27,3	823	1206
48	21	15,6	18,6	5	8,1	24,7	27,8	823	1206
49,0	32	15,6	16,5	5	7	24,7	27,3	823	1308
49,5	37	15,6	16,5	5	7	24,7	27,3	823	1206
54	19	15,6	16,5	5	7	24,7	27,8	823	1206
60	24	15,6	16,5	5	7	24,7	27,4	823	1308
61	23	15,6	19,4	5	9,6	24,7	27,8	823	1308
62	30	15,6	19,4	5	9,6	24,7	27,8	823	1206
62,5	23	15,6	19,4	5	9,6	24,7	27,8	823	1206
63,5	28	15,6	16,5	5	7	24,7	27,4	823	1308
64	28	15,6	16,6	5	7	24,7	27,8	823	1308
64,5	33	15,6	16,6	5	7	24,7	27,3	823	1308
65	23	15,6	18,4	5	8,1	24,7	27,8	823	1206
73	32	15,6	18,4	5	8,1	24,7	27,8	823	1206
74	27	15,6	16,6	5	7	24,7	27,8	823	1308
74,1	28	15,6	18,6	5	8,1	24,7	27,8	823	1206
75	28	15,6	16,5	5	7	24,7	27,4	823	1308
79	33	15,6	18,4	5	8,1	24,7	27,8	823	1206

for biostratigraphic purposes (Kojumdjieva et al. 1984), but the results were not published. Later the same materials were reanalyzed by (Ivanov and Lazarova, 2005) aiming to obtain information about fossil flora and vegetation structure. Scarce information about carpoflora from Elhovo Formation (incl. Izgrev Member) was reported in the overview of some Miocene floras by (Mai and Palamarev, 1997; Palamarev, 1990) and (Palamarev et al., 1999). Detailed pollen analyses has been recently performed by (Ivanov, 2009b) and is used for current reconstructions (Fig. 3).

The fossil flora identified during the micropalaeobotanic studies generally comprised representatives of 115 pollen taxa (Appendix 1.): 87 angiosperm pollen types from 50 families; 16 gymnosperm pollen types and 12 spore types (Ivanov, 2009b). Fossil flora is characterised by strong dominance of trees and shrubs, which is in contrast to the pollen flora from the outcrop Sinapovska River (SR-1). The last section showed a considerable pollen participation of herbaceous species and absence of representatives of spore plants. The herbaceous plants not only showed a high percentage participation (45.8 %), but considerable taxonomic diversity too (Ivanov et al., 2007b).

Analysis of the palynological data provided information on the probable climatic conditions during the sedimentation process. The palaeocli-mate reconstructions resulting from the application of the coexistence approach to the 19 palynofloras of core C-432 are shown in Fig. 3. The data from climate reconstruction for upper part of Elhovo Formation after (Ivanov et al., 2007b) – outcrop SR-1 (Sinapovska River) are used to correlate with recent data.

The present-day climate of Tundzha valley, Southeast Bulgaria is characterised by mean annual temperature (MAT) 12.2 ^{o}C, mean temperature of the coldest month (CMT) 0.9 ^{o}C, mean temperature of the warmest month (WMT) 22.7 ^{o}C, and mean annual precipitation (MAP) 541 mm (according to the Yambol Climatic Station, 143 m a.s.l.). The data for Elhovo Climatic Station, 130 m a.s.l. are as follow: MAT 12.3 ºC, TCM 1.1 ºC, WMT 22.9 ºC and MAP 545 mm (Stringmeteo, 2006-2009a; Stringmeteo, 2006-2009b; Velev, 1997).

Climate reconstructions based on palynological data from Izgrev Member of Elhovo Formation (the data obtained from core Trankovo C-432: Fig. 4; Table 1) display relatively stable climatic conditions for the entire time interval. The lower boundary of MAT coexistence intervals in all analysed pollen floras lies at 15.6°C. The upper boundary lies usually at 16.5°C, but higher values are also obtained (e.g. 18.4°C and 19.4°C) thus resulting in wider coexistence intervals. The middle values for the MAT are around 16°C except for some pollen floras from the bottom and middle part of the profile, which provide values ca. 17°C. Thus obtained

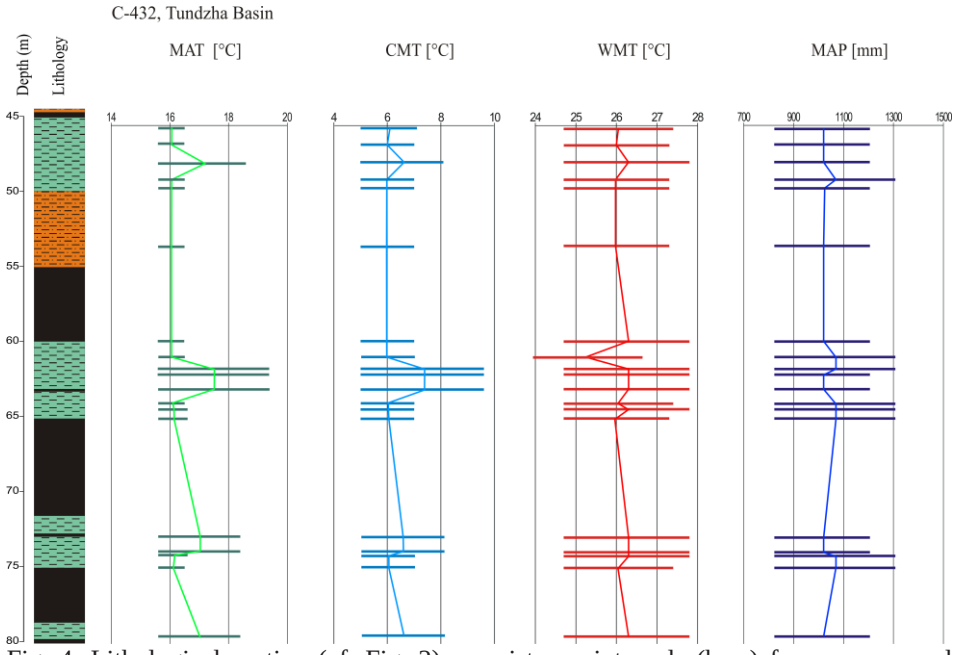

Fig. 4. Lithological section (cf. Fig. 2), coexistence intervals (bars) for mean annual temperature (MAT), and temperature of the coldest (CMT) and warmest month (WMT), and mean annual precipitation (MAT).

data for the annual tempera-tures shows relatively constant annual temperature during the sedimentation (Fig. 4). The invariability of this climate parameter and the lack of significant deviations testify to the absence of strong climate change.

The same is true for the winter temperatures. Coexistance intervals for CMT range mainly between 5.0°C and 9.0°C for most of the analysed microfloras (Fig. 4.). The most common middle values are 6.0°C. Only in sporadic cases higher values are obtained for the upper boundary, resulting in wider CA-intervals – 5.0-8.1°C and 5.0-9.6°C. In the upper part of the section, the upper CMT limit may decline to 7°C (at 15 m and 23 m in the profile). The lack of extreme winter temperatures was extremely important for the survival of palaeotropical plants, which required mild frost free winters.

Summer temperatures are in accordance with above mentioned results. The obtained data shows CA-intervals of 24.7-27.8°C and 24.7-27.3°C (Fig. 4.), while the middle values lies between 26.0-26.3°C. TWM show small oscillations of the upper limit of the intervals, which could not be interpret as significant climate change. Moreover, the results for annual and winter temperatures don't indicate increased seasonality and higher difference between winter and summer temperatures is not observed. Annual precipitation totals (middle values) are well above 1000 mm in the whole profile. The lower boundary of the coexistence intervals for MAP is at 823 mm and the upper is between 1206 and 1308 mm.

Summarizing the results obtained, it can be stated that a warm temperate climate persisted during the studied time period. Temperatures stayed at about the same level without significant fluctuations. Comparing to present climatic conditions it could state that temperatures were ca. 3-4°C higher than recent ones. The calculated MAP totals point to a permanently humid climate, with middle values above 1000 mm. Thus annual rainfalls during the studied time period were about twice higher as compare to recent levels of precipitation in the area of Tundzha Basin. The data obtained don't indicate any seasonally drier conditions.

The palaeoclimate data reconstructed using the NLR technique are over all supported by the broader vegetation data (Ivanov and Lazarova, 2005). For instance in most cases warm temperate and permanently humid conditions coincide with the presence of forest cover (mixed mesophytic forest with warmth-loving evegreens in the undergrowth). The calculated mean MAP total, commonly above 1000 mm, explains the rareness of xerophytic elements in the pollen spectra (Ivanov and Lazarova, 2005). Thus, all data indicate a very warm and humid climate.

These data coincide with the early Pontian warming trend recognised in Norethwest Bulgaria (Ivanov et al., 2002). Ivanov et al. (2002) point that after the late Maeotian cooling, the early Pontian begins with a warming trend. MAT reaches values of 15.6-17.2 ^{o}C, TCM lies between 5-7 ^{o}C, while MAP increases up to 1187-1308 mm. This event corresponds with the data obtained in current study.

Uncertainties of stratigraphical dating of the studied section do not allow direct correlation with climate curves available for other continental parts of Europe or global records, but work is in progress. However, if an earliest Pontian age can be assumed for the section, the data can be discussed in a European context. When compiling palaeoclimate data for the latest Miocene from various sources for different parts of Europe it is clear that the Elhovo region was characterized by favourable climate conditions with comparatively high MAT and mild winter temperature. Comparing temperatures (MAT, CMT) calculated for the Pontian of other areas (Ivanov et al., 2007a), the values obtained for the Tundzha Basin tend to be higher by a few degrees. This can be explained by a more southerly latitudinal position and/or a favourable microclimate caused by a small-scale relief. In the study area, MAP was apparently high when compared to other European regions.

The calculated values on the basis of the fossil macroflora from outcrop Sinapovska river (Ivanov et al., 2007b) had shown the annual temperatures within the range 14.4–15.8 °C, winter temperatures 3.7–5.8 °C, summer temperatures 25.6–26.4 °C, and the annual rainfalls 961–1179 mm. The values calculated on the basis of palynological data had shown wider CA-intervals: MAT 13.6–18.4 °C, CMT 2.4–9.4 °C, WMT 22.8–26,1 °C, and MAP 740–1206 mm. The wider interval of annual precipitation (740–1206 mm) might reflect diversity of the climatic conditions on a larger territory, including drier habitats (Ivanov et al., 2007b). The temperature values are by several degrees (1-2 °C) lower than the temperature values obtained in current study. This could correspond to slight cooling trend at the Pontian/Pliocene transition. Some dry-

ing is also possible. The expansion of herbaceous vegetation in outcrop SR-1 can be correlated with other late Neogene records in Bulgaria and surrounding areas (e.g. the upper part of the Staniantsi section – Utescher et al. (2009a). The increasing abundance of herbs combined with a low quantity of arboreal taxa, points to an opening of habitats, and probably decrease in mean annual precipitation.

5. Conclusions

Summarizing the results obtained it can be stated that a warm temperature climate with high rainfall and mild winter temperatures persisted in the time period regarded. Temperatures stayed about at the same level throughout the period of sedimentation of Izgrev Member of Elhovo Formation. All data indicate a very warm and humid climate without seasonally drier conditions. The early Pontian climate was about 3-4°C warmer than today, with rainfalls at least 300 mm higher that today. In general, these data coincide with the warming trend recognised in other regions of Bulgaria during the early Pontian.

The calculated climate values for the upper part of the Elhovo Formation (Ivanov et al., 2007b) shows some decrease in the annual and winter temperatures. A decrease of lower boundary of precipitations is also recorded. That could be attributed to a slight cooling trend at the end of Pontian, and possibly some drying.

Palaeoclimatic results shows that the climate in the Tundzha Basin in the period of sediment accumulation in the Elhovo Formation was warm temperate and permanently humid. Nevertheless the correlation of climate trends observed at Tundzha Basin with climate data from other late Miocene sedimentary successions is still tentative because of stratigraphic resolution, while the climate changes observed fit overall with observations from other regions of the European late Miocene.

Acknowledgements

The author is grateful to V. Mosbrugger and T. Utescher for the kindly provided access to the Palaeoflora database and Climstat software used for climate reconstructions. The comments from two anonymous referees greatly improved the manuscript. This work is a contribution to the Project B-1101 (NSF, Bulgaria) and to the International Network program NECLIME.

References

Akgun F., Kayseri M.S. and Akkiraz M.S., 2007. Palaeoclimatic evolution and vegetational changes during the Late Oligocene-Miocene period in Western and Central Anatolia (Turkey). Palaeogeography, Palaeoclimatology, Palaeoecology, 253(1-2): 56-90.

Akkiraz M.S., Kayzeri M.S. and Akgün F., 2008. Palaeoecology of Coal-Bearing Eocene Sediments in Central Anatolia (Turkey) Based on Quantitative Palynological Data. Turkish Journal of Earth Sciences, 17: 317-360.

Angelova D., Popov N. and Mikov M., 1991. Stratigraphy of the Quaternary sediments in the Tundzha depression. Rev. Bulg. Geol. Society, 52: 99-105 (in Bulgarian, English abstract).

Bakalov P. and Nikolov I., 1962. Les mammiferes du Tertiaire. In: Tzankov V. (ed.). Les fossiles de Bulgarie., 10, Bulg. Acad. Sci., Sofia: 1-160. (in Bulgarian).

Bruch A.A. and Gabrielyan I., 2002. Quantitative data of the Neogene Climatic Development in Armenia and Nakhichevan. Acta Univ. Carolinae - Geologica, 46(4): 41-48.

Bruch A.A. and Kovar-Eder J., 2003. Climatic evaluation of the flora from Oberdorf (Styria, Austria, Early Miocene) based on the Coexistence Approach. Phytologia Balcanica, 9(2): 175-185.

Bruch A.A., Uhl D. and Mosbrugger V., 2007. Miocene climate in Europe -- Patterns and evolution: A first synthesis of NECLIME. Palaeogeography, Palaeoclimatology, Palaeoecology, 253(1-2): 1-7.

Bruch A., Utescher T., Olivares C.A., Dolakova N., Ivanov D. and Mosbrugger V., 2004. Middle and Late Miocene spatial temperature patterns and gradients in Europe - preliminary results based on palaeobotanical climate reconstructions. Cour. Forsch.-Inst. Senckenberg, 249: 15-27.

Bruch A.A., Utescher T., Mosbrugger V., Gabrielyan I. and Ivanov D.A., 2006. Late Miocene climate in the circum-Alpine realm--a quantitative analysis of terrestrial palaeofloras. Palaeogeography, Palaeoclimatology, Palaeoecology, 238(1-4): 270-280.

Burchfiel C.B., Nakov R., Tzankov T. and Royden L.H., 2000. Cenozoic Extension in Bulgaria and Northern Greece: the Northern Part of the Aegean Extensional Regime. Geological Society, London, Special Publications, 173(1): 325-352.

Fauquette S. and Bertini A., 2003. Quantification of the northern Italy Pliocene climate from pollen data: evidence for a very peculiar climate pattern. Boreas, 32(2): 361-369.

Fauquette S., Guiot J. and Suc J.-P., 1998. A method for climatic reconstruction of the Mediterranean Pliocene using pollen data. Palaeogeography, Palaeoclimatology, Palaeoecology, 144(1-2): 183-201.

Fauquette S., Suc J.-P., Bertini A., Popescu S.-M., Warny S., Bachiri Taoufiq N., Perez Villa M.-J., Chikhi H., Feddi N., Subally D., Clauzon G. and

Ferrier J., 2006. How much did climate force the Messinian salinity crisis? Quantified climatic conditions from pollen records in the Mediterranean region. Palaeogeography, Palaeoclimatology, Palaeoecology, 238(1-4): 281-301.

Fauquette S., Suc J.-P., Guiot J., Diniz F., Feddi N., Zheng Z., Bessais E. and Drivaliari A., 1999. Climate and biomes in the West Mediterranean area during the Pliocene. Palaeogeography, Palaeoclimatology, Palaeoecology, 152(1-2): 15-36.

Fauquette S., Suc J.-P., Jiménez-Moreno G., Micheels A., Jost A., Favre E., Bachiri-Taoufiq N., Bertini A., Clet-Pellerin M., Diniz F., Farjanel G., Feddi N. and Zheng Z., 2007. Latitudinal climatic gradients in the Western European and Mediterranean regions from the Mid-Miocene (c. 15 Ma) to the Mid-Pliocene (c. 3.5 Ma) as quantified from pollen data, Geological Society Special Publication, pp. 481-502.

Gebka M., Mosbrugger V., Schilling H.D. and Utescher T., 1999. Regional-scale palaeoclimate modelling on soft proxy-data basis -- an example from the Upper Miocene of the Lower Rhine Embayment. Palaeogeography, Palaeoclimatology, Palaeoecology, 152(3-4): 225-258.

Ivanov D., 2009a. Palaeoclimatic reconstructions for the Late Miocene in Southwest Bulgaria based on palynological data. In: I. Bucur, E. Sasaran and D. Pop (Editors), Seventh Romanian Symposium of Paleontology, Cluj-Napoca, Romania, Presa Universitara Clujeana, pp. 56-58.

Ivanov D., 2009b. Vegetation and climate in Bulgaria during the middle and late Miocene (based on palynological data), DSc Thesis, Institute of Botany, Bulgarian Academy of Sciences, Sofia, 14 Tables, 105 Figs, 33 Plates, 350 pp.

Ivanov D., Ashraf A.R., Mosbrugger V. and Palamarev E., 2002. Palynological evidence for Miocene climate change in the Forecarpathian Basin (Central Paratethys, NW Bulgaria). Palaeogeography, Palaeoclimatology, Palaeoecology, 178(1-2): 19-37.

Ivanov D., Ashraf A.R., Utescher T., Mosbrugger V. and Slavomirova E., 2007a. Late Miocene vegetation and climate of the Balkan region: Palynology of the Beli Breg Coal Basin sediments. Geologica Carpathica, 58(4): 367-381.

Ivanov D.A., Ashraf A.R. and Mosbrugger V., 2007c. Late Oligocene and Miocene climate and vegetation in the Eastern Paratethys area (northeast Bulgaria), based on pollen data. Palaeogeography, Palaeoclimatology, Palaeoecology, 255(3-4): 342-360.

Ivanov D., Bozukov V. and Koleva-Rekalova E., 2007b. Late Miocene flora from SE Bulgaria: vegetation, landscape and climate reconstruction. Phytologia Balcanica, 13(3): 281-292.

Ivanov D. and Lazarova M., 2005. Late Miocene flora from Tundzha Basin. Preliminary palynological data. Compt. Rend. Acad. bulg. Sci., 58(7): 799-804.

Jiménez-Moreno G., Aziz H.A., Rodriguez-Tovar F.J. Pardo-Iguzquiza E. and Suc J.-P., 2007a. Palynological evidence for astronomical forcing in Early Miocene lacustrine deposits from Rubielos de Mora Basin (NE Spain). Palaeogeography, Palaeoclimatology, Palaeoecology, 252(3): 601-616.

Jiménez-Moreno G., Fauquette S. and Suc J.-P., 2008a. Vegetation, climate and palaeoaltitude reconstructions of the Eastern Alps during the Miocene based on pollen records from Austria, Central Europe. Journal of Biogeography, 35(9): 1638 - 1649.

Jiménez-Moreno G., Fauquette S., Suc J.-P. and Aziz H.A., 2007b. Early Miocene repetitive vegetation and climatic changes in the lacustrine deposits of the Rubielos de Mora Basin (Teruel, NE Spain). Palaeogeography, Palaeoclimatology, Palaeoecology, 250(1): 101-113.

Jiménez-Moreno G., Mandic O., Harzhauser M., Pavelic D. and Vranjkovic A., 2008b. Vegetation and climate dynamics during the early Middle Miocene from Lake Sinj (Dinaride Lake System, SE Croatia). Review of Palaeobotany and Palynology, 152(3-4): 270-278.

Jiménez-Moreno G., Rodriguez-Tovar F.J., Pardo-Iguzquiza E., Fauquette S., Suc J.-P. and Muller P., 2005. High-resolution palynological analysis in late early-middle Miocene core from the Pannonian Basin, Hungary: climatic changes, astronomical forcing and eustatic fluctuations in the Central Paratethys. Palaeogeography, Palaeoclimatology, Palaeoecology, 216(1): 73-97.

Kayseri, M.S. and Akgun, F., 2008. Palynostratigraphic, Palaeovegetational and Palaeoclimatic Investigations on the Miocene Deposits in Central Anatolia (Çorum Region and Sivas Basin). Turkish Journal of Earth Sciences, 17: 361-403.

Kojumdgieva, E., Stojkov, S. and Markova, S., 1984. Lithostratigraphy of the Neogene sediments in Tundzha Basin. Rev. Bulg. Geol. Society, 45(3): 287-295 (in Bulgarian).

Mai, D. and Palamarev, E., 1997. Neue paläofloristische Funde aus kontinentalen und brackichen Tertiärformationen in Bulgarien. Feddes Repertorium, 108(7-8): 481-506.

Mosbrugger, V., 1995. New methods and approaches in Tertiary palaeoenvironmental research. Abhandl. Staatl. Mus. Mineralog. Geol. Dresden, 41: 41-52.

Mosbrugger, V. and Utescher, T., 1997. The coexistence approach -- a method for quantitative reconstructions of Tertiary terrestrial palaeoclimate data using plant fossils. Palaeogeography, Palaeoclimatology, Palaeoecology, 134(1-4): 61-86.

Mosbrugger, V., Utescher, T. and Dilcher, D.L., 2005. Cenozoic continental climatic evolution of Central Europe. Proceedings of the National Academy of Sciences, 102(42): 14964-14969.

Nakov, R., Burchfiel, B.C., Tzankov, T. and Royden, L.H., 2001. Late Miocene to recent sedimentary basins of Bulgaria. Geological Society of America Map and Chart Series, MCHO, 88: 1-28.

Nikolov, I., 1985. Catalogue of the localities of Tertiary

Mammals in Bulgaria. Palaeontology, Stratigraphy and Litholology, 21: 43-62.

Palamarev, E., 1990. Grundzüge der paläofloristischen Paläosukzessionen im Spätmiozän (Sarmatien-Pontien) Bulgariens. In: E. Knobloch and Z. Kvaček (Editors), Palaeofloristic and palaeoclimatic changes in the Cretaceous and Tertiary, Prague, pp. 257-263.

Palamarev, E. and Bozukov, V., 2004. The macroflora of Neogene sediments in the Elhovo Formation (Southeast Bulgaria). Phitologia Balcanica, 10(2-3): 131-146.

Palamarev, E., Ivanov, D. and Bozukov, V., 1999. Paläoflorenkomplexe im Zentralbalkanischen Raum und ihre Entwicklungsgeschichte von der Wende Oligozän/Miozän bis ins Villafranchien. Flora Tertiaria Mediterranea, VI (5): 1-95.

Stringmeteo, 2006-2009a. Climate data for reference bulgarian stations (1961-1990, Monthly weather-fore-cast of NIMH). www.stringmeteo.com.

Stringmeteo, 2006-2009b. Climate data for reference bulgarian stations (Climate Reference Book: temperatures 1931-1970, precipitations 1931-1985). www.stringmeteo.com.

Syabryaj, S., Utescher, T., Molchanoff, S. and Bruch, A.A., 2007. Vegetation and palaeoclimate in the Miocene of Ukraine. Palaeogeography, Palaeoclimatology, Palaeoecology, 253(1-2): 153-168.

Temniskova-Topalova, D., Ivanov, D.A. and Popova, E., 1996. Diatom analysis on Neogene sediments from the Elhovo Basin in South Bulgaria. Geologica Carpathica, 47(5): 289-300.

Temniskova-Topalova, D. and Ognjanova-Rumenova, N., 1997. Description, comparison and biostratigraphy of the nonmarine Neogene diatom floras from Southern Bulgaria. Geologica Balcanica, 27(1-2): 57-81.

Traiser, C., Klotz, S., Uhl, D. and Mosbrugger, V., 2005. Environmental signals from leaves - a physiognomic analysis of European vegetation. New Phytologist, 166: 465-484.

Traiser, C., Uhl, D., Klotz, S. and Mosbrugger, V., 2007. Leaf physiognomy and palaeoenvironmental estimates – an alternative technique based on an European calibration. Acta Palaeobotanica, 47(1): 181-201.

Uhl, D., Bruch, A., Traiser, C. and Klotz, S., 2006. Palaeoclimate estimates for the Middle Miocene Schrotzburg flora (S Germany): a multi-method approach. International Journal of Earth Sciences, 95(6): 1071-1085.

Uhl, D., Mosbrugger, V., Bruch, A. and Utescher, T., 2003. Reconstructing palaeotemperatures using leaf floras - case studies for a comparison of leaf margin analysis and the coexistence approach. Review of Palaeobotany and Palynology, 126: 49-64.

Uhl, D., Traiser, C., Griesser, U. and Denk, T., 2007. Fossil leaves as palaeoclimate proxies in the Palaeogene of Spitsbergen (Svalbard). Acta Palaeobotanica, 47(1): 89-107.

Utescher, T., Djordjevic-Milutinovic, D., Bruch, A. and Mosbrugger, V., 2007. Palaeoclimate and vegetation change in Serbia during the last 30 Ma. Palaeogeography,Palaeoclimatology, Palaeoecology, 253 (1-2):141-152.

Utescher, T., Ivanov, D., Harzhauser, M., Bozukov, V., Ashraf, A.R., Rolf, C., Urbat, M. and Mosbrugger, V., 2009a. Cyclic climate and vegetation change in the late Miocene of Western Bulgaria. Palaeogeography, Palaeoclimatology, Palaeoecology, 272 1-2): 99-114.

Utescher, T. and Mosbrugger, V., 1990-2007. The Palaeoflora Database at http://www.palaeoflora.de.

Utescher, T., Mosbrugger, V. and Ashraf, A.R., 2000. Terrestrial climate evolution in northwest Germany over the last 25 million years. Palaios, 15(5): 430-449.

Utescher, T., Mosbrugger, V., Ivanov, D. and Dilcher, D.L., 2009b. Present-day climatic equivalents of European Cenozoic climates. Earth and Planetary Science Letters, 284(3-4): 544-552.

Velev, S., 1997. Contemporary air temperature and precipitation fluctuations in Bulgaria. In: M. Jordanova and D. Donchev (Editors), Geography of Bulgaria. Publishing House Bulg. Acad. Sci., Sofia pp. 145-150, (in Bulgarian).

Wolfe, J.A., 1993. A method of obtaining climatic parameters from leaf assemblages. US Geol. Surv. Bull, 2040: 1-71.

Zachos, J., Pagani, M., Sloan, L., Thomas, E. and Billups, K., 2001. Trends, rhythms, and aberrations in global climate 65 Ma to present. Science, 292(5517): 686-693.

Zdravkov, A., Kostova, I. and Kortenski, J., 2007. Properties and depositional environment of the Neogene Elhovo Lignite, Bulgaria. International Journal of Coal Geology, 71(4): 488-504.

Appendix 1. List of palynomorph found out in the sediments of the Elhovo Formation with percentage proportions and distribution of taxa (after Ivanov et al. 2007b and this study).

Pollen/Spore type	Core C-432, Trankovo, Tundzha Basin (depth in m)																			
	42,0	46,0	47,0	48,0	49,0	49,5	54,0	60,0	61,0	62,0	62,5	63,5	64,0	64,5	65,0	73,0	74,0	74,1	75,0	79,0	SR-1
Abies sp.	0	0,1	0	0	0	0,8	0	0	0	0	0	0,7	0,5	0,3	0	0,2	0,5	0,2	0,1	0,9	0
Acer sp.	0	0,5	0,8	0	0,7	1,1	1,7	1	1,4	1,3	0,8	0,7	1,2	0,3	0,8	0,5	0	0,7	0	1,1	0
Achillea sp.	0	0	0	0	0	0	0	0	0	0	0	0	0	0	0	0	0,7	1,3	0	0	0
Alisma sp.	2	0,1	0	0	0	0,3	0	0	0	0	0	0	0,2	0	0	0	0	0	0	0,1	0
Alnus sp.	0	0,5	0,4	9,6	0,5	0	1,3	1,6	1	1,1	0	1,1	1,7	1,7	1,2	0,9	1,9	2,4	1,4	1,5	6,3
Anacardiaceae	0	0,1	0,2	0,3	0,9	0,9	0	0,9	0,6	0,2	1,3	0,4	0,2	0,3	0	0,5	0,2	0,2	0	0,4	0
Apiaceae	0	0,2	0,9	0,3	0,2	0,5	0,2	0,1	0,6	0,9	0,3	0	1	0,7	0	0,5	0	0,9	0,1	0,3	1,8
Araliaceae & Hedera sp.	0	0,3	0,7	0	0	0,6	0,2	0,3	0	0,2	0	0	0	0,2	0,4	0	0	0	0	0,3	0
Artemisia sp.	0	0	0	0	0	0,3	0	0,6	0	0	0	0	0	0	0	0	0	0	0	0	2,7
Aster type	0	0	0	0	0	0	0	0	0	0	0,2	0	0	0	0	0	0	0	0	0	0,9
Asteraceae	0	0	0,2	0,3	0	0,2	0,4	0,6	0,2	0,4	6,3	0,7	0,7	1,7	0,4	1,1	3,1	0	0	0,1	0
Asteroideae	0	0	0	0	0	0	0	0	0	0	0	0	0	0	0	0	0	0	0	0	8,5
Betula sp.	0	3	2,8	3,3	0,9	2,3	0	1,1	3	2,4	3,7	3	3,7	5,1	1,6	2,9	2,1	4,1	2,8	2,6	1,8
Brassicaceae	0	0	0	0	0	0	0	0	0	0	0	0	0	0	0	0	0	0	0	0	0,4
Buxus sp.	0	0,7	3	0	2,4	2,6	0,6	0,1	0	0	0	0,7	0	0	0,4	0,7	0,7	0,4	0,2	0,7	0
Caprifoliaceae	0	0	0,2	0	0,6	0,5	0	0	0	0	0	0	0	0	0	0,2	0,2	0	0,1	0	0,4
Carpinus betulus type	0	0	0,1	0	0	0,7	0,4	1,3	0	1,1	0	1,1	1,2	1,4	0	0,7	1,4	1,5	1,2	4,9	2,2
Carpinus orientalis/Ostrya type	0	1,1	1,4	0,3	0,5	1,1	0	1,4	0,8	0,8	1	3,3	3,4	0,8	0,8	3,2	2,4	2,6	2	3,8	3,6
Carya sp. 1 & 2.	2	6,1	3,7	4,1	3,7	2,6	3,2	4,9	1	8,8	6,8	5,9	7,9	8,8	3,7	3,8	7,3	8,1	8,9	4,3	0
Caryophyllaceae	0	0,2	0,1	0,3	0,4	0,7	0	0	0,4	0,8	0	0,4	1,7	0,2	0,4	0,9	0,2	0	0,2	0,4	0,4
Castanea sp.	0	0,3	0,8	0,8	0	0,4	0	0	0,6	1,3	2,3	3,2	1,5	2,7	0,8	0,5	0,7	0,9	1,8	0,2	0,4
Castanopsis sp.	0	0	0	0	0	0	0	0	0	0	0	0,2	0	0	0	0	0	0	0	0	0
Cedrus sp.	0	0	0	0	0	0,4	0,6	0	0	0	0	0	0	0	2,9	0,5	0,7	0	0,2	0,2	0,4
Celtis sp.	0	0,3	0,7	0,3	0	0,1	0	0	0	0	0	1,1	0	0,2	0	0	0	0,4	0,1	0	0
Centaurea sp.	0	0	0	0	0	0	0	0	0,2	0,8	0	0	0	0	0	0	0	0	0	0,1	0,9
cf. Altingia sp.	0	0	0,2	0,3	0	0,6	0,4	0	0	0	0	0	0	0,5	0	0	0,2	0	0,2	0	0
cf. Euphorbia	0	0	0	0	0	0	0	0	0	0	0,1	0	0	0	0	0	0	0	0	0	0
cf. Glyptostrobus	32	0	0,4	1,4	1,5	0,7	1,1	1,3	1,2	1,5	1,3	1,9	2,5	3,2	6,1	3,2	1,7	0,4	2,1	0,9	0
cf. Keteeleria	0	0	0	0	0	0	0	0	0	0	0	0	0	0	0	0	0	0	0	0	0,4
Chenopodiaceae	0	0,1	0,8	0	0,5	1,3	0	0	1,4	1,9	3,4	1,9	0,2	5,1	0,8	1,1	0,7	0,7	0,2	0,7	11,6
Cichorioideae	0	0	0,2	0,3	0	0,2	0,4	0,6	0,2	0,2	1,3	0,7	0,7	1,7	0,4	1,1	0,7	0	0	0,1	1,4
Cornus sp.	0	1,4	1,7	0	0,5	0,6	0,2	0	0,4	0,9	0,5	0	0	0	0,4	0,7	0,2	0,2	0	0,1	0
Corrugatosporites sp.	0	0	0,2	0	0	0	0,2	0	0	0	0	0	0	0	0	0	0	0	0	0	0
Corylopsis sp.	0	0,1	1,7	0,6	0,4	1,8	0,4	0	0	0	0	0	1	0,3	0,8	0,9	0	0,9	0,2	0,3	0
Corylus sp.	0	2,2	0,5	0,3	1,6	1,3	0	0,7	1,6	1,3	0	0,4	2,5	1,2	0	3,4	0,7	1,7	1,1	2,3	2,7
Cupressaceae	2	0	0	0	0	0	0	0	0	0	0	0	0	0	0	0	0	0	0	0	0
Cyperaceae	4	0	1	0	0	0,7	0	0	0	0,4	0,5	0	0,2	0	0	0,4	0,6	0	0	0	0,4
Cyrillaceae/Clethraceae	0	0	0	0	0	0	0	0	0	0	0	0	0	0,5	0	0,2	0	0	0	0	0
Dipsaceae	0	0	0	0	0	0,1	0	0	0	0	0,3	0	0	0	0	0,2	0	0	0	0	5,4
Echinatisporis	0	0	0	0,3	0	0	0	0	0	0	0	0	0	0	0	0	0	0	0	0,2	0
Engelhardia sp.div.	0	5,9	7,8	11,8	9,1	5,4	9,4	10	3,6	5,6	5,2	1,9	2,9	4,6	5,7	1,1	2,4	10,1	2,5	3,1	0
Ephedra sp.	0	0,1	0	0	0,2	0	0,2	0	0	0	0	0	0	0	0	0	0	0	0	0	0
Equisetum sp.	0	0	0	0	0	0	0	0	0	0	0,1	0	0	0	0	0	0	0	0	0	0
Ericaceae	0	0,2	0	0,8	0,6	1,1	0,2	0,6	0,6	0,4	1	0	1,2	0,2	2	2,7	0,7	2	3,2	4	0
Eucommia sp.	0	0,4	1,9	1,4	0,5	0,6	0	1,4	1,2	1,3	0,5	0,4	0,5	1	0	1,6	1,2	0,2	1,2	2,5	0
Fabaceae	0	0	0	0	0	0	0	0	0	0	0	0	0	0	0	0	0	0	0	0	0,9
Fagus sp.	0	1,9	3	1,1	1	4,5	0,4	2,6	0,8	0,6	0	2,6	0,2	1	5,7	7,4	5,2	3,9	5	4,5	0,4
Fraxinus sp.	8	12	13,3	7,4	12,4	16,3	3	13,9	8,9	4,5	5,2	2,2	0,5	1,4	2,4	1,4	1,9	3,3	2,3	4,6	0
Humulus/Cannabis type	0	0	0	0	0	0	0	0	0	0	0	0	0	0	0	0	0	0	0	0	1,4
Ilex sp.	0	0	0,7	0	0	0,3	0	0	0	0,9	0	0	0	0	0	0,2	0	0	0	0	0
Juglans sp. 1 & 2.	0	0	0,2	0	0,4	0,3	0	0	0	0	0	0	0,5	0,2	0	0,9	0	0	0	0	0
Laevigatosporites	0	0	0,1	0,5	0,8	0,4	0,2	0	0,2	0,9	1,3	0	0	0,4	0	0,2	0	0	0	0	0
Liliaceae	0	0	0	0	0	0,1	0,2	0	0	0	0,8	0	0	0,5	0	0	0	0	0	0,1	0
Liquidambar sp.	0	0	0	0	0	0	0	0	0	0	0	0	0	0,5	0	0,2	0	0	0	0	0
Lonicera sp.	0	0	0	0	0	0	0	0	0	0	0	0	0	0	0	0	0	0	0	0	0,4
Lycopodium sp.	0	0,2	0	0	0,4	0	0	0,3	0	0	0	0,7	0	0	0	0	0	0	0,2	0	0
Magnolia sp.	0	0	0	0	0	0	0	0	0	0,2	0	0	0	0,5	0	0	0	0	0	0,3	0
Mentha/Salvia	0	0	0	0,8	0	0,2	0	0	0	0	0	0,4	0	0,2	0	0	0	0	0	0	0
Myrica sp.	0	3,2	1	3,5	0,2	1,3	0,4	0,3	0	0,8	0	0	0,7	0,2	0	1,6	0	3,7	1,4	0,9	0,4
Nuphar sp.	0	0	0	0,1	0	0	0	0	0	0	0	0	0	0	0	0	0	0	0	0	0
Nymphaeaceae	0	0	0	0	0	0	0	0	0	0	0	0	0	0	0	0	0	0	0	0	0,9
Nyssa sp.	0	0,2	0,9	0,3	0,4	0,6	0	0,6	2,4	0,9	1,6	2,2	2,5	2,5	1,2	3,8	3,1	1,3	1,4	2,6	0,4
Oleaceae	0	3,9	4,7	0	1,8	3,5	0	0	0,6	0	3,4	1,1	0	1	0	0	0	0,6	0,6	0,3	0,4
Osmunda sp.	0	0	0	0	0	0,2	0	0	0	1,1	0,5	0	0,2	0,3	0	0	0,4	0	0	0	0
Persicaria sp.	0	0	0	0	0	0	0	0	0	0	0,3	0,4	0,2	0	0	0	0	0	0	0	0
Picea sp.	0	0,4	0,3	0,6	1,2	1,1	3,6	1,6	3,8	1,7	1,6	4,4	2,5	2,5	1,6	1,4	0,9	0,6	0,6	3,8	0,4
Pinaceae ind.	2	0	0	0	0	0,1	0	0	0	0	0	0	0	0	0	0	0	0	0	0	0
Pinus diploxylon type	14	15,2	1,8	5,5	20,8	15,5	45	13,2	20,3	20,7	21,7	18,5	12,5	11,7	14,3	11,3	26,1	17,3	19,7	17,2	13,5
P. haploxylon/Cathaya	0	3,6	0,3	0,6	0	0,8	0,4	0,6	0,2	0	0	0	1,5	0,3	0,4	0,7	0	0,7	0,6	0,2	0,4
Pistacia sp.	0	0	0,2	0	0,9	0,2	0	0	0	0	0	0	0	0,2	0	0	0	0	0	0	1,4
Plantaginaceae	0	0	0	0	0	0	0	0	0	0	0	0	0	0	0	0	0	0	0	0	1,8
Platanus sp.	0	0,2	0,5	9,6	0	0,6	0,4	0	0	0,4	0,3	0	0	0	0,4	0,7	0	0,2	0	0,6	0,4
Platycarya sp.	0	0	0	0	0	0	0	0	0	0	0	0	0	0	0	0	0	0	0	0	0
Poaceae	0	1,4	2,8	0,6	1,8	1,7	0	0,4	1,4	0,6	0,3	1,5	0	2,5	1,6	3,8	5,5	1,5	3	1,8	6,7
Poaceae - Bambusoideae	0	0	0,3	0	0	0	0	0	0	0	0	0	0	0,4	0	0	0	0	0	0	0,4
Polygonum sp.	0	0	0	0	0,4	0,4	0	0,7	0	0	0	0	0	0	0	0,2	0	0	0,1	0,1	0
Polypodiosporites	0	1	0	0,3	0	0,1	0	0	0	1,4	0	0	0,2	0,3	0	0	0	0	0	0	0
Potamogeton sp.	0	0	1,3	0	0,4	0,3	0,2	0,3	0,2	0	0	0	0,5	0	0,4	0,2	0	0,5	0	0,7	0
Pteridium sp. & Pteridophyta	0	0	0	0	0	0	0,4	0	0	0	0	0	0	0	0	0	0	0	0	0	0
Pterocarya sp.1 & 2.	2	0,7	0,3	1,7	0,1	0,1	0	0	2	1,5	0	1,5	0,2	0,8	1,6	0,5	0	0,6	0,6	1,7	0,9
Quercus sp. 1 & 2.	4	7,5	7,1	6,6	11,1	5,7	1,7	6	1,2	1,7	0,5	1,9	0,5	0,7	1,2	0,9	0,9	1,5	3,3	2,7	3,1
Rosaceae	0	0,1	0,2	0	0	0,2	0	0	0	0	0	0	0	0	0	0	0	0	0,2	0,3	2,7
Rubiaceae	0	0	0	0	0	0,3	0	0	0	0	0	0	0,2	0	0	0	0	0	0	0	0,4
Salix sp.	0	3,6	6,3	1,1	0,9	0,5	0,2	0	7	0,9	0,5	0,4	0,2	0	0,4	0,2	0	0,6	0,7	0,4	0,9
Sapotaceae	0	0,5	0,2	0	0,6	0,3	0	0,3	1	0,4	0,3	0,4	0,7	0,3	0	0	0,5	0,2	0	0,1	0
Sciadopitys sp.	4	0	0,1	0	0,2	0,2	0,4	0,1	0	0	0	0,7	1,5	0,2	0	0	0,5	0	0,2	0	0
Selaginella sp.	0	0	0	0	0,2	0	0	0	0	0	0	0	0	0	0	0	0	0	0	0	0
Sequoia sp.	0	0	0	0	0	0	0	0	0	0	0	0	0	0,3	0	1,6	0	0	0	0	0
Sparganium sp.	0	0,2	1,9	0	0,2	1,5	0	3,1	1,4	0,5	0,8	0,7	0,2	5,2	2	7,2	5	1,2	0,2	1,1	0,9
Symplocos sp.	0	0	0,4	0	0	0,1	0	0	0	0,4	0,5	0,4	0,5	0	0	0,7	0,2	0	0,2	0,1	0
Tamarix sp.	0	0	0	0	0	0	0	0	0	0	0	0	0	0	0	0	0	0	0	0	0,4
Taxodiaceae	8	1,1	0,2	0	0,5	0,9	0	1,3	0,2	0,4	0,3	1,5	0,5	1,4	0,4	0	0,7	0,7	1,4	1,3	1,4
Thalictrum sp. & Ranunculaceae	0	0	0,1	0	0,2	0,4	0	0	0	0	0	0	0	0	0	0	0	0	0	0	0
Tilia sp.	0	0	0	0,3	0	0	0	0	0	0	0,6	0,5	0,7	0,7	0,3	0	0,9	0,2	0	0	1,4
Tricolporopollenites sibiricum Lubomirova	0	0,2	1,4	1,4	0	0,6	1,5	0,3	0	2,8	2,1	0,7	2,7	0,8	0,4	1,8	1,7	1,5	1,5	0,5	0
Tsuga sp.div.	2	1	1	0	1,3	2,1	4,1	3,3	2,8	4,3	3,7	1,1	0,7	0,7	1,2	1,4	0,9	2	0,9	3,4	0,4
Typha sp. & Typha/Sparganium	0	0,2	1,9	0	0,2	2,2	0	3,1	1,4	0,5	0,8	0,7	0,2	5,2	2	7,2	5	1,2	0,2	1,1	0,9
Ulmus sp.	2	12,9	12	15,7	12,4	7,2	13,2	19,4	19,7	8,3	13,1	20	27,3	19,1	29,8	20,9	16,4	15,7	18,5	10,7	3,6
Undeterminate polen	12	0,5	2,6	6,3	2	2,4	1,7	2,6	5,2	4,5	4,2	3,3	2	2,4	4,1	1,8	2,6	2,4	2,8	1,5	0
Urtica sp.	0	0	0,6	0	0	0	0	0	0	0	0	0	0	0	0	0,2	0	0	0,1	0,5	0
Verrucatosporites	0	0	0	0	0,1	0	0	0	0	0	0	0	0,5	0,4	0	0,4	0,4	0,5	0	0,1	0
Viburnum sp.	0	2,2	2,3	0	0,7	0,1	0	0,4	0	0,9	0	0	0	0	0	0	0	0,4	0	0,4	0
Vitaceae	0	0,5	0	0	0,2	0,1	0	0	0	0	0	0	0	0	0	0,5	0,5	0	0	0	0
Zelkova sp.	0	2,9	3,4	0,6	2,7	2,3	2,6	3,9	2,2	8,8	3,1	3,7	4,7	5,4	3,3	2,3	1,4	1,7	4,7	3,7	0
Botryococcus sp. (Algae)	0	0	0	0	0	0,2	0	0	0	0	0	0	0	0,5	0	0	0	0	0	0	0
AP	100	98	93,6	97,5	96,5	93,6	98,7	97	95,6	94,5	86,9	94,1	95,1	87,2	96,3	90,8	89,1	95,6	95,9	95,6	45,8
NAP	0	2	6,4	2,5	3,5	6,4	1,3	3	4,4	5,5	13,1	5,9	4,9	12,8	3,7	9,2	10,9	4,4	4,1	4,4	54,2
Loc. el.	7,4	1,8	6,3	1,1	2,4	5,7	1,1	6,7	3,1	4,8	3,8	2,2	2,4	11,9	4,3	15,6	11,5	3,6	0,7	3,3	2,3
AP+NAP	50	938	957	363	817	1082	469	697	497	532	383	270	407	592	245	444	422	542	813	1046	224

Scientific Annals, School of Geology, Aristotle University of Thessaloniki Proceedings of the XIX CBGA Congress, Thessaloniki, Greece	Special volume 100	279-286	Thessaloniki 2010

PALAEOENVIRONMENTAL RECONSTRUCTION AND CLIMATE CHANGE IN SOUTH EASTERN EUROPE (NEOGENE KARLOVO LIGNITES, CENTRAL BULGARIA)

Stefanova M.[1], Marinov S.P.[1] Zdravkov A.[2] and Kortenski J.[2]

[1] *Bulgarian Academy of Sciences, Institute of Organic Chemistry, Acad. G. Bonchev str. bldg. 9, BG-1113, Sofia, Bulgaria, maia@orgchm.bas.bg*
[2] *Department of Economic Geology, University of Mining and Geology "St. Ivan Rilski", 1700 Sofia, Bulgaria*

Abstract: Neogene Karlovo Basin, Central Bulgaria was comparatively studied with other Bulgarian lignites for palaeoenvironment assessment. Petrographic and chemical methods were used. The data allowed floral reconstruction at the region and assumption for the climate during the corresponding geological time. The data of geochemical and petrographic studies gave proves for the long-term evolution of the Late Neogene on the South Eastern Europe connected with the decrease in palaeotropical elements and increase in arctotertiary taxa. Conifers remained main coal-forming vegetation predominantly represented by *Pinaceae*. Biomarker assemblage assumed insignificant *Cupressaceae*/*Taxodiaceae* contribution. Monoaromatic angiosperm-derived triterpenoids with ursane/oleanane skeleton proved the presence of dicotyledonous angiosperm-derived organic matter in the palaeoplant taxa as well. Palaeoenvironmental conditions within the forest swamp should be determined as limnic, with varying water table and seasonal drying.

Key words: Neogene, Bulgaria, lignite, palaeoenvironment, petrography, biomarkers

1. Introduction

Palaeoclimate reconstruction is based on the pollen analysis and plant macrofossil record. It is advisable for climate changes restoration, i.e. temperature, humidity and their oscillation within the time, to be familiar with the vegetation during the corresponding geological period. Molecular organic geochemistry has the same target – to find relationship between registered organic compounds and specific taxa. Currently limited studies correlate biomarkers to modern taxa and try to draw systematic and phylogenetic relationships (Otto and Wilde, 2001; Hautevelle et al. 2006). Once sufficient and unequivocal information is available for source specific markers, palaeoclimatic reconstructions will be possible and floral diversities during certain geological ages can be proposed. Such data also will enhance the knowledge on coal precursors and their diagenetic transformations during coalification.

2. Study area

Karlovo Basin is the eastern-most basin in the Sofia coal province (Fig.1). It represents a tectonic graben bounded by the Middle Stara Planina Mountain to the north and the Sredna Gora Mountain to the south. The basin is filled with up to 350 m of Neogene sediments which overlie basement rocks composed of Precambrian and Paleozoic gneisses and granitoides. According to Angelova et al. (1991) the sedimentation was controlled by the formation and development of asymmetric basement blocks having different subsidence rates. The most significant tectonic movements occurred in the northwestern part of the graben, where the thickest Neogene sediments were deposited.

Sedimentation commenced in a fluvio-lacustrine environment with deposition of up to 15m of sandy gravels (Chounev et al., 1966; Fig. 2). Subsequently, the interfingering of sediments from different fluvial sources resulted in deposition of horizontally and vertically alternating layers of greenish to grey-blue silty to sandy clays and layers of unsorted sands and gravels (Fig. 2).

Later, block displacements established lacustrine environments in the center of the northwestern block of the Karlovo Graben and resulted in the

formation of up to 50m thick sediments, represented by several coal seams, diatomaceous clays and diatomites. Along the basin margin these interfingers with sandy sediments (Angelova et al., 1991). Temniskova et al. (1996) established multiple changes of benthic-epiphytic deep-water diatom species with planktonic ones which indicate frequent changes in water depth during the early stages of the deposition of the coal-bearing strata. Eleven coaly layers (Chounev et al., 1966) were formed, but only the topmost seam is up to 11m thick (Šiškov, 1985). Acidophilic diatom species suggested that coal formation occurred under acidic conditions.

3. Materials and methods

The present study is based on 24 samples from the main coal layer in Karlovo Graben. The samples originate from different drillings in the south-eastern part of the basin. Previously the samples were part of the studies of Kortenski and Dimitrov (1989), and Kortenski (1991) concerning the mineralogical and inorganic geochemical characteristic of the coal.

For the purpose of the present study, the samples from the neighboring drilling were combined into 3 bulk samples for the investigation of the organic geochemical composition of the coal. The position

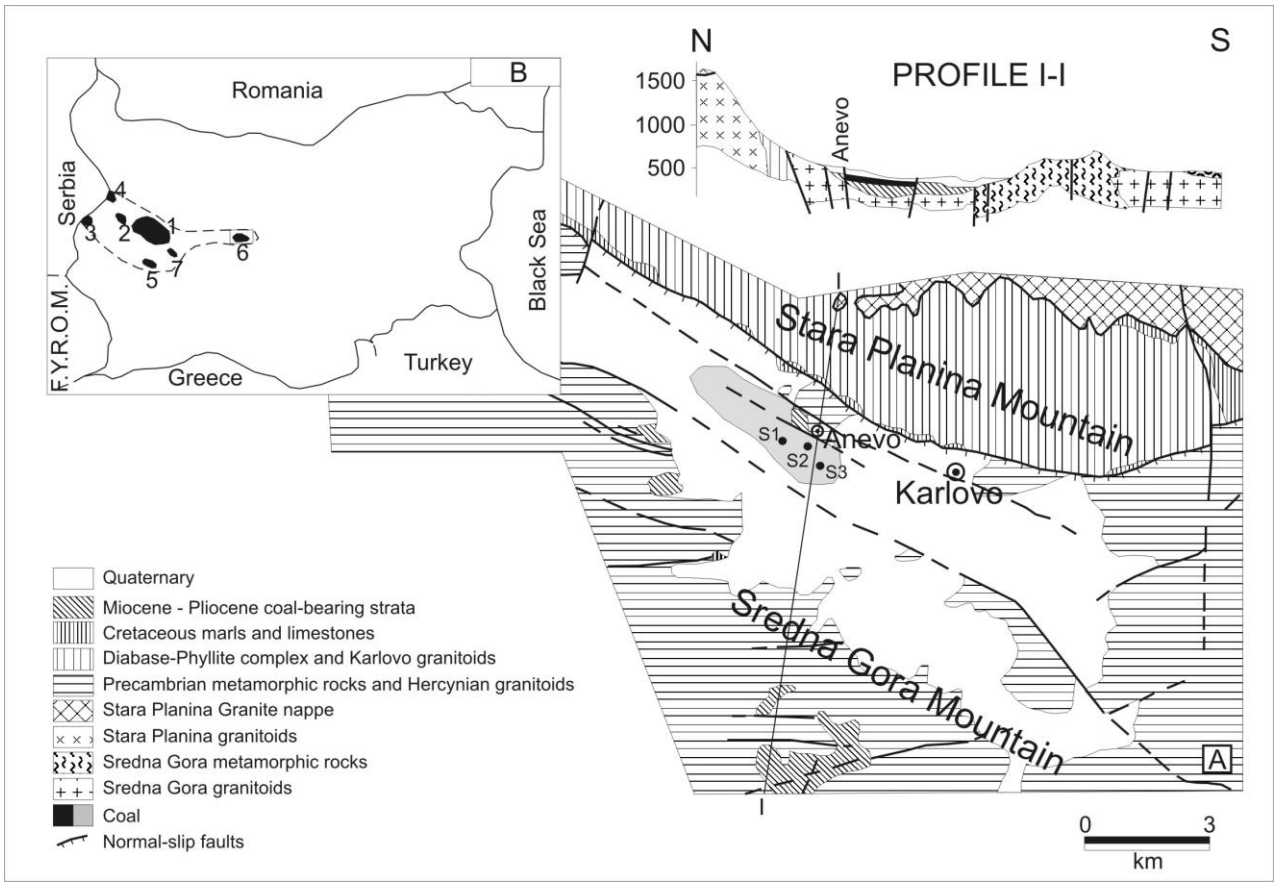

Fig. 1. Geological map (A) of the Karlovo graben (modified after Chounev et al., 1966; Angelova et al., 1991) and position of the basin within the Sofia coal province (C). S1, S2, S3 - the places of sampled; 1-Sofia basin; 2-Aldomirovtsi basin; 3-Belibreg basin; 4-Staniantsi basin; 5-Samokov basin; 6-Karlovo basin; 7-Chukurovo basin.

During the Late Pliocene, the lacustrine/palustrine depositional environment was replaced by a fluvial one. The latter resulted in the formation of alternations of sand, gravel, clay, and silt layers. These overlie the older washed-out lacustrine sediments with a sharp lithological boundary (Fig. 2; Angelova et al., 1991). The youngest deposits in Karlovo Basin are coarse-grained alluvial, proluvial, and talus sediments of Quaternary age.

of the samples within the coal basin is shown in Fig. 1.

For microscopic investigations, the samples were crushed to a maximum size of 1 mm, mounted in epoxy resin, ground and polished. Maceral analysis was performed by a single-scan method with Leica DM 2500 microscope using reflected white and fluorescent light. At least 350 points for each sample were counted.

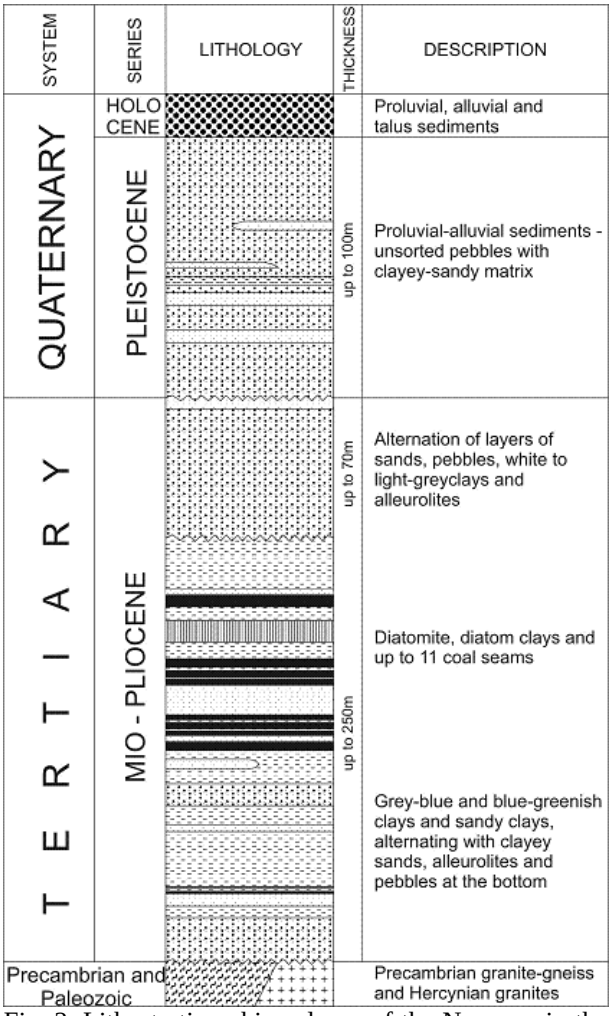

Fig. 2. Lithostratigraphic column of the Neogene in the Karlovo graben (modified after Chounev et al., 1966; Angelova et al., 1991).

The same protocol of bitumen preparation, separation and analysis as described in the previous paper for Chukurovo lignite is used (Stefanova et al., 2005). Individual compounds are identified by comparison of mass spectra with literature and library data. 2,4,6-Triethylbenzene is used as an inner standard for quantitative data interpretation. Contents of identified compounds are expressed in micrograms per gram "dry, ash free" coal sample (ug/g^{daf}).

4. Results and discussion

4.1. Maceral composition

The maceral composition of Karlovo lignite is dominated by the Huminite group macerals (Table 1). Their average contents in the bulk samples are around 80-80.8 %, but vary from 72.3 to 88.7 % in the individual samples. The organic matter is generally composed of groundmass, represented by both attrinite and densinite (Fig.3a) with contents reaching up to 82.5 % in the individual samples, but in the majority of the samples the amount of detrogelinite is mainly between 70 and 80%. Within the groundmass are scattered pieces of telohuminite macerals with different form and size. The subgroup is mainly represented by highly gelified eu-ulminite (Fig.3b, c) with contents varying significantly from 17.1 up to 50.5 %. Only small amount of it (about 4.6 to 6.7 %) is slightly less gelified and show transition to textinite (Fig. 3b). The latter is only a minor component of the organic matter in the studied lignite. Its average contents are between 4.6 and 6.7 %, but reach up to 10 % in some samples.

Unlike the other lignite basins in Sofia coal province, the studied lignite contains significant amount of liptinite macerals (from 16.7 to 18.2% - Table 1, and up to 24.9% in the individual samples). This is mainly due to the high contents of alginite (4.0 to 12.3%, Fig. 3a,e,f), and liptodetrinite (2.4 to 10.5 %, Fig. 3d). The rest of the macerals (microsporinite – Fig. 3f; cutinite – Fig. 3d; resenite, suberinite, fluorinite) from this group are usually an insignificant constituent of the organic matter with contents rarely exceeding 1 %.

Like most of the Tertiary coal basins around the world, Karlovo lignite contains only very small amounts of inertinite macerals – up to 2.5% (Table 1). The most abundant ones are funginite (Fig. 3a) with contents up to 2.7% in the individual samples, and inertodetrintie (up to 2.3% in the individual samples). The average contents of these macerals are however, much lower – around 1.0-1.5 % for the funginite and below 1.0% for the inertodetrinite (Table 1). In some of the samples can be observed also small lenses of fusinite and semifusinite, but usually their contents are less than 1%.

In general, the petrographic composition of the studied samples is similar to that established previously by Zdravkov et al. (2006). Based on the calculation of the maceral indices the palaeoenvironmental conditions within the forest swamp should be determined as limnic, with varying water table and seasonal drying.

4.2. Bulk characteristics

The data for extracts separated into aliphatic, aromatic and polar fractions on Silicagel column are summarized in Table 2. Different homologue series will be discussed separately.

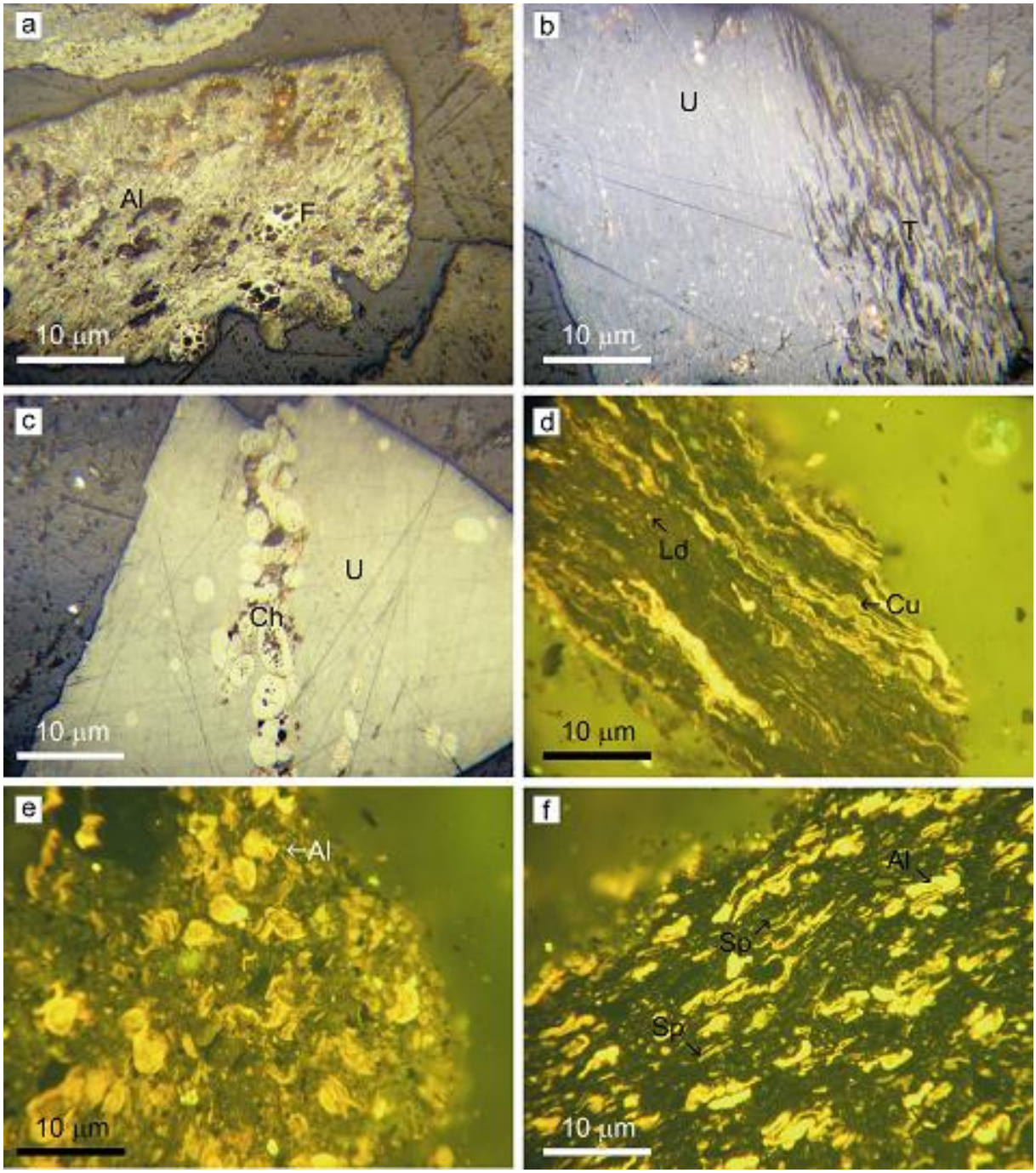

Fig. 3. Microphotographs of Karlovo lignite: a) Alginite (Al) and Funginite (F) in attrinite-densinitic groundmass, reflected white light, oil immersion; b) Highly gelified ulminite (U) in association with textinite (T), reflected white light, oil immersion; c) Highly gelified ulminite (U) with corpohuminite (Ch) bodies in former cell walls, reflected white light, oil immersion; d) Cutinite (Cu), associating with liptodetrinite (Ld) fragments, blue excitation light, oil immersion; e) Multiple alginite (A) bodies and fragments, blue excitation light, oil immersion; f) Alginite (A) and single microsporinite bodies (Sp), blue excitation light, oil immersion.

4.3. Aliphatic lipids

4.3.1. n-Alkane distribution

GC-MS reveals the presence of *n*-alkanes and terpenoids (Table 3, Fig.4) in the neutral fractions. *n*-Alkanes distribution is bimodal with two distinct maxima at *n*-C_{16} and *n*-C_{29}. The calculated values for CPI are S1= 3.5, S2 = 4.0 and S3= 2.0. The CPI magnitudes may be explained by the contribution of epicuticular wax from higher plants. There are at least two sources of *n*-alkanes: (a) shorter chains might be from algal or bacterial contribu-

tions to the palaeomire, and (b) the longer chains from terrestrial sources. The lower value calculated for sample S3, CPI = 2, comparing to the other ones, is an indication for the algal prevalence.

Table 1. Maceral composition of coal from Karlovo basin, % daf.

Sample	T	U	Ph	G	At	D	Hum	Sp	Cu	R	Sb	Al	Fl	Ld	Lipt	Fs	Id	F	Inert	MM
S1	5.1	33.3	2.6	0.8	31.0	*7.9*	80.7	0.7	0.7	1.0	0.3	8.3	0.6	5.5	17.1	0.1	0.6	1.5	2.2	23.5
S2	6.7	37.6	2.6	0.0	16.4	*17.5*	80.8	0.3	0.9	1.7	1.2	6.0	0.3	6.3	16.7	0.4	0.9	1.2	2.5	9.7
S3	4.6	32.3	3.4	0.2	27.5	*12.0*	80.1	0.4	1.0	0.6	1.0	8.0	0.0	7.2	18.2	0.1	0.6	1.0	1.7	19.3

T = Textinite; U = ulminite; Ph = Phlobaphinite; G = Gelinite; At = Attrinite; D = Densinite; Hum – Huminite group; Sp = Sporinite; Cu = Cutinite; R = Resinite; Sb = suberinite; Al = alginite; Fl = Fluorinite; Ld = Liptodetrinite; Lipt – Liptinite group; Fs = Fusinite; Id = Inertodetrinite; F = Funginite; Inert – Inerinite group; MM – mineral matter.

Pristane (Pr) is less abundant compared to phytane (Ph). This proportion is not typical for non-marine shales and coals because Pr is normally dominant in coal extracts. In our case the Pr/Ph ratio is < 1, which could be interpreted as an indication of a reducing environment during deposition.

Table 2. Bulk characteristics of samples and their bitumen extracts, in %.

Sample	Moisture	Ash	Bitumen				
			Yield	Fractions			Asph.
				Neutral	Arom.	Polar	
S1	6,9	30,2	2,2	10,3	15	65,3	1,6
S2	7,8	24,1	2,6	8,8	11,1	64,4	1,8
S3	7,7	23,7	2	18,2	11,5	64,5	1,3

4.3.2. n-Alkan-2-one distribution

A homologous series of long-chain acyclic *n*-alkan-2-ones with "odd" numbered homologues prevalence are determined in the extracts. The distributions of the long-chain *n*-alkanes and *n*-alkan-2-ones, i.e., *n*-C_{24} to *n*-C_{33}, are similar. All samples maximize at *n*-C_{31} and the "odd" homologues dominate. The similarity in distribution patterns suggests a product-precursor relationship. High quantities of isoprenoid C_{18} ketone (6,10,14-trimethyl-pentadecan-2-one) are registered as well. This ketone is supposed to be derived from microbial degradation of phytol and is often present in products of extraction or pyrolysis of fossil materials.

4.4. Terpenoids

4.4.1. Sesquiterpenoids

Hydrocarbons based on the cadinane skeleton are common constituents of resins, ambers, and petroleum with a terrigenous input component (Simoneit et al. 1986; Otto and Wilde, 2001). Subordinated quantities of sesquiterpenoid are determined. In all samples are registered cedrane and reduced cadalene derivatives.

4.4.2. Diterpenoids

Diterpenoids are distributed mainly in gymnosperms and in only a few angiosperms among contemporary plants. The "regular" abietane skeletal type of diterpenoids is represented by fichtelite and abietane (Fig.5). These compounds are often found in pine wood submerged in peat. The "regular" abietanes occur in all conifer families except *Phyllocladaceae*. The "phenolic" abietanes, i.e. ferruginol, sugiol, etc., are expected in the aromatic/polar fractions as in other Bulgarian lignites, i.e. Maritza-East, Chukurovo, etc. (Stefanova et al. 2002; Stefanova and Simoneit, 2008). There are no polar diterpenoids in the analyzed samples. A high preponderance of fichtelite and negligible contents of 16α(H)-Phyllocladane are registered in all samples. Minor quantities of partially aromatized abietane structures are also found (Fig.5).

Diterpenoids in Karlovo lignite are the dominant biomarkers in bitumen extracts but several peculiarities should be emphasized, namely: (i) subordinating quantities of 16α(H)-Phyllocladane (Fig. 5); (ii) and, total absence of polar diterpenoids;

4.4.3 Triterpenoids

Triterpenoids in fossils are hypothetically divided into two groups, hopanoids and non-hopanoids (Bechtel et al. 2005). Hopanoids are indicators of microbial activity while non-hopanoids are source-related components. Hopanoids in some Bulgarian lignites have been already discussed (Stefanova et al., 1995; 2005; Bechtel et al., 2005).

Non-hopanoids with lupane, ursane and oleanane skeletons are markers for a palaeoswamp with angiosperm predominance. The most abundant in samples under consideration are oleanane-type triterpenoids like β–amyrone. It should be noted that the presence of C-3 functionalized triterpanes (alcohols, acids, ketones, esters, etc.) makes them more susceptible to microbial or photochemical degradation to des-A-ring products (Des-A-lupane). A peculiarity of samples under study is

the appreciable quantity of Lupan-3-one, M^+ 426, m/z 205 (100%), m/z 383 (M^+- 43).

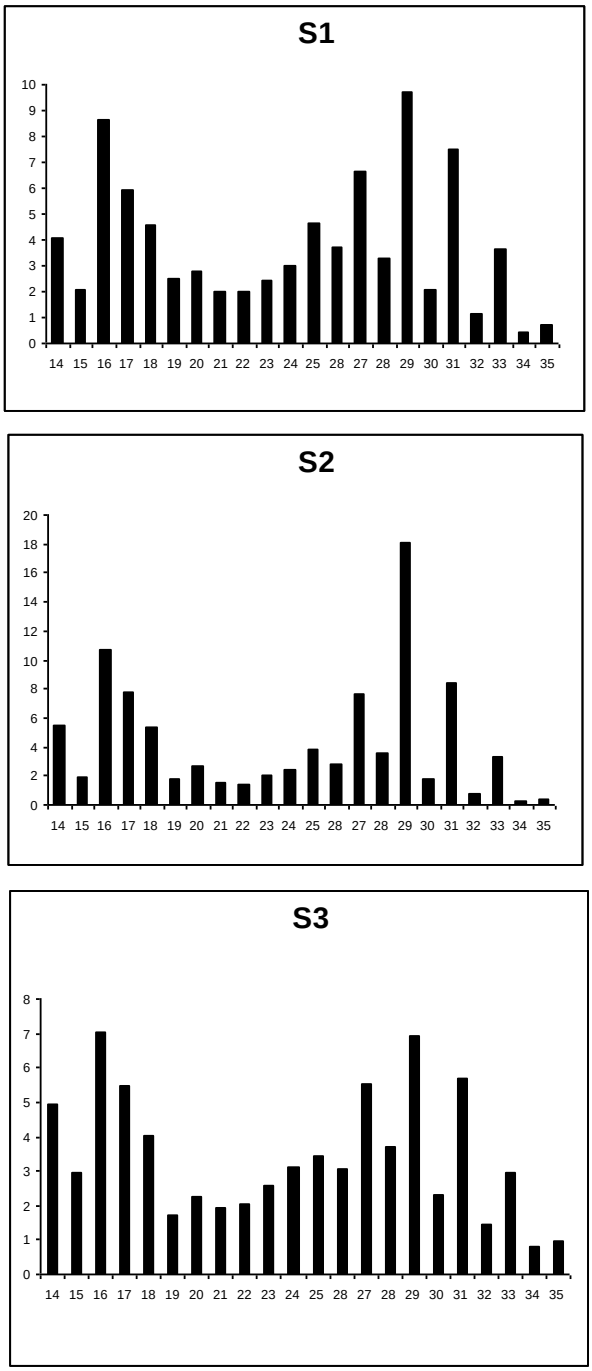

Fig. 4. Patterns of n-alkanes distributions in rel. % (numbers corresponds to the carbon numbers in alkanes).

Oxygenated pentacyclic triterpenoids, i.e., friedelin, α/β–amyrins/amyrones, are present in aromatic fractions. All abovementioned triterpenoids prevail in the surface waxes of the easily degraded leaves of angiosperms. The dominant triterpenoid in all aromatic fractions is friedelin which is a common component of epicuticular waxes (Logan *et al*., 1995). The same functionalized triterpenoid is already registered in the previous study dedicated to Chukurovo coal progenitor *Taxodium dubium* (Stefanova, 2004; Stefanova and Simoneit, 2008)

Monoaromatic angiosperm-derived triterpenoids with ursane/oleanane skeleton (SIM m/z 145) are with low abundance and distributed in neutral and aromatic fractions according to molecular mass, dinoroleana-1,3,5(10),13(18)-tetraene, (M^+ 376) and dinoroleana-1,3,5(10)-triene (M^+ 378). Higher homologue with M^+ 392 is tentative identified as well. Stout (1992) described these compounds as characteristic for Tertiary angiospermous lignite. It is presumed that all oleanane, ursane triterpenoids could be formed by a progressive amyrin aromatization. Triterpenoids and their monoaromatic analogues support the presence of appreciable dicotyledonous angiosperm-derived organic matter in the palaeoplant taxa of Karlovo lignite.

4.4.3.1. Hopanoids

The 22R-17α(H),21β(H)-homohopane ($H_{31\alpha\beta}$ M^+426) is the only prominent peak of the hopane distribution in SIM m/z 191 of neutrals. There are negligible quantities of $H_{27\beta}$, M^+ 370 and other H_{31} stereoisomers ($H_{31\beta\alpha}$ and $H_{31\beta\beta}$). The contribution of microorganism biomass during the diagenetic transformation of the parent organic matter can supply hopanoids.

In aromatic fractions SIM m/z 191 visualizes low quantities of hopanoid ketones, i.e. C_{27}, 17β(H)-trisnor-hopane-21-one (M^+ 384, maximal peak) and C_{29}, α-Adiantone (M^+ 412). One D-ring monoaromatic hopane with M^+ 364 is registered in neutral fractions.

4.5. Steroids

Stigmastan-3-one, M^+ 414 is present in all extracts. The C_{28} and C_{29} steroids are highly abundant in the

Table 3. Biomarkers contents, in microg/g daf coal

Sample	Alkanes	Terpenoids				Hopanes	Steranes	Friedelin
		Sesqui-	Di-	Ses-	Tri-			
S1	40,6	1,3	40,3	1,3	3,0	14,5	0,9	14,4
S2	17,2	0,0	47,6	0,8	1,1	10,9	0,7	14,4
S3	79,2	0,0	52,0	1,2	4,9	24,8	1,0	17,0

plant kingdom and reflect the input of detritus from higher plants (Oros and Simoneit, 1999). The steroids are nonspecific markers because sitosterol, the biological precursor, is ubiquitous in nature.

are abundant as in other Bulgarian lignites, i.e. Maritza-East, Chukurovo, Sofia coal-bearing deposits due to fichtelite and abietane. The total absence of polar diterpenoids is a hint for the lower

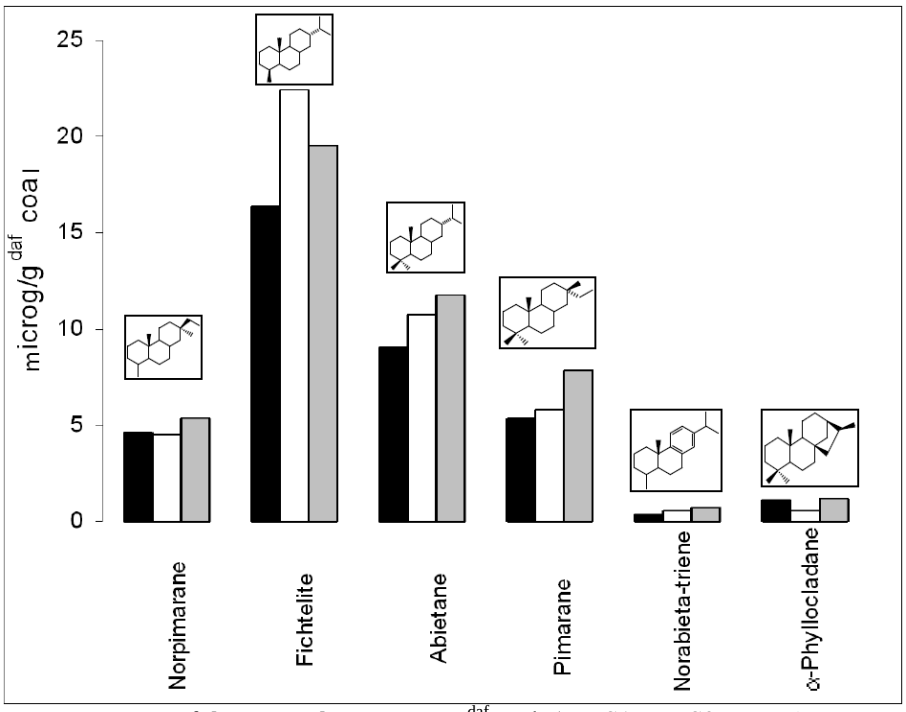

Fig. 5. Contents of diterpenoids in microg/g^{daf} coal. (■ – S1; □ – S2; ◘ - S3).

Coals contain lower quantities of steranes comparing to hopanes (by comparison of the intensities in the mass fragmentograms m/z 191 and m/z 217). Nevertheless, only in sample S3 m/z 217 visualizes the C_{27}, C_{28}, C_{29} whole range of steranes and diasteranes with strong dominance of 20R-$\alpha\alpha\alpha C_{27}$ homologue. The position in the triangular diagram for the relative contents C_{27} (40 %) C_{28} (28 %), C_{29} (32 %) indicates "estuarine or bay" formation of organic matter for S3 sample.

5. Implications for palaeovegetation

Karlovo lignites (Central Bulgaria) are well studied from geological, petrological and palaeobotanical point of view (Šiškov, 1985; Vălčheva and Trifonov, 1986; Stefanova and Valceva, 1994; Zdravkov et al. 2006). According to Ivanov and Slavomirova (2004) the age of the flora-bearing sediments covers the time span Pontian-Pliocene as is proven by geological data and diatom analysis. The biomarker assemblage of Karlovo lignite strongly differs from the other Neogene lignites in Bulgaria. The most striking peculiarity is the negligible content of tetracyclic diterpanes, i.e. 16α(H)-Phyllocladane). Diterpenoids

contribution of *Cupressaceae*/*Taxodiaceae* to the palaeomire. This coal progenitor is highly abundant in coal forming swamp but its importance declines with the advance of geological time. Inasmuch Karlovo lignite palaeoflora is from Upper Miocene and Pliocene the role of arctotertiary species in plant communities increases and becomes dominant in mesophytic forest. Respectively, it is supposed that *Cupressaceae*/*Taxodiaceae* gradually decreases due to drying and *Pinaceae* increases as better adapted to the colder and arider climate during Pliocene in Central Bulgaria. There are proves for the existence of flooded areas as well. Steranes are distributed in one of the samples and determines organic matter formed in limnic ecosystems. Angiosperms should not be neglected as there are mass spectral indications for the presence of *Quercus, Ulmus and Betula* in the palaeocommunites. Especially high *Betula* abundance could be assumed due to the presence of its biomarkers Des-A-lupane and Lupan-3-one.

6. Conclusions

The results of organic geochemical and petrographic study of Karlovo lignite (Central Bulgaria)

give us proves for the long-term evolution of the Late Neogene on the South Eastern Europe. The biomarker assemblages of samples under consideration are determined by the decrease in the palaeotropical elements and gradual increase in the arctotertiary taxa. Conifers remain main coal-forming vegetation predominantly represented by *Pinaceae*. Monoaromatic angiosperm-derived triterpenoids with ursane/oleanane skeleton prove the presence of dicotyledonous angiosperm-derived organic matter in the palaeoplant taxa. The palaeoenvirmental conditions within the forest swamp should be regarded as limnic with varying water table and seasonal drying.

Acknowledgements

The authors are grateful to the reviewers, DSc. D. Ivanov and anonymous one, for the remarks and recommendations which improved the text. The present study is financially supported by the Bulgarian Ministry of Education and Science through project No. VU 05/06.

References

Angelova D., Russeva M. and Tzankov Tz., 1991. On the structure and evolution of Karlovo Graben. Geotekton. Tektonofiz. Geodin., 23, 26–46 (in Bulgarian).

Bechtel A., Reischenbacher D., Sachsenhofer R.F., Zdravkov A., Kostova I. and Gratzer R., 2005. Influence of floral assemblage, facies, and diagenesis on petrography and organic geochemistry of the Eocene Bourgas coal and the Miocene Maritza-East lignite (Bulgaria). Organic Geochemistry, 36, 1498-1522.

Chounev D., Zagorchev I. and Kostov I., 1966. Pliocene in the plain of Karlovo. Rev. BGS, 27, 104–109 (in Bulgarian).

Hautevelle Y., Rymond M., Malartre F. and Trouiller A., 2006. Vascular plant biomarkers asproxies for palaeoflora and palaeoclimatic changes at the Dogger/Malm transition of the ParisBasin (France). Organic Geochemistry, 37, 610-625.

Ivanov D. and Slavomirova E. 2004. Palynological data on the Late Neogene vegetation from Karlovo basin (Bulgaria). First results. Comptes rendus de l'Academie bulgare des Sciences, 57, 65-70.

Kortenski J., 1991. Regularities in presence and distribution of trace elements in coal from Karlovo basin. Ann. UMG, 37, 249–259 (in Bulgarian).

Kortenski J. and Dimitrov A., 1989. Form of appearance and origin of mineral matter in the coal from Karlovo basin. Ann. UMG, 35, 171–179 (in Bulgarian).

Logan G.A., Smiley C.J. and Eglinton G., 1995. Preservation of fossil leaf waxes in association with their source tissues, Clarkia, Northern Idaho, USA. Geochimica et Cosmochimica Acta, 59, 751-763.

Oros D.R. and Simoneit B.R.T., 1999. Identification of molecular tracers in organic aerosols from temperature climate vegetation subjected to biomass burning. Aerosol Sci. and Technology, 31, 433-445.

Otto A. and Wilde V., 2001. Sesqui-, di- and triterpenoids as chemosystematic markers in extant conifers - a review. The Botanical Review, 67, 141-238.

Simoneit B.R.T., Grimalt J.O., Wang T.G., Cox R.E., Hatcher P. and Nissenbaum A., 1986. Cyclic terpenoids of contemporary resinous plant detritus and fossil woods, ambers and coals. Organic Geochemistry, 10, 877-889.

Šiškov G., 1985. Petrological characteristic of the Karlovo coal deposit. Comptes rendus de l'Academie bulgare des Sciences, 38, 883–886.

Stefanova M., 2004. Molecular indicators for Taxodium dubium as coal progenitor of Chukurovo lignite, Bulgaria. Bull. Geol. Soc. of Greece, 36, 342-347.

Stefanova, E., Valceva, S. 1994. Petrological characteristic of brown coal from Karlovo deposit in relationship with their briquetting. Annuaire de l'Universite de Sofia. Faculte de Geologie et Geographie, 84, 1, 49-63 (in Russian).

Stefanova M. and Simoneit B.R.T., 2008. Polar aromatic biomarkers of Miocene aged Chukurovo resinite and implication of the Taxodium dubium progenitor macrofossil. Int. J. Coal Geology, 75, 166-174.

Stefanova M., Magnier C. and Velinova D., 1995. Biomarker assemblage of some Miocene-aged Bulgarian lignite lithotypes. Organic Geochemistry, 23, 1067-1084.

Stefanova M., Oros D.R., Otto A. and Simoneit B.R.T., 2002. Polar aromatic biomarkers in the Miocene Maritza-East lignite, Bulgaria. Organic Geochemistry, 33, 1079-1091.

Stefanova M., Markova K., Marinov S.P. and Simoneit B.R.T., 2005. Molecular indicators for coal-forming vegetation of the Miocene Chukurovo lignite, Bulgaria. Fuel, 84, 1830-1838.

Stout S.A., 1992. Aliphatic and aromatic triterpenoid hydrocarbons in a Tertiary angiospermous lignite. Organic Geochemistry, 18, 51-66.

Temniskova D., Ognjanova N. and Popova E., 1996. Diatom analysis of the Neogene sediments from the Karlovo coal basin (Southern Bulgaria): II. Stratigraphy and palaeoecology based on silliceous microfossils. Phytol. Balc., 2, 13–28.

Välčheva S., Trifonov T., 1986. Petrological-technological evaluation of briqueting properties of coal from the Karlovo deposit. Annuaire de l'Universite de Sofia 80, 84-97 (in Bulgarian).

Zdravkov A., Sachsenhofer R.F., Kostova I. and Kortenski J., 2006. Reconstruction of paleoenvironment during coal deposition in the Neogene Karlovo Graben, Bulgaria. Int. J. Coal Geol., 67, 1, 79-94.

Special Session S15
Tertiary potassic and ultrapotassic magmatism along the Carpathian- Balkan-Dinaride chain: petrological processes and geodynamics

Scientific Annals, School of Geology, Aristotle University of Thessaloniki Proceedings of the XIX CBGA Congress, Thessaloniki, Greece	Special volume 100	287-295	Thessaloniki 2010

MINERALOGY OF THE PLIOCENE TRACHYTE AND ITS CARBONATITIC MINETTE INCLUSIONS IN OSTRVICA, F.Y.R. OF MACEDONIA

Yanev Y.[1], Boev B.[2], Iliev Tz.[1], Pecskay Z.[3], Karadjov M.[1] and Boev I.[2]

[1]*Geological Institute, Bulgarian Academy of Sciences, 1113 Sofia, Bulgaria; yotzo@geology.bas.bg; metodi@geology.bas.bg*
[2]*University "Goce Delčev", Štip, F.Y.R. of Macedonia; blazo.boev@ugd.edu.mk*
[3]*ATOMKI, Hungarian Academy of Sciences, 4001 Debrecen, Hungary; pecskay@namafia.atomki.hu*

Abstract: The trachyte at Ostrvica hill (age 3.21±0.10 Ma) in Vardar zone is the most evolved volcanics of the ultrapotassic Pliocene-Quaternary series in F.Y.R. of Macedonia. It is aphyric, with clinopyroxene and phlogopite microphenocrysts within a sanidine-anorthoclase groundmass. It contains inclusions of carbonatitic minette ranging in size from several mm to 6–7 cm. They are light coloured porphyric rocks, rich in vacuoles, composed of phlogopite and completely altered olivine(?) phenocrysts amongst acicular clinopyroxenes within a feldspar–calcite groundmass with abundant Fe-oxides and acicular apatite microlites. The inclusions are rimmed by a mm thick mixing zone composed of the same minerals but with intermediate composition between that of minette and trachyte. The clinopyroxenes are mainly diopside-augite with low Ti and Al content (with ^{6}Al only in the minette). Positive correlations are observed between Na and Fe^{3+}, Al and Ti, and negative one – between Al and Si. In the inclusions phlogopites the negative correlation between Mg# and ^{4}Al is found. The feldspars in the trachyte and minette inclusions are Ca-sanidine to Ca-anorthoclase, in the mixing zone – sanidine only. In the inclusions two plagioclase generations (An_{41} and An_{25}) exist. The estimated crystallization temperature of the minette clinopyroxenes is 1280–1180°C, of plagioclase (An_{41}) – 1130°C and in the hosting trachyte – 1080°C, at the pressures 6.9 and 7.7 kbar, respectively. The temperature of the feldspars crystallization (K-Na-feldspars and Pl_{24}) in the minette groundmass is 809–878°C. By analogy with other ultrapotassic volcanics from F.Y.R Macedonia it is suggested, that the discussed volcanics originated from phlogopite-bearing metasomatised mantle.

Key words: F.Y.R. of Macedonia, ultra-K series, trachyte, carbonatitic minette, magma mixing

1. Introduction

In the Northern Mediterranean domain of the Alpine orogen, from Spain to Syria, Cenozoic ultrapotassic (UK) volcanics, accompanied by rocks of the shoshonitic series, are widespread (review in Prelević et al., 2007). The UK volcanics in F.Y.R. of Macedonia (Yanev et al. 2003, 2008a,b; Altherr et al., 2004) belong to this series. They form the southern part of a NNW-SSE belt extended from Southern Hungary and across Serbia ends in F.Y.R. of Macedonia (in Vardar zone). The rocks are phonotephrites to ultra-K shoshonites (Mlado Nagorichane, Ejevo Brdo, Kureshnichka Krasta, Malino and Kishino), ultra-K latite (Gradishte) and high-Mg latite (Djurishte) dated from 3.24 to 1.47 Ma (Yanev et al., 2008a). The most evolved rocks are the trachytes at Nikushtak and Ostrvica hill (Fig. 1 and 2a). The latter contains inclusions of carbonatitic lamprophyre from several mm to 6–7 cm in size. The petrography and mineralogy of these inclusions and the hosting trachyte, as well as their age, are the subjects of the present communication. It is believed that it will complete the picture of the UK series in F.Y.R. of Macedonia and it will contribute to the clarification of their origin.

2. Methods

The petrographic studies of the rocks were performed by the classical methods, and the analyses of rock-forming minerals – by the Jeol 733 Superprobe at the Geological Institute, Sofia (analyst Tz. Ilyev) equipped with EDS (with ZAF corrections) at the following conditions: 15 kV, 1 nA beam current and 5 μm beam (standards: in Yanev et al., 2008b). To calculate Fe^{3+} in pyroxenes, a modified

version of the Papike et al. (1974) program was used on a charge-balance basis (kindly provided by P. Nimis, Padova University, Italy). The pyroxene components were calculated using the scheme of Yoder and Tilley (1962) complemented by White (1964) to divide the acmite and jadeite components. The pyroxene and plagioclase temperatures and pressures ware determined using the programs of Putirka et al. (2003) and Putirka (2005). The temperatures of groundmass feldspars were calculated using the geothermometer of Fuhrman and Lindsley (1988) at 1 kbar taking the values with difference between each equation <80^{o}C.

The chemical compositions of the trachyte and inclusions was determined by X-ray fluorescence at the Geological Institute (SRM-25, analyst S. Danev), and the carbonate content in minette – by gas sorption (analyst T. Popova, Niproruda Ltd, Sofia). The chemical composition of a powder sample (melted in Spectromelt-4 Merck) from the inclusions peripheral zone was analyzed by scanning of 5 areas (size 100x100 μm). The trachyte K–Ar age is determined on whole rock sample by Z. Pecskay. The analytical procedure is described in many papers (e.g. Yanev et al., 2008a).

3. Petrography

The Ostrvica trachyte (age 3.21 ± 0.10 Ma) forms an elliptical body (100x150 m) cutting Eocene flysch sediments 15 km NNW of Sveti Nikole town (Fig. 1). The trachyte is a grey aphyric rock, locally containing phlogopite phenocrysts up to 1.5x0.075 mm in size. Microphenocrysts of phlogopite and clinopyroxene are present in a dense groundmass made by microlites of the same minerals plus feldspars and accessories. The feldspar and phlogopite microlites are commonly oriented giving the rock trachytic texture. Phlogopite forms fine flakes, locally opacitized, with most common dimensions 0.2–0.4x0.02–0.045 mm. Clinopyroxene microphenocrysts are mostly acicular, up to 0.45–0.75x0.075–0.1 in size and the microlites are fine-acicular or isometric. The rock contains rounded quartz xenocrystals with diameter up to 1.5 mm, surrounded by a 0.15 mm reaction rim of fine acicular clinopyroxene. Some of them are entirely resorbed and only small lenses of pyroxene needles remain. Accessory minerals are magnetite, apatite and titanite, the latter reaching 0.6x0.225 mm in size.

The trachyte contains mm to 6-7 cm rounded inclusions of light-rusty to grey-brown rocks with rounded aggregates (diameter from 50 to 230 μm), probably of olivine completely replaced by alteration products and phlogopite flakes usually up to 0.75x0.075 mm (some to 4–5 mm). They are strongly opacitized, randomly oriented, forming a polygonal grid (Fig. 3a,b). In this grid are observed radial, rarely isometric aggregates of clinopyroxene microphenocrysts (up to 0.97x0.105 mm). Between them occur xenomorphic feldspars, skeletal clinopyroxene (diameter 20–40 μm) and phlogopite microlites. Some parts of the groundmass are rich in cryptocrystalline carbonate appearing together with the feldspars. We suppose that this carbonate is primary because it contains very small pyroxene microlites. The inclusions are very rich in vacuoles (from 50x50 to 240x120 μm), partly filled with secondary minerals. Skeletal apatite needles (up to 430x8 μm), "crosscutting" the clinopyroxene microphenocrysts and some alternation products (Fig. 3c), Ti-magmetite (with hercynite molecule) and ilmenite are accessories.

Fig. 1. Location map, after Yanev et al. 2008a. of the ultra- and high-potassic volcanic rocks in F.Y.R. of Macedonia and their K-Ar age in Ma (in parentheses).

Comparing the chemical compositions of the inclusions and their minerals (Tabl. 1-4), the quantities of latter can be estimated by a sample arithmetic procedure (alteration products excluding) as: clinopyroxene 42%, phlogopite+magnetite 25%, feldspars 21% (the carbonate quantity is 12% determined by a gas sorption). According to this mineral composition (Mitchell, 1995; Woolley et al., 1996) and the presence of carbonate >10% this is carbonatitic minette (Woolley and Kempe 1989). Such rocks have been described, among others, in Dubawnt (Canada, Peterson et al., 2002), in Jarangdihi with ~35% carbonate (India, Gupta et al., 2002).

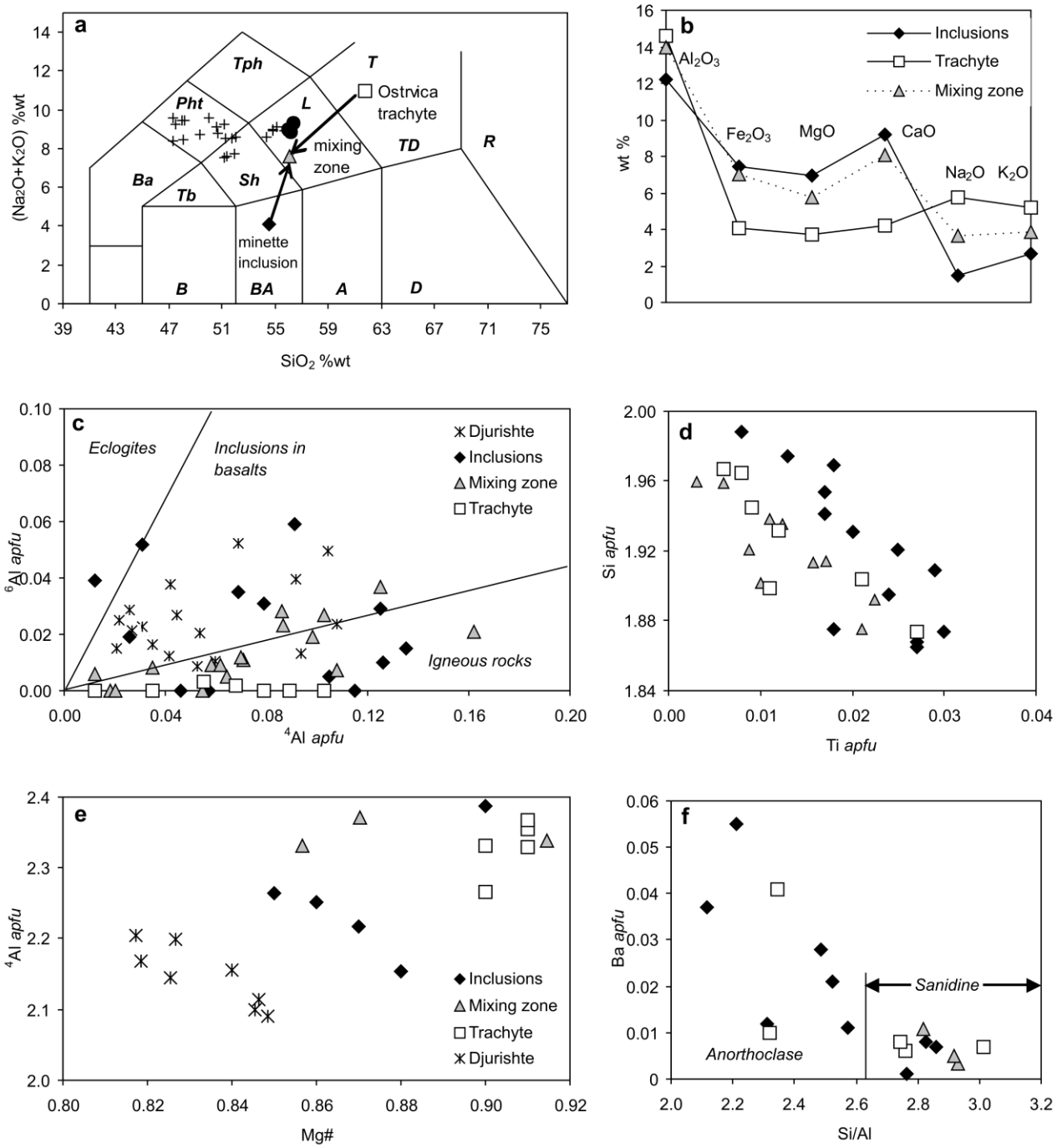

Fig. 2. a- TAS diagram (crosses, F.Y.R. of Macedonian UK volcanics and filed circles, Djurishte latites, after Yanev et al., 2008a); b- comparison between some oxides in studied volcanics; c and d – clinopyroxene diagrams (the fields are after Aoki and Kushiro, 1968; clinopyroxenes of Djurishte latites are after Yanev et al., 2008b); e- phlogopite diagram (Djurishte latites phlogopites are after Yanev et al., 2008b); f- Si/Al vs. Ba feldspar diagram.

The inclusions are rimmed by a dark grey zone up to 4–5 mm thick composed of clinopyroxene and rare phlogopite microlites in a sanidine groundmass. Sanidine in the darker part of the zone contains higher quantity of Fe, Mn and Mg (Tabl. 4). The clinopyroxene microlites are isometric (up to 0.18x0.12 mm) or short-prismatic (0.18x0.045 mm), commonly skeletal, with a central vacuole. Phlogopite forms microlites (from 0.15x0.015 to 0.3x0.1 mm) or rare microphenocrysts (0.8–0.9x0.1 mm).

4. Chemical composition

The trachyte is normative nepheline-bearing rock

(18.66%wt) containing equal quantity of Na_2O and K_2O (Tabl. 1). The inclusions are characterized by their low alkalis content, due to the almost complete decomposition of phlogopite. Because of this alteration and their specific lamprophyre mineral composition, it must not be classified accord-

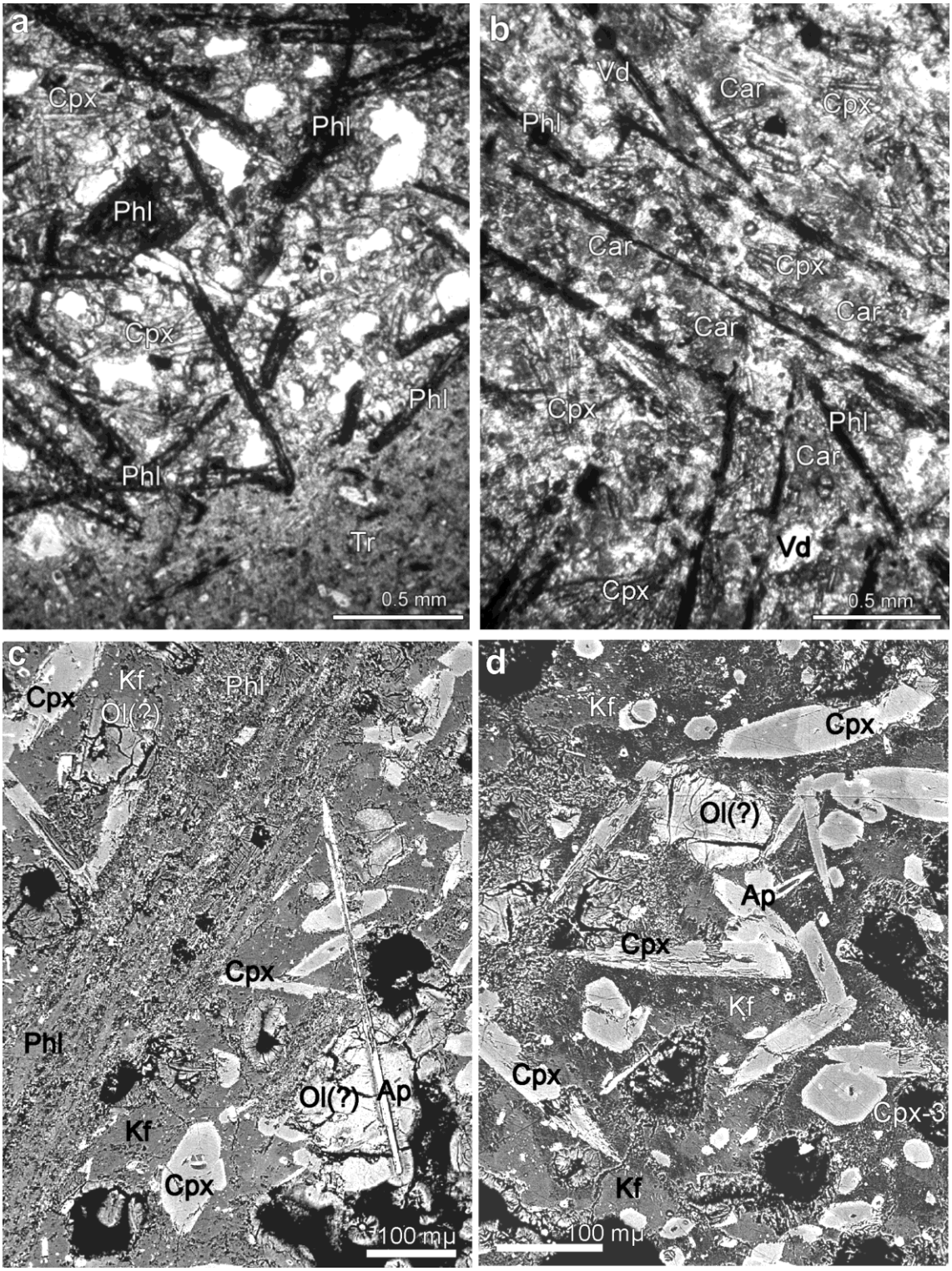

Fig. 3. Minette inclusions in the trachyte (Tr) – a and b, photomicrographs (plane-polarized light); c and d, back-scattered electron images. Phl, strongly altered phlogopite; Cpx, clinopyroxenes (in c and d, zoned and partly resorbed; the composition of Cpx-3 is presented in the table 2); Ap, skeletal apatite; Kf, K-Na-feldspars with different Ba content (in a an b – the white crystals in the groundmass); Ol?, completely altered olivine(?); Car, cryptocrystalline carbonate; Vd, voids (in c and d – the black spots).

ing to the TAS diagram (Woolley et al., 1996); however we plotted inclusions in such a diagram just for comparison with other volcanics from F.Y.R Macedonia (Fig. 2a). The composition of the zone, surrounding the inclusions, is transitional between trachyte and minette (Fig. 2b) and may be considered as product of mixing between the still liquid inclusions and the hosting trachytic magma. The mixing is suggested also by the rounded form of the inclusions and the absence of the sharp contact. This zone has a composition similar to the Djurishte latite (Yanev et al. 2008a), which is the only rock of shoshonitic affinity accompanied the UK volcanics from F.Y.R Macedonia. This latite has similar age (3.19 Ma, Yanev et al., 2008a) and it is exposed in the same region as the Ostrvica trachyte (Fig. 1).

Table 1. Whole-rock analyses

Rocks	Minette inclus.	Trachyte	Mixing zone
SiO_2	51,27	60,92	56,06
TiO_2	0,99	0,53	0,58
Al_2O_3	11,51	14,43	13,93
Fe_2O_3	7,03	4,05	7,01
MnO	0,24	0,07	0,09
MgO	6,56	3,69	5,72
CaO	12,61	4,18	8,09
Na_2O	1,36	5,70	3,68
K_2O	2,50	5,14	3,89
CO_2	5,57	n.d.	n.d.
Total	99,64	98,71	99,05

The studied minette inclusions actually are not UK rock, probably due to the alteration of the phlogopite. The majority of the minettes described in the literature are UK rocks excepting some minettes as those in Mexico (dykes in the Colima volcano, Luhr and Carmicael, 1981, in the volcanic fields of Ayutla and Tapalpa, Righter and Rosas–Elguera, 2001, of Mascota, Ownby at al., 2008 and Los Volcanos, Wallace and Carmichael, 1989), in Shahewen monzonitic pluton, Chine (Wang et al., 2007), in Qulitat Suweidi in Oman (Worthing and Nasir, 2008).

5. Mineral chemistry

5.1. Clinopyroxenes (Tabl. 2). They have a similar composition (diopside-augite) in all described rocks but those from the mixing zone occupy an intermediate position between the trachyte and inclusions pyroxenes. The more magnesian are the trachyte clinopyroxenes. In many crystals a zoning with respect to the $Mg \leftrightarrow Fe^{2+}$ substitution is observed, the periphery being richer in Fe component due to the decreasing crystallization temperature. There are, however, crystals with oscillatory zoning (Fig. 3d). The other elements as Ti and Mn do not reveal definite variations.

As in the rest of the volcanics of this series (Yanev et al., 2008b), the Al content in the described clinopyroxenes is likewise low (up to 0.1 *apfu*), slightly higher in the inclusions (up to 0.135 *apfu*), whereas in the mixing zone the values are intermediate. The lowest Al contents and respectively highest of Si are observed in the reaction pyroxenes around quartz xenocrystals. However, due to the high Si content, only in single cases there is an Al deficiency in the Si-Al tetrahedrons (mainly in the trachyte), which is compensated by Fe^{3+} (Hartman, 1969). In the inclusions and the mixing zone ^{6}Al is present (up to 0.059 *apfu*), in some cases even $^{6}Al > ^{4}Al$. Experiments prove that the $^{6}Al/^{4}Al$ ratio in silicate melts (in the crystallizing from them clinopyroxenes, respectively) increases with increasing pressure due to the increasing coordination of Al in the melt (Velde and Kushiro, 1978). In the inclusions clinopyroxenes (Tabl. 2) small quantities of jadeite component are formed, which is typical high-pressure molecule. Therefore, they plot in the field defined by Aoki and Kushiro (1968) for pyroxenes from mafic inclusions in basalts (Fig. 2c), where plot also the Djurishte latite pyroxenes. The pyroxenes from all UK volcanics cropping out in the F.Y.R. of Macedonia (Yanev et al., 2008b) and the studied trachyte are without or with low ^{6}Al content and they plot in the igneous rocks field.

The highest Na contain is found in low-Mg core (often resorbed – fig. 3d) of some zonal pyroxenes in the inclusions (up to 0.092 *apfu*, $J/J+Q = 0.05$). Na always participates in the clinopyroxene structure manly as acmite and in some cases as jadeite components. A weakly expressed positive correlation exists between Na and Fe^{3+}. The TiO_2 content is likewise relatively low without some regularity in its distribution in the individual pyroxene zones. Ti connects with Al in TAL ($CaTiAl_2O_6$) and rarely in NATAL components ($NaTiSiAlO_6$, Papike et al. 1974) determining the classical positive Al–Ti correlation related to the most important non-quadrilateral substitution in the pyroxene structure. The observed negative Al–Si correlation (Fig. 2d) resulted of $TiAl_2 \leftrightarrow MgSi_2$ exchange reaction.

Table 2. Microprobe analyses of clinopyroxenes

Rock	Minette inclusions											
	needle	needle	core-1	rim	core-2	rim	core-3*	interm.	interm.	interm.	rim*	core-4
SiO_2	50,46	52,47	51,41	50,43	51,83	54,21	50,45	53,88	51,66	54,73	51,92	53,07
TiO_2	0,97	0,59	0,85	1,09	0,90	0,46	0,63	0,66	1,04	0,28	0,73	0,61
Al_2O_3	2,63	1,04	2,54	3,10	2,50	1,05	3,50	1,94	3,45	1,19	2,38	1,33
FeO_{tot}	6,01	7,67	5,07	6,59	5,49	4,22	8,13	3,82	6,30	3,41	8,39	4,83
MnO	0,23	0,04	0,00	0,00	0,14	0,21	0,55	0,21	0,23	0,09	0,09	0,05
MgO	14,64	14,08	15,47	13,67	14,82	16,65	12,33	16,36	13,38	16,91	12,65	18,24
CaO	23,32	22,91	23,37	23,69	22,54	22,69	22,63	22,74	22,99	22,44	22,88	20,95
Na_2O	0,76	0,30	0,47	0,63	0,73	0,59	1,28	0,32	0,78	0,69	0,91	0,19
K_2O	0,18	0,55	0,17	0,18	0,05	0,05	0,15	0,03	0,09	0,10	0,01	0,10
Cr_2O_3	n.d.	n.d.	n.d.	n.d.	0,01	n.d.	n.d.	0,04	0,07	0,16	0,06	n.d.
Total	99,20	99,65	99,35	99,38	99,01	100,13	99,65	100,00	99,99	100,00	100,02	99,37
Mg#	0,92	0,78	0,92	0,87	0,86	0,89	0,82	0,88	0,81	0,90	0,76	0,90
Wo	48,4	47,2	47,8	49,5	47,4	46,0	48,6	46,7	49,2	46,1	48,6	41,8
Jd component					0,022	0,019		0,024	0,043	0,039	0,028	

*Cpx-3 on the fig. 3d (interm., intermediate zone)

Table 2 (continued)

Rocks	Mixing zone										Trachyte						
	microphenocryst	skeletal				core	interm.	rim	around quartz		microphenocryst						
SiO_2	53,02	51,86	51,23	52,56	51,86	51,39	50,02	52,94	52,87	53,69	52,47	54,84	52,59	50,46	53,46	50,96	52,36
TiO_2	0,45	0,82	0,56	0,32	0,62	0,37	0,74	0,41	0,12	0,23	0,34	0,23	0,43	0,97	0,28	0,76	0,41
Al_2O_3	1,61	2,68	2,49	1,27	2,62	2,69	3,65	1,64	0,42	0,47	1,31	0,28	1,61	2,36	0,81	2,03	1,85
FeO_{tot}	4,13	6,94	6,56	4,32	7,26	9,95	11,08	6,57	8,60	7,29	7,01	4,17	4,28	6,01	5,27	8,80	4,30
MnO	0,16	0,40	0,28	0,32	0,11	0,74	0,59	0,43	0,74	0,33	0,17	0,25	0,05	0,23	0,33	0,37	0,27
MgO	17,25	16,42	15,41	18,28	14,68	12,36	11,57	16,79	15,2	16,01	15,27	18,79	17,19	14,64	15,47	12,96	17,26
CaO	22,39	20,40	20,79	21,39	22,11	22,48	21,51	20,66	21,15	22,16	21,51	21,84	21,79	23,32	23,19	23,04	22,93
Na_2O	0,52	0,69	0,74	0,55	0,63	0,88	0,89	0,51	0,68	0,60	0,84	0,43	0,68	0,76	0,76	0,65	0,67
K_2O	0,01	0,15	0,07	0,03	0,00	0,06	0,02	0,05	0,00	0,06	0,03	0,18	0,05	0,18	0,11	0,15	0,02
Cr_2O_3	n.d.	n.d.	n.d.	n.d.	n.d.	n.d.	n.d.	n.d.	n.d.	n.d.	0,16	n.d.	0,12	n.d.	n.d.	n.d.	n.d.
Total	99,54	100,36	98,13	99,04	99,89	101,35	100,46	100,24	99,78	100,84	99,11	101,01	98,79	98,93	99,68	99,72	100,07
Mg#	0,90	0,90	0,88	0,95	0,84	0,78	0,73	0,87	0,80	0,84	0,91	0,87	0,95	0,91	0,90	0,80	0,97
Wo	45,0	41,6	43,7	42,9	45,8	46,8	46,0	41,7	43,1	44,4	42,9	44,5	44,4	48,6	47,2	47,9	45,9

5.2. Phlogopite (Tabl. 3). It shows low Ba and Ti contents. A negative correlation between Mg# and ^{4}Al is observed in the inclusions only (Fig. 2e); such a finding is found also in the Djurishte latite phlogopites. This correlation reflects the Ti+2Al=Mg+2Si substitution occurring at high temperature and pressure (Guo and Green 1990).

The inclusions phlogopites are almost completely opacitized (Fig. 3c) and their composition has been analysed only in the rare relics among magnetite crystals and the different alteration products.

5.3. Feldspars (Tabl. 4). They are Ca-sanidine to Ca-anorthoclase (according to the diagram of Smith and Brown 1988) in the trachyte and inclusions, and sanidine only in the mixing zone. The Ba content in sanidines is low whereas in the anorthoclases it reaches 0.55 *apfu* where a negative correlation between Ba and Si/Al ratio is observed (Fig. 2f). It is explained by $Ba^{2+}Al^{3+} \leftrightarrow K^{+}Si^{4+}$ substitution (Afonina et al., 1978). In the inclusions two plagioclase generations (An_{41} and An_{25}) also exist crystallizing at different temperatures (see below).

5.4. Carbonates. They are irregularly distributed in the minette groundmass. Most of them are calcite (average of 9 analyses: $CaCO_3$ 95.18, $MgCO_3$ 4.10, $BaCO_3$ 0.18, $MnCO_3$ 0.12, $FeCO_3$ 0.10 wt%) to high Mg calcite ($CaCO_3$ 69.75, $MgCO_3$ 29.00, $MnCO_3$ 1.85 wt%). Calcite sporadically appears also in other UK volcanics from F.Y.R Macedonia (in Ejevo Brdo and Kishino phonotephrites, Yanev et al., 2008b).

6. Crystallization parameters

The estimated crystallization temperature and pressure (Tabl. 5) of minette pyroxenes is 1280–1180°C (pressure 6.9 kbar), of plagiocalse (Pl_{41}) – 1130°C and of trachyte pyroxenes – 1080°C (pressure 7.7 kbar). This pressure explains the absence of orthopyroxene, which crystallizes at pressure

Table 3. Microprobe analyses of phlogopites

Rocks	Minette inclusions				Mixing zone					Trachyte			
SiO_2	39,37	39,79	40,43	41,87	39,96	38,75	40,00	40,05	40,62	40,56	40,02	40,40	40,62
TiO_2	1,48	1,83	2,11	1,60	1,50	1,90	1,99	1,48	1,60	1,64	1,76	1,52	1,78
Al_2O_3	13,43	13,35	13,30	14,21	14,70	13,59	14,08	14,32	14,20	14,66	14,33	14,38	13,69
FeO	6,37	6,97	5,84	5,56	4,80	6,74	4,19	6,50	4,41	4,26	4,41	4,64	5,02
MnO	0,00	0,18	0,11	0,28	0,00	0,05	0,05	0,00	0,00	0,11	0,00	0,00	0,00
MgO	22,28	22,42	22,89	22,55	24,31	22,63	25,14	24,46	25,18	24,83	24,76	24,60	24,37
CaO	0,04	0,10	0,07	0,24	0,20	0,26	0,22	0,00	0,04	0,25	0,19	0,29	0,54
Na_2O	1,11	1,00	0,88	0,45	0,73	0,64	1,06	0,61	0,94	0,75	0,81	0,51	0,62
K_2O	9,69	10,02	9,86	9,48	10,08	9,73	9,32	9,84	9,78	9,68	9,99	9,61	9,00
Cr_2O_3	n.d.	n.d.	n.d.	0,39	0,43	n.d.	n.d.	n.d.	0,17	0,41	0,49	0,40	0,11
BaO	0,35	0,10	0,04	1,06	0,46	0,47	0,01	0,38	0,41	0,18	0,18	0,43	0,31
LOI	5,87	4,25	4,47	2,31	2,82	5,26	3,95	2,34	2,64	2,68	3,05	3,24	3,94
Total	99,99	100,01	100,00	100,00	99,99	100,02	100,01	99,98	99,99	100,01	99,99	100,02	100,00
Mg#	0,86	0,85	0,87	0,88	0,90	0,86	0,91	0,87	0,91	0,91	0,91	0,90	0,90

Table 4. Microprobe analyses of feldspars

Rocks	Minette inclusions								Mixing zone			Trachyte				
									clear part	dark*						
Mineral	Ca-anorthoclase						sanidine	plagioclase	sanidine	Na-sanidine		Ca- anorthoclase			Ca-sanidine	
SiO_2	62,58	63,12	59,76	59,81	63,53	60,93	64,49	57,17	61,27	65,57	65,60	64,75	61,49	64,06	62,34	65,19	65,83
Al_2O_3	21,35	21,22	23,95	22,92	20,94	22,37	19,35	27,64	23,55	18,99	19,07	19,49	22,26	19,69	22,81	20,15	18,54
Fe_2O_3	0,12	1,06	0,34	0,52	0,16	1,08	0,70	0,40	0,64	0,52	0,38	0,49	0,48	0,84	0,62	0,21	0,56
CaO	1,72	4,19	2,90	2,38	2,02	4,34	0,77	8,63	4,86	0,38	0,87	1,44	2,21	1,31	3,38	0,89	1,13
Na_2O	5,26	5,98	6,32	4,71	5,42	6,40	4,89	6,30	7,22	4,74	4,95	5,63	6,68	6,24	7,43	5,80	4,65
K_2O	6,69	3,93	4,40	6,15	7,30	3,05	8,78	0,78	1,57	9,94	8,66	7,03	4,63	6,07	2,87	7,52	8,48
BaO	1,58	1,21	2,09	3,05	0,64	0,70	0,47	0,27	0,10	0,18	0,28	0,60	2,30	0,36	0,56	0,43	0,42
Total	99,30	100,71	99,76	99,54	100,01	98,87	99,45	101,19	99,21	100,32	99,81	99,43	100,05	98,57	100,01	100,19	99,61
An	9,0	21,3	14,8	13,1	9,8	22,2	3,8	41,2	24,6	1,8	4,3	7,2	11,2	6,6	16,7	4,4	5,8
Ab	49,5	55,0	58,4	46,7	47,8	59,2	44,1	54,4	66,0	41,3	44,5	50,9	61,0	57,0	66,4	51,6	42,8
Or	41,5	23,8	26,8	40,2	42,4	18,6	52,1	4,4	9,4	56,9	51,2	41,9	27,8	36,5	16,9	44,0	51,4
										*MnO		0,18					
										MgO		0,25					

more than 10 kbar (Barton and Hamilton 1982). The obtained data are comparable with the crystallization parameters of pyroxenes in the UK volcanics from F.Y.R Macedonia: temperature 1300–1150°C at pressure 6–8 kbar (Yanev et al., 2008a). The temperature of the feldspars crystallization in the minette groundmass (K-Na-feldspars and Pl_{24}) is 809–878°C. The carbonates crystallize between 650 and 1050°C when X_{CO2} in the remaining liquid of the SiO_2–CO_2 system reaches 0.83 (Otto and Wyllie, 1993).

7. Discussion on the rock genesis

The age of the Ostrvica trachyte and its major and trace elements composition (Altherr et al., 2004) define it as part of the UK volcanic series form F.Y.R of Macedonia. It is the most evolved member (with the trachyte from Nikushtak), but its composition is not ultrapotassic. It is assumed that this series originated from phlogopite-containing metasomatized mantle (Yanev et al., 2003, 2008a, b; Altherr et al., 2004) based on the hypothesis of Foley (1992) and others for the origin of high-K magmas.

Table 5. P and T estimations.

Rocks	T°C	P kbar
	Cpx/melt[1]	
Minette:		
core	1282	7,7
rim	1272	6,9
Mixing zone:		
core	1186	7,3
Trachyte:	1082	7,4
	Pl/melt[2]	
Minette:		
An_{41}	1132	n.d.

[1]after Putirka et al. (2003), [2]after Putirka (2005)

The present study suggested the presence of another type of magma in this series – that of the minette as in the Serbian Tertiary UK volcanics

(Prelević et al., 2004). The minette, irrespective of its minor quantities, commonly accompanies shoshonitic and UK magmas. Here it is characterised by high amount of volatile components (particularly CO_2), which make it very mobile and enabled mixing with the trachytic magma. The mixing zone around the minette inclusions is similar in chemical and mineral composition to the Djurishte latite, which is also not UK. It is possible that the latter originated from this mixing of these two magmas.

The lack of trace elements and isotopes data in the studied rocks does not allow to discuss the depth and processes of magma generation. Geobarotehrmometric data suggest that they began to crystallize into the crust at a depth of 20–22 km and at the above mentioned temperatures. The minette groundmass crystallizes at lower pressure and at about 250°C lower temperature.

References

Afonina G.G., Makagon V.M. and Shmakin B.M., 1978. Barium and Rubidium Bearing Potassic Feldspars. Nauka, Novosibirsk, 112p. (in Russian).

Altherr R., Meyer H.-P., Holl A., Volker F., Alibert C., McCulloch M.T. and Majer V., 2004. Geochemical and Sr-Nd-Pb isotopic characteristics of Late Cenozoic leucite lamproites from the East European Alpine belt (Macedonia and Yugoslavia). Contribution to Mineralogy and Petrology, 147, 58-73.

Aoki K. and Kushiro I., 1968. Some clinopyroxenes from ultramafic inclusions in Dreiser Weiher, Eifel. Contribution to Mineralogy and Petrology, 18, 326-337.

Barton M. and Hamilton D.L., 1982. Water-satured melting experiments bearing upon the origin of potassium-rich magmas. Mineralogical Magazine, 45, 267-278.

Foley S., 1992. Vein-plus-wall-rock melting mechanisms in the lithosphere and the origin of potassic alkaline magmas. Lithos, 28, 435–453.

Fuhrman M. and Lindsley P., 1988. Ternary feldspar modeling and thermometry. American Mineralogist, 73, 201-215.

Guo J. and Green T.H., 1990. Experimental study of Ba partitioning between phlogopite and silicate liquid at upper mantle pressure and temperature. Lithos, 24, 83-95.

Gupta A.K., Chathopadhyay B., Fyfe W.S. and Powell M., 2002. Experimental study on three potassium-rich ultramafic rocks from Damodar Valley, East India. Mineralogy and Petrology, 74, 343-360.

Hartman P., 1969. Can Ti^{4+} replace Si^{4+} in silicates? Mineralogical Magazine, 37, 366-369.

Luhr J.E. and Carmichael I.S.E., 1981. The Colima volcanic complex: Part II. Late Quaternary cinder cones. Contribution to Mineralogy and Petrology, 76, 127-147.

Mitchell R.H., 1995. Kimberlites, Orangeites and Related Rocks. Plenum Press, New York.

Otto J.W. and Wyllie P.J. 1993. Relationships between silicate melts and $CaO–MgO–SiO_2–CO_2–H_2O$ at 2 kbar. Mineralogy and Petrology, 48, 343-365.

Ownby S.E., Lange R.A. and Hall Ch.M., 2008. The eruptive history of the Mascota volcanic field, western Mexico: Age and volume constraints on the origin of andesite among a diverse suite of lamprophyric and calc-alkaline lavas. Journal of Volcanology and Geothermal Research, 177, 1077-1091.

Papike J.J., Cameron K.L. and Balfwin K., 1974. Amphiboles and pyroxenes: characterization of other than quadrilateral component and estimates of ferric iron from microprobe data. Geological Society of America. Abstracts with programs, 6, 1053-1054.

Peterson T.D., Van Breemen O., Sandeman H. and Cousens B., 2002. Proterozoic (1.85-1.75 Ga) igneous suites of the Western Churchill Province: granitoid and ultrapotassic magmatism in a reworked Archean hinterland. Precambrian Research, 119, 73-100.

Prelević D., Foley S.F., Cvetković V. and Romer R.L., 2004. Origin of minette by mixing of lamproite and dacite magmas in Veliki Majdan, Serbia. Journal of Petrology, 45, 759-792.

Prelević D., Foley S.F. and Cvetković V., 2007. A review of petrogenesis of Mediterranean Tertiary lamproites: A perspective from the Serbian ultrapotassic province. Geological Society of America. Special Paper, 418, 113-129.

Putirka K., 2005. Igneous thermometers and barometers based on plagioclase + liquid equilibria: Test of some existing models and new calibrations. American Mineralogist, 90, 336-346.

Putirka K., Mikaelian H., Ryerson F.J. and Shaw H., 2003. New clinopyroxene–liquid thermobarometers for mafic, evolved and volatile-bearing lava compositions, with applications to lavas from Tibet and the Snake River Plain, ID. American Mineralogist, 88, 1542-1554.

Righter K. and Rosas–Elguera J., 2001. Alkaline lavas in volcanic front of the Western Mexican Volcanic Belt: Geology and petrology of the Ayutla and Tapalpa volcanic fields. Journal of Petrology, 42, 2333-2361.

Smith J.V. and Brown W.S., 1988. Feldspar Minerals. Crystal Structure, Physical, Chemical and Microtextural Properties, v. 1. 2nd ed. Springer Verlag, N. York.

Velde B. and Kushiro I., 1978. Structure of sodium alumino–silica melts quenched at high pressure; infrared and aluminum K-radiation data. Earth and Planetary Science Letters, 40, 137-140.

Wallace P. and Carmichael I.S.E., 1989. Minette lavas and associated leucitites from the Western Front of the Mexican Volcanic Belt: petrology, chemistry, and origin. Contribution to Mineralogy and Petrology, 103, 470-492.

Wang F., Lu X.-X., Lo C.-H., Wu F.-Y., He H.-Y., Yang L.-K. and Zhu R.-X., 2007. Post-collisional, potassic monzonite–minette complex (Shahewan) in the Qinling Mountains (central China): 40Ar/39Ar thermochronology, petrogenesis, and implications for the dynamic setting of the Qinling orogen. Journal of Asian Earth Sciences, 31, 153–166.

White A.J.R., 1964. Clinopyroxenes from eclogites and basic granulites. American Mineralogist, 49, 883-888.

Woolley A.R. and Kempe D.R.C., 1989. Carbonatites: nomenclature, average chemical compositions and element distribution. In: Carbonatite Genesis and Evolution, Bell, K. (ed.), Unwin Hyman, London.

Woolley A.R., Bergman S.C., Edgar A.D, Le Bas M.J., Mitchell R.H., Rock N.M.S. and Scott Smith B.H., 1996. Classification of lamprophyres, lamproites, kimberlites, and the kalsilitic, melilitic, and leucitic rocks. Journal of the Mineralogical Association of Canada, 34, part 2.

Worthing M.A. and Nasir S., 2008. Cambro-Ordovician potassic (alkaline) magmatism in Central Oman: Petrological and geochemical constraints on petrogenesis. Lithos, 106, 25-38.

Yanev Y., Boev B., Doglioni C., Innocenti F., Manetti P. and Lepitkova S., 2003. Neogene ultrapotassic-potassic volcanic association in the Vardar zone (Macedonia). Comptes-rendus de l'Académie bulgare des Sciences, 56 (4), 53-58.

Yanev Y., Boev B., Doglioni C., Innocenti F., Manetti P., Pecskay Z., Tonarini S. and D'Orazio M., 2008a. Late Miocene to Pleistocene potassic volcanism in the Republic of Macedonia. Mineralogy and Petrology, 94, 45-60.

Yanev Y., Boev B., Manetti P., Ivanova R., D'Orazio M. and Innocenti F., 2008b. Mineralogy of the Plio-Pleistocene ultra- and high potassic volcanic rocks in Republic of Macedonia. Geochemistry, Mineralogy and Petrology, 46, Sofia, 35-67.

Yoder H.S.jr. and Tilley C.E., 1962. Origin of basalt magmas: An experimental study of natural and synthetic rock systems. Journal of Petrology, 3, 342-532.

Special Session S20
Marine mineralization associated with volcanic arc and other environments, with emphasis on the Aegean and Black Sea

Scientific Annals, School of Geology, Aristotle University of Thessaloniki Proceedings of the XIX CBGA Congress, Thessaloniki, Greece	Special volume 100	297-307	Thessaloniki 2010

FOSSILIZED MICROORGANISMS PRESERVED AS FLUID INCLUSIONS IN EPITHERMAL VEINS, VANI Mn-Ba DEPOSIT, MILOS ISLAND, GREECE

Ivarsson M.[1], Kilias S.P..[2] Broman C.[3] , Naden J.[4] and Detsi K.[2]

[1] *Department of Paleozoology, Swedish Museum of Natural History, Svante Arrheniusväg 9 Box 5000, 105 05 Stockholm, Sweden, magnus.ivarsson@nrm.se*
[2]*Department of Economic Geology and Geochemistry, Faculty of Geology and Geoenvironment, Panepistimiopolis, Zographou, 15784, Athens, Greece, kilias@geol.uoa.gr*
[3] Department of Geology and Geochemistry, Stockholm University, Geoscience Building, Svante Arrhenius väg 8C, 106 91 Stockholm, Sweden
[4] *British Geol Survey, Keyworth NG12 5GG, Notts , U.K.*

Abstract: Fossilized microorganisms preserved as fluid inclusions are found in barite–silica-Mn oxide veins in the marine rift basin-related Quaternary Mn-Ba deposit of Vani, Milos . Basin fill consists of 35-50 m thick sequence of glauconitic sediments sandwiched between volcaniclastic sandy tuffs, and, bedding-parallel barite–Mn oxide(–silica) horizons, pebble horizons, and massive gravel. Exhalative barite-rich deposits characteristic of sea-floor venting, such as white smoker(sulphate) structures in glauconitic sediments, feeder veins, bedding-conformable horizons, and extensive microbial mat- related structures in sandy tuffs, were recognized. The feeder veins host the microfossils and consist chiefly of banded barite and minor colloform quartz, Fe-oxyhydroxides, and hollandite-group minerals and MnO_2 phases, and display epithermal textures characteristic of open-space precipitation. Curvilinear, branched filamentous microfossils with distinct segmentation of septa and a turgid appearance of knob-like outgrowths occur associated with spheroidal spore-like microfossils and small twisted microstructures. Both filamentous and spheroidal microstructures are filled with aqueous (liquid ± vapour) and/or hydrocarbon phases. Oil and solid hydrocarbons in the fluid inclusions may represent decomposed biological material. Chitin was detected by the pigment Wheat Germ Agglutinin conjugated with Fluorescein Isothiocyanate (WGA-FITC) in some of the microfossils, indicating that they are fossilized fungi; a fungal interpretation is further supported by microfossil morphology. Smaller, often twisted filamentous microfossils with a simpler morphology in which chitin was not detected probably represent fossilized prokaryotes and, if so, prokaryotes and eukaryotes co-existed in the geothermal system of Vani. Fluid inclusion microthermometry shows that microfossils were trapped at temperatures of ~100°C in boiling water, probably evolved seawater. Preservation of microfossils occurred at shallow sub-marine conditions of <10 m depth. Our results show that fluid inclusions may contain valuable palaeobiological information and can be used both for establishing biogenicity but also for the reconstruction of the palaeoenvironment of fossilized microorganisms.

Keywords: fossilized fungi, chitin, WGA-FITC, epithermal vein, Milos, Vani

1. Introduction

Submarine, and subaerial volcanic and subvolcanic, hot-springs in both modern and ancient Earth exemplify the links between hydrothermal systems and microbial life (e.g. Harris et al. 2009 and references therein). Microorganisms are a common feature in both extant and extinct hydrothermal environments and recognised as an important agent in hydrothermal related geochemical and biogeochemical processes (e.g. Edwards et al., 2005; Ivarsson et al., 2008 and references therein; Dick et al., 2009). Hydrothermal systems are characterised by high rates of mineralization and may favour preservation of microorganisms which may host organic remains (Ueno et al., 2006). A recent study shows that fossilized microorganisms in combination with coexisting fluid inclusions in hydrothermal precipitates are a successful approach to reconstruct geobiological palaeoenvi-

ronments (Ivarsson et al., 2009). Fluid inclusions contain information about the fluid regime at the time of mineral formation, and microfossil entrapment, and are an excellent indirect tool to put the fossilized microorganisms in a physicochemical and palaeonvironmental context; however, it may be possible, yet very scarcely successful, to obtain biological information directly from inorganically formed fluid inclusions (Ueno et al., 2006).

In this paper we report of fluid inclusion bearing fossilized microorganisms in hydrothermal quartz from epithermal barite–Mn oxide(–quartz, chalcedony) veins of the Vani Mn-Ba, Milos, Greece. This is, to our knowledge, the first time fluid inclusions have been observed in, and described as the main constituent of, fossilized microorganisms. We use oil-bearing fluid inclusions to establish biogenicity of and to characterize the fossilized microorganisms as well as aqueous/vapour fluid inclusions as tools to describe the palaeoenvironment of the fossilized microorganisms. The fossilized microorganisms are interpreted as co-existing eukaryotes (fungi) and prokaryotes (bacteria or archaea).

2. Regional and local geologic setting

Milos is a recently emergent 2 Ma volcano of the Pliocene—modern South Aegean volcanic arc, that documents the transition between the submarine and terrestrial volcanic environments (Fig. 1) (Fytikas et al., 1986; Stewart and McPhie, 2006). Milos island comprises late Pliocene submarine volcanism and late Pleistocene to Holocene subaerial volcanism, which overly Miocene and lower Pliocene carbonate sedimentary successions. The volcanic rocks are calc-alkaline and range from basalt to rhyolite in composition, but are predominantly andesites and dacites. Moreover, Milos has an active high enthalpy geothermal system that vents in the shallow (<100 m) marine and terrestrial environments, and the island as a whole has been hydrothermally active for around 1.5 Ma (Fig. 1). Recent research on Milos island has identified a new metallogenic environment—namely mineralisation and geothermal activity associated with emergent volcanoes. Here—driven by magmatic heat—sea, meteoric and magmatic waters mix to produce geothermal systems that give rise to hybrid volcanic-hosted massive sulphide (VHMS) and continental epithermal mineralization (i.e. Profitis Ilias, Chondro Vouno, Fig. 1)(Kilias et al., 2001; Naden et al., 2005), and a diverse, submarine to terrestrial, suite of young and extremely well preserved mineralized palaeogeothermal systems. The latter are best represented by the Vani Mn-Ba deposit, in NW Milos (Fig. 1). Vani has been considered by previous workers as a stratabound Mn deposit formed by subsea-floor replacement of porous volcaniclastic rocks (Hein et al., 2000; Liakopoulos et al., 2001; Glasby et al., 2005), diagenetic processes (Skarpelis and Koutles, 2004) and submarine hotspring-type processes (Plimer, 2000). The following description is based on Kilias et al (2007), incorporates basic geological data from previous and presents some new data.

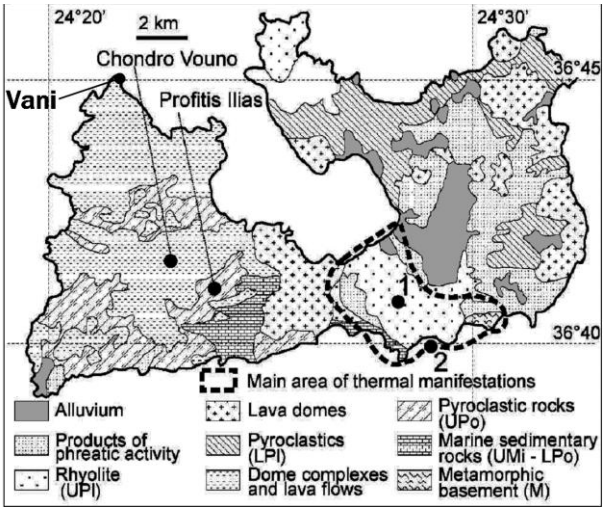

Fig. 1. Main geologic features of Milos Island plus location of Vani, hybrid VHMS-epithermal mineralization (Profitis Ilias and Chondro Vouno) and main surface manifestations of geothermal system—points 1 and 2 show the locations of the deep geothermal reservoir (Zephyria) and main shallow submarine geothermal system (Paleochori Bay), respectively. UPI—upper Pleistocene; LPl—lower Pleistocene; UPo—upper Pliocene; LPo—lower Pliocene; UMi—upper Miocene; M—Mesozoic (adapted from Fytikas et al., 1986 and Naden et al., 2005).

Vani deposit occurs in a 1 km long marine rift basin that was developed in a footwall of andesitic lava dome. The basin fill is 35-60 m-thick and consists of Upper Pliocene–Lower Pleistocene siliciclastic glauconitic sediments sandwiched between lower and upper volcaniclastic sandy tuffs/sandstones, bedding parallel barite–Mn oxide (–quartz, chalcedony) horizons, and lenses, pebble horizons, jaspilitic chert, gravel, capped by cherty mudstone with dessication cracks (Fig. 2). We have been able to recognized extensive microbial–possible cyanobacteria– mat related structures (see Noffke et al., 2001; Noffke, 2009) in the upper-

most sandy tuffs (Figs. 3, 4 and unpublished data); these have a variety of forms including structures on bedding planes (levelled bedding surfaces, microbial mat chips, and mat curls) as well as internal bedding structures (gas domes, thrombolitic and sponge pore fabrics, wavy and discontinuous laminae, and mat slump structures) indicative of nearshore intertidal to shallow-water conditions (Noffke et al., 2001).

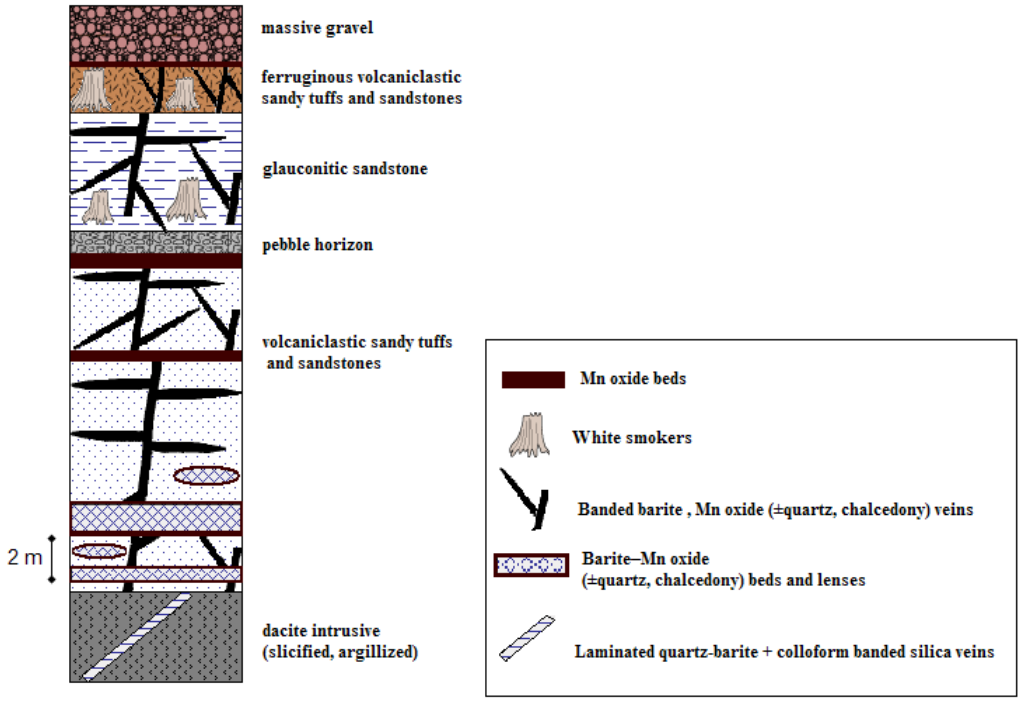

Fig. 2. Schematic stratigraphic section of Vani Mn-Ba deposit (modified after Liakopoulos et al., 2001 and Hein et al., 2000).

There is a important hydrothermal part to the Vani basin development. In addition to the extensive bacterial mats, features characteristic of sea-floor hydrothermal venting, such as white smoker (barite) structures and hydrothermal feeder veins, and hydrothermal mounds, have been recognized in Vani (Figs. 3, 4; Kilias et al., 2007, and unpubl. data). The feeder veins crosscut the sedimentary rocks and consist chiefly of banded open-space-grown of barite and minor colloform quartz, goethite, Fe-oxyhydroxides, and X-ray amorphous hollandite group-like minerals and MnO2–like phases; with the exception of the abundant barite, the vein displays complex and multiepisodic filling with epithermal textures characteristic of open-space precipitation (Hedenquist et al., 2000) (Fig. 3). Discordant colloform-banded epithermal-style stringer veins with the same mineralogy and exhibiting epithermal textures occur for several tens of meters stratigraphically below the sediments within silicified and argillised dacite hangingwall, and hyaloclastite. White smokers have two main modes of occurrence: (1) in massive glauconitic sediments they occur mostly in the form of subparallel vertical pipe-like "white"structures of variable length up to 30-40 cm, and diameter from 2 to 10 cm; individual tubes may have a barite±silica rim and a core filled with hummocky Mn oxide minerals and barite (Fig. 4A), (2) within the upper bedded sandy tuff the white smokers appear "black", and occur in the form of mound-shaped chaotic melange that at places may extend to tens of meters; the melange structure is Mn mineralized and consists of collapsed, toppled, eroded, and brecciated, white smoker chimneys and chimney rubble, debris and fragments, mixed with fragments of fossilised worm tubes, and microbial mat debris, all cemented by Mn oxide minerals and barite. Individual white smoker are hollow tubular structures, some up to 10 -15 cm wide, covered completely by Mn oxide minerals, with rims consisting of concentrically zoned thin Mn oxide layers, and hummocky outer surfaces completely cover by bead-like Mn oxide structures (Fig. 4B, C). Some smokers occur as isolated cylindrical structures consisting of barite-silica±Mn oxide minerals with a hollow core lined with barite ± Mn oxides, and buried in microbial mat debris (Fig. 4D).

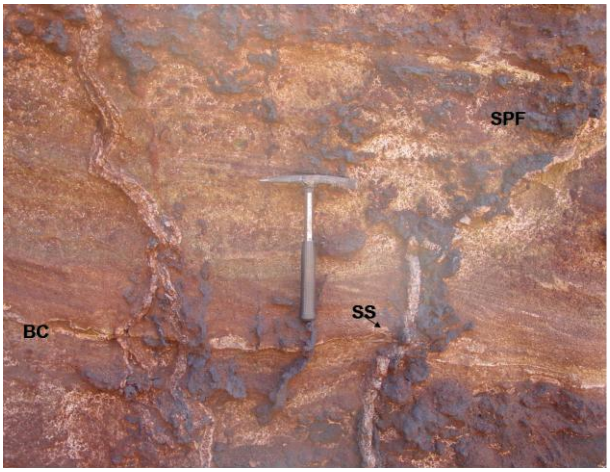

Fig. 3. Host rock of microfossils. Cross section of bifurcating, curvilinear banded barite–Mn oxide(±quartz, chalcedony) epithermal veins crosscutting finely bedded ferruginous sandy tuff, and bedding-conformable horizons with the same mineralogy(BC). Note, possible microbial mat related structures that may suggest syndepositional microbial activity (see Schieber et al. 2007; Noffke 2009): (a) sharply projecting fenestral (sponge pore) fabrics marked by Mn oxides exhibiting cauliflower-like thrombolitic fabrics (SPF)(i.e. biostabilization of the sediments by microbial mats); (b) sinoidal structures(SS) defined by crinkly, wavy and discontinuous barite laminae, denoting biofilm-imprinted rippled bed-surfaces.

The manganese mineralization exhibits a range of deposit styles including white-smoker analogous deposits, subseafloor-replacement and infilling deposits, microbial mat-related deposits, and structurally controlled colloform-banded epithermal-style stringer vein network style (Fig. 3, Kilias et al., 2007). A detailed description of Mn oxide mineralogy may be found in Liakopoulos et al. (2001), and Hein et al. (2000). Manganese minerals were deposited in two stages, and barite formed throughout the duration of Mn oxide mineralization at Vani (Hein et al. 2000; Liakopoulos et al. 2001). The presence of Mn–mineralized microbial mat-related deposits in this shallow marine environmet may suggest the possible role of cyanobacterial photosythesis in Mn^{2+} biooxidation and Mn-oxide biomineralization.

The ubiquitous presence of barite, coupled by the spatial coincidence of feeder-vein and bedding conformable barite-bearing units with white smokers of the same mineralogical composition(Figs. 3, 4), strongly suggest compatibility of the barite-Mn oxide(-silica) units of Vani with low-temperature white smoker (sulphate) deposition (Harris et al., 2009). Furthermore, the gravel unit that caps the Vani sediments contains clasts of dacite, epithermal-style colloform quartz, sandy tuff, manganiferous and ferruginous sandy tuff, and barite. This, coupled with the spatial association of white smokers with microbial mat features preserved within the siliciclastic sediments, suggest that white smoker-type activity, including the feeder veins, have been broadly contemporaneous with sediment accumulation and microbial mat growth in the Vani rift basin(see also Pirajno and Van Kranendonk, 2005). Due to remarkable similarities, Vani may be viewed as a modern analogue for the world's most ancient (3.49 Ga) microbial mats and stromatolites that have developed in association with barite-rich white smoker-type deposits in a shallow-water Early Archean geothermal system preserved in the North Pole Dome, W. Australia (Pirajno and Van Kradendonk, 2005; Harris et al., 2009)

3. Materials and Methods

Extensive fieldwork was conducted between 1996 and 2008 in the broader area around the abandoned open pit mine at Vani, in order to describe and decipher the relationships between sedimentary, hydrothermal and biological phenomena. Vein material for microfossil and fluid inclusion analysis was sampled from outcrops in the open pit. The samples were prepared as doubly polished wafers because these present certain advantages in microfossil studies in terms of better visibility, better light conditions, and an increased 3-dimensional view compared to ordinary thin sections (Ivarsson 2006), due to greater thickness (150–200 μm), and the possibility that the samples could be viewed from both sides.

For Raman spectroscopy analyses, a multichannel Dilor XY spectrometer was used with an incident laser beam of 514.5 nm and an Innova 70 argon laser as a light source.

For the detection of chitin in the microfossils a modified version of the staining method as detailed in Bonfante et al. (1987) was carried out. The pigment Wheat Germ Agglutinin conjugated with Fluorescein Isothiocyanate (WGA-FITC) under fluorescent microscopy was used. This is the first time that such a method is used in geological samples. Chitin is a component in fungal cell walls and not present in the cells of bacteria or archaea and thus WGA-FITC is commonly used to detect fungi or visually separate fungi from bacteria. For the fluorescence we used a Leitz DMRBE epifluorescent microscopy with a Leica DFC 280 camera. Microphotographs are taken in ultra violet light.

Fluid inclusionswere studied in the same wafers. Mirothermometric analyses were carried out using a Linkam TMSG600 heating-freezing stage calibrated using natural carbon-dioxide bearing fluid inclusions of known composition and commercially available chemical standards. Estimated analytical error is ±0.2ºC for low(<50ºC) and ±2 ºC for higher (>75ºC) temperatures.

4. Results and Discussion

4.1 Fossilized Microorganisms

This study has been conducted on barite-quartz interface in barite-Mn oxide(-silica) veins (Fig. 3). The veins consist chiefly of banded open-space-grown of barite and minor quartz, goethite, Fe-oxyhydroxides, and X-ray amorphous hollandite group-like minerals and MnO2–like phases. The barite is enclosed in a fine-grained quartz and has corroded surfaces which indicate that the barite predate the quartz (Fig. 5). Raman spectroscopy shows that the barite, as well as the quartz, is poorly crystalline at the quartz-barite interface. Various types of filamentous and spheroidal microstructures are found preserved in the poorly

Fig. 4. White smokers. A. Massive white smoker-bearing glauconite sandstone, overlying thinly bedded glauconite sandstone . Note white smokers on both sides of the hammer, and pebble horizon with dacite and quartz clasts coated by Mn minerals, at hammers head. The thinly bedded unit contains bedding-conformable barite-Mn oxide(±quartz) horizons; crinkly, wavy and discontinuous laminae may indicate microbial mats. White smokers are vertical, with cylindrical or tubular shape, variable width, and have no structural control; they have a barite and silica rim and a hollow core that may contain Mn minerals. B, C. Collapsed rubble of tubular Mn-oxide coated white smoker chimneys, chimney fragments, and chimney crusts, fossilised worm tubes, and microbial mat destruction structures; the unique microtextures of the Mn oxide deposits and the chimney crusts appear to have been produced by communities of diverse microorganisms inhabiting environments of venting at Vani. D. Isolated hollow barite(silica) white smoker filled with barite. Note cauliflower-like Mn oxides of possible biogenic origin.

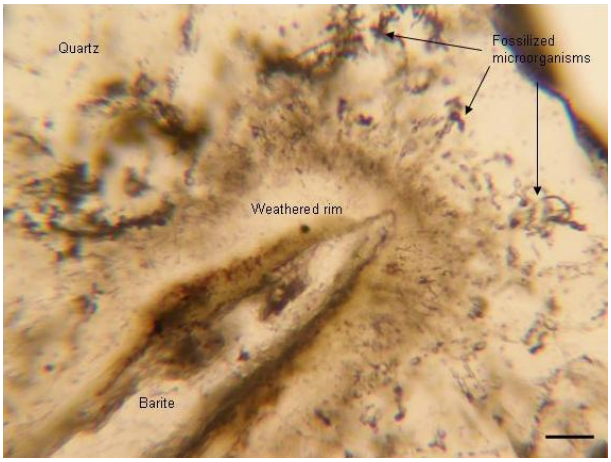

Fig. 5. Microphotograph of the barite-quartz interface. The barite is weathered which indicate that barite predated the quartz. High amount of microstructures at the interface. Scale bar 50 µm.

crystalline fine-grained quartz close to the quartz-barite interface (Fig. 5). The filamentous microstructures vary in size from only ~1 µm in diameter to ~15 µm in diameter (Fig. 6). The length of the small filamentous structures is ~10-20 µm and the length of the larger filamentous structures can range from ~20-200 µm. The morphology of the small filamentous microstructures is simpler with less branching, less segmentation and with a straight or twisted appearance compared to the larger filamentous structures that show more variation morphologically. The large type of the filamentous microstructures is curvi-linear, branched, and with distinct segmentation of septa. Many of the larger filamentous microstructures have a turgid appearance with knob-like outgrowths.

The spheroidal microstructures are between ~5-20 µm in diameter and are either circular or oval in

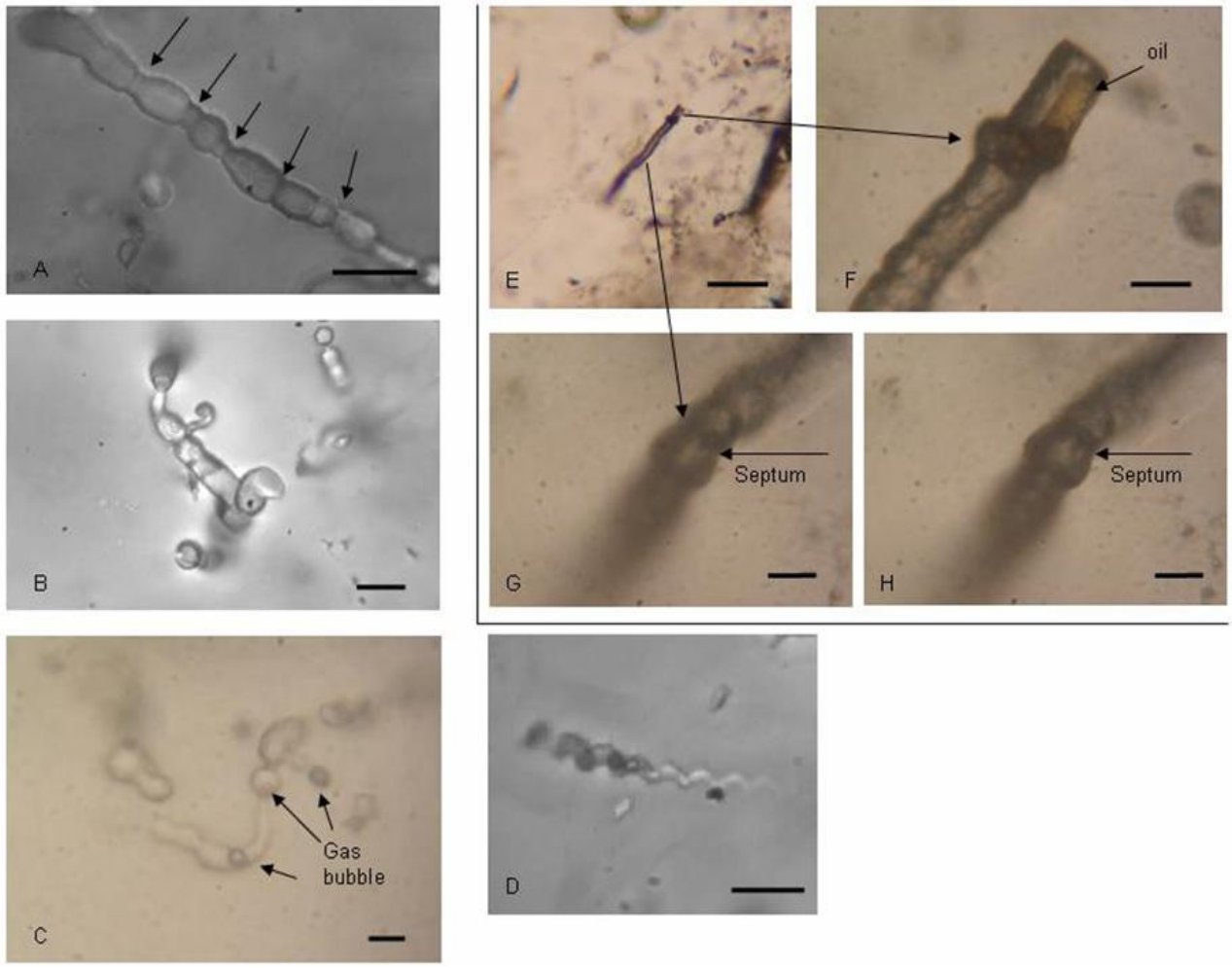

Fig. 6. Microphotographs of filamentous microstructures. A: Large filamentous microstructure with septa. B: Filamentous microstructure with knob-like outgrowths and/or associated spheroidal microstructures. C: Fluid inclusion bearing filamentous and spheroidal microstructures with transitions between the both types. Turgid appearance. D: Small, twisted microstructure. E-H: Large filamentous microstructure divided by septa, with and outgrowth at one end and a one or two phased oil inclusion. Scale bars: A, B, C: 10 µm, D: 5 µm, E: 100 µm, F, G, H: 10 µm.

shape (Fig. 7). Usually, they are bottle-shaped with a tail-like filamentous outgrowth at one end which results in a "spore-like" appearance. The oval microstructures can also be double which results in a "peanut"-like appearance. The spheroidal microstructures are highly associated with the filamentous structures and both types are sometimes combined and form transitions between each other.

Both the filamentous and the spheroidal microstructures are filled with aqueous (liquid ± vapour) and/or hydrocarbon phases. The hydrocarbon phase consists mainly of liquid hydrocarbons, but in a few cases also of solid hydrocarbons that coat the inner walls of the microstructures (Fig. 8). Raman spectra from a brownish solid phase within a filamentous microstructure with Raman bands at 2880, 2850, 1438 and 1295 cm-1 correspond to aliphatic hydrocarbons and may be assigned to evenkite (Jehlicka et al., 2009) (Fig. 9). In some of the larger microstructures chitin was detected with the pigment Wheat Germ Agglutinin conjugated with Fluorescein Isothiocyanate (WGA-FITC) under fluorescent microscopy (Fig. 10). Chitin is a component in fungal cell walls and not present in the cells of bacteria or archaea and thus WGA-FITC is commonly used to detect fungi or visually separate fungi from bacteria. We thus propose that the large microstructures observed represent fossilized fungi. The detection of chitin more or less rules out the possibility that the structures represent fossilized bacteria or archaea. Our interpretation is further supported by the close morphological resemblance with known fungi. The size, septa, branching and turgidity of the filamentous structures correspond more to the morphological appearance of fungi hyphae than filamentous bacteria. The size and morphology of the spheroidal structures are similar to fungal spores or fruiting bodies and their close association with the fossilized hyphae support this interpretation.

The presence of hydrocarbons in the microstructures does not directly support a fungal interpretation but, since the hydrocarbons probably represent thermally decomposed biological material, the presence of hydrocarbons indirectly support the biogenicity.

Microorganisms associated with hydrothermal systems are usually interpreted as prokaryotes belonging to the two kingdoms bacteria or archaea. Fungi are rarely reported from hydrothermal sub-seafloor environments. Marine fungi have been found in deep-sea sediments (Takami, 1999; Nagahama et al., 2003) and in association with hydrothermal vents on the seafloor (López-García et al., 2007) but never below the seafloor. Schumann et al. (2004) reported of fossilized fungi in carbonate filled veins in basalt from the North Pacific Eocene

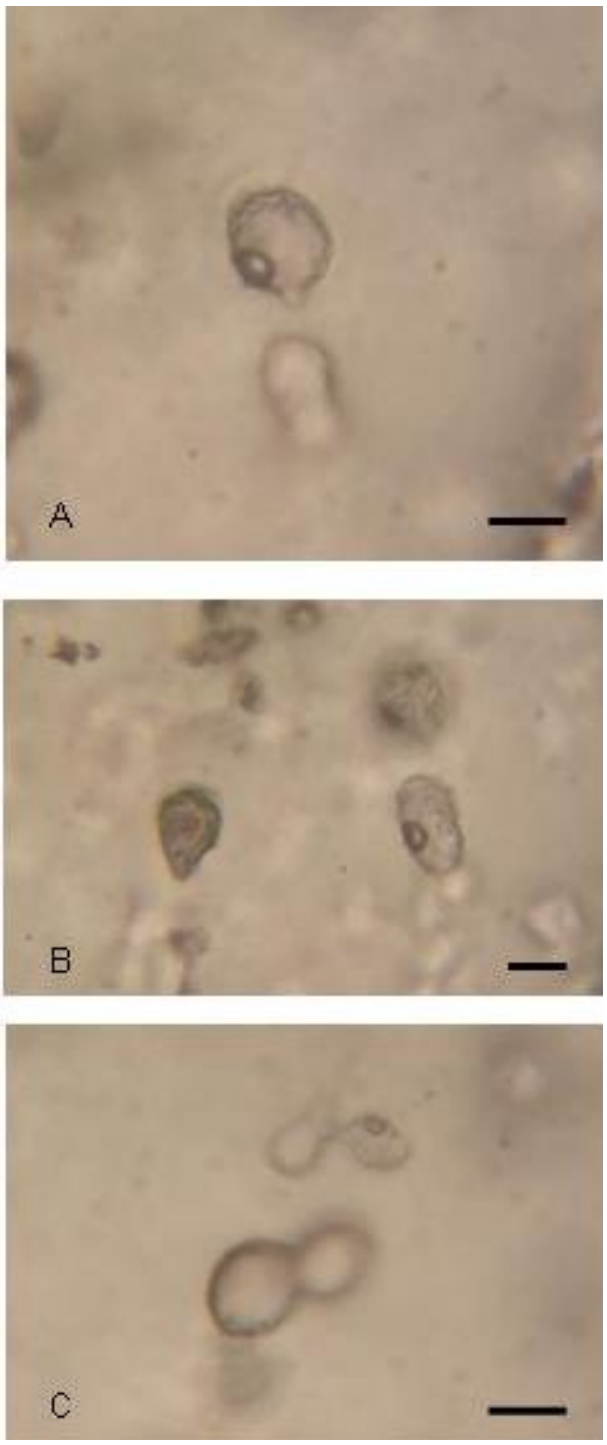

Fig. 7. Microphotographs of spheroidal microstructures. A: Speroidal microstructure with a "spore-like" appearance. B: Oval and "spore-like" microstructures. C: Spheroidal microstructures with a "peanut-like" appearance. Scale bars: A, B, C: 20 µm.

Crust and Reitner et al. (2006) reports of similar filamentous fungi structures in basalts from the Holocene oceanic basement from the Kolbeinsey Ridge (north of Iceland) at a depth of 1500 meters below sea level. These fossilized filamentous structures have been interpreted as fungi based on morphological observations only. The detection of chitin in the samples from Milos, is the first time a specific fungal biomarker has been detected in the fossilized fungi from hydrothermal environments.

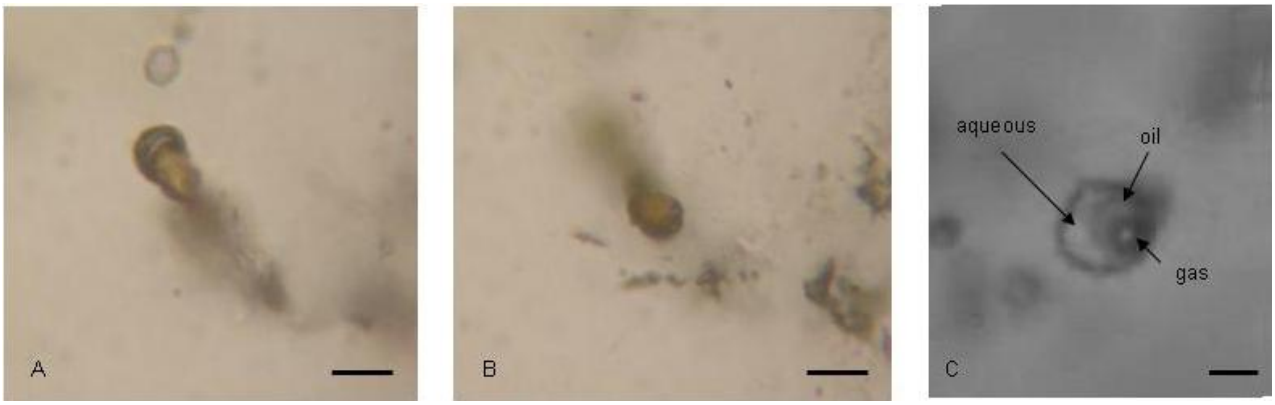

Fig. 8. Microphotograph of oil bearing inclusions. A, B: One or two phased oil inclusions. C: Three phase (gas, oil, aqueous) inclusion. Scale bars: 10 μm.

Fungi are known as an important geobiological agent in terrestrial environments where it lives in symbiosis with bacteria, algae and plants. The occurrence of fungi in sub-seafloor environments indicate that fungi might play an important role in more extreme environments as well, and this will need attention in the future.

The smaller microstructures, in which chitin not was detected, can not be interpreted as fossilized fungi but are most likely fossilized microorganisms as well. We argue this based on (1) the close resemblance morphologically to known microorganisms (Ehrlich 2002), (2) the presence of hydrocarbons, (3) the close association with the fossilized fungi, and (4) that the geological context is compatible with and known to harbour microorganisms (e.g. Harris et al. 2009, and references therein). Lack of chitin is not an evidence for prokaryotes, however, the size and morphology of the smaller microstructures correspond more to prokaryotes than eukaryotes. If this is the case our samples display co-existence between prokaryotes and eukaryotes in a hydrothermal system.

4.2. Fluid Inclusion Microthermometry

Fluid inclusions display the temperature and fluid regime in the system at the time of mineral formation and entrapment of the microorganisms. Small quantities of the hydrothermal mineralising fluid have been captured as fluid inclusions in barite and in the filamentous and the spheroidal microstructures in the fine-grained quartz. In neither of the studied fluid inclusions no signs of post-entrapment modifications like deformation, necking-down or leakage were noted. Microthermometry data on fluid inclusions in barite and the fluid-filled microfossils in quartz are comparable to previous published fluid inclusion data from the shallowest zone of the paleo-geothermal mineralization systems at Milos Island (Kilias et al., 2001; Naden et al., 2005). The present results show that barite was precipitated from a boiling solution at a temperature of around 100°C. Coexisting fluid inclusions have variable liquid/vapour ratios and show a large range of homogenisation temperatures, from 95° to 280°C with homogenisation to both liquid and vapour. This is typical for a heterogeneous system where fluid inclusions have trapped mixtures of various amounts of the residual liquid and the vapour phase. After freezing the inclusions, initial melting was observed within the interval -31° to -45°C, which is below the eutectic temperature of the NaCl-H_2O system and possibly suggests the presence of Ca or Mg salts in addition to NaCl. The final ice melting temperatures were measured between -0.7° (vapour phase dominated) and -12.4°C (residual liquid phase dominated) and correspond to salinities of 1.2 to 16.3 wt. % NaCl eq. (Bodnar, 1993). The aqueous fluid-filled filamentous and spheroidal microstructures in the quartz consist of one phase (liquid) or two phases (liquid and vapour). Homogenization of the two-phase inclusions took place in the range 109° to 144°C, the liquid-only inclusions are believed to have formed at approximately 100°C. The initial melting oc-

curred at similar temperatures as in the barite-hosted inclusions. Final ice melting temperatures were observed between -10.5 and -11.0°C and indicate a salinity of 14.5 to 15.0 wt. % NaCl eq. (Bodnar, 1993).

4.3. The palaeoenvironment and preservation of the microfossils

Our interpretation is that barite formed in boiling geothermal water at 100°C and at a shallow water depth (< 10 m). In previous studies of stable isotopes (D, O, Sr) on fluid inclusions from the epithermal mineralization system at Milos it was concluded that seawater was the main component in the geothermal system (Naden et al., 2005). In the present study, the high salinity of the fluid inclusions in barite is believed to represent the residual liquid phase of boiling seawater and implies that

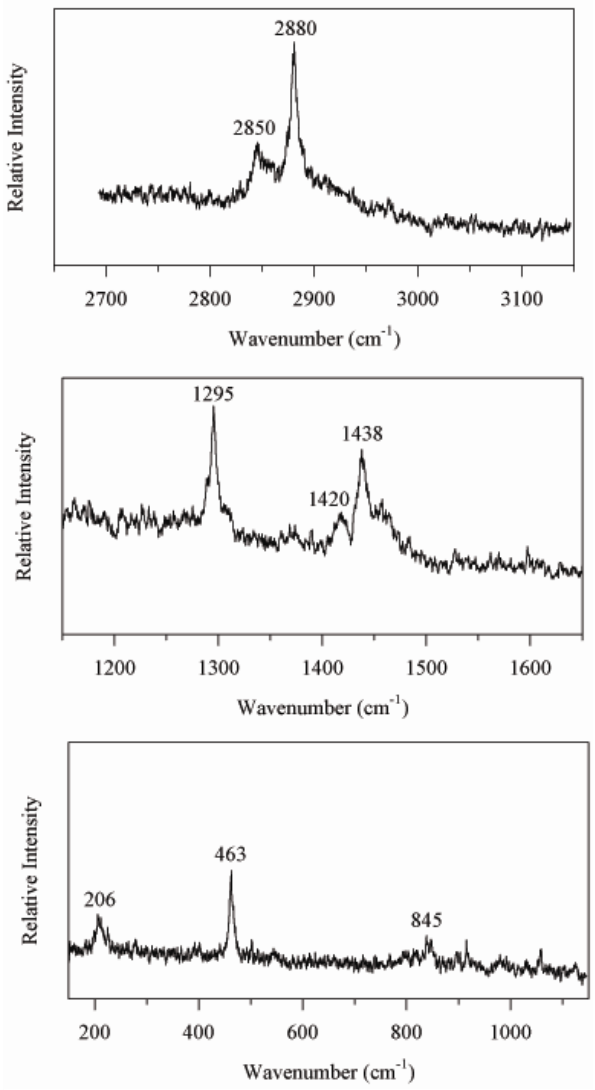

Fig. 9. Raman spectra of a solid hydrocarbon phase coating a microstrcucture.

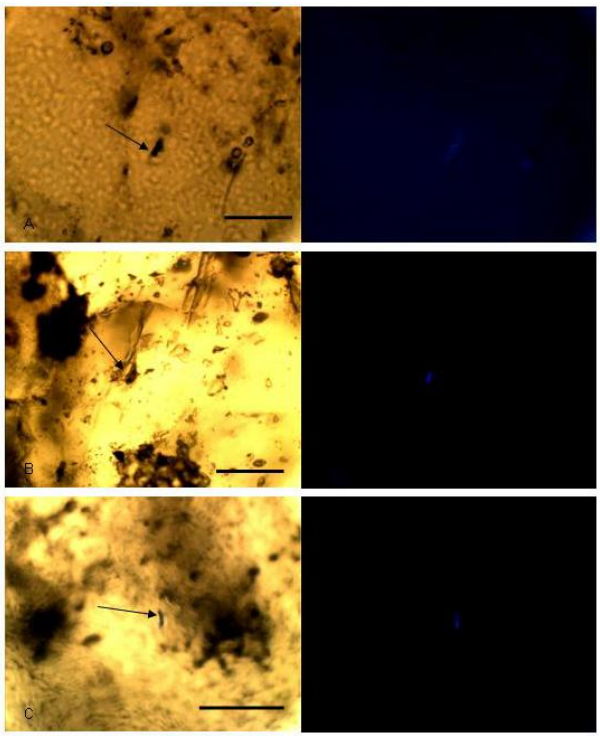

Fig. 10. Microphotographs showing detection of chitin in microstructures by the pigment WGA-FITC. Light microscopy to the left, fluorescence light to the right. Scale bars: 50 μm.

during barite precipitation the salinity of the water gradually evolved from seawater salinity to an elevated concentration (16 wt. % NaCl). The microorganisms were trapped in close association to the barite-quartz interface which suggest that they probably lived in the vicinity of the barite surface. This is supported by the mineralogical similarity of the unconformable feeder and white smoker structures with conformable barite-Mn oxide (–silica) horizons, and geological evidence for their spatial association with microbial mat features preserved within the siliciclastic sediments, which combined may suggest microbial colonization of sites near hydrothermal fluid flow and sea-floor venting. The corroded surface of barite may be the result of microbial sulphate reduction or just altered by the geothermal water. Hydrothermal environments are characterized by sudden pulses of hot fluids that are introduced to the system and it is not clear if the microorganisms existed during active boiling of the hydrothermal system or if they were present at a short period of somewhat cooler conditions. Ivarsson et al. (2009) showed that fluid inclusions associated with fossilized microorganisms do not necessarily represent the temperatures at which the microorganisms lived but merely the temperatures at which the microorganisms were trapped and

preserved. A new discharge of heated silica-rich water flowed into the system, the temperature increased to 100°C and the water started to boil. The silica was deposited as an amorphous accumulation in which the microorganisms were entombed and subsequently decomposed leaving water-filled cavities with preserved shapes of the original microorganisms on the inner walls. Some of the organic matter remained entrapped and still present in the microstructures as the detected liquid and solid hydrocarbons. With time the silica was transformed into the fine-grained poorly crystalline quartz with the microorganisms preserved as fluid inclusions.

5. Conclusions

We have showed how fossilized microorganisms preserved as fluid inclusions can be used in the process of establishing biogenicity of microfossils as well as a tool to describe the palaeoenvironment of the microfossils. Fluid inclusions have previously been suggested as important containers of paleobiological information in combination with the study of fossilized microorganisms (Ivarsson et al., 2009) but fluid-filled microfossils may be even more accurate from a paleobiological point of view and to our knowledge this is the first time it has been reported of. In our opinion these fluid inclusions contain more information than was covered in this paper and our recommendation is to study this type of fluid inclusions more intensely in the future.

Acknowledgements

Financial support from the University of Athens Special Account for Research Grants to S. P. Kilias (KA 70/4/3373, 70/4/6425) and the SEG Hugh Exton McKinstry fund (2006 and 2005) to K. Detsi is gratefully acknowledged. This work was in part funded by the Swedish National Space Board

References

Bodnar R.J., 1993. Revised equation and table for determining the freezing point depression of H_2O-NaCl solutions. Geochimica et Cosmochimica Acta, 57, 683-684.

Bonfante-Fasolo P. , Perotto S., , Testa B. and Faccio A.,1987. Ultrastructural Localization of Cell Surface Sugar Residues in Ericoid Mycorrhizal Fungi by Gold-Labeled Lectins. Protoplasma, 139, 25-35.

Dick G.J., Clement B.G.,. Webb S.M, Fodrie F.J., Bargar J.R., Tebo B.M., 2009, Enzymatic microbial Mn(II) oxidation and Mn biooxide production in the Guaymas Basin deep-sea hydrothermal plume. Geochimica et Cosmochimica Acta, 73, 6517-6530.

Edwards K.J., Bach W. and McCollom, T.M., 2005. Geomicrobiology in oceanography: microbe-mineral interactions at and below the seafloor: Trends in Microbiology, 13, 449-456.

Ehrlich H.L., 2002, Geomicrobiology, Marcel Dekker, New York.

Furnes, H., McLoughlin, N., Muehlenbachs, K., Banerjee, N., Staudigel, H., Dilek, Y., de Wit, M., Van Krankendonk, M., and Schiffman, P., 2008, Oceanic pillow lavas and hyaloclastites as habitats for microbial life through time – a review, in Dilek, Y., Furnes, H., and Muehlenbachs, K., eds., Links between geological processes, microbial activities and evolution of life, Springer, Modern approaches in solid Earth sciences, v. 4, p. 1-68.

Fytikas M., Innocenti F., Kolios N., Manetti P., Mazuolli R., Poli G., Rita F. and Villari, L., 1986. Volcanology and petrology of volcanic products from the island of Milos and neighbouring islets. Journal of Volcanology and Geothermal Research, 28, 297-317.

Glasby G.P., Papavassiliou C.T., Mitsis J., Valsami-Jones E., Liakopoulos A. and Renner R.M., 2005. The Vani manganese deposit, Milos Island, Greece: A fossil stratabound Mn-Ba-Pb-Zn-As-Sb-W-rich hydrothermal deposit. In Fytikas, M. and Vougioukalakis, G.E. (eds), Developments in Volcanology, Elsevier, Amsterdam, v. 7, p. 255-288.

Gold T., 1992, The deep hot biosphere: Proceedings of the National Academy of Sciences, 89, 6045-6049.

Harris A.C., White N.C., McPhie J., Bull S.W., Line M.A., Skrzeczynski R., Mernagh T.P. and Tosdal R.M., 2009. Early Archean hot springs above epithermal veins, North Pole, western Australia: new insights from fluid inclusion microanalysis. Economic Geology, 104, 793-814.

Hedenquist J.W., Arribas A. and Conzalez-Urien, E., 2000. Exploration for epithermal gold deposits. Reviews in Economic Geology, 13, 245-278.

Hein J.R., Stamatakis, M.G. and Dowling, J.S., 2000. Trace metal-rich Quaternary hydrothermal manganese oxide and barite deposit, Milos Island, Greece, Applied Earth Science, section B, 109, 67-76.

Ivarsson, M. (2006) Advantages of doubly polished thin sections for the study of microfossils in volcanic rock. Geochem. Trans. Geochemical Transactions, 7, 1-9.

Ivarsson M., Lausmaa J., Lindblom S., Broman C. and Holm, N.G., 2008. Fossilized microorganisms from the Emperor Seamounts: Implications for the search for a subsurface fossil record on Earth and Mar. Astrobiology, 8, 1139-1157.

Ivarsson M., Broman C., Lindblom S. and Holm, N.G., 2009. Fluid inclusions as a tool to constrain the preservation conditions of sub-seafloor cryptoendolith. Planetary and Space Science, 57, 477-490.

Jehlicka J., Edwards H.G.M. and Vitek, 2009. Assessment of Raman spectroscopy as a tool for the non-destructive identification of organic minerals and biomolecules for Mars studies. Planetary and Space Science, 57, 606-613.

Kilias S., Naden J., Cheliotis I., Shepherd T.J., Constandinidou H., Crossing J. and Simos, J., 2001. Epithermal gold mineralization in the active Aegean Volcanic Arc: the Profitis Ilias deposit, Milos Island, Greece. Mineralium Deposita, 36, .32-44.

Kilias S.P., Detsi K., Godelitsas A., Typas M., Naden J. and Marranitos, Y., 2007. Evidence of Mn-oxide biomineralization, Vani Mn deposit, Milos, Greece. In Andrew et al. (eds), Digging Deeper, Proceedings of the ninth Biennial SGA Meeting, Dublin.

Liakopoulos A., Glasby G.P., Papavassiliou C.T. and Boulegue, J., 2001. Nature and origin of the Vani manganese deposit, Milos, Greece: an overview. Ore Geology Reviews, 18, 181–209.

López-Garcí, P., Vereshchaka A. and Moreira, D., 2007. Eukaryotic diversity associated with carbonates and fluid-seawater interface in Lost-City hydrothermal field: Environmental Microbiology, 9, 546-554.

Naden J., Kilias S.P. and Darbyshire, D.P.F., 2005. Active geothermal systems with entrained seawater as modern analogs for transitional volcanic-hosted massive sulphide and continental magmato-hydrothermal mineralization: The example of Milos Island, Greece. Geology, 33, 541-544.

Nagahama T., Hamamoto M., Nakase T., Takaki, Y. and Horikoshi, K., 2003. Cryptococcus surugaensis sp. nov., a novel yeast species from sediments collected on the deep-sea floor of Suruga Bay. International Journal of Systematic and Evolutionary Microbiology, 53, 2095-2098.

Nora Noffke N., Gerdes G., Klenke T. and Krumbein W.E., 2001. Microbially induced sedimentary structures: A new category within the classification of primary sedimentary structures. Journal of Sedimentary Research, 71, 649-656.

Noffke N., 2009. The criteria for the biogeneicity of microbially induced sedimentary structures (MISS) in Archean and younger, sandy deposits. Earth Science Reviews, 96, 173-180.

Pirajno F., and Van Kranendonk M.J., 2005. Review of hydrothermal processes and systems on Earth and implications for Martian analogues. Australian Journal of Earth Science, 52, 329–351.

Reitner J., Schumann G. and Pedersen K., 2006. Fungi in subterranean environments, in Gadd, G.M., eds., Fungi in biogeochemical cycles, Cambridge University Press, New York, 377-403.

Schumann G., Manz W, Reitner J. and Lustrino, M., 2004.Ancient fungal life in North Pacific Eocene oceanic crust. Geomicrobiology Journal, 21, 241-246.

Skarpelis N. and Koutles, T., 2004. Geology of epithermal mineralization of the NW part of Milos Island: Greece, 5th International Symposium on Eastern Mediterranean Geology, Thessaloniki, Greece.

Stewart A.L. and Mcphie J., 2006. Facies architecture and Late Pliocene – Pleistocene evolution of a felsic volcanic island, Milos, Greece, Bulletin Volcanology, v. 68, p.703-726.

Takami H., 1999. Isolation and characterization of micro-organisms from deep-sea mud, in Horikoshi, K., and Tsujii, K., eds., Extremophiles in deep-sea environments, Springer-Verlag, Tokyo, .3-26.

Ueno Y., Yamada K., Yoshida N., Maruyama S. and Isozaki, Y., 2006. Evidence from fluid inclusions from microbial methanogenesis in the early Archaean era. Nature, 440, 516–519.

Scientific Annals, School of Geology, Aristotle University of Thessaloniki Proceedings of the XIX CBGA Congress, Thessaloniki, Greece	Special volume 100	309-315	Thessaloniki 2010

GEOLOGICAL SETTINGS AND CONDITIONS OF GENESIS OF VOLCANOGENIC DEPOSITS OF NON-FERROUS METALS IN PALEOISLAND ARC ENVIRONMENTS

Kekelia S[1]., Sosson M[2]., Kekelia M[1]., Asatiani G[1]., Kuloshvili S[1]., Sadradze N[1]., Gagnidze N[1]., Razmadze A[1].

[1]Department of Ores, A. Janelidze Institute of Geology, 0193, 1/9 M. Alexidze str.Tbilisi, Georgia, sergokekelia@yahoo.com;
[2] CNRS -GeoSciences Azur, UMR 6526 250 Rue Albert Einstein - Sophia Antipolis 06560 Valbonne – France, sosson@geoazur.unice.fr

Abstract: By the example of the Pontian-South Caucasian paleoisland arc actively functioning during the whole Mesozoic the authors consider the main peculiarities of spatial-temporal relationships between ores of non-ferrous metals and enclosing rocks, and discuss the conditions of the evolution of ore-magmatic systems. The authors' conclusions are substantiated by data on $^{87}Sr/^{86}Sr$ ratios, concentration of rare elements in enclosing volcanogenic rocks, isotopic ratio of sulfur and oxygen in ores, and results of thermobarogeochemical studies. The authors hold the opinion shared by many mining geologists that the main part of ore components in non-ferrous metal deposits was extracted from nearby magmatites enclosing and underlying mineralized zones. The solutions from which ores precipitated were, by their salinity, very close to sea water. The maximum temperature of ore formation at epigenetic deposits reached 400°C for copper ores and 280°C for barite-polymetallic ores, whereas the pressure did not exceed 200 bar. As for hydrothermal-sedimentary ores, they could most likely form at the sea bottom, at depths of 2-3km and maximum temperature no more than 300°C.

Keywords: the Pontides, the South Caucasus, Jurassic, Cretaceous, ore, non-ferrous metal

Within the Alpine-Himalayan mountain-fold belt there are known numerous fragments of paleoisland arcs and contiguous structures –back-arc and intra-arc basins. One of such paleoisland arcs is the Pontian-South Caucasian magmatic arc (fig.1). Volcanostructures situated within this arc host the largest and economically most important deposits of non-ferrous metals in the region. During the Alpine epoch, maximum volcanic activity in the eastern part of this belt (in Armenia and western Azerbaijan) occurred in Bajocian-Late Jurassic, whereas in the western part (Georgia and Pontides in Turkey) – in the Cretaceous time. Here, in areas that experienced the strongest tectonic stresses related to zones of large active faults, under the covergent interaction of lithospheric microplates (Pontian-South Caucasian and Iranian), intensive volcanism and hydrothermal activity took place accompanied by the appearance of considerable thermoanomalies in the earth crust (Biji-Duval et al., 1977; Monin and Zonenshain, 1987; Yilmaz et al., 1997).

During the convergence of above microplates, originally epigenetic volcanogenic and barite-polymetallic ores came into being (e.g.in Jurassic time in Armenia); later, in Late Cretaceous some copper, gold and barite-polymetallic deposits were formed in Georgia and the Pontides. The Pontides also host large-scale hydrothermal-sedimentary deposits, an example of which is the Çayeli deposit in eastern Turkey. At present, in the Eastern Pontides the following deposits are being exploited – Aşikoy (the Cyprus type of deposit), epigenetic deposits of Lahanos, Kutlular and Murgul, and the Kuroko-type Çayeli deposit. Estimated reserves of ores at the Çayeli deposit amount to 15.9 million tons averaging 4.4% copper, 6.1%zinc, 0.8g/t gold and 44g/t silver. All reserves of copper and zinc are concentrated within a single ore body that extends along the strike at a distance of 920m, maximum thickness being 100m (Altun, 1977). The ore-containing volcanostructure is made up of supra-ore basalts (pillow-lavas) alternating with limestones and "purple tuffs", and locally with propylitized dacites. This unit is overlain by massive sulfidic ores – sphalerite, chalcopyrite, pyrite. These ores are strongly brecciated and resemble

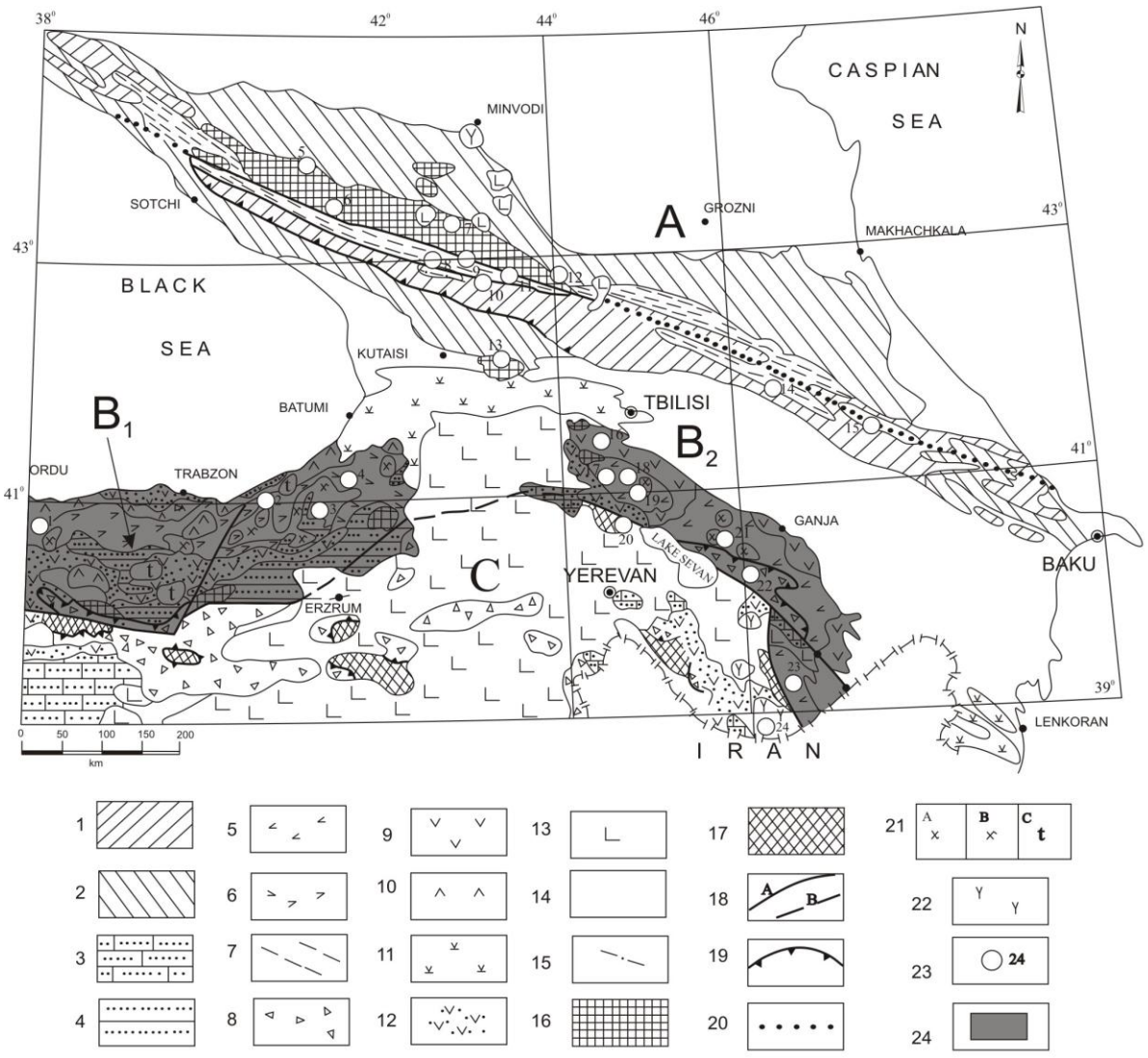

Fig. 1. Distribution of main metal-bearing deposits within the geological structures of eastern Turkey and the Caucasus. 1- Slope and rize of the South Caucasian microcontinent (Jurassic-Early Cretaceous, Greater Caucasus); 2- Shelf zones of the Scythian and South Caucasian microcontinents (Jurassic - Paleogene, Greater Caucasus); 3- Shelf zones of the North Iranian microcontinents (Cretaceous- Paleogene); 4- Shelf zones of the Pontian microcontinent (Early Jurassic, Eastern Pontides); 5- Lesser Caucasian ensialic island arc (Bajocian-Early Cretaceous); 6- Pontian ensialic island arc (Cretaceous); 7- Deep basins of marginal paleosea (Early-Middle Jurassic); 8- Oceanic zones in allochthonous occurrence. 9- Lesser Caucasian backarc volcanodepressions (Late Cretaceous); 10- Pontian backarc volcanodepressions (Late Cretaceous); 11- Intraplate riftogene volcanostructures (Eocene-Oligocene, Lesser Caucasus); 12- Eocene volcanodepressions superimposed on precollisional structures (Pontides, Lesser Caucasus, N. Iranian); 13- Young volcanic plateaus (Oligocene-Quaternary); 14- Orogenic troughs (Oligocene-Quaternary); 15- Terrigenous - volcanic rocks (Dizi series, Devonian-Triassic) intruded by Middle Jurassic granitoids; 16- Pre-Alpine basement of the Scythian and South Caucasian microplates (Pre-Cambrian (?) - Paleozoic); 17- Pre-Alpine basement of North Iran (North Iranian microplate, Pre-Cambrian - Paleozoic); 18- Tectonic sutures separating main geoblocks (represented by reverse faults and strike-slips, A - ascertained; B - proposed); 19- Thrusts; 20- Supposed boundaries between Scythian and South Caucasian microplates (overlain by thrust sheets); 21- Granitoids (a -Early Cretaceous, b - Late Cretaceous, c - Eocene-Oligocene); 22- Monzonites, syenites (Oligocene-Miocene); 23- Mineral deposits; 24- Fragments of paleoisland-arc. Main metal-bearing deposits of the Eurasian active paleomargin: 1 - Asikoy (Cu), 2- Lahanos (Cu, Zn, Pb), 3- Çayeli –Madenkoy (Cu, Zn), 4- Murgul (Cu, Zn), 5- Urup (Cu), 6- Kti-Teberda (W), 7- Tirni-Auz (W), 8- Lukhra (Au), 9- Tsana (As, Au), 10- Lukhumi (As), 11- Zopkhito (Au,Sb), 12- Sadon (Pb, Zn), 13- Chiatura (Mn), 14- Filizcay (Zn,Pb,Cu), 15- Kizil-Dere (Cu), 16- Madneuli (Cu,Zn, Pb, $BaSO_4$), 17- Alaverdi (Cu), 18- Shamlug (Cu), 19- Tekhut (Cu), 20-Megradzor (Au), 21- Dashkesan (Fe, Co), 22- Zot (Au), 23- Kafan (Cu), 24- Kadjaran (Mo, Cu). Microplates:Eurasian paleocontinent: A – Scythian, B – Pontian – South Caucasian (B_1 – Eastern Pontides, B_2 – South Caucasus); Afro-Arabian paleocontinent: C- North Iranian.

Kuroko-type ores in Japan. Çayeli ores are also close to "ore hills" of modern mid-oceanic ridges (MOR) and rifting zones of marginal basins, by their textural-structural characteristics and mineralogical zonality. In the course of the formation of the Çayeli ore body, simultaneously took place its destruction as a result of hydrothermal explosions. As a result, there were formed breccias of "black" (sphaleritic) ores that were healed, in most cases, by quartz-chalcopyritic substance ("yellow" ores). The ore body is overlain by a thin horizon of hematitous tuffites containing manganese minerals which, in turn, are overlain by andesite-basalts. Most of the scientists consider Çayeli ores to be hydrothermal-sedimentary products being an analogue of modern ores of MOR. At the same time, some authors assume that there is no complete similarity between ancient and modern ores (e.g. Ohmoto and Skinner, 1983). It is quite naturally since ancient ores during the long geological time experience deep structural and mineralogical transformations together with enclosing volcanogenic and sedimentary sequences.

Another type of hydrothermal-sedimentary mineralization in the Pontides is represented by the Aşikoy massive sulfide deposit, 2km west-northwest of Küre in northern Turkey. Here, ores are hosted by an allochthonous slab of volcanogenic and sedimentary rocks known in literature as"the Kure complex" (Guner, 1980; Ustaomer and Robertson, 1993; Çakir, 1995). It is generally accepted that the allochthone was transported onto the paleoisland arc structure from the marginal sea basin of the Paleothethys. Mineralization pattern and geological setting here are similar to those observed on the island of Cyprus – at the base of the section occur serpentinous peridotites that are successively overlain by gabbro, a diabase dyke complex and greenstone-altered basaltic pillowlavas. Above the latter there are coper-bearing massive sulfidic ores.

Examples of stokwork-veinlet deposits in the Pontides are Lahanos and Murgul whose mineralization pattern is very close to that observed in Madneuli, South Georgia.

The Georgian deposit Madneuli situated in the Bolnisi mining district in South Georgia represents a rather rare type of ore deposits in which gold, barite-sulfidic and copper ores belonging to temporally different stages are spatially clustered within a limited area. A volcano-tectonic depression (Bolnisi Cretaceous structure) that hosts the deposit represented a part of a back-arc basin. The volcanostructure is made up of three complexes that are the products of functioning during the Albian-Campanian time a number of various volcanoes (at first fissure-type and later composite stratavolcanoes) (Kekelia et al., 1993). The uppermost contrast basalt-andesite-rhyodacitic complex terminates volcanic activity in the Bolnisi Cretaceous structure. Most likely, that the comagmatites of this complex are granodiorites and granodiorite-porphyries discovered by drilling in the central part of the volcanodepression beneath the Madneuli quarry. Here productive are cupola-shaped rises squeezed on the slopes of large volcanic structures and consisting of rhyodacitic extrusions of the middle "rhyodacitic complex". The complex also contains ignimbrites and lavas and extrusions of rhyolites. The lower complex is made up of volcanogenic-sedimentary rocks with the predominance of intermediate (andesitic) volcanites.

Available data on the isotopic composition of strontium and concentrations of rubidium and strontium in mineralized rocks (Kekelia et al., 2004) indicate that basalts of the Bolnisi district (87Sr/86Sr=0.704910) were, most likely, products of undepleted mantle, rhyolites of Madneuli might have been the melt of the upper part of the crust ($^{87}Sr/^{86}Sr$=0.707739), whereas the rhyodacites of the Murgul deposit (Eastern Turkey) – products of the bottom of the earth crust ($^{87}Sr/^{86}Sr$=0.710269). Original data on various types of rocks, including rocks characteristic of the undepleted mantle are summarized by Abramovich et al., (1989).

In Armenia, some epigenetic copper and barite-polymetallic deposits hosted by Middle Jurassic volcanites have been exploited for a long time. These are Alaverdi, Shamlug, Akhtala and Kafan deposits. At the Alaverdi district, the geological section of Middle Jurassic productive series is represented by (from bottom to top): andesite and dacite lavas, tephroidal turbidites, piles of submarine colluvium, hyaloclastites, and a thin unit of chemogenic-sedimentary rocks. This ore-bearing sequence is overlapped by a Late Jurassic volcanogenic complex (Kekelia et al., 1993).

Copper veinlet-dispersed mineralization is characteristic of the Bolnisi, Alaverdi and Kafan deposits. At Madneuli, gold mineralization was found in secondary quartzites. Barite-sulfidic mineralization in Madneuli is developed in form of veins, veinlets and gently-dipping ore bodies. At the Alaverdi deposit, veinlet and veinlet-dispersed ore bodies are

located within narrow zones of quartz-sericite-chlorite metasomatites which are developed among widespread propylites.

Differences in ore characteristics from various parts of the paleoisland arc show strong dependence on the geodynamic regimes of specific metallogenic episodes. Below we propose a genetic model of the evolution of ore-generating systems of volcanogenic deposits of non-ferrous metals. The proposed model should be considered as a some abstraction that takes into account not the formal resemblance of individuals (ore bodies, ore deposits) but the standard course of processes proceeding in the system.

Isotopic-geochemical data (Franklin et al., 1984; Sinyakov, 1986; Kekelia et al., 1993) indicate the participation of a considerable amount of sea waters in the hydrosystems of volcanogenic deposits. Experimental studies (Hodgson and Lyndon, 1977; Grichuk et al., 1984) on the extraction of elements from rocks under PT-conditions corresponding to fluid functioning, assume it possible to regard both magmatic and sedimentary rocks as a source of metals for volcanogenic deposits.

Vast geological material collected under the study of the world ocean (Zonenshain and Kovalev, 1974; Rona, 1986; Grinberg et al., 1990; Elianova and Mirlin, 1990; Elianova, 1999) gives all reason to suppose that the large-scale ore-formation has been realized in case of proceeding some successive processes: (1) magma crystallization; (2) interaction between "aggressive" heated sea waters and magmatites, heat source being igneous rocks emplaced into volcanogenic-sedimentary complex; (3) stable functioning of a physical-chemical barrier in the area of hydrotherms discharge (depressions on the seafloor or closed structures in upper horizons of the earth crust).

Thus, volcanogenic deposits in island arc environments are distinguished by the following peculiarities:

1. Ore composition strongly depends on petrochemical features of rocks. For example, copper-zinc mineralization is usually associated with andesite-basalts and/or sodic rhyolites (Krivtsov, 1989). It has been noted that ore-bearing rocks of the mid-oceanic ridges often contain spherical oxidized-ore aggregates (Prokoptsev and Prokoptsev, 1990). Subalkaline lavas developed in rift valleys of MOR also contain sulfides as impregnation in clinopyroxene and feldspar phenocrysts (Akimtsev and Sharapov 1993). All these facts indicate that some magmatites were primarily productive.
2. Within the limits of ore-knots, ways of hydrotherm migration are marked by alterations in mineral composition of rocks. In down-going zones rocks are predominantly argillized, while upper and flank zones undergo strong propylitization.
3. Barite-sulfidic ores in secondary quartzites display vertical zonality (e.g. Madenuli). Stockworks of copper and copper-zinc ores are often overlapped by gypsum-anhydrite lenses. Similar picture is also characteristic of hydrothermal-sedimentary Kuroko-type deposits that was noted by Matsukama and Khorikosi (1973).
4. By their salinity hydrothermal solutions are close to sea water but in comparison with latter they are enriched in Fe, Ag, Pb, Cu and Zn (Mottl et al., 1979). Low salinity is a characteristic feature of fluids in zones of recent ore-formation (Bortnikov et al., 2004; Bortnikov and Vikentiev, 2005). Data on the Lesser Caucasian deposits (Kekelia et al., 1991; Kekelia et al., 1993) also confirm these observations. In the Lesser Caucasian deposits, the maximum temperature of mineral formation was established by the method of homogenization and was 410-390°C for copper and 280°C for barite-polymetallic deposits (Yaroshevich, 1985); pressure was equal to 150-200 bar (we used diagrams published by Shepherd et al., 1985). According to Arevadze et al. (1983) and Yaroshevich (1985), salinity of fluids in Madneuli from which copper and barite-zinc-lead ors were deposited, did not exceed 40g/l NaCl eq. The solutions were chloride-sulfatic potassium-sodic by composition. These data are confirmed by the results of chemical analyses of aqueous extracts from quartz, sulfides and barite.
5. The most favourable conditions for the stable accumulation of hydrothermal-sedimentary ores existed on the seafloor, at depths of 2-3km (Stackelberg, 1985; Gablina et al., 2000).
6. Data on the isotopic composition of hydrogen and oxygen in fluidal inclusions in quartz, barite and calcite from volcanogenic barite-polymetallic ores are interpreted in favor of the participation of both sea and meteoric waters in the ore-forming process, with the predominance of the former (Franklin et al., 1984; Yaroshevich, 1985; Krivtsov et al., 1987).

7. Data on isotopic composition of sulfides and sulfates are ambiguous and cannot be used for the identification of a sulfur source.

The evolution and functioning of hydrosystems in volcanic complexes can be conceived as follows: firstly, accumulation, in local depressions of back-arc and intra-arc basins, of volcanogenic-sedimentary, predominantly calc-alkaline sequences; then, after the decrease in volcanic activity (the stage of volcanostructure inversion), emplacement of intrusives took place whose crystallization occurred at a depth of about 2 km from the surface or 1 km – from the seafloor. Hydrothermal sedimentary ores by their mineral composition and structure have similarity with modern extint "black smokers". Mineral zonality in them can be explained by the re-distribution of ore-forming components as a result of destruction of "ore hills" and their subsequent diffusion from deeper to shallower levels (Hanington et al., 1986; Elianova, 1989).

In the Keramdec island arc (the south-west Pacific), volcanites host hydrothermal-sedimentary Kuroko type deposits (de Ronde et al., 2003). According to thermobarogeochemical studies, salinity of hydrothermal solutions here ranged from 2.2 to 3.9wt % NaCl eq. and the temperature of homogenization was 175-322°C. We adduce this example in order to demonstrate the uniformity of physical-chemical conditions of ore-forming processes, irrespective of the way of their deposition - epigenetic of hydrothermal-sedimentary.

At the seafloor conditions, destabilization of fluids occurs in connection with the temperature drop and oxidation of fluids. Taking into account the composition of suspended matter emanated by "black smokers" (pyrite, sphalerite, pyrrhotite), we may suppose that metals were transported in form of hydro-sulfidic complexes. Levels of ore-formation in epigenetic deposits are generally comparable with pipe zones of "black smokers" whose boundary anomalous physical-chemical parameters stipulated synchronous crystallization of anhydrite and iron sulfides. Such conditions are observed in zones of hydrosystems with minimum activity of oxygen coinciding with the lower boundary of barite stability, under equal activity of H_2S-SO_4^{2-} (Franklin et al., 1984); Tvalchrelidze, 1987; Kekelia et al., 2004). At barite-sulfidic deposits, the zonal distribution of metals is conditioned by a number of factors: (1) greater dependence of the solubility of copper minerals on temperature as compared with that of sphalerite and galena (Franklin et al., 1984); (2) different stability of complex compounds (Franklin et al. 1984; Ovchinikov 1988); (3) dependence of precipitation of metals on the concentration of S^{2-}; under equal concentrations of metals in solution, precipitation of copper and zinc demands higher content of H_2S than it needs for lead (Ganeev, 1989); (4) functioning of a H_2S- barrier whose efficiency is determined by low content of S^{2-} (Kraynov et al., 1988).

Under the conditions of hydrothermal-sedimentary ore accumulation when mineral zonality of "ore-hills" is a result of the recrystallization, solution and redeposition of ore matter, the stifling of the sulfide-forming process takes place where the therms reach zones with high partial oxygen pressure; in this case occurs the precipitation of oxides of Fe and Mn and formation of jasper rocks in the upper horizons of the deposit. It should be noted that the mechanism of ore accumulation on the seafloor – frequently-repeated deposition of ore matter – was decisive under the formation of volcanogenic massive sulfide deposits.

Several words about formation of gold-beraing quartz veins and veinlets at Madneuli. We assume that they were fromed simultaneously with the formation of explosive breccias (Kekelia et al., 1991; Kekelia et al., 1993). Precipitation of gold, quartz and minor sulfides in the secondary quartzites occurred during the destabilization of magmatogenic fluids. Heinrich (2005) studying Cu-Au porphyry deposits pointed out that the low-salinity magmatic waters are capable of transporting gold under high temperature regime. One of the main requirements for this, according to Heinrich, is the presence of a sufficient quantity of H_2S. Magmatic fluids under high pressure pass into liquid form, without heterogenous phase transition, and their influence on the surroundings is expressed by significant potassium and propylitic alterations.

In the long-functioning hydrothermal systems, gold-beraing low-sulfidic epithermal deposits are distinguished by a large proportion of meteoric waters. Gold could have penetrated into hydrosystems together with magmatic steamy-condensed fluids.

References

Abramovich I.I., Burde A.I. and Voznesenski V.D. 1989. Geodynamic reconstructions. Leningrad, Nedra, 278 p. (in Russian).

Altun Y. 1977. Geology of the Çayeli-Madenköy copper-zinc deposit and the problems related to mineralization. Ankara, Mineral Res. Expl. Bull., 89, p.10-24.

Akimtsev V.A., Sharapov V.N. 1993. Ore effusions of the rift valley of the middle-Atlantic ridge. Proceedings of the Academy of Sciences of Russia, 331, #3, p.329-331, (in Russian).

Arevadze D. V., Gogishvili V. G. and Yaroshevich V. Z., 1983. Geology and genesis of the Madneuli copper-polymetallic deposit (South Georgia). Geology of ore deposits, #6, p.10-22 (in Russian with English abstract).

Bortnikov N.C., Simonov B.A., Bogdanov I.A. 2004. Fluid inclusions in minerals of modern sulfur constructions: physical-chemical conditions of mineral formations and evolution of fluids. Geology of ore deposits, v. 46, #1, p.74-87, (in Russian).

Bortnikov N.C., Vikentiev I.V. 2005. Modern sulfur polymetallic mineral formation in the world ocean. Geology of ore deposits, v. 47, #1, p.16-50, (in Russian).

Biju-Duval B., Dercourt J., Le Richon X. 1977. From the Tethys ocean to Mediterranean seas; a plate tectonic model of the evolution of the western Alpine system. Histoire Structural de Bassins Mediterraneens, p.143-164.

Çakir Ü. 1995. Geological characteristics of the Aşiköy-Toykondu (Küre-Kastamonu) massive sulfide deposits. Mineral. Res. Expl. Bull., 117, Ankara, p.29-40.

de Ronde C.E.J., Faure K., Bray C.J., Chappell D.A., Ian C. Wright I.C. 2003. Hydrothermal fluids associated with seafloor mineralization at two southern Kermadec arc volcanoes, offshore New Zeland. Mineralium Deposita, 38, p.217-233.

Elianova E.A. 1989. Formation of composition and structure of ores during the modern and old sulfide generation. Soviet Geology. #12, p. 17-26, (in Russian).

Elianova, E.A. 1999. Formation of recent and ancient submarine pyrite ores: composition and structure. In: Popov V.E. (ed) Models of volcanogenic-sedimentary ore formation system. Abstracts of International Conference), St. Petersburg, p.26-27, (in Russian).

Elianova E.A. ,Mirlin E.G. 1990. The oceanic ore-genesis, Soviet Geology, #6, p.47-55, (in Russian).

Franklin, J.M., Lydon, J.W., Sangster, D.F. 1984. Base metal massive sulfide deposits of volcanogenic affinities. In: Skinner B.S. (ed) Genesis of Ore Deposits 2. Mir Publishers, p.39-252, (in Russian).

Gablina, I.F., Mozgova, N.N., Borodaev, Ju.C., Stepanova, I.V., Cherkashev G.A., Ilijin M.L. 2000. Associations of Cu sulphides in recent oceanic ores of the hydrothermal field Logachev (Mid-Atlantic ridge, 14°45N). Geology of Ore Deposits 42, #4, p.329-349, (in Russian).

Ganeev I.G. 1989. Material transportation by hydrothermal solutions. Proceedings of All-union mineralogical society, vol.1, p.3-16, (in Russian).

Grinchuk G.D., Borisov M.B., Melnikova G.L. 1984. Thermodynamic model of hydrothermal systems in the oceanic crust: evaluation of solution evolution. Geology of ore deposits, #4, p.3-23, (in Russian).

Grinberg I.C., Krasnov C.G., Ainimer A.U., Porshina I.M., Stepanova T.V. 1990. Hydrothermal sulfur mineralization in the ocean. Soviet Geology, #12, p.81-91, (in Russian).

Güner M. 1980. Sulphide ores and geology of the Küre area Pontid in N Turkey. Mineral Research and Exploration Bulletin, p.65-109.

Hannigton M.D., Peter J.M., Scott S.D. 1986. Gold in sea-floor polymetallic sulfide deposits. Econ. Geol.,vol. 81, p.1867-1883.

Heinrich Ch.A. 2005. The physical evolution of low-salinity magmatic fluids at the porphyry to epithermal transition: a thermodynamic study. Mineralium Deposita, 39, p.864-889.

Hodgson C.L., Lyndon S.M. 1977. The geological setting of the volcanogenic massive sulfide deposits and active hydrothermal systems: some implications for explorations. Canadian Mining Metallurgical Bull., v.70, p.95-106.

Kekelia S., Kekelia M., Otkhmezuri Z., Moon Ch., Ozgür N. 2004. Ore-forming systems in volcanogenic-sedimentary sequences by the example of non-ferrous metal deposits of the Caucasus and Eastern Pontides. Ankara (Turkey), Mineral. Res. Expl. Bull, 129, p.1-16.

Kekelia S.A., Ambokadze A.H., Ratman I.P. 1993. Volcanogenic deposits of non-ferrous metals of paleoislandarc systems and methods of their prognosis. Metsniereba Publications, 96 p., (in Russian).

Kekelia S.A., Yaroshevich V.Z., Ratman I.P. 1991. Geological and genetic models for Alpine volcanogenic non-ferrous deposits in the Mediterranean Metallogenic Belt. Geology and Geophysics 8, p.71-79, (in Russian).

Kraynov S.P., Matveev L.I., Solomin G.A. 1988. Geochemical conditions of lead and zinc sedimentation from brines in sedimentary basins on a sulfide barries. Geochemistry, 2, p.1708-1719, (in Russian).

Krivtsov A. L., Bogdanov I.V., Borodaevskaia M.B., Genkin A.D., Kurbanov N.K., Likhachev A.P., Mitachev I.F. (ed). (1987). Ore copper deposits – types and conditions of formation. Moscow, "Nedra". 197 p, (in Russian).

Krivtsov A.I. 1989. Applied metallogeny. Nedra Publications, p. 288, (in Russian).

Matsukama T., Khorikosi Ei. 1973. A review of Kuroko deposits in Japan. In: Tatsumi.T. (ed) Volcanism and ore formation. Mir Publishers, p.129-151, (in Russian).

Monin A.S., Zonenshain L.P. (eds.). 1987. History of the Ocean Tethys. Institute of Oceanology, 155 p., (in Russian).

Mottl M.J., Holland H.D., Corr R.F. 1979. Chemical exchange during hydrothermal alteration of basalts seawater. Experimental results for Fe, Mn and sulfur apecies. Geochim et acta. v43, p.869-884.

Ohmoto H. and Skinner B. 1983. The Kuroko and related volcanogenic massive deposits. Introduction

and summary of new finding. Econ. Geol., Monograph 5, p. 1-8.

Ovchinnikov L.N. 1988. Formation of ore deposits. Nedra Publications, 255 p., (in Russian).

Prokoptsev G.N., Prokoptsev N.G. 1990. Formation of metalliferrous hydrotherms at oceanic floor. USSR Academy of Sciences Transactions, Geological Series 4, p.34-44, (in Russian).

Rona P. 1986. Hydrothermal mineralization of spreading areas in the ocean. Moscow, Mir,160 p. (in Russian).

Shepherd T.J., Rankin A.H., Alderton D.H.M. 1985. A practical guide to fluid inclusion studies. Blaskie, Glasgow and London, 239 p.

Sinyakov V. I. 1986. General ore genesis models for endogenous deposits. Nauka Publications, Novosibirsk, 243 p., (in Russian).

Stackelberg I., 1985, Van and the shipboard scientific party. Hydrothermal sulfide deposits in back-arc spreading centers in the Southwest Pacific. BGC Circulair, 27, p. 3-14.

Tvalchrelidze A. G., 1987. Geochemical conditions of formation of massive sulfidic ores. Moscow, Nedra, 188p (in Russian with English abstract)

Ustaömer T., Robertson A.H.F. 1993. Late Paleozoic-Early Mesozoic marginal basins along the active southern continental margin of Eurasia: evidence from the Central Pontides (Turkey) and adjacent regions. Geological Journal, 120, p.1-20.

Yaroshevich, V.Z. 1985. Genetic features of the deposits of the Caucasus base ore formations according to data of isotopic studies. Abstract of dissertation. Tbilisi, 52 p.

Yilmaz Y., Tüysüz O., Yiðitbaþ E., Genç S., Şengör A.M.C. 1997. Geology and tectonic evolution of the Pontides. In: Robinson A.C. (ed) Regional and petroleum geology of the Black Sea and surrounding region. American Association Petroleum Geologists Memoir, 68, p.183-226.

Zonenshain L. P., Kovalev A. A. (ed). 1974. New global tectonics. Moscow, Mir, 471 p., (in Russian).

Special Session S21
Metallogeny along the Carpathian-Balkan region

Scientific Annals, School of Geology, Aristotle University of Thessaloniki Proceedings of the XIX CBGA Congress, Thessaloniki, Greece	Special volume 100	317-323	Thessaloniki 2010

PENTLANDITE MINERALIZATION RELATED TO ALBANIAN OPHIOLITES

Çina A.

Institute of Geosciences Polytechnic University of Tirana. Str.Don Bosko,Nr 60, E-mail:al_cina@yahoo.com

Abstract: The Jurassic ophiolites in Albania are characterized by several mineralization types including chromites, Fe-Ni-Cu sulfides and arsenides, Fe-Ti-minerals and minerals of the Platinum Group Elements (PGE). Pentlandite-bearing mineralization is related to upper mantle serpentinized harzburgites, chromitite deposits associated with upper mantle dunites, dunites of the supra-Moho zone, ultramafic-mafic intrusions (wehrlites, lherzolites, pyroxenites and gabbros) and to cumulate layered sequences of olivine-gabbros and gabbronorites. Pentlandite occurs in several mineral associations including Ni-bearing sulfides, Fe-Ni-Cu-Co-PGE-bearing sulfides and chromite + Ni-bearing sulfides + PGM. It accompanies chromite, olivine, pyrrhotite, chalcopyrite, cubanite, magnetite, native copper, valleriite, mackinawite, heazlewodite, millerite and PGM. The chemical composition of pentlandite (metal:sulfur ratios, Fe:Ni ratios and Co and PGE contents) is variable depending on the geological setting, mineral associations and textural relationships. It is suggested that the pentlandite-bearing mineralization hosted within chromitite deposits, related to upper mantle dunites and dunites of the supra-Moho zone, is of primary magmatic origin, but the one hosted within upper mantle serpentinized harzburgites, ultramafic-mafic intrusions and to cumulate layered sequences of olivine-gabbros and gabbronorites is genetically related to hydrothermal activity combined with serpentinization processes, which played an essential role for the remobilization of some elements from the host rocks and the transformation of primary sulfides and PGM.

Keywords: Albania, ophiolites, pentlandite, serpentinization, remobilization.

1. Introduction

Albania represents the connecting segment between the Dinarides and the Hellenides. The principal feature of Albanian geology is the presence of a widespread ophiolitic complex, related to important mineral deposits. This ophiolitic complex covers an area of about 4200km^2, representing one of the biggest exposures of oceanic lithosphere in the Mediterranean area. Triassic rifting was followed by intensive development of ophiolitic magmatism during the Middle Jurassic. The ophiolitic complex is partly covered by Cretaceous, Paleogene and Neogene sedimentary rocks. The Albanian ophiolitic complex is composed of two ophiolitic belts, a western and an eastern one, with a transitional zone displaying mixed petrologic features. The western ophiolite belt is characterized by the presence of high-Ti basaltic pillow lavas and corresponds to Jurassic oceanic lithosphere, constructed along a mid-ocean ridge (MORB ophiolite type). The ophiolites of the eastern belt include low-Ti volcanic rocks with geochemical features typical of Island Arc Tholeiites (IAT). The eastern ophiolite belt is considered to have been formed in a supra subduction zone (SSZ) (Shallo et al. 1995) by a high percentage of partial melting in the mantle source. This ophiolite belt is characterized by harzburgites-dunites (enriched in Mg and depleted in Si, Ca and Al as a result of a strong partial melting of the upper mantle), by the presence of supra-Moho dunites (some hundred meters thick), and finally the presence of a zone with ultramafic-mafic intrusions. In addition, in the two ophiolitic belts of the northern part of Albania, cumulate sequences of gabbroic rocks, quartz diorites, diorites and plagiogranites, as well as sheeted dykes and basaltic pillow lavas occur.

2. Mineralization

Harzburgites and dunites in the eastern ophiolite belt display a high chromite-bearing potential, whereas the mafic volcanic sequences include abundant copper-bearing mineralization. Pentlandite-bearing

mineralization within various associations of Fe-Ni-sulfides/arsenides, Fe-Ni-Cu-bearing sulfides and PGM is hosted either within upper mantle ultramafic rocks, or within ultramafic-mafic intrusions at the mantle-crust transition zone. The sulfide minerals occur as interstitial grains in chromitites of both upper mantle ultramafic intrusions and supra-Moho dunites and as Fe-Ni-Cu-mineralizations related to troctolite-gabbro sequences. The Fe-Ni- and Fe-Ni-Cu mineralization associated with PGM is situated mainly in the eastern ophiolite belt of Albania, particularly in Bulqiza and Kom-Tropoja ultramafic massifs. In the southern part of Bulqiza massif, pentlandite mineralization related to the supra-Moho dunites is composed of disseminated sulfides (1-5 vol. %) associated with disseminations and bands of chromite (Fig. 1). A similar PGE-bearing mineralization of disseminated Ni-sulfides is related to "black dunites" at the northwestern part of this massif, as well as with spatially associated ultramafic-mafic intrusions, such as plagioclase harzburgites, lherzolites, wehrlites and even gabbros. Within veins of gabbros crosscuting chromitite bodies, disseminations of Ni-Cu sulfides and native copper occur. At the Kom-Tropoja ultramafic massif pentlandite-

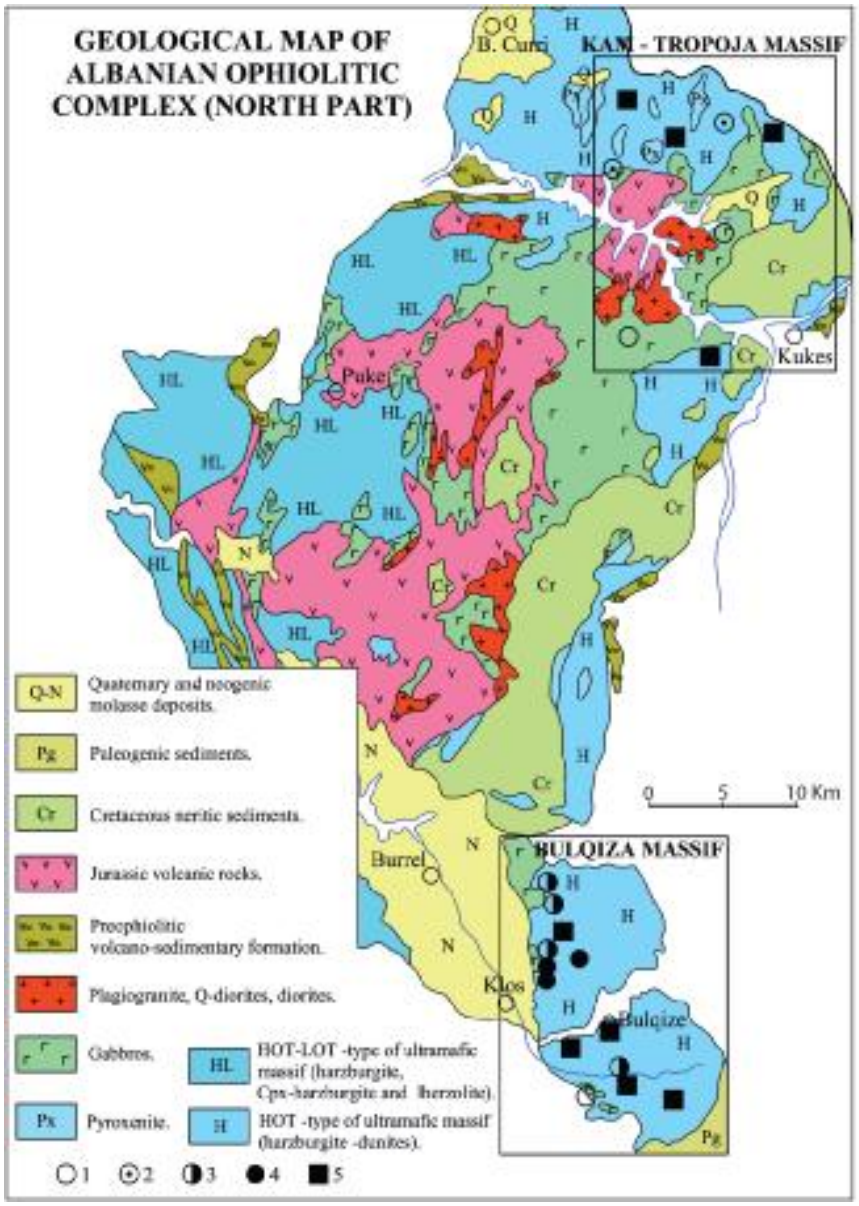

Fig. 1. Geological map of the ophiolitic complex of Albania, northern part. 1: Fe-Ni-Cu mineralization related to gabbro-troctolites; 2: Fe-Ni-Cu mineralization related to serpentinites; 3: Fe-Ni-Cu-PGE mineralizetion related to supra-Moho dunites; 4: Fe-Ni-Cu-PGE mineralization related to chromitites; 5: Chro-

bearing mineralization of the Fe-Ni-sulfide type is related to serpentinites. The lenticular ore bodies are composed of massive sulfide minerals, mainly pyrrhotite and pentlandite. These are the product of hydrothermal activity and serpentinization processes resulting of remobilization and modification of magmatic sulfides. Lenticular- to vein-shaped ore bodies, composed of Fe-Cu- Ni-rich massive sulfides are hosted within troctolite-gabbros in proximity to the ultramafic rocks.

Sulfides hosted within the dunites from the supra-Moho zone display the highest PGE contents ranging from 650-690 ppb to 2410 ppb and even 8400 ppb (Ohnenstetter et al. 1991; Karaj 1992; Burgath et al. 2002), with Pt/Pd ratios at 0.33. The Au content varies from 680 to 1600ppb. The chromite + sulfide ores are distinguished by the presence of low PGE contents (up to 820 ppb), higher Pt/Pd ratios (1.5 to 6), and very low Au contents. The Cu/(Cu+Ni)- and Ni/Co ratios for the Ni-sulfide ores from the supra-Moho dunites vary within values from 0.1 to 0.15, and from 20 to 25 respectively. These values are clearly distinct from similar mineralization in other Mediterranean regions (e.g. Tsangli/Eretria, Greece and Pevkos and Laxia to Mavrou/Limassol Forest, Cyprus). In contrast, the massive Fe-Ni-Cu sulfide mineralization related to serpentinites and troctolite-gabbro sequence displays intermediate Cu/(Cu+Ni) ratios (0.4 to 0.5), and high Ni/Co ratio (15 to 20), similarly to those from Cyprus and Greece ores, where later hydrothermal-serpentinization processes played a major role.

Table 1. Electron microprobe analyses of pentlandite and some other minerals from the ophiolitic complex of Albania (in wt. %, atoms).

Sample	1	2	3	4	5	6	7	8	9	10	11	12	13
	41C	215K	195K	279K	266K	993C	991C	992C	60C	997C	42C	46C	64C
S	30.87	32.12	32.19	33.44	30.67	33.50	32.40	32.40	32.70	35.90	0.39	34.84	26.42
As	0.12	-	0.11	0.03	0.06	0.01	0.02	0.02	-	-	-	0.06	0.26
Fe	38.14	44.09	39.53	21.97	19.48	40.90	34.90	37.70	24.60	58.30	26.41	1.06	0.30
Ni	27.86	22.42	26.15	44.69	31.86	22.40	18.70	19.90	19.50	3.85	72.10	56.83	71.03
Co	0.34	0.43	0.37	0.51	2.53	3.16	13.60	8.60	23.00	1.02	0.06	0.07	-
Cu	-	0.21	0.02	0.36	0.04	0.01	0.04	0.02	0.02	0.08	0.53	0.08	-
Os	-	0.04	-	0.41	0.14	-	-	-	-	-	-	0.19	-
Ir	0.15	-	0.29	-	13.12	-	-	-	-	-	-	-	-
Ru	0.07	-	-	-	0.42	-	-	-	-	-	-	-	-
Pt		0.51	0.11	-	-	-	-	-	-	-	-	-	-
Pd	0.03	-	-	0.12	0.33	-	-	-	-	-	-	0.22	-
Total	97.58	99.82	98.77	101.50	98.65	99.98	99.66	98.64	99.82	99.15	99.49	96.78*	99.55*
S	7.681	7.793	7.881	7.99	7.997	8.041	7.870	7.888	7.956	0.996		1.036	2.015
As	0.012		0.012		0.018							0.001	0.009
Fe	5.447	6.131	5.56	3.09	2.929	5.627	4.861	5.27	3.434	0.93	1.106	0.018	0.013
Ni	3.785	2.969	3.497	5.83	4.619	2.924	2.452	2.652	2.584	0.058	2.873	0.923	2.959
Co	0.046	0.057	0.049	0.062	0.357	0.411	1.802	1.19	3.026	0.015	0.002		
Cu		0.026	0.002	0.01	0.06					0.001	0.019	0.001	
Os		0.002		0.007	0.008							0.001	
Ir	0.006		0.012		1.034								
Ru	0.005				0.019								
Pt		0.02	0.04										
Pd	0.018			0.007	0.002							0.02	0.003
Atoms	17	17	17	17	17	17	17	17	17	2	4	2	5
M/S	1.21	1.186	1.152	1.109	1.12	1.115	1.162	1.135					
Fe/Ni	1.439	2.065	1.585	0.529	0.634	1.924	1.959	1.989	1.329				
Fe_9S_8	58.7	67.23	60.99	34.57	44.3	62.81	53.18	57.84	37.98				
Ni_9S_8	40.8	32.47	38.47	65.25	51.73	32.64	27.12	29.1	28.56				
Co_9S_8	0.5	0.3	0.54	0.18	3.97	4.55	19.7	13.06	33.46				

1-3: Pentlandite from sulfide mineralization related to supra-Moho dunites; 4, 5: Pentlandite from sulfide mineralization related to upper mantle chromitites; 6-8: Pentlandite from sulfide mineralization related to serpentinites; 9: Pentlandite from sulfide mineralization related to gabbro-troctolite; 10: Mackinawite from transformed pentlandite; 11: Awaruite; 12: Millerite; 13: Heazlewoodite. * The sample nr. 12 contains 3.52% Cr_2O_3 whereas sample nr. 13 contains 1.34% Cr_2O_3 which are excluded from the calculation of the analysis considered as contamination mixtures.

2. Mineral associations and textural features

According to the geological setting of the mineralization, pentlandite is associated to a large group of minerals, (e.g. chromite, magnetite, delafosite, pyrrhotite, chalcopyrite, cubanite, digenite, millerite, heazlewoodite, mackinawite, valleriite, native copper, awaruite, ferrite and PGM). Pentlandite from the Ni-sulfide mineralization related to the supra-Moho dunites is associated with chromite, magnetite, awaruite and native copper. It occurs, as interstitial, irregular shaped grains surrounding the chromite and olivine grains (Fig. 2a). In some cases, minute pentlandite grains are enclosed within chromite grains. Usually, the pentlandite grains are crosscut along cleavage planes by magnetite and ferrite veinlets and are surrounded by thin awaruite rims (Fig. 2b). Some native copper and delafosite grains occur in a serpentine groundmass, whereas fibrous aggregates of valleriite occur within pentlandite grains (Fig. 2c). The Fe-Ni-Cu-PGE sulfide mineralization related to the "black dunites" and ultramafic/mafic intrusions is composed of pyrrhotite, chalcopyrite, pentlandite, heazlewoodite, magnetite, native copper and PGM. Pentlandite is interstitial to chromitite surrounding and cementing chromite grains (Fig. 2d). Both minerals are crosscut by pyrrhotite and magnetite veinlets (Fig. 2e). Some composite pentlandite und sperrylite inclusions (Fig. 2f) occur within chromite grains. Minute pentlandite inclusions occur within laurite grains or the opposite (Fig 3a). The pyrrhotite,

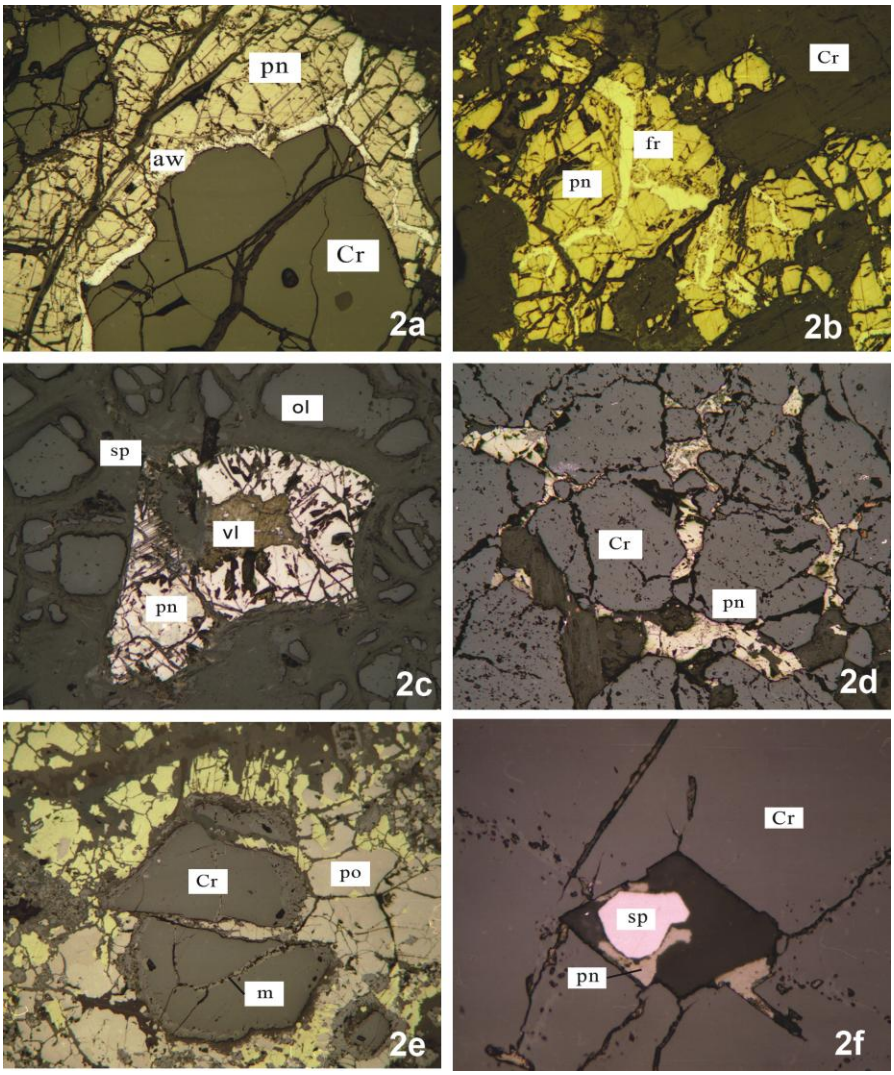

Fig. 2. (a) Intergranular pentlandite (pn) and chromite grains (cr) surrounded by awaruite rim (aw); (b) Ferrite veinlet (fr) crosscuting pentlandite grain (pn); (c) Pentlandite grain (pn) replaced by valleriite (vl).; (d) Pentlandite (pn) interstitial between chromite grains (cr); (e) Chromite grain (cr) intersected by pyrrhotite (po) and magnetite (m); (f) Composite inclusion of pentlandite (pn) and sperrylite (sp) included in chromite (Cr).

chalcopyrite and native copper occur within gabbro veins crosscutting chromitite ore. Pentlandite from the serpentinite-hosted sulfide mineralization is associated with hexagonal pyrrhotite, magnetite, native copper and mackinawite, valleriite. The groundmass is composed of pyrrhotite, whereas exsolved euhedral pentlandite grains occur as fine lenticular inclusions. The pentlandite grains are surrounded and intersected by magnetite and native copper (Fig. 3b). Usually, pentlandite is transformed partialy, into mackinawite (Fig. 3c, d).

Needle-like aggregates of valleriite fill cleavage planes of silicates (Fig. 3e). Pentlandite from the sulfide mineralization related to gabbro-troctolites is accompanied by pyrrhotite, cubanite, chalcopyrite, magnetite and mackinawite. Some small pentlandite grains included in pyrrhotite have an intensive pink color and higher reflectance index in comparison to usual pentlandite, being the result of its high Co content (up to 23 wt. %). Composite pentlandite and pyrrhotite lamellae are interpreted as exsolution products. Two types of pyrrhotite are distinguished, the first as groundmass and the second in the form of lamellae. Twinned chalcopyrite includes lamellae of cubanite and pyrrhotite as exsolution products (Fig. 3f).

3. The chemical composition of pentlandite

The chemical composition of pentlandite (met-

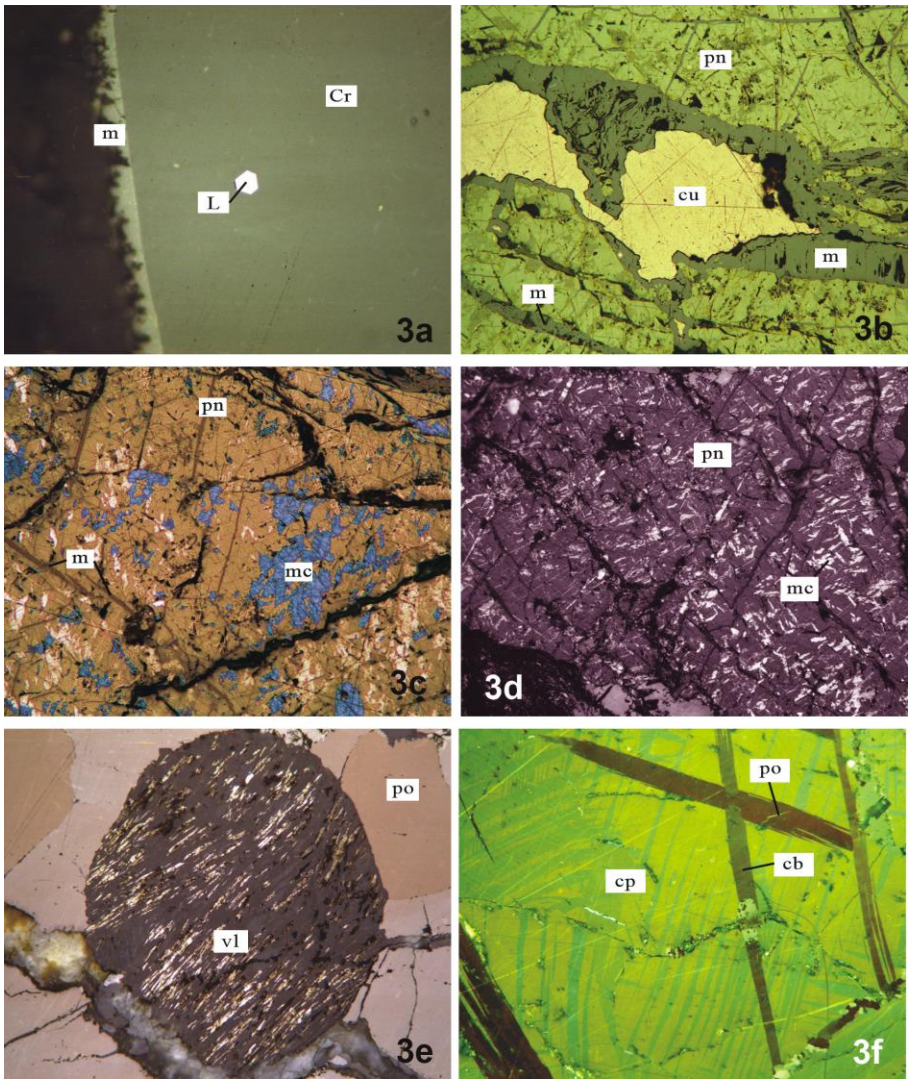

Fig. 3. (a) Euhedral polygonal laurite crystal (L) within a chromite groundmass (Cr); (b) Native copper (cu) surrounded by magnetite rim (m) within pentlandite (pn); (c) Pentlandite (pn) partially transformed into mackinawite (mc) (crossed nicols); (d) Pentlandite (pn) replaced along octahedral cleavage planes by mackinawite (mc) (crossed nicols); (e) Needles of valleriite (vl) along cleavage planes of silicate grain within coarse-grained pyrrhotite (po) (crossed nicols); (f) Pyrrhotite (po) and cubanite (cb) lamellae within twinned chalcopyrite groundmass (cp) (crossed nicols).

al/sulfur ratios, Fe/Ni ratios and Co, PGE contents) from various geological settings, associations and textural relationships, was examined by electron microprobe analyses at the MGA Department of B.R.G.M-Orleans and presented in Table 1. The metal/sulfur ratios vary from 1.115 to 1.210 (ideal ratio is 9/8 = 1.125). The Fe/Ni ratios are usually > 1 and reach values up to 2.065. In two samples the Fe/Ni ratios are <1 (0.529 to 0.634). According to the Co content pentlandite is characterized as low-Co (up to 0.5wt. %), medium-Co (from 2.53 wt. % to 3.16. %) and high- to very high-Co (from 8.5 wt. % to 23 wt. %) (Tab. 1). Another feature of pentlantide is the presence of PGE mainly Ir (up to 13.12 wt % according to Karaj 1992). Mackinawite derived from transformation of pentlantide, contains abundant Ni and Co (3.85 and 1.0 wt. % respectively, Tab. 1). Awaruite rimming pentlandite grains has Ni/Fe ratios 3:1. Millerite and heazlewoodite that associates the pentlandite have low PGE contents (Tab. 1).

There is a relationship between pentlandite composition and geological setting: The pentlandite related to supra Moho dunite + sulfide mineralization is Fe-rich containing up to 44.09 wt. % Fe (Tab. 1, analyses Nr 1-3, Fig. 4). The Ni content reaches values up to 27.86 wt. % and the Co content is very low (< 0.43 wt. %). Pentlandite from the massive pyrrhotite-pentlandite mineralization hosted within serpentinites, displays a similar to the above Fe and Ni contents. However, it is distinguished by higher Co contents ranging from 3.16-8.6 wt. % for granular pentlandite (Tab. 1, analyses 6 and 8), up to 13.6 wt. % for the fine lenticular exsolved inclusions of pentlandite hosted within pyrrhotite (Tab.1, analysis 7). Integranular pentlandite related to upper mantle chromitites displays the highest Ni contents (up to 44.09 wt. %), whereas the Fe contents are very low (up to 21.97 wt. %) (Tab. 1, analyses 4 and 5). Finally, the pentlantide from the pyrrhotite-cubanite-chalcopyrite association, related to gabbro-troctolites close to ultramafic rocks, is characterized by very high Co contents (up to 23 wt.%) and low Fe and Ni contents (Tab. 1, analysis 9, Fig. 4).

The following is a comparison of pentlandite compositions from the Albanian ophiolitic complex with those from ophiolites in other Mediterranean regions: Pentlandite of Tsangli/Eretria, Greece contains variable amounts of Co (from 2.8 wt. % to 28 wt. %), depending on its associations with chromite, magnetite or pyrrhotite (Economou and Naldrett 1984). The pentlantide from the Fe-Ni-Cu-Co mineralization of Pevkos/Limassol Forest, Cyprus contains relatively low Co abundances, whereas the Fe content predominates over Ni (Panayiotou 1980; Foose et al.1985; Thalhammer et al. 1986). These contents are almost similar to those from pentlandite related to chromitites and sulfides of serpentinites from Albania. The pentlandite of the Laxia to Mavrou, Cyprus sulfide mineralization is characterized by the highest Co contents (23.24 wt. %) and low Fe and Ni abundances (Thalhammer el al., 1986), similarly to pentlandite of massive sulfide mineralization related to gabbro-troctolites of Albania. It must be noted that pentlandite of Ivrea-Verbano (Italy) related to stratiform intrusions, has very low Co contents (0.6 to 1 wt. %) and is Fe-rich (Garuti et al. 1986), similar with pentlandite related to dunite + sulfide mineralization of Albania.

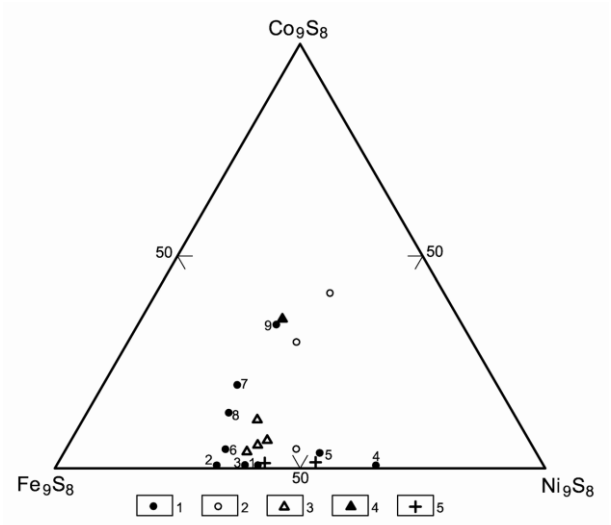

Fig. 4. Ternary Fe_9S_8-Ni_9S_8-Co_9S_8 plot of pentlandite compositions (in At. %) in Albanian and other Mediterranean ophiolites. 1. Pentlandite-bearing mineralization of Albania (dots 1-9); 2. Tsangli/Eretria, Greece (Economou and Naldrett 1984); 3. Pevkos/Limassol Forest, Cyprus (Panayiotou 1980; Foose et al., 1985; Thalhammer et al., 1986); 4. Laxia to Mavrou/Limassol Forest, Cyprus (Thalhammer et al., 1986); 5. Ivrea Verbano, West Alps, Italy (Garuti 1986).

4. Discussion

On the basis of the geological setting, ore body morphology, mineral associations, mineralogy and textural relationships, it can be concluded that the Ni-sulfide mineralization of the Albanian ophiolitic complex is not only the consequence of primary magmatic mineral-forming processes, but it is also related to processes of deformation, hydrothermal

alteration and serpentinization. The later processes caused remobilization of elements and transformation of primary minerals as a result of hydrothermal fluid circulation through the host rocks. The pentlandite-bearing mineralization from the Albanian ophiolitic complex can be subdivided into two types: (1) the Ni-sulfide mineralization related to chromite bands and disseminations hosted within supra Moho dunites, contain pentlandite grains are interstitial between chromite and olivine and are crosscut by magnetite, awaruite and ferrite veinlets. Pentlandite contains substantial amounts of Fe, resulting in very high Fe/Ni ratios (1.44 to 2.07 apfu) and it is characterized by remarkable low contents of Co (less than 1.0 wt. %). The ore is characterized by quite low Cu/(Cu+Ni) ratios (from 0.1 to 0.15), very high Ni/Co ratios (from 20 to 25) and high PGE contents (from 2410 ppb to 8400 ppb), with Pt/Pd ratios at 0.33 (Ohnenstetter et al. 1991; Karaj 1992). These geological-mineralogical features of Ni-sulfide mineralization related to supra-Moho dunites are indicative of a magmatic origin (Naldrett 1981). Similarly, the Ni-sulfide mineralization related to upper mantle chromitites is also suggested to be of primary magmatic origin. It is characterized by a predominance of Ni over Fe (Fe/Ni ratios from 0.53 to 0.63) and by high Ni/Co ratios in pentlandite. (2) The other type of pentlandite-bearing mineralization is represented by lenticular and vein ore bodies related to serpentinites along faults and troctolite-gabbro crustal sequences. The massive sulfide ores are composed of pyrrhotite and pentlandite, as well as pyrrhotite, cubanite, chalcopyrite associated with magnetite, mackinawite, valleriite and native copper, as secondary minerals. Based on the Cu/(Cu+Ni) ratios (0.4 to 0.5) and the Ni/Co ratio (~2), this mineralization is considered to be of a hydrothermal origin, as suggested for similar mineralization in other ophiolitic complexes in the Mediterranean region (Çina 1981, 1990; Foose et al. 1985; Thalhammer et al., 1986).

Acknowledgements

I am much obliged to Dr Panagiotis Voudouris for his hard effort to improve the manuscript and for his precious suggestions. I would also like to thank very much Dr Daniel Ohnenstetter for his useful assistance during electron microprobe analyses of pentlandite at MGA, BRGM, France.

References

Burgath K.P, Krauss U., and Moher M., 2002. Chromium ores and platinum-group element occurrences in Europe and Turkey: Inventory evaluation and possibilities Chronique de la Recherche Minière, 55-75 “last in series”.

Çina A., 1981. The influence of rock bearing hydrothermal vein deposits of copper ore of the ophiolitic belts of Albanides . UNESCO, Int. Symp. on Metallogeny of Mafic and Ultramafic Complexes. Athens, 1980.

Çina A., 1990. Sulphide and arsenide mineralization within the basic and ultrabasic rock of Albanian ophiolites. Oceanic Crustal Analogues, Symp.Troodos 1987, Nicosia Cyprus, 615-626.

Economou M., and Naldrett A.J, 1984. Sulfides associated with Podiform bodies of Chromite at Tsangli, Eretria, Greece. Mineralium Deposita 19, 289-297.

Foose M.P., Economou M., and Panayiotou A., 1985. Compositional and mineralogic contains on the genesis of ophiolite-hosted nickel mineralization in the Pevkos Area, Limossol Forest, Cyprus. Mineralium Deposita, 20, 234 -240

Garuti G., Fiandri P., and Rossi A., 1986. Sulphide composition and phase relations in the Fe-Ni-Cu ore deposits of the Ivrea-Verbano Basic complex (Western Alps, Italy). Mineralium Deposita, 22, 22-34.

Karaj N., 1992. Reportition des platinoides chromites et sulphures dans le massif de Bulqiza, Albania. Incidence sur le processus metallogeniques dans les ophiolites . These, Universite d‘Orleans, France, 379p.

Naldrett A.J., 1981. Nickel-Sulfide deposits: classification, composition and genesis. Economic Geology, 75, 628-685.

Ohnenstetter M., Karaj N., Neziraj A., Johan Z., and Çina A., 1991. Le potencial Platinifere des ophiolites: mineralizations en elements du groupe du platine (EGP) dans les massifs de Tropoja et Bulqiza, Albanie C.RAcad. Sci, Paris, 313ser II, 201-208.

Panayiotou A., 1980. Cu-Ni-Co-Fe sulphide mineralization Limassol Forest, Cyprus Ophiolite. Proc. Int. Ophiolites Symp, Cyprus, 102-116.

Shallo M., Çina A., and Turku I., 1995. Outline of metallogeny of the Albanian MOR and SSZ-type ophiolites. Workshop on Albanian ophiolites and related mineralization. Documents du BRGM 244. Ed. BRGM, France, 27-46.

Thalhammer O., Stumpfl E.F., and Panayiotou A., 1986. Postmagmatic, hydrothermal origin of sulfide and arsenide mineralization at Limassol Forest, Cyprus. Mineral. deposita 21, 95-105.

Scientific Annals, School of Geology, Aristotle University of Thessaloniki Proceedings of the XIX CBGA Congress, Thessaloniki, Greece	Special volume 100	325-332	Thessaloniki 2010

ARSENIC DISTRIBUTION IN LATERITE DEPOSITS OF THE BALKAN PENINSULA

Eliopoulos D.G. [1] and Economou-Eliopoulos M. [2]

[1] *Institute of Geology and Mineral Exploration (IGME), Sp. Loui 1, C Entrance, Olympic Village, GR-13677, Acharnai, Greece, eliopoulos@igme.gr*

[2] *Section of Economic Geology and Geochemistry, Department of Geology and Geoenvironment, University of Athens, Panepistimiopolis, GR-15784 Athens, Greece*

Abstract: The laterite deposits (Fe–Ni-laterite and bauxites) in the Balkan Peninsula are mainly located in the Mirdita–Sub-Pelagonian and Pelagonian geotectonic zones and are of great economic significance. These deposits have been affected by intense tectonism, which has created overthrusting, foliation, folding, and faulting. The investigation of arsenic in laterites is thought to be important for the ferronickel smelting process and the serious affect of the health. Minerals such as iron oxides and pyrite are of particular significance in controlling arsenic mobility, and hence aquifer contamination. Laterite samples from Ni-laterite deposits of Greece (Lokris, Vermio, Edessa, Olympos, Kastoria), Albania (Bitinca and Gouri- Perjuegjiun), Serbia (Rzanovo and Topola), bauxitic laterites and the Parnassos-Ghiona bauxite deposit were analyzed for major and trace elements, including arsenic (As). Arsenic concentrations for all laterite samples from the Balkan Peninsula range from < 2ppm to a few decades ppm. However, arsenic concentrations for the individual laterite occurrences and deposits from Aghios Ioannis vary significantly from <2 ppm to 2600 ppm. Arsenic in the Parnassos-Ghiona deposit ranges from <10 ppm in typical red colored ore to 900 ppm in yellow-grey colored ore. The latter type occurs along and near faults and constitutes a significant (approximately 30 vol. %) portion of the bauxite ores. They are characterized by the presence of abundant pyrite and micro-organisms. Elevated arsenic contents are mostly associated with Fe-oxides/hydroxides in Ni-laterites, showing enrichment in REE, Co, Ni, Th and U contents, and with Al-oxides in bauxites. The sulphur isotope compositions of Fe sulphides from the bauxite deposit show a range from +10.2 to –30.2 per mil. Most negative values were obtained from grey-coloured ore samples. The organic matter may be related to the source of arsenic and play a major role in controlling the redox conditions, since they can drive the formation of pyrite or Fe-oxides.

Keywords: Balkan Peninsula, Greece, arsenic, Ni-laterites, bauxites, organic matter

1. Introduction

Nickel, is a transition element of strategic significance, that is widespread as both siderophile (associated with iron) and chalcophile (associated with sulphur), and it is mined throughout the world from two types of ore deposits (a) laterites where the principal ore minerals are Ni- bearing iron oxides and hydrous nickel silicates and (b) magmatic sulphide deposits where the principal ore mineral is pentlandite [$(Ni,Fe)_9S_8$].The main world production comes from Russia, Canada, Australia and New Caledonia. The potential of Ferro-Nickel ore reserves in Greece is currently estimated to be in the range of 100 million tonnes, grading 1-1, 4 % Ni. The Fe–Ni-laterite deposits in the Balkan Peninsula are mainly found in the Mirdita–Sub-Pelagonian and Pelagonian geotectonic zones (Fig. 1) and are related to ophiolites of Upper Jurassic to Lower Cretaceous age. These deposits have been affected by intense tectonism, which has created overthrusting, foliation, folding, and faulting. This has resulted in the transportation of the laterite bodies, disrupting their continuity and in some cases mixing them with underlying rocks. The multistage deposition of the Fe–Ni ores, the redistribution of ore metals, the intense tectonism and the metamorphism, which have affected all the Ni-laterite deposits of Greece, have almost totally changed the initial mineralogical and chemical composition of the ores (Albandakis, 1980; Valeton et al., 1987; Eliopoulos and Economou-Eliopoulos, 2000).

Larko is the Hellenic Mining and Metallurgical Company for the extraction and processing of Ni. The mining operations are based at Psachna (north central Euboea Island), Aghios Ioannis (Lokris area) and Kastoria whereas the metallurgical plant is located at Larymna. Larko's production level corresponds to some 2-3% of the world total nickel output and is exported to various destinations in Western Europe. Based on bibliographic data, high As content (As>0.15%) in Ni-laterites is unacceptable in stainless steel production since it affects the ore quality. More specifically the higher portion of As in the feed, results to the higher As % content in the alloy (Zevgoles, 2004).

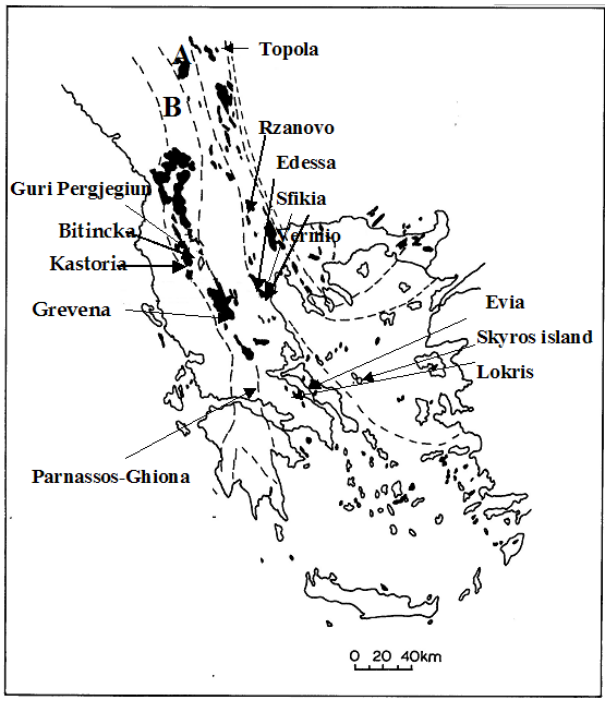

Fig. 1. Sketch map showing the Pelagonian (A) and Sub-Pelagonian (B) geotectonic zones of Greece, the distribution of ophiolites, and the location of the studied Fe-Ni-laterite and bauxite deposits.

The objective of this study is to define the As-distribution in Ni-laterites and bauxitic laterites in Greece and the Balkan Peninsula and bauxite deposits in Greece, using geochemical methods and mineral chemistry techniques in an attempt to explain its genetic significance and environmental impact.

2. Methods of investigation

Major elements were determined by atomic absorption at the University of Athens, and minor and trace elements by neutron activation analysis, at XRA Laboratories, Canada. The organic matter was determined at the University of Athens, following a wet oxidation method (Walkley- Black), using 1 N $K_2Cr_2O_7$ solution. The heat generated when two volumes of H_2SO_4 are mixed with one volume of the dichromate, assists the reaction. The remaining dichromate was titrated with ferrous sulphate. Mineralogical composition of the studied laterites was investigated by optical microscopy, and X-ray diffraction (XRD) using a Siemens D5005 power diffractometer.

The Electron microprobe analyses were carried out at the University of Athens using a Cambridge Microscan-5 instrument and a JEOL JSM-5600 scanning electron microscope, both equipped with automated energy dispersive analysis system, Link 2000 and ISIS 300 OXFORD, respectively, with the following operating conditions: accelerating voltage 20kV, beam current 0.5 nA, live time 50 secs, and a beam diameter of 1-2μm**.**

Sulphur isotopes were determined at Geochron Laboratories on representative bauxite samples (whole-rock) from the Parnassos-Ghiona deposit, in which the only detectable form of sulphur was Fe sulphide. Data were normalized to CDT with $^{34}S/^{32}S$ of 0.0450045.

3. Characteristic features of laterites

The majority of the Fe–Ni deposits in the Balkan peninsula are allochthonous, are developed on the Upper Jurassic–Lower Cretaceous serpentinized ultramafic ophiolites and are overlain by Tertiary molasses, such as the Kastoria and Bitincka deposits or Cretaceous limestones, such as the Tsouka (Lokris) deposit (Plastiras, 1979; Mountrakis, 1983; Valeton et al., 1987; Skarpelis et al., 1993). In the vicinity of the Aghios Ioannis laterite deposits the oldest volcanic rocks are a sequence of Triassic volcanic rocks consisting of several hundred meters of both mafic and acid pyroclastics and lavas at the Melidoni area, Lokris (Pe-Piper et al., 1981).

Commonly a goethite zone, is followed by the pelitic zone, characterized by fine-grained groundmass, composed of a pelitic matrix (goethite, hematite, clastic grains of quartz and chromite, as well as silicates), Mn-oxides (pyrolusite, lithiophorite). Pisolitic ore, overlies the pelitomorphic ore, and covers the whole section.

The Aghios Ioannis (Lokris) deposits lie on a karstified Jurassic limestone and are conforma-

bly overlain by Lower Cretaceous limestone. The Fe–Ni-laterite ore is mainly composed of goethite, hematite, Ni-bearing chlorite, illite, quartz, calcite, and chromite. The bauxitic-laterite contains mainly boehmite, gibbsite, kaolinite, goethite, and hematite. Chromite is usually found as very small fragments. Rutile, and sulphides (pyrite) and Ni-pyrite are also present, whereas smectite and takovite are more abundant towards the lowest part of the deposit (Alevizos, 1997; Veleton et al., 1987; Eliopoulos and Economou-Eliopoulos, 2000). Studied samples of re-worked Ni-laterite deposits from Lokris are composed by angular to rounded fragments of Fe-Ni laterite ore, saprolite, carbonate, silcrete, cemented by calcite, laterite material dominated by spheroidals, and redeposition of the laterite components towards and within the carbonate basement (Fig. 2).

Small Fe–Ni occurrences in the form of lenses (1x15 m) are found in the east Vermion, Edessa, Olympos, Sfikia and Skyros Island in Greece, Topola and Rzanovo, central part of the Kozuf Mountain, former Yugoslavia (Fig. 1). They are located at the contact of serpentinized harzburgites with Upper Cretaceous limestones–conglomerates or within the serpentinites themselves. Due to intense tectonism, the Fe–Ni-laterite occurrences are often entirely enclosed within serpentinized harzburgites, near to their contact with transgressive limestones (Mihajilovic et al., 1972; Macksimovic and Panto, 1982; Economou-Eliopoulos, 2003).

Bitincka and Guri-Perjuegjiun Ni-laterite deposits in Albania (Fig. 1) are located in the central and southern parts of the Mirdita zone. They have the characteristics of allochthonous deposits, lie on highly serpentizized peridotites and are unconformably overlain by Tertiary molasses the former and Cretaceous limestones the later (Xhomo et al., 1995; Eliopoulos and Economou-Eliopoulos, 2000).

The Parnassos-Ghiona geotectonic zone, including the major bauxite deposits of Greece, is part of the Mediterranean karst bauxite belt. These deposits are hosted within carbonate rocks and have been formed during different geological ages. Three bauxite horizons, B1, B2 and B3, can be distinguished (from the bottom to the top), which are intercalated with shallow-water limestone, within an Upper Jurassic to Middle Cretaceous sequence of the Parnassos-Ghiona zone. Typical bauxite ore of predominant coarse-grained layers with pisoliths and/or oolites and fine-grained layers is of dark red to red-brown color. However, there is a significant proportion (approximately 30 volume %) of yellow and grey to whitish bauxites, associated with faults and zones of high deformation (Papastavrou, 1986; Valeton et al., 1987; Laskou and Economou-Eliopoulos, 2007). There is a gradual change in their colour from red to black-grey extending in a distance of tens of meters (Fig. 3a). The most abundant mineral phases are boehmite or diaspore, hematite/goethite or pyrite. Sulphide veins crosscutting sulphide-rich zones (Fig. 3b) and thin-sulphide layers underlying a layer of organic matter between bauxite bodies and limestone cover is a characteristic feature as well. Thin-layered marine limestone on top of the bauxite horizons showing a dark colour and enrichment in organic material

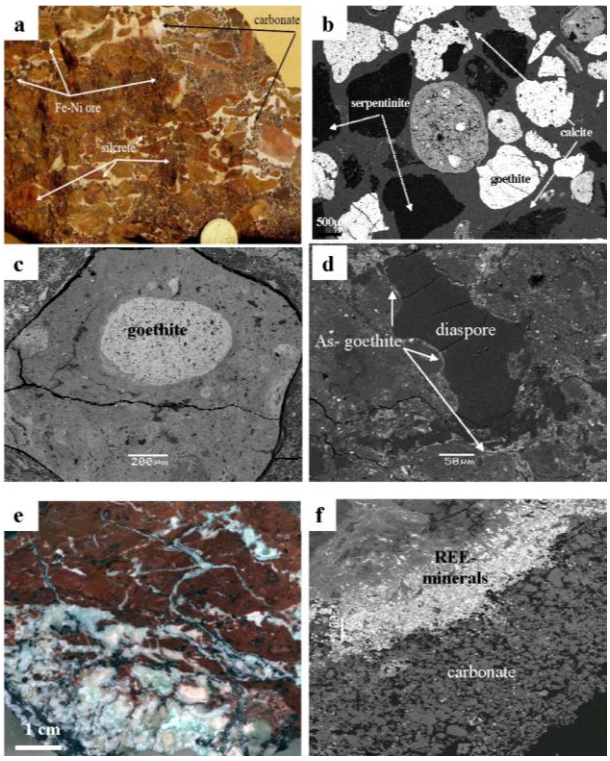

Fig. 2. Photos of re-worked Ni-laterite deposits from Lokris, showing a conglomerate composed of angular to rounded fragments of Fe-Ni laterite ore, saprolite, carbonate, silcrete, cemented by calcite and laterite material dominated by spheroidals (2a), and the re- mobilization and re-deposition of the laterite components towards and within the carbonate basement (2b). Back scattered electron SEM images from reworked Fe-Ni laterite derposit of Lokris, showing a general view of Fe-Ni ore (2c), containing chromite fragments of varying size and composition (light and dark gray) in a matrix of goethite (2d), As-bearing goethite of subsequent stage (2e) and abundant rare earth minerals (REE-minerals) towards the contact of the laterite with the limestone basement (2f).

Table 1. Electron microprobe analyses of Fe- and Al-oxides from Ni-laterites and bauxites.

	Ni-laterites					Bauxites		
wt%	Fe-oxides					Al-oxides		
SiO_2	2,58	1,87	2,38	2,47	2,81	0,81	0,87	0,34
Fe_2O_3	69,52	70,62	76,23	75,61	78,33	0,88	1,57	2,43
Al_2O_3	1,57	1,29	0,88	1,12	1,26	84,12	79,15	75,77
Cr_2O_3	n.d.	n.d.	n.d.	n.d.	n.d.	n.d.	0,42	0,22
TiO_2	0,26	4,85	0,71	0,24	n.d.	0,42	1,78	1,09
NiO	0,96	1,04	0,82	1,03	1,21	n.d.	n.d.	n.d.
As_2O_3	0,77	0,75	1,2	n.d.	n.d.	n.d.	1,39	n.d.
SO_3	0,74	0,89	0,73	0,51	n.d.	n.d.	n.d.	n.d.
Total	76,4	81,31	82,95	80,98	83,61	86,23	85,18	79,85

have been attributed stagnating and reducing conditions in coastal plains during tectonic down warping (Valeton et al., 1987). A layer of coal overlying the Parnassos-Ghiona B3 horizon has been studied recently (Kalaitzidis et al., 2009). Also, fossils of organic matter occur in Ni-laterite deposits of Edessa (Greece) and Katjeli (Albania), as Mn-bearing siderite having the form of plant fossils (Economou-Eliopoulos, 2003; Economou-Eliopoulos et al., 2003), resembling those in a laterite deposit on the south plateau of New Caledonia, characterized by the formation of a 4cm thick, Mn-rich siderite layer, which has the form of plant fossils (Golightly, personal communication). The remobilization/re-distribution of major and trace elements in Ni-laterite and bauxite deposits has been facilitated by the influence of bacteria (Fig. 3g, h). They may play a major role in controlling the redox conditions, since they can drive the formation of pyrite or Fe- oxides (Economou-Eliopoulos et al., 2003; Laskou and Economou-Eliopoulos, 2007).

4. Mineral chemistry

Although oolites seem to be a major component of the Ni-laterites, the microscopic examination and investigation using SEM/EDS analysis indicate that a concentric layering is lacking (Fig. 2). Rounded fragments of a pelitic matrix consist mostly of goethite containing clastic grains of quartz, chromite and chlorite (Fig. 2c, d) is suggesting a multistage re-deposition of Fe-Ni ore. Chromite exhibits a wide variation of the Cr/(Cr+Al) ratio ranging from 0.7 to 0.4. Rounded fragments of goethite containing clastic grains of various minerals, show a core with low aluminium and titanium contents, whilst outwards it is followed by a zone enriched in Al and Ti (Fig. 2c). Arsenic in such goethite ranges between 0.5 to 1.2 wt% As_2O_3 (Tab. 1, Fig. 2e). Arsenic in yellow-coloured bauxite is mostly hosted in Al-oxides, ranging between 0.6 to 1.4 wt% As_2O_3 (Tab. 1).

Bauxitic laterite from Aghios Ioannis (Nissi), Lokris shows the highest As and REE contents (Tab. 2) and it is characterized by the presence of abun-

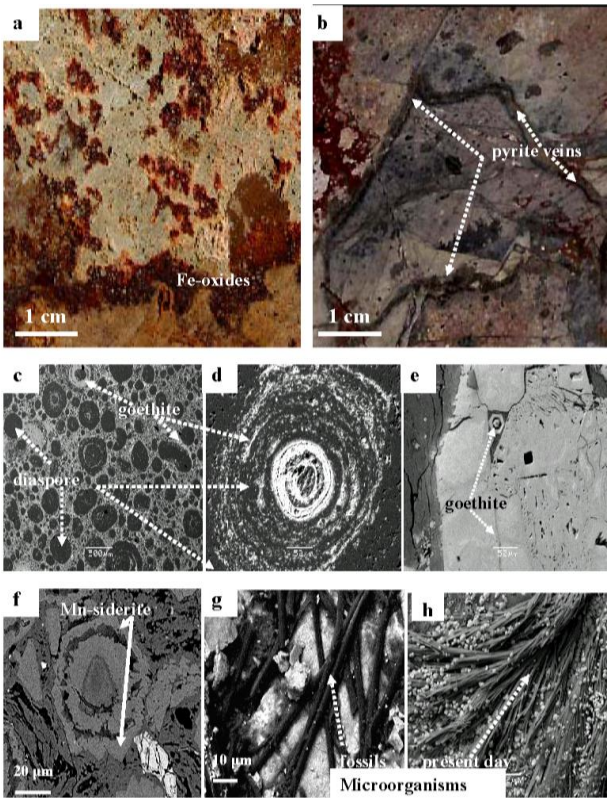

Fig. 3. Photograph of bauxite showing the transition zone between red and grey ore, and the occurrence of sulphide veins, from the Parnassos-Ghiona bauxite deposit (3a & 3b). Back scattered electron SEM images from the above zone (3c-h), showing the association of goethite and diaspore in pisoliths and matrix and their close association with filament-like microorganisms, either fossilized (3g) or present day microorganisms (3h). Fig. 3f shows a cross-section of Mn-siderite surrounding partially decomposed sticks of plant fossils, from a laterite deposit.

dant rare earth minerals (Fig. 2f). These minerals have been already described and reviewed along with the description of two new REE- minerals by Panto and Maksimovic (2001).

5. Whole rock chemistry

The whole rock analysis data have been published in previous papers (Eliopoulos and Economou-Eliopoulos, 2000; Economou-Eliopoulos et al., 2003). This study focuses on the distribution of arsenic in laterite samples from Ni-laterite deposits of Greece (Lokris, Vermio, Edessa, Olympos, Kastoria), Albania (Bitinca and Gouri Pergjegium), Serbia (Rzanovo and Topola), bauxitic laterites of Greece and bauxite deposit of Parnassos-Ghiona. Arsenic distribution shows a wide content range from lower than 2 to a few decades ppm (Tab. 2). However, arsenic concentrations for individual laterite occurrences and deposits of the Aghios Ioannis – Lokris area, Central Greece vary significantly and attain values up to 2600 ppm. The highest values were determined at the lowest part of the deposits lying on the karstified Jurassic limestone, and are accompanied by enrichment in rare earth elements (REE), Co, Ni, Th and U (Tab. 2; Economou-Eliopoulos et al., 1997). In addition these deposits are characterized by the presence of pellets rather than oolites or pisolites, due to the lack of a concentric development (Golightly 1981; Augustidis 1982), resulted from a multistage transportation and re-deposition of allochthonous Fe-Ni laterite material (Fig. 2). High As values were also determined in the Parnassos-Ghiona deposit ranging from <10 ppm in the typical red colored ore to 900 ppm in yellow-grey colored ore type (Fig. 3, Tab. 2). The common characteristic of all bauxite samples having elevated As content is their location near the top of bauxite horizons, associated with dark colour limestone which enriched in organic material and/or thin layers of coal (Kalaitzidis et al., 2009).

Total organic carbon (TOC) content in Ni-laterite samples from Lokris show relatively high As content ranging from 0.14 to 0.56 wt. %. TOC, while in grey-yellow coloured bauxite samples it reaches 2.8 wt. %, suggesting biological activity. Sulphur content ranges from 0.01 to 0.12 wt. % in Ni- laterite samples from Lokris, and from 0.06 to 18.2 wt. % in yellow-grey bauxites (Tab.3). The sulphur isotope compositions of Fe sulphides from the transitional zone between typical red-coloured and grey-whitish bauxite ore (sample 3B), grey- coloured (samples 3A and 4A) and a thin sulphide-layer from the top of the deposit, underlying the Cretaceous limestone (sample Sf.top1) show a wide range from +10.2 to –30.2 per mil (Tab. 3). The most negative values, obtained from grey-coloured samples, typical of sulphides formed by the action of bacteria (Laskou and Economou-Eliopoulos, 2007).

6. Discussion

Present data on the Fe-Ni ores feeding the metallurgical facilities indicate an As-enrichment up to a few thousands ppm As in the Aghios Ioannis laterite mines, although As in general in laterite deposits is lower than 10 ppm (Tab. 2). Such a variation seems to be consistent with the As variation from 0.1 to 0.5 wt% As in the metallurgical product (ferro-nickel alloy) of the Hellenic Mining and Metallurgical Company at Larymna (Zevgolis, 2004). The presence of elevated As contents in strongly re-worked Ni-laterites ores of Lokris (Fig.3; Tab. 1) and in the yellow-grey coloured bauxite ores occurring in a spatial association with organic matter, either micro-organisms (Fig. 3g, h) or layers of coal overlying bauxite ores (Kalaitzidis et al., 2009) suggest that the As-enrichment has taken place during a subsequent stage postdated that of the laterite re-deposition and that organic matter has played a significant role.

6.1. The role of organic matter-micro-organisms in the As-enrichment

The multistage development of the allochthonous laterite ores, by re-working and re-deposition in shallow sea environment is widespread in the Balkan Peninsula (Valeton et al., 1987; Alevizos, 1997; Eliopoulos and Economou-Eliopoulos, 2000). The development and characteristics of Fe-Ni laterite deposits are influenced by a number of geological and environmental factors including parent lithology, structure and alteration, and the conditions during deposition, diagenesis and meta-diagenesis stages. The role of the organic matter developed in stagnating and reducing conditions in coastal plains, (Valeton et al., 1987), which is a characteristic feature of certain Ni-laterites of Greece and Albania (Fig. 3f, g; Eliopoulos et al., 2003) and bauxites (Fig. 3g, h; Laskou and Economou-Eliopoulos, 2007; Öztürk et al., 2002) and in fluvial sediments in the Pilbara district of Western Australia (Freyssinet et al., 2005) seem to be of particular genetic significance. The stability of various iron oxides depends on

Table 2. Major and trace element content in representative Ni-laterite and bauxite samples from the Balkan Peninsula.

		wt%						ppm							
Location	Samples	SiO_2	Al_2O_3	Fe_2O_3	TiO_2	MgO	MnO	As	Ni	Cr	Co	Zn	ΣREE	Th	U
Ni-LATERITES															
GREECE	A.I.1	21,1	24,98	35,9	1,3	2,6	0,22	2600	5500	5100	1400	330	1367	10	7
Aghios Ioannis	A.I.2	15,9	16,1	42,1	0,35	1,25	0,55	1800	40000	4500	1400	340	6325	6	46
	A.I.3	23,1	18,8	35,1	1,24	3,4	0,1	200	27800	15100	430	300	480	5	66
	A.I.4	24,1	20,3	35,6	1,1	3,65	0,3	140	27500	12000	2200	350	438	12	13
	A.I.7	1,9	44	41,6	2,7	0,25	0,17	230	1500	5500	60	320	480	25	7
	A.I.11	34	8,6	42,5	0,4	3,4	0,3	120	7500	20000	510	270	80	2,2	<0.5
	A.I.14	23,5	6,85	54,5	0,25	2,85	0,21	14	7690	24300	570	270	42	1,1	<0.5
	A.I.16	31,2	7,1	44	0,35	4,37	0,3	52	9000	25100	520	250	54	1	<0.5
	A.I.Ts	8,5	5,15	69,8	0,05	2,3	0,2	4	13000	20500	450	320	2	<0.5	<0.5
Euboea Triada	E.Tr.1	25,6	5,6	45,1	0,13	0,3	0,12	2	100	20000	590	360	63	1,7	<0.5
	E.Tr.2	14,6	7,1	55,2	0,15	0,1	0,4	3	14000	17000	590	100	8,2	0,5	<0.5
	E.Tr.3	15,9	7,2	57,3	0,12	0,1	0,4	2	12000	22000	830	520	47	1,2	<0.5
Kastoria	Ka-5	3,8	3	77,6	0,03	0,55	1,7	3	8000	20000	330	370	0,5	<0.5	<0.5
	Ka-6	3,8	3	77,6	0,03	0,55	1,7	15	9100	15000	820	280	5,3	<0.5	<0.5
	Ka-7	4.5	1,8	68.1	0.03	0.80	0.79	17	7100	23000	420	390	3,6	<0.5	1.3
	Ka-8	4.05	3,4	78.20	0.10	0.60	0.30	14	4400	17000	330	320	4,2	<0.5	<0.5
Edessa	Ed.P.10	17,5	8,7	59,5	0,3	3,3	0,6	4	9500	9600	800	60	194	4	2,1
Olympos	OL.1	4,2	3,4	71,5	0,07	3,4	1,05	7	8600	91000	300	340	3	0,6	0,5
	OL.3	3,9	2,9	76,8	0,09	2,85	0,77	2	9300	82000	320	430	2,5	<0.5	2,3
	OL.5x	7	5,8	74	0,06	4,35	0,27	19	16000	20000	1200	850	32	1	0,6
Sfikia	Sf.G.1	7,5	5,1	80,9	0,15	2,05	0,26	3	9200	14000	1200	440	15	<0.5	<0.5
	Sf.G.5	25,3	1,6	52,9	0,1	8,4	0,33	6	12000	21000	920	530	8	<0.5	<0.5
E. Vermio															
Mavrolivado	A.K.	17,5	8,2	53,8	0,5	4,1	0,56	14	11000	14000	600	590	62	1,7	1,2
	A.K.1	17,5	29	36	1,28	3,6	0,37	57	5200	5500	400	700	294	19	4,2
Alonakia	AL.4	7,1	6,7	78,5	1,03	0,6	0,04	22	1400	16000	120	90	261	37	12,5
	AL.5	15,6	14,8	60,4	1,25	1,05	0,11	10	800	12000	100	80	113	22	5,1
Stournari	St.1	11,1	6,1	68,9	0,1	3,9	0,69	28	5300	21000	370	560	42	<0.5	<0.5
	St.2	15,1	7,5	54,8	0,15	11,5	0,49	22	6900	16000	1400	580	64	<0.5	2,8
Grevena	G.P.X.1	12,3	4,8	67,4	0,18	4,2	0,42	11	9700	13000	800	370	56	6,3	<0.5
Skyros island	Sk.3	11	7,4	69,7	0,21	2,4	0,36	24	9800	22000	360	60	2	3,6	1
	Sk.4	11,1	9,4	66,7	0,27	2,05	0,16	140	10000	23000	320	110	22	2,8	1
SERBIA															
Topola	Yu3	19,5	5,4	58,5	0,1	5,7	0,05	12	5500	21000	250	330	16	0,7	<0.5
	Yu4	20,8	5,2	61,65	0,3	3,8	0,1	2	9200	17000	250	90	10	0,6	0,8
Rzanovo	RZ1	29,6	5,4	41,3	0,4	8,8	0,2	3	5100	25000	260	150	18	1	<0.5
	RZ2	12,8	4,4	64,7	0,15	10,2	0,45	2	8200	15000	990	430	7	1	<0.5
ALBANIA															
Bitincka	B.43	17,1	2,3	56,6	0,03	5,68	0,2	11	16000	26000	960	650	33	1	4,1
	B.44	5,1	6,1	71,4	0,08	1,2	0,17	10	7200	17000	650	310	31	0,9	5
	B.45	7,9	6,8	66,5	0,05	1,4	0,8	5	13000	19000	2100	680	2	1,9	0,05
	B.46	6,1	6,5	69,8	0,05	1,34	0,3	3	9800	21000	410	410	2	<0.5	<0.5
Guri - Perjuegjiun	G.39	3,5	2,8	79,9	0,15	1,1	0,36	32	13000	22000	570	510	61	1,6	1,6
	G.40	4,1	3,9	77,3	0,1	0,7	0,26	31	35000	35000	550	400	8,6	<0.5	4,7
	G.41	3,9	2,9	81,4	0,13	0,75	0,29	25	6600	26000	390	180	2,2	<0.5	<0.5
BAUXITES															
Parnassos - Ghiona	P.-G.B.	1,4	60,1	23,1	2,9	0,2	0,1	50	650	1170	30	90	260	52	8
	P.-G.B2	1,2	52,8	21,8	2,4	0,1	0,02	300	490	950	50	18	72	41	9
	P.-G.B3	4,1	54,7	17,4	2,11	0,2	0,01	230	480	630	10	38	81	29	16
	P.-G.6	2,7	64,1	14,2	2,23	0,1	0,01	890	450	1100	12	25	125	60	7

physico-chemical conditions, such as pH, oxygen and sulphur availability, and the mechanism of biological activity. The abundant pyrite, in the case of grey or yellow-grey bauxite ore, appearing as a late diagenetic mineral compared to other iron minerals (goethite, hematite) within the bauxite

deposit, suggest a variation in the redox conditions (Hartog et al., 2004; Laskou and Economou-Eliopoulos, 2007). The presence of fine-grained minerals developed on the filament type bacteria of a bauxite sample (Fig. 3h) is consistent with experimental and *in situ* studies revealed that bacterial communities may dissolve primary rock-forming minerals to obtain essential nutrients and act as nucleation sites for the precipitation of secondary minerals (Baskar et al. 2003). The minerals may appear external to the microbial cell responsible for its genesis, on or in the cell envelope, or within the cell. Some microbial mineral formation is active and may involve direct enzymatic intervention or metabolic production of specific chemical reactants that cause precipitates (Baskar et al. 2003).

Table 3. Sulfur isotope composition of pyrite from the Parnassos-Ghiona bauxite deposit.

Sample	Description	S (wt%)	$\delta^{34}S$ CDT
3B	Transitional zone, red colar	4,1	(+) 10.2
3A	Transitional zone, gray colar	10,6	(-) 26.0
4A	Transitional zone, gray colar	8,4	(-) 29.7
Sf.top1	Thin layer of pyrite from the top	18,2	(-) 30.2

The restriction of arsenic in Fe, Al-oxides hosted in certain parts of Fe-Ni-laterite and bauxite deposits only (Tabs. 1& 3) may point to the existence of an As-source, such as organic matter developed during stagnating stage of the laterite evolution, and the existence of the physico/chemical conditions that facilitated their reaction.

6.2. Association of arsenic with Fe, Al-oxides

The elevated As-contents in certain Ni-laterite and bauxite laterites (Tab. 1) coupled with the existence of As-bearing goethite and Al-oxides (Tab. 3) suggest that the reaction between arsenic and both Fe- and Al-oxides is favorable in nature under certain circumstances. These analytical data are in a good agreement with the experimental literature data showing a significant sorption capacity of Fe- and Al-oxides for both As (III) and As (V) species (Gupta 1998; Smedley and Kinniburgh 2001; Pinon-Miramontes et al. 2003; USEPA 2004). The investigation of As (III) and As (V) sorption onto Al-rich and Fe-rich lateritic soil concretions (LC) has demonstrated that As (V) sorption onto iron oxides has a great dependence on pH. The equilibrium sorption capacity for As (III) is larger than that for As (V) over temperatures ranging from 25° to 60°C and that both As (III) and As (V) form inner-sphere complexes on Fe-rich LC. Arsenic (III) forms outer- sphere sorption mechanisms on Al-rich LC because there is no shift in pH (point of zero charge) even with an increase in As (III) concentration (Partey 2008). Furthermore, thermodynamic data such as free energy, entropy and enthalpy seems to contribute to the better understanding of the stability of As-bearing Fe, Al-oxides in nature. The negative "Gibbs free energy (ΔG°)" values for arsenite and arsenate sorption on Fe-rich LC are consistent with spontaneous reaction between the species and the medium. Also, positive "entropy (ΔS°)" values suggest the affinity of LC for the arsenic species in solution and positive enthalpy (ΔH°) values confirm that the sorption process is an endothermic process (Majzlan et al. 2000; Partey 2008). Therefore, the Fe and Al-oxides in laterites are considered of particular significance in controlling arsenic mobility, and hence aquifer contamination rather than they may be a source of environmental risk, due to the elevated As contents.

7. Conclusions

Although present study is in progress and much more research is required to define the controlling factors of the arsenic mobility during metadeposition and diagenesis of laterites, and its oxidation state (arsenate or arsenite), the available data leads to the following conclusions:

1. As in laterites is low (< 10 ppm) in general. Elevated arsenic contents were determined in the karst-type bauxitic- and Ni-laterite and are associated with epigenetic processes after their redeposition and diagenesis.

2. Arsenic is mostly associated with Fe-oxides/hydroxides in the Ni-laterites, showing enrichment in REE, Co, Ni, Th and U as well, and Al-oxides in bauxites.

3. The negative values obtained for the sulphur isotope compositions of Fe sulphides in grey bauxite ores (up to –30.2 per mil) confirm the sulphide formation by the action of micro- organisms.

4. The presence of organic matter, either plants or microorganisms plays a very crucial role to the stability or solubility of minerals and As-mobi-

lity, since they facilitate redox reactions, causing changes in the physicochemical conditions (pH, Eh).

Acknowledgements

P. Voudouris, of the Athens University, and an anonymous reviewer, are thanked for their constructive criticism and suggestions.

References

Albandakis N.D. 1980. The nickel-bearing iron-ores in Greece. UNESCO, IGCP 169 Inter.Symposium Metallogeny Mafic Ultramafic Complexes 1, 194-213.

Alevizos G. 1997. Mineralogy, geochemistry and origin of the sedimentary Fe –Ni ores of Lokris. PhD thesis, Technical University, Crete, 245 p (in Greek with English abstract).

Augustidis S.S. 1982. Atlas of sphaeroidal textures and structures and their genetic significance. Theophrastus Publications S.A., Athens.

Baskar S., Baskar R., Kaushik A., 2003. Role of microorganisms in weathering of the Konkan-Goa laterite formation. Current Science 85 (8), 1129–1134.

Economou-Eliopoulos M., 2003. Apatite and Mn, Zn, Co-enriched chromite in Ni-laterites of northern Greece and their genetic significance. Journal of Geochemical Exploration, 80, 41-54.

Economou-Eliopoulos M., Eliopoulos D., Apostolikas A. and Maglaras K., 1997**.** Precious and rare earth element distribution in Ni-laterites from Lokris area, Central Greece. In Mineral Deposits, Papunen (ed), Balkema, Rotterdam, 411-414.

Eliopoulos D. and Economou-Eliopoulos M., 2000. Geochemical and mineralogical characteristics of Fe–Ni and bauxitic-laterite deposits of Greece. Ore Geology Reviews, 16, 41– 58.

Freyssinet Ph., But, C.R.M., Morris R.C., Piantone P., 2005. Pre-forming processes Related to lateritic Weathering. Economic Geology, 100th Anniversary Volume, 681-722.

Gupta V.K., 1998. Equilibrium uptake, sorption dynamics, process development, and column operations for the removal of copper and nickel from aqueous solution and waste water using activated slag, a low-cost adsorbent. Industrial & Engineering Chemistry Research,37(1), 192-202.

Golightly J.P., 1981. Nickeliferous laterite deposits. Economic Geology, 75th Anniversary. Volume, 710–735.

Hartog N., Van Bergen P.F., De Leeuw J.W., Griffioen J., 2004. Reactivity of organic matter in aquifer sediment: geological and geochemical controls. Geochimica and Cosmochimica Acta, 68 (6), 1281–1292.

Kalaitzidis S., Siavalas G., Skarpelis N., Carla Viviane Araujo C. and Christanis C., 2009. Late Cretaceous coal overlying karstic bauxite deposits in the Parnassus-Ghiona Unit, Central Greece: Coal characteristics and depositional environment. International Journal of Coal Geology. In Press.

Laskou M. and Economou-Eliopoulos M. 2005. Microorganisms as fossils and present-day development in Ni-laterites and bauxites of the Balkan Peninsula. In: 8th SGA Meeting, Mao, J. & Bierlein, F.P. (Eds), "Mineral Deposits Research Meeting the Global Challenge" Beijing, August 18-21, 2005 (2), 1001-1004.

Macksimovic Z. and Panto, G. 1982. The main nickel-bearing phases in the Rzanovo deposit, Yugoslavia: chlorite, talc, stilpnomelan and gagnesioriebeckite. Bull. Acad. Serbe Sci. Arts, t. LXXII (23), 77-96.

Majzlan J., Navrotsky A. and Casey W. H. 2000. Surface enthalpy of boehmite. Clays and Clay Minerals, 48/6, 699-707.

Mihajilovic K., Yukovic M. and Rakic S., 1972. Magmatic iron and nickel ore deposits in Sumadija. Kongress Geology SFRJ, Zagreb (1970), 97-110.

Mountrakis D., 1983. The geological structure of the northern Pelagonian zone and the geotectonic evolution of the Internal Hellenides. PhD Thesis. University of Thessaloniki, 289 pp. Norton S., 1973. Laterite and bauxite formation. Economic Geology, 63, 353–361.

Öztürk H., Hein R.J. and Hanilci N., 2002. Genesis of the Dog¢ankuzu and Mortas Bauxite Deposits, Taurides, Turkey: Separation of Al, Fe, and Mn and Implications for Passive Margin Metallogeny. Economic Geology, 97, 1063-1077.

Papastavrou S., 1986. Greek bauxites. Mineral Deposits Research. IGME, Internal Report (in Greek, with English abstract), Athens, 30p.

Partey F.P., 2008. Mechanism of arsenic sorption onto laterite concretions. Ph.D., New Mexico Institute of Mining and Technology, Department of Earth and Environmental Science, 177p.

Pe-Piper G., Panagos A. and Varnavas S., 1981. The volcanic rocks of Melidoni (Locris). Neues Jahrbuch Mineralogie Abhandlungen, 143 (1), 102-111.

Plastiras V. 1979. The conglomerates and the underlying nickelif-erous ores of Ieropighi, Kastoria. Intern. Report. IGME _Inst. Geol. Miner. Explor.., Athens, 12 pp.

Skarpelis N., Laskou M., Alevizos G., 1993. Mineralogy and geochemistry of the nickeliferous lateritic iron-ores of Kastoria, N.W. Greece. Chem. Erde 53, 331–339.

Smedley P.L. and Kinniburgh D.G., 2001. A review of the source, behaviour and distribution of arsenic in natural waters. Applied Geochemistry, 17(5), 517-568.

Panto G. and Maksimovic Z., 2001. Two rare earth minerals in an unusual mineralization of the Nissi bauxite deposit. Acta Geologica Hungarica, 44/1, 81-93.

Pinon-Miramontes M., Bautista-Margulis R.G. and Perez-Hernandez A., 2003. Removal of arsenic and fluoride from drinking water with cake alum and a polymeric anionic flocculent. Fluoride, 36(2), 122-128.

USEPA 2004. Capital Costs of Arsenic Removal Technologies. U.S. EPA Arsenic Removal

Technology Demonstration Program Round 1 (EPA, 2004).

Valeton I., Biermann M., Reche R. and Rosenberg F., 1987. Genesis of Ni-laterites and bauxites in Greece during the Jurassic and Cretaceous, and their relation to ultrabasic parent rocks. Ore Geology Reviews, 2, 359-404.

Xhomo A., Arkaxhana A Bakalli F., Noka K and Ghejani P. 1995. Laterite mineralization related to ophiolite. Whorkshop on Albanian ophiolites and related mineralization. Documents du BRGM 244, 67-68.

Zevgolis E.N., 2004. The Evolution of the Greek Ferronickel Production Process. TMS International Laterite Nickel Symposium, North Carolina, USA, Proceedings, W. P. Imrie and D. M. Lane. (eds), pp. 619-632.

Scientific Annals, School of Geology, Aristotle University of Thessaloniki Proceedings of the XIX CBGA Congress, Thessaloniki, Greece	Special volume 100	333-341	Thessaloniki 2010

SOURCES OF BASE, PRECIOUS AND RARE METALS DURING THE TETHYAN PHANEROZOIC EVOLUTION OF THE CAUCASUS AND PONTIDES

Gugushvili V., Popkhadze N., Beridze T. and Khutsishvili S.

Ministry of Education and Science, Geological legal Entity of Public Law Al. Djanelidze Institute of Geology. 1/9 M. Alexidze str. Tbilisi 0193, Georgia,
gugushvili34@yahoo.com, nino_popkhadze@yahoo.com, tamara_beridze@yahoo.com and sofio_sofi@yahoo.com

Abstract: Base, rare and precious metal deposits are widespread in the Caucasus and Pontides regions. They are the result of the Phanerozoic evolution of the Tethys Ocean, of various geodynamic settings, including oceanic, intra-arc, back-arc and island arcs. The various types of mineralization are discussed in terms of the participation scale of sialic, basaltic crusts and mantle sources. In oceanic settings, cupriferous Cyprus-type deposits occur, where the source of Cu is the mantle. In intra-arc settings, Beshi type Cu-Zn deposits were formed; the source of Zn is interpreted to be basaltic crust. As for the island arc and back-arc settings, Cu-Pb-Zn porphyry, stockwork, VMS and vein deposits are common. The source of Pb is interpreted to be the sialic crust. The rare metals (Hg, W, Sb) are related to post-collisional settings, where sialic crust is important. Mo is also related mainly to post-collisional settings, and it subordinately participates in the island arc settings. Precious metal mineralization (Au and Ag) predominantly developed in island arc and post-collisional settings. Therefore, in the process of mantle depletion and crust formation precious metals (Au and Ag) mainly accumulated in the sialic crust.

Keywords: Tethys, Phanerozoic, metallogeny, Caucasus, Pontides.

1. Introduction

The Caucasus and Pontides are the result of the Phanerozoic evolution of the Tethys ocean. The process was terminated by post-collisional activity. The geodynamic development is clearly reflected in volcanic activity and base, precious and rare metals metallogeny. During the Paleozoic, the Tethys Ocean was located between the Afro-Arabian and Eurasian plates. During the Late Paleozoic, the oceanic slab started its north-verging subduction, the ocean closed during the Early Paleogene and is expressed by the Izmir-Ankara-Erzindjan-Sevan ophiolite suture zone.

The Phanerozoic evolution of the Caucasus and the Pontides is divided in pre-collisional and post-collision stages with a variety of geodynamic settings. During the pre-collisional stages, oceanic, intra-arc, back-arc and island arc settings were formed with associated metallogeny. After the closure of the ocean, the Caucasus and the Pontides evolved into collisional and post-collisional stages, and was consequently accompanied by a change of the character of metallogeny.

Base and precious metals in the various settings of the pre-collisional development are differently distributed: the oceanic setting is characterized by cupriferous ores, with subordinate Zn mineralization, and devoid of Pb. At the same time, seafloor occurrences of the oceanic setting generally contain only little gold and silver mineralization according to Rona and Scott (1993). In intra-arc settings, Cu-Zn mineralization contains subordinate gold, and in marginal sea-back-arc settings, Cu and Zn can be accompanied by galena and gold mineralization. Finally in island arcs, Cu, Pb, Zn, Au and Ag ores can be accompanied by significant and widespread galena mineralization. It is noteworthy, that rare metals such as Hg, W and Sb are absent in pre-collisional settings. The diversity of distribution of rare, non-ferrous and precious metals in the various geodynamic settings depends on the scale of participation of sialic, basaltic and mantle sources in the process of mineralization.

According to Hutchinson (1973), during the Archean, when the crust only existed as a protocrust

and the mantle was only weakly differentiated, only copper-zinc deposits were formed. Later, during the Proterozoic, when the sialic crust was developed, lead took part in the mineralization process and gained economic significance in volcanogenic massive sulfide (VMS) deposits.

Our aim is to examine mantle, basaltic and sialic crust influence on the character of mineralization in the Caucasus and Pontides region. Here during the process of Phanerozoic evolution, all types of geodynamic settings were present, including pre-collisional and post-collisional ones, with appropriate mineralization related to settings with predominant mantle, basaltic or sialic crust participation. The diversity of geodynamic situations, volcanic activity and ore formation of the region gives us an opportunity to consider and evaluate the rich variety of data.

2. Phanerozoic evolution and base, precious and rare metal metallogeny

The diversity of base, precious and rare metal deposits, which were formed during the Phanerozoic evolution of the Tethys described above are presented in Tables 1 and 2 and and Figures 1 and 2.

During the Late Paleozoic and Early Mesozoic in the Pontides, above a N-NW subducting slab, a minor ocean existed, with an ophiolite extrusion and MORB and island arc (IAT) tholeiites, confirmed by immobile element geochemistry. Here, the Kure complex consists of serpentinized perido-

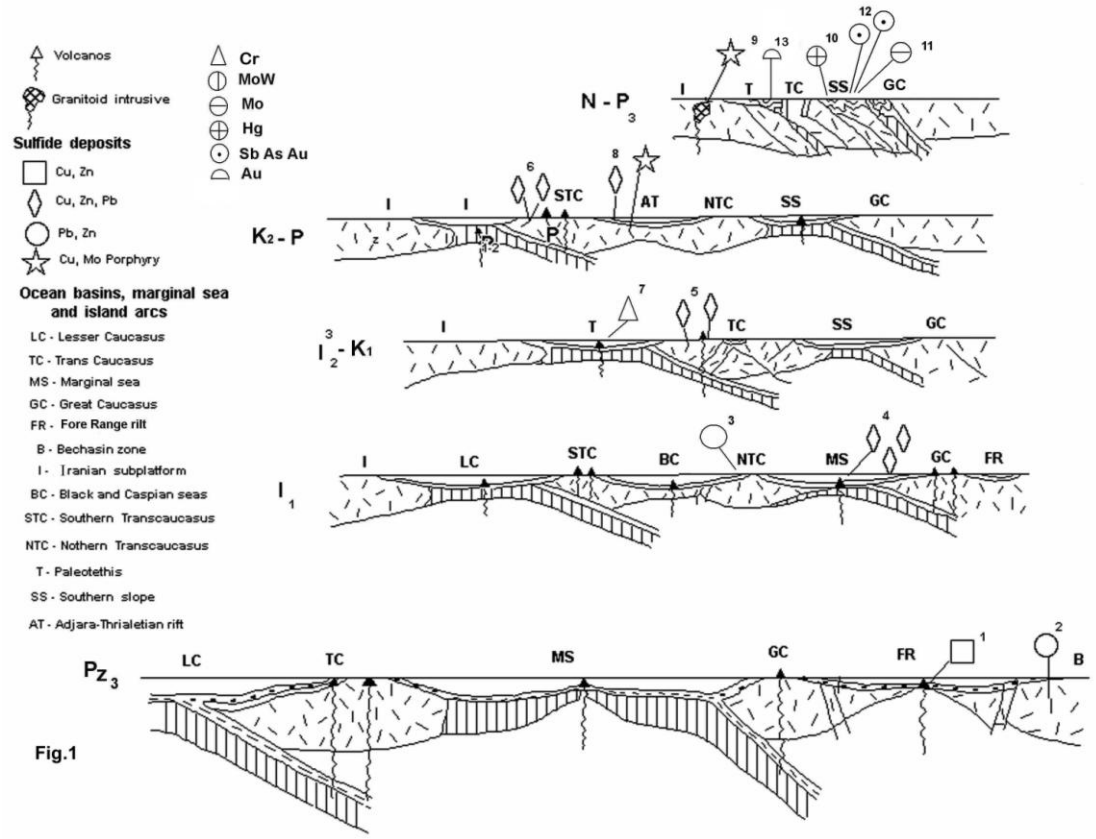

Fig.1

Fig.1 Palinspastic cross-section of the Caucasus according to Adamia et al. (1997) with nonferrous, rare and precious deposits related to different gaodynamic settings.
Precollision settings: 1. Cu-Zn Besshi type deposits of Urup group (intra-arc setting), 2. Pb-Zn vein deposits of Bechasin zone (island arc setting), 3. Pb-Zn vein deposits of Sadon, Kvaisa, Dzirsha groups (island arc setting), 4. Cu-Pb-Zn Filiz-Chai type deposits (backarc setting), 5. Cu-Pb-Zn VMS, porphyry, stockwork and vein type deposits od Somkhith-Carabakh zone (island arc setting), 6. Cu-Pb-Zn-Au porphyry, stockwork, epithermal and vein type deposits of Artvine-Bolnisi zone (island arc setting), 7. Cr vein and lens type deposits of Sevan-Akera suture zone (ocean setting), 8. Cu-Pb-Zn-Au porphyry, stockwork and vein type deposits of Ajara-Trialeti zone (island arc setting), 9. Cu-Mo porphyry deposits (Kajaran, Agarac), 10. Hg vein type deposits (Akhey, Avadhara), 11. Mo-W, Mo vein type deposits (Tirniauz, Karobi), 12. As-Sb-Au vein type deposits (Zopkhito,Lukhumi), 13. Au lode deposits (Zod, Meghrathzor).

tite at the base and is overlain by layered cumulate gabbros, passing upward into isotropic microgabbro and into a diabase sheeted dyke complex. The later is stratigraphically overlain by alternations of pillow lava, massive lava and lava breccias. Lava breccias are overlain by shales, which are interpreted as semi-pelagic sedimentary rocks according to Ustaomer and Robertson (1997). "Cyprus type" cupriferous pyrite deposits are found along the lava-sedimentary rock contact, and are expressed as disseminated and massive ores according to Guner (1980). The most significant deposits are: Asikoy and Bakibaba (Tab.3), massive sulfides consisting essentially of pyrite and chalcopyrite. Zn and Pb are only present as trace elements. Thus, the MORB mineralization of the Kure complex, which is a typical Cyprus type deposit, is characteristic for an oceanic setting.

The Beshi-type deposits of the intra-arc setting, related to the Urup group, are located in the fore-range of the Great Caucasus (Figs 1 and 2, Tab. 2). The intra-arc rift developed above a Paleozoic subduction, during the closure of the Great Caucasus minor ocean. The Paleotethyan branch is only represented by the allochtonous relic of its suture according to Adamia et al. (1981). The intra-arc rift is characterized by Paleozoic bimodal tholeiite-basalt-rhyolite volcanic activity and Au-bearing Cu-Zn Beshi type mineralization. The recent intra-arc rifts are similar to Fore Range basalts in K/Rb ratios and TiO_2 contents and enriched in the most lithophile and siderophile elements, as tholeiites of the Red Sea axial trough (Shavishvili 1983). The ores consist of copper-pyrite, copper-zinc, pyrite mineralization, with pyrite being prevalent (90-100%), and chalcopyrite and sphalerite being subsidiary (9%) according to Skripchenko (1972). Sialic crust material did not participate in the mineralization process, therefore the ores only contain Cu and Zn.

During the Lower Jurassic (Liassic), above the north-verging subduction zone, a back-arc rift appeared along the Southern Slope of the Great Caucasus and evolved into a marginal sea. It is characterized by the Filiz-chai group Cu, Zn, and Pb deposits, with subordinate gold mineralization (Figs. 1, 2; Tab. 1). The back-arc rifting here is associated with slow spreading without ophiolite extru-

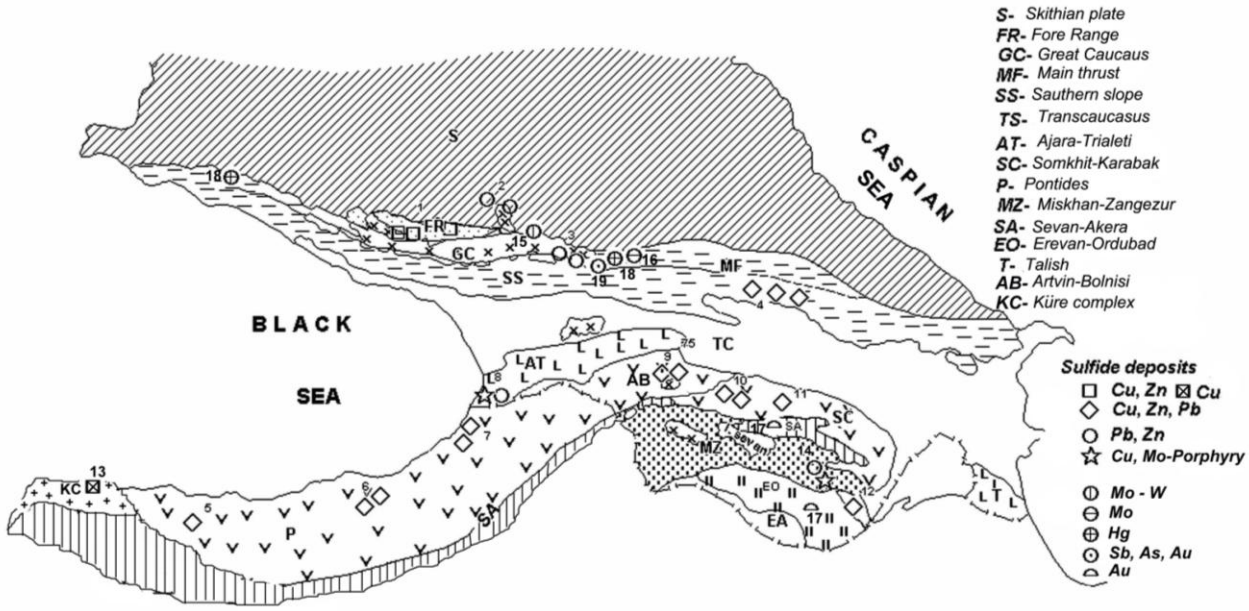

Fig.2 Geotectonic scheme of the Caucasus and Eastern Pontides with metallogeny of nonferrous, rare and precious metals deposits.

Precollision stage: 1. Urip group of Besshi type (Cu,Zn) deposits, 2. Pb, Zn – vein deposits of the Bechasin zone, 3. Pb, Zn vein deposits of Sadon group, 4. Filizchai type deposits, 5,6,7- (Lahanos, Madenkoy, Murgul VMS Kuroko type and polimetallic vein stockwork deposit of the East Pontides metalotect, 8- Cu-Mo porphyry and polymetallic vein deposits of Merisi group, 9- Au-Cu porphyry, Au –low sulfidation and vein and stockwork polymetallic deposits of Madneuli and Sakdrisi group. 10, 11, Cu-Pb-Zn VMS, vein and stockwork polymetallic and Cu porphyry deposit of Somkhit-Carabakh zone (Alaverdi group, Tekhut), 12- Kafan Cu porphyry deposit, 13- Cyprus type Cu deposits of Kure complex (Asikoy, Bakibaba), 14- Kajaran Cu-Mo porphyry and vein and stockwork polimetallic and stockwork deposit, 15- Tirniaus W-Mo vein and stockwork deposits, 16- Mo-Karobi, 17- Au lode and stockwork Zod and Maghradzor deposits, 18- Hg Akhei, Avadhara vein deposits, 19- Sb, As, Au Zopkhito, Lukhum vein deposits.

Table 1. Pre-collision metallogeny of the Caucasus and the Pontides

Metallogenic		Pre-collisional metallogenic unites							
Oceanic		Island arc		Intra arc		Deposits		Deposits	
		Deposits	Type of mineralization	Variscan	Type of mineralization	Deposits	Type of mineralization	Deposits	Type of mineralization
Variscan	VMS (Cu)	Okrila (Au)	disseminated veins (Au)	Urup, Khudes, Beskes	Beshi type VMS (Cu, Zn)			Asikoi,	VMS (Cu)
								Bakibaba	VMS (Cu)
							Filiz-chai type		
Alpine		Sadon, Zgid, Holst	vein, stockwork (Pb, Zn)			Filiz-chai Katkh, Artana	VMS (Cu, Pb,Zn) vein (Cu, Pb, Zn)		
	Early (Lias)	Dzirsha	vein (Pb, Zn)						
	Middle (Dogger, Malm)	Brdzirsha	stratabound (Pb, Zn)						
		Kvaisa	vein (Pb, Zn)						
		Alaverdi,	VMS (Cu, Pb, Zn)						
		Tekhut,	porphyry (Cu)						
		Kafan,	" – " (Cu, Pb, Zn)						
		Kedabeck,	" – " (Cu, Pb, Zn)						
	(Bajocian)	Karadag,	" – " (Au, Cu, Pb, Zn)						
		Kizilbulag,	" – " (Au, Cu, Ag)						
		Gosha	Stockwork and vein (Au, Cu, Ag)						
		Madneuli	porphyry, epithermal (Au,Cu, Pb, Zn)						
	Late (Senonian)	Sakdrisi						Shorja	vein, lens (Cr)
		Poladauri	vien (Fe)						
		Murgul	stockwork and vien (Cu, Pb, Zn)						
		Madenkoy	Kuroko type VMS (Cu, Pb, Zn)						
		Lahanos							
		Guzelaila	porphyry (Cu, Mo)						
		Balikasir Balia							
		Demirbaku	stokwork and vein (Pb, Zn, Ag, Au)						
		Altinoluk							
		Canakkale							
	(Eocene)	Merisi	porphyry (Cu, Ag, Pb, Zn)						
		Gujareti	vein, stockwork (Cu, Pb, Zn)						
		Dzama	skarn and porphyry (Fe, Au, Cu)						
		Algeti	vein (Mn)						

sions, and the seafloor was underlain by thin sialic crust according to Lomize and Panov (2002), which is thought to be source of lead in this setting, whereas the source of Zn are the subducted basaltic slab and slowly spreading basaltic crust. The tholeiites of the marginal sea are characterized by a low content of REE and a normal chondric distribution of Nb, Zr, Hf, and Y, but with slight distinct anomalies of Nb and Ti characteristic for island arc tholeiites. The ratio $^{87}Sr/^{86}Sr$ of 0.7034 is

consistent with MORB compositions and is typical of back-arc and intra-arc basins according to Tarney et al. (1977) and Lordkipanidze (1980). Typical calc-alkaline volcanic activity preceded the riftogenic tholeiitic volcanism and was postdated by calc-alkaline dacite and gabbro-diorite intrusive bodies according to Lordkipanidze (1980). The Filiz-chai Cu-Zn-Pb deposit consists of stratiform ore bodies. The mineralization consists of pyrite with subordinate sphalerite, galena, chalcopyrite and pyrrhotite, with minor quantities of marcasite, arsenopyrite, cobaltite, magnetite and goethite.

Mezo-Cenozoic island-arc settings were formed above the north-verging subducting slab of the Tethys Ocean in the Caucasus and the Pontides. The settings are characterized by calc-alkaline volcanism and basic metals Cu, Zn-Pb, precious metals Au-Ag and subordinate Mo mineralizations (Figs 1, 2; Tab.1). Jurassic – Bajocian VMS, porphyry, stockwork and vein type deposits occur in the Somkhit-Karabakh zone of the Transcaucasus. They include the Alaverdi group (Alaverdi, Shamlug, Akhtala), Tekhut, Kedabek, Karadag, Kizilbulag, and Gosha deposits (Figs 1, 2; Tab.1). The Somkhet-Karabakh zone is continuing to the northwest into the Artvin-Bolnisi and the Eastern Pontides zone (Fig.1), which represent a Cretaceous island-arc setting, with calc-alkaline volcanic rocks and Cu, Pb, Zn, Au and Ag mineralizations. The Artvin-Bolnisi zone includes the Madneuli, Tsiteli-Sopeli and Sakdrisi deposits interpreted as porphyry, epithermal low sulfidation, stockwork and vein deposits with economic reserves of Cu, Pb, Zn and Au (Fig. 2; Tab. 1).

The same volcanic activity with Cu, Pb, Zn and Au mineralization took place in the Eastern Pontides

Table 2: Post-collision metallogeny of the Caucasus

Metallogenic Epoch		Post-collisional Metallogenic Unites			
		Fold-Thrust Belt		Fore-lands	
		Deposits	Type of mineralization	Deposits	Type of mineralization
Alpine		Zod	Vein, stockwork		
			Au, Mo, Pb, Cu	Chiatura,	exhalative-sedimentary (Mn)
	Early			Chkhari,	
	(Oligocene)			Ajameti	
					exhalative-sedimentary (Cu, Au)
		Meghradzor	Au, Mo, Pb	Nakhchevan	
		Kajaran, Agarak	porphyry		
			(Mo, Cu, Pb, Zn, Au)		
		Avadhara,	vein (Hg)		
		Akhei	vein (Hg)		
		Tsana	vein, disseminated (As)		
	Middle				
	(Neogene)	Zopkhito	vein, disseminated		
			(Au, Sb, As, Pb)		
		Karobi	vein, (Mo)		
		Notsarula	vein, (Mo, W)		
		Tirniauz	vein, stockwork (Mo, W)		
		Lukhumi	vein, carline type (Sb, As, Au)		
	Late	Enguri	placer, (Au)	Araks	placer, (Au)
	(Quartenary)				
		Khrami	placer, (Au)	Ureki	placer, (Fe, Ti, V)

island-arc volcanic series, which include the Murgul group of subvolcanic base metal deposits, the Madenkoy and Lahanos Kuroko-type VMS and porphyry Mo-Cu deposits, Guzelaiala, as well as the Cheratepe gold-bearing polymetallic ores (Fig. 2; Tab.1). All of them contain essential, economic reserves of Pb derived from sialic crust and calc-alkaline volcanic rocks, as well as Cu and Zn derived from mantle and basaltic crust. At the same time in the island-arc setting of the southern slope of the Great Caucasus, Dogger-Malm Pb-Zn vein type and stratabound deposits were formed, whereas the Liassic Pb-Zn Sadon, Zgid and Holst vein type deposits were formed in the main range of the Caucasus. It is noteworthy that in all deposits there is a prevalence of galena.

In the Western Pontides, the Upper Cretaceous polymetallic stockwork and vein-type deposits Balikasir Balia, Demirbaku, Altinoluk, and Canakkale-Handeress were formed. The mineralization is related to calc-alkaline volcanic rocks and intrusives of an island-arc settings and are characterized by a high abundance of galena and precious metals (Tab.3).

In the Adjara-Trialeti folded zone (Fig.1, 2; Tab.1), characterized by a Late Eocene island-arc setting with calc-alkaline intrusive and volcanic series, Cu, Pb, Zn, Au and subordinate Mo porphyry and vein-type deposits of the Merisi group were formed. The sources of the non-ferrous metals are inferred to be the same as for the above-mentioned island-arc settings.

The volcanic host rocks of the island-arc deposits of the Caucasus and the Pontides are characterized by: low contents of LILE, REE and typical island-arc flat trends for heavy REE, negative anomalies of Nb, and Ti, normal chondritic contents of Zr, Hf and Y, and comparatively high $Sr/^{86}Sr$ ratios of 0.7041 to 0.7045 according to Lordkipanidze et al. (1988). Thus, the Caucasus and Pontides Phanerozoic pre-collisional stage mineralizations are related to oceanic (MORB), intra-arc, and back-arc and island-arc settings. In ocean and intra-arc settings, the mineralization is characterized by basaltic crust and mantle material sources for Cu and Zn. Whereas in island-arc settings and along the southern slope-marginal sea, Cu, Zn, Au and Pb mineralizations were sourced by mantle and sialic and basaltic crusts.

The post-collisional Oligocene and Neogene stages are characterized by fold thrust belts of the fore-range and the southern slope of the Great Caucasus and the Lesser Caucasus, where rare metals deposits with W, Hg, Mo, As, Sb, Pb vein-type, stockwork and porphyry deposits occur, including the W, Mo Tirniauz, Notsarula, Hg-Avadhara and Akhey Mo-Karobi, Sb, As, Au – Zopkhito and Lukhumi, and Mo, Cu, Pb, Zn Kajaran deposits (Figs 1, 2; Tab 2).

Occurrences of precious metals are known in the oceanic settings and in intra-arc and back-arc rifts; however the most significant mineralization and deposits are related to island-arcs and post-collisional settings. Hence, during the process of differentiation and depletion of the mantle, precious metals were distributed between the mantle, and the basaltic and sialic crusts, but mainly accumulated in the sialic crust. This is the reason why the most significant precious metals deposits are related to island-arc and post-collisional settings, where sources of sialic crust prevailed during the process of mineralization. For instance, the richest gold deposits of the Kuskokuim group of Alaska are related to the post-collisional stage and are located in post-accretion terranes according to Gray et al. (1997). The orogenic giant gold deposits of Muruntau, Cumtor, and Chulboi are associated with rare metal (W, Sb, Hg, Mo) mineralization, are also related to the post-collisional stage of the Tethyan ocean evolution. Hence, it is concluded that the sources of gold and rare metals are in the sialic crust.

Oceanic intra-arc and back-arc mineralization lack any Mo and rare metals, as well as Hg, W, and Sb. The highest grades and reserves of Mo are contained in the post-collisional porphyry deposits of Kajaran and Agarak (Tab.2). The post-collisional deposits contain high reserves and high grades of W, Sb, and Hg as well. The latter are totally absent in oceanic, intra-arc, back-arc and island-arc deposits.

By contrast to the belt-thrust structures, where hydrothermal Mo and rare metals deposits occur, the foreland of the Transcaucasus is characterized by Early Oligocene exhalative, sedimentary Mn deposits at Chiatura, Chkhari and Ajameti, and the Nakhchevan Cu-Au sedimentary deposits Finally, Quaternary Au-placers were formed in the valleys of Enguri and Khrami (Tab.2).

3. Discussion

The geodynamic setting of the Caucasus and the Pontides and the related metallogeny of the non-ferrous, rare and precious metals enable us to dis-

Table 3. Nonferrous, rare and precious metals deposits of the Caucasus and Pontides.

Source of mineralization	Reserves	Deposit age	Content of mineralization	Host rocks	Geodynamic setting	Source of mineralization	Reserves
1	2	3	4	5	6	7	8
Mantle	Ashikoy: 10.9mln.t	Late Paleozoic – Early Mezozoic	Cu	Tholeiite	Ashikoy	Mantle	Ashikoy: 10.9mln.t
Ashikoy			Trace elements:	basalt and			ore; grade:2.17%Cu
Bakibaba			Zn, Pb, V, Ni,	black shales			Bakibaba: 1.9mln.t
			Ti, Cd, Co, As				Middle – Upper
Mantle and	Urup: 770 th.t Cu,	Middle – Upper	Cu, Zn,	Basalt-rhyolite;	Urup	Great Caucasus	Devonian
basaltic crust	300 th.t Zn, 2t. Au, 10 th.t Ag, Khudes: 500 th.t Cu, 260 th.t Zn, 40t Co, 4t Au	Devonian	subordinate:	spilite-	Khudes	basaltic crust	300 th.t Zn, 2t. Au, 10 th.t Ag, Khudes: 500 th.t Cu, 260 th.t Zn, 40t Co, 4t Au
Khudes			Au, Ag, Co	andesite-dacite			
Filiz Chai type VMS	Southern slope of Great Caucasus	Lowe	Cu, Zn, Pb	Tholeiite	Back-arc rift	Mantle	Filizchai: 504 th.t Cu, 3.01 mln.t Zn, 1.2 mln.t Pb; 20t. Katsdag: 17.3 th.t Cu, 99.3 th.t Zn, 36.0 th.t Pb; Kizildere: 1.07 mln.t Cu, 3.2th.t Zn
Filiz Chai		Jurassic		basalts	Marginal sea,	basaltic and sialic crust	
Katsdag					with sialic bottom		
Kizil Dere							
Adange							
Kuroko type VMS	East Pontides	Upper	Cu, Pb, Zn	Dacite-rhyolite-andesite	Island	Sialic, basaltic crust.	Madenkoy: 23.06mln.t
Madenkoy		Cretaceous		tuffs	arc	calc-alkaline	ore; grade: 2.88%Cu, 0.32%Pb, 4.34%Zn
Lahanos						volcanics. mantle influence	Lahanos: 2.3 mln.t ore
							grade: 3.59%Cu
							2.38%Zn
							Pb is not calculated
Subvolcanic polimetallic	East Pontides	Upper	Cu, Pb, Zn	Dacite-rhyolite	Island	Sialic, basaltic crust.calc-alkaline volcanics. mantle influence	Murgul: 32 mln.t ore
stockwork		Cretaceous			arc		grade: 1.32%Cu,
Murgul							0.1%Zn, 0.05%Pb
Tumiscent stockwork	Lesser Caucasus	Upper Cretaceous	Cu, Pb, Zn,	Rhyolite dacite	Island arc	Sialic, basaltic crust.	Madneuli: 800 th.t Cu, 120 th.t Zn, 40 th.t Pb, 28 t Au, Tsiteli Sopeli: 316 th.t Cu, 24.4 t Au, 91.7 t Ag, 179 t Mo
polimetallic, gold-copperporphyry, gold (low sulfidation)			Au	tuffs		calc-alkaline	
Madneuli						volcanics. mantle influence	
Tsiteli Sopeli							
Polymetallic stockwork and vein deposits	West Pontides	Upper Cretaceous	Pb, Zn, Ag, Au	limestone	Island arc	Sialic, basaltic crust.	Balikesir Balia: 13.5 mln.t. ore
Balikasir Balia,				metaarcos,		calc-alkaline	grade: 4.40%Pb, 4.26%Zn;
Demirbaku				siltstones,		volcanics. and intrusive bodies.	Demirboku: 3.7 mln.t
Altinoluk				diabases, gabbros, schists, marbles of Permian Lower Triasian ages			grade: 3.91%Cu, 3.81%Zn, 0.25%Pb;
Canakkale-Handeresi							Altinoluk: 271 th.t ore
							grade: 8.21%Pb, 6.72%Zn, 25g/t Ag, 5g/t Au;
							Canakkale-Handeresi:
							3.7 mln.t. ore;
							grade: 5.24%pb, 2.05%Zn
Polymetallic stockwork VMS and vein deposits	Lesser Caucasus	Middle Jurassic	Cu, Pb, Zn	calc-alkaline volcanic series; andesites dacites, rhyolites	Island arc	Sialic, basaltic crust. calc-alkaline	Shamlug: 123 th.t Cu, 5 th.t Pb, 14 th.t Zn; Alaverdy: 125 th.t Cu, Pb and Zn are not calculated
Shamlug, Alaverdy, Akhtala, Kafan						volcanics. mantle influence	Akhtala: 6.5 th.t Cu, 19 th.t Pb, 5 th.t Zn
							Kafan: 145 th.t Cu Pb and Zn are not calculated
Molibdenum-copper porphyry deposits							
Guzelyayla	East Pontides	Upper Cretaceous	Cu, Mo	Calc-alkaline	Island arc	Sialic and basaltic crust and calc-alkaline volcanics and intrusive bodies, Mantle influence	186 mln.t. ore
				Volcanics: Basalt, andesite dacite			grade: 0.3% Cu
							0.012 % Mo
							Pb and Zn are not calculated
				Granodiorite and sienite diorite intrusives and Calc-alkaline		Calc-alkaline volcanics and intrusives	
				Volcanics: andesite, thachyandesite trachytes		mantle influence	
Merisi		Upper Eocene					
	Lesser Caucasus		Cu, Zn, Pb, Mo				74.8 th.t Cu, 11 th.t Zn, 9 th.t Pb, 859 kg Au, 15 t Ag
					Island arc		
Vein type	Southern Slope of the Great Caucasus	Dogger Malm	Pb, Zn	Black slates	Island arc	Basaltic and sialic crust	2,8 mln. t. ore;
Kvaisa							Pb 56.2 th. t.
Stratabound	"	"	Pb, Zn	Limestones and marls	Postcollision	Sialic crust	250 th.t. ore;
Brdzirsha							15,5 th.t. Pb;
							23,2 th.t. Zn
Vein type	"	Neogene	Hg	"	"	"	480 th.t.ore;
Avadhara							1353 t. Hg
Akhei	"	"	Hg	"	"	"	824 th.t. ore;
							2546 t. Hg
Karobi	"	"	Mo	Black shales	"	"	55 th.t. ore;
							50 t. Mo
Notsarula	"	"	Mo, W	"	"	"	10,8 th. t. ore;
							50 t. W; 2t Au
Lukhumi	"	"	Sb, As, Au	Calcareous sandstones siltsontes	"	"	150 th.t. ore;
							11,1 th.t. As; 1,8 th.t.Sb; 1,4 th.t.Au
Vein disseminated	"	"	Au, Sb, As, Ag	Black shales	"	"	231,4 th. T. ore; 27,4 th.t. Sb; 8,8 t. Au, 39t. Ag
Zophito							
Tsana	"	"	As	"	"	"	355 th.t.ore;
							55^{th}.t. As
Vein, stockwork	Forerange of the Great Caucasus	"	Mo, W	Granodiorite porphyry, rhyolite	"	"	5 mln.t Cu;
Tirniauz							1 mln.t.Mo;
							Pb and Zn are not calculated
Porphyry	The Lesser Caucasus	"	Cu, Mo, Zn, Pb	Granodiorite porphyry, montsonites	"	"	1.8 bil.t. ore;
Kajaran							4,48 mln.t. Mo
							Mo 0,25%
Vein, stockwork	"	Oligocene	Au, Mo, Pb, Cu	Granodiorite porphyry	"	"	16 mln.t ore,
Zod							125,5t.Au,
							160t. Ag
							Au 6,2 g/t,
							Ag 10 g/t
Vein, stockwork	"	"	Au, Mo, Pb,	Diorite	"	"	1,6 mln.t ore,
Mehradzor				porphyry			59,8t.Au,
							29,7t. Ag
							Au 8 g/t,
							Ag 10 g/t

cuss the sources of mineralization in the various settings. The mantle source of copper is evident for cupriferous Cyprus type deposits of oceanic settings. The Kure complex mainly consists of copper ores, and only traces of Zn and Pb. Mineralized fields of the modern ocean, investigated by Rona and Scott (1993) and Mozgova et al. (1999), predominantly contain copper, whereas zinc is subordinate and lead is absent or only present in traces. Gold and silver can also be present, but there are not any rare metals, such as Hg, W, Sb, or Mo. According to Hutchinson (1973), the formation of Zn-rich cupreous pyrite bodies in oceanic settings occurs during the early stage of rifting, when rifting between continental plates is small. In this setting, zinc may be derived from adjacent basaltic crust. Zinc contents decrease in younger (higher stratigraphic) bodies formed during subsequent stages, with more advanced rifting. Therefore, the source of zinc is in the basaltic crust and it is confirmed by the fore-range Beshi type Cu-Zn deposits of the Urup group related to intra-arc rifting. Zinc in the intra-arc setting may be extracted from the subducted basaltic slab causing stirring up mantle diapir and intra-arc rifting. However, zinc is also derived from rifted basaltic crust during spreading.

Lead mineralization is related to settings with active participation of sialic crust, such as island arcs and post-collisional settings. Economic lead mineralization is also known in the back-arc, marginal sea of the southern slope of the Great Caucasus, where participation of sialic crust is obvious. The marginal sea bottom is underlain by a thin sialic crust and calc-alkaline acid volcanic rocks according to Lordkipanidze (1980), and Lomize and Panov (2002), which is inferred to be source of lead in the Filiz-chai Pb-Cu-Zn deposit. Rare metals such as Hg, W, Sb, and Mo are related to island arc and post-collisional settings, where sialic crust is more predominant. Rare metal mineralization is typically absent in oceanic and intra-arc settings and is unknown in back-arc situations, where the role of sialic crust is subordinate.

The sources of precious metals (Au, Ag) mineralization are also interpreted to be ultimately of mantle and basaltic crustal source, because their subordinate mineralizations are present in oceanic mineralized fields according to Rona and Scott (1993) and in intra-arc and back-arc rifts of the Caucasus. However, the most significant gold mineralization occurs in island-arc and post-collisional settings, where sialic crust is predominant. Indeed, the richest gold deposits of the Caucasus are related to island arc post-collisional settings, including Madneuli, Sakdrisi, Cheratepe, Zod and Meghrazor (Fig.1; Tab.1). The giant gold deposits of Muruntau, Kumtor, Chulboi, Daugiztau, Amantaitau, etc. are related to the Altaid orogenic collage according to Yakubchuk et al. (2002), which corresponds to a post-collisional setting. The gold deposits are associated with rare metals, including W, Sb, Hg, and Mo. The mineralization is related to granitoid intrusions emplaced in the back-arc basin, carbon-rich sedimentary sequence. Magmatic events upgraded and added further precious and rare metals mineralization into structurally favorable traps.

4. Conclusions

The data about base, precious and rare metal mineralization in the various geodynamic settings during the Phanerozoic evolution of the Caucasus and the Pontides allows us to make the following conclusions:

1. The ultimate source of Cu must be mantle and ophiolites. This is confirmed by the Cyprus type oceanic rift deposits. They exclude any participation and influence of sialic crust during mineralization. The influence of basaltic crust source for Zn is subordinate, and occurs mainly during the first stages of spreading. Zn derived from the basaltic crust, is significant in intra arc mineralization. Au and Ag, participation is subordinate. Therefore in MORB and intra-arc settings Cu and Zn mineralizations are predominant.
2. The source of lead is in sialic crust and in calc-alkaline volcanic enriched with radiogenic lead. The content of lead in the basaltic crust and mantle is thought to be insufficient for producing essential galena mineralization.
3. In the island arc and marginal sea (back-arc rift) settings where sialic crust is widespread essential (economic) reserves of galena and precious metals occur, as well as Cu and Zn, because basaltic crust and mantle sources always participate in island arc ore formation.
4. The rare metal (Hg, W, Sb, and Mo) mineralizations are related to post-collisional settings as well as precious metals – Au and Ag where sialic crust is a major component.
5. Gold mineralization is common in all pre-collisional and post-collisional settings. However the most significant gold deposits developed in island arc and post-collisional settings with abundant sialic crust participation during mine-

ralization is prevalent. Therefore gold is accumulated in sialic crust and it is the main source of precious metals.

Acknowledgments

This study benefitted from financial support of the Georgian National Science Foundation (Grant 204) and the SCOPES program (IZ73Z0-128324). The authors are grateful to Dr. Robert Moritz and Johannes Mederer for reviewing and improving the paper and to Prof. Shota Adamia for valuable consultation on geodynamic processes in the Caucasus and Pontides.

References

Adamia Sh. A., Chkotua T., Kekelia M, Lordkipanidze M and Shavishvili I., 1981.Tectonic of the Caucasus and adjoining regions: implication for the evolution of the Tethys ocean. Journal of Structural Geology, 3, 437-447.

Adamia Sh. A, Ylmaz A, Lordkipanidze M, Shavishvili I, Chkotua T and Chabukiani A., 1997. Geodynamic evolution of the Black sea region. International Colloquium, Ankara, Turkey, 19-20 November, 8-9.

Gray I.E., Gent C. A. and Snee L.W. 1997. Epithermal mercury-antimony and gold-bearing vein bodies of Southwestern Alaska, Economic Geology. Monograph 9, 287-305.

Guner M. 1980. Massive Sulfide Ores and geology of Kure area, Pontides (N. Turkey), MTA Bulletin, 93/94, 65-109.

Hutchinson R. W. 1973. Volcanogenic sulfide deposits and their metallogenic significance. Economic Geology 68, 1223-1246.

Lomidze m. G.. and Panov d. I. 2002. Amagmatic initial stage of subduction at the Crimea-Caucasus margin of the Tethys. "Geotectonica" N4 (in Russian with English abstract), 78-92.

Lordkipanidze M.B. 1980. Alpine volcanism and geodynamic of the Central Segment of the Mediterranean Folder Belt. (in Russsian with English abstract) Tbilisi. " Metsniereba", 160p.

Lordkipanidze M.B., Meliksetian B. and Djrbashian R. 1988. Mesozoic-Cenozoic Magmatic Evolution of the Pontian-Crimean-Caucasian Region. France, Nouvelle série, Paris 154, 103-24.

Mozgova N.N., Efimov A.V., Borodaev Y.S., Krasnov, Cherkasov G,A., Stepanova T.V. and Ashadze A. M. 1999. Mineralogy and chemistry of massive sulfides from Logachev Hydrothermal field (140 45'N Mid-Atlantic Ridge). Exploration and Mining geology. I. M. Franklin, I.P. Richard ed., 8, N3, 4, 375-395.

Rona P.A. and Scott S.D.. 1993. Preface of the Special Issue on Sea from hydrothermal Mineralization: New Perspectives. Economic Geology. 88, 1933-1976.

Shavishvili I.D.. 1983. Variscan volcanism in the Caucasus. IGCP Project N 5, Newsletter, 169-179.

Skripchenko N.S. 1972. Hydrothermal-sedimentary sulfide ores of the Basaltoid Formations. (in Russian with English abstract), Moscow, 211p.

Tarney J., Saunders A.D.,Weaver S.D. 1977, Geochemistry of volcanic rocks from the island arcs and marginal basins of the Scotia arc region. In: Island arcs, deep sea trenches and back-arc basins. M. Talvani, W.C. Pitman III (Eds). Washington, p. 367 - 395

Ustaomer T. and Robertson A. (1997), Tectonic Sedimentary Evolution of the North-Tethyan Margin in Central Pontides of Northern Turkey. In: Regional and Pertoleum Geology of the Black Sea and surrounding region. Published by the American Association of Petroleum Geologist. Tulsa, Oklahoma, USA 74101, 255-290.

Yakubchuk A., Cole A., Seltman R.. and Shatov. 2002. Tectonic setting, characteristics, and regional exploration. Criteria for gold mineralization in the Altaid orogenic Collage: The Tian Shan Province as a key Example. Society of Economic Geologists, Special Publication 9,177-201.

Scientific Annals, School of Geology, Aristotle University of Thessaloniki Proceedings of the XIX CBGA Congress, Thessaloniki, Greece	Special volume 100	343-350	Thessaloniki 2010

FLUIDS RELATED TO REMOBILIZATION OF MESOZOIC SULFIDE MINERALIZATION IN THE EPTADENDRO-RACHI REGION IN EASTERN RHODOPE, THRACE, GREECE

Melfos V.[1], Chatzikirkou A.[2], Michailidis K.[1] and Voudouris P.[3]

[1]*Department of Mineralogy-Petrology-Economic Geology, School of Geology, Aristotle University of Thessaloniki, 54124, Thessaloniki, Greece, melfosv@geo.auth.gr*
[2] *Institute of Geology and Mineral Exploration (I.G.M.E),, Frangon Str. 1, 546 26, Thessaloniki, Greece*
[3]*Department of Mineralogy-Petrology, University of Athens, 15784, Athens, Greece*

Abstract: The copper sulfide mineralization in the Eptadendro and Rachi areas is hosted in the Upper Tectonic Unit of eastern Rhodope in Thrace. The orebodies are found along the contacts between granitoid intrusions and meta-ultrabasic-basic rocks, as well as within meta-ultrabasic-basic rocks. Two stages of mineralization have been identified: an initial stratabound stage which is considered to be of submarine volcanosedimentary origin and a later vein-type stage formed during a hydrothermal episode, related to the intrusion of the granitoids (trodhjemites and pegmatites), during Upper Cretaceous-Early Tertiary. It consists of pyrite, chalcopyrite, sphalerite, galena, hessite, bismuthinite, emplectite, tetradymite, aikinite, wittichenite, siegenite, millerite, bornite, pyrrhotite, covellite, magnetite, hematite and goethite, with chlorite, quartz, calcite and sericite being the main syn-ore gangue minerals. The mineralization has been affected at least by a greenschist facies metamorphic episode during Eocene-Oligocene. Although the sulfide mineralization is partly deformed and shows recrystallization textures, the data obtained from fluid inclusions demonstrate well the physical and chemical parameters of ore-forming environment during the latest hydrothermal event, caused by intrusion of the granitoids. Microthermometric studies showed three groups of fluid inclusions, corresponding to the distinct fluids involved in the mineral deposition and the pegmatite formation. The first group of fluid inclusions hosted in syn-ore quartz is characterized by relatively high homogenization temperatures (300° to 380° C, with a peak at 330° C) and low salinities (1.6 to 7.2 wt% NaCl equiv) and corresponds to the fluids of the main ore stage. The second group is distinguished by a drop in T_h (210° to 260°C) corresponding to the late ore stage associated with calcite formation, and salinities (3.2 to 6.3 wt% NaCl equiv) similar to the first group. The third group of fluid inclusions in the pegmatite is characterized by temperatures ranging from 300° to 390°C, and variable salinities (6.9 to 8.9 wt% NaCl equiv and 34.7 to 58.5 wt% NaCl equiv) suggesting a magmatic origin. The composition of these fluids is dominated by NaCl+KCl. Most probably these fluids were not related to the ore mineralization process.

Keywords: Fluid inclusions, hydrothermal fluids, copper sulfide mineralization, trondhjemites, Eastern Rhodope, Greece

1. Introduction

The copper sulfide mineralization in the Eptadendro and Rachi areas (Fig. 1) is hosted in the Upper Tectonic Unit (U.T.U.) of eastern Rhodope in Thrace (Chatzikirkou 2003; Chatzikirkou and Michailidis 2004). The rocks of U.T.U. are divided into meta-ultrabasics (serpentinites), metabasites (hornblendites, amphibolites, metagabbros), acidic rocks (granitoids and pegmatites) and marbles (Mposkos et al., 1989; Ricou et al., 1998; Mposkos and Krohe, 2000; Chatzikirkou, 2003). The meta-ultrabasic rocks are metamorphosed harzburgites, whereas the protoliths of the metabasites are andesitic- to sub-alkaline-basalts of tholeiitic affinity. The granitoids have an igneous origin, a calc-alkaline affinity, and their protoliths are trondhjemites.

According to Ashworth et al. (1988), Nesbit et al. (1988) and Chatzikirkou (2003) the mineralization is related to a fault zone of NE-SW direction. The orebodies are found along the contacts between the granitoid intrusions (mainly trondhjemites) and the meta-ultrabasic-basic rocks, as well as within the

meta-ultrabasic-basic rocks. Two stages of mineralization have been identified: an initial stratabound stage, which is considered of volcano-sedimentary origin and a later one of vein-type formed during a hydrothermal episode, related to the intrusion of the trondhjemites. The pegmatites are free from ore mineralization.

The orebodies exhibit a lenticular to tabular morphology and are concordant with the host rocks. Their length does not exceed 30 meters, while their thickness is less than one meter. The main ore mineral assemblage of the stratabound mineralization consists of pyrite and chalcopyrite, with minor magnetite and pyrrhotite, whereas the main syn-ore gangue minerals are chlorite and quartz. The vein type mineralization consists of pyrite and chalco-

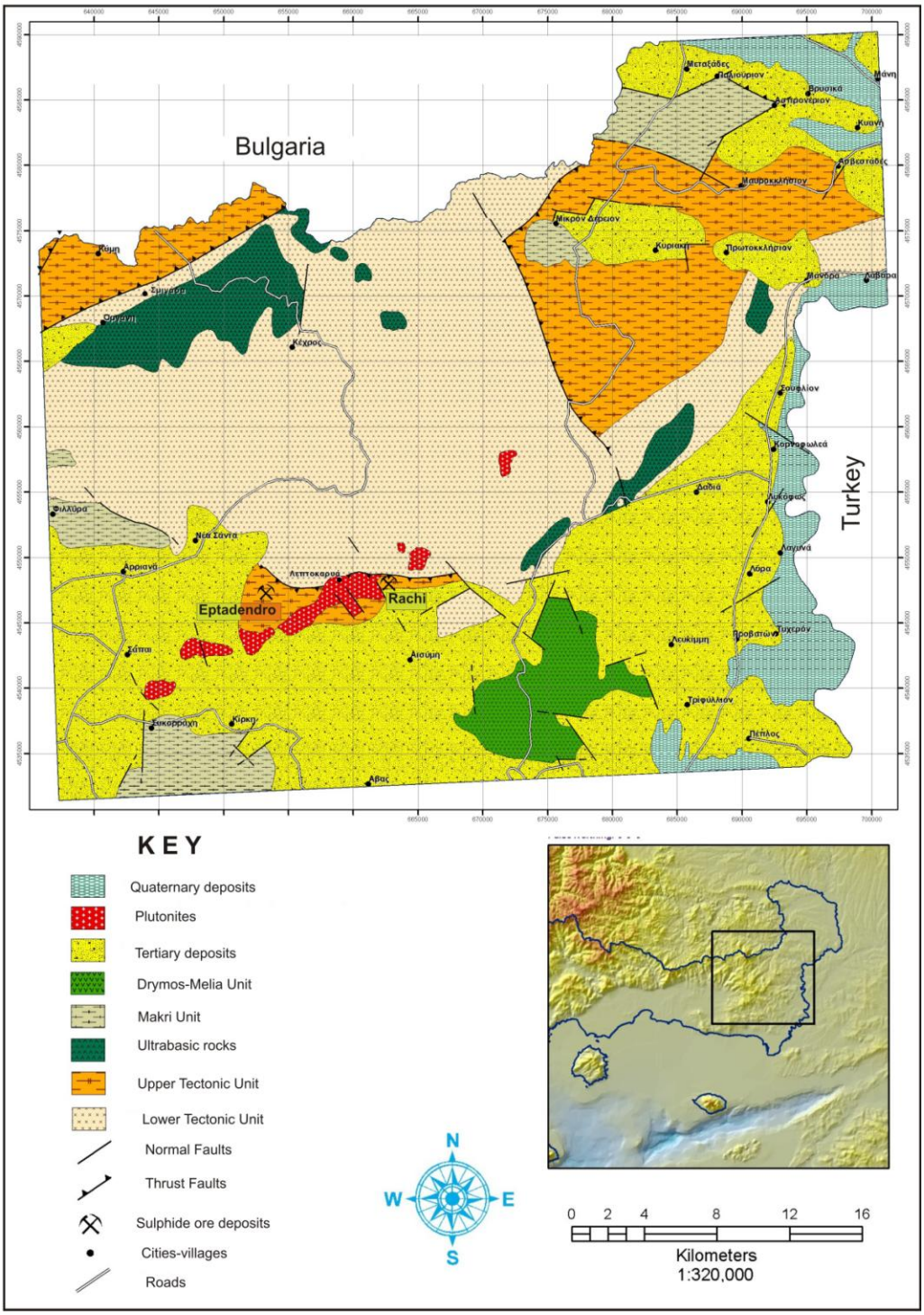

Fig. 1. Simplified geological map of the Eptadendro-Rachi ore district (Chatzikirkou 2003).

pyrite, with minor sphalerite, galena, magnetite and hematite and traces of hessite, bismuthinite, emplectite, tetradymite, aikinite, wittichenite, siegenite, millerite, bornite, pyrrhotite, covellite and goethite (Ashworth et al., 1988; Nesbit et al., 1988; Chatzikirkou, 2003; Chatzikirkou and Michailidis, 2004). Chlorite, quartz, calcite, and sericite are the main gangue minerals.

According to Chatzikirkou (2003) folding of thin mineralized layers, brittle or ductile deformation, annealing or porphyroblast formation of pyrite are typical metamorphic features confirming that the mineralization of both types has been affected by a series of metamorphic and deformation events.

Lead isotope characteristics confirmed that Pb is orogenic and was derived mainly from the crust and to a lesser extend from the mantle (Chatzikirkou, 2003). Besides, lead isotopes give an Upper Cretaceous to Eocene age for the ore mineralization. According to Chatzikirkou (2003) and Chatzikirkou and Michailidis (2004) these data suggest a metallogenetic stage related to the intrusion of the trondhjemites in the area. The $\delta^{34}S$ values for pyrite and chalcopyrite presented by Chatzikirkou (2003) vary between 1.2 and 4.6 ‰. These values give a temperature of ore formation of 293±34°C and indicate that sulfur probably precipitated from a fluid which might have been derived be of magmatic origin (~90%) and partly of seawater (~10%) origin (Chatzikirkou, 2003).

The current study further investigates the fluid inclusions in gangue syn-ore minerals and the acidic intrusions (trondhjemites and pegmatites) in the Eptadendro and Rachi areas, in an attempt to determine more precisely the ore-forming conditions. The mechanism and the physicochemical conditions of sulfide ore deposition are discussed in the context of the fluid inclusion data along with the genetic model proposed by Chatzikirkou (2003) and Chatzikirkou and Michailidis (2004).

2. Fluid inclusion study

Microthermometric measurements were conducted on carefully selected fluid inclusions hosted in: hydrothermal syn-ore quartz and calcite from the vein-type ore mineralization (four and two samples respectively), quartz from trondhjemite at the contact with meta-ultrabasic rocks (one sample), rock-forming quartz from the trondhjemite (one sample) and quartz from non-mineralized pegmatite (one sample).

Microthermometric data were obtained using a Leitz SM-LUX-POL microscope, equipped with a LINKAM THM-600/TMS 90 heating-freezing stage, housed at the Department of Mineralogy, Petrology and Economic Geology of the Aristotle University of Thessaloniki, Greece. Calibration of the stage was achieved using organic standards with known melting points (chloroform −63.5°C, naphthalene 80.35°C, Merck 135 135°C, saccharine 228°C, Merck 247 247°C) and ice (H_2O). The precision of the heating and freezing measurements were ±1°C and ±0.2°C, respectively. Fluid inclusion shapes and sizes, spatial relationships among inclusions, and minerals and number of constituent phases within inclusions were observed in nine doubly-polished thin sections prepared at the Institute of Geological and Mineral Exploration (IGME) of Greece. Routine heating-freezing runs were performed on a total of 421 fluid inclusions, including the 176 fluid inclusion measurements presented by Chatzikirkou (2003). The salinities were calculated based on the equations of state of Potter et al. (1978) and Bodnar (1993), whereas the FLINCOR program (Brown, 1989) was used to calculate salinities and densities from measured ice melting and homogenization temperatures.

3. Types of fluid inclusions

Fluid inclusions were evaluated using fluid inclusion types and fluid inclusion assemblages (FIAs) (Goldstein and Reynolds, 1994). The samples contain clear quartz and calcite which are intimately intergrown with the ore minerals. Fluid inclusions have regular or irregular shapes, and are isolated or are arranged in clusters and planes. Inclusions with negative crystal or rounded to elongated isometric shapes typically occur along crystal faces of quartz and calcite. They are assumed to be primary in origin with only a few considered as secondary, according to the criteria of Roedder (1984) and Bodnar (2003). Microthermometric measurements were conducted mainly on primary fluid inclusions and FIAs; inclusions that had been necked down or were secondary in origin were avoided. Fluid inclusions in calcite are rare, so that only a limited number of heating-freezing data were obtained.

At room temperature, only two phase liquid-vapor inclusions (Fig. 2 a-c) were identified: (i) in the ore-related quartz, (ii) at the contact between trondhjemites and meta-ultrabasic rocks and (iii) in the trondhjemite. Inclusions that were analyzed range in diameter between 3 and 42 μm and homogenize to liquid. The primary fluid inclusions have

relatively consistent liquid to vapor ratios (20-30 volume % vapor). The variability in homogenization temperature data may be due to real variability in the FIAs (Goldstein, 2003).

In the pegmatite's, two types of inclusions were recognized. Type 1 two-phase aqueous liquid-vapor inclusions (20 to 30% vapor) homogenize to the liquid state upon heating. They are the most common type of inclusions and have a maximum diameter of 45 μm. Type 2 inclusions are three phase liquid-vapor inclusions (10 to 15% vapor) that contain a colourless, isotropic cubic daughter mineral that is likely to be halite (Fig. 2 d). Rarely a second daughter mineral exists, being probably sylvite. The type 2 inclusions are up to 50 μm in diameter and homogenize to liquid by either disappearance of the vapor phase (type 2a) or dissolution of the daughter mineral (type 2b). The timing relationship (trapping time) between these two types of inclusions is unclear.

4. Microthermometry results

Microthermometric results and compositional data from the fluid inclusions are given in Table 1, and depicted in Figures 3 and 4. Homogenization temperatures of the fluid inclusions in syn-ore quartz from the Eptadendro and Rachi ore mineralization range from 275° to 422° C, with a peak at 330° C (Fig. 3a). First observable ice melting of fluids range from -21.6° to -20° C, suggesting that NaCl is the dominant salt component of the fluids (Crawford 1981; Shepherd et al. 1985). The final ice melting temperatures in the same inclusions range from -4.5° to -0.9° C, corresponding to salinities between 1.6 and 7.2 wt% NaCl equiv. Many inclusions in quartz can be grouped into FIAs, which have a constant liquid to vapor ratio (~25 %) and variable shapes, clustering along linear trends that do not cross cleavage or growth boundaries. FIAs showed restricted temperature ranges such as, 325°- 336° C, 331°-353° C and 344°-360° C, showing that the assemblages are true FIAs and, therefore, the inclusions probably represent the original trapping conditions and have not re-equilibrated.

Fluid inclusions in syn-ore calcite from the Epta-

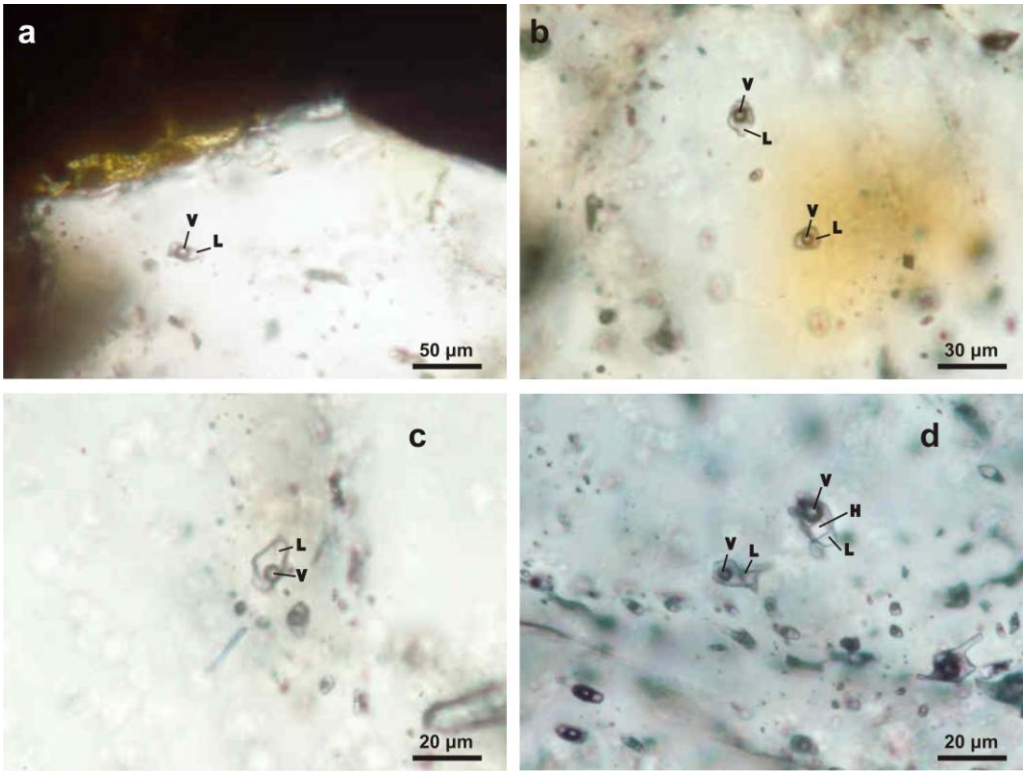

Fig. 2. Fluid inclusions in quartz from the sulfide mineralization at the Eptadendro-Rachi region. (a) Fluid inclusion of type 1 (two-phase aqueous inclusion) in quartz from the ore mineralization (sample E17). (b) Fluid inclusions of type 1 (two-phase aqueous inclusions) in quartz from the ore mineralization (sample E10). (c) Fluid inclusion of type 1 (two-phase aqueous inclusion) in quartz from the trondhjemite (sample F213). (d) Co-existing inclusions from the two types: two-phase aqueous inclusion (type-1) and three-phase halite-bearing aqueous inclusion (type 2). *L* Liquid, *V* vapor, *H* halite.

dendro and Rachi ore mineralizations exhibit T_h values between 154° and 257° C, with a peak at 240° C (Fig. 3a). These inclusions show final ice melting temperatures between -3.9° and -1.9° C, corresponding to salinities of 3.2 to 6.3 wt% NaCl equiv. An eutectic temperature of ~-21° C indicates that the dissolved salt is NaCl. Multiple populations of two-phase FIAs in calcite indicate restricted T_h: 224°-238° C, 230°-248° C, and 242°-256° C.

First observable ice melting of inclusions devoid of daughter crystals, in quartz of the pegmatite, range from -24.5° to -23.2° C, suggesting appreciable quantities of KCl in addition to NaCl (Shepherd et al. 1985). Final ice melting temperatures of type 1 inclusions range from -5.8° to -4.3° C (Table 1), which correspond to salinities of 6.9 to 8.9 wt% NaCl equiv. The homogenization temperatures (T_h) of type 1 fluid inclusions in quartz of the pegmatite, range from 267° to 388° C (Table 1) and display a bimodal distribution, with peaks at ~320° and ~370° C (Fig. 3c). Homogenization temperatures from 274° to >600° C were observed in the type 2 inclusions either by disappearance of the vapor bubble or dissolution of halite. Sylvite dissolution was observed between 174° and 226° C. Dissolution temperatures of halite in type 2 fluid inclusions (248° to 490° C) indicate a brine salinity of 34.6 to 58.4 wt% NaCl equiv. These data suggest that the hydrothermal fluids were saturated with respect to NaCl and KCl (Cline and Bodnar 1994).

Table 1. Homogenization temperatures, melting temperatures and salinities of the fluid inclusions from the Eptadendro and Rachi copper sulfide mineralizations.

Sample	Petrography	Area	Host mineral	Fluid inclusion types (homogenize to phase)	Homogenization temp. (°C) Number of measurements (n) (mean)[1]	Last melting temp. (°C) Number of measurements (n) (mean)[2]	Salinity (wt% NaCl eq) (mean)
E10	Ore mineralization	Eptadendro	qtz	*1* L+V→L	295 to 422 (91) (342)	-1.8 to -4.1 (48) (-3.1)	4.9 to 6.6 (5.5)
E17	Ore mineralization	Eptadendro	qtz	*1* L+V→L	325 to 415 (64) (348)	-2.1 to -4.5 (22) (-3.6)	3.6 to 7.2 (5.9)
F225	Ore mineralization	Rachi	qtz	*1* L+V→L	303 to 381 (26) (350)	-0.9 to -3.2 (26) (-2.2)	1.6 to 5.3 (3.8)
F275	Ore mineralization	Eptadendro	qtz	*1* L+V→L	275 to 361 (26) (330)	-0.9 to -2.9 (26) (-1.9)	1.6 to 4.8 (3.3)
F230	Ore mineralization	Rachi	ca	*1* L+V→L	154 to 257 (17) (229)	-1.9 to -3.9 (12) (-2.6)	3.2 to 6.3 (4.6)
F274	Ore mineralization	Eptadendro	ca	*1* L+V→L	155 to 253 (15) (226)	-1.9 to -3.8 (11) (-2.9)	3.2 to 6.1 (4.8)
A7	Contact between trondhjemites and ultrabasics	Eptadendro	qtz	*1* L+V→L	302 to 361 (72) (341)	-3.4 to -4.5 (36) (-4.0)	5.6 to 7.2 (6.5)
F213	Trondhjemite	Eptadendro	qtz	*1* L+V→L	245 to 429 (53) (341)	-2.0 to -4.2 (22) (-3.0)	3.4 to 6.7 (5.0)
F132	Pegmatite	Eptadendro	qtz	*1* L+V→L	267 to 388 (34) (341)	-4.3 to -5.7 (23) (-4.9)	6.9 to 8.9 (7.8)
				2 L+V+S→L	216 to 345 (22) (318)	248 to >600 (23) (445)	34.7 to 58.5 (53.4)

[1] The homogenization temperature corresponds to the temperature of the disappearance of the vapor bubble.
[2] The last melting temperature refers to the temperature of solid dissolution (> 248 °C) or last ice melting in a given inclusion;
qtz quartz; ca calcite; l liquid phase, v vapor phase; eq equivalent; n number of microthermometric analyses; avg average; temp temperature

Values of T_h in the contact between trondhjemite and meta-ultrabasic rocks, as well as in the trondhjemites were obtained from fluid inclusions in quartz (245° to 429° C), with a peak at ~330° C (Fig. 3b). These temperatures overlap with the T_h values (290° to 390° C) from the syn-ore quartz. Eutectic ice-melting temperatures of inclusions range from -21.0° to -20.1° C, suggesting that the dissolved salt is only NaCl. Final ice melting temperatures range from -4.5° to -2.0° C (Table 1), which correspond to salinities of 3.4 to 7.2 wt% NaCl equiv. Several clusters of fluid inclusions demonstrate FIAs that homogenized between 323° and 342° C, as well as 337° and 356° C, which overlap with the values of T_h in ore-mineralization stage (Figs 3a,b).

5. Discussion

Regarding the genesis of the mineralization in the

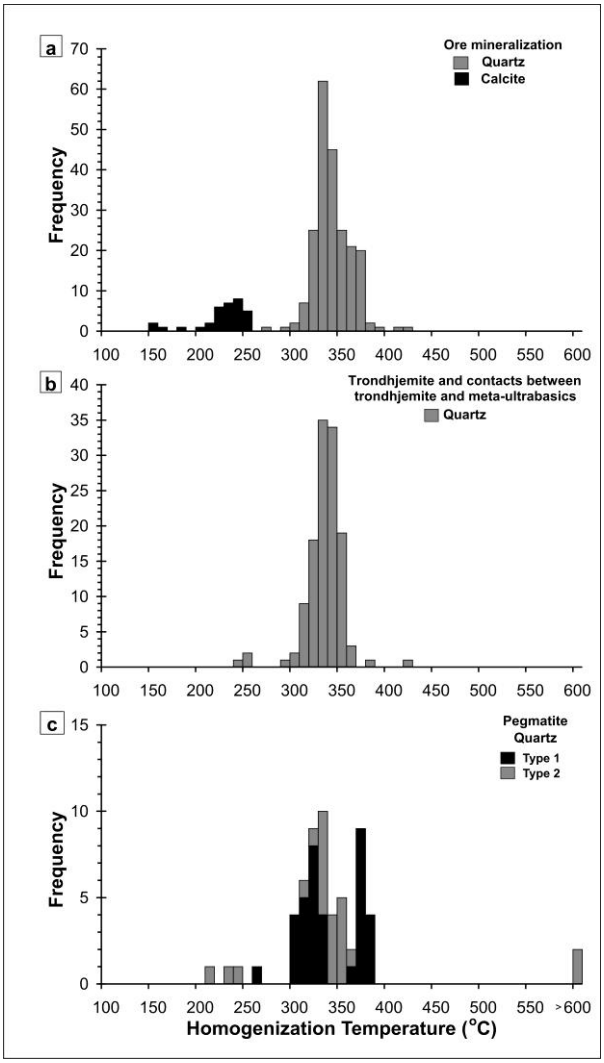

Fig. 3. Homogenization temperatures of fluid inclusions from the Eptadendro-Rachi region in the ore mineralization (a), in the trondhjemite and the contact between trondhjemite and meta-ultrabasic rocks (b) and in the pegmatite (c). *Type 1* two-phase liquid-rich aqueous inclusions. *Type 2* three-phase halite-bearing liquid-rich inclusions.

Eptadendro and Rachi areas, Chatzikirkou (2003) has suggested that the stratabound type mineralization hosted in the meta-ultrabasic-basic rocks is probably of Jurassic age and it was formed in a submarine environment. Seawater and to a lesser extent magmatic water circulating through faults and fissures of the ocean floor rocks has created a "hydrothermal convection system", which depleted metallic components from the host rocks and deposited them into the ocean floor.

During Upper Cretaceous, the intrusion of granitoids, mainly trondhjemites, created the remobilization of a part of the stratabound mineralization and the formation of the vein-type mineralization (Chatzikirkou, 2003). This is in agreement with the suggestion of Baziotis et al. (2008) that in the UHP Metamorphic Kimi Complex of East Rhodope, which is 25 km north east of the studied area, the amphibolitized eclogites are crosscut by tonalitic-trondhjemitic dykes of Early Tertiary times, at 65-63 Ma.

In addition, the magmatic fluids of these trondhjemites have added new amounts of mineralization with different elements. Consequently, all the types of mineralization have been affected at least by the greenschist facies metamorphic episode during the Eocene-Oligocene (Chatzikirkou, 2003; Chatzikirkou and Michailidis, 2004).

Fluid inclusions represent the only direct indication of ancient fluids in many crustal rocks. However, the rock may still have a completely different P–T evolution as fluid inclusion contents are seldom inert, and may have been subjected to post-trapping changes. Although the ores in the sulfide mineralization at the Eptadendro and Rachi areas are partly deformed and show some degree of recrystallization, the data obtained from the fluid inclusions demonstrate well the physical and chemical environment during the latest hydrothermal event caused by the intrusion of the trondhjemites during the Upper Cretaceous-Early Tertiary.

Based on the samples studied here, a plot of T_h values of fluid inclusions and FIAs versus salinity (Fig. 4a,b) suggests three groups, corresponding to the distinct fluids incorporated during the mineral deposition and the pegmatite formation. The first group of fluid inclusions hosted in syn-ore quartz is characterized by high values of T_h (300° to 380° C, with a peak at 330° C) and low salinities (1.6 and 7.2 wt% NaCl equiv) and represents the main ore stage which is associated with the intrusion of the trondhjemites.

The second group is distinguished by a drop in T_h (210° to 260 °C), associated with calcite formation, with similar salinities (3.2 to 6.3 wt% NaCl equiv) to the first group of inclusions. The composition of the fluids in these two stages remains the same, dominated by NaCl. The low salinities (1.6 to 7.2 wt% NaCl equiv) of the two ore stages can possibly be attributed to a mixing of ascending hydrothermal fluids and downward migrating dilute meteoric water. Such a process is very likely in a hydrothermal environment of shallow depth, with fault-controlled vein structure and causes ore deposition.

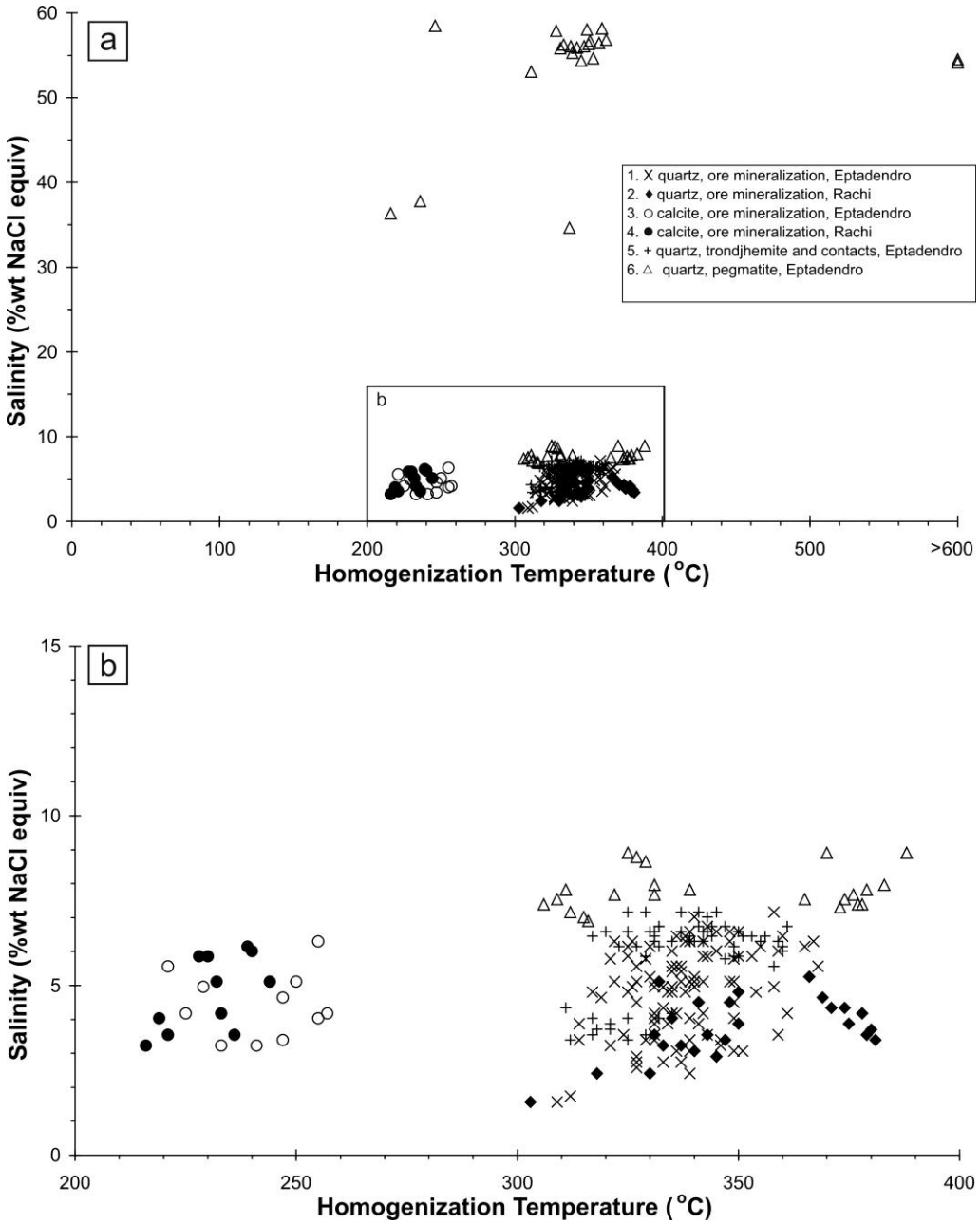

Fig. 4. Homogenization temperatures versus salinity plot for the fluid inclusions from the Eptadendro-Rachi ore mineralizations. Salinity was calculated using the equation of Potter et al. (1978) and Bodnar (1993).

The third group of fluid inclusions is related to the pegmatitic stage, which is free of mineralization. It is characterized by similar temperatures (300° to 390 °C) with the first ore stage, but variable salinities (6.9 to 8.9 wt% NaCl equiv and 34.7 to 58.5 wt% NaCl equiv). The composition of these fluids is dominated by NaCl and KCl documented by the first ice melting temperatures (T_e=-24.5° to -23.2°C), as well as by the presence of a second daughter mineral in the hypersaline fluids, possibly sylvite, in addition to halite. It is therefore most probable that these fluids were not related to the ore mineralization, although high salinity fluids can produce ore mineralization. They have a magmatic origin and are responsible for pegmatite formation, which is devoid of ore mineralization.

6. Conclusions

In the Eptadendro-Rachi ore district, a stratabound type mineralization hosted in meta-ultrabasic-basic rocks, probably of Jurassic age, was initially formed in a submarine environment. During Upper Cretaceous-Early Tertiary the intrusion of trondhjemites partly remobilized this mineraliza-

tion and contributed hydrothermal fluids to the formation of a vein-type mineralization. This mineralization was at least affected by a greenschist facies metamorphic episode during the Eocene-Oligocene.

Fluid inclusion data on gangue syn-ore quartz indicate that the ore mineralization was derived from hydrothermal fluids with low salinity (1.6 and 7.2 wt% NaCl equiv). Values of T_h from individual FIA vary from 300° to 380° C, with a peak at 330° C. These fluids represent the main ore stage of the vein type, which is related to the intrusion of the trondhjemites. A lower temperature ore stage, associated with the syn-ore calcite formation, is distinguished by a drop in T_h (210° to 260° C) and having similar salinities (3.2 to 6.3 wt% NaCl equiv) as the first group of inclusions. The composition of the fluids in these two stages is dominated by NaCl. A probable mixing of ascending hydrothermal fluids and downward migrating dilute meteoric waters generated the low salinity fluids.

Fluid inclusions in pegmatite quartz are characterized by temperatures from 300° to 390° C and variable salinities, 6.9 to 8.9 wt% NaCl equiv and 34.7 to 58.5 wt% NaCl equiv. The composition of these fluids is dominated by NaCl and KCl. They have a magmatic origin but probably they are not related to the ore mineralization.

Acknowledgments

Special thanks are due to Dr. H. Catchpole and Dr. K. Kouzmanov for carefully reviewing the manuscript and for their constructive comments and suggestions, resulting in significant improvements of this paper.

References

Ashworth K.L., Billet M.F., Constantinides D., Demetriades A., Katirtzoglou C. and Michael C., 1988. Base Metal Mineralization in the Evros Region, N.E. Greece. In: Base Metal Sulfide Deposits, Friedrich, G.H and Herzig, P.M. (eds), Springer-Verlag, Berlin-Heidelberg, 169-181.

Baziotis I., Mposkos E. and Perdikatsis V., 2008. Geochemistry of amphibolitized eclogites and cross-cutting tonalitic–trondhjemitic dykes in the Metamorphic Kimi Complex in East Rhodope (N.E. Greece): implications for partial melting at the base of a thickened crust. Int J Earth Sci (Geol Rundsch), 97, 459-477.

Bodnar R.J., 1993. Revised equation and table for determining the freezing point depression of the H_2O-NaCl solutions. Geochim. Cosmochim. Acta, 57, 683–684.

Bodnar R.J., 2003. Introduction to fluid inclusions. In: Fluid inclusions: analysis and interpretation, Samson, I., Anderson, A., and Marshall, D. (eds), Mineral. Assoc. Canada, Short Course, 32, 1-8.

Brown P.E., 1989. FLINCOR: A microcomputer program for the reduction and investigation of fluid inclusion data. Am. Mineral., 74, 1390-1393.

Chatzikirkou A. 2003 Study of the sulfide mineralization from Eptadendro and Rachi areas in Eastern Rhodope. Ph.D. Thesis, Aristotle University of Thessaloniki, 233p (in Greek with English abstract).

Chatzikirkou A. and Michailidis K., 2004. The Eptadendro and Rachi sulfide mineralization, Eastern Rhodope, Greece. Bull. Geol. Soc. Greece, 36, 397-405 (in Greek with English abstract).

Cline J.S. and Bodnar R.J., 1994. Direct evolution of brine from a crystallizing silicic melt at the Questa, New Mexico, molybdenum deposit. Econ. Geol., 89, 1780–1802.

Crawford M.L., 1981. Phase equilibria in aqueous fluid inclusions. In: Short course in fluid inclusions: applications to petrology, Hollister, L.S., and Crawford, M.L. (eds), 75-100.

Goldstein R., 2003. Petrographic analysis of fluid inclusions. In: Fluid inclusions: analysis and interpretation, Samson, I., Anderson, A., and Marshall, D. (eds), Mineral. Assoc. Canada, Short Course, 32, 9-53.

Goldstein R.H. and Reynolds T.J., 1994. Systematics of fluid inclusions in diagenetic minerals. SEPM Short Course 31, 199p.

Mposkos E. and Krohe A., 2000. Petrological and structural evolution of continental high pressure (HP) metamorphic rocks in the Alpine Rhodope Domain (N. Greece). In: Proceedings of the 3rd International Conference on the Geology of the Eastern Mediterranean (Nicosia, Cyprus), Panayides, I. et al. (eds), Geological Survey, Nicosia, Cyprus, 221–232.

Mposkos E., Perdikatsis V. and Liati A., 1989. Geochemical investigation of amphibolites from Eastern and Central Rhodope. Bull. Geol. Soc. Greece, 23, 413-427.

Nesbitt R.W., Billet M.F., Ashworth K.L., Deniel C., Constantinides D., Demetriades A., Katirtzoglou C., Michael C., Mposkos E., Zachos S. and Sanderson D., 1988. The geological setting of base metal mineralization in the Rhodope region, Northern Greece, In: Mineral deposits within the European Community, Boissonnas, J., and Omenetto, P. (eds), 499-514.

Potter R.W., Clynne M.A. and Brown D.L., 1978. Freezing point depression of aqueous sodium chloride solutions. Econ. Geol., 73, 284-285.

Ricou J.L., Burg J.P., Golfiaux I. and Ivanov Z., 1998. Rhodope and Vardar: The metamorphic and the olistostromic paired belts related to the Creataceous subduction under Europe. Geodin. Acta, 11, 285-309.

Roedder E., 1984. Fluid Inclusions. Rev Mineral, 12, 646p.

Shepherd T., Rankin A. and Alderton D., 1985. A practical guide to fluid inclusion studies. Blackie and Son, Glasgow, 239p.

Scientific Annals, School of Geology, Aristotle University of Thessaloniki Proceedings of the XIX CBGA Congress, Thessaloniki, Greece	Special volume 100	351-358	Thessaloniki 2010

A REVIEW OF AGE CONSTRAINTS OF EPITHERMAL PRECIOUS AND BASE METAL DEPOSITS OF THE TERTIARY EASTERN RHODOPES: COINCIDENCE WITH LATE EOCENE-EARLY OLIGOCENE TECTONIC PLATE REORGANIZATION ALONG THE TETHYS

Moritz, R.[1], Márton, I.[1], Ortelli, M.[1], Marchev, P.[2], Voudouris, P.[3], Bonev, N.[4], Spikings, R.[1] and Cosca, M.[5]

[1] *Section des Sciences de la Terre et de l'Environnement, University of Geneva, Rue des Maraîchers 13, 1205 Geneva, Switzerland, robert.moritz@unige.ch, istvan.marton@unige.ch, melissa.ortelli@unige.ch, richard.spikings@unige.ch*
[2] *Geological Institute of the Bulgarian Academy of Sciences, Acad. G. Bonchev Street, 1113 Sofia, Bulgaria, pmarchev@geology.bas.bg*
[3] *Department of Mineralogy-Petrology, University of Athens, GR-15784 Athens, Greece, voudouris@geol.uoa.gr*
[4] *Department of Geology and Paleontology, Sofia University St Kliment Ohridski, 15 Tzar Osvoboditel Bd., 1504 Sofia Bulgaria, niki@gea.uni-sofia.bg*
[5] *U.S. Geological Survey, Denver Federal centre, MS 963, Denver, CO 80225, U.S.A. mcosca@usgs.gov*

Abstract: The Tertiary Eastern Rhodopes are a major ore province within the Tethyan metallogenic belt. $^{40}Ar/^{39}Ar$ age data obtained in the past ten years are overviewed and discussed. It allows us to address some of the open questions and shed some new light on the sequence of ore-forming, magmatic and tectonic processes throughout the Eastern Rhodopes. Small to moderately sized ore deposits and prospects in the Rhodope Massif are hosted by high-grade metamorphic, continental sedimentary and igneous rocks. Sedimentary rock-hosted gold epithermal prospects are the earliest hydrothermal systems, hosted by Maastrichtian-Paleocene clastic rocks. Their $^{40}Ar/^{39}Ar$ ages vary between 37.55 ± 0.44 Ma and 34.71 ± 0.16 Ma, with the waning hydrothermal activity overlapping with the start of the oldest volcanism in the Eastern Rhodopes yielding $^{40}Ar/^{39}Ar$ ages ranging between 34.62 ± 0.46 Ma and 32.97 ± 0.23 Ma. Within a very short time between 32.13 ± 0.20 and 31.2 ± 0.4, Pb-Zn-dominated and Cu-Au-dominated epithermal prospects, respectively in the northern and the southern parts, were formed, and coincide with rhyolitic dikes emplaced at about 31.5 Ma. The Late Eocene-Early Oligocene post-orogenic magmatic and ore-forming evolution of the Eastern Rhodopes coincides with the time of collision at about 30-35 Ma of the African and Eurasian plates in the Caucasus and the Rif-Betic belts, when a dominantly subduction-dominated tectonic regime changed to a collision-dominated system, and the northward motion of the African plate slowed down, accompanied by an increasing southward slab retreat velocity in the Aegean Sea.

Keywords : epithermal, Cu-Au and Pb-Zn deposits, $^{40}Ar/^{39}Ar$ dating, Tertiary, Eastern Rhodopes

1. Introduction

The Tertiary Eastern Rhodopes are a major ore province within the Tethyan metallogenic belt (Fig. 1), with mining activities dating back to prehistoric times. Previous contributions (e.g. Arikas and Voudouris, 1998; Marchev et al., 2005) reported the characteristics of the different ore deposits and prospects, analyzed their fundamental relationships with magmatic and tectonic events, and discussed open questions related to ore-forming processes in the Eastern Rhodopes.

Some of the important debates about ore deposit genesis in the Eastern Rhodopes include the chronological relationship of epithermal ore formation between its northern, Bulgarian part, where magmatism has a more shoshonitic to high-K calc-alkaline nature and where epithermal deposits are dominated by Pb and Zn (Fig. 1: Spahievo, Madjarovo, Zvezdel), and its southern, Greek part (Fig. 1: Sappes, Perama, Kirki), where magmatism is predominantly calc-alkaline and the epithermal deposits are dominated by Cu and Au (Arikas and Voudouris, 1998; Marchev et al., 2005). A further debate relates to the nature of sedimentary rock-

hosted epithermal gold prospects located in Bulgaria, spatially associated with extensional detachment settings along exhuming gneiss-migmatitic domes (Fig.1: Ada Tepe, Rosino, Stremtsi), in particular whether there was any magmatic link during ore-formation in an area where ore deposits are otherwise typically associated to magmatic activity. Finally, Lescuyer et al. (2003), by comparing the similarity of the Bulgarian sedimentary rock-hosted prospect at Ada Tepe with the one at Perama in Greece along the Aegean Sea, partly hosted by sandstone (Fig. 1), also

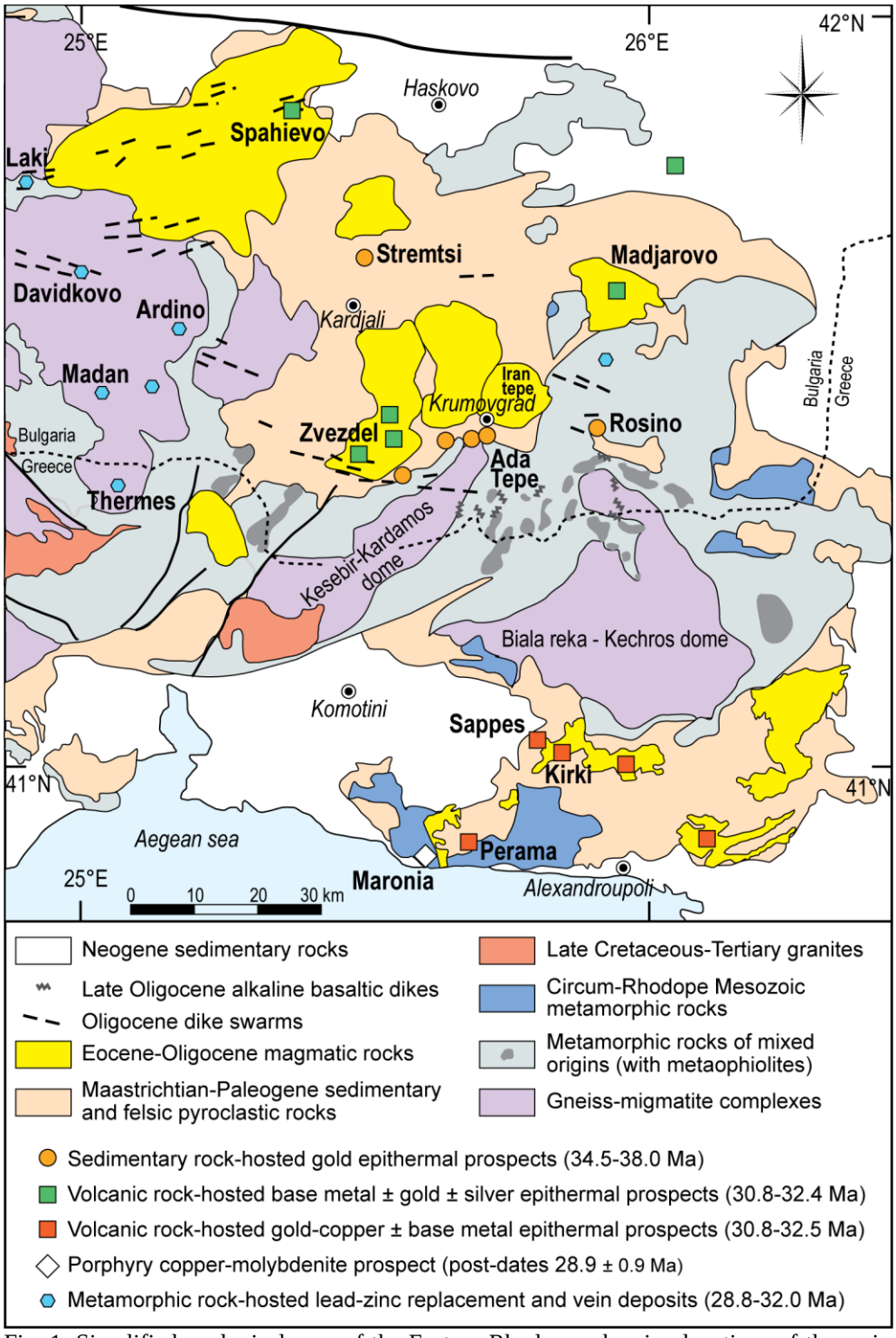

Fig. 1. Simplified geological map of the Eastern Rhodopes showing locations of the main epithermal and porphyry prospects and deposits (After Marchev et al., 2004b with additional information from Melfos et al., 2002, Marchev et al., 2005 and Voudouris, 2006).

opened the question about any possible genetic, temporal relationship among them.

Several new studies were undertaken recently in order to constrain some of the debates associated to the ore-forming processes in this province. In this contribution, we present an overview and discuss $^{40}Ar/^{39}Ar$ age data obtained over the past ten years, including data gathered more recently by a multidisciplinary research group focused on tectonics, magmatism, and ore deposit geology and geochemistry in the Eastern Rhodopes. This data set allows us to tackle the open questions mentioned above and permits to shed some new light on the sequence of ore-forming, magmatic and tectonic processes throughout the Eastern Rhodopes. In addition, we investigate the link of ore-formation in the Eastern Rhodopes with geodynamic changes, which occurred along the Tethys during the Late Eocene and Early Oligocene.

2. Regional geological and geodynamic setting

The Tertiary Eastern Rhodope Massif belongs to the Alpine-Himalayan orogenic belt and is interpreted as an accretionary complex, formed during Alpine convergence between the Adriatic-Apulian continental promontory of African affinity and the European Mosean plateform, within a north-dipping subduction system (Ricou et al., 1998). The evolution of the Rhodope Massif is commonly subdivided in two stages, including (1) a compressional stage, with thrusting and progressive thickening of the crust starting during Late Jurassic times (Bonev et al., in press), and culminating during the Middle Cretaceous (Burg et al., 1990), followed by (2) Late Cretaceous-Early Tertiary, syn- to post-orogenic collapse, as a result of unstability of the overthickened crust, which finally resulted in exhumation of deep metamorphic rocks along detachment faults (e.g. Bonev et al., 2006a), the formation of Late Eocene to Oligocene sedimentary basins filled with continental clastic rocks (e.g. Goranov and Atanasov, 1992), and widespread Late Eocene to Early Miocene basic to felsic magmatism (e.g. Arikas and Voudouris, 1998; Marchev et al., 2004a). The Palaeogene magmatism of the Central and Eastern Rhodopes culminated at about 30-35 Ma, and was accompanied by abundant ore-forming hydrothermal activity (Arikas and Voudouris, 1998; Marchev et al., 2005).

3. Major types of ore deposits and prospects of the Eastern Rhodopes

Small to moderately sized ore deposits and prospects in the Rhodope Massif are hosted by high-grade metamorphic, continental sedimentary and igneous rocks (Arikas and Voudouris, 1998; Marchev et al., 2005). The economically most significant ore deposits are Pb-Zn-Ag vein and marble-hosted replacement deposits of the Central Rhodopes within the Laki, Davidkovo, Ardino, Madan and Thermes ore fields (Fig. 1). They were formed between about 28.8 and 32.0 Ma, and are contemporaneous with the emplacement of felsic dike swarms, and are related to rapid tectonic and erosional denudation of metamorphic core complexes during late-orogenic collapse (Kaiser-Rohrmeier et al., 2004).

In the Eastern Rhodopes, epithermal deposits are hosted by volcanic centres of calc-alkaline, high-K calc-alkaline and shoshonitic composition. In the northern, Bulgarian part of the Eastern Rhodopes, epithermal deposits are Pb- and Zn-rich, with subsidiary Cu, Au and Ag, with predominantly intermediate-sulfidation fluid state characteristics, and are locally associated with low-grade Cu-Mo porphyry occurrences (Singer and Marchev, 2000; Marchev and Singer, 2002; Rice et al., 2007). The main ore districts are Spahievo, Madjarovo and Zvezdel (Fig. 1), which produced about 16.5 Mt of Pb-Zn ore during about 50 years (Marchev et al. 2005). A small gold mine remains in operation near Spahievo (Fig. 1). The epithermal deposits from the southern part of the Eastern Rhodopes located in Greece are characterized by Cu- and Au-enrichments with respect to the Bulgarian ones, and display gangue and ore paragenetic associations revealing high-sulfidation fluid states evolving progressively to later stage intermediate/low-sulfidation fluid states (Voudouris, 2006; Voudouris et al., 2006; Ortelli, 2009; Ortelli et al., 2009). They include the recently discovered Perama and Sappes prospects (Fig. 1; Michael et al., 1995; McAlister et al., 1999; Lescuyer et al., 2003).

A distinct group of epithermal gold-silver prospects, already mined during ancient times, are hosted by Maastrichtian to Paleocene syn-detachment, clastic sedimentary rocks overlying metamorphic basement rocks, located along the hanging-wall of detachment faults (Fig. 1: Ada Tepe, Rosino, Stremtsi; Marchev et al., 2004b; Bonev et al., 2006b; Noverraz et al., 2007; Márton 2009; Márton et al., 2010, submitted). The geometry of the epithermal prospects reveals both a lithological and a structural control. Ore formation was clearly associated with extensional tectonics

and with on-going supradetachment sedimentation. Ore deposition occurred variably as a consequence of boiling, fluid-rock interaction (fluid desulfidation) and fluid mixing, and explains the variation of paragenesis, geometry and other ore features among the sedimentary rock-hosted prospects. The sedimentary rock-hosted gold prospects display textural and mineralogical features characteristic of low-sulfidation deposits, although intermediate-sulfidation characteristics are also observed (Márton, 2009; Márton et al., submitted).

4. Overview of ages of major hydrothermal, tectonic and magmatic events since the Late Eocene

Figure 2 summarizes hydrothermal ore-forming, tectonic and magmatic events in the Eastern Rhodopes since the Late Eocene. Exhumation of gneiss-migmatite domes during crustal extension is the important process, which dominated the geological evolution of the Eastern Rhodopes during the Late Eocene, immediately before the onset of a sequence of diverse hydrothermal and magmatic events (Fig. 2). Retrograde metamorphism during exhumation with cooling muscovite ages were dated between 39.66 ± 0.47 and 39.28 ± 0.24 Ma in the Biala reka – Kechros dome, and between 38.13 ± 0.36 and 36.90 ± 0.36 Ma in the Keebir-Kardamos dome (Fig. 1; Bonev et al., 2006b, in press; Márton et al., 2010).

Sedimentary rock-hosted gold epithermal prospects are the earliest ore-forming events in various locations across the Eastern Rhodopes, and are hosted by Maastrichtian-Paleocene clastic sedimentary rocks at or close to the contact with underlying metamorphic basement rocks. Stremtsi (Fig. 1) yielded the oldest $^{40}Ar/^{39}Ar$ adularia age at 37.55 ± 0.44 Ma (Moritz et al. unpublished), and the youngest age was recorded for adularia from Ada Tepe, Bulgaria (Fig. 1) at 34.71 ± 0.16 Ma (Marchev et al., 2004b; Márton et al., 2010). The oldest volcanic event in the Eastern Rhodopes started at Iran Tepe, north of the town of Krumovgrad, Bulgaria (Fig. 1), and yields $^{40}Ar/^{39}Ar$ ages ranging between 34.62 ± 0.46 Ma and 32.97 ± 0.23 Ma, which overlap with one U-Pb zircon age obtained from the same location (Márton et al., 2010; Marchev et al., submitted).

Extensive shoshonitic and high-K calc-alkaline magmatic activity occurred at about 32 Ma (not shown in Fig. 2; see Singer and Marchev, 2000; Marchev and Singer 2002) throughout the northern Eastern Rhodopes and resulted in the formation of Pb-Zn dominated epithermal deposits at Madjarovo, Spahievo and Zvezdel, Bulgaria (Fig. 1), with $^{40}Ar/^{39}Ar$ ages between 32.13 ± 0.20 and 31.12 ± 0.35 Ma for epithermal ore formation (Singer and Marchev, 2000; Marchev and Singer, 2002; Marchev et al., 2005). At Spahievo (Fig. 1), an early, deeper porphyry Cu-Mo event yielded ages between 32.82 ± 1.06 and 32.61 ± 0.32 Ma (Singer and Marchev 2000). In the southern Eastern Rhodopes, near the Aegean Sea, porphyry-type Cu-Mo mineralization and Au-Cu±Pb±Zn epithermal ore formation in the Sappes-Kassiteres area, Greece (Fig. 1) occurred also during the Early Oligocene between 32.0 ± 0.5 and 31.2 ± 0.4 Ma (Ortelli, 2009) in an area dominated by calc-alkaline magmatism.

Rhyolitic dikes crosscutting the Kesebir-Kardamos dome (Fig. 1) yielded sanidine $^{40}Ar/^{39}Ar$ ages of 31.82 ± 0.20 and 31.27 ± 0.16 Ma (Marchev et al. 2004b; Marchev and Moritz unpublished), which overlap with epithermal ore-formation in the northern Madjarovo, Spahievo and Zvezdel and the southern Sappes-Kassiteres districts (Fig. 2). Magmatism is not so well constrained in the southern Eastern Rhodopes of the Greek territory. Rb-Sr and K-Ar geochronological data by Del Moro et al. (1988), Pècskay et al. (2003) and Christofides et al. (2004) show that magmatism also started during the Early Oligocene and continued until the Early Miocene (Fig. 2). A magmatic biotite $^{40}Ar/^{39}Ar$ age of a monzodiorite-diorite from Sappes-Kassiteres (Fig. 1) of 32.6 ± 0.5 Ma reported by Ortelli (2009; not shown in Fig. 2) confirms the Early Oligocene ages published by Del Moro et al. (1988), Pècskay et al. (2003) and Christofides et al. (2004).

5. Discussion and conclusions

The new $^{40}Ar/^{39}Ar$ age data obtained for the epithermal-porphyry system at Sappes-Kassiteres by Ortelli (2009) show that high- to intermediate/low sulfidation epithermal ore formation in Thrace, Greece was contemporaneous with epithermal ore-formation in Bulgaria at Spahievo, Madjarovo and Zvezdel (Fig. 2). The northern Pb-Zn-dominated epithermal prospects associated with shoshonitic to high-K calc-alkaline magmatism and the southern Cu-Au epithermal prospects located in a dominantly calc-alkaline magmatic area formed within a very short time interval between 32.13 ± 0.20 and 31.2 ± 0.4 Ma, and coincide with the emplacement of rhyolitic dikes within the Kesebir-Kardamos dome at about 31.5 Ma (Fig. 2).

Marchev et al. (2005) already discussed the genetic relationship of evolved silicic dikes and epithermal systems in the Bulgarian Eastern Rhodopes. The new age data for Sappes-Kassiteres (Ortelli, 2009) reveal that this genetic relationship is likely also the case for the epithermal deposits within the southern part of the Eastern Rhodopes, where rhyolitic dikes are spatially associated with a number

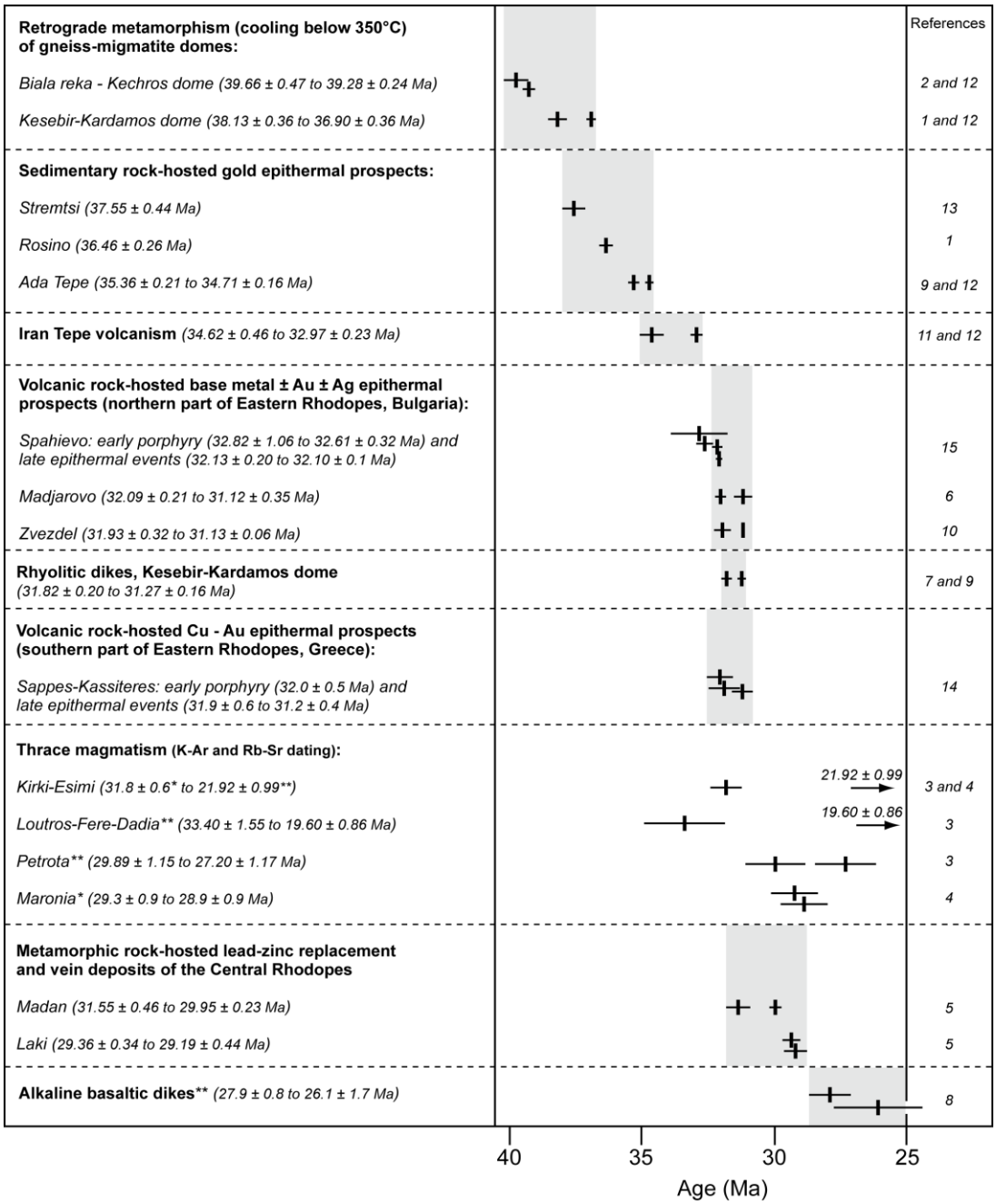

Fig. 2. Summary of the major tectonic, magmatic and ore-forming events in the Eastern Rhodopes since the Late Eocene. The data compilation shows absolute ages obtained by $^{40}Ar/^{39}Ar$ geochronology including 2s analytical errors, except when noted otherwise (see Thrace magmatism, Greece); *: Rb-Sr geochronology; **: K-Ar geochronology. For the sake of simplicity, if more than one age is available for a given location, then only the maximum and minimum ages are included in the figure. All ages are Ma. References: 1 – Bonev et al., 2006b; 2 – Bonev et al., in press; 3 – Christofides et al., 2004; 4 – Del Moro et al., 1988; 5 – Kaiser-Rohrmeier et al., 2004; 6 – Marchev and Singer, 2002; 7 – Marchev and Moritz, unpublished; 8 – Marchev et al., 1997; 9 – Marchev et al., 2004b; 10 – Marchev et al., 2005; 11 – Marchev et al., submitted; 12 – Márton et al., 2010; 13 – Moritz et al., unpublished; 14 - Ortelli, 2009; 15 – Singer and Marchev, 2000. See Figure 1 for locations.

of epithermal occurrences (e.g. Arikas and Voudouris, 1998; Voudouris et al., 2006; Ortelli, 2009; Ortelli et al., 2009). If one includes the ages of the early porphyry events in localities such as Spahievo, Bulgaria and Sappes-Kassiteres, Greece (Fig.1), it shows that ore-forming events started as early as 32.82 ± 1.06 Ma and 32.0 ± 0.5 Ma, respectively, thus yielding an overall ore-forming duration of about 3.5 m.y. throughout the entire Eastern Rhodopes for the volcanic-hosted Pb-Zn and Cu-Au epithermal and associated porphyry deposits. The long ore-forming time intervals recorded in each locality (e.g. Spahievo, Sappes-Kassiteres) reveal pulsed intrusive/volcanic and hydrothermal systems linked to the emplacement of multiple magmatic batches, because single porphyry-epithermal systems typically form only within 30 000 to 100 000 years (e.g. Harris et al., 2009).

The combined $^{40}Ar/^{39}Ar$ age data from the sedimentary rock-hosted gold epithermal prospects show that they constitute an independent hydrothermal system with respect to the volcanic rock-hosted epithermal deposits discussed above (Fig. 2). Based on the age data, formation of these hydrothermal systems also took place during an extended time of about 3.5 m.y., starting at Stremtsi at 37.55 ± 0.44 Ma and ending in Ada Tepe at 34.71 ± 0.16 Ma (Fig. 2). These deposits formed during on-going burial by supra-detachment, clastic sedimentary rocks, which was a process which could have supplied additional heat in addition to the one released from high geothermal gradients, typical for metamorphic core complex exhumation, necessary to sustain extensive ore-forming hydrothermal fluid circulation throughout the Maastrichtian-Paleocene sedimentary basins. The recent $^{40}Ar/^{39}Ar$ age data obtained by Márton et al. (2010) and Marchev et al. (submitted) reveal that the waning hydrothermal activity at Ada Tepe overlapped with starting volcanic activity at the Iran tepe centre (Fig. 2), located north of Krumovgrad (Fig. 1). This suggests that magmatism may have supplied heat, and possibly fluids and gold to the hydrothermal system as well. Nevertheless, this link is still not totally understood, because at other prospects, such as Rosino and Stremtsi (Fig. 1), contemporaneous magmatic activity remains to be demonstrated (Fig. 2). The absolute ages obtained so far (Fig. 2) indicate that the Bulgarian sedimentary rock-hosted systems at Ada Tepe, Rosino and Stremtsi (Fig. 1) have no genetic link with the partly sedimentary rock-hosted epithermal system of the Perama prospect, Greece (Fig. 1), as might be suggested by the comparison of Lescuyer et al. (2003), since the later prospect would be at least 3 m.y. younger than the Bulgarian ones.

The Late Eocene-Oligocene post-orogenic evolution of the Eastern Rhodopes coincides with the time of collision at about 30-35 Ma of the African and Eurasian plates in the Caucasus to the east and the Rif-Betic belts to the west, when a dominantly subduction-dominated tectonic regime changed to a collision-dominated system, and the northward motion of the African plate suddenly slowed down. In this locked subduction system, the southward slab retreat velocity increased in the Aegean Sea (Jolivet and Faccenna, 2000), from the Late Eocene trench position along the Eastern Rhodopes to the present-day position of the Hellenic Trench south of Crete (Jolivet et al., 2003 ; Jolivet and Brun, 2010). Thus, the roughly coeval, widespread formation over the entire Eastern Rhodopes of volcanic rock-hosted precious and base metal epithermal deposits, accompanied by minor porphyry mineralization at about 32 Ma, and preceded by sedimentary rock-hosted gold epithermal ore-formation in supra-detachment basins during exhumation of metamorphic core complexes, between about 38 and 34.5 Ma, coincides with major tectonic plate reorganization at the scale of the Tethys. The coincidence of ore formation in a short time interval in the Eastern Rhodopes and rapid geodynamic changes along the Tethys is analogous to other examples, where tectonic plate reorganization triggered major ore forming events (e.g. Cenosoic settings of southeast Asia and the West Pacific, Garvin et al., 2005). The prevailing extensional setting and geodynamic regime with a southward hinge retreat of the subducting plate also explains the small size of the porphyry systems in the Eastern Rhodopes, because formation of large porphyry systems is favoured in geodynamic settings characterized by slab flattening, contraction and crustal thickening (Cook et al., 2005; Sillitoe, 2008).

Acknowledgments

This study benefitted from financial support of the Swiss National Science Foundation (Grants 200020-101853 and 200020-113510) and the SCOPES program (IB7320-111046). We also would like to thank the support of Balkan Mineral and Mining (Dundee Precious Metals) and Cambridge Minerals Plc for support during field work, logistics, access to data and drilling material, and

for thoughtful discussions. Vasilios Melfos (Thessaloniki) and Kamen Bogdanov (Sofia) are thanked for their critical reviews.

References

Arikas K. and Voudouris P., 1998. Hydrothermal alterations and mineralizations of magmatic rocks in the southeastern Rhodope Massif. Acta Vulcanologica, 10, 353-365.

Bonev N., Burg J.P. and Ivanov Z., 2006a. Mesozoic-Tertiary structural evolution of an extensional gneiss dome - the Kesebir-Kardamos dome, E. Rhodopes, Bulgaria. International Journal of Earth Sciences, 95, 318-340.

Bonev N., Marchev P. and Singer B., 2006b. $^{40}Ar/^{39}Ar$ geochronology constraints on the Middle Tertiary basement extensional exhumation, and its relation to ore-forming and magmatic processes in the Eastern Rhodope (Bulgaria). Geodinamica Acta, 19, 265-280.

Bonev N., Spikings R., Moritz R. and Marchev P., in press. Evidence from the Kulidjik nappe for an early Alpine thrust tectonics in the Rhodope Massif, Bulgaria. Tectonophysics.

Burg J.P., Ivanov Z., Ricou L.E., Dimor D. and Klain L., 1990. Implications of shear-sense criteria for the tectonic evolution of the Central Rhodope Massif, southern Bulgaria. Geology, 18, 451– 454.

Del Moro A., Innocenti F., Kyriakopoulos K., Manetti P. and Papadopoulos P., 1988. Tertiary granitoids from Thrace (northern Greece): Sr isotopic and petrochemical data. Neues Jahrbuch für Mineralogie Abhandlungen, 159, 113-135.

Christofides G., Pècskay Z., Eleftheriafis G., Soldatos T. and Koroneos A., 2004, The Tertiary Evros volcanic rocks (Thrace, northeastern Greece): petrology and K/Ar geochronology. Geologica Carpathica, 55, 397-409.

Cook D.R., Hollings P. and Walshe J.L. 2005. Giant porphyry deposits: Characteristics, distribution, and tectonic controls. Economic Geology, 100, 801-818.

Garwin S., Hall R. and Watanabe Y. 2005. Tectonic setting, geology, and gold and copper mineralization in Cenozoic magmatic arcs of southeast Asia and the West Pacific. Economic Geology 100th anniversary volume, p. 891-930.

Goranov A. and Atanasov G., 1992. Lithostratigraphy and formation conditions of Maastrichtian-Paleocene deposit in Krumovgrad District. Geologica Balcanica, 22, 71–82.

Harris A.C., White N.C., Cooke D.R., Tosdal R.M. and Allen C.M. 2009. How fast can porphyry ore deposits form ? In: Proceedings of the 10th biennial SGA meeting, Townsville, Australia, August 2009, Williams, P. et al (eds), 279-281.

Jolivet L. and Facenna C. 2000. Mediterranean extension and the Africa-Eurasia collision. Tectonics, 19, 1095-1106.

Jolivet L. and Brun J.-P. 2010. Cenozoic geodynamic evolution of the Aegean. International Journal of Earth Sciences, 99, 109-138.

Jolivet L., Faccenna C., Goffé B., Burov E. and Agard P., 2003. Subduction tectonics and exhumation of high-pressure metamorphic rocks in the Mediterranean orogens. American Journal of Science, 303, 353-409.

Kaiser-Rohrmeier M., Handler R., von Quadt A. and Heinrich C., 2004. Hydrothermal Pb-Zn ore formation in the central Rhodopian dome, south Bulgaria: review and new time constraints from Ar-Ar geochronology. Schweizerische Mineralogische und Petrographische Mitteilungen, 84, 37-58.

Lescuyer J.L., Bailly L., Cassard D., Lips A.L.W., Piantone P. and McAlister M., 2003. Sediment-hosted gold in south-eastern Europe: the epithermal deposit of Perama, Thrace, Greece. In: Mineral exploration and sustainable development. Proceedings of the Seventh Biennal SGA Meeting, Athens 2003, Elioupoulos, D.G. et al. (eds)., 499-502.

Marchev P. and Singer B., 2002. $^{40}Ar/^{39}Ar$ geochronology of magmatism and hydrothermal activity of the Madjarovo base-precious metal ore district, eastern Rhodopes, Bulgaria. In: The timing and location of major ore deposits in an evolving orogen, Blundell, D. Neubauer, F. and von Quadt, A. (eds), Geological Society of London Special Publication, 204, 137-150.

Marchev P., Harkovska A., Pècskay Z., Vaselli O. and Downes H., 1997. Nature and age of the alkaline basaltic magmatism south-east of Krumovgrad, SE-Bulgaria. Comptes Rendus de l'Académie Bulgare des Sciences, 50, 77-88.

Marchev, P., Raicheva, R., Downes, H., Vaselli, O., Chiaradia, M., and Moritz, R., 2004a. Compositional diversity of Eocene–Oligocene basaltic magmatism in the Eastern Rhodopes, SE Bulgaria: implications for genesis and tectonic setting. Tectonophysics, 393, 301-328.

Marchev P., Singer B., Jelev D., Hasson H., Moritz R. and Bonev N., 2004b. The Ada Tepe deposit: a sediment-hosted, detachment fault-controlled, low-sulfidation gold deposit in the Eastern Rhodopes, SE Bulgaria. Schweizerische Mineralogische und Petrographische Mitteilungen, 84, 59-78.

Marchev P., Kaiser-Rohrmeier B., Heinrich C., Ovtcharova M., von Quadt A. and Raicheva R., 2005. Hydrothermal ore deposits related to post-orogenic extensional magmatism and core complex formation: The Rhodope Massif of Bulgaria and Greece, Ore Geology Reviews, 27, 53-89.

Marchev P., Kibarov P., Spikings R., Ovtcharova M., Márton I. and Moritz R., submitted. $^{40}Ar/^{39}Ar$ and U-Pb geochronology of the Iran Tepe volcanic complex, Eastern Rhodopes. Geologica Balcanica.

Márton I., 2009. Formation, preservation and exhumation of sedimentary rock-hosted gold deposits in the Eastern Rhodopes, Bulgaria. Ph.D. thesis, Terre et Environment, University of Geneva, 84, 163 p.

Márton I., Moritz R. and Spikings R., 2010. Application

of low-temperature thermochronology to hydrothermal ore deposits: formation, preservation and exhumation of epithermal gold systems from the Eastern Rhodopes, Bulgaria. Tectonophysics, 483, 240-254.

Márton I., Moritz R., Marchev P., Chiaradia M., Bonev N., Vennemann T., Kouzmanov K., Andrew C. and Hasson S., submitted,. Regional to local ore controls on the formation of Tertiary sedimentary rock-hosted gold deposits from the Eastern Rhodopes, Bulgaria. Economic Geology.

Melfos V., Vavelidis M., Christofides G. and Seidel E., 2002, Origin and evolution of the Tertiary Maronia porphyry copper-molybdenum deposit, Thrace, Greece. Mineralium Deposita, 37, 648-668.

McAlister M., Hammond J.M., Normand D. and Kampasakalis M. 1999. Discovery case history for the Perama Hill gold deposit, Greece. In: New generation gold mines '99, Case Histories of Discovery. Currie D., and Nielsen K. (eds),. Australian Mining Foundation Conference Proceedings, Perth, 39-49.

Michael C., Perdikatsis V., Dimou E. and Marantos I., 1995. Hydrothermal alteration and ore deposition in epithermal precious metal deposits of Agios Demetrios, Konos area, northern Greece. Proceedings, XV Congress of the Carpathian–Balkan Geological Association, Geological Society of Greece Special Publication 4, 778–782.

Noverraz C., Moritz R., Fontignie D., Kolev K., Marchev P., Vennemann T. and Spangenberg J., 2007. The Stremtsi gold prospect: a sedimentary rock-hosted, low sulphidation epithermal system in the Tertiary Eastern Rhodopes, Bulgaria. In: Digging deeper. Proceedings of the Ninth Biennal SGA Meeting, Dublin 2007, Andrew et al. (eds)., 141-145.

Ortelli O. 2009. Tertiary-Porphyry and epithermal association of the Sapes/Kassiteres district, Eastern Rhodopes, Greece. Unpublished M.Sc. thesis, University of Geneva, 87 p.

Ortelli M., Moritz R., Voudouris P. and Spangenberg J., 2009. Tertiary porphyry and epithermal association of the Sapes-Kassiteres district, Eastern Rhodopes, Greece. In: Proceedings of the 10th biennial SGA meeting, Townsville, Australia, August 2009, Williams, P. et al (eds), 536-538.

Pècskay Z., Eleftheriafis G., Koroneos A., Soldatos T. and Christofides G., 2003. K/Ar dating, geochemistry and evolution of the Tertiary volcanic rocks (Thrace, northeastern Greece). In: Mineral exploration and sustainable development. Proceedings of the Seventh Biennal SGA Meeting, Athens 2003, Elioupoulos, D.G. et al. (eds)., 1229-1232.

Rice C.M., McCoyd R.J., Boyce A.J. and Marchev P., 2007. Stable isotope study and the mineralization and alteration in the Madjarovo Pb-Zn district, south-east Bulgaria. Mineralium Deposita, 42, 691-713.

Ricou L.E., Burg J.P., Godfriaux I. and Ivanov Z., 1998. Rhodope and Vardar: the metamorphic and the olistrostromic paired belts related to the Cretaceous subduction under Europe. Geodinamica Acta, 11, 285-309.

Sillitoe R. H. 2008. Major gold deposits and belts of the North and South American Cordillera: Distribution, tectonomagmagtic settings, and metallogenic considerations. Economic Geology, 103, 663-687.

Singer B. and Marchev P., 2000. Temporal evolution of arc magmatism and hydrothermal activity, including epithermal gold veins, Borovitsa caldera, southern Bulgaria. Economic Geology, 95, 1155-1164.

Voudouris P., 2006. A comparative mineralogical study of Te-rich magmatic-hydrothermal systems in northeastern Greece. Mineralogy and Petrology, 87, 241-275.

Voudouris P., Tarkian M. and Arikas K. 2006. Mineralogy of telluride-bearing epithermal ores in the Kassiteres-Sappes area, western Thrace, Greece. Mineralogy and Petrology, 87, 31-52.

Scientific Annals, School of Geology, Aristotle University of Thessaloniki Proceedings of the XIX CBGA Congress, Thessaloniki, Greece	Special volume 100	359-367	Thessaloniki 2010

THE STRUCTURAL-METALLOGENIC MAPS OF ORE DISTRICTS OF F.Y.R. OF MACEDONIA

Volkov A.V.[1], Serafimovski T. [2], Alekseev V. Yu.[1] and Tasev G.[2]

[1]*Institute of geology of ore deposits, petrography, mineralogy and geochemistry of the Russian Academy of Science, IGEM RAS 119017, Staromonetny per., 35, Moscow, Russia, tma2105@mail.ru*
[2] *University "Goce Delcev"- Stip, faculty of natural and technical sciences of Institute of Geology, Goce Delcev 89, 2000, Stip, F.Y.R. of Macedonia, todor_s2000@yahoo.co.uk*

Abstract: The metallogenic characteristics, tectonic setting, and structure of F.Y.R. of Macedonian territory, Kozuf-Aridea and Kadica-Bucovic ore districts and its specific formation features are discussed in this paper on the basis of new results and data obtained by previous investigations. The interpretation of satellite images and morphostructural analyses were employed successfully for revealing the ore-concentrating structural features. The tectonic elements of the present-day topography were marked out and compared with the structural features that existed during the period of ore formation. The use of the present-day structural landforms of F.Y.R. of Macedonia for reconstruction of the tectonic elements of ore-bearing periods became possible after substantiating their inherited evolution. The ring structure occupies a special position in southern F.Y.R. of Macedonia and ore districts are controlled. Geological, geochemical, and morphostructural attributes allow interpretation of this structure as a center of long-term endogenous activity that evolved since the Jurassic-Cretaceous time.

Keywords: structural-metallogenic maps, morphostructural analysis, ore district, F.Y.R. of Macedonia, fault zones.

1. Introduction

The structural-metallogenic maps are traditionally a result of studying tectonics and metallogeny of large regions. In the Laboratory of Metallogeny of Ore Districts of IGEM RAS, various complex methods for verifying the geological structures in relation to metallogenetic ore districts on maps of 1 : 50 000, 1 : 200 000 and 1 : 500 000 scales are developed (Tomson et al., 1992; Volkov et al., 2006a).

When drawing up structural-metallogenic maps of orogenic districts, first of all, it is necessary to allocate potentially the ore-bearing structures, and the relation with the tectonic-magmatic episodes with the formation of ore mineralization. Recently, a Russian-F.Y.R. of Macedonian scientific team has carried out a comprehensive study of F.Y.R. of Macedonian territory, including Kozuf-Aridea and Kadica-Bucovic ore districts, under the agreement between the faculty of Geology and Mining of Stip, F.Y.R. of Macedonia, and the IGEM RAS.

2. Methods of map construction

The morphostructural analysis and the interpretation of satellite images are the most important methods of revealing the arch raisings. The methods of studying the relief become very effective in the paleoreconstructions of the inherited development of arch raisings. With the help of the interpretations of tectonic elements of a modern relief, the radial and concentric systems are the main indicators of arch raisings (Figs 1 and 2). Besides, for this purpose, interpretations of geochemical and geophysical data are also used. The various elements of the maps are important in discovering new metallogenic ore districts: intrusive-dome structures of various types reaching a diameter of 100 km, and break "through" zones, as systems of geological and tectonic anomalies (Fig. 3). Intrusive-dome structures are allocated with the same methods, as arc raisings. They are characterized by the radial-concentric forms of a relief created by complex combinations of new tectonic raisings and hollows, fixing intrusive-dome structures and depressions. In satellite pictures the break "through" zones are distinguished by linear anomalies of photo-tones. At the final stage, the special metallogenic analyses will be carried on, which will be based on the discrimination of the ore-formations ore

complexes and series, which are in space and time with the certain types of arch raisings, intrusive-dome structures and break “through" zones (Fig. 3). In addition the nature of metallogenic provinces related to tectonic structures of mineralization will be especially studied.

tural features, including superimposed ring and graben-like depressions, were outlined on the basis of interpretation of satellite images and morpho-structural analyses. The F.Y.R. of Macedonian Arch, which practically embraces the whole country, was recognized together with “daughter” ring

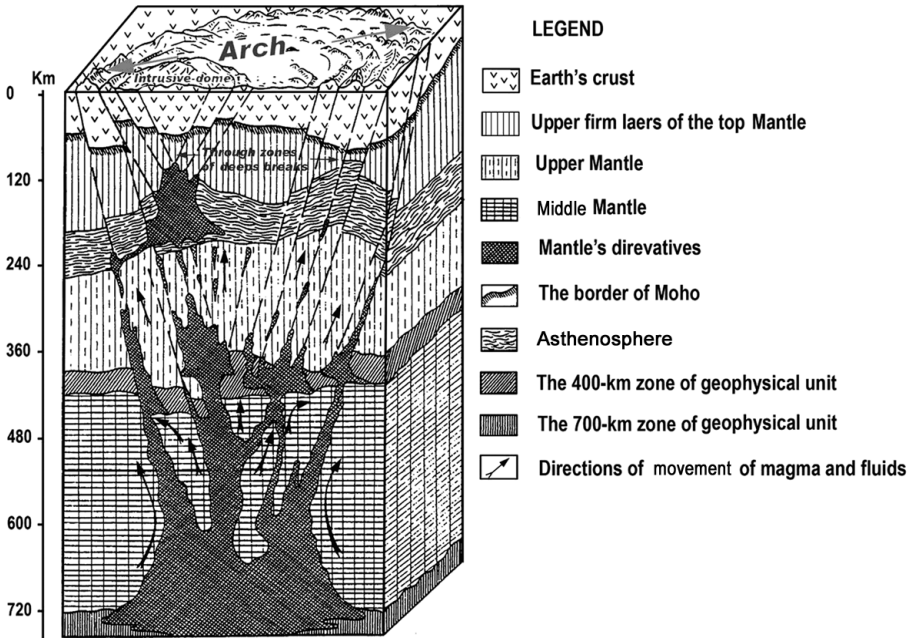

Fig.1. Genetic model of orogenic arched structure (Soloviev, 1978).

3. The structural-metallogenic map of the Republic of F.Y.R. of Macedonia

The F.Y.R. of Macedonia is located in the Serbo–Macedonian Massif of the Eurasian Tethys metallogenic belt (Fig. 4). The mineralizations are related to Cenozoic magmatic activity which is represented by volcanic and plutonic rocks in a dispersed spreading setting (Jankovic, 1993). Our previous joint studies with F.Y.R of Macedonian geologists concluded that the present-day tectonic structure of F.Y.R. of Macedonia reflects dislocations closely related to Cenozoic magmatism, which are connected with the formation of ore deposits (Tomson et al., 1998). A considerable part of the study area (Fig. 4) belongs to the Serbo-Macedonian and Pelagonian crystalline massifs separated by the Mesozoic Vardar Graben and to the reworked margins of these massifs: the West and East F.Y.R. of Macedonian margins, which were reactivated during Caledonian-Hercynian times and the Cenozoic, respectively.

According to our joint studies, F.Y.R. of Macedonia comprises fold-block systems, as well as superimposed and through-type structural features. A new structural work on the ore-controlling structures and through fault zones with important ore-controlling implications (Kochneva et al., 1997; Tomson et al., 1998).

In the present-day topography, the Cenozoic arched structure (250 x 300 km) has an oval to rounded shape. Its central part is relatively subsided (down to 1000-1500 m) and filled with Upper Cretaceous, Paleocene and Quaternary sedimentary rocks. The marginal part of the F.Y.R. of Macedonian Arch is uplifted to a height of 2000-2800 m on average. The dislocations within the arch are emphasized by the radial arrangement of the main tributaries of the Vardar River, which crosscut this structure. The main structural features of the arch are reflected in the isometric zoning of the anomalous gravity field: the central maximum is encircled by ring zones of gravity minima.

The comparison of the present-day structural features of the territory with geological and paleo-structural data shows that the main features of the F.Y.R. of Macedonian Arch are traceable since the Caledonian time. The presence of geological units of different ages suggests that the marginal belt of the arch, which consists of volcanic rocks and includes the largest ore deposits, is the most active

and long-lived part. Noteworthy is the widening of the marginal belt at the contrary of "daughter" ring structures of the second rank, as is observed in the vicinity of the Kratovo-Zletovo, Taimishte, and Alshar deposits (Fig. 4).

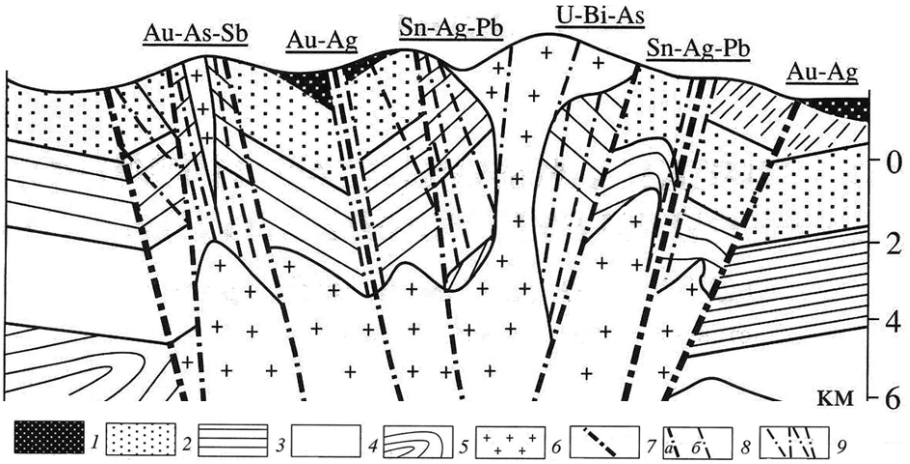

Fig. 2. Geological schematic section of the Maisk ore district showing an intrusive-dome structure of the Central Chuckotka, Russia. 1 - Relicts of volcanic rocks (Upper Cretaceous); 2 - Upper Triassic flysch sandstone-aleurolite deposits; 3 - Middle Triassic terrigenous aleurolite members; 4 - Lower Triassic greenschist members; 5 - Paleozoic terrigenous-carbonate basement rocks; 6 - Upper Cretaceous granite; 7 - Boundaries of the tectono-magmatic metallogenic zone; 8 - Deep-seated faults of the tectono-magmatic zone; 9 - Ore-localizing faults zones.

The Cenozoic reactivation involved mainly the eastern part of the F.Y.R. of Macedonian Arch (Tomson et al., 1998) and is reflected in the formation of the two faulting systems: NW-trending fault system relative to the Vardar Zone and the NE-trending transverse fault zones, which were active at the final stage of magmatic activity. Three NW-trending systems that control graben-shaped troughs, filled with Cenozoic sedimentary rocks, and one NE-trending fault zone, have been outlined from the interpretation of satellite images. Chains of local concentric central-type structures, many of which correspond to outcrops of Tertiary igneous rocks, are present along these NW- and NE-trending zones. The northwestern system controls the Cenozoic metallogenic zones (Fig.4).

The special implication of meridional fracture zones for localization of large ore deposits has been demonstrated by many researchers. Tomson et al. (1998) traced such meridional ore-controlling systems throughout Europe. The active role of such systems in localization of ore deposits was pointed out in neighboring Bulgaria (Vaptsarov et al. 1986). It is notable that such intersections provide zones of maximal permeability and cause ascent of mantle material. All economic deposits of F.Y.R. of Macedonia: Kratovo-Zletovo, Sasa-Toranica, Buchim, Taimishte, Rzanovo, and Alshar are controlled by such meridional zones.

The Oligocene-Miocene metallogenic zones recognized in the metamorphic sequences of the Serbo-Macedonian Massif are largely composed of Cenozoic tuffaceous-sedimentary and volcanic rocks and intruded by granitoid bodies and intermediate dikes. In total, three metallogenic zones make up an ore belt that extends westward to Serbia and southeastward to Greece and Bulgaria (Fig. 4). The characteristics of the metallogenic zones change and the igneous complexes and ores become progressively younger from southwest to northeast. There is a distinct correlation between age and composition of the ores. In addition, the ore mineralization changes in this direction from high- to low-temperature and from relatively low-sulfide to polysulfide types. The change in the ore composition may be associated with differentiations in the deep-seated magmatic chambers. Across the strike of metallogenic zones, the types of ore deposits change from magnetite skarn (Damian) to porphyry copper (Buchim) and further to copper-base metal (Kratovo-Zletovo) and base metal deposits (Sasa-Toranica). The age of the igneous rocks in the ore districts also changes towards the northeastern direction from 28.0-24.5 Ma (Buchim) to 27.2-16.0 Ma (Kratovo-Zletovo) and 24-12 Ma (Sasa-Toranica). Thus, the progressive change in the composition of the ore minerali-

zation is a consequence of rejuvenation and differentiation. These relationships suggest that there is a close link between the metallogenic zones.

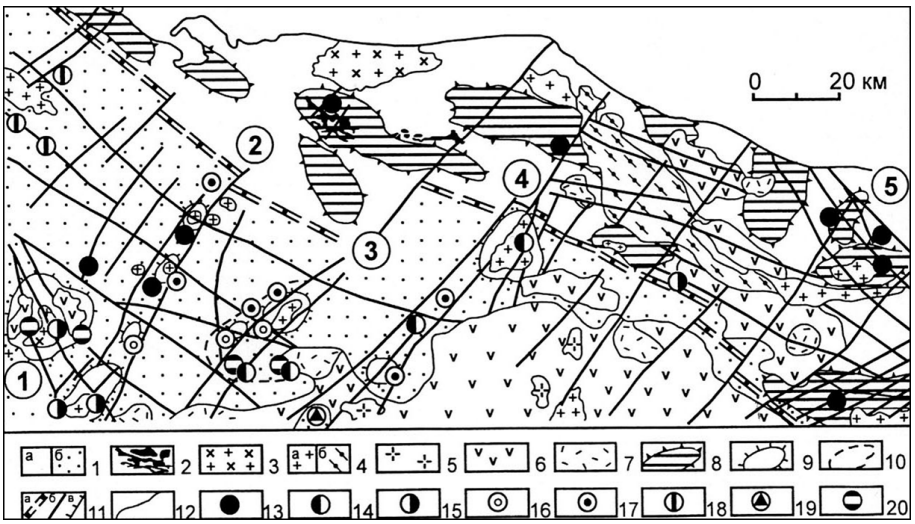

Fig. 3. Structural-metallogenic map of the Central Chukotka ore district. 1 – Mesozoic terrigenous sedimentary rocks (a), Paleozoic terrigenous-carbonaceous sedimentary rocks (b); 2 – Triassic dykes and sills of gabbro-diabase; 3 – Cretaceous granodiorites ; 4 - Cretaceous granites (a), granito-gneisses (b); 5 – Upper Cretaceous syenites, rhyolite-porphyries; 6 - Cretaceous andesite; 7 - Upper Cretaceous ignimbrite ; 8 - nucleus of Paleozoic tectonic raisings; 9 - intrusive-dome structures and separate domes; 10 – Maisk intrusive-dome structures; 11 - faults: a - Kuvet deep fault, b - slip-shifts, c - thrust; 12 - geological and geographical borders; 13 - 20 - deposits and occurrences: 13 – Au-quartz, 14 – Au-intrusion-related, 15 – Au-Ag-epithermal, 16 – Au-sulphidic disseminated, 17 – Sn-Ag-sulphidic, 18 - Sn-silicate, 19 – Cu-Mo-porphyry, 20 - Hg; *Figures in circles* – metallogenic zones: 1 - Palian; 2 -Karpung, 3 - Maisk; 4 - Matenvunay; 5 - Ruveem.

A model of this system at a depth may be viewed as a low-angle common seismic focal zone inclined southwestward (Tomson et al., 1998). The hypothetical focal zone could have served as a feeding channel for injection of magmas towards in northeast direction. Each new portion of magma and associated ore mineralization experienced compositional differentiation at a certain level of the seismic focal zone. The hanging wall of the zone moved southeastward. Particular blocks were detached along impaired zones with formation of grabens. The deep faults that bound the grabens could have reached the magmatic channel of the seismic focal zone to provoke the eruption of magmas and to stimulate ore formation.

The Kozuf-Aridea ore district which hosts a Pliocene mineralization, extends along the Greek - F.Y.R. of Macedonian border and is a significant ore deposit in southern F.Y.R. of Macedonia (Fig. 4). Volcanic structures and subvolcanic calc-alkaline intrusions are confined to NE-trending neotectonic faults. Igneous rocks are represented by calc-alkaline andesite and quartz latite. All subvolcanic intrusions of the Kozuf district are of the same age; intrusions at the Alshar deposit belong to the youngest phase, dated at 5.1-3.9 Ma (Boev and Serafimovski, 1998). The Kozuf-Aridea metallogenic zone is characterized by the development of a complex Au-As-Sb-Tl mineralization.

It is known that metallogenic zones in orogenic domains of fold systems are linear and oriented in two directions: along the strike of sedimentary sequences and across them. The metallogenic zones conformable with folding control plutonic bodies and deposits of the early orogenic stage, while the transverse metallogenic zones are accompanied by late orogenic mineralization and magmatism (Tomson and Polyakova, 2000). Thus, the system of northwestern zones in the F.Y.R. of Macedonian Arch may be referred to the early orogenic structural features, whereas the transverse Kozuf-Arid Zone is related to the late orogenic stage.

The Kadica–Bukovik ore district is located in the easternmost Surdulica–Osogovo–Pasos metallogenic zone characterized by the wide development of lead–zinc mineralization (Fig. 4). The zone incorporates systems of sheeted bodies and discordant dikes of quartz latites with an absolute age within 24–12 Ma. Recent discovery of the gold-bearing porphyry copper mineralization in the eastern Kadica ore district is inconsistent with its metallogenic specialization and previous metallogenic models of this belt (Tomson et al. 1998). To study this phenomenon, we carried out complex studies, which involved structural–geomorphological analysis of the ore district (Volkov et al., 2006a) and thermobarogeochemical study of the ore forming conditions.

4. Tectonic setting of the Carlin type Alshar deposit

The Pliocene volcanic-plutonic complex of calc-alkaline rocks of the Kozuf-Arid Zone was formed on a basement of Precambrian gneisses, Triassic sedimentary rocks (dominant), Jurassic ophiolites (gabbro-peridotite), and Cretaceous sedimentary sequences. The Precambrian albite gneiss with sporadic lenses of amphibolites forms the oldest rocks of the Kozuf-Arid Zone. Marble blocks are sporadically incorporated in gneiss. Paleozoic schist, phyllite, metasandstone, shale, and quartzite occur locally. The Triassic sequence occupies most of the area and is composed of two main facies: (1) limestone and dolomite and (2) mudstone and sandstone with sporadic dolerite and greenschist. The Jurassic sequence consists of limestone, sandstone, shale, quartzite, cherty shale, and a severely serpentinized dunite-harzburgite complex that hosts small podiform chromite bodies. Serpentinite is exposed as narrow tracts that have tectonic boundaries with the adjacent rocks. Their emplacement is related to diapiric processes. The Cretaceous sedimentary rocks are include Barremian-Albian conglomerate and Turonian limestone. The Upper Eocene sequence is composed of basal conglomerate overlain by flysch (siltstone, clay, and sandstone with limestone interbeds). Pliocene sedimentary and pyroclastic rocks are widespread around the Alshar deposit. They are composed of conglomerate and clayey sandstone with calca-

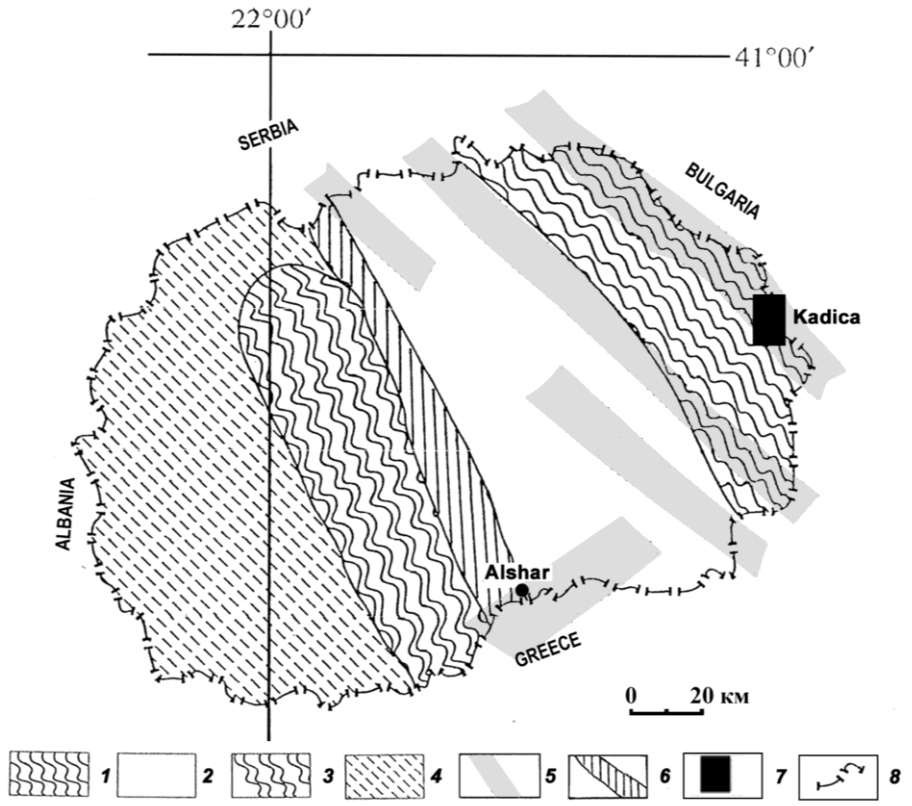

Fig. 4. Geotectonic units of F.Y.R. Macedonia. 1 - Serbo-Macedonian Massif; 2 - riftogenic Vardar Zone; 3 - Pelagonian Zone; 4 - West F.Y.R. of Macedonian region; 5 - Cenozoic metallogenic zones; 6 - Vardar metallogenic zone; 7 – Kadica–Bukovik area; 8 - F.Y.R. of Macedonian border.

reous clay interbeds. Volcano-sedimentary and pyroclastic rocks and clayey sandstone occur in some Pliocene basins north of the Alshar deposit. Quaternary sedimentary rocks form river terraces.

The Alshar deposit is located at the intersection of the Vardar and Kozuf-Arid metallogenic zones (Fig. 4) at the western flank of the Vardar Graben and the Pelagonian crystalline massif, approximately 50 km southwest of the town of Kavadarsi and 3 km from the Greek-F.Y.R. of Macedonian border. The ore field occupies an area of around 21 km^2. The tectonic setting of the ore district and the Alshar deposit itself was deduced from the results of morphostructural analyses and the interpretation of satellite images. First, the present-day structural grain of southern F.Y.R. of Macedonia was outlined. For this purpose, the traditional method of morphotectonic contour lines was used to generalize the topographic contour lines and drainage pattern. Structural features of different ranks were contoured from the analysis of present-day landforms of several orders.

The Alshar deposit is located in the upper flow of the Rozdenska River (the right tributary of the Crna River). The streams in the Rozdenska River basin form a radial-centripetal pattern (Fig. 5). The branched radial rivers and creeks are surrounded by arcuate ridges up to 1500-1800 m in height with arcuate valleys along their outer framework. Such an orographic pattern fits an endogenic ring structure 18 x 15 km in size with a relatively subsided inner part and an elevated outer belt. This ring structure is located at the intersection of two extended diagonal through fault zones: the northwestern zone, which is an element of the Vardar Zone and the northeastern zone deduced from linear shade anomalies in satellite images. This fault zone is emphasized by the rectilinear valley of the Bosavica River, by the present-day slope elements, and by a chain of dome-shaped structural features up to 10 km across. In addition, a system of very NE-trending young faults controls the Pliocene lava flows here. The Alshar ring structure is surrounded by a belt of daughter domes up to 5 km across. Each of these domes is comparable with associated ore-bearing central-type structures (Fig. 5). The three second-order domes located in Greece, south of the Alshar ring structure, are characterized by most complex structure and are contrastingly expressed in the present-day topography. By analogy with other regions studied previously (Figs 2 and 3), such structures control large ore districts and deposits (Volkov and Sidorov, 2001). The tectonic position of the Alshar deposit is emphasized by the configuration of geochemical ha-

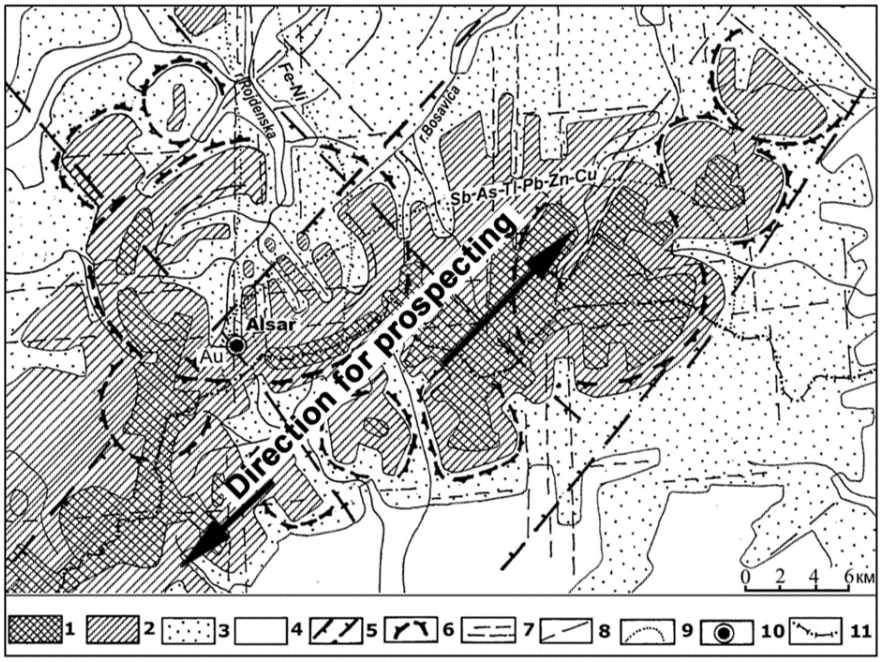

Fig.5. Structural-metallogenic map of the Kozuf-Aridea area and Alsar Carlin type deposit. Hypsometric levels: 1 - 1500-2000 m; 2 - 1000-1500 m; 3 - 500 -1000 m; 4 - lower than 500 m; 5 - zones of diagonal dispositions; 6 - borders of ring structures; 7 - deep orthogonal breaks; 8 - other breaks; 9 - geochemical anomalie; 10 – Alsar deposit; 11 - F.Y.R.O. Macedonian border.

los. A Fe-Ni halo extends along the Vardar Zone and an Sb-As-Tl-Pb-Zn-Cu halo corresponds to the young NE-trending fault system that crosses the Oligocene and Miocene metallogenic zones (Fig. 5). According to Jankovic (1993), the extensive and wide meridional fracture zone, which spreads radially relative to the center of the ring-structure, serves as a main ore-controlling tectonic line. We also traced a latitudinal fault zone, which is the fragment of an extended system interpreted in a satellite image.

The data obtained (Percival et al., 1990; Volkov et al., 2006b) show that the gold mineralization at the Alshar deposit is similar to that observed at the Carlin-type deposits in the western United States. Similar characteristics include: 1) the Au-As-Sb-Tl-Hg geochemical assemblage, 2) low Pb, Zn, Cu, and Ag contents in the ore, 3) widespread jasperoid and argillic metasomatic alterations of host siliciclastic-carbonate sedimentary rocks, and 4) the spatial relationship with fault zones. However the Alshar deposit differs from the Carlin-type deposits by the following features: 1) the Pliocene age of the mineralization, 2) extension of mineralization over younger volcanic rocks, 3) a high Tl grade in the ore, and 4) location of the ore field in a long-lived central-type magmatic structure (Fig. 5).

5. Tectonic setting of the Kadica Cu-porphyry ore field

Copper mineralization near the town of Pehchevo was recently discovered and preliminarily estimated. The Kadica deposit is found at the contact between Neogene quartz latites and the volcanosedimentary rocks of the Vlasina Group. Based on its characteristics, it is classified as a porphyry-Cu type, although some of the ore minerals and the wall-rock alteration are also typical for epithermal deposits (Volkov et al., 2006c). The Kadica–Bukovik ore district is located at the upper reaches of the Bregalnica, Pechevska, and Celevich rivers. The waterways form two systems: a centrifugal system in the upper flow of the Bregalnica River and a centripetal system in the Kadica plain. The northern part of the area represents moderate mountains (altitude up to 1700–1900 m). The relatively lower, southern part (up to 1000–1300 m) is crosscut by a wide sublatitudinal valley and numerous small water flows flowing into the main riverbed. From the north and east, the relatively lowered part of the area is surrounded by an arcuate ridge with an altitude ranging from 1600 to 1700 m. Radial-centripetal and radial-centrifugal patterns of waterflows in both the uplifted and lowered parts, make it possible to distinguish the intersecting oval southern (11 x 8 km) and northern (7.5 x 6 km) structures (Fig. 6). Altitude marks, erosion reworking, and alluvium accumulation, which are typical of the morphology of valleys and slopes, indicate a descending evolution of the southern oval and an ascending of the northern oval. Intersection of distinguished ovals is complicated, forming a ring structure with a diameter of 3.5 km. The central part of this structure coincides with the autonomous Bukovik Uplift elevated up to 1700 m. The most uplifted part of the Bukovik structure contains large occurrences of Pliocene volcanic rocks. The uplift is bounded by a ring depression belt, which is emphasized by arcuate valleys of the upper flows of the Celevich, Pechevska, and Rakovec rivers (Fig. 2). In the east, the structure is rimmed by an arcuate uplift 1700–1900 m high. It was found that the distinguished group of ring structures is localized at the intersection of two metallogenic zones: the base metal Surdulica–Osogovo–Pasos zone and the auriferous Kuzuf–Arid zone. The latter zone extends from the Alshar gold deposit (Percival and Radtke 1994) and contains Pliocene mineralization along the entire zone (Fig. 6). The Kuzuf–Arid metallogenic zone occupies a specific position at the southern end of F.Y.R. of Macedonia (Fig. 4). In addition to the Alshar deposit, this zone contains several Sb–As–Au-bearing mineralizations, porphyry copper deposits, and native sulfur occurrences. The intersection of the two aforementioned zones has a complex structure. For example, the Bukovik ring structure is located exactly at the junction of orthogonal fault systems revealed by linear tectonic elements of the modern relief. Meridional dislocations are traced as highly fissured belts, deciphered on the satellite images and expressed as accumulations of small linear elements of relief in the topographic map. Numerous latitudinal systems are emphasized by tectonic scarps, bends of large rivers, and modern graben-like depressions.

6. Conclusions

Our studies show that the Alshar deposit is confined to the central part of a ring structure, located at the intersection of two large diagonal fault zones, which host ore mineralizations of different ages. The deposit occupies a special structural position within southern F.Y.R. of Macedonia. Geological and morphostructural investigations indicate that this structure represents a center of long-

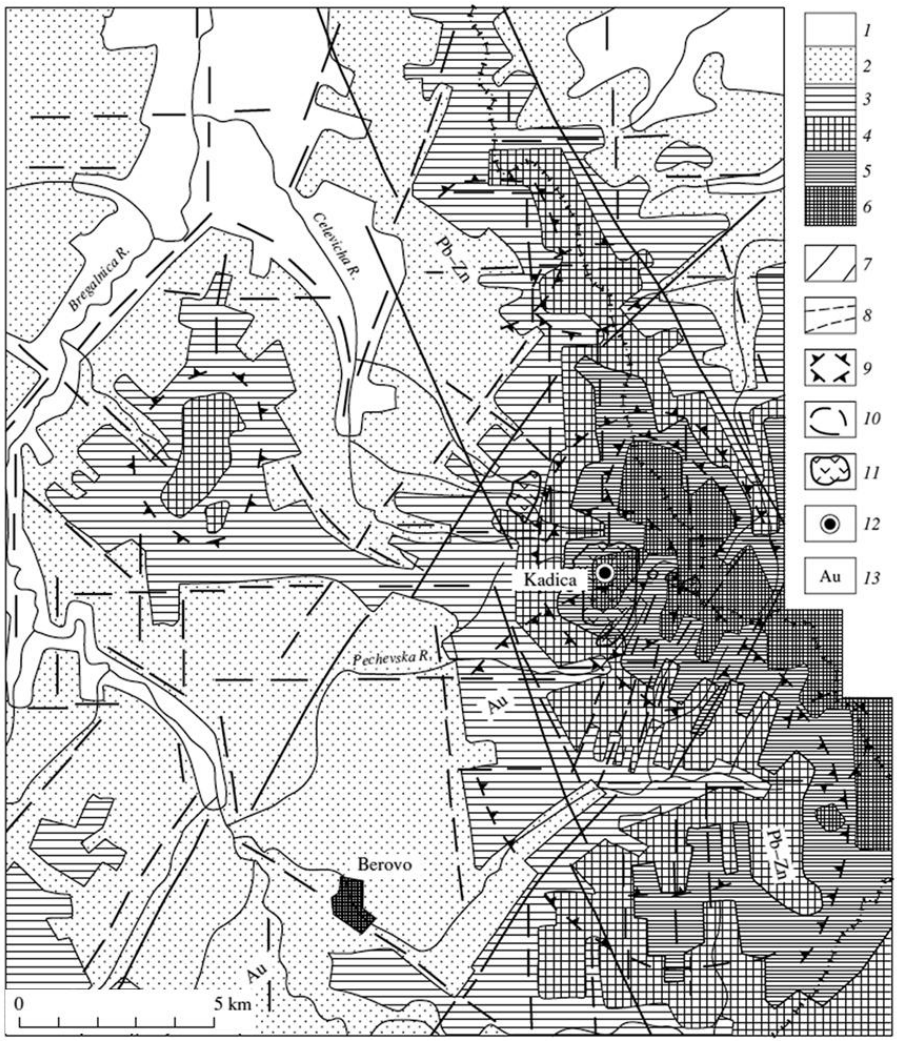

Fig. 6. Morphostructural scheme of the Kadica–Bukovik area. 1–6 - Hypsometric levels (m): 1 - below 800; 2 - 800–1000; 3 - 1000–1200; 4 - 1200–1500; 5 - 1500–1700; 6 - above 1700; 7 - metallogenic zones; 8–10 - structures deciphered from topographic maps and satellite images; 8 - linear dislocations, 9 - boundaries of ring structures, 10 - ring dislocations; 11 - outcrops of Pliocene volcanic rocks, 12 - Kadica deposit, 13 - specialization of metallogenic zones.

term endogenous activity, which started in the Jurassic–Cretaceous and evolved during subsequent periods. The Kadica ore field also occupies a specific structure position within Eastern F.Y.R. of Macedonia. It is confined to the central part of the ring structure, situated at the junction of two large orthogonal fault zones and corresponding to metallogenic zones of different ages (the base metal Surdulica–Osogovo–Pasos and the auriferous Kuzuf–Arid). The Kadica ore field is a promising area for the discovery of gold mineralization.

Acknowledgments

This study was supported by the Russian Foundation for Basic Research (project no. 08-05-00135a) and Program no. 2 "Evolution of the Lithosphere, Metallogenic Provinces…,"of the Division of Earth Sciences, Russian Academy of Sciences.

References

Boev B. and Serafimovski T., 1996. General Genetic Model of the Alshar Deposit. Proceeding of the Annual Meeting on IGCP Project 356 (Sofia), 1, 75-84.

Jankovic S., 1993. Metallogenic Features of the Alshar Epithermal Sb-As-Tl-Au Deposit. N. Jb. Miner. Abh. November, 25-41.

Kochneva N., Stojanov R., and Boev B., 1997. A Neogene's Orogenic Tectonic of East Macedonia (with Use of Morphostructural Analysis). Proceeding of Symposium. Stip-Dojran, 119-123.

Percival T. J., Radtke A. S. and Jankovic S. R., 1990. Gold Mineralization of the Carlin Type in the Alshar District, Macedonia, Yugoslavia. Proceeding of the

Eight Quadrennial IAGOD Symposium (Ottawa), 637-646.

Percival, T. J., Radtke, A., 1994, Sedimentary rock-hosted disseminated gold mineralization in the Alshar district, Macedonia // Canad. Mineralogist. 32: 649-655.

Soloviev V.V., 1978. Structures of Central type of territory of the USSR on geomorphologic data's. Leningrad, Nauka, 110 p.

Tomson H.N., Kravtsov V.S. and Kochneva N.T., 1992. Metallogeny of Orogens. Nedra, Moscow, 480 p.

Tomson H. N. and Polyakova O. P., 2000. Formation Succession and Direction Metallogenic Zone Migration with Reference to the Primorye Orogen, Dokl. Earth Sci. 375 (8), 1225-1228.

Tomson H. N., Serafimovski T., and Kochneva N. T., 1998. Cenozoic Metallogeny of Eastern Macedonia. Geol. Ore Deposits 40 (3), 175-183.

Vaptsarov K., Mishev N. and Kochneva N. T., 1986. Tectonic Elements in Present-Day Topography of Southern Bulgaria and the Recognition of Superimposed Deep Structures. Geology of the Balkans (Sofia), 3-19.

Volkov A. V. and Sidorov A. A., 2001. Unique Gold-Ore district in Chukchi Peninsula (SVKNII, Magadan) 180 p.

Volkov A. V., Serafimovski T., Kochneva N. T., Tasev G. and Tomson H. N., 2006a. The structural-metallogenic map of the Alshar district of Macedonia. Proceedings XVIII Congress of Carpathian-Balkan Geological Association. Belgrade: Sava Centar, 1, 648-650.

Volkov A. V., Serafimovski T., Kochneva N. T., Tomson H. N., and Tasev G., 2006b. The Alshar Epithermal Au-As-Sb-Tl Deposit, Southern Macedonia. Geol. Ore Deposits, 48 (3), 205-224.

Volkov A. V., Savva N. E., Sidorov A. A., Egorov V. N., Shapovalov V. S., Prokof'ev V. Yu., and Kolova E. E., 2006c. Spatial Distribution and Formation Conditions of Au-Bearing Porphyry Cu–Mo Deposits in the Russian Northeast. Geol. Ore Deposits 48 (6), 448-472.

Scientific Annals, School of Geology, Aristotle University of Thessaloniki Proceedings of the XIX CBGA Congress, Thessaloniki, Greece	Special volume 100	369-378	Thessaloniki 2010

MOLYBDENITE OCCURRENCES IN GREECE: MINERALOGY, GEOCHEMISTRY AND DEPOSITIONAL ENVIRONMENT

Voudouris P.[1], Melfos V.[2], Moritz R.[3], Spry P.G.[4], Ortelli M.[2], Kartal T.[5]

[1] *Department of Mineralogy-Petrology, University of Athens, 15784, Athens, Greece*
[2]*Department of Mineralogy-Petrology-Economic Geology, School of Geology, Aristotle University of Thessaloniki, 54124, Thessaloniki, Greece.*
[3] *Section des Sciences de la Terre et de l'Environnement, Université de Genève, Rue des Maraîchers 13, CH-1205 Genève,Switzerland*
[4] *Department of Geological and Atmospheric Sciences, 253 Science I, Iowa State University, Ames, IA 50011-3212, USA*
[5] *Mineralogisch-Petrographisches Institut, Univeristat Hamburg, Grindelallee 48, D-20146, Hamburg, Germany*

Abstract: Molybdenite occurs mainly in three mineralization types in Greece: (a) porphyry Mo-Cu-(±Te-Ag-Au), (b) reduced intrusion-related Mo-W systems (skarn, intrusion-hosted) and (c) shear zone-related Cu-Au-Bi-Mo. In porphyry-Mo-Cu prospects the molybdenite is the main ore constituent together with pyrite in quartz stockworks crosscutting sericite±carbonate altered porphyry stocks (dacite at Pagoni Rachi/Kirki, Myli/Esymi, Konos/Sapes, Melitena/Rhodopi and Stypsi/Lesvos; microgranite at Ktismata/Maronia; monzonite at Sardes/Limnos, Fakos/Limnos and Skouries/Chalkidiki). Reduced intrusion-related systems are characterized by the presence of molybdenite, pyrite and wolframite-scheelite in intrusion-hosted sheeted quartz veins and/or dissemination (granodiorite at Kimmeria/Xanthi, Plaka/Lavrion and leucogranite at Pigi/Kilkis and Seriphos) and skarn-hosted ores (Kimmeria/Xanthi). Finally in the shear-zone Stanos prospect molybdenite accompanies chalcopyrite, native Bi, Bi-tellurides and sulfosalts. The studied molybdenites display a wide spectrum of their rhenium content ranging from almost Re-free molybdenites at Stanos, to very low-Re molybdenite in the intrusion-related systems (Lavrion, Serifos, Pigia and Kimmeria), and high to ultrahigh-Re molybdenites in the northern Greek porphyries. The rare mineral rheniite (ReS_2), occurs along with Fe-Cu sulfides, Pb oxides, and native Sn in Pagoni Rachi and Konos prospects. Rheniite and high-Re molybdenite precipitated under oxidizing conditions and from relatively acid hydrothermal solutions, whereas Re-poor molybdenites are indicative of reduced conditions mostly dominant in the intrusion-related systems. At the northern Greek porphyry-Mo prospects, magmas previously enriched from their mantle source rocks were responsible for extreme contents of rhenium in molybdenite.

Keywords: Molybdenite, rheniite, mantle-crust origin, oxidizing vs reducing fluids.

1. Introduction

The Rhodope-Serbomacedonian- and Attic-Cycladic metamorphic belts in Greece comprise a number of styles of mineralization (base- and precious-metal porphyry, skarn, intrusion-related, shear zone-related, epithermal), which are in part genetically associated to arc-related magmatic rocks, and in part controlled by exhumation structures of high-pressure units in a back-arc setting (Arvanitidis and Constantinides, 1989; Arikas and Voudouris, 1998; Melfos et al., 2002; Skarpelis, 2002; Arvanitidis, 2003; Marchev et al., 2005; Voudouris, 2006; Tombros et al., 2007; Voudouris et al., 2008). Molybdenite occurs in a wide range of deposits/prospects, mainly those related to magmatic activity (porphyry-type, reduced intrusion-related), as well as deposits related to metamorphic or deformation processes (shear zone-related).

Previous studies reported the presence of Re-rich and Re-free molybdenite in various deposits/prospects in Greece and discussed the relationships between polytypism and rhenium content (Filippidis et al., 1986; Michailidis et al., 1993; Melfos et al., 1991; 2001). Recently, the extremely rare mineral rheniite (ReS_2) has been discovered in the Pagoni Rachi porphyry prospect (Voudouris et al., 2009), and this is the first occurrence of this mineral in a magmatic-hydrothermal deposit and only the second occurrence in the world after its type locality in the fumarolic sublimates in

Kudryavy volcano, Kurile islands (Korzhinsky et al., 1994). The study of Voudouris et al. (2009) indicated that the Re content of molybdenites from Pagoni Rachi is the highest ever reported (up to 4.70 wt.%), whereas the structural analyses demonstrated that they crystallized as the 2H polytype and not the 3R polytype, as previously hypothesized by Newberry (1979a, b) and others, thus suggesting that Re concentration does not correlate with a specific polytype. In addition the almost perfect linear correlation between the Mo and Re content of molybdenites from three northern Greek prospects (Pagoni Rachi, Maronia, Melitena) supports the concept previously proposed (e.g. Fleischer, 1959; Stein et al., 2001) that Re substitutes for Mo in the structure of molybdenite (Voudouris et al., 2009).

Despite the above mentioned mineralogical studies of molybdenite mineralization in Greece, an integrated documentation of molybdenum bearing ores has yet to be undertaken. The aim of the present study is to review all mineralogical data concerning molybdenites from various deposits/prospects in Greece (Fig. 1), to present new information concerning recent molybdenite discoveries, to evaluate their rhenium content and finally to discuss their origin.

2. Methods

Seventy eight thin and polished thin sections of host rocks and sulfide assemblages were studied with an optical microscope and a JEOL JSM 5600 scanning electron microscope equipped with back-scattered imaging capabilities, at the Department of Mineralogy and Petrology, University of Athens, Greece. The chemical composition of molybdenite was determined with a Cameca SX 100 wavelength-dispersive electron microprobe at the Department of Mineralogy and Petrology, University of Hamburg, Germany. Operating conditions were: 20 kV and 20

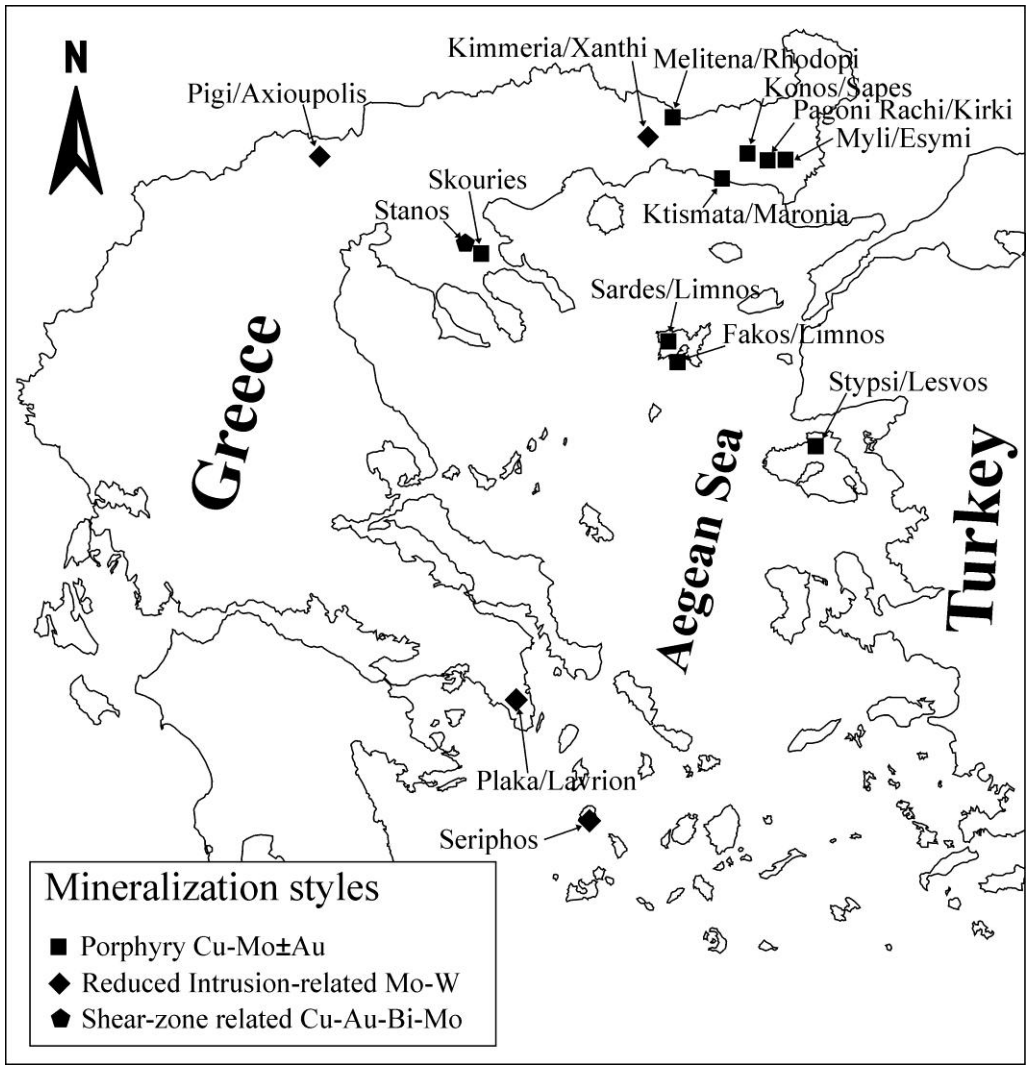

Fig. 1. Location map of the studied molybdenite occurrences in Greece.

nA, beam diameter <1 μm. The following X-ray lines were used: Mo*L*β, Re*M*α, Cu*K*α, Fe*K*α and S*K*α. Pure elements (for Re), pyrite and chalcopyrite (for Fe and S) and molybdenite (for Mo), were used as standards. The chemical composition of molybdenite and rheniite was also determined using a JEOL JXA 8200 electron microprobe at Iowa State University. The concentrations of the major and minor elements were determined at Iowa State University at an accelerating voltage of 15 kV and a beam current of 15 nA, with 10 seconds as the counting time (5 seconds on each background). The standards employed were metallic rhenium and molybdenum for Re and Mo, chalcopyrite for Cu, and synthetic pyrite for S.

3. Description of the mineralizations

All granitoid rocks are considered as post-collisional and mainly of sub-alkaline character. It follows a brief description of the mineralization studied.

3.1. Porphyry Mo-Cu- and Cu-Au deposits

Pagoni Rachi/Kirki: The Pagoni Rachi Mo-Cu-Te-Ag-Au prospect is genetically related to an Oligocene dacite porphyry stock (Arikas, 1981; Voudouris et al., 2009). Molybdenite-rheniite-pyrite-bearing quartz stockworks are related to sericitic alteration of the intrusion.

Konos/Sapes: In the Sapes area two porphyry-type mineralizing events, which are genetically related to microdiorite and dacite porphyries are recognized (Voudouris et al., 2006; Ortelli et al., 2009). The Konos Cu-Mo porphyry is hosted in a subvolcanic dacite and contains molybdenite-pyrite veins in host rocks affected by sericitic alteration (Ortelli et al., 2009). Rheniite, lead oxides and native Sn accompany molybdenite in the veins (Fig. 2a to c), (Ortelli, 2009; present study).

Myli/Esymi: The Myli Cu-Mo prospect similarly to Pagoni Rachi and Konos, is related to a dacite porphyry stock (Arikas, 1985). Molybdenite-pyrite-bearing quartz stockworks are related to sericite-carbonate alteration of the dacite. Molybdenite occurs as laths surrounding pyrite (Fig. 2e).

Ktismata/Maronia: The porphyry-Cu-Mo mineralization at Ktismata is genetically related to a microgranite porphyry body intruding the Middle Oligocene shoshonitic intrusive complex of Maronia (Papadopoulou, 2002). Molybdenite occurs within quartz stockworks crosscutting sericitic altered microgranite and is associated with pyrite, chalcopyrite, base metal sulfides and sulfosalts (Melfos et al., 2002).

Melitena: The Melitena porphyry-Mo prospect is hosted within a Tertiary intrusion of dacitic composition (Filippidis et al., 1986; Michailidis et al., 1993). Molybdenite forms disseminations and fissure fillings and is associated with quartz veinlets crosscutting the sericitic altered porphyry body together with pyrite, pyrrhotite, sericite, pyrophyllite, diaspore and aluminium-phosphate-sulfate minerals (Michailidis et al., 1993; Melfos et al., 2001).

Lesvos island: The Stypsi porphyry-Mo prospect (Voudouris and Alfieris, 2005) in the north-central part of the island is hosted by a high-K calc-alkaline dacite porphyry. A stockwork of grey to black silica veinlets crosscutting sericite-carbonate altered dacite, contain pyrite, chalcopyrite, bismuthinite, molybdenite and galena (Voudouris and Alfieris, 2005). Molybdenite occurs as laths surrounding pyrite (Fig. 2f).

Limnos island: Two bodies of quartz monzonite porphyry have intruded the volcanic and sedimentary rocks in the central part of Fakos peninsula, as well as near Sardes in the northwestern part of the island (Voudouris and Alfieris, 2005). The Fakos and Sardes prospects are telescoped porphyry-epithermal systems, where molybdenite occurs within a stockwork of quartz + pyrite veinlets crosscutting sericite-tourmaline altered monzonite and sedimentary rocks and overprinting earlier K-silicate alteration.

Skouries/Chalkidiki: The Skouries porphyry Cu-Au-Pd deposit is hosted by at least four monzonite porphyry phases (Eliopoulos and Economou-Eliopoulos, 1991; Kroll et al., 2002). Molybdenite occurs in late pyrite veinlets related to sericite-carbonate alteration of the porphyry stocks (Frei, 1995).

3.2. Reduced intrusion-related Mo-W deposits

Kimmeria/Xanthi: The Kimmeria ore district is characterized by an intrusion-related polymetallic system that includes intrusion-hosted sheeted quartz veins and stockworks crosscutting sericite-carbonate altered granodiorite, rich in pyrite, molybdenite, scheelite, wolframite, chalcopyrite as well as skarn ores enriched in chalcopyrite, magnetite, pyrrhotite and minor molybdenite (Fig. 2g) (Walenta and Pantzartzis, 1969; Vavelidis et al., 1990; present study).

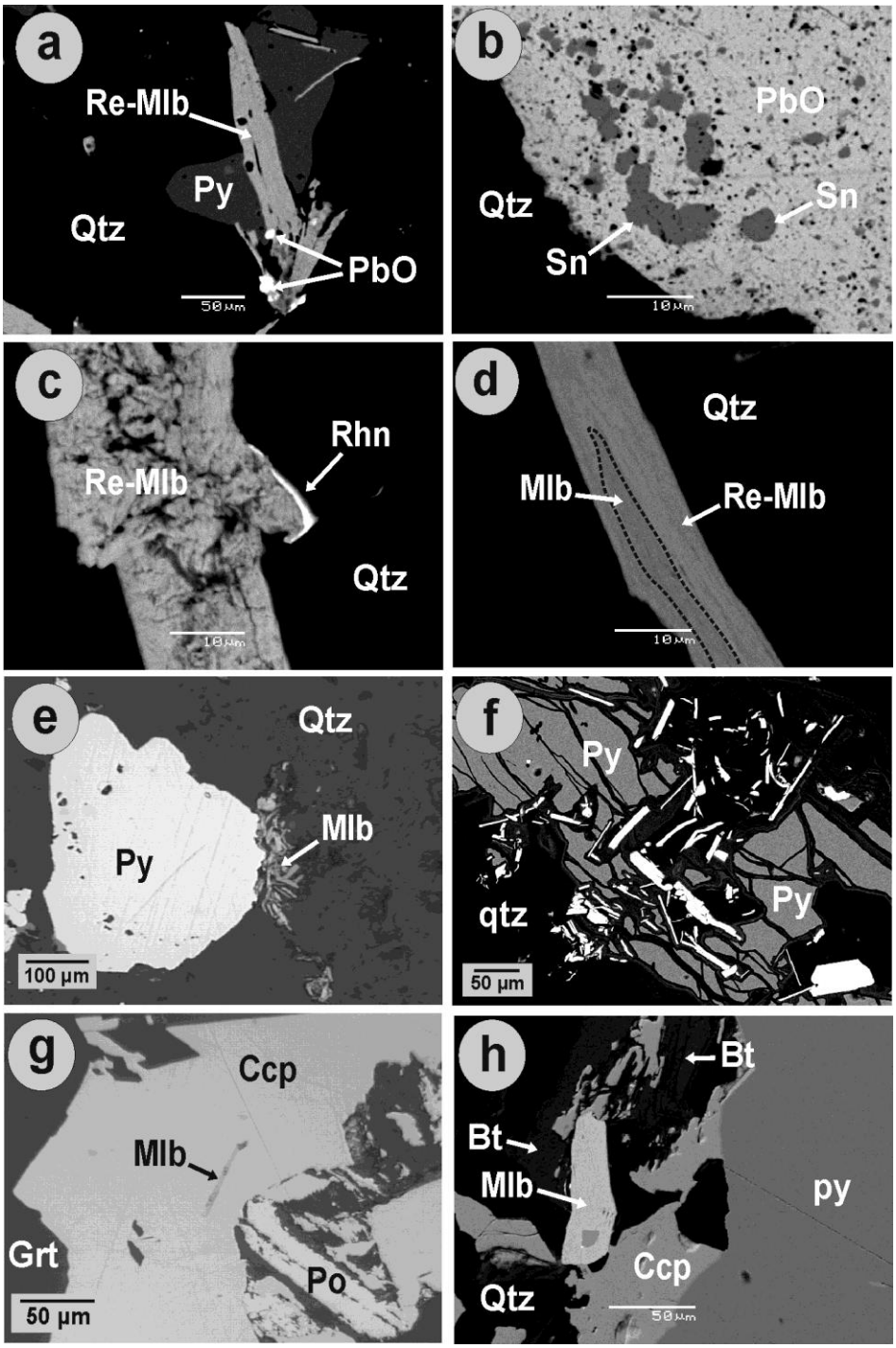

Fig. 2. Photomicrographs of molybdenite- and rheniite-bearing assemblages from various mineralization in Greece. (a) Rhenium-rich molybdenite (Re-Mlb) associated with pyrite (Py) and lead oxides (PbO) in quartz (Qtz) veinlet from the Konos/Sapes porphyry-Mo prospect (SEM–BSE image); (b) Native Tin (Sn) and lead oxide (PbO) from the Konos/Sapes porphyry-Mo prospect (SEM–BSE image); (c) Re-rich molybdenite (Mlb) and rheniite (Rhn) in quartz (Qtz) veinlet from the Konos/Sapes porphyry-Mo prospect (SEM–BSE image); (d) Rhenium-rich molybdenite (Re-Mlb) interfingered with Re-poor molybdenite (Mlb) in quartz (Qtz) veinlet from the Konos/Sapes porphyry-Mo prospect (SEM–BSE image); (e) Re-poor molybdenite (Mlb) surrounding pyrite (Py) in quartz (Qtz) veinlet from the Myli/Esymi porphyry-Cu-Mo prospect (SEM–BSE image); (f) Re-rich molybdenite (white flakes) surrounding pyrite (Py) in quartz (Qtz) veinlet from the Stypsi/Lesvos porphyry-Mo prospect (SEM–BSE image); (g) Chalcopyrite (Ccp) including Re-poor molybdenite (Mlb) and surrounded by pyrrhotite (Po) and garnet (Grt) in the intrusion-related Mo-W-Cu skarn prospect at Kimmeria/Xanthi (reflected light image); (h) Re-depleted molybdenite (Mlb) associated with chalcopyrite (Ccp) and biotite (Bt) postdating pyrite (Py) from shear-zone related Au-Bi-Cu-Te mineralization at Stanos/Chalkidiki.

Plaka/Lavrion: An intrusion-related polymetallic mineralization consisting of pyrite, molybdenite, chalcopyrite, pyrrhotite and minor scheelite, occurs within sheeted quartz veins and stockworks cross-cutting the granodiorite pluton of Plaka (Bonsall et al., 2007; Voudouris et al., 2008).

Pigi/Axiopolis: The Pigi Mo-deposit is related to the Upper Jurassic Fanos pluton, which is composed of high silica peraluminous leucogranites intruded the Mesozoic ophiolites of the Vardar zone (Christofides et al., 1990). Molybdenite is found within the leucogranites as disseminations and filling veinlets. Associated minerals are wolframite, pyrite, galena, quartz, sericite, chlorite, fluorite and kaolinite (Paraskevopoulos, 1958; Marakis and Skounakis, 1972; Michailidis et al., 1993).

Seriphos island: This study demonstrates the presence of an undeformed leucogranite at the southern part of Seriphos, composed of K-feldspar, quartz, minor plagioclase and biotite. Molybdenite occurs together with pyrite as disseminations and fracture fillings within fresh leucogranite.

3.3. Shear zone-related Cu-Au-Bi-Mo mineralization

Stanos/Chalkidiki: The Stanos mineralization is emplaced within a shear zone hosted in two-mica gneisses of the Serbomacedonian massif that records strong mylonitization and iron-potassic alteration with muscovite, biotite, chlorite and siderite (Voudouris and Sakellaris, 2008). The mineralization was formed in two stages: early pyrite, pyrrhotite and arsenopyrite deposition followed by a polymetallic assemblage including chalcopyrite, molybdenite (Fig. 2h), galena and Bi-Au-Te-bearing minerals contemporaneous with lower amphibolite/greenschist metamorphism (Voudouris and Sakellaris, 2008).

4. Composition of Re-bearing molybdenite

Representative electron-microprobe data of the molybdenites studied are presented in Table 1 and all data are plotted in the binary Re vs. Mo diagram (Fig. 3). Four groups of molybdenites are distinguished on the basis of their rhenium content: (a) Re-free molybdenites at Stanos/Chalkidiki, (b) very low-Re molybdenites (Re-content from 10 to 1310 ppm, average 206ppm) in the intrusion-related systems of Lavrion, Serifos, Pigi and Kimmeria, (c) intermediate- to high-Re molybdenites (Re-content from 300 to 10600 ppm, average 2302 ppm) in the porphyry-systems of Stypsi, Sardes, Fakos, Skouries and Myli, and (d) ultrahigh-Re

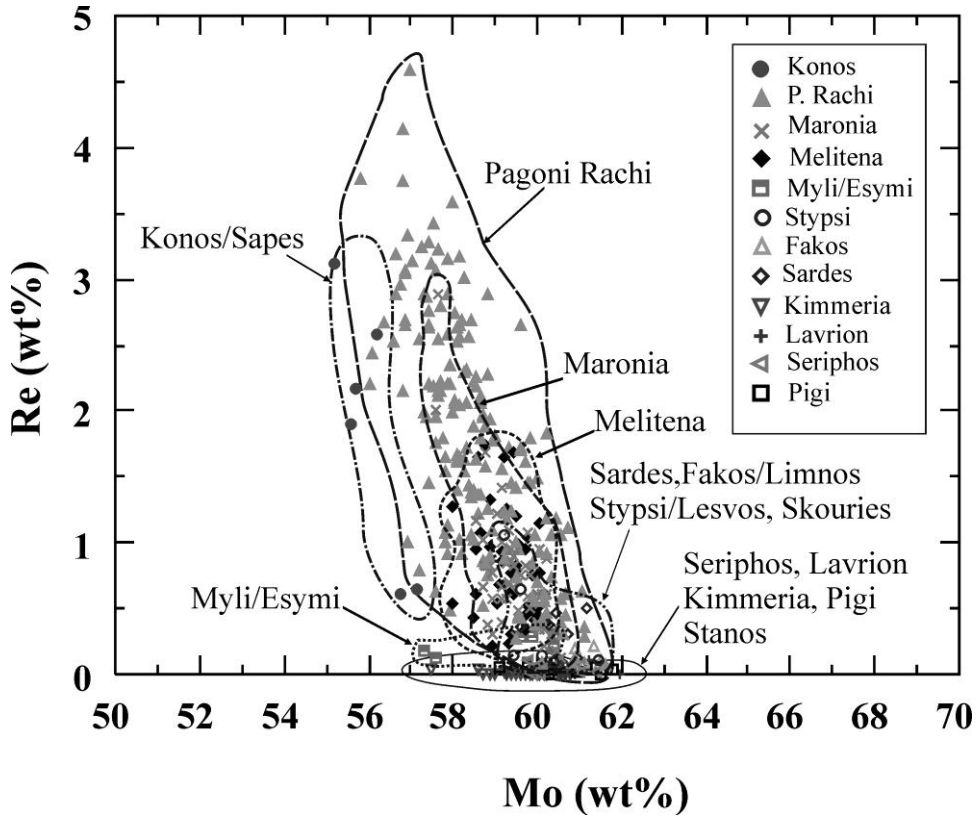

Fig. 3. Correlation diagram of rhenium (Re) and molybdenum (Mo) contents from the molybdenites from Greek occurences.

molybdenites in the northeastern Greek porphyries at Pagoni Rachi, Konos/Sapes, Melitena and Maronia (Re-content from 379 to 46900 ppm, average 13182 ppm). There is a correlation between the Mo and Re content of molybdenite supporting the concept that Re substitutes for Mo in the structure of molybdenite (Fig. 3). The Re content of molybdenite varies by more than 1 wt.% Re even within the same crystal (Fig. 2d) and it is highly likely that this heterogeneity is from the inhomogeneous distribution of rheniite (ReS_2) throughout the crystal. Rheniite was described recently from the Pagoni Rachi prospect (Voudouris et al. 2009). Rheniite also occurs in the Konos/Sapes deposit on grain boundaries of Re-rich molybdenite (Fig. 2c). Although Stein et al. (2001), Kosler et al. (2003) and Selby and Creaser (2001, 2004) suggested that Re must have redistributed or separated (decoupled) within molybdenite after formation, our study indicates that rheniite is not an exsolution-derived mineral from high-Re molybdenite (Voudouris et al., 2009).

5. Discussion

The Re content of molybdenite is controlled by several factors, including the composition of ore-forming solutions and host rocks, the nature and source of the host rock, the total amount of molybdenite in a given deposit, and the physicochemical conditions of ore formation (Berzina et al., 2005). Stein et al. (2001) related the Mo contents to mass balance considerations in which the Re content of molybdenite in Cu-Mo deposits was higher because of the restricted volume of molybdenite compared to that in Mo deposits. However, our study indicates that there is no clear relationship between Re content and molybdenite abundance, since molybdenite from the northern Greek porphyry Mo or Mo-Cu deposits (e.g. Pagoni Rachi, Konos/Sapes, Maronia, Melitena) is extremely enriched in Re. Relatively high Re concentrations, up to 0.35 wt.%, in the Majdanpek/Serbia and Elatsite/Bulgaria Cu-Mo porphyry deposits support a melt-metal source in fertile mantle and/or juvenile lower crust (Zimmerman et al., 2008). Mao et al. (1999) proposed that the rhenium contents in mo-

Table 1. Representative electron microprobe analyses (in wt. %) and atomic proportions of molybdenite from various known and new mineralization bd: below detection.

	Mo	Re	Fe	S	Total	Chemical formula (based on 3 apfu)
1	59.59	0.64	0.01	40.54	100.78	$Mo_{0.986}Re_{0.005}S_{2.008}$
2	59.23	1.06	bd	40.35	100.64	$Mo_{0.984}Re_{0.009}S_{2.007}$
3	60.13	0.14	0.02	40.11	100.40	$Mo_{1.001}Re_{0.001}Fe_{0.001}S_{1.997}$
4	60.26	0.38	0.34	39.87	100.85	$Mo_{1.002}Re_{0.003}Fe_{0.010}S_{1.985}$
5	61.20	0.52	0.17	39.66	101.55	$Mo_{1.017}Re_{0.004}Fe_{0.005}S_{1.973}$
6	56.81	3.75	0.12	38.85	99.53	$Mo_{0.973}Re_{0.033}Fe_{0.004}S_{1.991}$
7	58.80	0.76	0.10	39.32	98.98	$Mo_{0.997}Re_{0.007}Fe_{0.003}S_{1.994}$
8	59.21	1.65	bd	39.42	100.28	$Mo_{0.998}Re_{0.014}S_{1.988}$
9	60.20	0.39	0.01	39.86	100.46	$Mo_{1.005}Re_{0.003}S_{1.991}$
10	59.16	1.42	0.03	40.05	100.66	$Mo_{0.987}Re_{0.012}Fe_{0.001}S_{1.999}$
11	60.33	0.31	bd	39.60	100.24	$Mo_{1.011}Re_{0.003}S_{1.986}$
12	60.45	0.13	bd	40.35	100.93	$Mo_{1.000}Re_{0.001}S_{1.998}$
13	61.01	0.06	bd	38.86	99.93	$Mo_{1.032}Re_{0.000}S_{1.967}$
14	60.55	0.01	0.03	40.03	100.61	$Mo_{1.007}Re_{0.000}Fe_{0.001}S_{1.992}$
15	60.08	bd	0.02	39.63	99.73	$Mo_{1.009}Re_{0.000}Fe_{0.001}S_{1.991}$
16	60.92	0.03	0.04	40.06	101.05	$Mo_{1.010}Re_{0.000}Fe_{0.001}S_{1.988}$
17	61.77	0.04	0.02	39.81	101.63	$Mo_{1.024}Re_{0.000}Fe_{0.001}S_{1.975}$
18	60.92	0.19	nd	40.64	101.75	$Mo_{1.001}Re_{0.002}S_{1.998}$
19	61.50	0.11	nd	40.23	101.84	$Mo_{1.014}Re_{0.001}S_{1.985}$
20	59.75	0.10	nd	40.93	100.79	$Mo_{0.983}Re_{0.001}S_{2.016}$
21	60.70	0.02	nd	39.99	100.72	$Mo_{1.009}Re_{0.000}S_{1.990}$
22	59.84	0.33	nd	40.92	101.09	$Mo_{0.984}Re_{0.003}S_{2.013}$
23	60.08	0.04	nd	40.56	100.69	$Mo_{0.993}Re_{0.000}S_{2.006}$
24	56.18	2.59	bd	40.43	99.20	$Mo_{0.944}Re_{0.022}S_{2.034}$
25	57.17	0.65	bd	41.26	99.08	$Mo_{0.948}Re_{0.006}S_{2.047}$

1-3: Stypsi/Lesvos; 4,5: Sardes/Limnos; 6,7: Pagoni Rachi ; 8,9: Melitena; 10,11: Ktismata/Maronia; 12,13: Plaka/Lavrion; 14,15: Kimmeria/Xanthi; 16,17: Axioupolis/Kilkis; 18,19: Fakos/Limnos; 20,21: Seriphos; 22,23: Myli/Esymi; 24,25: Konos/Sapes

lybdenite decrease gradually from mantle sources, to mixtures between mantle and crust, and then to crust source. Furthermore, Stein et al. (2001) suggested that molybdenite in porphyry style deposits possess high Re contents if they are genetically related to the melting of mafic or ultramafic rocks, or if the source rocks involve mantle underplating or metasomatism. Deposits that are derived from intermediate crustal rocks generally contain molybdenite with lower Re concentrations (Stein et al., 2001). Molybdenite can occur with very low Re abundance (very low ppm and even ppb): Low ppb Re bearing molybdenites are quite common from intrusion-related systems like Mactung and Pogo deposits, as well as from highly evolved granite systems, especially in pegmatites (D. Selby, written commun. 2010). Low Re concentrations in molybdenite are also highly diagnostic of a metamorphic derivation (Stein, 2006).

Available geochemical and stable isotope data suggest that the Oligocene to Miocene plutonic rocks in northern Greece and associated porphyry mineralizations with high- and ultrahigh Re-molybdenites, have geochemical compositions indicative of a derivation from sub-continental lithospheric mantle and/or the lower crust, with a minimal contribution from the crust (Christofides et al., 1998, Pe-Piper and Piper, 2002). Slab breakoff resulted in the local ascent of asthenospheric mantle into mantle lithosphere and magma generation from a subcontinental lithospheric mantle, heterogeneously enriched by fluids and melts derived from previous subduction events (De Boorder et al., 1998; Pe-Piper and Piper, 2002). More precisely (a) a LILE- and LREE-enriched subcontinental mantle as the magma source of the Pagoni Rachi and Konos dacite magmas (Del Moro et al., 1988); (b) a lower crustal origin for the Maronia porphyritic microgranite (Papadopoulou, 2002); (c) a mantle source for the high-K calc-alkaline dacite porphyry at Stypsi (Pe-Piper and Piper, 2002); (d) dehydration melting of enriched metabasaltic amphibolite at the base of crust, triggered by rising mantle melts from both the asthenosphere and the enriched subcontinental lithosphere for the Limnos igneous rocks (Pe-Piper et al., 2009); and (e) a magma genesis in the upper mantle and subsequent crustal contamintation of the parental melts during emplacement for the Skouries deposit (Kroll et al., 2002). On the other hand, although Re-poor molybdenites (as present in the Kimmeria, Lavrion, Seriphos and Pigi prospects/deposits) should be indicative of magmas derived from crustal sources, available data are controversial: both a dehydration melting of lower crust without any contribution from mantle components, and a mantle origin with an important felsic component of crustal origin have been proposed for the formation of Xanthi granodiorite by Jones et al. (1992) and Christofides et al. (1998), and Lavrion granodiorite by Altherr and Siebel (2002) and Skarpelis et al. (2008). The source materials for the leucocratic granites of Fanos and Seriphos are suggested to be of crustal origin (Christofides et al., 1990; Iglseder et al., 2008). The lower Re-content in the intrusion-related systems of Lavrion, Kimmeria, Pigi and Seriphos is consistent with the reducing nature of mineralizing fluids as proposed by the experimental work of Xiong and Wood (2002) who suggested that reducing fluids containing sulfur have a lower capacity for transporting rhenium and, therefore, are not favorable for the formation of rhenium-enriched sulfide deposits. To form rhenium deposits, oxidizing fluids must be operative at some stage(s) of ore formation and this was the case for the ultrahigh Re deposits in northern Greece.

The coexistence of native Sn, lead-, lead-tin oxides and rheniite at Pagoni Rachi and Konos prospects is evidence that these phases formed directly from gas transport and precipitation as sublimates in a manner similar to that in the Kudryavy volcano, Kurile islands (Yudovskaya et al., 2006). According to Yudovskaya et al. (2006) the gas transport mechanism and the nano-scale phase formation allow coexistence of the reduced and oxidized phases of the transition metals. In the Kudryavy case, formation of native metals does not necessarily involve highly reduced fluids. Such nonequilibrium associations with coexisting various valence states are characteristic of high-temperature stages where the hydrothermal fluids exist as a gas phase, and mineral assemblages are precipitated as a result of gas transport reactions.

A rhenium release from the asthenospheric mantle wedge by subduction-related fluids and melts similarly to Kudryavy volcano, Kurile islands (Tessalina et al., 2008) could explain the enrichment of Re in the northern Greek magmatic systems.

Acknowledgements

We thank S. Heidrich and Alfred Kracher for their assistance with the electron microprobe at the Universities of Hamburg and Iowa State respectively. E. Michaelidis is especially thanked for his assis-

tance with SEM-EDS analyses at Athens University. This manuscript was significantly improved by the reviews of Anita Berzina and David Selby.

References

Altherr R. and Siebel W., 2002. I-type plutonism in a continental back-arc setting: Miocene granitoids and monzonites from the central Aegean Sea, Greece. Contributions of Mineralogy and Petrology, 143, 397-415.

Arikas K., 1981. Subvolcanic hydrothermal Mo-Cu-Pb-Zn mineralization in S.E. Rhodopes, Northern Greece: Petrology and geochemistry. Tschermaks Petrographische und Mineralogische Mitteilungen, 28, 189-205 (in German).

Arikas K., 1985. Hydrothermal alteration of subvolcanic rocks in Myli/ Esymi area: Mineralogy and geochemistry. Internal Report, I.G.M.E. Xanthi, (in Greek) 13p.

Arikas K. and Voudouris P., 1998. Hydrothermal alterations and mineralizations of magmatic rocks in the southern Rhodope Massif. Acta Volcanologica, 10, 353-365.

Arvanitidis N.D. and Constantinides D., 1989. Base and precious metal sulfide mineralization of the Greek Rhodope Massif. Geologica Rhodopica, 1, 298-305.

Arvanitidis N.D., 2003. Gold deposits in Greece: genetic types and economic perspectives. In: Mineral exploration and sustainable development. Millpress, Rotterdam, Eliopoulos D.G. et al. (eds), 941-943.

Berzina A.N., Sotnikov V.I., Economou-Eliopoulos M. and Eliopoulos D.G., 2005. Distribution of rhenium in molybdenite from porphyry Cu-Mo and Mo-Cu deposits of Russia (Siberia) and Mongolia. Ore Geology Reviews 26, 91-113.

Bonsall T.A., Spry P.G., Voudouris P., Seymour K.St., Tombros S. and Melfos V., 2007. Fluid inclusion and stable isotope characteristics of carbonate replacement Pb-Zn-Ag deposit in the Lavrion district, Greece. In: Mineral exploration and research: Digging deeper. Millpress, Rotterdam, Andrews C.J. et al. (eds.), 283-286

Christofides G., Soldatos T. and Koroneos A., 1990. Geochemistry and Evolution of the Fanos Granite, N. Greece. Mineralogy and Petrology, 43, 49-63.

Christofides G., Soldatos T., Elefthertiadis G. and Koroneos A., 1998. Chemical and isotopic evidence for source contamination and crustal assimilation in the Hellenic Rhodope plutonic rocks. Acta Volcanologica, 10, 305-318.

De Boorder H., Spakman W., White S.H. and Wortel M.J.R., 1998. Late Cenozoic mineralization, orogenic collapse and slab detachment in the European Alpine Belt. Earth and Planetary Science Letters, 164, 569-575.

Del Moro A., Innocenti F., Kyriakopoulos C., Manetti P. and Papadopoulos P., 1988. Tertiary granitoids from Thrace (Northern Greece): Sr isotopic and petrochemical data. Neues Jahrbuch für Mineralogie Abhandlungen, 159, 113-135.

Eliopoulos D.G. and Economou-Eliopoulos M., 1991. Platinum-group element and gold contents in the Skouries porphyry-copper deposit, Chalkidiki peninsula, N. Greece. Economic Geology, 86, 740-749.

Filippidis A., Vavelidis M., Michailidis K. and Evangelou, E., 1986. Re-rich and Re-poor molybdenite in the Melitena porphyritic intrusion, Rhodope massif. Fortschritte der Mineralogie, 64, 47.

Fleisher M., 1959. The geochemistry of rhenium with special reference to its occurrence in molybdenite. Economic Geology, 54, 1406-1413.

Frei R., 1995. Evolution and mineralizing fluid in the porphyry copper system of the Skouries deposit, northeastern Chalkidiki (Greece): evidence from combined Pb-Sr and stable isotope data. Economic Geology, 90, 746-762.

Iglseder C., Grasemann B., Schneider D.A., Petrakakis K., Miller C., Klötzli U.S., Thöni M., Zámolyi A. and Rambousek C., 2009. I and S-type plutonism on Seriphos (W-Cyclades, Greece). Tectonophysics, 473, 69-83.

Jones C.E., Tarney J., Baker J.H. and Gerouki F., 1992. Tertiary granitoids of Rhodope, northern Greece: magmatism related to extensional collapse of the Hellenic Orogen? Tectonophysics, 210, 295-314.

Korzhinsky M.A., Tkachenko S.I., Shumulovich K.I., Taran Y.A. and Steinberg G.S., 1994. Discovery of a pure rhenium mineral at Kudriavy volcano. Nature, 369, 51-52.

Kosler J.A., Simonetti A., Sylvester P.J., Cox R.A., Tubrett M.N. and Wilton D.H.C., 2003. Laser ablation ICP-MS measurements of Re/Os in molybdenite and implications for Re-Os geochronology. Canadian Mineralogist, 41, 307-320.

Kroll T., Muller D., Seifert T., Herzig P.M. and Schneider A., 2002. Petrology and geochemistry of the shoshonite-hosted Skouries porphyry Cu-Au deposit, Chalkidiki, Greece. Mineralium Deposita, 37, 137-144

Mao J., Zhang Z., Zhang Z., and Du A. 1999. Re-Os isotopic dating of molybdenites in the Xiaoliugou W(Mo) deposit in the northern Qilian Mountains and its geological significance. Geochimica et Cosmochimica Acta, 63, 1815-1818.

Marakis Gr. and Skounakis S., 1972. The physical properties of wolframite from Axioupolis Mo-occurences and their significance in the genesis of the Mo paragenesis. Annales Geologiques des Pays Helleniques, 24, 399-405 (in Greek).

Marchev P., Kaiser-Rohrmeier M., Heinrich C., Ovtcharova M., Von Quadt A. and Raicheva R., 2005. Hydrothermal ore deposits related to post-orogenic extentional magmatism and core complex formation: The Rhodope Massif of Bulgaria and Greece. Ore Geology Reviews, 27, 53-89.

Melfos V., Vavelidis M., Filippidis A., Christofides G. and Evagelou E., 1991. Re-rich and Re-poor molyb-

denite in the Maronia rhyolitic intrusion, Northeastern Greece. In: Source, Transport and Deposition of Metals (M. Pagel & J.L. Leroy, eds.), Balkema, Rotterdam, 775-777.

Melfos V., Voudouris P., Arikas K. and Vavelidis M., 2001. High Re concentrations in molybdenites from porphyry-Mo±Cu in Thrace (NE Greece). Bulletin of the Geological Society of Greece, 34, 1015-1022 (in Greek).

Melfos V., Vavelidis M., Christofides G. and Seidel E., 2002. Origin and evolution of the Tertiary Maronia porphyry copper-molybdenum deposit, Thrace, Greece. Mineralium Deposita, 37, 648-668.

Michailidis K., Filippidis A. and Kassoli-Fournaraki A. 1993. Polytypism and rhenium-contents of molybdenites from two Mo-deposits in northern Greece. In: Current Research in Geology Applied to Ore Deposits, Fenoll H.A., Torres-Ruiz and Gervilla (eds), 641-644.

Newberry R.J.J., 1979a. Polytypism in molybdenite (I): a non-equilibrium, impurity-induced phenomenon. Americal Mineralogist, 64, 758-767.

Newberry R.J.J., 1979b. Polytypism in molybdenite (II): relationships between polytypism, ore deposition/alteration stages and rhenium contents. Americal Mineralogist, 64, 768-775.

Ortelli M., 2009. Tertiary porphyry and epithermal association of the Sapes/Kassiteres district, Eastern Rhodopes, Greece. Unpublished M.Sc. thesis, University of Geneva, 87p.

Ortelli M., Moritz R., Voudouris P. and Spangenberg J., 2009. Tertiary porphyry and epithermal association of the Sapes-Kassiteres district, eastern Rhodopes, Greece, In: Smart Science for exploration and mining, Williams et al. (eds), 536-538.

Papadopoulou L., 2002. Mineral phase equilibria, crystallization conditions and evolution of the Maronia pluton, Thrace, Greece. PhD thesis, University of Thessaloniki, 336p (in Greek).

Paraskevopoulos G.M., 1958. Formation conditions of the molybdenite deposits at Axioupolis area. Annales Geologiques des Pays Helleniques, 9, 260-267 (in Greek).

Pe-Piper G. and Piper D.J., 2002. The igneous rocks of Greece. The anatomy of an orogen. Gebrüder Borntträger, Berlin-Stuttgart, 573p.

Pe-Piper G., Piper D.J., Koukouvelas I., Dolansky L.M. and Kokkalas S., 2009. Postorogenic shoshonitic rocks and their origin by melting underplated basalts: The Miocene of Limnos, Greece. Geological Society of America Bulletin, 121, 39-54.

Selby D. and Creaser R. A., 2001. Re-Os geochronology and systematics in molybdenite from the Endako porphyry molybdenum deposit, British Columbia, Canada. Economic Geology, 96, 197-204.

Selby D. and Creaser R. A., 2004. Macroscale NTIMS and mircoscale LA-MC-ICP-MS Re-Os isotopic analysis of molybdenite: Testing spatial restriction for reliable Re-Os age determinations, and implications for the decoupling of Re and Os within molybdenite. Geochimica et Cosmochimica Acta, 68, 3897-3908.

Skarpelis N., 2002. Geodynamics and evolution of the Miocene mineralization in the Cycladic-Pelagonian belt, Hellenides. Bulletin of the Geological Society of Greece, 34: 2191-2206.

Skarpelis N., Tsikouras B., and Pe-Piper G., 2007. The Miocene igneous rocks in the Basal Unit of Lavrion (SE Attica, Greece): petrology and geodynamic implications. Geological Magazin, 145, 1-15.

Stein H.J. 2006. Low-rhenium molybdenite by metamorphism in northern Sweden: Recognition, genesis, and global implications. Lithos, 87, 300-327.

Stein H.J., Markey R.J., Morgan J.W., Hannah J.L. and Scherstén A. 2001. The remarkable Re-Os chronometer in molybdenite: how and why it works. Terra Nova 13, 479-486.

Tessalina S.G., Yudovskaya M.A., Chaplygin I.V., Birck J.-L. and Capmas F., 2008. Sources of unique rhenium enrichment in fumaroles and sulphides at Kudryavy volcano. Geochimica et Cosmochimica Acta, 72, 889-909.

Tombros S., Seymour K.St., Williams-Jones A.E., and Spry P.G., 2007. The Genesis of Epithermal Au-Ag-Te Mineralization, Panormos Bay, Tinos Island, Cyclades, Greece. Economic Geology, 102, 1269-1294.

Vavelidis M., Michelidis K., Christofides G., and Boboti-Tsitlakides I., 1990. Geochemical study of placer gold and the gold-bearing skarn-type mineralization of Kimmeria area, Xanthi disctrict, NE Greece. Geologica Rhodopica, 2, 297-307

Voudouris P. 2006. A comparative mineralogical study of Te-rich magmatic-hydrothermal systems in northeastern Greece. Mineralogy and Petrology, 87, 241-275.

Voudouris P. and Alfieris D., 2005. New porphyry-Cu±Mo occurrences in northeastern Aegean/Greece: Ore mineralogy and transition to epithermal environment. In: Mineral deposit research: Meeting the global challenge. Springer, Berlin, Mao, J. and Bierlein F.P. (eds), 473-476.

Voudouris P. and Sakellaris G., 2008. The Stanos shear zone-hosted Cu-Au-Bi deposit, Chalkidiki/N. Greece: New mineralogical and textural data. Proceedings of the XIII International conference on thermobarogeochemistry and IV APIFIS symposium, Moscow, 1: 247-250

Voudouris P., Tarkian M. and Arikas K., 2006. Mineralogy of telluride-bearing epithermal ores in Kassiteres-Sappes area, western Thrace, Greece. Mineralogy and Petrology, 87, 31-52.

Voudouris P., Melfos V., Spry P.G., Bonsall T., Tarkian M. and Economou-Eliopoulos M., 2008 Mineralogy and fluid inclusion constraints on the evolution of the Plaka intrusion-related ore system, Lavrion, Greece. Mineralogy and Petrology, 93, 79-110.

Voudouris P., Melfos V., Spry P.G., Bindi L., Kartal T.,

Arikas K., Moritz R. and Ortelli M., 2009. Rhenium-rich molybdenite and rheniite in the Pagoni Rachi Mo-Cu-Te-Ag-Au prospect, northern Greece: implication for the Re geochemistry of porphyry-style Cu-Mo and Mo mineralization. Canadian Mineralogist, 47, 1013-1046.

Walenta K. and Pantzartzis P., 1969. The molybdenite deposit of Kimmeria, Xanthi, northern Greece. Erzmetall, 22, 272-278.

Xiong Y. and Wood S.A., 2002. Experimental determination of the solubility of ReS2 and the Re-ReO2 buffer assemblage and transport of rhenium under supercritical conditions. Geochemical Transactions, 3, 1-10.

Yudovskaya M.A., Distler V.V, Chaplygin I.V., Mokhov A.V., Trubkin N.V. and Gorbacheva S.A., 2006. Gaseous transport and deposition of gold in magmatic fluid: evidence from the active Kudryavy volcano, Kurile Islands. Mineralium Deposita, 40, 828-848.

Zimmerman A., Stein H.J., Hannah J.L., Kozelj D., Bogdanov K. and Berza, T. 2008. Tectonic configuration of the Apuseni-Banat-Timrok-Srednogorie belt, Balkans-South Carpathians, constrained by high precision Re-Os. Mineralium Deposita, 43, 1-21.

Special Session S23
Gemology

Scientific Annals, School of Geology, Aristotle University of Thessaloniki Proceedings of the XIX CBGA Congress, Thessaloniki, Greece	Special volume 100	379-383	Thessaloniki 2010

PRELIMINARY INVESTIGATIONS OF INCLUSIONS IN SOME TOPAZ CRYSTALS FROM VOLODARSK-VOLYNSKI MASSIF (WESTERN UKRAINE)

Dumańska-Słowik M., Natkaniec-Nowak L.ˈ Toboła T. and Bąk E.

Faculty of Geology, Geophysics and Environmental Protection AGH-University of Science and Technology, al. Mickiewicza 30, 30-059 Krakow, Poland, dumanska@agh.edu.pl, natkan@agh.edu.pl, tob@geolog.geol.agh.edu.pl

Abstract: The aim of this paper is the gemmological and microthermometric studies of colour types of topazes (colourless, light pink and blue) from pegmatites of the Volodarsk-Volynski massif (Western Ukraine). These topaz crystals are characterized by the presence of numerous solid and fluid inclusions, mainly of a secondary origin as well as the abundance of micropores. The solid inclusions include mainly albite, tourmaline, Fe-bearing mineral phases and probably organic matter. Among the groups of fluid inclusions, secondary two-phase (liquid-vapour) inclusions distinctly dominate over sparse inclusions of a primary origin. The measured values of temperature homogenization (T_h) for selected primary and secondary fluid inclusion assemblages ranges from 350-380°C and 322°C, respectively. Topaz from Volodarsk-Volynski Massif crystallized during hydrothermal stage in medium temperature conditions. The presence of different secondary and pseudosecondary fluid inclusions together with the traces of necking down processes, point that after the crystallization the topaz was also affected by mechanical, thermal and metasomatic processes.

Keywords: topaz, Volodarsk-Volynski, inclusion, homogenization temperature

1. Introduction

Topaz is a gem, which is commonly associated with acid igneous rocks of granite type and pegmatites, as well as pneumometasomatic and hydrothermal veins (e.g. tin-bearing greisens). Commonly it coexists with tourmaline, chrysoberyl, cassiterite, muscovite, fluorite, beryl and quartz (Abdel-Rehim, 1999). Important sources of topaz crystals are found in Brazil, the USA, Mexico, Russia, Pakistan, Madagascar and Australia. In Europe the finest topaz crystals are found in Volodarsk-Volynski, a village near Novograd-Volynski by the river Irsha (western Ukraine), a.k.a. "a stony heart of Ukraine". It is a centre of many precious gems as beryl, topaz, "rock crystal", labradorite and many others. Though this area is better known for gem-quality and interestingly etched yellow-green beryls, the topaz crystals of various colours are considered to be among the most beautiful in the world.

Four topaz samples from Volodarsk-Volynski massif (VVM) were the subject of gemmological studies. The crystals have been investigated by standard optical microscope, scanning electron microscopy (SEM) with backscattered electron (BSE) observations. The main aim of this work was to determine the complex characteristics of the topaz samples coming from VVM. More attention was paid to the presence of solid and fluid inclusions within the crystals.

Ukrainian topaz's promotion has been limited since the majority of papers concerning mainly geology and mineralogy of Volodarsk-Volynski massif, have been published in Russian or Ukrainian. Hence the authors of this paper hope the results of the gemmological studies of the topaz from western Ukraine contribute to the discussion on topaz group.

2. Geological setting

The VVM is the largest block of the anorthosite-rapakivi-granite Korosten Pluton, which is situated at the north-western part of the Ukrainian Shield. The extensive overview of the geology and geochronology of the Korosten complex was presented by Bogdanova et al. (2004). The VVM covers an area of ca. 1250 km^2 that makes up about

10% of the pluton. It is mainly composed of leucocratic large-grained gabbro-anorthosites in which anorthosites occur in the form of local bodies. Gabbro-norites, diabases, and ultrabasic rocks are present only in the periphery of the massif (Kravchenko, 2005).

The VVM was formed during two magmatic episodes at 1789.1 ± 2.0 Ma and between 1761 – 1758 Ma. Rapakivi granites constitute a more abundant group of rocks within the Korosten Pluton surrounding the VVM. Their emplacement took place 1767.4 ± 2.2 Ma ago (Amelin et al., 1994). In the western part of the massif at the contact zone of rapakivi granites with mafic rocks, miarolitic pegmatites occur abundantly. The Volodarsk-Volynski pegmatites are restricted to 0.3 to 1.5 km wide and 22 km long zone of the intrusion. They exhibit diverse mineral content and structures which are probably connected with their neighbour various basic and acid rocks (Koshil at al., 1991). Over 90 minerals, with gem-quality crystals as beryl, topaz, smoky quartz, amethyst, citrine and many others were identified in the miarolitic pegmatites of Volodarsk-Volynski massif.

Topaz forms usually prismatic crystals, of light blue, brownish-yellow and light pink colour. The crystals could appear from transparent to opaque. The presence of various mineral soild inclusions (e.g. fluorite, mica, columbite, albite, quartz) together with numerous fissures within the topaz crystals, is responsible for its non-transparent character (Koshil et al., 1991). Most of the topaz crystals show also etching effects. The Volodarsk-Volynski topaz can reach considerable sizes; the largest one weights 117 kg.

3. Analytical methods

Investigations of four differently coloured varieties of gem-quality topaz (T1, T2, T3, T4; see Table 1 and Figure 1) were carried out at the laboratories of the Department of Mineralogy, Petrography and Geochemistry and the Department of Economy and Mining Geology, Faculty of Geology, Geophysics and Environment Protection, AGH–University of Science and Technology in Kracow, Poland. All the samples were studied macroscopically. Standard optical examinations were carried out with an Olympus BX 51 polarizing microscope. The gemmological determinations of internal features, optical characteristics and luminescence under short- and long-wave radiation were carried out using Schneider equipment. Backscattered Electron (BSE) observations were performed on polished sections coated with carbon using a FEI Quanta 200 FEG scanning electron microscope with an EDS detector. The system was operated with 15 kV accelerating voltage and high – vacuum mode. Fluid inclusion analyses were carried out on double polished wafers (0.2 mm thick). Microthermometric measurements were conducted using a Linkam THMSG600 Geology Heating and Freezing Stage mounted on NIKON ECLIPSE E600 microscope. The measurements were carried out with the rate of 1 °C/min and with accuracy of 0.1 °C. The heating rate was 10°C/min and when approaching Th it was lowered to 0.5°C/min. T1 topaz sample was chosen for detailed fluid inclusion analyses.

4. Results

Specific gravity measured of all the 4 samples range from 3.3 to 3.5 g/cm^3. All crystals contain numerous inclusions of different kinds which affect their transparency. Some internal defects are visible with the naked eye. In T2 and T3 topaz crystals two kinds of solid inclusions were macroscopically observed, i.e. tiny, light creamy - feldspars and bigger, brown coloured - probably Fe-bearing minerals. In T1 topaz some aggregates of mineral crystals with characteristic prismatic or acicular habit can be found. Under immersion-

Table 1. Description and gemmological characteristics of topaz crystals from Volodarsk-Volynski Massif (western Ukraine).

Sample No./Parameter	**T-1**	**T-2**	**T-3**	**T-4**
Linear dimensions [length X width X height] (mm)	44 x 25	25 x 30	32 x 24	22 x 8
Colour	pale pink	colourless	blue	blue
Luminescence	Not observed	Not observed	Not observed	pale blue
Refractive Indexes	1.60-1.64	1.60-1.64	1.61-1.62	1.61-1.63
Pleochroism	Not observed	Not observed	pale blue- greenish	pale blue- greenish
Optical character	+	+	+	+
Specific gravity[g/cm^3]	3,51 zł	3,49 zł	3,30 zł	3,53 zł

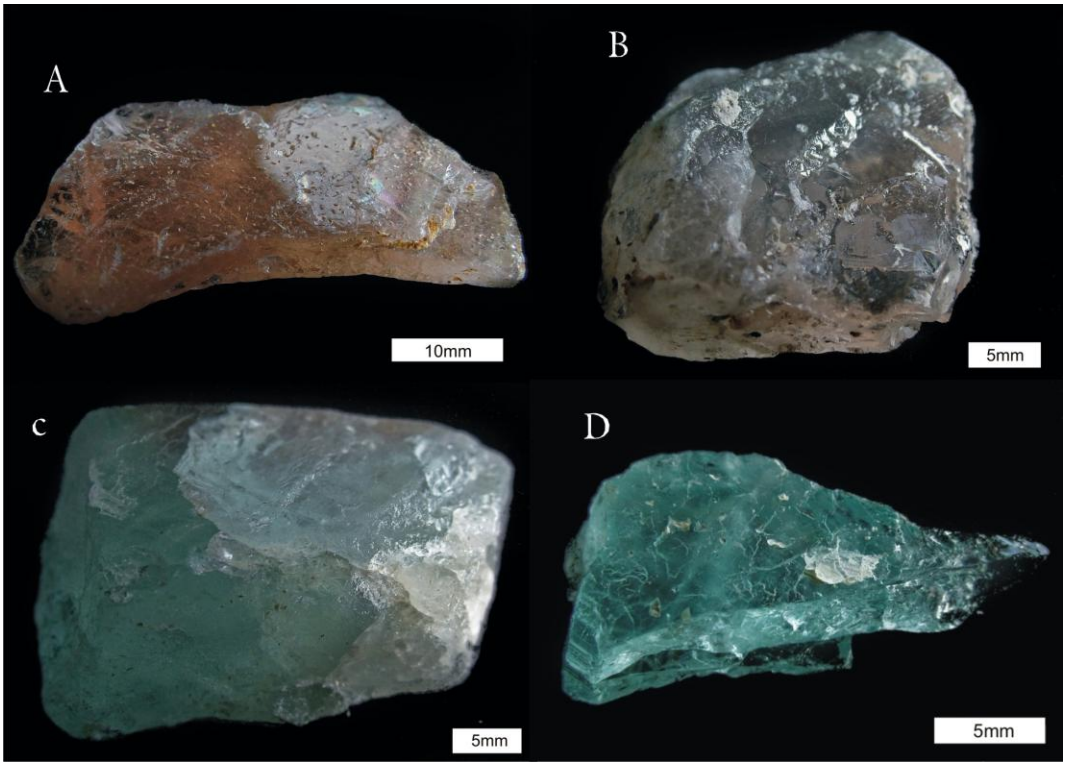

Fig. 1. Colour varieties of topaz crystals from Volodarsk-Volynski Massif (Ukraine); A-pale pink sample T1, B-colourless sample T2, C- blue sample T3, D-blue sample T4.

scope numerous fluid inclusions and growth zones can be identified within the topaz crystals. Under SW and LW UV -light only T4 crystal presents pale blue luminescence. The results cited above are summarized in the table 1.

T1 topaz crystal is rich in fluid inclusions assemblages (FIA) with sizes from 1 μm to 1 mm. Fluid inclusions studies revealed the presence of numerous inclusions of secondary and probably pseudosecondary origin as well as some relatively rare primary fluid inclusions. The distinction of pseudosecondary from secondary fluid inclusions seems difficult in this sample. Additionally, tiny primary inclusions with sizes from 1 to 3 μm are present sporadically within the T1 topaz from VVM (Fig. 2a). Fluid-inclusion's study also revealed the presence of oval in shape, two-phase liquid-vapor (L-V) inclusions with about 10% gas by volume at room temperature.

Moreover, secondary inclusions of the T1 sample, form diversified aggregates (Figs. 2b and c). The smaller oval inclusions are concentrated along craks' planes. Among them there are also bigger more elongated inclusions. The largest inclusions (up to 1mm in length) are usually oval and have characteristic "tails". They are most probably the oldest secondary fluid inclusions, identified within the topaz crystals, which had been changed in necking-down process.

The secondary inclusions are usually two-phase and exhibit a variable proportion of vapour to liquid (V/L). However, vapour phase prevails in most of them (Fig. 2c). Some fluid inclusions are composed mainly of gas (90% per volume) and only 10 wt% of liquid.

The scarcity of primary inclusions together with their small sizes, are both responsible for the difficulties in observation of the phases changes during heating. In order to avoid the effects of stretching, necking, and leaking, two groups of primary fluid inclusions (i.e. I-FIA and II-FIA) with consistent L/V ratios (Ermakov 1972; Roedder 1984, Goldstein and Reynolds 1994) from T1 topaz crystal were chosen for Th measurements. The group of inclusions I-FIA showing < 15% gas by volume at room temperature included eight inclusions with <10 μm in size. The homogenization temperatures revealed Ths from 362 to 380°C for I FIA. The II-FIA consisted of three tiny and spherically-shaped inclusions with <10 μm in size (Fig. 2a) with < 15% gas by volume too. The measured homogenization temperatures (T_h) range from 380 to 385°C for II FIA.

For microthermometric measurements were chosen

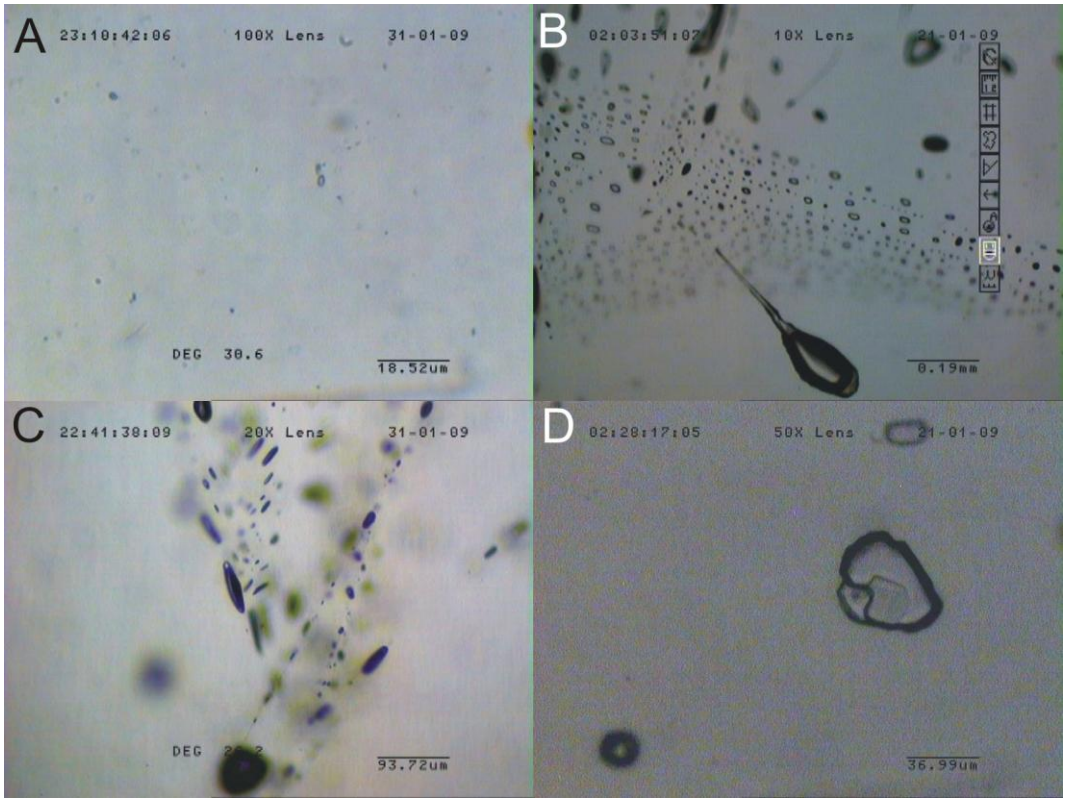

Fig. 2. A- Primary fluid inclusions in T1 topaz sample. B- Abundance of secondary fluid inclusions in T1 topaz sample. C- Fluid inclusions assemblage of secondary origin with the predominance of gas over liquid in T1 topaz sample D- Fluid inclusion with a daughter mineral in T1 topaz sample.

only the groups of secondary inclusion with sizes below 20 μm and which showing consistent L/V ratios (ca. 10% gas phase per volume). The determination of homogenization temperature for these inclusions can be an evidence for their sealing off before phase separation (Goldstein and Reynolds, 1994). Homogenization temperatures measurements revealed constant Th 322 °C for all analysed fluid inclusions.

The T1 topaz from VVM contains also single secondary inclusions with some daughter minerals. The cubic habit of this mineral suggests the possible presence of halite (Fig. 2d). All solid mineral phases occurring in this sample were identified with SEM-EDS. In homogeneous structure of topaz with crystallites from 40-50 μm in length, some micropores and rare mineral phases can be observed. Sodium plagioclase belongs to the most numerous inclusions (Fig. 3). Albite form tabular crystals with ca. 600 μm in length. Very tiny (1 μm long) Ce-bearing phases occur subordinately. In T2 topaz, black and long crystals with characteristic acicular or prismatic habit were observed (Fig. 4), being probably tourmaline. Gübelin and Koivula (1997) had already observed some tourmaline crystals within topaz matrix. Some inclusions filled with a black-brown mineral phase are irregularly scattered in the crystals. This mineral is an iron-rich phase. However, it is very probably that organic substance also appears in these solid aggregates. This could also be the potential cause of its pale blue luminescence under UV radiation.

5. Discussion and Conclusion

Detailed microscopic observations in one sample revealed the occurrence of plentiful secondary fluid inclusions with subordinate primary inclusions. Its secondary fluid inclusions with sizes from 10 μm to 1 mm usually form intersecting inclusion assemblages (FIA). Its fluid-inclusion petrography revealed mainly the presence of two-phase liquid-vapour (L-V) inclusions. Occasionally these inclusions show changeable L/V ratios, i.e. some of them are vapour - rich phase (ca. 90% gas by volume).

Microthermometric measurements on the T1 sample suggest that it was formed during the final pegmatite's crystallization in 362-385 ºC. Then it was probably affected by mechanical, thermal and metasomatic processes. The predominance of gas

over liquid phase and variable L/V ratios in secondary inclusions of the topaz indicates that the environment of fluid entrapment could probably had been changed from homegenic to heterogenic, with much amounts of gases. The values of homogenization temperatures measured for secondary and primary inclusions assemblages, which are approximate to each other, suggest that some cracks present in the topaz could be formed during crystallization of the mineral under hydrothermal conditions. However, studies on a bigger number of samples should be done in order to prove the results.

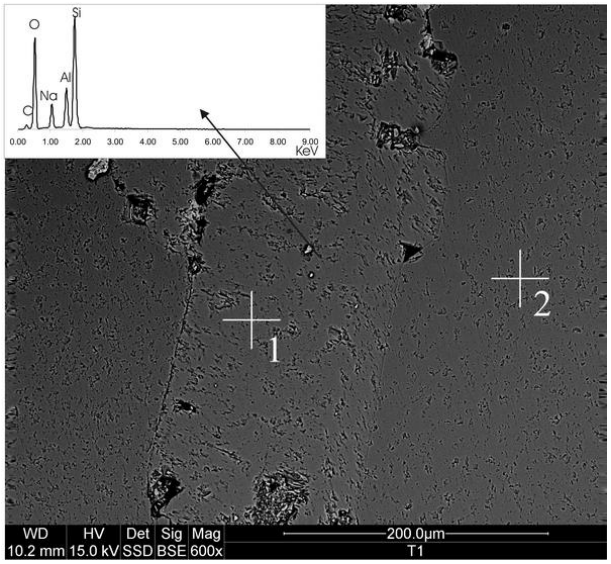

Fig. 3. Solid inclusion of albite (point no 1) in T1 topaz sample (point no 2), BSE image. In the inset is the chemical analysis diagram.

Solid inclusions of albite, tourmaline, Fe-bearing phases were identified within the four topaz crystals from VVM examined during this study. In one crystal potential evidence of organic matter's presence is observed. However, more studies should be done with other methods (e.g. Raman spectrometer), in order to verify this.

Acknowledgements

The authors are grateful to Adam Gaweł for performing SEM-EDS analyses. This work was financially supported by AGH-University of Science and Technology grants no 11.11.140.158

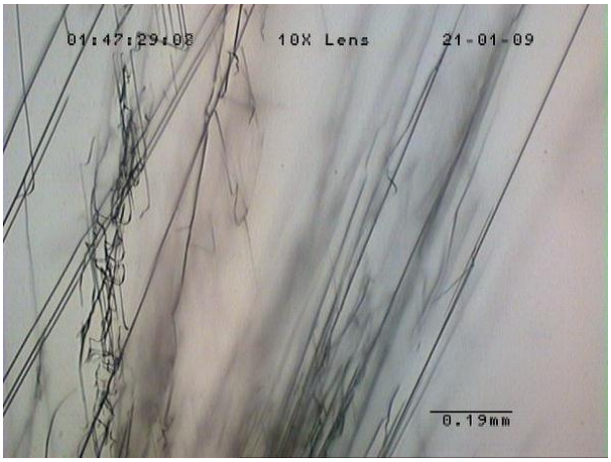

Fig. 4. Solid inclusions (probably of tourmaline) in T2 topaz.

References

Abdel-Rehim, A.M., 1999. Thermal analysis of topaz synthesis from kaolinite, Thermochimica Acta, 340-341.

Amelin Yu.V. Heaman L.M., Verkhoglyad V.M. and Skobelev V.M., 1994. Geochronological constraints on the emplacement history of an anorthosite-rapakivi granite suite: U-Pb zircon and baddeleyite study of the Korosten Complex, Ukraine. Contrib. Mineral. Petrol., 116, 411-419.

Bogdanova, S.V., Pashkevich, I.K., Buryanow, V.B., Makarenko, I.B., Orlyuk, M.I., Skobelev, V.M., Starostenko, V.I. and Legostaeva, O.V., 2004. The 1.80-1.74 Ga gabbro-anorthosite-rapakivi Korosten Pluton in the Ukrainien Shield: a 3-D geophysical reconstruction of deep structure, Tectonophysics 381, 5-27.

Ermakov N.P. 1972. Geochemical systems of inclusions in minerals, Nedra, Moscow, pp. 374.(in Russian).

Goldstein R.H. and Reynolds T.J. 1994. Systematics of fluid inclusions in diagenetic minerals. SEPM Short Course 31: 1-199.

Gübelin, E. and Koivula, J., 1997. Photoatlas of inclusions in Gemstones, ABC Edition, Zurich.

Koshil, I.M., Vasilishin, I.S., Pavlishin, V.I., and Panchenko, V.I., 1991. Geological structure and mineralogy of the pegmatites of Volynya, Ukraine, Lapis, 16 (10), 28-40.

Kravchenko S.N., 2005. First estimate for their age of a Mesoproterozoic paleomagnetic pole from the Volodarsk-Volynsky Massif, The Ukrainian Shield. Stud. Geophys. Geod. 49, 177-190.

Roedder E., 1984: *Fluid inclusions. Reviews in Mineralogy*. Min. Soc. Am., Washington, D.C., 646p.

Scientific Annals, School of Geology, Aristotle University of Thessaloniki Proceedings of the XIX CBGA Congress, Thessaloniki, Greece	Special volume 100	385-390	Thessaloniki 2010

THE TOKAJ MTS. OBSIDIAN – ITS USE IN PREHISTORY AND PRESENT APPLICATION

Hovorka D. and Illášová, Ľ.

Faculty of Natural Sciences, Constantine the Philosopher University in Nitra, 949 74, Nitra, Slovakia, dusan.hovorka@gmail.com, lillasova@ukf.sk

Abstract: Homogeneous acid volcanic glass of low water content has been an object of human attention since the prehistory. There exist archaeological evidences dealing with the use of obsidian from the Tokaj Mts. (eastern Slovak Republic and the north-eastern part of Hungary, as well) Late Tertiary volcanic province in the Late Palaeolithic. There at present exist attempts to use it as a jewelry raw material. Obsidian namely in combination with silver, nickel alloys and gold can be effectively used as a modern jewelry material.

Key words: Slovak Republic, obsidian, praehistory, nowadays utilisation

1. Introduction

One of typical geological processes, acted on the territory of the Slovak Republic, was Late Tertiary volcanic activity. Its various products are known from several volcanic mountains concentrated as a girdle on the inner side of the Carpathians belt. As far as its mineral and chemical composition is concerned, the rock products are represented by calc-alkaline clan, on isolated places also by alkaline basalts. Based on the geological surrounding of the site, where the lavas of the mentioned types penetrates the Earth´s surface, products of the volcanic activity have various appearances. One of the characteristic rock-types is the acid volcanic glass of the obsidian category. Disintegration of glassy lava bodies into blocks is the consequence of internal tension of the rhyolitic lava pouring into a water basin. Country rocks of the obsidian are various, mostly fine-grained mixed rocks of sedimentary as well as volcanic origin (= tuffites). Characteristic raw materials of prehistory –in archaeology cultures of the Palaeolithic– are very fine-grained till in observation by naked eyes amorphous siliceous matters and the acid volcanic glass - obsidian.

In the Tokaj Mts. (spread both on the territory of the Slovak Republic and Hungary) obsidian blocs are cropping out in the hilly area, or they are deposited several meters in depths. Individual blocks have dark, mostly blackish and greyish tints, in some cases also of deep-green, or brownish tint have been documented. Thin sections studies brought evidences of the presence of acid plagioclases as well as Na-K feldspars and in some spots also cristobalite radial crystals in discussed type of volcanic glass. Dark silicates, (namely dark micas) are represented mostly by their crystallites of 0,3 mm dimensions. Such our observations are in general agreement with those of Rózsa et al. (2003).

The most abundant obsidian blocks do occur just between the villages Viničky and Veľká Bara. Suitable environmental conditions enable the human tribes to settle this area already in the Palaeolithic. Archaeological excavations at sites of Cejkov, Kašov, Bara, Hrčel-Pivničky, and the others, offered plenty of stone implements made of obsidian. Archaeological aspects of the Tokaj Mts, obsidian are treated namely in papers by Janšák (1935); Bánesz (1961); Kaminská, (1995); Kaminská and Ďuda (1985) and Šiška (1999). In the very last time Illášová et al. (2008) published a little monograph devoted to the obsidian just from the Viničky site and the general characteristics of the area under consideration.

In Europe there are only several obsidian occurrences, but majority of them are known from the Eastern Mediterranean. So implements made of this characteristic raw material type occurring in the Tokaj Mts. were spread over the long distances in the neighbouring countries as well as in Germany and on Balkans. Evidences for this statement

are presented in papers by Warren et al. (1977), Williams (1983), Williams et al. (1984) and Rosania et al. (2008), resp. They are based (Williams and Nandris 1977) on similar chemical composition (main oxides, trace elements including REE, and isotopic data) of obsidian implements deposited in museums in Germany with obsidian from field occurrences just from the Tokaj Mts.

2. Background

From the geological point of view, obsidian occurrences are a part of extrusive body of rhyolitic lava 11–12 Ma, which under the postmagamtic hydrothermal activity is intensively secondary decomposed. So individual blocks of obsidian occurrences are present within the soft light-colored rocks of sedimentary and volcanic origin (=tuffites). On the Slovak Republic territory, Late Palaeolithic as well as Neolithic implements made of obsidian, as well as of other local raw materials –namely of limnoquartzite (= limnosilicite), occurring in the central Slovakia Žiar nad Hronom Late tertiary basin were described from the whole country territory (Hovorka and Illášová, 2002).

There exist written sources dealing with the raw material of chipped industry just from the Viničky area (see again Fig. 1). Obsidians (or the most probably ready-made implements) from this area were spread over practically the whole central and south-eastern Europe, where cutting tools and even untouched cores were found.

3. Material and Methods

The presented results are based on individual pieces of obsidian found on surface of vineyard of Viničky and Malá Bara willages. We have choosed, by naked eye, homogenous obsidian pieces with neither cracks nor zones of weathering. Obsidian pieces under consideration sized 2 to 12 cm. From the whole set of obsidian pieces we have choosed one hundred of them with stereoscopic microscope, for consequent cutting for cabochon and platelets. Realised laboratory tests proved the suitability of obsidian from Tokaj Mts. area for gemmological purposes for such conclusion is also the low amount (25-30%) of refuse from the total. All mentioned technologies have been realised in laboratories of DRAHOKAM Turnov (Czech Republik).

4. Results

Obsidians of the eastern Slovakia rank among the group of unaltered volcanic glasses generally with

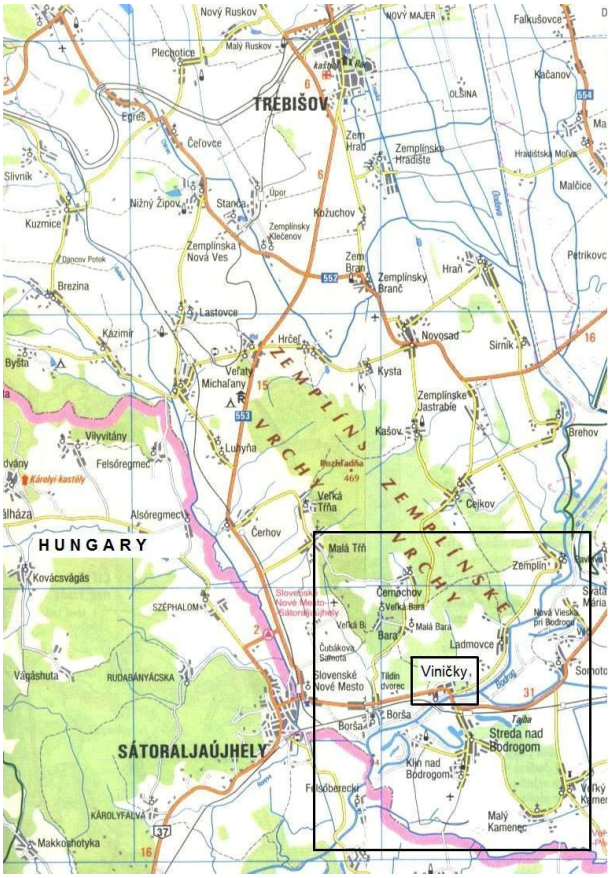

Fig. 1 Map of Tokaj Mts. and surroundings. Going north, except for Poland, Moravia (the easternmost county of the Czech Republic) and Bohemia, deposits of these obsidian-made tools and weapons are expected to occur up to the town Zauschwitz southward of Liptz (The Linear Pottery and Stroke Ware Cultures: Baumann and Fritzsche, 1973). On this place cutting tools, shaving blades and also untouched cores were found. The area covers the length of approximately 750 km. Other obsidian implements expected to come from the discussed area were found near Bodman (the northwestern Germany: Maier, 1955). Implements made of obsidian from the Zemplin county occurrences are traced southward to Macedonia and Balkan peninsula (850 km: Kilikoglou et al., 1996).

SiO_2 content about 75 %. The SiO_2 content in obsidians from the vicinity of Viničky village ranges from 74,65 to 75,79 % (Tab. 1); specifically from particular occurrences in the Viničky site (columns 1-5, Tab. 2). Higher acidity of local lavas led to higher SiO_2 content and lower H_2O content (0,01-0,66 %) in comparison with the world average (Šalát and Ončáková 1964). This is the reason of their higher devitrification resistance and at the same time of their technological suitability for production of decorative artefacts and jewelry, as well. Density of the Tokaj Mts. obsidians ranges between 2,3-2,4 g/cm^{-3}, porosity is noticeably un-

der 1 %, hardness at Mohs scale 5-5,5. Index of refraction is 1,48-1,51.

Fig. 2. Pieces of obsidian – the largest sized 10 cm in length - (a, up), obsidian of high quality (103 x 94 x 60 mm) - (b-down).

Obsidian pieces are of various sizes, which varied from 1 to 20 cm in diameter (Fig. 2a-b). Their colour is black, black-grey, in thin cuts grey to pale grey, sometime brownish. Production of jewelry and haberdashery are handicrafts. Banded obsidian forms are attractive. So-called silver obsidian varieties from here are known as well. Silvery shade is caused by the content of gaseous-fluid inclusions or crystallites. Fluid textures are pronounced.

For the practical use in the prehistory, types of homogeneous character (Fig. 3a-c) were mostly used. For ornamental purposes in subrecent and recent times dark obsidian with the presence of light microliths (representing accumulation of feldspars and cristobalite mostly of radial orientation and fine-grained character) are known; rarely also banded types, in which light stripes are present in prevailing dark obsidian. For obsidian a low content of water (below of 1 %) is characteristic.

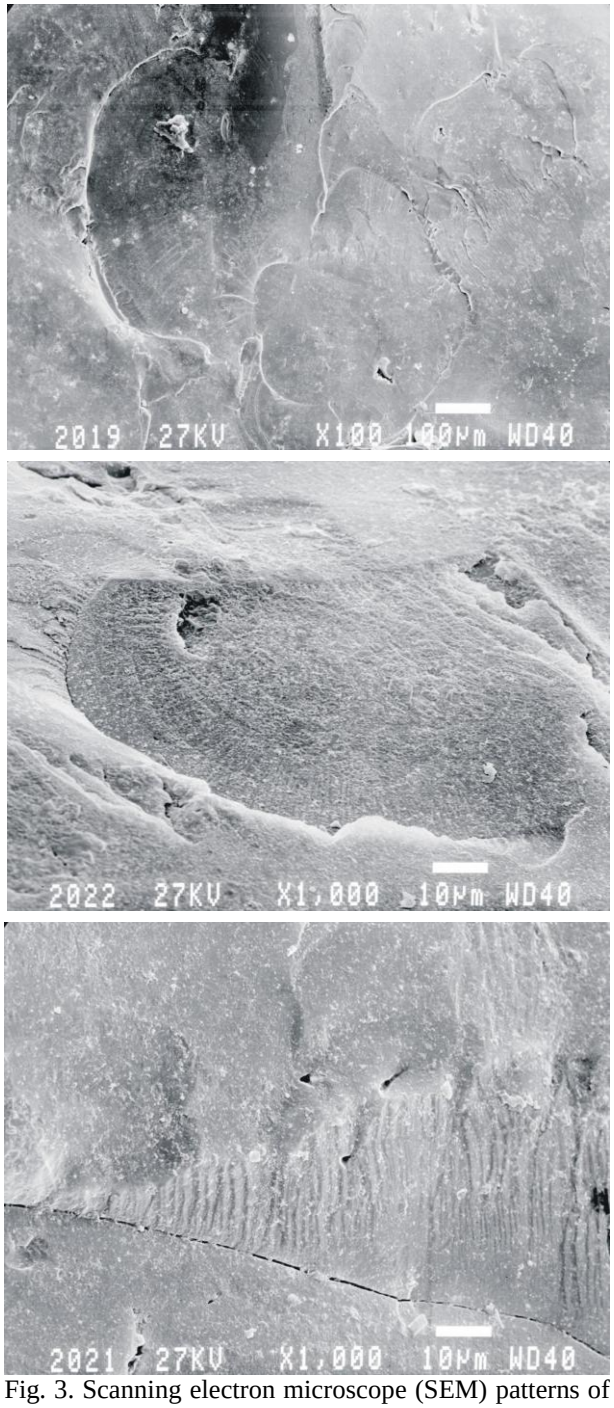

Fig. 3. Scanning electron microscope (SEM) patterns of obsidian from Viničky village. Patterns with non-distinct parallel orientation, low content microlit and for glasses typical splitting planes.

Jewelry and haberdashery production are kinds of traditional craft industry oriented at production of minute ornamental hangings and the various types of parts of weapons, decorations for human bodies, hair, clothes and others (necklaces, pendants and earings) and finally for small souvenirs making. They can occur in modern jewels in shape of mugle or faceted gems in order to represent Slovak decorative gems. From the above-mentioned aspects is clear that there should be paid more attention to the Tokaj Mts. obsidians especially because of its modern practical use as a raw material for decorative products.

Table 1. Obsidian – chemical composition from various occurrences.

Locality	**1**	**2**	**3**	**4**	**5**	**6**	**7**
SiO_2	74,14	74,59	72,8	69	73,8	75,9	69,7
TiO_2	-	0,11	0,1	0,57	0,13	0,25	0,37
Al_20_3	13,74	13,37	13	15,2	13,8	12,8	10,7
Fe_20_3	0,65	0,53	0,69	2,94	0,98	0,85	6,35
FeO	1,74	0,95	1,4	0,15	0,83	0,57	-
MnO	0,19	0,02	0,08	0,11	0,05	0,05	0,13
MgO	0,24	0,53	0,6	0,81	0,29	0,16	-
CaO	1,3	0,67	1,26	2,6	1,09	0,48	0,37
Na_2O	2,98	4,47	4,37	3,36	3,97	3,74	6,54
K_2O	4,31	4,51	5,04	4,12	3,98	4,2	4,52
H_2O^+	0,18	0,32	-	-	0,33	0,15	-
H_2O^-	0,05	0,04	-	-	0,07	0,01	-
P_2O_5	0,17	0,02	-	0,13	0,02	0	-
CO_2	-	0,22	-	-	-	0,05	-
S	-	-	-	-	0,05	-	-
s.ž.	-		0,2	-	0,33	-	-
Total	100,7	100,4	99,5	99	99,7	99,2	98,7

1 – Viničky, Tokaj county, Slovakia (Šalát, Ončáková 1964); 2 – Milos, Greece (Pesty, 1970); 3 – Lipari, Greece (Cobella et al., 1978); 4 – Sardínia, Italy (Coulon et al., 1978); 5 – Armenia (Karapetjan and Meliksenjan, 1981); 6 – Yellowstone, U.S (Laurse and Lanford, 1978); 7 – Rift-walley, Ethiopia (Gibson, 1970).

Obsidian is homogenous, suitable to cut and also to polish material. When it is dressed, presence of minute crystalline inclusions makes no obstruction; they even can be of some decorative quality in the raw material choice. Considering their homogeneity, losses at its cutting or polishing are relatively low. This is true when flat slices are cut from obsidians.

Verification of technological properties: losses caused by cutting into slices were watched together with those caused by polishing and other properties that can influence the final cut quality (Turnovec, 1985). We tested 500 g of obsidian fragments. Results of obsidian raw material recovery are comparable to commercial coloured chalcedonies, morion or smoky quartz.

Another way of the Tokaj Mts. obsidian dressing was simple tromling/tumbling of fragments. Massive fragments that had been freed from surface crust were put into tromling apparatus. The result was excellent and the recovery from the raw material was 90 %. In general, many minerals are convenient for tromling – massive and grainy as well as crystalline ones. This method is simple and undemanding.

The most common obsidian cuts are cabochons (Fig. 4). Losses caused by cutting and polishing in their production were examined (Tab. 3). As far as obsidians are partially transparent, they can be dressed also as faceted stones (Fig. 5) and made plates (Fig. 6). Convenient shapes are mainly step cuts, less brilliant cuts.

Table 2. Obsidian chemical composition: Viničky, Tokaj county, Slovakia

	1	2	3	4	5	6
SiO_2	74,59	68,51	66,93	75,1	75,4	75,75
TiO_2			0,4			0,02
Al_2O_3	13,44	15,6	15,74	14,07	14,15	13,73
Fe_2O_3	0,58	2,11	3,37	0,37	0,35	1,01
FeO	2,64	1,62	1,57	0,84	0,72	-
MnO	0,03		0,3	0,04	0,04	-
MgO	0,34	0,52	1,07	0,36	0,28	0,03
CaO	1,42	2,2	3,3	1,23	1,14	1,25
Na_2O	3,15	2,51	3,12	3,54	3,62	2,25
K_2O	3,05	0,55	3	4,37	4,36	4,92
P_2O_5	0,17	0,11	0,16	St.	-	
$+H_2O$						
$-H_2O$						
Total	100,36	100,39	100,36	100,12	100,24	100,36

Obsidian Viničky – various blocks (Šalát, Ončáková, 1964) in fine-grained volcaniclastics.

Obsidian blocks are homogeneous in color and composition. But there exists blocks, on the surface of which minute white flaky units (similar to the snow flakes) composed of cristobalite occur. Such types are called „flake obsidians“. Though obsidian is the product of rapid cooling of acid lavas, in the majority of thin sections minute crystals of biotite (dark micas) and magnetites (iron oxide) are visible there. Their distribution on the area of thin sections is irregular; size of individual crystals ranges within 20 - 200 μm.

Realised X-ray diffraction procedure (Illášová et

al., 2006) expressed on appropriate diffraction patterns shows any pronounced peaks. The only one wide reflection equal to 22,5^{o} 2Θ, which is equal to obsidians from the Melos and Lipary Islands (the eastern Mediterranean), as well as obsidian from Georgia. Among the analyzed set of obsidians from the European localities (Tab. 1) it is evident, that obsidians from the eastern Tokaj Mts. has the most acid character. So they are derivatives of the proper rhyolitic lavas (Biró et al., 1986; Bigazzi et al., 1990).

Fig. 4. Cut cabochon oval, (sized approximately: 10 x 8 x 5 mm) and cut cabochon – tear (length: 22 mm).

Another way of studied obsidian dressing was simple tromling/tumbling of fragments. Massive fragments that had been freed from surface crust were put into tromling apparatus. The result was excellent and the recovery from the raw material was 90 %. In general, many minerals are convenient for tromling – massive and grainy as well as cryptocrystalline ones. This method is simple and undemanding. As far as obsidians are partially transparent, they can be dressed also as faceted stones and made plates. Convenient shapes are mainly step cuts, less brilliant cuts.

5. Discussion and conclusion

During the last decade of the 20th century and the

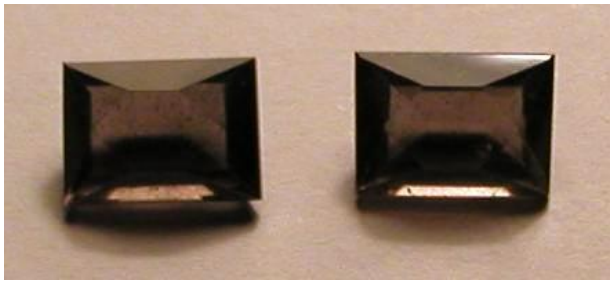

Fig. 5. Step square cut (sized approximately 12x10x5 mm).

Fig. 6. Oval plate (sized approximately30 x 20 x 5 mm)

first years of the 21st, in the European post communistic countries boom of precious stones as well as noble metals (namely gold and platinum) is evident. Elevated demand of precious stones, and jewelry is achieved in general of: a) elevated import of precious stones; b) synthetically made imitations of them, and c) use of new non-traditional precious and semi-precious stones.

Among such nontraditional semi-precious stones belongs also obsidian from the Tokaj Mts. (both on territories of the Slovak Republic as well as of Hungary) occurrences. Till now realised laboratory tests offer data on the appropriate quality of accidentally chosen blocks of obsidian for jewels production. Polished obsidian (mostly of cabochon morphology) in combination with silver and gold resp., are attractive, and what is important, not very expensive. To test the public interest for, from the obsidian made jewelry, several exhibitions of discussed type jewelry in Nitra (Ski) and Turnov (CSV) were organized (Illášová and Turnovec, 2004). Interest of the public was strong, i.e. - almost all presented obsidian-made jewels were sold. Accepting the renaissance of obsidian in a life of society, this raw material belongs to those ones, which have been used since pre-history and is used till present.

Table 3. Gemmological quality of Slovak obsidians

Variety cabochons:	**Pieces**	**Extract**	
	2, 643 g	40,80%	shape tear (15 x 7 x 4 mm)
	1,774 g	24,00%	length of triangle 14, 14 12 mm
	2, 186 g	25,20%	round, diameter 10 mm
	7, 464 g	26,1	round 2 piece diameter 10 mm
	6,038 g	86,7	cabochon 2 piece: round, diameter 10 mm, ovalny 5 x 7 mm
	5,593 g	46,30%	cabochon (4 piece) elipse 5 x 7 mm, 5 x 7 mm; round, diameter 10 mm and 10 mm
Extract in percentage from 4,3 g raw material: from 36 % to 47 %, sporadic different			
Variety fazets:	**Pieces**	**Extract**	
	2,618 g	36,31%	
	1,912 g	23,53%	
	2,28 g	21,35%	
	7,39 g	22,08%	
	6,22 g	44,40%	
	5,721 g	40,13%	
Extract in percentage at fazetes shape (common step square or rectangle) from 4,36 g raw material is from 28 to 49 %, sporadic different			
Flat plates:	500 g	31-57%	

References

Bánesz L., 1961. Prehľad paleolitu východného Slovenska. Slovenská Archeológia, IX. Bratislava, Veda, SAV, 33-44.

Baumann W., Fritzsche C., 1973. Ein weiterer Tiergefäßfund in der bandkeramischen Siedlung von Zauschwitz. Kr. Borna, Ausgrabungen und Funde 18, 63-70.

Bigazzi G., Marton P., Norelli, P. and Rozložník, M., 1990. Fission track dating of Carpathian obsidians and provenance identification. Nuclear track and radiation measurements, 17, 3; 301-306.

Biró T. K., Poszgau I., Vladár A., 1986. Electron beam microanalyses of obsidian samples from geological and archaeological sites. Acta Archeol. Acad. Sc. Hungaricea, 38. Academiai Kiado, Budapest, 257-278.

Hovorka D., Illášová Ľ., 2002. Anorganické suroviny doby kamennej. UKF Nitra, 201 p.

Illášová Ľ., Turnovec I., 2004. Východoslovenské obsidiany a jejich využití. Bull. mineral., petrolog. Nár. Muzea, Praha, 11, 150-152.

Illášová Ľ., Spišiak J. (edts.), 2006. Geochémia prírodných skiel. Zborník z konferencie Prírodné sklá a kremité hmoty. Sept. 2004 Nitra-Viničky. Edícia prírodovedec č. 213, UKF Nitra, 52-73.

Illášová Ľ., Jamrichová E., Spišiak J., Turnovec I., 2008. Sopečné sklo z Viničiek. Čo je zdrojom sily a kvality tokajského. Edícia Prírodovedec č. 317, Nitra, UKF FPV, 64 s.

Janšák Š., 1935. Praveké sídliská s obsidiánovou industriou na východnom Slovensku. Bratislava, 85 p.

Kaminská Ľ., 1995. Katalóg štiepanej kamennej industrie z Hrčeľa-Pivničiek a Veľatoch. Supl. 4, Slov. Archeol. Spol. pri AÚ SAV, Nitra , AÚ SAV, 95 p.

Kaminská Ľ., Ďuďa R., 1985. K otázke významu obsidiánovej suroviny v paleolite Slovenska. Archeologické rozhledy, 37, Praha, ČAV, 121-129.

Kilikoglou V., Bassiakos Y., Grimanis A. P., Souvatis K., Pilali-Papasteriou A., Papanthimou-Papaefthimiou A., 1996. Carpathian obsidian in Macedonia, Greece. Journal of Archaeological Science, 23, 343-349.

Maier R. A., 1955. Keramik der Baden Kultur aus Ufersiedlungen des Bodensees, Germania 33, 155-173 p.

Rosania, C.N., Boulanger, M.T., Biró, K.T., Ryzhow, S., Trnka, G., Glascock, M.D., 2008. Revisiting Carpathians O sidian. Antiquity, 82, 318.

Rózsa, P. Z., Edlekes, Gy., Szöxor, Simon, A., Simulak, J., Uzonyi, I. and Kiss, Á. Z. 2003. Phynocrysts in obsidian glasses. J. of Radioanalytical and Nuclear Chemistry, 256, 2, 329-337.

Šalát, J., Ončáková, P. 1964. Perlity – ich výskyt, petrochémia a praktické použitie. Bratislava : SAV, 148 s.

Šiška, S. 1999. Sídliska s obsidiánovou industrious. Nitra : SAV, Východoslovenský pravek 5, 65-82.

Turnovec, I. 1985. První zkušenosti s těžbou tuzemských šperkových surovin. Hornická Příbram Drahé kameny, Příbram, 16-30.

Warren, S.E. – Williams, O. – Nandris, J. 1977. The sources and distribution of obsidian in Central Europe. – Intern. Symp. on Archaeometry, Pensylvania.

Williams, O. and Nandris, J. 1977. The Hungarian and Slovak sources of archaeological Obsidian: an interim report on further fieldwork, with a more on tektites. J. Arch. Sci., 4, 207-219.

Williams, C., Thorpe, O., Waren, S.E., Nandris, J.G. 1984. The distribution and provenance of archaeological obsidian in Central and Eastern Europe. J. Archaeol. Sci., 11, 183-212.

Williams, C. 1983. Obsidian im Neolithikum nd Äneolithikum Europas. Ein Überblick. Germania, 61, 2, 327-351.

Scientific Annals, School of Geology, Aristotle University of Thessaloniki Proceedings of the XIX CBGA Congress, Thessaloniki, Greece	Special volume 100	391-397	Thessaloniki 2010

GEM MINERALS AND MATERIALS FROM THE NEOLITHIC AND CHALCOLITHIC PERIODS IN BULGARIA AND THEIR IMPACT ON THE HISTORY OF GEMMOLOGY

Kostov R.I.

Department of Mineralogy and Petrography, Faculty of Geology and Prospecting, University of Mining and Geology "St. Ivan Rilski", 1700 Sofia, Bulgaria, rikostov@yahoo.com

Abstract: Studies of prehistoric (Neolithic to Chalcolithic period) artefacts from the territory of Bulgaria during the past decade revealed a lot of specific gem and decorative minerals and materials: nephrite, malachite, serpentinite, turquoise, jadeite, jet, carnelian, agate and jasper (including heliotrope). Nephrite artefacts in Bulgaria, as well as in some other countries on the Balkans, are widespread during the Neolithic and rare during the Chalcolithic – the nephrite sources are under discussion. A Balkan "nephrite culture" is introduced, which is supposed to be the earliest in the world, compared to the well known Chinese "nephrite cultures". The Varna Chalcolithic necropolis (middle of the V mill. BC) is known with the earliest and largest amount of gold artefacts in the world, including also some copper objects from the copper mines near Stara Zagora. A large amount of beads are also identified as made by malachite (in rare cases with azurite), serpentinite, carnelian, agate, coal (jet), marble and shells. Some of the carnelian beads from Varna display 16+16 facets along their elongation, which is the first record for a constant and complex faceting of hard mineral known so far. An early prehistoric weight system links mineral beads and gold artefacts (the weight unit "van" is introduced, 0.4 g = 2 carats). The first report of turquoise beads for SE Europe is related to the Orlovo prehistoric site (Haskovo district). The "Thracian stone" in ancient sources is identified also as heliotrope, which is known since the Chalcolithic in the Eastern Rhodopes. Some of the artefacts are masterpieces of art and as stage of perfection, thus pointing to the Balkans as a cradle of prehistoric gemmology.

Keywords: nephrite, malachite, serpentinite, jadeite, turquoise, carnelian.

1. Introduction

Archaeomineralogy (archaeological mineralogy; mineralogical archaeology) is an important interdisciplinary science, which is related to the study of archaeological objects of a natural mineral or rock composition, as well as of their sources (including in the broad sense the mineralogical, technological, economic and cultural approach). In certain cases archaeomineralogy is linked also to gemmology (archaeogemmology) as a science for the study of natural and artificial raw materials, which have been used for some sort of jewellery or decorative purposes since the dawn of humankind to modern times (mineral species and aggregates; rocks; bioobjects; glass and pottery, mineral pigments as well as metals and alloys) (Kostov, 2003). Archaeomineralogy can be viewed as part of geoarchaeology as a broader scientific field for application of all the different branches of Earth sciences during archaeological searching, prospecting and study of sites, monuments or artefacts.

A large amount of stone artefacts (lithic material from the Neolithic and Chalcolithic) from museum collections in Bulgaria are studied with respect to specific in colour or genesis minerals and mineral aggregates.

2. Materials and Methods

Among the Neolithic sites are found many nephrite objects, which are considered rare during the next Chalcolithic period. Beside the metal (suggested as the earliest and largest gold treasure; copper) and non-metal (minerals, rocks, pottery, pigments, bioobjects) artefacts in the Chalcolithic graves (V mill. BC) from Varna (as well as in the Durankulak necropolis to the north) in Bulgaria (The First Civilization, 1982; Ivanov and Avramova, 2000; Kostov, 2005b; Gergova and Kostov, 2008 and references therein) are found numerous beads of

different shape and composition. The hardest beads are made of red chalcedony (carnelian) and agate. Other mineral beads are made or malachite, serpentinite, coal (jet) and carbonate material (marble or shells) of different shape. The largest amounts of shells used for decorative purpose are those made from *Dentalium spp*. Turquoise was identified to be used as beads for the first time in southern Bulgaria and heliotrope for small lithic tools in the Eastern Rhodopes – in both cases with local material. The origin of jadeite artefacts is under discussion.

The mineral beads or larger stone (mineral and rock) artefacts have been identified and studied by X-ray powder analysis (TUR-M62 and DRON-2: University of Mining and Geology "St. Ivan Rilski", Sofia), optical microscopy (stereomicroscope MBS-9 and Olympus CZ-61), and in some cases (nephrite) – by microprobe analysis (SEM JEOL-SUPERPROBE 733; Geological Institute, Bulgarian Academy of Sciences, Sofia) and electron paramagnetic resonance (EPR; JEOL FA100; Institute of Catalysis, Bulgarian Academy of Sciences, Sofia), as well as by their color. Their morphometrical characteristics and physical properties are compared to similar artefacts on the Balkan Peninsula and elsewhere (Kostov, 2007a). The mineral artefacts are compared also to the known gem and decorative minerals and aggregates, which are described on the territory of Bulgaria (Petrussenko and Kostov, 1992).

3. Results and Discussion

Nephrite. Nephrite $Ca_2(Fe,Mg)_5Si_8O_{22}(OH)_2$ is a Fe-Mg bearing silicate mineral with a double-chain structure, which is classified in the group of amphiboles (a massive fine fiber variety with an intermediate composition in the tremolite-ferroactinolite series). It is known mainly with a pale green or dark green colour. In some cases small black inclusions can be found in the green aggregates, which are attributed to magnetite and other spinel-type minerals. Nephrite and jadeite are both unified in gemmological literature, as well as to some old and popular science papers, as nephrite-jade and jadeite- jade respectively. However, the term jade is not a valid scientific name for nephrite.

According to archaeological data nephrite objects are spread throughout the Neolithic and Chalcolithic period (~VII-V mill. BC in Bulgaria). Recent observations and redeterminations in museum collections revealed a lot of nephrite samples which have been mislabeled or unidentified from a mineralogical point of view (Kostov, 2005a; 2007a and references therein). Small axes and chisels with a fine polish represent the dominant part of nephrite artefacts. Among the artefacts can be found ritual zoomorphic (frog-like) figurines or amulets, two of them with a 4-fold (swastika type) rotational symmetry from the Early Neolithic sites at Kurdjali and Kovachevo (Kostov, 2007a; Fig. 1). A unique and finely polished scepter, 36.4 cm long, found at the Early Neolithic site at Galabnic near Sofia is supposed to be nephritoid (serpentinite) or nephrite-bearing (Kostov, 2007a). Most of the nephrite artefacts are located in Southwest Bulgaria – they have been found mainly in archaeological sites

Fig. 1. Nephrite artefact (axe fragment, 4.6x3.6x0.9 cm) N30939; Kovachevo, Blagoevgrad region, Early Neolithic (left; photo R. Kostov) and zoomorphic nephrite amulet N4532; Regional Historical Museum Kurdjali, Early Neolithic, 4.2x3.7 cm (right; photo V. Alexeev).

along the Struma valley with the largest number and variety of finds from the Kovachevo prehistoric site. Seventeen nephrite artefacts (represented mainly by small axes) are described throughout the Early Neolithic to Late Chalcolithic at the Karanovo prehistoric site in Central Bulgaria (Kostov and Lang, 2005). At the Varna II Chalcolithic necropolis, a fine nephrite "hair pin" is found with dimensions 12.1x0.7 cm (Kostov et al., 2003).

Electron paramagnetic resonance (EPR) spectroscopy of nephrite from Neolithic artefacts found at sites along the Struma valley revealed three main types of signals: a weak signal of Fe^{3+} (g~4.3; in supposed tetrahedral sites in the structure), a strong and broad signal due to iron-bearing phases and/or Fe^{3+}-Fe^{2+} clusters (g~2) and a 6-component signal from Mn^{2+} (g~2). The EPR data, as well as the microprobe data (including the inclusions), are considered as useful for determination of groups of nephrite samples from at least two possible deposits (occurrences) on the territory of Southern Bulgaria or some other Balkan countries (Kostov, 2007a; 2009).

Neolithic nephrite artefacts, including an amulet, are reported also from Serbia (Antonovic and Stojanovic, 2009), as well as from some other Balkan countries (Kostov, 2007a). No nephrite deposits are known from geological publications in the Balkan region so far, despite of the favorable geological setting with a lot of ultrabasic (serpentinite) exposures. One possible source has to be confirmed in Turkish Thrace, linked to the Yenikoy melange (Özbek, 2009). The well known European nephrite deposits in Poland, Switzerland and Italy have been (re)discovered in the late XIX and early XX centuries, and do not provide information or can not be related to trade routes on the Balkans in prehistoric times. As the Early Neolithic on the Balkans is dated about the VII-VI mill. BC, thus the observed nephrite objects as part of the Balkan prehistoric area are considered as representatives of the earliest "nephrite culture", long time before the well known "nephrite cultures" (Hemudu; Hongshan; Liangzhu; Longshan) in Neolithic China or in the Russian Federation (Kitoi; Glaskovo) (Kostov, 2005a; 2007a).

Jadeite. Jadeite $NaAlSi_2O_6$ belongs to the pyroxene group. In prehistory jadeite artefacts are spread during the Neolithic in Western Europe and on the British Isles (see D'Amico et al., 1995). Such artefacts are known from several archaeological sites in Bulgaria, but their origin as far as from the Alps (Errera et al., 2006; Pétrequin et al., 2009) is under discussion (Kostov, 2007a). The mineral is not found in Bulgaria, but is known from occurrences in Turkey and F.Y.R. Macedonia.

Malachite. Malachite $Cu_2(CO_3)(OH)_2$ is a wide spread copper carbonate mineral. Among the nonmetallic jewellery objects from grave N3 of the Chalcolithic necropolis Varna II is a necklace of short cylindrical mainly malachite beads (in a single case – a bead with admixture of azurite $Cu_3(CO_3)_2(OH)_2$, and in several other cases – with admixtures of cuprite Cu_2O) (Kostov et al., 2003). The study of the nonmetallic mineral artefacts of gemmological interest found in the prehistoric cemetery at Durankulak (NE Bulgaria) display similar beads and admixtures (Kostov and Dimov 2003; Fig. 2).The malachite short cylindrical beads have an average weight of 0.06 g and 0.20-0.25 g. Malachite beads are known since the VII mill. BC from Jericho in the Near East and from Ergani-Cayonu Tepesi and Catalhouk in Turkey (Savascin 1986). In Bulgaria malachite artefacts are reported since the Neolithic and related to malachite are the big copper deposits Mechi Kladenets (Ai Bunar) of Chalcolithic age near Stara Zagora – supposed to be the earliest for Europe.

Serpentinite. Serpentinite is a rock composed mainly by chrysotile $Mg_3Si_{21}O_5(OH)_4$, antigorite $(Mg,Fe)_3Si_2O_5(OH)_4$ and lizardite $Mg_3Si_2O_5(OH)_4$, formed after ultrabasic rocks. This rock is widely used as raw material in the Neolithic and Chalcolithic of Bulgaria. At the Kovachevo prehistoric site the serpentinite artefacts are ~50% among the lithic materials (Kostov, 2007a). The serpentinites

Fig. 2. Malachite (with azurite bead in the middle) beads in a necklace from the Durankulak necropolis, Historical Museum Dobrich NK1441-3, diameter of beads 0.2-0.5 cm (photo V. Alexeev).

are dark-coloured, almost black. They are represented mainly by antigorite, in some cases with talk, and small black oxide inclusions. A fine reel-holder (3.2x3.1 cm; 50.85 g) made of dark serpentinite, probably intended to be used in the drilling process, is known from the Chalcolithic necropolis Varna II (Kostov et al. 2003). Pale green serpentinite short cylindrical beads from the Varna Chalcolithic necropolis have an average weight of 0.025 g and 0.07 g and similar beads are described from the near-by Durankulak site (Kostov and Dimov, 2003).

Turquoise. Turquoise $CuAl_6(PO_4)_4(OH)_8.4H_2O$ is a copper-bearing phosphate mineral with a distinctive blue or bluish green colour. Turquoise was identified among beads from the prehistoric (Neolithic to Chalcolithic) Orlovo site near the town of Haskovo in southern Bulgaria (Kostov et al., 2007). The finds at Orlovo of polished beads and bored bead blanks of turquoise (Fig. 3) suggest a local prehistoric bead workshop for this prestigious material. The most reliable source for the raw material is the Spahievo Pb-Zn ore field south-west of Haskovo, where turquoise mineralization has been found both during underground mining and at the surface as small veinlets. The turquoise beads are considered as the earliest report of this gemmological material in southeast Europe.

Coal (Jet). The gemmological name jet is generally employed in most countries for a black hard, fossilized coniferous wood, which is capable of being carved and can be highly polished. Jet is an amorphous organic non transparent substance with a brown streak and 2.5-4 hardness on the Mohs scale. Coal beads are found both in the Durankulak (Kostov and Dimov, 2003) and Varna (Kostov, 2007a) necropolis. At the second site they are represented by short cylindrical (the smallest beads are with mean weight 0.003, 0.006 and 0.009 g) and barrel-shaped beads (mean weight 0.015, 0.022 and 0.06 g). In previous works they are published as made of lignite, but recent studies point to jet, due to the law refractive values and microscopic observation (Kostov et al., 2010).

Fig. 3. Turquoise bead (1.2x0.7x0.3 cm) from the Orlovo prehistoric site, Regional Historical Museum Haskovo (photo I. Petrov).

Carnelian and agate. Among the metallic (gold and copper) and non-metallic artefacts found in graves from the Chalcolithic sites at Durankulak and Varna are numerous beads of a carnelian and agate composition (Fig. 4). Three main morphological types of beads have been described: type 1 – elongated barrel-shaped; type 2 – elongated with trapezohedral facets; type 3 – short cylindrical. The carnelian and related beads of type 2 have a "constant" number of 32 facets, 16+16 on both sides on the elongation of the bead (the form is a truncated 16-fold trapezohedron), which is considered the earliest in Chalcolithic times complex type of faceting on a hard mineral as quartz (chalcedony is 6.5-7 on the Mohs scale). In the hole of a single carnelian bead a gold mini-cylinder (~2x2 mm) was found, probably with the purpose to tighten up some sort of strip.

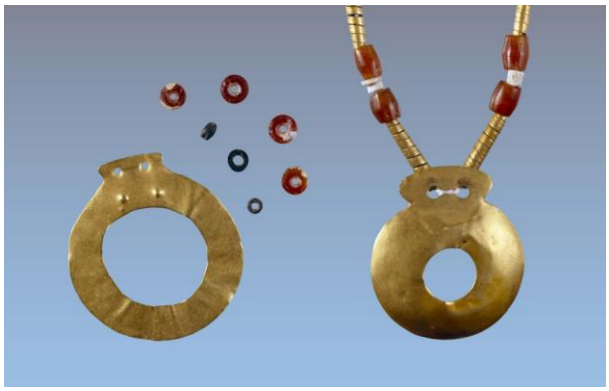
Fig. 4. Gold ring shaped (diameter 3.8 and 3.6 cm) and spiral artefacts, mineral (4 short cylindrical and 4 barrel and faceted red carnelian and 3 white carbonate) and 3 black jet beads from the Varna Chalcolithic necropolis, NI.2771, graves N97 and N254 (photo V. Alexeev).

The mean dimensions (length to width) for the types 1and 2 beads is 1.29 (weight 0.40 g) and for type 3 – 0.54 (weight 0.15 g) (Kostov and Dimov, 2003; Kostov and Pelevina, 2008). Three main types of colour have been distinguished visually among the carnelian beads: orange red, red and

dark red. It has been suggested that the uniform dark red colour may have resulted from a process of heating of pale red or pinkish coloured carnelian beads (for Indian carnelian see Kenoyer, 1997). Such technique for improving the colour of gemstones is known even today for carnelian in Asia Minor, Iran, Pakistan and India ("mekke tasi", Savascin, 1986). Several operations of manufacture have been suggested for the described carnelian beads – pecking, shaping, faceting, polishing, drilling and tumbling.

The social and symbolic meaning of the chalcedony beads are studied – in the Durankulak necropolis they are distributed equally among male and female graves and in the Varna I necropolis they are typical for the symbolic graves (cenotaphs). In both cases the chalcedony beads are associated with gold and copper objects, as well as with pottery and bone or shell artefacts – they are considered as prestigious jewellery objects (Kostov and Pelevina 2008). The origin and trade routes of carnelian is not yet clarified.

The aesthetic value of brilliance and colour among the Varna mineral beads has been discussed (Chapman, 2007; Gaydarska and Chapman, 2008). Probably all of the beads are linked to a complex weight system among each material and between the different mineral and metal substances (Kostov, 2004; 2007a). The gold objects from the Chalcolithic necropolis at Varna are assumed to be the "oldest gold of mankind" according to their number and quantity. Analysis of the measured weight of the different types of gold artefacts (beads, appliqués, rings, bracelets, pectorals and diadems; Fig. 4) has revealed at least two weight units of 0.14-0.15 and 0.40-0.41 g in correspondence to the carnelian beads weight (Kostov, 2004; 2005b). The second weight is suggested as a basic "Chalcolithic unit" (=2 carats) with the name "van" (from the first letters of Varna necropolis). The weight units as applied to the golden objects are supposed to be the earliest in history and related in later times to other weight units in the Near East, Mesopotamia and Ancient Egypt.

Jasper (including heliotrope). Jasper of different colour is spread in Bulgaria mainly in the Eastern Rhodopes and West Srednogorie regions (Petrussenko and Kostov, 1992). Small red jasper of jasperoid beads are known from the prehistoric Durankulak necropolis (Kostov and Dimov, 2003). Heliotrope (bloodstone; dark green jasper with red spots) is another rare material, which has been found at the Chalcolithic workshop at Sedlare in the Eastern Rhodopes. The "Thracian stone" in ancient sources (Pliny the Elder) is identified also as heliotrope, probably traded in the past from the same area (Kostov, 2007b).

4. Conclusions

Archaeomineralogical studies of prehistoric (Neolithic to Chalcolithic period) artefacts from the territory of Bulgaria revealed a lot of specific (important to the history of gemmology) gem and decorative minerals and materials as nephrite, malachite, serpentinite, turquoise, jadeite, coal (jet), carnelian, agate and jasper (including heliotrope).

Nephrite artefacts are known from prehistoric sites since the Early Neolithic and they "disappear" at the end of the Chalcolithic period. For gemmologists the precision and symmetry of the objects as well as the perfection in the final polishing is a surprise. The possible nephrite sources in Bulgaria, as well as in some other countries on the Balkans are under discussion. A Balkan "nephrite culture" is introduced, which is supposed to be the earliest in the world, compared to the well known Asian "nephrite cultures".

The Varna Chalcolithic necropolis (middle of the V mill. BC) is known as the place with the earliest and largest amount of gold artefacts in the world, including also some copper objects from the copper mines near Stara Zagora. A large amount of mineral beads are also identified as made from malachite (in rare cases with azurite), serpentinite, carnelian, agate, coal (jet), marble and shells. Some of the carnelian beads from Varna display 32 (16+16) facets along their elongation, which is the first record for constant and complex faceting of hard mineral known so far. An early prehistoric weight system links mineral beads and gold artefacts and the weight unit "van" is introduced (0.4 g = 2 carats).

The first report of turquoise beads for SE Europe is related to the Orlovo prehistoric site (Haskovo district) with a local source. The "Thracian stone" in ancient sources has been identified also as heliotrope, which is known since the Chalcolithic in the Eastern Rhodopes.

The territory of contemporary Bulgaria and the Balkans in general can be suggested as a homeland of developing of prehistoric (Neolithic and Chalcolithic) jewellery craft and trade (different mineral beads and other artefacts, faceted beads, precious

minerals and bioobjects, gold and copper), which is of importance both for the European and world history of gemmology.

Acknowledgements

The author wish to thank the following colleagues, who assisted or helped in different manner the archaeomineralogical studies: Dr. J. Chapman (Durham, England), Dr. B. Gaydarska (Durham, England), Assoc. Prof. Dr. M. Gurova (Sofia), Dr. M. Grebska-Kulova (Blagoevgrad), Assoc. Prof. Dr. I. Kostova (Sofia), Dr. F. Lang (Salzburg, Austria), Prof. Dr.Sc. M. Lichardus-Itten (Paris, France), Assoc. Prof. Dr. Ph. Machev (Sofia), Prof. Dr.Sc. V. Nikolov (Sofia), Dr. V. Slavchev (Varna), Assoc. Prof. Dr. N. Zidarov (Sofia), V. Alexeev (Sofia), A. Bakamska (Pernik), J. Boyadjiev (Varna), M. Christov (Sofia), T. Dimov (Dobrich), V. Genadieva (Kyustendil), I. Kulov (Blagoevgrad), O. Pelevina (Varna), I. Petrov (Haskovo) and P. Zidarov (Sofia).

References

Antonović D. and Stojanović A., 2009. The nephrite amulet from Zmajevac (Cerovac, Central Serbia). Archäologisches Korrespondenzblatt, 39, 2, 183-191.

Chapman J., 2007. The elaboration of an aesthetic of brilliance and colour in the Climax Copper Age. In: Stephanos Aristeios. Archäologische Forschungen zwischen Nil und Istros. Lang, F., Reinholdt, C. and Weilhartner, J. (eds), Wien, 65-74.

D'Amico C., Campana R., Felice G. and Ghedini M., 1995. Eclogites and jades as prehistoric implements in Europe: A case of petrology applied to Cultural Heritage. European Journal of Mineralogy, 7, 1, 29-41.

Errera M., Hauzeur A., Pétrequin P. and Tsonev Ts., 2006. Étude spectroradiométrique d'une hache trouvée à Svoboda, district de Chirpan (Bulgarie). Interdisciplinary Studies, 19, Sofia, 7-24.

The First Civilization in Europe and the Oldest Gold in the World – Varna, Bulgaria. 1982. Nippon Television Network Cultural Society, 135p (in Japanese and English).

Gaydarska B. and Chapman J., 2008. The aesthetics of colour and brilliance – or why were prehistoric persons interested in rocks, minerals, clays and pigments? In: Geoarchaeology and Archaeomineralogy, Kostov, R.I., Gaydarska, B. and Gurova M. (eds), Proceedings of the International Conference, Sofia, 29-30 October 2008, Publishing House "St. Ivan Rilski", Sofia, 63-66.

Gergova D. and Kostov R.I., 2008. Role of Bulgaria in the history of world's jewellery art. In: Field Trip Guide Book. International Conference "Geoarchaeology and Archaeomineralogy". Sofia, 29-30 October 2008. Sofia, 11-19.

Ivanov I. and Avramova M., 2000. Varna Necropolis. The Dawn of European Civilization. Agató Publishers, Sofia, 55p.

Kenoyer J.M., 1997. Trade and technology of the Indus valley: new insides from Harappa, Pakistan. World Archaeology, 29, 2, 262-280.

Kostov R.I., 2003. Precious Minerals: Testing, Distribution, Cutting, History and Application (Gemmology). Pensoft, Sofia-Moscow, X, 453p (in Bulgarian).

Kostov R.I., 2004. Prehistoric weight system among the golden objects of the Varna Chalcolithic necropolis. Geology and Mineral Resources, 3, 25-28 (in Bulgarian with an English abstract).

Kostov R.I., 2005a. Gemmological significance of the prehistoric Balkan "nephrite culture" (cases from Bulgaria). Annual of the University of Mining and Geology, 48, Part I, 91-94.

Kostov R.I., 2005b. Precious and decorative minerals from the Eneolithic necropoli in Northeastern Bulgaria and their significance in the history of gemmology. In: Proceedings of the Jubilee International Conference "80 Years Bulgarian Geological Society", Sofia, 205-208.

Kostov R.I., 2007a. Archaeomineralogy of Neolithic and Chalcolithic Artefacts from Bulgaria and their Significance to Gemmology. Publishing House "St. Ivan Rilski", Sofia, 126p., I-VIII (in Bulgarian with English abstract).

Kostov R.I., 2007b. Notes and interpretation on the 'Thracian stone' in ancient sources. Annual of the University of Mining and Geology, 50, Part I, 99-102.

Kostov R.I., 2009. Electron paramagnetic resonance (EPR) spectroscopy of nephrite (from Neolithic artefacts from SW Bulgaria). Annual of the University of Mining and Geology, 52, Part I, Geology and Geophysics, 115-120.

Kostov R.I. and Dimov T., 2003. Mineralogical and gemmological characteristics of non-metallic jewellery objects from the prehistoric cemetery on the west bank of the Durankulak Lake (NE Bulgaria). Geology and Mineral Resources, 10, 23-29 (in Bulgarian with English abstract).

Kostov R.I. and Lang F., 2005. Nephrite artefacts from the Karanovo prehistoric site, Bulgaria. Geology and Mineral Resources, 9, 35-39.

Kostov R.I. and Pelevina O., 2008. Complex faceted and other carnelian beads from the Varna Chalcolithic necropolis: gemmological analysis. In: Geoarchaeology and Archaeomineralogy, Kostov, R.I., Gaydarska, B. and Gurova M. (eds), Proceedings of the International Conference, Sofia, 29-30 October 2008, Publishing House "St. Ivan Rilski", Sofia, 67-72.

Kostov R.I., Pelevina O. and Slavchev V.S., 2003. Mineralogical and gemmological characteristics of the nonmetallic jewellery objects from the Middle Eneolithic necropolis Varna II. Geology and Mineral Resources, 9, 23-26 (in Bulgarian with English abstract).

Kostov R.I., J. Chapman J., Gaydarska B., Petrov I. and Raduntcheva A., 2007. Turquoise – archaeomineralogical evidences from the Orlovo prehistoric site (Haskovo district, Southern Bulgaria). Geology and Mineral Resources, 7-8, 17-22.

Kostov R.I., I. Kostova I. and Pelevina O., 2010. Coal (jet) beads from the Varna Chalcolithic necropolis (V mill. BC). In: Der Varna Gräberfeld. Vol. II. Slavchev, V.S. (ed.), Archäologie in Eurasien. Deutsches Archäologisches Institut, Eurasien-Abteilung, VML Verlag Marie Leidorf GmbH, Rahden/Westf. (submitted)

Petrussenko S.I. and Kostov R.I., 1992. The Precious and Decorative Minerals in Bulgaria. Bulgarian Academy of Sciences, Sofia, 90p (in Bulgarian).

Özbek O., 2009. Raw material procurement in Thrace in Neolithic societies: comparing settlements in Turkey and in Bulgaria. In: Interdisciplinary Studies on Mediterranean Ancient Marble and Stone. Ph. Jockey (ed.). Maisonneuve & Larose, Maison méditerranéenne des sciences de l'homme, 879-896.

Pétrequin P., Cassen S., Errera M., Tsonev Ts. and Dimitrov K., 2009. Les haches en roches alpines en Bulgarie. In: Jade. Colloque International. Besançon, 24-26 septembre 2009, Résumés des Communications, 47-49.

Savascin Y., 1986. Anatolia: gems from the past. Lapidary Journal 32, 12, 42-44.

Special Session S24
Natural stones, usage and testing

Scientific Annals, School of Geology, Aristotle University of Thessaloniki Proceedings of the XIX CBGA Congress, Thessaloniki, Greece	Special volume 100	399-405	Thessaloniki 2010

CLIMATE CHANGE AND WET WINTERS: TESTING THE DIFFUSION OF SOLUBLE SALTS IN BUILDING STONE UNDER SATURATED CONDITIONS

McCabe S.[1], Smith B.J.[1], McAlister J.J[1]., Viles H.A.[2], Curran J.M.[3] , Crawford T.[4]

[1] *School of Geography, Archaeology and Palaeoecology, Queen's University Belfast, BT7 1NN, UK*
[2]*School of Geography and the Environment, Oxford University Centre for the Environment, Oxford OX1 3QY, UK*
[3] *Consarc Design Group, Belfast, BT7 2JD, UK*
[4] *Geography Department, Methodist College, Belfast, BT9 6BY*

Abstract: Controls on stone decay processes are rapidly changing as a result of changing climate. As such, there is a need to understand decay, not just in a dynamic world, but also in a world where the nature of the dynamics themselves are changing. Future climate change scenarios for the northwest of the United Kingdom (NW UK) typically project both increased short-term uncertainty in day-to-day weather conditions and an underlying trend towards wetter, warmer and longer winter conditions. The result of this is that natural stone used in buildings and monuments is wet for long periods of time – over a wet winter, it is possible that entire blocks become saturated. Usually the movement of salts is associated with moisture flux, but this paper investigates an alternative mechanism of salt movement – when blocks are saturated and a concentration gradient is set up, ions must move by diffusion. Because of the increasingly likely scenario of block saturation (in NW UK), this paper proposes a way of testing salt diffusion through natural building stones, modified and refined from studies testing chloride diffusion in concrete, to determine how quickly salts may diffuse through natural stone and any associated deleterious chemical effects. A concentration gradient is set up, whereby salts diffuse through a saturated sandstone sample from a 'cell' containing a 0.55 molar solution to another 'cell' containing de-ionized water. The increase in concentration in the cell containing de-ionized water can be measured at intervals using Ion Chromatography. Preliminary tests have shown that both salt and stone types are important controls for the rate of diffusion. Emphasis is placed on the need to adapt laboratory studies to more accurately reflect the environmental conditions under investigation.

Keywords: Climate change, salt weathering, ion diffusion

1. Introduction

Controls on stone decay processes are rapidly changing as a result of changing climate. As such, there is a need to understand decay, not just in a dynamic world, but in a world where the nature of the dynamics themselves are changing (Smith et al., 2008), and thus, a need to adapt stone decay experiments in the laboratory to reflect the environmental conditions being investigated. Future climate change scenarios for the northwest of the United Kingdom (NW UK) typically project both increased short-term uncertainty in day-to-day weather conditions and an underlying trend towards wetter, warmer and longer winter conditions (Betts, 2002; Hulme et al., 2002). Buildings appear to have responded to these changing climatic conditions by 'greening' – recent observations have shown an increase in algal 'greening' of external sandstone walls (a material that has shown itself to be particularly sensitive to changes in environmental regime, especially moisture related) in many places in the NW UK (Smith et al., 2004) (see Fig. 1a and 1b). The authors hypothesize that this is caused by a combination of increased moisture and decreased air pollution, and thus reflects recent changing environmental conditions. Beyond this blatant aesthetic and physical change, it is likely that chemical weathering will be enhanced in the NW UK due to increased 'time-of-wetness' (Viles, 2002; Smith et al., 2004). Prolonged and more deeply penetrating wetness should also affect other agents of decay through allowing deep-seated salt penetration and surface algal colonisation.

Fig. 1. Greening of sandstones as a response to increased 'time-of-wetness', St. Mark's Church, Belfast (see also Smith et al., 2004). Greening represented by shading – a (up) shows greening related to surface roughness, b (down) shows patchy greening on a facade.

There is a need in current research to more directly relate changing climatic conditions to effects on a building façade. A first attempt to relate future climate change to effects on built heritage has been carried out in the Noah's Ark project (http://noahsark.isac.cnr.it), using one Global Climate Model (GCM) and one emission scenario. One of the aims of the Noah's Ark project was to research, predict and describe the effects of climate change on Europe's built cultural heritage over the next 100 years. However, the project "does not involve downscaling" (Grossi et al., 2007) and there are, therefore, inherent difficulties in applying the results to 'site specific' localities. Initial work by the Noah's Ark project produced model-based maps of changing sandstone moisture contents showing current very dry conditions across Europe and even drier trends in future (NOAH's ARK, 2007). However, variability in climate across, for example, the UK, is difficult to pick up in these outputs. This is illustrated in the fact that UK-specific studies (for example, Crawford, 2007), using statistical downscaling, do predict increases in winter wetness in NW UK over the next 50 to 100 years that will exaggerate the moisture content of stone masonry. GCMs are simply not appropriate for answering these questions – they were developed to predict synoptic-scale, general circulation patterns of the atmosphere (Crawford, 2007). Thus, the relevance of GCMs decrease as resolution increases – to understand how the changing climate will impact sites or buildings, they are of little use. Predicting the impacts of future climate change on surface and deep-seated wetness of sandstone masonry is a highly complex task, and necessitates downscaling global predictions to a local level and consideration of probabilistic models.

2. Downscaling

"So-called 'downscaling' techniques have… emerged as a means of bridging the gap between what climate modellers are currently able to provide and what impact assessors require" (Wilby and Wigley, 1997, 530).

"Even if global climate models in the future are run at high resolution there will remain the need to 'downscale' the results from such models to individual sites or localities for impact studies" (DOE, 1996). Statistical downscaling consists of a search in observed climate baselines for a statistical relationship between the surface climate variable to be downscaled ('predictand') and the potential 'predictors' (frequently the large-scale upper air variables) and a subsequent application of that relationship to GCM-produced data for future climate change (Huth, 2005). The approach is based on the concept that regional climate is conditioned by two factors: the synoptic climate state, and local physiographic features. Thus, local climate information is derived by first determining a statistical model which relates large-scale climate variables to local characteristics. Then the large-scale output from a GCM experiment is fed into this statistical model

to estimate corresponding local climate variables (Wilby et al., 2002; Wilby and Dawson, 2004; Crawford, 2007).

Projecting future climate change in the NW UK is far from straightforward. Large prediction uncertainty is related to choice of climate model, choice of emissions scenario, and choice of downscaling technique. However, several robust downscaled predictions have emerged from work carried out by, for example, Crawford (2007). Temperatures are likely to increase across all months (though for weathering in the NW UK, this is possibly a secondary concern behind the role of moisture). Precipitation regimes are likely to become much more seasonal, as a function of wetter winters and markedly drier summers (see Fig. 2, illustrating increased seasonality in precipitation across different models and emission scenarios at a site in the west of Northern Ireland, Killyclogher). The number of extreme rainfall events, and their contribution to the overall total, is likely to increase in winters in response to a more zonal synoptic pattern, with increases also found in late summer in response to convective activity (Crawford, 2007).

3. Weathering implications of wetter winters

Investigations into how salt weathering impacts natural stone have largely focused on how soluble

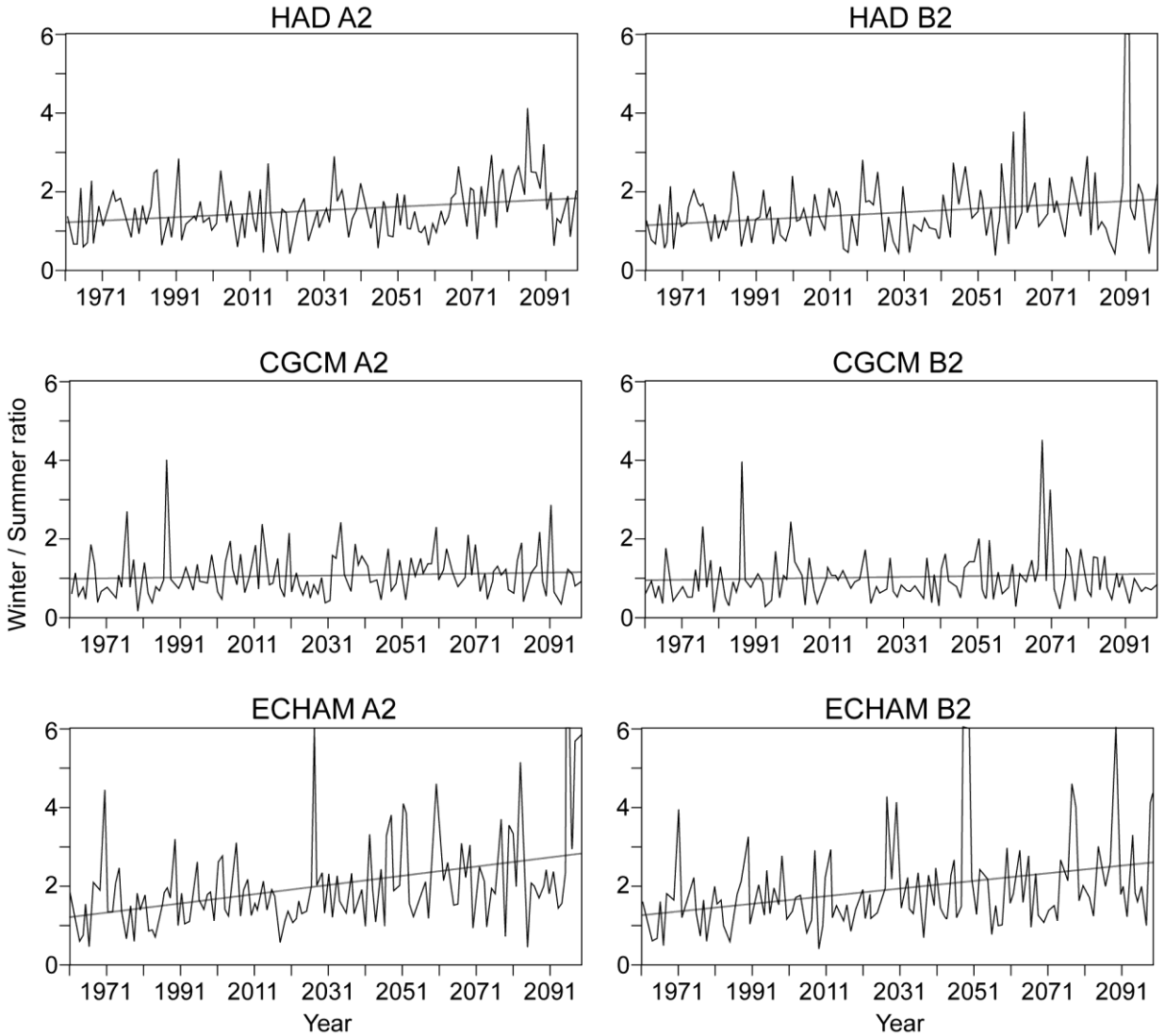

Fig. 2. Shows projected increasing seasonality in precipitation (expressed as a winter/summer ratio) across different models (HAD/CGCM/ECHAM) and emission scenarios (A2/B2) for a site in west NI (Killyclogher) – a trend mirrored to varying degrees around the NW UK (from Crawford 2007). HAD = HADCM3, UK Met Office's atmospheric Unified Model; CGCM = CGCM2, the second version of the Canadian Centre for Climate Modelling and Analysis Coupled Global Climate Model; ECHAM = ECHAM4, the fourth in a series of models derived from the European Centre for Medium-Range Weather Forecasts model.

salts move into stone via moisture flux, with periodic wetting events quickly followed by drying (Goudie, 1986; Smith and McGreevy, 1988; Smith et al., 2005; McCabe et al., 2007; McCabe et al., 2008) – essentially, wetting and drying of the stone surface zone. However, with climate change bringing longer, wetter winters in the NW UK, it is likely (and reported anecdotally by architects) that the increased 'time-of-wetness' of stone blocks will, and may already be leading to block saturation. Essentially, during wet winters, a block may remain saturated for long periods of time (Turkington and Smith, 2000). Indeed, Smith et al. (2004) have posited that a positive feedback is setup, whereby algal growth (encouraged by the presence of moisture in the stone) keeps the block beneath it damp. This leads to the question, how do soluble salts behave if blocks become saturated and there is no moisture flux? Turkington and Smith (2000) have demonstrated complete salt penetration of entire sandstone blocks from a building in Belfast, coinciding with inconsistent anion/cation ratios suggesting the importance of ion diffusion of salts during periods of saturation. Diffusion in solution is the process whereby ionic or molecular constituents move from an area of high concentration (activity) to an area of low concentration (activity) under the influence of random kinetic motion of the constituent molecules or ions. Diffusion occurs without any bulk water movement. If the solution is flowing, diffusion is a mechanism along with dispersion that can cause the mixing of molecular and ionic constituents. Diffusion ceases when there is no concentration gradient. Testing of this phenomenon is widespread in the study of chloride movement in concrete or brick (Shaát, 1994; Poupeleer et al., 2003). However, studies of this kind have perhaps neglected the diffusion of soluble salts within natural building stones – possibly because moisture movement is more rapid in such porous materials, but also linked to the dogma that wetting and drying results in an almost constant flux of moisture, and that this is restricted to an alternating frequently wetted and thoroughly dried outer layer of stonework. It should be noted that, in an homogeneous material, ultimate uniformity of salt concentration may be achieved, but this is unlikely in a mineralogically heterogeneous material – in this case it is likely that localized concentration within the stone may emerge as anions, in particular, are fixed by, for example, clay minerals or organics.

This paper suggests a method, adapted and refined from the study of chloride diffusion in concrete, to test the diffusion of salts within sandstones – the rate at which the ions move and the possible deleterious chemical effects that their passage might have on the stone itself (for example, the dissolution and transportation of amorphous cementing agents such as silica or iron). With reference to the increasing seasonality of precipitation, it would be remiss not to make mention of the potential implications of summer drying following winter saturation – complete drying out of a block in the summer months (along with salts that have been allowed to move deep into the block interior during a wet winter) can mean that crystallized salts become trapped deep within stone, causing damaging sub-efflorescence that can fuel retreat of the blocks surface following loss of surface material (see Smith et al., 2002 for a detailed conceptual model of block retreat).

4. Method – diffusion cells

Several methods have been proposed to investigate salt diffusion. Techniques include the use of different tracer solutions and various experimental set-ups. Non-intrusive methods such as dual-energy gamma radiation and magnetic resonance imaging (MRI) have proven quite successful. However, due to high expense and limitations for the large size (dimension) of physical models, these techniques are not employed on a routine basis to measure fluid flow in porous media. One area where method development has progressed is in reinforced concrete studies since chloride ingress is the main cause of rebar corrosion. A rapid chloride permeability test was introduced that used an electric current to accelerate the diffusion process (Whiting, 1981). This method was later adapted to introduce effective or apparent diffusion coefficients where both salt flow and chemical reactions between salt ions and cement paste were taken into account.

The method proposed is an adaptation of that outlined by Poupeleer et al. (2003). Cell A is filled with salt solution (0.55 molar in preliminary tests), while cell B is filled with de-ionised water. Between the two cells, a sample of saturated stone sits (preliminary tests were carried out on 20mm thick samples of Dumfries Sandstone and Portland Limestone, but different thicknesses may be used), with the rounded edge sealed with silicon. See Table 1 for a summary of stone characteristics. Because of the concentration gradient set up by this apparatus (see Fig. 3 for a schematic representa

Table 1. Characteristics of Dumfries Sandstone and Portland Limestone (after Warke and Smith, 2007).

Stone Type	Porosity (%)	Permeability mD)	Description
Dumfries Sandstone	18 - 25	Range: 200 - 1000 Mean: 600	Permian quartz and iron-rich red sandstone with well-defined bedding. Quartz 52%, feldspars 10.5%, clays 18% (smectites) and mica 1%
Portland Limestone	13 - 26	Range: 1 - 150 Mean: 15	Jurassic oolitic limestone. Calcite 57.8%, quartz 2.3% and clays 13.5%

tion), ions diffuse from cell A to cell B, through the porous stone sample. For high-durability concrete studies, this is very time-consuming (Poupeleer et al., 2003). This is not so with, for example, sandstone, which is generally much more porous and readily permits the movement of ions from one cell to the other. The use of IC to analyse the solution at regular intervals is a more refined and sensitive approach than conductivity meters used in previous concrete studies, allowing for early detection of ion diffusion and a much more accurate and absolute understanding of the phenomenon.

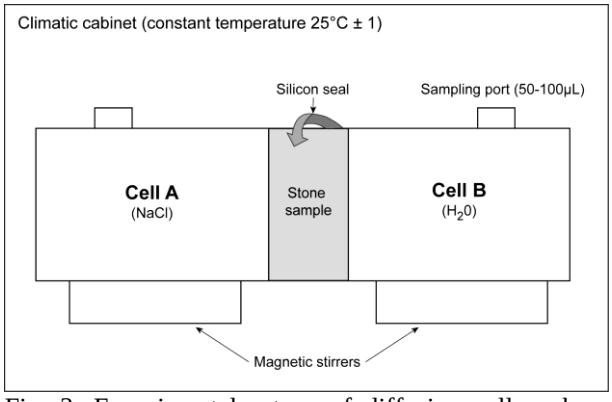

Fig. 3. Experimental set-up of diffusion cells, where ions diffuse through a stone core from cell A (salt solution) to cell B (de-ionized water)

The experiment set-up requires the following assumptions:

1. The solution in the cell outside the stone sample is well mixed (this can be achieved with magnetic stirrers within the cells)
2. Concentration measurements of the vessel solution are made using a minimum volume (50-100µL) for ion chromatography analysis of chloride and other anions (nitrate, sulphate) when mixed salt solutions are included in the experiment
3. The water within the matrix of the core is immobile (the stone remains saturated)
4. The temperature of the solutions in the cells is constant (achieved by a climate cabinet)
5. Sorption is negligible

5. Preliminary Results

Fig. 4 shows the results for diffusion rates of chloride in Dumfries sandstone and Portland limestone. Preliminary tests using the methods described above (using 20mm thick stone sample of Dumfries Sandstone and Portland Limestone) show that salts diffuse through natural sedimentary stone relatively rapidly (when compared to dense concrete samples) – within a day, IC detects an increase in Chloride concentration in cell B in the test using Dumfries Sandstone (a range of 77.04 – 133.3 ppm/day from 3 different samples, explained by the large range in permeability, or connectivity of pores, exhibited by Dumfries Sandstone, Table 1). The rate of diffusion differs for different stone types, based on specific stone characteristics (porosity, permeability) – chloride diffuses much more slowly through the less permeable Portland Limestone (30.1 ppm/day). The type of salt (choride/sulphate/nitrate) also has an impact on diffusion rate. Previous work (discussed in Smith et al. 2005) has shown that chloride ions diffuse through the stone faster than sulphate ions (taking about 5 days to move through the sample), conforming with previous studies on sandstone buildings that showed chloride typically dispersed throughout blocks and sulphate concentrated near exposed faces (Turkington and Smith, 2000).

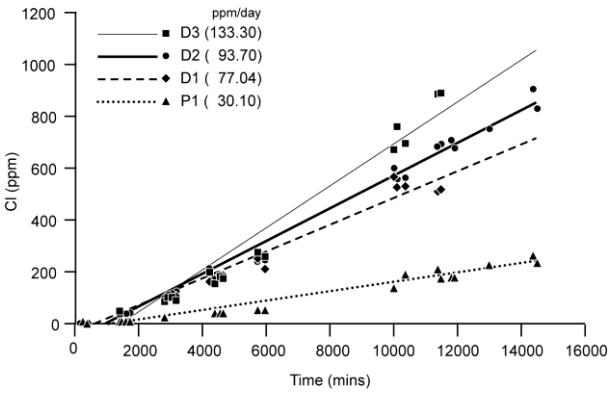

Fig. 4. Diffusion rates for 3 samples of Dumfries Sandstone (D1, D2 and D3), and Portland Limestone (P1). Measurements were made by placing a 20mm thick and 100mm diameter stone sample between an ionic source (0.55 NaCl) and a neutral solution and measuring ion content of the neutral solution side at regular intervals using Ion Chromatography (IC)

6. Discussion

"The chemical behaviour of soluble salts is at the heart of salt weathering and must be understood before a real appreciation of how salts cause damage can be gained" (Goudie and Viles, 1997). To understand salt weathering fully, an appreciation of chemical damage is necessary. With most current research in this area focusing on mechanical damage through crystallization/hydration, this perspective can become lost. Thus, one recent study on salt weathering stated that "if salts are presented in porous system of masonry materials in the form of solution, they are mostly not dangerous" (Pavlik et al., 2008). However, if chemical damage is to take place, it is necessarily when the salt is in solution. The majority of sandstones are largely composed of crystallized quartz (SiO_2) grains. These grains are usually cemented together by silica in a less well-crystallized (amorphous) form. This cement may also contain iron oxides or hydroxides. Silica polymorphs undergo hydrolysis ($SiO_2 + 2H_2O = H_4SiO_4$) and it has been shown that the dissolution rates of quartz and amorphous silica are increased 50-100 times when alkali and alkaline earth cations are introduced into otherwise pure solutions (Icenhower and Dove, 2000). Thus, the weakening of inter-granular bonds of amorphous silica by salts in solution is an essential ingredient in paving the way for physical damage manifesting itself in granular disintegration when crystallization does occur. While the effect of cations on the dissolution rate of silica has been thoroughly investigated, however, only a few studies have been carried out on the impact of anions – one important study has shown the solubility of amorphous silica to increase in the presence of sulphate (Bai et al., 2009), but this area requires further work.

Supporting this perspective of damage caused by salt in solution, another recent investigation into irregular silica cementation and the strength of a particular sandstone when wet and dry showed that compressive strength was significantly reduced (from 'moderately strong' to 'weak') when masonry was wet for long periods of time (Nespereira et al. *in Press*). Thus, another area that would provide a fuller understanding of the impact of ion diffusion on sandstones, not seen in previous concrete and porous media studies, is in the detailed geochemical analysis of the final solution in cell B (Fig. 3). Analysing the final solution will give an understanding of what is being removed from the stone by salt in solution.

Future work, then, will involve the final cell B solution being analysed for Si, Al and Fe concentrations after ion diffusion using various single electrolytic solutions and their mixtures. Sensitive colorimetric techniques are being developed for Si and Al while Fe will be determined using atomic absorption spectrometry. Sensitive colorimetric techniques are chosen since the availability of the ICP atomic emission spectrometry technique is still limited and costly. The ICP technique also suffers serious drawbacks when high levels of salts are present in solution. Detection limits of 0.005 and 0.02 mg/L are possible for Al and Si respectively using colorimetric analysis. These techniques will be employed in an attempt to study the mobility of the above cations plus Ca, Mg, Na and K as a result of the diffusion process. The experimental set-up outlined could also enable a study of the effects of different electrolytic/organic acid mixtures on sandstone as a result of the ion diffusion process.

7. Conclusions

- In response to changing environments, the nature of decay processes change
- Downscaled projections show increased seasonality in precipitation for sites in the NW UK, across different models and emission scenarios
- In NW UK, longer wetter winters mean that sandstone blocks in buildings may become saturated for long periods of time
- Increased seasonality means that complete drying out of blocks in summer following winter saturation could leave damaging sub-efflorescences deep within the stone
- There is a need to adapt laboratory testing of stone to reflect the changing nature of decay regimes – the authors suggest the outlined ion diffusion test method as a means of understanding how soluble salts move in sandstone under saturated conditions and the chemical damage that can be done to the stone while the salts are in solution
- Diffusion rates vary with type of salt and stone properties – future work will be carried out on salt mixtures, different stone types, and the analysis of the dissolution of cementing agents, for example, amorphous silica and iron

Acknowledgements

Thanks to Gill Alexander for help in the preparation of figures. This research was funded by EPSRC grant EP/G01051X/1 (and partly by the Dept of Employment and Learning, NI).

References

Bai S., Urabe S., Okaue Y., Yokoyama T. 2009. Acceleration effect of sulfate ion on the dissolution of amorphous silica. Journal of Colloid and Interface Science 331, 551-554.

Betts N. L, 2002. The climate of Northern Ireland. In: Smyth, A., Montgomery, W. I., Favis-Mortlock, D. and Allen, S. (eds), Implications of Climate Change for Northern Ireland: Informing Strategy Development. Norwich, The Stationary Office Ltd, 26 – 42.

Crawford T., 2007. Future climate change: modelling the implications of shifts in rainfall characteristics for runoff in Northern Ireland. Unpublished PhD Thesis, Queen's University Belfast.

Deprtment of the Environment, 1996. Review of the potential effects of climate change in the United Kingdom. HMSO, London, p. 247.

Goudie A. S., 1986. Laboratory simulations of 'the wick effect' in salt weathering of rock. Earth Surface Processes and Landforms, 11, 275-285.

Hulme M., Jenkins G. J., Lu X., Turnpenny J. R., Mitchell T. D., Jones R. G., Lowe J., Murphy J. M., Hassell D., Boorman P., McDonald R. and Hill S., 2002. Climate Change Scenarios for the United Kingdom: The UKCIP02 Scientific Report, Tyndall Centre for Climate Change Research, School of Envirnmental Sciences, Univ. of East Anglia, Norwich, UK, 120 pp.

Huth R., 2005. Downscaling of humidity variables: a search for suitable predictors and predictands, International Journal of Climatology 25, 243 – 250.

Icenhower I.P. and Dove P.M., 2000. The dissolution kinetics of amorphous silica in sodium chloride solutions: effect of temperature and ionic strength, Geochim. Cosmochim. Acta, 64, 4193-4203.

McCabe S., Smith B. J. and Warke P. A., 2007. Preliminary observations on the impact of complex stress histories on the response of sandstone to salt weathering: laboratory simulations of process combinations. Environmental Geology, 52, 251-258.

McCabe S., McKinley J. M. and Smith B. J., 2008. Simulating initial stages of salt accumulation and organisation within building sandstones. In: Lukaszewicz, J. W., Niemcewizc, P. (eds), 11th International Congress on the Deterioration and Conservation of Stone. Nicolaus Copernicus University Press, Torun, 173-180.

Nespereira J., Blanco J. A., Yenes, M. and Pereira D., In Press. Irregular silica cementation in sandstone and its implication on the usability as building stone. Engineering Geology, *in press*.

Pavlik Z., Michalek P., Pavlikova M., Kopecka I., Maxova I., and Cerny R., 2008. Water and salt transport and storage properties of Msene sandstone, Construction and Building Materials 22, 1736 – 1748.

Poupeleer A. S., Carmeliet J., Roels S. and Van Gemert D., 2003. Validation of the salt diffusion coefficient in porous materials. International Journal for Restoration of Buildings and Monuments, 9, 663-682.

Shaát A., 1994. Int. Conf. on Corrosion and Corrosion Protection of Steel and Concrete, 446-460.

Smith B. J. and McGreevy J. P., 1988. Contour scaling of a sandstone by salt weathering under hot desert conditions. Earth Surface Proc. and Landforms, 13, 697-705.

Smith B. J., Turkington A. V., Warke P. A., Basheer P. A. M., McAlister J. J., Meneely J. and Curran J. M. 2002. Modelling the rapid retreat of building sandstones: a case study from a polluted maritime environment. In: Seigesmund, S., Weiss, T. & Vollbrecht, A. (eds), Natural Stone, Weathering Phenomenon, Conservation Strategies and Case Studies: 347 – 362, Special Publications 205. London: Geological Society.

Smith B. J., Warke P. A. and Curran J. M., 2004. Implications of climate change and increased 'time-of-wetness' for the soiling and decay of sandstone structures in Belfast, Northern Ireland. In: Prikryl, R. (ed.), Dimension Stone, Taylor&Francis Group, London, 9-14.

Smith B. J., Warke P. A., McGreevy J. P. and Kane H. L., 2005. Salt weathering simulations under hot desert conditions: agents of enlightenment or perpetuators of preconceptions? Geomorphology, 67, 211-227.

Smith B. J., Turkington A. V. and Curran J. M. 2005. Urban stone decay: the great weathering experiment? Geological Soc. of America, Special Paper, 390, 1-9.

Smith B. J., Gomez-Heras M. and McCabe S., 2008. Understanding the decay of stone-built cultural heritage. Progress in Physical Geography, 32, 439-461.

Turkington A. V. and Smith B. J., 2000. Observations of three-dimensional salt distribution in building stone. Earth Surface Processes and Landforms, 25, 1317-1332.

Warke P. A. and Smith B. J. 2007. Complex weathering effects on durability characteristics of building stone. In: Prikryl, R. and Smith, B. J. (eds), Building Stone Decay: From Diagnosis to Conservation, Geological Society, London, Special Publications, 271, 211 – 224.

Wilby R.L., and Wigley T.M.L., 1997. Downscaling general circulation model output: a review of methods and limitations. Progress in Physical Geography 21, 530-548.

Wilby R., and Dawson C. W., 2004. Using SDSM version 3.1 – a decision support tool for the assessment of regional climate change impacts. Version 3.1 User Manual, Nottingham, Environment Agency of England and Wales.

Wilby R., Dawson C. W., and Barrow E. M., 2002. SDSM – a decision support tool for the assessment of regional climate change impacts, Environmental Modelling & Software, 17, 147 – 159.

Whiting,D., 1981. A rapid measurement of chloride permeability of concrete, Public Roads, V. 45(3), 101-112).

Scientific Annals, School of Geology, Aristotle University of Thessaloniki Proceedings of the XIX CBGA Congress, Thessaloniki, Greece	Special volume 100	407-411	Thessaloniki 2010

SPATIAL DISTRIBUTION OF SALT PENETRATION IN WEATHERED SANDSTONE

McKinley J.[1], Keaney A.[1], McCabe S.[1]., Curran J.[2] and Smith B.[1]

[1]*School of Geography, Archaeology and Palaeoecology, Queen's University Belfast, BT7 1NN, UK, j.mckinley@qub.ac.uk, akeaney04@qub.ac.uk, stephen.mccabe@qub.ac.uk, b.smith@qub.ac.uk*
[2]*Stone Conservation Services, Consarc Design Group, 4b Cromac Quay, Belfast, BT7 2JD, Joanne.Curran@consarc-design.co.uk*

Abstract: This research investigates the importance of the spatial distribution of salts in the weathering process of stone decay. The relationship between salt penetration and the intrinsic rock property, permeability, is examined to elucidate the ingress and egress of salt solution in masonry sandstone. The accelerated weathering trial simulates pre-loading a sandstone block with a 10% salt solution (equal parts NaCl and $MgSO_4$) during a wet winter followed by dried out in summer. Permeability data measured from horizontal slices through the block are correlated with salt data from IC analysis. Results indicate relatively high surface permeability values and salt crystallization on exposure to air. The effect of salts blocking pores and reducing permeability is evident in a reduction in permeability in the near surface zone where permeability and (sulphate and chloride) salt data are correlated. At greater depth, continual wetting with salt and subsequent heating increases permeability and pore connectivity of the sandstone block. Salt crystallization enlarges and fractures pores, enabling the ingress and movement of soluble chloride salts. The stone's intrinsic properties (permeability and porosity) have been changed by salt weathering, ultimately leading to deterioration and accelerated stone decay.

Keywords: Salt weathering, sulphate, chloride, probe permeametry, sandstones, correlation matrix.

1. Introduction

The breakdown of masonry sandstone has been extensively researched due to its significance in architectural and archaeological conservation (e.g. Mottershead, 1994; Smith and Warke, 1996; Smith et al., 2002). Mechanical decay in sandstones in polluted urban environments is attributed to salt concentration through crystallization, thermal expansion/concentration, and hydration/dehydration (Warke and Smith, 2000; Turkington and Smith, 2000). Previous work has alluded to an oversimplification in current modeling of salt solution fluctuation that fails to address moisture movement from within masonry stone (Bluck and Porter, 1991; Warke and Smith, 2000) and stresses the importance of modeling building stones as three-dimensional features (Turkington and Smith, 2000). The decay of natural masonry materials such as sandstone can be unpredictable and is related to the variability of the intrinsic properties of the stone, such as permeability, porosity and mineralogy (McKinley et al., 2006), and the mobility of the salts in the weathering process (Warke and Smith, 2000). The interaction between these properties has implications for moisture movement and salt input, output and storage. Any attempt to model the decay dynamics of natural building stone must take into account the impact of the spatial variability of the stone properties on the ingress and egress of salt solution. In this paper the spatial distribution of salts in weathered sandstones is investigated and the relationship between salt penetration and permeability, a key trigger factor of stone decay.

2. Materials and Methods

Sandstone blocks of dimensions 20x20x20 cm were used to represent building stones in accelerated weathering trials. Peakmoor Sandstone, a medium-grained sandstone of Carboniferous age, was used which is representative of a stone type used frequently in construction and restoration programmes (BRE, 2000). Predictions for future temperate climates envisage warmer and wetter winters (Crawford, 2007, Viles, 2002). The implications for building stones are that blocks will remain damp for long periods of time during winter months. As a result soluble salts may migrate

through a block, and entire building stones potentially could be contaminated with damaging salts in a relatively short time (Smith et al., 2004). The weathering simulation used in this paper was designed to simulate the scenario where a masonry building stone is 'loaded' with salt during a wet winter and then completely dried out in summer. The weathering simulation involved pre-loading a sandstone block with a 10% salt solution (equal parts NaCl and $MgSO_4$) by capillary rise through one face, and subsequent drying out with a heat lamp from the same face. The block was placed in a salt solution (2 cm deep and topped up as necessary) for 48 hours. Following removal from the salt solution the block was dried for 6 hours by a heat lamp directed at the block face which had been immersed in the solution. This encouraged capillary rise of the solution to the 'back' face of the block. Limited ingress and egress of moisture and salts to one exposed face more closely simulates the situation of a building stone (Smith and McGreevy, 1988).

Following the weathering simulation, the block was cut horizontally at 2 cm intervals resulting in 10 slices through the block to characterize the rock properties and salt distribution of the sandstone block in three dimensions. Non-destructive and destructive techniques were applied to the weathered block. Probe permeametry is a non-destructive technique that measures pressure decay as a function of time, enabling the determination of gas permeability. An unsteady-state Portable Probe Permeameter PPP250^{TM} (Core Laboratories Instruments, 2001) was performed on the block before each slice was cut. In the technique, initial flow pressure declines as gas flows into the stone surface and the decay versus time is recorded and used to calculate permeability from the pressure decay curve (Jones, 1992). The PPP250 has an aperture radius of 8 mm producing an approximate effective penetration depth at each position of between 17.6 mm and 32 mm (2.2-4 times the radius; Goggin et al., 1986; Goggin et al., 1988; Jensen et al., 1994; Tidwell and Wilson, 1999).

Ion chromatography (IC), thin section and scanning electron microscopy (SEM) facilitated the structural and mineralogical characterization of the weathered sandstone. The use of a 10 x 10 cm sampling grid, giving 100 sample points for each slice, resulted in permeability measurements at the same relative positions as samples taken for destructive analysis. This provided a spatial dataset and the potential to quantify the relationship between permeability and salt distribution of the weathered block.

3. Results and Discussion

Quartz formed the predominant detrital framework mineral in the fresh Peakmoor sandstone. Feldspars formed the second most volumetrically important detrital framework mineral. The major feldspar type present was albite with subordinate microcline (as determined by XRD analysis). XRD analysis, thin-section petrography and SEM analysis confirmed the presence of illite and kaolinite as diagenetic clay phases. Kaolinite was the most volumetrically significant diagenetic clay. Results from the weathering simulation show variable permeability at different depths in the salt-loaded block. Figure 1 shows mean permeability values (Fig. 1a) and mean salt (SO_4 and Cl) concentration (Fig. 1b) at increasing depths in the sandstone block. The inset figure (Fig. 1c) provides greater detail for mean concentrations of SO_4 and Cl (ppm) below the surface layer of the block.

High permeability was observed for the surface slice (range 62 -120 mD; mean 84 mD) but permeability values were reduced at 2 and 6 cm depth (Fig. 1a; mean 56 and 57 mD for 2 and 6 cm depth respectively). Permeability increased at greater depth in the block with a maximum mean value of 90 mD at 18 cm depth. IC analysis indicated extensive salt concentration in the surface layer of the salt-loaded block. High concentrations of sulphate (SO_4) and chloride (NaCl) were indicated in the surface slice following salt-loading (Fig. 2). Results showed concentrations of 8515 ppm and 1018 ppm for Cl and SO_4 respectively (Fig. 1b). The large quantity of salts rapidly diminished at 2 cm depth where a mean concentration of 445ppm and 449 ppm was recorded for Cl and SO_4 respectively. The amount of SO_4 observed in the block remained relatively constant from a depth of 4 cm (range 530 to 460 ppm) to 12 cm when the concentration is reduced to 362 ppm. Lowest concentration of sulphate was recorded at depth in the salt-loaded block (Fig. 1c; 181 ppm at 18-20 cm depth). This pattern of salt concentration through the block is not replicated by chloride in that although IC results indicate a decrease in chloride concentration immediately under the surface layer (Fig. 1c; 445 ppm), the quantity of chloride remains relatively constant with increasing block depth (range 507 to 428 ppm) until at depth of 16 cm when an increase in chloride is observed. A

concentration of 1018 ppm is recorded at a depth of 18 cm in the salt-loaded block.

The correlation matrix between salts indicate a correlation between salt concentration in the surface layer of the block where high quantities of both salts were found (Tab. 1; correlation coefficient = 0.68.) However strongest correlation is found at a depth of 4 – 6 cm in the salt-loaded block (correlation coefficient = 0.7 to 0.91). This coincides with the observed decrease in salt quantities (Fig.1c) and shows that the salts are acting in a similar way between 4 and 6 cm depth in the block. After this depth the salts act in different ways and show weaker correlations and an inverse relationship as sulphate salts decrease through the block but chloride salts were found to increase towards the base of the block (Tab. 1). The correlation between permeability and salts data show strongest spatial cross correlation at a depth of 4-6 cm in the salt loaded sandstone block (correlation coefficient = 0.35 and 0.37 for SO_4 and Cl respectively).

The block weathered in the accelerated salt simulation trial provided detail on the three dimensional changes in the sandstone. Once the block was loaded with salt solution to simulate the complete wetting of a building block during a damp winter, a heat lamp was directed at the block face which had been immersed in the solution. Permeability measured from the horizontal slices was used to correlate with salt data. Results from permeability measurement and salt data indicate relatively high surface permeability values (84mD) and high salt

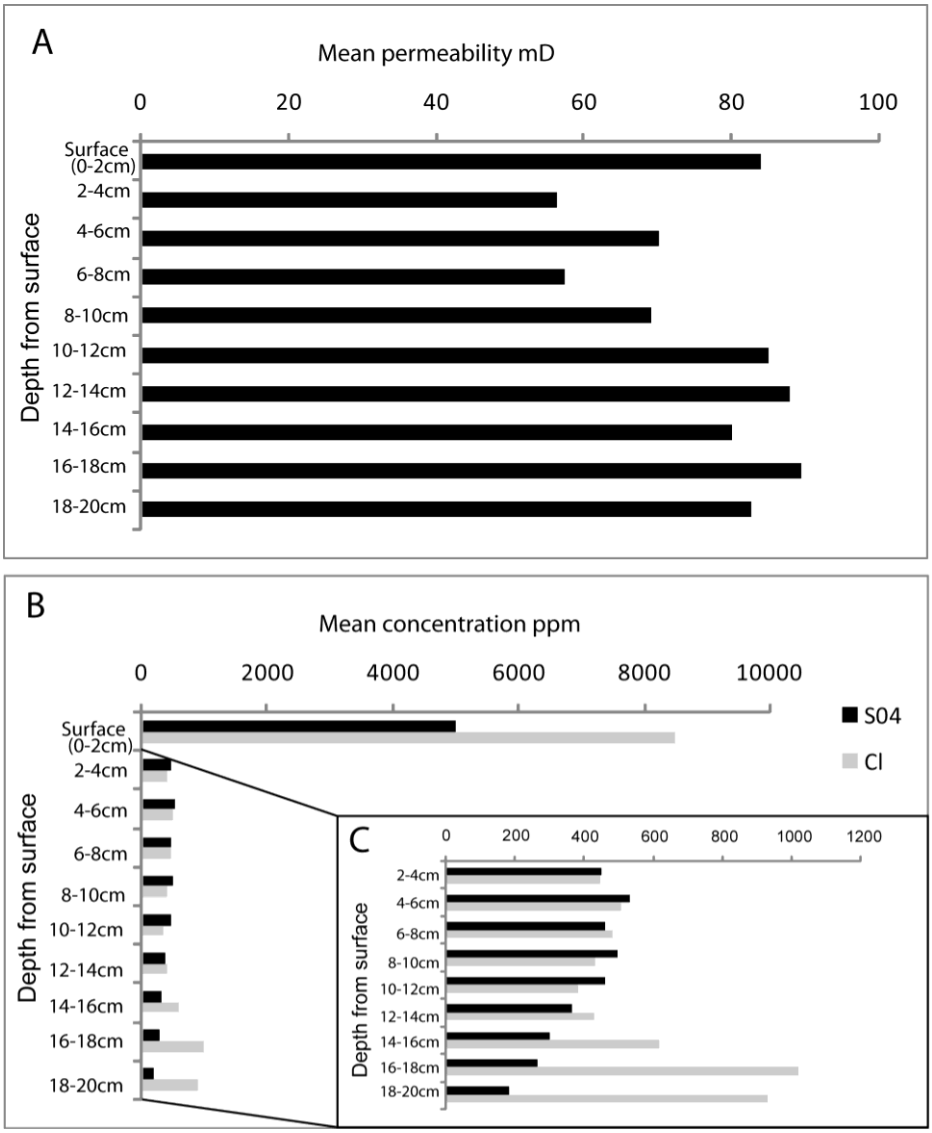

Fig. 1. Graphs showing A) permeability mD; B) salt (SO_4 and Cl) concentration at different depths in the sandstone block. Inset C) shows (SO_4 and Cl) concentration at different depths below the surface of the block.

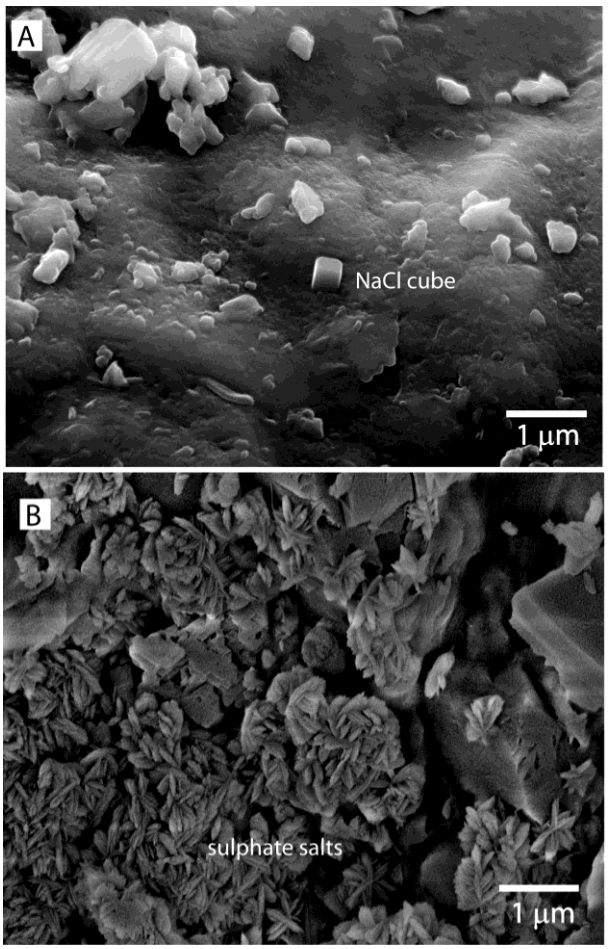

Fig. 2 SEM micrographs of salt-loaded block showing A) NaCl cube and B) sulphate salts.

concentrations related to salt crystallization on exposure to air. At this stage salt concentration is not strongly related to permeability. High salt concentration can be related to an efflorescence observed on the block surface produced as salt was drawn back to the surface on heating with the heat lamp. This would be expected to block surface pores and reduce permeability. The effect of this is not obvious in surface permeability but is more evident in the reduction in permeability below the rock surface where both salt solutions and permeability data are more strongly correlated. The results suggest that, initially high permeability values are reduced with the build up of salt concentration in the near-surface zone (2 – 6 cm depth). At greater depth in the block (at 12cm depth) continual wetting with salt and heating appears to be effective in increasing permeability and consequently pore connectivity, enabling the ingress and movement of salt and moisture more effectively through the stone. The findings indicate that chloride salts are more abundant than sulphates at this depth in the block.

The findings from this study concur with and build on previous research (e.g. Warke and Smith, 2000; Turkington and Smith, 2000) in that the research aims to elucidate the importance of the spatial distribution of salts in the weathering process of stone decay. The results indicate that continual wetting with salt laden rain followed by drying out produces a salt residue in the form of a zone of accumulation of chloride and sulphate salts in the surface zone. Salt crystallization on the surface may re-establish stability because surface pores are blocked (surface efflorescence blocks pores). Permeability is reduced in the near surface zone minimizing the ingress of moisture and salts. At this depth salt crystallization is controlling permeability. The results of this study indicate, however, that this stability is temporary and at greater depth (10 - 12 cm depth) permeability begins to increase due to crystal expansion. Salt crystallization enlarges and fractures pores, increasing the mobility potential of moisture and salts. This acts as a

Table 1: Correlation matrix for sulphate (SO_4) and chloride (Cl) salts.

Salts		Sulphate (SO_4)									
	Depth from surface	Surface 0-2 cm	2-4 cm	4-6 cm	6-8 cm	8-10 cm	10-12 cm	12-14 cm	14-16 cm	16-18 cm	18-20 cm
Chloride (Cl)	Surface 0-2 cm	.68*	.39*	.42*	.35*	.31	-.23	-.24	.04	-.11	-.29*
	2-4 cm	.06	.91*	.80*	.80*	.69*	.08	-.03	.29	-.08	-.72*
	4-6 cm	.06	.84*	.85*	.74*	.68*	.14	.05	.36	-.09	-.72*
	6-8 cm	.04	.77*	.67*	.70*	.67*	.22	-.01	.33	.08	-.61*
	8-10 cm	.01	.75*	.71*	.61*	.66*	.34	.08	.28	.12	-.54*
	10-12 cm	-.06	.79*	.73*	.64*	.57*	.37*	.18	.17	.12	-.56*
	12-14 cm	-.08	.75*	.69*	.63*	.60*	.27	.27	.31	.15	-.53*
	14-16 cm	-.03	.61*	.61*	.50*	.55*	.24	.13	.44	.04	-.49*
	16-18 cm	.03	.42*	.41*	.22	.27	.33	.37*	.24	.64*	-.17
	18-20 cm	-.18	.58*	.50*	.42*	.45*	.13	-.03	.15	.02	-.45*

Symbol * indicates correlation is significant at the 0.05 probability level.

zone of transition that enables the inward migration of salt. At depth in the weathered block, there is an observed increase in permeability and a zone of accumulation of chloride salts (18 – 20 cm depth). Stresses exerted by the expansion of salt crystals in confined pore spaces, and subsequent hydration during periods of drying, have increased pore connectivity and hence permeability enabling the ingress of soluble chloride salts. The stone's intrinsic properties (permeability and porosity) have been changed by the salt weathering, ultimately leading to deterioration and accelerated stone decay.

4. Conclusion

This paper presents a three-dimensional examination of a sandstone block following a salt weathering trial to investigate the spatial distribution of salts in zones of accumulation, transition and concentration. The implications of the study are that continual wetting with salt solution and drying enables the ingress and movement of salt and moisture through the stone. The movement of salt depends on the composition and mobility of the salt solution; both sulphate and chloride salts accumulate in the near surface zone. At greater depth chloride salts are effective in changing the intrinsic properties (permeability and porosity) of the stone and concentrate at much deeper levels in the stone. Ultimately this may result in accelerated stone decay. The results from this study are currently being validated against weathered stone masonry provided by an ongoing building restoration programme.

Acknowledgements

This research was funded by EPSRC grant EP/E049648/1.

References

Building Research Establishment (BRE) 2000. Technical Data Sheet Peakmoor Sandstone (http://projects.bre.co.uk/ConDiv/stonelist/peakmoor.html).

Bluck B.J. and Porter J. 1991. Sandstone buildings and cleaning problems. Stone Industries, April, 21-27.

Core Laboratories Instruments, 2001. PPP250TM Portable Probe Permeameter, Operators Manual.

Crawford T. 2007. Future climate change: modelling the implications of shifts in rainfall characteristics for runoff in Northern Ireland. Unpublished PhD Thesis, Queen's University Belfast.

Goggin D.J., Chandler M.A., Kocurek G. and Lake L.W. 1986. Patterns of permeability in Eolian Deposits. 5th Symposium on Enhanced Oil Recovery, Tulsa, SPE/DOE 14893, 181-188.

Goggin D.J., Thrasher R.L., and Lake L.W. 1988. A theoretical and experimental analysis of minipermeameter response including gas slippage and high velocity flow effects. In Situ, 12, 79-116.

Jensen J.L., Glasbey C.A. and Corbett P.W.M. 1994. On the interaction of geology, measurement and statistical analysis of small-scale permeability measurements. Terra Nova, 6, 397-403.

Jones S.C. 1992. The Profile Permeameter: A new, fast, accurate minipermeameter. 67th Annual Technical Conference and Exhibition of the Society of Petroleum Engineers. Washington, DC, SPE 24757, 973–983.

McKinley J.M., Warke, P.A., Lloyd, C.D., Ruffell A.H. and Smith B.J. 2006. Geostatistical analysis in weathering studies: case study of Stanton Moor building sandstone. Earth Surface Processes and Landforms, 31, 950-969.

Mottershead D.N., 1994. Spatial variation in intensity of alveolar weathering of a dated sandstone structure in a coastal environment, Weston-super-Mare. In: Rock Weathering and Landform Evolution, Robinson, D.A. Williams, R.B.G. (eds), Wiley, Chichester, 151-174.

Smith B.J. and J.P. McGreevy. 1988. Contour scaling of a sandstone by salt weathering under hot desert conditions. Earth Surface Processes and Landforms, 13, 697 – 705.

Smith B.J. and Warke P.A. 1996. Processes of Urban Decay, Dunhead, London.

Smith B. J., Turkington A.V., Warke P. A., Basheer M., McAlister J.J., Meneely J. and Curran J.M. 2002. Modelling the rapid retreat of building sandstones: a case study from a polluted maritime environment. Geological Society of London Special Publication, 205, 339–354.

Smith B. J., Warke P.A. and Curran J.M. 2004. Implications of climate change and increased 'time-of-wetness' for the soiling and decay of sandstone structures in Belfast. Northern Ireland. In: Dimension Stone, Prikryl R. (eds), London, Taylor & Francis Group, 9 – 14.

Tidwell V.C. and Wilson J.L. 1999. Permeability upscaling measured on a block of Berea sandstone: results and interpretation. Mathematical Geology, 31, 7, 749-769.

Turkington A.V. and Smith B.J. 2000. Interpreting spatial complexity of decay features on a sandstone wall: St Matthew's Church, Belfast. In: Stone Decay: Its Causes and Controls, Smith B.J. and Turkington A.V. (eds), Shaftesbury, Dunhead Publishing, 149-166.

Viles H.A. 2002. Implications of future climate change for stone deterioration. In: Natural Stone, Weathering Phenomenon, Conservation Strategies and Case Studies. Special Publications, Seigesmund S., Weiss T. and Volbrecht A. (eds). London: Geological Society, 205, 407 – 418.

Warke P.A. and Smith B.J. 2000. Salt distribution in clay-rich weathered sandstones. Earth Surface Processes and Landforms, 25, 1333-1342.

Scientific Annals, School of Geology, Aristotle University of Thessaloniki Proceedings of the XIX CBGA Congress, Thessaloniki, Greece	Special volume 100	413-419	Thessaloniki 2010

HIGH ACIDIC SULPHATE SALT PRODUCTION ON THE CAVE WALL IN THE YOSHIMI HYAKU-ANA HISTORIC SITE, CENTRAL JAPAN

Oguchi C.[1], Takaya Y.[2], Yamazaki, M.[3], Ohnishi R.[3], Thidar A[4]. and Hatta T.[5]

[1] *Geosphere Research Institute, Saitama University, 338-8570, Saitama, Japan, ogchiaki@mail.saitama-u.ac.jp*
[2] *Research Facility Center for Science and Technology, University of Tsukuba, 305-8577, Ibaraki, Japan,*
[3] *Department of Civil and Environmental Engineering, Saitama University, 338-8570, Saitama, Japan,*
[4] *Graduate School of Science and Engineering, Saitama University, 338-8570, Saitama, Japan,*
[5] *Japan International Research Center for Agricultural Sciences, 305-8686, Ibaraki, Japan,*

Abstract: Acidic sulfates such as aluminum sulfates and ferric sulfates are often observed on the wall of tuff or volcanic rocks in Japan. We investigated wall surfaces of an artificial cave dug from 1941 to 1945 in the Miocene tuff. The cave locates in the historic site of Yoshimi Hyaku-Ana which is ancient graves of 6-7 centuries. The cave was suffering from severe salt efflorescence and deterioration of its cause. Salts are much in dry winter but less in humid summer. We set up twelve investigation points for monthly monitoring of temperature and humidity. Fallen salts and debris at each point were also collected monthly from November 2008 to December 2009. Main salt minerals, detected by XRD, are hard and granularly effloresced alunogen ($Al_2(SO_4)_3.17H_2O$) on the walls near the entrances, and gypsum was found on the inside walls in the humid summer. On the contrary, powdery effloresced halotrichite ($FeAl_2(SO_4)_4.22H_2O$), sodiumalum ($NaAl(SO_4)_2.12H_2O$) and epsomite ($MgSO_4.7H_2O$) were detected in the dry winter. Jarosite ($KFe_3(SO_4)_4.(OH)_8$) minerals were observed on iron hydroxide stains on the walls in every season. Halotrichite, sodiumalum and epsomite damaged the walls most severely especially in the dry winter. The amount of salts and debris from the inner wall were greater than those from near entrances.

Keywords: alunogen, jarosite, sulphate, salt weathering, tuff, Yoshimi-Hyaku-Ana.

1. Introduction

Salt weathering due to sulphate salts causes sometimes severe deterioration on stone monuments and natural rock walls (Goudie and Viles, 1997; Winkler, 1994). Salt weathering itself is generally categorized into physical weathering but chemical reaction sure to be observed before the salt crystallyzation. These processes are sometimes investigated from the aspect of water-rock interaction. Seki and Sakai (1987) studied a decay of rock-cliff Budda sculpted on Miocene tuff caused by sulphate salts of gypsum, thenardite (Na_2SO_4), epsomite ($MgSO_4{\cdot}7H_2O$) and mirabilite ($Na_2SO_4{\cdot}10H_2O$). Kuchitsu (1992) studied Japanese cultural important building made by brick covered with plaster and insisted that deterioration on the building occurred when evaporates such as aphthitalite ($K_3Na(SO_4)_2$), thenardite, trona ($Na_3H(CO_3)_2{\cdot}2H_2O$) and thermonatrite ($Na_2CO_3{\cdot}H_2O$) formed inside the building materials. Origin of sulphates of Seki and Sakai (1987)'s case was internal of rock, however, that of Kuchitsu (1992)'s case is external such as acid rain water with SO_4^{2-} ion.

Japan is volcanic country and Japanese cultural properties or historic sites are often sculpted on the tuff cliff. Thus, these cultural properties are suffering from sulphate attack. It is important to investigate sulphate mineral production for not only the purpose of characterization themselves but also aiming at conservation of stone monuments. In this study, monitoring of salt weathering and environmental condition as well as salt description were made at the Yoshimi-Hyaku-Ana Historic Site, central Japan.

2. Study Area

The Yoshimi-Hyaku-Ana historic site locates at the central Saitama Prefecture, central Japan (Fig. 1). The topography of Saitama Prefecture is largely divided by the western mountainous area neighboring the Kantō Mount Range of Paleozoic and Mesozoic systems and the eastern alluvial low-

lands formed by Arakawa River. The historic site exists on the branch of the Hiki hills, the Yoshimi hill, with an area of east-west length of 2.5 km and south-north length of 3 km at 50-80 a.s.l. According to the Matsumaru and Hayashi (1980), the hill composes of metamorphic rocks such as amphibolite, ultramafic rocks and crystalline schist in the center, sandstone, conglomerate, mudstone and tuff of Miocene Kosono formation in the northeast part, and tuff, mudstone and sandstone of Miocene Fukuda formation in the southwest part. Two faults are considered to run between the two members, which covered with Pleistocene Monomiyama conglomerate. The rocks are pale gray, fine tuffacious mudstone and sandstone, which contains feldspars, quartz, volcanic glass and its altered clay minerals.

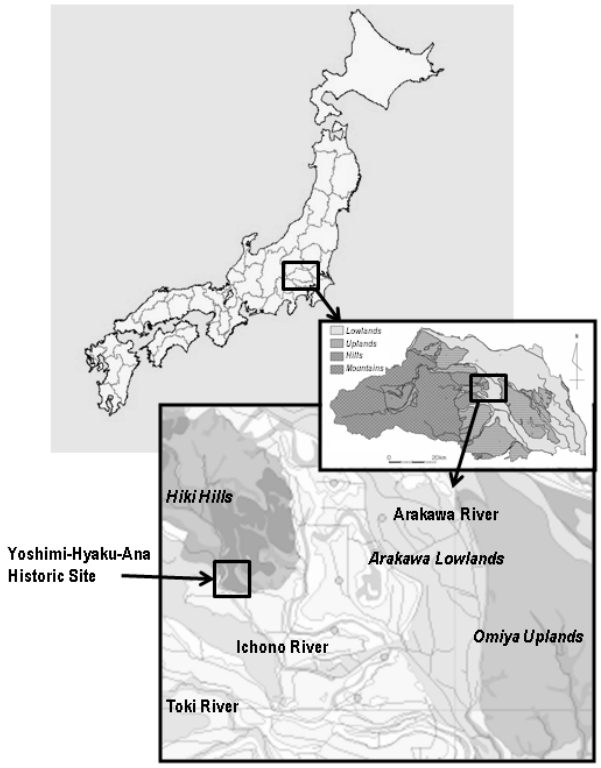

Fig. 1. Location of Yoshimi-Hyaku-Ana Historic Site.

The Yoshimi-Hyaku-Ana historic site is a graveyard of 6 to 7 century, which is one of the national cultural properties in Japan. The numbers of the graves exceed 200 (Kanaidzuka, 1986) and they distribute on the western slope of the Yoshimi Hill. The size of each grave is ca. 4 m in diameter and 2.2 m in height (Fig. 2). The entrance of each grave had a large stones to shut the inside and outside, although they disappeared anymore. At the foot of graveyard, there are larger artificial caves with a size of 4 m diameter. The caves were dug by Japanese and Korean workers during World War II for purpose of Military use and occupy large areas under the Yoshimi Hill. A small river, Ichino River, flows in the west side of the Yoshimi Hill. The water level is 5 m below the artificial cave floor, and thus the caves have not experienced to be affected by river water.

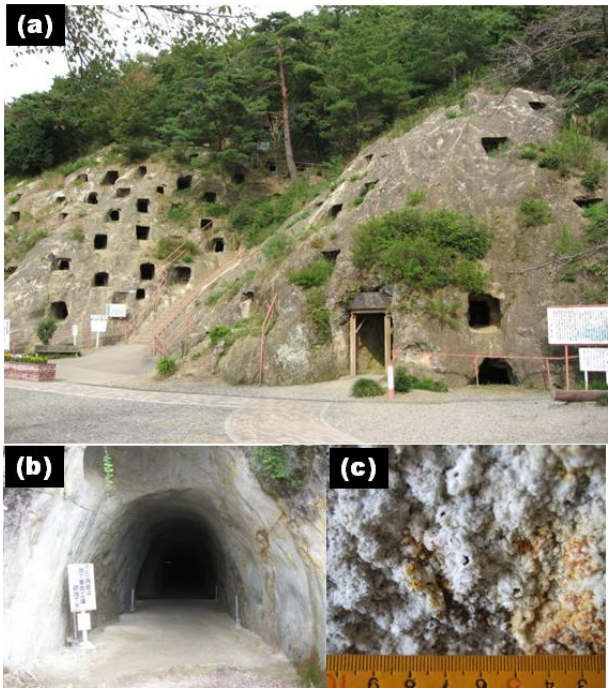

Fig. 2 Overview of Yoshimi-Hyaku-Ana Historic Site (a) and artificial cave entrance (b).

Salts are observed on the both wall of the graveyards and military cave. However, much salts effloresced on the wall of military cave. Especially near the entrance of the artificial cave, much salt are observed. In the previous literatures, description of the salt efflorescence or evaporates were made (Horiguchi, 1975; Chiba et al., 1975; Kuchitsu and Ozaki, 1999; Horiguchi et al., 2000). Horiguchi et al. (2000) investigated salt types and identified them into alunogen, halotrihite, jarosite and gypsum. Kuchitsu (1999) also detected these minerals and considered the relationships between salt efflorescence and deterioration of the wall. However, these researches are not enough to consider quantitative amount of salt and debris formation.

3. Monitoring of Environmental Conditions

Figure 3 shows the plane map of the military cave. We set the twelve investigation points; Points 1-4 were located along the corridor A, Points 5-8 were located along the corridor B and Points 9-12 were

located the corridor C. The corridor B runs perpendicular to corridors A and C which run straight from two cave entrances to the inside. In each point salt collecting trays with a size of 21×9×3 cm were set and environmental data were collected in nearly one month interval from January 2008 to December 2008 (Jan 22nd , Feb 26th, Mar 27th, May 7th, Jun 6th, Jul 10th, Aug 11th, Sep 16th, Oct 21st, Dec 2nd). Environmental condition such as air temperature, air relative humidity, wall temperature was also measured on each monitoring dates using multi-environmental meter (Nihon Shintech Co. Ltd.; AHLT-100) and infrared thermometer (A&D Co. Ltd.; AD-5613A).

Environmental data are shown in figure 5. In February, temperature of all investigation points of the cave wall showed below 5ºC (Fig. 5a). They increased and exceeded 20 ºC in August. There were no variation of each point except for spring. Points 1 and 3 showed higher temperature during March to July, which might be caused by sunlight from the west. Air temperature near each point showed similar as wall temperature (Fig. 5b). The values of air temperature were by 2-3ºC higher than those of wall temperature. The reason of low temperature in June was rainy season in Japan. Relative humidity (RH) of each point varied especially in February and September (Fig. 5c). In February, the RH of the Points 1-4 were 38-45%, whereas those of the Points 11 and 12 were more than 60%. The values of points 5-8 showed around 50%. The Points 11 and 12 are close to the entrance 1 which is covered with branches of trees. In June, the RH of all points exceeded 80%. The cave wall contained much moistures and salts at all the investigation points diffloresced. The RH decreased in mid summer to autumn. The RH values showed 70-80% in September and 60-70% in October. The variability of RH showed similar to February; Points 1-4 had higher RH, Points 9-12 had lower RH and Points 5-8 had intermediate RH values.

4. Monitoring of Salt Efflorescence and Salt Type Indentification

General observation of each point is explained below and the pictures of representative points, Points 2 and 8, are shown in figure 4. Points 1-4 have many salts from December to June. The salts

Fig. 3. Plane map of the artificial cave.

are white or yellow and their shapes are bubble scab with a diameter of 3-5 mm. In June the salts contain much moisture and in August most of salts were disappeared. The amounts of salts are larger in Point 2 than those in Point 1. Points 5-8 have less salts than points 1-4 and points 9-12. Changes in salt efflorescence are not clear, however, the amount of salts gradually increase from December to June. Powdery salts are observed in these points. Points locate next corridor to the points 1-4. These points shows intermediate characteristics of points 1-4 and 9-12. Points 11 and 12 are much salt efflorescence than the points 9 and 10.

Salts collected directly from the rock wall at each investigation point. They were identified using X-ray powder diffraction (Rigaku Co. Ltd.; RAD-X system). The operating conditions were X-ray target of CuKα, tube voltage of 40 kV and tube current of 25 mA, scan spped of 2.00^{o} / min and 0.5^{o}–0.3mm–0.5^{o} slits.

Results are shown in figure 6. At Point 2, alunogen ($Al_2(SO_4)_3 \cdot 17H_2O$) and halotrichite ($FeAl_2(SO_4)_4 \cdot 2H_2O$) was detected from January to July, then it disappeared but gypsum ($CaSO_4 \cdot 2H_2O$), quartz (SiO_2) and albite ($NaAlSi_3O_8$) was identified.

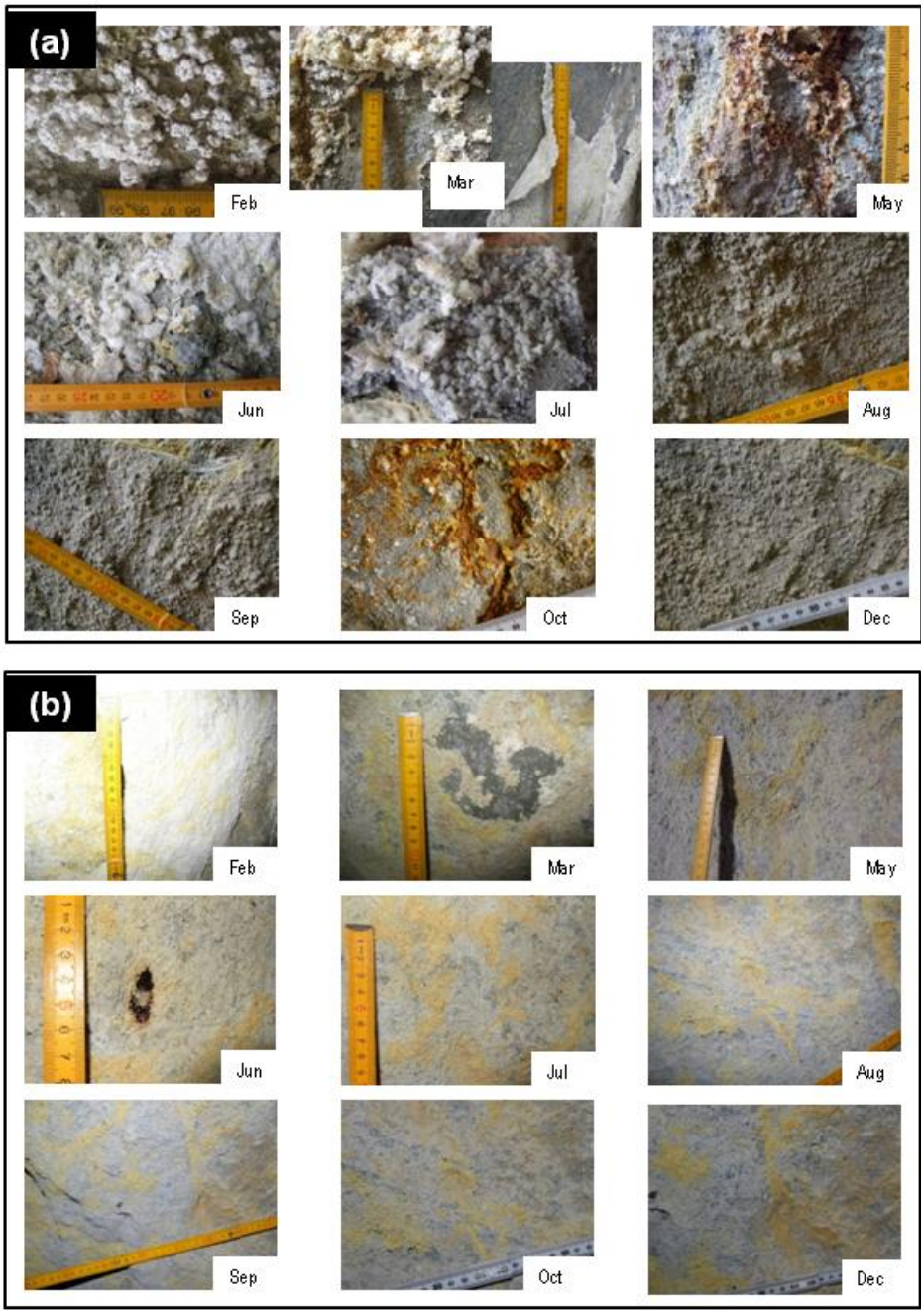

Fig. 4. Salt efflorescence of the rock wall. (a) Point 2 and (b)Point 8.

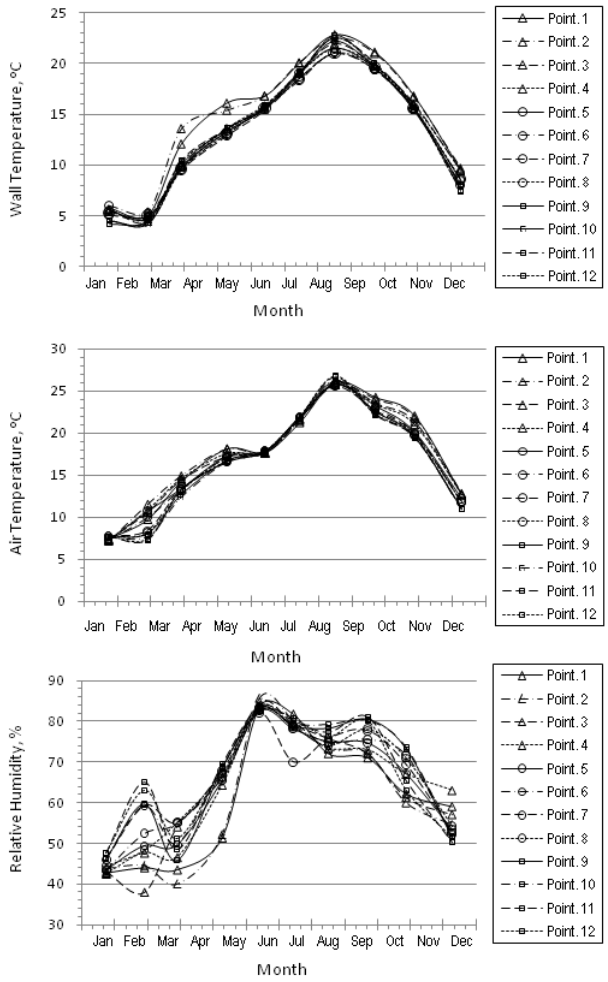

Fig. 5.Environmental condition of the investigation points. (a) Wall temperature, (b) Air temperature and (c) Air relative humidity.

Quartz and albite are originated by rock forming minerals. In December gypsum disappeared and alunogen and halotrichite come again. At Point 8, sodium alum ($NaAl(SO_4)_3{\cdot}12H_2O$), halotrichite and small amount of gypsum were detected from January to May. From June to October, jarosite ($KFe(SO_4)_2(OH)_6$) and gypsum were dominant accompanied by small amount of quartz and albite. At Point 12, alunogen as well as small amounts of sodium alum and gypsum were detected from January to May. From June to September, gypsum and sodium alum as well as small amount of quartz and albite are identified.

5. Monitoring of Debris Production

Fallen salts and debris were collected using the tray set at each investigation point when every field work made. They were brought to the laboratory and the total weight of salts and debris of each point was measured. Then, the salt and debris were oven dried at 110 ºC for 24 hours and weighed again. After that enough distilled water pored and dissolved the salts. The solution was sucsion-filtrated using the 0.1μm filter paper and Büchner funnel. Finally, the remains were oven dried at 110 ºC for 24 hours and weighed again, resulting net-weight of debris. Figure 7 shows the results. At the Points 1-3, there were much debres in May to Augst, but the Points 4 had little debris. Points 1 has extremely large amount of debris. Debris falled in spring (from March to June) contains much moisture, whereas those falled in summer (June to August) did not contain moisture. The debris amounts of Points 2 and 4 were comparatively stable throughout the year. There are few debris production from the cave wall along Points 2 and 4, whereas there are much debris production from teh wall along Points 1 and 3. At Points 5-8, especially Points 6 and 8, had the largest amount of debris than another points. Salt weathering occurred and

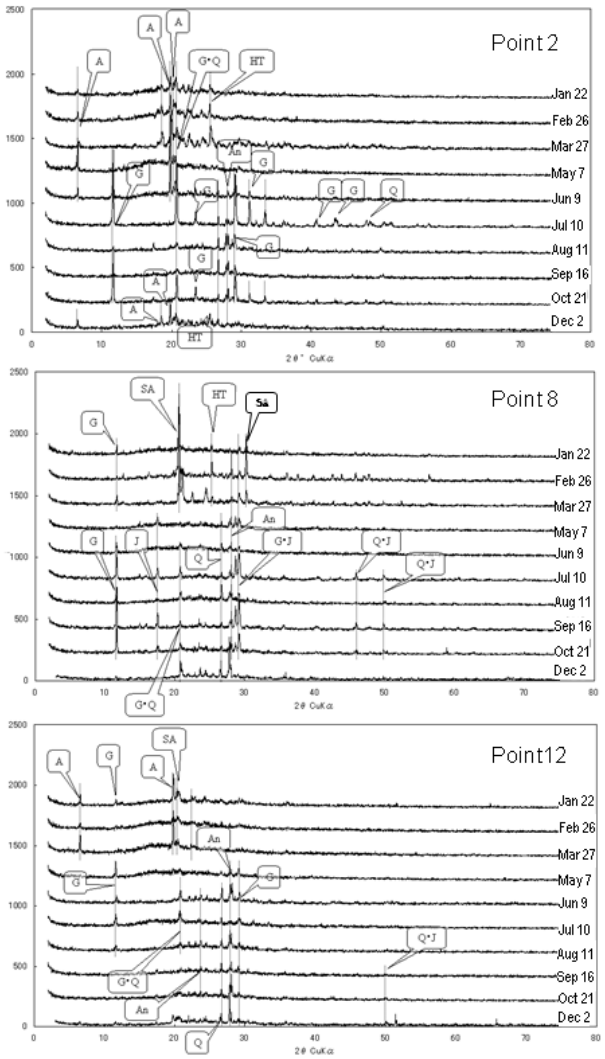

Fig. 6. X-ray diffraction of sampled salts. (a) Point 2, (b) Point 8 and (c) Point 12.

debris production are significant in winter and spring. Until June, they were stopped. The debris were fine powder, which was different from Points1-4 and Points 9-12. Debris production of Points 9-12 started in the beginning of winter and the maximum production was between winter to spring. Dibris were sporadically fell down during summer to autumn.

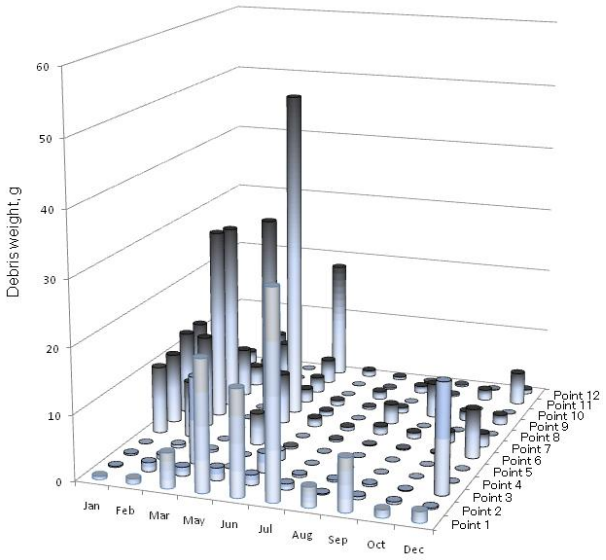

Fig. 7. Seasonal difference of debris production of each investigation point.

6. Discussion

Above these findings, it is confident that there are salt weathering occurred inside the Yoshimi caves, although the process is very slow. The types of salts were different from surrounding environments, reflecting the amount of debris production of each investigation points. There are much salt in humid summer and small amount of salt in dry winter. Especially at the Points 1-4, alunogen ($Al_2(SO_4)_3 \cdot 17H_2O$) crystallized from September and the peak period of the crystallization was February. Debris starts falling down from March. Thus, decrease of humidity plays an important role to crystallize of salt minerals and succeeding defflorescence occurred in the high humid season in summer.

Secondary, dominant salt type was different depending on the location of the cave. Points 5-8 are different from Points 1-4 and 9-12. Alunogen are dominant at the former location, whereas halotrichite ($FeAl_2(SO_4)_4 \cdot 2H_2O$) and sodium alum ($NaAl(SO_4)_3 \cdot 12H_2O$) are dominant at the latter location. The differences of the characteristics of the efflorescence of these salts are that alunogen tends to appear near the entrance of the cave, whereas the other salts occur at it inside of the cave. Alunogen is considered to prefer dryer condition rather than the other salts. Gypsum also occurred at Points 5-8, which complements to this interpretation.

Considering the relationships between salt type and debris production, there are time-lag when alunogen produce debris. Alunogen keeps itself on the rock wall for a long time, and then it falls down when the RH rise and the rock wall highly moisturized. However, halotrichite and sodium alum do not have time-lag to produce debris. As soon as they crystallize on the rock wall and they break the rock material powdery. In order to elucidate these phenomena, it will be necessary to consider more strict investigation.

According to Nordstorm (1982) compiled aluminium behaviour in natural water and insisted that alunogen are formed by evaporation under the strong acid environment. This assertion indicates that alunogen tends to occur near hot springs or secondary mineralization of mines. Actually the pH paper tests on salt debris solution showed around pH 2. The cave was artificially cut about 60 years ago and since then the direction of ground water movement gather to the tunnel caves.

The formation process of strong acid environment is often considered to be pyrite oxidation. Although pyrite was not detected from the rocks of the cave, pyrite might be contained in the rock mass of Yoshimi Hill, most of which is Miocene tuff and metamorphic rocks. When pyrite oxidizes, it produces much hydrogen ion. The ion has the ability to dissolve most of elements. Thus, water-rock interaction progresses and secondary minerals, salts, are formed. The origin of salts are considered to be cave opening, change in groundwater direction, dissolution and oxidation of pyrite, acid production and salt mineral formation. Salt type differs from its sensitive process of their environmental production, they damage to rocks by salt weathering.

7. Conclusions

Yoshimi-Hyaku-Ana Historic Site is suffering from severe salt weathering. The salts detected were sulphate minerals of alunogen, gypsum, jarosite, halotrichite and sodiumalum. These sulphates effloresced in different environmental conditions. Alunogen prefers to crystallise near the entrance of the artificial cave from dry winter to the

beginning of humid summer, whereas gypsum and sodiumalum prefer to effloresce inside of the cave with little environmental changes in the same season. Halotrichite prefers to crystallise more moisturized environment. These sulphates originated from tuff which contains pyrite that dissolved and produced strong acid. Seasonal debris production of this cave also monitored. Alunogen produced much debris when it disappeared in the beginning of humid summer. However, gypsum and sodiumalum produced powdery debris continuously when they crystallized.

Acknowledgements

We are grateful to Mr. Ota in Yoshimi archaeological centre for allowing us to field work. This study was supported by the Science Research Fund of the JSPS (No. 18680054).

References

Goudie A. and Viles H., 1997. Salt Weathering Hazards, John Wiley & Sons, Chichester, 241p.

Horiguchi M., 1975. Geology of Saitama Prefecture. Tsukiji Shokan, Tokyo, 258p (In Japanese).

Horiguchi T., Nakata M., Shikazono N. and Honma H., 2000. Occurrence and formation process of alunogen and salt accumulation on the surface of tuff in Yoshimi Hills, Saitama Prefecture, Japan. Journal of the Mineralogical Society of Japan, 29, 3-16 (In Japanese with English abstract).

Kanaidzuka R., 1986. Yoshimi no Hyaku Ana. Kyoikusha, Tokyo, 285p (In Japanese).

Kuchitsu N., 1992, On the evaporites observed in the Museum Meiji-Mura, Aichi Prefecture, Japan. Journal of Mineralogym Petrology and Economic Geology, 87, 388-391 (In Japanese with English abstract).

Kuchitsu N. and Ozaki T., 1999. The evaporates observed at the Yoshimi Caves Historic Site, Japan. Journal of the Geological Society of Japan, 105, 266-272 (In Japanese with English abstract).

Matsumaru K. and Hayashi A., 1980. Neogene Stratigraphy of the eastern marginal areas of Kanto Mountains, Central Japan. Journal of the Geological Society of Japan, 86, 4, 225-242. (In Japanese with English abstract)

Nordstorm D. K., 1982, The effect of sulphate on aluminium concentrations in natural waters: some stability relations in the system Al_2O_3-SO_3-H_2O at 298 K. Geochemica et Cosmochemica Acta, 43, 681-692.

Seki Y. and Sakai H., 1987, Salt crystallization decay of the rock-cliff Budda sculpture and water-rock interaction at Daifukuji Temple, Tateyama, Chiba central Japan. The Journal of the Japanese Association of Mineralogists, Petrologists and Economic Geologists, 82, 269-279 (In Japanese with English abstract).

Tiba T., Saito Y. and Matsubara S., 1975. Acid Tuff from Yoshimi Hills, Saitama Prefecture, Japan. Bulletin of National Science Museum, Series C (Geology), 1, 111-117 (In Japanese with English abstract).

Winkler E. M., 1994, Stone in Architecture (Third ed.). Springer Verlag, Berlin, 313p.

Scientific Annals, School of Geology, Aristotle University of Thessaloniki Proceedings of the XIX CBGA Congress, Thessaloniki, Greece	Special volume	421-428	Thessaloniki 2010

THE CURRENT STATE OF CONSERVATION OF ROMANIAN STONE MONUMENTS

Sandu I.[1,2], Brânzilă M.[3], Iancu O.-G.[3], Sandu I.G.[4], Vasilasche V.[1] and Sandu A.V.[2,4]

[1]*Arheoinvest Interdisciplinary Platform,"Al. I. Cuza" University, Bvd. Carol I, no. 11, 700506 Iaşi, Romania;*
[2]*Romanian Inventors Forum, Str. Sf. Petru Movila, no 3, Bl. L11, III/3, 700089 Iaşi, Romania*
[3]*Department of Geology, ,"Al. I. Cuza" University, Bvd. Carol I, no. 11, 700506 Iasi, Romania;*
[4]*Department of Material and Ingineering Science, "Gh. Asachi" Techn.University, Bvd. D Mangeron 73, 700050, Iaşi,Romania*

Abstract: The paper deals with aspects concerning the conservation degree of Romanian stone monuments, of different periods affected by natural and anthropogenic causes, with consequences on the historical development of the region. There are discussed main phenomena related to their present state, the stone from monuments restored/preserved, respectively, the recently discovered ones, on which no interventions have been performed. The analysis of these stones was achieved, through a correlation between the destruction and alteration factors, specific to the Romanian region and their casuistics and consequences of the degradation and deterioration phenomena. Also, for their analysis the nature and characteristics of the stone have been considered, along with the procedures of manufacturing, restauration, identifying some anomalies and inadequate interventions, already notorious.

Keywords: indigenous stone, conservation state, old Romanian monument, restoration and preservation

1. Introduction

Since ancient times, stone as construction material was preferred over other natural materials, due to some advantages such as: resistance to exogenous factors, availability, good workability, favoring the development of human communities. In Romania, the main sources of stone were mainly from quarries in the region of the Carpathian and Dobrogea Mountains, specific to orogenic rocks, then from the plateau areas of Moldova, Transylvania, Oltenia, Muntenia, Dobrogea Central and South soft rocks, especially sedimentary (Sandu et al., 2009).

In the paper, a number of monuments from different periods and in different states of conservation, from the entire territory of Romania, have been selected (Fig. 1). Thus, the paper presents a number of phenomena determining their present state, differentiated in some monuments restored/preserved and others on which there are no interventions.

There are also discussed the main factors of deterioration and degradation of these lythotypes, specific to Romanian territory, with their consequences and casuistics. The nature and characteristics of the stone have been analysed, along with the manufacturing technologies and the restoration principles and procedures.

2. The indigenous stone used in monuments

2.1. At the manufacturing of the monument

The rocks used in architectural historical buildings belong to three main categories of hardness (Mihailescu and Grigore, 1981; Sandu et al., 2009): *hard, compact or rocky* (granite, granodiorit, syenite, porphyry, andesite, gabrou, basalt, quartzite, crystalline schists, crystalline limestones and marbles, travertine, sandstones); s*oft, consolidated* (clay, marl, gypsum) and *detritic, non-consolidated* (sand, gravel, ballast).

Hard rocks were generally used as split stone, carved and brut in several constructions mainly underground (foundations, tunnels, cellars, galleries), but also on the ground, especially nearby quarries. During the work, the stone was used both as apparent, highly processed through molding, highlighting its natural features and as stone inside the masonry. Some rocks in this category (marbles and other natural limestones, travertines, sandstone) were used for ornamental elements, cladding and sculptures.

Consolidated *soft rocks* were used primarily to obtain ceramic products (bricks, tiles, tubes for feed pipes and sewage) and plastering. Their manu-

facturing technology involved thermal processes, leading to the improvement of the physical-mechanical properties, so that allowed their use with hard rocks or in wet aggressive systems.

The non-consolidated detritic rocks were used for preparing mortars, concretes, plasters, decorative cast frames, road building and access roads, the pavements and some foundations. They required a

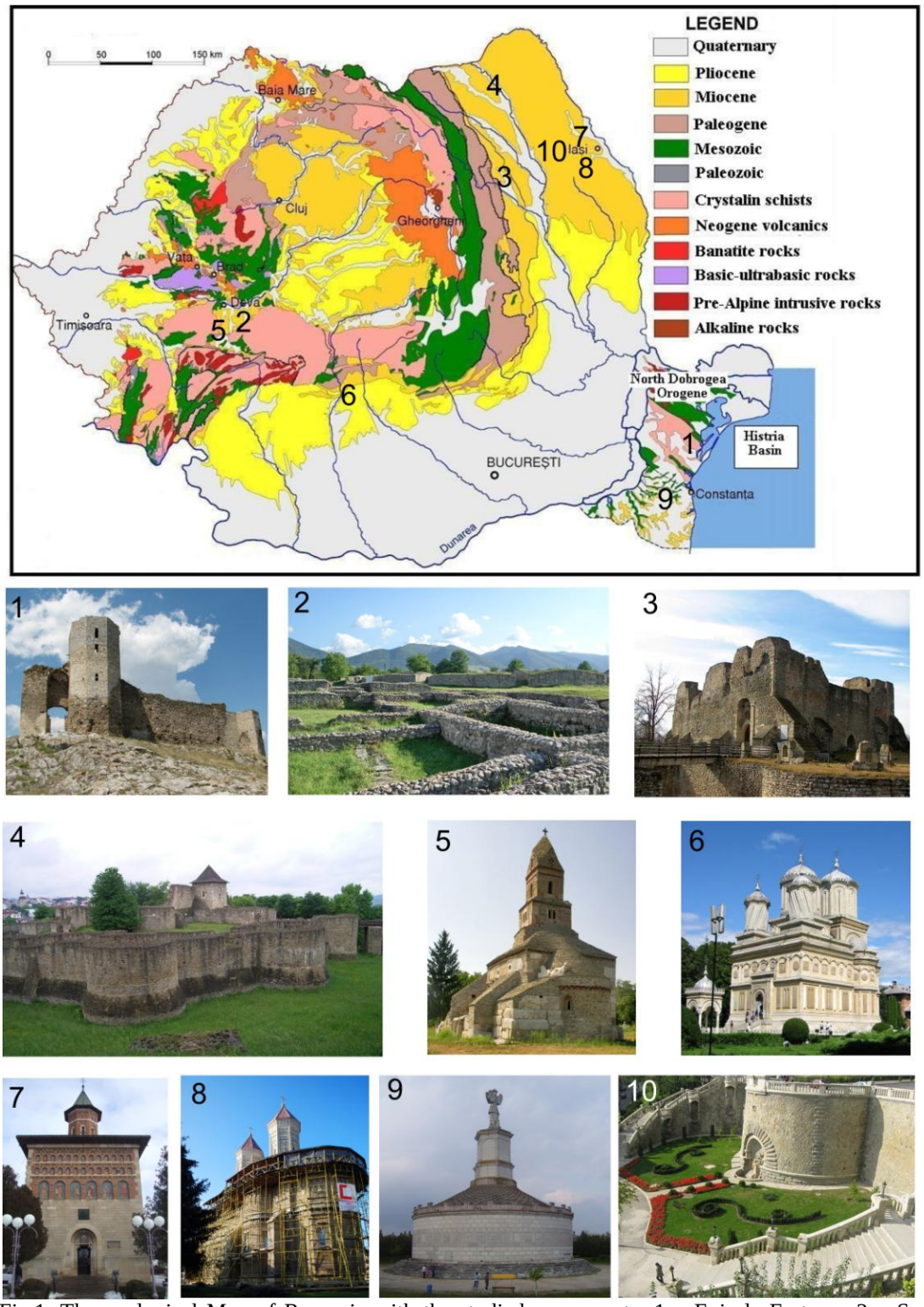

Fig.1. The geological Map of Romania with the studied monuments: 1 – Enisala Fortress, 2 – Sarmisegetuza, 3 – Neamt Fortress, 4 – Suceava Fortress, 5 – Densus Church, 6 – The Cathedral of Curtea de Arges, 7 – St.Nicolas Church Iasi, 8 – The Three Saints Hierarchs Church in Iasi, 9 – Tropaeum Traiani, 10 – Râpa Galbenă (Elisabeta Esplanade) .

specific binder (at the beginning the hydrated lime and later, the cement) which allowed them to become more resistant to environmental factors by monolitization.

2.2. During restoration

In the interventions of restoration of the monuments in Romania two appproaches were adopted: that of architect André Lecomte de Nouy (who restorated monuments such as the Cathedral of Curtea de Arges, Three Hierarchs and St. Nicholas of Iaşi) today considered an inappropriate intervention, the other approach was the one accepted by universally recognized rules today (minimal intervention on the material, opportunity, compatibility, readability, reversibility).

The stone used in restoration in an inappropriate way, without respecting a set of technological rules, has brought great damage to monuments or simply has not survived in the work. According to current principles of restoration, the new stone must be compatible to the original material, in terms of strength, density, color etc. Therefore, the stone chosen to achieve this condition, in terms of geochemical, physical-structural, mechanical but also hydrous characteristics, has to correspond to the original. In general, the restoration simply replaced broken or damaged stones, touching the strength, but also the aesthetics of the monument (Sandu, 2008; Sandu et al., 2006). The most difficult problem that arose in this regard was the exhaustion of old quarries; therefore finding new sources of stone resembling to the old one became difficult, leading to the increase of the costs.

3. Deterioration and degradation of monuments

Generally speaking, stone monuments from the Carpatho-Balkan region were affected, besides the environmental agents (humidity, temperature, air currents, precipitation, air pollution, microbiological organisms etc.) and some risk factors specific to Romania, from the *calamity* or *cataclysms group*, such as: earthquakes, landslides, floods, storms, hail, fire, lightning, explosions, drought and freeze, but also from the *entropic catastrophe* group like those provoked by vandalism, wars or revolutions, accidents, leading to lack of materials, damage, collapse or demolition, cracking, erosion, exfoliation etc. Their deterioration and degradation occur also because of some *endogenous factors*, related to: material, technology implementation and defects. Besides those, the shape and structural complexity of the monument, its age and state of preservation (Sandu, 2008; Sandu et al., 2006) have to be considered.

The stone degradation of the old monuments in Romania was determined by the buildings morphology (sculptures, facades, cornices, balconies, frames of windows) and also the mode of exposure (position towards the cardinal points, towards the weather phenomena, the fundation system influenced by soil or surface/ underground waters). The alteration and destructions are specific to the typology of stone and monument, being influenced by agents or exogenous factors only to a certain extent, their effects depending on the nature, intensity and duration of their action and how to interfere or overlap. All stones and their derivatives, no matter how strongly they were, submitted to continuous alteration and destruction: the first affects their physical state and the second, their chemical nature. The stone type and all the characteristics of its environment determined the specificity, rate and duration of these processes. Some stone materials remained unaffected over the years, while other materials were strongly affected (wood, by rotting, created voids or niches in walls, floors etc., reducing the ensemble strength). Few works of art are homogeneous in terms of component materials (Sandu et al., 2009).

The most important processeses to which old stone monuments were subjected, especially those abandoned, are: stealing, demolition/collapse, fracturing, grinding or splitting/erosion, cracking, fragilization, coming off, desagregation and others. They generated specific effects, commonly seen in some stones, like for sandstone and limestone "powdering weakening" and "separation through plates"; old cracks for marble and gemstones. There are often noticed a series of other processes, like monolitization, fouling of organic products resulting from "aero-foil" processes of the smog and soot or of metabolic products (micetes, algae, lichens, mosses, insects, birds etc.). Grinding by errosion processes have severely weakened the stone. Cumulative effects, such as iridescent, fouling or efflorescence deposits forming the so-called *patina*, continously altered them in an evolutive process. Crystallization of salts caused the surface powdering, cracking and even total disintegration, leading to losses of material through shrinkage, detachments, swelling etc., effect encountered at most part of the monuments. A specific case in Romania is the presence in the oldest monuments of iron ox-

ides in sandstones and crystalline limestone, derived from sedimentary pyrite, which under the influence of microbiological factors moved the iron oxides and gypsum, the early processes leading to alteration by acid-basic disolution, coupled with redox processes. Some damage and degradation were also due to inadequate maintenance and treatment, both during the work and in the preservation/restoration processes or after vandalism.

The degradation of buried stone in the foundations of buildings or archaeological sites, was due to the underground and surface water with high chemical and physical loading, but also to microbiological activity and soil processes (related to the excavation, processing soil subsidence and landslides, earthquakes, crop plants and trees). Generally, the stone used as such, shaped or sculpted, finished by polishing, provoqued micro-destructions, with evolutive decay. The placement of the stone in bulding, sometimes by foreign craftsmen unaware of the environmental aggression or of the inappropriate functions for the structure (for filling or resistance), without taking into account the durability and compatibility led to a number of evolutive processes, some of there errors becaming notorious. Different stones had different behaviors and deterioration-degradation rates, depending on the aggressiveness of the environment and anthropogenic factors. However, one of the most aggressive environmental factors, often met in Romania, remains the humidity. The moisture or humidity content is defined by two terms: humidity in the environment, measured by relative humidity (RH), humidity of a material, measured in percent by weight (moisture content). The two types of humidity can be correlated through the term *hygroscopicity*. This is the *reversible humidity* of a material, which is exchanged with the environment. Because stone is a hydrophilic material, sudden and large variations in environmental conditions (humidity, temperature, rainfall and rising water surface), have generated a series of destructive processes of structural and chemical alteration, coassisted or not by the microbiological heat or radiation, especially light. All types of water that affect majorly the behavior of a stone can generate different alteration and destruction ways. Water acted directly (through hydrogels, cristalohidrates, selective dissolution of minerals, recrystallization) on the stone, but also through the materials found in contact (soil, mortar, plaster, metals, organic materials), when their mobile chemical load has made its mark. The behavior of the stones according to the alteration is directly related to the phenomena of hydrous transfer (Sandu, 2008; Sandu et al., 2009).

The use of stone in the architectural buildings reports another phenomenon with serious consequences for the conservation of historical monuments: the "removal" of the stone from archaeological sites or abandoned buildings and their use in a new work (e.g. Church of Densus stone raised in 1280 with stones taken from the Dacian fortress Sarmisegetuza but also from different camps or Roman tombstones). The positive part of this example is that although several elements have been preserved (we refer here to the tombstones, altars, capitels), probably in other circumstances, they would have been destroyed. The phenomenon is similar to transhumance of objects or monuments in other areas of museum sites. It is known that after a transfer, the monument loses a number of elements and economic functions. So in our case, somewhere similar to the great museums of the world, who gathered artifacts from other places, it was allowed a better preservation of them, but with diminished patrimonial value (Sandu et al., 2009).

4. Conservation state of representative monuments

4.1. Non-restored or partially restored monuments

Many old monuments recently discovered or those keeping few original elements (only the foundations and partially the walls) have not yet been studied, either because of the lack of financial resources or because of scientific and historical reasons. The best case for some of them, was after 1860, when archaeological excavations were performed. Some of them were abbandoned, in an unnatural way because of the lack of protection systems, others have been robbed, for new buildings. After The Second World War, with the introduction of modern laws concerning the protection of cultural heritage and archaeological values, a number of inventories and preventive measures have been taken. Among these, it is worth mentioning: the ruins of medieval fortress Enisala of Dobrogea, Sarmisegetuza of Transylvania, the fortresses of Neamț and Suceava in Moldova.

Enisala medieval fortress is located at 2 km from the Enisala town on a limestone hill dominating the Babadag and Razelm lakes area (Mănucu-Adameşteanu, 1980). The history of the city and the nearby settlement is illustrated also by the

names they used to have: Vicus Novus, translated to New Village, and the Slavic name Novoe Selo, which the Turks changed into Yeni - Sale. The fortress is situated in an archaeological complex with numerous archaeological remains coming from the Neolithic to the Middle Ages. The archaeological excavations have been begun in 1939 and continued with minor interruptions, during 1970-1998. Medieval period corresponds to two levels of living. First, prior to fortification building, was dated on archaeological material from the late XIIIth – XIVth century. The second level corresponds to the period raising the walls. The fortress was built for military purposes, defense and surveillance of roads on water and on land, in the second half of XIVth century. Based on construction techniques, archaeological material and historical realities has been hypothesized that only interested in raising a fortress in the system of fortifications in northern Dobrogea, directed towards the sea for naval traffic control, were Genovese merchants who were holders of the monopoly of navigation on the Black Sea. Between 1397-1418, during the reign of Mircea the Old, the city was part of the defensive system of the Romanian Country, and after the conquest by the Ottomans in 1419/1420 there was installed a Turk military garrison. The city was abandoned after Turkish domination advancing beyond the mouths of the Danube (1484). The Fortress has a polygonal irregular plan (Fig. 1.1), following the sinous relief of the Jurassic massive on which lies and from which career has been excavated the needed construction material. Enclosure walls, towers and bastions, partially preserved and restored, are conserved on a height of 5 to 10 m. A particular architectural element is the main gate bastion, of oriental origin, with double arch frequent in the Middle Ages and used by Byzantine builders to various buildings in the Balkans but also in Romania. Since the city is abandoned for a long time, many elements of the building structure are lacking, many were stolen, others were totally degraded and lost. A series of photographs of archaeological discharge, partial structural ordering and reintegration, were made and reflect the overall integrity of the monument to be included in the museums circuits.

Sarmisegetuza was the most important Dacian military, religious and political center. Build on the top of a 1.200 m high mountain, the fortress was the core of the strategic defensive system in the Orastie Mountains, comprising six citadels, of which the most important is Sarmisegetusa Director and Ulpia Traiana Sarmisegetusa (Daicoviciu, 1984; Glodariu, 1988). Sarmisegetuza Director is the name of the capital of pre-Roman Dacia, from which the most remarkable is Big Rounded Sanctuary and The Andesito Sun. Most of the archeologists assert that the city was raised in between the 3rd and the 2nd century BC, while others sustain that it would be at least 600 years older. One of the reasons of this dispute could be the striking resemblance of the Big Rounded Sanctuary with those of Stonehenge. It seems that the same architect has conceived them both, the only difference being that the one from Orastie is smaller. At about 40 km away from Oraştie Mountains, in the county of Sarmisegetuza, in the South-West of the Hateg Depression, there are the ruins of the other fortress bearing the same name, capital of Roman Dacia, also called Ulpia Traiana Sarmisegetuza, founded by the governor Terentius Scaurianus between 108–110. For two centuries, it represented the political and administrative center of the province of Dacia. The sieges of the governor, of the administration, of the financial system, of the military, economic and religious centers were situated inside the fortress. During the rule of Emperor Hadrian (117-138), Sarmisegetuza was called Colonia Ulpia Traiana Sarmisegetuza, and then during the period 222-235, to its name was added the epithet of metropolis.

In these, stones from geological formations developed in Hateg Depression were used, mainly of Cretaceous age sedimentation, but also crystalline limestones and marbles, coming from the nearby areas, were used. To all these, andesite slabs used mostly in sanctuaries, but also to some pavements for access roads, are added. The last years operations were focused onto archaeological dowload, coherent ordering and reintegration of stone blocks in their original building shape, with remaking of pavements and acccess routes, allowing a better highlighting of the structure and monuments disposal within the complex (Fig. 1.2).

Neamț Fortress was rumored to have been built, in the XIIIth century, by the Teutonic Knights, against Tatar incursions. In 1476, after defeating the Moldavian armies in the Battle of Valea Albă, the Ottoman Empire Sultan Mehmet IInd forced Steven the Great to retreat here (Fig. 1.3). The place was battlefield between Turkeys and Moldovians, the garrison being almost totally destroyed (Giurescu, 1976; Iijima and Dumbrava, 2005).

The building material for the walls, but also for

some annexes is represented by blocks of limestone, shale and especially so-called type Kliwa sandstone, the Cretaceous and Oligocene. All these materials came from nearby quarries, opened in deposits of the Carpathian Flysch.

In 1866, the fortress was declared a historical monument. Reinforcement of the wall works, made between 1968-1972, led by renowned architect Stefan Bals, aimed at the preservation and maintenance of the monument as it is, without reconstruction of missing parts. In the absence of certain information, some terraces were performed just useful to visiting in good condition. In the past years some walls have been raised, especially the inside ones, the shape of cavity. The stone used in the restoration process was purchased from the same sources with the original one.

Suceava Fortress (Fig. 1.4) was built by the prince Petru I Muşat, by the end of the XIVth century, with thick walls and semicircular bastions. The plan of the stone fortress is square-shaped (Iijima and Dumbrava, 2005). Excavations uncovered ceramic plates and disks used for interior and exterior decoration, for secular and religious aims. Following the destructions caused by Turkish and Polish incursions, Stephen the Great fitted the fortress with an inner courtyard with semicircular bastions and a new stone ditch, adapting the old fortresses to the new military technique program. It is essential to remind that the first excavations were carried out by the end of the XXth century by C.A. Romstorfer (Giurescu, 1976; Daicoviciu, 1984; Glodariu, 1988).

The fortress was built with stone, extracted from local quarries, near the town, such as sandstone and limestone whose geological age is placed in the Sarmatian age. Inside the walls, there are also blocks of sandstone and limestone coming from the mountain area of Carpathian Flysch.

The fortress was restored especially in the outer walls, which were largely reunited, using stone coming from the same sources with the original stone.

4.2. Restored Monuments

Regarding the interventions of restoration of some stone monuments in Romania, we encounter three totally different situations: very old monuments built of stone coming from other monuments, monuments restored according to the old principles, through total demolition and reconstruction following the initial plans – André Lecomte de Nuoy and restored monuments according to the modern principles, accepted worldwide.

4.2.1. Old monuments built of stone coming from other monuments

Typical example for Romania is the ***Church of Densus*** (Fig. 1.5), where it is considered that on the setting of the present day church, there was once a Dacian temple dedicated to Zamolxis, upon which the conquering Romans built a temple dedicated to the god Mars. After the Roman administrative withdrawal, the temple became in the IVth century AD, a Paleo-Christian church. Its present form dates from the beginning of the XIIth century and is considered the oldest church in Romania and South East Europe.

Observations on the building material show that it comes from stones taken from Dacian fortress of Sarmisegetuza but also from various Roman camp or tombstones. These stones were used fully or partially shaped by carrying out an original architectural system, which kept intact the old stone ornamentation.

4.2.2. Monuments restored after now outda-ted principles

The Cathedral of Curtea de Argeş (early XVIth century) is one of the most famous churches in Romania (Fig. 1.6), restored by an old principle of André Lecomte de Nuoy. It resembles a very large and elaborate mausoleum, built in Byzantine style, with Moorish arabesques (Dragut, 2000).

Building material consists of native stone, brought from the nearby quarries. The sleek and shaped stone facade and also the foundation blocks, are made of numulitic limestones, which come from the Albesti quarries near Campulung Muscel, are of Eocene age and following diagenesis processes have taken appropriate structure and texture to be processed and even carved. Inside the church there also marble columns (e.g.: crystalline limestones) probably from Greece.

It is known that the founder was Prince Neagoe Basarab (1512-1521), Prince Ioan Radu completed the work in 1526. Along the years, the cathedral was submitted to several restoration works: Prince Şerban Cantacuzino in 1681, Joseph, the first bishop, in 1804. The present form was given both by the French architect André Lecomte du Nouy and the Romanian architect Nicolae Gabrilescu, whose restoration works were completed in 1885

and in 1886 it was reconsecrated. The cathedral is faced with pale grey limestone, easily chiselled but hardening on exposure. The interior is of brick, plastered and decorated with frescoes.

St. Nicholas Church of Iaşi, built between 1491-1492 by Stefan cel Mare and rebuilt in the late XIXth century (between 1890 - 1904) by French architect André Lecomte du Nouy, is the oldest religious edifice in Iasi which has been preserved until today (Fig. 1.7).

The exterior architecture gathers in the most harmonious way, the stone, brick and tiles, disposed in polychrome enamel discs. The initial building material was used only partially in the restoration, since the church have been entirely demolished, the wall stone being largely replaced by brick. The inside of the church belongs, entirely to the last restoration.

The Three Saints Hierarchs Church in Iasi was built between 1637-1639 by Vasile Lupu (Fig. 1.8). The church became renowned for the extraordinary lacery in stone which adorns the facades, from bottom to the top of the derricks. One can count over 30 non-repeating registers of decorative motives. Western architectural elements (Gothic, Renaissance) are combined with the Eastern style, of Armenian, Georgian, Persian, Arabian or Ottoman inspiration, in a totally bold conception, whose result is a harmonious ensemble. The effusive scenery makes the church resemble a shrine of architectonic proportions, especially conceived to protect the Saint Parascheva's relics (1641). After the 1882 restoration, the original fresco was detached, some fragments still being kept today in the monastery's museum.

Although in the restoration process led by Lecomte du Nouy in a fashion of the time, the church was demolished and part of its annex buildings (which were removed) and the most of the church's original materials from its structure, were reused at the rebuilding of the edifice involving other materials.

Native stone quarry near Iasi is found in the thick walls, but exterior plaques, blocks from the wall base and ornaments are numulitic limestone. These limestones come from the same quarries from Albesti near Campulung Muscel, where limestone for Curtea de Arges was extracted. The sculptured stone plaques are mainly new, there were kept just a few old stone cladding, but they are carved on the rear face. It is known that many elements, as the huge horologe in the gate's tower were taken to Paris after restauration in 1882.

4.2.3. Monuments restored after modern principles

Tropaeum Traiani Adamclisi (Fig. 1.9) is a monument built in 109 inside Roman Civitas Tropaensium, in Inferior Moesia (Dobrogea), to commemorate Roman Emperor Traian's victory over the Dacians, from 102, in the Battle of Tapae. Before Traian's construction, an altar existed there, and its walls were inscribed the names of 3,000 legionaries and auxiliaries (servicemen) who had died in 92. Traian's monument was inspired by the Augustus mausoleum, and was dedicated to the god Mars Ultor in 107/108 AD. On the monument there were 54 metopes depicting Roman legions fighting against enemies; most of these being preserved in the museum nearby.

The original monument disintegrated a long time ago. The present edifice is a reconstruction dating from 1977 entirely made of different stone from initial one (neosoic age calcars).

The nearby museum contains many archaeological objects, including parts of the original Roman monument. From the original 54 metopes, 48 are in the museum and 1 is in Istanbul.

Rapa Galbena or **Elisabeta - Esplanade** from Iaşi (Fig. 1.10) has been included on the list of historical monuments since 2004 and restored in 2007. The construction was completed in1906. The area is affected by many springs keeping the humidity in the monument, needing periodical restorations. The main part in the degradation of stone of this monument was played by the air pollution (exhaust), ground waters (chemical charge, especially nitrates) and abusive use of sodium chloride during the winter, which led to massive erosion. A first technical solution adopted in 1906 for the collection of the springs was a special sewage discharge into Bahlui river.

Stone is the main element used in construction. It came from multiple sources, from the beginning. Some came from the quarries that valued the sarmatian deposits from Moldavia, and other, especially older blocks, came from the quarries of the Carpathians Flysch. At the last restoration in 2007, were preferred rocks coming from Tg.Ocna (siliceous sandstone, yellowish, with a high amount of iron oxides, which gives a reddish color). Deposits from which this sandstone (called Kliwa sandstone) comes from, have an Oligocen age.

5. Conclusions

This paper focused on a number of Romanian old monuments, from different periods, describing

their state of conservation due to natural and anthropogenic causes, as consequences of the specific social-historical development in the area. Thus, the study shows the main phenomena related to their present state, differentiated in monuments restored/preserved and the ones less known, on which the preservation-restoration has not been performed. There are presented the stone types and procedures used in restauration during time, identifying some anomalies and inadequate interventions, which have become of notoriety.

Acknowledgments

This work was supported at "Al.I.Cuza" University of Iasi by projects CNMP PN II 31-059/2007 and CNCSIS IDEI cod 423.

References

Daicoviciu H., 1984. Colonia Ulpia Traiana Augusta Dacica Sarmizegetusa, Ed. Sport-Turism, Bucureşti, 198 p.

Drăguț V., 2000. Encyclopedic Dictionary of Romanian Medieval Art (Dicționar enciclopedic de artă medievală românească), Ed. Meridiane, Bucureşti, 166-169.

Giurescu C.C., Giurescu D.C., !976. Romanians History (Istoria Românilor), vol. II, (1352-1606), Ed. Ştintifică si Enciclopedică Bucuresti, 154-192 pp.

Glodariu I., 1988. Dacs Fortresses and Settlements in the Orastiei Mountains (Cetăți și așezări dacice în munții Orăștiei), Ed. Sport-Turism, Bucureşti, 159 p.

Iijima B., Dumbrava V., 2005. Stefan der Große – Fürst der Moldau. Symbolfunktion und Bedeutungswandel eines mittelalterlichen Herrschers. Leipziger Universitätsverlag, Leipzig, 203 p.

Mănucu-Adameşteanu Gh., 1980. Medieval Necropola of Enisala, Preliminary Report (Necropola medievală de la Enisala. Raport preliminar), Peuce, VIII, Tulcea, 473-496.

Mihailescu N.St., Grigore I., 1981. Mineral Resources for construction materials in Romania (Resurse minerale pentru materiale de constructii in Romania), Ed.Tehnica, Bucuresti, 380 p.

Sandu I., Brânzilă M., Sandu I.G., 2009. Scientific Conservation of the Stone Monuments (Conservarea stiintifica a monumentelor de piatra)**,** "Al.I.Cuza" University Press, Iaşi, 314 p.

Sandu I., 2008. Degradation and Deterioration of the Cultural Heritage (Deteriorare si Degradarea Bunurilor de Patrimoniu Cultural), Vol. I and II, "Al.I.Cuza" University Press, Iaşi, 462 and 538 p.

Sandu I.G, Sandu I., Dima A., 2006. Modern Aspects Concerning the Conservation of Cultural Heritage (Aspecte moderne privind conservarea stiintifica a patrimoniului cultural), vol.III.Ed. Performantica, Iaşi, 502 p.

Special Session S25
Weather modification

Scientific Annals, School of Geology, Aristotle University of Thessaloniki Proceedings of the XIX CBGA Congress, Thessaloniki, Greece	Special volume 100	429-435	Thessaloniki 2010

STUDY OF A MESOSCALE CONVECTIVE COMPLEX OVER WESTERN AND SOUTHERN BALKANS

Foris D.

Meteorological Applications Centre. Hellenic Agricultural Insurance Organization, Macedonia Airport, 55103, Thessaloniki, Greece, d.foris@elga.gr

Abstract: The purpose of this study is to thoroughly examine the conditions leading to the development of a mesoscale convective complex (MCC) on 24 May 2009 that affected the western and southern Balkan peninsula, its features and the manifestation of its activity at the surface. To this end, data from a variety of sources were used, such as weather maps, surface records and upper-air soundings, a hailpad network, satellite, lightning, precipitation and radar data. First, the evolution of the system was described, in terms of the track, timing, and areal extent. Second, the synoptic and thermodynamic environment that favored its development was studied. Special features at the surface, such as a cold pool and a mesohigh, were documented by surface observations. Finally, successive satellite, lightning and radar imagery revealed the organization of the system. All data together document well the categorization of this system as an MCC.

Keywords: mesoscale convective complex, western and southern Balkans, cold pool, mesohigh.

1. Definition

The concept and definition of MCC adopted worldwide are based on satellite imagery. Maddox (1980) proposed a definition based on areal extent and depth, as determined by the temperature of its capping cloud cover. More precisely, what is required is (a) a continuous cloud shield with IR temperature $\leq$ 241 K that must have an area $\geq$ 100,000 km^2, (b) an interior cold cloud region with temperature $\leq$ 221 K that must have an area $\geq$ 50,000 km^2, (c) these conditions must be met for a period $\geq$ 6 h and (d) the eccentricity of its shape must be $\geq$ 0.7 at the time of maximum extent.

An alternative definition, including dynamics, was proposed by Cotton et al. (1989) reading as follows: "a mature MCC represents an inertially stable mesoscale convective system which is nearly geostrophically balanced and whose horizontal scale is comparable to or greater than λ_R, the Rossby radius of deformation".

2. Special features and conceptual model

The climatology of MCCs indicates that they develop both in the tropics and midlatitudes, over land and sea. In midlatitudes they appear during spring and summer over continents, usually in late evening and night. They acquire their maximum extent (mature stage) around local midnight and dissipate just before sunrise. They often produce strong surface winds and lightning activity, heavy precipitation and big hail.

MCCs evolve from the merging of the anvils of neighboring orogenic cumulonimbus of meso-β scale organization, which leads to the formation of a stratiform cloud layer extending from the melting level up to the tropopause. A cold pool of meso-β dimensions is thus created due to precipitation evaporation and downdraft outflow. The level of strongest upward motion and of maximum heating then shifts upward to 300 hPa level (Wetzel et al., 1983). Finally, after sunset, a cooling of the cloud canopy occurs due to radiative effects (Fritsch and Brown, 1982). All these factors favor upscaling, namely the transition of the system to the meso-α scale.

The conceptual model distinguishes two regimes: a leading narrow area of strong convection and an extended trailing area of stratiform precipitation. The airflow is characterized by a warm, moist, low-level jet, an ascending front-to-rear flow of unstable air and a strong descending rear-inflow jet (Johnson et al., 1989). A mesohigh is generated in the boundary layer due to the cold pool at the surface, a mesolow in midlevels due to the stretching

of the air column resulting from cooling at low levels and heating aloft and a mesohigh at tropopause level due to the mesoscale ascent in the stratiform area.

3. Track, timing and extent

The system started as a complex of 4-5 convective cells in the south end of the Pannonian Plain, the triggering mechanism being the orographic uplift along a line between the Dinaric Alps and the Carpathian Mountains. When the anvils of the individual cumulonimbus merged to form the MCC, the system started to move towards SSE and dissipated over south Aegean Sea, leaving its signature as a cyclonically rotating vortex (a PV anomaly) or MCV (mesoscale convective vortex) in the form of spiral cloud bands in the middle troposphere.

Surface observations (METARs) from weather stations along the track marked thunderstorm activity at 10:00 UTC over Belgrade, at 12:30-13:30 over Nis, at 14:30-16:00 over Skopje, at 18:00-19:00 along the line Florina-Thessaloniki-Kavala, at 19:30 over Larissa and finally at 20:00-21:00 over Lamia and Volos, Greece. Thereafter, the system started to dissipate gradually. The total length of its track was about 950 km.

Individual storms started to develop at about 10 UTC. The MCC formed at 15 UTC, reached maturity at 18 UTC and started dissipating at 21 UTC, its duration (6 h) lying within the typical values. The MCV (Bader et al., 1995), on the other hand, lasted for several hours (9 h), until 06 UTC next morning.

Individual thunderstorm organization started as a meso-β scale feature, whereas the MCC resulted in meso-α scale. At maturity time the system had a more or less oval shape, its eccentricity being $\varepsilon \approx 0.75$, the area covered by the cirriform anvil was estimated to be about 235,000 km^2 (at 241 K) and the corresponding area covered by overshooting tops reached about 90,000 km^2 (at 221 K), as identified by enhanced IR imagery. These values are within the standard theoretical extent and shape, according to the MCC definition. It is to be noted that large MCCs acquire a horizontal scale comparable to Rossby radius of deformation, which for midlatitudes (where earth's rotation dominates) is 300 km. This value agrees indeed with the area of 300 X 300 = 90,000 km^2 found above.

4. The pre-storm environment

The large-scale environment characterizing the MCC genesis region shows a pronounced anticyclonically curved jet streak to the north of the MCC (Maddox, 1983). Favorable conditions also comprise absence of synoptic forcing, weak vertical shear of the horizontal wind and a large convective available potential energy (CAPE). Necessary requirements also include strong warm advection (WA) at low levels and existence of abundant moisture through a deep layer of the troposphere, resulting in strong potential instability (Cotton et al., 1989).

These features were actually verified, in the case under consideration, with the aid of a variety of data. First, a jet streak was present at 250 hPa to the NNE of genesis area at 00 UTC (Fig. 1). Second, a warm air mass of 20^{o}C at 850 hPa at the same time from Central Mediterranean was advected towards NNE into the region (Fig. 1). As for the vertical profile, the most representative sounding of Belgrade at 12 UTC (Fig. 2) was examined. This showed a weak vertical shear, moisture all the way

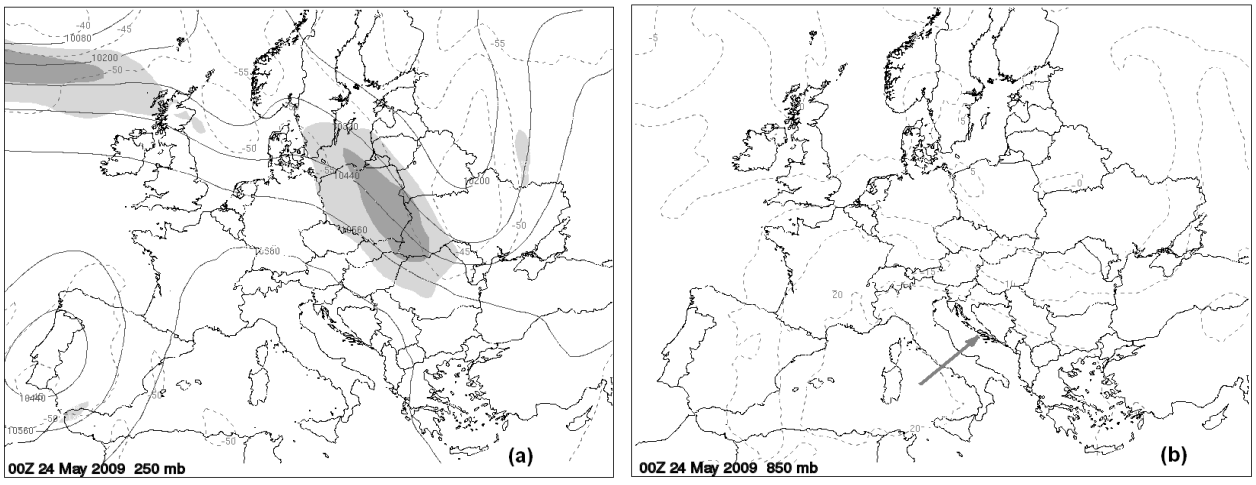

Fig. 1. Maps of (a) 250 and (b) 850 hPa at 00 UTC of 24-5-2009 depicting the pre-storm environment.

up to about 300 hPa, significant instability with CAPE = 995 J kg^{-1} and high enough instability indices (KI = 32 ^{o}C and TT = 50 ^{o}C).

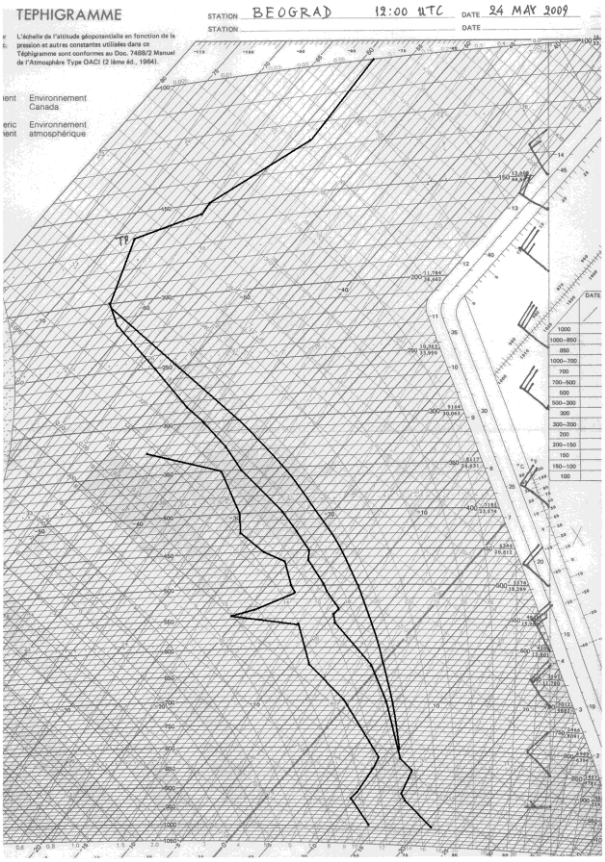

Fig. 2. Belgrade 12 UTC sounding of 24-5-2009.

5. Manifestation at the surface

Surface observations along the track revealed several common features, like the significant drop in temperature and pressure, strong winds and heavy precipitation. A temperature drop of 8^{o}C in 2 h was observed in Belgrade, of 9^{o}C in 1.5 h in Nis and of 12^{o}C in 1.5 h in Skopje. Wind gusts up to 40 kt were also recorded in Skopje.

Surface manifestations of MCC features were documented from two automatic meteorological stations installed west of Thessaloniki, namely Galatades (north) and Meliki (south). Graphs of the daily march of temperature at both stations (Fig. 3) show a considerable drop in temperature, indicative of the cold pool which was created near the surface. This, in turn, formed a mesohigh in the pressure field, marked in the graph by the significant rise in pressure after its drop. The mesohigh is not an anticyclone, since there exists no anticyclonic circulation, and its extent usually ranges from 100 to 500 km (Djuric, 1994). This extent was in the present case estimated to be 200 km, from the mean velocity of the system (50 km h^{-1}) and the time elapsed (4 h) for the pressure to adjust to the average prestorm passage value. The MCC passage was also manifested in the wind speeds recorded, where successive spikes indicated surface gust fronts and consequent divergence from the individual convective cells. Heavy rainfall, resulting from the leading convective cells (27.2 mm in half-an-hour) was recorded, followed by 6.2 mm in one hour due to the trailing stratiform precipitation.

The MCC moves typically partly with the environmental wind, but deviates from it, since new convective cells develop on the side with the most

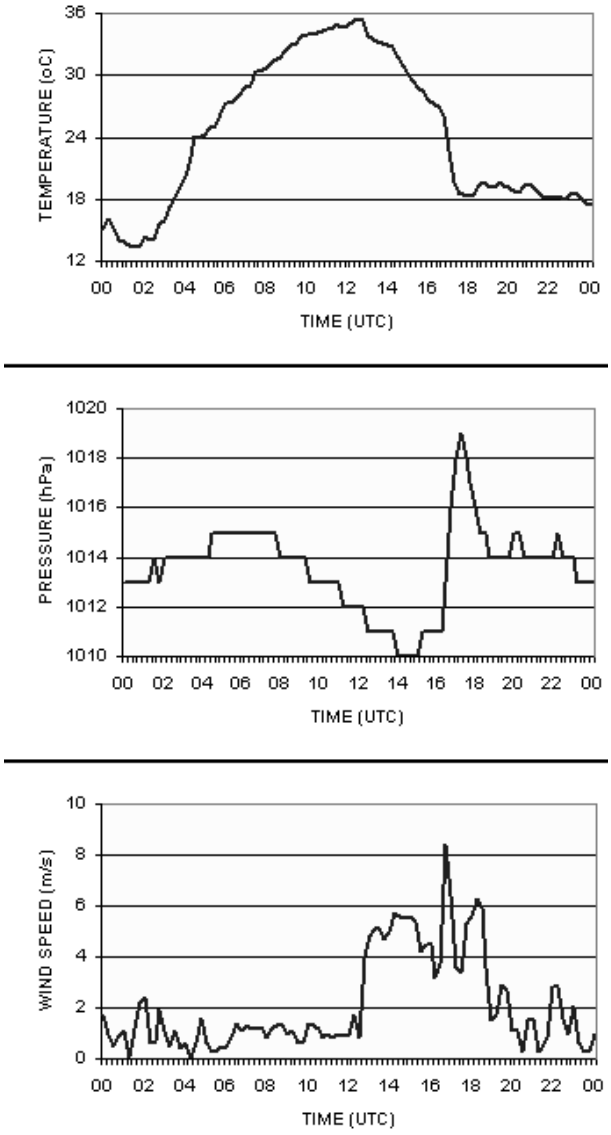

Fig. 3. Meliki (south station) daily records of 24-5-2009 for temperature, pressure and wind speed. Similar graphs exist for Galatades (north station).

low-level warm inflow (Djuric, 1994). In the present case, the steering wind was from 320°, while the actual motion was from 340°. New cells developed in the west end of the line of convective cells, according to warm advection from Adriatic Sea. The MCC moved at 14 m s^{-1}, much faster than average (5 m s^{-1}), that is why flash flooding did not occur, since precipitation was not delivered over the same area but, instead, was distributed over a long stretch.

6. Satellite, lightning and radar history

Satellite IR (11.2 μ) images (Fig. 4) reveal the special features related to MCC lifecycle. At 13 UTC the individual convective clouds could be easily identified, while at 15 UTC the anvils emanating

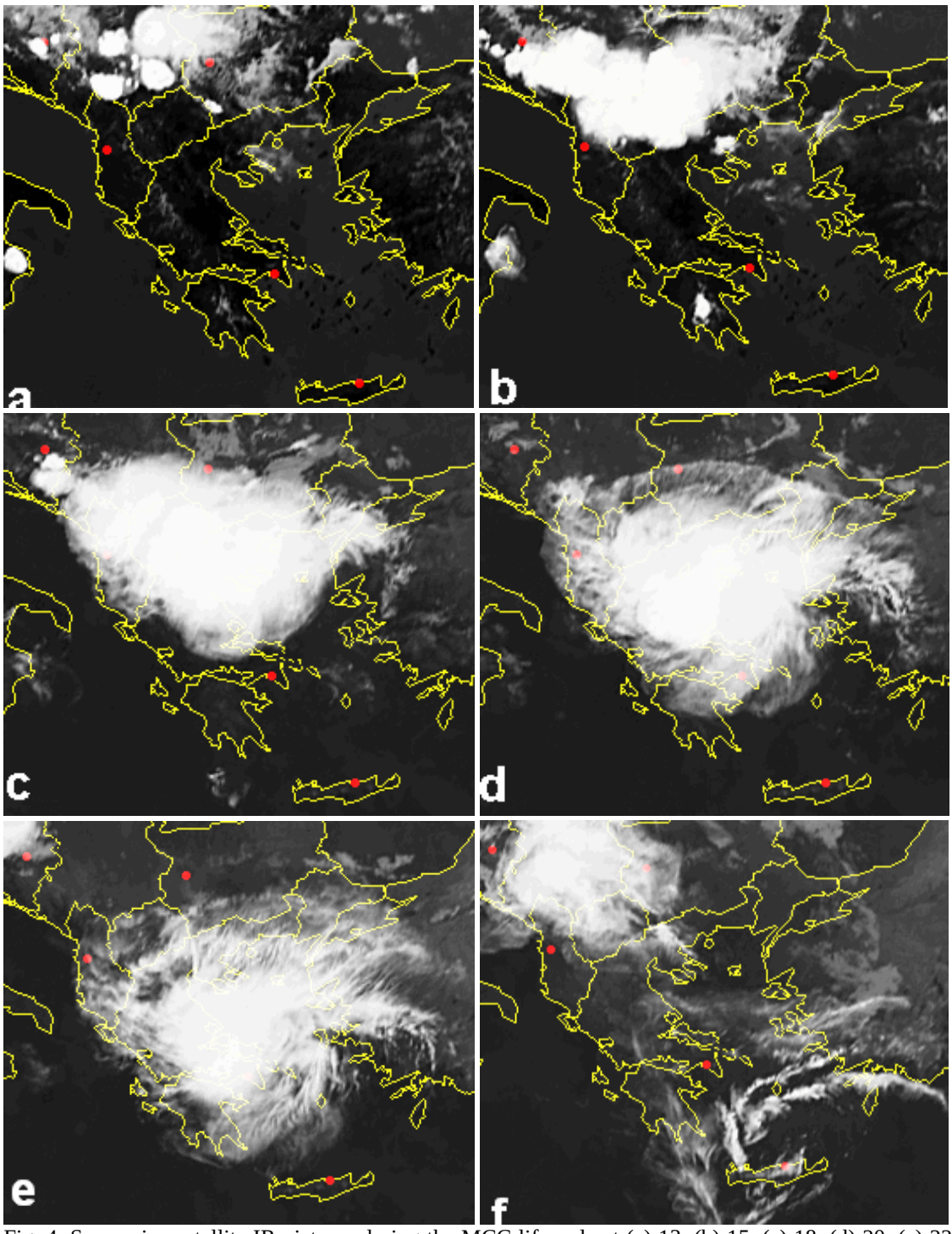

Fig. 4. Successive satellite IR pictures during the MCC lifecycle at (a) 13, (b) 15, (c) 18, (d) 20, (e) 22 UTC of 24-5-2009 and (f) of 04 UTC of 25-5-2009.

from meso-β thunderstorm elements merged. At 18 UTC the MCC reached maturity and its maximum extent (from Sarajevo to Athens), while at 20 UTC the dissipation stage started from the MCC outer cirriform boundary. Dissipation continued at 22 UTC inwards, with spiral bands becoming evident. At 04 UTC the MCV signature was the remnant of the system. At the same time, a new, weaker and smaller MCC appeared to follow the same path. This is not unusual, since MCCs may form in episodes on several consecutive days (Wetzel et al., 1983).

Lightning activity (Fig. 5) is exclusively related to convective cells. Each picture represents the total lightning that occurred within the previous hour. Thus, at 17 UTC, this indicates the alignment of leading thunderstorms along an arc-shaped line, with the convex toward the leading edge (Houze, 1993). At 19 UTC the maximum lightning activity took place, just after the MCC had reached maturity, in compliance with the time of transition from convective to stratiform precipitation (Goodman and MacGorman, 1986).

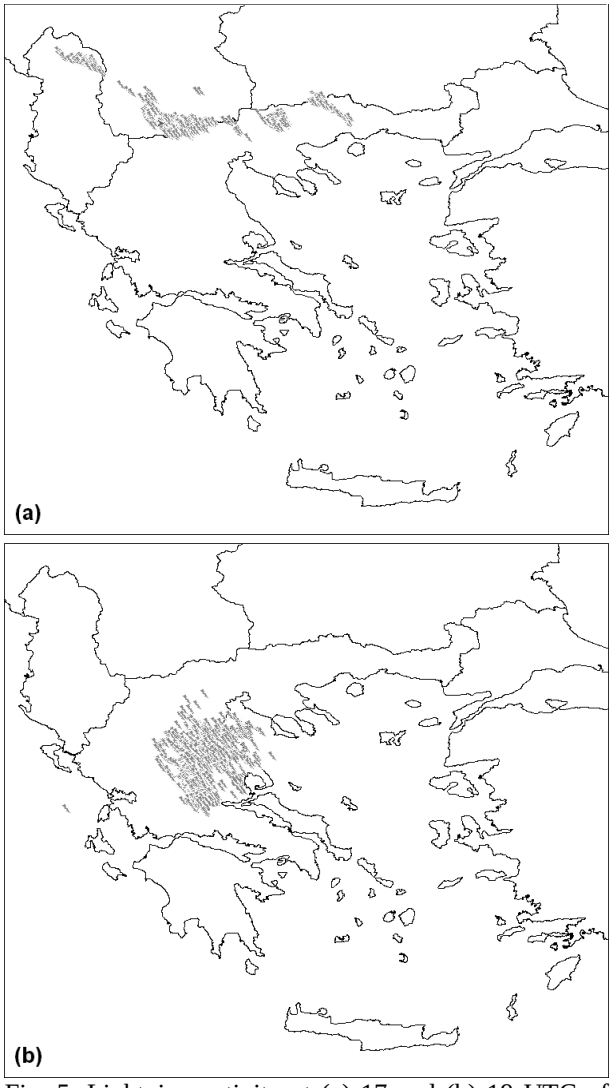

Fig. 5. Lightning activity at (a) 17 and (b) 19 UTC of 24-5-2009.

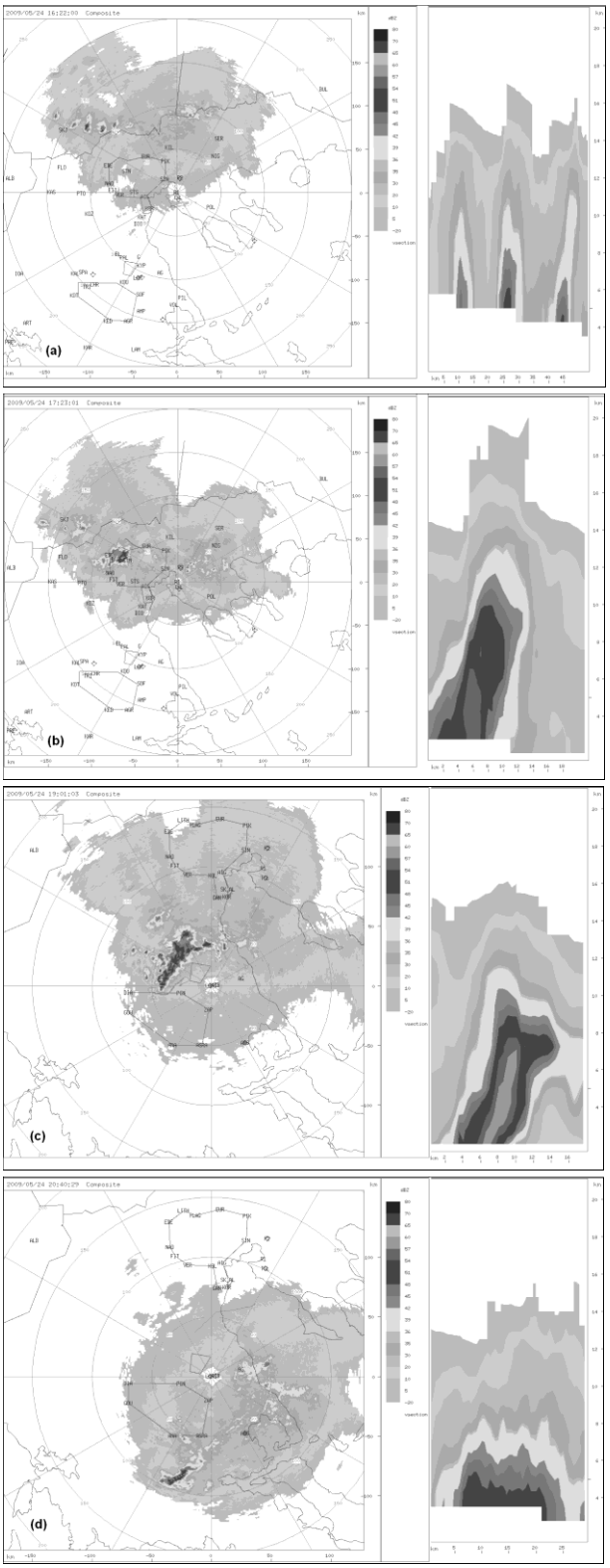

Fig. 6. Successive radar CAPPIs and cross-sections at (a) 16:22, (b) 17:23, (c) 19:01 and (d) 20:30 UTC of 24-5-2009.

Radar imagery (Fig. 6) reveals MCC features beneath the anvil shield. Two S-band radars located at Thessaloniki and Larissa were monitoring the track of the system with the aid of the radar recording system TITAN. At 16:22 UTC a west-to-east alignment of leading convective elements was recorded, with the decaying ones to the east and the newly formed ones to the west, in agreement with the warm inflow region. This is a typical pattern of the asymmetric development of convective elements on the leading edge (Houze, 1993). At 17:23 UTC a particular thunderstorm NW of Thessaloniki reached the maximum recorded height of 16 km (as seen in the relevant cross-section) and pea-size but quite dense hail was recorded on hailpads installed in this area. At 19:01 UTC, close to maturity, the pattern of convective cells changed to a NNE-SSW orientation, and the maximum reflectivity of 62 dBZ was then recorded. At 20:30 UTC the stratiform precipitation dominated, marked by moderate reflectivities (Cotton and Anthes, 1989) and the presence of bright band, typical of this precipitation type. All horizontal sections were taken at -5^{o}C and the echo was more or less circular with a diameter of 200 km.

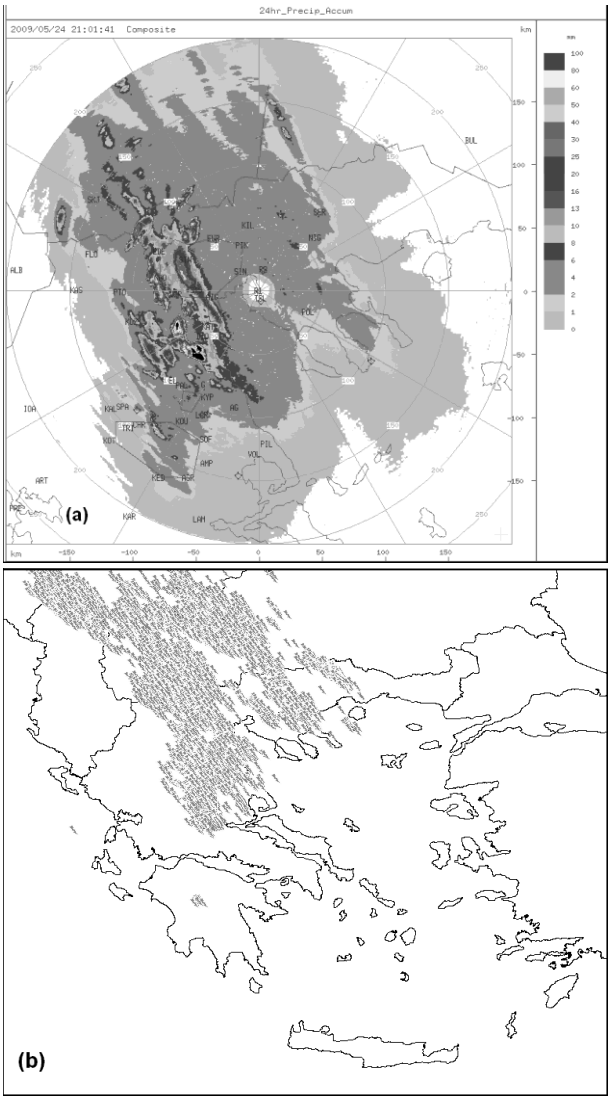

Fig. 7. Precipitation accumulation (a) and total lightning (b) during MCC lifecycle.

It has to be noted here that the convective elements of the system were seeded for almost 3 h close to maturity time (between 17 and 20 UTC), with three aircraft missions that delivered a total of 13270 g of seeding material (silver iodide being the seeding agent). Apparently, seeding had no or little effect. This is due to the violent turbulence the aircrafts encountered that prohibited their approach to the appropriate areas for effective seeding.

The accumulated precipitation over the MCC lifecycle (Fig. 7) shows a maximum of more than 100 mm near the place where maturity occurred. The precipitation pattern reveals the motion of the system and is in good accordance with the total lightning activity recorded (Fig. 7).

Moreover, radar data indicate a mean velocity of 49,2 km h^{-1} (maximum 59), a mean maximum reflectivity of 53 dBZ (maximum 62) and top height of 13 km (maximum 16) at maturity. Maximum vertically integrated liquid water (VIL) was 108.3 kg m^{-2} and hail mass aloft reached a maximum of 452 ktons.

7. Conclusions

Mesoscale convective complexes are important atmospheric phenomena. Due to their large size and long duration they are driven by a combination of interacting cumulus, mesoscale and larger scale dynamic and thermodynamic processes and affect their environment long after their decay.

Indeed, most of the features exhibited by the system of 24 May 2009 agree with what was predicted by the MCC conceptual model. It was orogenic in nature, acquired an oval shape with classical dimensions and produced heavy precipitation, hail and strong lightning activity. The initiation and maturity timing and the duration were also correct. There was evidence of the cold pool and mesohigh and the synoptic and thermodynamic environment was as expected. Finally, satellite and radar data revealed all the relevant features. All the above conclusions place the system of 24 May 2009 unquestionably in the typical MCC regime.

References

Bader M.J., Forbes G.S., Grant J.R., Lilley R.B.E. and Waters A.J., 1995. Images in Weather Forecasting. Cambridge University Press, 499p.

Cotton W.R. and Anthes R.A., 1989. Storm and Cloud Dynamics. Academic Press, Inc., 883p.

Cotton W.R., Lin M.S., McAnelly R.L. and Tremback C.J., 1989. A composite model of mesoscale convective complexes. Mon. Wea. Rev., 117, 765-783.

Djuric D.,1994. Weather Analysis. Prentice-Hall, Inc., 304p.

Fritsch J.M. and Brown J.M., 1982. On the generation of convectively-driven mesohighs aloft. Mon. Wea. Rev., 110, 1554-1563.

Goodman S.J. and MacGorman D.R., 1986. Cloud-to-ground lightning activity in mesoscale convective complexes. Mon. Wea. Rev., 114, 2320-2328.

Houze R.A.Jr., 1993. Cloud Dynamics. Academic Press, Inc., 573p.

Johnson R.H., Chen S. and Toth J.J., 1989. Circulations associated with midlatitude, mesoscale convective complexes. Mon. Wea. Rev., 117, 942-959.

Maddox R.A., 1980. Mesoscale convective complexes. Bull. Am. Meteorol. Soc., 61, 1374-1387.

Maddox R.A., 1983. Large-scale meteorological conditions associated with midlatitude, mesoscale convective complexes. Mon. Wea. Rev., 111, 1475-1493.

Wetzel P.J., Cotton W.R. and McAnelly R.L., 1983. A long-lived mesoscale convective complex. Part II: Evolution and structure of the mature complex. Mon. Wea. Rev., 111, 1919-1937.

Special Session S26
Measurements and modeling of biologically active UV solar radiation: towards balancing between risks and benefits

Scientific Annals, School of Geology, Aristotle University of Thessaloniki Proceedings of the XIX CBGA Congress, Thessaloniki, Greece	Special volume 100	437-443	Thessaloniki 2010

OVERVIEW OF THE UV ACTIVITIES IN BELGIUM SINCE THE END OF THE EIGHTIES

Gillotay D., Bolsée D., Depiesse C. and Stevens F.

Belgian Institute for Space Aeronomy, 3, Avenue Circulaire B-1180 Brussels BELGIUM, dgill@oma.be

Abstract An overview of the UV activities in Belgium is presented including the balloon borne, Space borne and ground based measurements (at 5 stations) of the global and direct Solar irradiance. Main results in terms of biologically active UV are discussed in relationship with the main factors of influence as Ozone, Clouds and Aerosols. Positive UV effective doses trend (+0.6 % /Year) is discussed in correlation with the ozone negative trend (-0.2 % /year) and more favorable meteorological conditions. Finally, some information are on the future activities namely, the UV indices predictions in real conditions.

1. Introduction

Since more than thirty years, the Belgian Institute for Space Aeronomy (BISA) is interested in the interaction between Solar radiations and the atmosphere with as main goal, a better understanding and modeling of the atmospheric physics and chemistry.

2. Balloon borne od Space borne activities.

During the seventies, a series of stratospheric balloon-borne campaigns where performed to measure the "extraterrestrial" solar spectrum and its variations in the UV range as a function of the main solar cycle. (Simon et al., 1981). The error on the estimation of the residual absorption due to the remaining atmosphere (above 40 km) was a major obstacle to very high precision spectra. Nevertheless stratospheric balloon flights provide a relatively cheap tool to access quasi-extraterrestrial solar irradiances and concentration profile of minor constituents (measured during the ascending or descending phase of the flight).

At the end of the seventies, BISA designed, in collaboration with the Service d'Aéronomie, CNRS (France) and the observatories of Heidelberg and Hannover (Germany) an instrument called SOLSPEC (Solar Spectrum) for the first international space mission SPACELAB 1. It consisted in three double spectro-radiometers (UV, Visible and IR) mounted on a single scanning mechanism, equipped with internal calibration lamps for absolute intensity scale and wavelength scale verifications. The successive versions of this instrument took part to four short (~10 days) space flights (Spacelab 1 in 1983, Atlas 1, 2 and 3 during the 1992-1994 period) and a mission of eighteen months onboard of Eureca 1 in 1993-1994. A third generation of SOLSPEC is presently, since February 2007, on the ISS as major part of the SOLAR payload.

More detailed information will be founded in Thuillier et al., 1992; 1996; 1997; 1998; 1999; 2009. Figure 1 illustrates the solar spectrum measured by SOLSPEC during the Atlas 1 and ISS missions.

3. Ground based activities

At the end of the eighties, satellite measurements confirmed the depletion of stratospheric ozone, which educe the efficiency of this natural UVB filter.

In order to verify the potential increase of UVB at the ground level, to study the penetration mechanisms in the atmosphere and to establish a reliable UVB climatology, the BISA Solar Radiation Group has developed, in the framework of European programmes, ground based UVB monitoring stations.

The penetration of solar UV radiation through the atmosphere depends on the solar zenithal angle (SZA), the ozone overhead column and other at-

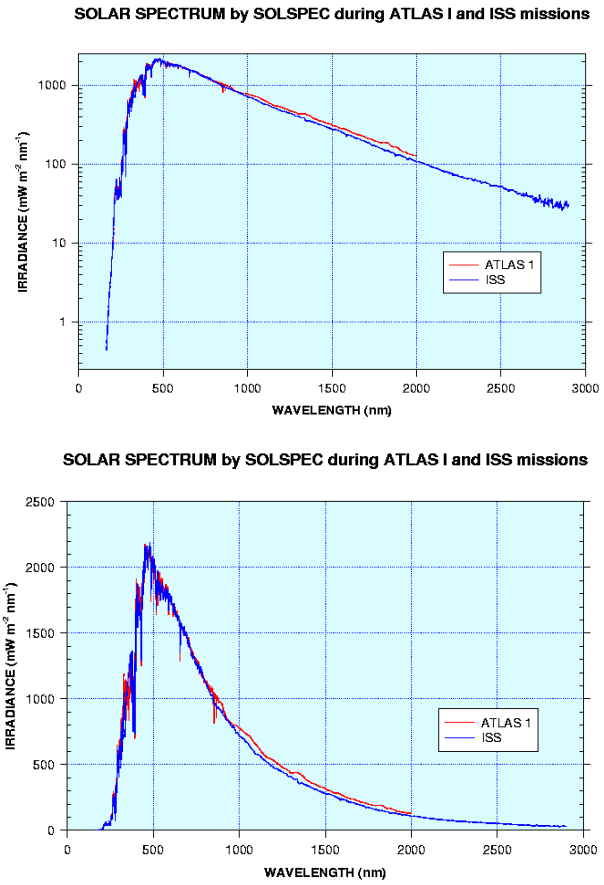

Fig. 1. Extra-terrestrial Solar Spectrum measured by SOLSPEC during the Atlas 1 and ISS missions.

mospheric absorbers and scatters such as clouds and aerosols. In particular, clouds are responsible for a great deal of the observed irradiance variability. The interpretation of observed UV-B time series, and e.g. the detection of possible trends due to human activity, requires the correct understanding of the effects of these different 'factors of influence' and a detailed study of their evolution with time. The instrumentation is described in the next section. The Royal Meteorological Institute (KMI/IRM) using a Dobson and a Brewer spectroradiometer, (De Muer and De Backer, 1992), measures total ozone at Uccle. Ozone, temperature and relative humidity profiles are obtained by balloon soundings, also provided by KMI/IRM. The cloud fraction and type as well as the ground meteorological parameters (pressure, temperature, horizontal visibility, pluviometry,…) are monitored routinely at the station sites. Since 2000, clouds are directly monitored by two different instruments: the Total Sky Imager (TSI, from YES) providing clouds cover fraction by analysis of visible CCD camera pictures, and the CIR13 and CIR4 (Atmos-Fr /IASB-BIRA – Be) measuring by thermal infrared radiometry the temperature of the sky dome (IR – 8-14 µm) providing cloud cover fraction and ceiling altitude.

UV measurements in Uccle (Brussels) Belgium are available since April 1989 by combining the BISA measurements and data from KMI/IRM. The major results are presented and discussed in terms of correlation between the UV-B irradiance and the main atmospheric parameters like Ozone, Clouds cover, Aerosols, … Potential trends are also presented and discussed.

4. Experimental

4.1. Ground based monitoring stations

The BISA automated stations are located at Uccle, a residential area in the Brussels suburbs (lat.: 50°48'N, long: 4°21'E, Alt.: 105m), at Redu-Transinnes, in an agricultural area (lat.: 50°00'N, long: 5°09 'E, Alt.: 450m), at Ostende, close to the North Sea, (lat.: 51°14'N, long: 2°56'E, Alt.: 0m), at Virton in a small city area, (lat.: 49°34'N, long: 5°32 'E, Alt.: 250m) and at Mol, in a forest environment (lat.: 51°13'N, long: 5°05 'E, Alt.: 75m)

They are respectively operational since mid-March 1993 (Uccle), mid-June 2004 (Redu), April 2006 (Ostende), December 2007 (Virton) and December 2008 (Mol). The location of the 5 stations are mapped on in figure 2.

Uccle is the main station equipped with a large variety of equipment:

The core instruments of the main station are two double monochromator (modified HD10, Jobin-Yvon and Bentham DTM300). It includes also four filter radiometers (SPUV-10, UVMFR-7 and MFR7 from Yankee Environmental System, (YES), GUV 511C from Biospherical Instruments) and four pyranometers (YES), two in the UV-B range (UVB-1), one in the UV-A (UVA-1) and the last covering the wavelength range from the UV-A up to the near IR (TSP-700). In addition to these radiometric captors, 2 types for instrument to measure clouds (TSI and CIR) are also deployed as well as a meteorological station (RM Young) to measure the basic environmental parameters.

The two spectro-radiometers (HD10 modified and Bentham), with their optical axis pointing the zenith direction, are fitted with a Lambertian Teflon diffuser (2 p sr field of view) measures the total solar irradiance (diffuse + direct), with a nearly perfect cosine response. One scan, in perfect simultaneity is performed with each spectro-radiometer every 15 minutes for SZA smaller than 100°.

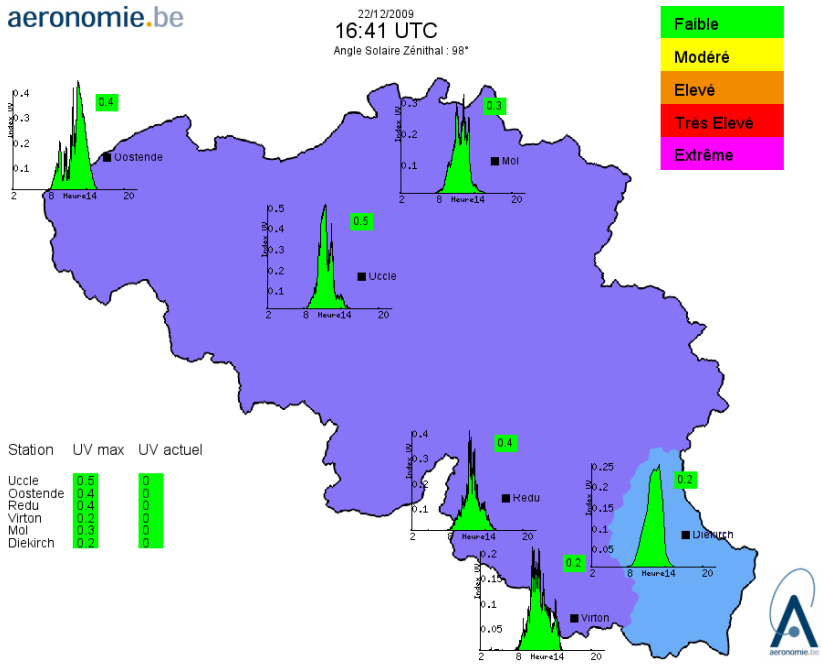

Fig. 2. Map localizing the 6 stations of the Belgium-Luxemburg network.

The 10-channels filter radiometer (SPUV-10, YES) measures the direct solar irradiance from 300 nm to 1040 nm. It is mounted on a sun tracking system. This radiometer is designed to provide direct solar irradiance measurements from which the ozone total column and the atmospheric turbidity (the optical depth of aerosols in clear sky conditions) can be deduced.

GUV 2511, MFR7 and UVMFR-7 are respectively 6, 7 and 7 channels 2 p sr filter radiometers. The MFR-7 and UVMFR-7 equipped with a shadowing band are designed to perform direct and diffuse quasi-simultaneous measurements of the solar irradiance, from which complementary information on ozone and aerosols can be deduced. The pyranometers cover the full range of the solar spectra scanned by the monochromators. It permits a direct measurement of integrated doses with a much higher time sampling (1 mean integrated measurement every minute). One of the UV-B meters is shadowed in order to measure the diffuse component of the solar irradiance.

Finally, KMI/IRM perform UV-B measurements with a Brewer (Mk II) single mono-chromator from 280 to 325 nm, initially at noon (from April 1989 to December 1990) and on an hourly base (January 1991 – today). A schematic view of the IASB station is shown in figure 3.

The four other stations are equipped with GUV 2511, 6 channels filter radiometers, a set of three pyranometers (UVB, UVA and TSP), a meteo station, and a CIR to measure cloud cover and ceiling.

4.2. Calibration and quality control of the data

Periodical absolute calibration is performed in a dark room using five different NIST-FEL 1000W standard lamps. Furthermore, stability is periodically checked by means of a Transportable Lamp System (TLS) developed specifically in our laboratory. It consists of five 200 W quartz-halogen lamps and a Mercury low-pressure source, mounted on a carrousel inside a movable container. In the field, the different lamps are successively placed and automatically aligned with the entrance optics of the instruments. With both 'standards' the uncertainties can be estimated to be less than ±5% over all the wavelength range. This estimation was confirmed during the previous European Inter-comparison Campaign (Gardiner et al., 1993). Moreover, the coherency of the data set is verified by comparing the filter radiometer and broadband measurements with the corresponding convoluted spectral measurements.

4.3. Time series of measurements

Erythemal doses at noon at the 5 stations are evaluated from both sets of broadband and narrowband measurements in addition to the spectral UV-Visible measurements weighted by the CIE action spectrum. (McKinlay and Diffey, 1987). The KMI/IRM data set is corrected to take into account the lack of spectral measurements between 325 and 400 nm. The comparison of the different

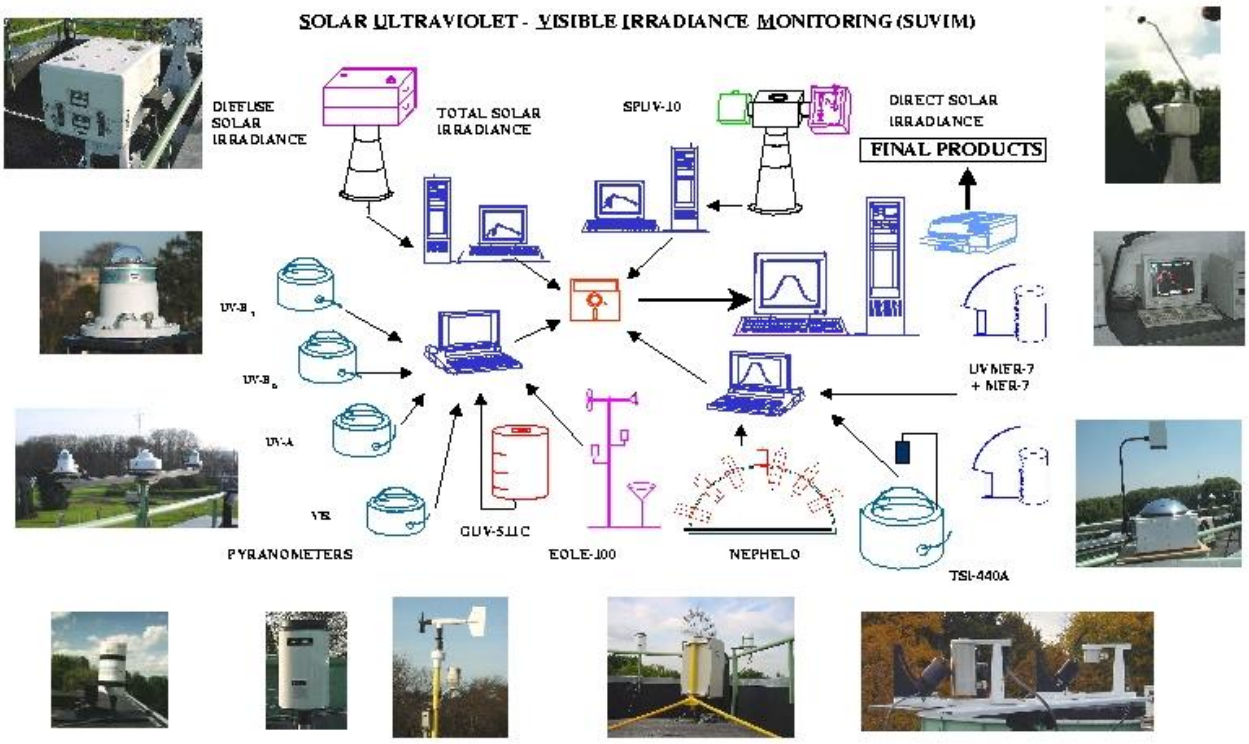

Fig. 3. Schematic view of the Uccle UV station.

spectral data sets gives a good agreement (within 5%) for most of the cases over the overlap period (1993-2001). Nevertheless, in some occasions, the discrepancy can reach 20-25%. This is probably due to 1) the unperfected synchronism between the measurements and 2) the correction of the Brewer measurements which does not take into account the modification of the cloud cover during one scan duration. Comparison of erythemal doses obtained from integrated measurements and spectral measurements gives the same agreement of around 5 %. Figure 4 illustrates the available time series and shows their seasonal variation. The peak values are achieved in June, corresponding to the smallest SZA of the year and relatively low ozone columns. The scatter within the seasonal fluctuation can be ascribed to changes in cloud coverage, see for example Gillotay,(1996) and Gillotay et al., (2001) and variations of aerosols type and optical depth.

5. Factors of influence

The two most important factors limiting the penetration and explaining the day-to-day variations of the UV-B radiation to the Earth's surface are the ozone and the cloud coverage ans aerosols. These three 'factors of influence' will be detailed in the next sections.

5.1. Ozone

Figure 5 illustrates the anti-correlation between ozone total column and UV-B integrated irradiance corrected for the effect of cloud cover. The applied correction is relatively simple: it consists in the ratio UV-B/UV-A that takes into account, as a first approximation, the effect of clouds as a neutral filter, combined with a corrective factor to describe the non-neutral effect of clouds in the shorter wavelengths of the spectrum.

A discrete ordinates radiative model (Stamnes et al., 1988) has been used to simulate the experimental data and to verify the anti-correlation function between ozone and UV-B.

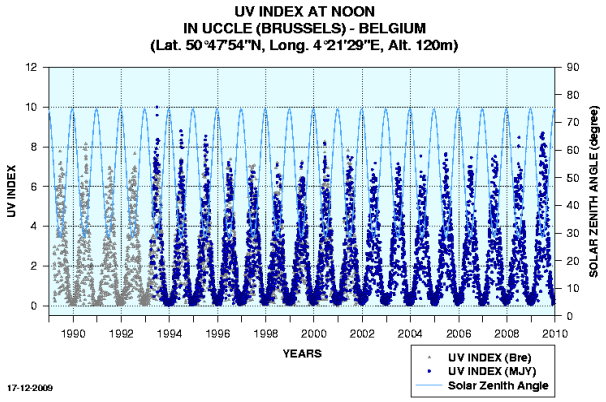

Fig. 4. Time series of the erythemal doses at Uccle.

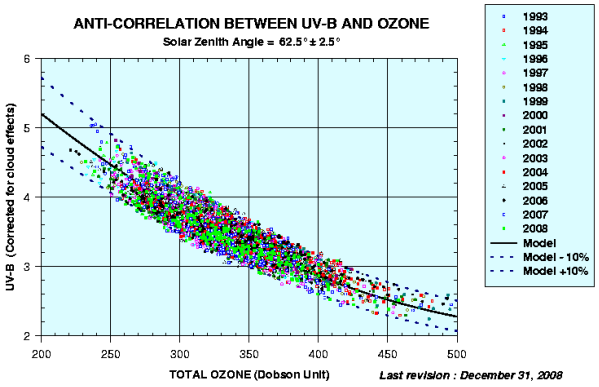

Fig. 5. Anti-correlation between ozone and UV-B.

The extraterrestrial flux is a combination of the SUSIM spectrum below 350 nm (Van Hoosier et al., 1984) and the Neckel and Labs spectrum (Neckel and Labs, 1984) up to 600 nm. The wavelength dependence of the aerosol optical properties follows the parameterization of WCP (WCP, 1986) for typical continental mixtures. This choice is motivated by air pollution lower in Uccle than in typical urban centers. The weak dependence of cloud extinction and asymmetry factor is parameterized following the procedure developed by Slingo (1989).

A good agreement (better than 5%) between experimental data and the simulation has been established for SZA between 30° and 70° in clear sky condition. The discrepancies between modeled and experimental data increase generally with the SZA and might exceed 10% at high SZA in the visible range. Figure 5 shows clearly that (i) the anti-correlation factor observed experimentally is well reproduced by modeling and (ii) practically all the experimental conditions are included within a ± 10% limit vs the predicted values. This 10 % variation can easily be explained by considering the error in the ozone measurements (2-5%), the unsophisticated correction of the cloud layer effects (5 %) and error licked to aerosols type and optical depth (2-5%).

5.2. Clouds

In order to investigate the role of clouds as a function of wavelength, average spectra for well-defined conditions (complete overcast, similar zenith angles) have been derived from the

observations, and compared with a corresponding clear sky spectrum. The average cloud transmission ratios for SZA=30 ° are displayed in figure 6, and compared to a modeled transmission ratio. A 1-km low cloud with an optical depth equal to 5.0 has been assumed. Despite the large variability of the cloud impact, a consistent picture is found. The attenuation is lowest in the UV-A, and highest in the ozone absorption bands (UV-B) because of the increased multiple scattering and tropospheric ozone absorption caused by cloud. The attenuation increases into a lesser extent in the visible range, reflecting the lesser importance of Rayleigh diffusion at higher wavelengths.

Finally, the average attenuation of sunlight by different type of clouds can be also directly estimate from the pyranometers data. As expected, the attenuation by cirrus clouds (high altitude) is found to be very small. In contrast, low clouds (mainly stratocumulus) reduce solar irradiance by about a factor 5 on average. A more detailed study on this topic are given in Gillotay et al, (2002). This attenuation is found to increase monotonously with the Solar zenith angle in the UV-A and UV-B ranges, but not for the total integrated irradiances (300-3000 nm). These last results have to be examined in the more detailed future modeling studies.

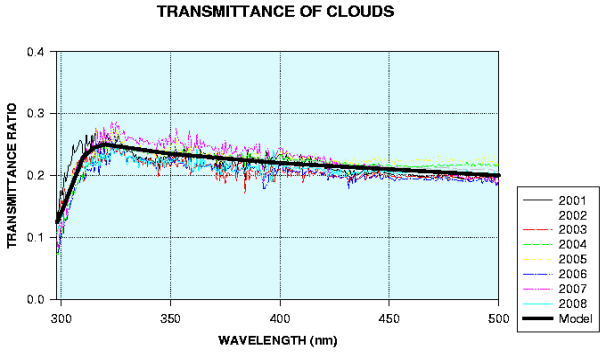

Fig. 6. Ratio of fully cloudy (8 Octas) to clear sky irradiance.

5.3. Aerosols

Aerosols have also a significant role in the attenuation of the UV flux at the Earth surface.

In Belgium, in general, and more particularly in Brussels, we observe usually a mixture of continental and maritime aerosols, with optical depth (at 500 nm) ranging from 0.05 to 0.3 as shown by the "Cimel" measurements performed at the Institute (Herman C., 2010), available on aeronet. In some specific cases we observe (i) continental aerosols during stable eastern wind conditions, (ii) maritime aerosols during stable western wind conditions and (iii) urban aerosols during high urban pollution episodes, usually accompanied by high tropospheric ozone concentrations.

Table 1 summarized the aerosols effect on the penetration of biologically active UV radiations (UV index). As we could expect, effect of aerosols is more pronounced for high solar zenith angle; due to the longer optical path in the atmosphere. It is also evident from Table 1 that "Urban" aerosols type has a most lager impact than the other types, probably due to the presence of small particles and specific absorber like ozone and peroxides.

Table 1. Effect of Aerosols on the UV index for various aerosols types and optical depths at two Solar Zenith Angle conditions.

SZA & Ozone	25°	306 DU			70°	306 DU		
Optical depth	0	0.1	0.2	0.3	0	0.1	0.2	0.3
Maritime	8.50	8.25	8.07	7.91	0.79	0.70	0.67	0.66
Relative	*1.00*	*0.97*	*0.95*	*0.93*	*1.00*	*0.89*	*0.85*	*0.83*
Continental	8.50	8.16	7.87	7.62	0.79	0.69	0.65	0.63
Relative	*1.00*	*0.96*	*0.92*	*0.90*	*1.00*	*0.87*	*0.82*	*0.80*
Mixture	8.50	8.20	8.00	7.77	0.79	0.70	0.66	0.64
Relative	*1.00*	*0.97*	*0.94*	*0.91*	*1.00*	*0.88*	*0.84*	*0.81*
Urban	8.50	7.75	7.08	6.47	0.79	0.64	0.57	0.52
Relative	*1.00*	*0.91*	*0.83*	*0.76*	*1.00*	*0.81*	*0.72*	*0.66*

6. Trends

The bring to light of potential trends of UV-B radiation at the Earth's surface due to human activity is of high interest for the public health medical community as well as for all the scientists interested in the effects of UV-B on biology and material sciences.

The aim of this section is just to illustrate what can be deduced from a 14-years period of UV-B monitoring. Figure 7 illustrates the high variability of UV-B effective doses on a monthly base mainly due to the variability of meteorological conditions.

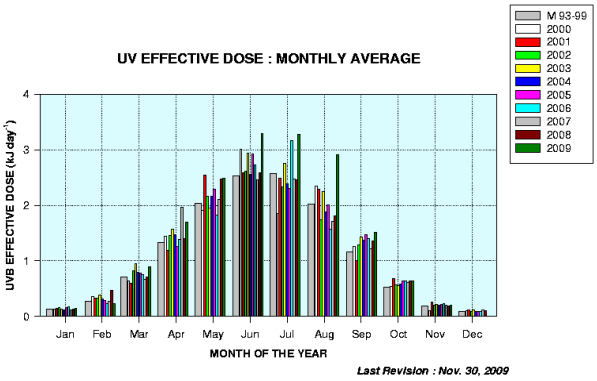

Fig. 7. UV-B effective monthly averaged doses in Uccle (Brussels) Belgium.

Figures 8 and 9 give an idea of the potential trends of UV-B and ozone in Brussels. UV-B trends show an increase of 0.6 % per year that looks coherent with the ozone trends of 0.2 %.

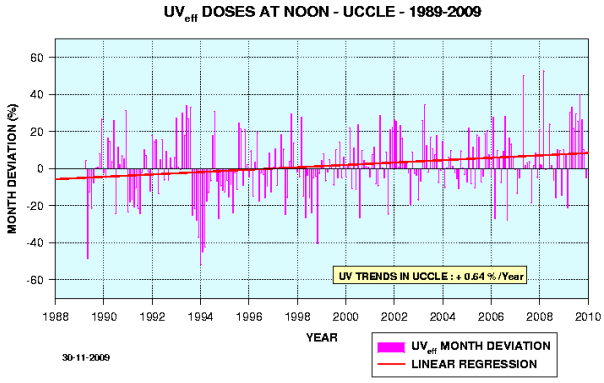

Fig. 8. UV-B trends in Brussels 1989-2002.

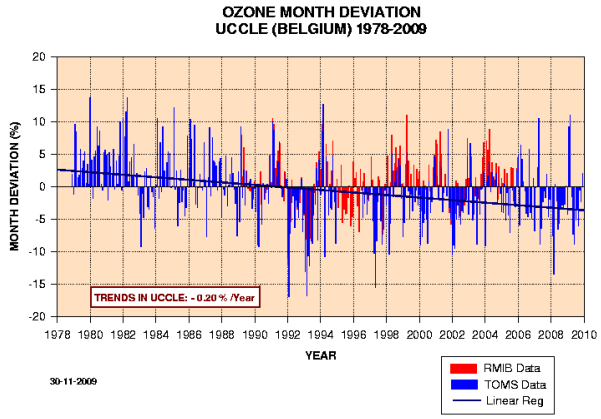

Fig. 9. Ozone trends in Brussels (1978-2002) by combining TOMS/OMI and KMI/IRM data.

Part of the UV positive trend can be ascribed to more frequent long sunny periods observed in Brussels since 2-3 years. (See for example the periods Jun → Aug 2009, Feb 2008, Apr 2007 and Jul 2006 on figure 7)

7. Future activities

The measurement of erythemal doses and the diffusion to the community of information on measured UV indices is probably very interesting, but the main expected information is an accurate predictive value of these indices at 24, 48 or 72 hours, taking into account the most reliable meteorological predictions, correct ozone values and the climatologic particularities of the different area of a country.

That is the goal of the BISA Solar radiation team for the next years: to provide UV indices prediction in real conditions.

This activity will be carried out, in collaboration

with our colleagues from Luxemburg. Different tools are already tested and the first results are promising.

8. Conclusion

These results, presented above, show the consistency of both our model and experimental data. They provide a first understanding of the UV-B climatology in Belgium that could be extrapolated to the 50°-latitude area. An extended period of measurements is necessary to improve the preliminary trends given above. Nevertheless the increase of UV-B radiation seems to be real and needs to be explored in more details.

Acknowledgments

The authors are very grateful European Union for their financial supports in the framework of European UV programs (e.g. SUVDAMA & EDUCE) and to Dr H. De Backer for providing ozone and UVB data.

References

De Muer, D., and H. De Backer, 1992, Revision of 20 years of Dobson total ozone data at Uccle(Belgium): Fictitious Dobson total ozone trends induced by sulfur dioxide trends, J. Geophys.Res., 97, 5921-5937.

Gardiner B.G., Webb A.R., Bais A. F., Blumthaler M., Dirmhirn I., Forster P., Gillotay D., Henriksen K., Huber M., Kirsch P.J., Simon P.C., Svenoe T., Weihs P. and Zerefos C.S., 1993, European Intercomparison of ultraviolet spectroradiometers, Environ. Technol., 14, 25-43.

Gillotay D., 1996, UV monitoring in Belgium: Past, present and future. in Measurements and Trends of Terrestrial UVB Radiation in Europe, (Ed. B. L. Diffey), pp. 41-53.

Gillotay D., D. Bolsée, 2001, The UV climatology in Belgium from UV Field monitoring, , in IRS'2000: "Current Problems in Atmospheric Radiation", Eds W.L. Smith & Y.M. Timofeyev, St. Petersburg, Russia, 24-29 July, 2000, pp 1162-1165, A Deepak Publishing,.

Gillotay D., T. Besnard and Y. Labaye, 2002, Impact of cloud spatial distribution on solar UV radiation transfer., in proceedings of 11th conference on Cloud Physics, Ogden, UT, USA, 3-7 June.

Herman C., 2010, private communication

Neckel, H., and D. Labs, 1984, The Solar Radiation Between 3300 and 12500 A, Solar Physics, 90, 205-258.

McKinlay, A.F; and B.L. Diffey 1987, A reference action spectrum for Ultraviolet induced erythema in human skin. CIE J. 6 p; 17-22

Simon, P.C., R. Pastiels, D. Nevejans and D. Gillotay, 1981, Balloon observation of solar ultraviolet irradiance during solar cycle 21., in Proceedings of the symposium on Solar Constant and Spectral Distribution of Solar Irradiance, eds J. London and C. Fröhlich, IAMAP Third Scientific Assembly, Hamburg (FRG), August 1981, 95-102,

Slingo A.S., 1989, A GCM parametrization for the shortave radiative properties of water clouds, J. Atmos. Sci., 46, 1419-1427.

Stamnes, K., S. C. Tsay, W. J. Wiscombe, and K. Jayaweera, 1988, Numerically stable algorithm for discrete-ordinate-method radiative transfer in multiple scattering and emitting layered media, Appl. Opt., 27, 2502-2509.

Thiullier G., M. Herse, P.C. Simon, D. Gillotay and W. Peetermans, 1992 , Solar spectral irradiance measurements between 180 and 3200 nm by the SOLSPEC/ATLAS I instruments. Extended abstract in the "American Geophysical Union, 1992 Fall meeting", pp 427, (published as a supplement of EOS, October 27, 1992)

Thuillier G., M. Herse, P.C. Simon, D.Labs, H. Mandel and D. Gillotay, 1996, Observation of the Visible solar spectral irradiance from 350 to 850 nm during the ATLAS 1 mission by the SOLSPEC spectrometer., accepted at the "17th International Workshop, National Solar Observatory/Sacramento Peak, Sunspot New-Mexico, USA, June 17-21.

Thullier G., M. Herse, P.C. Simon, D.Labs, H. Mandel and D. Gillotay, 1997, Observation of the UV solar spectral irradiance between 200 and 360 nm during the ATLAS 1 mission by the SOLSPEC spectrometer. Solar Phys., 171, 283-302.

Thullier G., M. Herse, P.C. Simon, D.Labs, H. Mandel D. Gillotay and T. Foujols, 1998, The visible solar spectral irradiance from 350 to 850 nm as measured by the SOLSPEC spectrometer during the ATLAS I mission. , Solar Phys., 177, 41-61.

Thullier G., M. Herse, P.C. Simon, D.Labs, H. Mandel D. Gillotay, W. Peetermans and T. Foujols, 1999, The SOLSPEC Experiment: Recent Results and Future Investigations on Board the International Space Station Alpha. in Space Technology and Applications International Forum- 1999, (Eds. M. S; El-Genk), pp 211-216.

Thuillier G., T. Foujols, D. Bolsée, D. Gillotay, M. Hersé, W. Peetermans, W. Decuyper, H. Mandel, P. Sperfeld, S. Pape, D. R. Taubert and J. Hartmann, 2009, SOLAR/SOLSPEC: Scientific Objectives, Instrument Performance and Its Absolute Calibration Using a Blackbody as Primary Standard Source, Solar Physics, 257-1, 185-213.

Van Hoosier, M., J.D. Bartoe, G. Brueckner, and D. Prinz, 1988, Absolute solar spectral irradiance 120 nm-400 nm (Results from the Solar Ultraviolet Spectral Irradiance Monitor-SUSIM Experiment on board Spacelab 2), Astro. Lett. and Communications, 27, 163-168.

World Climate Programme (WCP), 1986, A preliminary cloudless standard atmosphere for radiation computation, WMO Report WMO/TD No. 24, World Meteorological Organisation.

Special Session S28
Geotourism

Scientific Annals, School of Geology, Aristotle University of Thessaloniki Proceedings of the XIX CBGA Congress, Thessaloniki, Greece	Special volume 100	445-452	Thessaloniki 2010

THE GEOTOURIST DEVELOPMENT ON THE EXAMPLE OF THE AREA OF JASIENIOWA MT. (WESTERN CARPATHIANS FLYSCH, POLAND)

Dmytrowski P. and Górna M.

Department of General Geology, Environment Protection and Geotourism, AGH University of Science and Technology, al. Mickiewicza 30, 30-059 Krakow, Poland, pdmytrowski@geol.agh.edu.pl, mgorna@geol.agh.edu.pl

Abstract: The interpretation of geo(morfo)logical phenomena and processes as well as the transmission of geoscientific knowledge to the general public are the essential tasks of geotourism. The proper development of the geotourist sites is a tool for their accomplishment. This paper presents the model of geotourist development which consists of planning and creation of infrastructure (basic and supporting) and the promotion of sites. The basic infrastructure includes the interpretative materials, geotourist trails as well as technical facilities ensuring the safety and comfort of sightseeing. The elements of proposed model are shown on the example of the area of Jasieniowa Mt. (Cieszyn Foothills). The outcrops located in the selected region represent the oldest sedimentary rocks in the Polish Carpathians Flysch, which are the Vendryne Formation and the Cieszyn Limestone Formation. Within the scope of geotourist development, the geotourist trail and information panels were designed, as well as the location of the protective and supporting facilities was proposed.

Keywords: geotourist development, interpretation, Cieszyn Foothills.

1. Introduction

For many tourists, the abiotic nature is not as valuable and worth attention as living animals or plants. Therefore, the issue of presentation and promotion of "rocky" sites is such an important task. The transmission of information linked with Earth's history and emphasizing the significance of the geological environment are the essential roles of new branch of tourism called geotourism (Hose 2000; Słomka and Kicińska-Świderska, 2004). The actions for proper adaptation of sites for geotourism are defined as the geotourist development. It is a part of a much broader concept which is the tourist management (see Rogalewski, 1974 for definition). The aim of this article is to propose a pattern and to characterize the individual elements of the geotourist development and then to present them on the example of Jasieniowa Mt. area. The outcrops located there are of great importance for preservation geodiversity in supra-regional scale, as well as they are distinguished by geotourist (Waśkowska-Oliwa et al., 2008) and educational potential (Górna, 2009). At the moment, they are not adapted to geotourism's aims.

2. Methodology

The main goal of the geotourist development is creation of appropriate infrastructure that ensures the protection and proper operation of the sites, to satisfy tourists' needs, especially in the field of geoeducation, and also sites publicity. The formation of new geotourist attractions (tourist products), as well as the encouraging people to visit them should be a result of these actions. The proposed model of geotourist development assumes the planning and creation of infrastructure and the promotion of sites (Fig. 1).

However, before the geotourist development enters into the planning stage, the inventory and valorization of sites should be carried out. The inventory includes an accurate description of sites or phenomena in terms of geology, geography and tourism. The result of valorization shows the educational usefulness of sites and their geotourist attractiveness (Alexandrowicz et al., 1992; Dmytrowski and Kicińska, 2009).

With the detailed characteristics of the selected sites, we can move forward to the planning stage. It is worth emphasizing that the scheme of geotourist development should be consistent with legal regulation and consulted with the organs of the self-government administration. The estimate of the future tourist movement and its impact on the

both biotic and abiotic nature is an important element of planning. The visits of tourists and recreationalists in the geological environment and the existence of infrastructure can result in increase of erosion, degradation of sites (friable rocks) and vegetation, acts of vandalism, littering or noise. The role of planning and the future management is to reduce the adverse impacts (Newsome and Dowling, 2006). Moreover, this assessment is helpful during selecting the appropriate infrastructure and also it may become the determinant of the profitability of investment (in the case of entrance fee).

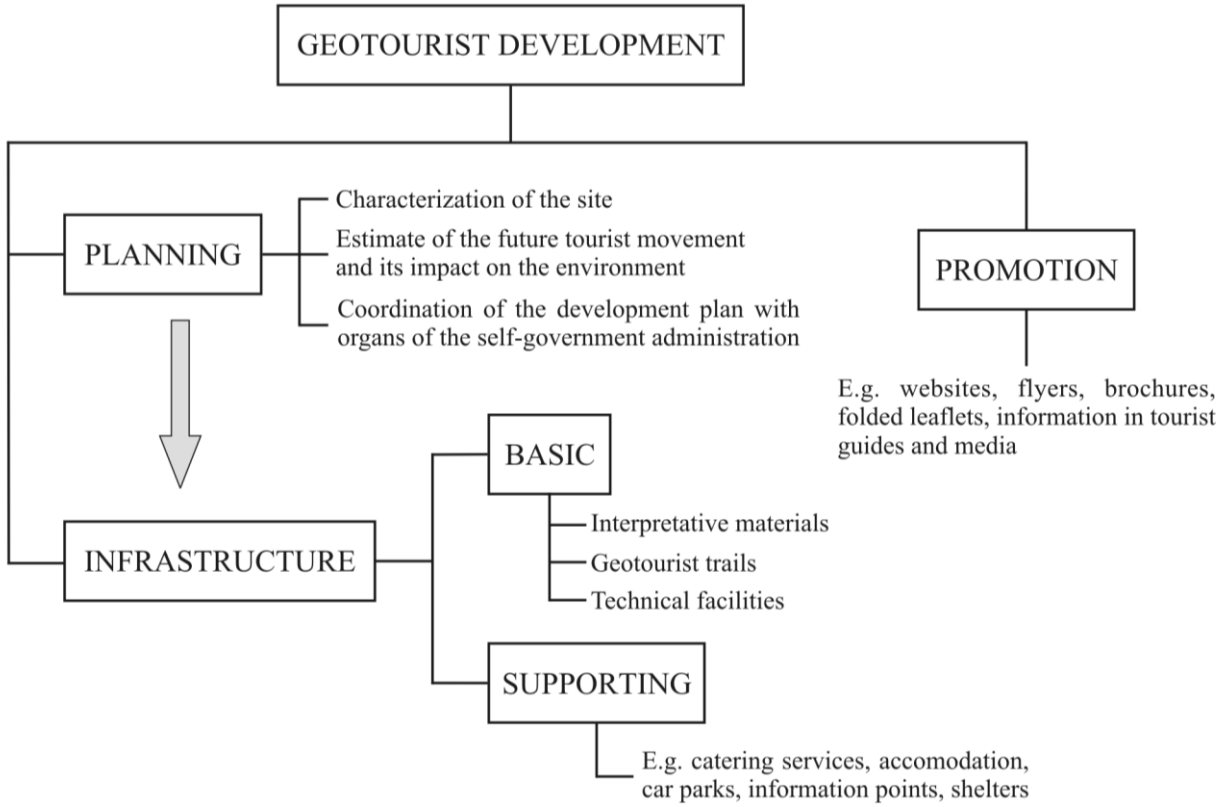

Fig. 1. The model of geotourist development.

Every geotourist site has a different nature, but almost everyone (if the result of valorization proves it) is suitable for geotourist development. The fundamental component of this development is infrastructure (understood as the elements of permanent nature) which consists of basic and supporting infrastructure. The first includes interpretative materials, geotourist trails and technical facilities aiding sightseeing.

Interpretative materials are essential at any geotourist sites. Their overriding function is interpretation, but they are also used for providing "facts" to the public. The outdoor panels, interactive touch panels, models, computer animations or displays can be rated among the group of the most common interpretative materials. Some of these components are useful for tourists on-site, other can be available only off-site, for example in information centers. It is important to note that others forms of interpretative materials, which have not permanent nature, are also popular and useful. In this case, guidebooks (rather for specialists), packet-sized booklets or site leaflets, videos or slide shows should be considered as the most crucial. The on-site outdoor panel is the most often used form of interpretative materials so it is worth to devote more attention to it. This form is particularly intended for a wide range of non-specialists recipients. The authors' research suggests that usually the information on panels is too scholarly, complex, unclear and visually unattractive to visitors. The ideal interpretative panel should be characterized by being graphic-rich and text-poor. The text should be written in a way that can be easily read and understood. Graphics should add explanations, show details which could be otherwise overlooked, and not repeat what tourists can see themselves. Applied colouring should harmonise with surroundings and simultaneously attracts tourist's attention. Materials as well as construction should be

consistent with local architecture. It is also essential to pay attention to panel location. Panels should be accessible and placed at suitable distance from sites. More details with regard to the rules of designing and location of panels are provided by Hose (2000). It is worth noticing that the text should be written in the language of the country of site's location, as well as in language known by the majority of foreigners, usually in English. Multilingual descriptions are particularly important if the sites are located in borderland. Then, the good practice is to use the language of the neighbours.

The geotourist trails are other elements of the basic infrastructure. Predominantly, it is a walking trail among several geotourist sites. The descriptions of them are available in the form of booklets or on-site panels. This trail has to be marked and has adequate protection and facilities for visitors. Furthermore, the kind of trail, issues, time of covering the distance, degree of difficulty and equipment requirements must be specified. It should also be possible to hire the geotourist guide, and in justified cases, sightseeing with guide should be obligatory (for example in mines or caves) (Kicińska-Świderska and Słomka, 2004).

The technical facilities are designed both for ensuring the safety and comfort during sightseeing and protection of site. Adequate preservation of ground, for the sake of tourist's safety, applies primarily to the mines, tunnels, caves, quarries, phenomena and processes occurring today (for example volcanic activity) etc. While the protection of sites, by imposing restrictions to tourists' motion, is of particular importance in case of places legally protected. The most common technical facilities are: the direction signs, warning notices, railings, handrails, fences, stairs, which are installed in places where difficulties in exploring may appeared (precipices, chasms, steep climbs), as well as observation and view platforms. Furthermore, in many cases it is necessary to provide lighting system. This concerns mainly caves, mines and tunnels, and also buildings constructed from rocks or other sites which sightseeing by night may be a great attraction.

It should be noticed that the scope of infrastructure depends on the specificity of sites, thus not all elements of basic infrastructure have to be created.

The supporting infrastructure is quite a wide range of constituents which are designed to assist basic infrastructure. It includes mostly car parks, catering services, shelters, benches and tables, dustbins, sanitation, accommodation and information points. Each component of the infrastructure, both basic and supporting, should be properly integrated in landscape, so that not to be too conspicuous and not to obscure the sites or view.

The promotion is the last element of the proposed model of the geotourist development. Appropriate publicity of sites may be a key to attract and educate a large number of visitors and provide economic benefits to local residents. The aim of promotion is "selling the sites", that is to encourage tourists to visit the geotourist sites by providing information about their unique qualities. Nowadays, the most proper place for this task is the Internet. Creating a website presenting the geotourist site or trail is the basis for promotion and easily accessible source of information, not only in tourism. Other forms of publicity may be small flyers, folded leaflets or brochures (available in local authorities' seats and tourist information points), articles in local as well as specialist newspapers and broadcast in local media. Additionally, placing the markers, for example logos, on tourist maps and general information in tourist guides can also support the promotion.

3. Case study

3.1. Research area

The region of Jasieniowa Mt. is located in the south part of the Cieszyn Foothills, which is numbered among the Śląskie Foothills, in the Western Outer Carpathians. The examined area lies within the administration of Śląskie province and Cieszyn district. Goleszów is a village situated at the foot of the Jasieniowa Mt. (Kondracki, 2002). The important tourist centres as Cieszyn and Ustroń are situated at the distance of no more then 10 km from considered region.

The described area is built of the flysch deposits of Cieszyn Subunit (the lower part of the Silesian Nappe). This subunit includes the oldest deposits of the Outer Carpathians, which are traditionally called the Cieszyn Beds. Among them, the following deposits can be distinguished: Lower Cieszyn Beds- Vendryne Formation (Kimmeridgian- Tithonian), Cieszyn Limestones- Cieszyn Limestone Formation (Upper Tithonian- Lower Valanginian) and Upper Cieszyn Shales- Cisownica Shale Member (Valanginian- Hauterivian) (Golonka et al. 2008). In the vicinity of Jasieniowa Hill, the outcrops of the two oldest formations can be ob-

serve. The Vendryne Formation is developed as dark gray to black marls with rare intercalations of redeposited limestones. This pre-flysch deposits represent the chaotic type of sedimentation (Słomka, 1986; Ślączka and Kamiński, 1998; Golonka and Waśkowska-Oliwa, 2007). The deposits of the Cieszyn Limestone Formation are lithologically unique (calcareous flysch) and have begun the series of flysch sedimentation in Polish Carpathians, thus there are the example of the oldest deposits of turbiditic currents. The occurrence of this formation is restricted only to the western, marginal part of the Outer Carpathians, between Soła and Olza rivers. It is generally represented by white or light grey limestone beds interbedded with grey marly shales. The limestones are diverse, from pelitic and thin-bedded in lower part of the sequence, to detrital, coarse grained, and thick-bedded in upper part (Peszat, 1967; Słomka, 1986; Ślączka and Kamiński, 1998; Golonka and Waśkowska-Oliwa, 2007).

Several abandoned quarries, where the limestones were mainly exploited, can be found on the slopes of Jasieniowa Mt. The biggest one, situated on the eastern slope, because of its exceptional scientific value, belongs to the Polish list of representative geosites selected for the Europen Network- the Global Geosites Project (Alexandrowicz, 2006). Moreover, it should be emphasized, that this quarry has been protected as the documentary site since April 2009.

3.2. Results- the proposal of geotourist development

The proposal of the development, in considered case, focuses primarily on the basic infrastructure which includes: delineating the geotourist trail

Fig. 3. The outcrop of marly shales representing the pre-flysch deposits, abandoned marl quarry.

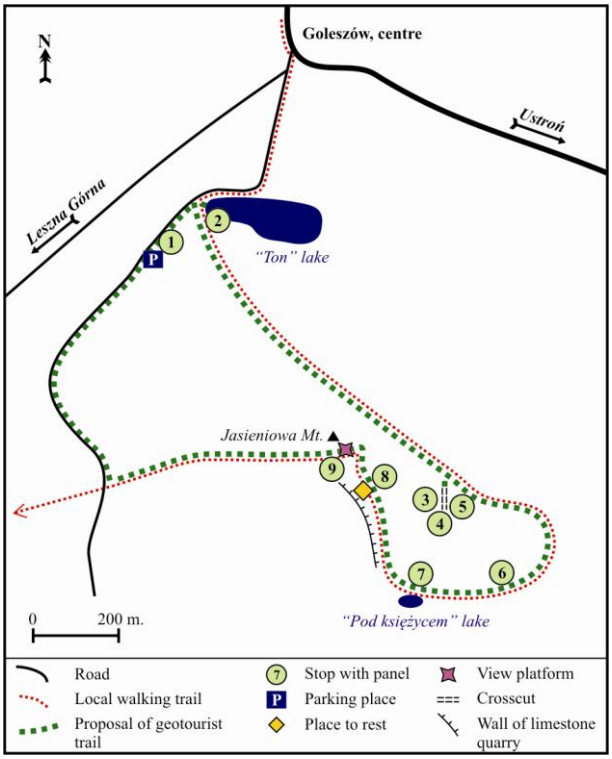

Fig. 2. The sketch map of proposed geotourist trail "Jasieniowa Mt." together with location of interpretative panels.

with stops, the location of the necessary technical facilities and the design of information panels. The parking place and place to rest are the elements of supporting infrastructure, which are provided for this project. The proposed trail has an overall cognitive and educational character. This initiative enables to acquaint visitors with geological structure of this region, rocks which can be found here, and history of abandoned quarries. The issue of geoconservation is also brought up. Moreover, it leads through the forest and several view points, which allow the tourists to spend time close to nature and to enjoy the beauty of the landscape.

The length of the trail is 3,5 km, the estimated time of covering the distance is 1,5 hour (on foot, the time for stops and rest is not included) and the total climb is 100 m. This suggested geotourist trail coincide with the fragment of the local walking trail called "Jasieniowa". It is intended for individual visitors, as well as for tourist groups, particularly schoolchildren.

The geotourist trail and also the location of sites and stops are shown on figure 2. The trail begins nearby the complex of small ski jumps, to the south-west of the centre of Goleszów. There is a possibility of parking there. Then it leads to the first abandoned quarry. In the past the marls were

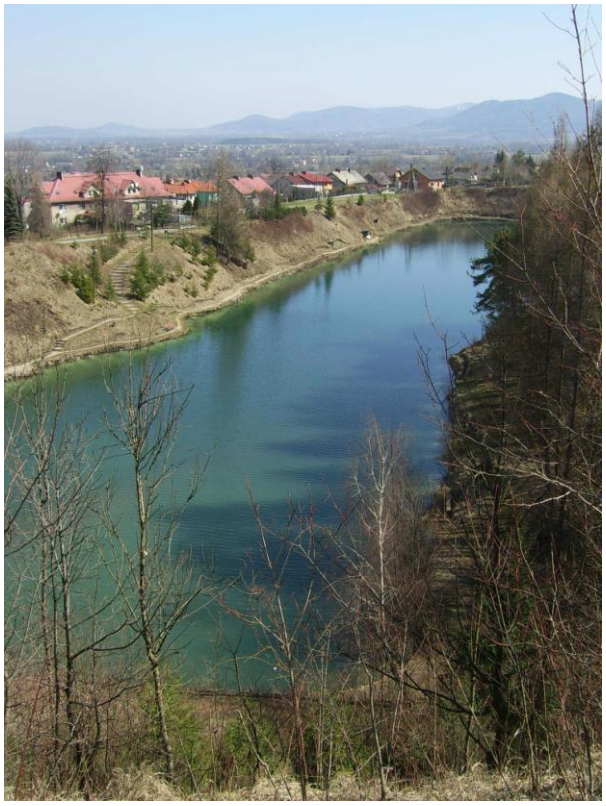

Fig. 4. The view on the abandoned marl quarry with the "Ton" lake, farther Goleszów and the summit of Beskid Śląski Mts.

exploited here, today the void is filled with water. The walk around the lake called "Ton" is an opportunity to observe the small occurrences of marls, which represent the Vendryne Formation (Fig. 3). From above the quarry stretches the view on the lake, Goleszów and the summits of Beskid Śląski Mts. (Fig. 4). The following interesting site on the trail is called by local people "ravine". It is a crosscut in the ridge of Jasieniowa Mt. which was used to export the stone from a nearby quarry to cement plant in Goleszów. Currently, the 20 m high walls of crosscut are a convenient place to observe the rocks belonging to the Cieszyn Limestone Formation (Fig. 5). The trail goes further to the biggest in considered area, abandoned limestone quarry. It is partly cover with vegetation, but the fragments of 30 m high and over 200 m long rock walls are still visible (Fig. 6a). In the lower part of this quarry the small, temporary lake called "Pod księżycem" can be found (Fig. 6b). A small forest clearing, picturesquely located in the upper part of the quarry is an perfect place to rest. After a short climbing, almost from the top of Jasieniowa

Fig. 5. The general view on the crosscut in the ridge of Jasieniowa Mt. The layers of limestones intercalated by marly shales are visible.

Fig. 6. The abandoned limestone quarry with outcrop of the thick-bedded limestones (a) and the temporary lake called "Pod księżycem" (b).

Mt., one can enjoy the wide and attractive view of the Cieszyn Foothills and the Beskid Śląski Mts. In the end, the trail returns to the parking place. Fallowing stops were situated on the trail:

1. Geotourist trail "Jasieniowa Mt."
Scope of information: general information about the geotourist trail, its main aims, a sketch map with trail and location of stops, issues of panels at stops.

2. The old marls quarry and "Ton" lake.
Scope of information: what are marls, the use of marls, the outline of history of exploitation, current use of quarry.

3. The Carpathian flysch.
Scope of information: basic information about flysch, what is called flysch, its origin, idea of nappe, region of Jasieniowa Mt. on geological map of the Polish Carpathians Flysch, the Cieszyn Beds as the oldest deposits of the Polish Carpathians Flysch.

4. The Cieszyn limestones.
Scope of information: the variety of Cieszyn limestones, their origin, the ways of identifying their age.

5. The traces in rocks.
Scope of information: what are trace fossils and hieroglyphs (Fig. 7).

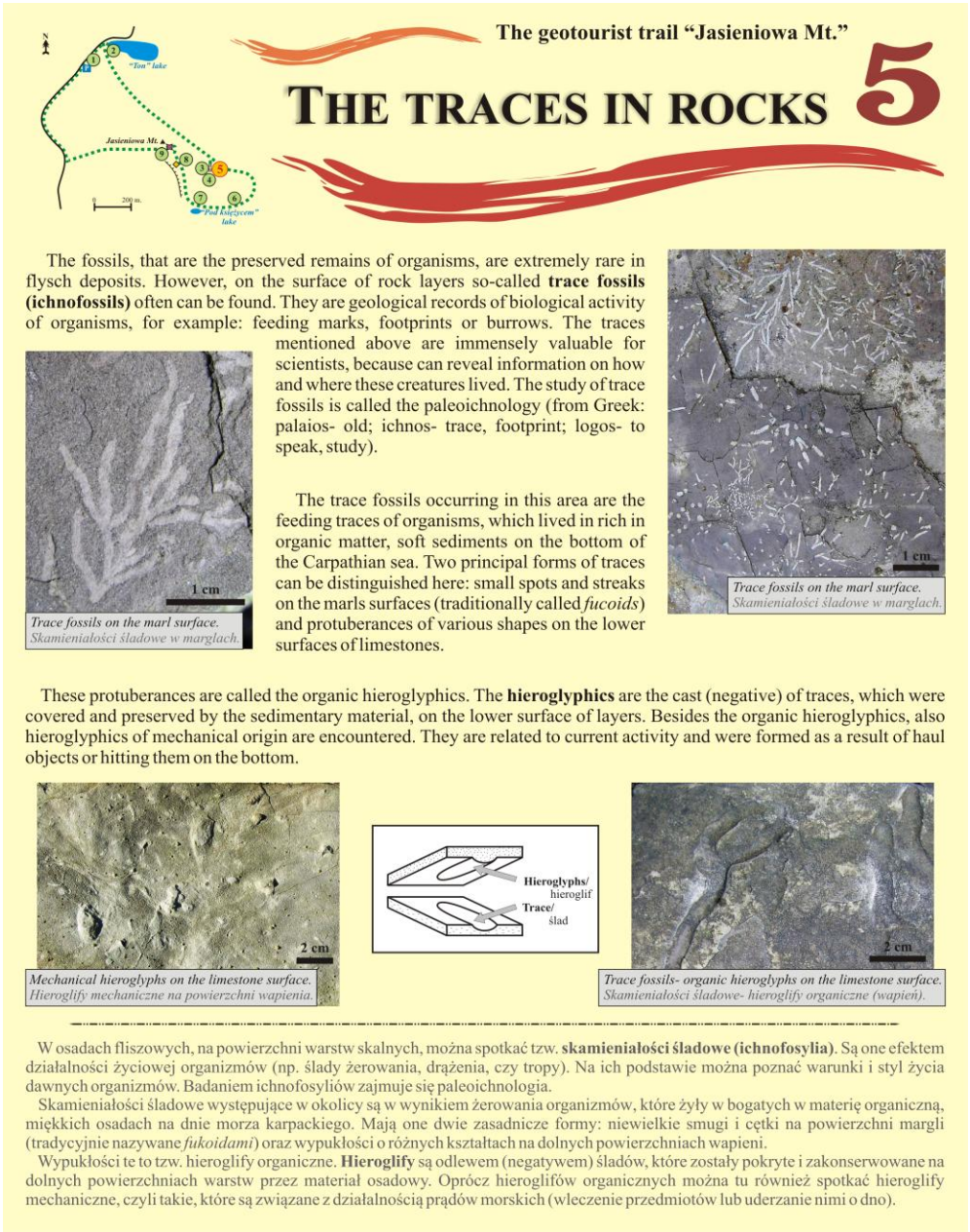

Fig. 7. A design of one of the interpretative panels.

6. The history of limestone exploitation.
Scope of information: outline of history of limestones exploitation in this region, the use of limestones, the transportation of stone- the traces of the narrow gauge railway.

7. The „Pod księżycem" lake
Scope of information: how the origin of lake is explained.

8. The protection of abiotic nature.
Scope of information: the reason for abiotic nature protection, the documentary site, the reason of protection of this limestone quarry.

9. The view point.
Scope of information: „geological view"- combination of view with geology of this region, relation between relief and geological structure.

The following technical facilities are indispensable components of this project: railings over the marl quarry and along the crosscut, the stairs with handrails nearby the 2nd, 7nd and 9th stop and the view platform below the summit of Jasieniowa Mt. Moreover, the shelter, benches, tables and dustbins at the place to rest and the parking place belong to the suggested elements of the supporting infrastructure.

The best form of promotion of described geotourist trail is the website as well as the folded leaflets which should be available at least in tourist information points in Ustroń, Cieszyń and Wisła. In order to present the initiative to local residents, the authors suggest to run the articles in local newspaper.

4. Conclusions

The proper interpretation of geological features and processes is a key to making geotourism accepted by general public. That is why the appropriate development of valuable geotourist sites is responsible so significant and action.

In the considered case, marking the geotourist trail together with the proper facilities as well as placing on-site interpretative panels are the most appropriate way of development. This solution allows visitors to acquaint with the values of selected sites to a sufficient extend. Moreover, completing the project will surely contribute to increase attractiveness of Goleszów commune, and also enrich the tourist offer of entire region.

References

Alexandrowicz Z., 2006. Framework of European geosites in Poland. Nature Conservation, 62, 63-87.

Alexandrowicz Z., Kuśmierz A., Urban J., and Otęska-Budzyn J., 1992. Evaluation of inanimate nature of protected areas and objects in Poland. PIG. Warszawa (in Polish with English abstract and summary).

Dmytrowski P. and Kicińska A., 2009. Geotourism valuation of unbiotic objects and their signification in prospect of geopark development. Problemy ekologii krajobrazu (in Polish with English abstract) (in print).

Golonka J. and Waśkowska-Oliwa A., 2007. Stratygraphy of the Polish Flysch Carpathians between Bielsko-Biała and Nowy Targ. Kwartalnik AGH Geologia, 33, 4/1, 5-28 (in Polish with English abstract and summary).

Golonka J., Vašíček Z., Skupien P., Waśkowska-Oliwa A., Krobicki M., Cieszkowski M., Ślączka A. and Słomka T., 2008. Lithostratygraphy of the Upper Jurassic and Lower Cretacerous deposits of the western part of the Outer Carpathians (discussion proposition). In: The deposits from the turn of the Jurassic and Cretaceous in the Western Flysch Carpathian of the Polish-Czech borderland, Jurassica VII, 27-29.09.2008- Żywiec/Stramberk, Krobicki, M. (ed.), Kwartalnik AGH Geologia, 34, 3/1, 9-31 (in Polish with English abstract and summary).

Górna M., 2009. The geosites of Cieszyn Foothills- the proposal for protection and education. In: Interdisciplinary Topics in Mining and Geology. IX PhD Students' Scientific Conference. Szklarska Poręba, 25–27.05.2009, Milczarek, W. (ed.), Scientific Papers of the Institute of Mining of the Wrocław University of Technology, 126, Series: Conferences, 53, 132-142 (in Polish with English abstract).

Hose T. A., 2000. European „geotourism"– geological interpretation and geoconservation promotion for tourists. In: Geological Heritage its Conservation and Management, Barettino, D., Wimbledon, W.A.P. and Gallego E. (eds), Madrid, Spain, 127-146.

Kicińska-Świderska A. and Słomka T., 2004. The construction of geotourist routs. Folia Turistica, 15, 179-184 (in Polish with English abstract).

Kondracki J., 2001. Regional geography of Poland. Wyd. Nauk. PWN, Warszawa, 321 (in Polish).

Newsome D. and Dowling R., 2006. The scope and nature of geotourism. In: Geotourism, Dowling, R. and Newsome, D. (eds), Oxford, UK, Elsevier/ Heineman Publishers, 3-25.

Peszat Cz., 1967. The lithological development and conditions of sedimentation of the Cieszyn limestones. Prace Geologiczne PAN, Warszawa, Wyd. Geol., 44, 1-111 (in Polish with English summary)

Rogalewski O., 1974. Tourist management. Wydawnictwa Szkolne i Pedagogiczne, Warszawa (in Polish).

Słomka T., 1986. Statistical approach to study of flysch sedimentation- Kimmeridgian-Hauterivian Cieszyn

Beds- Polish Outer Carpathians. An. Soc. Geol. Pol., 56, 277-336 (in Polish with English abstract and summary).

Słomka T. and Kicińska- Świderska A., 2004. The basic concepts of geotourism. Geoturystyka/Geotourism, 1 (1), 5-7 (in Polish with English abstract).

Ślączka A. and Kaminski M.A., 1998. A Guidebook to Excursions in the Polish Flysch Carpathians. Kraków, Grzybowski Foundation, Special Publication, 6, 36-40.

Waśkowska-Oliwa A., Krobicki M., Golonka J., Słomka T., Ślączka A. and Doktor M., 2008. Sections of the oldest sedimentary rocks in Polish Flysch Carpathians as geotourist objects. In: The deposits from the turn of the Jurassic and Cretaceous in the Western Flysch Carpathian of the Polish-Czech borderland, Jurassica VII, 27-29.09.2008- Żywiec/Stramberk, Krobicki, M. (ed.), Kwartalnik AGH Geologia, 34, 3/1, 9-31 (in Polish with English abstract and summary).

Scientific Annals, School of Geology, Aristotle University of Thessaloniki Proceedings of the XIX CBGA Congress, Thessaloniki, Greece	Special volume 100	453-458	Thessaloniki 2010

GEOLOGICAL AND GEOMORPHOLOGICAL VALUES OF THE CASTLE HILL GEOLOGICAL AND EDUCATIONAL TRAIL SITUATED IN SZANDA (NORTHERN HUNGARY)

Dobos A. and Gali.Z

Department of Environmental Sciences, Eszterházy Károly College, 3300 Eger, Hungary
dobosa@ektf.hu, zoltan.gali80@gmail.com

Abstract: This article is about results of cadastre of unique geological and geomorphological values in the Castle Hill, in Hungary. The Castle Hill situated in Szanda (528,6 m) has preserved *the remnant of the dyke ridge developed during the Miocene volcanism (16-14 million years) in the Cserhát Mts., the special geological structure and landforms of the dyke and anthropogenic aspects of the mining activity.* We would like to show these particular geological structures and landforms with a *geological and educational trail extended new stages for tourists* today. During our field works, geological and geomorphological values of the Castle Hill have been mapped and surveyed by the *Cadastre data sheet of unique landscape values*. We have made detailed description of different objects, we have taken photographs of them, we have mapped the route of the new, more detailed geological trail and the topographic situation and landscape values of the stages. Where it was possible, we have measured dips and strikes. Our aim was to cadastre and survey unique geological and geomorphological values of this important *nature protection territory*. Our investigation has explored 28 new geological outcrops and landform values and these can be built to the route of the older geological and educational trail.

Keywords: Northern Hungary, the Cserhát Mts., andesite dykes, geological and geomorphological values, nature protection, geotourism

1. Introduction

The nationwide investigation, the classification and qualification of the Earth Scientific Values began in 1999 in Hungary. Lot's of geological, geomorphological and educational trail have been created in our country since that time. In this article we would like to introduce ***the Castle Hill situated in Szanda***, which has special geological (dyke) structure and many earth scientific values. This study area can be found in the Cserhát Mts, in the North Hungarian Mountains, 21 kilometres far away from Balassagyarmat. The dyke ridge characterised with the special NW-SE strike direction (Fig. 1.) has risen from its surroundings with 120 metre relative height next to Szanda and Szandaváralja. The Castle Hill is situated along the microlandscape border of the Central Cserhát Mts. and the Terényi foothill area (Marosi and Somogyi 1990). This territory, the doubled summit of the Castle Hill can be reached along the "blue" hiking trail from Becske, Szanda and Szandaváralja. We can find a large non-working mining site in the territory of the Peter Hill. The 20 ha area of the Castle Hill and the Peter Hill with mining sites were declared as a "*local importance nature protection area*" in 1976, then they were categorized as a "*most important nature protection area*" situated in the Bükk National Park in 2004 (275/2004. (X. 8.) Order in Council). ***The geological and educational trail of the Castle Hill*** is generally in neglected situation, but the Castle Hill and its surroundings are popular excursion site for tourists.

2. Materials and Methods

At the first stage of our investigation we gathered the geological, geomorphological and topographical maps and bibliography of the study area. We have done the research work on the field, where we have surveyed and cadastred the unique geological and geomorphological values of the Castle Hill, we have filled in the form of the Cadastre data sheet of unique landscape features (Hungarian Standard No. 20381/1999), we have made detailed

description of different objects, we have taken photographs of them, we have mapped the route of the new, more detailed geological and educational trail and the topographic situation and landscape values of the stages. During our field research work, we have measured new dips and strikes. Our results have been represented by CorelDraw 12 and Golden Software SURFER 8.0 programs. Our aim was to investigate the geological and geomorphological development and fundamentals of the study area and to cadastre and survey unique geological and geomorphological values of this *important nature protection territory*.

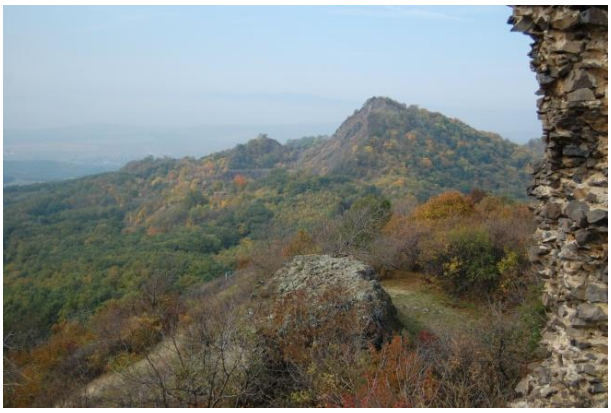

Fig. 1. The dyke ridge situated in direction of NNW and SSE in the Peter Hill (quarry) and the Castle Hill.

3. Results and Discussion

3.1. Geological built up and fundamentals

The series of Oligocene (38-24 million years) grey and greenish grey coloured clays, claymarls, sands and glaukonite sandstones are built up the territory of the Szőr-part (Fig. 2.) and southern Szőlőkalja (end of the vineyard) next to the Castle Hill. These sediments refer to the shallow sea situation (Szécsény Schlier Formation, Pétervására Sandstone Formation) (Noszky 1940, Gyalog 2005). Somewhere, brown coal layers were deposited into the mentioned sedimentary layers (Becske – brown coal). In correspondence of Szava Orogenic Phase, more important denudational period appeared at the border of the Oligocene and the Miocene in the North Hungarian Mountains. The Szécsény Schlier F. and Pétervására Sandstone F. could be showed in the Cserhát Mts. during the Lower Miocene. ***Miocene Ottnangian staged*** (Lower Helvetian stage) (20-19 million years) terrestrial sediments were deposited next to the Castle Hill and the Peter Hill in direction of NW and SE. Because of the appearance of the marsh, new brown coal sediments and layers were developed here. Lot's of mud were sedimented in these layers and after that gravels were accumulated here. The gravel can be found in the overlying bed. Some sand, sandstone layers and Schlieren were deposited on the gravel layers (Noszky 1940).

A large, longer than 10 km fissure was developed with NNW-SSE direction into the Oligocene and the Lower Miocene sediments in case of the Szanda Hill and the Peres Hill (Fig. 2.). This fissure was filled in by thin ***andesite dyke*** in the Miocene Lower Badenian stage (Lower Tortonian stage) (14,3 – 13 million years). In consequence of ***the labial volcanic activity*** long and thin ***andesite nappe*** (Láng 1967) was developed here (Hasznosi Andesite F., Gyalog 2005.). Three summits could be found along the main part of this dyke ridge in the Szanda Hill originally. The Peter Hill was situated at the western part of the Castle Hill and it had larger andesite nappe and two 545 m height summits above the sea level. The body of the ***pyroxene andesite dyke*** passed through ***hydrothermal dykes and*** hydroandesite has explored by the mining activity (Noszky 1940, Csalagovits). The eastern,

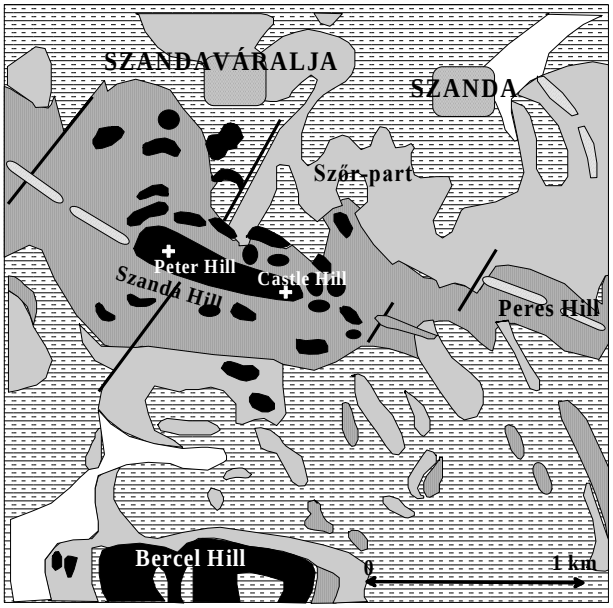

Fig. 2. The geological map of the study area (based on Noszky 1940).

528,6 metre high summit of the Castle Hill is built up with ***pyroxene andesite dyke and smaller andesite nappe***. These rocks were deposited above Upper Oligocene clayey sands. The dyke ridge of the Castle Hill continues toward east in the Peres Hill (Fig. 2.). The Miocene gravel layers can be investigated under the andesite nappe of the Castle Hill in original deposition and thickness. That is why the Szanda Hill can be categorised as ***a residual. Pleistocene loess and slopeclay*** can be found at the edge of the pediment surface of the Castle Hill and the Peter Hill, where the surface has been dissected by erosional and derasional valleys. ***Holocene fluvial gravel, sand, mud and clay*** were deposited in the territory of alluviums and in valleys of surrounding settlements.

3.2. Landscape development and geomorphological surfaces

The ridge of the andesite nappe and the dyke situated in direction of NNW and SSE were originated from the Miocene and after that they were ***eroded and peneplanated*** by exogenic processes during the ***Upper Miocene Sarmatian (14,3 – 11,5 million years) and Pannonian stages (11,5 – 5 million years).*** Therefore the dyke structure has appeared on the surface and it has eroded upon the surrounding territory and it has lowered. New denudated period was probably during the Miocene Sümegium period (8,5 – 8 million years) and at the border of the Miocene and the Upper Pliocene Bérbaltavárium period (5,6 million years). At that time, ***pediments*** began to develop under the semiarid climatic condition (Schweitzer F., 1993) at the edge of hills. Today, we can see and investigate the pediment of Villanyium period clearly, which was developed at the border of the Pliocene and the Pleistocene (1,8 – 1,4 million years) around the Castle Hill. Derasional valley heads cut into this surface during the Pleistocene.

This Villanyium pediment was dissected by derasional and erosional valleys later, that is why it could be observed and investigated at the edge of the Castle Hill in direction of NE, SE, N and S. (Fig. 3.). During the Pleistocene (1,8 – 0,01 million years) *glacial periods*, the frost weathering, the formation of cryoplanation walls/frost-riven cliffs, tors, periglacial sorted talus slopes, stone fields, cryoturbation processes, derasional valleys, forms of gelisolifluction and the formation of fluvial terraces were developed. During the *interglacial periods*, the chemical weathering, the formation of forms of solifluction, and the deepening and creating of the valleys or development of new fluvial terraces were dominated (Láng 1967, Martonné Erdős 2003). In the Holocene period (0,01 million years - todays), the deepening of erosional valleys and water cuts, mass movements, the denudation of older surfaces, and the movements and the accumulation of Holocene sediments in alluviums and basins can be recognised. Wider alluviums develops along the streams (Gólya stream).

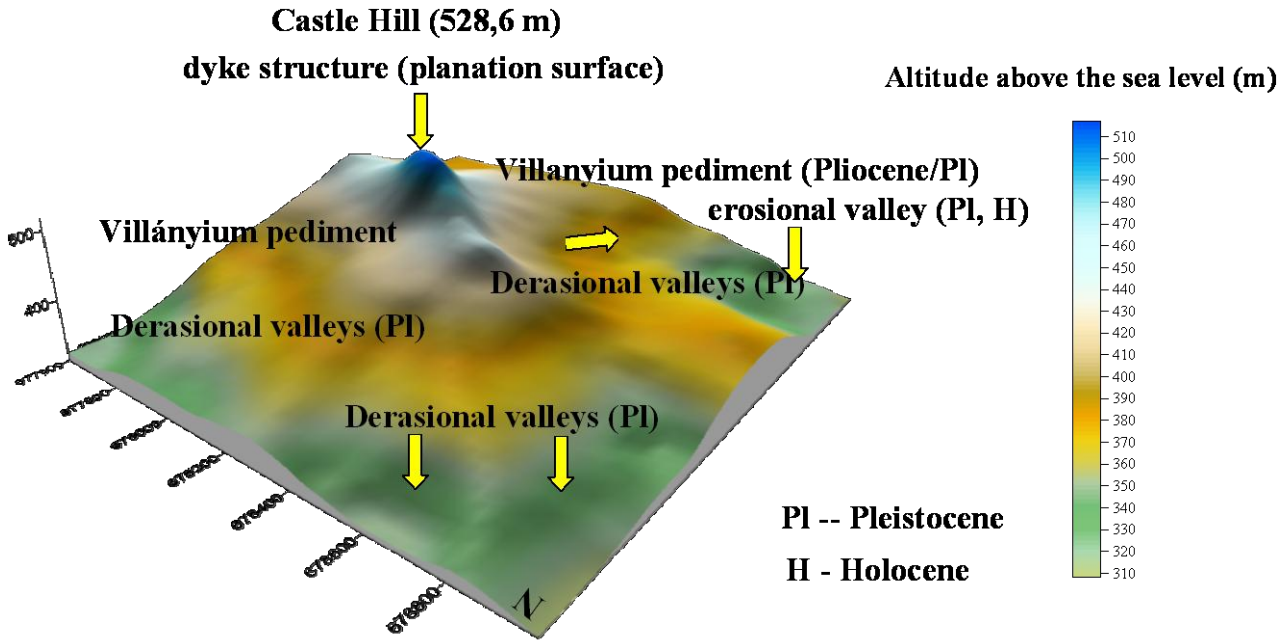

Fig. 3. The geomorphological surfaces of the Castle Hill in Szanda (Northern Hungary, Cserhát Mts.) (Dobos and Gali, 2009).

3.3. Surveying and cadastre of geological and geomorphological values

The geological and educational trail was planned and built up in the Castle Hill in 1996 (Cene 1996). This geological trail can show the *thick bedded, columned and foliated andesite outcrops*, the *processes of denudation of andesite in the Pleistocene and the Holocene, and the landforms of mining activity* (Fig. 4.). The older geological and educational trail can present the following geological values in case of different stages:

(15/I) – 5-8 m wide, 2-3 m height ***small quarry***, where grey coloured, andesite columns are situated in dip of 70-80° and strike of SW direction. (16/II.) – ***rock stream*** built up with thicker and thinner, 1,5 metre long andesite columns. (III.) – ***smaller mining site*** (20 x 30 metres), where volcanic landforms could not be seen because of its neglected situation. (IV.) – the territory of important ***rock stream and cylindrical andesite columns.*** (12/V.) – The most beautiful ***outcrop of the columned andesite*** in the Castle Hill, where we can investigate the central part of the labial volcanism. (VI.) – ***The outcrop of the thick bedded andesite*** with dip of 20-30° (This is the deepest section of the labial volcanism.). (VII. or 11.) – The ***canyon*** developed by mass movements and the dissection of volcanic nappe.

We began the cadastre of unique geological and geomorphological values of the Castle Hill in the summer of 2009. We used the *Hungarian Standard* (Hungarian Standard No. 20381/1999.) and *its cadastre data sheet and its system of landscape values* and *our cadastre data sheet and the category of geological and geomorphological values*, which has improved during nature protection research work in the Bükk Mts. (Dobos et al., 2001). We strived for present the most important and the most characteristic geological structures, outcrops and landforms of the Castle Hill during our investigation. We can fail to point out such stages along "blue" hiking trail and its surroundings, where the dyke structure, its landforms and the remnant of geomorphological surfaces and landforms created during the Pleistocene and the Holocene periods can be investigated well. We can show the most important and the most characteristic geological and geomorphological values by development of older geological and educational trail along the hiking route used by tourists (Fig.4.). The mapped and measured geological and geomorphological values or unique landscape values can be seen in Table 1.

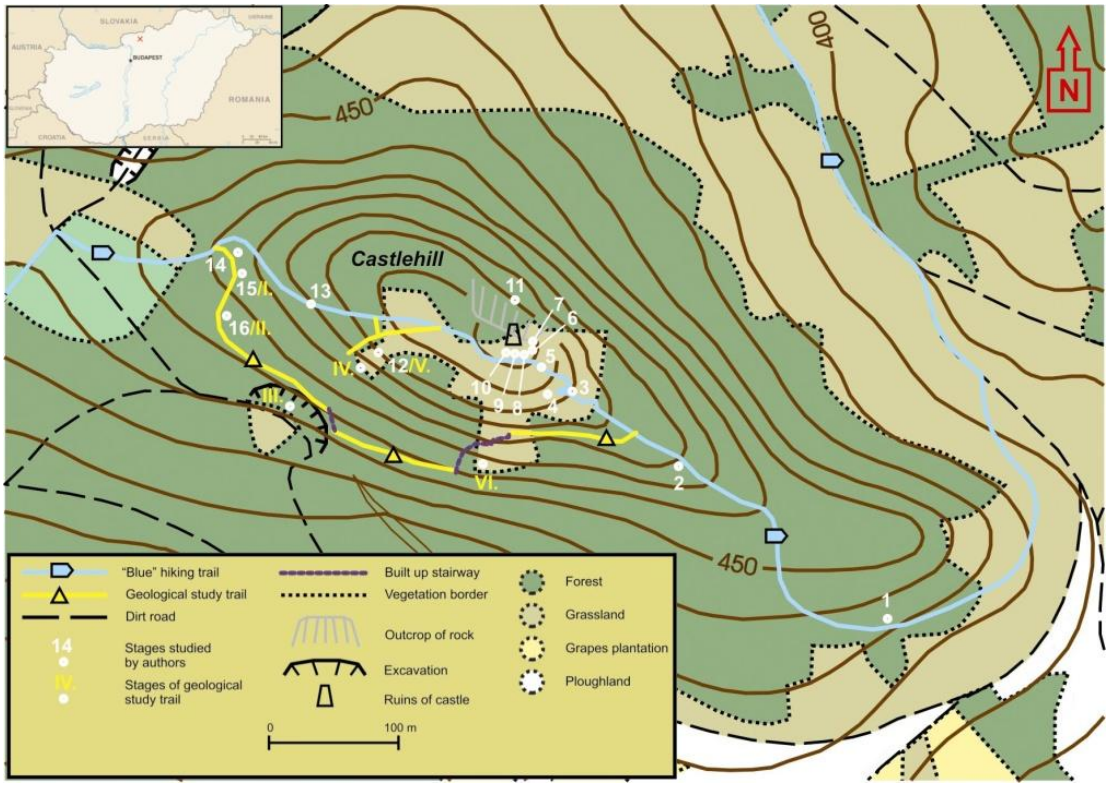

Fig. 4. The stages of the geological and educational trail and the new stages marked out along the "blue" hiking trail in the Szanda Hill (Gali and Dobos, 2009).

Table 1. The unique landscape values of the Castle Hill situated in Szanda

Number	Mark	The name of the unique landscape value	The type of the unique landscape values (Dobos A. et al, 2001)	Genetical date of rocks and landforms
1	SZD1/A	Outcrop of pyroxene andesite	2.1.2.	Miocene, Lower Badenian stage: 16-14 million years
	SZD1/B.	Frost-riven cliffs, remnants of frost-riven cliffs, series of talus cones	2.9.2.	Pleistocene
	SZD1/C	rockfall (mass movement)	2.5.1.	Pleistocene, Holocene
2	SZD2/A	Outcrop of pyroxene andesite: thick-bedded and foliated types	2.1.2.	Miocene, Lower Badenian stage: 16-14 million years
	SZD2/B	Cryoplanation terraces	2.9.2.	Pleistocene
3	SZD3/A	Outcrop of pyroxene andesite, thick bedded types	2.1.2.	Miocene, Lower Badenian stage: 16-14 million years
	SZD3/B	Bedding plane and the rim of beds	2.4.1.	Upper Miocene, Pliocene and Quaternary
4	SZD4/A	Outcrop of columned pyroxene andesite	2.1.2.	Miocene, Lower Badenian stage: 16-14 million years
	SZD4/B	Outcrop of columned pyroxene andesite, Bedding plane and the rim of beds	2.4.1.	Upper Miocene, Pliocene and Quaternary
5	SZD5	Outcrop of pyroxene andesite, Foliated types	2.1.2.	Miocene, Lower Badenian stage: 16-14 million years
6	SZD6/A	Outcrop of pyroxene andesite, foliated and thick bedded types	2.1.2.	Miocene, Lower Badenian stage: 16-14 million years
	SZD6/B	Folds and faults, discordance	2.4.1. 2.4.2.	Miocene Lower Badenian stage, younger structural movements
7	SZD7/A	Outcrop of pyroxene andesite, thick bedded types	2.1.2.	Miocene, Lower Badenian stage: 16-14 million years
	SZD7/B	Folds and faults	2.4.1. 2.4.2.	Miocene Lower Badenian stage, younger structural movements
8	SZD8/A	Outcrop of pyroxene andesite,	2.1.2.	Miocene, Lower Badenian stage: 16-14 million years
	SZD8/B	Folds and faults	2.4.1. 2.4.2.	Miocene Lower Badenian stage, younger structural movements
9	SZD9/A	Outcrop of pyroxene andesite, thick and thin bedded types	2.1.2.	Miocene, Lower Badenian stage: 16-14 million years
	SZD9/B	Folds and faults	2.4.1. 2.4.2.	Miocene Lower Badenian stage, younger structural movements
10	SZD10/A	Outcrop of pyroxene andesite, bedding plane	2.1.2.	Miocene, Lower Badenian stage: 16-14 million years
	SZD10/B	Folds and faults, anticline	2.4.1. 2.4.2.	Miocene Lower Badenian stage, younger structural movements
11	SZD11	Polygenetical canyon	2.12.2.	Tertiary, Quaternary
12	SZD12/A	Outcrops of columned pyroxene andesite	2.1.2.	Miocene, Lower Badenian stage: 16-14 million years
	SZD12/B	Periglacial block facies	2.9.2.	Pleistocene
	SZD12/C	Periglacial stone streams	2.9.2.	Pleistocene
13	SZD13	Series of talus slopes	2.9.2.	Pleistocene
14	SZD14	Cryoplanational walls, periglacial talus slope	2.9.2.	Pleistocene
15	SZD15	Outcrop of pyroxene andesite, quarry	2.1.2.	Miocene, Lower Badenian stage: 16-14 million years
16	SZD16	Cryoplanational walls, remnants of frost-riven cliffs, and talus cones and stone stream	2.9.2.	Pleistocene

Conclusions

The Castle Hill (528,6 m) situated in Szanda has preserved *the remnant of dyke ridge developed during the Miocene volcanism (16-14 million years) in the Cserhát Mts.*, *its special geological structure and landforms and anthropogenic aspects of quarry*. During our research work, we have investigated and categorised 12 different outcrops of andesite, 7 landforms of folds and faults, 1 rock fall (mass movement), 7 periglacial landforms and 1 polygenetical canyon among Earth Scientific Values in the study area.

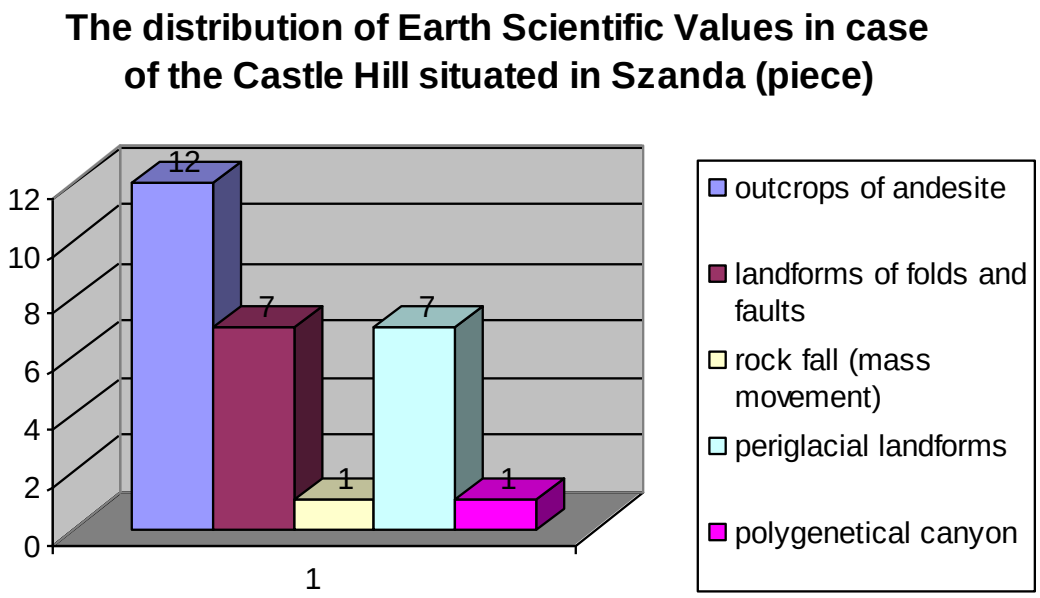

Fig. 5. The distribution of Earth Scientific Value categories in case of the Castle Hill in Szanda.

These cross sections, outcrops and landforms (Fig. 4. and 5.) simply reflect the most important phases of geological development and remnants of landforms in the study area. We suggest to showing and building up these unique geological and geomorphological values in case of the geological and educational trail in the Castle Hill for the future.

References

Cene J., 1996. The Landscape Development Plan of neglected andesite quarry of the Castle Hill situated in Szanda, GEOTEAM Research and Entrepreneurial Ltd., Eger, 24p. (in Hungarian)

Dobos A., Gasztonyi É., Kozák M., Püspöki Z., Sütő L., Szabó J. 2001: Cadastre data sheet of geological and geomorphological values, in: Szabó J. and Sütő L. 2005. Some questions and practical methods of the unique landscape cadastre in case of the Cserehát Mts., (insert) in: Dobos A. and Ilyés Z. 2005. The Protection of Geological and Geomorphological Values, Eger, 81-100. (in Hungarian)

Gyalog L., 2005. Explanatory note for the geological map of Hungary, 1:100 000, Hungarian Geological Institute Explanatory notes, Budapest, 188p. (in Hungarian)

Láng S., 1967. The Physical Geography of the Cserhát Mts., Geographical Monographs, Publishing House of the Hungarian Academy of Sciences, Budapest, 1-375. (in Hungarian)

Hungarian Standard No. 20381/1999. Nature protection. Cadastre of unique landscape features, Hungarian Standard Association, 1999. August, Budapest, 1-8.

Marosi S. and Somogyi S., 1990. The cadastre of the microlandscape units in Hungary II., The Hungarian Academy of Sciences, Research Institute of the Earth Science, Budapest, 1023p. (in Hungarian)

Martonné Erdős K., 2003. The Physical Geography of the Hungary I. for students of Geography, University of Debrecen, Publisher of Kossuth University, Debrecen, 245p. (in Hungarian)

Noszky J., 1940. The geological fundamentals of the Cserhát Mts., The geology of Hungarian Landscapes/3., Hungarian Royal Geological Institute, Budapest, 283p.

Schweitzer F. 1993. Landscape development in the Pannonian Basin at the border of the Upper Tertiary and Quaternary, Thesis of Dissertation, Budapest, 1-27. (in Hungarian with English abstract)

Scientific Annals, School of Geology, Aristotle University of Thessaloniki Proceedings of the XIX CBGA Congress, Thessaloniki, Greece	Special volume 100	459-466	Thessaloniki 2010

THE BEST GEOTOURISTIC OBJECTS OF THE SILESIAN UNIT, OUTER FLYSCH CARPATHIANS IN THE VICINITY OF KRAKOW, POLAND

Doktor M., Golonka J., Waśkowska A. and Słomka T.

AGH University of Science and Technology, Department of General Geology, Environmental Protection and Geotourism, Mickiewicza Ave 30, 30-063 Kraków; Poland,doktor@geol.agh.edu.pl, jan_golonka@yahoo.com, waskowsk@agh.edu.pl; slomka@geol.agh.edu.pl

Abstract: The Outer Carpathians are built up of a stack of nappes and they are trust over the southern part of the North European platform. The Silesian Nappe occupies central part of the Outer Carpathians and it is built of sedimentary facies represented continues succession of Late Jurassic to Early Miocene times. In sedimentary profile are written successively stages of development of Silesian Unit on the background of evolutionary stadia of the geodynamic development of the Northern Carpathians from syn-, post-rift to synorogenic phase. The best outcrops (legible, good-preserved and accessible for the group of tourists) to examine the Silesian rocks are presented and included into the trail. The sites highlight stratigraphy and sedimentology of Silesian Unit, from Jurassic to Neogene, elements of structural geology, petroleum systems (source rocks, reservoir rocks, seals), geotouristic important objects and history of human activities in the Carpathians, especially of mining and oil industries. The proposed trail traverse the Silesian Nappe in Polish sector of West Carpathians between Kraków, Cieszyn and Ciężkowice area.

Key words: Polish Outer Carpathians, Silesian Nappe, geoturistic objects

1. Introduction

The authors attempt to provide the review of the most important and significant geotouristic attraction within the **Silesian Unit, Outer Flysch Carpathians**. The idea of this paper is derived from raising importance of geotourism as well as from the international geological meetings, which were conducted in the Carpathians in the XXI century. The programs of these meetings included several field trip guides aimed for the highlights of the Outer Carpathians designed for the international audience interested in the various subject of geology and geotourism. We selected the best geological outcrops and geotouristic sites, which can be visited during short 1 day to two weeks visit in the Polish Carpathians. The sites highlight stratigraphy and sedimentology of Silesian Unit, from Jurassic to Neogene, elements of structural geology, petroleum systems (source rocks, reservoir rocks, seals), geotouristic important objects and history of human activities in the Carpathians, especially of mining and oil industry. There are organized according to their age from oldest to youngest, illustrating geodynamic development of the Silesian Unit through time. The Jurassic - Early Cretaceous deposits were a subject of classic XIX century studies by Hohenegger (1861). The formation names were derived from this classic work, the exact definition were reworked during 150 years of studies by many Polish and Czech geologists (see the review in Golonka et al., 2008 a,b).

2. The Silesian Unit within the Outer Carpathians

The Outer Carpathians (Fig. 1B) are built up of a stack of nappes and thrustsheets spreading along the Carpathians, built mainly of up to six kilometers thick continual flysch sequences, representing the time span from Jurassic to Early Miocene. All the Outer Carpathian nappes are thrust over the southern part of the North European platform covered by the autochthonous Miocene deposits of the Carpathian Foredeep on the distance of 70 km, at least (Ślączka et al., 2006). Boreholes and seismic data indicate that the distance of the Carpathian overthrust was at least 60 km. During overthrusting movement the northern Carpathians nappes became uprooted from the basement and only their basinal parts were preserved. The succession of the nappes from the highest to the lowest is as follows: Magura Nappe, Fore-Magura group of nappes, Si-

lesian Nappe, Subsilesian Nappe and Skole (Skiba) Nappe (Fig. 1A).

The Silesian Unit (Nappe) occupies central part of the Outer Carpathians, pinching out below the most internal nappes. Sedimentary facies of the Silesian Unit represent continuous succession of deposits of age interval from Late Jurassic to Early Miocene. The oldest sediments of the Silesian Unit are known only in Moravia and Silesia areas in the Western Carpathians. They were deposited within proto-Silesian basin representing synrift - postrift stages of the geodynamic development of the Northern Carpathians (Golonka et al., 2008a,b). The basinal successions represent mainly passive margin turbidites. Alkaline magma (teschenites association rocks) intruded these turbiditic sequences (Ślączka et al., 2006; Golonka et al., 2008a,b).

The Vendryně Formation (Kimmeridgian-Tithonian/Early Berriasian) represents the oldest deposits of this zone (Fig. 1A). It is covered by the Cieszyn Limestone Formation (Late Tithonian - Middle Valanginian). The younger Hradište Formation is Middle Valanginian - Barremian. Two members were distinguished within the Hradište Formation: Cisownica Shale Member and Piechówka Sandstone Member. The Hradište Formation is covered by Veřovice Formation (Aptian) represented by black shales rich in organic matter.

During latest Early Cretaceous proto-Silesian Basin was reorganized, turned into the Silesian Basin and went into synorogenic phase of geodynamic development. The Lhoty Formation (Albian) represents the oldest synorogenic flysch-type deposits. The Mikuszowice Chert Member is distinguished within this formation. During the Late Cretaceous and Paleocene in the Silesian Basin took place sedimentation of sandy turbidites often thick-bedded, that represent the Godula and Istebna beds. Their complete thickness is estimated in the western sector of the Polish Carpathians for about 4500m. The thick-bedded sandstone (Ciężkowice Sandstones) or variegated shales sedimentation took place up to the Middle Eocene and later was replaced by thin-bedded shaly-sandstone flysch of the Hieroglyphic Beds. All clastic material of Godula and Istebna beds as well as of the Ciężkowice Sandstones was derived from southwest, from the Silesian Ridge. During the Oligocene the Menilitic and Krosno beds were developed. Then in the southern part of the Silesian Basin in some levels formed olistostromes (Cieszkowski et al., 2003). The sedimentation of the Krosno Beds was finished in the Early Miocene (Fig. 1A).

3. Selected geotouristic objects

3.1. Vendryně Formation (1)

The oldest sediments of the Silesian Unit can be examined along the Olza River Bank near the village Wędynia (Czech name Vendryně) – the type locality for the Vendryně Formation (locality (1) on Fig. 1B). Here we see dark grey marly shales with a few intercalations of redeposited detrital limestones containing fragments of macrofauna e.g. echinoderms and mollusks (Fig. 1C). The shales display chaotic structures, indicating that these sediments represent slump deposits derived from the adjacent carbonate platform, where pelitic sediments formes. The Vendryně Formation rocks represent synrift deposits, corresponding to the initial opening of proto-Silesian basin at the end of Jurassic period (Ślączka et al., 2006; Golonka et al., 2008a,b).

3.2. Cieszyn Limestone Formation with teschenite intrusions (2)

Cieszyn Limestone Formation rocks are splendidly exposed in the Jasieniowa Hill abandoned quarry (Ślączka and Kaminński 1998, Waśkowska-Oliwa et al., 2008) (locality (2) on Fig. 1B). The local touristic-educational trail lead from the Goleszów town to the quarry, displaying section through calcareous turbidites (Fig. 1D). The clastic material comprising the detrital limestones was derived from the adjacent shallow water calcareous platform, while to a large extent the pelitic limestones represent a *Coccolithus - Nannoconus* microfacies similar to the maiolica Alpine microfacies. The lower surfaces of the beds are covered with numerous sole marks, mainly of organic origin, and on surfaces of internal laminae organic traces (called fucoids), of varied size are often visible. In the upper part of the profile we can observe intercalations of thick- and very thick-bedded, graded, coarse-grained and conglomeratic limestones. The coarse basal part of these limestones consists of organic detritus (fragmented shells of lamellibranches, aptychi, crinoids, urchin spines, along with algae and gastropods). Quartz grains, fragments of dark Tithonian limestones, and Carboniferous coal are also present, indicating that the erosion in source area reached already the basement of the Jurassic calcareous rocks.

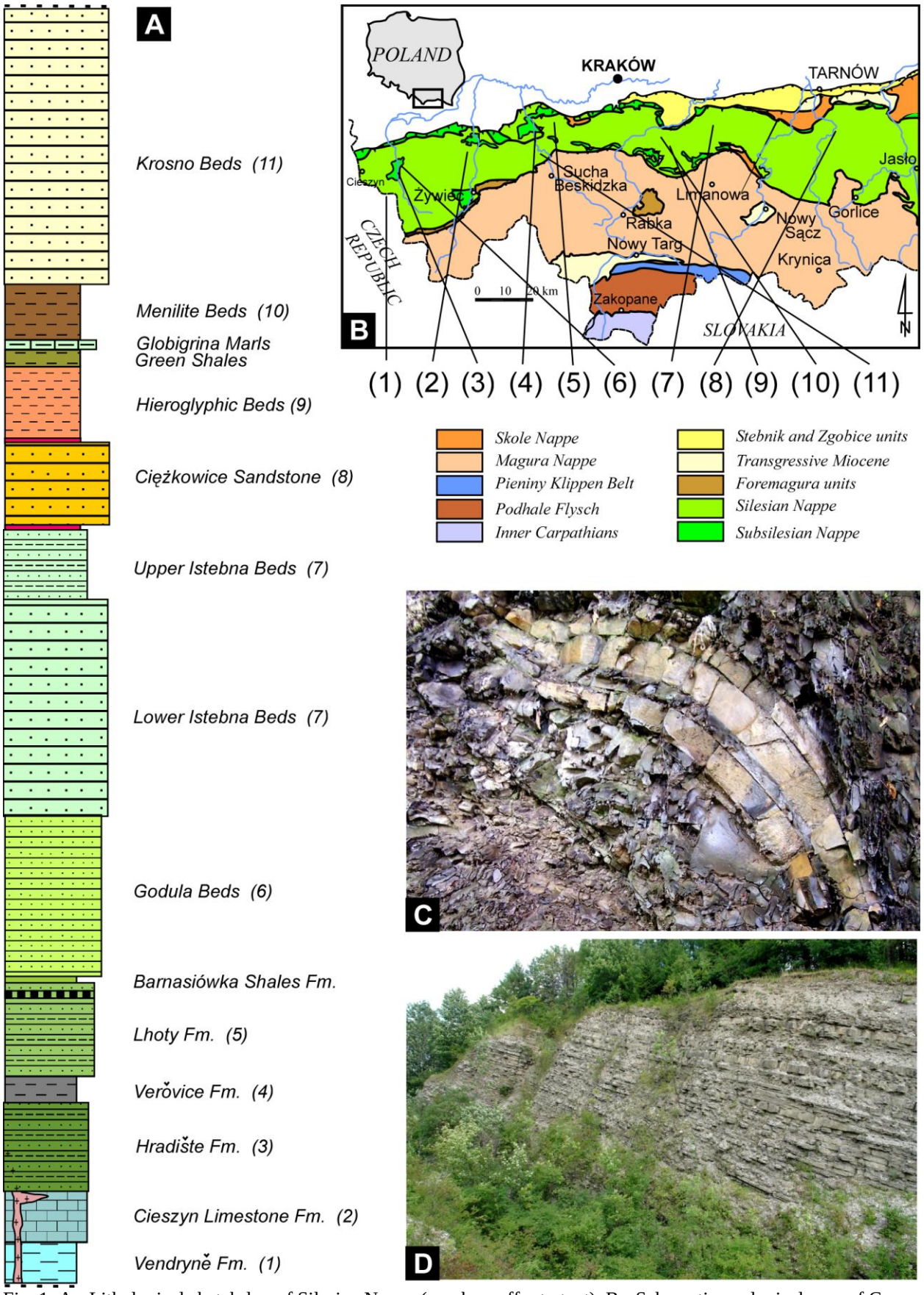

Fig. 1. A - Lithological sketch-log of Silesian Nappe (number reffer to text). B - Schematic geological map of Carpathians; C - Vendryně Fm. (1), Vendryně; D - Cieszyn Limestone (2), Goleszów.

The strongly folded and faulted Cieszyn Limestone Formation with teschenite intrusions can be observed in the natural outcrops along the Soła River in Żywiec. This object is located near the famous Żywiec brewerey, founded by Habsburgs, which produces the best and most famous Polish beer, well known not only in Poland (Ślączka and Kaminski, 1998). The Żywiec outcrop was selected as one of the best eleven geosites in Poland (Słomka et al., 2008). The outcrop displays calcareous turbidites consisting of thin-, medium- and occasionally thick-bedded detrital and pelitic limestones, usually graded, with parallel and cross lamination and occasionally with small sole marks. Marls and marly shales intercalate limestone layers. Limestone beds comprise several debris-flow and submarine slump deposits including numerous fragments and pebbles of detrital and pelitic limestones, organodetrital limestones, marly shales and metamorphic rocks. Pebbles are randomly arranged in a mass of structureless hard marly silt. The Soła river sequence of the Cieszyn Limestone Formation represents a more proximal part of a vast submarine fan while more distal parts are exposed on Cisownica Hill. The teschenite sills in contact with the beds of graded limestone are exposed on the right bank of the Soła river.

3.3. The Hradište Formation (3)

The Hradište Formation (Eliaš et al., 2003) was formerly known as Upper Cieszyn Beds and Hradište (Grodziszcze) Sandstones (e.g. Ślączka et al., 2006) or Tešin-Hradište Formation (Picha et al., 2006). Two members are distinguished with the Hradište Formation (Golonka et al., 2008a): Cisownica Member (Upper Cieszyn Beds) and Piechówka Member (Grodziszcze Sandstones). Good exposure of rocks proposed as stratotype for Cisownica Member (Hauterivian-Barremian, locally Aptian) is located in the Czantoria valley in Cisownica village. Thise post-rift turbiditic sequence consist of dark grey marly and calacreous shales (Ślączka and Kaminski, 1998; Waśkowska-Oliwa et al., 2008). This shales are interbedded by thin-bedded, laminated dark calacreous sandstones and contain also numerous spherosiderites. The layers of detritic limestones sporadically occur within the sequence. The spherosyderites were mined until XIX as the iron ore.

The name Piechówka Member is derived from the name of hamlet in Żegocina (Golonka et al., 2008; Krobicki et al., 2008; Waśkowska-Oliwa et al., 2008) (locality (3) on Fig. 1B). The quarry near this hamlet is the type locality for this lithostratigraphic unit. It was selected as of the best eleven geosites in Poland (Słomka et al., 2008), it is also one of the geosites included on the Polish database constructed by Polish Academy of Sciences Institute of Nature Preservation as a part of the IUGS Global GEOSITES project, carried out by the European Association for the Conservation of the Geological Heritage (ProGEO) (Alexandrowicz 2006). The informational plate, designed by Late Dr. Tadeusz Leśniak is located at the entry of quarry (Fig. 2A). It contains detailed description of the site history and geology. The profile exposes 50 m thick turbiditic sediments with alternating sandstones and shales and typical sedimentary structures like graded bedding, horizontal lamination flow structures and flute marks indicating a northeastward direction of transport. Coarse-grained sandstones contain fragments of redeposited rocks, Carboniferous coal among the others. The sandstones are intercalated by grey shales. Fragments of aptychi have also been found.

3.4. Veřovice Formation (4)

The Veřovice Formation belongs to typical Black Cretaceous organic-rich deposits. Its stratotype is located in Veřovice village, in Czech Republic (Golonka et al., 2008a). The best exposures in Poland serving as a reference section is exposed in the Wieprzówka cascade site in Rzyki village near Andrychów (Kamiński and Ślączka, 1998) (locality (4) on Fig. 1B). The stream valley was deeply dissected by fluvial erosion forming a series of scenic waterfalls and revealing the Lower Cretaceous Veřovice and Lhoty formations. The rocks of Veřovice Formation in Wieprzówka profile are developed as carbonateless, black and heavy-grey, organic-rich shales, locally siliceous with rare intercalations of thin- and very thin-bedded laminated coarser siltstones, fine-grained sandstone, occasionally with spherosiderites (Fig. 2B). The host a variety of tectonic deformations. We can easily identify faults and folds of different geometry. These deformations results from the Miocene Alpine tectonic movements, which formed the Silesian Nappe as part of the Carpathian Mountains. The formation's rocks were deposited during the Early Cretaceous, under the *Oceanic Anoxic Event* (OAE) conditions. Transgressions related to the highest Phanerozoic sea-level and the upwelling contributed to the excessive nutrient supply. The Carpathian basins were producing a large amount of organic matter, preserved due to sedimentary

conditions and to limited supply of terrigeneous material. The Rock-Eval analysis of the Verovice Formation from Rzyki revealed the *Total Organic Carbon* – TOC reaching 2.31 wt % (Golonka et al., 2008c).

3.5. Lhoty Formation (5)

The outcrops of Lhoty Formation are located in the forest slopes of Lanckorona Hill, next to main square of beautiful small town Lanckorona and ruin of historical castle (locality (5) on Fig. 1. B). The old quarries are accessible by the foot-path bearing the name "Alley of Lovers", marked by brown signs, passing historical cottages, and well known by locals and tourists. The exposed Albian-Cenomanian synorogenic flysch sequence contains of thin- and medium-bedded fine-grained siliceous sandstones interbedded by thin grey and dark shales (Ślączka and Kaminski, 1998). The upper part of Lhoty Formation – Cenomanian Mikuszowice Chert Member is exposed behind monumental cottage Pan Tadeusz and in the old quarry in northern part of Lanckorońska Hill (stop on the local foot-path). The gray-bluisch cherts with paralell lamination in sandstones layers are the characteristic features of this member.

3.6. Godula Beds (6)

Sandstones of Godula Beds were mined for a long time as building stones used locally as well as in numerous building in Krakow and industrial Silesia area (Bromowicz et al., 1976; Rajchel, 2005; 2008). Numerous quarries were established, most of them are abandoned now. The Ustroń quarry provide an example of such abandoned quarry used in the past as garbage dump, now cleaned and accessible as perfect geoturistric object (localty (6) on Fig. 1B). It is located on the slopes of Czantoria Mountiain within town limits of Ustroń, famous spa town with numerous hotels and touristic attractions. Thick-bedded turbiditic and fluxoturbiditic greenish sandstones prevail in the quarry (Ślączka and Kaminski, 1998) (Fig. 2C). They represent synorogenic stage of the Silesian Basin development. The areas surrounding this basin were uplifted and supplied clastic material. These material represent basement rocks as well as previously deposited turbiditic sequences. Well visible submarine slumps can be observed in the quarry. They contain large olistolith of redeposited Lhoty Formation.

The thick (up to 2000-3000 meters) Godula sandstones build the Beskid Śląski mountain range, many spectacular rocks are exposed within this mountains (Alexandrowicz, 2008). The best known is Malinowska Rock accessible by foot tourist trail from Salmopolska Pass between Wisła and Szczyrk. The coarse-grained sandstones and conglomerates (Malinowska Skała Conglomerate – stratigraphic unit within Godula Beds) builds several meters high rock cliff.

3.7. Istebna Beds (7)

The splendid outcrops of rocks known typical for Istebna beds (Senonian – Palaeocene), known as Brodziński Stones (Alexandrowicz, 2008; Krobicki et al., 2008) are accessible by educational trail (blue signs) located west of Lipnica Murowana (locality (7) on Fig. 1B). It starts at the parking lot near the country inn (Karczma) offering delicious regional specialties and leads southward across the woods covering the Paprotna Hill. The area is a classic study site and has high educational value especially, for demonstrating rock relief, sedimentary structures typical of fluxoturbidites, and geological setting of rocks (tors) in the zone of Istebna Formation sandstones as well as lithostratigraphic position in the deposit succession of the Silesian Unit (Fig. 2D). The shape of tors has depend on the lithology and lamination of sandstones, the direction of joints as well as on their position with respect to the morphological elements (Alexandrowicz, 2008). The differentiated bedding of deposits, domination of coarse-grained material and traces of submarine erosion characterise fluxoturbidites accumulated by high density turbidite current and debris flows. Features of these sediments are particularly well visible on tors' walls subjected to selective weathering. The Istebna sandstones of Silesian Unit were utilized in outcrops and quarries during past many centuries in local architecture as building stones.

3.8. The Ciężkowice Sandstones (8)

The best place to examine the Ciężkowice Sandstones is their type area – Ciężkowice surroundings (locality (8) on Fig. 1. B). The Ciężkowice Sandstones are important for exploitation providing perfect reservoir rocks in the cradle of Polish petroleum industry since XIX century. Ciężkowice Sandstones consists of four about 100 m thick sandy complexes interbedded by variegated, muddy shales with rich foraminiferal assemblages pointing the Eocene age. Sandstones are usually thick-bedded, fine- to coarse-grained and conglomeratic with many erosinal structures.

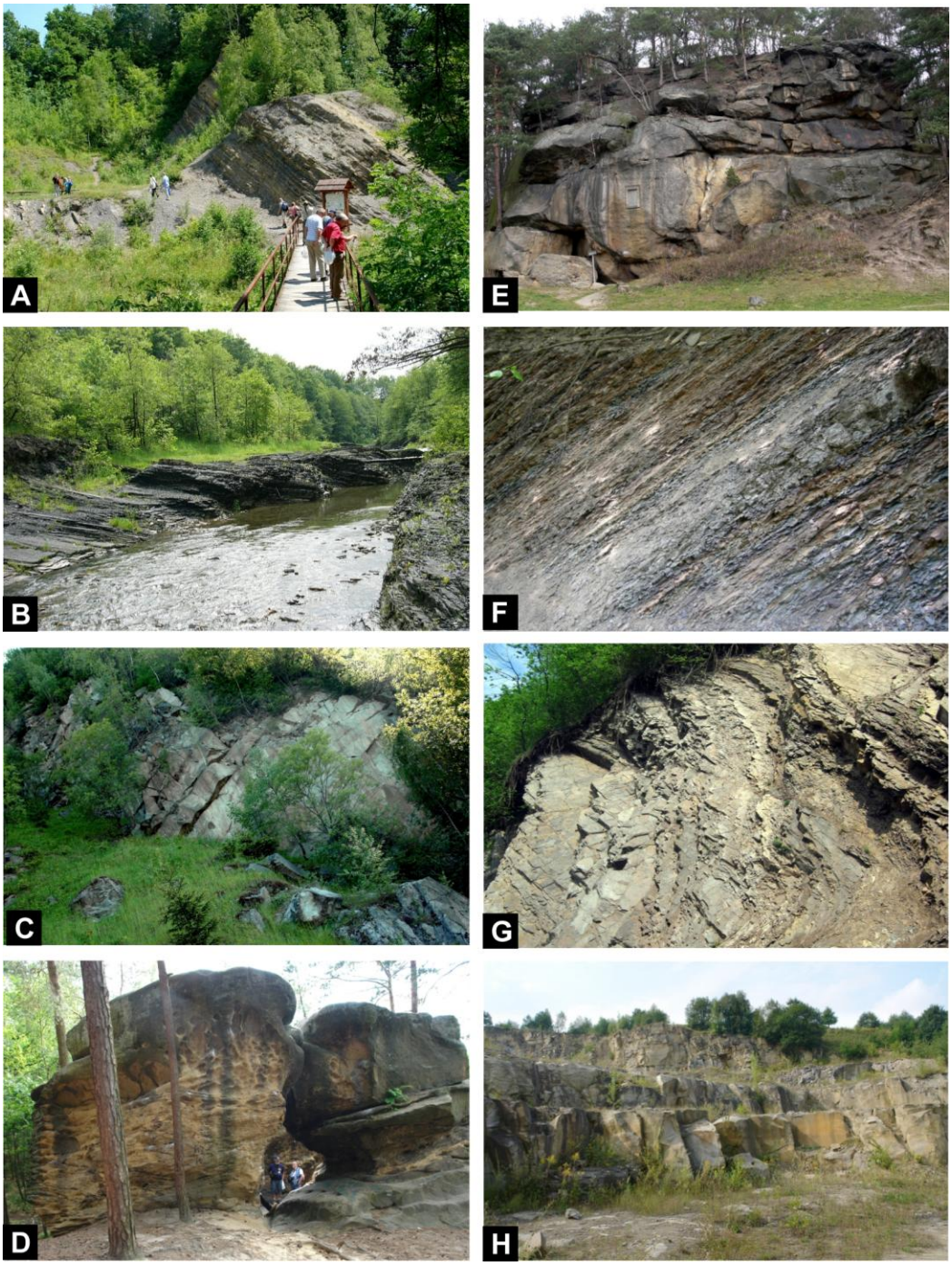

Fig. 2. The best outcrops of Silesian Nappe in Polish sector of West Carpathians. A - Hradište Fm., Żegocina; B - Veřovice Fm., Rzyki near Andrychów; C - Godula Beds, Ustroń; D - Istebna Beds, Lipnica Murowana; E - Ciężkowice Sandstone, Ciężkowice; F - Hieroglyphic Beds, Krzeszów; G - Menilite Beds, Kobielnik; H - Krosno Beds, Mucharz.

Weathering of the Ciężkowice Sandstones produced scenic landforms, as e.g. ”The Petrified Town” (Skamieniałe Misto) in Ciężkowice village or ”The Spinners” (Prządki) near Krosno town. In Ciężkowice various landforms built of eroded Ciężkowice Sandstones form a wide belt, up to 300 meters long on the western slopes of the Skała Hill (367 m a.s.l.) gently descending towards the Biała Dunajecka River (Fig. 2E).

All these landforms were carved along the joint systems cutting steeply dipping, thick layers of the Ciężkowice Sandstones, which reveal diversified resistance against weathering. At the surfaces of

particular rocks numerous hollows and niches are visible, caused by differential weathering.

The landforms are protected by law as one of the oldest nature reserves in the whole Carpathians. The reserve is connected by tourist trail with the Ciężkowice town located about 1.5 km northward. Due to attractiveness and reasonable tourist infrastructure the site is the most popular and most commonly visited Ciężkowice Sandstones exposure in the whole Carpathians (Gruszka, 2008).

3.9. Hieroglyphic beds (9)

The natural outcrops are located in both banks and bottom of Stradomka river in western part of Szczyrzyc Synclinorim (Beskid Wyspowy Mt. Range), opposite of the Devil Stone and hermitage in Krzesławice spot (locality (9) on Fig. 1B). The Upper Paleocene variegated (green) shales occur as green, gray (sporadically with red cherry layers) 100 m thick claystones. Hieroglyphic beds overlaying variegated shales are represented by gray shales with rare thin bedded, fine-grained siliceous sandstones often with parallel- and/or cross lamination and common hieroglyphs (both: organic and mechanic) on the layers bottoms (Fig. 2F). Biostratigraphical analysis from this locality indicates Early – Late Eocene age. Numerous thin layers of betonites in the central part of profile between alternating grey and brown shales with are testimony of volcanic activity during the Middle Eocene times. The outcropped profile is around 150 m thick.

3.10. Menilite beds (10)

Menilite beds (Oligocene) known as main source-rocks for Carpathian oils (Kotarba and Kołtun, 2006) are well exposed in the old quarry in Kobielnik located on the right bank of Kobielnik stream (west slope of Świnia Hill), (Beskid Wyspowy Mt. Range), (locality (10) on Fig. 1B). Brown siliceous organic-rich, bituminous shales, often with muscovite, containing numerous fish fossils prevail in this outcrop. The siliceous menilitic marls and complex of dark thin-bedded cherts, sandstones and shales outcrop in the lower part of profile in the Kobielnik stream (Fig. 2G). Occasionally the thin-medium-bedded sandstones fine- to coarse-grained (with quartz, feldspars, shall and sandy clasts, metamorphic and magmatic rocks as well as coal) are present in the upper part of the profile. The sandstones represent locally reservoir rocks within self-contained petroleum system. Sometimes they are overfilled by oil seeping along joint fractures.

3.11. Krosno Beds (11)

Krosno Beds represent the youngest rocks within the Silesian Unit (Picha et al., 2006; Ślączka et al., 2006). They were formed during Oligocene – Early Miocene synorogenic to postorogenic stages of the geodynamic development of the Outer Carpathians, displaying transition from flysch to molasse. The previously deposited turbiditic sequences were included into accretionary prism, uplifted and eroded together with older basement rocks, supplying material into Krosno Beds. Krosno Beds are widespread in the eastern part of the Polish Outer Carpathians. Near Krakow they are well exposed in the area south of Wadowice, between Beskid Mały and Beskid Makowski mountain ranges (locality (11) on Fig. 1B). In Mucharz quarry thick bedded lower (Oligocene) Krosno sandstones are exposed (Fig. 2H). They contain numerous sedimentary structure, like cross and convolute bedding, lamination, erosional channels, flute casts and other tool marks on the layers bottoms, locally submarine slides. These sandstones were deposited in distributary channels of the inner fan and lobes of the outer fan on the continental rise of Carpathian Basin. They were mined for centuries supplying building stone for local churches, mansions and other buildings.

4. The proposed itinerary

Kraków – Lanckorona – Kalwaria – Wadowice – Rzyki – Bielsko-Biała – Cieszyn – Wędrynia – Goleszów – Ustroń – Wisła – Malinowska Skała – Szczyrk – Żywiec – Mucharz – Kraków – Dobczyce – Stradomka – Kobielnik – Żegocina – Lipnica Murowana (Brodziński Stones) – Ciężkowice – Wieliczka – Kraków.

This itinerary start and ends in Krakow (Unesco World Heritage Site, well known for its Old Town and Royal Castle) and its Balice airport. It includes also historic towns like Lanckorona, Kalwaria Zebrzydowska (another Unesco World Heritage Site), Wadowice (Pope John Paul II birthplace), Bielsko-Biała, Cieszyn (oldest time in southern Poland), and Żywiec (famous brewery and Habsburg palace), Dobczyce (with famous castle on the banks of lake), Wieliczka (famous ancient salt mine also on Unesco World Heritage list). It passes numerous splendid wooden churches, the best known is located in Lipnica Murowana (again Unesco World Heritage Site). It also goes through

scenic mountain ranges. We propose one hiking trip to the Malinowska Skała Mountain in Beskid Śląski. Another mountain tops in Beskid Śląski, Mały, Makowski and Wyspowy are accessible by many foot trails and also by lifts, like from Bielsko-Biała to Szyndzielnia, from Ustroń to Czantoria and from Szczyrk to Skrzyczne.

The user could treat each geotouristic and touristic site separately, according to his or hers desire and interest, starting from Katowice, Zakopane or Ostrava in Czech Republic.

Acknowledgments

This work was supported by AGH grant 11.11.140.447.

References

Alexandrowicz Z., 2006. Framework of European geosites in Poland. Nature Conservation, 62: 63-87.

Alexandrowicz Z., 2008. Sandstone rocky forms in Polish Carpathians attractive for education and tourism. Przegląd Geologiczny, 56 (8 PART 1): 680-687.

Bromowicz J., Gucik S., Magiera J., Moroz-Kopczyńska M., Nowak T. and Peszat C., 1996. Carpathian sandstones and their resources significance and utilization perspectives. Zesz. Nauk. AGH, Geologia, 2: 3-95 (in Polish).

Eliáš M., Skupien P. and Vašíček Z., 2003. Návrh úpravy litostratigrafického členění nižší části slezské jednotky na českém území (vnější Západní Karpaty). Sborník vědeckých Prací Vysoké Školy báňské -TU, Řada hornicko-geologická, Monografie 8: 7-14.

Golonka J., Krobicki M., Waśkowska-Oliwa A., Słomka T., Skupien P, Vašíček Z., Cieszkowski M. and Ślączka A., 2008a. Lithostratigraphy of the Upper Jurassic and Lower Cretaceous deposits of the western part of Outer Carpathians (discussion proposition). In: Krobicki M. (ed.). Utwory przełomu jury i kredy w zachodnich Karpatach fliszowych polsko-czeskiego pogranicza. Kwartalnik AGH. Geologia 34: 9-31 (in Polish with English abs).

Golonka J., Krobicki M., Waśkowska-Oliwa A., Vašíček Z. & Skupien P, 2008b. Main paleogeographical elements of the West Outer Carpathians during Late Jurassic and Early Cretaceous times. In: Krobicki M. (ed.). Utwory przełomu jury i kredy w zachodnich Karpatach fliszowych polsko-czeskiego pogranicza. Kwartalnik AGH. Geologia, 34: 61-72 (in Polish with English abs).

Golonka J., Matyasik I., Skupien P., Więcław D., Waśkowska-Oliwa A., Krobicki M., Strzeboński P. and Vašíček Z., 2008c. Upper Jurassic – Lower Cretaceous source rocks in the western part of the Flysch Carpathians. In: Krobicki M. (ed.). Utwory przełomu jury i kredy w zachodnich Karpatach fliszowych polsko-czeskiego pogranicza. Kwartalnik AGH. Geologia, 34: 73-81 (in Polish with English abs).

Gruszka I., 2008. Natural values and their protection status in the Pogórze Ciężkowickie. Kwartalnik AGH. Geologia, 35(2/1), 77-86. (in Polish with English abs)

Hohenegger L. 1861. Die geognostischen Verhältnisse der Nordkarpathen in Schlesien und den angrenzenden Teilen von Mähren und Galizien, als Erläuterung zu der geognostischen Karte der Nordkarpathen. Justus Perthes, 8: 1-50. Gotha.

Kotarba M. J. and Koltun Y. V., 2006. The origin and habitat of hydrocarbons of the Polish and Ukrainian Parts of the Carpathian Province. In: Golonka J. & Picha F. J. (eds), The Carpathians and their foreland: geology and hydrocarbon resources. American Assoc. of Petroleum Geologists Memoir, 84: 395-442.

Krobicki M., Golonka J., Cyran K., Leśniak T., Strzeboński P. and Toboła T., 2008. Field Trip. Marginal part of Western Carpathians and Carpathian Foredeep. In: Słomka T. (Ed.) 4th International Conference Geotour 2008 "Geotourism and Mining Heritage", 26-28 June 2008 , Kraków, Poland. AGH University of Science and Technology; Faculty of Geology, Geophysics and Environmental Protection, IAGt - International Association for Geotourism: 81-112.

Picha F., Stráník Z. and Krejčí O., 2006. Geology and Hydrocarbon Resources of the Outer West Carpathians and their foreland, Czech Republic.In: Picha F. and Golonka J. (eds), The Carpathians and their foreland: Geology and hydrocarbon resources. American Association of Petroleum Geologists, Memoir, 84: 49-175.

Rajchel J., 2005. The stony Cracow. Spojrzenie geologa. Uczelniane Wydawnictwa Naukowo-Dydaktyczne AGH (in Polish).

Rajchel J., 2008. The Stony Cracow: Geological valors of its architecture. Przeglad Geologiczny, 56: (PART 1): 653-662.

., Mayer W., Słomka E., 2008. Development of geoturism in Poland and examples of geosites from the Catalogue of geotouristic objects in Poland. Przeglad Geologiczny, 56 (8 PART 1): 588-594.

Ślączka A. and Kaminski M. A., 1998. A Guidebook to excursions in the Polish Carpathians: Field Trips for Geoscientists. Grzybowski Foundation Special Publication, 6, 1–173.

Ślączka A., Kruglow S., Golonka J., Oszczypko N. and Popadyuk I., 2006. The General Geology of the Outer Carpathians, Poland, Slovakia, and Ukraine. In: Picha F. & Golonka J. (eds), The Carpathians and their foreland: Geology and hydrocarbon resources. American Assoc. of Petroleum Geologists, Memoir, 84, 221-258.

Waśkowska-Oliwa A., Krobicki M., Golonka J., Słomka T, Ślączka, A & Doktor M., 2008. Sections of the oldest sedimentary rocks in Polish Flysch Carpatians as geotouristic objects. In: Krobicki M. (ed.). Utwory przełomu jury i kredy w zachodnich Karpatach fliszowych polsko-czeskiego pogranicza. Kwartalnik AGH. Geologia, 34, 83-121(in Polish with English abs).

Scientific Annals, School of Geology, Aristotle University of Thessaloniki Proceedings of the XIX CBGA Congress, Thessaloniki, Greece	Special volume 100	467-472	Thessaloniki 2010

THE MANAGEMENT OF A SUSTAINABLE TOURISTIC ACTIVITY AT THE LACU-ROŞU TOURISTIC RESORT – WITHIN THE "BICAZ GORGE– HĂŞMASUL MARE" NATIONAL PARK

Dombay Şt., Magyari-Sáska Zs. and Seer M.

Babeş-Bolyai University, Faculty of Geography, Gheorgheni University Extension, Str. Grădina Csiky Nr. 53, 535500 Gheorgheni, jud. Harghita, Romania, dombay.istvan@gmail.com, zsmagyari@gmail.com, seermihaly@yahoo.com

Abstract: The "Bicaz Gorge – Hăşmaşul Mare" Natural Park belongs to the Central Group of the Eastern Carpathians, it is located in the Hăşmaşul Mare Mountains. Due to its natural characteristics, geological, biological, zoological, components, these 2128 ha, in 1980, then in 1995, were denounced as Natural Reservation by the County Council. In 2000, under the 5th law, 3rd paragraph, of National Territorial Planning and Administration, the 6575 ha, of The "Bicaz Gorge – Hăşmaşul Mare" region was declared a Natural Park, altogether with the Lacu Rosu Lake Tourism Resort. In the management of the "Bicaz Gorge – Hăşmaşul Mare" Natural Park we should consider three points of criteria: the management of the inland, the management of border areas (buffer areas), the management of the surrounding settlements, around the national park.

Keywords: Natural Park, sustainable tourism, Lacu-Roşu, SWOT analysis

1. Approaching Lacu-Roşu

The tourist resort, is situated 35 km from the town of Bicaz and 25 km distance from the town of Gheorgheni, over the Pângărați pass (1254 m), that is part of the national road 12C, that connects Transylvania to Moldavia.

Jurisdictionally belongs to the town of Gheorgheni. The appearing and development of the resort is closely linked to this town. Gheorgheni was first mentioned in 1332 in a papal census. Its development through time is closely related to the development of the sekler society's development. Its harsh and cruel history (social ranking – horsemen, footman, serfhood – the Mongol invasions, plague, Austrian dominance, the 1848 revolution, the first and second World Wars, the slow evolution of capitalism, centralization of power, socialist economy, the disappointments that fallowed the 1989 changes and the not so favorable climate) led to the closing in of the population, that became weary, suspicious and held back.

The 25,000 people, who live in Gheorgheni, are in majority Hungarians, and the town is the biggest one in the Gheorgheni basin, and an important starting point to numerous touristic attractions (Borsec, Praid, Sovata, Lacu-Roşu Lake, Miercurea Ciuc).

On the eastern side of the city, near the road that leads to the Lacu-Roşu Lake, lies the 77m long, 33m wide, elliptical shaped Both Castle, which was built at the end of the 15th century and the beginning of the 16th century, and its tale has to do with Rákóczi Ferenc the 2nd's revolution. Further up the Belchia creeks valley, near the 4th Km, another cheek enters the main stream, where a fine tourist resort was established, where wooden cabins and huts, a motel, ski slopes for beginners, a lake measuring half a hectare awaits the adventurers. At the 5 Km mark there was established the finest and best established ski slope of the region, with ski lift in the lower part of the course.

Further upstream at km 6 and 7 two more creeks join the Belchia, the Cerbul spring (5+800m), and the Cianod brook (6+600m) and the water collector of the town is located. After this the main brook heads north.

The next important stop is located at Km 9, where a fine restaurant is located at the juncture of the Moghioroş brook with the Belchia brook, from here the road ascends 300m, in just 15 km, to the

Pângărați pass (1257m), located under the Pângărați peak, from where one can have an outstanding panorama over the whole valley and mountain range.

The Pângărați Peak is an important point, from here marked trail (red stripe) leads to the Călimani mountains, fallowing the main crest of the Giurgeului Mountains. The trail marked with a blue stripe leads the adventurers to the Ceahlău Reservation. The red stripe that heads south west, fallows the main crest of the Hăşmaş Mountains and leads to the Ciuc Mountains.

Descending from the Pângărați pass, we travel near pine forests, and beautiful brooks, on some of these were constructed alluvium stopping dams, and finally as we reach Km 21 we have the first glimpse of the Lacu-Roşu Lake, and in the background we see the Suhardul Mic.

One of the Hungarian travelers, Orbán Balázs, in its book: "A Székelyföld leírása" (the description of Sekler country) relates that the view that greats any tourist is as catching as any unforgettable view of the Swiss Alps, or north Italy's landscapes, not as big, but remarkably beautiful and breathtaking (Fig. 1).

Fig 1. Weekend houses at Red Lake.

The road passing the Oii brook arrives on the right side of the lake, fallows the shoreline of the lake till we reach Km 25, where we will find the boat renting small harbor.

The trail that fallows the Oii brooks valley, leads to the Poiana Albă Peak, from where the tourists can reach the main crest of the Hăşmaş Mountains, that leads to the mountain cabin at the Piatra Singuratică (Lonley) Peak, on the trail marked with a red stripe.

2. The origin of the lake

Though the lake is relatively young, its origins are still disputed. In the time of its formation no commercial roads led through its valleys, it was difficult to reach it, a document mentions it in 1835, from the town of Bicaz (Dombay, 1998).

Geologist, Bányai János, argues the year 1837, Herbich Ferenc argues 1838 for the formation year of the lake, when an earthquake was noted in January, 1838, that was repeated in February. Maybe this contributed to the landslide that means the origin of the lake. The arguments about the year 1837, talk about the heavy rains and storms in 1837, mentioned by Puskás Ferenc from Ditrău, in its work: "Borszék Története" (History of Borsec Spa).

There are several examples of lakes formed behind massive landslides, is the natural dams are consisted of porous weak materials, the life of the formed lakes is little, they are formed rapidly, and just as they appear they disappear. The Lacu-Roşu Lake has is in a more fortunate situation, its dam is still strong in spite of the harsh meteorological conditions, holding back the water behind it.

Even now we can notice the landmass blocking the valley of the Bicaz River, at the foot of the Suhardul Mare Mountain (Fig. 2).

Fig 2. Suhardul Mare Mountain.

3. How did it get its name?

Some writers noted the lake as "Lacu-Roşu" meaning Red Lake, the name appearing in the works of Károly Benkő (1853), Ferenc Herbich (1866), but the last author in 1878 names it: "Lacul Ucigaş" meaning "Killer lake". Orbán Balázs is the one who uses the name *Killer Lake* more frequently, and due to him it became so well spread in com-

mon knowledge. Probably it got its name from the Ghilcoş Mountain, (Killer Mountain), its name-origin is much older, mentioned as part of the Lázár Family's estate, in 1773.

4. The legend of the lake

Orbán Balázs (1871) does not mention in its work the origin of the lake, this matter is firstly presented by Nándor Urmánczy, in 1895, according to him an old sekler fisherman told him the story about the lakes origin.

A villain living in the Suhardul Mare cave, kidnapped the beautiful Ferenc Anikó, the girl cried so much that the walls of the cave opened and the spirit of the mountain took the girl into its depths, the villain became very angry and with its club rammed the wall of the cave so hard that the whole mountain collapsed. The legend has a couple of variants, known in the common knowledge now.

5. The lakes position and limits

The longer branch of the lake, formed behind the natural barrier is north oriented, the shorter branch is east-west oriented. At its beginning the lake's longer branch reached as far back as Veresszakál massif, of the Luhaşul Mountain. Nowadays the southern part of the lake the Oii-Lacu-Roşu-Licas brooks confluence forms, which are well sedimented and swampy. In the east the slopes of the Ghilcoş Mountain (1384m), in the west the Licaş corner foothills border the lake.

6. The dimensions of the lake

The original dimensions of the lake are presently uncertain, Ferenc Herbich tried to measure the lake, but he warns the readers about the inaccuracy of his measurements in 1859. His measurements were noted and recalculated (750 fathoms long <750*1.83m>, 120 fathoms wide <120*1.83m>, its surface 56*0.57 hectares). By the 1864 census, the surface of the lake is noted as being 36*0.57 hectares. The depth of the lake wasn't measured just estimated by the height of the tree trunks that emerge from the water, having figures between 15-40 m.

Accurate measurements were done by Ion Pişotă and A. Năstase in 1955, and since 1966, these are the figures on which all calculations rely on. The scientifically done measurement's only defect is that the resulted geometrical form after the measurements didn't correspond with the pictures drawn about the shores of the lake.

Since then the figures and area of the lake is constantly changing, and this requires periodical renewing of the existing database.

In 2002 professor Pándi and crew from the University of Babeş Bolyai, Faculty of Geography, remeasured the lake, the Oii Brook branch measures 900 m, average width 134 m. The Suhard brook branch of the lake measures 438 m long, width 62 m, maximum with 83m. The lakes surface measures 116532 m^2, its volume 643704 m^3, its perimeter 3044 m, its maximal depth 9.63 m close to the outflow (Pándi and Magyari, 2003).

The lake extends in two directions, southwards (on Oii brook) and westwards (on Suhard brook). Its shape is close to a boot or a letter L (Fig. 3).

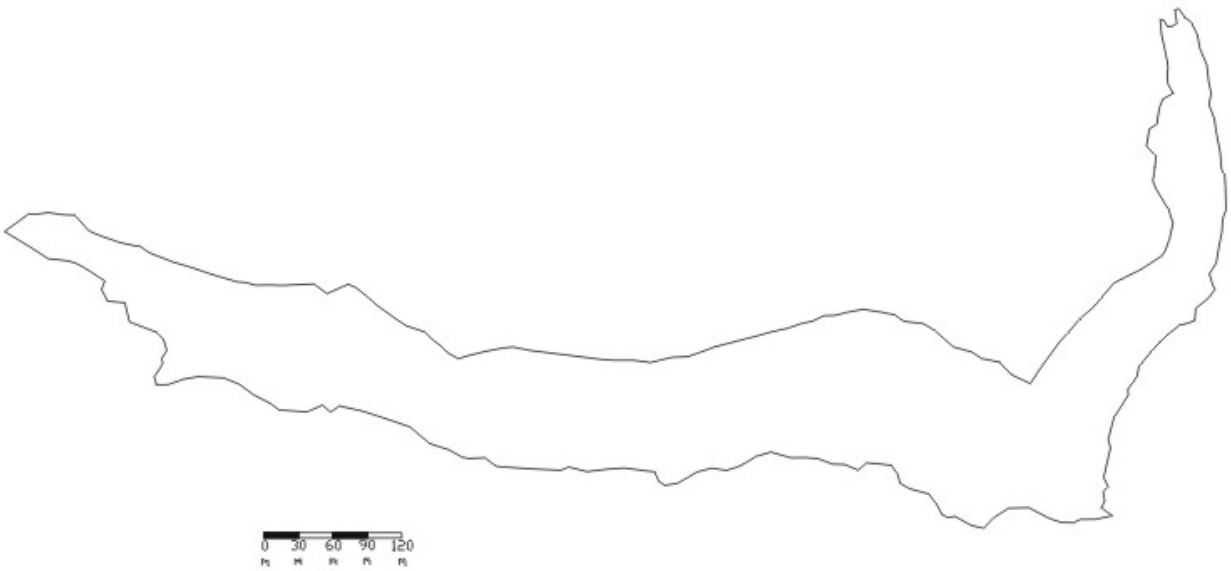

Fig 3. The actual shape of Lacu-Roşu.

The slide that blocked the valley of these brooks, the trees in the lower part of the slopes were covered by the lake's waters, and are still standing in the lake, as remnants of the old forests that existed there. The water, that exits the lake, is the spring of the Bicaz River (Fig. 4).

Fig 4. The Bicaz brook.

The lake is supplied by four major brooks: Oii, Suhard, Piatra Roşie and Licaş, a smaller one: Ghilcoş Brook, and 13 temporary watercourses.

In rainy seasons the watercolor is reddish, brownish, in dry seasons is light green and transparent.

7. The extinction of the lake

From extinction the lake can be saved for a while but not for good. In the beginning just after its birth the lake lost some of its water because of the barriers constitution, the upper, less resistant and soluble soil was first diluted and transported, then the remaining rock formations were segmented and cut through. When the level of the lake reached the less soluble and hard rocks of the barrier, its decrease diminished, and by this the only extinction factor that remained is the siltation of the lake (Ciangă, 1997).

All the affluent bring a lot of alluvium, that is deposited at their entrance in the lake, factor enforced by the tree cuttings and logging done in the area.

The most dangerous brook is the Oii, but the other 3 major brooks contribute to this phenomenon. Initially all 4 entered individually the lake, but now, the Ghilcoş brook enters the Oii, and the Roşu Brook after joining with the Licaş brook also end up in the Oii brook. So alluvium catching artificial dams were made to slow down the siltation of the lake. On the Ghilcos brook a barrier was made in 1913, on the Piatra Roşie and Oii brooks dams were made in 1954, but the one on the Oii was destroyed in 1975 and on the Suhard one wasn't built so far.

Another factor that leads to the slow extinction of the lake is the extension of the back vegetation. Some shallow areas, are covered by Potamogeton natans. In swampy areas plants like Sparganium erectum, Glyceria, Equisetum fluviatile, Poa trivialis and Ranunculus repens find home.

To the extension of the vegetation the logs that become loose from the bottom of the lake contribute largely. On these logs after a while other plants raise roots, contributing to the view of the area but destroying it in the same time as well. So human intervention just delays these processes, but it can not stop them.

On the other hand, the industrial activities contribute for quite some while to the degradation of the lake (Roşu, 1980). Since 1895, when the first mill, and barracks for the workers were built on the southern part of the lake, and the first pub and store was established, a lot of sawdust and other leftovers got into the lake, and by the building of the roads that lead through the gorge today, after the explosions all the materials were washed into the lake.

The originality and charm of the lake is affected by the choked forest's disappearance. Limestone is deposited on the tree trunks, algae and other dissolved minerals cover the trees, after a while changing their balance, they detach and then float on the surface, drifting to the entrances of the brooks, where they get stuck in the shallows. And some boating tourists contribute to this as well, to enlarge the visitable areas (Dombay, 2002).

Otto Herman in 1871 writes about the flooded forests death: the pine trees struggled with the new, unnatural conditions, but eventually died. Slowly the needles fell off the branches, the bark of the trees fell off, and the elements of the nature whitened out the remaining trunks. They look like skeleton arms rose to the skies asking for an answer (Fig. 5).

By the development of tourism a great amount of trash landed in the vicinity of the lake (plastic, glass, paper, domestic garbage, rubber, metals, etc.).

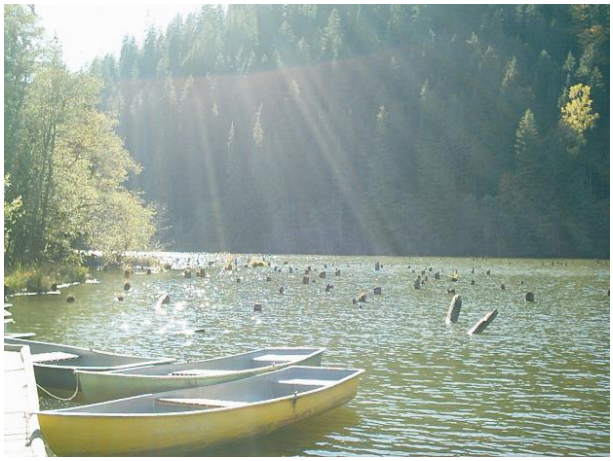
Fig 5. The Red Lake.

8. The natural values of the lake and surrounding area

The forces of nature formed a breathtaking landscape here in the Hăşmaş Mountains, presenting a varied relief (Tab. 1), with narrow corridors and steep walls, dolinas, underground water systems, caves, uvalas, rock slides, etc. the classification of the caves (Ciangă, 2001):

- Licaş cave (gully hole): its entrance on the top on the Licaş Peak (1675m), thought bottomless, formed is limestone vertically, its depth 51 m, from its 8 m wide entrance the gully hole is 37.5 m deep, where a permanent ice and snow formation can be found.
- The Piatra Vitoş tectonic cave (1609), in the eastern part of the limestone mountains, formed by three caves having tens of m in depth.
- The caves along the Bicaz river, numerous, more then 51, the most significant one is the Ghiocelul (Snow flower) cave, measuring 28 m in length, 26 m wide, discovered in 1973. Initially it was full of stalactites, stalagmites and pillars, but till it was made reservation it was destroyed.

After the last glacial age this area was and is a resting point in the path of the migrating flocks of birds.

9. Protected plants and wildlife

Plants: edelweiss, yew tree, globe flower, thyme, Romer grass, primrose, etc.

Animals: lynx, chamois, brown bear, muscardine, weasel.

Birds: crow, black woodpecker, tichodroma.

10. SWOT analysis

Strong points:
- lies near a main national road;
- rare and protected natural resources:
  - numerous relief formations in limestone: Suhardul Mic, Cupaş, Şugău cave;
  - unique natural resource: Romania's only naturally formed barrier lake;
  - a healthy climate, long lasting snow (till april);
  - rich and protected wildlife;
  - rich in birdlife;
  - specific mountain vegetation, rare, endemic plants, area suitable for multiple purpose forms of tourism:
    - resting tourism;
    - adventure tourism;
    - climbing tourism on the 47 acknowledged and marked trails;
    - winter sport tourism;
    - speotourism;
    - hunting parties;
    - fishing;
    - ecotourism;
    - transition tourism.

Weak points:
- concerning the general infrastructure and equipments:
  - the bad condition of the roads;
  - the absence or the aging of the existing drinking water system;
  - the absence of a filtering station;

Table 1. The "Bicaz Gorge-Hăşmaşul Mare" National Parks protected areas

Location	Area (ha)	Category	Notes
Bicaz-Hasmas national Park	6937.09	Protected area	No local administration
Licas cave	5	Speological reservation	Belongs to the National Park
Bicaz Gorge, Lacul Rosu Lake	2128	Natural reservation	
Hasmasul Mare, Piatra singuratica Peak, Fekete hagymas Mountains	800	Natural reservation	
Buffer area			Holds the refiries of the Natural Park
Transit area			Holds the agricultural and lived areas in the vecinity.

- bad street lighting;
- the absence of centralized heating;
- the bad management of waste dumping, collection and disposal.

- other needs and lack of equipment:
  - appropriate health care;
  - cultural infrastructure;
  - safe parking spaces;
  - the degradation of the majority of the housing facilities;
  - constructions raised illegally;
  - administrative problems raised in the dispute of the drawing of the county borders with the neighboring county;
  - entertainment, relaxation and recovery facilities;

The strong points and the weak points give enough information so that we can start working on a management program (Tab. 2) on efficient and sustainable touristic activities.

Table 2. A management plan for a sustainable touristic activity within the Bicaz-Hasmasul Mare Natural Park

Required steps	**Goals**
The building of a visiting center within the park	Functioning an information center.
Putting together information packages and selling them.	Harmonized advertisement.
Presenting the plant life of the N.P.	Posting the rules of personal conduct, and decreasing inappropriate behavior.
A better usage of local means of transportation.	Better, environmentally friendly means of transportation.
Improving the road conditions.	Controlling the movement of tourists.
Marking camping grounds, walking and biking trails.	Monitoring the active touristic activities.
Building appropriate housing facilities.	Improving the housing conditions.
Improving the quality of services provided: tour guides, equipment rentals.	Involving the local population in these activities.
The introduction of ecotourism.	Attracting specific groups of tourists with special interests.
Studying the behavior of the tourists.	Decreasing the negative impact of tourism upon the environment.
Interviewing with questioners.	Interviewing the tourists about their needs and comments.
Integrating the activities in a national and international system.	Establishing information points at the entering points of the N.P.
Marking the boating routes on the lake.	Protecting the flora and fauna of the lake.

References

Ciangă N., 1997. Tourism in Easter Carpathians (in Romanian), Cluj University Press, Cluj, Romania.

Ciangă N., 2001. Romania. Tourism Geography I. (in Romanian), Cluj University Press, Cluj, Romania.

Dombay Șt., 1998. The Recreation Spas in Harghita county (in Romanian with English abstract), "Dimitrie Cantemir" Ecological University, Târgu-Mures, Romania.

Dombay Șt. et all, 2002. The rehabilitation of tourism in Lacu-Roșu (in Romanian), Romanian Ministry of Tourist research, Bucharest, Romania.

Orbán B., 1871. Description of Székelyföld (in Hungarian), Tettey Nándor and co., Pest, Hungary.

Pandi G., Magyari Zs., 2003. The creation of batimetrical maps using computer. The Lacul Rosu model. (in Romanian with English abstract) Studia Universitatis "Babes-Bolyai", Geographia, XLVIII, 2, Romania.

Roșu Al., 1980. Physical Geography of Romania (in Romanian), Didactic and Pedagogical Press, Bucharest, Romania.

***, 1984. Geography of Romania. Physical Geography (in Romanian), Romanian Academic Press, Bucharest, Romania.

Scientific Annals, School of Geology, Aristotle University of Thessaloniki Proceedings of the XIX CBGA Congress, Thessaloniki, Greece	Special volume 100	473-482	Thessaloniki 2010

UNDERGROUND GEOTOURISTIC ROUTES IN THE MAŁOPOLSKA DISTRICT

Dzięgiel M.

Upper Silesian High School of Business (GWSH), Katowice, Poland, md@ip.krakow.pl

Abstract: In the Małopolska District two underground routes located in old mine workings have been opened to the public. They were developed in the Forecarpathian Basin, in the salt mines in Wieliczka and Bochnia. The salt deposits are hosted in Tertiary - Miocene formations accompanied by anhydrites, gypsum and clays. From the south, these formations are surrounded by the sandstones and shales (flysch), which belong to the Carpathian Foredeep. In both the salt mines in the tourists visit the old mine workings, mainly in the form of spacious chambers and galleries. In those mines the visitors experience a small boat trip across the underground sweet lakes. In Bochnia's salt mine visitors are also carried by the historical underground railway along 1km distance. Those salt mines are very popular underground health resorts. People ill of breathing system can spend there some time for inhalation.

Keywords: geotourism, mine, working, salt

1. Introduction

Salt mining in the Małopolska District has been known from the medieval times. It was exploited from the underground in two towns, Wieliczka and Bochnia (Fig. 1) since the late XIIIth century. Both in Wieliczka and Bochnia it was stopped in 1996 for the economical reason. Wieliczka is situated very close to Cracow. Bochnia is 30 km east from Cracow (Fig. 1).

Some parts of the old, closed salt mines in the Małopolska District have already been opened for the public. Up today, there have been made sightseeing underground routes there. In such a way, the salt mines in Wieliczka and Bochnia were transformed into museum complexes. The visitors can see there plenty of very nice chambers and galleries, the most interesting workings and experience the boat trip across the underground sweet lakes.

In Bochnia's salt mine are some more attractions. The historical underground railway carries the visitors along the distance of 1 km there. There is also an underground playground for basket-ball, a room for rehabilitation and a bedroom.

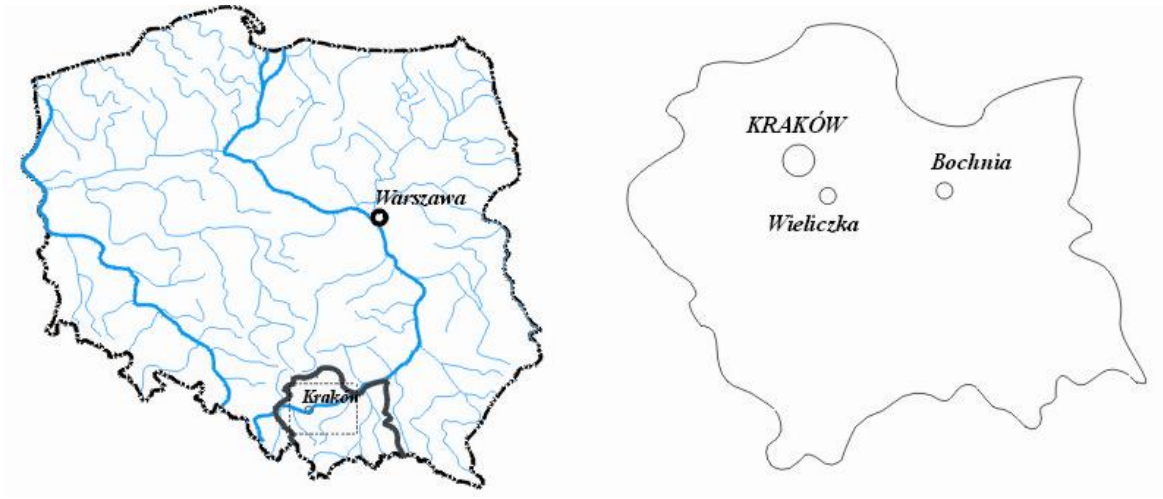

Fig. 1. Location of the Małopolska District and some of its cities and towns.

The salt mine in Wieliczka is so interesting and important that it has already been known all over the Europe for decades and ages. In Bochnia, it was opened for the public much later than in Wieliczka but it can also become popular all over the world.

2. Geological structure of the northern part of the Małopolska District area

Both Wieliczka and Bochnia are located on the border between the Forecarpathian Basin and the Carpathian Foredeep (Fig. 2, 3, 4, 5). The area between Wieliczka and Bochnia is composed of Upper Jurassic, Cretaceous, Tertiary – Miocene and Quaternary sediments. The Upper Jurassic rock is limestone there (Fig. 3). It is covered by the Miocene - Badenian formation, hosting salt deposits, which occur all over the area.

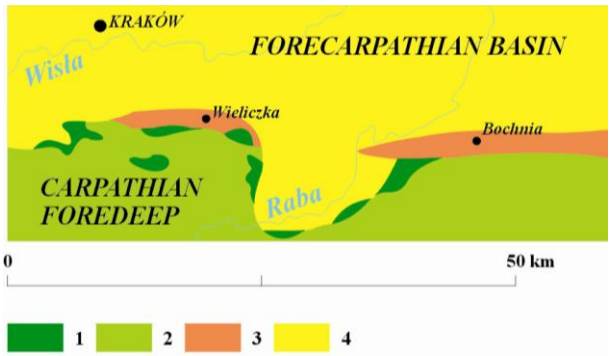

Fig. 2. Forecarpathian Basin and Carpathian Foredeep (Książkiewicz, 1972). 1- Under Silesian Nappe (Cretaceous), 2- Silesian Nappe (Creataceous), 3- Salt deposit (Miocene), 4- Autochtonic Miocene.

The Miocene–Badenian formation around Wieliczka and Bochnia is divided into four stratigraphic series: the Skawina beds, Wieliczka beds, Chodenice beds and Grabowiec beds. The Skawina beds include dark clays and marl claystones (Garlicki 1968; Połtowicz 1977). The Wieliczka beds include the main salt seams in this region. They consist of halite, anhydrite and gypsum with addition of clays and claystones. The full profile of this unit is outcropped in the salt mine in Wieliczka. Its thickness is of 30 – 100 m (Fig. 3). That series is characterised by cyclic evaporate system comprising five series. Those are evaporates of Proszówki, Łężkowice, Bochnia, Kłaj and Szczepanów (Garlicki, 1994). Their thickness is 4 – 30 m on average. The evaporates of Proszówki and Szczepanów are the most important ones. The Proszówki evaporates consist clays and sulphatate sediments. The Szczepanów evaporates include anhydrites and marl claystones with halite. There also happens to occupy some tuffs and bentonites among the clastic sediments (Fig. 4, 5) (Garlicki, 1979; Wiewiórka, 1979; Bukowski et al., 1996; Bukowski, 1999; 2000). Salt seams located close to the Carpathian Foredeep are especially tectonically disturbed and often over folded (Poborski, 1952; Poborski and Skoczylas-Ciszewska, 1962; 1963; Połtowicz, 1977). The Chodenice beds are composed of grey claystones with some tuffs. Their thickness does not exceed a few hundred meters (Olszewska, 1999). The Grabowiec beds consist of sands and clays. Their thickness is also about a few hundred meters (Aleksandrowicz, 1962; Garlicki, 1968; Peryt and Piwocki, 2004).

In the southern part of the Forecarpathian Basin, occur flysch rocks belonging to the Carpathian Foredeep. These are mainly sandstones, mudstones, shales and marls. They belong to the Silesian and Sub Silesian nappe. The whole described area is covered by Quaternary weathered loams, river sands and gravels (Fig. 2,3,4,5).

Miocene salt seams were deeply folded under the pressure of the Carpathian orogen (Książkiewicz, 1972; Jodłowski, 2000). In Wieliczka, two kinds of salt deposits are distinguished: sedimentary and blocked (Fig. 3). In Bochnia, flysch rocks occur also in the central part of two steep salt folds (Fig. 4).

3. Salt mine in Wieliczka

The origin of salt mining in the area of the present town of Wieliczka took place probably in the Middle Neolithic (3 500 BC). It is supposed by the old traces of the first plant in which salt was manufactured from the brine just there. Large-scale salt mining in Wieliczka began in the 1280s. The Goryszowski shaft connected with that was then discovered in the courtyard of Żupny Castle in Wieliczka (Piotrowicz, 1968; Reguła, 1969).

The golden age of Cracow's salt mines was between XVIth and mid-XVIIth century. Production exceeded 30,000 tonnes then and the salt was exploited at three levels. During that period, eight shafts were on. Among them was the Daniłowicz Shaft, which is currently used for tourist purposes (Fig. 7, 8). In result of prolonged wars, plagues and the accompanying natural disasters the safety work was neglected by the miners (Długosz, 1958; Keckowa, 1965).

Under Austrian management (1772-1918) salt production was greatly increased, which made the great

development of the Wieliczka salt mine again. New technology of mining operation was found. It was mechanized by the new steam and electric machines. Professional engineering staff was beginning to be employed and the first tourist route there was created (Markowski, 1978; Dziwik, 1980).

After a time, salt exploitation was becoming extensive, so current safeguarding started to be neglected. In result of that, the stability of the rock mass and the condition of the mine were broken down. It was even planned to flood the salt mine after the Second World War. The exploitation was

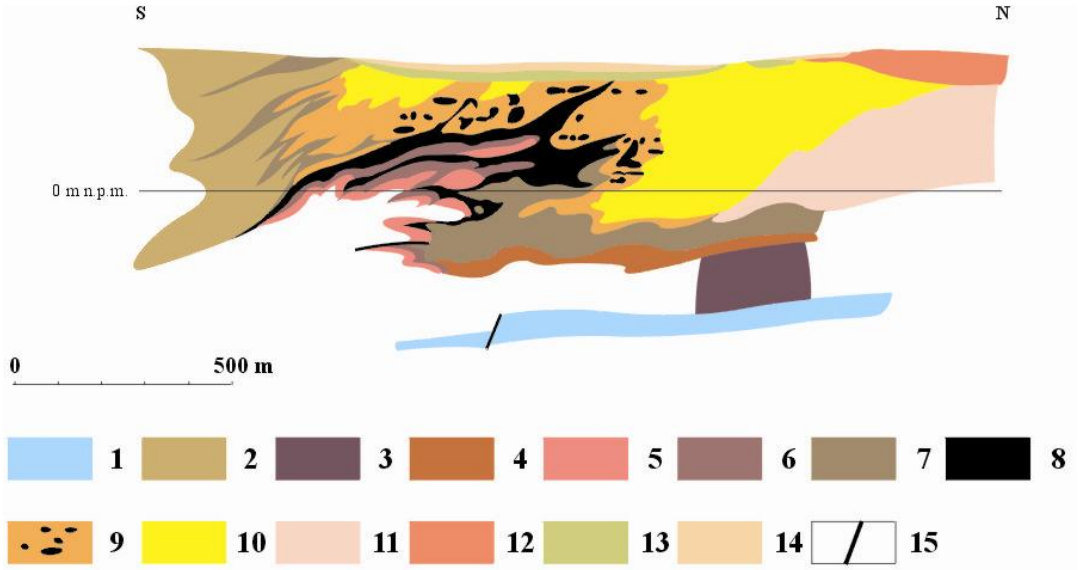

Fig. 3. Cross section through the salt deposit in Wieliczka (Poborski, Skoczylas-Ciezewska, 1968. 1-Upper Jurassic (limestone), 2-Carpathian flysch, 3-11-Lower Badenian, 3-5-under salt beds (3-marly clay, 4-sandy clay, 5-conglomerate and sandstone, 6-anhydrite clay with green salt, 7-anhydrite clay, 8-sedimentary salt, 9-salt clay with blocky salt, 10-clay with flysch material, 11-Chodenice clay, 12-Grabowiec beds (Upper Bademian), 13-gypsum, 14-Quaternary, 15-faults.

A new modern salt-boiling plant in Wieliczka was installed in 1913. It created a number of workplaces and prospects for the increase of salt production for a long time, especially in the inter-war Second Polish Republic. It was possible because of the new technology of salt leaching under ground.

going to be finished in 1964 (Piotrowicz, Grzesiowski, 1977) and was completely over in the mid 1996.

At present, the picturesque old salt workings serve tourism, museum and health purposes. The number

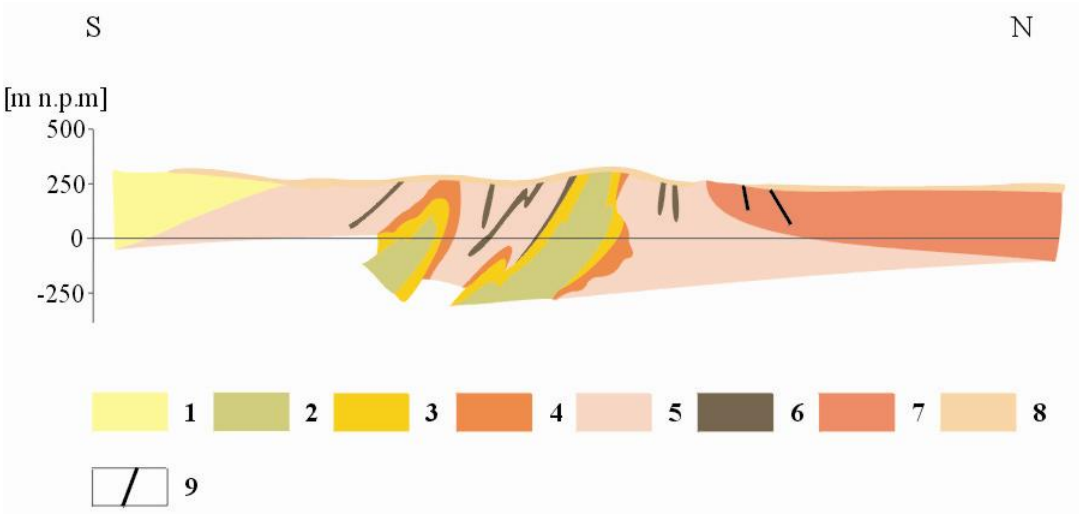

Fig. 4. Cross section through the salt deposit in Bochnia (Poborski, 1952). 1-flysch of the Carpathian Foredeep, 2-flysch in the centre of the salt folds, 3-sediments under salt deposits, 4-salt sediments, 5-Chodenice beds, 6-tuff in Chodenice beds, 7-Grabowiec beds, 8-Quaternary cover, 9-faults.

of the old excavations is growing very fast. During seven ages, 26 surface and 180 smaller shafts connecting different levels of the mine were excavated. The exploitation of the salt deposit was made on the nine levels on between 57 – 327 meters under ground. In consequence, 2 350 chambers and over 240 km of galleries were carved. For better protection of the most valuable excavations, a historic zone has been delimited in the salt mine in Wieliczka. Up to 2004, it embraced 218 galleries and 190 chambers al levels I – V. Over 20 of them is available for the visitors in the Tourist Route (levels I – III) and 16 at the Museum of Cracow's Salt works (level III) (Jodłowski, 2000).

In the Spalone Chamber tourists can be reminded that methane explosions were a very great danger for the mine in the old times. There is illustrated the work of the experienced miners, named "penitents" who burnt out the colourless gas accumulating under the chamber ceiling. They were doing so with torches on the long poles, crawling on the floor of the excavations (Majka, 1996) (Fig. 7).

The Sielec Chamber presents authentic device used for salt transportation in underground galleries (Fig. 7). The old miners used wooden carts, named "Hungarian dogs", chests, and special sledges. Fine salt was put into barrels and carried on the

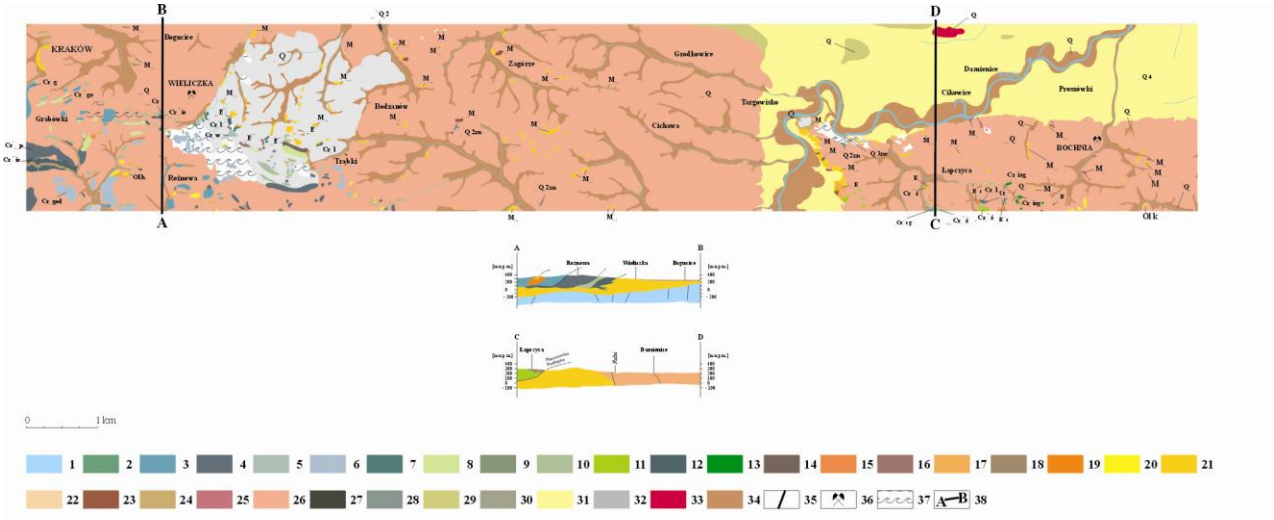

Fig. 5 Geological map of the area between Wieliczka and Bochnia (Burtan, 1954, Skoczylas-Ciszewska, Burtan, 1954)
1 - limestone (J) *2* - Cieszyn Lower beds (arrow sandstone and shale (Cr cg)) (Silesian nappe) *3* - Grodzisk beds (shale) and Cieszyn Upper shale (Cr g) (Silesian nappe) *4* - Grodzisk beds in general (thick grain sandstone and conglomerate (Cr p)) (Silesian nappe) *5* - Wierzów shale (shale) (Cr w) (Silesian nappe) *6* - Lower spong beds in general (shale and sponge (Cr ged) (Silesian nappe) *7* - Lgota beds in general (sandstone and shale) (Cr l) (Silesian nappe) *8* - sponge beds in general (shale and sponge) (Cr ge) (Sub Silesian nappe) *9* - patchy shale (Cr) (Silesian nappe) *10* - patchy marl (Cr) (Silesian nappe) *11* - Żegocina marl (Cr ż) (Sub Silesian nappe) *12* - Istebna beds (Tomaszkowice sandstone) (Cr is)) *13* - Upper Istebna beds in general (sandstone and conglomerate (Cr isg) (Sub Silesian nappe) *14* - green shale and siderite (E) (Sub Silesian nappe) *15* - Ciężkowice sandstone (E) (Sub Silesian nappe) *16* - siliceous and glauconitic (E) (Sub Silesian nappe) *17* - patchy shale (E) (Sub Silesian nappe) *18* - patchy shale (E) (Sub Silesian nappe) *19* - menilite shale (with chert) (OE) (Sub Silesian nappe) *20* - Krosno beds in general (sandstone and shale) (Olk) (Silesian nappe) *21* - Chodenice beds in general (grey and black clay with tuff) (M) (Tortonian) (Tortonian = Lower Badenian) *22* - tuff (M) (Tortonian) *23* - gypsum (M) (Tortonian) *24* - Bogucice sand (sand from Bogucice and Rajsko) (M) (Tortonian) *25* - Grabowiec beds in general (sand and shale clay) (M) (Tortonian) *26* - dusty loam (Q) (Plejstocene) *27* - water glacier sand (Q 2) (Plejstocene) *28* - the highest terrace gravel (Q 2zn) (South Poland Glacier) *29* - "mixed" gravel (Q 3) (Middle Poland Glacier) *30* - the old high terrace gravel (Q 3zw) (Middle Poland Glacier) *31* - loam and gravel of low accumulation terrace (Q 4) (Baltic Glacier) *32* - weathered loam (Q) (Plejstocene/Holocene) *33* - dune sand (pk Q) (Plejstocene/Holocene) *34* - river sediment in general (gravel, sand and mud) (Q) (Holocene) *35* - fault/overlap *36* - salt mine *37* - landslide *38* - cross-section line

The tourist route in the mine is about 3,5 km long. It runs through quite a number of chambers and galleries (Fig. 6). The most interesting among them are: the Mikołaj Kopernik Chamber, the Spalone Chamber, the Sielec Chamber, the Casimir the Great Chamber, the Pieskowa Skała Chamber, the Kunegunda Traverse, the St. Kinga's Chapel, and the Józef Piłsudski Chamber. First, the visitors go down by steps to the depth above 50 m underground (Fig. 6).

The Mikołaj Kopernik Chamber has taken its name after the famous astronomer. He was one of the first visitors in that salt mine (Fig. 7). His salt monument was placed in the chamber on the 500th anniversary of his birth. The chamber, carved in a salt block is secured by wooden casings (Majka, 1996).

carts. Large blocks of salt were rolled on the wooden platforms (Majka, 1996).

In the XVIth century, miners began to use horses for help in transporting salt into the surface. It is illustrated in the Casimir the Great Chamber, in the centre of which a horse – drawn Saxon wheel tread can be seen (Fig. 7). It could transport salt rolls even up to two tones in weigh (Majka, 1996).

The Pieskowa Skała Chamber is considered as one of the most beautiful places in the mine. The great space of the chamber links two adjacent levels of the salt stratified deposit, whose exploitation was started in the XVIIth century. In the chamber, some parts of the stairs carved in salt have been preserved (Fig. 7). Old miners carried fine salt in special bags or wooden troughs along such stairs (Majka, 1996).

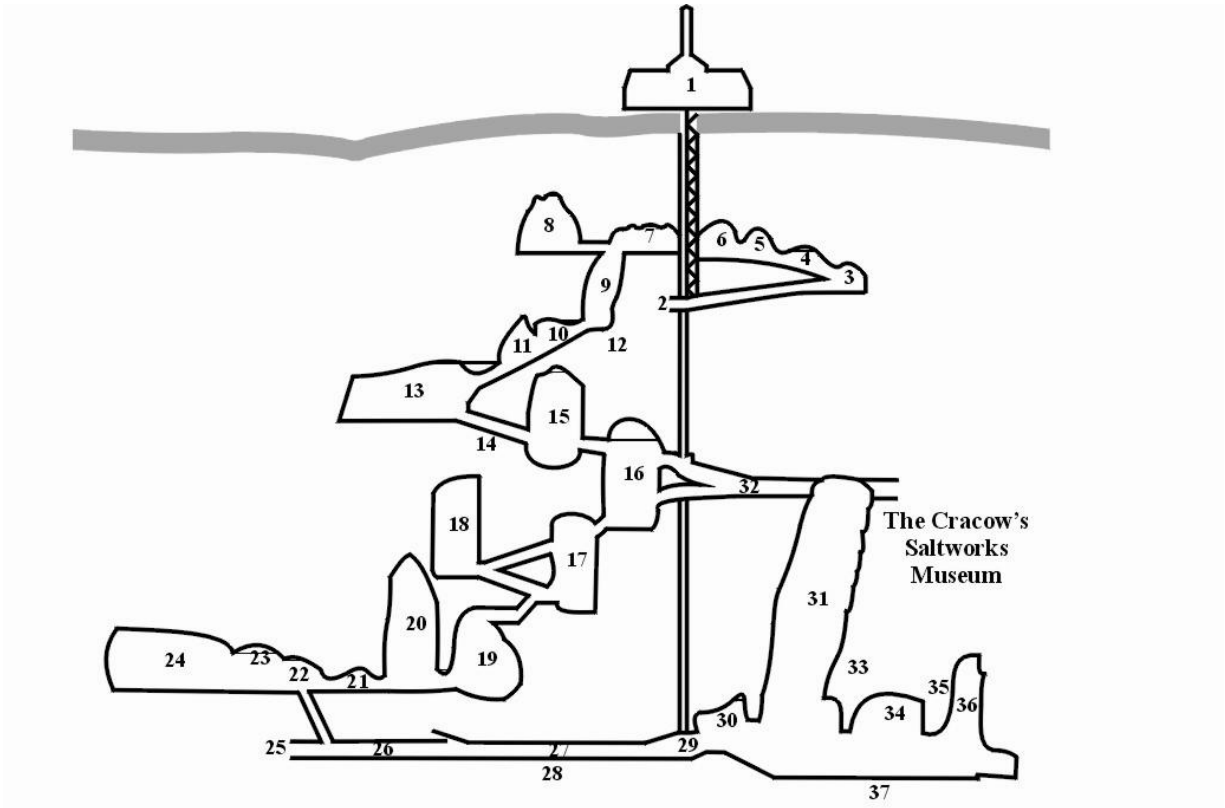

Fig. 6 Chambers on the tourist route in the salt mine in Wieliczka (Jodłowski, 2000):
1 - The Daniłowicz Shaft
Level I: *2* - The Daniłowicz Shaft Bottom *3* - The Mikołaj Kopernik Chamber *4* - The Janowice Chamber *5* - The St. Anthony's Chapel *6* -The Spalone Chamber *7* - The Sielec Chamber *8* - The Casimir the Great Chamber *9* - The Pieskowa Skała Chamber
Upper Level II: *10* - The Kunegunda Shaft Bottom *11* - The Holy Cross Chapel *12* - The Kunegunda Traverse
Lower Level II: *13* - The St. Kinga's Chapel *14* - The Barącz Slipway *15* - The Barącz Chamber *16* - The Michałowice Chamber *17* - The Weimar Chamber *18* - The Drozdowice Chamber
Kazanów split-level: *19* - The Józef Piłsudski Chamber *20* - The Stanisław Staszic Chamber *21* - Treasurer *22* - The Wisła Chamber
Level III: *23* - The Witold Budryk Chamber *24* - The Warszawa Chamber *25* - The Juliusz Słowacki *26* - The Jan Haluszka Chamber *27* - The Izabela Chamber *28* - The Anthony Longitude *29* -The Daniłowicz Shaft Bottom *30* - The Jan Długosz Chamber *31* - The Saurau Chamber *32* - The Harańcza Transverse *33* - The Kraj Chamber *34* - The Modena Chamber *35* - The Miejska Chamber *36* - The Maria Teresa Chambers *37* The Russegger Chambers

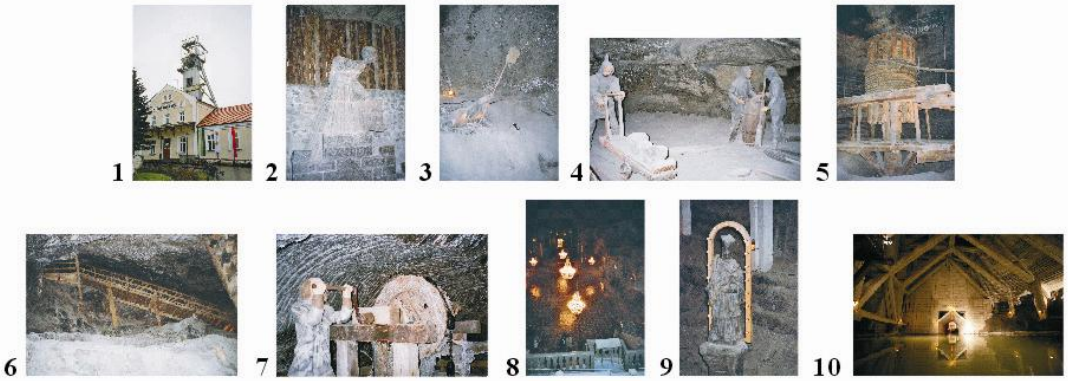

Fig. 7 Photos of the salt mine in Wieliczka:
1 - The Daniłowicz Shaft (author) *2* - The Mikołaj Kopernik Chamber (author) *3* - The Spalone Chamber (author) *4* - The Sielec Chamber (author) *5* - The Casimir the Great Chamber (author) *6* - The Pieskowa Skała Chamber (author) *7* - The Kunegunda Traverse (author) *8* - The St. Kinga's Chapel (author) *9* - The St. Kinga Sculpture (author) *10* - The Józef Piłsudski Chamber (http://www.kopalnia.pl)

In the Kunegunda Transverse, the method of the salt mine dehydratation is shown (Fig. 8). In the old times, water was first directed to vats and special tanks. Then it was directed through water troughs, piper to the main reservoir located by the shaft. In the end, water was drawn to the surface (Majka, 1996).

Te St. Kinga's Chapel is a very spacious chamber carved in a block of salt (Fig. 7). It has been a place of worship since 1896. The chapel chancel is decorated by a few sculptures of the New Testament scenes. Apart from them, there are also some statues of the last saint people. Among them is St. Kinga (Fig. 8), thanks of whom the salt mine was created, according to a legend. This sculpture was made as a gift of thanks for the canonizing of the Blessed Kinga by pope John Paul II in Stary Sącz in 1999. Large salt chandeliers illuminate the chapel. It is one of the most impressive and opulent underground temples in Europe (Majka, 1996).

The Józef Piłsudski Chamber (Fig. 8) was created by combining two adjacent green salt workings. In the early XIXth century, the Austrians connected the twin chambers with a 10-m tunnel when the first tourist route was being set up. There were also built wooden stairs and platform. The bottom of the chamber was filled with brine. At present, raft crossing through the tunnel is the additional attraction provided for tourists (Majka, 1996).

4. The salt mine in Bochnia

The Bochnia Salt Mine is the oldest one in Poland and the oldest industry in Europe. The salt deposit in Bochnia was discovered in 1248. It happened completely accidentally, while deepening brine wells and some salt rocks were met at a depth of 50 – 60 m. Since then Bochnia has become economically attractive. When Bolesław the Chaste, reigning in the city of Cracow and Sandomierz at that time, got known about salt discovery in his duchy, he bought out all the land around the place of discovery. Thanks to his investments and the help of Cistercians from Wąchock, the first mineshafts in Bochnia named "Sutoris" and "Gazaris" could be established in 1255 (Kobiela, 1999; Flasza, 2005; Bielak, 2007).

However, salt exploitation in Bochnia proved to be much more difficult than in Wieliczka. It was because of a very complicated geological structure of those salt deposits (almost vertically occurring salt rocks) combined with highly diversified and unusual shape of post-exploit caverns, and corridors. This untypical structure was caused by Carpathian's orogen pressure. In XIVth century, for the first time in deep mines, the connections between the mineshafts at a depth of 70 m were made in the salt mine in Bochnia. There were also galleries and smaller shafts. The salt was manually separated from the rest of the cube-shaped blocks with the help of pickaxes and splitting wedges. Then it was put into the ceramic forms and after that the salt fragments closed in barrels were drawn up. In between XVth - XVIth century the horses have been used for help in transportation of heavy blocks in Bochnia's salt mine.

The period of the reign of the king Casimir the Great was the most fruitful in the mine's history as the citizens of Bochnia were awarded with country's highest privileges. The mineshaft named "Regis" was constructed then, which made possible to discover some new rich salt deposits and build the Poland's first staff hospital – shelter for the sick miners. It was done due to numerous accidents occurring in the mine just then.

The salt mine in Bochnia played a vital role in the area's industrial growth and provided hundreds of citizens with work. Among them were not only miners but also carriers responsible for salt transport. As for industries existing thanks to the salt mine, there were mainly blacksmiths, coopers and rope makers.

In the XVth century, the salt exploitation reached the depth of 300 m what made the miners go even deeper in the search of salt. At the same time large salt seams were discovered in the western part of the deposits, due to which the "Campi" shaft was constructed. That shaft became the main one just in XVIth century and the salt mining was concentrated in that part of its deposit. The most significant crisis came together with the Swedish Deluge, in the XVIIth century.

The economic situation of salt evaporation ponds in Bochnia was improved only in the XVIIIth century when the system of the underground routs created in result of exploitation was rearranged by Jan Borlach, an outstanding land surveyor, who was invited to Bochnia. Consequently, two main corridors: "August" at the depth of 200 m and "Podmoście" 300 m underground were come into existence. That let salt extraction be much easier and more effective and put the mine's crisis to an end. In the XIXth century, some modern techniques were in usage, mainly dynamite, steam machine and steel line.

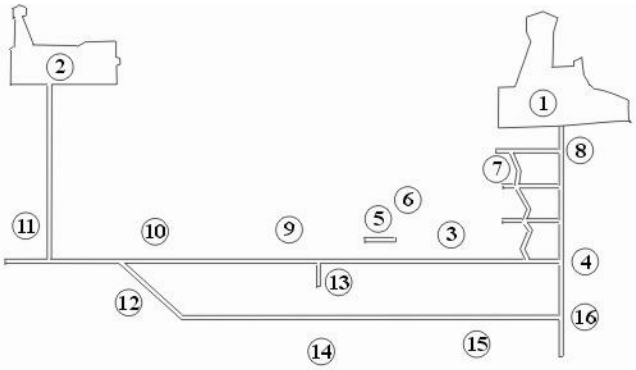

Fig. 8 The Sightseeing Route in the Bochnia salt mine (Bielak, 2007):
1 - The Sutoris Shaft *2* - The Campi Shaft *3* - The Mysiur Stable *4* - Level IV August
5 - Interlevel Chamber Dobosz *6* - The Christian Chamber *7* - Regis Stairs *8* - Level III Wernier
9 - The St. Kinga's Chapel *10* - A water trademill *11* - The Kołdras Chamber *12* - A slide
13 - The Ważyn smaller shaft *14* - The Ważyn Chamber *15* - A water wheel *16* - Level VI Sienkiewicz

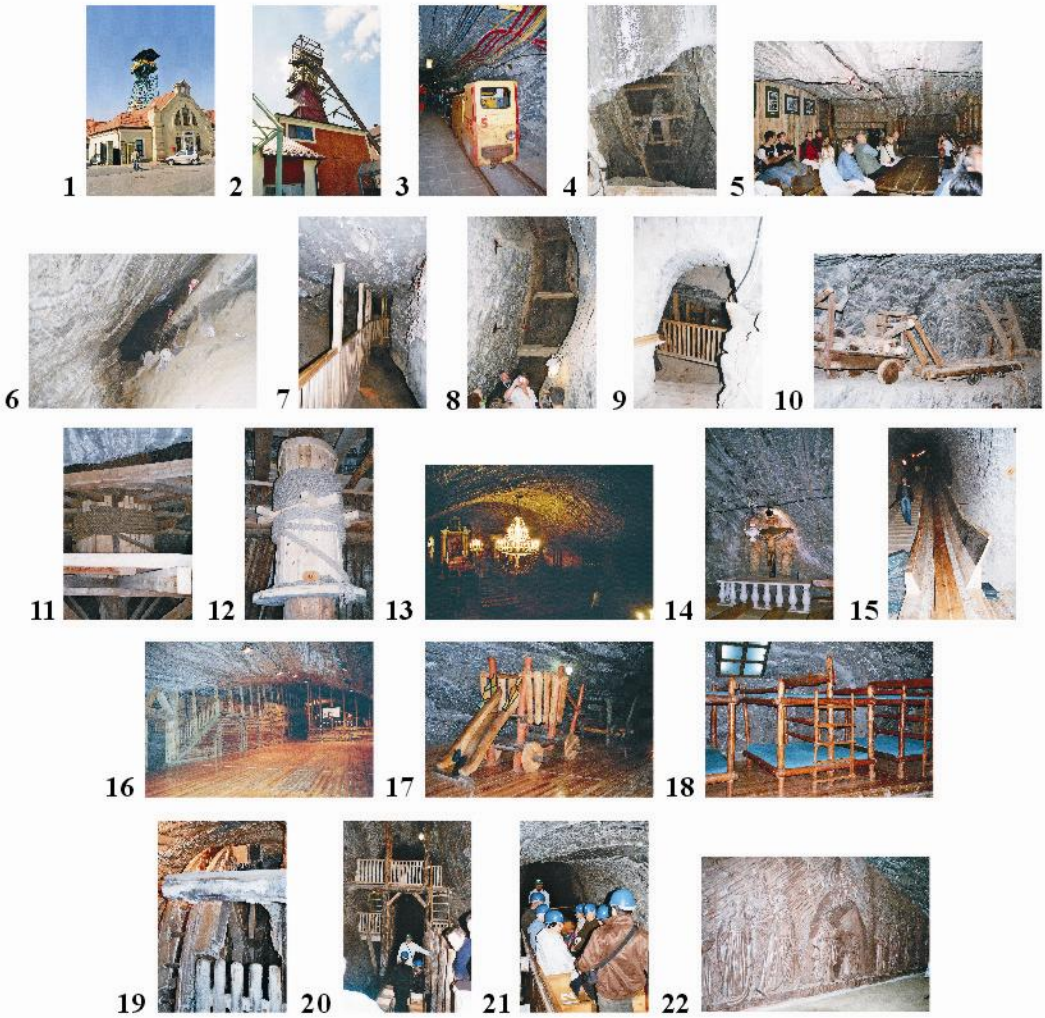

Fig. 9 Photos of the Sightseeing Route in the Bochnia salt mine (by author):
1 - The Sutoris Shaft *2* - The Campi Shaft *3* - Underground railway *4* - Old working miners *5* - The Mysiur Stable
6 - Old miners burning out methane (in the Interlevel Chamber Dobosz) *7* - Interlevel Chamber Dobosz
8 - The Christian Chamber *9* - Regis Stairs *10* - Old carts *11* - The Treadmill Chamber *12* - The Rabsztyn Chamber
13, 14 - The St. Kinga's Chapel *15* - A slide *16, 17* - The Ważyn Chamber *18* - The bedroom for bathers in the Bochnia Underground Health Resort *19* - A water wheel *20, 21* - Chamber 81 *22* - The Cross Way Relief (Level IV August)

After the World War II the salt miners revamped their extracting methods. With the help of electricity installment in the sixties, they could reach the depth of 470 m and the horses were no longer needed. In 1981 some mine excavations were taken under protection by one of the regional monuments restoring agencies in order to maintain its beauty.

The salt exploitation was over in the nineties, because the industrial plant "Solvay" in Cracow was closed in 1990. The resource of salt had been provided just for that plant. In the meantime the mine workers started adopting Bochnia's salt workings to be used for recreational and tourist purposes. Thus underground tourist rout and health resort was already created in 1995 (Charkot and Jaworski, 1992; Borkowski, 2000; Flasza, 2005; Bielak, 2007).

The tourist route in Bochnia's salt mine is about 2,5 km long. It involves a few chambers connected with drifts and smaller shafts (Fig. 8,9). First, the visitors go down by lift of the "Campi" shaft to the Level August, 212 m underground. Then they are carried by the underground railway to the "Sutoris" shaft. Its line runs down the Level August, on the distance of 1 km (Fig. 8, 9). Then the visitors start from there walking through old, very interesting, salt workings.

The Mysiur Stable (Fig. 8,9) was for keeping horses working in the mine safe. At present, this chamber is used as a place for conferences, trainings and parties.

The Interlevel Chamber Dobosz (Fig. 8,9) is situated 20 m above the Level August. It shows mainly the work of the miners burning out methane in the chamber's upper part. There can be also seen some carts used for carrying blocks of salt along the slides.

The Christian Chamber (Fig. 8,9) is a typical kind of working in the Bochnia salt mine. It has a specific vertical, narrow, and soaring shape, what results from the vertical pattern of salt deposit in the area. There are some traces of miner's work with the help of small pickaxes on the chamber's walls.

The chamber with a treadmill is the room where the visitors can watch methods of transportation of very big salt blocks, 150 - 450 kg in weigh. The horses were used for that. A water treadmill is a tool for dehydrating of the Rabsztyński smaller shaft (Fig. 8,9).

Regis stairs (Fig. 8,9) consist of 11 sections of different lengths and gradients. There are plenty of places to rest. Their length is 320 m of total and they are the only ones in the mine that lead round the shaft. The miners were walking up and down those stairs until 1923.

The St. Kinga's Chapel (Fig. 8,9) is the mine's biggest chapel preserved in a very great condition. The fact that mine work is very dangerous accounts for the religious climate in the mine. That's why there used to be plenty of chapels on the main communication routes. Up to now, there are many of the salt sculptures of saint people.

A slide connecting Level August with the Ważyn Chamber long on 140 m, is one of the biggest tourist attractions in the mine. The slide is situated on the drift along which the salt was transported from the Ważyn Chamber to the Level August.

The Ważyn Chamber is the most spacious chamber in Bochnia's salt mine. This room serves for recreational and health purposes. It is situated 248 m below surface and divided into 5 segments being long on 255 m in total. At present, the chamber is adopted for sport field (playground), attractions for children (Fig. 10), gastronomy, disco and bedroom for 260 people. There is also a restaurant and a souvenir shop. The tourists can ask a guide to rent a sports equipment there too. The room is also used on the various occasions such as conferences, symposia, trainings, theatrical performances, concerts, and other parties. People with some illnesses, especially of breath system can spend a time in the chamber, because there are quite suitable climate conditions there.

A water wheel is situated at Ważyn Level. That device served for pulling the brine out of the mine.

At the end of the visit in the Bochnia Salt Mine, tourists can have a raft ride on the distance of 120 m in the Chamber 81. It is situated 230 m underground. In the middle of XXth century, there were performed some experiments with wet mining. Thus, there are traces of them in the form of underground streams and lakes. That's why this additional tourist attraction is possible. After the ride the tourists can watch a very beautiful relief of the scene of the Cross Way on the Level August wall (Charkot, Jaworski 1992, Borkowski 2000, Flasza 2005, Bielak 2007).

5. Conclusions

Described underground geoturistic objects in salt deposit in the Malopolska District belong to the

most interesting sites not only in Poland but also in Europe. Both of them were acknowledged as the National History Monuments by the decree of the President of Poland, the Wieliczka Salt Mine in 1994 and the Bochnia Salt Mine in 2000 (http://www.kopalniasoli.pl). In addition, the Wieliczka Salt Mine was inscribed in UNESCO's First World List of Cultural and Natural Heritage (http://www.kopalnia.pl). All the underground geoturistic objects in the Małopolska District have become very popular mainly because the excavations of these old mines, in the form of galleries and chambers have been very well prepared for the visitors to watch them. In this way, the tourists can now imagine themselves the original picture of all those mines and the atmosphere among the miners in the past when they were working. It is possible thanks to the old exploiting machines exhibited in these objects, and the old underground railway in Bochnia's salt mine. In the author's opinion, all these objects described in the paper deserve to have a name as the most popular monuments in the world.

There is also one more underground salt mine open for tourists in Poland. It is situated in Kłodawa in Wielkopolska District. The structure of both the salt deposit and the salt workings in Kłodawa are quite different than in these in Bochnia and Wieliczka.

References

Alexandrowicz S. W., 1962. Microfaunistic levels of the Lower Tortonian sediment near Miechow and Działoszyce. [Summery of the ref.] Report of the Scientific Commission Assembly of Polish Scientific Academy in Cracow, VII-XII 1961, 446-448, Cracow (in Polish with English abstract)

Bielak P., 2007. Tourist guide – Poland from the close site. Bochnia and around, Progres, 55 pp. (in Polish with English abstract)

Borkowski K., 2000. The adaptation of the industrial objects for tourism needs. In: Integra IITF no. 1 (in Polish with English abstract)

Bukowski K., 1999. Difference between Badenian salt sediments in Wieliczka and Bochnia by new data. Works of National Geological Institute, 168, 43-56. Warsaw (in Polish with English abstract)

Bukowski K., 2000. Geochemistry and age determination of Badenian evaporates from Wieliczka and Bochnia salt mines (Poland). 8th World Salt Symp, vol. 1, 101-105, Elsevier, Amsterdam

Bukowski K., Wójtowicz A., Durakiewicz T., 1996. First results of hornblende dating as the material for radiometric age defining by K/Ar method. III Polish Scientific Session, Mineral and rock dating, 13-17, UMCS Lublin (in Polish with English abstract)

Burtan J., 1954. Geological Map of Poland in Detail, M-34-77A WIELICZKA. National Geological Institute. Warsaw (in Polish with English abstract)

Charkot J., Jaworski W., 1992. Characteristics of antique excavations in Bochnia's salt mine. In: Studies and materials on the history of salt mines in Poland. Vol. XVII, Ministry of Culture and Art, Department of Cultural Activities, Museum of Krakow Salt, Wieliczka (in Polish with English abstract)

Długosz A., 1958. Salt mining history in Wieliczka. SMDNP, 7-64 (in Polish with English abstract)

Dziwik K., 1980. The history of salt industry in Polish lands in between 1772-1918. SMDŻ, vol. 9, 99-140.

Flasza J., 2005. Bochnia. Guide to Town. Magistrate of Bochnia, 160 pp. (in Polish with English abstract)

Garlicki A., 1968. Miocene Podkarpacie autochthonic salt sediments located between Skawina and Tarnów. Bulletin of the Geological Institute, 215, 5-77. Warsaw (in Polish with English abstract)

Garlicki A., 1979. Sedimentation of Miocene salt in Poland. Works of the Geological Scientific Commission of the Polish Scientific Academy in Cracow, 119, 66 pp., Cracow (in Polish with English abstract)

Garlicki A., 1994. Salt sediment in Upper Silesia and Bochnia. Geological Review, 42, 9, 752-753 (in Polish with English abstract)

Jodłowski A., 2000. Salt work in Wieliczka. Museum of Salt work. Wieliczka, 193 pp. (in Polish with English abstract)

Keckowa A., 1965. Salt deposits in Cracow countryside up to 18th century. SDGH, vol. 10. (in Polish with English abstract)

Kobiela S., 1999. Salt mine in Bochnia, In: Bochnia News No. 3 (in Polish with English abstract)

Książkiewicz M., 1972. Geological composition of Poland, vol. IV, Tectonics, p. 3, Carpathians, Geological Edition of Geological Institute. Warsaw (in Polish with English abstract)

Majka J., 1996. Guidebook on the Salt Mine "Wieliczka" and the underground museum. Wieliczka (in Polish with English abstract)

Markowski I., 1978. Development of the space of the salt mine in Wieliczka. SMDŻ, vol. 7, 7-28.

Olszewska B., 1999. Biostratygraphy of the Neogene of Forecarpathian Basin by the new micropaleontological data. Works of the National Geological Institute, 168, 9-28. Warsaw (in Polish with English abstract)

Peryt T. M., Piwocki M. (red.), 2004. Geological composition of Poland, vol. I, Stratygraphy, p. 3a, Kenosoic, Paleogene, Neogene. Polish Geological Institute. Warsaw (in Polish with English abstract)

Piotrowicz J., 1968. The problems of the origin and the oldest times of salt mining in Poland. SMDŻ, t. IX, 173-234 (in Polish with English abstract)

Piotrowicz J., Grzesiowski J., 1977. Museum of Cracow's Salt Work in Wieliczka – origin and development. SMDŻ, vol. VI, 13-32 (in Polish with English abstract)

Poborski J., 1952. Salt deposit in Bochnia on the geological background of the countryside. Bulletin of Geological Institute, 78, 160 pp. Warsaw (in Polish with English abstract)

Poborski J., Skoczylas-Ciszewska K., 1962. Tectonics of the Miocene salt deposit in Western Podkarpacie. Report from the Scientific Commission Assembly of Polish Scientific Academy in Cracow, 6, 2, 528-530. Cracow (in Polish with English abstract)

Poborski J., Skoczylas-Ciszewska K., 1963. Miocene of the sediments in the Carpathian Foredeep zone near Wieliczka and Bochnia. Annual of Polish Geological Association, 33, 3, 339-348. Cracow (in Polish with English abstract)

Połtowicz S., 1977. Remarks on the salt deposit in Wieliczka and Barycz tectonic development. Annual of the Polish Geological Association, 47, 2, 279-299, Cracow (in Polish with English abstract)

Reguła K., 1969. Probable brine machines in the period from Late Latin till Early Roman in Wieliczka at the stage XI. In: Archaeological investigation made by the museum of Salt Works in Wieliczka in 1969, 14-19. Wieliczka (in Polish with English abstract)

Skoczylas-Ciszewska K., Burtan J., 1954. Geological Map of Poland in Detail, M-34-77B BOCHNIA. National Geological Institute. Warsaw (in Polish with English abstract)

Wiewiórka J., 1979. Main tuff levels in the salt mine in Wieliczka. Report from the Assembly of the Scientific Commission in Polish Scientific Academy in Cracow. 21, 1, 176-178, Cracow (in Polish with English abstract)

http://www.kopalniasoli.pl

http://www.kopalnia.pl

Scientific Annals, School of Geology, Aristotle University of Thessaloniki Proceedings of the XIX CBGA Congress, Thessaloniki, Greece	Special volume 100	483-489	Thessaloniki 2010

THE GEOTOURIST ASSESSMENT OF THE VOLCANIC SITES IN VTÁČNIK MTS. (SLOVAKIA, WESTERN CARPATHIANS)

Górna M. and Golonka J.

Department of General Geology, Environment Protection and Geotourism, AGH University of Science and Technology, al. Mickiewicza 30, 30-059 Krakow, Poland, mgorna@geol.agh.edu.pl, jan_golonka@yahoo.com

Abstract: The evaluation of resources is one of the most important tasks of geotourism research. This paper presents the method of geotourist assessment, which was applied on the example of sites presenting the Neogene volcanic activity within Vtáčnik mountain range. Two stages of assessment are proposed: inventory and valorization. The inventory includes identification of resources, initial selection and characterization. During the valorization, a researcher uses the point bonitation method and takes into account the following indicators: scientific value, location and additional values. The result of valorization process is presented in table which allows comparison and categorization of the selected sites. The assessment of considered region revealed, that selected sites like rock walls, rock forms, abandoned quarries and hills with ruins are characterized by high or medium geotourist value. Consequently, Vtáčnik is an example of area of a great potential for geotourism development.

Keywords: geotourist assessment, Neogene volcanism, Vtáčnik Mts.

1. Introduction

Geotourism, understood as a combination of applied geology and active tourism (Słomka and Kicińska- Świderska, 2004), is a way to promote geological heritage among general public (Hose, 2000). Geotourism research is a multidisciplinary activity encompassing primarily recognition of geotourist potential. The assessment of entire regions and single sites is a key element of geotourist potential, furthermore, it is particularly important for the future geotourism management. The results of the assessment enable to compare and classify the sites and offer suggestions for their promotion, protection and development. The aim of this paper is to present the pattern of geotourist assessment on the example of the volcanic sites in Vtáčnik.

2. Methodology of geotourist assessment

The sites, which belong to the sphere of geotourism interest, can be divided according to their individual features into the following categories:

- geotourist resources- all elements which relates to geotourism,
- geotourist sites- resources which are characterized by science, educational and aesthetic value; they can be potential destination of geotourist excursions,
- geotourist attractions- places/ sites which are appropriately developed and promoted.

In order to identify the resources and select the most valuable geotourist sites out of them, the assessment process is essential. This procedure includes two stages: inventory and valorization. The first step consists of identification of potential sites, their initial selection and characterization. During the second step, numerical assessment is assigned to the features of selected sites, on the basis of established criteria. The results of valorization allow comparison of the sites and creating the ranking list which can be useful with regard to future protection, geotourist development or other initiatives.

2.1. Step 1- inventory

One of the essential aims of this stage is to determine the amount and the types of sites in the described area. This task is executed on the basis of literature data and field work. During the initial selection, location, accessibility for tourists and condition of outcrop are taken into consideration. This process also includes the detailed descriptions of each of selected sites, that is: location (with GPS co-ordinates), information on geology and geomorphology, accessibility, present uses and infrastructure, protection, condition of outcrop (visibil-

ity), other information (cultural, historical values) and photographic documentation. The data collected here are indispensable for the next stage of assessment.

2.2. Step 2- valorization

This part of assessment is carried out with using the point bonitation method. This method assumes the assignment of the numerical values (points) to individual features of the site, according to the established criteria and scale (Sołowiej, 1992). The framework of valorization is based on 3 principal and 13 secondary indicators (Tab. 1). Part of the criteria was taken from existing literature on related field (for example: Otęska-Budzyn, 1992; Pralong, 2005; Reynard et al., 2007). The scale value is from 1 to 2 (for 3 indicators) or from 1 to 3 (for 10 indicators). The value of feature may equals 0 when it is below the proposed criteria. The sum of all indicators determines the total value of sites (maximum 36) which are taken into account under final categorization. Consequently, the sites with scores over 70% of maximum total value can be considered as sites with high geotourist value, the sites with scores between 69 and 40 %- as sites with medium geotourist value and the sites with scores under 39%- as sites with low geotourist value in the assessed area. The results of valorization stage should be recorded in a table.

3. Case study

3.1. Research area

The mountain range Vtáčnik constitutes a western part of the Slovenské stredohorie, in the Inner Western Carpathians (Figs. 1, 2). It extends between Previdza by the Nitra river and Žarnovica by the Hron river (Nacher et al. 2004). The central part of Vtáčnik is included in the Ponitrie Pro-

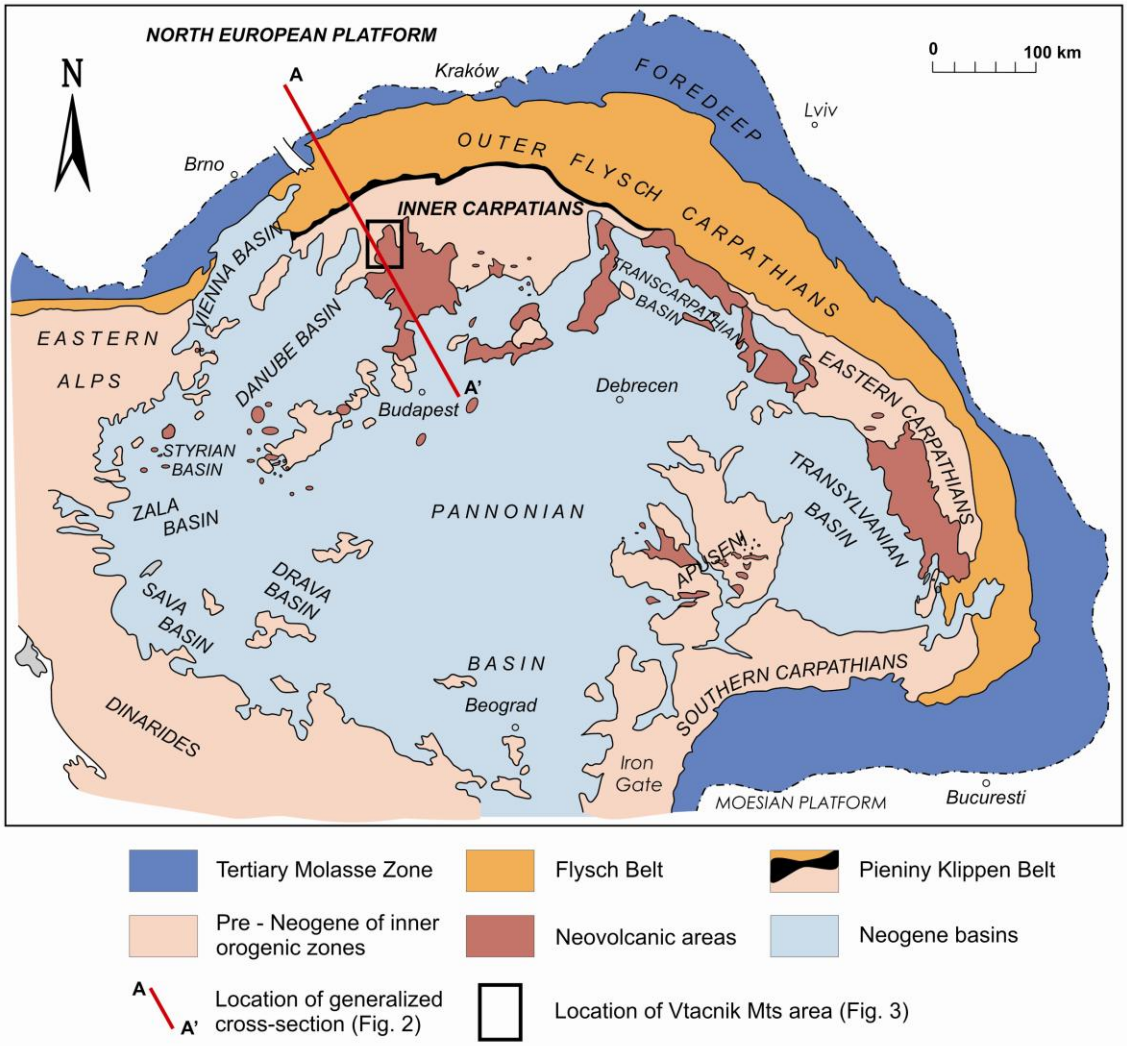

Fig. 1. Tectonic sketch map of the Alpine-Carpathian-Pannonian-Dinaride basin system (after Kováč et al., 1998) with location of Vtáčnik area and generalized cross-section A-A'.

tected Landscape Area. Moreover, 20 individual protection forms like reserves or natural monuments can be found within the considered region.

Vtáčnik is the second highest volcanic mountain range of Slovakia. It is located in the north-west part of the area called the Central Slovakia Volcanic Field (Fig. 1). The Neogene volcanic activity was contemporaneous with the origin of the horst and graben system induced by back-arc extension processes (Šimon 1999; Konečný and Lexa 2002). According to Seghedi et al. (2004) the subduction-related calc-alkaline magmatism responsible for the first (Badenian) phase of Central Slovakia Volcanic Field was followed by asthenosphere derived magmatism widespread in the Carpthian-Pannonian region (Figs. 1, 2). Decompressional melting of old asthenosphere upwelling replaced lower lithosphere or heating and melting former subducted slabs. The volcanic rocks rest on variable Mesozoic and Paleogene deposits. The remnants of the Vtáčnik stratovolcano cover the prevailing part of described area. In the south and east the remnants of the Štiavnica and Kremnica stratovolcano also can be found. The oldest volcanic rocks (Lower/ Middle Badenian) are the products of explosive-effusive activity of the Štiavnica stratovolcano which reached the south part of this region. During the Late Badenian to Early Sarmatian the subsidence of the large Kremnica graben was accompanied by floods of basaltic, pyroxene and leucocratic andesite flows and then by amphibole-pyroxene andesite flows. The andesite Vtáčnik stratovolcano was formed from the Early to Middle Sarmatian, as a result of the most significant volcanic activity in this region. The extensive rhyolitic volcanism took place during the Late Sarmatian to Early Pannonian, mainly in south. The Ostrovica dykes and necks are the remnants of the youngest manifestation of volcanic activity in considered region (Pannonian) (Konečný et al. 1983; Šimon 2000). The most common rocks are the pyroxene andesites. The basaltic andesites, rhyolites, dacites, volcanic tuffs and breccias are rarely occur. The present relief of Vtáčnik is a result of the neotectonic movement and denudation processes.

Vtáčnik is characterized by a large number of the representative, valuable and magnificent rock outcrops which are the witnesses of geological history and can be use in geotourist context.

3.2. Results of geotourist assessment

Within the range of Vtáčnik four groups of sites are distinguished: rock walls (4), rock forms (small and single outcrops were passed over) (33), abandoned quarries (3) and hills with ruins (2). All of them are generally located in the northern part of the described area (Fig. 3). Predominantly, the outcrops are the relics of andesite lava flows. The rock walls can be found in the main and lateral ridge of the range. The most spectacular walls are 1000 m long (Biely Kameň) and 80 m high (Hrádok, fig. 4). The rock forms are located nearby the ridge and on sides of valleys. They were formed by the selective weathering of rock of vertical fissures and platy jointing and/or by gravitational slopes slide (Vitek 1986). Several sites can be called the rock cities- with rocks towers, gates and windows (Kláštorská skala, fig. 5, Končitá). In several cases, the block fields called stone seas appear at the foot of the rock forms (Jaseňová skala, Krivá skala). The frost weathering was the reason of their origin. In the abandoned quarries, the andesites (in Vel'ká Lehôtka and Župkov) and the rhyolites (Štamproch in Nová Baňa, fig. 6) were

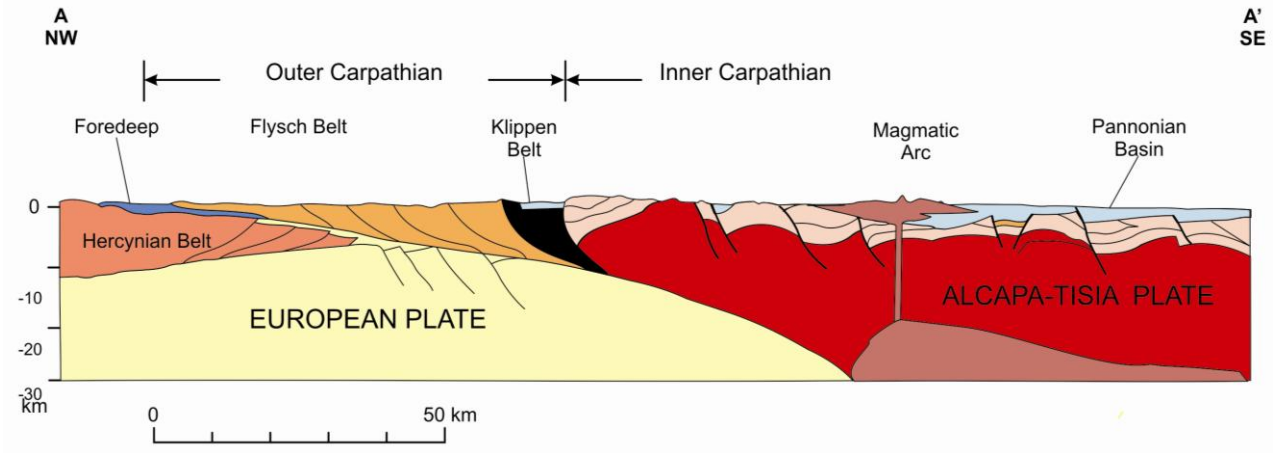

Fig. 2. Generalized cross-section A-A' across Carpathian-Pannonian region (after Picha, 1996). Cross-section location on figure 1.

exploited. It is worth emphasizing that the stone from Štamproch quarry often occurs as an element of buildings in Nová Baňa and vicinity. In the case of hills with ruins, rock ground was considered, as well as the material used to building. Both Gothic castles were built from local andesite rocks. The ruins in Revištské Podzámčie (Fig. 7) are in better condition then in Podhradie (Sivý Kameň).

As it turned out, the most magnificent rock walls and quite a lot of rock forms and quarries are unavailable because of restriction of legal protection, their location (away from tourist trails) or lack of access (relief, vegetation). Out of 42 sites, 15 were selected to further characterization.

The results of the second stage of assessment and categorization of sites are presented in table 2. Six sites obtained the score over 70% of maximum total value and they were recognized as the most valuable for geotourism. The middle geotourist value was attributed to nine sites. The Hrádok-magnificent rock wall with a small abandon quarry appears to be the most valuable geotourist sites in the assessed region (Fig. 4). It is worth noticing that no site in Vtáčnik is developed with a view to geotourism. It is also essential, that 11 sites are under legal protection, 7 of them because of geologi-

Table 1. The indicators and their numerical assessment used during valorization process.

Scientific value (maximum 12) Sc		
Rareness in relation to the area	1	Site one from several similar
Rar	2	One of the most important
	3	The only occurrence
Condition of outcrop (visibility)	1	Partly covered with vegetation, partly damaged as a result of human activity or natural processes
Con	2	Partly covered with vegetation
	3	Well exposed
Ilustrativeness	1	Low illustrativeness
Ilu	2	Good example of geo(morfo)logical feature or processes
	3	Excellent example of geo(morfo)logical feature or processes
Diversity of geo(morfo)logical features/ processes	1	Low diversity
	2	Medium diversity
Div	3	High diversity
Location (maximum 12) Lo		
With respect to tourist trails	1	More then 200 m from tourist trail, easy to find
TT	2	Less then 200 m from tourist trail
	3	By tourist trail
With respect to roads (accessible by car)	1	Between 2,5 and 5 km from parking place
Ro	2	Between 1 and 2,5 km from parking place
	3	Less then 1 km from parking place
With respect to support service (accommodation, catering)	1	Between 10 and 15 km
	2	Between 5 and 10 km
SS	3	Less then 5 km
Accessibility	1	Difficult, only with special equipment
Acc	2	Difficult for some tourists
	3	Available for all tourist
Additional values (maximum 12) Add		
Aesthetic value	1	Low
Aes	2	Medium
	3	High
		Subjective value, based on visual singularity of outcrop, quality of panorama, attractiveness forms
Development and use	1	Present use as tourist/cultural/other site
DU	2	Present use as geological site (element of educational trail)
	3	Present use as geotourist site (with interpretative materials)
Access to geological information	1	Difficult access or only scientific knowledge
AI	1,5	Access to general information (Internet, tourist guidebooks)
	2	Easy access, special geotourist publications
Legal protection	1	Protected as a part of larger area
LP	1,5	Individual protection as historical, nature site
	2	Individual protection as geo(morfo)logical site
Cultural/ historical value	To 2	Historical value- 1
CH		Cultural value- 1

cal values. The relation between geotourism and geoconservation affects the popularization of Earth science. Thus, the protected areas are predisposed to practise geotourism (Alexandrowicz, 2006).

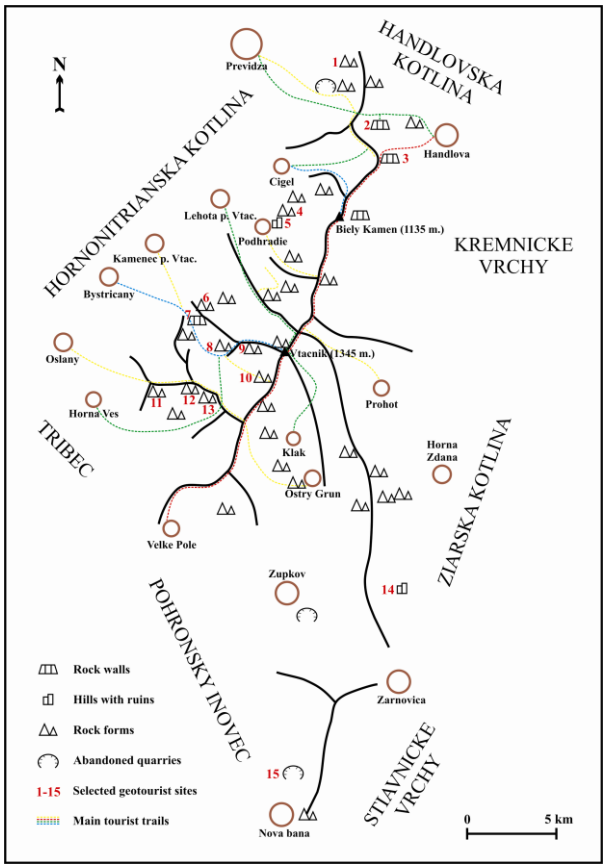

Fig. 3. The sketch map of Vtáčnik with location of the identified and selected sites. 1-Hradisko, 2-Malý Grič, 3-Velký Grič, 4-Krivá skala, 5-Sivý Kameň, 6-Končitá, 7-Hrádok, 8-Jaseňová skala, 9-Kostolik, 10-Kláštorská skala, 11-Žarnov, 12-Sladná skala, 13-Buchlov, 14-Revištské Podzámčie, 15-Štamproch. For map location see fig. 1.

4. Discussion

This paper focuses on assessment process from the perspective of geotourism. The proposed method, with quantitative and qualitative aspects, allows an overall and detailed assessment which results can be comparable. Its framework bases on two stages: inventory (with identification, initial selection and description) and valorization (with numerical assessment and classification). The valorization includes 3 principal and 13 secondary indicators. In the case of geotourist assessment, it was affirmed, that the scientific value is as crucial as location or additional values. The most attractive geotourist sites should be valuable, as well as picturesque, unusual and conveniently located. It is worth emphasizing that the criterion like size of site was not

Fig. 4. Hrádok- the highest rock wall in Vtáčnik, remnant of the andesite lava flow.

considered. In the case of Vtáčnik initially only sites with the size distinguishing them from the surroundings were taken into account, thus this feature was not considered as a significant one during the following valorization. The gathering all results into one table facilitate the quick comparison of sites, their total values and also their assessment of each of established indicators. The disadvantage of the propagated point bonitation method is an element of subjectivity because the given value depends on the opinion of the assessor.

Fig. 5. The part of rock city Kláštorská skala. Well developed platy jointing is visible.

Fig. 6. Štamproch abandoned quarry- the only selected outcrop of rhyolite.

Fig. 7. The andesite hill with ruins of the Gothic castle in Revištské Podzámčie.

However, elaborated criteria and scale allow recognizing the general assessment as relatively objective.

geotourist attractions. Moreover, the project of geotourist trail in this region should be considered.

Tab. 2. The result of geotourist assessment of volcanic sites in Vtáčnik.

Indicators / Sites	Rar	Con	Ilu	Div	∑ Sc	TT	Ro	SS	Acc	∑ Lo	Aes	DU	AI	LP	CH	∑ Add	Total value	
Hrádok	2	3	3	3	11	3	2	3	2	10	3	1	1,5	1	1	7,5	28,5	HIGH GEOTOURIST VALUE
Končitá	2	2	2	3	9	3	3	3	3	12	2	1	1,5	2	0	6,5	27,5	
Krivá skala	2	2	3	3	10	1	3	3	3	10	2	1	1,5	2	0	6,5	26,5	
Sivý Kameň	1	2	2	3	8	1	3	3	3	10	3	1	1,5	2	1	8,5	26,5	
Buchlov	2	2	2	3	9	3	1	2	3	9	2	2	1,5	2	0	7,5	25,5	
Kláštorská skala	2	3	3	3	11	3	0	2	3	8	3	1	1,5	1	0	6,5	25,5	
Jaseňová skala	2	2	3	3	10	3	1	2	3	9	2	2	1	1	0	6	25	MEDIUM GEOTOURIST VALUE
Revištské Podzámčie	1	1	2	3	7	1	3	3	3	10	3	1	1,5	0	1	6,5	23,5	
Sladná skala	0	2	2	2	6	3	1	2	3	9	2	2	1,5	2	0	7,5	22,5	
Kostolik	0	2	2	3	7	3	1	2	3	9	2	2	1	1	0	6	22	
Štamproch	3	2	2	3	10	1	2	3	3	9	2	0	0	0	1	3	22	
Hradisko	0	2	1	1	4	1	3	3	3	10	1	1	1,5	2	1	6,5	20,5	
Malý Grič	1	2	1	2	6	3	1	3	3	10	2	1	1,5	0	0	4,5	20,5	
Žarnov	0	2	1	1	4	3	1	2	3	9	1	2	1,5	2	0	6,5	19,5	
Velký Grič	1	2	1	1	5	3	1	3	3	10	1	1	1,5	0	0	3,5	18,5	

5. Conclusions

The presented method is distinguished by two main advantages: simplicity and comprehensiveness. What is more, it can be applied to diverse areas, independently of their size or number and kind of sites in their limits. With using this method, the assessment of volcanic sites in Vtáčnik was carried out. On the basis of its results, it was affirmed that a large number of sites related with Neogene volcanic activity are characterized by geotourist potential. Thus, several sites with the highest value should be properly developed and promoted as

Acknowledgements

This work was funded within the confines of research nr 10.10.140.575

References

Alexandrowicz Z., 2006. Geopark- nature protection category aiding the promotion of geotourism (Polish perspectives). Geoturystyka/ Geotourism, 2(5), 3-12.

Hose T.A., 2000. European geotourism- geological interpretation and geoconservation promotion for tourists. In: Geological Heritage: Its Conservation and Management, Barretino, D., Wimbledon, W.A.P. and Gallego, E. (eds), Sociedad Geologica de Espana/Instituto Technologico GeoMinero de Es-

pana/ProGEO, Madrid, 127-146.

Konečný V. and Lexa J., 2002. Evolution of the Central Slovakia Neogene Volcanic Field related to the horst/graben structure. In: Proceedings of XVIIth Congress of CBGA, Bratislava, 1-4.09.2002, Michalik, J., Šimon, L. and Vozár, J. (eds), Geologica Carpathica, special issue, 53, on CD.

Konečný V., Lexa J. and Planderová E., 1983. The stratigraphy of the central Slovakia neovolcanic field. Západné Karpaty, series Geologia, 9, 1-203 (in Slovak with English abstract and summary).

Kováč M., Nagymarosy A., Oszczypko N., Ślączka A., Csontos L., Marunteanu M., Matenco L. and Márton, M., 1998. Palinspastic reconstruction of the Carpathian-Pannonian region during the Miocene. In: Geodynamic development of the Western Carpathians, Rakús M. (ed.), Geological Survey of Slovak Republic, Dionýz Štúr Publishers, Bratislava, 189-217.

Nacher A., Styczyński M., Cisowski B. and Klimek P., 2004. Slovakia. The Carpathian heart of Europe. Wyd. Bezdroża, Cracow (in Polish).

Otęska-Budzyn J., 1992. Functions of protected areas and objects in Earth sciences education and popularization. Ochrona Przyrody/ Nature Conservation, 50, cz. I, 129-169 (in Polish with English abstract and summary).

Picha F.J., 1996. Exploring for hydrocarbons under thrust belts: a challenging new frontier in the Carpathians and elsewhere. American Association of Petroleum Geologists, Bulletin, 89, 1547-1564.

Pralong J.P., 2005. A method for assessing tourist potential and use of geomorphological sites. Géomorphologie: relief, processus, environnement, 3, 189-196.

Reynard E., Fontana G., Kozlik L. and Scapozza C., 2007. A method for assessing scientific and additional values of geomorphosites. Geographica Helvetica, 3, 148-158.

Seghedi I., Downes H., Szakács A., Mason P.R.D., Thirlwall M.F., Rosu E., Pecskay Z., Márton E. and Panaiotu C., 2004. Neogene–Quaternary magmatism and geodynamics in the Carpathian–Pannonian region: a synthesis. Lithos, 72, 117-146.

Słomka T. and Kicińska- Świderska A., 2004. The basic concepts of geotourism. Geoturystyka/Geotourism, 1 (1), 5-7 (in Polish with English abstract).

Sołowiej D., 1992. Basics of assessment methodology of the natural environment of human being. Wyd. Nauk. UAM, Poznań (in Polish).

Šimon L., 1999. Volcanism and sedimentation in the north-western part of the Cantral Slovak Neogene Volcanic Field. Geologica Carpathica, Special issue, 50, 137-140.

Šimon L., 2000. Evolution of volcanics of the Vtáčnik Mts. in the Central Slovakia Neogene volcanic field. Mineralia Slovaca, 32, 227-229.

Vitek J., 1986. The geomorphology of andesite rock forms in the Vtáčnik Mountain Range, Central Slovakia. Sbornik, Československe Geograficke Společnosti, 91, 1, 15-27 (in Slovak with English abstract and summary).

Scientific Annals, School of Geology, Aristotle University of Thessaloniki Proceedings of the XIX CBGA Congress, Thessaloniki, Greece	Special volume 100	491-502	Thessaloniki 2010

PHENOMENON OF MUD VOLCANOES IN WESTERN ROMANIA AS A GEOTURISM OBJECT

Madeja G. and Mrowczyk P.

Department of General Geology, Environmental Protection and Geoturism, Faculty of Geology, Geophysics and Environmental Protection, AGH University of Science and Technology, Al. Mickiewicza 30, 30-059 Kraków, Poland
madeja@geol.agh.edu.pl, mrowczyk@geol.agh.edu.pl

Abstract: The biggest mud volcanoes in Europe are located in eastern Romania, in the center of the Carpathian Foredeep, in the anticline structure called Berca-Arbanasi extending for 20 km north-southward. The volcanoes are located there in four zones: Beciu, Paclele Mici (PMI), Paclele Mari (PMA) and Fierbatori at a distance about 20 km northwest from Buzau. In 1924 the volcanoes PMI and PMA received the status of geological reserve, and nowadays are one of the major geotourism attractions in the country. The volcanoes in both regions are either cone- or pie- shaped. In the mud samples drawn from both regions the separation of fractions was carried out. It indicates that the muddy substance is composed mainly of grain fraction of 0.5-0.18mm and 1.0-0.5mm. The mineral composition, determined by means of polarizing microscope on fraction 0,5-0,18mm in both regions, indicates that prevailing, however distinct in percentage share, minerals are the following: quartz grains, claystones and mudstone fragments. This identification was confirmed by X-ray pattern, which showed the mud volcanoes transport mostly mud composed of clay minerals represented by illite-smectite. Chemical analyses performed using ICP method showed that volcano waters are composed of mud mixed with salty waters. Moreover, chemistry of these waters collected from the two separate volcanoes are different too, and the main elements are the following: B, Ba, Br, Ca, I, K, Li, Na, Mg and Sr. Results of chemical analyses confirm various sources of salty waters as well as their migration across various evaporites present below volcanoes. The research shows significant differences between these two apparently identical objects, making them even more attractive as far as geotourism values are concerned. Establishing an appropriate geotourism infrastructure would serve at least three purposes: enriching the aesthetic impressions after visiting the region, allowing tourists to get to know the differences and enhancing the educational offer of the reserves.

Keywords: Romania, Carpathian Foredeep, mud volcanoes, mineral composition, geoturism

1. Introduction

1.1 General information about mud volcanoes

Mud volcanoes are defined as geological features through which agrillaceous material is altered and transported from the Earth's interior and expelled onto its surface. Mud volcanoes can be found almost everywhere on Earth. They are commonly associated with compressional tectonics at convergent margins (Higgins and Saunders, 1974; Barber et al., 1986; Kopf et al., 1998 cited in Kopf, 2003). Their density shows a positive correlation with (1) thick, rapidly deposited sediments consisting of high clay mineral component as (Yassir, 1989 cited in Kopf, 2003), (2) sediment overpressuring due to hydrocarbon formation (Hedberg, 1974; Lavrushin et al., 1996 cited in Kopf, 2003), (3) a structural association with tectonic shortening dehydration (Moore and Vrolijk, 1992 cited in Kopf, 2003) and/or earthquake activity (Sondhi, 1947 cited in Kopf, 2003), (4) fluid emission such as gas, brines, water from mineral dehydration (Moore and Vrolijk, 1992 cited in Kopf, 2003) and gas hydrate dissociation (Milkov, 2000 cited in Kopf, 2003), and (5) polymictic assemblages of the surrounding rock present in the ejected argillaceous matrix (Robertson and Scientific Party of ODP Leg 160, 1996; Kopf et al., 1998 cited in Kopf, 2003).

There are about 700 mud volcanoes known in the world, and almost half of them can be found in

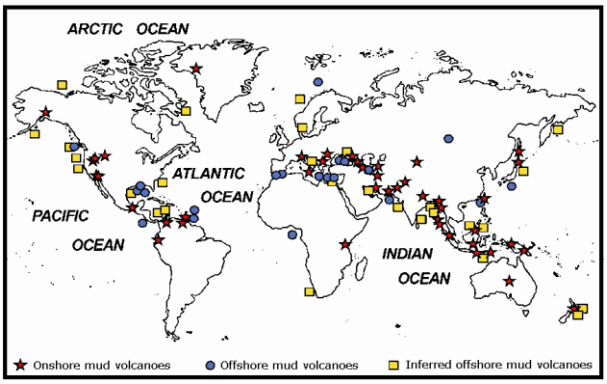

Fig. 1. Distribution of mud volcanoes worldwide (modified from Milkov 2003).

Azerbaijan. The other ones were also discovered in Turkmenistan and in the south-Caspian region, in Australia, Taiwan, China, Pakistan and Iran. Only a few are found in Europe: in the south-west of Ukraine, in Southern Italy and Sicily, and in Romania. It is also worth noticing that mud volcanoes can form both onshore and offshore (Fig. 1) (http://azer.com/aiweb/categories/magazine/ai151_folder/151_articles/151_mud_volcanoes.html).

The size of mud volcanoes ranges from a few centimeters to several meters of width, and from a few centimeters to 500-700 meters of height, whereas the biggest offshore mud volcano reaches the diameter of 30 km and about 2 km of relative height (Kopf, 2002).

Generally, mud volcanoes have the shape of cones (Fig. 2) or pies (Fig. 3). The former, depending on the viscosity of the muddy substance, exhibit various inclinations from 35 - 40˚, and sometimes are characterized by the presence of parasitic cones on the slopes. The latter, are characterized by slight inclination of slopes - <5˚, and become cylindrical or irregular in shape. Both forms may occur in active or fossil form (Kopf, 2002).


Fig. 2 Example of cones in Paclele Mici region (Madeja 2009).

The substance flowing out of mud volcanoes can be both watery, thus such outflows are constant and accompanied by characteristic bubbling, however, at times they can be viscid, sticky and therefore, more spectacular eruptions of discarding fireballs can take place. Frequently, slight traces of oil accompany the discard (http://azer.com/aiweb/categories/magazine/ai151_folder/151_articles/151_mud_volcanoes.html).


Fig. 3 Example of pie in Paclele Mari region (Mrowczyk 2009).

Interestingly, mud volcanoes due to their specificity are not long-lasting objects (in a geological time), and are susceptible to erosive factors. At the same time, new cones or pies begin to form, and therefore the landscape, where mud volcanoes occur, changes constantly, creating more and more fascinating forms.

1.2 The outline of the geological structure of Romania

There are three main tectonic units in Romania: the south-western part of the East European Plate (EEP) called Moldavian Platform, Moesian micro-

plate (MP) and Intra-Alpine micro-plate (IAP). IAP is a core component of the Alpine orogen, which includes the Eastern Carpathians, the Southern Carpathians and the Apuseni Mountains. Besides, IAP also includes depressions such as Pannonia and Transylvania. The boundaries draw between the major tectonic units: TT zone (Teisseyre-Tornquist), extending NW-SE separating EEP and IAP, as well as major crustal faults separating MP from EEP and IAP. The area where all three boundaries of tectonic units meet is called Vrancea Region, and is characterized by high seismic and geodynamic activity (Baciu, 2007) (Fig.4).

There is the Carpathian Foredeep filled by thick Neogene molassic sediments located in the outer part of the Eastern and Southern Carpathians. On the basis of geologic and tectonic features, three sedimentary basins were distinguished there: Moldavian Basin, Focsani Basin and Getic Basin. The biggest thickness of sediments reaching 8000m is observed in Focsani Basin, on the other two indexes reach 3000m (Baciu, 2007).

Romania is a country characterized by moderate tectonic activity, and receives earthquakes at depths of 5 to 30 km. However, within its borders, there is one of the most tectonically active areas in Europe, where magnitudes of earthquakes reach

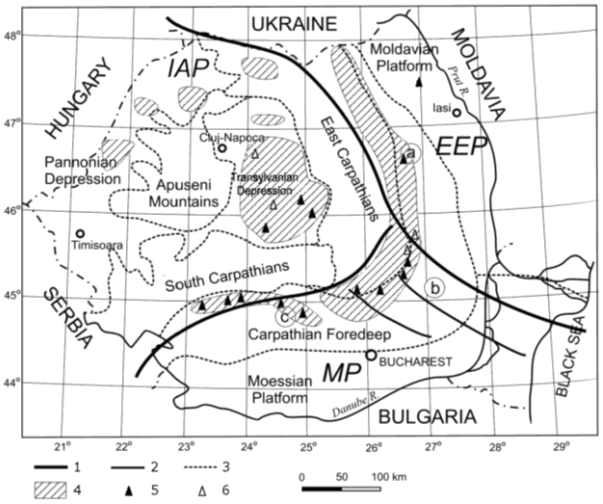

Fig. 4. Geotectonic units in Romania and distribution of mud volcanoes and hydrocarbon seeps in Romania. 1-limits between lithosperic plates (microplates); 2- major faults; 3- limits between main structural units; 4- hydrocarbon seepage areas; 5- mud volcanoes; 6- Dry macroseeps; EEP - East European Plate; IAP - Intra-Alpine Microplate; MP – Moessian Microplate; a - Moldavian Basin; b - Focsani Basin; c - Getic Basin (modified from Baciu, 2007).

7.7, and their hypocenters are located at 70 to 180km underground. It is in already mentioned Vrancea Region (Baciu, Etiope, 2005).

Romania also possesses is well-stocked in deposits of hydrocarbons (Fig. 4). Two of the richest regions are the Flysch Carpathians and the Carpathian Foredeep, where almost 110 deposits are located, and where the majority of mining has been taking place for the last 150 years. Research indicate that the age of these deposits dates back to Paleogene-Pliocene. Moreover, the hydrocarbons deposits are known from Moesian Platform, where over 125 structures, rich in natural gas and oil, were found at depths of 350 to 4900m, and exhibit a large age span: from the Devonian to the Pliocene (Paraschiv, 1979 cited in Baciu, 2007). Other, less important, Miocene gas deposits, were discovered in the western part of the Moldavian Platform. Furthermore, Transylvanian Depression is regarded as the biggest provider of natural gas for the Central and Eastern Europe (Baciu, 2007).

In Romania mud volcanoes are located in Carpathian Foredeep, Transylvanian Depression and Moesian Platform. The main aim of this paper is to describe mud volcanoes located in Carpathian Foredeep as a geoturism object.

1.3 Mud Volcanoes in Romania

The largest mud volcanoes in Romania are those located in the center of the Carpathian Foredeep, more precisely in the anticline structure called Berca-Arbanasi, of north-south orientation and 20 km long. Numerous faults occur in the anticline intersecting impermeable salt formations drawing on hydrocarbon deposits, enabling natural gas and mud to expel onto the surface (Etiope, 2004, Baciu, 2007).

Volcanoes are located there in four zones: Beciu, Paclele Mici (45°21’29.08”N, 26°42’44.47”E), Paclele Mari (45°20’22.17”N, 26°42’25.65”E) and Fierbatori, 20km North-West of Buzau (Fig.5). The distances, in straight line from specific zones, can be illustrated in the following way: Beciu-Paclele Mici - 3km, Paclele Mici - Paclele Mari - 2km; Paclele Mari - Fierbatori - 5km (Fig. 5). Two regions: Paclele Mici (PMI) and Paclele Mari (PMA) received the status of geological reserve in 1924 and they will be the subject of subsequent discussion (Etiope, 2004).

Paclele Mari and Paclele Mici regions are located in the central part of anticline, where strike-slip

fault intersects the axis of this anticline (Fig. 5). Paclele Mari (Fig. 6) region is a plateau 1.8km long and 3km wide and 80m high, whereas Paclele Mici (Fig. 7) is a slightly smaller plateau: 1.3km long, 1km wide, and 60m high. The surface of 1.62km^2 is covered by products originating from Paclele Mari volcanic activity, whereas the surface of Paclele Mici has only 0.62km$^{2.}$ The active volcanoes in Paclele Mari cover 0.22km^2 while in Paclele Mici 0.16km^2 (Baciu, 2007). In both regions over 60 holes emit methane: 62 holes in Paclele Mari expels 300 tons of methane to the atmosphere yearly, while 65 holes in Paclele Mici emit 255 ton/year. Methane comes out onto the surface through pores in ground in the following amounts: Paclele Mari 430 ton/year Paclele Mici 128 ton/year (Etiope, 2004). In both regions the volcanoes have cone shapes, and are 10m high, some of them have parasitic cone shapes, too. Furthermore, muddy substance reaches the surface through pies of 3 to 10m in diameter (Baciu, 2007).

In Fierbatori region (Fig. 5), located in the southern part of the discussed anticline feature, the surface, covered by products of volcanic activity, has 0,09km^2. Mud coming out to the surface is relatively watery there and has the shape of pies, and few small, rather flat cones (Baciu, 2007). What is more, large emission of methane through pores in ground is also noticed there. The first recorded eruption of muddy substance there took place in 1881 (Cobalcescu, 1883 cited in Etiope, 2004).

The smallest surface area, less than 0.01 km^2, covered by deposits from mud volcanoes (in form of pies), is located in the northern part of anticline, in the area of Beciu (Fig. 5). However, it was in this region that the biggest outflows took place in the past. A significant eruption occurred in November 1976, and 1 meter-"pillar" of mud eruption was seen for 24hours, and during 30 days of volcanic activity there 5000 tons of muddy material got out to the surface (Sencu, 1985 cited in Etiope, 2004). Slightly smaller, but also well- remembered event

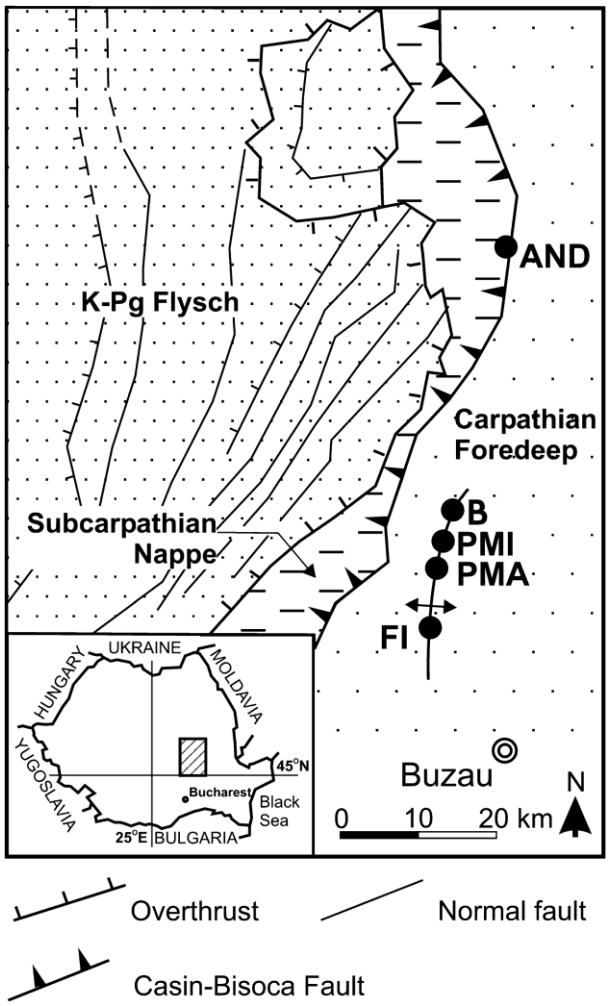

Fig. 5. Sketch map of the geostructural setting of the study area. AND-Andreiasu, B–Beciu, PMI-Paclele Mici, PMA-Paclele Mari, FI-Fierbatori (modified from Etiope 2004).

took place a year later when the local earthquake, which reached the magnitude of 7.2, was accompanied by 6h -mud eruption (Sencu, 1985 cited in Etiope, 2004).

The total surface of the four discussed areas, covered by products of volcanic activity, is estimated for 2,5km^2, whereas the total methane emission, according to research data, accounts for 1200 ton/ year (Etiope, 2004 cited in Baciu, 2007).

Fig. 6. Paclele Mari region (Madeja 2009).

Fig. 7. Paclele Mici region (Mrowczyk, 2009).

Furthermore, in the north-east of Beciu, there is a small village Andreiasu (Fig. 5) which is a natural reserve for the self-burning exhalations of gas-known as "Focul viu" (live fire). These fires burn all the time, and their columns can reach 1m high. The occurrence of fire is connected with a fault Casin-Bisoca located there (Etiope, 2004; Baciu, 2007). Geology of ground: hard marl, sandstones and volcanic tuffs do not favor mud formation, and therefore only natural gas (mostly methane), around 50 ton/year, is emitted to the surface of 400m^2 , and small amount of water (Baciu, 2007).

In the table 1 it is shown the composition of gas emitted in percentage terms in the discussed areas.

Table 1. Gas composition and He isotopes of the macro-seeps in Romania (PMI-Paclele Mici, PMA-Paclele Mari, FB-Fierbatori, AND-Andreiasu) (Baciu 2007).

	He (ppmv)	N_2 (%V)	CH_4 (%V)	CO_2 (%V)	3He/4He
PMI	24	2.8	94.9	2.3	$6.1x10^{-8}$
PMA	25.1	15.3	82.7	2	$6.1x10^{-8}$
FB	14.3	6.2	91.2	2.5	$2.1x10^{-8}$
AND	10.3	2.2	95.8	2	$4.3x10^{-8}$

2. Materials and methods

The material for investigation was collected to glass containers as samples of mud coming from the volcano. The samples were spread at laboratory using following sieves: 2mm, 1mm, 0,5mm, 0,18mm. Each fraction was then dried and prepared for analysis.

Coarse fractions were tested using digital as well as polarizing light microscope. Mineral composition of fractions was determined after counting of 500 grains at each sample. Results were collected in tables and illustrated in the form of diagrams.

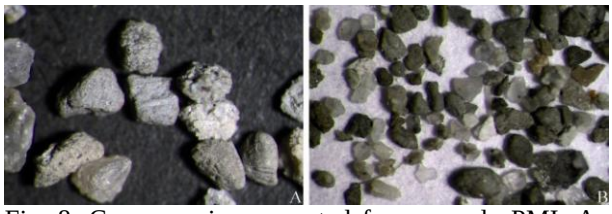

Fig. 8. Coarse grains separated from sample PMI. A–rounded fragments of rocks, B–fragments of rocks (dark grey) mixed with sharp grey and milky quartz . Digital microscope, magnification 20x.

Table 2 Separation of fractions in samples PMI and PMA.

	<0,18mm	0,5-0,18mm	1-0,5mm	1-2mm
PMI	99,33%	0,62%	0,04%	0,01%
PMA	99,63%	0,32%	0,05%	0%

Fine, clay fraction was observed under Jeol 540 SEM and examined using X-ray diffraction method.

3. Results and Discussion

3.1 Sample PMI

Natural sample represented clayey mud of grey color. Separation of fractions showed that sample was composed mostly of grains 0,5-0,18mm and 1.0-0,5mm (Tab. 2). Microscopic observation performed by digital microscope showed the presence of rock fragments as well as sharp grains of gray and milky quartz (Fig. 8, 9). However, it did not answer question concerning petrological character of rocks fragments, therefore further investigation was performed by use of polarizing light microscope.

Further investigation showed that fragments of rocks as well as quartz are main components of

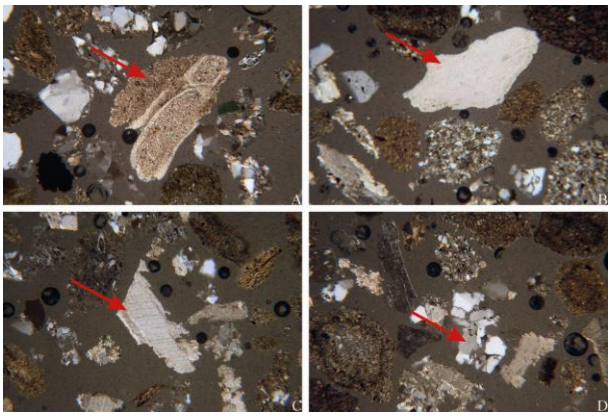

Fig. 9. Microscopic picture of coarse fractions separated from sample PMI. A–grain of limestone containing foraminifera, B–fragment of cortex bone, C-fragment of calcite monocrystal, D-fragments of fine sandstone and claystones. Polarizing light microscope, polaroides X, magnification 80 x.

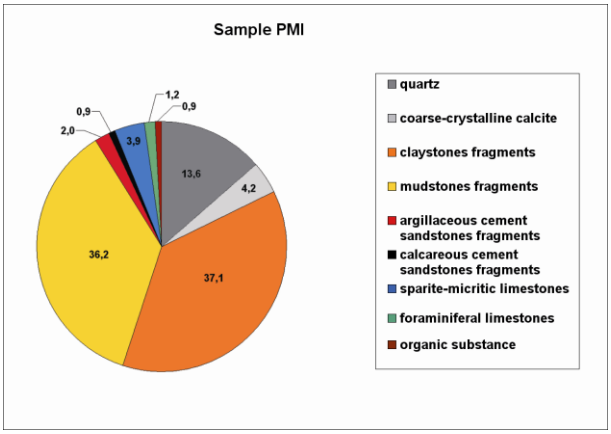

Fig. 10. The diagram showing mineral composition of fraction 0,5-0,18mm selected from sample PMI.

this fraction (Fig. 9, Tab. 3, Fig. 10).

Investigation of fine fractions performed using SEM microscope showed that they were composed of clay flakes mixed with fine quartz (Fig. 11). This identification was confirmed by X-ray pattern. X-ray examination of natural orientated sample showed the illite and mixed smectite-illite minerals as main clay components of sample (Fig. 12). On the other hand, detrital material was represented mainly by quartz, calcite and traces of feldspars. The value d_{hkl} = 7.6A confirms the presence of gypsum, however this mineral was present most probably in fraction < 0.18mm because in coarser fractions tested using polarizing light microscope gypsum was not identified.

The presence of mixed illite-smectite clay minerals was confirmed additionally by X-ray examination

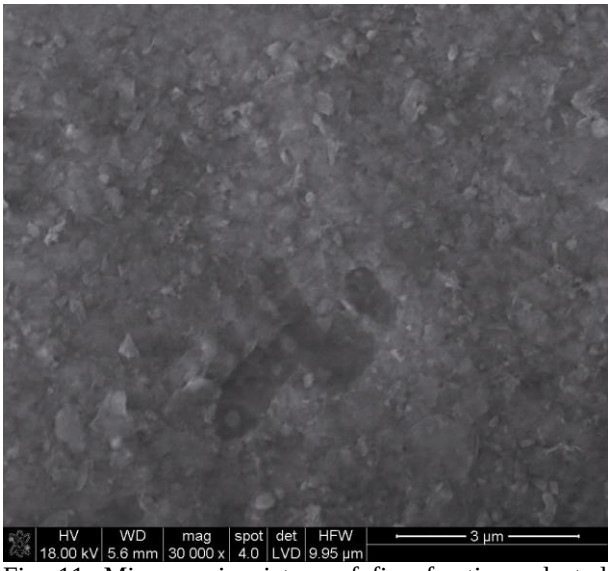

Fig. 11. Microscopic picture of fine fraction selected from sample PMI. One can see small flakes of clay minerals present together with fine grains of quartz. SEM. Magnification 30 000x.

of sample after glycole (Fig. 13) where two small peaks showing values d_{hkl} about 13.8 and 14.2A can be perceived.

Chemical analyses performed using ICP method showed that volcano waters are composed of mud mixed with salty waters. Moreover, chemistry of these waters collected from the two separate volcanoes were different (Tab. 4, 5). Differences concerned major as well as minor components of salty waters suggesting two various wags of water mineralization. Waters of sample PMI contained more Na whereas sample PMA contained more Ca. These differences suggest that PMI mud volcanoes were supplied by waters penetrating salt layers and waters from PMA volcanoes were connected with limestones ore rock containing higher amount of calcium. Waters from the PMA volcanoes contained additionally more Mg, Sr and K but the content of Br and J was at both waters similar confirming the connection of volcanoes waters with evaporate systems (Fig. 14).

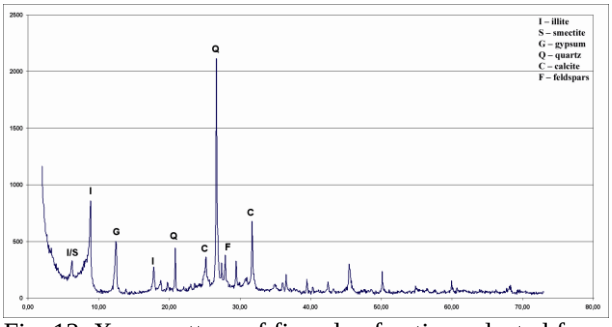

Fig. 12. X-ray pattern of fine clay fraction selected from sample PMI.

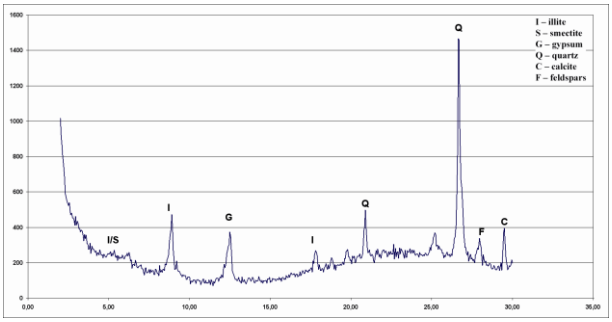

Fig. 13. X-ray examination of sample PMI after glycole.

3.2 Sample PMA

Sample represented soft, gray clay with admixture of fine mud fraction (Tab. 2). Investigation confirmed that tested sample did not contain grains bigger than 1mm. Finer material was of similar character as observed in sample PMI however, more quartz and less fragments of rocks could not be perceived (Fig. 15).

Table 3. Mineral composition of fraction 0,5-0,18mm selected from sample PMI and PMA.

		PMI	PMA
minerals			
	quartz	13,6	45,0
	coarse-crystalline calcite	4,2	1,7
clastic rocks fragments			
	claystones fragments	37,1	23,3
	mudstones fragments	36,2	19,4
	argillaceous cement sandstones fragments	2,0	3,8
	calcareous cement sandstones fragments	0,9	2,6
limestones fragments			
	sparite-micritic limestones	3,9	1,2
	foraminiferal limestones	1,2	1,8
evaporites fragments			
	fine-crystalline gypsum	0,0	0,5
igneous rocks fragments			
	rhyolite character effusive rock frament	0,0	0,3
organic substance	organic substance	0,9	0,4

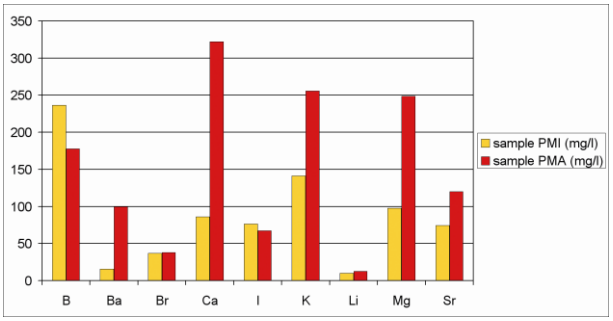

Fig. 14. Diagram showing content of main elements at tested waters from mud volcanoes.

A more detailed observation performed by polarizing light microscope confirmed quartz and rocks fragments as the main components in this fraction (Fig. 16, Tab. 3, Fig. 17).

X-ray pattern of natural sample showed a general mineral composition similar to composition of sample PMI, however, it contained slightly more clay minerals represented mostly by illite (Fig. 18, d_{hkl} = 10.1A). The content of other identified minerals such as quartz and feldspars was similar to a sample PMI, but it contained less carbonates represented by calcite (Fig. 18, d_{hkl} = 3,85A, 3.03A). Gypsum was present in this sample at fraction > 0.18mm and was identified under microscope observation. The amount of coarse grains was small (Tab. 3). This fact confirmed that gypsum was also present in fine fraction.

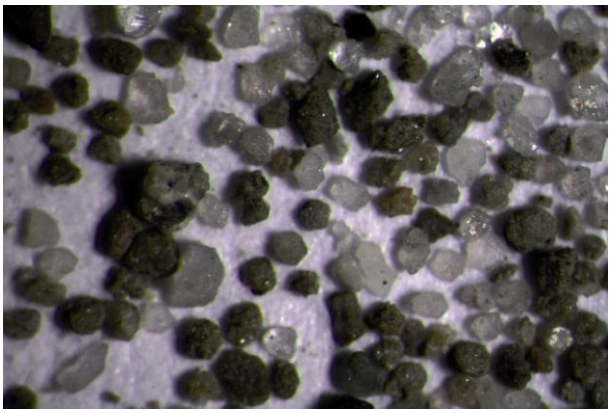

Fig. 15. Fraction 0,5-0,18 mm selected from sample PMA. Digital microscope, magnification 20x.

X-ray pattern of orientated natural (Fig. 18) and not orientated sample (Fig. 19) confirmed quartz and clay minerals to be the main component.

4. Conclusions

Examination showed that the mud volcanoes transports mostly mud composed of clay minerals represented by illite-smectite. Together with clay minerals one can determine quartz and rocks fragments, present at various proportions, in volcanoes mud. Salty waters transported by mud volcanoes are chemically differentiated too.

Obtained data i.e. results of chemical analyses confirm various sources of salty waters as well as their migration across various evaporites present below volcanoes.

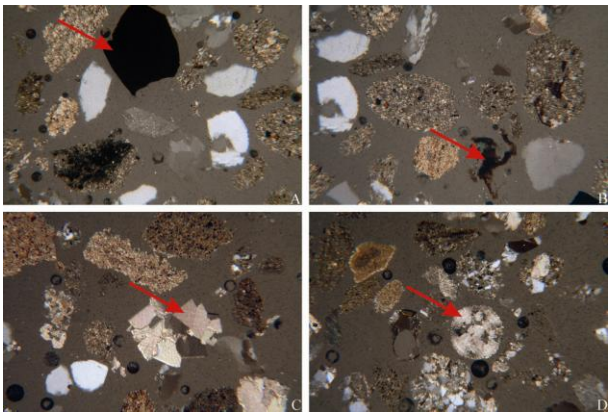

Fig. 16 Microscopic picture of coarse fractions separated from sample PMA. A-black fragment of organic matter (charcoal?), B-fragments of claystones and mudstones together with irregular fragment of organic matter, C-aggregates of calcite crystals grains of quartz and fragments of claystones, D-skeleton of foraminifera mineralized with calcite between grains of mudstones and claystones. Polarizing light microscope, polaroides X, magnification 80x.

Table 4 Chemical composition (mg/l) of waters from mud volcanoes.

	PMI	PMA		PMI	PMA
Ag	0.003139	0.002056	**Mn**	0.019799	0.051006
Al	0.112184	0.480066	**Mo**	0.060520	0.017069
As	0.071971	0.090101	**Na**	15430.000	17810.000
B	236.2961	178.0153	**Ni**	0.015888	0.016025
Ba	15.734322	99.995579	**P**	1.470154	0.894768
Be	0.000181	0.000271	**Pb**	0.004990	0.031456
Bi	0.000757	0.000682	**Rb**	0.145275	0.336015
Br	36.986726	37.823335	**Sb**	0.006419	0.002936
Ca	86.265110	322.38698	**Se**	0.148906	0.100473
Cd	0.000324	0.000898	**Si**	12.500321	10.206566
Co	0.002561	0.002570	**Sn**	0.001077	0.000754
Cr	0.270529	0.345542	**Sr**	74.236739	120.285076
Cs	0.000355	0.001520	**Te**	0.000640	0.001001
Cu	0.239583	0.285641	**Tl**	0.000381	0.000197
Fe	0.541477	1.864679	**U**	0.000283	0.000872
Ga	0.308273	1.265757	**V**	0.075059	0.092024
Hg	0.031424	0.022678	**W**	0.228601	0.000628
I	76.716075	67.336015	**Y**	0.000474	0.001355
K	141.148990	255.560988	**Zn**	0.073695	0.136326
Li	10.252115	12.687268	**Zr**	0.001215	0.000334
Mg	97.786107	248.445632			

Mineral composition of volcanoes mud as well as chemical composition of their salty waters suggest their good features for utilization. Because of this there is necessity to continue investigation of mud volcano region as potential area for balneology and recreation.

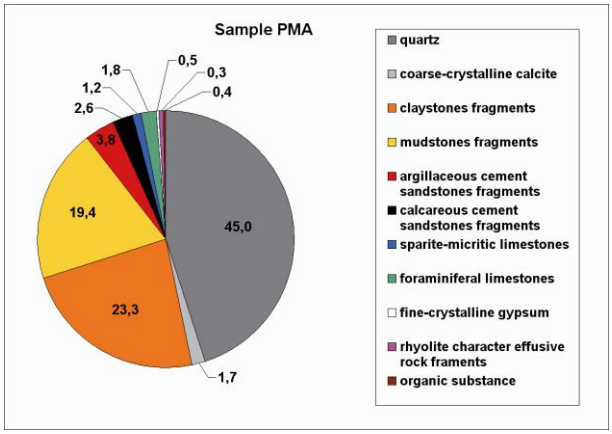

Fig. 17. The diagram showing mineral composition of fraction 0,5–018mm selected from sample PMA.

5. Current state of geoturism development

The observations made in July, 2009 clearly indicate that touristic infrastructure in the region of mud volcanoes is rather underdeveloped. The marking of access roads to the volcano areas is virtually non-existent. Occasional signposts, only in Romanian language, often force tourists to guess where to go. Although the way to Paclele Mici is relatively easy to decipher, it is difficult to get to Paclele Mari on the other hand. The roads to Beciu or Fierbatoni are not labeled at all. Reaching Beciu requires several hours marching, or possessing off-road vehicle as the road is a very low quality. However, getting to Fierbatoni seems almost impossible for an average tourist, as even the locals do not know the way.

Table 5 Anions containing in sample PMI and PMA.

	Cl (mg/l)	HCO_3 (mg/l)
PMI	25094,84	2249,314
PMA	32054,67	917,318

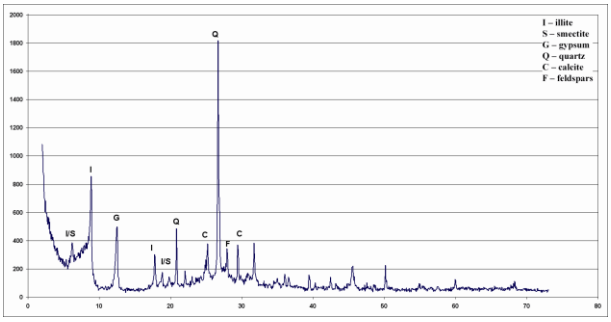

Fig. 18. X-ray pattern of fine clay fraction selected from sample PMA.

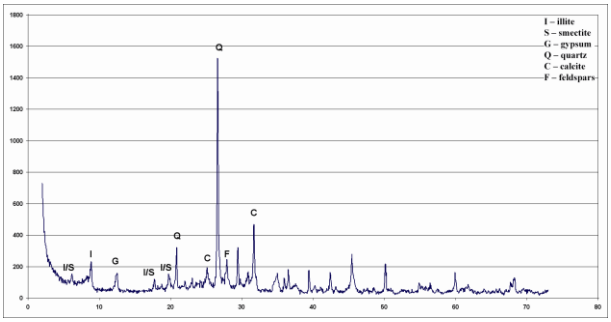

Fig. 19. X-ray pattern of not orientated sample PMA.

There is a guest house with restaurant nearby the reserve PMI, but the quality of rooms and bathrooms does not meet the Europeans standards, although the establishment is relatively new. Berca offers more possibilities of accommodation and catering.

Tourists must pay to enter PMI and PMA reserves. PMI volcanoes are located next to access road, and there is also a small car park there. The only English source of information can be purchased in a form of a brochure, however the books about volcanoes and souvenirs from the region are available only in Romanian language. Right behind the entrance gate, there are two information boards, one concerns terms of use of the reserve, in the other there is a map of attractions in nearby localities. However, the problem arises here as well, as both boards are in Romanian language.

General information about mud volcanoes

Mud volcanoes are defined as geological features through which agrillaceous material is altered and transported from the Earth's interior and expelled onto its surface. The size of mud volcanoes ranges from a few centimeters to several meters of width, and from a few centimeters to 500-700 meters of height, whereas the biggest offshore mud volcano reach the diameters of 30 km and about 2 km of relative height (Kopf 2002).

Generally, mud volcanoes have the shape of cones or pies. The former, depending on the viscosity of the muddy substance, exhibit various inclinations from 35 - 40° , and sometimes are characterized by the presence of parasitic cones on the slopes. The latter, are characterized by slight inclination of slopes <5°, and become cylindrical or irregular in shape. Both forms may occur in active or fossil form (Kopf 2002).

The substance flowing out of mud volcanoes can be both watery, thus such outflows are constant and accompanied by characteristic bubling, however, at times they can be viscid, sticky and therefore, more spectacular eruptions of discarding fireballs can take place. Frequently, slight traces of oil accompany the discard.

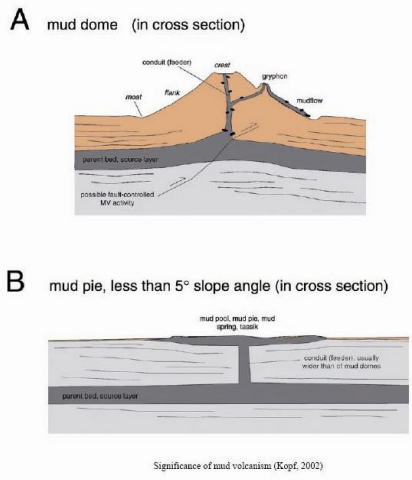

Significance of mud volcanism (Kopf, 2002)

Mud volcanoes in the world

There are about 700 mud volcanoes known in the world, and almost half of them can be found in Azerbaijan. The other ones were also discovered in Turkmenistan and in the south-Caspian region, in Australia, Taiwan, China, Pakistan and Iran. Only a few are found in Europe: in the south-west of Ukraine, in Southern Italy and Sicily, and in Romania. It is also worth noticing that mud volcanoes can form both onshore and offshore.

Mud volcanoes are commonly associated with compressional tectonics at convergent margins (Higgins and Saunders 1974; Barberet al. 1986; Kopf et al. 1998 cited in Kopf 2003). Their density shows a positive correlation with (1) thick, rapidly deposited sediments consisting of high clay mineral component (Yassir 1989 cited in Kopf 2003), (2) sediment overpressuring due to hydrocarbon formation (Hedberg 1974; Lavrushin et al. 1996 cited in Kopf 2003), (3) a structural association with tectonic shortening dehydration (Moore and Vrolijk 1992 cited in Kopf 2003) and/or earthquake activity (Sondhi 1947 cited in Kopf 2003), (4) fluid emission such as gas, brines, water from mineral dehydration (Moore and Vrolijk 1992 cited in Kopf 2003) and gas hydrate dissociation (Milkov 2000 cited in Kopf 2003), and (5) polymictic assemblages of the surrounding rock present in the ejected argillaceous matrix (Robertson and Scientific Party of ODP Leg 160 1996; Kopf et al. 1998 cited in Kopf 2003).

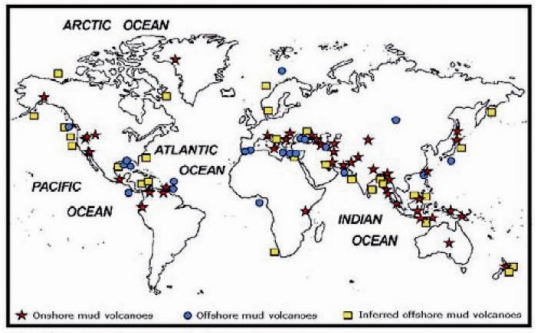

Worldwide distribution of mud volcanoes (modified from Milkov, 2003)

Mud volcanoes in Romania

In Romania mud volcanoes are located in Carpathian Foredeep, Transylvanian Depression and Moesian Platform. The largest mud volcanoes in Romania are those located in the center of the Carpathian Foredeep, more precisely in the anticline structure called Berca-Arbanasi, of north-south orientation and 20 km long. Volcanoes are located there in four zones: Beciu, Paclele Mici (45°21'29.08" N, 26°42'44.47" E), Paclele Mari (45°20'22.17" N, 26°42'25.65" E) and Fierbatori, 20km North-West of Buzau. The distances, in straight line from specific zones, can be illustrated in the following way: Beciu-Paclele Mici - 3km, Paclele Mici – Paclele Mari – 2km; Paclele Mari – Fierbatori – 5km. Two regions: Paclele Mici and Paclele Mari received the status of geological reserve in 1924.

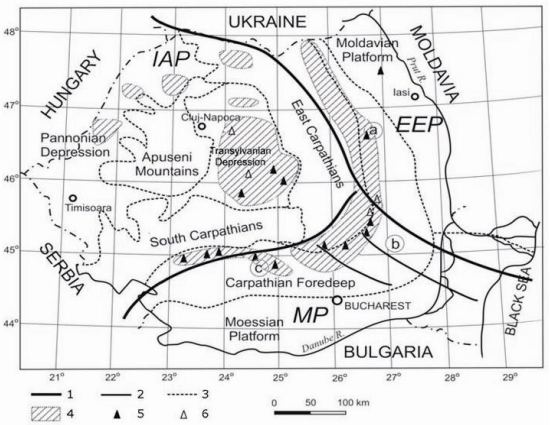

Geotectonic units in Romania and distribution of mud volcanoes and hydrocarbon seeps in Romania. 1 - limits between lithosperic plates (microplates); 2 - major faults; 3 - limits between main structural units; 4 - hydrocarbon seepage areas; 5 - mud volcanoes; 6 - Dry macroseeps; EEP - East European Plate; IAP - Intra-Alpine Microplate; MP – Moessian Microplate; a - Moldavian Basin; b - Focsani Basin; c - Getic Basin (modified from Baciu 2007).

Fig. 20. Information board proposition "General information about mud volcanoes" (Mrowczyk and Madeja, 2009).

Mud volcanoes in Paclele Mari region

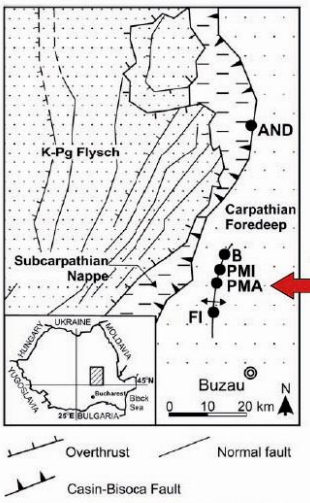

Sketch map of the geostructural setting of the study area. AND-Andreiasu, B–Beciu, PMI-Paclele Mici, PMA-Paclele Mari, FI-Fierbatori (modified from Etiope 2004).

Paclele Mari and Paclele Mici regions are located in the central part of anticline, where strike-slip fault intersects the axis of this anticline. Paclele Mari region is a plateau 1.8km long and 3km wide and 80m high. The surface of 1.62 km^2 is covered by products originating from Paclele Mari volcanic activity. The active volcanoes in Paclele Mari cover 0.22km^2 (Baciu 2007). The volcanoes have cone shapes, and are 10m high, some of them have parasitic cone shapes, too. Furthermore, muddy substance reaches the surface through pies of 3 to 10m in diameter (Baciu 2007). 62 holes in Paclele Mari expels 300 tons of methane to the atmosphere yearly. Methane comes out onto the surface also through pores in ground in the amounts 430 ton/year. The composition of gas emitted in PMA are: CH_4 (82,7%), N_2 (15,3%), CO_2 (2%) and sprinkling He (Etiope 2004).

Natural sample represented soft, gray clay with admixture of fine mud fraction: grains 0,5-0,18mm (99,63%) and 1.0-0,5mm (0,32%). Main components of fraction 0,5-0,18mm are quartz (45%), fragments of claystones (23,3%) and mudstones (19,4%). Volcanoes waters are composed of mud mixed with salty waters. Main elements at tested waters from mud volcanoes are: Ca, K, Mg, B, Sr,Ba, I, Br and Li. So great amount of Ca suggesting that waters from PMA volcanoes are connected with limestones ore rock containing higher amount of calcium.

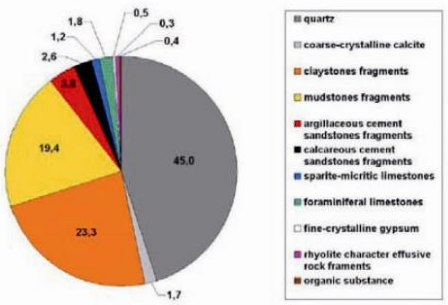

The diagram showing mineral composition of fraction 0,5 - 0,18mm

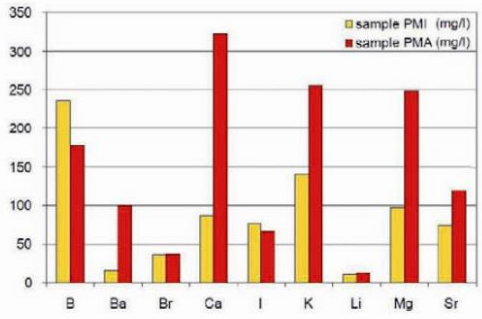

Diagram showing content of main elements at tested waters from mud volcanoes

Fig. 21. Information board proposition ”Mud volcanoes in Paclele Mari region” (Mrowczyk and Madeja, 2009).

Mud volcanoes in Paclele Mici region

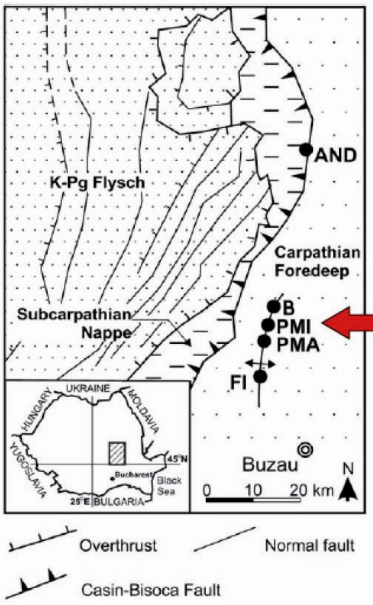

Sketch map of the geostructural setting of the study area. AND-Andreiasu, B–Beciu, PMI-Paclele Mici, PMA-Paclele Mari, FI-Fierbatori (modified from Etiope, 2004).

YOU ARE HERE

Paclele Mari and Paclele Mici regions are located in the central part of anticline, where strike-slip fault intersects the axis of this anticline. Paclele Mici region is a plateau 1.3km long, 1km wide, and 60m high. The surface of 0.62km^2 is covered by products originating from Paclele Mici volcanic activity. The active volcanoes in Paclele Mici cover 0.16km^2. The volcanoes have cone shapes, and are 10m high, some of them have parasitic cone shapes, too. Furthermore, muddy substance reaches the surface through pies of 3 to 10m in diameter (Baciu 2007). 65 holes in Paclele Mici expels 255 tons of methane to the atmosphere yearly. Methane comes out onto the surface also through pores in ground in the amounts 128 ton/year. The composition of gas emitted in PMA are: CH_4 (94,9%), N_2 (2,8%), CO_2 (2,4%) and sprinkling He (Etiope 2004).

Natural sample represented clayey mud of grey color, composed mostly of grains in fractions 0,5-0,18mm (99,33%) and 1.0- 0,5mm (0,62%). Main components of fraction 0,5-0,18mm are fragments of claystones (37,1%) and mudstones (36,2%) as well as quartz (13,6%). Volcanoes waters are composed of mud mixed with salty waters. Main elements at tested waters from mud volcanoes are: Na, B, K, Mg, Ca, Sr, Br, Ba, Li. So great amount of Na suggesting that PMI mud volcanoes are supplied by waters penetrating salt layers.

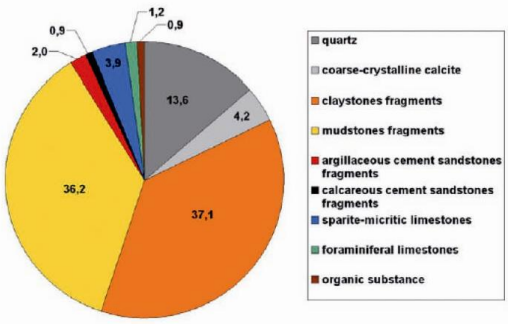

The diagram showing mineral composition of fraction 0,5-0,18mm

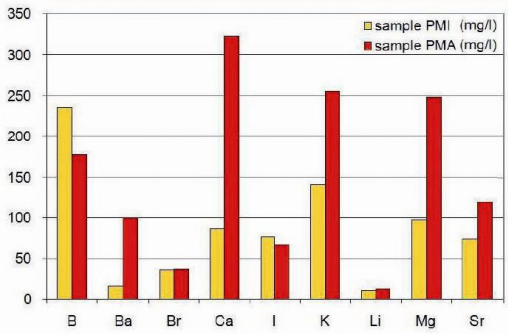

Diagram showing content of main elements at tested waters from mud volcanoes

Fig. 22. Information board proposition ”Mud volcanoes in Paclele Mici region” (Mrowczyk and Madeja, 2009).

It is advisable to ask for access road to PMA while visiting PMI, as the only existing sign can be missed easily, which is confirmed by a small number of visitors there. After reaching a small booth, located on a peripheral road, it is necessary to take a 20-minute walk still along an unmarked path to get to the volcanoes. Nevertheless, things are going to be changed in a near future, as some part of the path has already been lined with stones which makes it easier to move around. There are neither information boards, nor souvenirs in PMI.

Geotourism infrastructure in the discussed region is almost non-existent. It is a great pity as this type and class of object that belongs to major geotourism attractions in Romania, and whose values have been appreciated for 86 years, should possess such infrastructure. According to the definition a geotourism object can or/and may become an object of touristic interest if well promoted and easily accessed (Słomka and Kicińska-Świderska, 2004). Undoubtedly, PMA and PMI volcanoes fit the definition. Development of geotourism infrastructure in MV region would certainly broaden visitors' knowledge about the earth and processes present in its nature. More and more often tourists ask themselves when, why and how such geological object was created, thus an appropriate infrastructure even in the form of information boards and folders would provide them with the answers and thereby elevate the importance of the object.

In the discussed region, it would be enough to put up one or two information boards upon entrance to the reserve, providing a comprehensive geoinformation for an average tourist, without causing any damage to the landscape. To achieve as smallest interference into the landscape as possible, the boards should be two-sided and contain the same information in both languages (Romanian and English), so that every tourist has an equal opportunity to know their content. Well-selected information, photos and drawings would enrich aesthetic experience obtained from the visit to this extraordinary place.

Although there are many publications about mud volcanoes, they are not available to public. Therefore, the next step of development in PMI and PMA zones should concern the creation of a folder, including geological information about mechanisms of formation and activity of mud volcanoes, their correlation with occurrence of earthquakes, and some pieces of information about regional geology. Furthermore, it should contain data concerning: hydrocarbon migration, diversified mineral composition of mud from PMI and PMA, as well as water chemistry. The following figures show examples of information boards (Fig. 20, 21, 22).

Establishing an appropriate geotourism infrastructure in PMI and PMA mud volcanoes areas, enabling tourists to know the differences between the two presented herein regions would not only enrich the aesthetic impressions remaining after visiting these fascinating places, but also would enhance the educational offer of the reserves.

Acknowledgments

We would like to express our gratitude to Professor Maciej Pawlikowski for his help in carrying out and analyzing the results obtained from this study.

References

Baciu C., Caracausi A., Etiope G. and Italiano F., 2007. Mud volcanoes and methane seeps in Romania: main features and gas flux, Annals of Geophysics, 50 (4).

Baciu C, Etiope G., 2005. Mud volcanoes and seismicity in Romania, Martinelli G. and Panahi B. (eds.), Mud Volcanoes, Geodynamics and Seismicity, 77–87 Springer.

Etiope G., Baciu C., Caracausi A., Italiano F. and Cosma C., 2004. Gas flux to the atmosphere from mud volcanoes in eastern Romania, Terra Nova, 16, 179–184.

Kopf A., 2002. Significance of mud volcanism, Reviews of Geophysics, 40(2), 1005.

Kopf A., 2003. Global methane emission through mud-volcanoes and its past and present impact on the Earth's climate, Springer-Verlag.

Milkov A., Sassen R., Apanasovich T. and Dadashev F., 2003. Global gas flux from mud volcanoes: A significant source of fossil methane in the atmosphere and the ocean., Geophysical Research Letters, 30 (2), 1037.

Słomka T. and Kicińska-Świderska A., 2004. The basic concepts of geotourism. Geoturystyka/Geotourism, 1 (1), 5-7 (in Polish with English abstract).

Special Session G29
Promoting geoconservation in South-Eastern Europe – Geoparks

Scientific Annals, School of Geology, Aristotle University of Thessaloniki Proceedings of the XIX CBGA Congress, Thessaloniki, Greece	Special volume 100	503-512	Thessaloniki 2010

BUZAU LAND GEOPARK. STEPS IN BUILDING A NEW GEOPARK IN ROMANIA

Andrasanu A.

Department of Geology and Palaeontology, Faculty of Geology and Geophysics, University of Bucharest, 1, Nicolae Balcescu Bd., sect.1, Bucharest, Romania, mesajalex@yahoo.com

Abstract: Rapid development of geopark concept and positive results of existing geoparks have generated in Romania both the official recognition of geopark as distinctive protected area and the increase of interests of new territories to develop geoparks. Based on a local initiative and a grass root effort a new geopark project has been launched in Romania: The Buzău Land Geopark. Located in the South-eastern part of Romania (Fig. 1), the territory covers about 1100 sq kilometers, comprises 18 mayoralties and a population of 45000 inhabitants. Unique geological sites like: mud volcanoes, amber deposits, salt caves and oil springs are present. Sedimentary rocks folded and overthrusted are depicting a geological history covering more than 70 million years. The paper is presenting the main steps taken so far in building the new geopark. The approach is based on our previews experience in Hateg Geopark and in other geoparks members of the European Geoparks Network. The process comprises: interdisciplinary research studies, stakeholders identification, local heritage evaluation, and sustainable development strategy design, establishing the basic requirements for a brand development, correlation with local projects and initiatives and design of training courses for the geopark team. This approach allowed us to identify the optimal territory for the geopark, to create a framework for partnership, local needs identification and to set-up clear objectives for sustainable use of local resources. The commitment of local communities has generated national projects dealing with public awareness, cultural events, promotion, and informal education. All these are valuable elements to prove the rightness of the geopark concept and its capacity to join around groups and stakeholders from different areas of interest.

Keywords: geopark, Romania, Buzau Land, sustainable development

1. Introduction

The geopark concept as we know it today is the result of continuous efforts of few dedicated specialists and of innovation and cooperation of different teams and territories across Europe. Key elements of the concept development are synthesized bellow:

a) Innovative approaches in using local geological heritage as main resource for socio-economic development in LEADER territories from France, Germany, Greece, Spain then Italy, Great Britain and other countries (Frey, 2003; Martini, 2003; Zouros, 2003, Zouros, 2004);

b) Continuous development of geoconservation activities especially after the *1st International Symposium on the Conservation of our Geological Heritage* and of the *4th International meeting of the Earth Science Conservation – European Working Group*, held in Digne, France, in 1991 that adopted the *Digne Declaration*;

c) The need for a practical use in geotourism, education and public awareness of all geological assets identified and classified by different geopark teams, working groups of ProGEO, specialists from natural parks and museums and other professional geological associations (Brilla et al., 1999; Hose, 1999; Page, 1999; Fassoulas, 2003; Kollman, 2003; Macadam, 2003; Watson, 2003; Weber, 2003);

d) The need for an integrated approach and a beter understanding of the close connection of natural environment and socio-economic needs for sustainable development plans designe and for local Agenda 21 as required Rio the Conference in Brazil, in 1992.

The beginning of European Geoparks Network (EGN) started in 1996, and was clearly stated in 2000 as a result of an international project among four territories focused on their geological heritage

(Zouros & Martini, 2003, Zouros, 2004; Frey et al., 2006). UNESCO`s division of Earth Sciences supported from the beginning the process and had a first attempt to launch a new programme and a geopark label in 1997 when a first guidelines was issued (Patzak & Eder, 1998). UNESCO watched and sustained the process and, based on the European experience and results, extended the concept worldwide in 2004 (UNESCO, 2004, 2008) when the Global Geopark Network (GGN) was set up. The geopark approach of geoconservation proved to be very efficient and now EGN has 35 members from 13 countries and GGN has 63 members from 19 countries.

A Geopark creates appropriate methods to raise the awareness for the geological heritage of our planet and developes new strategies in nature conservation and local development. During the 2nd UNESCO International Conference on Geoparks, held in Belfast, in 2006, Guy Martini (2006) launched the provocation of a complete new vision of geopark concept and management and suggested to some of the oldest geoparks to develop inside their territory experimental zones called "geopark - phase II".

Hateg Country Dinosaurs Geopark (HCDG) was the first geopark in Romania (Fig.1). Established in 2004 as a natural park, it joined EGN and GGN in 2005. HCDG is the result of a grass root effort which started in 2001. It`s development followed since the beginning the EGN Charta, and UNESCO`s reccomandations but adapted to local social and economic realities (Grigorescu & Andrasanu, 2003). The territory of Hateg Geopark is a good example of the geodiversity of Carpatho – Balkan region. Geological evolution of the area covers more than 500 million years and the network of geosites comprises: granite outcrops and boulders, bauxite quarries, reef limestone, volcanic structures, Mesozoic and Cenozoic continental and marine fossils, karst and cave systems. The territory contains one of the latest assemblages of dinosaurs in the world, internationally unique and commonly known as the "dwarf dinosaurs of Transylvania" (Grigorescu, 2005).

Our experience in Hateg Geopark set-up and management and in other geoparks reveal that for the South East European countries there are special economic and social conditions we have to take into consideration in the process of building a geopark (Grigorescu & Andrasanu, 2006).

Hateg Geopark experience generated in Romania a new approach in nature conservation, Romania beeing one of the first countries to recognise the geopark as a distinct protected area according to the Act no. 57/ 2007. Also geodiversity become part of management plans in several natural and national parks and new geopark initiatives and projects were launched: Mehedinti Plateaux Geopark (South Carpatians) is already recognised as natural park, Buzau Land Geopark (southern part of East Carpathians) is near to become official a geopark (Andrasanu, 2008). and a new initiative for Baia Mare Geological and Mining Park (northern part of East Carpathinas) was launched in 2009 (Kovacs & Fulop, 2009).

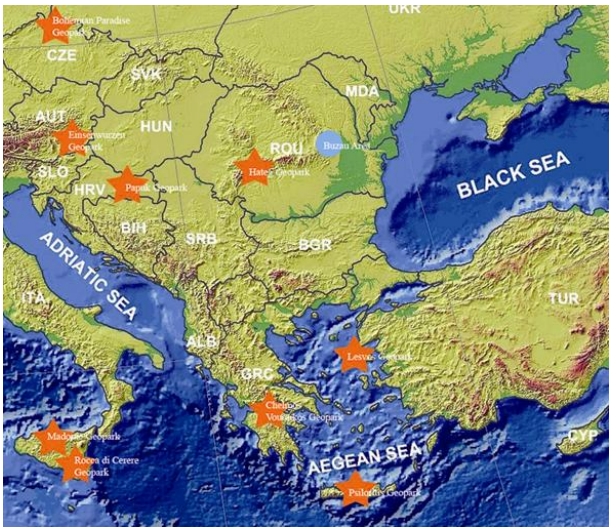

Fig. 1. Location of the Buzau Geopark area. The stars point geopark members of the European Geoparks Network (modified after EGN map, 2009).

The Buzău Land Geopark project is an initiative of the Buzau County Council in partnership with the University of Bucharest and is supported by other local and national bodies and institutions. Located in South East of Romania, in the Carpathian bend zone, the territory endorses unique geological places and phenomenon, a high biodiversity, five Natura 2000 sites, and a well preserved cultural heritage. All these assets recommend the area to be well fitted to become a geopark.

2. Materials and Methods

Our research approach in geopark project development was focused in keeping a balance among the requirements of what an international geopark means, the local socio-economic and cultural realities and the need to create a base for further European funded projects and initiatives.

Cooperation and partnership development between institutions and private individuals, both from the public and private sectors, together with governmental and non-governmental organizations was the first step we taken so far. Three levels of partnerships and working groups were created: i) first one is that of decision makers and stakeholders; ii) the second one comprises national and local institutions with specialists from different areas of competence able to develop and sustain research studies; iii) and the third group is made of local enthusiastic people able to create a link among different teams and between specialists and local communities.

The second step was the evaluation of the partner`s interest and a work plan development (table 1). Interdisciplinary teams of specialists in geology, biology, anthropology, ethnography, sociology, tourism, education were established in order to produce detailed research studies of the whole area. The objective was to identify the territorial system components, their relationships, social and economical needs, and to assign a role and relative priority to each identified need (Andrasanu, 2007).

The third step was to analyse the results of preliminary studies for 36 mayoralties (more than 200 villages) foreseen to be part of the geopark. This activity offered us the possibility to evaluate the potential of geopark development and further management in the frame of the Buzau County and its neighbouring areas. This evaluation is important if we take into consideration that a geopark territory overlaps an organic context of tangible and intangible realities. Physical structures, such as geodiversity and biodiversity, are linked to local cultural identity. In respect to that the geopark area has to be coherent from the social, administrative and cultural point of view and to be a key element to support and strengthen local identity (Andrasanu & Grigorescu, 2006). The results of all these analysis indicated the need to select for the Buzau Land Geopark only 18 mayoralties (about 156 villages) from the 36 foreseen initially.

Table 1. The partnership working plan.

Objectives	Results	Assumptions
R1. Mapping proposed Geopark with relevant levels of protection	Map provided and endorsed by relevant local, national and international authorities and institutions	Results of surveys provide bulk of necessary technical information Realistic available data
R2 Complete inventory of geological, biological archaeological, cultural asets	Inventory provided and endorsed	Results of surveys provide bulk of necessary technical information
R3 Recreation / tourism opportunities (carrying capacity & infrastructure) analysed and sustainable financing resources identified	Identify the main element to support tourism development (tangible and intangible); SWOT Analysis for existing tourism activities Design the framework for a Management visitor plan; Identification of a brand	Appropriate co-operation with stakeholders; Funding opportunities available; Existing strategies for tourism development, commitment to applay them and appropriate local and national fund resources or chemes
R4 Small business development, analyse opportunities for small business development within Geopark framework, training and funding opportunities identified	Analyse of different local initiatives, projects, strategies, web pages; Questionaires, interviews with stakeholders, decision makers, local people; Intercomunal association to support the projects	Appropriate co-operation with stakeholders; Funding opportunities available; Realistic local development plans and political commitment; Prevoius co-operation projects of local stakeholders
R5 Provision of all necessary documents / guidelines and costs for registration and management of the geopark	Structure of the geopark documentation; Develop a Charta (Strategical famework) for the local communities; Develop the geopark brand : Buzau Land Geopark; Partnership with mass-media	Appropriate co-operation with stakeholders; Local initiative, existing associations and community projects; Policy makers and local stakeholders support the brand development and incorporate it in other initiatives
R6 Provision of all necessary documents for registration of the geopark as a protected area	Documents provided and endorsed; Local and national partnership for education, research and management	Local resources for geopark management; Project team; Charismatic person to represent the geopark
R7 Provision of all necessary documents for joining national network, EGN, GGN	Documents provided and endorsed; Management structure, financial resources, development plans, local partnerships	Commitment of local communities; Results and impact in geopark management

The fourth step was dedicated to detailed interdisciplinary studies for the selected villages and a SWOT analysis for tourism and community projects. The fifth step was to provide and endorse documentation for geopark official recognition and to set up a strategy to support local sustainable development. The sixth step was to identify the basic elements required to create the "Buzau Land Geopark" Brand and to sustain the project by national partnership projects. The Buzau Geopark Intercommunity Association was created to foster the geopark project in partnership with local and national institutions, universities and museums.

3. Results

Field research and documentation allowed us to map and inventory the components of the geopark geodiversity, biodiversity and cultural assets and to provide documents for further plans and projects.

The Romanian Carpathians are part of a complex structure formed in response to the Triassic to Tertiary evolution of three continental blocks. The first two are represented by Tisza (the Internal Dacides) and Dacia (the Median Dacides) the third one by Eastern European, Scythian and Moesia platforms. The blocks were separated by two oceanic domains, the Transylvanides and the Outer Dacides (Ceahlau – Severin) (Sandulescu, 1984; Csontos and Vörös, 2004; Schmidt et al., in press, Vasiliev et al., in press). Cretaceous and Miocene events led to the deformation of these units and their related sediments. According to different interpretation several structural units were identified (Sandulescu, 1984): Transylvanides, Piennides, Median Dacides, Outer Dacides, and Moldavides. The geopark territory is partially overlapping the Moldavides (Tarcau Nape and Subcarpathian nappe) and the thrusted internal foredeep. The geologic map (Fig. 2) shows a faulted and folded geological setting of flysch deposits of the Tarcau

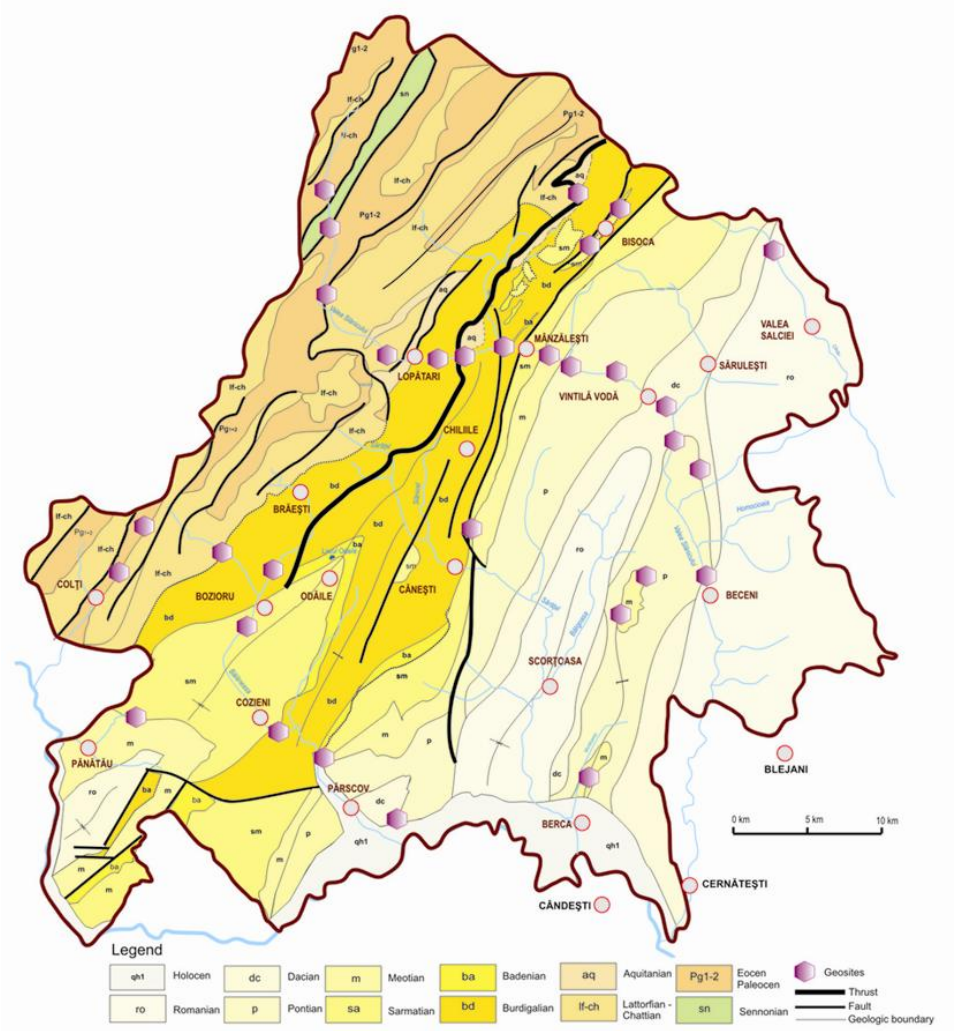

Fig. 2. Geologic map of the Buzau Land Geopark territory (after IGR, Covasna and Prahova maps, Sc. 1:200000).

Nappe (Sennonian – Lower Miocene), marls, sandstone, salt and gypsum of mollase type deposits of Subcarpathian Nappe (Lower – Middle Miocene) and sandstone, marls of marine, lacustrine, deltaic and fluviatile environments of the thrusted internal foredeep (Upper Miocene – Holocene). Associated fauna of invertebrate's fossils and sedimentary structures are characteristic for the last part of Tethys Basin Evolution, the transition to Paratethys (Dacic Basin) and the intermittent connections with other basins. A well documented sedimentary record of Messinian Crisis event and of the Miocene / Pliocene boundary in Paratethys are well represented along the Slanicul de Buzau Valley (Krijgsman et al., in press). The area is well known for its comprehensive Pontian, Dacian and Romanian deposits and also for few outstanding geological assets like Romanian amber, salt diapirs and mud volcanoes.

The Colti amber, Oligocene in age, is famous for its variety in color from yellow to black and insect's fossils remains and was described for the first time as *rumanit*. Samples of amber and a collection of documents and tools from a former local mine are exhibited in Colti Museum (Fig. 3).

Fig. 3. Examples of local geodiversity: mud volcanoes in Piclele Mari (left); Colti amber (center); salt Hills in Meledic area (right).

The salt deposits (Aquitanian) outcrop along faults and diapir structures in different locations. The largest area is in Meledic hill where salt like exo and endo karst structures could be seen (Fig. 3), fresh water lakes and typical salt habitats, all of them quite well preserved. The salt was a local trade product but also an important factor in generating natural hazards.

The biggest mud volcanoes in Romania are located on the Berca-Arbanasi hydrocarbon bearing structure (Eastern Carpathians Foredeep). The Paclele Mari (PMA) and Paclele Mici (PMI) areas were declared natural reserves since 1924 (Baciu & Ettiope, 2003) and now are part of a larger Natura 2000 SCI site. Their activity is generally quiescent with some intermittent explosive activity up to one meter high generating a peculiar landscape and a special habitat for halophile plants (Fig. 3).

Geopark biodiversity was shaped by the geological and climatic evolution of the Carpathians in connection to North Dobrogea and Black Sea areas. The geopark territory is covering three biogeographic regions: steppic, alpine and continental. Field studies allowed us to identify 77 habitats types, a great number of species listed in different national and European directives for nature conservation and few endemic species: *Euscorpius carpathicus, Nitraria shoberi and Artemisia santonicum.*

One of the most impressive historical and archeological characteristic is done by the 30 caves digged since VI century (?) by orthodox Christians in soft Oligocene sandstone beds. Hard living conditions and isolation of this small monastic community made people to call the area „Romanian Athos" (Fig. 4). The map from figure 5 presents a selection of natural and cultural sites of the Buzau Land Geopark.

4. Discussion

Rich geological and biological diversity often coincides with cultural diversity, and the conservation and management cannot be undertaken without the involvement of people closest to these resources. The main objectives of a geopark are: i) to respect and protect local cultural values; ii) to strengthen identification of the population with their area; iii) to foster socio-economic development that is culturally and environmentally sustainable. A successful geopark has a balanced construction, in terms of surface, resources and support and a good management structure. To build a Geopark means a bottom-up process, based on a

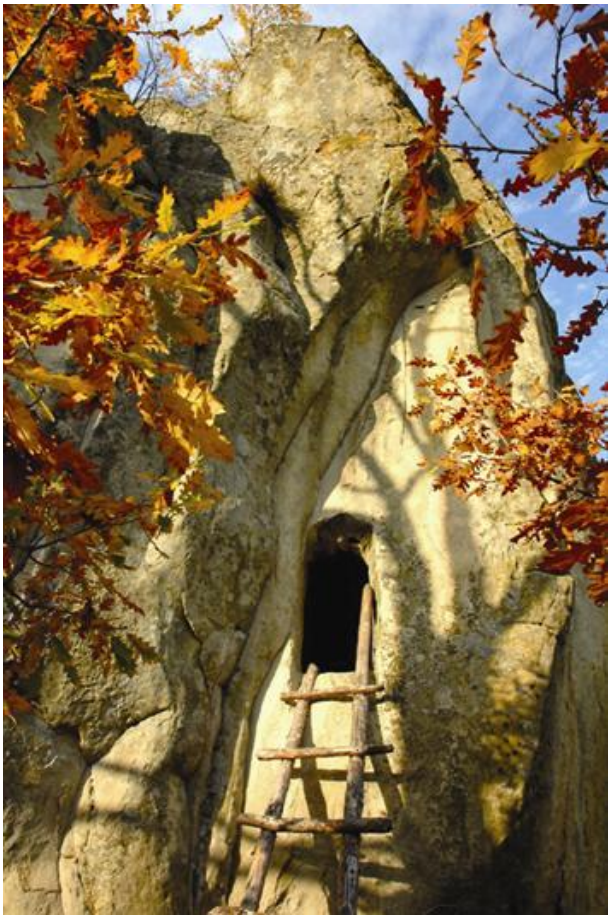

Fig. 4. Entrance of the "DionisieTorcatorul Cave" part of an ancient orthodox monastic settlement (photo credit M Mincu).

strong multi task-force concept and political will with long-term financial support. Effective management requires a strong commitment of local communities and administrations. To create a successful geopark one of the key point is to identify its optimum territory. An optimum territory could be defined by the following conditions:

1) Relevant network of significant and valuable geological, biological, cultural sites, with a balanced distribution and worthing to be preserved in a sustainable way;

2) A territory enough large to foster sustainable socio-economic development. A small territory of few communities has no natural, social and financial resources to support a geopark. A large territory is difficult to be managed in a sustainable way and generates conflicts with other development projects or land use plans;

3) A geopark territory has a cultural value being a distinct place of interaction between nature and people, a record of past and present activities and a place of local identity made by tangible and intangible values.

4) The associate communities have strong cultural, social and economic affinities. The management process requires a continuous consultation with relevant statutory bodies, to guarantee effective conservation and to adopts its own territorial policy for sustainable regional socio-economic and cultural development;

5) Geopark`s border is overlapping the administrative border of associate communities. Geopark management needs organizational arrangements to involve public authorities, local communities, private interests, and both research and educational bodies in partnership projects that cover the whole geopark territory.

The Buzau Land is a territory of continuous cultural influence of the three Romanian provinces: Transylvania, Moldavia and Wallachia. Being mainly a remote rural area these influences were continuously adapted and transformed to local characteristics in different degrees and generated cultural, social and economic differences among the communities. Field research, meetings of partners, public debates allowed us to identify local values, cultural affinities and the commitment of different structures to participate in geopark development. The results indicate that the initial territory of 36 mayoralties foreseen by county administration for a future geopark is not an optimum one due to the following considerations:

The initial territory is too large, about 30% of the county surface (Fig. 6), being a potential source of unbalanced development and conflicts. The high mountain area in Northwest is very sparsely populated and our recommendation is for that part to be integrated into a regional national park;

There is an unbalanced distribution of the geological, biological and cultural sites. The Eastern and Southern parts left out are mostly agricultural areas with less geological and biological sites of interest;

Due to geographical position an historical evolution there are communities with strong influence, cultural affinities and commercial connections in the neighboring regions Transylvania, Wallachia and Moldavia (Fig. 7). This context generates a lack of commitment or interest for different communities to work together within a geopark

The selected territory considered being optimum for geopark development and management comprises 18 mayoralties representative for what was historical called "Buzau Land". These communities are strongly bound by cultural, commercial,

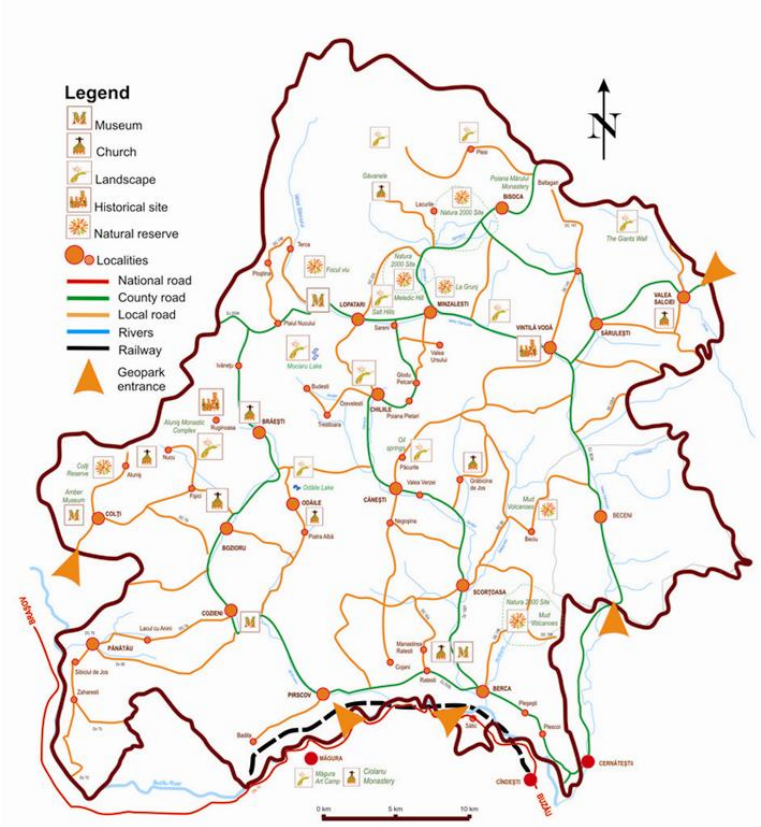

Fig. 5. Natural and cultural sites of the Buzau Land Geopark (selection).

social activities and traditions, and already developed common projects. The selected territory for Buzau Land Geopark is quite homogenous from the economic point of view (Fig. 8), is covering an area of about 1100 sq km and a population of 45000 inhabitants, most part of them still living in a traditional way (Fig. 9).

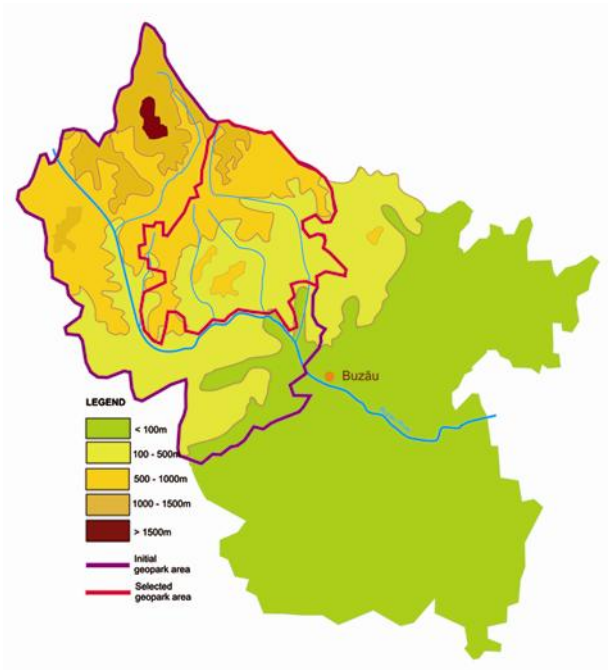

Fig. 6. Buzau County relief map presenting the borders of the initial and the selected geopark areas.

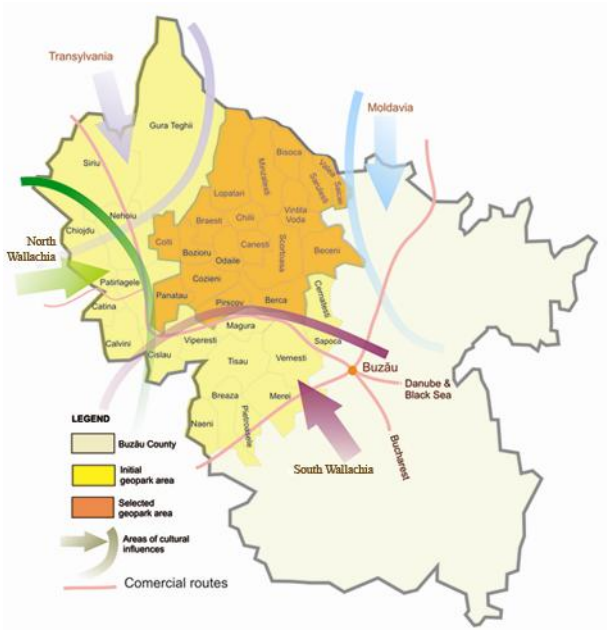

Fig. 7. Local identity is a key issue in geopark management and common projects implementation. For Buzau Geopark heterogeneous areas with strong influence from neighboring regions were lefted apart after cultural and socio-economic analysis.

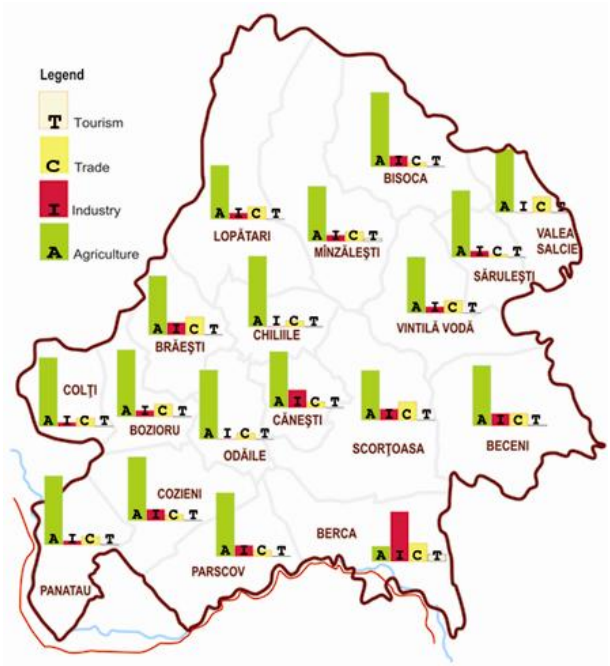

Fig. 8. Synthesis of the main incomes for local communities of the geopark. The sum of the four activities represents 100%. Note the small amount of incomes from tourism, less than 5%.

The selection process of the optimum territory was a crucial point in geopark development and allowed us to plan future common activities and especially to focus on projects aiming to strengthen local identity. The geoparks border is overlapping the administrative borders of the associate localities and different development documents like Geopark Charta or Geopark Management Plan will be easier implemented with the full support of local administrations and policy makers.

A detailed SWOT analysis of the geopark territory was the base for a strategical framework for sustainable use of local resources: the Geopark Charta. In concordance with the LEADER initiative of local communities, the document identified the main axis of territorial development, possible projects, partnerships and financial resources. Members of the Action Local Group are partners of the geopark team. The 18 mayoralties set-up an Intercommunity Association in order to implement the identified projects, correlate different initiatives and manage the future geopark and to assure a political and administrative support for the geopark.

The results we have mentioned completed the inventory of the Geopark in accordance with the conditions of Romanian legislation that regulate the declaration of an area as official Geopark.

Fig. 9. Local people are still living in a traditional way (photo credit I. Piturescu).

5. Conclusions

To fulfill the dual objectives of geo-conservation and the fostering of local socio-economic development that is socially and environmentally sustainable for Buzau Geopark our approach was based both on experience of different European geoparks and Hateg Geopark and we presented few basic ideas in approaching a geopark set-up:

The territory of the geopark has to comprise a relevant number of geological, biological, cultural sites, with significance both for scientific and local communities and worthing to be preserved;

The territory of the geopark has to be quite homogenous from cultural, economic and social point of view and its border to overlap the administrative borders of the partnership communities;

The need for detailed interdisciplinary research studies to identify the territorial system components, their relationships, social and economical needs and assign a role and relative priority for each one related to local identity valorization;

Use of the research results and multi-stakeholders approach to develop social, economic and cultural projects and to support active participation and involvement of local communities;

Create local, national and international partnerships for formal and informal education, public awareness, projects development and to promote the area and its values;

Develop a brand for the geopark territory in order to strengthen local identity and to valorize local innovative approach, in our case “Buzau Land Geopark”;

Each territory has its own identity, and also is part of a national and international context. For Romania and other South East European countries is important to adapt the geopark concept to their context of socio-economic evolution, European development programs and the need to foster local identity.

This approach has generated in Buzau area a framework for partnership, local needs identification, set-up of clear objectives for sustainable use of local resources. Strong support of local communities generated partnerships for national projects dealing with public awareness, cultural events, promotion, and informal education.

Buzau Land Geopark territory is fulfilling the requirements to become a geopark and all the steps we have already taken so far created the base for its official recognition. The geopark territory comprises a rich geodiversity and peculiar geological phenomena are representatives for the established geological framework items of Carpato- Balkan area and Europe, as were defined by different ProGEO initiatives (Wimbledon et al, 1998) and can aspire to play its own role as an international geopark.

Acknowledgements

I would like to thank to Laurentia Conda, Ioana Daia, Dana Alexandrescu, Gabriela Leonida, Dorel Rusti, and Claudia Baltatoiu for their help with socio-economic, anthropological, ethnographical and biological studies. This work was supported by the Ministry of Education and Research, Partnership Programs (PN2), projects 31-030/2007 and 91-017/2007 and by Buzau County Council and Geomedia Centre, University of Bucharest.

References

Andrasanu A., 2007. Basic concepts in geoconservation. In: Mesozoic and Cenozoic vertebrates and Paleoenvironments - Tributes to the career of Dan Grigorescu. Ars Docendi, Bucharest, p. 37- 41.

Andrasanu A., 2008. Buzau Geopark. Building a new aspiring geopark, Proceedings of the 3rd International UNESCO Conference on Geoparks, Osnabruck, Germania: 15;

Andrasanu A., Grigorescu D., 2006. The role of Geoparks in strengthens local identity. In: Proceedings of The Second UNESCO International Conference on Geoparks, Ireland de Nord, Belfast, 25.

Baciu C., Etiope G., 2005. Mud volcanoes and seismicity in Romania. In: Mud Volcanoes, Geodynamics and Seismicity, Martinelli G., Panahi B., (eds). Springer, 11 – 89.

Brilla J., B., Dias G., Mendes A., Henriques R., Azevedo I., Pereira R., 1999. The Geological Heritage of the Peneda Ceres National Park (NW Portugal) and its electronic Divulgation. In: Towards the Balanced Management and Conservation of the Geological Heritage in the New Millenium, Barretino D., Vallejo M., Gallego E. (eds). Sociedat Geologica de Espana, Madrid, 313 – 315.

Csontos L., Vörös A., 2004. Mesozoic plate tectonic reconstruction of the Carpathiandevelopment. In: NHM of Petrified Forest. Proceedings of 2nd International Symposium of Natural Monuments and Geological Heritage, Lesvos, 29 – 44.

Fassoulas C., 2003. Psiloritis Natural Park: Capabilities for education and development of hinterland. In: NHM of Petrified Forest. Proceedings of 2nd International Symposium of Natural Monuments and Geological Heritage, Lesvos, 260 – 268.

Frey, M-L., 2003. Geopark Vulkaneifel: Geopotential, touristic valorization and sustainable Development. In: NHM of Petrified Forest. Proceedings of 2nd International Symposium of Natural Monuments and Geological Heritage, Lesvos, 29-44.

Frey M.L., Schafer, K., Buchel, G., Patzak, M., 2006. Geoparks – a Regional, European, Global policy. In: Geotourism, Dowling, R.K., Newsome, D., (edts), Elsevier, Oxford, 95 – 117.

Grigorescu D., Andrasanu A., 2003. Hateg Dinosaurs Geopark – A new strategy for sustainable development in Romania. In: Proceedings of the 4th European Geoparks Network Meeting on the development of Geoparks, Crete, 123 – 127.

Grigorescu D., Andrasanu A., 2006. European Geoparks and sustainable development of the regions: a case study Hateg Country Dinosaurs Geopark of Romania. In: Proceedings of The Second UNESCO International Conference on Geoparks, Ireland de Nord, Belfast, 7.

Grigorescu D., 2005. Rediscovery of a "forgotten land". The last three decades of research on the dinosaur-bearing deposits from the Hateg Basin, Acta Palaeontologica Romaniae, 5, Ars Docendi, Bucuresti,191-204.

Hose T.A., 1999. European Geotourism – geological interpretation and geoconservation promotion for tourists. In: Geological Heritage - its conservation and management. D. Barettino, W.A.P. Wimbledon and E. Gallego (eds.) Madrid, (Spain), 127-146.

Kollman H., 2003. Geoturism in Nature Park Styrian Eisenwurzen, Austria. In: NHM of Petrified Forest. Proceedings of 2nd International Symposium of Natural Monuments and Geological Heritage, Lesvos, 121 – 125.

Kovacs M., Fulop A., 2009. Baia Mare Geological and Mining Park – a potential new Geopark in north western part of Romania. In:Studia Universitas Babes–Bolyai, series Geologia, 27 – 32.

Krijgsmana W., Stoica M., Vasilieva V., Popov V., in press. Rise and fall of the Paratethys Sea during the

Messinian salinity crisis. Earth and Planetary Science Letters.

Macadam J., 2003. Potential European geoparks, and the present state of Geotourism, Geoconservation, and Geo-education in Cornwall, south-west Britain. In: NHM of Petrified Forest. Proceedings of 2nd International Symposium of Natural Monuments and Geological Heritage, Lesvos 135-145.

Martini G., 2003. Presentation of the Reserve Geologique de Haute Provence. In: NHM of Petrified Forest. Proceedings of 2nd International Symposium of Natural Monuments and Geological Heritage, Lesvos, 25 – 28.

Martini G., 2006. Geoparks …The future? The Second UNESCO Geoparks Conference. Belfast, oral presentation.

Page K., 1999. Sites and their use. In: Towards the Balanced Management and Conservation of the Geological Heritage in the New Millenium, Barretino D., Vallejo M., Gallego E. (eds). Sociedat Geologica de Espana, Madrid, 28 – 31.

Patzac M., Eder W., 1998. UNESCO Geopark. A new Programme – A new UNESCO Label. Geologica Balkanica, 28, 3-4, Sofia, 33 – 37.

Sandulescu M., 1984. Geotectonics of Romaniei, Ed Tehnica, Bucharest, 334 p (in Romanian with English abstract).

Schmid S.M., Bernoulli D., Fugenschuh B., Matenco L., Schaefer S., Schuster R., Tischler M., Ustaszewski K., in press. The Alps – Carpathians – Dinarides connection: a compilation of tectonic units. Eclogae Geologicae Hervetiae.

UNESCO, 2004. Operational Guidelines for the World Heritage Convention, Paris. In: www.unesco.org/.../geopark/2004guidelinesJuneendorsed.pdf (30.12.2009).

UNESCO, 2008. Operational Guidelines for the World Heritage Convention, Paris. In: www.unesco.org/.../geopark/2008guidelinesJuneendorsed.pdf (30.12.2009).

Vasiliev I., Mațenco L., Wout K. , in press. The syn and post collisional evolution of the Romanian Carpathian foredeep: New constraints from anisotropy of magnetic susceptibility and paleostress analyses. Tectonophysics.

Watson R., 2003. Marble Arch Caves and Cuicagh Mountain Park. In: NHM of Petrified Forest. Proceedings of 2nd International Symposium of Natural Monuments and Geological Heritage, Lesvos, 107 – 108.

Weber J., 2003. The Bergstrasse – Odenwald – Public relations. Geo – Education and Products. In: Proceedings of the 4th European Geoparks Network Meeting on the development of Geoparks, Crete, 137 – 139.

Wimbledon W. et al., 1998. A first attempt at a GEOSITE Framework for Europe – an IUGS initiative to support recognition of world heritage and European geodiversity. Geologica Balkanica, 28, 3-4, Sofia, 5-32.

Zouros N., 2003. The Petrified Forest of Lesvos – Greece: Principles and problems for a sustainable management. In: NHM of Petrified Forest. Proceedings of 2nd International Symposium of Natural Monuments and Geological Heritage, Lesvos, 45 – 63.

Zouros N., 2004. The European Geoparks Network. Geological heritage protection and local development. Episodes, Vol. 27, no. , 165 – 171.

Zouros N., Martini G., 2003. Introduction to the European Geoparks Network. In: NHM of Petrified Forest. Proceedings of 2nd International Symposium of Natural Monuments and Geological Heritage, Lesvos, 17 – 21

Scientific Annals, School of Geology, Aristotle University of Thessaloniki Proceedings of the XIX CBGA Congress, Thessaloniki, Greece	Special volume 100	513-518	Thessaloniki 2010

VULNERABLE GEOSITE PROTECTION AND MANAGEMENT IN GEOPARKS - A CASE STUDY OF TAFONE IN LESVOS PETRIFIED FOREST GEOPARK

Zouros N. [1] and Gumus E. [2]

[1] *European Geoparks Network Coordinator, Member of UNESCO Geoparks Bureau, University of the Aegean, Department of Geography, Mytilene GR-81100 GREECE, nzour@aegean.gr*
[2]*University of the Aegean, Department of Geography,Mytilene GR-81100 GREECE, egumus@geo.aegean.gr*

Abstract: Geoparks consists of a number of adjacent geosites which have different attributes in terms of value (scientific, educational, aesthetics) and vulnerability. In the Lesvos Petrified Forest Geopark area, beyond the fossilized plants which constitute a natural monument of international value, there are many other sites of interest in terms of geology, geomorphology, ecology and local traditions. Coastal geosites of the Lesvos Petrified Forest are of significant geomorphological, aesthetic, educational and touristic value including cliffs, collapsed boulders, tafoni structures and cavernous weathering forms. Tafoni are widespread on the Miocene volcanic formations on Sigri coast. Miocene volcanics are hosting the silicified plants of the Petrified Forest; a protected natural monument of international value and beauty. Due to their importance and fragility the Natural History Museum of the Lesvos Petrified Forest adopted special measures for the protection and conservation of the tafoni structures of the territory. The research activity in the costal area of western Lesvos island led to the inventory of tafoni. As a consequence of the research some endangered tafoni were brought to the museum for protection, conservation and exhibition. This tafoni exhibition introduces the museum visitors to the processes forming the external surface of our planet.

Keywords: Geopark, Vulnerable geosite management and protection, Lesvos Petrified Forest, Tafoni, Cavernous weathering

1. Introduction

Till recently nature management, protection and conservation attempts were mostly concerned with the biotic environment (flora and fauna). The non-living earth heritage was somehow neglected from the management priorities, even if included were not because of their geological or geomorphological importance but the visual appeal as scenery.

A Geopark is a nationally protected area containing features of geological significance, rarity or beauty, which safeguards and sustainably manages the geological heritage of the earth (Zouros, 2008). Geoparks consists of a number of adjacent geosites which have different attributes in terms of value (scientific, educational, aesthetics) and vulnerability.

Vulnerability is a debate surrounded concept because of the semantics of and the understanding of the term (Mcfadden et al., 2007). In environmental aspects; vulnerability is related to the magnitude of the impact, the adaptation or toleration capacity of the receiver, and the acceptable level of decomposition. Geoparks have a holistic approach in protected areas conservation and management. Geoparks in order to ensure a comprehensive protection of the Earth heritage sites adopt a management plan including the recognition, assessment and protection of the earth heritage monuments present in their territory.

2. Lesvos Petrified Forest Geopak

The Petrified Forest Geopark is situated on the western part of Lesvos island in the North Aegean Sea. The Lesvos Petrified Forest Geopark is one of the four founders of the European Geoparks Network established in 2000 (Zouros et al., 2008). It is well known for its large numbers of petrified trunks in immense beauty. The outstanding fossil of the Petrified Forest which indicates an ancient subtropical eco-

system reveals the last 20 million years history of the Aegean area (Velitzelos and Zouros, 2007). In the Lesvos Petrified Forest Geopark area, beyond the fossilized plants which constitute a natural monument of international value, there are many other sites of interest in terms of geology, geomorphology, ecology and local traditions. Coastal geosites of the Lesvos Petrified Forest are of significant geomorphological, aesthetic, educational and touristic value including cliffs, collapsed boulders, tafoni structures and cavernous weathering forms. The Lesvos Petrified Forest is awarded by a number of international awards on protection and conservation of the earth heritage as far as its successful management on geotourism development which has concrete socio economic results for local development.

3. Tafoni structures

"Tafoni" (singular: tafone) is a Corsican word that means window (Tschang, 1969). Tafoni have caused human curiosity for a long time. One of the oldest known depictions of such features are presented in the "Spring Fresco" excavated in Akrotiri, Greece dating 3500 years ago (Hejl, 2004). Tafoni are characteristic cavernous weathering features in various sizes and have arch shaped entrances, concave inner walls, overhanging margins and fairly smooth gently sloping, debris-covered floors (Mellor et al., 1997).

Science arbitrarily classifies tafoni according to their size, shape and location. The nomenclature for pitted and cavernous weathering was not harmonized throughout most of the twentieth century, but the word 'tafoni' has now become standard for all such pits, large and small (Norwick and Dexter, 2002). The same method is followed in this study that 'tafoni' refers to all cavernous weathering features. Several attempts were made to classify and explain tafone formation (Turkington, 2005; Uzun, 1995 and Tschang, 1969).

Although they are characteristic to the Mediterranean region they are found in many parts of the world, particularly in dry semi-arid environments but also hyper arid and cold arid desert environments as well as in the mild coastal zones, and even on the Mars surface as proved by the observation made by the Viking 1 Landers (Parsons et al., 2005).

The origin of the tafoni formation is a long debate. In 1930's scientist believed that tafoni were aeolian formations (Popoff and Kvelberg, 1938), however Young (1986) argued that salt weathering was the effective factor.

New researches claims tafoni formation as a self-reinforced weathering process characterized by positive feedback of mineral disintegration (ie.carbonates) and salt crystallization (Philips, 2004; Turkington, 2005; and Erginal, 2007).

Last of all, tafoni formation is result of selective or differential weathering on the rock surface driven by inherit internal variations of the rock structure (composition, strength, lithology) and the external exploiting effects of physical, biotic and chemical factors (Dragovich, 1969).

4. Materials and methods

The research area is situated at the Sigri Village; the western coast of Lesvos Island. Although the whole coastline seems to have tafoni features; for an intense survey, the research area was limited from the Plaka Petrified Forest Park till the peninsula of Sarakina, south of Sigri village (Fig. 1).

The tafoni evaluation and validation process mostly depends on field observations. More than 200 tafoni were measured in dimensions, directions and locations and the gained data were extracted to the tables and diagrams for further analyses (Fig. 2).

These statistical data were used to understand the development phases of the cavernous weathering in the research area. Directional (compass) measurements were used analyze the effect of the insolation and sea as a salt source on the tafoni development. Lichen effects on tafoni of the shaded areas were examined by stereoscopic microscopes. Finally the tafoni on the Sigri Castle walls were measured in order correlate the speed of the coastal tafoni development.

5. Tafoni of the Lesvos Petrified Forest Geopark

Cavernous weathering forms have a wide distribution in the warm and partly arid coastal regions of Greece (Kelletat, 1980). Lesvos Petrified Forest Geopark protected area as well bears wide variety of tafoni in terms of origin, size, distribution, parent material. Dimensional measurement comprises two different rock types and locations; one of them is on the coarse ignimbrite layers, the other one is on the bedrocks. Most of the tafoni that were sub-

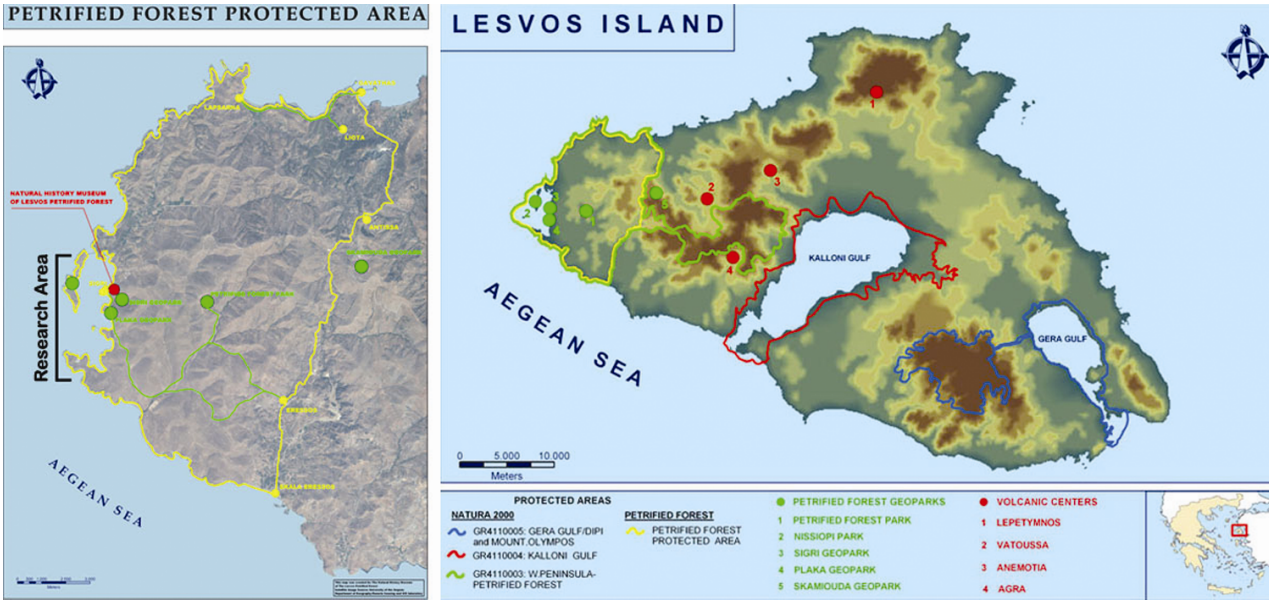

Fig. 1. Location map of research area and Lesvos Petrified Forest Geopark.

jected to this research were less than one meter in scale. As they represent different stages of cavernous weathering they are invaluable clues to understand the phases of erosion processes. The two of them shown below are characteristic samples of tafoni development on andesitic rocks (Fig. 3).

Tafone distribution is highly variable in Lesvos Petrified Forest Geopark coastal area. They develop on the ground rocks, at the lateral surfaces of bedrocks or overhanging over the cliffs (Fig. 4).

The microclimatic conditions and variety of the parent material led the development of very distinct types of tafoni in a relatively small area. Thus in one side of a cliff, salt crystallization can be the driving force, while biogenic activities of the lichens and the wind are dominant on the shaded side.

Most of the tafoni are in a zone not more than 10 meters far from the shoreline. This zone is the most prominent environment for tafoni development due to the strong insolation and splashing water as a salt source. This zone is also under mechanical erosion of waves. Tafoni structures similar to those formed on volcanic boulders along the Sigri coast are also formed on the stones walls of the Sigri castle walls, which was built by the Ottoman navy admiral Suleyman Pasa in 1760 (fig.5).

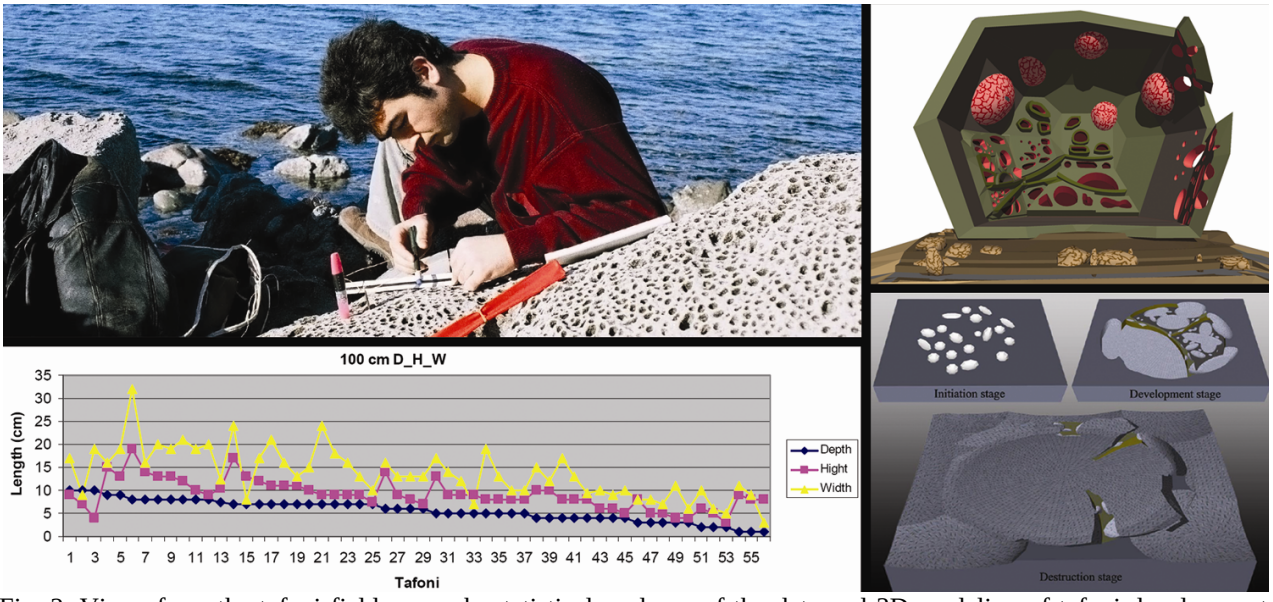

Fig. 2. Views from the tafoni field research, statistical analyses of the data and 3D modeling of tafoni development phases on the coastal geosite of Lesvos Petrified Forest Geopark.

Fig. 3. Two characteristic tafoni formations on andesitic rocks on Plaka Park coastal geosite.

The Sigri castle was mostly build with local volcanic rocks which enabled to create a relative dating of the coastal tafoni and their development phases. The mesurements assumed 0.2 mm weathering per year for the coastal tafoni according to the size/date correlation of Sigri Castle wall tafoni.

6. Protection of vulnerable tafoni in Lesvos Petrified Forest Geopark

Lesvos Petrified Forest Geopark launched a broad initiative for the identification and mapping of the various sites of interest in its territory (Zouros, 2007).

The geosite inventory provides an overall image for the tafoni in terms of distribution, threads and vulnerability. Tafoni which developed on the pyroclastic cliffs were very unstable and continuously collapsing. Tafoni bearing andesitic boulders along the Sigri coast are much less solid than they seem. The pyroclastic formation including andesitic boulders which are in the range of the waves were continuously eroded before the tafoni complete their development phases. The erosion process results in falling or rolling of tafoni bearing rocks. Due to the inner cavities, micro scale decomposition caused by salt crystallization, dissolution and removal of the rock cement by capillarity mechanically weakens the rock. In order to protect some of the spectacular tafoni boulders were carried to the museum (Fig. 6).

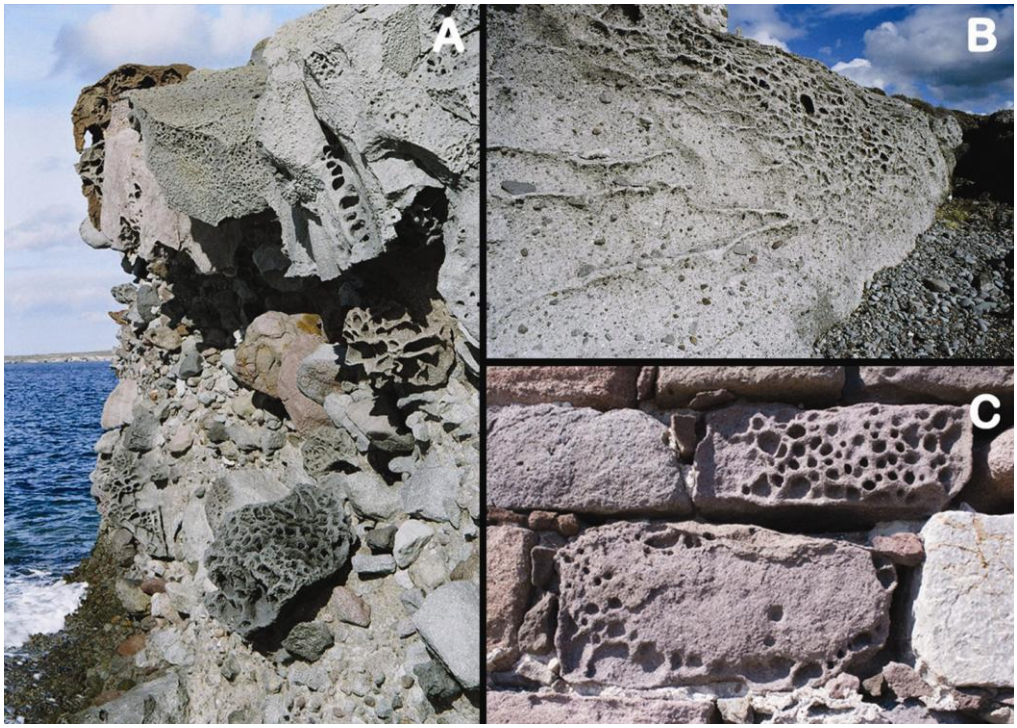

Fig. 4. Various tafoni distribution on the coastal geosite of Lesvos Petrified Forest Geopark (A: Andesitic boulders on cliffs, B: Coarse-grained pyroclastic layer, C: Sigri Castle wall).

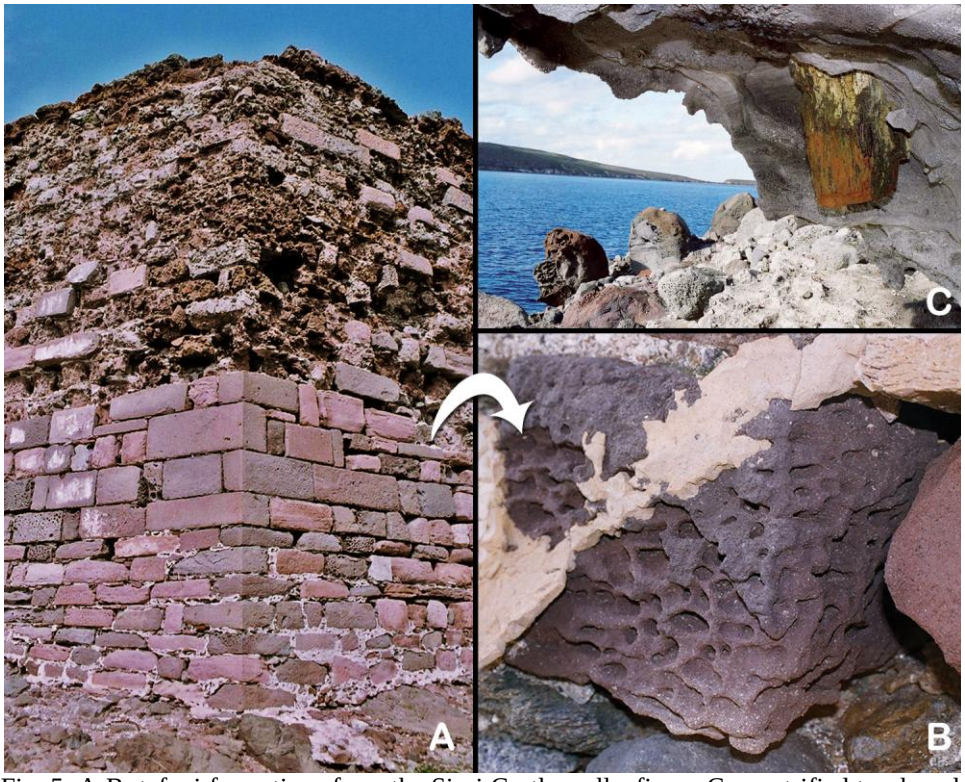

Fig. 5. A-B: tafoni formations from the Sigri Castle walls, figure C: a petrified trunk and tafoni on the same formation. A unique image of Geoparks comprehensive perspective.

A big boulder with tafone structures was found on the coastal area of the Plaka Park, 4.20 m above sea level. It has a large visor and the inside was almost eroded and removed. Just some merged inner alveols and the outer crust remained over time. The vertical circumference was 1.8 m and the horizontal circumference was 2.20 m. The entrance was 50 cm in height, 65 cm in width and 40 cm in


Fig. 6. Andesitic boulders with tafoni structures at the museum.

depth. Its inward buckled cavern floor was so fragile that in some parts the thickness of the rock separating two different tafoni development surfaces was less than 5 mm. The tafone was very thin in the crust and become almost empty with the successive weathering processes. It was connected with the cliff on a small neck less than 20 cm^2 thick. Another endangered tafone boulder was on the cliff of Plaka Park. This tafone bears well developed samples of honey comb cavities and a characteristic surface crust created by the precipitation of internal minerals carried to surface by capillarity. This sample was also about to collapse to the sea but because of its size and weight. The tafone was also carried to the museum without any considerable damage of the very fragile honey comb cavities. Both tafoni are now being visited in the museum.

7. Discussion

The tafoni structures of the Lesvos Petrified Forest Geopark are geosites with aesthetic, educational and scientific value. Moreover, different aspects of tafone development in the Geopark reveal strong linkage to the cultural and geological history of the territory.

The "Tafoni" approach of the Lesvos Petrified Forest Geopark was a successful instance of vulnerable geosite protection and management. The tafoni of the Petrified Forest protected area was documented and depending on this inventory, threatened or vulnerable tafoni were carried to the museum for protection and exhibition.

Beside the scientific importance, Tafoni have other benefits to be used as a touristic attraction or as an educational material for the students.

References

Dragovich D., 1969. The origin of cavernous surfaces (tafoni) in granitic rocks of southern South Australia: Zeitschrift fuer Geomorphologie, 13, 163-181.

Erginal A.E., Gonuz A., Bozcu M., Ates S.A. and Cetiner Z., 2007. The first findings on the origin of alveolar disintegration at the western shores of Gelibolu. Mineral Resource Exploration. Bulletin, 134, 27-34.

Gumus E. and Zouros N., 2008. Cavernous Weathering in Sigri Area, Lesvos Island, Greece, Proceedings of International Conference on Studying, Modeling and Sense Making of Planet Earth, 1-11.

Hejl E., 2005. A pictorial study of Tafoni development from the 2nd millennium BC. Geomorphology, 64, 87-95.

Kelletat D., 1980. Studies on the age of honeycombs and tafoni features. Catena, 7, 317-325.

Mcfadden L., Nicholls J.R and Rowsell P.E., 2007. Managing Coastal Vulnerability.Elsevier, London, 262p.

Mellor A., Short J. and Kirby S.J., 1997. Tafoni in the El Chorro area, Andalucia, Southern Spain. Earth Surface Processes and Landforms, 22, 817-833.

Norwick S.A. and Dexter L.R., 2002. Rates of development of tafoni in the Moenkopi and Kaibab Formations in Meteor Crater and the Colorado Plateau, Northeastern Arizona. Earth Surface Process and Landforms, 27, 11-26.

Parsons R.L., Head J. W. and Marchant, D.R., 2005. Weathering pits in the Antarctic dry valleys, insolation-induced heating and melting and application to Mars. Lunar and Planetary Science, 36, 1138.

Tschang H., 1969. Geomorphological observations on the tafoni forms of Honk Kong. The Chung Chi Journal, 9, 32-51.

Turkington V.A. and Jonathan D.P., 2004. Cavernous Weathering, Dynamical Instability and Self-Organization. Earth Surface Processes and Landforms. 29, 665-675.

Uzun A., l998. Weathering Forms on Sandstones Directly Exposed to Sea Effects in Gelincikburnu and Its Surroundings (South Coast of the Black Sea). Z. Geomorphology, 42, 233-244.

Velitzelos E. and Zouros N., 2007. The Petrified Forest of Lesvos, Topio Publications, Athens, 155p.

Young R.W., 1986. Tower karst in sandstone: Bungle Bungle massif, northwestern Australia. Z. Geomorphol. 30, 189-202.

Zouros N., 2005. Assessment, protection and promotion of geomorphological and geological sites in the Aegean area, Greece. Géomorphologie: relief, processus, environment, 3, 227-234.

Zouros N., 2007. Geomorphosite assessment and management in protected areas of Greece. The case of the Lesvos island – coastal geomorphosites. Geographica Helvetica. 3, 169-180.

Zouros N. 2008. Guide to the Plaka and Sigri Petrified Forest Park. Natural History Museum of the Lesvos Petrified Forest, Lesvos, 136p.

Zouros N., Ramsay T., Mc Keever P. and Patzak M., 2008. European Geoparks, Natural History Museum of the Lesvos Petrified Forest, Lesvos, 163p.

Special Session S30
Underwater geoarchaeology: an interdisciplinary field bridging marine geosciences and underwater archaeology

Scientific Annals, School of Geology, Aristotle University of Thessaloniki Proceedings of the XIX CBGA Congress, Thessaloniki, Greece	Special volume 100	519-524	Thessaloniki 2010

UNDERWATER GEOARCHAEOLOGICAL SURVEY IN FRONT OF THE DANUBIAN ISLAND "PACUIUL LUI SOARE" (ROMANIA) USING REMOTE SENSING TECHNIQUES – PRELIMINARY RESULTS

Caraivan G.[1], Fulga C.[1], Chera C.[2]

[1] *National Institute of Marine Geology and Geo-ecology (GeoEcoMar), Constanta, Romania: bd. Mamaia no. 304, cod 900581, Constanta, Romania, gcaraivan@geoecomar.ro; cfulga@geoecomar.ro*
[2] *Museum for National History and Archeology Constanta, Place Ovidiu 12, 900745, Constanta, Romania, anroed@hotmail.com*

Abstract: On the Danubian island "Pacuiul lui Soare", between 355 and 357 km, there are the ruins of a Byzantine fortress from the X-XIII centuries, most of which has already been eroded by the Danube river. A seismoacoustic survey which was carried out along the Danube in front of the island, showed the presence of the fortress ruins under the river waters. Further geo-archaeological survey is required in the studied area, aiming to a better understanding of the island evolution and of the fortress history as well.

Keywords: seismo-acoustic survey, underwater geo-archaeology, Byzantine fortress, Danube River.

1. Introduction

On the Danubian island "Pacuiul lui Soare", between the landmarks: NE-44° 8' 05.48"N; 27°28' 14.33"E and SW-44° 7'44.65"N; 27°28' 02.60"E, there are the ruins of a Byzantine fortress from the X-XIII centuries, most of which has already been eroded by the Danube river (Fig. 1; Fig.1a).

In the north-east end of the island, in a dense forest, one can see just a tenth of the ruins of the old Byzantine fortress, the rest being under the river waters. The fortress was built between the years 972–976, by the troops of Emperor John Tzimisces and reflects the strength of Byzantine rule in the Lower Danube and the greatness of the Macedonian dynasty emperors.

Although no Roman archaeological level was identified up to date, it is assumed that the Byzantines built the fortress on the ruins of an older city, reusing building material and also putting into practice a new technique that has demonstrated competence and ability of manufacturers.

Under a non-consolidated alluvial substrate, there were two possibilities to stabilize the walls foundation: (i) a deep foundation, which required a large effort or a woody (oak beams) sub- construction that also requires a large amount of stone (Barnea and Stefanescu, 1971), or (ii) the wall foundation was made of burned oak stakes, than stuck in the ground at some intervals, over which manufacturers had placed oak beams arranged longitudinally and transversely. The vacant spaces were filled with mortar (masonry) - a mixture of lime, gravel and stone grated/shredded tuna (Barnea and Stefanescu, 1971). In the case of "Pacuiul lui Soare" Byzantine fortress the latter approach was used.

Modern underwater remote sensing techniques introduce many advantages to the underwater archaeology, particularly to the detection of submerged man-made structures of archaeological interest (Panin et al., 1977). This work presents the preliminary results of a seismo-acoustic survey in the Danube River for the detection of the ruins of a Byzantine fortress on the river floor.

2. Material and methods

In the fall of 1987, a sedimentological and seismo-acoustic survey was carried out by GeoEcoMar on the Romanian Danube trail. Seismo-acoustic profiling was conducted by ultrasonic survey method with continuous recording (vertical sonar). A high-frequency transmitter generates a sound wave that propagates through the layer of water

Fig. 1. Romania-Danube-“Pacuiul lui Soare” Island and the Byzantine fortress.

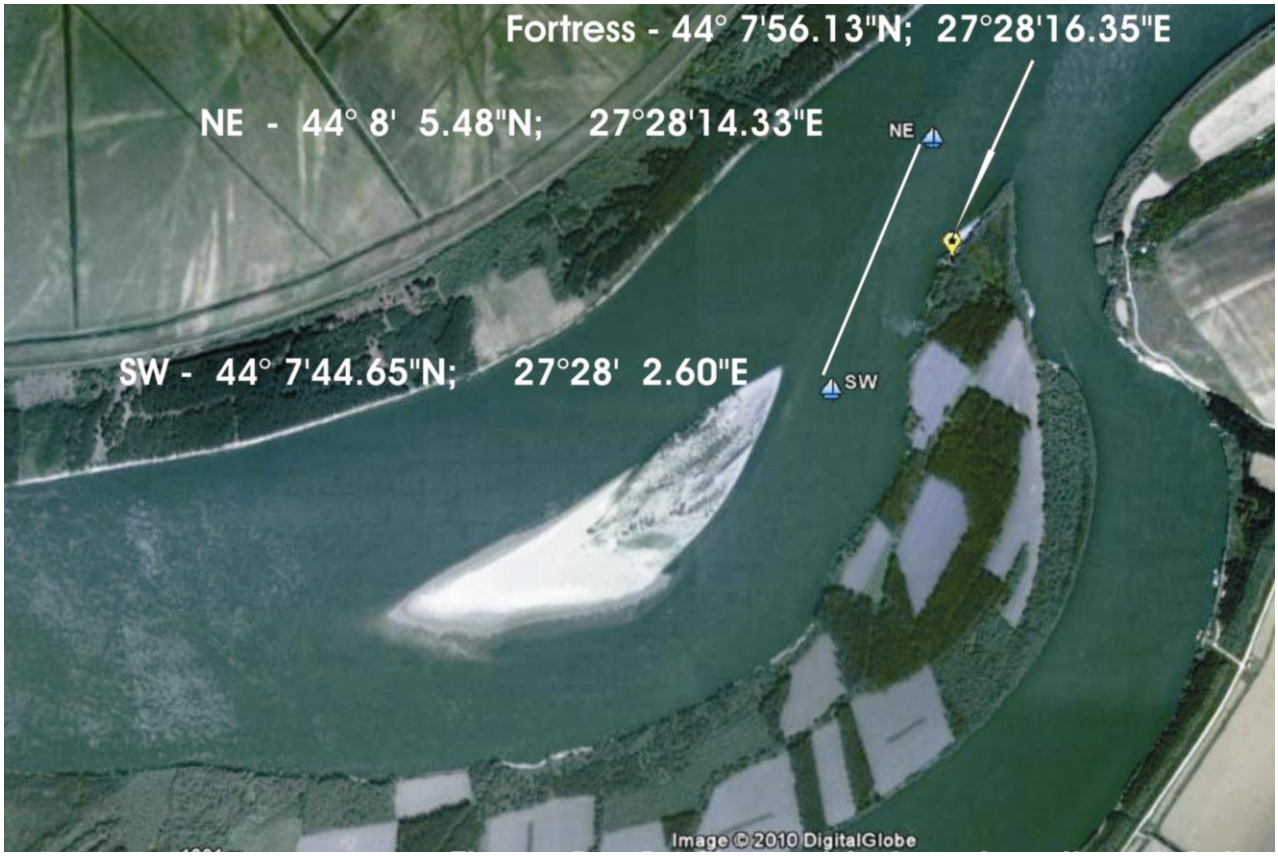

Fig. 1a. Profile and fortress location details.

with a speed of about 1500 m / sec, then reflected on the interface water / sediment, being received by a transducer (hydrophone), located in the same place with the transmitter. The pulse length, generated by the transmitter, was milliseconds order of magnitude, and the issue rate of 1 second. The bottom reflected signal was recorded on electro-sensitive paper, obtaining a continuous profiling during the vessel trackline. An Ocean Sonics vertical sonar ORS-219, with dry recording paper and working emission frequency of 8 KHz, was used. The equipment was mounted on a tug of 600 hp, with maximum draft of 1.80 m. The speed of research vessel considered optimal, was about 13 km/h. The vessel route followed river sailing line at the proximity of the "Pacuiul lui Soare" (Fig. 2). The position and the navigation of the vessel were carried out using a DGPS system with an accuracy of less than 1 m.

3. Results and Discussion

The interpretation of the seismo-acoustic profile, obtained when passing along the underwater continuation of the fortress, showed an informative vertical picture of the Danube bed. Perpendicular to the northern wall of the fortress a mound-like feature is obtained on the seismo-acoustic profile. This feature appears a sharp rise of the Danube bottom having a length of about 40 m and a height of 9 m compared to the surrounding river bottom. The minimum water depth of the river at the area was only 4.5 m. This feature is developed on a bathymetric background of 14-15 m. The acoustic character on the seismo-acoustic profile suggests the hard nature of the raised feature, compared with the usual "anti-dune" morpho-dynamic structure of the sedimentary bed (Fig. 3). The presence of well shaped depressions on the Danube bottom bed, downstream and upstream of the underwater raised feature illustrates the hydrodynamic conditions, induced by undermining and flooding of the fortress walls (Fig. 3). Upstream of the main bed lifting, small positive ruin shaped irregularities are found on the Danube bottom, with a height ranging from 1.00 to 1.50 m (see Fig. 3, and Fig. 3a, in the right half of the seismo-acoustic profile, see the scale of the depth, below the sketch of profile lines. Seismo-acoustic profile also showed 2-3 subbottom discontinuous reflectors from 3 to 5 m below the river bottom, indicating the existence of lenses of different lithological characteristics. The Byzantine fortress walls which are located on the

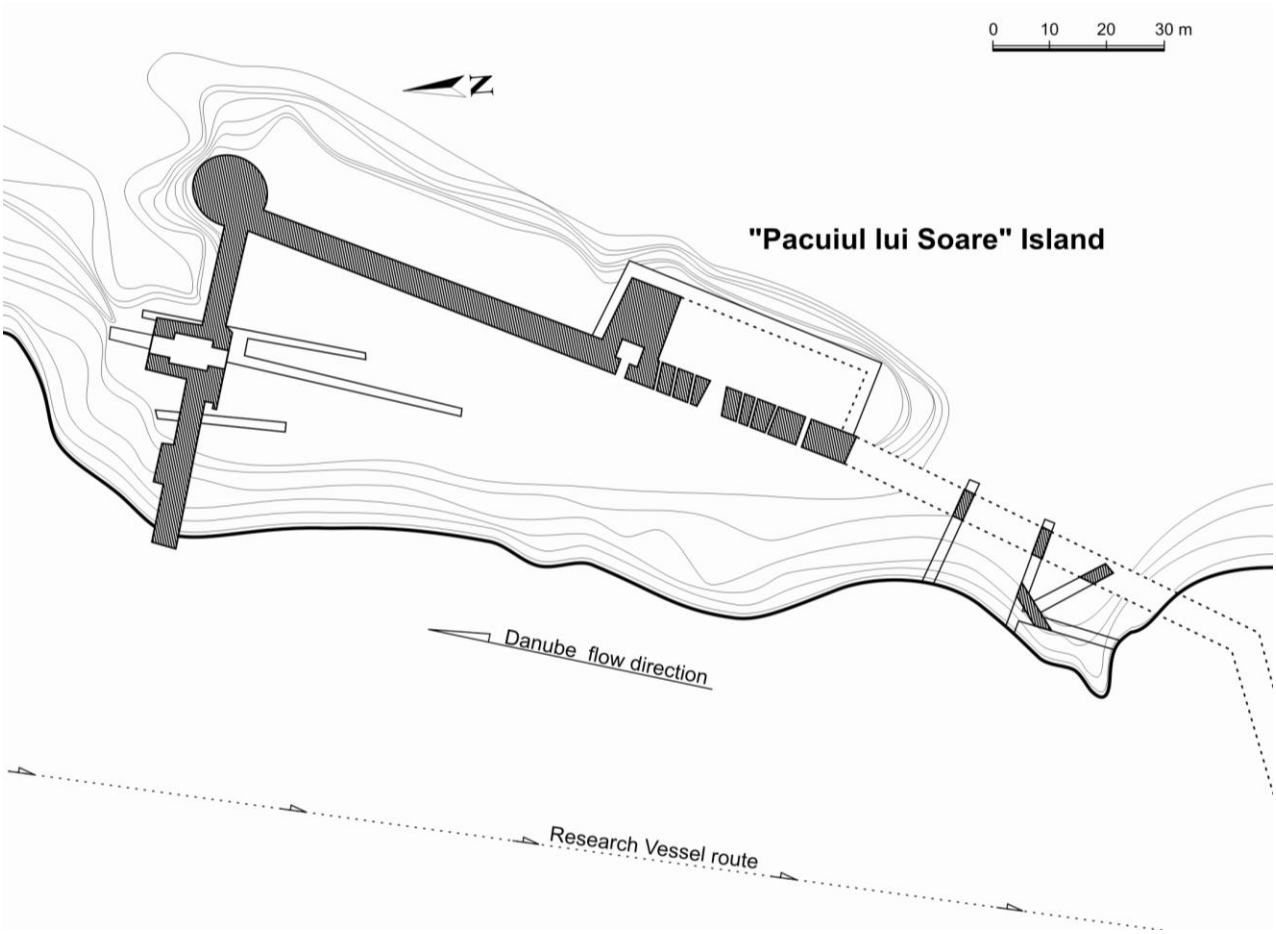

Fig. 2. “Pacuiul lui Soare” Fortress GPS position - 44° 7'56.13"N; 27°28'16.35"E.

island of “Pacuiul lui Soare” end abruptly at the bank of the Danube,

suggesting the underwater continuation of the ruins under the Danube River waters. Seismo-acoustic survey conducted on the Danube River near the “Pacuiul lui Soare” island brings an important geophysical argument supporting this hypothesis.

The sub bottom discontinuous reflectors identified on the seismo-acoustic profile could represent the woody bed foundation, on which the fortress walls

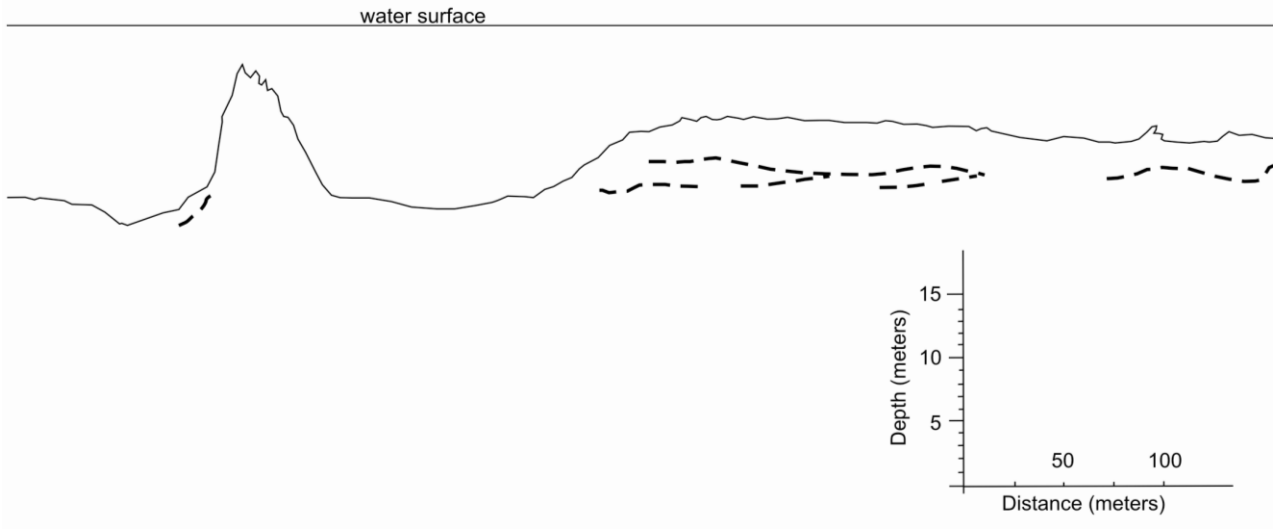

Fig. 3. The profile from NE to SW, between: NE - 44° 8' 05.48"N; 27°28'14.33"E and SW - 44° 7'44.65"N; 27°28' 02.60"E.’

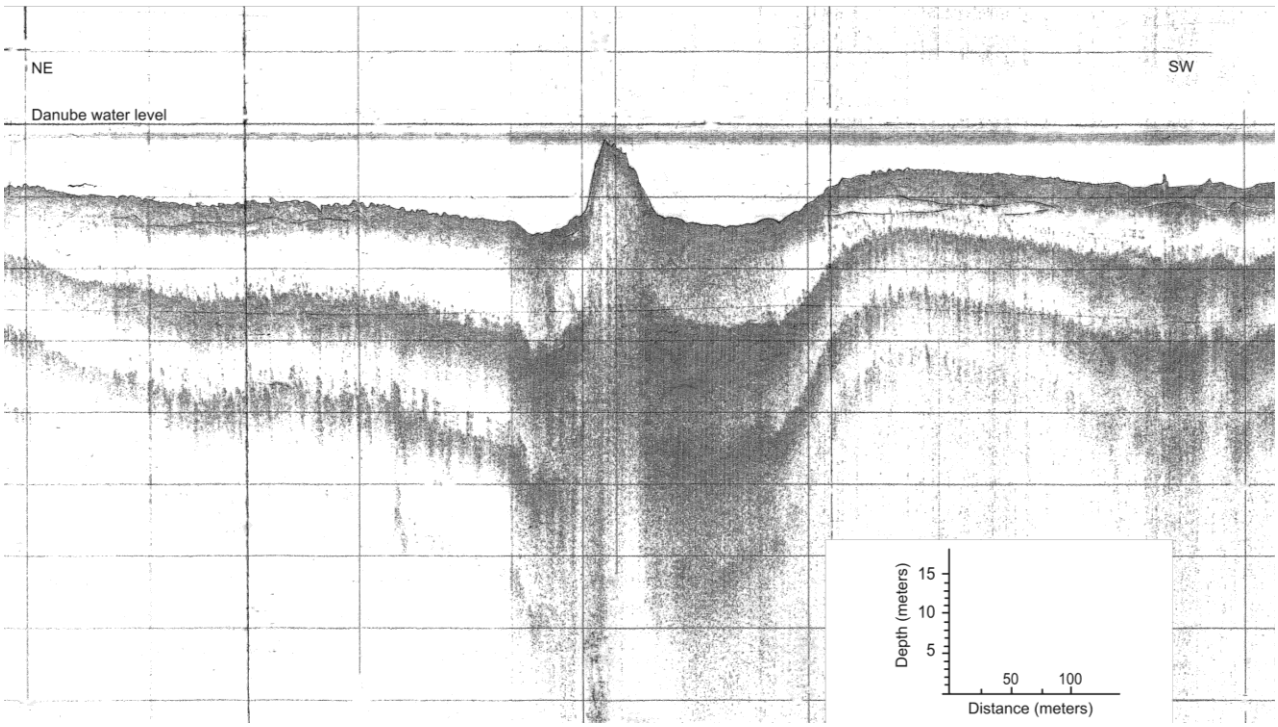

Fig. 3a. "Pacuiul lui Soare" Island and Fortress – Image of the original seismo-acoustic profile.

were built. By changing of the Danube flow regime, the left side of the island was subject to enhanced erosion, causing sub digging of the foundation structure. In 2003, when the Danube water was at very low levels, the network of wood beams was clearly visible.

On the eastern right bank of the "Pacuiul lui Soare"island (or the other name, "Dervent" island), where a narrow branch separates the island from the Dobrogean land, the erosion was much less. Therefore, the constructive structures could maintain in good condition (for example, wharf, see Fig.2 and 4). The underwater seismo-acoustic survey which was carried out in front of the "Pacuiul lui Soare" island fortress, provide a clear argument to support the hypothesis that the remains of city extend in the underwater area. Therefore, further geo-archaeological research is required in the stud-

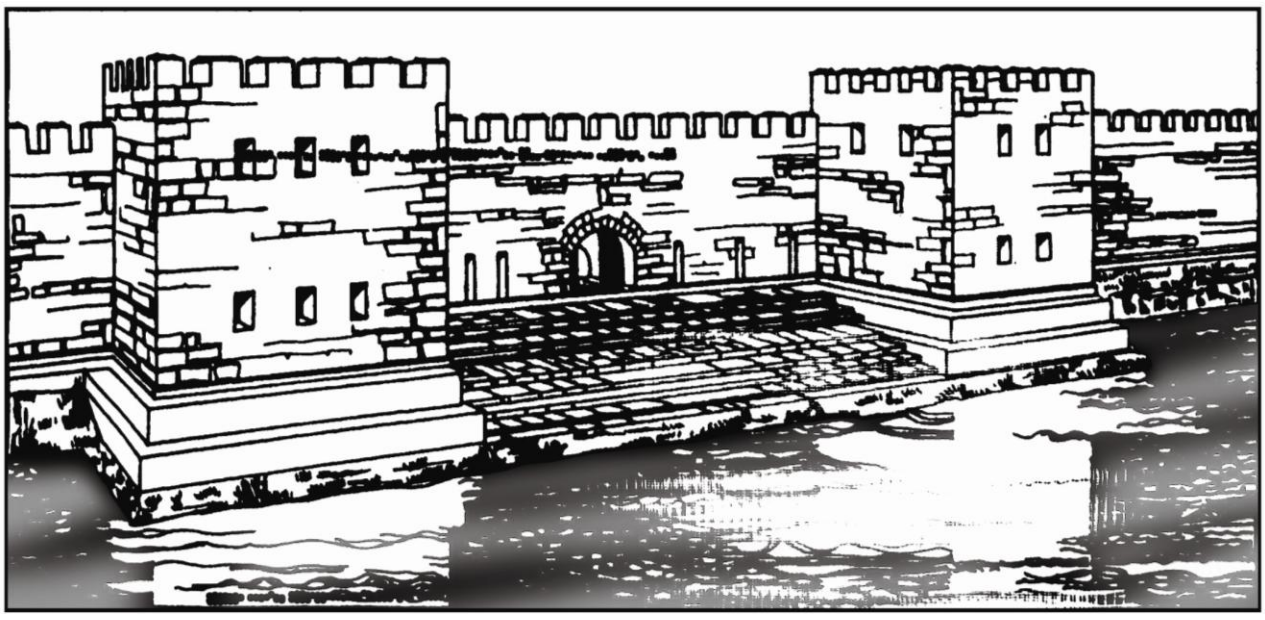

Fig. 4. Wharf reconstruction proposal (arh. Mira Dordea Voitec).

ied area, through a comprehensive interdisciplinary program, involving sedimentological and geophysical studies, in conjunction with direct observations (ground truthing), specific to underwater archaeology. The proposed survey will lead to a better understanding of the history of the city as well as the sedimentary-hydrodynamic evolution of the island.

References

Barnea I, Stefanescu St., 1971. The history of Dobrogea. Vol.III. Byzantines, Romans and Bulgarians at the Lower Danube, Ed. Academiei RSR, Bucharest, 440 p.

Panin N., and al., 1977. Bathymetrical research on the Black Sea continental shelf., St. cerc. geol., Geophysics., Geogr., Tome 15, p.57-73

Special Session S32
The use and applications of GPS and InSAR to geohazards across South-Eastern Europe

Scientific Annals, School of Geology, Aristotle University of Thessaloniki Proceedings of the XIX CBGA Congress, Thessaloniki, Greece	Special volume 100	525-533	Thessaloniki 2010

THE USE OF GNSS TECHNOLOGIES FOR APPLICATION IN MINING, GEOLOGY AND GEODESY IN BULGARIA

Kostyanev S.[1], Valev G.[2], Majdrakov M.[1], Jelev V.[1], Avdev S. [3], Bliznakov A.[4], Stoyanov V.[1], Atanasova E. [5]

[1]*University of Mining and Geology;*
[2]*University of Architecture, Civil Engineering and Geodesy;*
[3]*Geology and Geophysics Corporation;*
[4]*New Bulgarian University;*
[5]*Sofia University "K. Ochridski"*

Abstract: A review on the use of GPS technologies for application in mining and geology on territory of Bulgaria is presented in this paper. Some particular results concerning the application of GPS in opencast mining in Bulgaria are presented and analyzed. The essentials of them are periodical survey of mine working; investigation of slope strain; management of output and transportation of mining mass. In the area of geology and geophysics are discussed some results on application of GPS on: geological mapping and assaying; gravity investigations; deformation of earth's crust; investigation of landslide processes; coordination of platforms for oil and gas production etc. Plans for future work on the above issues are discussed too. The problem of the combined processing of GPS and other types of classical geodetic measurements concerning the higher accuracy of the result is still topical. In the proposed paper a better accuracy in the vertical component of the GPS-networks has been sought. It is suggested that the results from the spirit levelling expressed by heights should be used. Observation equations of heights (orthometric or normal) can be included in the mathematical model for processing of GPS measurements. In these equations a simplified model of geoid (quasigeoid) is involved. A numerical example for the combined processing of GPS measurements with EDM and spirit levelling heights has been presented. The results confirm the expected higher accuracy of the height component.

Keywords: GNSS Technologies Application

1. GPS application for geological targets on the Bulgarian territory

1.1. Introduction (history)

Computer systems application for representation of geographically related geological information during the geological investigations on Bulgarian territory was initiated in 1995 by the experts of the Derectorate "Geology and subsurface protection" of the Ministry of Environment and Waters (MEW) by means of purchase of the program product MapInfo. Later MEW introdused the requirenment all map materials to be submited by application of MapInfo, ArcView or AutoCad both from the state and private (including foreign) firms fulfiling geoprospecting on the territory of Bulgaria. The usage of GIS is the main reason for introduction of the Global Positioning System (GIS) in geological practice. The first attempt was done in 1995 by the Irish company of "Navan" completing prospecting works on several licenced area in Bulgaria. The supplied Trimble GPS receptors turn to be difficult to carry and useless in the daily field work of the geologists.

In the period of 1998-2001 MEW bought the software products of ESRI ArcViewGIS and ArcVewInfo, necessary for the processing of the immense geological information preserved in the National Geofund. Several GPS receptors was bought as well.

In the period of 1999-2000, in the frames of projects financed by the European Community (Phare Program), two GIS laboratories was equiped in the departments "Geology and prospecting of mineral resources" and "Geology and paleontology" of the University of Mining and Geology "St. Ivan Rilski" – Sofia. Software product ArcView 3.1 of ESRI was purchased. In addition three GPS receptors of Garmin were supplied. Up to date these laboratories have been applied mainly for research work. In the nearest future they will be incorporated in the frames of the courses of "Field geology

(geological mapping)" and "Prospecting of mineral resources". At the moment the students get some ideas about the Global Positioning System and GPS receptors during the practice of "Field geology".

- protected areas and objects in the frame of task financed by the Ministry of Environment and Waters related to the completion of register and cadastre of the Bulgarian geological phenomena and so on.

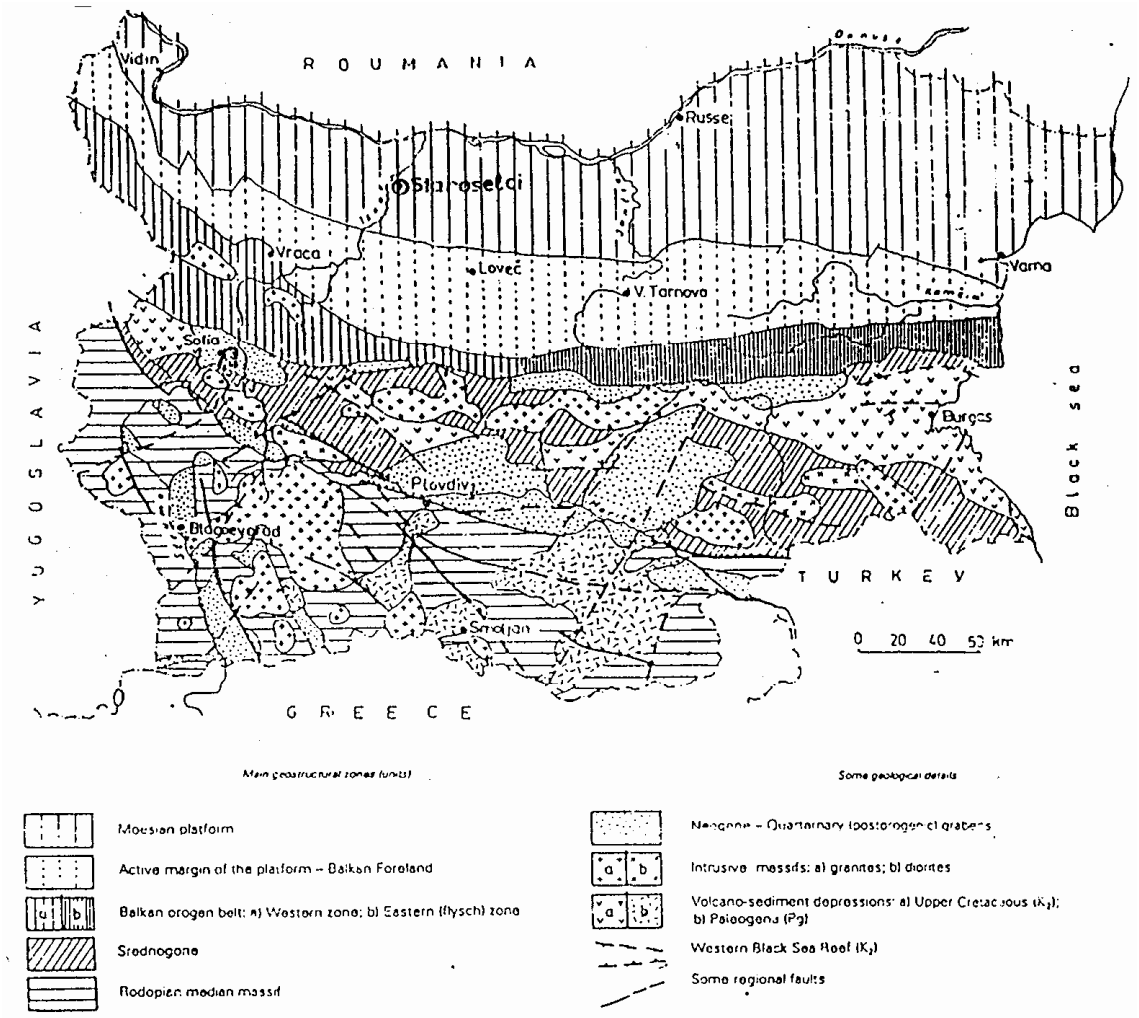

Fig.1.Geostructural scheme of Bulgaria.

1.2. Application

GPS is applied in the field of geology to receive coordinated relations of objects as follows:

- outcrops of the geological mapping;
- profile lines and pickets of the reconnaissance geoprospecting as well as of the preliminary prospecting (e.g. in the soil and rock sampling);
- lithogeochemical samples in the stream-sediment sampling, used for searching of goldbearing areas and structures as well as for environmental tasks;
- boreholes, trenches and prospecting shafts during the detailed exploration of industrial minerals and most of the types of ore deposits (excluding the vein type that reqiures higher accuracy);

1.3. Scales

The requirement for accuracy of the geological maps of Bulgaria is 1 mm independantly of the map scale (Bairaktarov et al., 1995). The conditional state geological mapping on the territory of Bulgaria fulfills in scale 1:25 000 i.e. the admissible mistake is up to 25 m. Maps in scale of 1:10 000 and 1:5 000 are used in the reconnaissance geoprospecting as well as in the preliminary exploration. The admissible errors are accordingly 10 and 5 m. GPS receptors of Garmin (e.g. GPS 12, GPS 12 CX, eTrex, eTrex Summit etc.) are oftenly used in the field works due to their low price. In favorable conditions (good constellation of the

visible satellites) their accuracy drop down below 5 m. It satisfies entirely the needs of the field geoprospecting works mentioned above.

1.4. Problems

The principal problem is the discrepancy between the GPS coordinates and the coordinates of the topographic maps of Bulgaria elaborated for industrial application. In practice this problem is resolved by GPS coordinate determination of several characteristic objects (topographic repers) existing on the maps followed by a computer correction of the rest map data using some of the GIS products (e.g. the extention of ArcViewGIS, Spatial analyst).

Another problem is the level inaccuracy (so called Z coordinate). In some of the recent models of Garmin GPS receptors (e.g. eTrexSummit) this problem is resolved by means of an additional build in barometric altimeter. The rest of receptors require field calibration using a topographic reper of known level.

1.5. Perspectives

The world process of globalisation as well as the pre-accession strategy of Bulgaia urges an integrated aproach to the collection and application of geographically related information. In the field of geology this process of unification is traditional. But the new technologies have elaborated a number of more rapid and more effective methods to do this. The Global Positioning System (GPS) improves permenantly. Permanently improve and GPS receptors and their accuracy increases. Electronic notebooks are elaborated (e.g. palmtop type) with interface both to GPS receptors and mobile phones. Moreover, there are laptops which work do not depend on the weather. They possess installed software ArcViewGIS that apart from the integration of all field documentation allows both geological maps compilation and decission making in real time (in the field). In fact, the dream of the field geologist is reached. But for the Bulgarian geologists it is still unreal due to its very high price.

2. GPS application in the open pits

Recently, GPS-technologies have often been used in the open pits in Bulgaria. This fact is due to a number of circumstances as follows:

- GPS-measurements do not depend on the visibility between the points as well as on the presence of points of higher class;
- GPS allows the measurements of the three coordinates;
- Many receivers with different class of accuracy existed.

The receivers of higher class are mainly used in inventing and supporting of mine surveying models of the open pits. The most important applications are as follow:

2.1. Establishing of local geodetic networks

The advantages of GPS technologies are very clearly expressed in pits, which embrace significant areas, situated in plain relief (e.g. Maritsa-East pit in Bulgaria) and isolated small pits (e.g. numerous quarries for building materials and facing rocks in Bulgaria).

Maritsa-East lignite deposit is situated in the southeastern part of the Upper-Thracian lowland. The minefield embraces a territory of 250 km2 between the villages of Aprilovo, Rassimanovo, Gledachevo, Kovachevo, Gradets, Mednikarovo and Obruchishte (Fig. 2). The proven coal reserves are 3,5 milliard tons. Two open pits are exploited in the Maritsa-East basin: “Troyanovo-North” and “Troyanovo-3” (Fig. 3, Fig. 4) which feed three electric power stations. This complex produces 30% of the total electrical energy of Bulgaria.

Maritsa-East is e complicated industrial object with entirely completed energical cycle: from the coal mining to the production of electrical energy and briquettes. Production related technological processes cause versatile impact on the environment. This impact is expressed mainly in destruction of the relief forms, soil and vegetation overburden, alienation of fertile lands etc. Large areas have been affected by significant deformations, which make the classical methods for development of stable networks inefficient.

2.2. Development of surveying base and detail surveying

GPS advantages are significant in surveying of underwater mining (aquatorial surveying works). In Bulgaria it is applied for surveying of dam bottoms (of course, in combination with echo sounding.

It is useful to apply GPS for studying of deformational processes especially in large mine fields.

Larger GPS-technology application in open pits is impeded by factors, which are not inherent to the system, but to the Bulgarian conditions as follows:

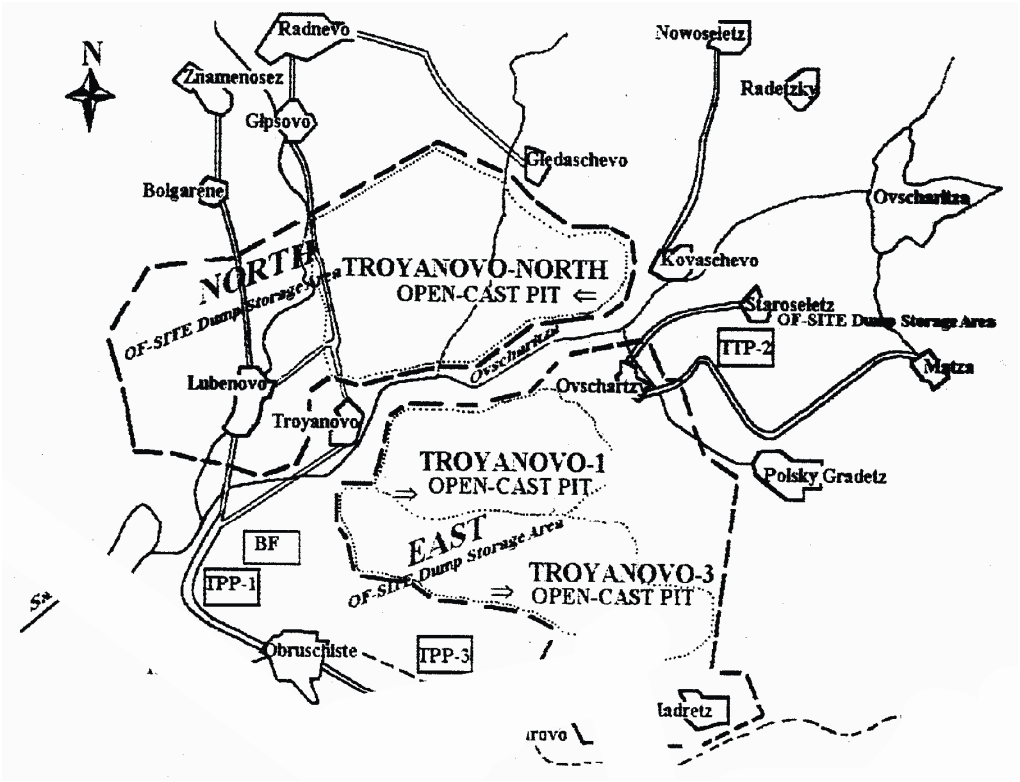

Fig.2.Schematic map of Maritsa-East lignite deposit region.

2.2.1. The high price of the receptors especially of these ones working in real time. This problem could be resolved by a relevant policy: leasing, attraction of sub-executors etc.

2.2.2. GPS determines the coordinates in projections and on ellipsoids, which are different from Bulgarian ones. That is why a transformation of the obtained data is required. In the future with the implementation of the new coordinate system BGS 2000 and the ellipsoid WGS84 it could be expected direct receiving of the coordinates.

The receptors of low class of accuracy (1-5 m) are used in the open pits for operative management of the autotransport (e.g. in the "Assarel" open pit). It

Fig.3.Open pit "Troyanovo-North".

is perspective these systems to be included in the totally automized systems for management both the quality and quantity of the production in real time.

Fig.4.Open pit “Troyanovo-3”.

By introduction of differential corrections, GPS-receptors of low accuracy could be used for current surveying of the situation of the mine workings in unfavorable weather conditions (fog, rain etc.), for coordination of geological samples and so on.

3. Some geodetic application of the GPS in Bulgaria

3.1. Combined processing of the GPS measurements with classical geodetic measurements

There are many publications on the problem of the combined processing of different types of measurements (classical and from space techniques), (Hein, 1981; Valev and Minchev, 1989; 1994; 1995; Valev et al., 1997) and others.

In the mentioned papers, the problem about the combined processing of GPS measurements (baselines) with results from different classical geodetic measurements: horizontal directions, zenith distances, slope distances, astronomical coordinates, astronomical azimuths, height differences are discussed. There are also program realisations of different algorithms on this problem.

In the case of a combined adjustment of GPS data with some of the classical geodetic measurements, the best way is to use slope distances, measured with EDM. But the inclusion of distances despite their high precision leads to the increasing only of the accuracy of the horizontal component. The accuracy of the vertical component is unchanged. And this is namely the weak point of the GPS measurements. The vertical accuracy neither of the horizontal angles nor the astronomic azimuths increases. The accuracy increases when zenith distances, heights or height differences from spirit levelling are included in the adjustment model of GPS measurements. It is known that the zenith distances are measured with a low accuracy because of the vertical refraction and we have to accept some hypothesis about the atmospheric pressure. The use of zenith distances also requires an introduction to the astronomic coordinates of the points. But when we use height differences from spirit levelling the main problem is that we have to introduce some hypothesis for the geoid and to accept the stipulation that the adjacent points between which height differences are measured are situated not far from each other. Depending on the complexity of the gravity field as well as on the complexity of the geoid that distance can be restricted to 3- 4km. Besides that the use of the height differences requires the introduction of astronomic coordinates. The problem in combining of GPS measurements with zenith distances and height differences rises with the difference between the astronomic system and WGS84.

The problem of the use of results from spirit levelling expressed in heights in some height system is not discussed very detailed and in our opinion is not enough developed. However, if heights from sprit levelling and gravimetric data are used the accuracy of height component will increase considerably.

The heights h can be obtained from levelling and

gravimetric measurements through the gravitational potential W

$$h(orth) = (Wo - W)/gm$$

or

$$h(norm) = (Wo - W)/\gamma m$$

Geopotential difference (Wo - W) has been obtained as follows

$$Wo - Wa = \int_0^a g.dh = \sum_0^a gi.hi$$

The weak point of the problem is that we have to know the undulation. However, we have the possibility of dividing the territory in small regions and of applying some simplified suitable model of geoid (quasigeoid), for example

$$dh = C0 + C1.\varphi + C2.\lambda,$$

where φ and λ are geodetic coordinates of the point, belonging to the same region and Co, C1, C2 are coefficients specific for the region. Instead of geodetic coordinates λ and λ we can replace them with the linear quantities B and L calculated from the formulae

$$B = M.(\varphi - \varphi o); \quad L = N.\cos(\varphi).(\lambda - \lambda o),$$

where φo and λo are the geographic coordinates of some central point of the territory, and M, N - main radii of curvature.

It is possible to introduce more complicated models of geoid (quasigeoid), for example

$$H - h = Co + C1.B + C2.L + C3.B2 + C4.B.L + C5.L2 + \ldots$$

Whereas in the classical 3D adjustment it is supposed the level surfaces were concentric spheres in the proposed method the level surfaces are not parallel and a deviation along the parallel and the meridian is supposed.

On the base of the above presented method algorithms for combined adjustment of GPS measurements, slope distances and orthometric (normal) heights are written as well as their computer realization. An experience is performed and from the results it is obvious that the accuracy of the coordinates increases. However, the familiar problem which heights are more convenient to be for use is still under discussion.

Numerical example

67 GPS baselines with Leica System 200 receivers, 89 slope distances with Mecometre 5000 and heights of 25 points by spirit levelling have been measured in the network, shown on the Figure 6. Using the above described procedure the network has been adjusted once - as a pure GPS network, second - as a GPS network, combined with slope distances and several combinations of GPS data with slope distances and heights. In the last case, with three types of data, several combinations with different a priori standards for the adjustment have been performed. For each variant, a posteriori standards for each type of measurements have been derived.

Coefficients of the Geoid Model are derived

Co = 35.4543 m ±0.0032 (m),

C1 = -6.251319356 (mm/km) ± 0.000395920 (mm/km),

C2 = 41.759181949 (mm/km) ± 0.000659620 (mm/km).

Estimations for whole (entire) network

Mean square error of the space position

Mp = ± 3.18 mm

Mean square error of the horizontal position

Mxy = ± 1.05 mm

Mean square error of the height position

Mh = ± 2.99 mm

3.2. A new Reference System and its introducing in Bulgaria

A new geodetic projectional coordinate system has suggested to be distributed on the territory of Bulgaria. It is a conformal conic projection with two standard parallels and a basic meridian. It is uniform for the whole country and calculated with the parameters of the ellipsoid of WGS84. The most appropriate parameters and formulae for calculation have been chosen. The orientation of the ellipsoid will be carried out on the basic of the points, defined on the territory of Bulgaria as a result of the performed EUREF campaigns. This system is named SYSTEM 2000. It is planned to build a fundamental GPS networks, consisting of about 400 basic points. Requirements and a technology for measuring and adjustment of the network have been worked out. There is planned a further densifying of this network so that the new coordinate system is used effectually.

3.3. Geodynamic research of the Mirovo Salt Deposit, NE Bulgaria

The Mirovo salt deposit is located approximately

5km southeast of the town of Provadija, in the Varna province, Bulgaria. That is a unique natural phenomenon with its origin, composition, location and geophysical characteristics. The Mirovo salt diapir has a depth of approximately 4 000 m and its top is 15 to 20 m deep. The diaper has a base area of the order of 200 km2 and generally has the shape of a truncated cone. Approximately 73% of the diapir are Sodium Chlorid, the remainders comprising insoluble elements and other evaporites, irregularly distributed through the salt mass. It was excavated in 1919. The method of boring is applied at present in the salt pits (more than 30 utilized bore-holes) and more specifically the method of underground salt leaching through which one major raw material for the Devnya chemical plants is produced – brine.

It is a geodynamic project, which was attracting researcher's interest. A dense network (Fig. 5) of 26 stable pillars and many leveling benchmarks is designed and built-up especially to monitor movements and deformations in the deposit area using precise angular and distance measurements, spirit leveling and GPS. Part of the pillars– outside the central zone – control the detailed over the salt body. Twenty campaigns, after the initial observations in 1990, were taking place. The aim is to examine how far exploration of rock salt is connected to local seismic activity because recently earthquakes occur here more frequently and with increasing strength. To give an idea what the magnitude of the deformations is, these solutions are compared also to the campaign, accomplished in June 1990.

The general trend of terrain deformations is subsidence of the central zone (Fig. 6) and, as a by-product, shortening of the distance between the center and the outer margin. Increasing residuals with time span is due to the time-dependent components, whereas the constant part gives an accuracy estimate.

The components of the isotropic plane deformations of earth blocks in the region of the geodynamic polygon are calculated by the final element method and by the relative linear deformations at suitable sides of the network. The calculation results are the base for a variable analysis of deformation processes in the investigated region.

It is necessary to point out that the deformation intensity for the period investigated is higher than the average critical values of the earth crust. Taking into consideration the shortness of the temporary interval, for which research has been done, the received extreme values of deformations should

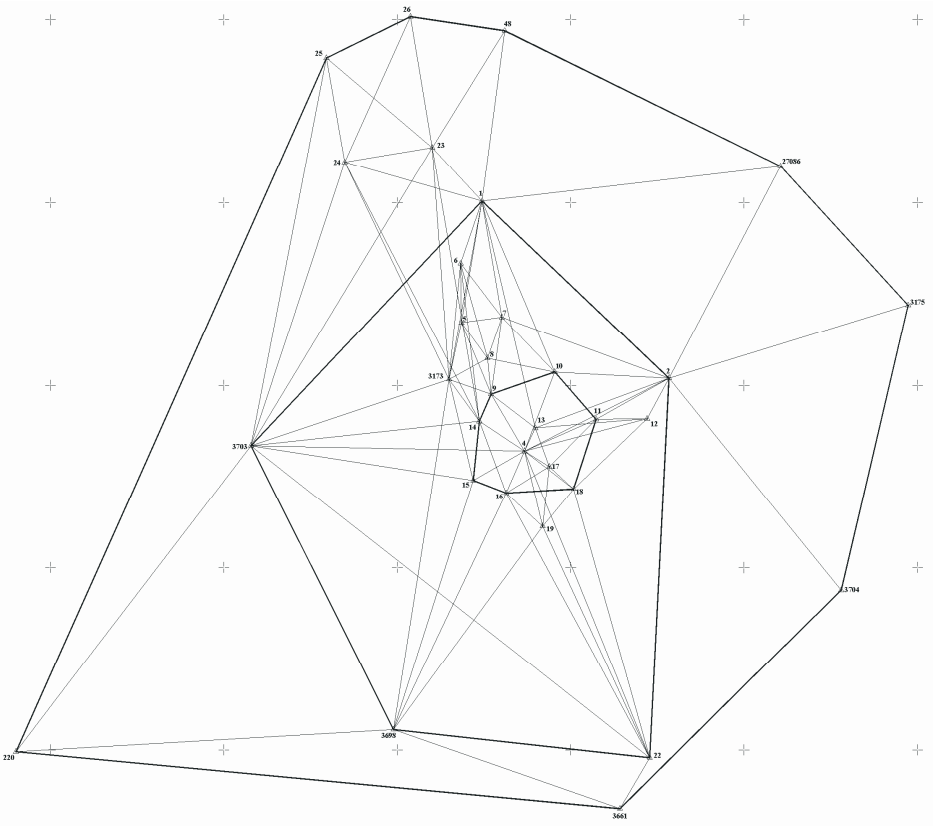

Fig.5.Geodynamic Network.

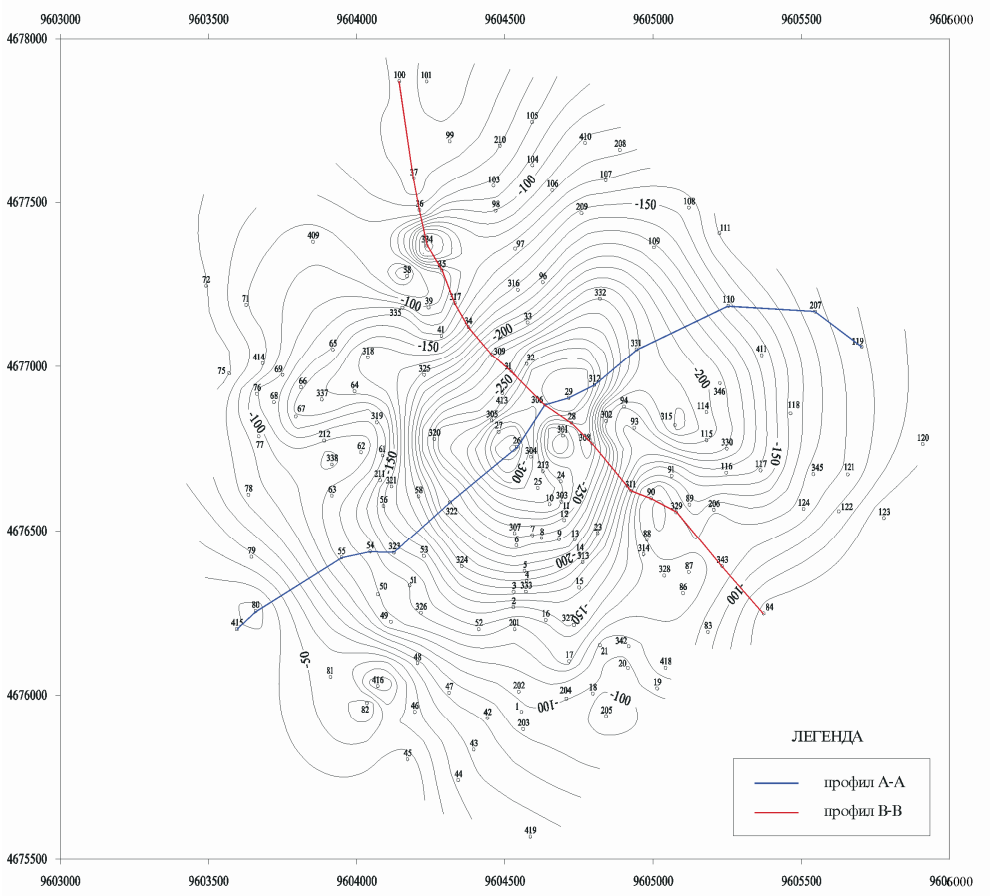

Fig.6.Subsidence in the Mirovo Salt Deposit.

not ease us, especially in the salt mirror. However, it is necessary to determine what part of the total value of deformation is the one of technogenetic character and what is the part, which is of tectonic origin. The necessity of such determination in the near future is supported by the fact that a great part of the axes of deformation sections are in NW-SE direction, a direction characteristic of the whole country. Additional specifications are necessary to the activity and the territory detachment of the tectonic processes in the region, and especially to those, which could become generators of seismic occurrences. A final and definite answer to these questions could not be given for the time. The reason for this opinion is the relatively small amount of information, which prevents us from creating a full concept on the mechanism and the genetic peculiarities of dynamic and deformation processes in the region.

3.4. GPS technology application in monitoring of landslides

We have successfully applied GPS technology in monitoring of landslides on the entire territory of North Bulgaria. These are the regions of Orjahovo, Orsoja, Gabrovo, Cibar, Somovit, Kneja, Lom, and Varna.

3.5. Application of new technology in the surveying and mapping of the Danube River

According to the PHARE-project „Morphological Changes and Abatement of Negative Effects on a Selected Part of the Danube River", a surveying experiment has been carried out. The task of the experiment includes surveying and mapping of a selected reach of the river applying new technologies including GPS use. Many scientists and specialists from Austria, Bulgaria and Romania have participated in the project. The team leader has been the Institute of Hydrology and Water Resource Management, University of Technology, Vienna.

The project's aim is to establish the preconditions for remedial actions. This includes the following tasks:

Development and application of modern methodology and technology including GPS use for surveying and mapping of the Danube River.

Generation of precise maps of the riverbed from historical and current measurements.

Assessment of morphological and hydrological situation and its development for planning of remedial actions, based on a common view and perception of the major processes.

It is proposed, that all Danube countries should use a uniform co-ordinate and height systems for all control points, benchmarks and gauges, situated along the river banks and on the islands. The bases of these systems are EUREF and UELN. Results, such as maps of the River Danube, GIS-applications, etc. have to be prepared in Lambert conic map projection.

More details and some other applications in geodesy are given it the paper "Some aspects of GNSS applications in Bulgaria" by Dr Milev, prof. Valev at all.

4. Conclusions

The using of the Global Navigation Satellite System in Bulgaria has been started since 1980. Numerous established surveying and other firms are equipped with modern GPS hard and software. Presently nearly fifty geodetic receivers are in use in Bulgaria. The scope of its application is increasing continuously. Many scientists, engineers and specialists are applying this technology for different purposes. The GPS technology is studied by the students from the Universities. Several conferences, workshops and symposiums on this topic have carried out in Bulgaria. A lot of papers and theoretical works have presented from Bulgarian autors.

Acknowledgements

Without the assistance and cooperation of Bulgarian mining & geological exploration company personel in the allowing access to geological and GPS data this work would have been impossible. Thanks to all of them. A part of these results are debated with colleagues in United Nations/United States of America workshop on "The use and application of global navigation satellite systems". Thanks to all of them. The development and application of modern methodology and technology including GPS used for surveying and mapping of Danube river successful can be used and for surveying of Black sea coast. Just such problems are working in 7FP project "Up-grade Black sea scientific network", N226592, who financed this investigation. Thanks.

References

Bairaktarov I., S. Boyadjiev, I. Vaptzarov, N. Vardev, V. Valkov, D. Dimov, K. Doncheva, V. Zhelev, Zh. Ivanov, N. Katskov, R. Marinova. T. Marinov, L. Filipov, C. Chembersky, G. Cheschitev. 1995. Methodological requirenments for the geological mapping on scale 1:25 000, the geomorphological mapping on scale 1:50 000 and the attendant prospecting of mineral resources. – Committee of Geology and Mineral Resources, 155 pp.

Geoprecise Engineering Ltd. Geodynamical Investigations of Mirovo Rock Salt Deposit by Geodetic Methods. Annual Reports, 2000. GEOSOL Ltd. Provadia.

Kostyanev S., 1994, Mathematical Modeling of Stationary Geophysical Fields in Gradient Media (Monograph), Sofia, 134 pp.

Kostyanev S., 1999, Mathematical Modeling of Geophysical Fields in Gradient Media (Monograph), Sofia, 200 pp.

Kostyanev S., 1999, Mathematical methods in geophysics (Textbook), Sofia, 450 pp.

Mazhdrakov M., 2001. Mine Surveying. Methods of mine surveying in open pits. – Sofia (in Bulgarian).

Milev G., Valev G., 1999. GPS Applications in Bulgaria. Sucsess Die to Many-sided Opportunities. GIM Intertnational. The Worldwide Magazine for Geomatics. March '99, Vol. 13, p.66-67.

Stoynov V., Valev G., Minchev M., 1992. Current tasks of the national geodetic measurements. . Geodesy, cartography and land management. 2. (in bulgarian).

Valev G., Minchev M. 1994. Common adjustment of GPS observations and Classical geodetic measurements. Symposium of the IAG Subcommission for the EUREF, Warsaw, June 8-11, 1994

Valev G., Minchev M., Combined Adjustment of GPS and Classical Network Data. Paper presented at the Symposium of IAG Subcommission for EUREF. Helsinki, May 5 -10,1995.

Valev G., Minchev M., Gabenski P., 1997. Again on the problem about the combination of the GPS measurements and data from classical geodetic networks. High Military Scool, Shumen. (in bulgarian).

Valev G., Vassileva K., Kastreva, P., 1999. Combined processing of GPS measurements with heights derived from spirit leveling. Third Turkish-German Joint Geodetic days "Toward a Digital Age". June 1-4,1999, Istanbul.

Valev G., Stoeva P., Janev G., 1999. Geodynamic researches of the Mirovo Salt Deposit near Provadija. 5th Conference "Mechanical behavior of Salt - Mecasalt 5". Bucharest, August 9-11 1999.

Valev G., Yanev G., Rajnov G., 2000. Geodynamic researches of the Mirovo Salt Deposit near Provadia, NE Bulgaria. Special symposium on Sinkholes and unusual subsidences over solution-mined caverns and salt and potash mines, 15 – 18 October 2000, San Antonio, Texas, USA.

Scientific Annals, School of Geology, Aristotle University of Thessaloniki Proceedings of the XIX CBGA Congress, Thessaloniki, Greece	Special volume 100	535-545	Thessaloniki 2010

CONTRIBUTION OF INSAR AND KINEMATIC GPS DATA TO SUBSIDENCE AND GEOHAZARD MONITORING IN CENTRAL MACEDONIA (N. GREECE)

Mouratidis A.[1, 2], Briole P.[2], Astaras A.[1], Pavlidis S.[3], Tsakiri M.[4], Ilieva M.[2], Rolandone F.[5] and Katsambalos, K.[6]

[1] *Department of Physical and Environmental Geography, Aristotle University of Thessaloniki, 54124 Thessaloniki, Greece, amourati@geo.auth.gr, astaras@geo.auth.gr*
[2] *Laboratoire de Geologie, Ecole Normale Superieure (ENS), 24 rue Lhomond, 75231 Paris Cedex 05, France, mouratidis@geologie.ens.fr, pierre.briole@ens.fr, ilieva@geologie.ens.fr*
[3] *Department of Geology, Aristotle University of Thessaloniki, 54124 Thessaloniki, Greece, pavlides@geo.auth.gr*
[4] *Department of Cadastre-Photogrammetry-Cartography, Aristotle University of Thessaloniki, 54124 Thessaloniki, Greece, martsaki@topo.auth.gr*
[5] *Laboratoire de Tectonique, Universite Pierre et Marie Curie (Paris VI), 4 place Jussieu 75005 Paris, France, frederique.rolandone@upmc.fr*
[6] *Department of Geodesy and Surveying, Aristotle University of Thessaloniki, 54124 Thessaloniki, Greece, kvek@eng.auth.gr*

Abstract: SAR interferometry (InSAR) is a relatively new, but well established, remote sensing technique that can be used for geodetic observations and whose basic principles and applications have been well documented. On the other hand, the Global Positioning System (GPS) has been utilized as a standard geodetic tool for several decades. The objectives of this study were (a) to implement ENVISAT/ASAR interferometry, in order to monitor subsidence/deformation phenomena, as well as (b) to discuss the potential of integrating extensive kinematic GPS (KGPS) measurements with InSAR or other remote sensing data for geohazard and other geoscience applications. For the above purposes, a region in N. Greece that presents great scientific interest was chosen, including (a) the broader area of Kalohori, located at the extension of the western end of the city of Thessaloniki, which is part of the 2500-year old Thessaloniki coastal plain and has been dominated by subsidence phenomena for several decades and (b) Mygdonia basin, a basin of tectonic origin located approximately 30Km east of Thessaloniki, which constitutes the most seismically active region in Northern Greece. InSAR processing of 19 ENVISAT/ASAR images, spanning the 2002-2007 period, was carried out via the ROI_PAC software and 117 interferograms were computed and enhanced, by estimating coherence over space and time and applying different filtering strategies, in order to monitor the rate and extent of the subsidence around Kalohori. Extensive KGPS measurements were carried out in the broader study area and more than 60,000 data were collected. Results from ENVISAT/ASAR Interferometry for the Kalohori area are primarily discussed, whereas issues associated with other interesting signals, detected in the broader area of Thessaloniki, that verify suspected deformation, previously revealed by ERS SAR Interferometry, are also addressed. Finally, issues and challenges of integrating KGPS and remote sensing data are discussed, leading to the final conclusions.

Keywords: InSAR, Kinematic GPS (KGPS), subsidence, geohazards, Central Macedonia, Greece

1. Introduction

SAR interferometry (InSAR) is a remote sensing technique which exploits the phase differences of at least two complex-valued (amplitude and phase) SAR images acquired from different orbit positions and/or at different times. Basic principles and applications of SAR Interferometry have been well documented (e.g. Zebker and Goldstein 1986; Gabriel and Goldstein 1988; Gabriel et al. 1989; Massonnet and Feigl 1998; Bamler and Hartl 1998; Hanssen 2001; Zhou et al. 2009). The information derived from interferometric datasets can be used to measure several geophysical quantities, such as topography, deformations (volcanoes, earthquakes etc.) (e.g. Massonnet et al. 1995), landslides, gla-

cier flows, ocean currents and vegetation properties.

InSAR has been successfully implemented in subsidence studies (e.g. Avallone et al. 1999; Raucoules et al. 2005; Lopez-Quiroz et al. 2009) and has proven to be a very useful technique in monitoring the rate and spatial extent of such deformation phenomena.

On the other hand, the Global Positioning System (GPS) has been utilized as a standard geodetic tool for several decades. Kinematic GPS (KGPS) data covering small areas have been used in Greece for terrain creation and analysis, along with classical surveying techniques (e.g. Pikridas et al. 2004), but the integration of extensive KGPS measurements with remote sensing data for geoscience applications has not yet been sufficiently explored.

The objectives of this study were (a) to implement ENVISAT/ASAR interferometry, in order to monitor subsidence/deformation phenomena, as well as (b) to discuss the potential of integrating extensive KGPS measurements with InSAR or other remote sensing data for geohazard and other geoscience applications.
For the above purposes, a region in N. Greece that presents great interest for various scientific research disciplines, including geological and earthquake applications, subsidence and other geophysical or environmental studies, is chosen.

2. Study area

The broader area of interest is located in Central Macedonia, Northern Greece (Fig. 1), in the vicinity of the city of Thessaloniki, which is the second most populated city in Greece (about 1,000,000 habitants). The relief of the study area varies from completely flat areas to mountainous regions with steep slopes. Elevation values vary from zero (and in some cases a few meters below mean sea level) to up to a maximum of 1201m (Hortiatis/Kissos). Vegetation consists mainly of agricultural areas (51%), shrubs (21%), forests (12%) and pastures (7%) (Greek Ministry of Agriculture 1994). Two areas of particular interest for this study are the basin of Mygdonia and the Kalohori area.

Mygdonia Basin, located approximately 30Km east of the city of Thessaloniki, is a basin of tectonic origin named after the former homonymous lake (Mygdonia lake), which included the contemporary lakes of Koroneia (Lagadas) and Volvi (Fig. 1). This basin constitutes the most seismically active region in Northern Greece and has been the epicentral area of the most recent severe earthquake (1978, Ms=6.5). Dominated by a N-S extensional stress (Martinod et al., 1997), Mygdonia and its complex structure, as well as the surrounding area, have been the subject of several multidisciplinary studies (see Vamvakaris et al., 2006; Chatzipetros et al., 2005 and references therein).

On the other hand, the evolution of the broader Kalohori area, in the eastern extension of the city of Thessaloniki, is directly connected to the evolution of the Thessaloniki coastal plain. The latter is a 2500-year old delta, occupying an area of about 2000Km^2 (Fig. 2). The plain is mainly drained by two major rivers (Axios and Aliakmon) that form

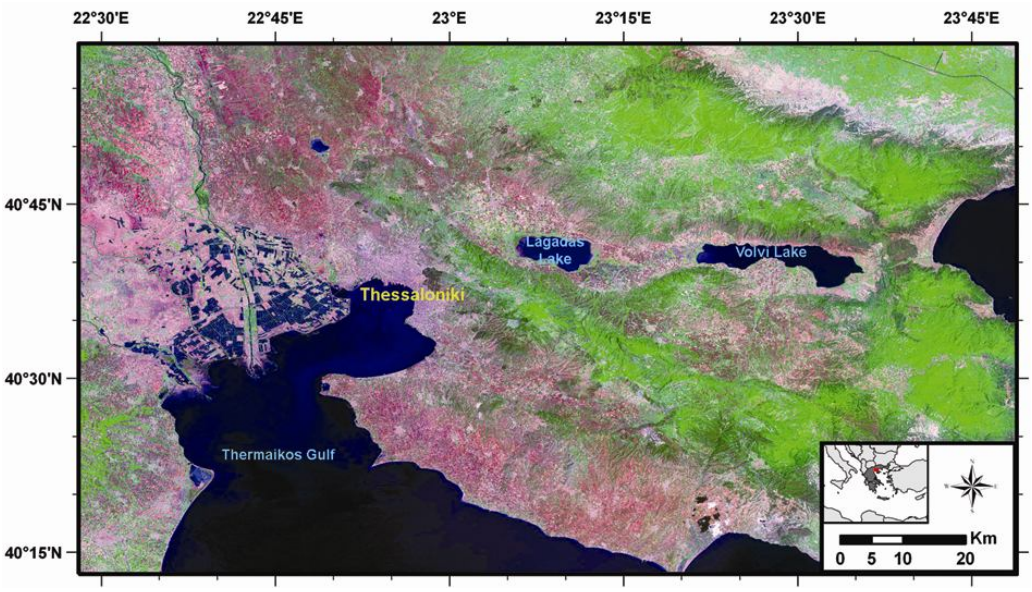

Figure 1. Broader study area.

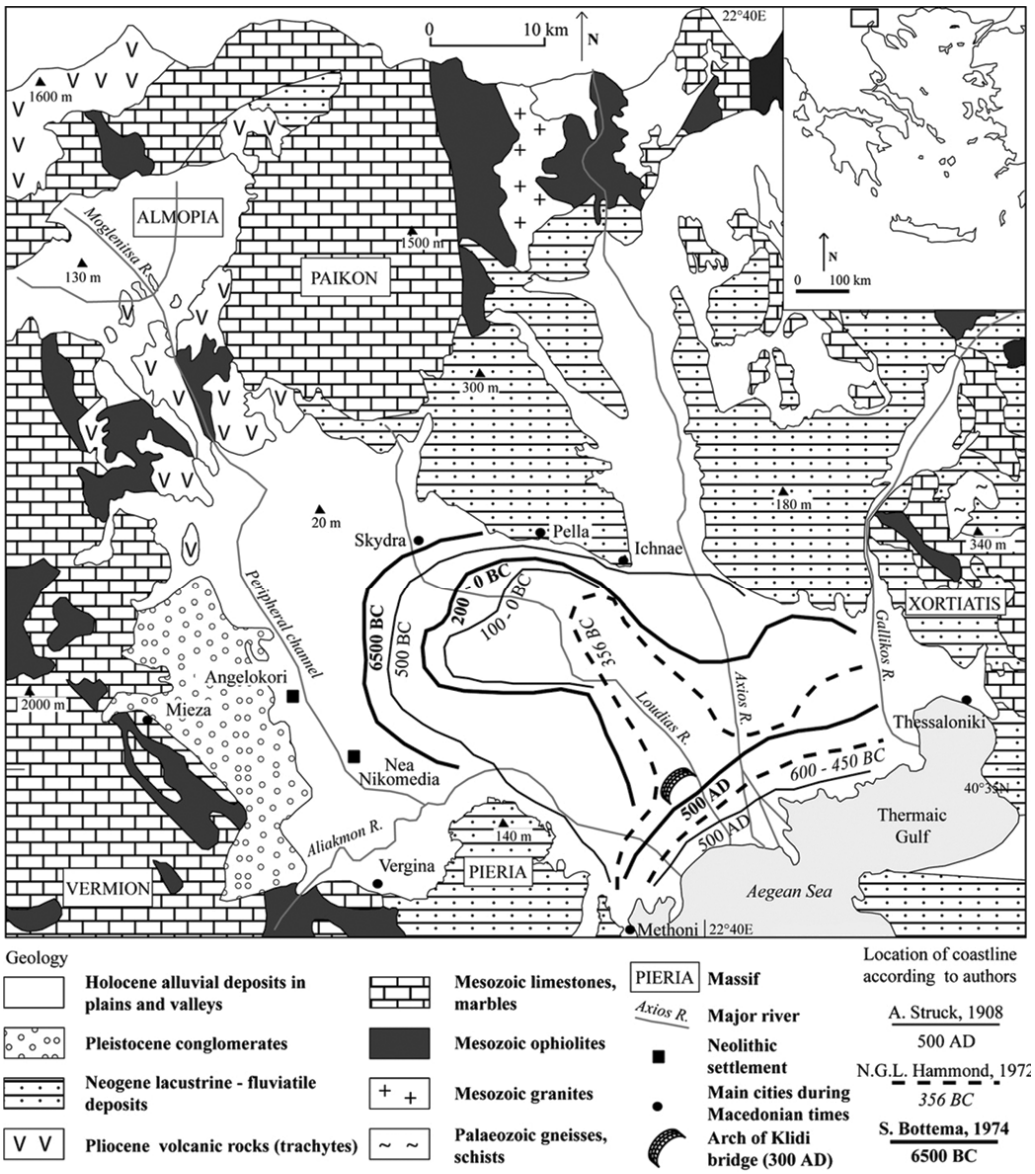

Figure 2. Geology of the Thessaloniki Plain and location of the coastline, according to palaeogeographic reconstructions by contemporary authors (Ghilardi et al. 2008).

deltas and secondarily by two smaller rivers (Gallikos and Loudias) (Astaras and Sotiriadis 1988).

During the era of Alexander the Great (≈ 500 B.C.), the city of Pella was located by the sea, but in time, the increasing river sediment discharge and the continental uplift caused the gradual regression of the sea and the relocation of the coastline by approx. 50Km in SE direction (Fig. 2). Today, elevations down to a few meters below MSL occur in the area (near Kalohori). Turning to the geological background of the region (Fig. 2): Mesozoic limestones, marbles, schists, phyllites, granites and ultrabasic rocks prevail in the mountains; Neogene to Pleistocene sediments occur in the hills and Holocene alluvial deposits in the plains and valleys (Astaras and Sotiriadis 1988; Ghilardi et al. 2008).

Part of this 2500-year old coastal plain, the broader area of Kalohori (Fig. 3), has been dominated by subsidence phenomena for several decades, occurring at velocities in the order of a few cm/yr (Andronopoulos et al. 1991; Stiros 2001; Psimoulis et al. 2008).

The first signs of subsidence in Kalochori were noticed in 1965 in the form of a progressive marine invasion. In 1969, during a period of intensive rainfall, the seawater reached the southern houses of the village. The first two efforts of building embankments failed, as the constructions collapsed in 1973 and 1979 respectively. In 1980, a new larger

Figure 3. Overview of the Kalohori - Thessaloniki area (source: Google Earth™).

dam was constructed, providing apparent security to Kalochori. Since then, several events of damage and extensions of the embankment occurred, but the main construction man-aged to resist the deformation caused by the subsidence and the dynamic loading of sea waves. This protective barrier is combined with an extensive surface drainage network and several pumping stations to prevent the inland region from flooding (Loupasakis and Rozos 2009). Still, several flooded areas were never reclaimed (Fig. 4).

According to Loupasakis and Rozos (2009), taking into consideration the geological, geotechnical and hydrogeological setting of the wider Kalochori region and the historical background of the subsidence, it is clear that the excessive deformations is mainly attributed to the overexploitation of confined aquifers in the area. Although most of the studies converge to that interpretation, some authors have suggested alternative sources that have possibly contributed to the subsidence phenomena, like the consolidation of sediments, coastal erosion and sea level rise.

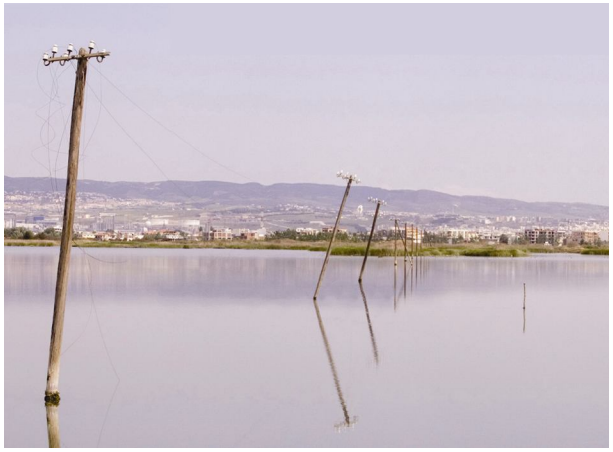
Figure 4. Contemporary view of flooded areas near Kalohori.

3. InSAR measurements

The dataset used consisted of 19 ENVISAT/ASAR descending (track 279) images (ESA Category-1

project ID: 4482), spanning a period between 2002 and 2007 (Fig. 5). InSAR processing was carried out via the ROI_PAC (Repeat Orbit Interferometry Package) software, developed by JPL (NASA) and CalTech (California Institute of Technology).

As expected, the coherent pixels are concentrated in and around urban areas and in particular in the vicinity of the city of Thessaloniki. This analogy is more obvious if the coherence map is compared to an amplitude ASAR image (Fig. 10).

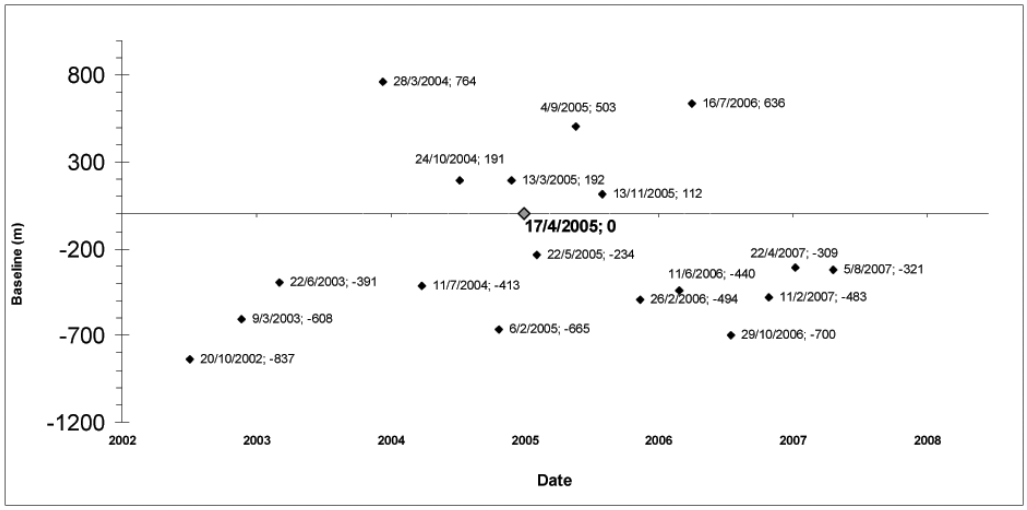

Figure 5. ENVISAT/ASAR available dataset (track 279, descending).

In total, 117 differential interferograms were successfully computed, some of the most interesting of which are subsequently presented (Fig. 6).

Orbital fringes were removed using orbital information provided by the Department of Earth Observation and Space Systems (DEOS) of the Delft University of Technology and topographic contribution was removed using the 3-arc second SRTM DEM (Farr and Kobrick 2000).

A considerable number of the computed interferograms, with temporal baselines between 5 months and 2.5 years and perpendicular baselines between 11m and 260m, clearly indicate the presence of a noisy deformation pattern around Kalohori (Fig. 7).

Additionally, some week signals south of Oreokastro, between the ring road of Thesaloniki and the Egnatia road, are present in several interferograms. These signals present consistency in time that is unlikely to be attributed to random atmospheric effects, which are generally correlated in space but not in time (Mouratidis et al. 2010b).

The next step was to estimate the phase coherence in space and time (Fig. 8), on the basis of the 117 ASAR interferograms. Due to the redundancy of data incorporated in the calculations, a coherence map of increased reliability was constructed (Fig. 9).

All interferograms were particularly noisy, as a result of the loss of coherence in most non-urban areas, thus making the steps of interferogram filtering and unwrapping quite challenging.

Due to fact that despite the improvements of various methods, phase unwrapping is still difficult, risky and potentially damaging (Ferretti et al. 2007) and taking into account the noisy interferograms produced in this study, it was decided to interpret the wrapped products. This conservative approach limits the practical use of the interferograms, as the displacements along the SAR line of sight cannot be calculated for each pixel, but on the other hand there is no risk of "damaging" the interferogram or introducing noise that could be misinterpreted as signal. Combined with a large number of computed interferograms, this approach has the potential of providing less, but reliable information and results.

Concerning the interferogram filtering, after experimenting with various techniques, a two-step approach was adopted; the first step was to remove non-coherent pixels, by determining a coherence threshold using the coherence map. The second step was to apply an adaptive 5x5 Gamma filter, in order to enhance the visual result (Fig. 11). By further confining the interferogram to the area of interest, the final products were derived (Fig. 12 & 13).

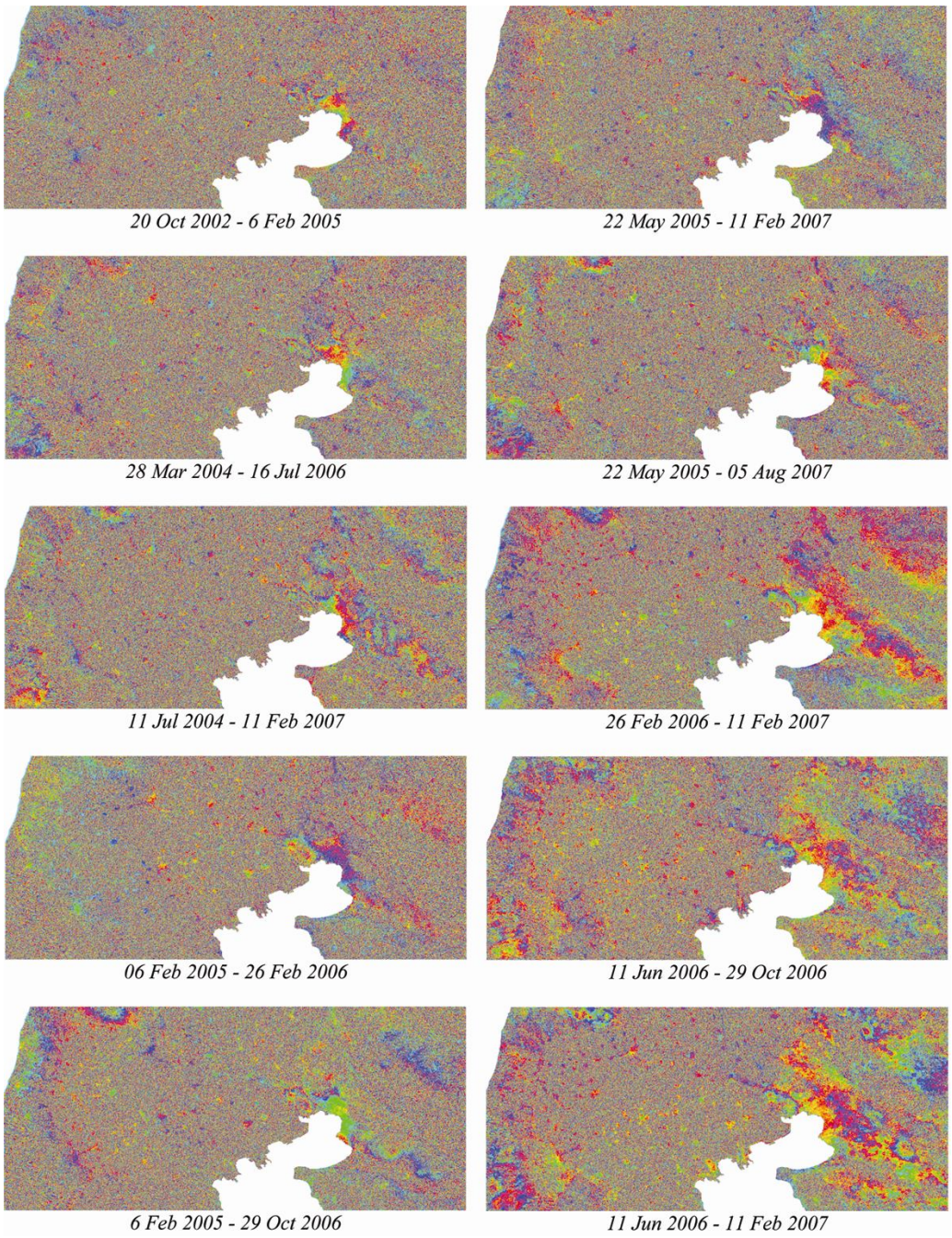

Figure 6. Selection of computed wrapped differential interferograms.

4. Collection and processing of Kinematic GPS data

In January and February 2008, for the purposes of supporting relevant remote sensing research efforts conducted by Mouratidis (2010a, b), a four-day kinematic GPS campaign was carried out in the broader area of the city of Thessaloniki (Fig. 14), using two Topcon™ GB-1000 dual frequency GPS and GLONASS (the latter data were not used in this study) receivers. Sampling rate was selected to 1sec. The reference stations were chosen each day accordingly, so as to facilitate the receiving of the satellite signals (open horizon, no obstructions, etc.) and at the same time to ensure a maximum distance of 20Km from the rover, in order to minimize atmospheric contributions to the GPS signal. In total, three different locations had to be used for the reference station. In order to have some backup reference station, a Leica RS500 GPS receiver located in the University of Thessaloniki (approximately in the centre of the study area) was set to collect data at 1sec interval during the period of measurements.

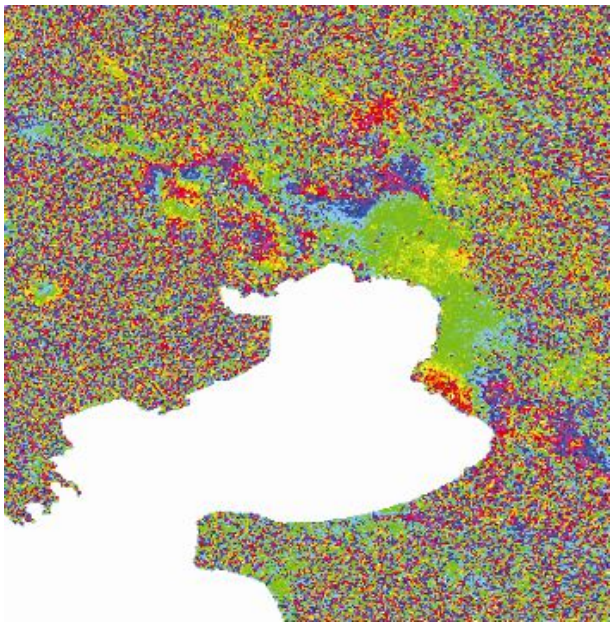

Figure 7. Area of interest, as visualized on the 6 Feb 2005 - 29 Oct 2006 interferogram.

The GPS antenna of the rover was securely mounted on the top of a vehicle that was used for all measurements (Fig. 15). During data collection, the speed of the vehicle had been targeted to remain below 60Km/h, in order to both ensure the stability and safety of the antenna and also to have at least one measurement every 15m. In practice, the mean speed of the vehicle did not exceed 40Km/h, providing a much denser volume of data than theoretically expected (approx. 1 point/11m).

In general, there is a good correlation of data collection density and relief, in the sense that a flat relief is well recorded with relatively sparse measurements, while mountainous areas demand denser sampling. These conditions are in practice well met, since the speed of the vehicle is by default regulated by the character of the road, which is in turn controlled by the quality of the terrain.

With the above configurations and considerations, more than 60,000 points were collected, within approximately 22 hours (approx. 720 Km driven), providing a density of measurements in the order of 20 points Km^{-2}.

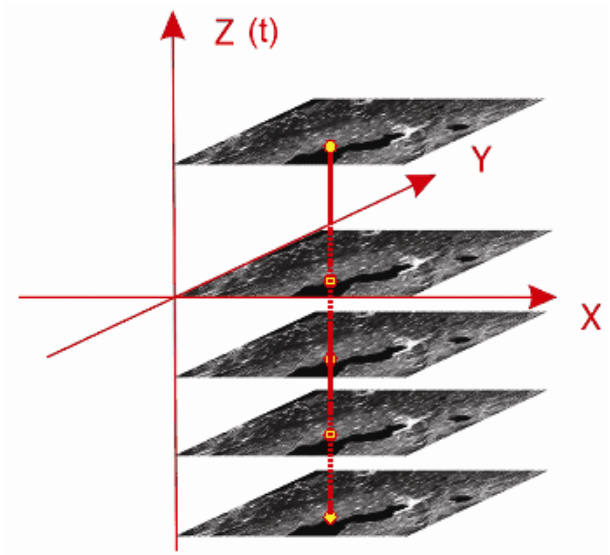

Figure 8. Concept of coherence estimation in space and time.

Post-processing of the kinematic GPS data was carried out with Ashtech™ Precise Navigation (PNAV™) software, after calculating reference station coordinates, using data from the European Reference Frame (EUREF) Permanent Network (EPN). WGS'84 datum was used for all calculations and GPS geometric heights were converted into orthometric heights by subtracting the height of the geoid (with reference to the WGS84 ellipsoid) in the area of interest, which according to Andritsanos et al. (2000), the University NAVstar COnsortium (UNAVCO) website (http://sps.unavco.org/geoid) and the Hellenic Mapping & Cadastral Organization (O.K.X.E.) is

Figure 9. Coherence map based on 117 ASAR data.

approximately 43m. The distribution of errors for the processed KGPS points is presented in fig. 16.

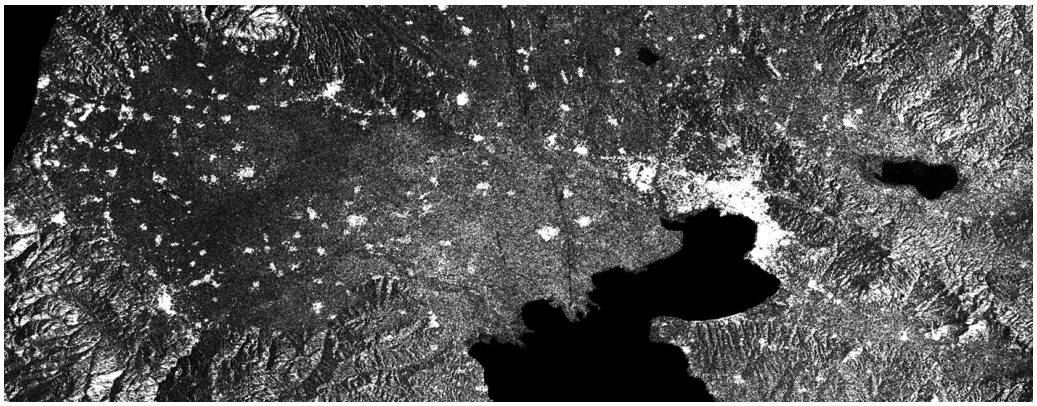

Figure 10. Amplitude image of ASAR data used.

5. Results and Discussion

The 117 computed ENVISAT/ASAR interferograms of the broader Thessaloniki area, spanning the 2002-2007 period, are particularly noisy, mainly due to the loss of coherence in the non-urban parts of the study area, but also due to random atmospheric influences, which prevent the "clean" and full forming of fringes. Nevertheless, the large number of computed interferograms and a-priori information support the results and assist in the identification of subsidence on several interferograms.

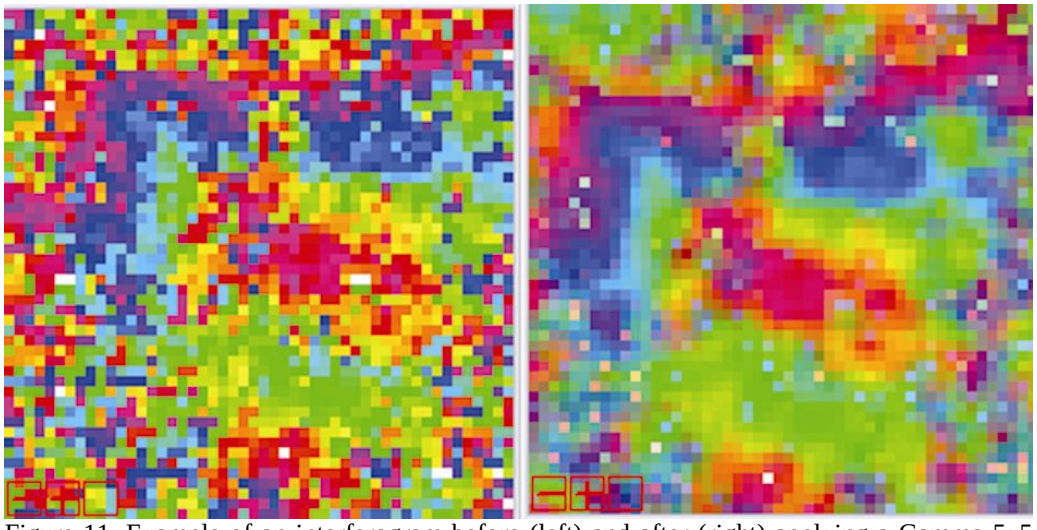

Figure 11. Example of an interferogram before (left) and after (right) applying a Gamma 5x5 adaptive filter.

Using the coherence map to eliminate non-coherent pixels and subsequently filtering the wrapped interferogram improves the final products considerably.

According to the results of ENVISAT/ASAR interferometry implemented in this study, the mean subsidence rate, between 2002 and 2007, in the Kalohori area is estimated to be no more than 3cm/yr (approx. 1 fringe/yr), a result which is consistent with the rates suggested in previous studies, incorporating data until 2002 (Badelas et al. 1996; Doukas et al. 2004; Stiros 2001; Raucoules et al. 2008). This denotes that the phenomenon is still in progress.

On the other hand, the city of Thessaloniki appears to be relatively stable, since no deformation pattern is detectable in any of the 117 computed interferograms.

Additionally, several ENVISAT/ASAR interferograms indicate that a deformation pattern, originally drawn from of ERS InSAR (Raucoules et al. 2008), in the NNW suburbs of Thessaloniki (Oreokastro area) is not opportunistic. Instead, it

reflects an on-going phenomenon of unclear origin, requiring further investigation.

nominal accuracy down to a few meters (e.g. Mouratidis 2010b; Mouratidis et al. 2010a).

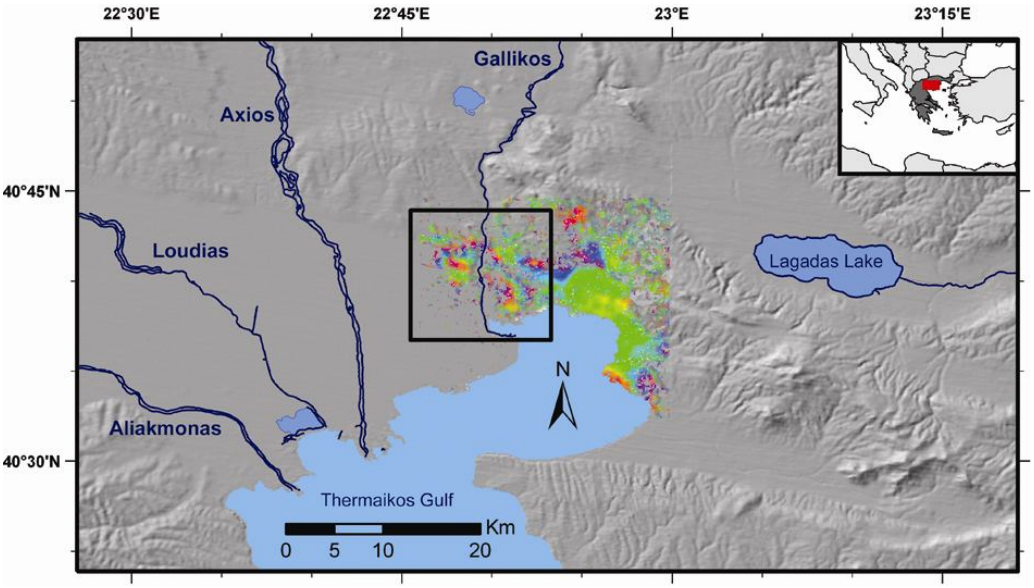

Figure 12. Filtered interferogram (6 Feb 2005 - 29 Oct 2006) draped over a shaded relief map of the study area.

Concerning the KGPS data, as shown by Mouratidis (2010b), they can be successfully used for recognizing reliable Ground Control Points (GCPs) in remote sensing imagery of the visible and infrared part of the electromagnetic spectrum. SAR and InSAR products can also benefit in this respect, by the recognition of GCPs in the amplitude images, which can later on be directly related to the interferometric phase images.

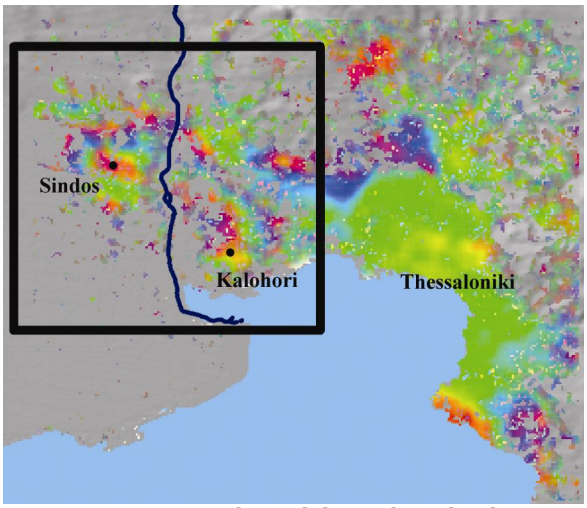

Figure 13. Zoom in the Kalohori-Thessaloniki area, on the 6 Feb 2005 - 29 Oct 2006 interferogram.

Nevertheless, the most straightforward application of such extensive KGPS datasets is related to the validation of practically any elevation data of

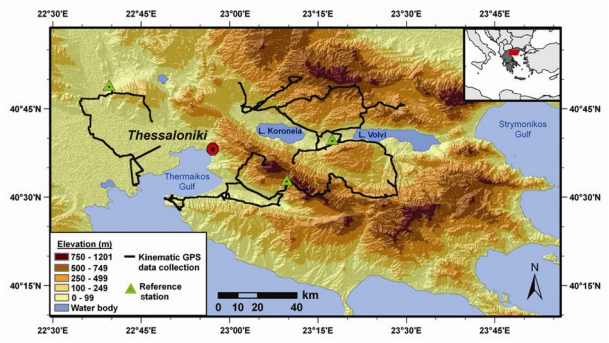

Figure 14. Kinematic GPS (KGPS) measurements conducted in the broader region of interest.

Figure 15. Rover receiver antenna (b, c) mounted on the top of the vehicle (a) that was used during the KGPS measurements. One of the 2 identical Topcon™ GB-1000 receivers that were used is also depicted (d).

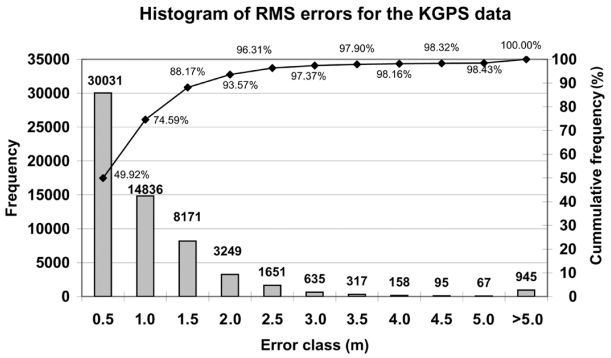

Figure 16. KGPS data accurary after post-processing. RMS is <0.5m for approx. 50% of the data, whereas almost 90% of the data have an accuracy better than 1.5m. Only 1.5% of the data are of relatively low accuracy (RMS>5m).

Although it has to be anticipated that some of the collected KGPS data will be insufficient in terms of accuracy for some applications, there will still be enough reliable points left to work with. The success of a KGPS campaign will strongly depend on the type of equipment available and the planning of the measurements, but also from the type of terrain and land cover in each study area.

6. Conclusions

ENVISAT/ASAR interferometry has demonstrated that subsidence in the Kalohori area has been continuing in the 21st century at approximately the same rates (a few cm/yr) as before. Taking into consideration the existence of below-MSL elevations and the general trend for global sea level rise caused by climatic change, the risks and issues associated with subsidence and marine invasion in the vicinity of Kalohori are expected to aggravate in the next few decades.

The time and effort needed to carry out an extensive KGPS campaign is rather small, compared to the potential applications of the collected data and their diachronic value.

A large number of KGPS data collected is an independent dataset that can be used for various applications. Apart from validating DEMs, other ways of using these datasets have been proposed but there is still a need for optimization of the synergy with InSAR data and other remote sensing images. The tools that will facilitate the use of KGPS data in remote sensing studies are yet to be developed and more innovative applications are yet to be discovered.

Acknowledgements

The European Space Agency (ESA), Ecole Normale Superieure (ENS), the Aristotle University of Thessaloniki (AUTH), the Greek State Scholarships Foundation (IKY) and Universite Pierre et Marie Curie (Paris VI), are gratefully acknowledged for making this work possible by providing data, knowledge, facilities, human resources & funding.

References

Andritsanos V.D., Fotiou A., Paschalaki E., Pikridas C., Rossikopoulos D. and Tziavos I.N., 2000. Local Geoid Computation and Evaluation. Physics and Chemistry of the Earth, 25, 63-69.

Andronopoulos B., Rozos D. and Hadzinakos I., 1991. Subsidence Phenomena in the Industrial Area of Thessaloniki, Greece. Land Subsidence 200, 59-69.

Astaras T.A. and Sotiriadis L., 1988. The Evolution of the Thessaloniki-Giannitsa Plain in Northern Greece during the last 2500 years - From the Alexander the Great Era Until Today. Lake, Mire and River Environments during the last 15000 years. Balkema, Rotterdam, 105-114.

Avallone A., Zollo A., Briole P., Delacourt C. and Beauducel F., 1999. Subsidence of Campi Flegrei (Italy) detected by SAR Interferometry. Geophysical Research Letters, 26, 2303-2306.

Badelas A., Savvaidis P., Ifadis I. and Doukas I., 1996. Monitoring of ground subsidence in the area of Kalohori by using a high precision leveling control network. Technical Report, Research Committee, Aristotle University of Thessaloniki, 2853, 157.

Bamler R. and Hart P., 1998. Synthetic aperture radar interferometry. Inverse Problems, 14, R1–R54.

Doukas I., Fotiou A., Ifadis I.M., Katsambalos K., Lakakis K., Petridou - Chrysohoidou N., Pikridas C., Rossikopoulos D., Savvaidis P., Tokmakidis K. and Tziavos I.N., 2004. Displacement field estimation from GPS measurement in the Volvi area. FIG Working Week, May 22-27, 2004, Athens, Greece.

Farr T.G. and Kobrick M., 2000. Shuttle Radar Topography Mission produces a wealth of data. Amer. Geophys. Union Eos, 81, 583-585.

Ferretti A., Monti-Guarnieri A., Prati C., Rocca F. and Massonnet D., 2007. InSAR Principles: Guidelines for SAR Interferometry Processing and Interpretation, ESA TM-19, ESA Publications Division, Noordwijk, The Netherlands.

Gabriel A.K. and Goldstein R.M., 1988. Crossed orbit interferometry: theory and experimental results from SIR-B. Int. J. Remote Sens., 9, 857-72.

Gabriel A.K., Goldstein R.M. and Zebker H.A., 1989. Mapping small elevation changes over large areas: differential radar interferometry. J. Geophys. Res., 94, 9183-91.

Ghilardi M., Fouche E., Queyrel F., Syrides G., Vouvalidis K., Kunesch S., Styllas M. and Stiros S., 2008. Human occupation and geomorphological evolution of the Thessaloniki Plain (Greece) since mid Holo-

cene. Journal of Archaeological Science 35, 111-125.

Greek Ministry of Agriculture, 1994. Forestry map (1:200,000) of the Prefecture of Thessaloniki, Forestry Service of Greece.

Hanssen R. F., 2001. Radar Interferometry: Data Interpretation and Error Analysis. Springer, Berlin, 328 p.

Lopez-Quiroz P., Doin M.-P., Tupin F., Briole P., Nicolas J.-M., 2009. Time series analysis of Mexico city subsidence constrained by radar interferometry. Journal of Applied Geophysics, 69, 1-15.

Loupasakis C. and Rozos D., 2009. Finite-element simulation of land subsidence induced by water pumping in Kalochori village, Greece. Quarterly Journal of Engineering Geology and Hydrogeology, 42, 369–382.

Massonnet D., Briole P. and Arnaud A., 1995. Deflation of Mount Etna monitored by spaceborne radar interferometry. Nature, 375, 567-570.

Massonnet D. and Feigl K., 1998. Radar interferometry and its application to changes in the earth's surface. Rev. Geophys., 36, 441-500.

Mouratidis A., 2010a. Contribution of -GPS and GIS-assisted spaceborne Remote Sensing in the Morphotectonic research of Central Macedonia (N. Greece). Ph.D. thesis, Aristotle University of Thessaloniki (in Greek with English summary).

Mouratidis A., 2010b. Production and validation of DTM from high resolution (SPOT-5/HRG) satellite imagery with the support of kinematic GPS data. Diploma thesis, Faculty of Rural and Surveying Engineering, Aristotle University of Thessaloniki (in Greek with English summary).

Mouratidis A., Briole P. and Katsambalos K., 2010a. SRTM 3 arc second DEM (versions 1, 2, 3, 4) validation by means of extensive kinematic GPS measurements: A case study from N. Greece. Int. J. Remote Sens. (in press).

Mouratidis A., Briole P., Ilieva M., Astaras T., Rolandone F. and Baccouche M., 2010b. Subsidence and deformation phenomena in the vicinity of Thessaloniki (N. Greece) monitored by ENVISAT/ASAR interferometry. Proceedings of Fringe 2009 Workshop: "Advances in the Science and Applications of SAR Interferometry", 30th November - 4th December 2009, ESA/ESRIN, Frascati, Rome, Italy. ESA Special publication on CD-ROM (SP-677).

Pikridas C., Spatalas S., Tokmakidis K. and Tsoulis D., 2004. Terrain creation and analysis using information from GPS and classical techniques. INGEO 2004 and FIG Regional Central and Central European Conference on Engineering Surveying, 11-13 November 2004, Bratislava, Slovakia.

Psimoulis P., Ghilardi M., Fouache E. and Stiros S., 2007. Subsidence and evolution of the Thessaloniki plain, Greece, based on historical leveling and GPS data. Engineering Geology, 90, 55-70.

Raucoules D., Colesanti C. and Carnec C., 2005. Use of SAR interferometry for detecting and assessing ground subsidence. C. R. Geoscience, 339, 289-302.

Raucoules D., Parcharidis I., Feurer D., Novalli F., Ferretti A., Carnec C., Lagios E., Sakkas V., Le Mouelic S. and Cooksley G., 2008. Ground deformation monitoring of the broader area of Thessaloniki (Northern Greece) using radar interferometry techniques. Natural Hazards and Earth System Sciences, 8, 779-788.

Stiros S.C., 2001. Subsidence of the Thessaloniki (northern Greece) coastal plain, 1960-1999. Engineering Geology, 61, 243-256.

Zebker, H.A. and Goldstein R.M., 1986. Topographic mapping from interferometry synthetic aperture radar observations. J. Geophys. Res., 91, 4993-4999.

Zhou X., Chang N.B. and Li S., 2009. Applications of SAR Interferometry in Earth and Environmental Science Research. Sensors, 9, 1876-1912.

Author index